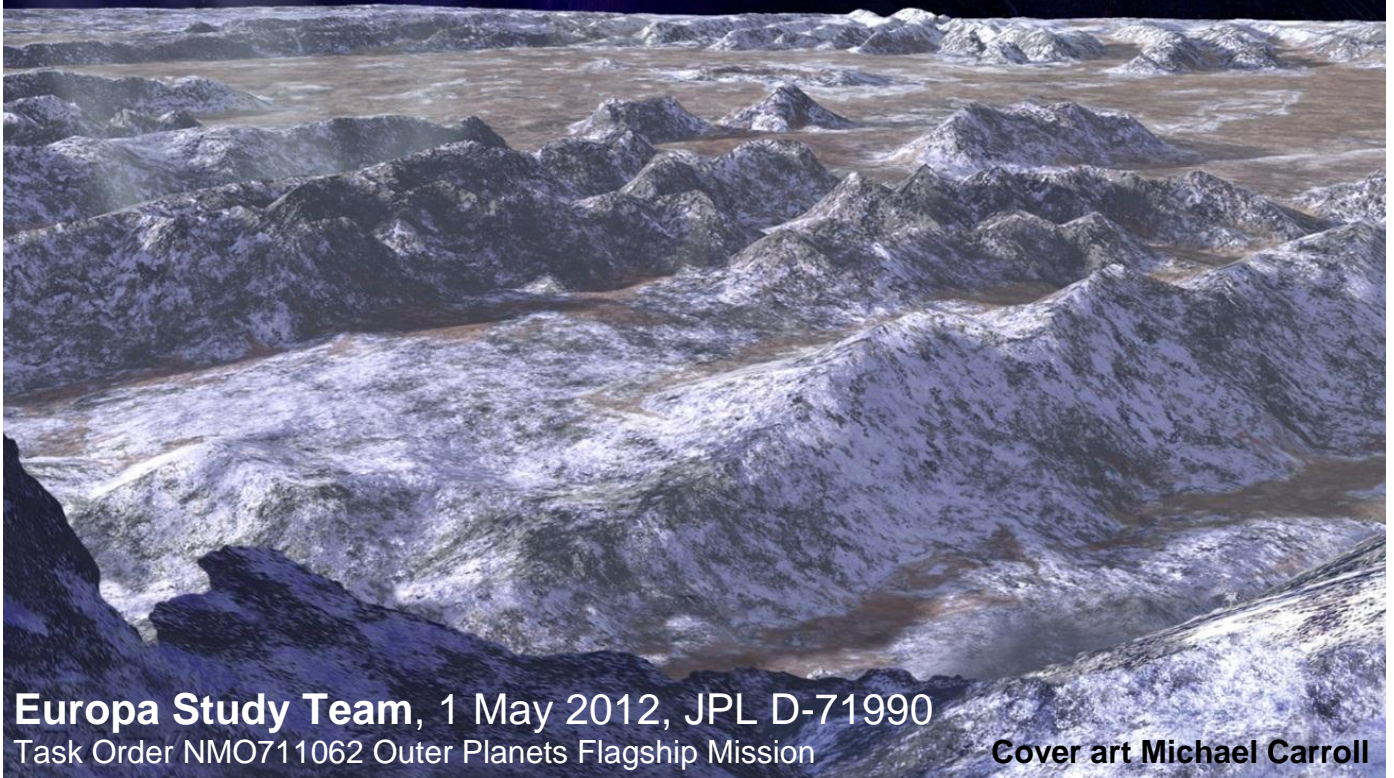National Aeronautics and Space Administration

EUROPA STUDY 2012 REPORT

Europa Study Team, 1 May 2012, JPL D-71990
Task Order NMO711062 Outer Planets Flagship Mission

Cover art Michael Carroll

National Aeronautics and Space Administration

EUROPA STUDY 2012 REPORT
EXECUTIVE SUMMARY

Europa Study Team, 1 May 2012, JPL D-71990
Task Order NMO711062 Outer Planets Flagship Mission

Cover art Michael Carroll

ES. EUROPA STUDY 2012 REPORT: EXECUTIVE SUMMARY

Contents

ES.   EUROPA STUDY 2012 REPORT: EXECUTIVE SUMMARY

ES.1 Executive Summary

ES.1.1 Introduction

Four hundred years ago, Galileo's discovery of Jupiter's four large moons forever changed humanity's view of the universe, helping to bring about the Copernican Revolution. Today one of these Galilean moons may again revolutionize science and our sense of place, for hidden beneath Europa's icy surface is the most promising home for extant extraterrestrial life within our reach.

This new appreciation began to unfold in 1995, when a spacecraft named in Galileo's honor arrived at the Jupiter system to follow up on earlier Voyager discoveries. As part of its mission, the Galileo spacecraft could provide only tantalizing samplings of data at Europa (Figure ES.1.1-1); nonetheless, it provided strong evidence for a deep global ocean beneath Europa's icy crust, leading to speculation on the potential for life within icy moons.

Meanwhile, over the last quarter century we have learned that Jupiter-like planets are common around other stars, and perhaps many have icy moons like Europa. Understanding Europa—one of the most geophysically fascinating and astrobiologically promising bodies in our solar system—is therefore vital to understanding the habitability of worlds throughout the galaxy.

A mission targeting Europa would be needed to pursue these exciting discoveries using close-up observation with modern instrumentation designed to address the habitability of Europa. Over the last decade, NASA has considered several mission options for exploring Europa, convening a series of Science Definition Teams (SDTs), composed of experts from the scientific community, to hone the highest priority science objectives for Europa.
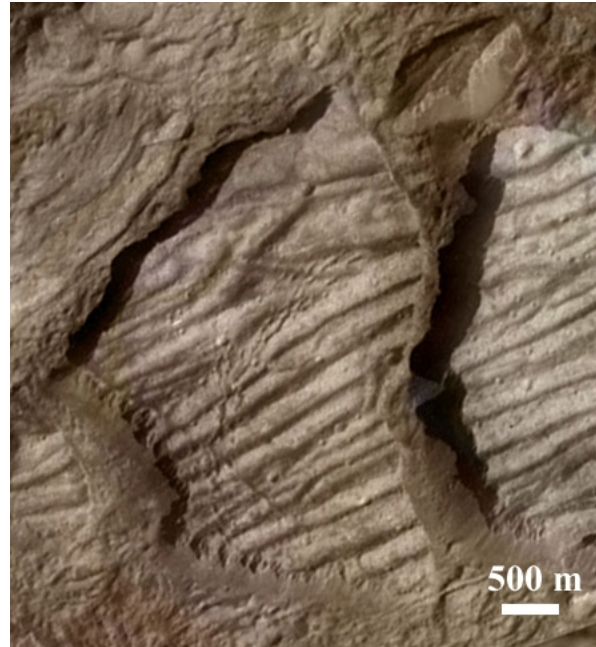

Figure ES.1.1-1. Europa's surface shows a landscape scarred by tectonic and icy volcanic events. This image of the Conamara Chaos region at 11 m per pixel implies that portions of the surface have been broken up into giant plates. This event is inferred to have happened in Europa's geologically recent past. The dark reddish material may be derived from the ocean.

By 2008, technical studies culminated in a mature Pre–Phase A mission concept, the Jupiter Europa Orbiter (JEO), as part of a joint NASA–ESA Europa Jupiter System Mission (EJSM). The JEO concept was further refined throughout 2009 and 2010 in a pre–Phase A mode. The March 2011 Planetary Science Decadal Survey concluded that the science contribution of such a mission would be of paramount importance, comparable to the entire proposed Mars Sample Return campaign. It stated, "Because of this ocean's potential suitability for life, Europa is one of the most important targets in all of planetary science" (Space Studies Board 2011, p. 271).

However, because of serious concerns over mission cost, based on NASA's independent cost estimate, the Decadal Survey also recommended that "NASA should immediately undertake an effort to find major cost reductions for JEO, with the goal of minimizing the
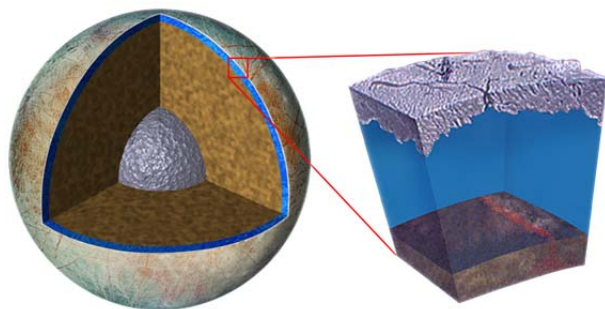
Figure ES.1.2-1. Europa is believed to have a relatively thin ice shell above a 100-km-thick global ocean—equivalent to twice the volume of all of Earth's oceans—in direct contact with a rocky mantle below. Oxidants from the surface above and chemicals from the rocky mantle below might be able to supply the ocean water with the required chemistry and energy for life.

size of the budget increase necessary to enable the mission" (Space Studies Board 2011, p. 5). To that end, NASA Headquarters promptly enlisted a new Europa SDT, and directed the Europa Study Team to examine a set of reduced-scope options for exploring Europa. Independent cost and technical reviews were to be performed on all study results. What follows is a summary of these results.

ES.1.2 Habitability of Europa as Motivation for Future Missions

Europa is a prime candidate in the search for present-day habitable environments in our solar system. Europa is unique among the large icy satellites (Figure ES.1.2-1) because it probably has a saltwater ocean today beneath an ice shell that is geodynamically active and relatively thin (several kilometers to several tens of kilometers thick). The combination of irradiation of its surface and tidal heating of its interior could make Europa a rich source of chemical energy for life. Perhaps most importantly, Europa's ocean is believed to be in direct contact with its rocky mantle, where conditions could be similar to those on Earth's biologically rich sea floor. Hydrothermal zones on Earth's seafloor are known to be rich with life, powered by energy and nutrients that

result from reactions between the seawater and the warm rocky ocean floor.

Life as we know it depends on three principal "ingredients": 1) a sustained liquid water environment; 2) essential chemical elements (e.g., C, H, N, O, P, S) that are critical for building life; and 3) a source of energy that could be utilized by life (Figure ES.1.2-2). For Europa, current assessment of these three broad requirements for life can be summarized as: 1) a likely internal global ocean, which has likely existed for over 4 billion years, and potentially water pockets within the ice shell; 2) elements derived from the primordial chondritic composition of the satellites, plus delivery by asteroids and comets over time; and 3) oxidants at the surface, and possible hydrothermal activity at the ocean floor as driven by tidal heating, suggesting that the cycling of chemical energy into Europa's ocean over geological time is vital to understanding its habitability.

These "ingredients" and the scientific issues surrounding them define three themes of *water*, *chemistry*, and *energy* that permeate discussions of Europa's potential habitability. Europa may meet these minimum require-
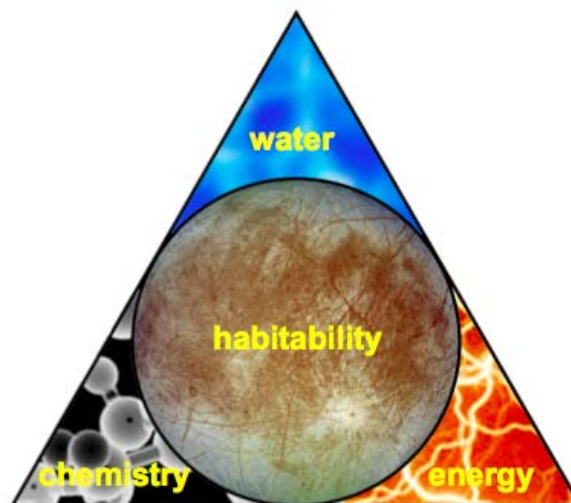

Figure ES.1.2-2. The three "ingredients" for life—water, chemistry, and energy—are key to understanding Europa's habitability, and they are developed into themes that permeate the Europa mission concepts.

ments, but the processes that shape Europa's ice shell, and the exchange processes between the surface and ocean, are poorly understood. Indeed, even the existence of a subsurface ocean, while suspected, is not yet proven. With this in mind, the four categories of scientific investigation most relevant to understanding Europa's habitability are:

Ocean: Existence, extent, and salinity of the ocean and its relation to the deeper interior;

Ice Shell: Existence and nature of any subsurface water within or beneath the ice shell, heterogeneity of the ice shell, and the nature of surface-ice-ocean exchange;

Composition: The chemistry and distribution of salts, any organics, and other compounds, and their relationships to ocean composition;

Geology: The characteristics and formation of surface features, including sites of recent or current activity, and implications for water reservoirs and satellite evolution.

ES.1.3 Europa Mission Study

To address and answer the key questions about Europa's habitability, a dedicated Europa mission would be required. To that end, a study was conducted starting in April 2011 to define options for Europa mission concepts. A Europa SDT guided the science definition, and a combined Jet Propulsion Laboratory (JPL) and Applied Physics Laboratory (APL) study team performed the technical work.

The SDT was tasked with reformulating the science of a Europa mission to achieve compelling science while ensuring reduced risk and scope from past studies. The SDT approached the task by identifying an over-arching goal, key science objectives, and science investigations to best address those objectives, with examples of appropriate measurements that could be carried out at Europa to address the science investigations.

The SDT determined that there is a clear division among the key science questions and associated investigations (Table ES.1.3-1), where some are best conducted from Europa orbit, others best achieved through multiple flybys, and the remainder best addressed through a landed mission. To characterize the extent of the ocean and its relation to the deeper interior, scientists need systematic geophysical measurements of gravity, topography, and magnetic field: measurements best obtained from an orbital platform. An orbital platform also permits uniform geological mapping. In comparison, observations to characterize the ice shell, understand the surface composition, and perform high-

Table ES.1.3-1. Key Europa science questions and associated mission platforms.

Science Question	Orbiter	Multi-Flyby	Lander
1. What are the characteristics of Europa's ocean?	✓	*	✓
2. How thick is the icy shell?	✓	✓	✓
3. Is there near-surface water within the ice shell?		✓	✓
4. What is the global distribution of geological features?	✓	✓	
5. Is liquid water involved in surface feature formation?		✓	
6. Is the icy shell warm and convecting?		✓	✓
7. What does the red stuff tell us about ocean composition?		✓	✓
8. How active is Europa today?		✓	✓
9. What is the plasma and radiation environment at Europa?			
10. What is the specific nature of organics and salts at Europa?			✓

✓ Mission concept explicitly addresses the science question.
* Relevant science could be addressed with modest mission modifications.

resolution targeted geological observations are data-intensive and require high-mass, high-power instruments, so these are best carried out from a spacecraft that makes multiple flybys of Europa, transmitting data back to Earth during long orbital petals. Only a lander could accomplish evaluation of the detailed surface chemistry and mineralogy to best understand the detailed nature of near-surface organics and salts, as these investigations require *in situ* sample analyses.

Any of these three mission options would provide high caliber, compelling science that would change paradigms in our understanding of the nature and habitability of icy worlds. Each is intended to fly completely independently, without a requirement for any other mission.

Each mission option has a common goal:

Explore Europa to investigate its habitability.

A Europa *Orbiter* Mission would chiefly perform geophysical measurements ("water" science). A Europa *Multiple-Flyby* Mission would concentrate on performing remote measurements that address the "chemistry" and "energy" science. A Europa *Lander* Mission would concentrate on *in situ* "chemistry" science.

ES.1.4   Orbiter Concept

ES.1.4.1   Orbiter Science

The orbiter concept is tailored to the unique geophysical science that requires being in orbit at Europa. This includes confirming the existence of an ocean and characterizing that ocean through geophysical measurements of Europa's gravitational tides and magnetic induction response. It also includes mapping of the global morphology and topography of the satellite, to reveal its geological evolution.

The objectives, investigations, and model planning payload of the Orbiter Mission are

Table ES.1.4-1. Objectives, investigations, and model planning payload for a Europa Orbiter concept.

Goal	Objective		Investigation	Model Planning Payload	Theme		
					W	C	E
Explore Europa to investigate its habitability	Ocean	Characterize the extent of the ocean and its relation to the deeper interior.	Determine the amplitude and phase of gravitational tides.	Radio Subsystem, Laser Altimeter	✔		
			Determine Europa's magnetic induction response.	Magnetometer, Langmuir Probe	✔	✔	
			Determine the amplitude and phase of topographic tides.	Laser Altimeter, Radio Subsystem	✔		
			Determine Europa's rotation state.	Laser Altimeter, Mapping Camera	✔		
			Investigate the deeper interior.	Radio Subsystem, Laser Altimeter, Magnetometer, Langmuir Probe	✔	✔	✔
	Geology	Understand the formation of surface features, including sites of recent or current activity to understand regional and global evolution.	Determine the distribution, formation, and three-dimensional characteristics of magmatic, tectonic, and impact landforms.	Mapping Camera, Laser Altimeter	✔		✔

Note: Shaded check marks illustrate that the objectives directly address the themes of water (W), chemistry (C), or energy (E).

summarized in Table ES.1.4-1. Science objectives are listed in priority order, and the investigations within each objective are listed in priority order. The implied model planning payload are all low mass, low power, and low data rate, and thus well-matched to the technical demands of operating in Europa orbit. The Orbiter Mission concentrates on the water theme, as related to habitability, while addressing chemistry and energy themes as well.

ES.1.4.2 Orbiter Mission Concept

The Europa Orbiter Mission concept would deploy a highly capable, radiation-tolerant spacecraft (Figure ES.1.4-1) into orbit around Europa to collect a global data set to map the moon's surface morphology, its tidal cycle through gravity fluctuations, and its ocean induction signature through investigation of Europa's interaction with the Jovian magnetosphere. These measurements would be performed from a 100 km, 2- to 4-p.m. local solar time, near-polar orbit over the course of a 30 day science mission. The model planning payload assumed for the Europa Orbiter Mission (Table ES.1.4-2) consists of a notional set of remote-sensing instruments (Laser Altimeter and Mapping Camera), *in situ* instruments (Magnetometer and Langmuir
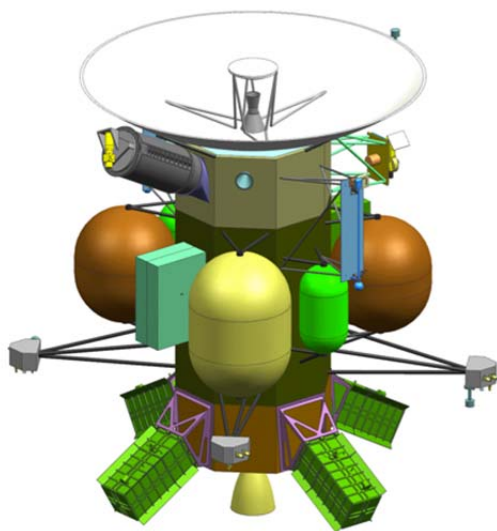
Probe), and a telecommunications system that provides Doppler and range data for accurate orbit reconstruction in support of geophysical objectives.

ES.1.4.3 Orbiter Mission Design

The Orbiter Mission starts with the spacecraft launch on an Atlas V 551 that places it on a 6.5 year Venus–Earth–Earth Gravity Assist (VEEGA) interplanetary trajectory before performing the Jupiter Orbit Insertion (JOI) burn. After JOI, fifteen gravity-assist flybys of Ganymede and Calisto are used over the course of 18 months to reduce orbital energy and align the trajectory with Europa; this mission design balances total radiation dose for the spacecraft with the amount of ΔV required. A Europa Orbit Insertion (EOI) burn places the spacecraft directly into a 100 km, circular, near-polar science orbit. After a short checkout period, science observations are conducted for 30 days. This orbit and the mission duration were chosen to meet the science objectives for gravity science, laser altimetry, and mapping (Figure ES.1.4-2).
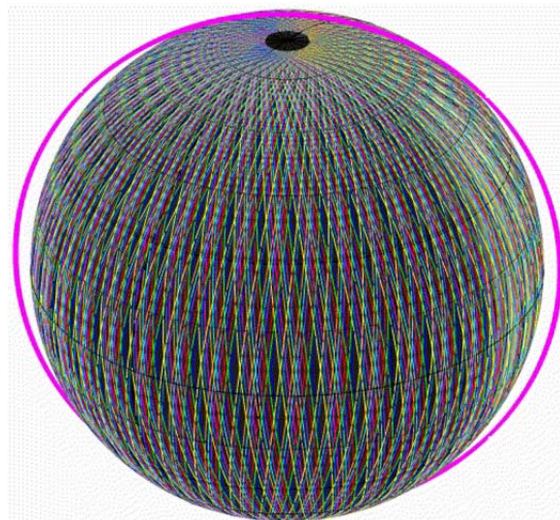
Figure ES.1.4-2. From a 100 km, circular, near-polar science orbit (pink circle), at the end of 30 days, the Orbiter Mission would create a dense network of Laser Altimeter profiles (equatorial spacing about 25 km), and it images essentially the entire surface in stereo (at about 100 m/pixel resolution). Each color represents those profiles obtained during a given 3.55 day orbit of Europa around Jupiter.

Figure ES.1.4-1. The Europa Orbiter Mission flight system provides a robust platform to collect and transmit science data.

Table ES.1.4-2. Capable science instruments for the Europa Orbiter concept draw on previous flight designs.

Instrument	Characteristics	Similar Instruments	
Laser Altimeter (LA)	**Time-of-Flight Laser Rangefinder** Time-dependent topography as a function of Europa's position in its tidal cycle, along with tidal amplitude for ocean detection and ocean characteristics, at better than 1 m vertical resolution.	NEAR NLR; MESSENGER MLA; LRO LOLA	
Mapping Camera (MC)	**Pushbroom Imager with fixed color filters and along-track stereo channel** Imaging at better than 100-m/pixel spatial resolution and 30-m vertical resolution at better than 300 m/pixel spatial scale. Panchromatic plus three color bands.	MRO MARCI; Nozomi MIC; MPL/MSL/MARDI; MESSENGER MDIS; New Horizons MVIC	
Magnetometer (MAG)	**Dual 3-axis Fluxgate Magnetometer** Two sensors located on a 10-m boom to determine the induction response from the ocean. Measurement rate of 8 vectors/s and sensitivity of better than 0.1 nT.	MESSENGER MAG; Galileo MAG	
Langmuir Probe (LP)	**Dual Langmuir Probe** Characterization of the local plasma and electric field to support the MAG determination of Europa's magnetic induction response, using booms 1-m long oriented 180° apart over a full 4π steradian field.	Rosetta LAP; Cassini RPWS	

ES.1.5 Multiple-Flyby Concept

ES.1.5.1 Multiple-Flyby Science

The Europa Multiple-Flyby Mission concept concentrates on remote sensing science that can be accomplished through multiple close flybys of Europa. This includes exploring Europa's ice shell for evidence of liquid water within or beneath it, in order to understand the thickness of the ice shell and potential material pathways from the ocean to the surface and from the surface to the ocean. The mission concept also includes exploration of the surface and atmospheric composition of Europa, in order to address ocean composition and habitability. Detailed morphologic and topographic characterization of Europa's surface are included as well.

The objectives, investigations, and model planning payload of the Multiple-Flyby Mission are summarized in Table ES.1.5-1.

Science objectives are listed in priority order, and investigations within each objective are listed in priority order. The Multiple-Flyby Mission instruments are heavy, require significant operating power, and generate large volumes of data. The multiple-flyby mission design allows for high-data-rate science collection followed by days of playback time, while greater mass margins afforded by foregoing Europa orbit insertion enable shielding to lower the radiation dose in the spacecraft avionics vault.

The Multiple-Flyby Mission concentrates on the chemistry and energy themes, as related to habitability. It also addresses the water theme by probing for water within the ice shell and investigating the relationship of surface chemistry and geology to subsurface water.

Table ES.1.5-1. Objectives, investigations, and model planning payload for the Europa Multiple-Flyby concept.

Goal	Objective		Investigation	Model Planning Payload	Theme		
					W	C	E
Explore Europa to investigate its habitability	Ice Shell	Characterize the ice shell and any subsurface water, including their heterogeneity, and the nature of surface-ice-ocean exchange.	Characterize the distribution of any shallow sub-surface water and the structure of the icy shell.	Ice-Penetrating Radar, Topographical Imager	✓		✓
			Search for an ice-ocean interface.	Ice-Penetrating Radar, Topographical Imager	✓		✓
			Correlate surface features and subsurface structure to investigate processes governing material exchange among the surface, ice shell, and ocean.	Ice-Penetrating Radar, IR Spectrometer, Topographical Imager	✓	✓	✓
			Characterize regional and global heat flow variations.	Ice-Penetrating Radar	✓		✓
	Composition	Understand the habitability of Europa's ocean through composition and chemistry.	Characterize the composition and chemistry of the Europa ocean as expressed on the surface and in the atmosphere.	IR Spectrometer, INMS	✓	✓	
			Determine the role of Jupiter's radiation environment in processing materials on Europa.	IR Spectrometer, INMS		✓	✓
			Characterize the chemical and compositional pathway's in Europa's ocean.	IR Spectrometer, INMS	✓	✓	
	Geology	Understand the forma-tion of surface features, including sites of recent or current activity, and characterize high science interest localities.	Determine sites of most recent geological activity, and characterize high science interest localities.	Topographical Imager	✓		✓

Note: Shaded check marks illustrate whether the objectives directly address the themes of water (W), chemistry (C), and energy (E).

ES.1.5.2 Multiple-Flyby Mission Concept

The Multiple-Flyby Mission concept (Figure ES.1.5-1) would deploy a highly capable, radiation-tolerant spacecraft into a long, looping orbit around Jupiter, performing repeated close flybys of Europa to collect information on ice shell thickness, composition, and surface geomorphology.

The model planning payload (Table ES.1.5-2) consists of four instruments: a Shortwave Infrared Spectrometer, an Ice-Penetrating Radar, a Topographical Imager, and an Ion and Neutral Mass Spectrometer (INMS). Except for calibration and maintenance, these instruments are operated during each Europa flyby. The nominal Multiple-Flyby Mission would perform 32 flybys of Europa at altitudes varying from 2700 km to 25 km.
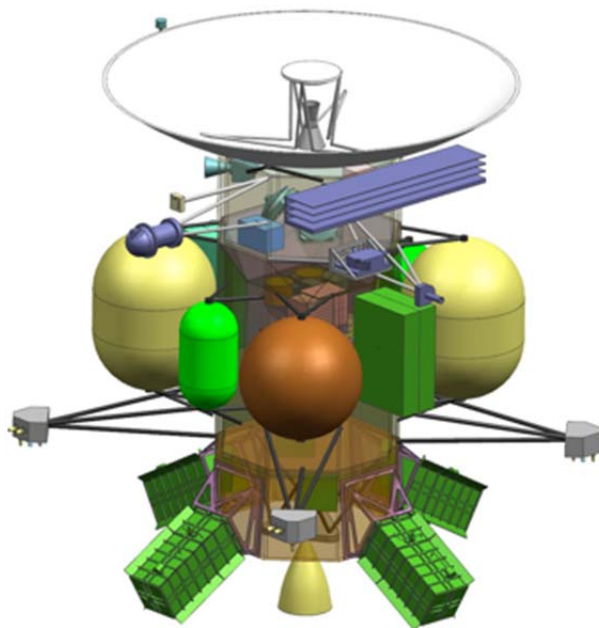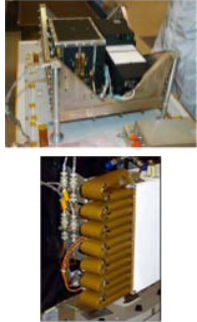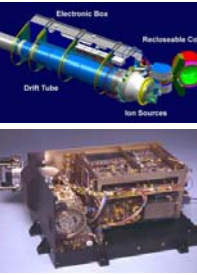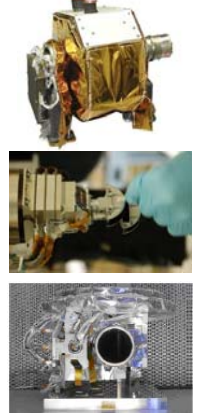

Figure ES.1.5-1. The Europa Multiple-Flyby Mission flight system provides a robust platform to collect, store, and transmit a high volume of science data.

Table ES.1.5-2. Capable science instruments for the Europa Multiple-Flyby concept draw on previous flight designs.

Instrument	Characteristics	Similar Instruments	
Ice-Penetrating Radar (IPR)	**Dual-Mode Radar Sounder** Radar sounding of the ice shell, with a higher-frequency band designed to provide high spatial resolution (footprint and depth) for studying the subsurface above 3 km depth at 10 m vertical resolution. A low-frequency band can penetrate much deeper to search for the ice-ocean interface or the hypothesized transition between brittle and ductile ice in the deep subsurface, at a depth of up to 30 km at 100 m vertical resolution.	Mars Express MARSIS; MRO SHARAD	
Shortwave Infrared Spectrometer (SWIRS)	**Pushbroom Spectrometer** Reflectance spectra for surface composition at ~10 km/pixel resolution for global mapping, and scans at better than 300 m/pixel. 10 nm spectral resolution from 0.85 to 5.0 µm.	Chandrayaan M3	
Ion and Neutral Mass Spectrometer (INMS)	**Reflectron Time-of-Flight Mass Spectrometer** Elemental, isotopic, and molecular composition of Europa's atmosphere and ionosphere by means of mass spectrometry during close flybys.	Rosetta ROSINA; Cassini INMS	
Topographical Imager (TI)	**Panchromatic Stereo Pushbroom Imager** Stereo imaging to characterize geological landforms, and assistance in removal of clutter noise from Ice-Penetrating Radar off-nadir surface topography.	MRO MARCI; MESSENGER MDIS; New Horizons MVIC	

ES.1.5.3　Multiple-Flyby Mission Design

The Multiple-Flyby Mission starts with the spacecraft launch on an Atlas V 551 that places it on a 6.5 year VEEGA interplanetary trajectory before performing the Jupiter Orbit Insertion (JOI) burn. After JOI, the spacecraft would perform four additional Ganymede gravity assists over 11 months to lower its orbital energy with respect to Jupiter and set up the correct flyby conditions (lighting and relative velocity) at Europa. The spacecraft would then embark on an 18 month Europa science campaign.

A unique multiple-flyby mission design allows for building up over time a regionally distributed network of flyby locations across Europa's entire globe (Figure ES.1.5-2, top). Remote-sensing instruments are able to observe Europa with flyby coverage similar to orbiting the body (Figure ES.1.5-2, bottom). This is analogous to how the Cassini mission at Saturn has been able to garner a global picture of Titan through repeated flybys.

This mission design achieves the science requirement of regionally-distributed global coverage of Europa with intersecting, daylit flyby trajectories. This results in 32 science flybys of Europa.

ES.1.6　Lander Concept

ES.1.6.1　Lander Science

The Europa Lander Mission concept concentrates on science observations that can best be achieved by *in situ* examination of Europa from its surface. Chiefly, this means sampling Europa's dark reddish material (Figure ES.1.6-1) to understand its detailed composition and chemistry, to best understand the specific nature of salts, any organic materials, and other contaminants. It also means geophysical prospecting of Europa through seismology and magnetometry, in order to probe the satellite's ice shell and ocean. From the surface, it is possible to perform *in situ*
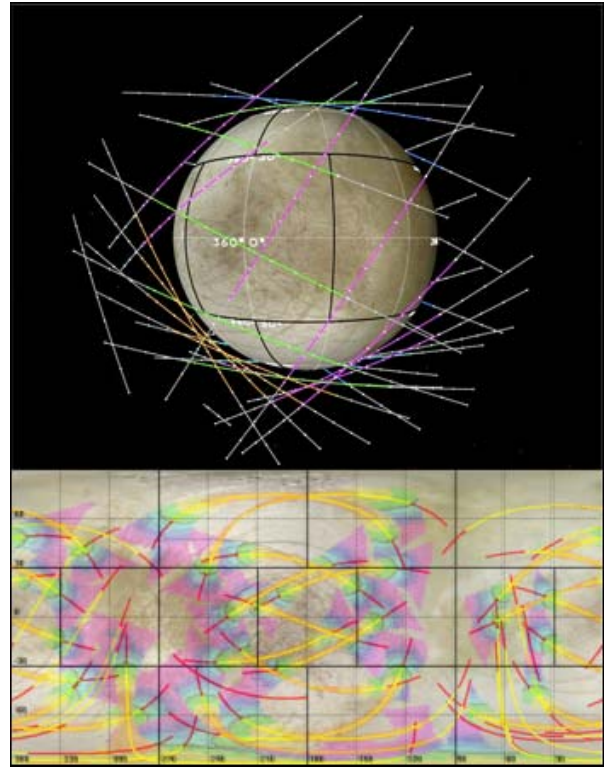
Figure ES.1.5-2. Unique mission design enables the Europa Multiple-Flyby Mission to obtain network-like mapping coverage approaching that of an orbiter. *Top:* Multiple fly-by paths envelop Europa after 32 spacecraft passes. *Bottom:* These multiple flybys provide globally distributed regional coverage by the instruments: arcing trajectory paths are shown for spacecraft altitudes of 25–400 km (red) and 400–1000 km, and pastel colors illustrate stereo imaging coverage by the Topographical Imager from 200 m/pixel (violet) down to 25 m/pixel (orange) for each daylit path.

characterization of the surface at a human scale, to "see" the surface as if standing upon it.

The objectives, investigations, and model planning payload of the Lander Mission are summarized in Table ES.1.6-1. Science objectives are listed in priority order, and investigations within each objective are listed in priority order. The highest priority composition objectives require a sampling and sample handling system to obtain icy material from the surface (0–2 cm depth) and near-surface (5–10 cm depth) and bring it to the instruments for analysis. Given the challenges of data return from and long-term survival on the surface, the

Table ES.1.6-1. Objectives, investigations, and model planning payload for the Europa Lander concept.

Goal	Objective		Investigation	Model Planning Payload	Theme W	C	E
Explore Europa to investigate its habitability	Composition	Understand the habitability of Europa's ocean through composition and chemistry	Characterize surface and near-surface chemistry, including complex organic chemistry to constrain ocean composition and understand the endogenic processes from which it evolves.	Mass spectrometer, Raman Spectrometer		✔	✔
			Characterize surface and near-surface chemistry, including complex organic chemistry to constrain the exogenic processes and material fluxes that affect ocean composition.	Mass spectrometer, Raman Spectrometer		✔	✔
			Constrain the context of compositional measurements.	Site Imager, (Reconnaissance Imager), Microscopic Imager	✔	✔	✔
	Ocean & Ice Shell	Characterize the local thickness, heterogeneity, and dynamics of any ice and water layers	Constrain the thickness and salinity of Europa's ocean.	Magnetometer, Multi-Band Seismometer Package	✔	✔	
			Constrain the thickness of ice and the thickness of any water layers in the region.	Magnetometer, Multi-Band Seismometer Package	✔		
			Search for local heterogeneity of the ice and any subsurface water.	Multi-Band Seismometer Package	✔	✔	
			Characterize Europa's seismic activity and its variation over the tidal cycle.	Multi-Band Seismometer Package	✔		✔
	Geology	Characterize a locality of high scientific interest to understand the formation and evolution of the surface at local scales	Constrain the processes that exchange material between the surface, near-surface, and subsurface.	Site Imager, (Reconnaissance Imager), Microscopic Imager	✔	✔	✔
			Constrain the processes and rates by which the surface materials (regolith and bedrock) form and evolve over time.	Site Imager, (Reconnaissance Imager), Microscopic Imager	✔	✔	✔
			Understand the regional and local context of the landing site.	Site Imager, (Reconnaissance Imager)	✔	✔	✔
			Constrain the physical properties of the surface and near-surface at the landing site to provide context for the sample.	(Reconnaissance Imager,) Microscopic Imager, Engineering data		✔	

Note: Shaded check marks illustrate whether the objectives directly address the themes of water (W), chemistry (C), and energy (E).

Lander science is accomplished by instruments with low data volume requirements, along with data editing and compression. The Lander Mission concentrates on the chemistry theme, as related to habitability, while addressing water and energy themes as well.

ES.1.6.2 Lander Mission Concept

The lander mission concept (Figure ES.1.6-1 and Figure ES.1.6-2) would deploy a robust, highly capable, radiation-tolerant soft Lander to the surface of Jupiter's moon Europa to perform *in situ* investigation of surface and near-surface composition and chemistry, seismological and magnetic study of local and regional ice and ocean thickness and dynamics, and high-resolution imagery of landing site and sample morphology. The model planning payload on the landed element (Table ES.1.6-2) consists of six instruments: a Mass Spectrometer, a Raman Spectrometer, a Magnetometer, a Multiband Seismometer Package, a Site Imaging System, and a Microscopic Imager.
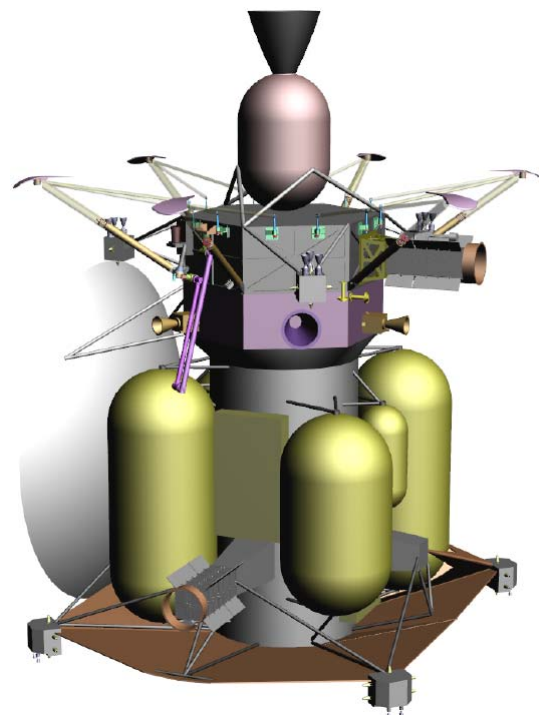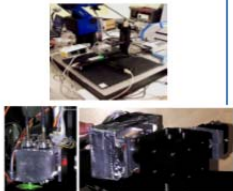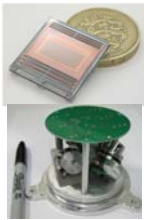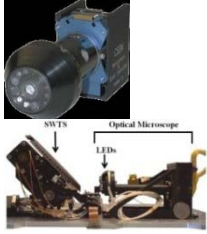

Figure ES.1.6-1. The integrated spacecraft with Carrier and Lander elements provides reconnaissance, safe landing, and *in situ* science in a single mission.

Table ES.1.6-2. Capable science instruments for the Europa Lander concept draw on previous flight designs.

Instrument	Characteristics	Similar Instruments	
Mass Spectrometer (MS)	**Quadrupole mass spectrometer** Evolved gas analysis, pyrolysis, and gas chromatography for determining the composition of the Europa's surface and near surface, through measurement of two obtained samples. Abundances will be retrieved of organics (as low as 1 ppb) and inorganics (as low as 1 ppm).	Huygens GCMS; MSL SAM; Rosetta COSAC	
Raman Spectrometer (RS)	**Raman infrared line spectrometer** Characterization of surface and near-surface chemistry, including complex organic chemistry, through measurement of shift in the wavelength of the scattered laser light due to vibrations in mineral structure, across a spectral range of 900 nm–1.5 μm.	New development; some similarity to ExoMars RS and MMRS	
Multiband Seismometer Package (MBS)	**Six 3-axis MEMS seismometers** Thickness of ice and water layers through seismic analysis, and characterization of seismic activity level and its variation over the tidal cycle.	New development; some similarity to ExoMars SP sensors and COTS seismometers	
Magnetometer (MAG)	**3-axis fluxgate magnetometer** Ocean thickness and salinity though measurement of the magnetic induction signal generated in Europa's ocean as a response to Jupiter's magnetic field.	MESSENGER MAG; Galileo MAG	
Site Imaging System (SIS)	**Dual stereo color imagers** Stereo landform mapping of the landing site from near the Lander to the horizon, including the sample acquisition location.	MER Pancam	
Microscopic Imager (MI)	**Wide-angle close-focus camera** Wide-angle, close-focused camera to provide high-resolution images of the collected samples to characterize ice grains and non-ice materials within the samples.	MSL MAHLI; Phoenix MECA; MER Microscopic Imager; Beagle 2 Microscope	
Reconnaissance Camera (RC)	**Engineering panchromatic narrow-angle camera** Camera on the Carrier element for high-resolution imagery of candidate landing sites from Europa orbit prior to Lander deployment, and to image Lander on surface to provide context for the landed measurements. Resolution 0.5 m/pixel from 200-km altitude.	MRO HiRISE	

These investigations would be performed during a 30 day science campaign from a single location on the surface of Europa. There is also one instrument on the Carrier element: a Reconnaissance Camera to aid landing site selection. The information needed to select a safe landing site is not available from the Galileo and Voyager database. Without a precursor mission, the science landing zones would be selected from several candidates identified before launch and narrowed to one zone after a 30 day on-orbit landing site reconnaissance campaign and site selection process determines the preferred landing site for safe Lander deployment (Figure ES.1.6-2).

ES.1.6.3 Lander Mission Design

The Lander Mission would start with the spacecraft launch on a Delta IVH Launch Vehicle that places it on a 6.5 year VEEGA interplanetary trajectory before performing the Jupiter Orbit Insertion (JOI) burn. After JOI, the spacecraft would perform eleven gravity-assist flybys of Ganymede and Calisto over
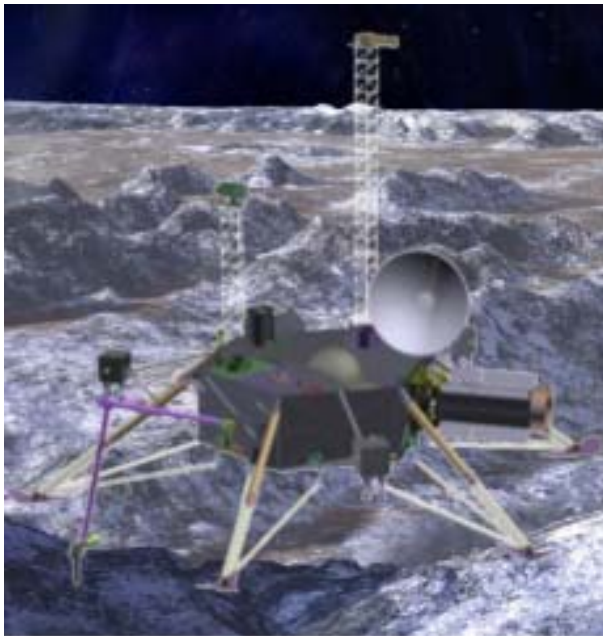
Figure ES.1.6-2. The Lander (deployed surface configuration) provides a reliable platform for completing the baseline science objectives. (Background artwork by Michael Carroll.)

about 1.5 years to lower its energy with respect to Europa, at which point a Europa Orbiter Insertion (EOI) is performed. This mission design was selected to reduce the total radiation dose on the lander, which minimizes lander mass. This is important because additional lander mass penalizes the lander wet mass and the carrier wet mass. The spacecraft is placed into a 200 km circular, near-polar, orbit, for landing sight reconnaissance. After 30 days, a safe landing site is selected and the landing sequence is initiated. Then the periapsis is lowered to 5 km, where the Lander is released to perform its deorbit, descent, and landing sequence. After separation, the Carrier returns to the 200 km circular orbit to perform data-relay functions and to take images of the resultant landing site. The Carrier remains in orbit for the mission duration (nominally 30 days).

ES.1.7 Key Architectural Concepts

The Europa spacecraft would employ a modular configuration (Figure ES.1.7-1), which provides distinct programmatic advantages. Implementation flexibility is gained through parallel integration paths, module-level integration during Phase C testing, and isolation of implementation issues at the module level. A modular approach minimizes peaks in the project funding profile and allows greater flexibility in phasing of module implementation schedules.

The spacecraft design uses a nested shielding configuration (Figure ES.1.7-2) that reduces the radiation dose at critical electronic components to existing geosynchronous part tolerances. The spacecraft design uses a radiation design factor of two (thus assuming that the end-of-life radiation experience by components is twice as great as the modeling predicts). Upon flight system assembly, the avionics vault is placed into a cavity within the propulsion module. The components in the avionics vault gain shielding from neighboring
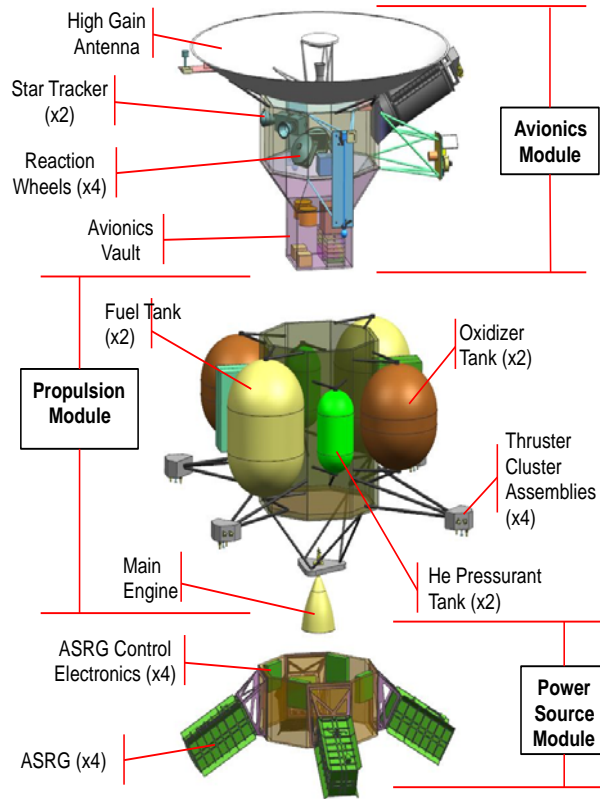
Figure ES.1.7-1. The Europa modular design simplifies integration and test (Orbiter spacecraft shown).

components and structure, while the propellant provides additional radiation shielding.

An additional benefit of the nested configuration is an efficient thermal design, which uses waste heat from the avionics vault to warm the propellant without additional heaters.

For electrical power, each spacecraft would utilize Advanced Stirling Radioisotope Generators (ASRGs), which are a NASA technology development to advance the efficiency of radioisotope power systems (RPS). The ASRGs would provide stable power output throughout all mission phases and life, while reducing the amount of plutonium-238 fuel required as compared to previous RPS designs.

All three mission concepts have good–to-excellent technical margins for this stage of the development process (Table ES.1.7-1).
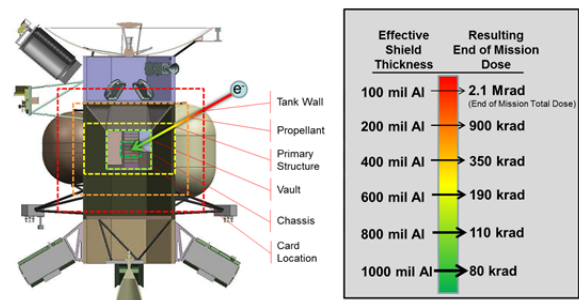
Figure ES.1.7-2. The nested shield approach reduces the radiation dose seen by the electronics and allows the use of heritage hardware (Orbiter spacecraft shown).

ES.1.8 Cost Estimating Methodology

To estimate the cost of each mission concept, JPL used its institutional cost estimation process applicable for the design maturity of a concept study in early formulation. This process focuses on using parametric cost models, analogies, and other non-grassroots estimating techniques. For the three mission concepts, the tools and methods used include the following:

- SEER and PRICE, commercial off-the-shelf (COTS) tools that have been calibrated to the most relevant JPL planetary missions
- NASA Instrument Cost Model (NICM) for the payload (at 70% confidence level, to be conservative)
- NASA Space Operations Cost Model (SOCM)
- Institutional wrap factors based on analogous historical planetary missions

Table ES.1.7-1. All three spacecraft have excellent (blue) or good (green) technical margins.

Technical Parameter	Orbiter	Multi-Flyby	Lander
Mass Margin	42%	48%	29%
Power Margin	39%	39%	38%
Data Return Margin	39%	80%	86%
Radiation Design Factor	2	2	2

- 40% reserves applied for Phases A–D and 20% for Phases E–F

The Europa Study Team vetted the integrated cost rollup and detailed basis of estimate (BOE), and reviewed the results for consistency and reasonableness with the mission design, WBS, and NASA requirements to ensure that technical and schedule characteristics were accurately captured and a consistent cost-risk posture utilized. Analog missions were used as an additional cross-check. Table ES.1.8-1 summarizes the cost estimate for each mission option. The results are reasonable and conservative, as deemed by the independent review board and by the Aerospace Corporation, as described next.

Table ES.1.8-1. Cost Elements for Each Mission Option

Mission Option	Cost Estimate (FY15$, No LV)
Orbiter	$1.6B
Multiple-Flyby	$1.9B
Lander	$2.8B

ES.1.9 Independent Review

An independent review board was formed to provide a technical assessment, including risks, of the proposed mission concepts. The board had a broad range of expertise and was led by Scott Hubbard (Chair), Orlando Figueroa, and Mark Saunders, who are each retired NASA Headquarters personnel. The board met on November 15, 2011 to review both the orbiter and flyby concepts, and then on March 15, 2012 to review the lander concept and to consider responses to previous requested actions. The science, technical, and management details of the three mission concepts were presented in detail at these reviews. The board deemed both the orbiter and flyby concepts as viable within the cost estimate with low risk. The board concluded that a landed mission is not viable without a precursor mission that would first determine Europa landing surface characteristics; otherwise, active sample acquisition combined with landing safely on an unknown terrain was deemed to be too risky.

The science and technical overviews of the Orbiter and Multiple-Flyby Mission concepts were presented to an open community meeting of the Outer Planets Assessment Group (OPAG) on October 19, 2011. Both Orbiter and Multiple-Flyby options were received very favorably and were enthusiastically endorsed by OPAG.

The science and technical overview of the Lander Mission concept were presented at open meeting of OPAG on March 29, 2012. OPAG viewed the lander science as exciting science; however, the concept was considered infeasible in the short term due the cost magnitude and the need for technology maturation.

The Aerospace Corporation was contracted to perform an independent cost verification. They performed an Independent Cost Estimate (ICE) and a Cost and Technical Evaluation (CATE) for each mission concept, to serve as an independently derived check against the Europa Study Team estimates. Members of the Aerospace Corporation attended both independent review team sessions in order to gather data for their cost estimates. The Europa Study Team interacted with the Aerospace Corporation to assure that any misunderstandings were clarified and reconciled. The results of the Aerospace Corporation results showed excellent correlation with the Europa Study Team estimated costs. The Aerospace Corporation review showed no schedule or cost threats for the Orbiter and Multiple-Flyby mission options. The Lander mission option was determined to have minimum cost and schedule threats. The Aerospace ICE and CATE results are summarized in Table ES.1.9-1.

Table ES.1.9-1. Aerospace ICE and CATE estimates for each mission option.

Mission Option	Aerospace Independent Cost Estimate (ICE) (FY15$, No LV)	Aerospace Cost and Technical Evaluation (CATE) (FY15$, No LV)
Orbiter	$1.7B	$1.8B
Multiple-Flyby	$2.1B	$2.1B
Lander	$2.8B	$3.0B

ES.1.10 Summary

Three unique science mission concepts were examined in detail by a joint science and engineering team. Any of the three would be a scientifically compelling mission that would change paradigms in our understanding of the workings and potential habitability of icy worlds, in our Solar System and beyond.

These mission options use superb architectural concepts, which utilize a nested shielded design to enable the use of standard space equipment and parts, minimize the number of instruments necessary to achieve outstanding science, have significant margins to accommodate risk, and employ a modularity approach that increases schedule and test flexibility.

The Lander Mission concept is believed to be unaffordable in the current federal budget environment and has associated mission risks that are deemed unacceptable without further development. Both the Orbiter Mission and Multiple-Flyby Mission concepts are found to be fully consistent with Decadal Survey and NASA Headquarters direction. The independent review board concluded: "Both the Orbiter and Multiple-Flyby mission concepts satisfied the 'existence proof' test as missions that met Europa science requirements, could be conducted within the cost constraints provided and have substantial margins." Overall, we conclude that the Multiple-Flyby Mission concept has the greatest science return per dollar, and it is our recommended option.

EUROPA STUDY 2012 REPORT
INTRODUCTION

Europa Study Team, 1 May 2012, JPL D-71990
Task Order NMO711062 Outer Planets Flagship Mission

Cover art Michael Carroll

Europa Study 2012 Report: Introduction

Contents

A. EUROPA STUDY 2012 REPORT: INTRODUCTION

A.1 NASA Headquarters Direction

The 2011 Planetary Decadal Survey recommended an immediate effort to find major cost reductions for a Europa mission by decreasing the mission scope. To that end, in April 2011, NASA's Planetary Science Division (PSD) directed the pre-project office to conduct a study to revise the JEO mission to meet the NASA cost target of $2.25B ($FY15). Science and technical descopes were to be utilized to achieve this goal in such a manner that the results could be validated via independent review on all study results.

The study was to abide by the following ground rules:

- Cost: All cost analyses shall use $FY15. An estimate of the cost for the minimum science mission is one of the objectives of this study. A discussion of the descopes and their cost impact if new technologies are utilized must also be provided.
- Science Objectives: The primary science objective of the mission concept is Europa. The science content of the EJSM JEO concept presented to the Decadal Survey is expected to be descoped. A science "floor" must be established for which any other descope(s) will make the mission not worthwhile to pursue.
- International Contributions: The study shall limit international contributions to no more than half of the payload.
- Launch Vehicle: The study shall delineate the cost of all potential launch vehicle options both presently available and projected to be available, but these costs are not to be included in the target.
- Power System: The study shall use the Advanced Stirling Radioisotope Gen-

erator (ASRG) as the power system for the spacecraft. The number of ASRG units is not specified but should be minimized. The study should assume ASRG cost of $50M per unit.
- Science Definition Team: The study shall utilize a small well focused Science Definition Team (SDT) to provide guidance on the scientific objectives, measurements, and priorities for the mission concept. The SDT shall be composed of US scientists only and shall be kept to a reasonable size. An ESA observer may be attending some meetings but is not expected to contribute.

For the remainder of FY11, the study team was to assess the feasibility of a limited number of mission concepts, including, but not limited to, a Europa orbiter that takes as its starting point the descope path in the 2008 final report (as recommended by the Decadal Survey) and a Jupiter orbiter with a large number of Europa flybys. NASA expects the product of this detailed study to consist of a final report that provides sufficient detail to undergo independent review. The PSD is expected select a single concept for detailed study in FY12.

A.2 Europa Science Overview

A.2.1 Background

Europa and her sibling satellites were discovered by Galileo in 1610, but nearly 400 years passed before any detailed views of their surfaces were seen and the uniqueness of the Galilean satellites was revealed. The physical and orbital properties of Europa are summarized in Table A.2.1-1. In the 1960s, ground-based telescopic observations determined that Europa's surface composition is dominated by water ice, as are most other solid bodies of the outer solar system.

The Pioneer 10 and 11 spacecraft flew by Jupiter in the 1970s, but the first spacecraft to

Table A.2.1-1. Properties of Europa.

Discovered	1610
Discoverers	Galileo Galilei, Simon Marius
Mean Distance from Jupiter	671,100 km
Radius	1560.8 ±0.5 km
Mass	(4.8017 ±0.000014) x 10^{22} kg
Density	3.014 ± 0.005 g/cm^3
Orbital Period	85 hours (3.551 Earth days)
Rotational Period	85 hours (3.551 Earth days)
Orbital Eccentricity	0.0094
Orbital Inclination	0.469 degrees
Visual Geometric Albedo (Avg.)	0.68
Escape Velocity	2.026 km/s
Spacecraft Visitors	Voyager 1 (March 1979) Voyager 2 (July 1979) Galileo (Jul 1994–Jan 2002)

image the surfaces of Jupiter's moons in significant detail were the Voyager 1 and 2 spacecraft. Voyager 1's closest approach to Jupiter occurred in March 1979, and Voyager 2's in July of the same year. Both Voyagers passed farther from Europa than any of the other Galilean satellites, with the best imaging resolution limited to 2 km per pixel. These images revealed a surface brighter than that of Earth's moon, crossed with numerous bands and ridges, and with a surprising lack of large impact craters or high-standing topography.

Despite the resolution limitations, the images were of high enough quality that researchers noted some of the dark bands had opposite sides that matched each other extremely well, like pieces of a jigsaw puzzle. These cracks had separated, and ductile dark icy material appeared to have flowed into the opened gaps, suggesting that the surface has once been mobile. The relative youth of Europa's surface was suggested by a lack of large impact craters—Voyager images showed only a handful—which are expected to build up over time as a planetary surface is constantly

bombarded by meteorites over billions of years until the surface is covered in craters. A lack of craters implies that something has erased them—such as icy volcanic flows, or viscous relaxation of the icy crust. The patterns of some of the longest linear features on the surface did not fit with predicted simple models of global stresses that might arise from tidal interactions with Jupiter. However, if the shell was rotated back by several tens of degrees, the patterns fit exceptionally well to a model of "nonsynchronous rotation," by which the icy surface has slowly migrated with respect to the satellite's tidal axes. This mechanism probably requires a ductile or liquid layer between the surface ice and the deeper interior. Combined with the observations of dark bands, there were tantalizing hints that perhaps Europa had a warm interior at some time in the past, and perhaps still has today. Theoretical models of tidal heating of Europa suggested that a global subsurface ocean might exist within Europa today.

These intriguing findings led to a strong sense of anticipation for the Galileo mission, which launched from the Space Shuttle Atlantis in 1989 and entered orbit around Jupiter in 1995. The primary mission included observations of each the four Galilean satellites as the spacecraft passed by. Despite severe data rate limitations of the Galileo mission because its main antenna did not open, information from Galileo was so intriguing that the mission was extended to make 12 total close flybys of Europa. Data from the Galileo mission included images of Europa at a range of scales, and included magnetic measurements that strongly imply the presence of an induced magnetic field that implies a saltwater ocean beneath the surface today.

The ocean on Europa most likely formed early in the moon's evolution. During the formation of our solar system, the growing gas giant planet Jupiter pulled material from the solar nebula in nearly primordial form. Thus, the material incorporated into the Galilean satel-

lites was probably similar in composition to the asteroids of the outer asteroid belt, containing ice, silicates, carbonaceous material, and nickel-iron metal. The Galilean satellites formed by aggregation of these solids, with the proportion of ice varying with distance from the warm protoplanet Jupiter.

Europa formed as a mostly rocky satellite (density = 3.0), able to accrete sufficient volatiles to form a ~100 km thick outer layer of H_2O. If the Jovian subnebula were cold enough, some lower-temperature condensates such as CO_2 could have been incorporated as Europa formed. Europa's early heat of accretion, combined with heat from radioactive decay, would have warmed the satellite's interior and formed a primordial ocean, which was likely reduced and sulfidic. Thermal and geochemical evolution would have caused some oxidation of the ocean through time, forming sulfates. Tidal heating of Europa—repeated squeezing as the satellite orbits its parent planet each 3.55 days (85.2 hours)—is sufficient to maintain Europa's liquid beneath a skin of ice ocean over the age of the Solar System.

A.2.2　Habitability of Europa—Motivation for Future Missions

Europa is a prime candidate in the search for present-day habitable environments in our solar system. It is probable that this planet-sized moon has a saltwater ocean today beneath a relatively thin and geodynamically active icy shell (Figure A.2.2-1). Europa is unique among the large icy satellites because its ocean is believed to be in direct contact with its rocky mantle, where conditions could be similar to those on Earth's biologically rich sea floor. Hydrothermal zones on Earth's sea floor are known to be rich with life, powered by energy and nutrients that result from reactions between the seawater and the warm rocky ocean floor.

Life as we know it depends upon: 1) liquid water; 2) complex organic and inorganic compounds that contain nitrogen, phosphorus, sulfur, iron and certain trace elements; and 3) a photo- or chemical-energy source (Figure A.2.2-2). Europa appears to meet these minimum requirements for life, and it is distinguished among the bodies of our Solar System by the potential presence of enormous volumes of liquid water and geological activity that promote the exchange of surface materials with the sub-ice environment. However, the processes that shape Europa's ice shell, and the exchange processes between the surface and ocean, are poorly understood. Indeed, even the existence of a subsurface ocean, while suspected, is not yet proven.

A.2.2.1　Water

The likelihood that Europa has a global subsurface ocean hidden beneath a relatively young icy surface has profound implications in the search for past or present life beyond Earth. Europa is the natural target for the first focused spacecraft investigation of the habitability of icy worlds. Its candidate sources of chemical energy for life, direct ocean-mantle contact, a relatively thin ice shell, and potentially active geology that exchanges surface and oceanic material make it a recognized top

Figure A.2.2-1. Europa's surface shows a landscape marked by tectonic and icy volcanic events. This image shows ridges and bands that crisscross the icy surface, and spots that expose warm ice and/or water that erupted from below.
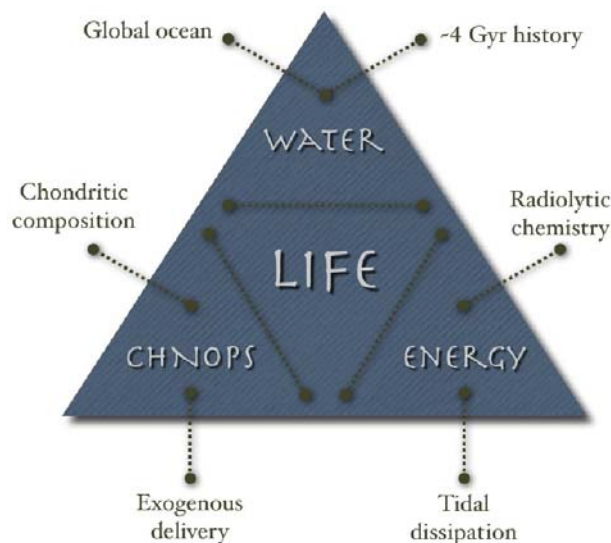
Figure A.2.2-2. Pyramid of habitability. Our present understanding of the conditions for life could be distilled down to three broad requirements: 1) a sustained liquid water environment (an internal global ocean, which has likely existed for over 4 billion years); 2) essential chemical elements (e.g., C, H, N, O, P, S) that are critical for building life (derived from primordial chondritic composition of the satellites, plus delivery by asteroids and comets over time); and 3) a source of energy that could be utilized by life (oxidants at the surface, and possible hydrothermal activity at the ocean floor as driven by tidal heating). The cycling of chemical energy into an icy satellite's ocean over geological time is key to understanding habitability of the satellite. Figure courtesy Kevin Hand.

priority for exploration.

Galileo observations confirmed Europa's surface as sparsely cratered and therefore young. Models for the formation of its abundant linear tectonic features suggest that the icy shell is relatively thin and responds to intense tidal flexing. Tidal deformation in Europa's ice could create briny pockets associated with salty impurities and partially melted zones.

These and other lines of evidence are consistent with an ocean many tens of kilometers deep beneath an ice shell a few to tens of kilometers thick, all underlain by a rocky seafloor in direct contact with ocean water, possibly supplied in chemical nutrients by

hydrothermal activity. The potential for areas within the ice shell hosting salty fluids and the occurrence of hydrothermal systems driven by tidal heating make for a favorable environment for prebiotic chemistry or for microbial life. Cycling of water through and within the ice shell, ocean, and upper rocky mantle, could maintain an ocean rich with the chemistry conducive to life.

A.2.2.2   Chemistry

At present, Europa may hold the Solar System's best prospects for life beyond Earth, based on complementary surface and subsurface chemistry. Understanding Europa's chemistry relates to understanding its geophysical energy and the ability of Europa's water to serve as a medium for facilitating chemical reactions. These coupled interactions constitute the most likely source for elements essential for life, including C, H, N, O, P, and S.

Irradiation of Europa's icy surface is responsible for production of O_2, H_2O_2, CO_2, SO_2, and probably other oxidants yet to be discovered. At present, few constraints exist for mechanisms and timescales for delivery of these materials to the subsurface, where they could power life. Meanwhile, cycling of ocean water through seafloor minerals could replenish the water with biologically essential reductants, which are the other half of the necessary redox reaction for life. Combined geophysical and compositional factors, with a yet-uncertain role for tidal heating, may lead to ocean habitability.

A.2.2.3   Energy

Europa is unique for the extraordinary amount of tidal heat energy predicted to occur in its interior to drive interior geochemistry, coupled with energy in the form of Jupiter's intense radiation environment that generates an oxidant-rich surface chemistry. Physical cycling of energy at Europa is arguably the greatest uncertainty in assessing the satellite's habitability: the uncertain mechanisms of surface-ice-ocean exchange are critical to

providing chemical energy to the ocean. Assessing the exchange processes between the ice shell, ocean, and underlying rocky interior is necessary for understanding Europan habitability.

Hydrothermal activity at Europa's seafloor may determine ocean chemistry and global cycling of ocean water. Tidal flexing and resultant energy input to Europa's ice shell are responsible for creating conditions that could drive solid-state convection in the ice, and fracturing and destabilization of brittle ice at Europa's surface. These geological processes may determine the nature and extent of chemical exchange between Europa's surface and its subsurface ocean.

A.3   Europa Mission Study

To address and answer the key questions about the Europa's habitability, a dedicated Europa mission is needed. To that end, this study

report details work performed since April 2011 in defining Europa mission concepts. A Europa Science Definition Team (SDT) guided the science, and a combined Jet Propulsion Laboratory (JPL) and Applied Physics Laboratory (APL) study team performed the technical work. This document is a combined SDT and technical report of the mission concepts that were studied by the Europa Study Team.

The Europa Study Team initially converged on studying an orbiter and a multiple-flyby mission concept. In autumn 2011, NASA Headquarters directed that a lander mission concept also be investigated. Complete study results for the three mission concepts (Figure A.3-1) are contained in Section B (Orbiter), Section C (Multiple-Flyby) and Section D (Lander) of this report. Both the Orbiter and Multiple-Flyby Mission concepts are fully compliant with Decadal Survey and

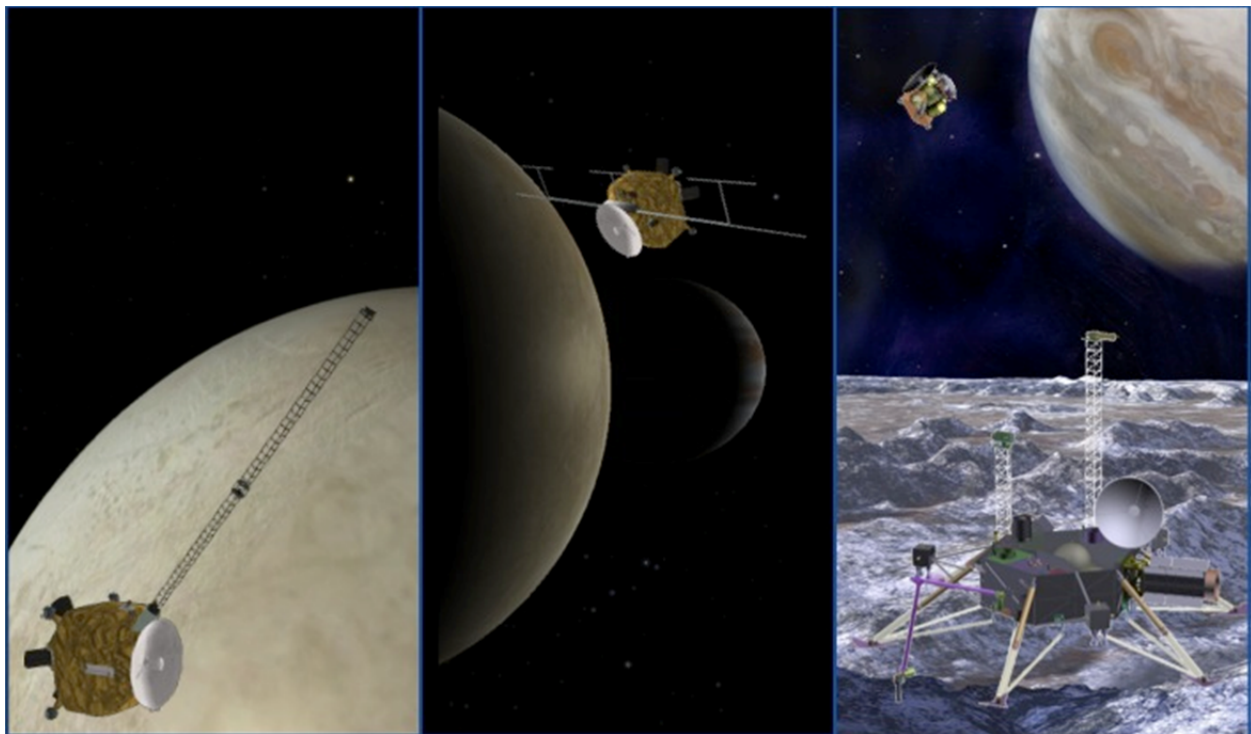**Figure A.3-1.** Europa Orbiter Mission (left panel) would perform geophysical measurements ("water" science). The Multiple-Flyby Mission (middle panel) would concentrate on performing remote measurements that address the "chemistry" and "energy" science. The Europa landed mission (right panel) would perform detailed *in situ* characterization of a Europan landing site assessing key habitability science objectives.

NASA Headquarters direction. However, the Lander Mission concept was found to exceed the NASA total cost guideline and has associated mission risks that are deemed unacceptable at this time.

A.3.1 Science Definition Team Process

The NASA Headquarters tasked the Europa SDT with formulation and definition of the science goals, objectives, investigations, and example measurements for reduced-cost Europa mission concepts (flyby, orbiter, and lander) that maximize the science value per dollar. To carry out this task, SDT members and a chairperson were appointed from the scientific community to represent a broad range of Europa science interests (Table A.3.1-1). An initial group was assembled to evaluate concepts that achieve science objectives from Europa or Jupiter orbit, leading to the formulation of the Orbiter and Multiple-Flyby Mission concepts. When the scope of the study was expanded to include an evaluation of a lander concept, five additional members were added to the SDT for this study phase.

The SDT approached the task by identifying an overarching goal, key science objectives, science investigations to best address those objectives, and examples of appropriate measurements that could be carried out by each platform to address the science investigations. Presentations were heard from the SDT members, and from the other members of the scientific and engineering communities invited to provide complementary expertise. To perform its tasks, the SDT was organized into Objective Working Groups (Ocean and Ice Shell, Composition, and Geology), each with a lead and a deputy, who served as principal points of contact for formulating the science traceability for the Orbiter and Multiple-Flyby Mission concepts. For the Lander Mission concept, Cross-Cutting Working Groups were also formed, for the topical areas of Astrobiology, Instruments, and Landing Sites. Each of these cross-cutting groups was composed of members from each of the three Objective Working Groups, to ensure full cross-communication.

Table A.3.1-1. Europa Science Definition Team.

Member	Inst.	Role
Fran Bagenal	U. Colorado	Plasma
Amy Barr	Brown U.	Geophysics
Bruce Bills	JPL	Geophysics
Diana Blaney	JPL	Composition
Don Blankenship	U. Texas	Ice shell
Will Brinckerhoff*	GSFC	Astrobiology
Jack Connerney	GSFC	Magnetometry
Kevin Hand*	JPL	Astrobiology
Tori Hoehler*	Ames	Astrobiology
William Kurth	U. Iowa	Plasma
Melissa McGrath	MSFC	Atmosphere
Mike Mellon*	SWRI	Ice Physics
Jeff Moore	Ames	Geology
Robert Pappalardo	JPL	Chair, Study Scientist
Louise Prockter	APL	Deputy, Geology
David Senske	JPL	Deputy, Geology
Everett Shock*	ASU	Geochemistry
David Smith	MIT	Geophysics

*SDT augmentations for the lander mission study.

Table A.3.1-2. Europa Science Definition Team meetings 2011–2012.

	Date	SDT Activity	Location
2011	2-3 May	Considered Europa objectives and mission design trades, and converged on Orbiter and Multiple-Flyby Mission concepts	Pasadena, CA
	23–24 Jun	Provided feedback on initial Orbiter and Multiple-Flyby mission designs, and iterated on model payloads and mission requirements	Pasadena, CA
	22-23 Aug	Finalized Orbiter and Multiple-Flyby Mission science traceability, model payloads, and mission requirements	Pasadena, CA
	17-18 Oct	Developed initial objectives and investigations for Lander Mission	Pasadena, CA
	29-30 Nov	Derived preliminary lander model payload and science mission requirements	Boulder, CO
2012	31 Jan–2 Feb	Determined baseline vs. floor science and finalized Lander Mission model payload and mission requirements	Pasadena, CA

The 2011-2012 activities of the SDT are summarized in Table A.3.1-2, which provides an overview of the meetings convened during the study phase, from the spring 2011 through May 2012. Throughout the study, technical team members worked closely with the SDT to understand and iterate on mission requirements imposed by science. This process aimed for mission concepts that were realistic within the target resources while preserving the high-level scientific objectives.

The SDT was requested to reformulate a Europa mission, using JEO as a basis of comparison, that achieves compelling science but represents a descope from past studies. It became clear that there is a division between the key science investigations best conducted from Europa orbit and those best achieved through multiple flybys. To characterize the extent of the ocean and its relation to the deeper interior, systematic geophysical measurements of gravity, topography, and magnetic field are needed, and are best obtained from an orbital platform. An orbital platform also permits uniform geological mapping. In comparison, observations to characterize the ice shell, understand the surface composition, and perform high-resolution targeted geological observations are quite data intensive and require high-mass, high-power instruments, so these are best carried out from a spacecraft that makes multiple flybys of Europa, broadcasting data back during long orbital petals. Only a lander could accomplish evaluation of the detailed surface chemistry and mineralogy to best understand the detailed nature of near-surface organics and salts, requiring the *in situ* sample analyses. All three of these mission options could provide high caliber, compelling science that would change paradigms in our understanding of the nature and habitability of icy worlds.

A.3.2   *Independent Review Process*

The science and technical overviews of the Orbiter and Multiple-Flyby Mission concepts were presented to at an open community meeting of the Outer Planets Assessment Group (OPAG) on October 19th, 2011. Both concepts were received very favorably and enthusiastically endorsed by OPAG. The science and a technical overview of the lander concept were presented at open meeting of OPAG on March 29th, 2012. OPAG viewed the lander science as exciting science; however, the concept was considered infeasible in the short term due the cost magnitude and the need for additional technology maturation.

An independent review board was formed to provide a technical assessment, including risks, of the proposed mission concepts. In making this assessment, the board was asked to consider:

- Ability of the mission element to satisfy the science objectives
- Mission design approach
- Robustness of the mission element and the associated system architectures
- Robustness of mission element and system margins and compliance with JPL design principles
- Proposed scope, including available options, as consistent with the funding target value to complete the mission element
- Cost risk
- Project planning risks, including design, environment mitigation plans, integration and test plans, schedule, and margins

Members of the review board are listed in Table A.3.2-1. The Board provided written reports detailing the findings of their independent technical and cost reviews, including any requests for actions as recommended by the board. The board met on November 15, 2011 to review both the orbiter and flyby concepts. The board again met on March 15, 2012 to review the lander concept and to consider responses to previous requested actions. The science, technical, and manage-

Table A.3.2-1. Independent Review Board.

Review Board Member	Institution and Role
Scott Hubbard	NASA (Ret.), Chair
Orlando Figueroa	NASA (Ret.), former Director for Mars Exploration
Mark Saunders	NASA (Ret.), Former Director of NASA Independent Program Assessment Office
Dave Nichols	JPL, Systems Engineering
Jeff Srinivasan	JPL, Telecommunications
Barry Goldstein	JPL, Avionics
Cindy Kahn	JPL, Mechanical Systems
Gentry Lee	JPL, Solar System Chief Engineer
Will Devereux	APL, Head of Engineering
Douglas Eng	APL, System Engineering
Rosaly Lopes	JPL, Science (Orbiter & Flyby)
Leslie Tamppari	JPL, Science (Lander)

ment details of the three mission concepts were presented in detail at these reviews. The board deemed both the orbiter and flyby concepts as viable within the cost estimate with low risk. The board deemed the lander concept as a challenging assignment to the study team in that a large amount of work was completed in short amount of time, and they commended the study team in exposing the challenges and risks of a Europa lander, but they concluded that a landed mission is not viable without a precursor mission that would first determine Europa landing surface characteristics: otherwise, active sample acquisition combined with unknown terrain is too risky to fly the lander mission. The board written reports are contained in Sections B.4.5, C.4.5, and D.4.5.

Aerospace Corporation was contracted to perform an Independent Cost Estimate (ICE) for each mission concept, to serve as an independently derived check against the Europa Study Team estimates. Members of the Aerospace Corporation attended both independent review team sessions in order to gather data for their cost estimates. In addition, the Europa Study Team populated a data package provided by the Aerospace Corporation, detailing mission technical and programmatic information. The Europa Study Team interacted with the Aerospace Corporation to assure that any misunderstandings were clarified and reconciled. The results of the Aerospace Corporation ICE results showed excellent correlation with the Europa Study Team estimated costs. The Aerospace Corporation's written reports are contained in Sections B.4.4, C.4.4, and D.4.4.

A.4   References

Space Studies Board, 2011. Visions and Voyages for Planetary Science in the Decade 2013–2022. The National Academies Press, Washington, DC.

National Aeronautics and Space Administration

EUROPA STUDY 2012 REPORT
EUROPA ORBITER MISSION

Europa Study Team, 1 May 2012, JPL D-71990
Task Order NMO711062 Outer Planets Flagship Mission

Cover art Michael Carroll

Europa Study Final Report—Orbiter

Contents

B. ORBITER MISSION

The Europa Orbiter Mission would explores Europa to investigate its habitability, delivering cost-effective, low-risk science.

Executive Summary

Background

The 2011 Planetary Science Decadal Survey recommended an immediate effort to find major cost reductions for the Jupiter Europa Orbiter (JEO) concept. To that end, NASA Headquarters appointed a Science Definition Team (SDT) and directed the Europa Study Team, guided by the SDT, to redefine a set of minimal science missions to Europa. The cost target was $2.25B ($FY15, excluding launch vehicle) and additional guidelines were levied, as described in §A. Independent cost and technical review was to be performed on all study results. These studies, independent reviews, and all deliverables were delivered to NASA Headquarters on May 1, 2012.

One of these mission concepts, a Europa Orbiter Mission, is well suited to addressing the
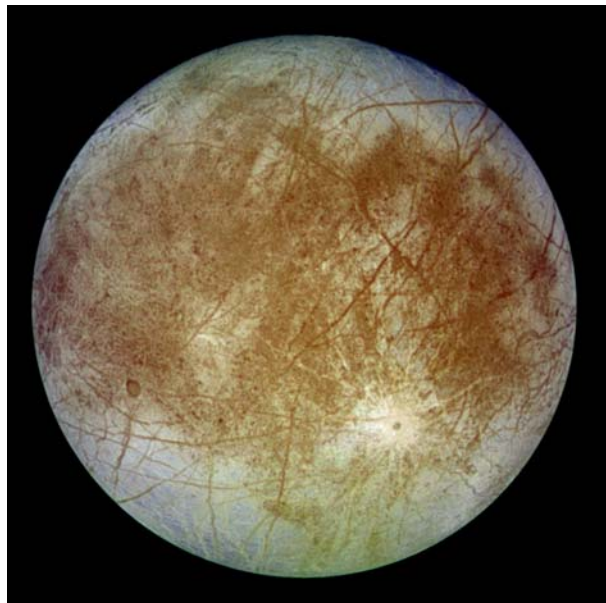
Figure B-1. Europa: a world of rock, ice, and water the size of the Earth's moon. The 2011 Planetary Decadal Survey identifies exploration of Europa as "the first step in understanding the potential of the outer solar system as an abode for life" (Space Studies Board 2011, p. 1).

ocean and geology themes of Europa exploration. It would involve a spacecraft low circular polar orbit around Europa, uniformly covering the entire moon to form global imagery, gravity and magnetometry data sets allowing investigation of the interior ocean, ice shell and surface geology. This concept, as detailed below, represents the combined effort since April 2011 of the SDT and a technical team from the Jet Propulsion Laboratory (JPL) and Johns Hopkins University's Applied Physics Laboratory (APL).

Rationale for Orbiter Science

The 2003 Planetary Decadal Survey, "New Horizons in the Solar System," and 2011 Planetary Decadal Survey, "Vision and Voyages" (Space Studies Board 2003, 2011), both emphasize the importance of Europa exploration. The 2011 Decadal Survey discusses the likelihood of contemporary habitats with the necessary conditions for life, stressing the inherent motivation for "a Europa mission with the goal of confirming the presence of an interior ocean, characterizing the satellite's ice shell, and understanding its geological history" (Space Studies Board 2011, pp. 1–2).

Understanding the global-scale structure of Europa, with emphasis on the ocean, along with the distribution of landforms is key to evaluating the habitability of this moon. Within this goal, the Orbiter Mission objectives—(1) to characterize the extent of the ocean and its relation to the deeper interior and (2) to understand the formation of surface features, including sites of recent or current activity, and characterize high-science-interest localities— require global data sets obtained under relatively uniform conditions. As such, these data sets are best suited to collection from a platform that is in orbit around Europa. Within this report, the science to be achieved is discussed, the data types that are needed, and the means by which they can be acquired. The Europa Orbiter Mission would be directly responsive to the Deca-

dal Survey's recommendations for Europa science.

Science Objectives

Understanding planetary processes and habitability is a key driver for Europa exploration. Thus, the goal adopted for the Europa Study is to "Explore Europa to investigate its habitability." The phrase "investigate its habitability" recognizes the significance of Europa's astrobiological potential. "Habitability" includes characterizing any water within and beneath Europa's ice shell, investigating the chemistry of the surface and ocean, and evaluating geological processes that might permit Europa's ocean to possess the chemical energy necessary for life (Figure B-2). Understanding Europa's habitability is intimately tied to understanding the three "ingredients" for life: water, chemistry, and energy. The Europa Orbiter Mission objectives are categorized in priority order as exploration of Europa's ocean and exploration of Europa's geology to understand their contributions to the ingredients for life.

The complete traceability from top level mission goal and objectives to example measurements and the model instruments that could accomplish them is compiled and contained in this report. The example measurements and the notional instruments are provided as a proof of concept to demonstrate the types of measurements that could address the investigations, objectives, and goals. These are not meant to be exclusive of other measurements and instruments that might be able to address

the investigations and objectives in other ways. The model planning payload selected for the Europa Orbiter Mission consists of a notional set of remote-sensing instruments (Laser Altimeter [LA] and Mapping Camera [MC]), in situ instruments (Magnetometer [MAG] and Langmuir Probe [LP]), and a telecommunications system that provides Doppler and range data for accurate orbit reconstruction in support of geophysical objectives. NASA will ultimately select the payload through a formal Announcement of Opportunity (AO) process.

A traceability matrix (Foldout B-1 [FO B-1]), with its overarching goal to "Explore Europa to investigate its habitability," provides specific objectives (in priority order), along with specific investigations (in priority order), and example measurements (in priority order) for each investigation. Each objective and its investigations are described in this report, along with the corresponding example measurements that could address them.

Architecture Implementation

Careful analysis and detailed understanding of the science objectives and traceability matrix led the team to determine that an orbiter mission architecture is the optimal approach to satisfying the science objectives in the most cost-effective, lowest-risk manner. This approach allows the acquisition of a uniform, well controlled data set, while exposing the flight hardware to a lower radiation dose compared to JEO.

The mission concept has been designed to provide global coverage of the Europan surface by means of a circular polar orbit. This orbit, in association with an instrument scan platform, allows mapping coverage across all latitudes at uniform lighting conditions with concurrent acquisition of magnetometry and gravity science measurements. Science measurement requirements are fully met with the current mission design with several areas of further refinement available to improve overall

Figure B-2. Diagram of Europa's subsurface ocean: our Solar System's best chance for extant life beyond Earth?

mission robustness. The Europa Orbiter Mission instruments are light, require only a modest amount of power and produce a data at a modest and manageable rate. These characteristics are ideal for deployment into Europa orbit where insertion mass, power requirements and data return constraints dominate. Additionally, science operations are very repetitive, which leads to low-cost operations. The instrument interface and accommodations allow for delivery late in system-level integration and test, providing program flexibility.

The flight system (Figure B-3) uses a modular architecture, which greatly facilitates the implementation, assembly, and testing of the system. The 3-axis-stabilized spacecraft would utilize four Advanced Stirling Radioisotope Generators (ASRGs) for power. A innovative propulsion system accommodation, along with a Juno-style electronics vault and a nested shielding strategy, would provide significant protection from the radiation environment, allowing the use of existing parts qualified for Earth geosynchronous or medium earth orbit applications. Europa planetary protection requirements would be met through system-level dry-heat microbial reduction in a thermal-vacuum chamber at the launch site. Technical margins for the mission design are extremely robust, with 43% mass margin, 39% power margin during science operations, and 71% downlink margin.

Schedule and Cost

A top-level development schedule is shown in
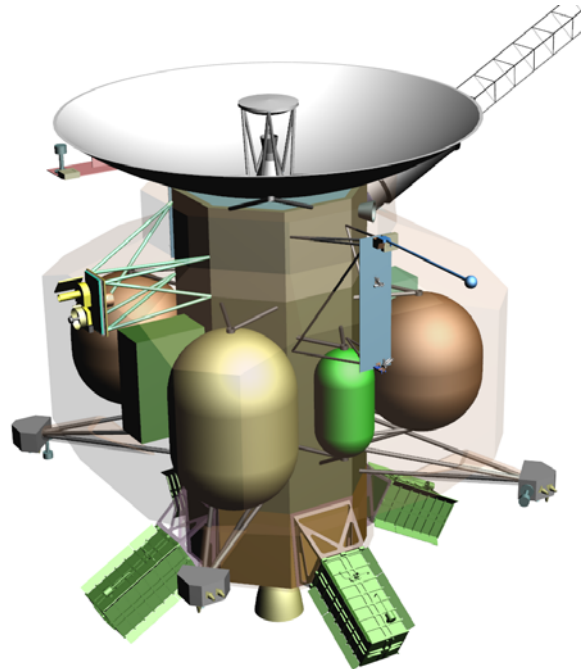
Figure B-3. The Europa Orbiter Mission flight system provides a robust platform to collect and transmit science data.

Figure B-4. The phase durations are conservative and draw on experience from previous outer planets missions. This schedule would enable front-loading of requirements development, significant time for instrument development to understand the actual design implications for radiation and planetary protection, and a flatter than typical mission funding profile, all consistent with newly drafted NASA NPR 7120.5E requirements.

The Orbiter Mission study used a model based costing methodology deriving driving flight
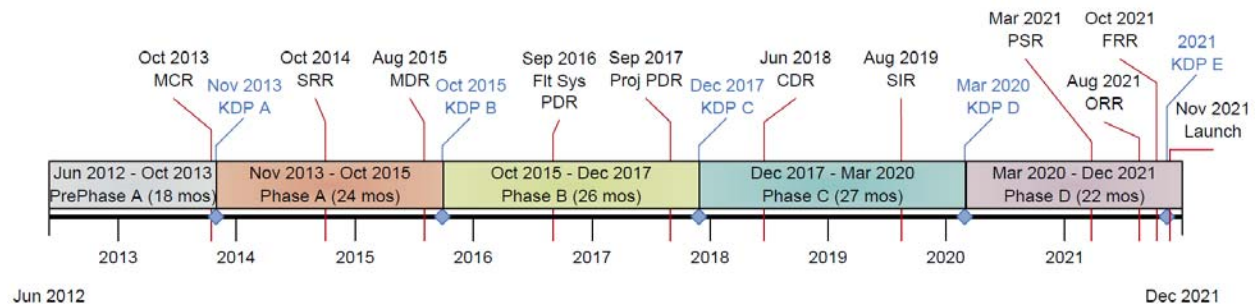
Figure B-4. Top-level development schedule with conservative durations provides appropriate time to address radiation and planetary protection challenges.

system costs from two cost models (PRICE-H, SEER) and payload costs from the NASA Instrument Cost Model (NICM). Experience based percentage wrap factors were then applied to derive supporting Work Breakdown Structure (WBS) elements. JPL Team X estimates were obtained as internally independent validation of the estimated cost and the Aerospace Corporation was retained to perform an external independent CATE cost estimate. The mission Phase A–E lifecycle cost is estimated to be $1.7B (FY15$, w/o Launch Vehicle), 70th-percentile confidence. The Aerospace Corporation performed an independent cost analysis and found $1.8B (FY15$, w/o Launch Vehicle).

Summary

The challenge from NASA and the Decadal Survey has been met with the Europa Orbiter Mission concept. The Europa Orbiter Mission is in compliance with NASA Headquarters direction and guidelines. It has been descoped relative to JEO, yet still retains exceptional science merit. The mission design is conservative with large margins, and meets the NASA cost target$2.25B (FY15$, w/o Launch Vehicle). The Europa Orbiter Mission was presented to the Outer Planets Assessment Group (OPAG) in October 2011, to extremely positive community feedback. An independent technical review of the Europa Orbiter Mission concept was conducted, chaired by Scott Hubbard . The key findings were:

- The overall approach to modularity and radiation shielding was universally lauded as a creative approach to reducing technical risk and cost;
- No engineering "showstoppers" were identified;
- The Orbiter concept satisfied the "existence proof" test as a mission that met Europa science requirements, could be conducted within the cost constraints provided and has substantial margins;

- Two technical risks were identified: ASRG and radiation mitigation for instrument detectors.

The review board's report is included in Appendix B.4.4.

NASA Headquarters Guidelines

Key guidelines from NASA Headquarters included the following:

- Science Objectives: The primary science objective of the mission concept is Europa. The science content of the Europa Jupiter System Mission (EJSM) JEO concept presented to the Decadal Survey is expected to be descoped. The mission concepts are expected to represent the minimum science missions that are at or very near the acceptable science "floor" below which the mission concept is not worth pursuing at the cost estimate.
- International Contributions: The study shall limit international contributions to no more than half of the payload.
- Launch Vehicle: The study shall limit its launch vehicle options to those expected to be available and approved for nuclear payloads by 2020. The study shall delineate the launch vehicle cost, but these costs are not to be included in the cost target.
- Power System: The study shall limit the power systems under consideration to solar arrays, ASRGs, batteries, or any combination thereof. The number of ASRG units available is not specified, but should be minimized. The study should assume an ASRG cost of $50M/unit.
- Science Definition Team: The study shall utilize a small, well-focused SDT to provide guidance on the scientific objectives, measurements, and priorities for the mission concept. The SDT shall be composed of US scientists only and shall be kept to a reasonable

size. A European Space Agency (ESA) observer might be attending some meetings, but is not expected to contribute.

- Presentations of the mission to the science community, including but not limited to OPAG and other advisory groups as requested by HQ.

B.1 Science of the Orbiter Mission

B.1.1 Orbiter Science

Europa is a potentially habitable world that is likely active today. As outlined in this section, there are many well-defined and focused science questions to be addressed by exploring Europa. Both the 2003 Planetary Decadal Survey, *New Horizons in the Solar System,* and the 2011 Planetary Decadal Survey, *Vision and Voyages,* emphasize the importance of Europa exploration (Space Studies Board 2003, 2011). Both Decadal Surveys discuss Europa's relevance to understanding issues of habitability in the solar system, stressing this as the inherent motivation for Europa exploration.

"The first step in understanding the potential of the outer solar system as an abode for life is a Europa mission with the goal of confirming the presence of an interior ocean, characterizing the satellite's ice shell, and understanding its geological history" (Space Studies Board 2011).

Understanding Europa's habitability is intimately tied to understanding the three "ingredients" for life: water, chemistry, and energy (see §A). A spacecraft in orbit around Europa is an excellent platform to understand the global-scale structure of Europa, with emphasis on the ocean, the distribution of landforms, and evaluation of the link between the interior and the surface. To fulfill these types of investigations, a focus on geophysical and geologic measurements is required, necessitating global data sets obtained under relatively uniform conditions. These data are best suited to be collected from orbit around Europa. In this

section, we discuss the science background of an orbiter mission that concentrates on geophysical measurements to address Europa's habitability.

B.1.1.1 Ocean

As it orbits Jupiter, Europa is continually flexed, tugged, and deformed by the gravity of this gas giant. Consequently, the satellite's response of bending, breaking, flowing, heating, and churning enable the characteristics of its ocean and ice to be observed and inferred. Europa also experiences the varying magnetic field of Jupiter, which generates induction currents in the satellite's interior and reveals the conductivity structure through its response. These external influences, in addition to Europa's internal thermal and chemical properties, create the possibility that Europa's interior is volcanically active. Geophysics both dictates and elucidates the characteristics of Europa's ocean, as well as its ice shell and deeper interior.

The surface of Europa suggests recently active processes operating in the ice shell. Jupiter raises gravitational tides on Europa, which 1) contribute to thermal energy in the ice shell and rocky interior (Ojakangas and Stevenson 1989, Sotin et al. 2009), 2) produce near-surface stresses responsible for some surface features (Greeley et al. 2004), and 3) might drive currents in the ocean. Although relatively little is known about the internal structure, most models include an outer ice shell underlain by liquid water, a silicate mantle, and iron-rich core (Anderson et al. 1998, Schubert et al. 2009). Possible means to constrain these models include measurements of the gravitational and magnetic fields, topographic shape, and rotational state of Europa, each of which includes steady-state and time-dependent components. Additionally, the surface heat flux and local thermal anomalies might yield constraints on the satellite's internal heat production and activity. Taken together, results from measuring a range of geophysical parameters would be fundamental to characterizing

the ocean and the overlying ice shell and would provide constraints on deep interior structure and processes.

B.1.1.1.1   Gravity

Observations of the gravitational field of a planetary body provide information about the interior mass distribution. For a spherically symmetric body, all points on the surface would have the same gravitational acceleration; in those regions with more than average mass, however, gravity would be greater. Lateral variations in gravitational field strength, therefore, indicate lateral variations in internal density structure.

Within Europa, principal sources of static gravity anomalies could be those due to 1) ice shell thickness variations, 2) topography on the ocean floor, or 3) internal density variations within the silicate mantle. If the ice shell is isostatically compensated, it would only yield very small anomalies. Gravity anomalies that are not spatially coherent with ice surface topography are presumed to arise from greater depths. Radio Doppler tracking over repeat orbits at 100- km altitude could resolve seamount ridges or other topographic features hundreds of kilometers wide on the ocean floor; note, however, that unique determination of the nature of these features would require additional knowledge acquired via other geophysical measurements (e.g., high-order induced magnetic field measurements).

One of the most diagnostic gravitational features is the amplitude and phase of the time-dependent signal due to tidal deformation (Moore and Schubert 2000). The forcing from Jupiter's gravitational field is well known, and Europa's tidal response would be much larger if a fluid layer decouples the ice from the interior, permitting the unambiguous detection of an ocean and characterization of the ocean and the bulk properties of the overlying ice shell. With an ocean that decouples the surface ice from the rocky interior, the amplitude of the semi-diurnal tide on Europa is roughly 30 m,

which is in clear contrast to the ~1 m tide in the absence of an ocean (Moore and Schubert 2000). Because the distance to Jupiter is 430 times the mean radius of Europa, only the lowest degree tides are expected to be detectable. Figure B.1.1-1 illustrates the degree-two tidal potential variations on Europa during a single orbital cycle. The tidal amplitude is directly proportional to this potential.

B.1.1.1.2   Topography

Characterizing Europa's topography is important for several reasons. At long wavelengths (hemispheric-scale), topography is mainly a response to tides and possibly shell-thickness variations driven by tidal heating
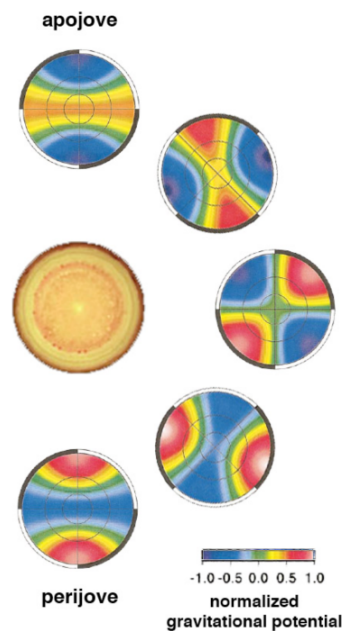
Figure B.1.1-1. Europa experiences a time-varying gravitational potential field as it moves in its eccentric orbit about Jupiter (eccentricity = 0.0094), with a 3.551-day (1 eurosol) period. Europa's tidal amplitude varies proportionally to the gravitational potential, so the satellite flexes measurably as it orbits. This adaptation of a figure from Moore and Schubert (2000), looks down on the north pole of Jupiter as Europa orbits counterclockwise with its prime meridian pointed approximately toward Jupiter. Measuring the varying gravity field and tidal amplitude simultaneously allows the interior rigidity structure of the satellite to be derived, revealing the properties of its ocean and ice shell.

(Ojakangas and Stevenson 1989, Nimmo and Manga 2009) and is, thus, diagnostic of internal tidal processes. At intermediate wavelengths (hundreds of kilometers), the topographic amplitudes and correlation with gravity are diagnostic of the density and thickness of the ice shell. The view of Mars provided by the MOLA laser altimeter (Zuber et al. 1992) revolutionized geophysical study of that body; if similar measurements were achieved, then the same advancement of our understanding of Europa would be expected. The limited topographic information currently available shows Europa to be very smooth on a global scale, but topographically diverse on regional to local scales (Schenk 2009). At the shortest wavelengths (kilometer-scale), small geologic features would tend to have topographic signatures diagnostic of formational processes.

B.1.1.1.3   Rotation

Tidal dissipation within Europa probably drives its rotation into equilibrium, with implications for both the direction and rate of rotation. The mean rotation period should almost exactly match the mean orbital period, so that the sub-Jupiter point would librate in longitude, with an amplitude equal to twice the orbital eccentricity. If the body behaves rigidly, the amplitude of this forced libration is expected to be ~100 m (Comstock and Bills 2003); however, if the ice shell is mechanically decoupled from the silicate interior, the libration could be three times larger. Similar forced librations in latitude are due to the finite obliquity and are diagnostic of internal structure in the same way. The rate of rotation would also change in response to tidal modulation of the shape of the body and corresponding changes in the moments of inertia (Yoder et al. 1981).

The spin pole is expected to occupy a Cassini state (Peale 1976), similar to that of Earth's Moon. The gravitational torque exerted by Jupiter on Europa would cause Europa's spin pole to precess about the orbit pole, while the orbit pole in turn precesses about Jupiter's spin pole, with all three axes remaining coplanar. The obliquity required for Europa to achieve this state is ~0.1 degree, but depends upon the moments of inertia and is, thus, diagnostic of internal density structure (Bills 2005, Bills et al. 2009).

Obtaining a wide variety of different geophysical observations, all relevant to the internal structure of Europa, reduces the ambiguity inherent in interpretations of measurements.

B.1.1.1.4   Magnetic Field

Magnetic fields interact with conducting matter at length scales ranging from atomic to galactic. Magnetic fields are produced when currents flow in response to electric potential differences between interacting conducting fluids or solids. Many planets generate their own stable internal magnetic fields in convecting cores or inner shells through dynamos powered by internal heat or gravitational settling of the interior. Europa, however, does not generate its own magnetic field, suggesting that its core has either frozen or is still fluid but not convecting.

Europa is known to respond to the rotating magnetic field of Jupiter through electromagnetic induction (Khurana et al. 1998, 2009). In this process, eddy currents are generated on the surface of a conductor to shield its interior from changing external electric and magnetic fields. The eddy currents generate their own magnetic field—called the induction field—external to the conductor. This secondary field is readily measured by a magnetometer located outside the conductor.

The induction technique exploits the fact that the primary alternating magnetic field at Europa is provided by Jupiter, because its rotation and magnetic dipole axes are not aligned. It is now widely believed that the induction signal seen in Galileo magnetometer data (Khurana et al. 1998) arises within a subsurface ocean in Europa. The measured signal was shown to remain in phase with the primary field of Jovi-

an origin (Kivelson et al. 2000), thus unambiguously proving that the perturbation signal is a response to Jupiter's field.

Although clearly indicative of a Europan ocean, modeling of the measured induction signal suffers from non-uniqueness in the derived parameters because of the limited data. From a short series of measurements, such as those obtained by the Galileo spacecraft, the induction field components cannot be separated uniquely, forcing assumptions that the inducing signal is composed of a single frequency corresponding to the synodic rotation period of Jupiter. Unfortunately, single frequency data cannot be inverted to determine independently both the ocean thickness and the conductivity. Nevertheless, the single frequency analysis of Zimmer et al. (2000) reveals that the ocean must have a conductivity of at least 0.06 S/m. Work by Schilling et al. (2004) suggests the ratio of induction field to primary field is 0.97, from which Hand and Chyba (2007) infer that the ice shell is <15 km thick and the ocean water conductivity >6 S/m (see also Hand et al. 2009).

The large uncertainty in the conductivity estimates of the ocean water results from the poor signal-to-noise (S/N) ratio of the induction signature obtainable from relatively short segments of Galileo flyby data. Observations from a Europa orbiter could improve the S/N ratio of the induction field by several orders of magnitude.

To determine the ocean thickness and conductivity, magnetic sounding of the ocean at multiple frequencies is required. The depth to which an electromagnetic wave penetrates is inversely proportional to the square root of its frequency. Thus, longer period waves sound deeper and could provide information on the ocean's thickness, the mantle, and the metallic core. Electromagnetic sounding at multiple frequencies is routinely used to study Earth's mantle and core from surface magnetic data (Dyal and Parkin 1973, Parkinson 1983). Recently, Tyler et al. (2003) and Constable and

Constable (2004) demonstrated that data from orbit could be used for electromagnetic induction sounding at multiple frequencies. In the case of Europa, the two dominant frequencies are those of Jupiter's synodic rotation period (~11 hr) and Europa's orbital period (~85 hr). Observing the induction response at these two frequencies would likely allow determination of both the ocean thickness and the conductivity.

Some remaining key questions to be addressed regarding Europa's ocean, bulk ice shell properties, and deeper interior include:

- Does Europa undoubtedly have a subsurface ocean?
- What are the salinity and thickness of Europa's ocean?
- What is the internal structure of Europa's outermost H_2O-rich layers?
- Does Europa have a non-zero obliquity and, if so, what controls it?
- Does Europa possess an Io-like mantle?
- Does Europa exhibit kilometer-scale variations in ice shell thickness across the globe?

B.1.1.2 Geology

By understanding Europa's varied and complex geology, the moon's past and present processes are deciphered, along with implications for habitability. An understanding of Europa's geology provides clues about geological processes on other icy satellites with similar surface features, such as Miranda, Triton, and Enceladus.

The relative youth of Europa's surface is inherently linked to the ocean and the effects of gravitational tides, which trigger processes that include cracking of the ice shell, resurfacing, and possibly release of materials from the interior. Clues to these and other processes are provided by spectacular surface features, such as linear fractures and ridges, chaotic terrain, and impact craters.

B.1.1.2.1   Linear Features

Europa's unusual surface is dominated by tectonic features in the form of linear ridges, bands, and fractures (Figure B.1.1-2). The class of linear features includes simple troughs and scarps (e.g., Figure B.1.1-2g), double ridges separated by a trough, and intertwining ridge-complexes. Whether these represent different processes or stages of the same process is unknown. Ridges are the most common feature type on Europa and appear to have formed throughout the satellite's visible history (Figures B.1.1-2j and l). These ridges range

from 0.1 to > 500 km long, are as wide as 2 km, and could be several hundred meters high. Cycloidal ridges are similar to double ridges, but form chains of linked arcs.

Most models of linear feature formation involve fracturing in response to processes within the ice shell (Greeley et al. 2004, Kattenhorn and Hurford 2009, Prockter and Patterson 2009). Some models suggest that liquid oceanic material or warm mobile subsurface ice squeezes through fractures to form the ridge; other models suggest that ridges form by fric-
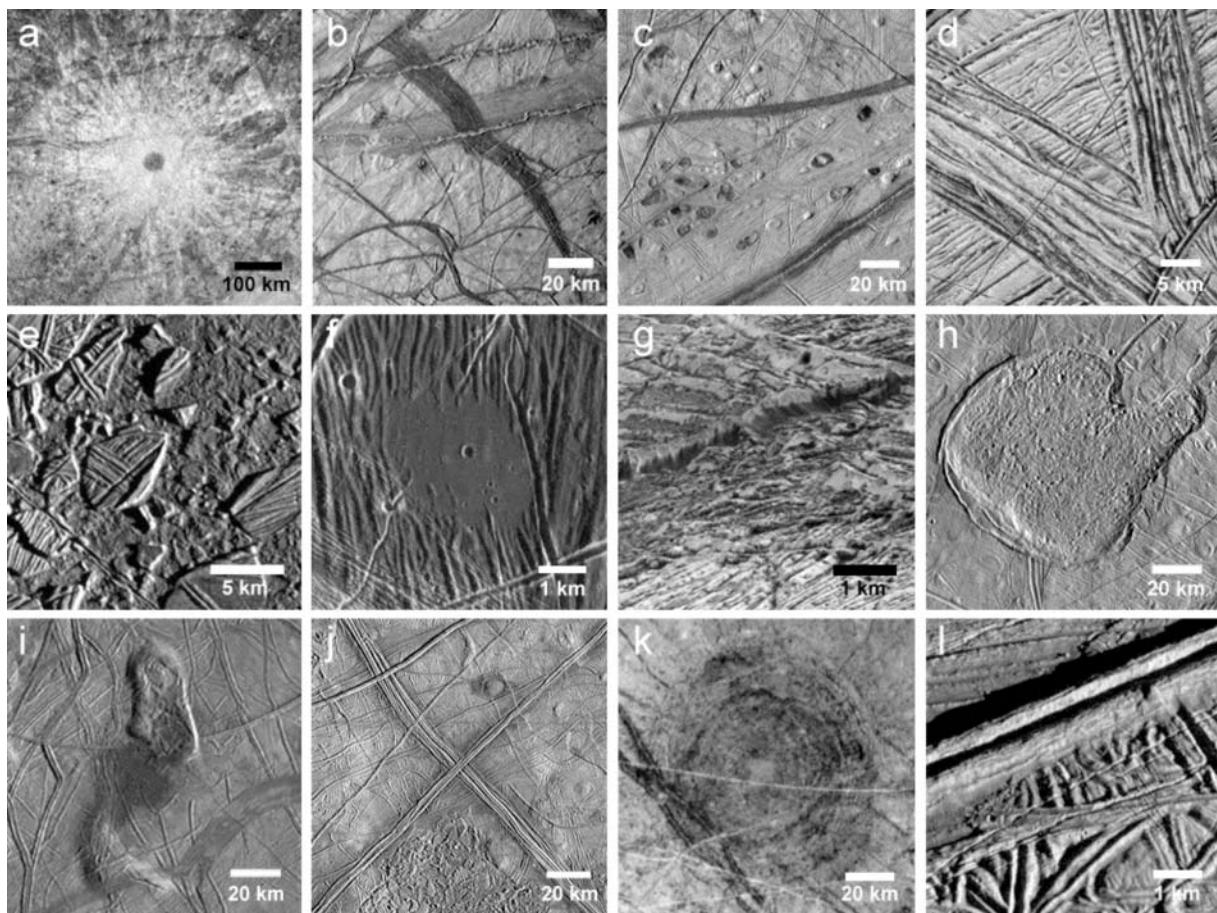
Figure B.1.1-2. Europa is a cryological wonderland, with a wide variety of surface features. Many appear to be unique to this icy moon. While much was learned from Galileo, it is still not understood how many of these features form or their implications for Europa's evolution. Shown here are: (a) the impact crater Pwyll, the youngest large crater on Europa; (b) pull-apart bands; (c) lenticulae; (d) pull-apart band at high resolution; (e) Conamara Chaos; (f) dark plains material in a topographic low, (g) a very-high resolution image of a cliff, showing evidence of mass wasting; (h) Murias Chaos, a cryovolcanic feature that has appears to have flowed a short distance across the surface; (i) the Castalia Macula region, wherein the northernmost dome contains chaos and is ~900 m high; (j) a regional view of two very large ridge complexes in the Conamara region; (k) a Tyre impact feature, showing multiple rings; and (l) one of Europa's ubiquitous ridges, at high resolution.

tional heating and, possibly, melting along the fracture shear zone. Thus, ridges might represent regions of material exchange between the surface, ice shell, and ocean, plausibly providing a means for surface oxidants to enter the ocean. Some features, such as cycloidal ridges, appear to initiate as a direct result of Europa's tidal cycle (Hoppa et al. 1999).

Bands reflect fracturing and lithospheric separation, much like sea-floor spreading on Earth; most bands display bilateral symmetry (e.g., Sullivan et al. 1998) (Figures B.1.1-2b and d). Their surfaces vary from relatively smooth to heavily fractured. The youngest bands tend to be dark, while older bands are bright, suggesting that they brighten with time. Geometric reconstruction of bands suggests that a spreading model is appropriate, indicating extension in these areas and possible contact with the ocean (Tufts et al. 2000, Prockter et al. 2002).

The accommodation of extensional features remains a significant outstanding question regarding Europa's geology. A small number of contractional folds were found on the surface (Prockter and Pappalardo 2000), and some sites of apparent convergence within bands have been suggested (Sarid et al. 2002); these features are, however, insufficient to accommodate the extension documented across Europa's surface. Although some models suggest that ridges and local folds could reflect such contraction, the current lack of global images, topographic information, and knowledge of subsurface structure precludes testing these ideas.

Fractures are narrow (from hundreds of meters to the ~10-m limit of image resolution) and some exceed 1000 km in length. Some fractures cut across nearly all surface features, indicating that the ice shell is subject to deformation on the most recent time-scales. The youngest ridges and fractures could be active today in response to tidal flexing. Young ridges might be places where there has been material exchange between the ocean and the

surface and would be prime targets as potential habitable niches.

B.1.1.2.2   Chaotic Terrain

Europa's surface has been disrupted to form regions of chaotic terrain, as subcircular features termed lenticulae, and irregular-shaped, generally larger chaos zones (Collins and Nimmo 2009). Lenticulae include pits, spots of dark material, and domes where the surface is upwarped and commonly broken (Figures B.1.1-2c and f). Pappalardo et al. (1998, 1999) argued that these features are typically ~10 km across and were possibly formed by upwelling of compositionally or thermally buoyant ice diapirs through the ice shell. In such a case, their size distribution would imply the thickness of the ice shell to be at least 10–20 km at the time of formation.

An alternative model suggests that there is no dominant size distribution and that lenticulae are small members of chaos (Greenberg et al. 1999), formed through either direct material exchange (through melting) or indirect exchange (through convection) between the ocean and surface (e.g., Carr et al. 1998). Thus, global mapping of the size distribution of these features could address their origin.

Chaos is generally characterized by fractured plates of ice that have been shifted into new positions within a background matrix (Figure B.1.1-2e). Much like a jigsaw puzzle, many plates could be fit back together, and some ice blocks appear to have disaggregated and "foundered" into the surrounding finer-textured matrix. Some chaos areas stand higher than the surrounding terrain (Figures B.1.1-2h and i). Models of chaos formation suggest whole or partial melting of the ice shell, perhaps enhanced by local pockets of brine (Head and Pappalardo 1999). Chaos and lenticulae commonly have associated dark, reddish zones thought to be material derived from the subsurface, possibly from the ocean. However, these and related models are poorly constrained because the total energy

partitioning within Europa is not known, nor are details of the composition of non-ice components. Subsurface sounding, surface imaging, and topographic mapping (e.g., Schenk and Pappalardo 2004) are required to understand the formation of chaotic terrain and its implications for habitability.

B.1.1.2.3   Impact Features

Only 24 impact craters with diameters of ≥10 km have been identified on Europa (Schenk et al. 2004), reflecting the youth of the surface. This is remarkable in comparison to Earth's Moon, which is only slightly larger but far more heavily cratered. The youngest Europan crater is thought to be the 24-km-diameter Pwyll, (Figure B.1.1-2a), which still retains its bright rays and likely formed less than 5 Myr ago (Zahnle et al. 1998, Bierhaus et al. 2009). Complete global imaging would provide a full crater inventory, allowing a more comprehensive determination of the age of Europa's surface and helping to identify the very youngest areas.

Crater morphology and topography provide insight into ice layer thickness at the time of the impact. Morphologies vary from bowl-shaped depressions with crisp rims, to shallow depressions with smaller depth-to-diameter ratios. Craters of up to 25–30 km in diameter have morphologies consistent with formation in a warm but solid ice shell, while the two largest impacts, Tyre (Figure B.1.1-2k) and Callanish, might have punched through brittle ice approximately 20 km thick into a liquid zone (Moore et al. 2001, Schenk et al. 2004, Schenk and Turtle 2009).

B.1.1.2.4   Geological History

Determining the geological histories of planetary surfaces requires identifying and mapping surface units and structures and placing them into a time-sequence.

In the absence of absolute ages derived from isotopic measurements of rocks, planetary surface ages are commonly assessed from impact crater distributions, with more heavily cratered regions reflecting greater ages. The paucity of impact craters on Europa limits this technique. Thus, superposition (i.e., younger materials burying older materials) and cross-cutting relations are used to assess sequences of formation (Figueredo and Greeley 2004, Doggett et al. 2009). Unfortunately, only 10% of Europa has been imaged at a sufficient resolution to understand temporal relationships among surface features; for most of Europa, imaging data is both incomplete and disconnected from region to region, making the global surface history difficult to decipher.

Where images of sufficient resolution (better than 200 m/pixel) exist, it appears that the style of deformation evolved through time from ridge and band formation to chaotic terrain (Greeley et al. 2004), although there are areas of the surface where this sequence is less certain (e.g., Riley et al. 2000). The mechanism for the change in geological style is uncertain, but a plausible mechanism for the change is one in which Europa's ocean is slowly cooling and freezing out as the ice above it is thickening. Once the ice shell reaches a critical thickness, solid-state convection may be initiated, allowing diapiric material to be convected toward the surface. A thickening ice shell could be related to a waning intensity of geological activity.

Given the relative youth of Europa's surface, such a fundamental change in style might seem unlikely over the last ~1% of the satellite's history, and its activity over the rest of its ~4.5 billion year existence could only be speculated. Four possible scenarios have been proposed (see Figure B.1.1-3):

   (a) Europa resurfaces itself in a steady-state and relatively constant, but patchy style.

   (b) Europa is at a unique time in its history, having undergone a recent major resurfacing event.

   (c) Global resurfacing is episodic or sporadic.
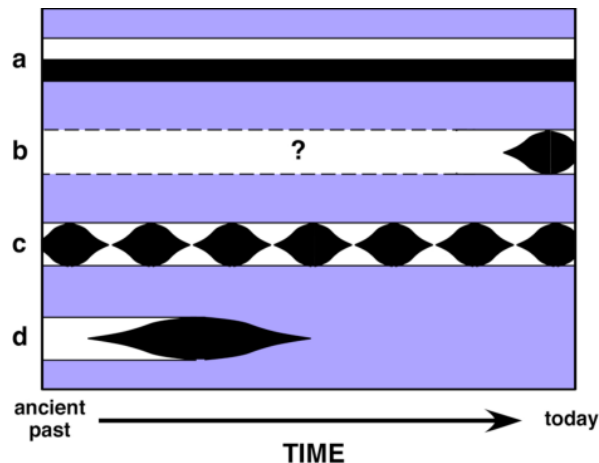
Figure B.1.1-3. Possible evolutionary scenarios for Europa's surface: (a) steady-state, relatively constant resurfacing; (b) the satellite is at a unique time in history, with a recent major resurfacing event; (c) global resurfacing is episodic or sporadic; and (d) the surface is older than cratering models suggest. After Pappalardo et al. (1999).

(d) Europa's surface is actually much older than current cratering models suggest (Zahnle et al. 2003).

From the standpoint of the dynamical evolution of the Galilean satellite system, there is good reason to believe that Europa's surface evolution could be cyclical. If so, Europa could experience cyclical variations in its orbital characteristics and tidal heating on time scales of perhaps 100 million years (Hussman and Spohn 2004).

Global imaging, coupled with topography, would enable these evolutionary models to be tested. Europa's surface features generally brighten and become less red through time, so albedo and color could serve as a proxy for age (Geissler et al. 1998, Moore et al. 2009). Quantitative topographic data (Schenk and Pappalardo 2004) could provide information on the origin of geologic features and might show trends with age. Profiles across ridges, bands, and various chaotic terrains would aid in constraining their modes of origin. Moreover, flexural signatures are expected to be indicative of local elastic lithosphere thickness at the time of their formation and might provide evidence of

topographic relaxation (e.g., Nimmo et al. 2003, Billings and Kattenhorn 2005).

Some remaining outstanding questions related to Europa's geology include:

- Do Europa's ridges, bands, chaos, and/or multi-ringed structures require the presence of near-surface liquid water to form?
- Where are Europa's youngest regions?

B.1.2 Orbiter Traceability Matrix

As outlined in Section B.1.1, multiple well-defined and focused science questions can be addressed by exploring Europa to understand the potential for life in the outer solar system. Interrelated physical processes and habitability are key drivers for Europa exploration. Thus, the goal adopted for the Europa orbiter mission concept is:

Explore Europa to investigate its habitability.

This goal implies understanding processes, origin, and evolution. These include testing the numerous scientific questions described above. "Investigate its habitability" recognizes the significance of Europa's astrobiological potential. "Habitability" includes confirming the existence and determining the characteristics of water below Europa's icy surface, investigating the evolution of the surface and ocean, and evaluating the processes that have affected Europa through time. A Europa orbiter supplies critical information for investigating the extent of Europa's ocean and the cycling of energy from its interior to its surface.

The Europa orbiter mission objectives flow from the key science issues outlined above. These objectives represent a key subset of Europa science best accomplished by a Europa orbiter mission. These objectives are categorized in priority order as:

O. Europa's Ocean: Characterize the extent of the ocean and its relation to the deeper interior.
G. Europa's Geology: Understand the formation of surface features, including

sites of recent or current activity to understand regional and global evolution

The traceability matrix, complied in Foldout B-1, maps the orbiter objectives (in priority order) to specific investigations (in priority order within each objective) to address the overarching mission goal. The specific measurements for each investigation are also listed in priority order. The orbiter objectives and investigations are discussed in detail in Sections B.1.2.1 and B.1.2.2.

B.1.2.1   Europa's Ocean

Galileo observations—in particular, the magnetometer data—provide evidence that the presence of a sub-surface ocean is very likely. Given the critical importance of such an ocean to Europa's astrobiological potential, it is important to first confirm its existence.

In the likely instance that an ocean exists, several geophysical measurements would place constraints on its depth, extent, and physical state (e.g., salinity). Several of these techniques would also help to characterize the deeper interior structure of Europa (the mantle and core). Doing so is important because of the coupling that takes place between the near-surface and deeper layers: for instance, an Io-like mantle implies a vigorously convecting ocean and a relatively thin ice shell. The investigations and corresponding measurement techniques are as follows.

B.1.2.1.1   *Investigation O.1: Determine the amplitude and phase of the gravitational tides.*

Perhaps the most direct way of confirming the presence of an ocean is to measure the time-variable gravity and topography due to the tides raised by Jupiter. In the absence of an ocean, Europa's ice shell would be coupled directly to the rocky core, and the time-dependent tidal surface displacement would be a few meters (Moore and Schubert 2000). If, on the other hand, Europa has a liquid water ocean beneath a relatively thin ice shell, the displacement amplitude would be 30 m over one orbit (Figure B.1.2-1). The surface displacement would also cause a measurable periodic gravity signal. Thus, measurement of the tidally driven time-variable topography or gravity (described by the Love numbers h_2 and k_2, respectively) would provide a simple and definitive test of the existence of a sub-ice ocean.

The Love number k_2 is estimated from the time-variable gravitational field of Europa. Simulations show that measurements of the Doppler shift of the spacecraft radio signal could be used to estimate k_2, the mantle and ice shell libration amplitudes and phase lag angle, and the static gravitational field parameters, which are estimated along with the spacecraft trajectory information (Wu et al. 2001). Simulations adding altimetry measurements show that the tidal Love number h_2 could also be estimated (Wahr et al. 2006).

Observations from many orbits are required to estimate the body gravity field, including the tidal response, because the spacecraft orbit has to be determined at the same time. Orbit determination is improved by crossover analysis using altimetry measurements. If the spacecraft measures different distances to the same spot on the surface during different orbits, then (neglecting tides) the change must be due to the changing spacecraft altitude. In this manner, the spacecraft position could be accurately determined as at Mars (Neumann et al. 2001). This approach could also take into account the fact that the surface undergoes periodic displacements, due to tides and librations.

In addition to testing the ocean hypothesis, h_2 and k_2 could be used to investigate the ice shell thickness. Figure B.1.2-1 shows how these quantities vary with ice shell thickness and rigidity. Based on simulations of plausible internal structures, measurement uncertainties of ±0.0005 for k_2 and ±0.01 for h_2 would permit the actual k_2 and h_2 of Europa to be inferred with sufficient accuracy such that the combination places bounds on the depth of the ocean and the thickness of the ice shell (Wu et al. 2001, Wahr et al. 2006).

Goal	Objective	Investigation	Measurement	Model Instrument	Mission Constraints/Requirements	Water	Chemistry	Energy
Explore Europa to investigate its habitability	Characterize the extent of the ocean and its relation to the deeper interior	O. Ocean	O.1 Determine the amplitude and phase of gravitational tides.	O.1a Measure degree two-time dependent gravity field, to recover k_2 amplitude at Europa's orbital frequency to 0.003 absolute accuracy, and the phase to 1 degree.	Radio Subsystem (RS)	(1) Low altitude (100 km; < 200 km should be sufficient), circular, near-polar (within 5° to 10° of the pole) orbit, for at least 30 days (baseline), 18 days (floor); (2) Range-rate measurements with an accuracy better than 0.1 mm/s at 60 sec integration time to determine spacecraft orbit to better than 1-meter (rms) in radial direction over several tidal cycles; (3) Several "unperturbed" days for the data arcs (preferably at least one rotation of Europa) for gravity. Limit spacecraft momentum dumping or thrusting to an interval of 3 to 4 days, if possible.	✔		
				O.1b Determine topographic differences from globally distributed repeat measurements to recover spacecraft altitude at crossover points to 1-meter vertical accuracy.	Laser Altimeter (LA)	(1) Low altitude (100 km; < 200 km should be sufficient), circular, near polar (within 5° to 10° of the pole) orbit, for at least 30 days (baseline and floor); (2) Near continuous global ranging to the surface with 10-cm accuracy (baseline); floor of 20-cm accuracy; (3) Range-rate measurements with accuracy better than 0.1 mm/s at 60-sec integration time.	✔		
				O.1c Determine the orbital position of Europa's center of mass, relative to Jupiter, during the lifetime of the mission to better than 10 meters.	Radio Subsystem (RS)	(1) Low altitude (100 km; < 200 km should be sufficient), circular, near-polar (within 5° to 10° of the pole) orbit, for at least 30 days (baseline), 18 days (floor); (2) Range-rate measurements with an accuracy better than 0.1 mm/s at 60 sec integration time to determine spacecraft orbit to better than 1-meter (rms) in radial direction throughout the lifetime of the orbiter; (3) Limit spacecraft momentum dumping or thrusting to 3 to 4 days, if possible.	✔		
			O.2 Determine Europa's magnetic induction response.	O.2a Measure three-axis magnetic field components at 8 vectors/s, and a sensitivity of 0.1 nT, near-continuously to determine the induction response at multiple frequencies (orbital as well as Jupiter rotation time scales) to an accuracy of 0.1 nT.	Magnetometer (MAG)	(1) Low altitude (100 km; < 200 km should be sufficient), circular, near-polar (within 5° to 10° of the pole) orbit, for at least 30 days (baseline), 18 days (floor).	✔	✔	
				O.2b Characterize the local plasma density, temperature and flow to constrain (in conjunction with modeling) the contribution from currents not related to the surface and ocean.	Langmuir Probe (LP)	(1) Low altitude (100 km; < 200 km should be sufficient), circular, near-polar (within 5° to 10° of the pole) orbit, for at least 30 days; (2) Operation in "sweep" mode to measure ion currents; (3) 4π coverage (multiple probes with differential measurements); (4) Cover approximately 12 hours of local time (Europa local time) by spanning noon to dusk (or dawn) on the dayside hemisphere, which would also capture midnight to dawn (or dusk) on the nightside hemisphere.	✔		
				O.2c Determine electric field vectors (near DC to 3 MHz), and measure electron and ion density, as well as electron temperature, for local conductivity and electrical currents determination	Langmuir Probe (LP)	(1) Low altitude (100 km; < 200 km should be sufficient), circular, near-polar (within 5° to 10° of the pole) orbit, for at least 30 days; (2) Operation in "sweep" mode to measure ion currents; (3) 4π coverage (multiple probes with differential measurements); (4) Cover approximately 12 hours of local time (Europa local time) by spanning noon to dusk (or dawn) on the dayside hemisphere, which would also capture midnight to dawn (or dusk) on the nightside hemisphere.	✔		
		O.3 Determine the amplitude and phase of topographic tides.	O.3a Determine topographic differences from globally distributed repeat measurements at varying orbital phases, with better than or equal to 1-meter vertical accuracy, to recover h_2 to 0.01 (at the orbital frequency).	Laser Altimeter (LA)	(1) Low altitude (100 km; < 200 km should be sufficient), circular, near polar (within 5° to 10° of the pole) orbit, for at least 30 days (baseline and floor); (2) Near continuous global ranging to the surface with 10-cm accuracy (baseline); floor of 20-cm accuracy; (3) Range-rate measurements with accuracy better than 0.1 mm/s at 60-sec integration time.	✔		
				O.3b Measure spacecraft velocity to constrain the position of the spacecraft to better than 1 meter (rms).	Radio Subsystem (RS)	(1) Low altitude (100 km; < 200 km should be sufficient), circular, near-polar (within 5° to 10° of the pole) orbit, for at least 30 days (baseline), 18 days (floor); (2) Range-rate measurements with an accuracy better than 0.1 mm/s at 60 sec integration time to determine spacecraft orbit to better than 1-meter (rms) in radial direction throughout the lifetime of the orbiter; (3) Limit spacecraft momentum dumping or thrusting to 3 to 4 days, if possible.	✔		

☐ Floor

▨ Baseline only

Water: Water in its liquid form as pertaining to habitability as an oxidizer and medium for the transport of chemical constituents.
Energy: Energy that supports and fosters a means for potential metabolism to be established and sustained.
Chemistry: The constituents that foster and sustain the processes and environment for metabolic activity.

		Objective	Investigation	Measurement	Model Instrument	Mission Constraints/Requirements	Water	Chemistry	Energy
Explore Europa to investigate its habitability	O. Ocean	Characterize the extent of the ocean and its relation to the deeper interior	O.4 Determine Europa's rotation state.	O.4a Determine the mean spin pole direction (obliquity) to better than or equal to 10 meters, through development of an altimetry corrected geodetic control network from imaging at better than or equal to 100-m/pixel.	Laser Altimeter (LA), Mapping Camera (MC)	(1) Low altitude (100 km; < 200 km should be sufficient), circular, near polar (within 5° to 10° of the pole) orbit, for at least 30 days (baseline and floor); (2) Near continuous global ranging to the surface with 10-cm accuracy (baseline); floor of 20-cm accuracy; (3) Range-rate measurements with an accuracy better than 0.1 mm/s at 60 sec integration time; (4) Near-uniform lighting conditions preferred. To the extent possible, imaging should be at solar incidence angles greater than 45°. Ideally the incidence angle would be 70°; (5) Baseline: ≥80% global mapping at better or equal 100 m/pixel; Floor: ≥80% global mapping at better or equal 200 m/pixel.	✔		
				O.4b Determine the forced nutation and the amplitude of the forced libration of the spin pole at the orbital period to better than or equal to 1 meter, through development of a geodetic control network to better than or equal to 10-meter spatial scale at multiple tidal phases.	Laser Altimeter (LA)	(1) Low altitude (100 km; < 200 km should be sufficient), circular, near polar (within 5° to 10° of the pole) orbit, for at least 30 days (baseline and floor); (2) Near continuous global ranging to the surface with 10-cm accuracy (baseline); floor of 20-cm accuracy; (3) Range-rate measurements with accuracy better than 0.1 mm/s at 60-sec integration time.	✔		
			O.5 Investigate the deeper interior.	O.5a Resolve the static gravity field to degree and order 20 (floor); 30 (baseline) or better.	Radio Subsystem (RS)	(1) Low altitude (100 km; < 200 km should be sufficient), circular, near-polar (within 5° to 10° of the pole) orbit, for at least 30 days (baseline), 18 days (floor); (2) Range-rate measurements with an accuracy better than 0.1 mm/s at 60 sec integration time to determine spacecraft orbit to better than 1-meter (rms) in radial direction; (3) Several "unperturbed" days for the data arcs (preferably at least one rotation of Europa) for gravity. Limit spacecraft momentum dumping or thrusting to an interval of 3 to 4 days, if possible.	✔		
				O.5b Make topographic measurements to resolve coherence with gravity to degree 20 (floor); 30 (baseline) or better, with better than or equal to 1-meter vertical accuracy.	Laser Altimeter (LA)	(1) Low altitude (100 km; < 200 km should be sufficient), circular, near polar (within 5° to 10° of the pole) orbit, for at least 30 days (baseline and floor); (2) Near continuous global ranging to the surface with 10-cm accuracy (baseline); floor of 20-cm accuracy; (3) Range-rate measurements with accuracy better than 0.1 mm/s at 60-sec integration time.	✔		
				O.5c Characterize the local plasma density, temperature and flow to constrain (in conjunction with modeling) the contribution from currents not related to the surface and ocean.	Langmuir Probe (LP)	(1) Low altitude (100 km; < 200 km should be sufficient), circular, near-polar (within 5° to 10° of the pole) orbit, for at least 30 days; (2) Operation in "sweep" mode to measure ion currents; (3) 4π coverage (multiple probes with differential measurements); (4) Cover approximately 12 hours of local time (Europa local time) by spanning noon to dusk (or dawn) on the dayside hemisphere, which would also capture midnight to dawn (or dusk) on the nightside hemisphere.	✔		✔
				O.5d Measure three-axis magnetic field components at 8 vectors/s with a sensitivity of 0.1 nT.	Magnetometer (MAG)	(1) Low altitude (100 km; < 200 km should be sufficient), circular, near polar (within 5° to 10° of the pole) orbit, for at least 30 days (baseline and floor).	✔	✔	✔
	G. Geology	Understand the formation of surface features, including sites of recent or current activity to understand regional and global evolution	G.1 Determine the distribution, formation, and three-dimensional characteristics of magmatic, tectonic, and impact landforms.	G.1a Constrain regional and global stratigraphic relationships by determining surface morphological characteristics at ~100-m/pixel scale.	Mapping Camera (MC)	(1) Near-uniform lighting conditions preferred. To the extent possible, imaging should be at solar incidence angles greater than 45°. Ideally the incidence angle would be 70°; (2) Baseline: ≥80% global mapping at better or equal 100 m/pixel; Floor: ≥80% global mapping at better than or equal to 200 m/pixel.	✔		✔
				G.1b Determine topography at better than or equal to 300-m/pixel horizontal footprint resolution (elevation posting from 100-m/pixel image data) and better than or equal to 30-meter vertical resolution (presumably through stereo imaging coverage), over as much of the surface as feasible.	Mapping Camera (MC), Laser Altimeter (LA)	(1) Stereo imaging: either have sufficient along-track or cross track FOV so that adjacent tracts cover at least half of each other for stereo, or else image the surface twice, the second time off nadir; (2) Laser altimetry is preferably simultaneous with imaging; (3) Baseline: ≥80% global mapping at better or equal 100 m/pixel; Floor: ≥80% global mapping at better or equal 200 m/pixel.	✔		✔

	Floor
	Baseline only

Water: Water in its liquid form as pertaining to habitability as an oxidizer and medium for the transport of chemical constituents.
Energy: Energy that supports and fosters a means for potential metabolism to be established and sustained.
Chemistry: The constituents that foster and sustain the processes and environment for metabolic activity.

Figure B.1.2-1. Sensitivity of Love numbers k_2 (left) and h_2 (right) to ice shell thickness and rigidity, with the assumption of a subsurface ocean. For the same curves that depict h_2, the right-hand axis shows the amplitude ζ_{tidal} (which is half of the total measurable tide) as a function of ice shell thickness. For a relatively thin ice shell above an ocean, the tidal amplitude is $\zeta_{tidal} \sim 15$ m (total measureable tide ~30 m), while in the absence of an ocean $\zeta_{tidal} \sim 1$ m (Moore and Schubert 2000). Solid curves show the h_2 and corresponding ζ_{tidal} for an ice shell rigidity of μ_{ice} $=3.5 \times 10^9$ Pa, while the dotted lines bound a plausible range for ice rigidity. A rocky core is assumed, with a radius 1449 km and rigidity $\mu_{rock} = 10^{11}$ Pa, and the assumed ice + ocean thickness =120 km. Triangles show the reported values from Moore and Schubert (2000), which did not include a core. Figure courtesy Amy Barr.

B.1.2.1.1.1   *Measurement Techniques—Radio Subsystem and Laser Altimetry*

To detect the radio Doppler shift caused by the spacecraft motion in the line-of-sight to Earth, two frequency bands have been considered. X-band (near 8 GHz) would be used for spacecraft commanding and Ka-band (near 32 GHz) would be used for transmission of spacecraft data to Earth. With the X-band uplink, Doppler measurement accuracy is limited by fluctuations in the solar plasma. An accuracy of 0.1 mm/s for 60 s integration times is typical, but varies as a function of solar elongation.

Doppler-only simulations (Wu et al. 2001) show that the Love number k_2 could be determined with an accuracy of approximately 0.0005, or 0.25%, using either X/X or X/Ka Doppler tracking over 15 days when fit simultaneously with the Europa gravity field, librations, and spacecraft trajectory. In the same estimation the radial position of the spacecraft could be determined to an accuracy of 2 m, close to the desired orbit reconstruction accu-racy, but about 10 times worse than currently being achieved with Mars orbiting spacecraft using much longer data arcs (Konopliv et al. 2006). The expected accuracy in determining k_2 is easily sufficient to distinguish between an ocean-bearing and ocean-free Europa.

Range-rate measurements would also permit precise determination of the position of Europa's center of mass relative to Jupiter during the lifetime of the mission. This is necessary for determining the spacecraft orbit to better than 1-meter (rms) throughout the orbiter lifetime.

The Love number h_2 is derived by measuring the time-variable topography of Europa; specifically, by measuring topography at crossover points. This measurement can be readily achieved with a laser altimeter (Figure B.1.2-2); in fact, the technique has been demonstrated for the Earth (Luthcke et al. 2002 2005) and Mars (Rowlands et al. 1999, Neumann et al. 2001). After ~30 days in orbit about Europa, the sub-spacecraft track would form a reasonably dense grid (~25-km spacing
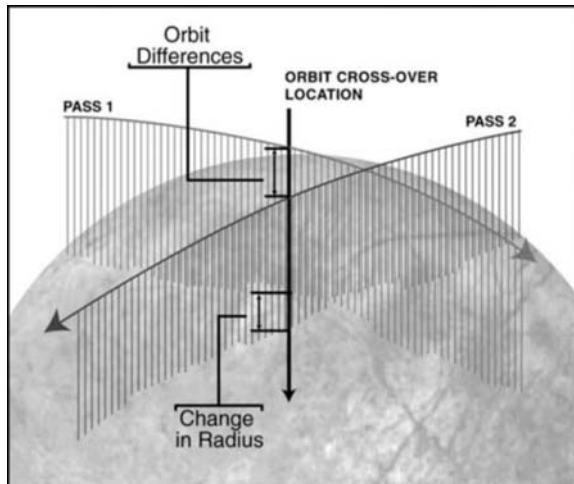
Figure B.1.2-2. Illustration of the cross-over technique. The actual change in the radius of Europa due to tidal and librational motions is determined by measuring altitude from the spacecraft to the surface and by accounting for the distance of the spacecraft from the center of mass by means of Doppler tracking (Wahr et al. 2006).

at the equator), comprised of a number N of (~340) great circle segments over the surface of Europa in 30 days. Each of the N arcs intersects each of the remaining N-1 arcs at two roughly antipodal locations; at these cross-over locations, the static components of gravity and topography should agree. As illustrated in Figure B.1.2-2, differences in the measured values at cross-over points are equal to the sum of actual change in radius caused by tides and libration, combined with the difference in orbital altitude, along with any errors in range to the center of the body or orbital position. The errors are dominated by long wavelength effects and could be represented by 4 sine and cosine terms in each orbital component (radial, along track, and cross track). The tidal effects in gravity and topography have known spatial and temporal patterns and could each be represented globally by two parameters: an amplitude and a phase. The librations are effectively periodic rigid rotations with specified axes and periods and, again, an amplitude and a phase parameter.

B.1.2.1.2　Investigation O.2: Determine Europa's magnetic induction response.

The strongest current evidence for Europa's ocean is the induction signature apparently generated by Jupiter's time-dependent magnetic field interacting with a shallow conductive layer, presumably a salty ocean. However, because the Galileo spacecraft was effectively measuring the induction response at a single frequency during its flybys, only the product of the layer thickness and conductivity could be established. By contrast, an orbiter could determine both thickness and conductivity by measuring the induction response at multiple frequencies.

Europa is immersed in various low-frequency waves that could be used for magnetic sounding, some of which arise from Io's torus at the outer edge of Europa's orbit. Waves of different frequencies penetrate to different depths within the satellite and exhibit different induction responses. Dominant frequencies occur at the synodic rotation period of Jupiter (period ~ 11 hr) and the orbital period of Europa (period = 3.55 days = 85.2 hr). Over a broad range of parameter space, the induction curves at two frequencies intersect (Khurana et al. 2002). In this range, the ocean thickness and conductivity (which constrains the salinity) could be determined uniquely. In order to sound the ocean at these two frequencies, continuous data are required from low altitude over times of at least one month.

B.1.2.1.2.1　Measurement Technique—Magnetometry & Plasma Measurements (Langmuir Probe)

Magnetometry requires near-continuous observations from Europa orbit for at least 8–10 eurosols (i.e., at least one month). A high cadence of 8 vectors/s is required to remove the effects of moon-plasma interactions from the data, and knowledge of spacecraft orientation is required to 0.1°. In addition, measurements of the electron and ion density, electron temperature, and electrical currents (Langmuir

Probe) generated in Europa's vicinity are necessary to facilitate removing their contributions from the measured magnetic field.

B.1.2.1.3   Investigation O.3: Determine the amplitude and phase of topographic tides.

The time-dependent tidal deformation of Europa's surface, characterized by the Love number h_2, provides a strong test for the existence of an ocean. It could also be used in conjunction with the k_2 Love number to constrain the ice shell thickness.

B.1.2.1.3.1   Measurement Technique—Laser Altimetry and Radio Subsystem

The method to achieve the desired measurements is through quantifying topographic differences at the same surface point while Europa is located at different positions in its orbit. The details of how this can be accomplished are described in section B.1.2.1.1.2.

B.1.2.1.4   Investigation O.4: Determine Europa's rotation state.

Europa's rotation pole position and its librations in both longitude and latitude would be determined as part of the orbit determination and crossover analysis necessary to determine h_2 and k_2 (Sections B.1.2.1.1). These quantities all depend on Europa's internal structure; thus, they provide additional, largely independent, constraints on the presence or absence of an ocean and the polar moment of inertia B. This latter quantity contains information about the distribution of mass within the satellite.

Librations in longitude and latitude are driven by the non-zero eccentricity and obliquity of the satellite, respectively. The amplitude of forced librations in longitude gives the combination (B-A)/C for the principal moments of inertia A < B < C, as has been done for Earth's Moon (Newhall and Williams 1997). The quantity (B-A) depends on the degree-two static gravity coefficients, which would be determined to high accuracy, and, thus, the polar moment of inertia C could be determined. If the ice shell is decoupled from the

interior by an ocean, the libration amplitude would be a factor of three larger than for a solid Europa (Comstock and Bills 2003). Similar constraints would be provided by determination of the latitudinal libration amplitude.

If there is an ocean, there might be two librational signals: one from the ice shell and another from the deeper interior. The shell's signal would be revealed in both gravity and topography data, whereas the deeper signal would appear only in the gravity.

Europa's obliquity—the angular separation between its spin and orbit poles—provides another constraint on its polar moment of inertia B. If its spin state is tidally damped, the obliquity is expected to be ~0.1° (Bills 2005), with the exact amplitude depending on C (Ward 1975, Bills and Nimmo 2008).

B.1.2.1.4.1   Measurement Technique—Laser Altimetery and Mapping Camera

The dynamical rotational state (spin rate and orientation, libration amplitudes) of Europa would be determined using Doppler tracking data and a laser altimetry crossover technique supplemented by a geodetic control network derived from imaging data at better than 100 m/pixel. Initially assuming both steady rotation and zero obliquity, the cross-over analysis described above (Section 1.2.1.1.2) would be used to adjust the spacecraft orbit estimate and to determine the dynamical rotation as well as the tidal flexing of Europa.

B.1.2.1.5   Investigation O.5: Investigate the deeper interior.

Whether Europa's silicate interior is Io-like and dissipative or cold and inactive has important consequences for the likely thickness of the shell and for silicate-ocean interchange. Clues to the nature of the deeper interior could be obtained from gravity, topographic, and magnetic observations.

Static gravity observations, made using the same techniques as outlined above, could be used to investigate the topography at the silicate-ocean interface. Figure B.1.2-3 illustrates
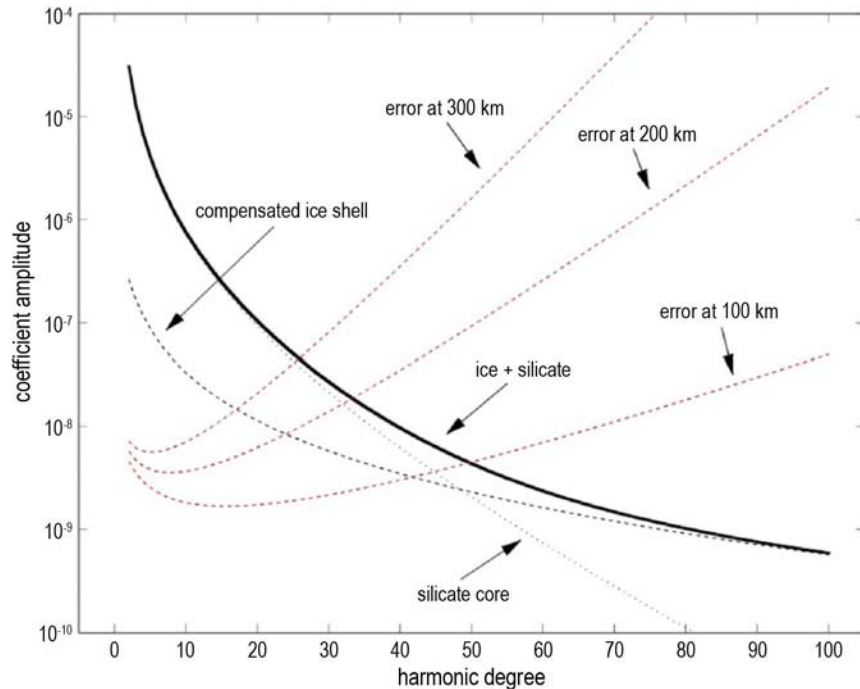
Figure B.1.2-3. Models of Europa's gravity spectrum, assuming an ice shell 10-km thick with isostatically compensated topography above an ocean and a silicate interior with a mean surface 100 km below the ice surface. The variance spectra of the ice topography and silicate gravity are assumed similar to those seen on terrestrial planets (Bills and Lemoine 1995). The signal has contributions from the silicate mantle and ice shell. The error spectra represent 30 days at fixed altitude and reflect variations in sensitivity with altitude. The error spectra at different orbital altitudes do not have the same shape because the longer wavelength anomalies are attenuated less at higher altitudes. During a few days at these altitudes, the improvement is linear with time; for longer times, repeat sampling leads to improvement proportional to square root of time.

the estimated gravitational spectrum for Europa, with separate contributions from an ice shell and a silicate interior, along with simulated error spectra for 30 days of tracking at each of three representative orbital altitudes (see Wu et al. 2001). To be conservative, only the X-band error estimate has been used. The recovered gravity errors are smaller at lower altitudes because the spacecraft is closer to the anomalies and, thus, experiences larger perturbations.

At long wavelengths, the gravity signal is dominated by the silicates. Because the water-silicate density contrast likely greatly exceeds density variations within the mantle, long-wavelength gravity anomalies would

provide evidence for sea-floor topography and might point to the existence of seamounts or volcanic rises. Such long-wavelength gravity anomalies might also result in potentially measurable surface topographic variations (as with the sea surface on Earth).

At shorter wavelengths, the signal is dominated by shallower ice-shell contributions and the topography and gravity should be spatially coherent (Luttrell and Sandwell 2006). Isostatically supported topography in the ice shell produces a gravity anomaly that is larger for thicker shells. If the wavelength at which the transition from silicate-dominated to ice-dominated signals could be determined, this would provide a constraint on the thickness of the ice shell (assuming isostatic compensation). Such a transition is potentially detectable at a 100-km orbit altitude.

B.1.2.1.5.1   *Measurement Technique— Radio Subsystem, Laser Altimetry, Magnetometry & Plasma Measurements (Langmuir Probe)*

Time-dependent gravity and static topography measurements might also provide constraints on Europa's deep interior: for instance, a fluid-like Love number ($k_2 \sim 2.5$) would imply a low-rigidity mantle and core, as well as a subsurface ocean.

Magnetometer measurements of very low-frequency magnetic variations (periods of several weeks) would shed light on the magnetic properties of the deep interior, including

Table B.1.2-1. Hypothesis Tests to Address Selected Key Questions Regarding Europa's Ocean and Interior.

Example Hypothesis Questions	Example Hypothesis Tests
Does Europa undoubtedly have a subsurface ocean?	Measure the gravity field at Europa over the diurnal cycle.
What are the salinity and thickness of Europa's ocean?	Determine the magnetic induction signal over multiple frequencies to derive ocean salinity and thickness.
What is the internal structure of Europa's outermost H_2O-rich layers?	Use measurements of the time-variable topography to derive the Love number h_2, to relate the ice shell and ocean layer thicknesses.
Does Europa have a non-zero obliquity and, if so, what controls it?	Use gravitational and topographic measurements of the tides to infer obliquity, which, in turn, constrains moments of inertia, especially in combination with libration amplitude(s).
Does Europa possess an Io-like mantle?	Magnetic and/or gravitational inferences of the ice shell thickness constrain how much heat the silicate interior is producing; magnetometer inferences of ocean salinity constrain the rate of chemical exchange between silicates and water and the conductivity structure of the deep interior; time-variable gravity place bounds on the rigidity of the silicate interior.
Does Europa exhibit kilometer-scale variations in ice shell thickness across the globe?	Measure high degree and order gravity field and topography to determine coherence

the core. For instance, a partially molten, Io-like mantle is expected to have a higher conductivity than a cold, inactive interior. Such measurements need to be taken over a period of several months. Simultaneous plasma measurements are necessary to remove the effects of moon-plasma interactions from the data.

The key outstanding questions relating to Europa's ocean could be linked to and addressed by the investigations described above, as summarized in Table B.1.2-1.

B.1.2.2   Europa's Geology

Europa's landforms are enigmatic; there exist a wide variety of hypotheses for explaining the formation of these landforms. The search for geologic activity is significant for understanding Europa's potential for habitability, especially with respect to the question of how material is transported between the surface and the subsurface, including the ocean.

B.1.2.2.1   Investigation G.1: Determine the distribution, formation, and three-dimensional characteristics of magmatic, tectonic, and impact landforms.

Geologically active sites are the most promising for astrobiology. Europa's continuous tidal activity leads to predictions that some landforms might be actively forming today and are the most likely locations for near-surface liquid (see Section B.1.2.1). The most promising regions for current activity are 1) regions of chaos wherein thermally or compositionally buoyant diapirs rise to the surface or 2) cracks that have recently formed in response to tidal stresses. Low-albedo smooth-plains material associated with some chaotic terrains might be subsurface material (such as brines) that have been emplaced onto the surface (Collins and Nimmo 2009, Schmidt et al. 2011); these locations might therefore, represent sites of high scientific interest. Recently or currently active regions are expected to best illustrate the processes involved in the formation of some surface structures, showing pristine morphologies and distinct geologic relationships, and, perhaps, exhibiting associated plume activity such as that seen on Enceladus.

Determining the relative ages of Europa's surface features allows the evolution of the surface to be unraveled. Indication of relative age comes from the stratigraphy, derived from cross-cutting and embayment relationships, and the relative density of small primary impact craters. These relationships enable a time history to be assembled within regions that can be extrapolated globally across Europa. Without a global map, the relative ages of different regions cannot be determined because they cannot be linked; this is the current problem in

understanding Europa's stratigraphy based on Galileo imaging.

B.1.2.2.1.1 Measurement Technique—Mapping Camera

Of first-order importance is characterization of surface features—their distribution, morphologies, and topography—at regional scales to understand the processes by which they formed. Galileo images demonstrate that regional-scale data (~100 m/pixel), is excellent for a geologic study of Europa; however, less than 10% of the surface was imaged at better than 250 m/pixel (Figure B.1.2-4). Near-global coverage (>80% of the surface) at 100 m/pixel would ensure characterization of landforms across the satellite.
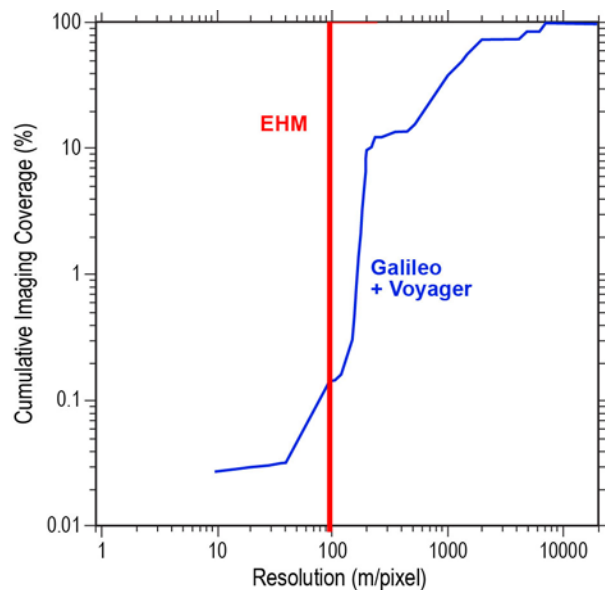
Figure B.1.2-4. Cumulative imaging coverage of Europa's surface as a function of imaging resolution, illustrating the improvement of planned EHM imaging coverage relative to that from Voyager and Galileo combined.

Topographic mapping through stereo images (and correlated with laser altimetry data) at a regional scale can permit construction of digital elevation models with vertical resolution of ~30 m and horizontal resolution of 300 m, which would greatly aid morphologic characterization and geological interpretation. Stereo imaging could be achieved through horizontal overlap of adjacent Mapping Camera image tracks, resulting in approximately 30-m vertical-height accuracy with 100 m/pixel wide-angle camera images.

The key outstanding questions relating to Europa geology can be addressed by the Objective G investigations described above are summarized in Table B.1.2-2.

B.1.3 Science Instrument Complement

B.1.3.1 Mission Goal Relation to Core Measurements and Instrumentation

The overarching goal of an orbiter mission is to determine the habitability of Europa. As such, the recommended scientific measurements and scientific payload follow objectives (§B.1.1) of examining the presence of liquid water (the occurrence and extent of a subsurface ocean) and the regional and global geologic history (stratigraphic history, geologic processes, and exchange of material between the subsurface ocean and the surface). In this way, the payload links tightly with the three science themes that relate to Water, Chemistry, and Energy. In particular to Europa, the presence of a subsurface ocean, the overall structure and thickness of the ice shell and the exchange of material between the subsurface (ice shell and ocean) and the surface layer over time, followed by the physical evolution of the surface, leads to a complex story of Europa

Table B.1.2-2. Hypothesis Tests to Address Selected Key Questions Regarding Europa's Geology.

	Example Hypothesis Questions	Example Hypothesis Tests
G.1	Do Europa's ridges, bands, chaos, and multi-ringed structures require the presence of near-surface liquid water to form?	Imaging to determine the style of surface deformation and the links to interior structure and water.
G.1	Where are the youngest regions on Europa and how old are they?	Stereo imaging to determine detailed stratigraphic relations on a global scale.

habitability. Unraveling this story requires an integrated package of instruments that work ideally and effectively in coordination. An orbiter mission offers unique abilities to observe the surface and unambiguously address the goal of understanding Europa's habitability.

The recommended science measurements and payload utilize the strengths of each archetypal instrument and technique to address key questions:

- What is the depth and salinity of the ocean, ice shell thickness and structure, and pathways by which ocean water may exchange with the surface?
- What are the geological signatures of surface-ocean exchange of materials and the surface history observed at scales of hundreds of meters?

B.1.3.2   Integration of Instrument Categories

Coordination and integration of observations and measurements acquired by different instruments is central to determining Europa's habitability. Spatially or temporally coordinated observations greatly enhance the scientific value of the mission. For example, obtaining clear insight into the internal structure of Europa requires various types of measurements working in concert. Probing the interior of Europa requires knowledge of the subsurface distribution of mass as manifested in variations of the gravity field. Combining this with time-dependent assessment of topographic due to tides and estimates of ocean salinity as derived from induced magnetization, a full picture of the ocean and ice shell is achieved. With this view in hand, global imaging provides a means to decipher the surface signature of interac-

tions between the icy crust and the watery interior. In this way the suite of instruments integrates to address the broader questions of habitability in a way that cannot be accomplished by each instrument alone.

B.1.3.3   Instrument Payload

The choice of instruments for the scientific payload is driven by the need for specific types of measurements that trace from the overarching goal of Europa's habitability, as detailed in the Europa orbiter traceability matrix (Fold-out B-1). These measurements focus on the geophysical characteristics of Europa's ocean and overlying ice shell along with the global-scale structure and stratigraphic history of exchange between the subsurface ocean and the observed surface. These fundamental measurements drive the recommendation of model instruments. These include active (such as topographic ranging) along with passive measurements (such as context imaging, magnetometry and gravity science). The notional payload (Table B.1.3-1) defined by the Science Definition Team (SDT) is the minimum required to achieve the required science objectives. Thus, it represents both the baseline and floor set of instruments. It was the SDT's judgment that more tolerable descopes would reflect a reduction in capability rather than the elimination of a specific instrument.

These model instruments work in concert to fully realize the value of data collected. For example, The Radio Subsystem (RS) would be used for gravity tracking of the spacecraft to determine gravity tides and the static field to probe the deep interior. Simultaneously, over a period of at least 5 Eurosols (18 days), the Laser Altimeter (LA) would determine surface

Table B.1.3-1. Scientific instruments of the model payload.

Model Instrument	Key Science Investigations and Measurements
Radio Subsystem (RS)	Gravitational tides and static gravity field to determine interior mass distribution to and characterize an interior ocean.
Laser Altimeter (LA)	Time-dependent topography as a function of Europa's position in its tidal cycle.
Magnetometer (MAG)	Magnetic measurements to derive ocean thickness and bulk salinity.
Langmuir Probe (LP)	Plasma correction for magnetic measurements
Mapping Camera (MC)	Formational mechanisms of surface features on regional to global scales

Table B.1.3-2. Potential enhanced instruments, not included in baseline model payload.

Model Instrument	Key Science Investigations and Measurements
Ion and Neutral Mass Spectrometer (INMS)	Atmospheric composition and chemistry through mass spectrometry.

elevations which, at crossover points, would be used to derive amplitude variations as a function of tidal cycle and the response to the ocean. Just as important as the LA and RS measurement, the Magnetometer (MAG) and Langmuir Probe (LP) would measure the time-variable induced magnetic field and plasma environment respectively so as to constrain the ocean salinity and hence the ice and water layer thicknesses. As the spacecraft makes successive orbits of Europa, the Mapping Camera (MC) would build up a global visual picture of Europa. Combining the image data with LA measurements, a three-dimensional view of geologic features, their stratigraphic relations and association with the deeper crustal processes can be achieved. The geophysical investigations achievable from an orbiter would fundamentally advance the state of knowledge and understanding of the habitability of Europa.

B.1.3.4 Europa Composition science from an Orbiter Mission

One additional instrument was considered by the SDT as potentially attractive to enhance the scientific return of a Europa Orbiter Mission by addressing composition science (Table B.1.3-2). However, this was not included in the baseline model payload because the Flyby Mission would be the more appropriate platform for the associated measurements. If an Orbiter Mission were chosen for Europa, then consideration of this valuable instrument might be made in considering the optimal payload for an Orbiter mission, to address a portion of the composition science.

The science of the Europa Flyby Mission (§C) includes investigation of the composition and chemistry of the surface and atmosphere. The potential inclusion of an Ion and Neutral Mass Spectrometer (INMS) on an Orbiter mission

would allow the first *in situ* assessment of the chemistry of material derived from the surface. Taken in concert with the ocean focused Orbiter measurements, inclusion of an INMS would provide insight into processes of interaction between the ocean, ice shell, and surface.

The sections that follow will provide details of the mission implementation approach and discuss the specific characteristic of each instrument.

B.2 Orbiter Mission Concept

B.2.1 Orbiter Study Scope and Driving Requirements

The purpose of the 2011 Europa Orbiter Mission study was to determine the existence of a feasible, cost effective, scientifically compelling mission concept. In order to be determined feasible, the mission had to have the following qualities:

- Accommodate the measurements and model payload elements delineated in the Science Traceability Matrix.
- Launch in the 2018-2024 timeframe w/ annual backup opportunities
- Use existing Atlas V 551 launch vehicle or smaller
- Utilize ASRGs. No limit on number, but strong desire to minimize ^{238}Pu usage
- Mission duration < 10 years, launch to EOM
- Use existing aerospace radiation hardened parts rated at 300 krad or less
- Optimize design for cost; looking for minimal cost while achieving baseline science
- Maintain robust technical margins to support cost commitment

The study team's strategy in investigating this concept was to develop a well-defined, well-documented architecture description early in the mission life cycle. From that architecture space, more compact design solutions were favored to reduce shielding and overall system mass. Hardware procurement, implementation, and integration were simplified by using a modular design. Mission operation costs were reduced by increasing system robustness and fault tolerance to allow for extended periods of minimally monitored operations during the long interplanetary cruise. Radiation dose at the part level was reduced to currently existing aerospace part tolerances. Specifically, the part total dose was reduced to levels demonstrated by geosynchronous and medium earth orbit satellites components.

Together, it was felt that each of these strategies contributes to an overall reduction in mission cost while maintaining a compelling, high reliability mission.

B.2.2   Orbiter Mission Concept Overview

The orbiter mission concept centers on deploying a highly capable, radiation tolerant spacecraft into orbit around the Jovian moon Europa to collect a global data set mapping the moon's surface morphology, measuring its tidal cycle through gravity fluctuations, and measuring its ocean induction signature through investigation of Europa's interaction with the Jovian magnetosphere. These measurements are performed from a 100 km, 2-4pm local solar time near-polar orbit over the course of a 30-day science mission.

A representative Orbiter mission would launch from Cape Canaveral Air Force Station in November 2021 and spend 6.5 years travelling in solar orbit to Jupiter. During this time, the mission would perform gravity assist flybys of first Venus then two flybys of Earth before swinging out to Jupiter. All terrestrial body flybys would have altitudes greater than 500 km.

Jupiter orbit insertion occurs in April 2028 when the vehicle performs a nearly 2-hour main engine burn to impart a 900 m/s velocity change on the spacecraft. This maneuver places the spacecraft in an initial 200 day Jovian orbit. An additional burn at apojove raises the perijove altitude and reduces the orbital period. The spacecraft then performs fifteen gravity assist flybys of Ganymede and Callisto over the course of eighteen months to reduce orbital energy and align the trajectory with Europa.

A 600 m/s Europa Orbit Insertion (EOI) burn places the spacecraft directly into a 100 km circular near-polar orbit. After a short checkout period, science observations begin. The spacecraft is oriented to point the high gain antenna (HGA) at Earth continuously during this time. A scan platform allows nadir pointing of the mapping camera and laser altimeter while maintaining HGA on earth-point. During the sunlit side of each orbit, the high resolution mapping camera collects 94 km wide swaths of imagery below the orbiter while the laser altimeter collects vertical topography data at 26 measurements per second throughout the orbit. Simultaneously, the magnetometer monitors changes in the local magnetic field as the spacecraft orbits Europa and Europa orbits Jupiter. Finally, maintaining continuous HGA-to-Earth pointing allows high precision radio science measurements of changes in Europa's gravitational field, a measurement expected to give significant insight into Europa's tidal amplitude and cycle.

The science measurement campaign would last a minimum of 30 days forming a statistically significant magnetic and gravitation data set for model correlation and allowing for at least eight opportunities to map any given location on Europa's surface. Extended mission objectives are possible and could be executed until critical spacecraft functionally is lost due to exposure to the intense radiation environment surrounding Europa. The spacecraft would be decommissioned by either commanding active

deorbit to the surface or by passive orbital decay due to third body gravitational perturbations.

B.2.3 Orbiter Mission Elements

The Orbiter mission would be composed of a flight system and a ground system. The ground system is responsible for planning, testing, transmitting and monitoring all command sequences executed by the flight system, monitoring the flight system's health, and planning and executing any anomaly recovery activities required to maintain system health and mission robustness.

The flight system is a modularly designed spacecraft composed of three main modules: Avionics, Propulsion, and Power Source.

The Avionics Module hosts the bulk of the flight system's powered elements including the computers, power conditioning and distribution electronics, radios, and mass memory. These units are housed in a vault structure that provides significant radiation shielding. The upper section of the Avionics Module is called the Upper Equipment Section and hosts the batteries, reaction wheels, and star trackers, as well as the payload elements.

The Propulsion Module supports the fuel, oxidizer, and pressurant tanks, as well as the pressurant control assembly and the propellant isolation assembly. Four thruster clusters supported by tripod booms at the base of the Propulsion Module each contain four 1-lb reaction control system thrusters and one 20-lb thrust vector control thruster. The main engine would be mounted to a baseplate suspended from the bottom of the Propulsion Module main structure.

The Power Source Module would be composed of a ring and four vibration isolation systems each supporting an Advanced Stirling Radioisotope Generator (ASRG). The control boxes for the ASRGs would be mounted directly to the Power Source Module's main ring structure.

B.2.4 Orbiter Mission Architecture Overview

Architecturally, the flight system's modular design offers several advantages and efficiencies. First, the Avionics Module is designed to place radiation sensitive components in a central vault structure. Centralization of sensitive components provides significant self-shielding benefits from passive spacecraft components that are then enhanced by the vault structure. Late in the integration flow, the Avionics Module is stacked onto the Propulsion Module. This configuration places the avionics vault structure in the core of the spacecraft; surrounded on all sides by the Propulsion Module's structure and propellant tanks. During the majority of the mission, these tanks would contain a significant amount of propellant. This configuration allows propellant to act as additional radiation shielding. In this way, dedicated, single purpose radiation shielding mass is minimized while still providing an internal vault radiation environment comparable to the doses received by geosynchronous satellites after a 20-year mission.

Additionally, the central vault avionics configuration allows waste heat from the avionics to be applied directly to keeping the propellant warm eliminating the need for dedicating significant electrical power to propellant tank heaters. There is sufficient heat emitted by the avionics to keep the propellant above 15 deg C for the life of the mission.

Finally, the modular design allows for a flexible procurement, integration, and testing strategy where each module is assembled and tested separately with schedule margin. Delays or problems on one module do not perturb the testing schedules of the other modules.

B.2.5 Science Instrumentation

A viable science instrument planning payload will provide the required science measurements, can be accommodated on the spacecraft, and can be implemented to operate successfully in the mission environment using only current technology.

B.2.5.1   Planning Payload

The Europa Orbiter planning payload, while notional, is used to quantify engineering aspects of the mission and spacecraft design and to define the operational scenarios required to obtain data necessary to meet the science objectives. For the purposes of this study, instruments were defined to demonstrate a viable approach to 1) meeting the measurement objectives, 2) performing in the radiation environment, and 3) meeting the planetary protection requirements. Therefore, instrument descriptions are provided here to show proof of concept. Heritage or similarities discussed refer to instrument techniques and basic design approaches. Physical and electrical modifications of previous heritage designs will be required for all instruments to function within the context of the mission requirements. These modifications are all judged feasible with current technology, and reasonable resource allocations are included in the mass and cost estimates. Instrument performance estimates assume only currently available detector technology. Developments costs have been included in the cost estimates, but their projected performance improvements have not been assumed in these performance calculations. Alternative instrument concepts and tech-

niques that meet the mission objectives might be selected via NASA's AO process. Such options can be accommodated in the present concept. The instrument capabilities presented here are not meant to prejudge AO solicitation outcome.

The model planning payload selected for the Europa Orbiter study consists of a notional set of remote sensing instruments, *in situ* instruments, and a telecommunications system that provides Doppler and range data for accurate orbit reconstruction in support of geophysical objectives. Instrument representatives on the SDT (or identified by SDT members) were utilized extensively to understand the requirements for each instrument. Table B.2.5-1 presents the estimated resource requirements for each instrument and for the total planning payload.

Table B.2.5-2 summarizes the instruments and their capabilities. A more detailed mass estimate for each instrument is included in the Master Equipment List (MEL, Section B.4.3) as input for the NASA Instrument Cost Model (NICM).

B.2.5.1.1   Payload Accommodation
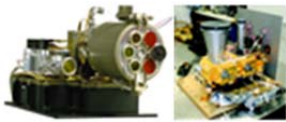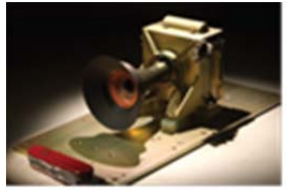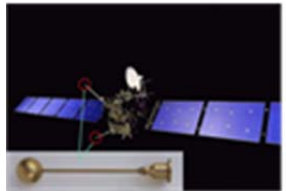
All remote-sensing instruments in the planning payload require view in the nadir direction

Table B.2.5-1. Europa Orbiter planning payload resource requirements and accommodations are met by the Europa Orbiter spacecraft.

Instrument	Un-shielded Mass (kg)	Shielding Mass (kg)	Total Mass (kg)	Operating Power (W)	Instantaneous Telemetry Bandwidth (kbps)	Telemetry Interface	Science Electronics Chassis Board Ct.	Field of View	Pointing
Laser Altimeter (LA)	5.5	4.7	10.2	15	2	SpaceWire	2	0.029° dia. spot	Nadir
Mapping Camera (MC)	2.5	1.5	4.0	6	126	SpaceWire	1	50° × 0.049°	Nadir
Magnetometer (MAG)	3.3	0.0	3.3	4	4	SpaceWire	1	N/A	
Langmuir Probe (LP)	2.7	0.0	2.7	2.3	2	SpaceWire	2	Omni Electrons: 4π	
Total All Instruments	**14.0**	**6.2**	**20.2**	**27.3**			**6**		

Note: Resource requirements for the transponder used for radio science are carried as part of the spacecraft telecommunications system (see Section B.2.7.6.1).

Table B.2.5-2. Capable science instruments draw on previous flight designs.

Instrument	Characteristics	Similar Instruments	
Laser Altimeter	**Time-of-Flight Laser Rangefinder** Transmitter: 1.064 µm laser Detector: Avalanche Photodiode Resolution: better than 1 m vertical Spatial: 50-m laser spot size, 26-Hz pulse rate	NEAR NLR MESSENGER MLA LRO LOLA	
Mapping Camera	**Pushbroom Imager** with fixed color filters and along-track stereo channel Detector: CMOS or CCD line arrays (5) Detector size: 1024 pixels wide Color bands: 560, 760, 950 nm Spatial resolution: 85 m from 100-km orbit FOV: 50° cross track; IFOV: 0.85 mrad	MRO MARCI Nozomi MIC MPL/MSL/MARDI MESSENGER MDIS New Horizons MVIC	
Magnetometer	**Dual 3-axis Fluxgate Magnetometer** Boom: 10 m Sensor location: 5 m and 10 m from S/C Dynamic range: 3000 nT Sensitivity: 0.1 nT Sampling resolution: 0.01 nT Maximum sampling rate: 32 Hz	MESSENGER MAG Galileo MAG	
Langmuir Probe	**Dual Langmuir Probe** Local plasma density, temperature, and flow Electric field vectors (near-DC to 3 MHz) Electron temperature Coverage: 4π steradian Booms: 1-m oriented 180° apart; at least one sensor always free of S/C wake	Rosetta LAP Cassini RPWS	

when in orbit around Europa, as shown in Figure B.2.5-1. Because the Orbiter spacecraft has adopted a fixed high-gain antenna (HGA) and the gravity science requires nearly continuous Doppler tracking with the HGA pointed to Earth, the remote sensing instruments are mounted on a two-axis gimbaled platform to permit continuous nadir viewing and cross-track orientation of the camera field of view (FOV). The LP requires a wide, unimpeded FOV and is located to minimize obstructions to that field of view. Instrument mounting and accommodation requirements are summarized in Table B.2.5-2.

The Europa Orbiter Mission design calls for a near-circular, high-inclination orbit around Europa with local time such that the HGA end of the spacecraft is pointed close to the Sun while keeping the gimbaled platform side oriented toward Europa. This geometry provides favorable viewing direction for thermal

radiators to dark space. The science payload is expected to contain instruments with detectors requiring cooling to as low as 170 K for proper operation while dissipating around 300 mW of heat. Cooling to this level can be accomplished via a passive radiator, mounted so that its view is directed away from the Sun and Europa at all times. Jupiter will move across the radiator FOV every 3.5 days, subtending a small portion of the radiator FOV but presenting only a minor transient perturbation to instrument thermal system performance.

The remote sensing instruments will require spacecraft pointing control to better than or equal to 2°, stability to 5 mrad/s, and reconstruction to 0.9 mrad. Pointing requirements are driven by the MC; however, these pointing requirements are less demanding than the HGA pointing requirements. To achieve the Europa geophysical science objectives connected with characterizing the topographic
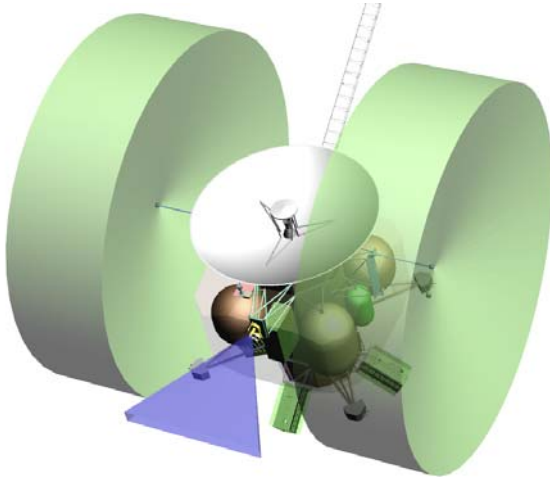
Figure B.2.5-1. The spacecraft configuration provides clear instrument FOVs.

Figure B.2.5-2. Instrument electronics are colocated for efficient radiation shielding.

tides, the Europa Orbiter orbit must be reconstructed to an accuracy of 1 m in the radial direction. To achieve this level of accuracy, Doppler radio tracking must be performed for several orbits(5~10 orbits), unperturbed by thruster firings.

The payload data rate is sufficiently low that an onboard science data storage volume of only about 2 Gb is needed to cover for the loss of a single DSN station pass. This volume is readily available on current generations of the RAD750 computer card without requiring an additional solid-state recorder. The notional planning payload block diagram (Figure B.2.5-2) assumes a data system architecture with SpaceWire interfaces baselined for all instruments.

The project will support the instrument AO process by providing NASA HQ with a Proposal Information Package (PIP) and any other advice as requested. To ensure compatibility between the selected instruments and the Orbiter flight system, the PIP is expected to specify a common instrument interface, provide an approved parts list, offer housing of instrument electronics in a centralized radiation-shielded vault, and require compatibility with Dry Heat Microbial Reduction (DHMR).

The instrument electronics are currently baselined to be accommodated with each instrument, shielded separately. However, the spacecraft concept accommodates an additional science chassis that can house all of the payload electronics, as well as perform some of the data reduction for IPR. This approach results in a conservative mass estimate, adding further margin in radiation shielding. Further trades need to be conducted on the benefits of a separate science chassis and its functionality. Since the presented model payload is notional, the payload trade will have to be re-evaluated once the flight instruments are selected.

B.2.5.1.2 *Radiation and Planetary Protection*

The severe radiation environment at Europa presents significant challenges for the science instruments, as does the need to meet the planetary protection requirements outlined in Section B.2.9.2. These challenges have been addressed by a notional payload architecture that efficiently implements radiation shielding and the use of radiation-hardened parts throughout the payload. A thorough study of both the radiation effects and the impact of planetary protection protocols on detectors was conducted for the 2008 JEO study by a Detector Working Group (DWG). The DWG developed a methodology for determining the required radiation

shielding for successful instrument operation in the severe transient radiation environment at Europa, assessed degradation of detectors due to total dose and displacement damage effects, and assessed the compatibility of candidate detectors with the planetary protection protocols. The DWG determined that there were no major issues associated with the types of detectors included in this planning payload.

Payload Architecture

The mission radiation design point is 1.56 Mrad behind 100 mils of aluminum shielding (Si) without a design margin, as shown in Section B.2.9.1. Note that energetic particle fluxes are high at Europa; therefore, sensors and supporting electronics require significant shielding. The most mass-efficient approach to providing radiation shielding is to centrally locate as much of the instrument electronics as possible, minimizing the electronics that must be co-located with the sensor portion of the instrument. The planning payload design presented here assumes instrument partitioning in this manner, as shown in Figure B.2.5-1**,** and includes a science electronics chassis implemented using the industry standard 6U Compact PCI form-factor. Space for six electronics boards is baselined, with radiation shielding sufficient to allow the use of components hardened to 300 krad without additional spot shielding. Internal partitioning of the science electronics is baselined to provide electrical isolation between instruments and to mitigate electromagnetic interference (EMI).

Detector Radiation Noise Methodology

The impact of radiation-induced transient noise on detectors was analyzed by estimating the number of high-energy electrons and protons penetrating the radiation shield and assessing their effect on the detector material. The flux of incident electrons reaching the detector for different radiation shielding thicknesses T can be estimating by applying the cutoff energy E determined from

$$E(\text{MeV}) = [T(\text{gm/cm}^2) + 0.106]/0.53$$

(Zombeck 1982) to the external integral electron flux. For 1 cm of Ta shielding, an estimated 4.3×10^5 electrons/cm^2·s and 50 protons/cm^2·s would reach the detector while in orbit at Europa. The predominance of electrons in the Jovian environment is the determining factor for the detector radiation shielding analysis presented in subsequent sections.

Detector Working Group

The DWG concluded that the radiation and planetary protection challenges facing the planning payload are well understood. The question of detector survivability and science data quality is not considered to be a significant risk provided appropriate shielding is allocated to reduce cumulative TID, DDD, and instantaneous electron and proton flux at the detector. The full DWG assessment report can be found under separate cover (Boldt et al. 2008). Specific activities to support early education of potential instrument providers regarding the complexity of meeting radiation and planetary protection requirements were identified, and a series of instrument workshops was completed as part of the JEO study effort.

Planetary Protection Protocols

The approach to planetary protection compliance for the Europa Orbiter Mission is presented in full in Section B.2.9.2 and can be summarized as follows:

- Prelaunch sterilization to control the bioburden for areas not sterilized in flight
- In-flight sterilization via radiation prior to Europa Orbit Insertion (EOI)

The preferred method of sterilization is DHMR. Our plan is to sterilize the entire spacecraft upon completion of the flight assembly. Current planetary protection protocols include a time vs. temperature profile ranging from 125°C for 5 hours to 110°C for 50 hours.

Early in the instrument selection process, the project will generate and disseminate planetary protection guidelines to potential instrument providers, thereby allowing these providers to adequately address planetary protection issues. A mid-Phase B Payload Planetary Protection Review is baselined so that issues and mitigation strategies can be identified and addressed. Instrument-specific planetary protection concerns will be addressed in subsequent sections.

B.2.5.2 Instrument Descriptions

B.2.5.2.1 *Laser Altimeter*

The notional Laser Altimeter (LA) is a diode-pumped Cr:Nd:YAG Q-switched laser transmitting at 1.064 μm with an optical receiver and time-of-flight (TOF) sensing electronics. The notional design employs elements of the Lunar Orbiter Laser Altimeter (LOLA), the Mercury Laser Altimeter (MLA), and the NEAR Laser Rangefinder (NLR). The LA baselined for the Europa Orbiter is tailored to satisfy the following science requirements, as identified in Section B.1:

- Topographic differences to 1-m vertical accuracy at globally distributed crossover points at varying Europa orbital phases.
- Better than or equal to 10-cm ranging accuracy (to allow for ~1-m spacecraft orbit determination accuracy).

Simultaneous ranging with stereo imagery is desired.

Instrument Description

The notional LA includes a 0.5-mrad beam expander to produce a single 50-m laser spot from the 100-km orbit. A pulse rate of 26 Hz provides contiguous spots and 50-m along-track resolution, assuming a 1300-m/s ground track rate from the 100-km orbit. With each orbit crossing every previous orbit twice, in the course of 30 days more than 500,000 points are available for crossover analysis.

The notional laser transmitter is based upon the "Heritage Laser" developed by the multi-year NASA Laser Risk Reduction Program (LRRP) (Seas et al. 2007) and shown in Figure B.2.5-3. The Heritage Laser design incorporates elements of the MLA and LOLA instruments and lessons learned from the LRRP effort itself. The baseline characteristics of the passively Q-switched, diode-pumped Cr:Nd:YAG laser allow up to 30-mJ, 6-ns pulses at rates of up to 150 Hz. For the Europa Orbiter, a nominal output of 2.7 mJ at 26 Hz is baselined, maintaining similarity to the LOLA laser transmitter. The Cr:Nd:YAG slab is assumed to be side pumped with a gallium arsenide (GaAs) diode array at 809 nm, similar to that used by NLR.

The notional optical receiver is based on a scaled version of the lightweight reflective telescope used by NLR and shown in Table B.2.5-2. The output of the telescope is passed through a spectral filter and presented to an avalanche photodiode (APD) operating in linear mode with gain of ~100 (per NLR) to minimize radiation effects.
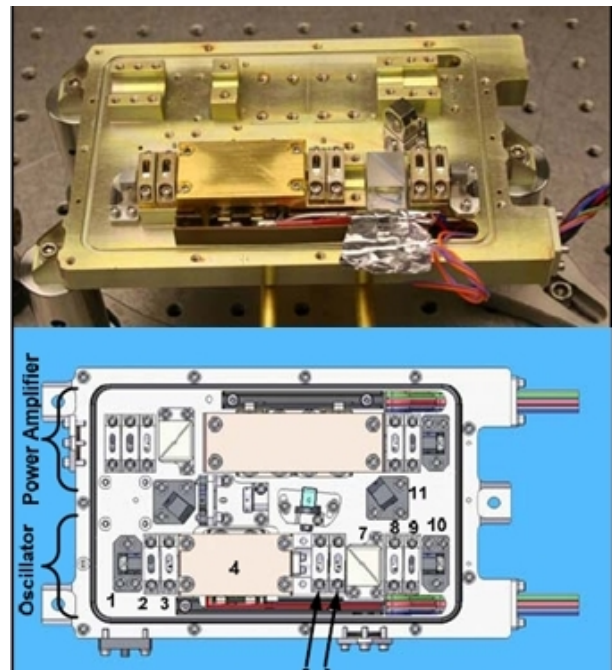
Figure B.2.5-3. The heritage laser developed by the NASA Laser Risk-Reduction Program is baselined for the notional Europa Orbiter Laser Altimeter.

Telescope sizing is obtained by comparison to the NLR link analysis, which assumes a 15-mJ transmitter, 8.9-cm-diameter receiver telescope with ~50-cm^2 unobscured collecting area, and 15% surface albedo. While initially designed for a 50-km range, NLR achieved a 95% probability of detection for a single shot at 160-km range using 15 mJ of transmit power (vs. the initially specified 5 mJ) (Cole et al. 1997). Scaling for lower transmit power (2.7 mJ is assumed per the LOLA transmitter), a range of 200 km, and a surface albedo of 67% at Europa, an unobscured collecting area of ~100 cm^2 is required for the notional LA. Assuming the same obscuration ratio as the NLR telescope, a 12.5-cm-diameter receiver telescope is baselined for Europa Orbiter. Comparisons to MLA and LOLA link analysis provided similar results.

The notional TOF system is a low-power design based on the range measurement system used by MLA, which employs a coarse counter (5 MHz) and precision timing offset measurements made using multiple radiation hardened TOF ASICs to achieve timing resolution equivalent to a 2-GHz counter (Cavanaugh et al. 2007). A commandable range gate masks system noise during laser firings and masks transient background radiation noise in the APD detector. The MLA range-measurement scheme can acquire and downlink multiple returns per shot, and this system can be

adapted to directly measure return pulse dilation to correct for topographically induced range-walk. The MLA range error budget (Cavanaugh et al. 2007) totals 1 m rms, with errors dominated by spacecraft orbit knowledge errors (0.75 m) and spacecraft pointing angle uncertainty (0.13 mrad). The expected performance of the Europa Orbiter spacecraft (≤1-m radial orbit knowledge with Ka-band and 0.25 mrad pointing uncertainty) allows the notional LA to meet the 1-m rms vertical-accuracy requirement.

A conceptual physical diagram of LA is shown in Figure B.2.5-4. The laser transmitter and optical receiver are located on the nadir-facing gimbaled platform of the spacecraft. The laser transmitter power supply, TOF system, system controller, and spacecraft interface electronics are packaged as two 6U cPCI boards and located in the science electronics chassis, which provides radiation shielding sufficient for components tolerant of 300 krad.

Radiation Effects and Shielding

The LA laser transmitter contains four main components requiring radiation shielding: GaAs laser diodes, a Cr:Nd:YAG laser slab, a LiNbO3 Q-switch, and the fiber optic pickoff that provides the start pulse to the TOF system. The significant radiation issue for GaAs laser diodes is proton displacement damage. Testing with 5.5-MeV protons to a level of 6×10^9 MeV/g, beyond the expected Europa
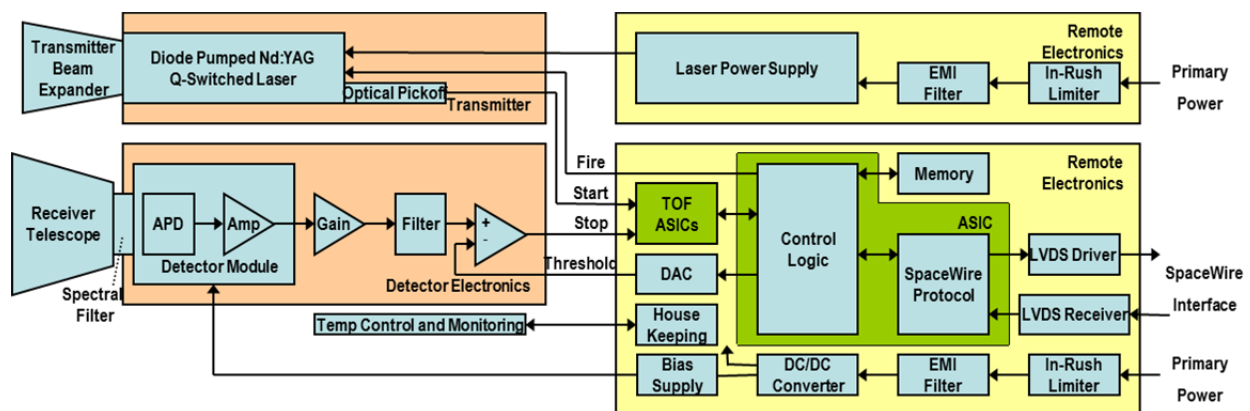
Figure B.2.5-4. The notional Laser Altimeter block diagram shows the remote electronics in a radiation-shielded enclosure.

Orbiter end-of-mission dose, showed only a minor shift in threshold current and no change in quantum efficiency (Johnston 2001). The significant radiation issue for Cr:Nd:YAG is total dose. Testing to 500 krad showed a negligible change in output power, with the level of Cr_3^+ doping a determining factor (Rose et al. 1995). Significant radiation issues for $LiNbO_3$ are total dose and displacement damage. Gamma irradiation of $LiNbO_3$ to levels far beyond that expected by Europa Orbiter showed a minimal change of insertion loss (Tsang and Radeka 1995). No corresponding data on displacement damage were reviewed for this study. The significant radiation issue for fiber optics is total dose. Testing observed only a 0.5 dB/m transmission loss in single-mode Ge-doped fiber optics after irradiation with 1×10^6 gray (Gy) (Henschel et al. 1995). While an exhaustive survey of radiation test results for the materials required for the LA laser transmitter is beyond the scope of this study, sufficient information has been reviewed and summarized in Boldt et al. (2008) to indicate the feasibility of operating a laser transmitter for the duration of the Europa Orbiter Mission. Based on this information, shielding of the LA laser transmitter to a level allowing use of materials tolerant of 400 krad is assumed.

The LA optical receiver uses an APD operating in linear mode to detect the return signal from the laser transmitter. Both silicon and germanium devices experience dark current increases due to total dose and proton damage and are susceptible to transient background radiation, which can create a signal larger than that produced by the optical return. The large detector area, typically 0.5 mm^2, results in a high probability of a transient radiation event during the period of the range gate, assumed to be 67 µs for this analysis, and corresponding to an altitude range of 10 km. With 1 cm of Ta shielding, an estimated 4.3×10^5 electrons/$cm^2 \cdot s$ and 50 protons/$cm^2 \cdot s$ reach the APD through the shield while in orbit at Europa.

With the notional detector area and range gate, an estimated 14% of laser firings will be corrupted by background radiation. Increasing the shielding to 3 cm of Ta reduces the estimate to ~1.5% of laser firings. This level of shielding reduces the total dose seen by the detector to 10 krad and requires a detector tolerant of 20 krad, assuming 2× design margin. At this level of dose, dark current increases are modest (Becker et al. 2003) and can be accommodated by electronic adjustments and detector cooling.

Resource Estimates

The mass estimate for the LA is based on NLR (5 kg), adjusted for receiver telescope size, the mass of LRRP Heritage Laser, and radiation shielding of the laser transmitter, APD detector and detector electronics. The LRRP Heritage Laser, implemented with an aluminum chassis, is ~1.1 kg, with ~300-mil chassis walls (equivalent to 0.125 cm Ta) and interior dimensions of ~13×9×2 cm. To allow components tolerant to 300 krad, 0.3 cm of Ta shielding is required. The additional 0.175 cm of Ta shielding for the LA laser transmitter is estimated at 0.94 kg. Shielding of the APD (a small device) with 3 cm of Ta is estimated at 2.96 kg. Shielding of the detector electronics (assumed to require an 8×8×2 cm interior volume) with 0.2 cm Ta (1-Mrad components) is estimated at 0.6 kg. Shielding of the fiber optic is allocated 0.2 kg, resulting in an overall mass estimate for the notional LA of 10.2 kg.

The power estimate for the LA is 15 W based on NLR and assumptions for simplification of LOLA from a five-spot, five-receiver system to a single-spot, single-receiver system. The telemetry rate is estimated at 2 kbps, which allows output of ~75 bits per shot. A 100% duty cycle is assumed in Europa orbit.

Planetary Protection

Planetary protection concerns can be met for the LA through dry heat microbial reduction. Temperature effects on the nonimaging reflective optics are not considered to be an issue.

Temperature effects on the laser transmitter materials themselves are not likely to be problematic, although maintaining alignment of the transmitter components over a wide temperature range will require careful design and a thorough test program.

B.2.5.2.2   Radio Science

The Europa Orbiter spacecraft telecommunications system includes redundant small deep-space transponders (SDSTs) that receive commands from Earth tracking stations at X-band and transmit data to Earth at Ka-band, a configuration used on the Deep Space 1 and Kepler projects. The SDST also supports X/Ka Doppler range and delta-differential one-way range (ΔDOR) for orbit determination. The SDST-based Doppler measurement accuracy is better than 0.1 mm/s for a 60-s integration time. Downlink tracking arcs free of spacecraft perturbations are required over several orbits, and range-rate measurements spanning several Europa tidal cycles are required. As discussed in Section B.1, simulations (Wu et al. 2001) show that these measurements can determine the radial component of the orbit about Europa to 1-m accuracy as well as allow determination of gravity and tidal parameters to useful accuracies. The approach to accommodation and radiation protection for the telecomm subsystem elements are addressed in Section B.2.7.6.1.

B.2.5.2.3   Mapping Camera

The MC consists of a wide-angle camera with basic functionality similar to that of the MRO Mars Color Imager (MARCI), the Nozomi Mars Imaging Camera (MIC), and MPL/MSL Mars Descent Imager (MARDI) instrument shown on Table B.2.5-2. The MC imager will be used in Europa orbit to provide global stereo landform mapping and to enable a search for evidence of surface/subsurface material exchange. The MC baselined for Europa Orbiter is tailored to satisfy the following science measurement requirements identified in Section B.1:

- Global stereo mapping:
  - Better than 100-m/pixel spatial resolution from a 100-km orbit.
  - 30-m vertical resolution at ≤300 m/pixel spatial scale.
  - Greater than 80% surface coverage.
- Color imaging:
  - Better than 100-m/pixel spatial resolution from a 100-km orbit.
  - Panchromatic plus three color bands.

Instrument Description

Collection of a global map with 100-m spatial resolution within 3 Eurosols (~35% of the nominal mission at Europa) requires an image swath width >80 km. This swath width results in a requirement for >800 pixels cross-track; a 1024-pixel-wide line array image sensor operating in pushbroom mode is baselined to allow for ample cross-track swath overlap for robust inter-swath tiepointing. The 1024-pixel-wide image sensor results in an instrument FOV of ~50° full angle. A compact wide-angle refractive telescope similar to that of the MARDI instrument and a detector configuration similar to that of the New Horizons Multispectral Visible Imaging Camera (MVIC) are baselined. The notional MC has a 0.85-mrad IFOV to produce an 85-m pixel footprint at nadir and 120-m cross-track pixel footprint at the edge of the swath from the 100-km orbit. The radiation-shielded focal plane, similar to that of the New Horizons MVIC shown in Figure B.2.5-5, is envisioned to include 5 separate line arrays: four nadir viewing (one panchromatic and 3 color bands) plus one offset to view ~40° forward or aft of nadir to enable near-simultaneous in-track stereo coverage. Vertical resolution provided by stereo imaging from the 100-km orbit is shown in Figure B.2.5-6. A digital elevation model (DEM) vertical resolution of 30-m is achieved at a stereo convergence angle of 40º. Fixed-color filters superimposed directly on the color line arrays satisfy the color imaging requirement with a minimum of complexity. The color and
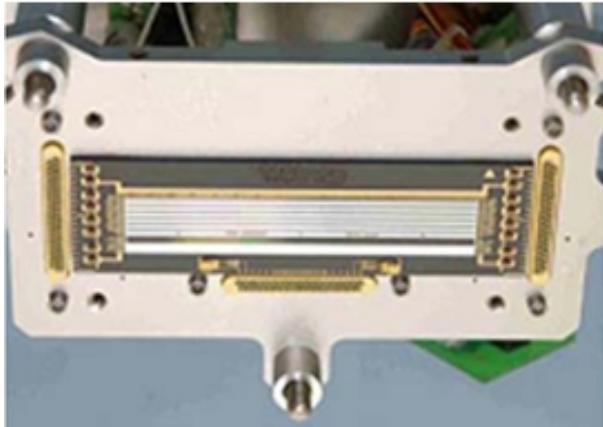
Figure B.2.5-5. The New Horizons MVIC detector, which contains multiple line arrays on a single substrate, is indicative of the notional MC detector.

stereo bands can be operated or not, as selected by ground command.

Preliminary MC performance analysis has been completed using the pixel characteristics (quantum efficiency, 13-μm pixel size, 100-Ke$^-$ well depth) of the e2v CCD47-20BT image sensor used by the New Horizons Long-Range Reconnaissance Imager (LORRI) instrument as *an example* of the performance expected from the MC image sensor. The measured LORRI system readout noise of 20 electrons was assumed, although the LORRI pixel readout rate is considerably higher than that required for the MC (1.2 MHz vs. 13.3 kHz). Nominal selections for the color filters are

- Band #1: 540-580 nm.
- Band #2: 730-790 nm.
- Band #3: 900-1000 nm.

The wavelength-dependent quantum efficiency of the CCD47-20BT (*example only*) indicates that the line arrays for Band #1 and Band #2 will receive ~1/10 of the illumination of the panchromatic channel, while the line array for Band #3 will receive ~1/20 of the illumination. To balance the exposure times between the panchromatic and color channels, a neutral density filter, nominally ND-1, can be assumed in lieu of independent exposure control for each line array element.
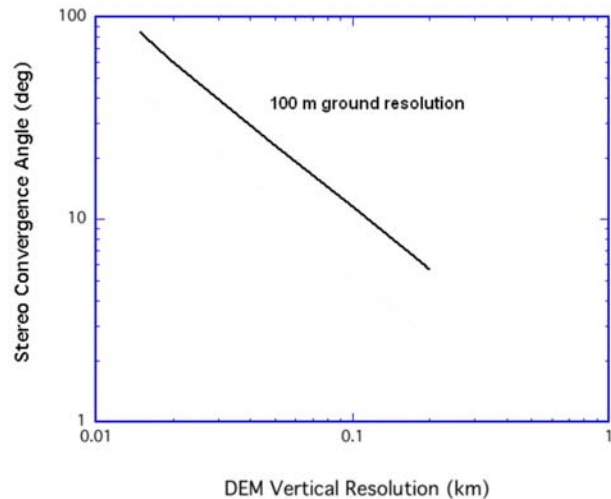
Figure B.2.5-6. The predicted MC vertical resolution obtained by stereo imagery based on parallax computations and use of modern auto-correlators will meet the science measurement requirements for surface topographic mapping.

Assuming a 15-mm focal length telescope with 3-mm aperture (*f*/5), an ND-1 filter on the panchromatic channel, an optical efficiency of 75%, and a surface reflectance of 30%, a 50-Ke$^-$ signal level is reached in ~25 ms, or ~40% of the 63-ms integration time available while moving one pixel along track. Barring radiation-induced transient noise, this exposure results in a very high SNR (>200) driven by photon noise rather than system noise and allows for longer exposure times over low-contrast surfaces. The performance of Band #1 and Band #2 will be similar to that of the panchromatic band with an ND-1 filter applied. The SNR of Band #3, which receives about half the light of the other bands, is ~160.

A conceptual physical block diagram of the MC is given in Figure B.2.5-7.

Consistent with the instrument architecture described in Section B.1.3.3, minimal electronics are packaged at the focal plane with the detector. The signal chain shown in the focal plane electronics contains elements required for a charge-coupled device (CCD) image sensor (clock drivers, correlated double sampler, A/D conversion) that either are unnecessary or are typically implemented within a
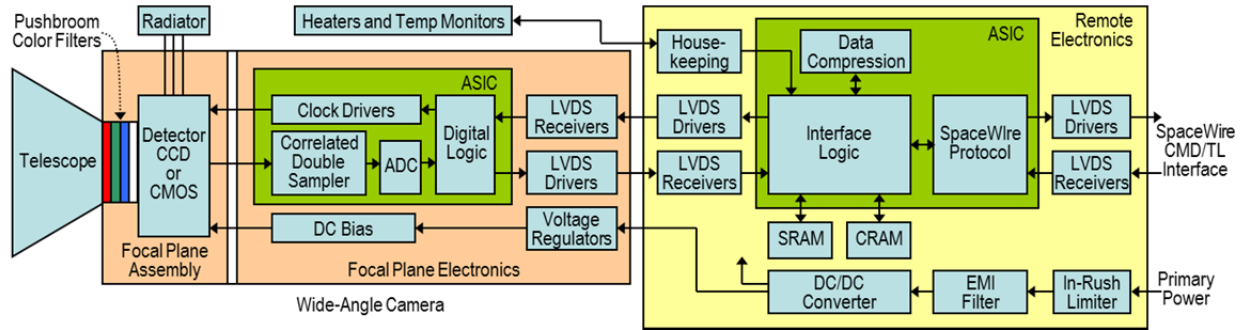
Figure B.2.5-7. Block diagram of the notional MC locates remote electronics in a radiation-shielded enclosure.

complementary metal-oxide semiconductor (CMOS) active pixel sensor (APS) device. A highly integrated CMOS APS device is an ideal solution, as it minimizes components at the focal plane that require radiation shielding.

A passive thermal design is baselined for the MC with an cold space facing radiator used for detector cooling.

The MC is baselined with one electronics board (6U cPCI format) housed remotely in the science electronics chassis. The board provides DC/DC power conversion for both the camera and the electronics board itself. Data compression is assumed to be wavelet based, with commandable degrees of compression. Radiation-hardened static RAM (currently available as 16-Mb devices) is included for buffering incoming imager data, data compression intermediate products, and incoming and outgoing SpaceWire command and telemetry data.

Radiation Effects and Shielding

To protect the MC image sensor from total dose, displacement damage, and transient radiation noise, radiation shielding with 1 cm of Ta, comparable to that used by the Galileo Solid-State Imager (SSI), is baselined. Radiation dose analysis indicates a ~35 krad total dose behind 1 cm of Ta shielding, which, assuming a required design margin of 2, allows use of detectors tolerant of 70 krad. While a CMOS APS device is favored for the notional Europa Orbiter MC due to its potential for high radiation tolerance, this dose level allows a choice of silicon device technologies, includ-

ing CMOS APS, P-channel CCD, and (arguably) N-channel CCD. Shielding mass of 1.5 kg is allocated for a 1-cm Ta, 5×3×4 cm enclosure similar to that shown in Figure B.2.5-8, which is designed to house a STAR1000-based CMOS APS and its interface electronics.

The impact of radiation background noise on the MC has been analyzed by estimating the number of high-energy electrons and protons penetrating the 1-cm Ta shield and assessing their effect on the silicon detector. An estimated 4.3×10^5 electrons/cm^2·s would reach the detector through 1 cm of Ta shielding. For a typical silicon image sensor, each incident electron can be expected to generate an average of 2000 signal electrons in the detector (per Boldt et al. 2008). Assuming 13-μm pixels and a maximum exposure time of 63 ms for the notional MC, a "hit rate" of 4.6% of pixels per integration time is expected in orbit at

Figure B.2.5-8. Ample radiation shielding encloses a miniature focal plane assembly for a STAR1000 CMOS APS.

Europa. With the assumption that the signal-electrons generated by the incident particles are concentrated on a single pixel, the method of calculating the SNR adopted for the Galileo SSI camera can be employed (Klaasen et al. 1984). Based on empirical data, the radiation-induced noise is approximated as 35×SQRT (mean radiation signal per pixel). For a 4.6% hit rate and 2000 electrons per hit, the radiation-induced noise would contribute 340 electrons to the MC SNR calculation if the radiation noise were uniformly distributed across the array. This would reduce the average MC SNR to ~120 (~70 for the 950-nm band). However, since >90% of the pixels would be unaffected by radiation-induced signal, they would retain their normal SNR value, while a small minority of pixels would have severely reduced SNR (~25), most of which can be repaired during ground processing. The number of incident protons reaching the detector through the 1 cm Ta shield can be estimated using the external integral 100-MeV flux level at Europa. The expected 50 protons/cm^2·s, when combined with 13-μm pixels and a maximum 63-ms exposure time, result in a hit rate of 0.0053% of pixels per integration time in orbit at Europa. While the proton is expected to cause a strong signal (~10,000 signal-electrons) in a pixel or pixel group at the impact site, the low number of occurrences, ~5 per 1-Mpixel image, and the strong signal are expected to have no significant impact on Europa science after ground-based post-processing to remove artifacts.

The MC electronics present no significant radiation concerns beyond those particular to the detector, and use of parts tolerant to 300 krad is assumed. Total dose and displacement damage effects on optical materials can be mitigated through use of a combination of fused silica and radiation-hardened glasses. In a system with a refractive telescope, the telescope itself acts as a "forward shield" for the image sensor, with the remainder of the image sensor surrounded by radiation shielding mate-rial. In a system with a reflective telescope, a folded off-axis design can act as a "baffle" for radiation shielding of the detector, enabling shielding of the image sensor from all radiation input angles.

Resource Estimates

Mass estimates for the MC (4 kg including 1.5 kg of radiation shielding) are derived from similarity to the camera subassemblies of the Mercury Dual Imaging System (MDIS) on the Mercury Surface, Space Environment, Geochemistry, and Ranging (MESSENGER) mission and from estimated values for the harness mass and the 6U cPCI electronics boards. Power estimates for WAC (6 W) are based on measured values of the MESSENGER MDIS camera subassemblies and New Horizons LORRI electronics.

For an orbital ground track speed of 1300 m/s in the 100-km orbit, the MC line period is 63 ms. Assuming 12 bits/pixel from each of the line arrays, the MC uncompressed data rate is 189 kbps per channel, and the compressed data rate (with compression factor of 3 assumed) is 63 kbps/channel or 126 kbps for simultaneous stereo.

Planetary Protection

Planetary protection concerns for the MC will be met through dry heat microbial reduction. Temperature effects on optical materials, optical mounts and the image sensor will be a key aspect of the component and material selection process.

B.2.5.2.4   Magnetometer

The notional Magnetometer (MAG) measures the magnetic field at Europa with sufficient sensitivity to resolve the induction signal generated in Europa's ocean as a response to Jupiter's magnetic field. Operation in Europa orbit for an extended period allows sounding at multiple frequencies to determine ocean thickness and conductivity. Performing a role similar to that of the Galileo MAG, the notional MAG is adapted from more recent designs,

such as the MESSENGER MAG, and from ongoing developments in ASIC design for highly integrated MAG electronics. The MAG baselined for Europa Orbiter is tailored to satisfy the following science requirements identified in Section B.1:

- Characterize the magnetic environment at Europa to determine the induction response from the ocean:
  - Measurement rate: 8 vectors/s.
  - Measurement sensitivity: better than 0.1 nT.

Instrument Description

The notional MAG contains two sensors located on a 10-m boom: one at the tip and the other at the halfway point. The dual-MAG configuration can quantify and separate the spacecraft field from the background field, thereby improving the overall sensitivity of the system. The dual sensors also provide a level of redundancy once inflight calibrations are performed to assess the spacecraft-generated magnetic field. The expected magnetic field range over the full Europa Orbiter Mission is 0–500 nT. To achieve the required sensitivity, a magnetic cleanliness program is required to limit the magnetic field of the spacecraft at the 10-m point of the boom to <0.25 nT, with variation of <0.05 nT. An analysis of the effect of using ASRGs as the spacecraft power source confirmed that this level of cleanliness could be achieved with a 10-m boom.

The notional MAG sensors use three orthogonally mounted ring-core fluxgate sensors and are based on the MESSENGER MAG sensor assembly shown in Figure B.2.5-1. The sensors are excited by an AC signal that is also used to synchronously detect the signals from the fluxgate sensors. In an analog fluxgate MAG, the output from each synchronous detector is applied to an integrator, which supplies the feedback current used to null the field seen by the sensor. The output of the integrator is directly proportional to the component of the magnetic field along each orthogonal axis

and is sampled by a high-bit-count A/D converter. In a digital fluxgate MAG, the output from each synchronous detector is applied to an integrator whose output is digitized by an A/D converter. All subsequent filtering is done in the digital domain, and feedback to null the field seen by the sensor is generated by a D/A converter.

Digital fluxgate MAGs capable of meeting the Europa Orbiter science requirements have been demonstrated (O'Brien et al. 2007), and substantial progress has been made in developing a MAG front-end ASIC (MFA) that incorporates a complete MAG signal chain, including synchronous detection, high-bit-count $\Sigma\Delta$ A/D converters, digital filtering, $\Sigma\Delta$ D/A converters for sensor feedback, and basic output data formatting into a single device (Valavanoglou et al. 2007). Although current versions of MFA do not meet all of the Europa Orbiter radiation requirements, with further development this technology is likely to be available for Europa Orbiter; consequently, this approach is baselined for the notional MAG instrument.

A conceptual physical block diagram of the notional MAG is shown in Figure B.2.5-9. A single 6U cPCI electronics board located in the science electronics chassis contains ASICs for MAG signal processing, spacecraft interface electronics, and a low-voltage power supply.

Fluxgate sensors suffer from small drifts in their zero levels that require periodic calibration. During the Cruise Phase, calibrations can be achieved using the rotational nature of the interplanetary magnetic field. Once inside Jupiter's magnetosphere, slow spacecraft spins around two orthogonal axes will be required every 2 to 4 weeks.
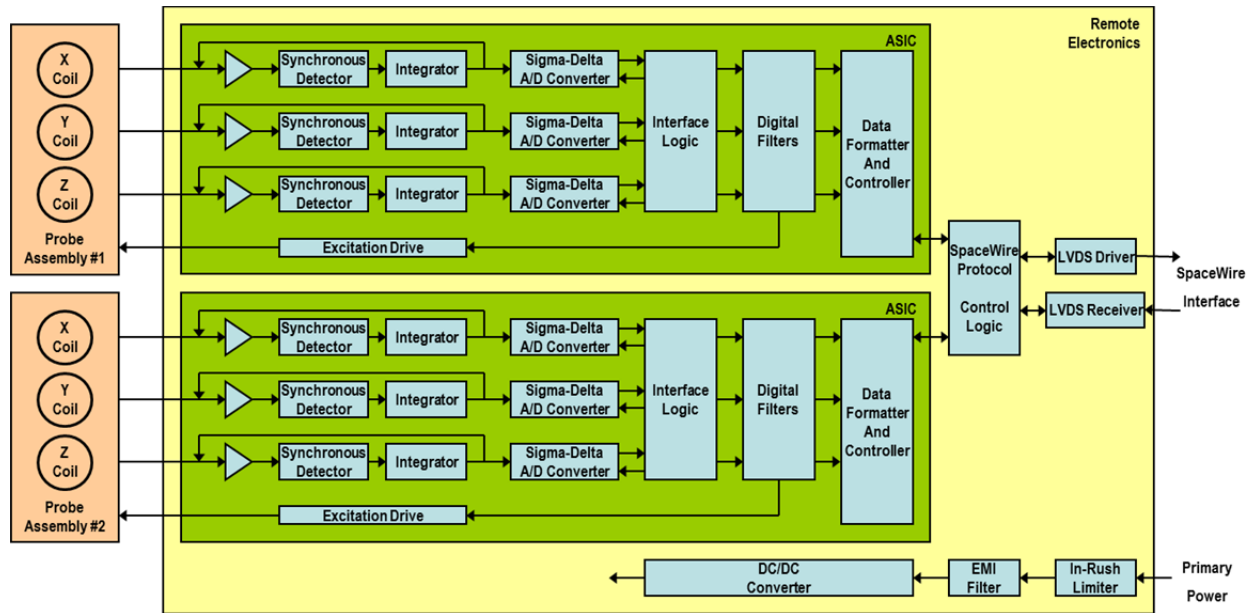
Figure B.2.5-9. Block diagram of the notional MAG locates remote electronics in a radiation-shielded enclosure.

Radiation Effects and Shielding

Fluxgate MAG sensors contain no active electrical parts and, with proper selection of materials, present no issues in meeting the Europa Orbiter radiation requirements. The notional MAG electronics are located in the science electronics chassis, which provides radiation shielding sufficient for components hardened to 300 krad. A fully radiation-hardened MAG signal-chain ASIC similar to the current MFA is assumed for the notional Europa Orbiter MAG.

Resource Estimates

The mass estimate for the notional MAG is based on the as-built mass of the MESSENGER MAG sensor (250 g), the as-built mass per unit length of the MESSENGER MAG harness (113 g/m), and the estimated mass of a 6U cPCI board. The total mass estimate for MAG is 3.3 kg, slightly more than half of which is required by harnessing. The estimated 19.2 kg mass of the supporting boom and deployment structure is not included in this instrument mass estimate, but rather included in the engineering structures mass rollup. See section B.4.3 for the Master Equipment List.

MAG power dissipation is estimated at 4 W based on scaling measured performance of the MESSENGER MAG for two probes. The MAG telemetry rate is estimated at 4 kbps based on scaling of the MESSENGER MAG telemetry rate for a higher sampling rate (32 Hz max) and two sensors.

Planetary Protection

Planetary protection concerns for MAG will be met through dry heat microbial reduction. With proper selection of materials for the MAG sensor, no issues are expected.

B.2.5.2.5   Langmuir Probe

The notional dual Langmuir probe (LP) instrument will characterize the local plasma and electric field in order to support the MAG determination of Europa's magnetic induction response. The LP will satisfy the following science measurement requirements identified in Section B.1:

- Electron number density (N_e) up to 10^6 cm^{-3}, sampled at frequencies from 0 (dc) to 20 kHz.
- Ion density up to 10^6 cm^{-3} for sampling frequencies up to 1 Hz.

- Electron temperatures (T_e) in the range of 0.01 to a few eV for sampling frequencies up to 1 Hz.
- Ion drift speed (v_{di}) in the range 1-200 km/s, depending on density, for sampling frequencies up to 1 Hz.
- Electric field component (1 Hz to 3 MHz).
- The differential electric field between the two probes.
- The spacecraft potential over a range of ±100 V for sampling frequencies up to 1 kHz.

Coverage will extend over a full 4π steradian field. No DC field measurements are possible, as the probes would be too close the spacecraft body and photo-electrons would interfere. A similar LP concept is described in Wahlund et al. (2005) for the Jupiter Icy Moons Orbiter study.

Instrument Description

The notional LP sensors are 5-cm-diameter spheres mounted on 1-m long booms (see Figure B.2.5-10). Since the plasma densities in Europa orbit are assumed to be large (>10 cm^{-3}), 1-m long low-mass sticks can be used for the booms. The notional LP is similar to the probes flown on Rosetta and as part of the Cassini RPWS instrument. The LP booms will be stowed for launch and deployed once in space. The LP preamps must be located within ≤3 m of the sensors. This constraint can be met
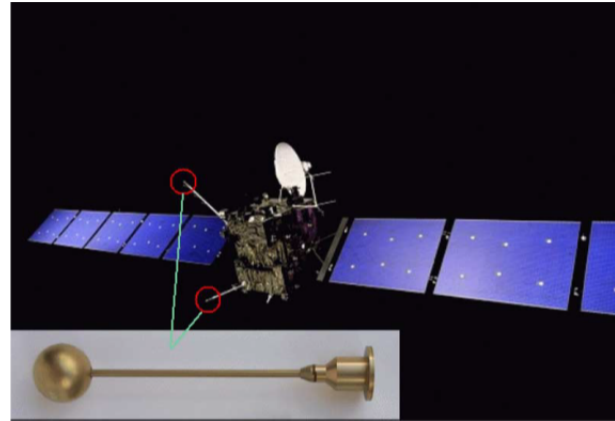
Figure B.2.5-10. The dual Langmuir Probe instrument on board Rosetta. A similar setup is considered for the Europa Orbiter.

while housing the preamps with the rest of the LP electronics in the shielded science electronics vault. Dedicated DC/DC conversion is needed, as well as a DPU. In addition, the LP needs bias control and an analyzer board. Two 6U cards will hold the expected electronics. A conceptual physical diagram of the notional LP is shown in Figure B.2.5-11.

Radiation Effects and Shielding

A rad-hardened MEMS wafer-level-packaging miniaturized preamplifier (as is currently under development at the Swedish Institute of Space Physics, Uppsala) is envisioned to be housed in the remote shielded vault with the rest of the electronics. All other parts required are rad-hard to ≥100 krad.
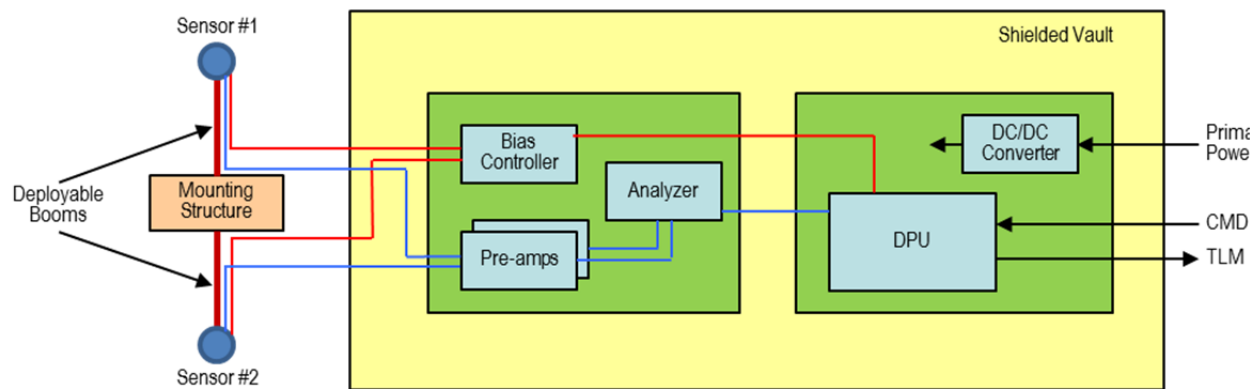
Figure B.2.5-11. Block diagram of the notional LP locates remote electronics in a radiation-shielded enclosure.

Resource Estimates

The estimated LP mass is approximately 2.7 kg. Power consumption is 2.3 W. Telemetry can be varied between 100 bps and several kbps according to availability; 2 kbps is baselined. The preferred mounting would have the first probe located roughly in the ram direction and the second probe at least 90° away from ram. This objective is met by orienting the two booms 180° apart and mounting them on structures that place the deployed sensors far enough out from the spacecraft that a minimum of 15° clearance from the spacecraft structure wake (plasma relative velocity vector) is provided to at least one sensor for all orbital geometries (see Figure B.2.5-1). Spacecraft EMI/EMC cleanliness will be required at levels comparable to those of Rosetta and/or Cassini.

Planetary Protection

The LP can tolerate the EHM dry-heat microbial reduction plan.

B.2.6   Mission Design

A robust mission design is presented, offering healthy margins to accomplish the high-value scientific observations that are best made from orbit around Europa.

The trajectory design goal for this Europa Orbiter Mission study was to show the feasibility of a Europa Orbiter mission that meets the SDT on-orbit observation and measurement requirements as outlined in the traceability matrix (Foldout B-1). The focus for this study was to deliver sufficient mass into orbit around Europa to accommodate the necessary science instruments while minimizing flight time and total ionizing dose[1] (TID).

The Europa Orbiter Mission flight system assumes a launch on an Atlas V 551 from Cape Canaveral Air Force Station on a Venus-Earth-Earth gravity assist (VEEGA) interplan-

---

[1] Total ionizing dose Si behind a 100-mil Al, spherical shell.

etary trajectory. After a cruise of 6.37 years, the spacecraft would fly by Ganymede just prior to performing Jupiter Orbit Insertion (JOI) via a large main engine maneuver. The spacecraft would then perform additional Ganymede, Callisto and Europa flybys over about 1.5 years to lower its energy with respect to Europa, at which point a relatively low-ΔV Europa Orbit Insertion (EOI) burn is performed. EOI places the spacecraft into a near-polar, near-circular 100-km altitude orbit, where science operations will be conducted for 30 days. The orbit maintenance ΔV of 5 m/s per month is small enough that the spacecraft could remain in orbit for several more months while in good health. Planned end-of-mission is impact on Europa's surface, which occurs due to natural orbit decay over one to two months, or which could be commanded, if impact in a particular region is desired. Foldout B-2 depicts a summary of the mission design.

For discussion of data acquisition scenarios, data return strategies, and communication strategies, see Section B.2.7.7.3.

B.2.6.1   Mission Overview and Phase Definitions

The general descriptions of each mission phase and the related activities are summarized in Table B.2.6-1.

B.2.6.2   Launch Vehicle and Launch Period

In the baseline mission design used for study purposes, Atlas V 551 would launch the spacecraft with a maximum C_3 of 15.0 km^2/s^2 during a 21-day launch period opening on November 15, 2021. The optimal launch date within the launch period is November 21, 2021 (Figure B.2.6-1). The date of Jupiter arrival is held fixed throughout the launch period, incurring only a negligible penalty while simplifying the design of the tour in the Jovian system. The launch vehicle and launch period parameters are shown on Foldout B-2. The launch vehicle performance is taken as that specified in the NASA Launch Services (NLS)-II Con-

Table B.2.6-1. Mission phase definitions and descriptions.

Phase	Subphase	Activity	Start–End
Interplanetary	Launch and Early Operations	Begins with the launch countdown, launch, initial acquisition by the DSN, checkout and deployment of all major flight-system subsystems, and a moderate maneuver to clean up trajectory errors from launch vehicle injection.	Nov./Dec. 2021 + 30 days
	Cruise	Science instrument calibrations, Venus and Earth gravity-assist flyby operations, annual spacecraft health checks, trajectory correction maneuvers, and operations readiness tests (ORTs).	Jan. 2021–Oct. 2027
	Jupiter Approach and JOI	Training, and ORTs for all mission elements in preparation for JOI and Jovian tour. This phase includes the Ganymede (G0) flyby ~12 hours before JOI and ends with completion of JOI which puts the spacecraft into a ~200-day orbit.	Oct. 2027–Apr. 2028
Jovian tour	PJR	Perijove Raise Maneuver near apoapsis of the first Jovian orbit counteracts solar gravitational perturbations and targets Ganymede for the first flyby of the tour.	Apr-2028–Jul. 2029
	Pumpdown	Series of Ganymede, Callisto and Europa flybys to reduce orbital energy around Jupiter, reduce v-infinity at Europa, and obtain the phasing necessary to achieve the desired plane for the orbit around Europa.	
	Endgame and EOI	Two consecutive Europa flybys. The first puts the spacecraft first on a 4:3 resonant return to Europa, and the second in a 6:5 resonant return for EOI. A v-infinity leveraging maneuver is performed on each resonant transfer to reduce v-infinity at Europa for EOI. In the final approach to Europa, multi-body effects are exploited to reduce the EOI maneuver further still.	
Europa Orbit		Science observations and orbital operations. EOI puts the spacecraft in a ~100-km circular, polar orbit with ~2-hr period. The sun-beta angle is 70 deg. Groundtrack has a 3-eurosol repeat. Orbit maintenance maneuvers every 3.5 days or longer.	Jul. 2029 (1 month)
Spacecraft Disposal		Europa impact due to natural orbital eccentricity growth from Jupiter perturbations: the period remains stable, causing the periapsis to drop.	Aug.-Sep. 2029

tract, which includes, in particular, a performance degradation of 15.2 kg/yr for launches occurring after 2015. The spacecraft propellant tanks are oversized enough to permit them to be loaded up to the launch vehicle capability. The flight system is designed to launch on any given day in the launch period without reconfiguration or modification.

B.2.6.3   Interplanetary Trajectory

The baseline trajectory used for the Europa Orbiter Mission is a VEEGA (Foldout B-2 and Table B.2.6-2). Cruise navigation would use Doppler and range observations from the Deep Space Network (DSN). The deep-space maneuver (DSM) ΔV required on the optimal day of the launch period is zero, but is about 80 m/s at the start of the launch period and
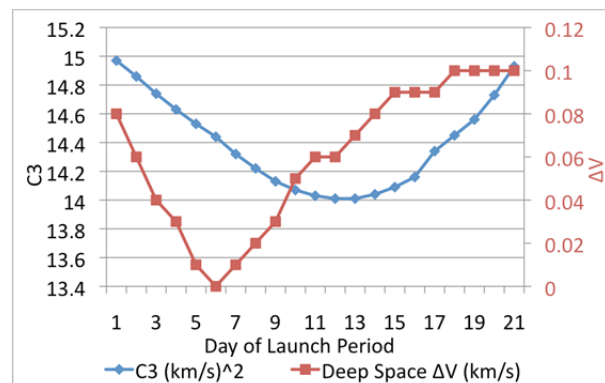
Figure B.2.6-1. Baseline interplanetary launch period

reaches its highest level of 100 m/s on the last day. The DSM occurs on the Earth-Venus leg of the trajectory. The interplanetary trajectory design would comply with all required National Environmental Policy Act (NEPA) assess-

Europa Orbiter Mission Design: Low-ΔV and Low-Radiation Mission to Explore Europa and Investigate its Habitability from Low-Altitude Orbit

A) Interplanetary Phase: VEEGA Trajectory (6.37 years)

VGA
(5/14/22)

EGA-1
(10/24/23)

EGA-2
(10/24/25)

Launch
(11/21/21)

JOI
(4/4/28)

Jupiter's
Orbit

B) Pre-JOI Ganymede Flyby
(Reduces JOI ΔV by ~400 m/s)

Ganymede
Gravity Assist
(500-km altitude)

JOI
(1-hr burn)

Sun

Satellite positions plotted at
time of Ganymede gravity assist

C) Tour Phase (1.3 years)
Energy reduction from large, ~200-day initial orbit

Sun

PJR

D) EOI
Short burn arc, minimal gravity losses

Thrust

Number of accesses is between 1 and 4
after a repeat cycle (11 days)

Jupiter occultation gap
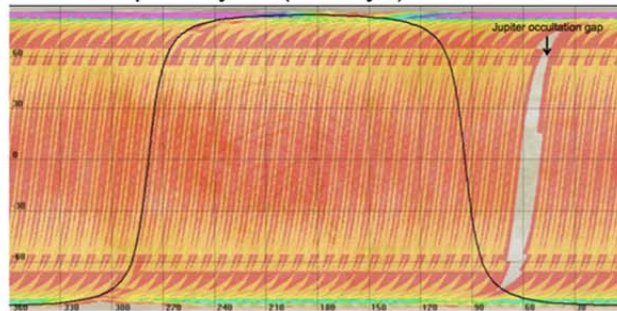
Ground tracks after a repeat cycle (11 days)
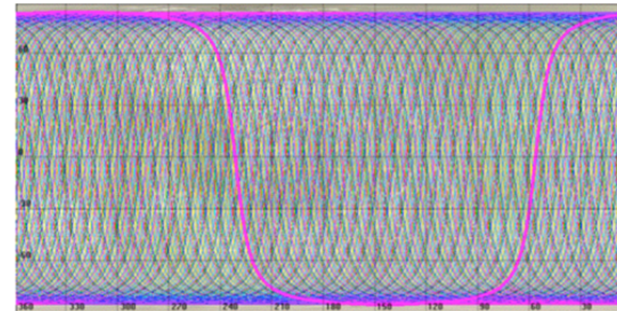
Ground tracks after one repeat
cycle (11 days)

Launch	VGA	EGA-1	EGA-2	JOI	EOI	End of Prime Mission

INTERPLANETARY					JOVIAN TOUR	
2021	2022	2023	2024	2025	2028	2029

Disposal
or extended
mission

Key Parameters	Value
Launch Vehicle	Atlas V 551
Earth to Jupiter Trajectory	VEEGA
Earth Launch Period	11/15/21 to 12/05/21
C3 (Max), R.A., Dec.	15 km²/s², 334.5°, 11.7°
Jupiter Arrival Date	4/3/2028
Jupiter Arrival V-infinity	5.6 km/s (maximum)
JOI Earth Range	4.52 AU
JOI Periapsis Range	12.8 R_j
Jupiter Capture Orbit Period	206 days
Tour	4/4/28–8/12/29 (1.3 yrs.)
EOI	8/12/29
Primary Europa Science	8/12/29-9/12/29
Average Orbit Altitude, Inclination, Period	100 km, 95°, 126 min
Initial Orbit Node	4 p.m.
End of Mission	Europa Impact >10/12/29

Range to Jupiter (R_j)

Callisto

Ganymede

Europa Orbit

TID Si behind 100 mil Al (krad)

Days past JOI
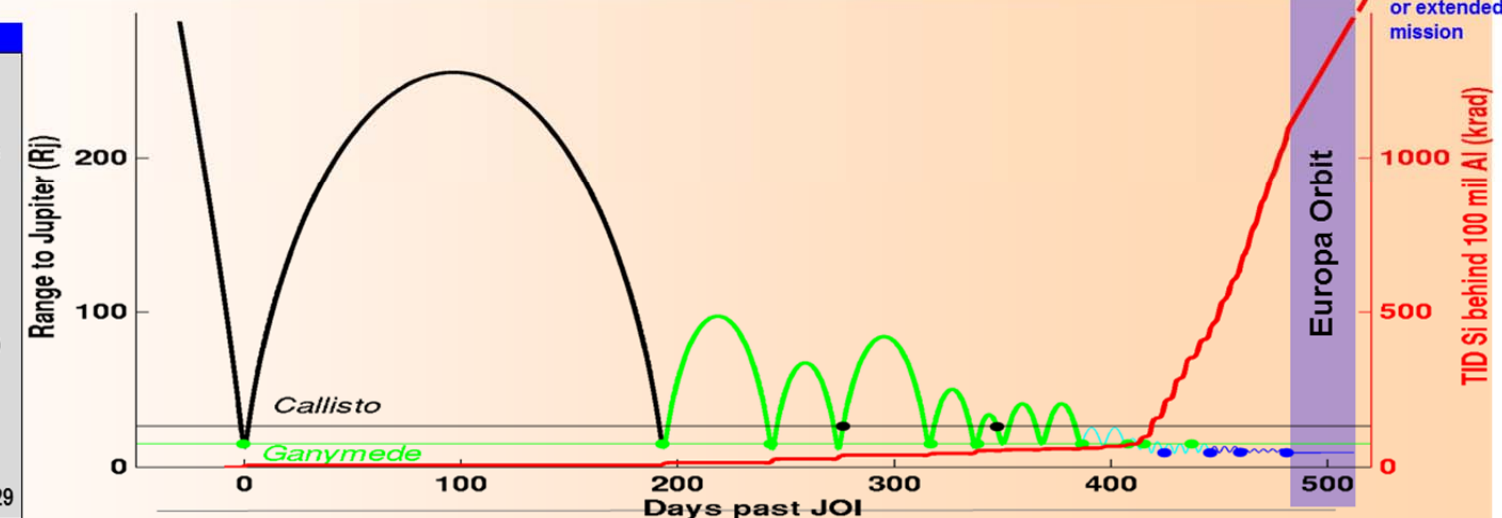
ment and safety analysis (see Section B.2.9.3). An aim-point-biasing strategy would be used for the Earth flybys. The nominal flyby altitudes of Venus and Earth do not vary significantly over the launch period and are relatively high, as seen in Table B.2.6-2. For comparison, Cassini flew by Earth at an altitude of 1166 km, and Galileo at altitudes of 960 and 304 km.

A 500-km flyby would be performed at Ganymede about 12 hours before JOI, thereby saving about 400 m/s of ΔV (compared to the case of no Ganymede flyby). The JOI maneuver lasts about 1 hour and occurs at perijove at a range of 12.8 Rj, which is in the less intense, outer regions of the radiation belts. Gravity losses are negligible due to the small angle subtended by the burn-arc.

B.2.6.4　Backup Interplanetary Trajectories

Besides the baseline trajectory described above, many trajectory options are available, offering at least one launch opportunity every calendar year through 2024. The results of a comprehensive search of all 1-, 2-, 3-, and 4-gravity-assist trajectories are shown in Figure B.2.6-2. The best candidates from the search are shown in Table B.2.6-3, which includes launch period effects. The table shows, for each trajectory, the optimal launch date of the launch period, the flight time to Jupiter, the expected maximum C_3 over the launch period, the launch vehicle capability at maximum C_3 for the indicated launch year

(NLS-II contract), the propellant required for flying the mission (assuming the full launch vehicle capability is used), the maximum dry mass (i.e., the difference between the two preceding numbers), and the propellant required to fly the mission assuming the CBE value for the dry mass. In all cases, the CBE ΔV from Table B.2.6-7 is used.

It is worth noting that two types of commonly considered trajectories do not appear in the short list of Europa Orbiter Mission trajectories because of their relatively poor mass performance. The first type is the ΔV-Earth gravity assist (ΔV-EGA), which is a V_∞ leveraging type of trajectory involving a large maneuver near aphelion before the first Earth flyby). For the ΔV-EGA, the maximum dry mass that can be delivered in the years 2019–2027 is about 1360 kg (about 800 kg less than the "Max Dry Mass" numbers in the short list, Table B.2.6-3). The required C_3 is in the range 25–30 km^2/s^2, and the flight time is typically 4–5 years, corresponding to a 2:1 ΔV-EGA (4.5 years for the maximum-dry-mass case).

Table B.2.6-2. Baseline VEEGA interplanetary trajectory (for optimal launch date).

Event	Date	V_∞ or ΔV (km/s)	Flyby Alt. (km)
Launch	21 Nov 2021	3.77	-
Venus	14 May 2022	6.62	3184
Earth	24 Oct 2023	12.07	11764
Earth	20 Oct 2025	12.05	3336
G0	03 Apr 2028	7.37	500
JOI	04 Apr 2028	0.858	12.8 Rj

Table B.2.6-3. Short list of interplanetary trajectories, including launch period effects. Baseline trajectory is in bold; other listed trajectories represent viable backup opportunities.

Launch Date	Flyby Path	TOF to JOI (yrs.)	C_3 (km^2/s^2)	Atlas V 551 Capability (kg)	Max MEV Prop Mass (kg)	Max Dry Mass (kg)	Prop for CBE Dry Mass (kg)
25 Mar 2020	VEE	6.03	15.6	4456	2247	2209	1373
27 May 2021	VEE	6.87	14.5	4541	2424	2117	1546
21 Nov 2021	**VEE**	**6.37**	**15.0**	**4494**	**2303**	**2191**	**1419**
15 May 2022	EVEE	7.22	10.2	4935	2696	2239	1626
23 May 2023	VEE	6.18	16.4	4339	2272	2067	1484
03 Sep 2024	VEE	6.71	13.8	4562	2477	2085	1604
01 Aug 2026	VEE	6.94	10.0	4893	2632	2261	1571
21 Jul 2026	VEE	6.15	15.2	4400	2311	2089	1493
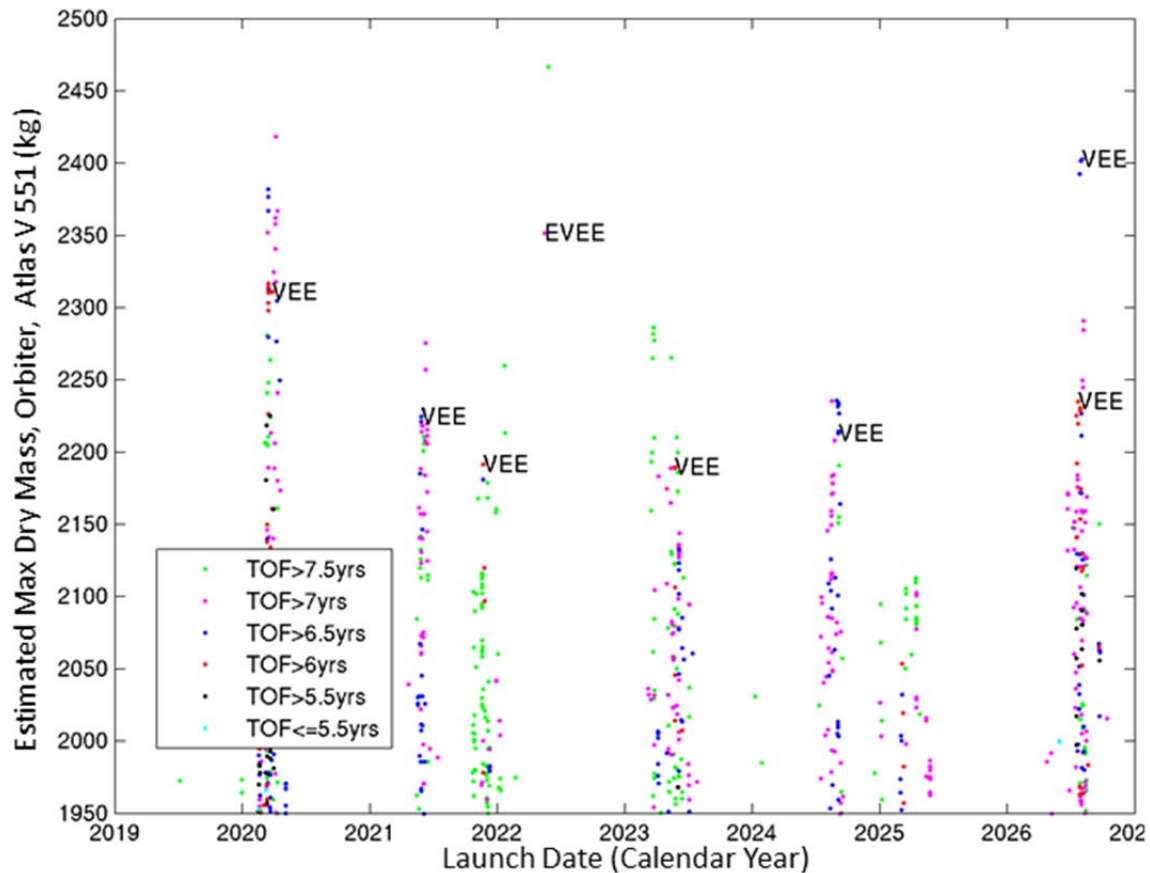
Figure B.2.6-2. Interplanetary trajectory options.

The second type is the Venus-Earth Gravity Assist (VEGA), involving a large maneuver after the Venus flyby. For flight times of around 4.4 yrs, the maximum dry mass for the VEGA is about 1440 kg. For flight times around 5.4 yrs, approaching the VEEGA flight times, the maximum dry mass becomes about 1810 kg. Thus, these two trajectory types significantly underperform in terms of delivered mass compared to the typical VEEGA trajectory. To save some flight time, these trajectory types may be considered in later phases of the mission design, once the vehicle mass is better characterized, assuming it does not grow significantly from current levels.

B.2.6.5   Jovian Tour

The three outer Galilean satellites are exploited as gravity-assist bodies to reduce greatly the ΔV required for Europa Orbit Insertion. Adding Io gravity assists would reduce the

mission ΔV still further, but would involve higher radiation dose and longer flight times. Although the net mass trade between propellant mass and shielding mass would favor using Io gravity assists, the system mass margin was already high enough to make the addition of Io unwarranted. Conversely, shortening the tour will typically add ΔV and reduce flight times and radiation dose. The approximate trade-offs are summarized in Table B.2.6-4.

In this design, we assume a tour analogous to the 99-35 tour that has been designed in previous studies [Johannesen & D'Amario 1999]. Tour 99-35 starts with a 200-day orbit post-JOI. On this first Jovian orbit, a perijove raise maneuver (PJR) is performed near apoapsis to counteract perturbations from the Sun's gravity and to target G1, the first flyby of the tour. To keep radiation exposure low, perijove

Table B.2.6-4. Trade-offs between Flight-time, deterministic ΔV, and TID (Si behind 100 mil Al, spherical shell) for various types of tours as compared to the concept baseline tour

Flight Time (delta yrs)	ΔV (delta km/s)	TID (delta Mrad)	Type of Tour
		JOI-to-EOI, inclusive	
0	> 5.5	~0	No tour, direct insertion to Europa Orbit from interplanetary trajectory
0.25	4	~0	Callisto gravity assists and v-infinity leveraging
0.5	3	~0	Further Callisto gravity assists and v-infinity leveraging
1	2.5	0.1–0.5	Callisto and Ganymede gravity assists (no endgame)
1.5	1.5	0.8–1.2	Callisto, Ganymede, and Europa gravity assists (4:3, 6:5 endgame)
2.5	1.3	1.7	Callisto, Ganymede, Europa and Io gravity assists

ranges are kept high while the orbital period is reduced through Ganymede and Callisto flybys, as shown in the Tisserand Plot in Foldout B-2. By the time of the first Europa flyby, the period has been reduced substantially to about 5.5 days, giving a relatively low v-infinity at Europa. After four phasing orbits and a further Ganymede flyby, a second Europa flyby is performed, which marks the beginning of the tour endgame, whose purpose is to reduce the v-infinity (and hence EOI ΔV) even further. The first part of the endgame is a 4:3 resonance with Europa (approximately 4 Europa revolutions while the spacecraft does 3), followed by a Europa flyby that puts the spacecraft on a 6:5 resonance. On each of the resonances, a small leveraging maneuver is done near an apoapse to reduce the v-infinity at Europa. On the final approach to EOI, multi-body gravitational effects (from Jupiter and Europa) are exploited to give a final, substantial reduction to the EOI ΔV. The tour events and EOI are shown in Table B.2.6-5.

The 1.1 Mrad radiation exposure in tour 99-35 is taken as a design point for this study, although it is foreseen that approximately 300 krad can be eliminated without impacting the mission ΔV by shifting the phasing orbits to

Table B.2.6-5. Flybys of representative tour 99-35, which has a multi-body, v-infinity-leveraging endgame to reduce EOI. Maneuvers are impulsive.

Event		Days to EOI	Altitude (km)	ΔV or V_∞ (km/s)
Ganymede	1	289.18	100	6.15
Ganymede	2	239.12	2243	6.22
Callisto	3	205.55	1117	6.40
Ganymede	4	165.24	577	5.19
Ganymede	5	143.79	493	5.19
Callisto	6	134.72	607	4.00
Ganymede	7	95.51	127	2.49
Ganymede	8	74.09	1413	2.49
Ganymede	9	66.98	2533	2.48
Europa	10	57.48	4134	2.60
Ganymede	11	44.73	122	1.68
Europa	12	36.34	100	1.57
Leveraging ΔV		29.52		0.118
Europa	13	22.51	6654	0.93
Leveraging ΔV		11.50		0.071
Europa	14	0.06	1765	Elliptical periapsis
EOI		0	100	0.450

the earlier parts of the tour that lie outside of the radiation belts [Grebow et al., 2011; Campagnola et al., 2012]. The correct phasing is needed so that the approach trajectory to EOI is in the plane of the desired science orbit. Also, ΔV can be expended to perform EOI earlier if radiation exposure becomes a more pressing concern.

B.2.6.6   Europa Orbit, and Orbit Maintenance

After EOI and associated clean-up maneuvers, the spacecraft is in a roughly 100-km circular, near-polar, science orbit with a node of 4pm. The finite burn losses for EOI are minimal as shown in Table B.2.6-6.

Table B.2.6-6. Gravity losses for EOI, CBE case and Maximum Dry Mass case (launch vehicle capability fully utilized)

	CBE Dry Mass w/ CBE Prop	Max Dry Mass Case
ΔV impulsive	450 m/s	450 m/s
ΔV finite burn	455 m/s	460
Gravity Loss	5 m/s	10 m/s
Gravity Loss, fractional	1 %	2 %
Burn Duration	4 minutes	6 minutes

Weekly orbit maintenance maneuvers are sufficient to control the growth of the eccentricity, which occurs mainly due to Jupiter's gravity, and will fine-tune the orbit period for repeat ground tracks. The total ΔV needed for maintenance for a month is only 5 m/s. The maneuver frequency and magnitude can be reduced further still if the orbital eccentricity vector is properly set once the main gravity harmonics of Europa are estimated. The prime science mission ends 30 days after EOI. The TID for a month in the science orbit is about 360 krad, a figure which accounts for the shielding effect of Europa, bringing the total unshielded (i.e. behind 100 mil Al) TID at end of prime mission to about 1.46 Mrad.

B.2.6.7 Navigation in the Jovian System

The navigation strategy and statistical ΔV are based on experience with Galileo and Cassini. A full-blown navigation study with precise maneuver locations and covariances is beyond the scope of this study. The main uncertainties early in the Jovian cruise are the satellite ephemerides. The maneuver execution errors and perturbing ΔVs are much less significant by comparison, except for the large JOI and EOI burns. Thus, up to three statistical maneuvers are envisioned per orbit around Jupiter: About three days after a flyby, near apoapsis, and about three days before a flyby. A cleanup maneuver will be done a few days after JOI to counteract errors both from the 500-km G0 flyby and from JOI itself. Similarly, EOI will have a cleanup maneuver done about 6 to 12 hours after the main burn to give sufficient

time for ground-based orbit determination. Two-way Doppler and range are assumed for orbit determination. Optical navigation is not assumed, but will be studied as a navigation trade option because it has the potential to offer lower statistical ΔVs, closer flybys and hence possibly shorter cruise and lower radiation exposure.

B.2.6.8 Potential Extended Mission(s)

Given a healthy spacecraft at the end of the Europa Orbiter prime mission (and support from NASA HQ), various options may be considered, depending on the findings of the prime mission and on the propellant reserves available. Extended mission options may include for example:

- Lower orbits for improved mapping and remote sensing
- Long life-time orbits or stable orbits for observing longer temporal variations
  - Higher polar orbits (longer lifetime)
  - Low-inclination, stable orbits (assuming significant propellant remains)
- Highly elliptical orbits with very low periapses

B.2.6.9 Spacecraft Disposal

Without active maintenance, low, circular orbits above about 40 degrees inclination will naturally impact the surface of Europa due to eccentricity growth (the orbital period does not have any significant secular change). Starting in the science orbit, it would take at least a month for an uncontrolled spacecraft to impact Europa. Thus, if the spacecraft becomes nonfunctional, it will eventually impact the surface of Europa at a random location. Alternatively, it may be decided after the prime mission to set a still-functioning spacecraft on a deliberate impact course with a specific spot on the surface. There will almost certainly not be sufficient propellant remaining at the end of the prime mission to enable the spacecraft to

Table B.2.6-7. Orbiter ΔV summary.

Activity	CBE ΔV (m/s)	MEV ΔV (m/s)	Comments
Launch Injection Cleanup	20	20	Estimate to correct injection errors from launch vehicle
Earth Bias DV	50	50	Needed for final correction of deliberate aim-point bias away from the earth. ~25m/s/E-flyby. May be performed separately or integrated with other TCMs.
Deep Space Maneuver	100	150	Maneuver on Earth-Earth leg near aphelion. Baseline launch period variation goes from 0m/s up to 100m/s
IP statistical & ΔV cleanup	50	50	Multiple small maneuvers
JOI at 12.8 Rj, 500-km G0 flyby	880	900	200-day initial orbit. Includes 3% for cleanup & minimal gravity losses.
Perijove Raise	40	80	Counteracts solar perturbations, targets G1 flyby
Pump-down phase Statistical	120	120	~8 m/s per flyby (conservative) (~15 flybys, incl. endgame). Expected average per-flyby: 3m/s. Deterministic ΔV can usually be avoided.
Endgame ΔV	188	200	4:3, 6:5 resonance sequence. ΔVs near an apoapse on each leg.
EOI ΔV, impulsive	450	600	100 km circular orbit
EOI ΔV gravity loss	25	30	<~5% for Max mass case and 890N engine
EOI cleanup	10	15	~2% of EOI, probably multiple maneuvers
Orbit Maintenance	5	5	Estimate: ~5 m/s per month, 100km circular orbit
Reserve	0	55	
TOTAL	**1940**	**2275**	

escape from Europa. Thus, impact with Europa is the ultimate fate of the spacecraft, which clearly has spacecraft sterilization implications.

B.2.6.10   Orbiter Mission ΔV

Table B.2.6-7 summarizes both the current best estimate (CBE) and maximum estimated value (MEV) for the total ΔV needed to execute the Europa orbiter mission. The two totals are comprised of both computed values (DSM, JOI, PRM and the tour's deterministic ΔV) and estimated values (launch injection cleanup, Earth bias ΔV, interplanetary statistical and cleanup ΔV, tour statistical and cleanup ΔV, EOI cleanup, orbit maintenance).

See the Master Equipment List (MEL, Sec B.4.3) for calculations of propellant loading based on ΔV and thruster usage.

B.2.7   Flight System Design and Development

The Orbiter flight system, a capable spacecraft tailored to the Orbiter science objectives, has high heritage and a low-complexity payload.

The Europa Orbiter Mission Flight System is described first in overview, identifying key components and features, then in detail at the module level. The module description overview discusses cross-cutting subsystem concepts followed by detailed descriptions of the three flight system modules: Avionics, Propulsion and Power Source. Finally, technical resource budgets are described followed by a description of the module and flight system level integration and testing concept.

B.2.7.1   Flight System Overview

The conceptual flight system (see Figure B.2.7-1) is comprised of three modules stacked along the Z axis. From top to bottom these are

- Avionics Module—comprising the telecom section (dominated by the 3 m high gain antenna), the upper equipment section containing the payload, and the avionics vault.
- Propulsion Module—containing the tanks, propellant, plumbing, valves and engines

- Power Source Module—Housing the ASRGs, their control electronics and the launch vehicle adapter.

Instruments

The Orbiter Mission flight system is configured to support the following notional science instruments:

- Mapping Camera (MC).
- Laser Altimeter (LA).
- Magnetometer (MAG).
- Langmuir Probe (LP).

The MC and LA are mounted on a two-axis gimbaled platform for nadir pointing during the Europa orbit. The MAG is accommodated on a 10 m boom to provide separation from the spacecraft and to collect magnetic field data in many orientations. The LP is deployed on a 1 m boom to reduce measurement disturbance from spacecraft surface charging. In addition to these four instruments, the flight system X/Ka band telecommunication system supports the Europa gravity science investigation without requiring functionality beyond what is already needed to support nominal communications.

Attitude Control

The Orbiter flight system is three-axis-stabilized in all phases of flight. Stabilization is achieved through the use of inertial measurement and star measurement for attitude determination and thrusters and reaction wheels for attitude control.

Data Handling

During an orbit, the volume of science data collected is relative small (~200 MB). This data is stored in the RAD750 radiation-hardened RAM prior to downlinking; the RAD750 is part of the Command and Data Handling Subsystem (C&DH).

Power

The power source for this spacecraft is four ASRGs. The power system is sized to accommodate the failure of one Stirling engine (each
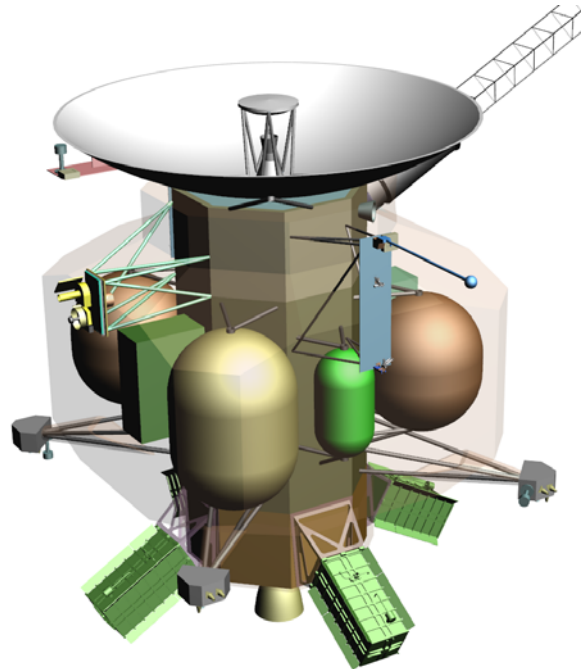
Figure B.2.7-1. The flight system (with transparent thermal shroud) provides a robust platform to collect, store, and transmit high volumes of science data.

ASRG uses two Stirling engines). Excess power is stored in an internally redundant 59-Amp-hour lithium-ion battery or dumped as heat through a thermal shunt. For transient mission phases that require more power than produced by the ASRGs in steady state, additional power is temporarily drawn from the battery.

Thermal

To minimize the power demand of the spacecraft (driven by a desire to minimize the number of ASRGs), the spacecraft was designed to minimize the use of electrical heaters. To achieve this goal, the heat from spacecraft electronics is captured inside a thermal shroud surrounding the Propulsion Subsystem providing enough heat to keep the propellant near room temperature without the need for supplemental electrical heaters. The concept includes 30 radioisotope heater units (RHUs) and/or variable radioisotope heater units (VRHUs) that will be used in extremities and select locations (e.g., thruster cluster assemblies) when heat from the avionics vault is not

available to minimize the need for electrical heaters.

Telecommunications

The Telecomunications Subsystem is designed to support the gravity science investigation and real-time transmission of science data communicated back to Earth while in Europa orbit. This system consists of X-band uplink for commands, X-band downlink for low-data-rate telemetry, and Ka-band downlink using the fixed 3-meter HGA for high-data-rate telemetry.

Propulsion

The Propulsion Subsystem provides delta-V and attitude control, momentum management, trajectory correction, Jupiter Orbit Insertion (JOI), and EOI. To support these activities, the Propulsion Subsystem utilizes a dual-mode, bipropellant architecture. The fuel, oxidizer, and pressurant tanks are distributed around the core of the spacecraft to provide radiation shielding to the internal electronics. During Phase A, a risk assessment will be performed on potential micrometeoroid damage to the tanks; if necessary, the thermal shroud can be upgraded with standoff Whipple/bumper shields. The tanks are sized for maximum propellant for spacecraft on the Atlas 551 and can support up to 2.28 km/s of ΔV. The engines consist of one 890-N main engine, four 90-N thrust vector control (TVC) thrusters, and sixteen 4.4-N (eight primary, eight redundant) attitude-control thrusters. Each of the four thruster control assemblies (TCA) contains 4 attitude control thrusters and 1 TVC thruster.

Redundancy

The spacecraft uses a redundancy philosophy similar to that of Cassini: that is, the flight system is redundant with selected cross strapping. The instruments are single string. The structure, main engine, and TVC are also single string; these single-string elements will undergo a risk assessment in Phase A to determine whether the risk is acceptable.

Radiation

This mission has very demanding total dose radiation requirements (1.56 Mrad (Si) behind 100 mils Al). To support the use of standard aerospace EEE parts, the design uses a multi-layered radiation shield. Most of the spacecraft electronics are housed in a vault (similar to that on the Juno spacecraft). This vault is also buried inside the spacecraft to benefit from shielding provided by spacecraft elements such as the batteries, the structure, tanks, propellant (during Jupiter cruise), and ASRGs. Inside the vault, components will be exposed to less than 150 krads end-of-mission total dose. Parts not capable of meeting even this reduced total dose requirement with proper derating, can be accommodated using additional box level shielding, box and card placement to provide additional self-shielding, and parts-level spot shielding.

B.2.7.1.1   Flight System Configuration

The engineering configuration of the spacecraft is shown in Figure B.2.7-2. The left side of the figure is the CAD model without the thermal shroud and with the instruments stowed. The right side of the figure is a cross section of the same configuration.

Figure B.2.7-3 shows the spacecraft with the 10-m MAG boom and the LP deployed, and with the thermal shroud. The left side of the figure shows how the HGA and thermal shroud protect the spacecraft from the high solar flux during the Venus flyby portion of the interplanetary cruise. The few elements exposed to the solar flux are the LGA, the thruster clusters, and the LP. These three elements can survive without shading the heating that occurs during the Venus flyby.

B.2.7.1.1.1   Avionics Module

The topmost portion of the Avionics Module is the telecommunications section. It is composed of a fixed 3-meter HGA, the medium-gain antenna (MGA), one of three low-gain antennas (LGAs) and associated waveguide and amplifiers. Below the HGA is the upper
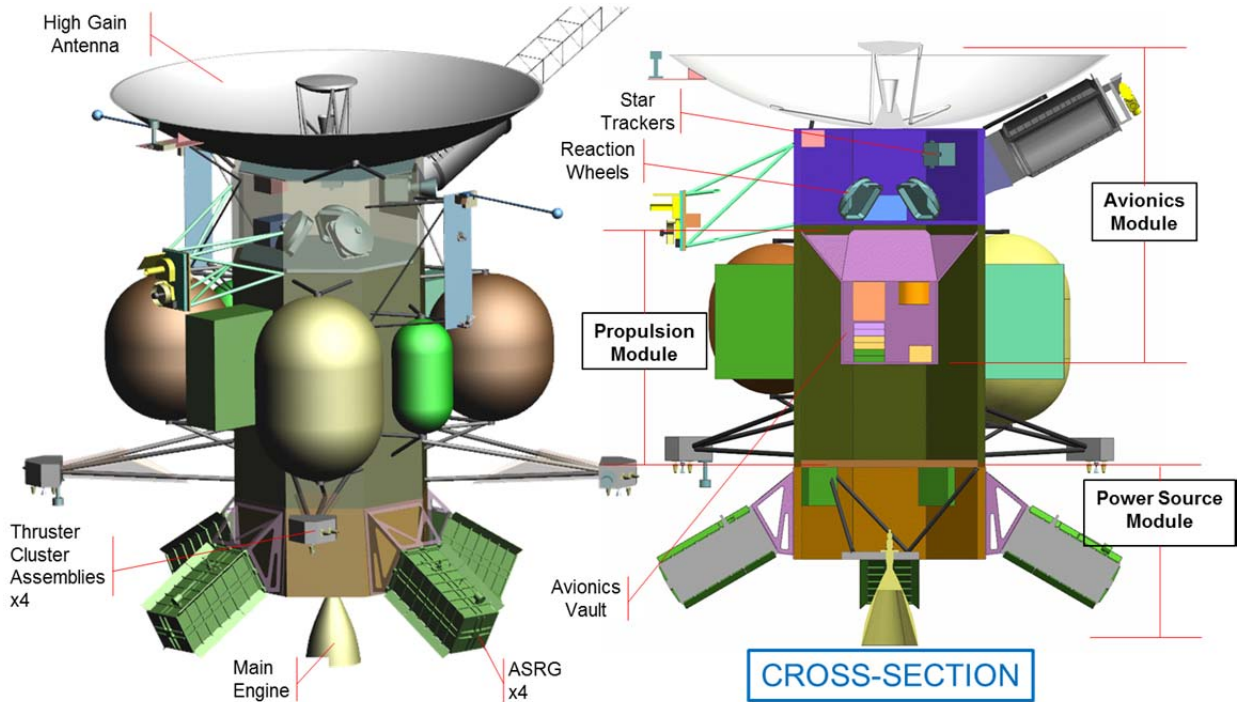
Figure B.2.7-2. The modular configuration shown provides maximum radiation shielding for the electronics (note that the thermal shroud is not shown).
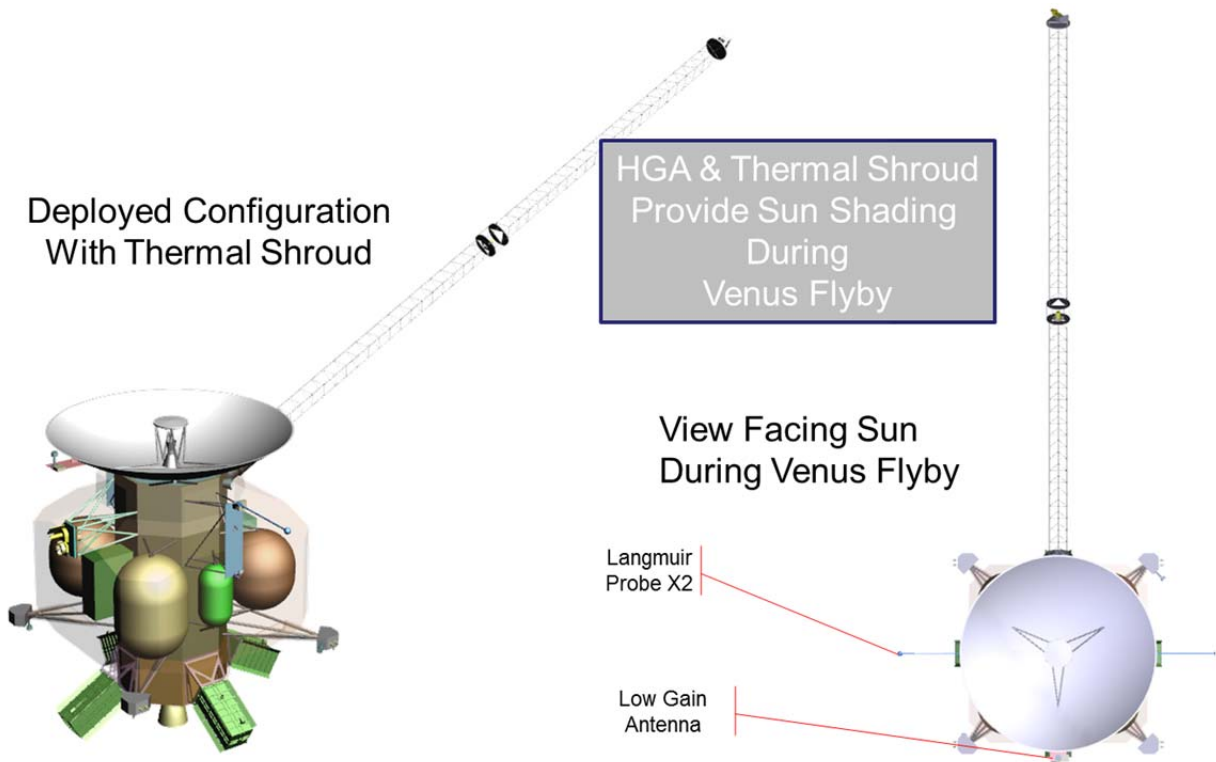
Figure B.2.7-3. The flight system configuration with thermal enclosure and deployed instrumentation.

equipment section. This section holds the instruments, science electronics chassis, reaction wheels, and star-trackers. At the bottom of the Avionics Module is the avionics vault section; inside the vault is a majority of the spacecraft avionics. Note that the vault sits inside the Propulsion Module to maximize the radiation shielding from the tanks, structure, and propellant. The Avionics Module attaches to the Propulsion Module. Until the Avionics Module is mated with the Propulsion Module, all components in the Avionics Module sections are accessible for testing, troubleshooting or rework without significant impact to the System Integration plan. After spacecraft integration, a de-mate operation from the Propulsion Module will enable access to the vault.

B.2.7.1.1.2   Propulsion Module

The Propulsion Module contains the fuel tanks, oxidizer tanks, and pressurant tanks as shown in Figure B.2.7-2. At the bottom of the Propulsion Module are four thruster clusters holding the attitude-control thrusters; these are supported to maximize the moment arm for attitude control. The main engine is physically attached to the Propulsion Module but protrudes down through the central ring of the Power Source Module after mating. This design allows end-to-end testing of the fully plumbed and sealed Propulsion Module. It also allows system integration of the Propulsion Module to the Avionics and Power Source Modules without breaking the final, tested plumbing configuration.

B.2.7.1.1.3   Power Source Module

The Power Source Module supports the four ASRGs and their control electronics. The ASRG units would be mounted on the end of a support structure that supports them radially and slightly canted away from the spacecraft. This is to improve the ASRGs thermal view to deep space to improve ASRG efficiency. The support structures also house a passive vibration damping system tuned to the ASRG oscillation frequency of around 100 Hz. This sys-

tem would greatly reduce the vibration transmitted through the spacecraft structure to vibration sensitive components such as the star tracker and optical instruments. The launch vehicle adapter is attached to the underside of the Power Source Module's primary ring.

A main goal of modularizing the ASRG assembly from the rest of the flight system is to decouple the heavily guarded and regulated ASRG fueling and assembly process from the rest of the system. The concept allows for the Power Source Module to be assembled and tested independently from the rest of the spacecraft, only mated to the system at the last possible moment at the launch site before fairing installation. This helps ensure the safest possible handling of the ASRGs.

B.2.7.1.2   System Block Diagram

Figure B.2.7-4 shows the system block diagram for the Orbiter spacecraft. The top box is the Avionics Module. The middle box is the Propulsion Module. The bottom box is the Power Source Module. Note that items like electrical heaters and temperature sensors are distributed across all of the modules. The legend shows the key interface types between elements.

The Avionics Module holds the majority of the spacecraft avionics. Inside the vault are the C&DH electronics, power electronics, pyro/propulsion drive electronics, inertial measurement units (IMUs), RWA electronics, and SDSTs. Outside the vault are the instruments, science electronics chassis and the following GN&C components: RWA mechanical assemblies, Sun-sensors, and stellar reference units (SRUs). The power subsystem components outside the vault are the shunt radiator and battery. The telecom subsystem components outside the vault are the TWTAs, the coax, the waveguide, switches, and antennas.

The Propulsion Module is an integrated structure comprising all of the tanks (fuel, oxidizer, pressurant), the plumbing, the pressurization control assembly (valves, filters, sensors, etc.),
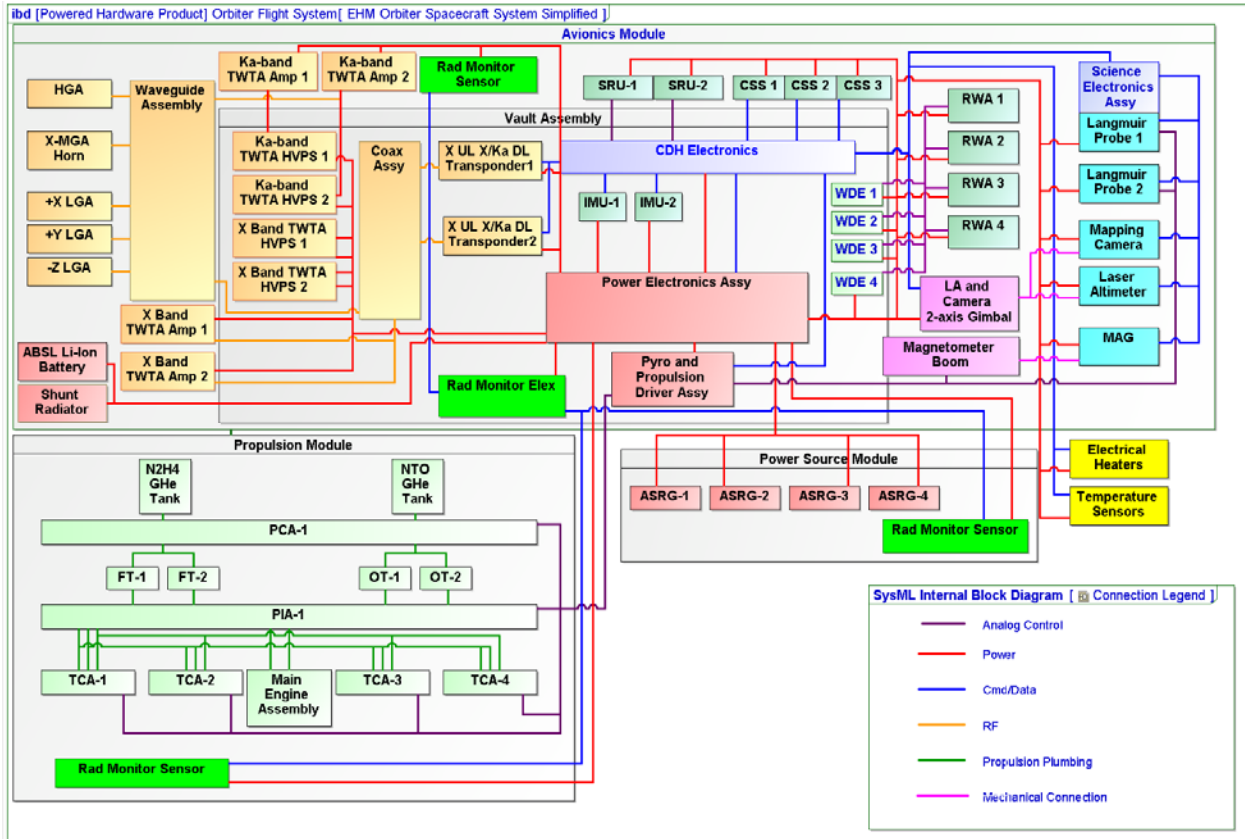
Figure B.2.7-4. The system block diagram shows the simple interfaces between the spacecraft modules

the propellant isolation assembly (valves, filters, sensors, etc.), the thrusters, and the main engine.

The Power Source Module is an integrated structure with the launch vehicle adapter and ASRGs. The ASRG consists of the power sources and the control electronics.

Note that some of the boxes (e.g., C&DH) do not show redundancy because they are internally redundant.

B.2.7.1.3   Flight System Key Drivers

Table B.2.7-1 shows the key drivers that flow down to the flight system from the science measurements.

Gravity science measurements drive radio Doppler observation of the spacecraft while in orbit around Europa. Long, continuous data sets (i.e. radio Doppler measurements of the spacecraft through several Europa orbits without non-gravitational perturbations from

thruster firings) are highly desired with 24 hour continuous data sets required as a minimum. This requirement drives RWA momentum sizing, telecom performance requirements and power system requirements.

Magnetic field measurements levy two drivers on the flight system design: the system and subsystem design must meet stringent magnetic cleanliness requirements and the magnetometers must be deployed away from the spacecraft. Two magnetometers—one at 5 m along the boom and the other at 10 m—are used to enable post processing removal of any residual spacecraft magnetic field bias.

Charged particle measurement using the Langmuir Probe has two drivers on the flight system design. The system and subsystem design must meet stringent EMI requirements andLP must be deployed away from the spacecraft to provide a clear FOV to the plasma.

Table B.2.7-1. The spacecraft driving requirements from the science measurements are mature and have been vetted through numerous Science Definition Team meetings.

Science Measure	Requirement	GN&C	Telecom	Power	CDH	Prop	Thermal	Mech
Gravity Science	Provide continuous "arcs"	RWA Sizing/ Desat Freq	Continuous	# of ASRGs				
	0.1 mm/sec performance		X up, Ka down					
Magnetometry	Provide magnetically clean spacecraft		EMI	EMI	EMI			Deploy two mag
Langmuir Probe	Provide EMI clean spacecraft		EMI	EMI	EMI			
	"FOV" of Plasma (not in Wake of Spacecraft)							Deploy
Mapping Camera	Simultaneous with LA & Gravity Science							Gimbal system
	Stereo Imaging		3-m HGA Ka down		Data Storage			
	Strip overlap & alignment							
Laser Altimetry	Simultaneous with Gravity Science & Mapping Camera							Gimbal system
	10-cm accuracy							

The MC and LA levy several drivers on the flight system. Imaging the surface while simultaneously collecting gravity science with a body-fixed HGA necessitates the use of a two-axis gimbal platform. The surface map creation in stereo is the driver on data storage and downlink; it drives the size of the data storage in the C&DH subsystem and drives the size and power of the telecommunication subsystem. The mapping strip overlap and alignment requires tight pointing knowledge from the GN&C subsystem. The 10-cm accuracy requirement on the LA drives tight pointing knowledge from the GN&C subsystem.

Table B.2.7-2 shows the key drivers that flow down to the flight system from the mission design.

The Venus flyby is a driver for the spacecraft thermal design and results in an approach wherein the spacecraft points the HGA towards the Sun; this enables the HGA and the thermal shroud to shade the vehicle.

During inner-solar-system cruise, there are two key drivers on the flight system design. Commanding and telemetry during this inner-solar-system cruise require an X-band system for uplink and downlink using near-4π steradian coverage from the LGAs. This type of telecom approach is needed since the spacecraft cannot always point the HGA to Earth because of thermal constraints.

During the outer-solar-system cruise, commanding and telemetry require an X-band system for uplink and downlink using the MGA.

During the outer-solar-system cruise and Europa orbital phase, the cold conditions drive the thermal design of the spacecraft. To minimize electrical heater power demand, the internal heating from the electronics is captured within the thermal shroud to keep the spacecraft equipment within flight allowable temperatures. External elements will require electrical heaters or VRHUs.

JOI and EOI are autonomous critical events that drive robust system fault protection. This flows down to the subsystems, resulting in a fault tolerant architecture that allows faults to be detected and isolated so that recovery can

Table B.2.7-2. The flight system incorporates design elements that flow down from the mission drivers.

Mission Design	Driver	System	GN&C	Telecom	Power	CDC	Prop	Thermal	Mech
Venus Flyby	Thermal control							Shade with HGA & shroud	
Inner Solar System Cruise	Command & Telemetry								
	Earth Flybys with ASRG	Fault Protection							
Outer Solar System Cruise/Jupiter Cruise/Europa	Command & Telemetry		Sun sensors						
	Thermal Control							Thermal Shroud/ RHU/VRHU	
JOI/EOI	Critical Event	Fault Protection	Dual string/ Hot Sparing	Dual string/ Hot Sparing	Dual string/ Hot Sparing	Dual string/ Hot Sparing	TVC Size Engine Size		
TCM/Europa Orbit Maintenance	Navigation			Doppler					
Jupiter Cruise + Europa Orbit	Radiation	Fault Protection	<300 krad parts	<300 krad parts	<300 krad parts	<300 krad parts			Vault & Config

occur rapidly and without terminating the orbit insertion sequence.

Since the mission has several trajectory correction maneuvers (TCMs), both deterministic and statistical, the onboard communication system must support Doppler tracking to enable navigation on the ground.

The Jupiter cruise and the Europa orbital phase drives one key flight system requirements: a large radiation total dose of approximately 1.56 Mrad (Si) (behind100 mil Al) is accumulated during these phases with periods of high peak flux; part selection and shielding, sensor noise tolerance and fault-protection requirements.

B.2.7.2   Structures and Mechanisms

The overall configuration (Figure B.2.7-5) starts with the Avionics Module at the top, followed by the Propulsion Module and the Power Source Module at the bottom. The primary structure (Figure B.2.7-6) consists of these three octagonal modules. Each module's structure is based on an aluminum forging machined from the outside. Aluminum was chosen because it provides the best balance
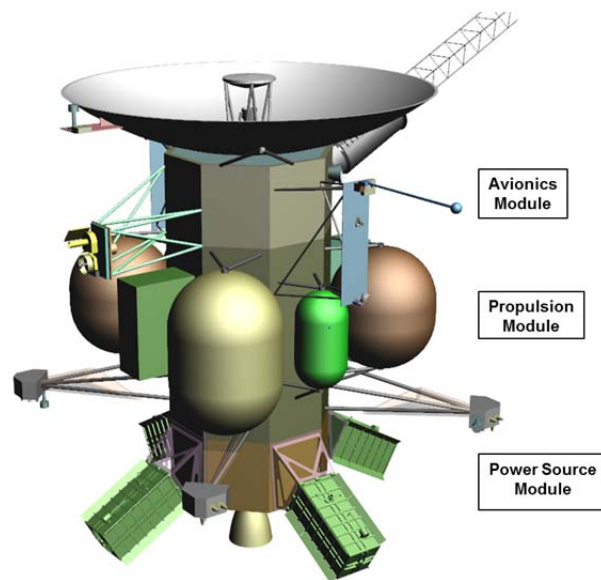
Figure B.2.7-5. Structures and mechanisms configuration.

among weight, strength, stiffness, and radiation-shielding and is easily worked into a lightweight, high-strength, and stiff structure. When all three modules are stacked, they form a superstructure that is able the meet the Atlas V launch vehicle's load and frequency requirements.
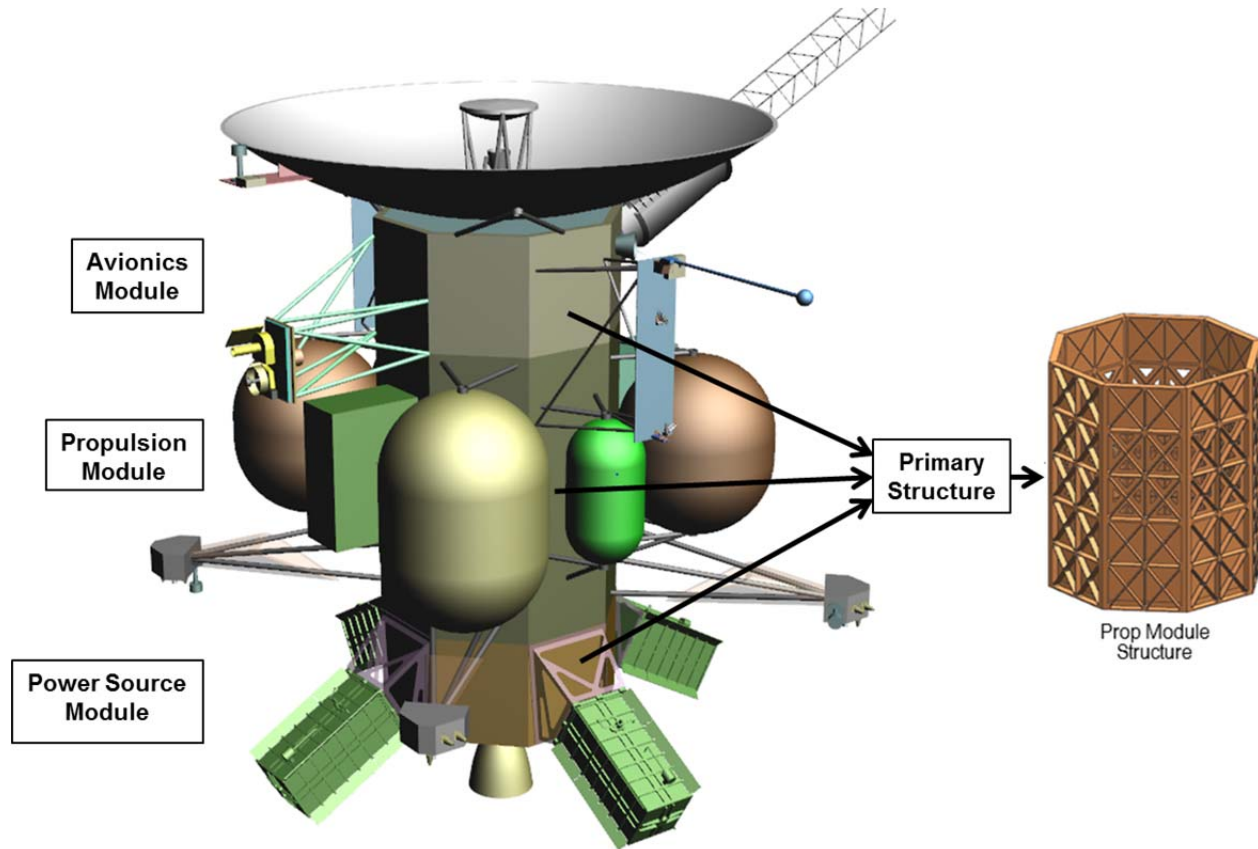
Figure B.2.7-6. Orbiter primary structure.

All brackets, struts, secondary structures, and mechanisms are mechanically grounded to the primary structure. Loads for these appendages are determined using the Atlas V mass acceleration curve.

The orbiter's primary mechanisms are the instrument two-axis gimbal, the LP's deployment system and the MAG boom deployment mechanism (Figure B.2.7-7).

The structures and mechanism do not require any new technology. Designs from past missions can be adapted to meet all of the structural and functional requirements for the Europa Orbiter.

B.2.7.2.1   Key Mechanical Drivers

- First mode fundamental frequency: 8 Hz
- Primary structure lateral launch acceleration: 2 G

- Atlas V mass acceleration curve for appendages
- Isolate spacecraft at least 20 Hz from Stirling converter operation frequency (102 Hz)

B.2.7.3   Orbiter Thermal Control

The thermal design uses, to the fullest extent practicable, waste heat, insulation, and louvers to control temperatures. This approach consumes little to no operational heater power, is low-mass, and has a flight-proven heritage.

B.2.7.3.1   Key Thermal Drivers

- Maintain the propulsion system and battery within allowable flight temperature (AFT) ranges of 15°C to 50°C and 10°C to 25°C, respectively.
- Maintain all instruments within the AFT limits.
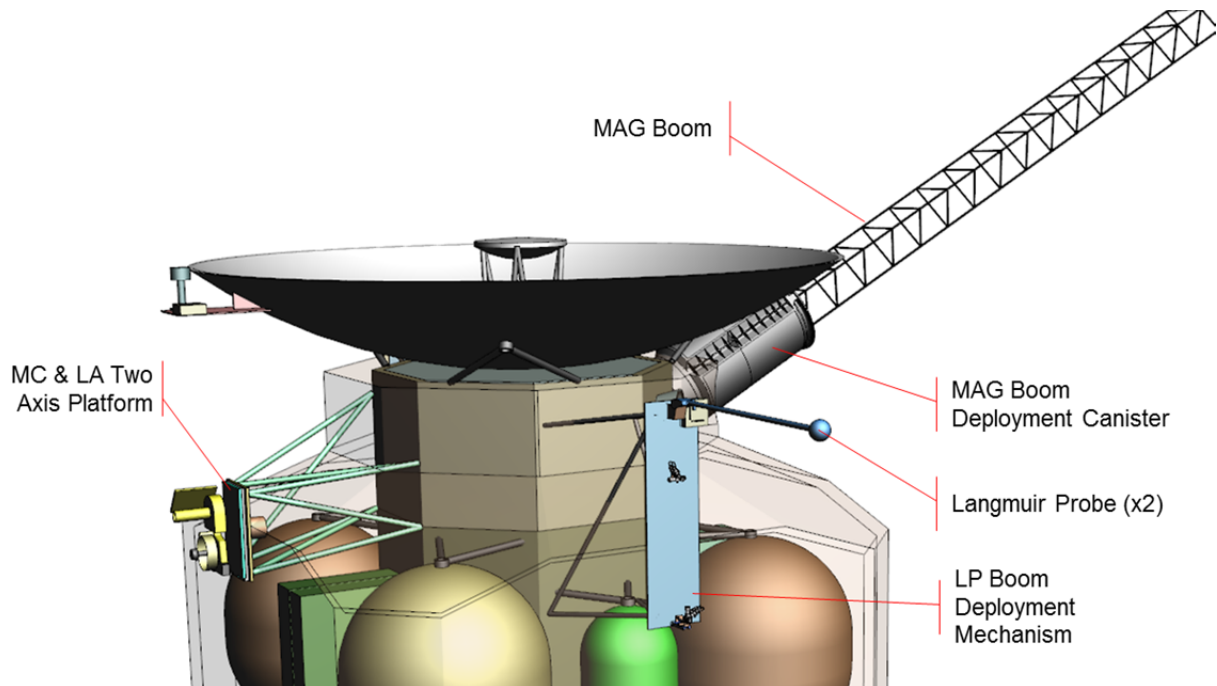
Figure B.2.7-7. Laser altimeter and MC and LP.

- Accommodate the variation in environmental heat loads from Venus at 0.7 AU to Jupiter at 5.2 AU (i.e., 2.0 to 0.04 Earth Suns).
- Tolerate limited transient off-Sun exposure at less than 1 AU during fault conditions or trajectory maneuvers.
- Minimize replacement heater power at outer cruise and Jupiter.

B.2.7.3.2   Thermal Design

Figures B.2.7-8 and B.2.7-9 show the primary thermal components of the spacecraft. A lightweight thermal shroud surrounds the propulsion tanks and associated plumbing. Consisting of multilayered insulation (MLI) supported by a latticework, this shroud creates a radiative cavity around the tanks. A clearance of 100 mm between the propulsion components and shroud provides adequate view factors for radiation.

Waste heat from the avionics vault and Advanced Stirling Radioisotope Generator (ASRG) electronics radiates into the cavity and warms the propulsion system. Openings in the primary structure allow heat to radiate from the vault onto the tanks and into the cavity.

A temperature-regulation system is necessary to accommodate the variation in environmental loads and internal dissipations. Accordingly, louvers over external radiators on both ends of the spacecraft regulate the cavity temperature to maintain acceptable vault and propulsion temperatures. Heat from the vault and ASRG electronics, coupled with louvers on the mounting structure, warms the shroud in the cold case and rejects excess heat to space in the hot case, producing acceptable temperatures on the propulsion system and vault.

This system of waste heat and louvers requires no additional electrical heaters for normal operation. With an MLI external area of 26 m^2 and a nominal effective thermal emissivity of 0.01, acceptable tank temperatures occur with a 200-W heat flow. During the mission, 290 W to 418 W is available from the avionics vault and ASRG electronics. Hence, the heat balance is always positive. Fault conditions, where the avionics may be off and waste heat is low, make survival heaters necessary on the
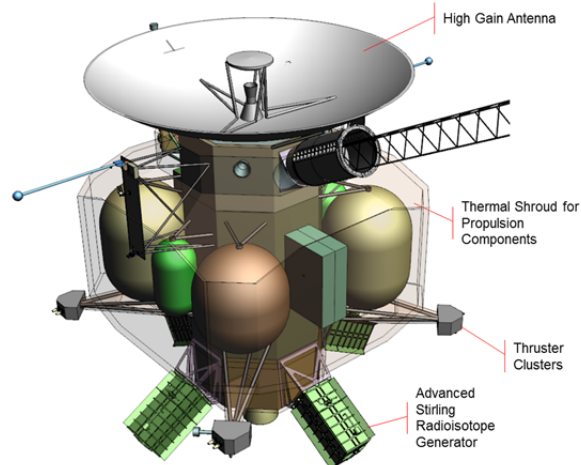
Figure B.2.7-8. Orbiter spacecraft with thermal shroud surrounding propulsion tanks.

Figure B.2.7-9. Orbiter spacecraft with thermal shroud removed.

vault. Survival operation will be studied in Phase A.

The high-gain antenna (HGA) performs an important thermal-control function: It shades the spacecraft from the Sun during the hot conditions near Venus. At Venus, the spacecraft is oriented such that the HGA faces the Sun. This orientation preserves the heat balance on the thermal shroud and louvers. If necessary to tolerate a loss-of-attitude fault at Venus, a hybrid MLI layup with five external layers of embossed Kapton protects against high exterior temperatures. Off-Sun illumination and the impact on temperatures will be studied during Phase A of the project.

A separate thermal-control zone with a dedicated radiator and louver controls the temperature of the battery. This is accomplished by locating the battery in the upper equipment section of the Avionics Module mounted directly to a space exposed bulkhead with a dedicated louver.

Variable radioisotope heating units (VRHUs) control the temperature of the thruster clusters. Local heating from the VRHUs is required due to the remote location of the thrusters. Each VHRU consists of two to three individual RHUs mounted in a rotating cylinder. One half of the cylinder is painted white while the other half is insulated. A bimetallic spring positions

the cylinder to radiate heat into the thruster cluster when the cluster is cold, or out to space when the cluster is warm. There are four VHRUs per thruster cluster with a total of ten individual RHUs per cluster. Four thruster clusters yield a total of sixteen VHRUs and 40 individual RHUs. This design tolerates a failure mode where one VHRU is stuck fully open or fully closed.

Instrument thermal control is individually customized via local radiators and heaters to maintain acceptable temperatures.

Risk exists, as in any thermal-control system, where thermal performance is affected by workmanship. The effective emissivity of MLI is a notable example. For the Europa Orbiter, this risk is mitigated by design and by test. Margin in the active louver system provides tolerance for hardware variations. Also, thermal development tests of the louvers and critical areas of MLI reduce risk to acceptable levels.

B.2.7.3.3   *Heritage*

The thermal design for the Europa Orbiter follows that of Cassini. In the Cassini design, the propulsion system was enclosed in a shroud that formed a radiative cavity. Heat for

the Cassini shroud came from radioisotope thermoelectric generators (RTGs), whereas on the Europa Orbiter spacecraft the heat comes from the avionics vault and the ASRG electronics. VRHUs control the temperature of the thruster clusters for both Cassini and Europa Orbiter. HGA shading protected the Cassini spacecraft from solar loading at Venus and will do the same here. Other thermal hardware, such as louvers, heaters, MLI, and platinum resistance thermometers, also have good heritage based on the flight experience of prior JPL missions.

B.2.7.3.4 Heat Balances for Three Governing Conditions

The inner cruise takes the spacecraft near Venus. In this 0.7-AU hot condition, the high-gain antenna points toward the Sun to shade the rest of the spacecraft and prevent overheating. Side-facing louvers automatically control the internal temperatures. All of the heat from the ASRG electronics, 72 W, radiates off the lower louver, and 68 W of the vault power radiates off the upper louver, as shown in Figure B.2.7-10.

The orbiter experiences cold conditions when in orbit about Europa without communications. In this cold science mode, the vault power is 169 W. This low level of waste heat is fully used to warm the thermal shroud. Hence, the upper louver is closed. In addition, 31 W of waste heat from the ASRG electronics conducts into the central structure. The remaining 41 W from the ASRG electronics radiates off the lower louver, as shown in Figure B.2.7-11.

Power levels change again for orbit insertion and trajectory correction maneuvers. In this high-power condition, the vault dissipates 346 W. Consequently, the upper louver rejects 146 W while the lower louver rejects 72 W, as shown in Figure B.2.7-12.

Passive thermal control of the propulsion tanks and adjacent lines is by radiation into the thermal shroud. This is the same approach that was used on Cassini. At Jupiter, in the worst-case cold condition, thermal equilibrium occurs with a heat flow of 200 W from the inner structure into the shroud and out through the insulation. An initial thermal analysis shows that the propulsion tanks remain within 25°C to 40°C, in compliance with their AFTs, without direct heating or active control. Fig-

Figure B.2.7-10. Heat balance for inner cruise.
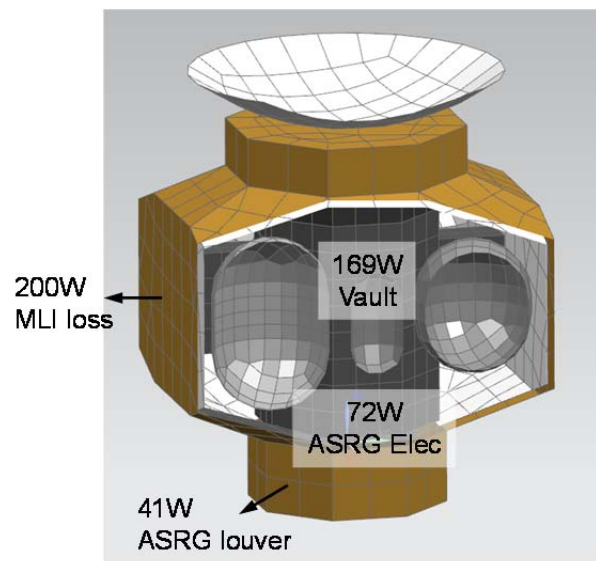
Figure B.2.7-11. Heat balance for Europa orbit with communications off.
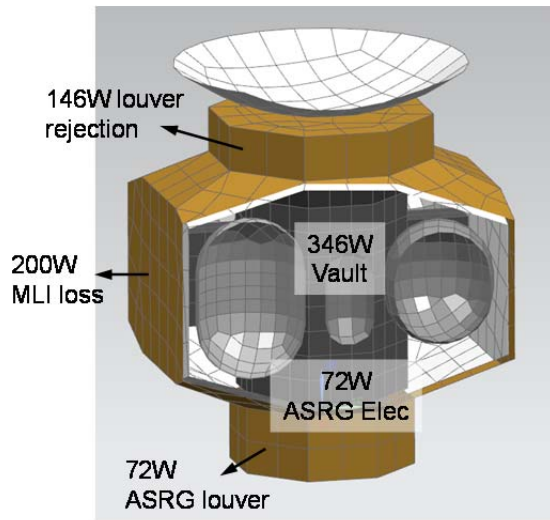
Figure B.2.7-12. Heat balance for orbit insertion and trajectory correction maneuvers.

Figure B.2.7-13. Tank temperatures.

ures B.2.7-13 and B.2.7-14 show predictions of the tank temperatures.

B.2.7.4   Propulsion Module

B.2.7.4.1   Propulsion

This propulsion subsystem, specifically designed for long-life outer-planet missions, will provide the impulse and reliability necessary to meet the needs of the Europa Orbiter Mission.

The Europa Orbiter spacecraft propulsion subsystem is a dual-mode bipropellant system. The propellants are hydrazine (N_2H_4) and nitrogen tetroxide (NTO). The hydrazine fuel and nitrogen tetroxide oxidizer are used by the bipropellant main engine, and the hydrazine fuel alone is used by the monopropellant reaction-control subsystem (RCS) thrusters and thrust vector control (TVC) thrusters. Figure B.2.7-15 shows a schematic of the propulsion subsystem.

B.2.7.4.1.1   Key Performance Drivers

The key drivers of the design of the propulsion subsystem are typical of those for outer-planet missions, with the possible exception of the desire to configure the system to take advantage of the propulsion subsystem mass to provide radiation shielding to sensitive elec-

Figure B.2.7-14. Predicted tank temperatures, showing only the tanks.

tronics. The key drivers for the propulsion subsystem are to

1. Provide delta-V for maneuvers, including the JOI and EOI maneuvers.
2. Provide thrust vector control during main engine operation.
3. Provide for attitude control when the spacecraft is not using reaction wheels.
4. Provide for reaction wheel unloading.
5. Configure the system to maximize radiation shielding of the spacecraft electronics.
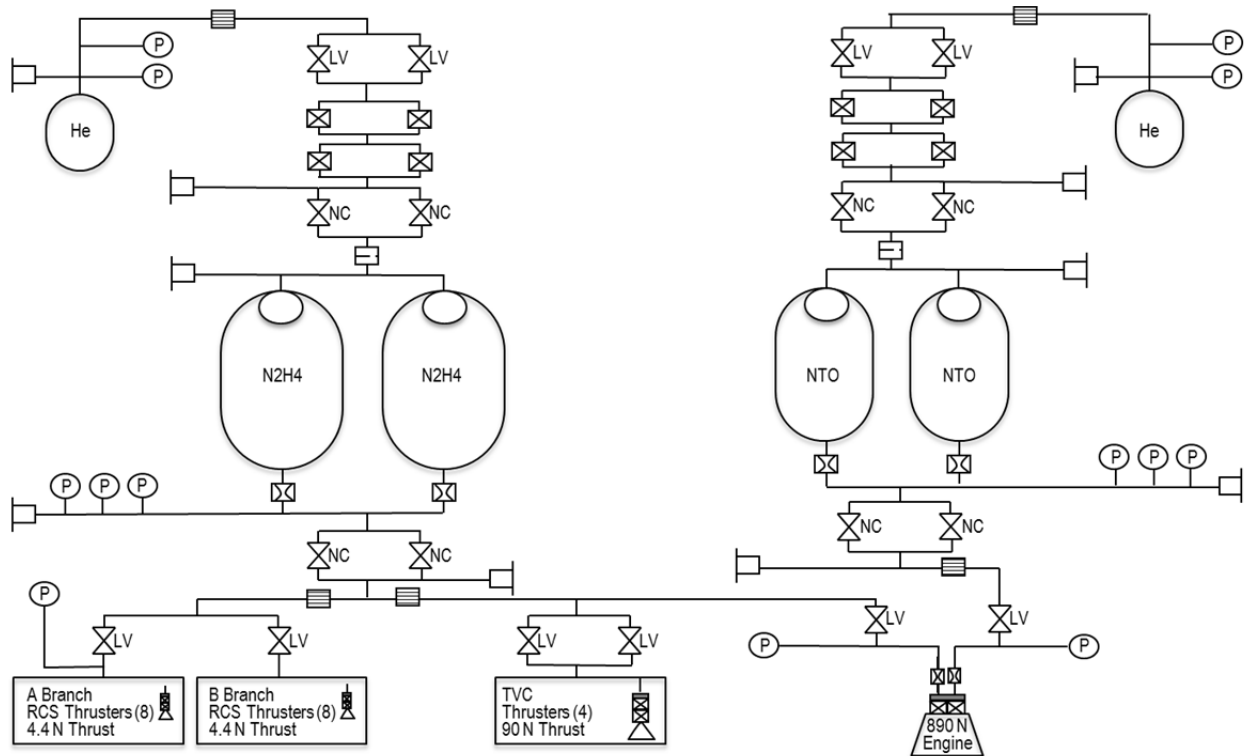
Figure B.2.7-15. Dual-mode, bipropellant propulsion subsystem schematic.

B.2.7.4.1.2   Propulsion Module Configuration

Figure B.2.7-16 shows that the Propulsion Module configuration is based on a core octagonal structure with the propellant tanks, pressurant tanks, and component plates mounted on the exterior sides of the octagonal structure. This configuration is driven by the desire to maximize the radiation shielding for the spacecraft electronics, mounted on the avionics module and located internal to the Propulsion Module core structure. Note that the propulsion components' plates are mounted perpendicular to the core structure (see Figure B.2.7-16). This is done because there is insufficient real estate to mount the component plates in a more traditional fashion (i.e., parallel) without increasing the length or diameter of the Propulsion Module. It was decided not to mount the component plates to an interior wall of the Propulsion Module because of limited accessibility during ATLO.

A single main engine, mounted using struts at the bottom of the Propulsion Module and pro-truding through the Power Source Module, provides for primary delta-V. The RCS and TVC thrusters are mounted on four thruster cluster assemblies (TCAs), which in turn are mounted on struts extending away from the spacecraft. This configuration is very similar to that of the Cassini RCS. Each TCA contains four RCS thrusters (two primary and two redundant) and a single TVC thruster. The RCS thrusters are redundant, in that there are two strings of eight thrusters. Each string of eight thrusters is isolated by a single latch valve. The RCS thruster configuration provides for coupled thrust about the Z-axis (roll) and uncoupled thrust in pitch and yaw, identical to the Cassini configuration. Both the main engine and TVC thrusters are single-string in the current concept. A detailed trade of complexity vs. redundancy will be conducted in Phase A to confirm or modify this decision.
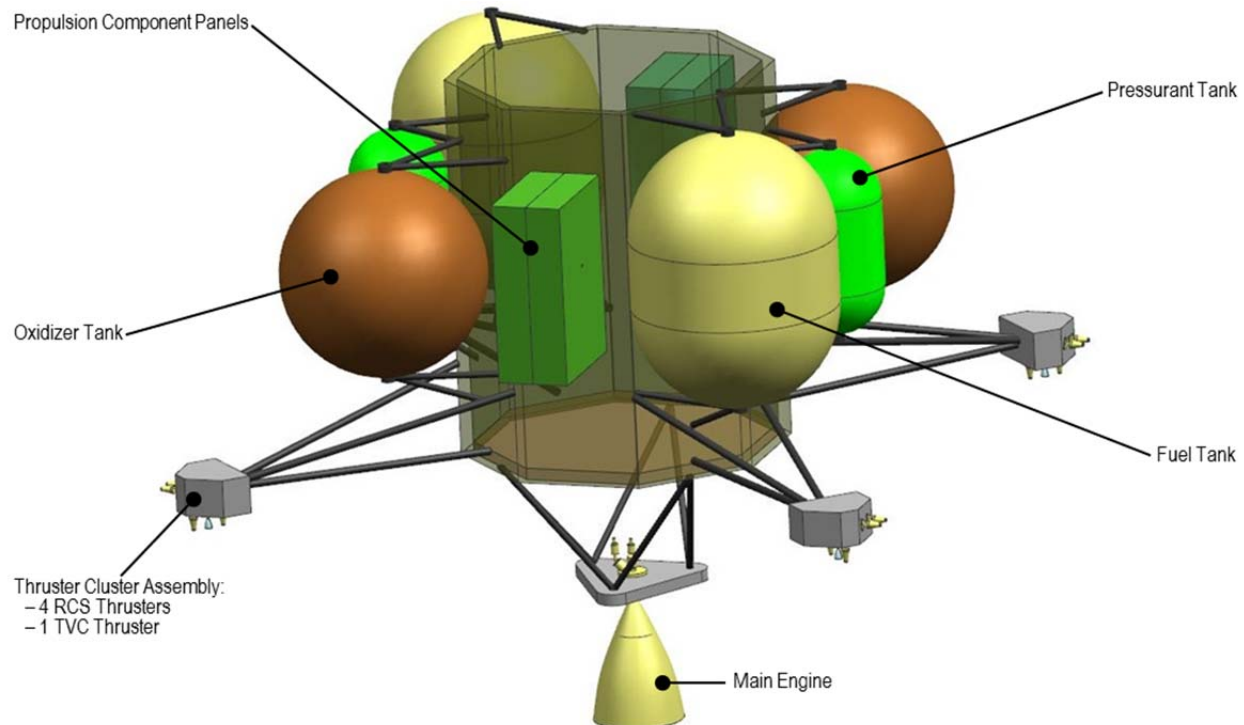
Figure B.2.7-16. Propulsion module configuration.

B.2.7.4.1.3   Propulsion System Design

Engines and Thrusters

An 890-N (200-lbf) main engine operating at a nominal mixture ratio of 1.0 with a minimum specific impulse of 323 seconds has been baselined for the Orbiter Mission concept. As currently planned, the engine is required to support a JOI maneuver on the order of 60 minutes and an EOI maneuver on the order of 25 minutes.

It should be noted that the engine interior wall will most likely have an oxidation-protective coating, which could be subject to micrometeoroid damage. The actual risk of failure and time to failure caused by damage is unknown, and likely indeterminate. The presented concept does not include an engine cover but the design does not preclude its addition either. The decision to include an engine cover will be reevaluated during Phase A.

The TVC thruster currently assumed for the Orbiter spacecraft is the Aerojet MR-107T thruster (or equivalent), providing approxi-

mately 90 N (20 lbf) of thrust. A preliminary analysis has been performed by ACS personnel showing that this thruster provides adequate control authority for the vehicle during main engine operation. The RCS thruster currently assumed is the Aerojet MR-111 thruster (or equivalent), providing approximately 4.4 N (1 lbf) of thrust. Both thrusters are qualified for flight and have high heritage.

Pressurization System

The baselined pressurization system allows for independent pressurization and regulation of the oxidizer and fuel tanks. Rather than using a traditional mechanical regulator, this system uses a set of four solenoid valves configured to be parallel and series-redundant (i.e., quad-redundant), allowing for electronic regulation using pressure transducer feedback. Flight software (FSW) would provide closed-loop control using pressure transducers measuring tank pressure. Three pressure transducers would be polled to protect from a transducer failure scenario. There are several advantages of this system over a more traditional pressuri-

zation system using mechanical regulators, especially for long-duration outer-planet missions:

1. Separate pressurization and regulation of the oxidizer and fuel tanks eliminates the risk of propellant vapor mixing in the pressurization system. It also eliminates the need for numerous check valves and pyro-valve isolation, reducing dry mass.

2. Elimination of the mechanical pressure regulator reduces the risk of regulator leakage. The series-redundant solenoid valves are less susceptible to leakage than are mechanical regulators.

3. The design allows for active control of the oxidizer and fuel tank pressures. This is advantageous because the oxidizer-to-fuel mixture ratio can be adjusted during the mission. It allows for more accurate control of mixture ratio, which in turn allows one to reduce residual propellant.

The schematic in Figure B.2.7-15 shows that the quad-redundant solenoid valves are isolated above by parallel redundant, high-pressure latch valves and below by parallel redundant, normally closed pyro valves. The pyro valves would remain closed until first use of the regulators is required.

Systems similar in concept to this have been used in the past on other spacecraft (e.g., MiTEx Upper Stage, Clementine, GeoLite, and Orbital Express).

Propellant and Pressurant Tanks

The propellant tanks are sized for a total propellant load of 2250 kg. This assumes the maximum launch capability of the Atlas V 551 LV on the 20 November 2021 launch window, providing a delta-V of 1.940 km/s. Table B.2.7-3 shows the rack-up of propellant, including residual and ACS propellant. The selected hydrazine tanks are 117 cm (46.0 in.) high by 89 cm (35.1 in.) in diameter (6% ullage), and the oxidizer tanks are a

89-cm (35.1-in.)–diameter sphere. The fuel tanks are based on the ATK P/N 80399-1 tank. The oxidizer tank is based on the ATK P/N 80350-1 tank.

The pressurant tanks are essentially off-the-shelf tanks and significantly oversized for the current propellant load. The pressurant mass load is 5.5 kg. The pressurant tank sizing will be optimized as the design matures.

Propellant Isolation

The propellant tanks are isolated from the thrusters using parallel redundant, normally closed pyro valves and low-pressure latch valves. The design provides sufficient mechanical inhibits to meet KSC launch safety requirements.

Careful design of the propellant tank surface-tension propellant-management devices (PMDs) and the venturis downstream of the tanks will be necessary in order to prevent propellant transfer between the two tanks, or preferential draw of propellant from one tank. It may be necessary to take more positive measures to prevent propellant transfer, such as the addition of latch valves to isolate the propellant tanks from each other when not in use. Further detailed analyses will be required before this design can be finalized.

B.2.7.4.1.4   Heritage

The majority of the components used in the Orbiter propulsion system are flight qualified and considered off-the-shelf. This includes the RCS thrusters, TVC thrusters, service valves,

Table B.2.7-3. Maximum propellant load case for Orbiter spacecraft propellant tank sizing.

Required Propellant	Mass (kg)
Propellant load for 1.940 km/s delta-V	**2054**
Hydrazine (MR=1.0)	1027
NTO	1027
Hydrazine for TVC	101
Allocation of ACS propellant (N_2H_4)	40
Hydrazine residual/hold up (2.5%)	29
NTO residual/hold up (2.5%)	26
Total hydrazine	1197
Total NTO	1053
Total Propellant Load	2250

pressure transducers, filters, and latch valves. As discussed above, the baselined main engine will require a full qualification program. Regarding the propellant tanks, it is the study team's intent to size them based on a heritage design that makes use of qualified hemisphere forgings. The current design makes use of a 89-cm (35.1-in.) tank, but will likely require a change in length of the cylindrical section. In addition, a new PMD for the oxidizer and fuel tanks will need to be designed and integrated. Hence, the propellant tanks will likely require a new qualification test program. The study team is taking a similar approach with the pressurant tanks, using a qualified design that best meets the requirements for the Europa Orbiter Mission.

The pressurization system, which makes use of electronic regulation, will need to go through a program that develops and qualifies it as an integrated system, including the propulsion hardware, controller, and FSW.

B.2.7.4.2   Propulsion Module Structure

The Propulsion Module (Figure B.2.7-17) supports the fuel tanks, attitude-control thrusters, propellant-isolation assembly (PIA), pressurant-control assembly (PCA), and main engine. The propulsion fuel tanks are supported by bipod and tripod combinations and are attached to the primary structure. The main engine is attached at the bottom and extends
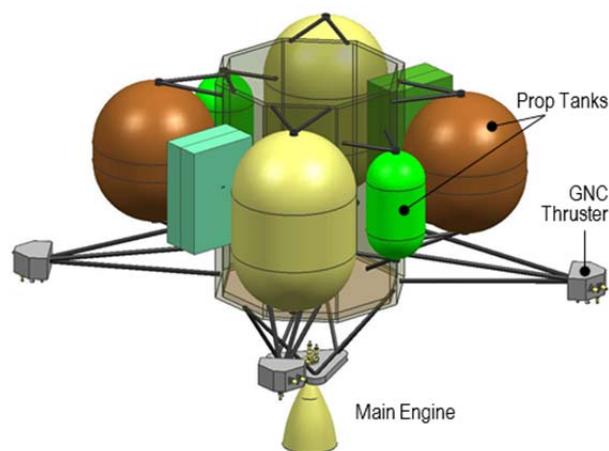
Figure B.2.7-17. Propulsion module.

through and below the Power Source Module. Four thruster clusters are supported at the ends of four tripods and are located as far from the spacecraft's center of mass as the launch vehicle fairing envelop will allow. This configuration maximizes thruster-control authority, and minimizes both plume-impingement forces and fuel required. The PIA and PCA are attached together, back to back and parallel to each other. The PIA/PCA assembly is in turn attached to the Propulsion Module's primary structure.

The Propulsion Module's primary structure has triangular holes in the wall at the location where the warm avionics has a radial view to the propulsion tanks. These holes allow for a direct radiation path to the tanks. In this region, the primary structure's wall thickness is increased to compensate for the holes. The necessary radiation shielding is still maintained due to the position of the tanks and the thickness of the vault.

B.2.7.5   Power Source Module

The Power Source Module (Figure B.2.7-18) would contain four ASRGs, the ASRG mounting structure and the launch vehicle adapter. Each ASRG provides a power and command interface to the spacecraft. The Power Source Module would be delivered directly to the launch site for integration. The thermal dissipation of the ASRGs inside the primary structure contributes to the overall thermal input inside the thermal shroud of the spacecraft. The main engine assembly of the Propulsion Module goes through the center of the Power Source Module with a thermal shroud protecting against the heat of the engine.

B.2.7.5.1   Power Source

The spacecraft power source interface is to an industry-standard defined power bus with 22 to 36-V range defined at the load interface. The power bus architecture is a direct energy transfer, with the power source interfacing with the power subsystem in the Avionics
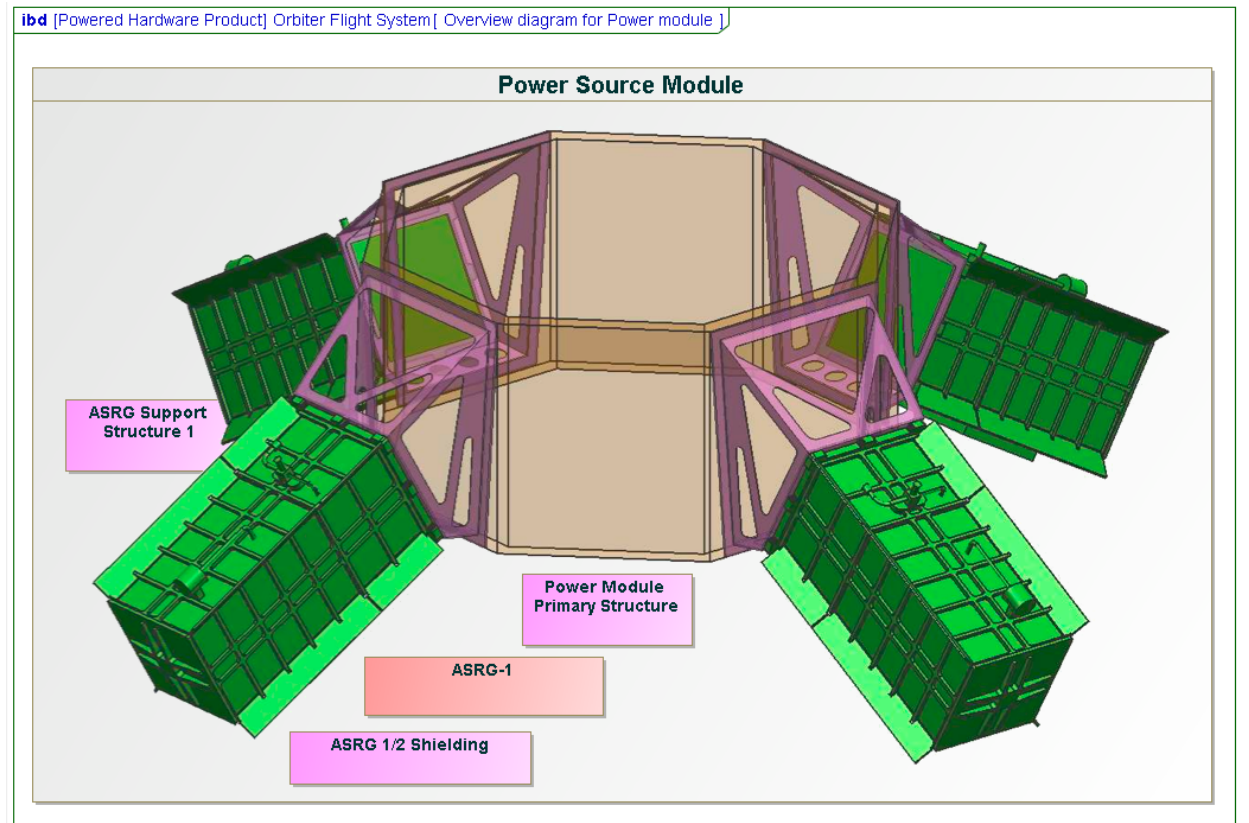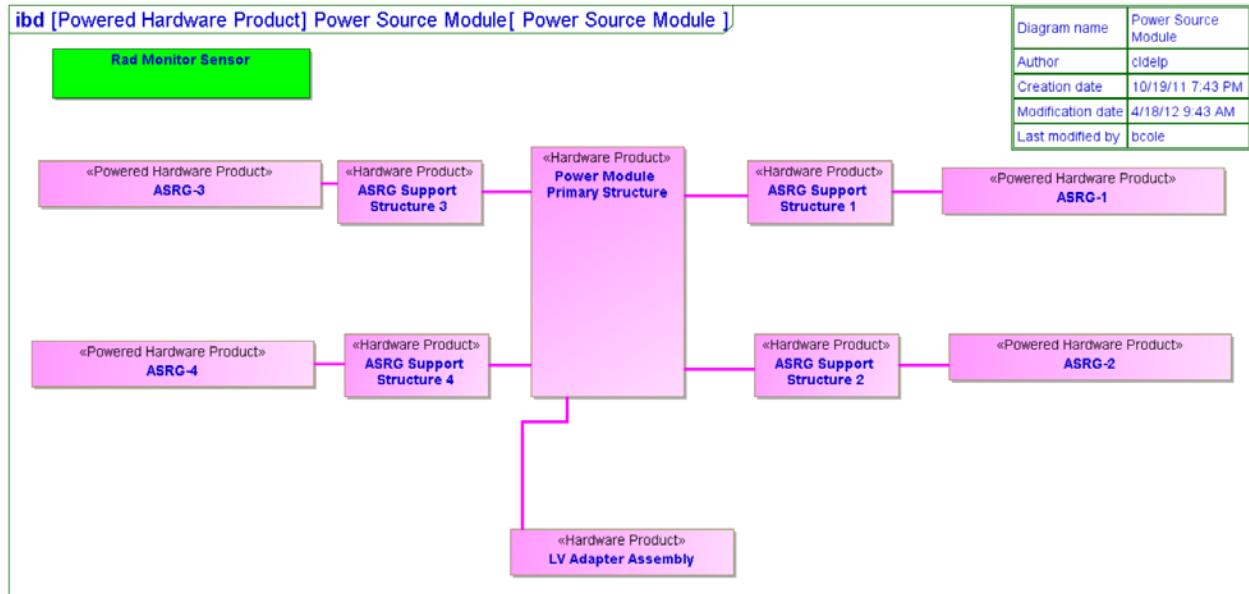
Figure B.2.7-18. Power Source Module block diagram as represented in the system model.

Module. The power subsystem electronics provides the power bus regulation.

Power Source Drivers

The key performance drivers for the power source are:

1. Provide 396 W at EOM after a single Stirling engine failure. (Each ASRG has two Striling engines)
2. Provide a constant power over the nominal power bus voltage operating

range of 22 to 34 V as defined at the power source output.

3. Survive with a power bus voltage over the 34 V and less than 40 V for an indefinite period of time.

4. Provide a diminished power for the power bus voltage less than 22 V to support a bus overload recovery.

The power source is the combined contribution of four ASRGs.

B.2.7.5.2   ASRG

ASRG Functional Description

Each ASRG (Figure B.2.7-19) consists of two General Purpose Heat Source (GPHS) modules, two ASRG Stirling converters (ASCs), a generator housing assembly (GHA), a shunt dissipater unit (SDU), and an ASC controller unit (ACU).

The GPHS contains plutonium dioxide fuel pellets and is designed to meet all necessary safety and handling requirements. The GPHS produces a range of 244 Watts thermal (Wt) to 258 Wt at encapsulation when the fuel mixture is set in the pellet and placed in the module. From the point of encapsulation, the GPHS thermal output degrades with the radioactive decay rate of plutonium-238, which is approximately 0.8% per year. The study team is assuming that the average GPHS encapsulation will be 3 years before launch.

The ASC converts the thermal energy from the GPHS to AC electrical current using a piston and linear alternator. The ACU rectifies the AC power to DC power and provides it to the power bus with a constant power I-V curve over the power bus voltage range controlled by the spacecraft. The constant power I-V curve
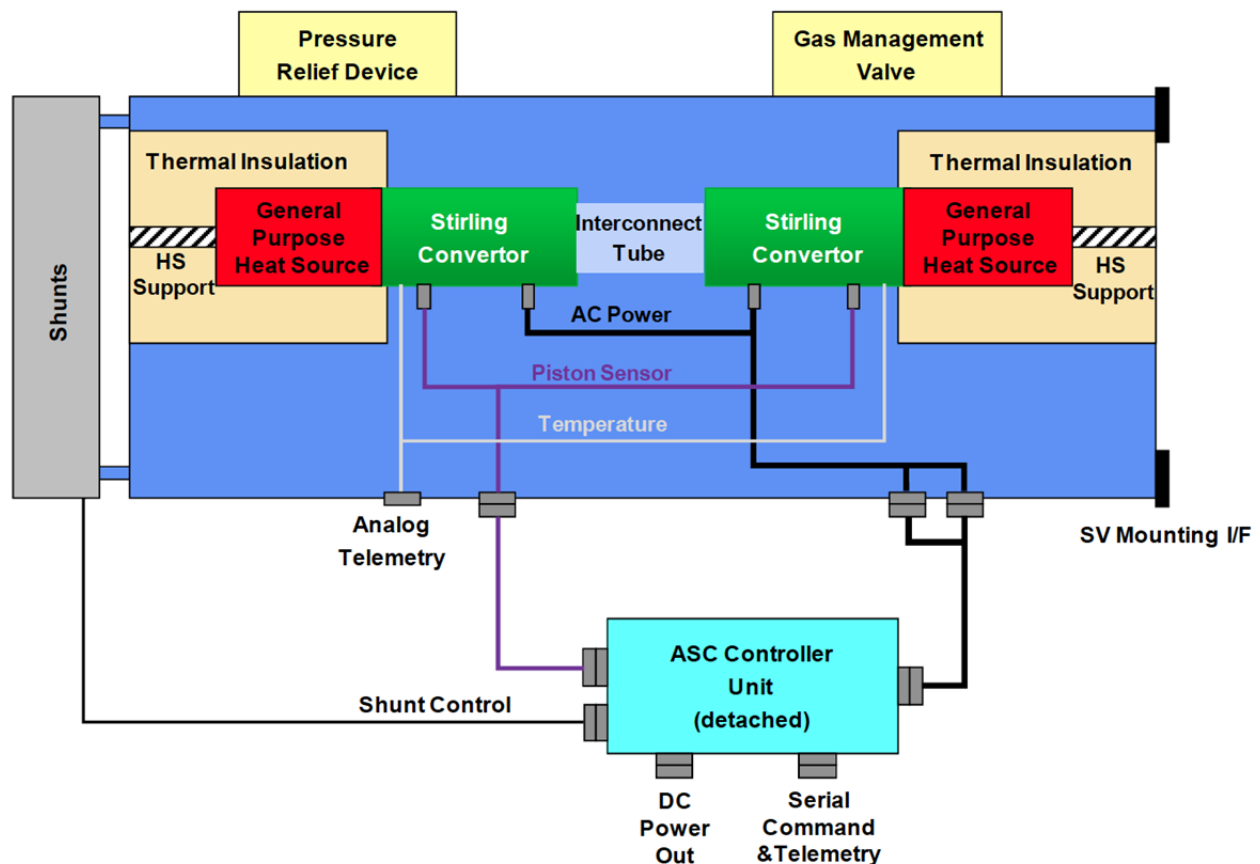
Figure B.2.7-19. The ASRG block diagram includes all functional elements that make up the ASRG, with the detached controller that provides the electrical interface with the spacecraft [HS=Heat Source].
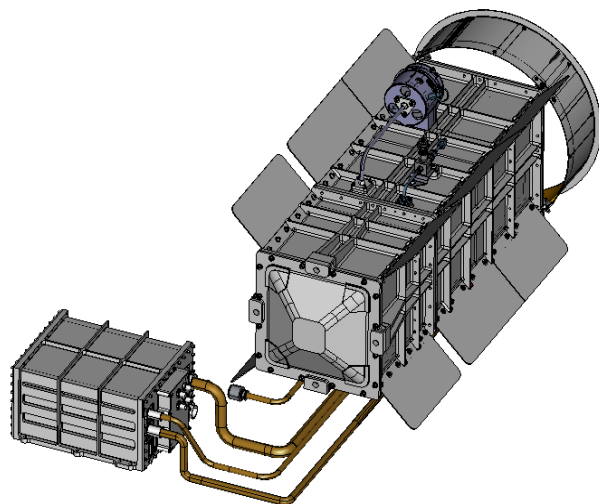
Figure B.2.7-20. ASRG CAD model shows the detached controller with cabling and outboard shunt radiator.

allows for more than one ASRG to be connected to the same power bus and share the power.

The ASRG protects itself if the bus voltage goes outside of the specified range of 22–34 V at the ASRG output. The ACU disengages the output from the power bus and shunts the power to the attached radiator if the bus voltage exceeds 35 V ±1 V. The internal ASRG shunt regulator is independent of the spacecraft shunt regulator used to regulate the power bus. The ASRG shunt radiator is on the outboard end of the GHA and is used only for the off-nominal bus voltage. The power system maintains the bus voltage range at less than 34 V at the ASRG interface to prevent the disengagement. The ASRG reengages once the bus voltage drops back into the range. The ASRG provides a current limited to 3.5 A if the bus voltage drops below 22 V, enabling the system to recover by charging the battery.

The ACU is detached from the GHA (Figure B.2.7-20) and mounted on the inside of the Power Source Module primary structure.

The ACU is single-fault-tolerant with N+1 architecture (Figure B.2.7-21). The ACU needs to be within 3 meters due to impedance constraints from the controller. The ACU also
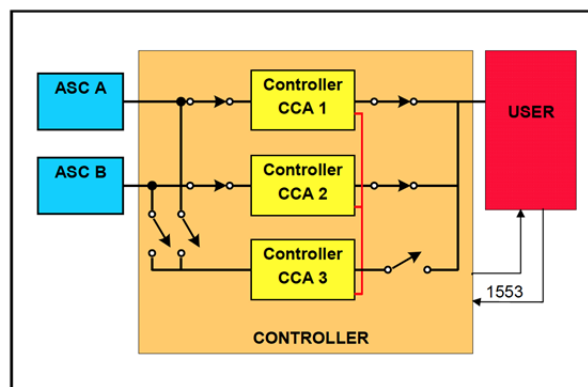
Figure B.2.7-21. ASC controller unit block diagram shows the spare controller # 3 that the internal fault protection switches to with the detection of a failure.

needs to be greater than 1 meter away to reduce self-generated radiation levels.

The ACU has internal fault protection to switch automatically to the spare controller board with the detection of a fault. ACU components are currently rated to 50 krad (radiation design factor of 2) total end of mission dose and would need significant additional shielding for use in the Europa Orbiter Mission environment. This additional shielding is included in the system level mass rollup.

B.2.7.5.2.1   ASRG Performance

The ASRG output power is a function of time and environment. The power graphs below show power output of the four ASRGs, with degradation due to natural decay of the plutonium dioxide fuel as a function of time from encapsulation, and assuming each GHA has a direct view to space (Figure B.2.7-22). The total power current best estimate (CBE) is with the nominal specified GPHS thermal output of 250 Wt at encapsulation. The total power specification is from the ASRG user guide with a BOM power at 130 W, failure of a single Stirling converter after launch, and 1% degradation per year. The lowest expected value (LEV) is with the minimum specified GPHS thermal output at 244 Wt at encapsulation, 1% degradation per year, and failure of a single Stirling converter after launch. The main difference between the Department of Energy
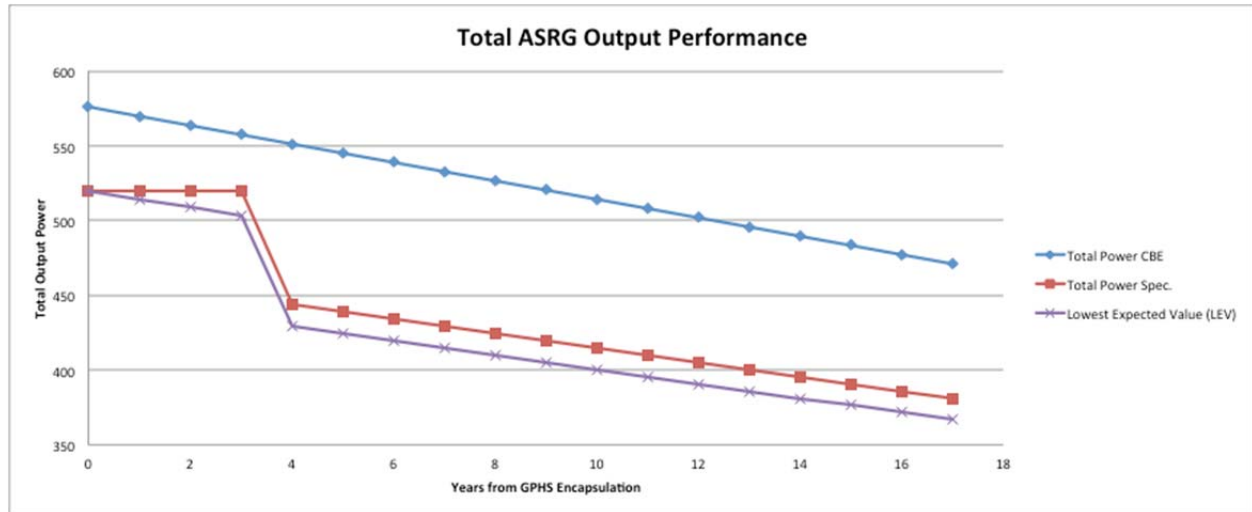
Figure B.2.7-22. From the comparison of the ASRG Output CBE to the specification and the LEV with a failure after launch, the LEV degrades performance from GPHS encapsulation; however the specification defines BOM after launch and degrades from that point on.

(DOE) specification and the Europa Study Team's LEV is that the study team chose to start the 1% degradation per year 3 years prior to launch at the average GPHS encapsulation date. With the Europa Orbiter Mission duration at 11 years, the study team expects at least 396 W at EOM.

The curve above assumes a direct view to space with a sink temperature equivalent to 4 K. The power output graph below shows the degradation as the sink temperature increases due to the environment (Figure B.2.7-23).

The spacecraft configuration uses the high-gain antenna and thermal blanket envelope to shade the ASRGs from the Sun within 1 AU. For the changing environment of launch, inner cruise, and Venus gravity assist, a command is sent to the ASRG to adjust the internal operational set point to make sure the ASRG is safe from over temperature which will impact the output power. This operation is independent of the power bus voltage set points controlled by the spacecraft. The spacecraft has adequate power margin for the expected environmentally impacted mission phases. The operation of the ASRG is covered in the ASRG Users Guide.
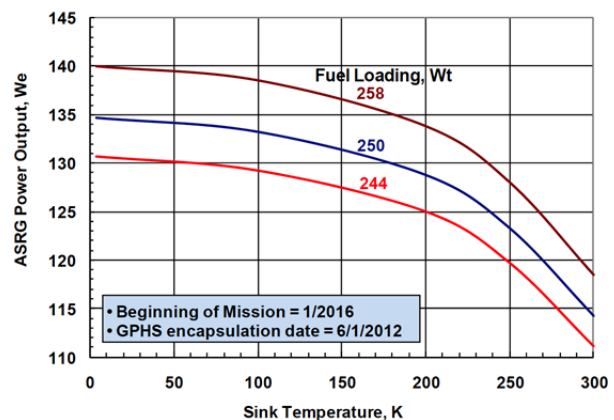
Figure B.2.7-23. ASRG output power vs. sink temperature shows that depending on the environment the output power will degrade. The ASRG power output power will depend on the view to space.

B.2.7.5.3   Structure/LVA

The four ASRGs and their avionics reside would on the Power Source Module (Figure B.2.7-24). The Propulsion Module's main engine assembly passes through the center but does not directly attach to the Power Source Module's primary structure.

Each ASRG has two opposing and cycling advanced Stirling converter (ASC) pistons. Because they oppose each other, vibration is greatly reduced. If one of these pistons failed to function, the single piston's vibration could
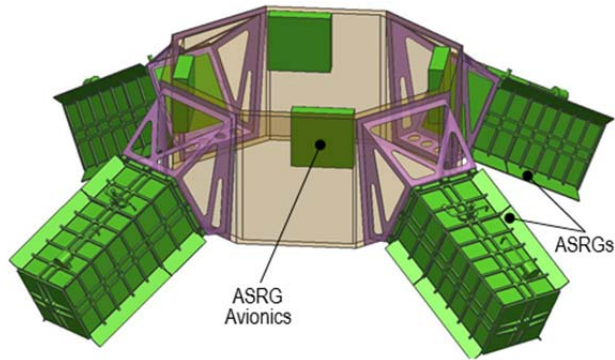
Figure B.2.7-24. Power module.

couple into the structure and imparted large loads on the spacecraft.

In the event of a failed ASC piston, the interface makes use of compression spring assemblies oriented parallel to the long axis of the ASRG. These spring assemblies provide a compliance that yields a 20-Hz axial frequency. At 20 Hz this spring mass system will not couple in with the ASC's frequency of 102 Hz. While the interface is designed to be compliant (20 Hz) axially, the stiffness is still high enough to ensure positive margin for the springs stress when exposed to ASRG launch accelerations.

Because the Power Source Module is the bot-

tommost module, it will experience the largest moment loads during launch. This will require its primary structure to have a slightly greater wall thickness than the propulsion and Avionics Modules.

At the bottom of the Power Source Module is the launch vehicle adapter (LVA, Figure B.2.7-25). The LVA provides for a transition between the octagonal geometry of the Power Source Module and the circular Marmon clamp separation interface.

B.2.7.6   Avionics Module

The Avionics Module concept results in radiation shielding that enables the use of standard aerospace industry radiation-tolerant parts.

The Avionics Module will be described in this section of the report. After an overview of the module, the following subsystems included in the Avionics Module will be discussed:

- Telecom
- Power
- Guidance, Navigation, and Control
- Command and Data Handling
- Software
- Structure, along with instrument accommodation
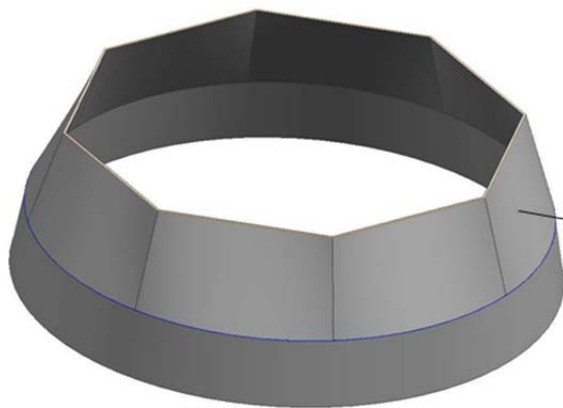
Figure B.2.7-25. Launch vehicle adapter.
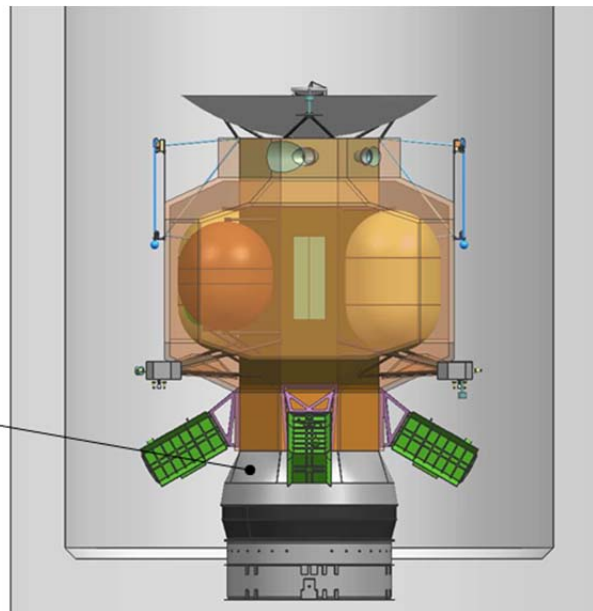
Avionics Module Overview

The key design goals for the Avionics Module are:

- A modular design for parallel integration and test with propulsion and Power Source Modules

- A vault to shield a majority of the spacecraft electronics

- Enabling of late integration of instruments

- Simple interfaces with Propulsion and Power Source Modules

Figure B.2.7-26 shows the configuration of the Avionics Module. This module consists of three separate sections: the telecom section, the upper equipment section, and the vault section.

Figure B.2.7-27 shows the system block diagram of the Avionics Module. The red interfaces are 28-V power; the blue interfaces are data; and the gold interfaces are RF.

Inside the vault are the C&DH electronics (this box is internally redundant), the RWA electronics, the power electronics (this box is internally redundant), the pyro/propulsion drive electronics (this box is internally redundant), two block-redundant IMUs, and two block-redundant small deep-space transponders (SDSTs). Outside the vault are the instruments (MAG, LP, MC and LA) and science electron-

Figure B.2.7-26. The three sections of the Avionics Module (telecom, upper equipment, and vault) are configured for simple interfaces to enable parallel integration and test.

ics chassis. Also outside the vault are the following GN&C components: RWA mechanical assemblies, Sun-sensors, and SRUs. All the elements outside the vault are individually shielded for total-dose radiation; in the case of instrument and star-tracker detectors, the shielding also mitigates the effect of the electron flux. The Power Subsystem components outside the vault are the shunt radiator and battery (internally redundant). The Telecom Subsystem components outside the vault are the TWTAs, the coax, the waveguide, switches, and antennas configured in a single-fault-tolerant configuration for Ka-band and X-band communication.
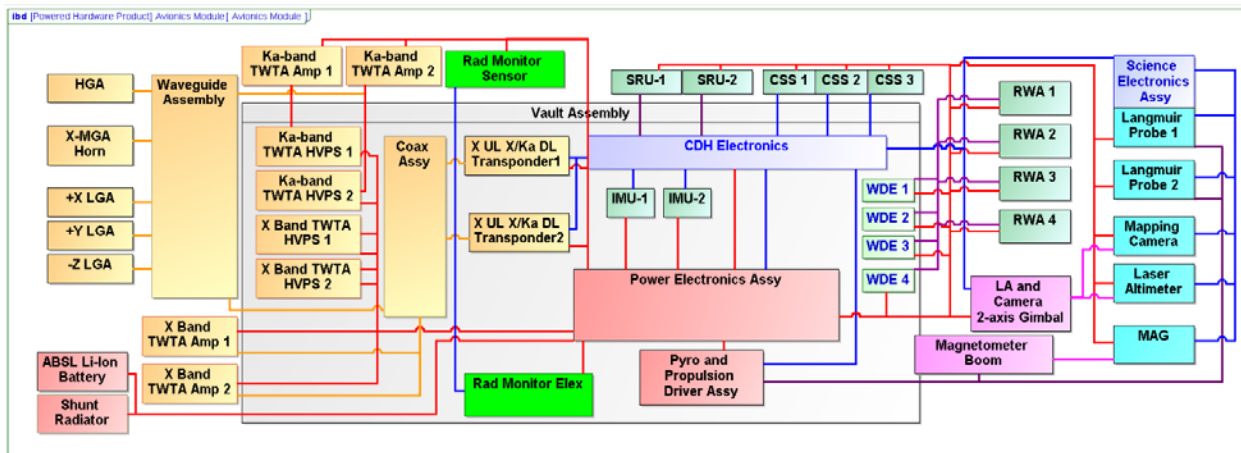
Figure B.2.7-27. The system block diagram shows a majority of the spacecraft electronics protected in the vault.

B.2.7.6.1   Telecom Subsystem

The telecom subsystem performs a triple role for the spacecraft: two-way communications with Earth, Earth-to-spacecraft ranging to support navigation as well as precision Doppler velocity measurements for Gravity Science.

B.2.7.6.1.1   Driving Requirements

There are a number of driving requirements for the subsystem. It must accept uplinked commands through all post launch mission phases as well as send to Earth engineering telemetry and science data. Key data rates required are

- Engineering telemetry: ~2 kbps
- Uplink commanding: ~1 kbps
- Safe mode commanding: ~7.8 bps
- Safe mode telemetry: ~10 bps
- Science data return: ~108 kbps

Implicit in these requirements is communications with the Deep Space Network (DSN) 34-m subnet for routine communications and the 70-m subnet for emergency/safe mode communications.

For Gravity Science, the Telecom System must meet a residual Doppler velocity requirement of 0.1 mm/sec at 60 second integration times. This is met through the subsystem's nominal two-way coherent communications mode through the HGA and the use of the DSN's 34m subnet.

The telecom subsystem is also required to be single-fault-tolerant. This drives the telecom subsystem architecture to include redundant transponders (small deep-space transponders [SDSTs]), redundant X-band and Ka-band travelling-wave tube amplifiers (TWTAs), a complex waveguide transfer switch (WTS) network, as well as a set of low- and medium-gain antennas. One X-band low-gain antenna (LGA) and the medium-gain antenna (MGA) are tolerant of a single WTS failure. Even though there is a single High Gain Antenna (HGA), the HGA features the capability of two

downlink polarizations for fault tolerance to a single failure in the telecom subsystem's transmitter/receiver hardware chain.

B.2.7.6.1.2   Subsystem Features

The implementation of the telecom subsystem includes X-band uplink and downlink capabilities as well as a Ka-band downlink. The Ka-band downlink enables the mission to meet science data volume requirements concurrently with stringent requirements for DC power. While the downlink data volume requirements could be met with X-band alone (assuming a much more powerful X-band TWTA), a trade study between available DC power and science data volume return informed the selection of a more DC-power-efficient architecture for high-rate science data. For the Europa Orbiter Mission, the use of Ka-band for high-rate science downlink directly reduces the number of ASRGs required to meet mission objectives.

The telecom subsystem features a 3-m-diameter X/Ka-band high-gain antenna (HGA), three LGAs, an MGA with dual polarizations, redundant 25-W (RF power) Ka-band TWTAs, redundant 20-W (RF power) X-band TWTAs, redundant SDSTs, and a complement of microwave waveguide and coax elements. The SDSTs are X-band uplink and downlink capable as well as Ka-band downlink capable. There is no capability or driver for Ka-band uplink.

B.2.7.6.1.3   Block Diagram

As shown in the telecom subsystem block diagram (Figure B.2.7-28), the equipment configuration is based upon many years of deep-space communications heritage. For example, the -Z LGA is fault-tolerant to a single WTS failure; this provides a robust fault-tolerance posture for communications during the inner-cruise portion of the mission when the spacecraft is required to use its HGA as a sunshield. The LGA configuration enables communications through all cruise periods out to approximately 2 to 3 AU from Earth after which the MGA takes over the safe-mode and
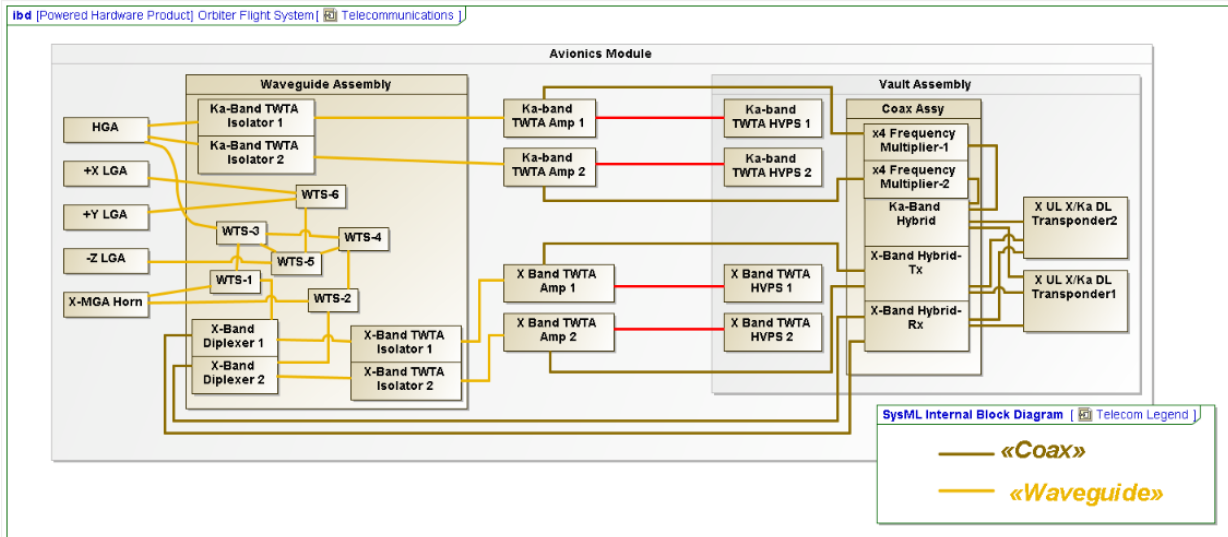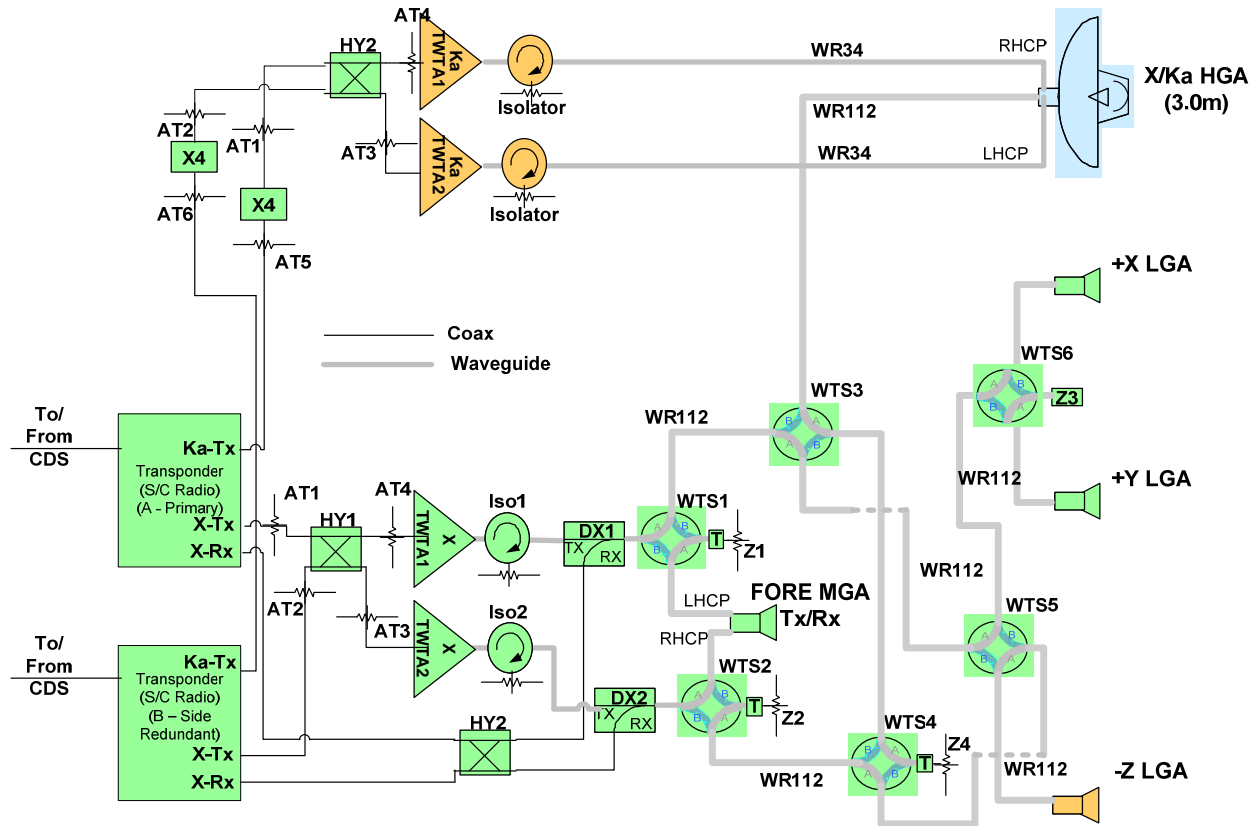
Figure B.2.7-28. The telecom subsystem provides robust fault-tolerance through a simplified architecture that minimizes potential for single-point failures.

general cruise communications. Ka-band downlink redundancy is provided through the use of redundant hardware chains and downlink antenna polarizations. This simplified architecture promotes a more robust system

fault-tolerance than could be achieved with the inclusion of an additional WTS to switch between the redundant downlink TWTAs. Similarly, for the X-band uplink an RF hybrid is used (HY2) in place of a WTS. This alone eliminates a potential single-point failure in

the critical X-band uplink path. Similarly the MGA has dual polarizations that enable single fault tolerance safe mode communications at Europa. Overall the Telecom Subsystem presents a robust fault tolerance and presents a low risk posture for the mission.

B.2.7.6.1.4   Equipment Heritage

Hardware heritage comes from a number of previous missions. The HGA will be similar to the Juno HGA, but scaled up from Juno's 2.5-m-diameter HGA to 3 m. The Europa Orbiter Mission's HGA will leverage technology developed for the Juno HGA reflector (Figure B.2.7-29) to meet the surface-tolerance requirements for precision Ka-band pointing and efficiency.

The Juno HGA optics will be redesigned to improve Ka-band performance for the Europa Orbiter's high-rate downlink communications requirements.

The TWTAs have heritage from multiple JPL missions: Juno, Dawn, and MRO (X-band) and Kepler (Ka-band). A good example here is the X-band TWTA for the Dawn mission, shown in Figure B.2.7-30. We propose to leverage a long history of downlink TWTAs designed specifically for the requirements of deep-space missions.

The concept proposes to use the SDST, a very mature product, to provide the mission-critical uplink and downlink function. The SDSTs have heritage from Juno (X/X/Ka-bands), Dawn (X-band), MRO (X/X/Ka-bands), MSL (X-band), Kepler (X/X/Ka-bands), and others. A candidate SDST, flown recently on the Dawn mission, is shown in Figure B.2.7-31. Due to the extensive heritage inherent in the SDST product line, the use of the SDST lowers the overall residual mission risk.

B.2.7.6.1.5   Characteristics and Sizing

The telecom subsystem downlink data rate must be at least 108 kbps during Europa science operations. The telecom link budget is designed to meet this requirement with the parameters shown in Table B.2.7-4.

The HGA is body-fixed to the spacecraft and requires a ≤1-mrad pointing accuracy to meet
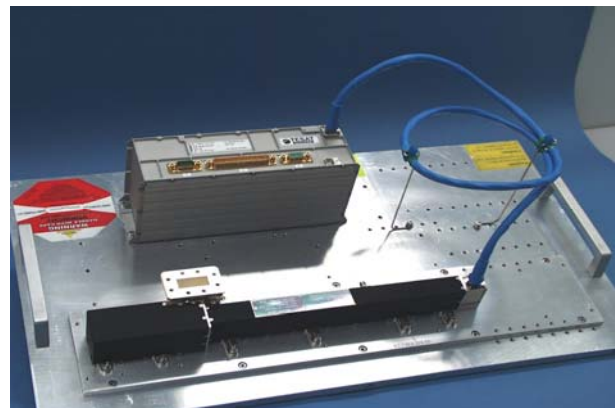
Figure B.2.7-30. Candidate X-band TWTA (flown on MRO, MSL, and Dawn).

Figure B.2.7-29. Juno's 3-m HGA (X/Ka-band) provides the basis for the Europa HGA.

Figure B.2.7-31. The SDST product line provides the mission-critical communications link to Earth.

Table B.2.7-4. Telecom link budget.

Parameter	Required Capability	Notes
Throughput Rate (worst case)	108 kbps	Average = 1.2 × worst case
Gravity Science Residual Doppler	≤0.1 mm/sec @ 60 second integration	Met with Two-Way Coherent Mode
TWTA RF Power	25 W (Ka), 20 W (X)	2× for Power Dissipation
HGA Diameter	3.0 m	Body fixed HGA, 60% efficiency
HGA Pointing Error	≤1.0 mrad	Reaction-wheel control
DSN Weather	90% cumulative dist.	
Canberra Elevation	20°	Worst-case, fixed
Earth S/C Range	5.5 AU	Average mission design
Hot Body Noise	16 K	About 0.6 dB loss
Turbo Coding	Rate=1/6, 8920-bit frame	
TWTA to HGA Losses	2 dB	Conservative estimate
Link Margin	3 dB	Per Institutional guidelines
SEP Angle	20°	Worst-case assumption
Operational Configuration	X-band up, Ka-band down	X-band downlink for safe mode & cruise
Hardware Configuration	X-band up, X/Ka-band down 3 LGAs, MGA, HGA, TWTAs	Possible X-band SSPA in lieu of TWTA

communications throughput requirements. A conservative approach was taken with the telecom link by requiring 3 dB margin minimum and by making conservative estimates of individual contributors to the link. Parameters such as RF losses in the downlink path, DSN station performance due to low station elevations, link degradation at low Sun–Earth pointing (SEP) angles and Jupiter's hot-body noise at Ka-Band are all taken into account. Overall, the X-band and Ka-band communications links are conservative and robust.

The LGA complement provides full 4π-steradian coverage; this enables command uplink at any spacecraft attitude. Spacecraft communications during the inner cruise portion of the mission (<1 AU solar distance) use a single-fault-tolerant LGA (-Z LGA). The distances to Jupiter, however, prevent LGA communications at the required safe mode rates. To meet safe mode communications rate requirements, an MGA is needed. All high-rate communications are performed through the HGA. Turbo coding at rate = 1/6 is also part of the baseline communications architecture.

B.2.7.6.2 Power

The Orbiter Power subsystem electronics and energy storage provide the power bus regulation and distribute power to the loads.

B.2.7.6.2.1 *Power Performance Drivers*

1. Single-fault-tolerance.
2. Provide energy storage mission load profile.
3. Provide power bus regulation.
4. Provide battery charge control.
5. Distribute power to the loads.
6. Actuate valves.
7. Fire pyro events.

B.2.7.6.2.2 *Power Subsystem Description*

The power subsystem electronics regulates the power bus and distributes power to the loads on the spacecraft. The power subsystem will provides energy storage to cover the transient load profiles of the different Orbiter Mission scenarios. It is single-fault-tolerant, using a combination of block-redundancy with cross-strapping and some majority-voted functions. It provides the valve-drive and pyro-firing functions with range and mission safety inhibits for the hazardous functions.

The power subsystem consists of an ABSL Li-ion battery, a shunt radiator, a shunt driver slice (SDS), two multimission power switch slices (MPSSs), two power bus controllers (PBCs), two power converter units (PCUs), two pyro-firing cards (PFCs), and four propulsion drive electronics slices (PDEs) (Figure B.2.7-32).
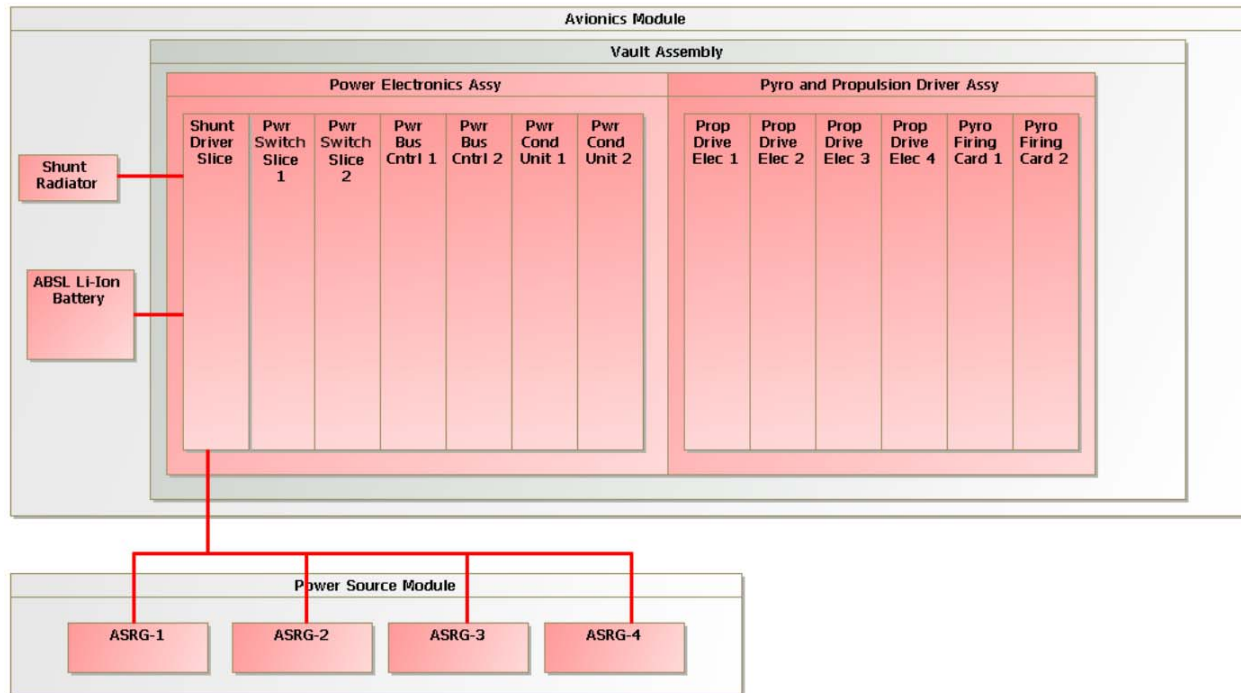
Figure B.2.7-32. Power subsystem block diagram is captured in the SysML model. The figure shows that the battery and shunt radiator are outside the vault.

B.2.7.6.2.3 Power Control

The PBC slices provide the SpaceWire command interface to C&DH. The PBC provides a low-power serial data bus to all of the other power electronics slices. It converts the commands from C&DH via the SpaceWire interface and distributes them to other slices through the low-power serial data bus. The PBC collects the power subsystem telemetry and makes it available to C&DH via the SpaceWire interface.

The PBC contains the control algorithms for regulating the power bus by commanding the shunt switches in a shunt regulator. The ASRG power source has a constant power I-V curve over a power bus voltage range of 22 to 34 V at the ASRG output. The control function senses the current in the battery and adds or subtracts shunt current to limit the battery charge current to a C/5. The PBC commands discrete shunt driver switches in the SDS that drive power to the shunt radiator to control the power bus. The current regulation will taper to 0 current at the voltage set point correlating to the desired state of charge. Power analysis uses 32.8 V as the 100% state of charge for the selected Li-Ion battery technology. The PBC has several commanded set points to set the battery at the desired state of charge.

The energy storage technology used for this study is the same small-cell ABSL Li-ion battery used on the Soil Moisture Active Passive (SMAP) mission (Figure B.2.7-33). The battery is configured with eight cells in series to get the desired bus voltage operating range, and 52 cells in parallel to get the desired 59 Ah of energy storage at the beginning of life. It has a capability of 40 Ah at EOM after a single-string failure, including degradation for life, discharge rate, and operating temperature. The reference scenario that defines the energy storage for the Orbiter Mission is the 2-hour JOI, which requires 13 Ah at 10°C with a 6.5-A discharge rate. The JPL Design Principles (DPs) allow for a 70% depth of discharge (DOD), making a 19-Ah battery adequate for the Orbiter Mission (JPL 2010a).
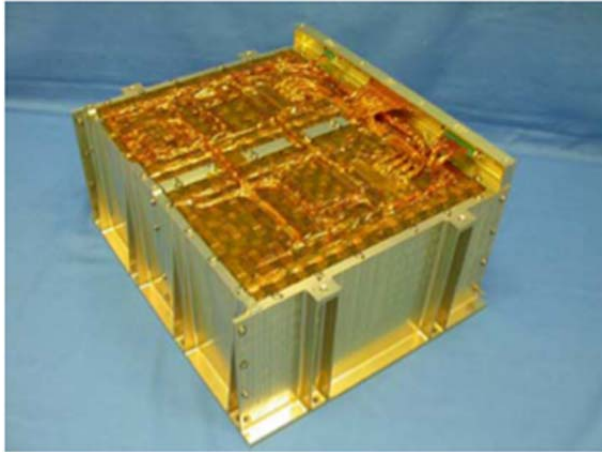
Figure B.2.7-33. Small-cell ABSL reference battery is the same size as the SMAP battery configured with 8 cells in series and 52 strings in parallel (Model Number 8S52P).

The small-cell battery approach does not implement individual cell monitoring and balancing due to the matched cell behavior; however, a trade between the large cell with cell balancing and the small cell needs to be studied for this lifetime. This will be considered in Phase A.

B.2.7.6.2.4　　Power Distribution

The power distribution function is a combination of centralized power switches in the MPSS and distributed power switches on the primary side of each PCU. This combination enables the system to optimize the mass of the cabling by using centralized switches for heater buses and other loads that do not require a PCU and distributed switches for each PCU, reducing the point-to-point cabling for the major subsystems. The slice packaging approach enables the addition of centralized power switches while impacting only the mechanical footprint and cabling without modifications to a chassis or backplane. The command and telemetry interface is handled by the addition of addresses on the serial bus implemented in cabling. The thermal interface scales with the mechanical footprint.

Independent high- and low-side switches prevent any single failure from resulting in a stuck-on load. Commanding is cross-strapped

to the power switches through each PBC such that no single failure will prevent the commanding of any power switch. Each set of load switches is part of the load fault-containment region regardless of the location as a centralized or distributed switch.

B.2.7.6.2.5　　Power Conversion

The power conversion function for each subsystem uses a distributed point of load (POL) architecture (Figure B.2.7-34). The approach has a single isolated power converter on the PCU board, providing an intermediate power bus voltage that is distributed to each subassembly in the subsystem. The front end of each subassembly can cross-strap the intermediate power bus and provide on and off capability with fault protection to enable low-power operating modes and improve subsystem fault-containment regions. The primary side power switch is controlled by the power subsystem, and the POL regulators are commanded by the subsystem.

B.2.7.6.2.6　　Pyro Firing and Valve Drive

The pyro-firing and valve-drive functions are provided by a set of centralized power switches in the power subsystem electronics commanded by C&DH via the PBC. The PFCs are fail-safe off, with two cards providing the block-redundancy. Each PFC fires 32 NASA Standard Initiators (NSIs) from a protected load power bus that provides all of the safety inhibits required for launch. The PFC controls the current into each NSI, with an overall capability to fire six simultaneous events.

The PDE actuates the valves for the main engine and the ACS thrusters. The PDE also switches power from the protected load bus with the necessary safety inhibits in place. The PDE is fail-safe off with the single-fault-tolerance provided by a block-redundant set.

B.2.7.6.2.7　　Power Subsystem Heritage

The power subsystem uses the same architecture as SMAP, and many of the slice designs are the same. The power bus control algorithm
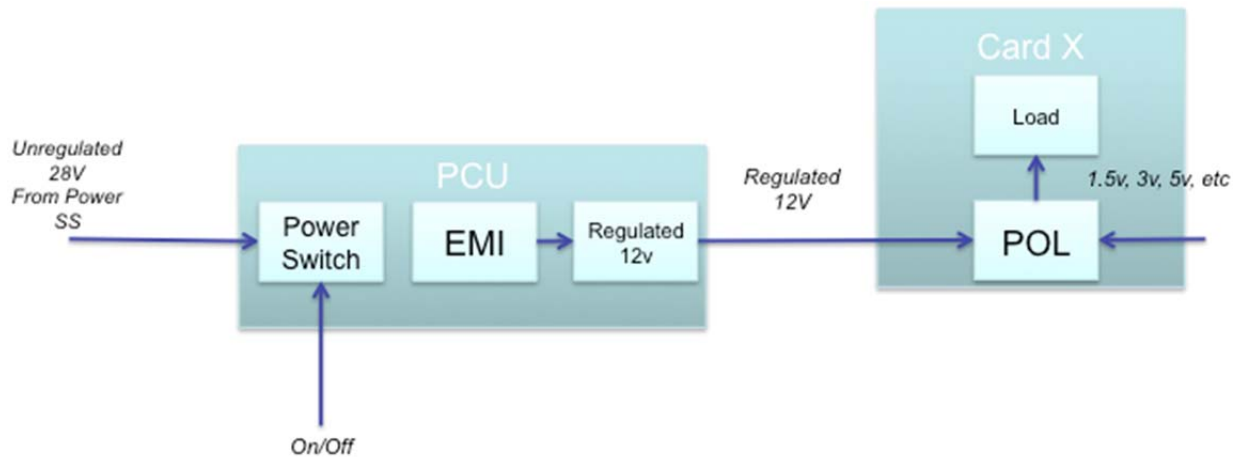
Figure B.2.7-34. POL power conversion architecture shows the primary power bus interface with distributed switch controlled by the power subsystem. The distributed POL converters are controlled by the local subsystem.

is the same as used on SMAP, as is the slice packaging design and designs for the PFC and PDE. The MPSS is the high-side and low-side variant of the design used on SMAP. The PBC has a new command interface, but the control of the shunt regulator is the same as for SMAP. The ABSL battery is the same design as used on SMAP, and the cell technology has flight heritage with Kepler.

B.2.7.6.3   Orbiter Guidance, Navigation, and Control (GN&C)

The Orbiter GN&C provides a stable platform for science data collection and telemetry transmission.

Functional Drivers

The GN&C subsystem provides three-axis attitude control through all mission phases to meet the instrument and engineering pointing needs. During TCMs, EOI, or JOI, when the fixed main engine is used, the GN&C provides thrust vector control using dedicated TVC thrusters mounted on the thruster clusters. During Europa orbital science, the spacecraft points the HGA towards Earth to downlink the science data/perform gravity science while using a two-axis gimbal to nadir point the LA/MC.

Features

The C&DH subsystem hosts GN&C software, which is developed in a GN&C design and simulation environment. The RWA, IMU, and

SRU are heavily shielded from radiation, allowing the use of standard space products. The SRU head with detector is shielded to reduce the electron/proton flux so that 4th magnitude and brighter stars can be tracked. The Europa Study team analyzed attitude determination capabilities in the Europa environment and demonstrated a pointing-knowledge capability exceeding the requirements for HGA pointing. All known targets will be stored onboard, enabling ephemeris-based tracking; Cassini experience indicates that this reduces the operation complexity. Finally, the use of thrusters for TVC reduces the development cost for a gimbaled engine and reduces the number of unique interfaces on the vehicle.

Key Characteristics

Table B.2.7-5 shows the key characteristics of the GN&C subsystem. The RWA sizing of 25 Nms is driven by environmental momentum accumulation. This was sized based on vehicle inertias and a desaturation rate of twice per day. Figure B.2.7-35 shows the thruster configuration. The attitude-control thruster sizing of 4.45 N provides a sufficiently small minimum torque impulse for deadband attitude control during interplanetary cruise (or safe mode). The TVC thruster sizing of 40 N provides sufficient control authority for up to a 9-centimeter shift of the vehicle center of mass

Table B.2.7-5. The GN&C subsystem design provides an agile platform with precise pointing control.

Item	Value	Sizing
RWA Momentum	25 Nm	Handle gravity gradient momentum accumulation
Attitude-Control Thruster Size	4.45 N	MTIB for deadband control during cruise/safe mode [spell out, as in FB chapter]
TVC Thruster Size	40 N	TVC control for CM offset
Ka Pointing	1 mrad	Support HGA link budget at required data rate with 3 dB of margin
X Pointing	112 mrad	MGA communication while Sun-pointing
LA Pointing Knowledge	1.7 mrad	Pointing knowledge induced altitude error, derived from science traceability requirement
MC Pointing Knowledge	5 mrad	Mapping strip alignment, 1% of FOV

during the mission. Ballast mass is also included in the MEL to provide initial CM/CG alignment. For attitude control and TVC, a thrust-moment arm of approximately 2 meters is used.

The 1-mrad pointing is a radial, three-sigma number derived from the telecom link analysis. Based on error budget analysis of the inertial and stellar reference assemblies in the expected radiation environment, this can be met with a capability of 0.25 mrad (per axis, three-sigma) pointing knowledge. The attitude knowledge is driven by the radiation capability of the SRUs. The X-band pointing for safe mode is 112 mrad based on a beam width that allows Sun-pointing with Sun-sensors while still communicating with Earth from Europa. The pointing knowledge to support laser altimetry is derived as an error budget allocation from the 10-cm accuracy requirement. The pointing knowledge to support surface mapping strip alignment is derived as an error budget allocation from the 1% FOV accuracy requirement.

Block Diagram

Figure B.2.7-36 shows the block diagram of the GN&C Subsystem. At the center of the
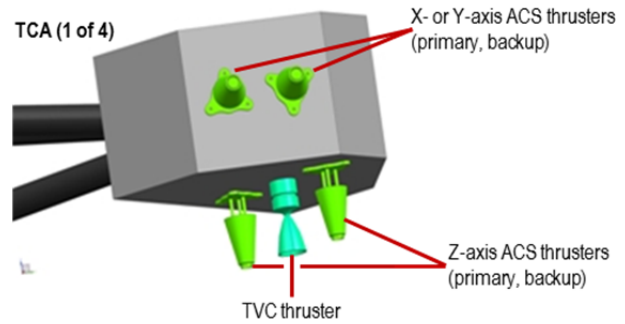
Figure B.2.7-35. The Orbiter thruster configuration leverages the proven Cassini approach.

subsystem is the FSW that resides in the RAD750 processor within the C&DH electronics. For Sun-pointing modes of operation, the Sun vector with respect to the vehicle reference frame is provided by the three Sun sensors distributed on the Avionics Module to provide near-4π steradian coverage; if there are any gaps in the coverage, a spiral scan attitude maneuver can quickly bring the Sun into a sensor's FOV. For precise attitude determination, a combination of inertial measurements corrected by stellar updates is provide by the IMUs in the radiation vault and shielded SRUs outside the vault.

For precision attitude control, three of four RWAs are used; these are desaturated as needed by the attitude-control thrusters. The RWA wheel-drive electronics are in the vault; mechanical assembly is outside the vault. For less precise attitude control during cruise or during safe mode, the attitude-control thrusters can be used. For attitude control during TCM, EOI, or JOI (when the main engine is fired), the TVC thrusters are used for pitch/yaw control, while the attitude-control thrusters are used for roll control.

The architecture is cross strapped such that any SRU can be used with any IMU to provide the attitude information to any computer. Attitude control can occur with any three of four RWA or with any set of 8 block-redundant thrusters.
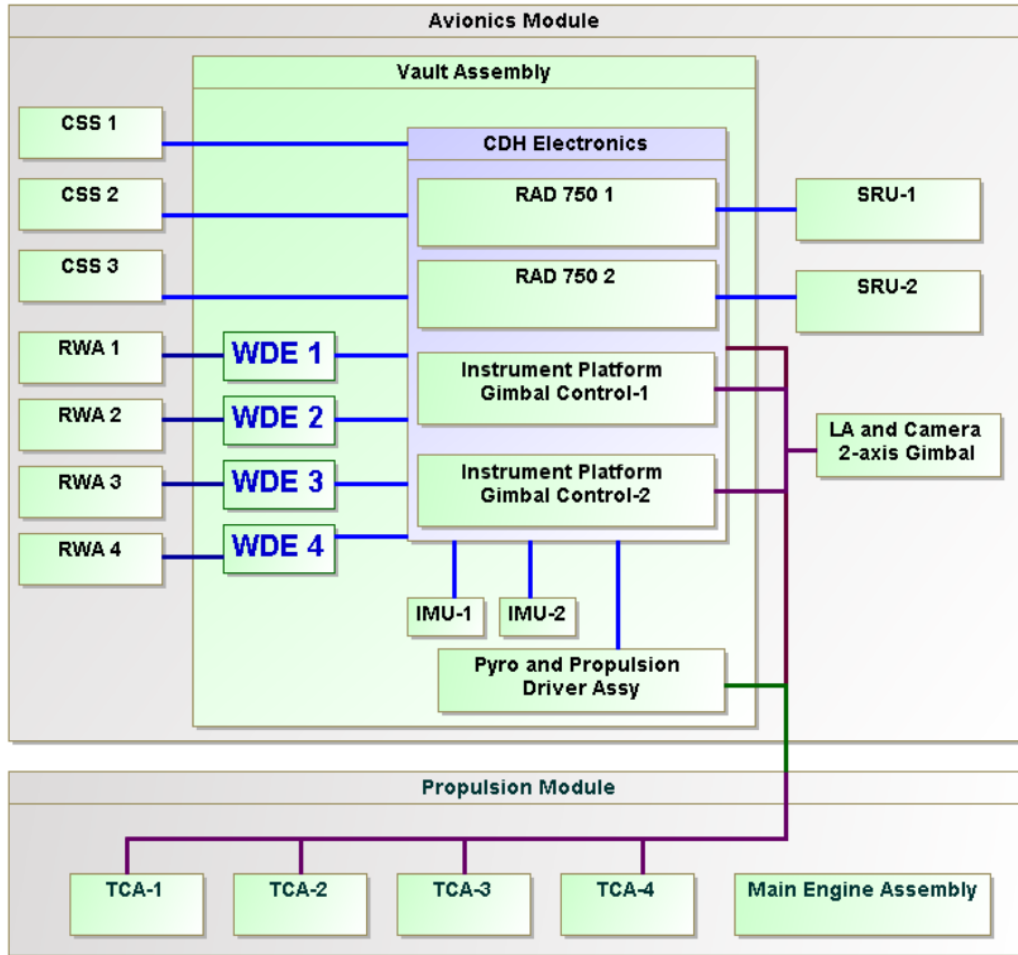
Figure B.2.7-36. The GN&C subsystem is redundant and cross strapped to provide robust fault tolerance to radiation events.

Heritage

Given the radiation shielding provided by the spacecraft, the GN&C subsystem can use standard space GN&C products with high TRL. Table B.2.7-6 shows the GN&C hardware items and the approach to deal with radiation.

B.2.7.6.4   Orbiter Command and Data Handling Subsystem

The Orbiter C&DH provides a cross-strapped and redundant radiation-hardened platform to support the data storage and processing needs of orbiter science.

Performance Drivers

The key performance drivers of the C&DH are as follows:

Table B.2.7-6. Standard high-TRL GN&C hardware ensures radiation shielding.

Item	Radiation Approach
RWA	Sensitive wheel-drive electronics in the vault Mechanical assembly radiation-hardened by design
Sun-Sensor	Radiation-hardened by design
Stellar Reference Unit	Shielding for flux and total dose
Inertial Measurement Unit	In vault

- The design should be single-fault-tolerant and cross strapped to enable the C&DH to fail operational.
- The design should allow swapping to enable rapid transition of control during a fault. A RAD750 single-board computer (see Figure B.2.7-37) was se-

lected to leverage the processor flight heritage, radiation hardness, and JPL's extensive experience with this processor.

- The onboard data storage should accommodate buffering science data for 1 missed DSN pass.

Features

The C&DH electronics box is a single box that is internally redundant. Given the use of SpaceWire (see Figure B.2.7-38) as the primary interface, there is no need for a backplane or motherboard within the box; this increases the C&DH box reliability. A standard-size chassis of a 6 U×220 mm cards was selected to enable the use of heritage single-board computers and to provide sufficient board area for the I/O and memory cards. Time broadcast and synchronization are part of the SpaceWire standard; therefore, no external timing network is required. The remote I/O handles all the low-level interfaces, such as analogs, discretes, and serial I/O; this I/O also provides the telecom interface, critical relay commanding, and processor swap functions. The I/O is multiplexed through the SpaceWire interface chip; this radiation-hardened chip includes an embedded processor to accommodate programmable I/O functions. The I/O circuits are standard designs from other JPL spacecraft. The RAD750 RAM provides 512 Mbits of storage using radiation harden RAM; this supports science data storage and program execution. The power-conditioning unit (PCU) takes in unregulated 28 V off the power bus, provides EMI filtering, and converts the power to a regulated 12 V that is distributed to each card in the box. The PCU on/off switch is controlled by the Power Subsystem. The local card on/off is software controlled via the processor and commands issued via the remote I/O.

Block Diagram

The system block diagram is shown in Figure B.2.7-39. This diagram shows the cards in the C&DH box. The box is internally redun-

Figure B.2.7-37. The RAD750 provides high heritage for both the C&DH electronics and FSW designs.
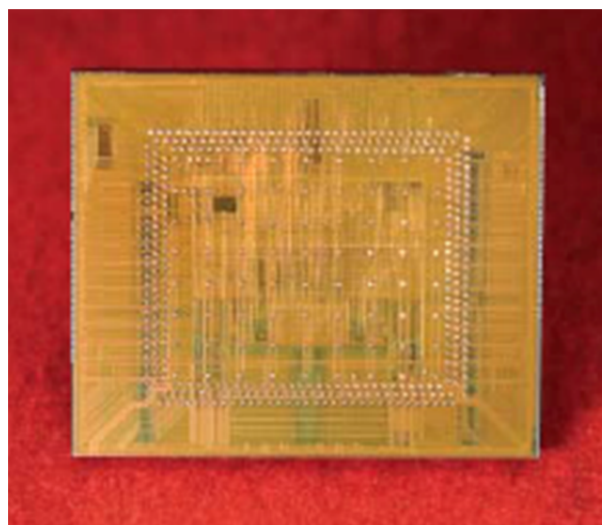
Figure B.2.7-38. The SpaceWire interface chip is radiation hardened and provides a high-speed standard interface to the cards in the C&DH.

dant and cross strapped (both data and power). SpaceWire supports multiple topologies (e.g., star or daisy chain). The box consists of two RAD750 single-board computers with a SpaceWire router, two remote I/O cards, and two PCUs. The remote I/O cards interface to the single board computer via SpaceWire. Hosted in the CDH chassis and using the PCU are the remote instrument electronics. This
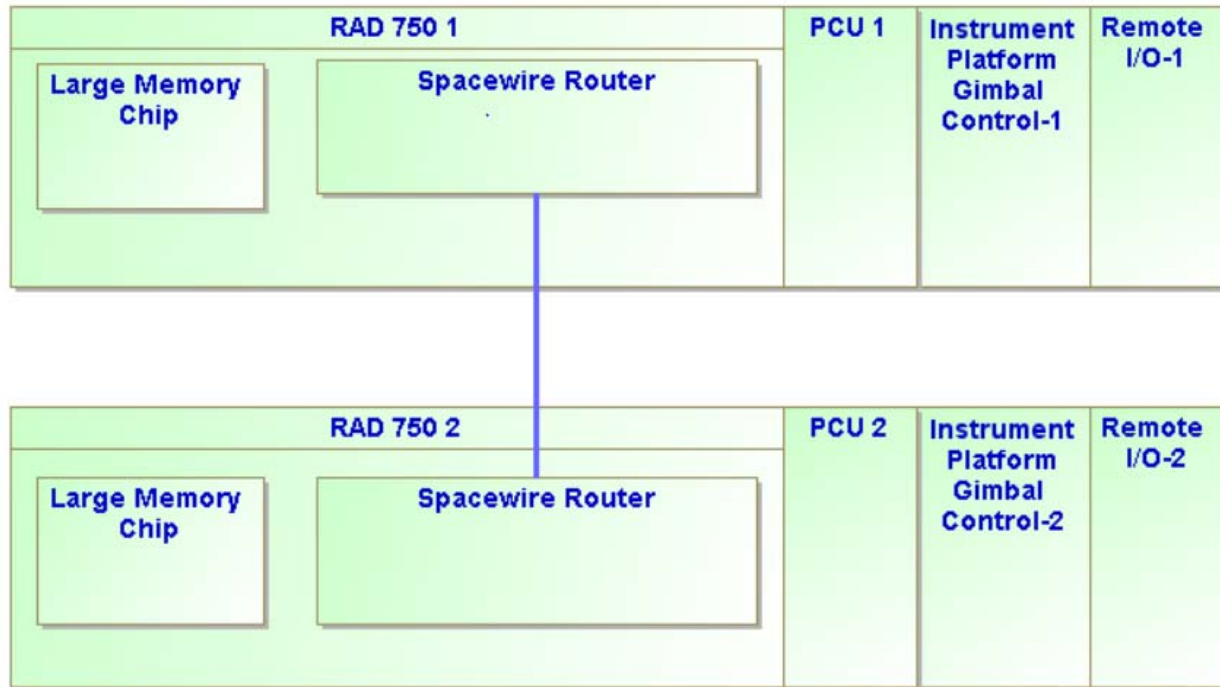
Figure B.2.7-39. The C&DH is redundant and cross strapped to provide robust fault tolerance.

integration provides significant savings on mass (including shielding).

Heritage

The C&DH electronics does not require any new technologies. The RAD750 single-board computer with SpaceWire is an off-the-shelf product. The SpaceWire interface chip is an off-the-shelf product. The I/O circuits and power supply have analogs on previous projects. The 6 U×220 m packaging standard has been qualified and used on previous projects.

B.2.7.6.5   Software

Highly reliable software for mission-critical applications is essential for this long-life mission. The FSW baseline extends JPL's long heritage in FSW architecture development, and is implemented in accordance with JPL requirements for NASA Class B (non–human-space-rated) software development. JPL has established a set of institutional software development and acquisition policies and practices as well as Design Principles (DPs) that apply to mission-critical and mission-support software. These practices conform to NASA Software Engineering Requirements, NPR 7150.2 (NASA 2009b) and are an integral part of the JPL DPs and Flight Project Practices (FPPs) (JPL 2010a, b). All Europa Orbiter Mission FSW would be developed in accordance with JPL institutional policies and practices for deep space missions, including JPL's Software Development Requirements (JPL 2010c), which address all Capability Maturity Model Integration (CMMI) process areas up to maturity level 3. Software identified as safety-critical will comply with safety-critical requirements, regardless of software classification. Software safety-criticality assessment, planning, and management will be performed for all software, including new, acquired, inherited, and legacy software and for supporting software tools. Software is identified and documented as safety-critical or not safety-critical based upon a hazard analysis conducted prior to start of development activities.

Key functions allocated to software include system command and control, health and safety management, attitude control (maintaining concurrent HGA Earth pointing during telecom sessions), science platform articulation, science data collection, onboard data management, reliable delivery using Consultative Committee for Space Data Systems (CCSDS) File Delivery Protocol (CFDP), and thrust vector control during critical propulsion maneuvers. Onboard ephemeris-based pointing and the use of CFDP help to simplify operations and thus reduce long-term operations costs. None of these capabilities are seen as new technology, and significant algorithm and architecture heritage is available from Cassini, MSL, SMAP, MESSENGER, and other missions.

Flight software also has a key role in system fault management. Critical activities are expected to include post launch separation, detumble, acquisition, JOI, EOI and Europa orbit science data acquisition. Once in Europa orbit the sequence of behaviors intentionally becomes very repetitive and synchronous with the orbit. During this phase software controls the camera articulation, HGA pointing, and data acquisition and management required for surface mapping, all roughly comparable to MRO except that these behaviors repeat at a more demanding rate than experienced in previous missions, and occur in the hostile radiation environment around Europa. Moreover, coverage objectives require most of the orbital science campaign to complete with minimal disruption. For this reason the FSW coordinates a system fault-management approach, consistent with current best practices, aimed at protecting essential resources, but trying to maintain scheduled operations using automatic fault responses such as resetting devices, switching to redundant devices, or selectively trimming subsets of planned activities.

The FSW is organized in a layered architecture, as shown in Figure B.2.7-40.

The Platform Abstraction layer interfaces directly with the hardware. This layer contains drivers that provide control, and data abstractions to the device-manager and services layers. The drivers communicate with the hardware using the device-specific syntax and protocol, allowing higher layers of software to interact with these devices using system-standard communication protocols and message formats. Notably, the use of industry-standard SpaceWire as a common hardware communications medium reduces the number of different device types that must be supported, with commensurate reductions in software system complexity. Furthermore, the ability of SpaceWire interface devices to buffer data and perform other control functions in hardware (as demonstrated by MESSENGER) is expected to further reduce the complexity and time-criticality of the FSW implementation.

The Platform Abstraction layer also encapsulates the real-time operating system, device drivers, and all interprocess communications, leveraging flight heritage with the RAD750 platform and all JPL missions since Pathfinder. The commercial operating system provides real-time task scheduling, memory management, and interfaces to I/O devices immediately associated with the processor board.

The Behaviors layer includes software elements that perform closed-loop control around specific system behaviors. These behaviors are typically responsible for the management of one or more hardware devices or subsystems, as well as integrated behaviors associated with them, such as attitude control. Closed-loop behaviors also incorporate fault detection and localized fault management capabilities.

Behavior coordination is provided in a separate Coordination layer that can sequence and coordinate the control of underlying behaviors. This layer is also responsible for coordinating any fault responses at a system level.

The MetaControl layer provides services for initializing and supervising reliable operation of the rest of the software and computing system and for supporting external commanding

Figure B.2.7-40. Flight software benefits from appropriate reuse and evolution within a layered architecture.

and configuration (such as changing system behavior from the ground).

Instrument-embedded software is developed by instrument providers and tested locally using a spacecraft simulator (see Testbed Approach). It is delivered with the instruments. Some engineering devices may also include embedded software. All other software is developed in-house.

B.2.7.6.6 Structure

The Avionics Module (Figure B.2.7-41) supports the majority of the avionics, batteries, science instruments, star-trackers, Sun-sensors, and reaction wheels. The vault houses and shields the avionics components that are most sensitive to radiation and extends below the Avionics Module's interface with the Propulsion Module. This configuration optimizes radiation-shielding by making use of the exist-

ing structure in all directions: From the top the octagonal primary structure, reaction wheels, and batteries provide shielding; from the sides the primary structure, tanks, and thermal enclosure provide shielding; and from the bottom the Power Source Module's primary structure and main engine provide shielding, complementing the vault's thick walls. Waste heat from the avionics is allowed to radiate out from the vault to help maintain the propulsion tanks at their required temperatures.

The topmost part of the Avionics Module is also octagonal. The vault is box-shaped. The tapering structure that connects the upper part of the Avionics Module to the vault is composed of machined stringers fastened to sheet-metal panels. An octagonal ring is fastened to the top of the module, and a square interface ring is fastened to the bottom.

The vault consists of six machined panels that are fastened together, with access panels integrated to allow for installation and removal of the avionics. The batteries and reaction wheels reside within the upper section of the Avionics Module.

Instrument Accommodation Structures

The science instruments on the Orbiter are the LP, LA, MC, and MAG. They are all external-
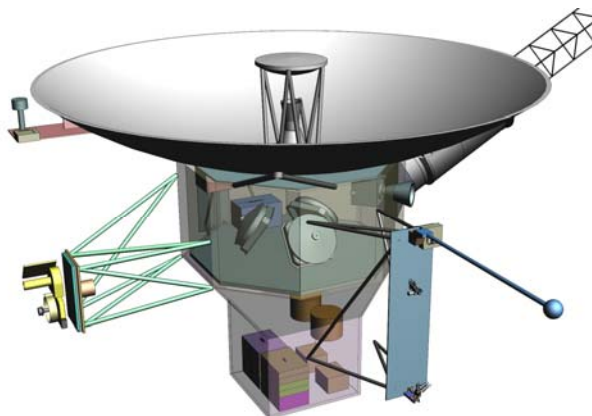
Figure B.2.7-41. Avionics module.

ly mounted on the upper section of the Avionics Module.

The LP is passively deployed using a compression spring-based mechanism configured to allow for rotation. This mechanism is based on a device used on MER to retract cables at the cruise stage separation interface. There are launch restraints at the base and end of the probe, held in place by ¼-inch separation nuts. When the probe reaches end of travel it is latched at full deployment.

The LA and MC are attached to a two-degree-of-freedom gimbal mechanism. On one axis there is a rotating table, driven by a motor and gearbox actuator. The second degree of freedom is driven by a linear actuator.

The MAG boom extends axially. A rate-limiting eddy-current damper at the base of the boom can act as an attenuator. This attenuator is similar to the one currently used on MSL. The attenuator limits the end of travel loads to the required levels.

Thermal Section Structures

The thermal enclosure (Figure B.2.7-42) consists of blankets made from aluminized Kapton, aluminized Mylar, and Dacron net separa-
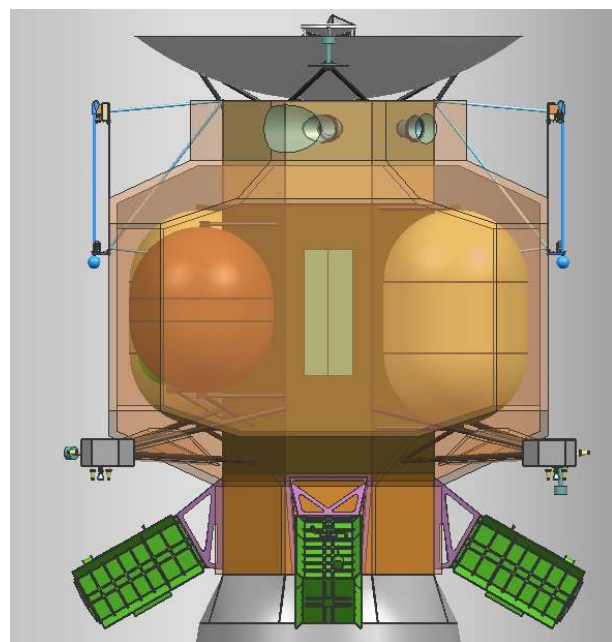
Figure B.2.7-42. Thermal enclosure.

tors, supported by a lightweight, carbon-fiber tubular frame.

B.2.7.7   Technical Budgets

Three primary technical margins are addressed here: mass, power/energy, and data balance.

Other key technical margins are covered elsewhere in this report: Radiation tolerance margin is treated in Section B.2.6.1.

The approach to technical resources in this study has been to model what is well understood, and then include conservative margin based on past experience to account for items not known well enough to model.

To minimize cost and schedule risk, the concept strives to achieve high levels of technical margin wherever possible.

B.2.7.7.1   MEL and Mass Margins

The mass margin follows the definitions and conventions specified in the JPL Design Principles, Section 6.3.2 (JPL 2010a). The earliest milestone at which the Design Principles specify a mass margin, however, is the Project Mission System Review (PMSR), when 30% is required. In consideration of the fact that the Europa Orbiter Mission concept is in a much earlier phase, pre–Mission Concept Review (MCR), we have set a more conservative policy of 40% mass margin for this report. This is consistent with the expected evolution of JPL's institutional guidance. The method of calculating the Design Principles margin is shown in Table B.2.7-7.

The dry mass current best estimate (CBE) includes tanks sized to carry the maximum propellant load, radiation shielding, and the launch vehicle adapter (LVA). Each of these is discussed in more detail below.

Use of "Max Propellant"

The Design Principles explicitly require that the propellant load assumed for the margin calculation be that amount of propellant needed to provide the required ΔV for the maximum possible launch mass on that launch vehicle (LV) (JPL 2010a). In addition, the dry mass of the propellant tanks reflects tanks sized for this maximum propellant load. This approach gives an accurate reading of the overall dry mass margin, *assuming* that the flight system grows to the maximum launchable mass.

Table B.2.7-7. Europa Orbiter Mission mass margin.

Orbiter Mass Margin				
T. Bayer 24 Apr 2012	LAUNCH			
Orbiter Model - Final Report Update	Flight System Mass, kg			
	CBE	Cont.*	MEV	
Laser Altimeter	10	50%	15	
Langmuir Probe	3	50%	4	
Magnetometer	3	50%	5	
Mapping Camera	4	50%	6	
Payload	20	50%	30	
Power	56	21%	68	
C&DH	19	30%	25	
Telecom	94	30%	122	
Structures	561	27%	715	
Thermal Control	44	30%	57	
Propulsion	193	28%	247	
GN&C	62	29%	80	
Harness	70	50%	105	
Radiation Monitor	8	30%	10	
ASRGs (4)	164	46%	239	
Spacecraft	1271	31%	1668	
Flight System Total Dry	1291	32%	1698	Max Prop
Bipropellant	1129		1837	2054
TVC Monopropellant	101		101	101
ACS Monopropellant	40		40	40
Pressurant	6		6	6
Residual and Holdup	32		49	55
Propellant	1308		2033	2256
Flight System Total Wet	2599		3731	
Capability (21-Nov-21 VEEGA)	Atlas V 551:		4494	
System Margins				
JPL DWP (Capability - Max Prop - CBE Dry) / (Capability - Max Prop)			42%	

*Using ANSI/AIAA Guide G-020-1992, "Estimating and Budgeting Weight and Power Contingencies for Spacecraft Systems", applied at the component level.

Specifically, in Table B.2.7-7, propellant mass is computed from the ΔV required for the 21 November 2021 Venus-Earth-Earth gravity assist (VEEGA) trajectory. The CBE propellant is computed using the CBE dry mass and CBE ΔV. The maximum expected value (MEV) propellant is computed using the MEV dry mass and the MEV ΔV. The max propellant is computed using the maximum possible dry mass and the CBE ΔV.

Radiation Shielding

The model tracks the amount of shielding necessary to protect each piece of sensitive electronics. This mass is accounted for at the appropriate level of assembly (card, box, or module), and shown as a payload and engineering total in Table B.2.7-7.

Launch Vehicle Adapter

A standard Atlas LVA is assumed. The mass shown in Table B.2.7-7 includes both the part that remains with the spacecraft and the part that remains with the Centaur upper stage but is considered "payload mass" for the purpose of LV performance.

This margin calculation adds "growth contingency" mass to the CBE masses to arrive at an MEV and the propellant required for that mass, and then compares this value to the LV capability. For determination of contingency factors, the Europa Study Team has used the ANSI/AIAA Guide G-020-1992(American National Standards Institute 1992), applied at

the component level. This specifies the *minimum* contingency factor based on project phase and component sizing and maturity, and allows a higher factor where the project deems it appropriate. The guideline is generally consistent with traditional JPL practice, but provides a more rigorous grounding through its use of historical data.

As can be seen in Table B.2.7-7, the Europa Orbiter Mission has excellent mass margins. A more detailed mass breakdown can be found in the Master Equipment List (MEL) Section B.4.3.

B.2.7.7.2   PEL and Power/Energy Margins

The Power Equipment List (PEL) contains the CBE with a contingency for maturity. The Orbiter Mission power modes are based on the mission scenarios. Europa Orbiter Mission policy is to maintain 40% of the power source capability after a single failure as power margin on the load for all mission power modes. Each mission mode is assessed against the policy. The transient modes are assessed with the power margin on the load and the DPs DOD of actual battery capacity with a single failure (JPL 2010a). Summary results of the mission mode power analysis are shown in Table B.2.7-8.

The PEL provides the current best estimate (CBE) power output and the lowest expected value (LEV) sum output of the ASRG power source for each mission mode. The power

Table B.2.7-8. Orbiter power analysis compares the power source capability to the estimated load for all phases of the mission. There are two mission modes that rely on the battery, and the DOD is displayed.

	EHM Orbiter Power Analysis							
	ASRG Power, W		Flight System Power, W				SS or	Max Bat
Mission Phase	Spec	LEV	CBE	Cont.	MEV	Margin, %	Transient	DoD, %
Launch	426	334	172	28%	221	48%	SS	
Inner Cruise	535	420	224	19%	266	47%	SS	
Inner Cruise (Safe)	535	420	244	45%	354	42%	SS	
Outer Cruise	514	403	228	46%	334	43%	SS	
Outer Cruise (Safe)	**514**	**403**	**244**	**40%**	**341**	**39%**	**SS**	
Orbit Insertion/TCM	505	396	356	59%	566	40%	Transient	15%
Europa—Communications	505	396	241	68%	405	40%	Transient	13%
Europa—No Communications	505	396	180	98%	358			
Decommissioning	505	396	221	-44%	123	44%	SS	

source estimate takes into account a degraded performance of the ASRG during launch due to the environmental conditions inside the shroud. The LEV of the ASRG assumes a failed Stirling converter after launch, effectively producing the power of 3.45 ASRGs versus a nominal 4.0 ASRGs.

The PEL contains a line item for each load, estimating a CBE load value, an estimated contingency based on maturity, and a maximum expected load value (MEV). Each mode is identified in the PEL, along with a summation of all of the loads that are powered on in that mode. The mission mode total is compared to the power source capability for each mission mode, with the power margin calculated per the DPs approach of (Capability − CBE) / Capability (JPL 2010a). The transient modes are modeled to estimate the battery DOD with the actual battery capacity.

All mission mode power budgets currently meet the Europa Orbiter Mission 40% margin policy with the exception of outer cruise safe mode, in which the power margin is slightly below policy at 39%. Since safe mode is considered steady state, additional battery capacity does not provide additional margin. Several

options will be examined in Phase A to improve power margin in this mode and it was judged that 39% margin is adequate to assess mission concept feasibility.

The two transient modes are the orbit insertion/TCM and Orbiter science. Orbit insertion is the defining mode for the battery sizing due to the long JOI burn of 1 hour. The battery capacity is estimated to be 40 Ah with a 14-A discharge at 10°C at EOM. The load profile and battery DOD are shown in Figure B.2.7-43.

The JPL DPs allow for a 70% DOD for events such as orbit insertion that are less than 100 cycles (JPL 2010a).

The next transient mode is the science orbit mode, in which the X and Ka band amplifiers are turned on for a continuously for 72 hours to support gravity science. After the continuous track, the X and Ka band amplifiers are 50% duty cycled for the next five orbits until the battery is recharged (see Figure B.2.7-44).

The dominant factor to the Orbiter science mode is the continuous operation of Telecom, driving a 40% DOD for the Orbiter Science with the 72-hour continuous track. The JPL
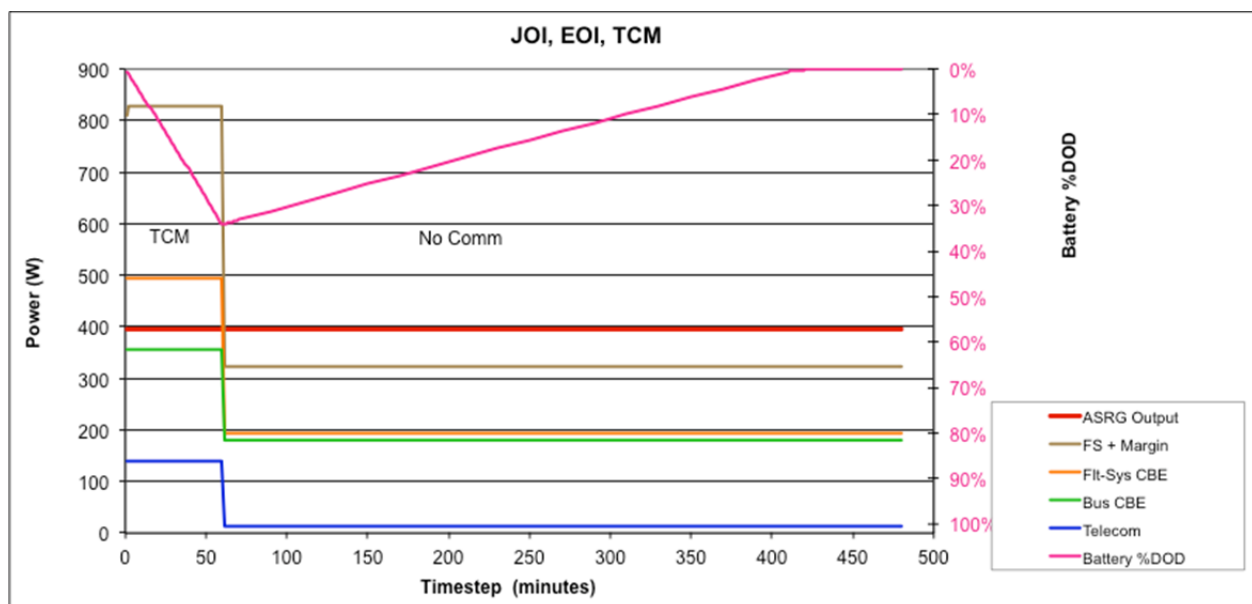
Figure B.2.7-43. JOI power analysis shows a 1-hour discharge of the battery using the Europa Study policy of 40% margin on the load profile.
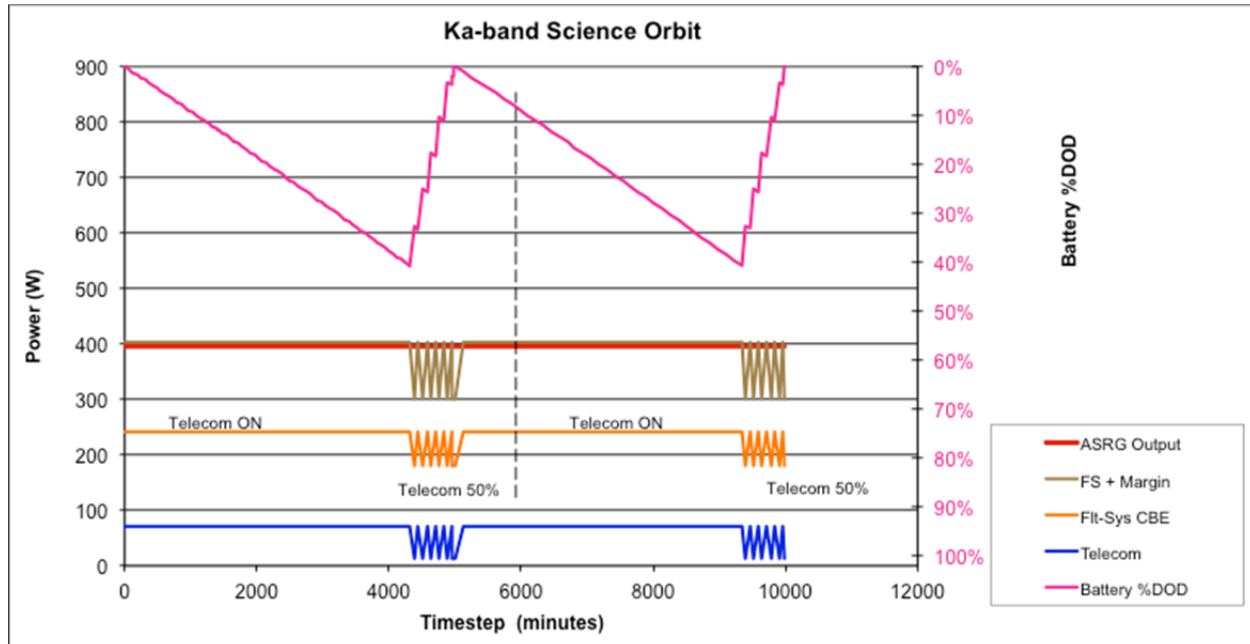
Figure B.2.7-44. Orbiter science mode power profile shows that the system is power-negative with Telecom On for a continuous track of 72 hours for gravity science and then a 50 duty cycle to recharge the batteries.

DPs allow for a 60% DOD for less than 5000 cycles. There is an opportunity to adjust the size of the battery to reduce mass if necessary (JPL 2010a).

B.2.7.7.3   Data Balance

Mission data balance is analyzed primarily for the science operations scenario described in Section B.2.1. This is considered to be the driving case for data balance because this is the only time when all science instruments are operating apart from some short-duration calibration and checkout during cruise or the Jovian tour.

The target 100-km science orbit is a near-polar orbit (95-degree inclination) with a solar phase angle intended to optimize the surface lighting for imaging, and minimize Earth occultation so that gravity science can obtain the longest possible continuous Doppler measurements. In the notional mission concept the geometry of this orbit and mission timing allows for continuous spacecraft visibility from Earth except when Europa is occulted by Jupiter. The orbit would also be maintained so that the MC could obtain a near-complete surface map in 3 Eurosols. At all times during this phase the

HGA maintains Earth pointing, and the instrument platform maintains nadir pointing. The 2-axis instrument platform also keeps the FOV of the MC oriented perpendicular to the ground track.

During the science phase of the mission all instruments would be continuously powered, and the MAG, LP, and Laser Altimeter instruments are operated continuously. The MC collects stereo imaging data during the sunlit half of each orbit (additional data margin can be obtained by eliminating overlap coverage of polar regions on later orbits, but the redundant coverage is included in the balance for now to keep operations simple).

Downlink is continuous and concurrent with gravity science for 34 orbits, followed by six orbits during which telecom is operated at only a 50% duty cycle to allow batteries to recharge. Data would be transmitted on Ka band to maximize downlink throughput. Continuous ground tracking would be provided during this mission phase using 34m DSN stations. Mission data balance is shown in Table B.2.7-9. This analysis assumes that only one stereo

surface map (80% coverage) is needed to meet the science baseline and that the notional orbit would achieve this in 3 Eurosols.

Per orbit downlink margins are shown in Table B.2.7-10 for orbits with continuous telecom. Not shown, but also included in the 549 Mbits of data accumulated, are engineering data collected at 2 kbps. Downlink capacity is computed using the Ka link budget described in Table B.2.7-4, which was computed for a worst-case range of 5.5 AU, and DSN elevation angle of 20 degrees, and then multiplied by a factor of 1.2 to the ability to step downlink bit rates over each pass to maximize the throughput.

The C&DH subsystem provides 256 Mbytes of solid-state storage into which all science data are recorded during observations. When telecom is operating, downlink data is retrieved from storage and queued for transmission by the data manager. Stored data would be managed as products (files) in the onboard store, and the CCSDS File Delivery Protocol (CFDP) would be used to ensure reliable transport of this data to the ground. At the average downlink rate of 129 kbps data would

accumulate on the ground at a rate of about 3.7 Gbit/pass, or 11.1 Gbit/day during the science mission, or about 334 Gbit for the entire science mission.

B.2.7.8 Module Development, Integration, and Test

The modular approach for the spacecraft allows parallel testing before delivery to system integration and test at a higher level of integration than was possible for previous spacecraft.

The spacecraft is comprised of the Avionics Module, the Propulsion Module, and the Power Source Module.

Development of the spacecraft modules begins with the design and fabrication of a developmental test model (DTM) of the spacecraft structure. The DTM is populated with appropriate mass mockups as required to properly represent the mass properties of the spacecraft. After assembly, a full set of structure qualification tests is to be performed, including static loads, modal survey and pyro-shock testing. The DTM is also be used later as a "trailblazer" to ensure that all facilities (such as the launch site and LV) and mechanical ground support equipment (MGSE) characteristics are compatible. Because the DTM components are built to the same drawings as flight, elements of the DTM could also be used as surrogates for the flight structure, if required.

As the DTM program progresses, the flight model (FM) structural components are fabricated and delivered to the module teams (Avionics Module, Propulsion Module and Power Source Module) for integration with active components and secondary structure, and for

Table B.2.7-9. Orbiter Mission Data Balance.

	Gbit
30-day mission data for MAG	10.6
30-day mission data for LA	5
30-day mission data for LP	5.3
30-day mission data for Eng	5.3
Data for one stereo map	38.4
Total mission baseline data (one map)	90
Mission downlink capacity	310
Downlink capacity margin	71%

Table B.2.7-10. Data Balance and Margin.

	MC	LA	MAG	LP	Total/Orbit
Raw data rate (Kbps)	375	1.95	4	2	
On-time per orbit (%)	50	100	100	100	
Data reduction factor	3	1	1	1	
Effective output rate (Kbps)	63	1.95	4	2	
Average data per orbit (Mbit)	472.6	14.7	31	15.5	549
Average downlink rate (Kbps)					129
Downlink time required (hour)					47
Downlink time available (hour)					77.5
Downlink margin					39%

module-level testing, including environments, prior to the start of system integration and test. 2 months of schedule margin is allocated for the structure deliveries to the Module Development Teams, and a minimum of 1.5 months schedule margin is allocated for the delivery of the tested flight modules for system integration. Since the Avionics Module is the most complex functionally, 3.5 months of margin are allocated in recognition of its schedule criticality to System Integration and Test.

The module concept adopted for the spacecraft permits testing, both functional and environmental, to be performed with flight cabling and flight structure at a higher level of integration prior to delivery than has been performed on similar previous missions, such as Cassini. Development of more highly integrated modules allows more parallel path testing, reducing the number of interfaces that need to be verified at the system level, compared to a project like Cassini, where individual components and subsystems were delivered and integrated during System Integration and Test.

The major deliveries to system integration are the Avionics Module (consisting of the upper equipment section with science instruments (see below), the avionics vault and its contents, and the telecom assembly), the Propulsion Module (with tanks, other propulsion components, and harnessing), and the Power Source Module. The Power Source Module is populated with advanced Stirling radioisotope generators (ASRG) that are electrically heated to permit realistic testing and evaluation of the end-to-end power delivery system for the spacecraft. Emulations of other modules at electrical interfaces will be used to support module-level integration in each case.

All module deliveries are planned to occur at the start of System Integration and Test to maximize flexibility. The Upper Equipment Section is initially delivered with Engineering-Model (EM) Science Instruments. The Flight Model (FM) science instruments are delivered later as shown in the System Integration and Test flow,

permitting any interface or performance issues to be resolved before the flight deliveries.

B.2.7.8.1   *Testbed Approach*

Consistent with longstanding practice, the Europa Orbiter Mission has adopted a system integration approach that is supported by an additional set of software and hardware testbeds, enabling early and thorough integration of key hardware and software interfaces prior to ATLO. This development and validation approach begins with scenario development during formulation and design, and progresses incrementally to system validation using an ever-growing battery of regression tests that verify and validate system architecture as it is designed and developed. Figure B.2.7-45 depicts the proposed testbeds described in the following paragraphs.

Since science instruments are likely to be developed externally, instrument developers must be provided with a testbed environment that includes an emulator for engineering subsystems (hardware and software) that simulates the power, data, and control interfaces with which the instrument must integrate. This ensures that all interface issues have been resolved prior to delivery, thereby helping to keep the ATLO work focused on system integration and on the concerns that can be verified only in an assembled system context. Similar subsystem assembly testbeds are provided for early integration testing of major subsystems (telecom, propulsion, power, etc.).

A high-fidelity model-based simulation capability (known as the workstation test set [WSTS] on MSL and SMAP) is baselined for FSW development test and verification. This includes but is not limited to fault management development and test, attitude control system-level verification and validation (V&V), and mission activity development and test; so several groups will exploit this capability, which can be replicated cheaply as often as necessary. The software simulation of hardware must be of sufficient fidelity to allow seamless

Instrument TB

- For development, qualification, & acceptance of each integrated instrument
- Project provides ▪ common items (PCU, power switch, BIU, PoL…) & S/C Sim

Chassis

S/C Sim | Instrument Elex' (BIU, PoL…) | PCU

BTE | Instrument Detector

Flight

Subsystem Assembly TB

- For development, qualification, & acceptance assembly, and for subsystem I&T
- BTE and test software
- EMs

Avionics/FSW Integration TBs

- For early system integration, and for FSW verification
- Augmented Avionics Integration TB
- Rotate through…
  - Flight units
  - Instrument elex' EMs
  - Simulations
- SSE
  - External interfaces and emulators, as needed

Workstation TBs

- For unit and integration testing
- Workstation-based with fully simulated environment
- Replicated many times

Mission System TB

- For system verification and ORTs
- Full H/W redundancy
  - EM of C&DH, ACS, Pwr
  - Includes ASRG elex' EM
  - Emulation* in SSE for absent items

Flight Operations Support TB

- For ORTs, procedures, FSW updates, anomaly resolution
- System TB reduced as appropriate

Avionics Module Integration & Test

- Full modular system integration & verification
  - Functional
  - Environments

- Uses System TB SSE and LCE, as needed

Figure B.2.7-45. System integration testbeds. [Define bus interface unit (BIU), launch control equipment (LCE), spacecraft support equipment (SSE). Pester Arden. (will put in acronym list).]]

migration of FSW and test cases from simulation to hardware-in-the-loop testbeds. This capability is important and necessary because certain software services are needed to support the instrument testbeds and the testing and integration of devices. Therefore, emphasis will be placed during hardware testing on validating simulation model fidelity.

The first workstation-based spacecraft simulator version will be available in time to support development of the first FSW release, and will progress with expanded capability, as needed to support testing of subsequent FSW builds. It will be available on all software developers', systems engineers', and testers' workstations.

Capabilities will include closed-loop spacecraft behaviors operating in both nominal and off-nominal modes. These simulators are built to allow for interchangeability between software models and hardware engineering models (EMs) later in the "hardware-in-the-loop" testbeds in a manner that is transparent to the FSW and to test scripts, at least at the interface level. This enables use of the same test scripts whenever the testbed models are interchanged with EMs or hardware emulators.

In addition to the simulation capability described above, the Europa Orbiter Mission would have three system testbeds. The first two are the Avionics/FSW integration

testbeds, which are similarly configured with single string avionics. These support the development and test of ground support equipment (GSE) hardware and software, the development and validation of test scripts, and the maturation of databases, such as command and telemetry dictionaries. First on line is the Real-Time Development Environment (RDE), which is dedicated to GSE hardware and software development and test. The next instance of this testbed, the Flight Software Testbeds (FSWTBs), becomes available later in the development process to allow V&V to proceed in parallel with FSW development. The third system testbed is the Mission System Testbed (MSTB), a full redundant, high-fidelity testbed dedicated to system V&V, FSW fault management tests, mission system tests, and ATLO support.

These system testbeds include the C&DH, GN&C, power, telecom, and harness subsystems, as well as Ground Data System (GDS) hardware and software. The EM versions of all flight system engineering subsystems and instruments will pass through these testbeds for integration and interface verification and the testbeds can support flight hardware testing, if needed. The V&V simulation environment can offload the hardware-in-the-loop testbeds and use the EM integration effort to help evaluate model fidelity. The simulation environment interfaces and procedures are compatible with those of the hardware testbeds. These testbeds are also used to train test analysts to support system testing, as well as to support ATLO procedure development and anomaly investigation. All FSW versions are verified on the system testbeds prior to being loaded onto the flight system during ATLO or flight operations. The flight system testbed transitions to operational use for this purpose after launch.

B.2.7.8.2   System Integration and Test

The conservatively derived system integration and test program is based on actual durations from the Cassini project. Launch operations *durations are based on actuals from the MSL project along with operations unique to the Europa Orbiter Mission.*

The System Integration and Test (SI&T) Phase, described graphically in Figure B.2.7-46, would begin with the delivery of the flight Avionics Module components, Propulsion Module, and Power Source Module for system integration. The Avionics Module components, consisting of the telecom assembly, Upper Equipment Section (with EM science instruments) and the Avionics Vault, is integrated initially using extender cables. These permit access to circuits for integration and troubleshooting, as well as for connection of direct access equipment needed for closed-loop operation of the Attitude Control Subsystem during mission scenario and comprehensive performance testing. During integration, interface signal characteristics are measured and recorded for comparison with requirements.

Even though traditional EMC/EMI system engineering methods would be employed during development, the early integration of the telecom subsystem permits monitoring of spectral characteristics as other hardware is added to the system for detection and identification of any interfering spurious signals. A thorough telecom functional test is included in the flow to establish baseline performance while operating with the rest of the Avionics Module.

Europa Study System Integration & Test

12-19-11
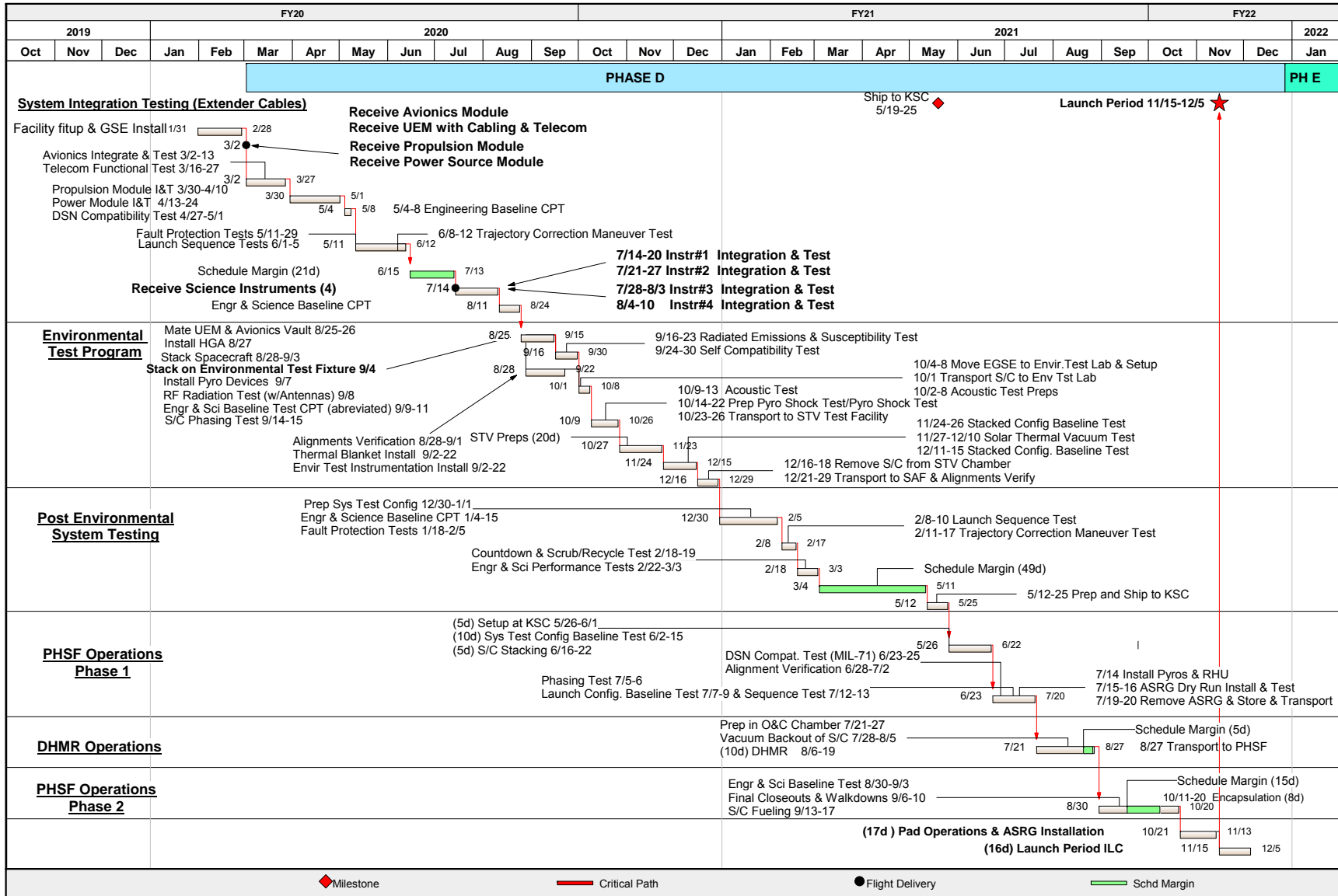
Figure B.2.7-46. The comprehensive ATLO program is based on as-run durations from the Cassini and MSL projects plus JPL-required schedule margins.

The Propulsion Module is electrically integrated through extended cables next in the flow to demonstrate signal characteristics to propulsion valves and thrusters, and to perform an initial verification of proper phasing. The design of the extender cables and the layout of the modules in the test facility address cable length issues, as appropriate. Phasing of propulsion components (as well as G&C components) is repeated after spacecraft stacking to remove any influence of the extender cables.

Finally, the Power Source Module is electrically integrated through extended cables. Plans call for fully functional ASRGs that are electrically heated and can be used to verify end-to-end performance, as well as to verify integration procedures that will be used for the flight ASRG integration at KSC.

A Deep Space Network (DSN) compatibility test is performed at this point (with the DSN compatibility test trailer) followed by an Engineering Baseline Comprehensive Performance Test (CPT). This and other configuration-dependent baseline tests are performed throughout the ATLO program in order to detect performance changes resulting from either trending or environments.

A series of fault management tests is performed to establish correct operation of the fault management system software in conjunction with associated hardware detections and responses.

The first mission scenario test is the launch sequence test, executed both nominally and with selected fault and off-nominal conditions. Subsequently, a trajectory correction maneuver test (including orbit insertion) is performed in both nominal and off nominal conditions. Other capabilities of the spacecraft to support required operational modes, science observations, and other noncritical mission scenarios will be incorporated in CPT(s) rather than in specific scenario tests so that spacecraft capabilities are fully established, rather than merely performing point-design mission scenario

verifications. Since all operations described above are first-time events, one-month schedule margin is included at this point to prevent any delay to the science instrument integration.

At this point, any remaining science instruments are delivered and integrated into the Avionics Module, replacing their EMs that have been serving as surrogates throughout system testing. An Engineering and Science CPT follows integration, with all spacecraft components present to establish the performance of the spacecraft before reconfiguration for environmental test.

The environmental test program starts with the mechanical and electrical integration of the upper equipment section, avionics vault and the telecommunications assembly to complete the Avionics Module. Stacking of the Propulsion Module, Power Source Module, and Avionics Module to each other, stacking the spacecraft on the Launch Vehicle Adapter (provided by the Launch Service) and the installation of pyro devices needed for pyro-shock testing. An Abbreviated Baseline CPT is performed, as well as an RF radiation test using the flight antennas, and a phasing test to demonstrate proper phasing without extender cables. This is the first time the spacecraft is in a flight-like electrical and mechanical configuration.

Radiated emissions and radiated susceptibility tests are then performed, as well as a self-compatibility test. This is followed by an alignment verification to establish pre-environmental alignment data. Thermal blankets (including the thermal shroud) and environmental test instrumentation are installed after the spacecraft is stacked.

The spacecraft is then transported to the Environmental Test Lab (ETL), where acoustics tests and pyro-shock tests are performed. The pyro-shock test also verifies the LV separation mechanical interfaces.

The spacecraft is then moved to the 25-foot Space Simulator, where a baseline test is performed to verify configuration and performance prior to starting solar thermal-vacuum (STV) tests. The STV test is primarily a verification of worst-case hot and cold performance, as well as selected thermal balance conditions. Additional tests (such as science instrument modes that require vacuum conditions) are performed during thermal transitions, if they are not otherwise required for the worst-case thermal tests that verify margins required by JPL Design Principles and Flight Project Practices (JPL 2010a, b).

After STVtest, the spacecraft is transported back to the Spacecraft Assembly Facility (SAF), where post-environmental alignment verifications are performed. The Engineering and Science CPT is repeated for post-environmental performance verification. Launch sequence tests, trajectory correction maneuver tests, countdown and scrub/recycle tests, and engineering and science performance tests are performed prior to shipment to KSC. Two months of schedule margin are included at this point to protect the ship date and KSC operations. Shipment to KSC is performed at the module level because of the large size of the stacked spacecraft and to permit access to direct access signals for the final comprehensive performance testing at KSC.

After arrival at the KSC Payload Hazardous Servicing Facility (PHSF), the spacecraft modules, interconnected with extender cables, are put through a System Test Configuration Baseline CPT to reestablish the health of all spacecraft systems. Spacecraft stacking is then performed, followed by a DSN Compatibility Test with MIL-71, alignment re-verification, and a final Phasing Test using the launch version of flight software. A Launch Configuration Baseline Test is performed, followed by a Launch Sequence Test from prelaunch through early cruise. Flight pyrotechnic devices (excluding those for spacecraft separation) are installed. A dry-run installation of the flight

ASRGs is performed as well. After the flight ASRGs are removed and secured, the spacecraft is transported to the KSC Operations and Checkout (O&C) facility for dry heat microbial reduction (DHMR). The descriptions of operations with the ASRG assume that they can be handled in similar fashion to the MMRTG used on Mars Science Laboratory (MSL). These operations will be refined as the ASRG requirements and development proceed.

At the O&C the spacecraft is installed in an existing thermal chamber in the O&C high bay. Vacuum bakeout of the spacecraft is performed, followed by backfill to an appropriate convective atmospheric environment for heating (either nitrogen or filtered air at the preference of the Planetary Protection Engineer). Spacecraft temperatures are elevated and verified, at which point the DHMR operation is conducted. Because of uncertainty in the durations of each of these operations, five days of schedule margin are allocated at this point. Over one month of schedule is allocated to the end-to-end DHMR operation. The spacecraft is then transported back to the PHSF. Conservative planetary protection handling is planned beyond this point, consistent with a spacecraft that could impact Europa.

At the PHSF, a baseline test is performed to confirm the status of all spacecraft systems after DHMR. Since the ASRGs would not be present, the spacecraft will be powered by ground support equipment power supplies. Final spacecraft closeouts and walk-down inspections are performed, followed by propellant and pressurant loading of the Propulsion Module. Three weeks of schedule margin are included at this point to protect the date of delivery to the LV for integrated operations.

At this point, the spacecraft is ready for integrated operations with the LV, including mating to the flight LVA, encapsulation with the fairing, transport to the launch pad, and fueled ASRG installation for flight, countdown, and launch.

Durations for most of the spacecraft test operations (including setup, reconfiguration, preps, and transportation) are based on actual "as-executed" durations from Cassini. Cassini was used as a reference because its ATLO plan was executed without any holiday work, or any work on a holiday weekend, minimal Saturday work, and a nominal five-day-per-week, single-shift operation. Integrated operations with the LV are based on actuals from MSL, which had similar operations with the same/similar LV and integration of an MMRTG. These estimates have been informed by MSL complications of MMRTG installation inside the MSL aeroshell and implementation of required cooling systems. Cooling may not be required for the Europa Orbiter Mission, given the characteristics of ASRGs.

The ATLO flow described above has not been optimized to incorporate opportunities for parallel operations, except in the case of preparations for environmental testing, where such operations are customary. The flow described also includes the 20% schedule margin at JPL, and one day per week schedule margin at KSC, as required by the JPL Design Principles (JPL 2010a).

B.2.8   Mission Operations Concept

Europa and its vicinity is a challenging and hazardous environment for operating any science mission. The central guiding theme of mission operations is to deliver the spacecraft to Europa safely, and fully capable of conducting science observations. No other activities are allowed to drive the design of the operations systems and concepts. For the Orbiter Mission, operations consist of repeated measurements made via one orbital template that is replicated over multiple orbits.

Operations development has drawn much wisdom from the many NASA-wide studies of Europa exploration from as early as 1997. In addition, two key studies in 2008 were conducted to capture relevant lessons learned from past and present operations missions, incorpo-

rating members from JPL, APL, and NASA Ames (Clark, 2008). These studies focused in particular on flight and ground system capabilities needed to simplify science operations; early development of flight and ground concepts to ensure appropriate implementation; and postlaunch activities and development to ensure functional capabilities and simplified operations. All of the operations assessments, from the many studies and scenario work of highly experienced engineers, emphasize early consideration of operability issues in the system architecture and design. All system trades (spacecraft, operations, science, etc.) are treated as mission trades to work toward the best cost/risk for the overall mission, rather than optimizing a single element and unknowingly adding significant cost/risk to another.

B.2.8.1   Operations Concept— Interplanetary and Jupiter Cruise

After launch, mission focus is on the checkout, characterization, and deployment of all flight systems. In the first few weeks of cruise, coverage is continuous, driven by real-time commanding for schedule flexibility based on the high variability associated with early checkout activities. Once postlaunch checkouts are complete, the mission transitions to interplanetary cruise.

Interplanetary cruise is quiescent, save for elevated activity required for gravity assists and maneuvers. The spacecraft is minimally operated, with basic telemetry expected only once per week; however, 24-hour coverage is expected around maneuvers, and daily to continuous tracking is expected prior to gravity assists, particularly for nuclear safety maneuvers prior to gravity assists involving Earth. After JOI, instrument characterization and checkout resume, and operations readiness tests (ORTs) and instrument calibrations could be conducted during Jupiter system flybys prior to Europa orbit.

B.2.8.2   Operations Concept—Science Phase

The Orbiter Mission science phase, described in Section B.3.1, begins after Europa Orbit Insertion and circularization and is achieved via 30 days of operations at Europa. Each orbit has a very similar geometry; simple, repeated observations flowing from one conceptual design are capable of delivering all of the science goals. The Europa orbit geometry that will be used is shown in Figure B.2.8-1.

The science phase concept is a 30-day mission at an altitude of 100 km. The inclination is 95°, and at a 4:30 pm local solar time as shown in Figure B.2.8-1, near-constant communications with Earth are possible, for the spacecraft never enters occultation by Europa (though it does by Jupiter). The Laser Altimeter, LP, MAG, and Radio Science experiments can be on nearly all the time, except for maneuvers and Jupiter occultation (because both the spacecraft and Europa are occulted). Imaging is conducted on the day-side (shown by the yellow swath in Figure B.2.8-1).

There are many candidate repeat orbits available for use in accomplishing global mapping. The best repeat orbits have a comfortable swath-to-swath overlap, complete the repeat quickly, and are close enough to Europa to satisfy resolution requirements. Figure B.2.8-2 shows the candidate repeat cycles for the Europa Orbit Mission. The best option, marked in

Figure B.2.8-1. Europa orbit geometry as seen from Earth.
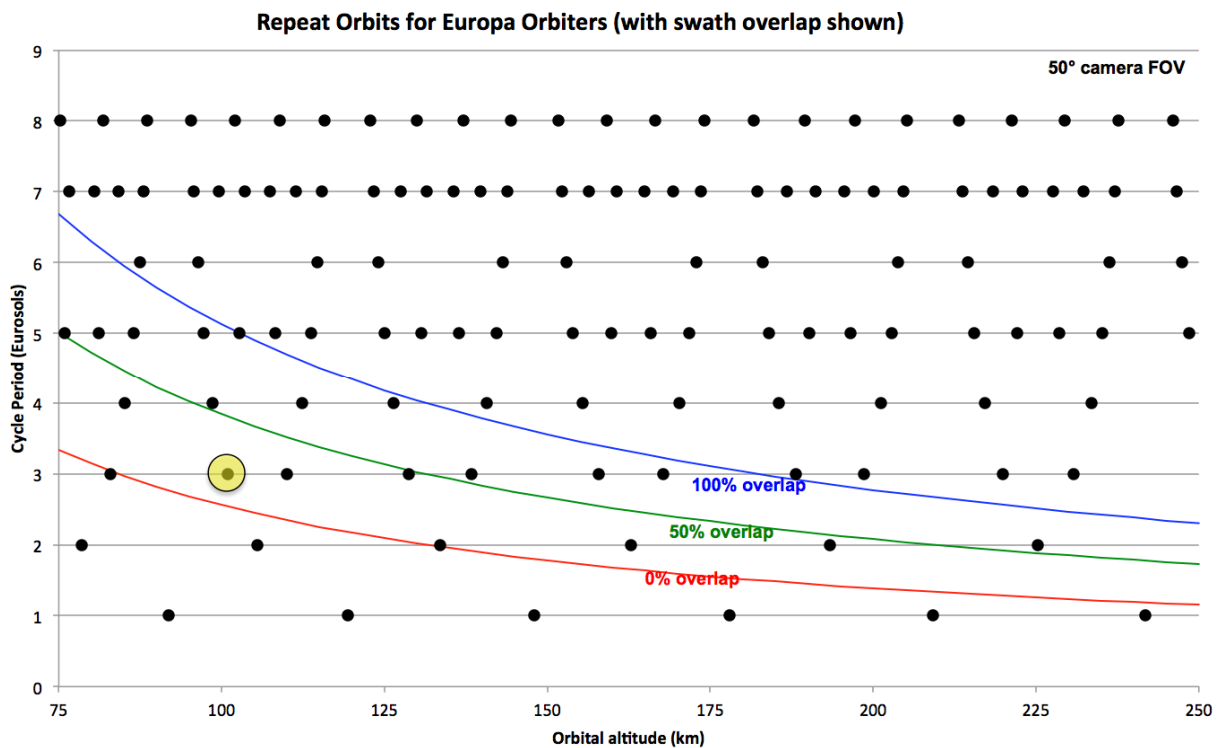
Figure B.2.8-2. Candidate repeat orbits.

the figure with a yellow circle, is a 122:3 repeat orbit; that is, 122 orbits of Europa are executed over 3 eurosols (about 11 days). This repeat cycle gives a swath-to-swath overlap of 18% at the equator at the end of the cycle. Since this repeat cycle only takes 11 days, continuing the cycle would provide up to three opportunities to map each point on the surface over the 30-day mission.

Imaging might be curtailed at the poles after the first Eurosol, as the groundtracks converge and higher overlap is achieved. At the equator, the overlap is 18% from one Eurosol to the next; however, above about 50 degrees latitude, only every other swath need be imaged for full coverage; and above about 65 degrees latitude, only every fourth swath is needed for full coverage. This strategy might be utilized to conserve resources (power, data) if needed, or to enable other operations, such as maneuvers.

Figure B.2.8-3 illustrates the imaging coverage achievable after one repeat cycle of 11 days. The only gap shown is that due to occultation by Jupiter, as the satellite (and spacecraft) passes into shadow.

Figure B.2.8-4 shows the Laser Altimeter spacing and coverage after the full 30-day science phase. Equatorial spacing of 25 km is achieved by allowing the groundtracks to drift after the first imaging repeat cycle.

The data collection and pointing profile is identical in nature for each orbit, save for curtailing of imaging coverage over time. No negotiation for resources or case-by-case optimization is necessary.

The orbiter concept employs frequent to continuous coverage for data downlink. The spacecraft is Earth-pointed except for trajectory correction maneuvers (TCMs), with science playback, engineering telemetry, and two-way navigation during DSN passes. Instruments that require pointing to the surface are on a two-gimbal science platform. The data balance described in Section B.2.4 allows for reasonable DSN tracking and healthy data volume margin in returning each orbit's science observations.

Simple, repeated operations are sufficient to
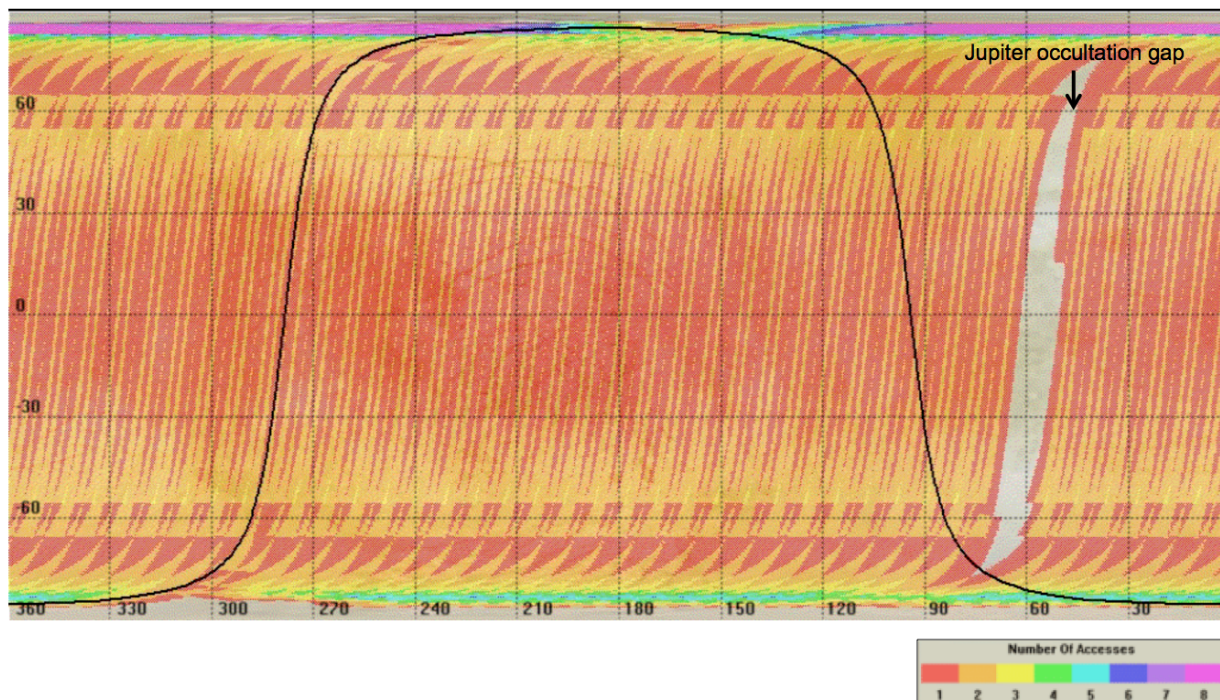
Figure B.2.8-3. Imaging coverage after one repeat cycle.
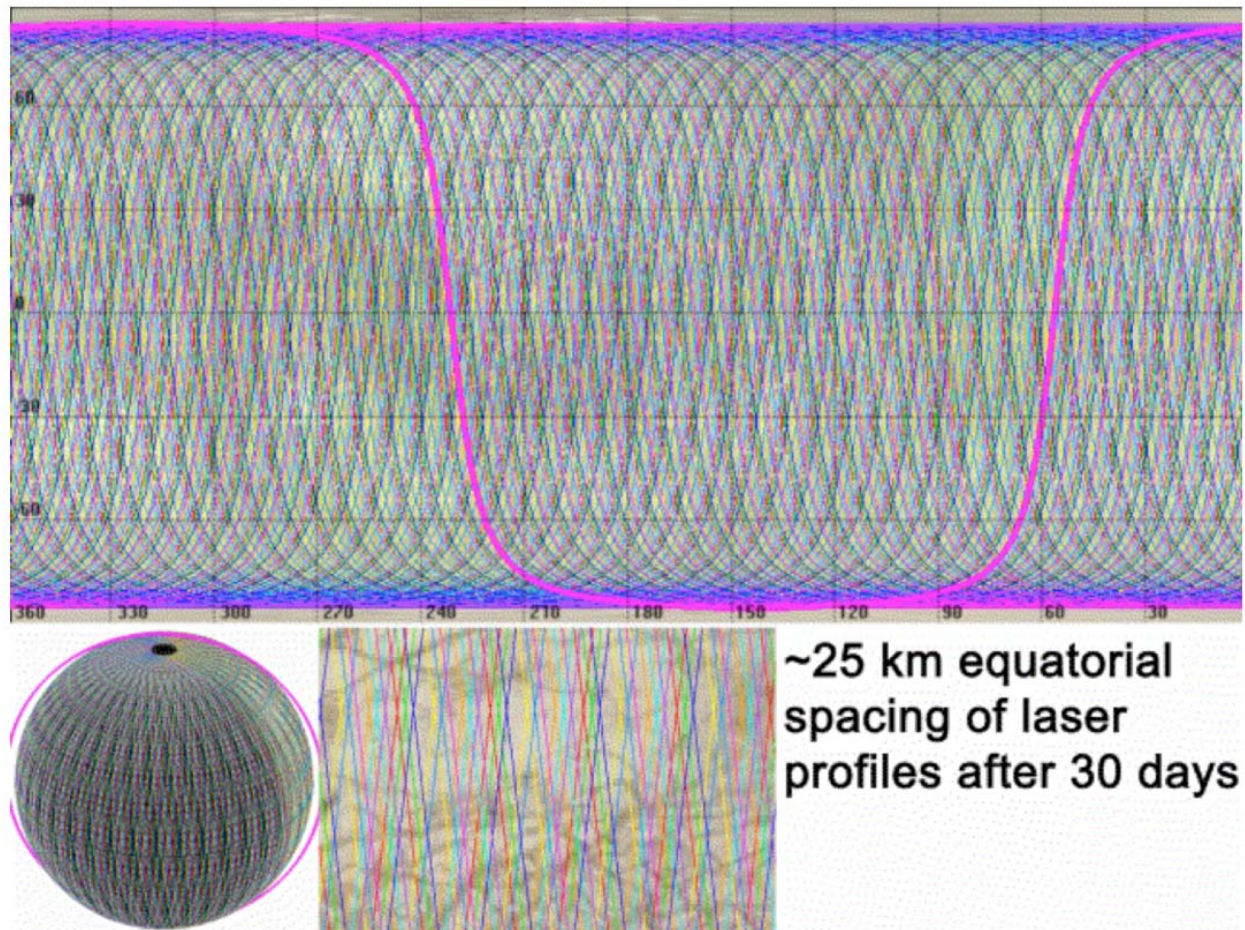
Figure B.2.8-4. Laser Altimeter coverage after one repeat cycle.

accomplish the above operations concepts. All orbits follow a single science profile of activities. There is no optimization per orbit or sharing of pointing or data volume, so negotiation is negligible. Maneuvers occur every few days; overall, activity intensity is low, with mostly continuous, simply sequenced background activities.

B.2.8.3 Development Supporting Europa Operations

Early consideration of operability issues in the system architecture and design is of great importance. The Europa Flyby Mission plans significant operations scenario development during Phases A-D. Science operations will be a strong element of the prelaunch flight systems engineering. Science operations scenarios will be developed early and at a level of detail that permits flight system design choices to be

assessed thoroughly. Operations and ground system architecture, requirements, models, and software will be developed to a level sufficient to support prelaunch development and flight system trade studies. Science planning tools will be developed such that they can be used to evaluate the ground and flight system requirements and capabilities. Based on these preparations, refinements can then be made much more confidently in cruise and throughout the mission to this unified ground and flight system architecture and its software requirements.

Modeling will be conducted to simulate representative operations in deep space, including Europa flyby operations. The ATLO phase includes testing of at least one representative operational sequence to be used during Europa encounters. These efforts, though they add early cost, should bring net savings to the

project over all life cycle phases because they make possible more efficient operations, and uncover problems at a time when something can be done to mitigate them.

Opportunities for process improvement are built into the schedule after launch. A long cruise period presents some challenges, among them the risks of personnel attrition and ground system obsolescence. However, the varying level of intensity—lower between gravity assists, for example—also offers opportunities to improve processes, software, IT infrastructure, and operations concepts and the science template for Europa observations. A Europa Orbiter Mission project would aim to fill the "bathtubs" between major events in cruise with periods of further development and training. The Europa Orbiter Mission would strategically defer some operations development until after launch. Doing so has several advantages. First, it obviates the need to staff the project up for major cruise events and down afterwards. Second, it allows the project to take advantage of improvements in technology as they become available and to work with a flight team more likely to be present during later operations than is the flight team in place at launch. Third, it affords the flight team enticing opportunities to contribute to the design of the operations system, improving staff skill and possibly retention as team members choose to remain with the project in part to see their efforts bear fruit in Europa orbit. Finally, it ensures that the operations team on the line during science operations is deeply familiar with the system, such that disruptions from faults or radiation issues can be handled in an expeditious, reliable, and expert manner.

Staffing levels should remain at approximately the late Phase D workforce level through launch and initial checkouts, after which it can drop to a more sustainable cruise staffing level. Cruise staffing should be relatively flat thereafter, with a moderate increase in development staff in the later portion of interplanetary cruise. Because the navigation team must

be fully capable for JOI, they would staff up to Jupiter cruise levels no later than six months before JOI. Spacecraft system and subsystem support needed to support navigation and maneuvering would also be added at this time. Other operations teams would staff up at around JOI to prepare for EOI, finalize the orbital science operations plan and supporting software, with the first ORTs for Europa science operations beginning 4 to 6 months after JOI.

B.2.9 *Systems Engineering*

Through key investments in infrastructure, engineering products, and team-building, the Europa Study Team is well positioned to move into pre-project formulation.

This section outlines the overall systems engineering approach and plan. The subsections that follow address three specific systems engineering challenges: radiation, planetary protection, and nuclear safety.

In general the Europa Orbiter Mission can be said to have the following technical and programmatic characteristics:

- Technical
    - Functioning in the presence of radiation flux, SEEs, radiation damage to parts and materials
    - Satisfying planetary protection of the Europan ocean, as well as of Ganymede and Callisto, from delivered bioburden
    - Lifetime and reliability over a long mission
    - Maintaining conservative resource margins
    - Integrating a suite of competitively selected science instruments from a diverse field of providers
    - Integrating radioisotope power sources
    - Contrasting thermal environments at Venus flyby and Jupiter
    - Critical orbit insertion at Jupiter and Europa

- Intense science operations schedule at Europa after years of unhurried cruise
- Keeping a 10-year-plus "corporate memory" of the requirements, detailed design, and the rationales for design choices

- Programmatic
  - Succeeding in a cost- and cost-profile-constrained environment
  - Coordinating the efforts of a large, diverse engineering team
  - Integrated the project and design with competitively selected instruments
  - Accommodating development and maturation issues of the radioisotope power sources
  - Multi-institution and potential multinational partnerships (JPL, APL, PIs)

To help address these concerns, the following overarching systems engineering objectives have been set for formulation:

- By System Requirements Review (SRR), produce a Baseline System Specification (L1-L3 Baseline; L4 Preliminary; L5 Key and Driving), a committed systems engineering schedule and cost profile, and a committed mission architecture.
- By Preliminary Design Review (PDR), produce a released set of procurement specifications, a fully developed preliminary design, and a committed project schedule and cost.

Institutional project and line management is uniformly committed to making major strides in systems engineering, supporting and enforcing the following approach:

- Exercise rigorous engineering discipline. Expect engineering rationale to be documented as complete and logical chains of thought, and in appropriate

tools (Mathematica/Maple not Power-Point; IOMs not emails)

- Make use of emerging new systems engineering capabilities as appropriate, including system modeling language standards and tooling, model integration and exchange standards and tooling, and Web-based report generation.
- Starting from the beginning, build persistent and evolvable artifacts.
- Starting from the beginning, build a core team of systems engineers who can faithfully promulgate the architecture later as the project grows.
- Proactively align with forthcoming NPR 7120.5E (NASA 2012).
- Emphasize architecture and design space exploration through MCR. An architectural approach keeps the team properly focused on the "why," and design space keeps us properly focused on the concept rather than a point design. In this endeavor, trusted models and analytical tools are essential investments.
- Make decisions by a process that is explicitly guided by Architecture, is timely and responsive, is transparent to all stakeholders, and includes balanced consideration of multiple experienced viewpoints.

The Europa OrbiterOrbiter Mission is well positioned to move into pre-project formulation. The Europa Study Team has made key investments in infrastructure, engineering artifacts, and team-building, as described below:

- Infrastructure has been under development for the long term. Already set up and in initial use are a collaborative Systems Modeling Language (SysML) environment (MagicDraw/Teamwork Server), a collaborative architecture development environment (Architecture Framework Tool), the project doc-

ument repository (DocuShare), and the project workflow management system (JIRA).

- Key plans and processes are in place. Key parts of the architecture description are in preliminary form, as outlined in this report. The core of a system model is established.
- Our team processes and practices are maturing. Cost estimates, some technical margin estimates, and mechanical configuration changes have been improved over past practice.

From this strong starting point, a plan that achieves robust maturity at SRR and PDR has been constructed. The sketch of this plan, expressed as key artifacts per life-cycle phase through PDR, is shown in Tables B.2.9-1 through B.2.9-4. In these tables the changes from one table to the next are shown in **bold**

blue font, and the parentheticals following the artifact names denote required maturity levels:

- (A): Approach is defined, and possibly a sketch of the artifact.
- (K&D): Key and Driving cases are identified and covered.
- (P): Preliminary. A full version for review and discussion leading to a baseline version.
- (B): Baseline. The artifact is under configuration control.
- (U): Update.

After PDR, systems engineering focus changes from development to implementation: managing change control process, while maintaining architectural integrity; implementing I&T and V&V programs; and preparing for flight operations.

Table B.2.9-1. Present maturity of systems engineering artifacts.

At Tech Review	Systems Engineering Plan: Key Artifacts per Life-Cycle Phase Artifact Type					
SCOPE	**Plan**	**Scenario**	**Model**	**Analysis & Sim**	**Report**	**Spec**
Program (L1)						L1 Rqmts (K&D)
Project (L2)	Arch Dev Plan (P) SEMP (A) Model Mgt Plan (A)	Driving Mission (K&D)	Trajectory (P) Science Margin (A) Data Margin (P) FS Radiation (P)	Delta-V/Prop (P) Science Margin (A) Data Margin (P) FS Radiation Life (P)	Concept Report (P) Msn Arch Descr (P) Ops Concept (A) Tech Assessment (A) Eng Dev Assess (A) Top Risks (A)	L2 Rqmts (A) Env Definition (A)
System (L3)		Flight Sys Ops (K&D)	FS Functional (P) FS Physical (P) FS Shielding (P) FS Power (P) FS Static Mech (P) FS Thermal (P) FS Telecom Link (P) FS Attitude Ctrl (P)	FS Mass Margin (P) FS Shield Mass (P) FS Pwr Margin (P) FS Mass Props (P) FS Therm Balance (P) FS Link Margin (P) FS Pntg Margin (P)		L3 Rqmts (A)
Subsystem (L4)			Power (K&D) Thermal (K&D) Propulsion (K&D) Telecom (K&D) Avionics (K&D) Structure (K&D)	Power Bus Sim (P) Therm Balance (P) JOI Perf (A) EIRP, G/T (P) C&DH Throughput (A) LV Static Envel (P)		
Component (L5)			Radiation Effects (P) DHMR Effects (P)	Component Life (P) Parts/Matl Issues (P)	Approved Parts (A) Approved Matls (A)	

Legend (right margin): Blue = Change · (U) Update · (B) Baseline · (P) Preliminary · (K&D) Key & Driving · (A) Approach

Table B.2.9-2. Maturity of systems engineering artifacts at MCR.

At MCR	Systems Engineering Plan: Key Artifacts per Life-Cycle Phase Artifact Type						
	Plan	Scenario	Model	Analysis & Sim	Report	Spec	
Program (L1)						L1 Rqmts **(P)**	
Project (L2)	Arch Dev Plan **(B)** SEMP **(P)** Model Mgt Plan **(P)** **Integr Plan (A)** **V&V Plan (A)**	Driving Mission **(P)**	Trajectory **(B)** Science Margin **(B)** Data Margin **(B)** FS Radiation **(B)**	Delta-V/Prop (P) Science Margin **(P)** Data Margin (P) FS Radiation Life (P) **Rqmt Traceability (P)**	Concept Report **(B)** Msn Arch Descr (P) Ops Concept **(P)** Tech Assessment **(P)** Eng Dev Assess **(P)** Top Risks **(P)**	L2 Rqmts **(P)** Env Definition **(P)** **External ICDs (K&D)** **Intersystem ICDs (K&D)** **S/C–P/L ICD (K&D)**	**Blue = Change**
System (L3)		Flight Sys Ops **(P)**	FS Functional (P) FS Physical (P) FS Shielding (P) FS Power (P) FS Static Mech (P) FS Thermal (P) FS Telecom Link (P) FS Attitude Ctrl (P) **FS Behavior (P)** **FS Fault Contnmt (P)**	FS Mass Margin (P) FS Shield Mass (P) FS Pwr Margin (P) FS Mass Props (P) FS Therm Balance (P) FS Link Margin (P) FS Pntg Margin (P)		L3 Rqmts **(K&D)** **Intra-FS ICDs (K&D)**	(U) Update
Subsystem (L4)			Power **(P)** Thermal **(P)** Propulsion **(P)** Telecom **(P)** Avionics **(P)** Structure **(P)**	Power Bus Sim (P) Therm Balance (P) JOI Perf **(P)** EIRP, G/T (P) C&DH Throughput **(P)** LV Static Envel (P)			(B) Baseline
Component (L5)			Radiation Effects (P) DHMR Effects (P)	Component Life (P) Parts/Matl Issues (P)	Approved Parts **(P)** Approved Matls **(P)**		(P) Preliminary

(Legend, right column, reading down: Blue = Change · (U) Update · (B) Baseline · (P) Preliminary · (K&D) Key & Driving · (A) Approach)

SCOPE (vertical label on left)

Table B.2.9-3. Maturity of systems engineering artifacts at SRR.

At SRR	Systems Engineering Plan: Key Artifacts per Life-Cycle Phase Artifact Type						
	Plan	Scenario	Model	Analysis & Sim	Report	Spec	
Program (L1)						L1 Rqmts (B)	
Project (L2)	Arch Dev Plan (U) SEMP (B) Model Mgt Plan (B) Integr Plan (P) V&V Plan (P) **S/W Mgt Plan (P)**	**Mission Plan (K&D)**	Trajectory (U) Science Margin (U) Data Margin (U) FS Radiation (U)	Delta-V/Prop (B) Science Margin (B) Data Margin (B) FS Radiation Life (B) Rqmt Traceability (B)	Concept Report (U) Msn Arch Descr (B) Ops Concept (B) Tech Assessment (B) Eng Dev Assess (B) Top Risks (B) **Instrument AO PIP (B)**	L2 Rqmts (B) Env Definition (B) External ICDs (B) Intersystem ICDs (P) S/C-P/L ICD (P)	**Blue = Change**
System (L3)		Flight Sys Ops (B)	FS Functional (B) FS Physical (B) FS Shielding (B) FS Power (B) FS Static Mech (B) FS Thermal (B) FS Telecom Link (B) FS Attitude Ctrl (B) FS Behavior (B) FS Fault Contnmt (B)	FS Mass Margin (P) FS Shield Mass (P) FS Pwr Margin (P) FS Mass Props (P) FS Therm Balance (P) FS Link Margin (P) FS Pntg Margin (P) **FS PRA (A)** **FS Func FMECA (A)** **FS TAYF Exceptions (A)**	**Ground Sys Arch (P)** **Payload Arch (P)**	L3 Rqmts (B) Intra-FS ICDs (P) **Procurement Specs (P)**	(U) Update (B) Baseline (P) Preliminary (K&D) Key & Driving (A) Approach
Subsystem (L4)			Power (B) Thermal (B) Propulsion (B) Telecom (B) Avionics (B) Structures (B)	Power Bus Sim (P) Therm Balance (P) JOI Perf (P) EIRP, G/T (P) C&DH Throughput (P) LV Static Envel (P)		**L4 Rqmts (P)** **Intrasubsystem ICDs (P)**	
Component (L5)			Radiation Effects (B) DHMR Effects (B)	Component Life (P) Parts/Matl Issues (P)	Approved Parts (P) Approved Matls (P)		

(SCOPE — vertical label along left side)

Table B.2.9-4. Maturity of systems engineering artifacts at PDR.

At PDR	Systems Engineering Plan: Key Artifacts per Life-Cycle Phase Artifact Type						
	Plan	Scenario	Model	Analysis & Sim	Report	Spec	
Program (L1)						L1 Rqmts (B)	Blue = Change
Project (L2)	Arch Dev Plan (B) SEMP **(U)** Model Mgt Plan **(U)** Integr Plan **(B)** V&V Plan **(B)** S/W Mgt Plan **(B)**	Mission Plan **(P)**	Trajectory (U) Science Margin (U) Data Margin (U) FS Radiation (U)	Delta-V/Prop **(U)** Science Margin **(U)** Data Margin **(U)** FS Radiation Life **(U)** Rqmt Traceability **(U)** **Mission Fault Tree (P)**	Concept Report (U) Msn Arch Descr **(U)** Ops Concept **(U)** Tech Assessment **(U)** Eng Dev Assess **(U)** Top Risks **(U)** Instrument AO PIP (B)	L2 Rqmts (B) Env Definition (B) External ICDs (B) Intersystem ICDs **(B)** S/C–P/L ICD **(B)**	(U) Update
System (L3)		Flight Sys Ops **(U)**	FS Functional (B) FS Physical (B) FS Shielding (B) FS Power (B) FS Static Mech (B) FS Thermal (B) FS Telecom Link (B) FS Attitude Ctrl (B) FS Behavior (B) FS Fault Contnmt (B)	FS Mass Margin **(B)** FS Shield Mass **(B)** FS Pwr Margin **(B)** FS Mass Props **(B)** FS Therm Balance **(B)** FS Link Margin **(B)** FS Pntg Margin **(B)** FS PRA **(P)** FS Func FMECA **(P)** FS TAYF Exceptions **(P)**	Ground Sys Arch **(B)** Payload Arch **(B)**	L3 Rqmts **(B)** Intra-FS ICDs **(B)** Procurement Specs **(B)**	(B) Baseline
Subsystem (L4)			Power (B) Thermal (B) Propulsion (B) Telecom (B) Avionics (B) Structures (B)	Power Bus Sim **(B)** Therm Balance **(B)** JOI Perf **(B)** EIRP, G/T **(B)** C&DH Throughput **(B)** LV Static Envel **(B)**	**Subsys Des Desc (P)** **P/L Design Desc (P)**	L4 Rqmts **(B)** Intrasubsystem ICDs **(B)**	(P) Preliminary
Component (L5)			Radiation Effects (B) DHMR Effects (B)	Component Life **(B)** Parts/Mat Issues **(B)**	Approved Parts **(B)** Approved Matls **(B)**	**L5 Rqmts (P)**	(K&D) Key & Driving

(A) Approach   (K&D) Key & Driving   (P) Preliminary   (B) Baseline   (U) Update

SCOPE

B.2.9.1   Radiation

The effects of radiation on the spacecraft are mitigated by the efficient use of inherent shielding provided by the spacecraft itself and additional dedicated shield mass, combined with radiation-tolerant materials and electronics.

The Europa Orbiter spacecraft would be exposed to naturally occurring and self-generated radiation from launch to the end of mission. The self-generated radiation, composed of neutrons and gamma rays, is evolved from the natural decay of nuclear fuel used in the Advanced Stirling Radioisotope Generators (ASRGs). The naturally occurring radiation encountered during the cruise phase between launch and Jupiter Orbit Insertion (JOI) consists of solar flare protons and background galactic cosmic ray heavy ions. Between JOI and the end of the mission, the spacecraft is exposed to protons, electrons, and heavy ions trapped in the Jovian magnetosphere.

The radiation encountered during the mission can affect onboard electronics, nonmetallic materials, thermal control materials, and surface coatings by depositing energy through ionization, henceforth called total ionizing dose (TID), and can cause noise in science instrument and star-tracker detectors due to the intense proton and electron flux encountered in the Jovian system. The expected accumulated TID from launch to end of mission as a function of effective aluminum shielding thickness is shown in Table B.2.9-5. Peak electron and

proton fluxes for the mission are shown in Table B.2.9-6.

The selection of electronic parts with respect to their radiation tolerance and reliability in the Europa radiation environment will be achieved through a combination testing and analysis. The minimum acceptable total ionizing dose hardness of electronic devices will be 100 kilorad. The minimum single event effects (SEE) hardness will be documented in a Parts Program Requirements (PPR) document. A combination of radiation testing (TID, DDD, and SEE) of electronic devices and buying vendor guaranteed radiation hardened parts that meet the minimum TID and SEE requirements will ensure that robust electronics will be used in spacecraft and instrument electronics. Radiation testing will be done at industry standard high dose rates and at low dose rate for electronic devices types that are susceptible to Enhanced Low Dose Rate Sensitivity (ELDRS) effects (primarily bi-polar devices). Electronic part parameter degradation observed during radiation testing will be documented and used as input into the spacecraft and instrument electronics end of mission Worst Case Analysis (WCA). Electronic devices that do not meet the minimum TID and SEU hardness requirements will not be used within the spacecraft electronics or instruments unless approved by a requirements waiver.

The selection guidelines of non-metallic materials for radiation susceptibility and reliability has been documented in a report entitled, "Materials Survivability and Selection for Nuclear Powered Missions" by Willis [*JPL D-34098*].

Table B.2.9-5. Expected Orbiter Mission accumulated total ionizing dose as a function of shield thickness.

Aluminum Thickness (mil)	Total Ionizing Dose (krad Si)				
	Electron	Photon	Proton	ASRG	Total
100	1500	5.3	51.7	1.3	1560
200	685	6.0	12.1	1.3	704
400	258	7.0	2.1	1.3	268
600	134	7.6	1.0	1.3	140
800	80.5	8.1	0.6	1.3	90.5
1000	53.4	8.4	0.4	1.3	63.5
1200	37.9	8.7	0.3	1.3	48.2
1400	28.1	8.8	0.2	1.3	38.4
1600	21.6	8.9	0.2	1.3	32.0

Table B.2.9-6. Expected Orbiter Mission peak electron and proton flux.

Particle Energy (MeV)	Flux (#>Energy cm^{-2} sec^{-1})	
	Electron	Proton
10	1.6E6	1.5E5
20	4.6E5	2.8E4
30	2.1E5	7.3E3
50	7.0E4	6.9E2
100	1.5E4	1.5E1

Detailed evaluations will be performed for these materials after exposure to end of mission radiation environment to ensure end of life performance requirements are met. Radiation testing will be performed for materials which do not have available radiation data.

The Europa Orbiter mission will develop an Approved Parts and Materials List (APML) for the purpose of identifying standard parts approved for flight equipment developed under the project's cognizance. The APML will be populated with EEE parts and materials, as well as many critical parts such as sensors, detectors, power converters, FPGAs, and non-volatile memories. Each entry will be accompanied with a Worst Case Datasheet (WCD) and application notes describing proper use of the part at selected radiation levels. Dissemination of this information early in the design process is critical to enable the spacecraft electronics and instrument providers to adequately design for the radiation environment.

Every approved part listed on the APML will meet the reliability, quality, and radiation requirements specified in the PPR. The APML will be updated as new radiation data become available. Parts not listed as approved on the APML are defined as non-standard parts and will require a Non-standard Part Approval Request (NSPAR) for use in the Europa Orbiter mission. All non-standard parts will be reviewed, screened, and qualified to the requirements of PPR.

Every part on the APML will be approved by the Parts Control Board (PCB). The PCB recommends and approves parts for inclusion in the APML. Criteria will be based on absolute need, the number of subsystems requiring the part, qualification status, TID, Single Event Effects (SEE), and procurement specification review. Mission designers should use standard parts to the maximum extent possible so that they can reduce the radiation testing and qualification expenditure to the minimum.

Radiation-induced effects on instrument detectors and other key instrument components can ultimately impact the quality and quantity of the mission science return and the reliability of engineering sensor data critical to flight operations. High-energy particles found within the Europa environment will produce increased transient detector noise as well as long-term degradation of detector performance and even potential failure of the device. Transient radiation effects are produced when an ionizing particle traverses the active detector volume and creates charges that are clocked out during readout. Radiation-induced noise can potentially swamp the science signal, especially in the infrared wavebands where low solar flux and low surface reflectivity result in a relative low signal. Both TID and DDD effects produce long-term permanent degradation in detector performance characteristics. This includes a decrease in the ability of the detector to generate signal charge or to transfer that charge from the photo active region to the readout circuitry; shifts in gate threshold voltages; increases in dark current and dark current non-uniformities, and the production of high-dark-current pixels (hot pixels or spikes). It is important to identify and understand both the transient and permanent performance degradation effects in order to plan early for appropriate hardware and operations risk mitigation to insure mission success and high-quality science returns.

A JEO Detector Working Group (DWG) was formed in FY08 to evaluate the detector and laser components required by the planning payload and stellar reference unit. The DWG participants included experienced instrument, detector, and radiation environment experts from APL and JPL. For each technology required for the payload, the DWG (i) reviewed the available radiation literature and test results, (ii) estimated the radiation environment incident on the component behind its shield, and (iii) assessed the total dose survivability (both TID and DDD) and radiation-induced

transient noise effects during peak flux periods. The assessment included the following technologies: visible detectors, mid-infrared and thermal detectors, micro-channel plates and photomultipliers, avalanche photodiodes, and laser-related components (pump diode laser, solid-state laser, fiber optics).

The DWG assessment, reported in "Assessment of Radiation Effects on Science and Engineering Detectors for the JEO Mission Study" [JPL D-48256], concluded that the radiation challenges facing the JEO notional payload and SRU detectors and laser components are well understood. With the recommended shielding allocations, the total dose survivability of these components is not considered to be a significant risk. In many cases, the shielding allocation was driven by the need to reduce radiation-induced transient noise effects in order to meet science and engineering performance requirements. For these technologies—notably mid-infrared detectors, avalanche photodiode detectors, and visible detectors for star tracking—the extensive shielding (up to 3-cm-thick Ta) for transient noise reduction effectively mitigates all concern over total dose degradation. For the remaining technologies, more modest shielding thicknesses (0.3–1.0 cm Ta, depending upon the specific technology) were judged to be sufficient to reduce the total dose exposure and transient noise impact to levels that could be further reduced with known mitigation techniques (detector design, detector operational parameters, algorithmic approaches and system-level mitigations). The DWG conclusions reached for the JEO are applicable for the science detectors and the SRU onboard the Europa Orbiter mission.

A rigorous "test-as-you-fly" policy with respect to detector radiation testing, including irradiation with flight-representative species and energies for TID, DDD, and transient testing, will be adopted for the Europa Orbiter mission.

The Jovian electron environment also causes dielectric materials and ungrounded metals to collect charge on spacecraft external surfaces and within the spacecraft. This causes transient voltage and currents in the spacecraft when an electrostatic discharge (ESD) event occurs. Surface charging effects are mitigated by limiting the differential charging of external materials. This is accomplished by using materials that have surface coatings and treatments that allow the accumulated charges to bleed to spacecraft ground. A significant number of such surface materials have been used extensively in severe charging environments for spacecraft with long lifetimes (typically geosynchronous communications spacecraft, but also Juno) and are usable for the Europa Orbiter Mission. These materials include

- Carbon-loaded Kapton thermal blankets
- Indium-tin-oxide-coated gold Kapton thermal blankets
- Germanium-coated, carbon-loaded Kapton thermal blankets
- Electrostatic-conductive white paint
- Electrostatic-conductive black paint
- Composite materials
- Metallic materials

When surface discharge does occur, the voltage and current transients are mitigated by shielding around harness lines and using interface electronic devices that can tolerate the energy from ESD-induced transients that couple into the harness center conductors.

Internal ESD is controlled by shielding to reduce the electron flux present at dielectric materials within the spacecraft (typically circuit boards) and by limiting the amount of ungrounded metal (ungrounded harness conductors, connector pins, device radiation shields, part packages). The shielding required to reduce the TID to acceptable levels for the Europa Orbiter Mission is more than sufficient to reduce the electron flux enough to preclude discharge events to circuit boards. Grounding

of radiation shields, part packages, harness conductors, and connector pins through ESD bleed wires or conductive coatings limits the ungrounded metals to small areas that cannot store enough energy to cause discharges that can damage electronic devices.

The surface and internal charging methodology has been used extensively in a severe charging environment for spacecraft with long lifetimes and was used specifically on the Juno project.

The spacecraft's exposure to radiation is attenuated to acceptable levels by providing shielding between the external environment and the sensitive materials and electronic parts in the spacecraft. Most of the spacecraft electronics are placed in a shielded vault. Payload electronics and sensor heads external to the vault have shielding tailored for their design and location on the spacecraft. Science instrument detector shielding to suppress radiation-induced background noise and permanent damage effects is achieved through a combination of instrument-level shielding for detector support electronics and internal high-Z material shielding for the detector devices.

Efficient use of dedicated shield mass is achieved through a nested shield design, shown in Figure B.2.9-1. Spacecraft structure and placement of the propulsion subsystem hardware (fuel tanks, oxidizer tanks, helium pressurant tanks, and propellant that remains in the tanks after JOI) provide significant collateral shielding to the electronics packaged within the vault. The vault's wall thickness and material composition, 5.3-mm-thick aluminum, limit the Orbiter Mission TID to 150 krad for the enclosed electronics. Localized shielding at the assembly level reduces the Orbiter Mission TID from 150 krad to 50 krad at the device level for all electronics.

The dedicated shield mass for the Orbiter Mission is a total of 167 kg, as shown in Table B.2.9-7. The shield mass was calculated based on a detailed radiation transport analysis
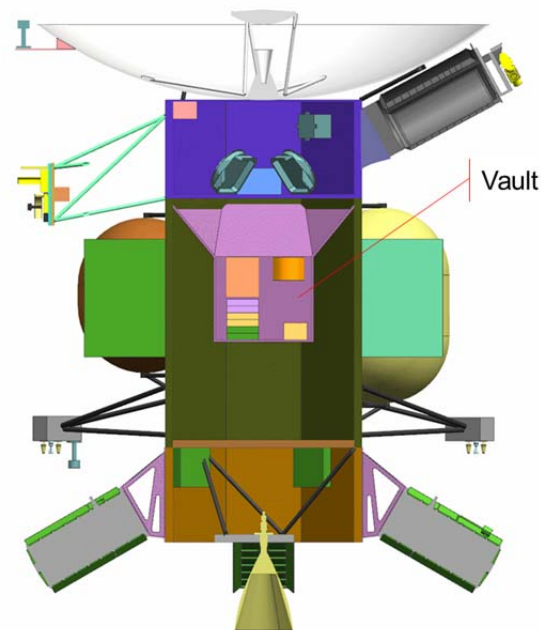
Figure B.2.9-1. Orbiter Mission electronics are shielded by the spacecraft structure, propulsion tanks, and a dedicated electronics vault.

that takes into account the spacecraft configuration shown in Figure B.2.9-1; material composition and thickness of the spacecraft structural elements and propulsion tanks; and the locations of electronic units and science instruments. Analysts used the following process:

1. Generate spacecraft element configuration and locations from a CAD model.
2. Explicitly calculate the shielding effectiveness of materials used in spacecraft structure, propulsion tanks, electronics unit chassis, dedicated vault, and added electronics assembly shielding based on material composition, density, and location using the NOVICE radiation transport code. For this analysis, the propulsion tanks are modeled with 436 kg of fuel and oxidizer in the tanks for the portion of the mission between Jupiter Orbit Insertion (JOI) and Europa Orbit Insertion (EOI). After EOI, the propellant tanks are modeled as empty tanks.

3. To minimize the cost and risk of assuming electronic parts with higher radiation tolerance, assume all spacecraft electronics to use 300-krad-tolerant electronic parts.

4. Understand science instrument electronics co-located with detectors to have radiation tolerances that are instrument-specific (see Section B.2.2).

5. Through adjustments to assembly-level shielding mass, shield all spacecraft electronics assemblies to a TID of 150 krad or less at end of mission (i.e., to account for environmental uncertainty, they are given a radiation design factor [RDF] greater than or equal to 2 at the end of the mission).

6. Shield science instrument electronics to have a minimum RDF of 2 for TID at the end of the mission.

7. To minimize cost, use aluminum shielding for all spacecraft electronics except science instrument and star-tracker detectors.

8. To minimize the radiation-induced noise at the detector location, shield science instrument and star-tracker detectors using high-atomic-number materials (such as tantalum) (see Section B.2.2).

9. At the individual assembly level, to allow the use of off-the-shelf electronics without modification, wrap shielding around each assembly rather than integrating it into the assembly chassis.

10. Model circuit boards within the electronic assemblies as unpopulated boards. (Modeling component layouts on boards will be performed as the project progresses into Phase B. Including component layout in the radiation transport model will further reduce TID at the device level.)

Significant opportunities to reduce the dedicated shield mass have been identified alt-

Table B.2.9-7. Calculated shield masses to reduce the mission TID below 150 krad within each assembly.

Item	Shield Mass (kg)
Vault Structure	40.6
C&DH Subsystem	4.3
Power Subsystem	9.8
MIMU (2)	7.8
SDST (2)	4.7
WDE (4 slices)	3.5
Ka HVPS (2)	5.4
X HVPS (2)	4.8
ASRG (5)	48.2
Star-Tracker (2)	13.7
Pressure Transducer (10)	3.9
Science Electronics	13.7
Topographic Imager	1.5
Laser Altimeter	4.7
Orbiter Mission Total	167

hough they have been unexercised at this time. These opportunities include the following:

1. Change electronics unit placement within the vault to protect units with lower-TID-capable electronic parts.

2. Place electronics cards within units to provide the lowest local TID at the part level.

3. Use a more efficient shield material than aluminum.

4. Add rigor to the radiation transport model by including populated boards and individual device shielding.

5. Integrate the shielding into the electronics chassis.

6. Use multiple-material layered shielding.

The shield masses in Table B.2.9-7 have been incorporated into the spacecraft MEL.

B.2.9.2   Planetary Protection

NASA Planetary Protection policy (NPR 8020.12C [NASA 2005]) specifies requirements for limiting forward contamination in accordance with Article IX of the 1967 Outer Space Treaty.

As Europa is a body of extreme interest to the astrobiological community as a possible loca-

tion for the emergence of extra-terrestrial life, contamination of Europa with Earth-derived biology must be carefully avoided.

The mission's plan for responding to planetary protection requirements is to perform Dry Heat Microbial Reduction (DHMR) on as much of the spacecraft as possible, as late in the integration flow as possible. DHMR involves raising the bulk temperature of the spacecraft above the survival threshold for microbes and their spores. For materials contamination reasons, this bake out is typically done in vacuum or inert gas (nitrogen). To the extent possible, all spacecraft components will be designed to accommodate late integration DHMR without disassembly or recalibration. However, components or instrumentation unable to comply with DHMR requirements may be removed and sterilized through other means.

The extent to which DHMR sterilization and subsequent recontamination must reduce the spacecraft bioburden before liftoff is greatly influenced by the expected impact of post-launch sterilization processes and contamination probabilities. These include:

a) Probability of organism survival during interplanetary cruise
b) Probability of organism survival in the Jovian radiation environment
c) Probability of impacting Europa
d) Probability of organism survival on the surface of Europa before sub-surface transfer
e) The duration required for transport to the Europan subsurface
f) Organism survival and proliferation after subsurface transfer

Each of these factors will be carefully examined to determine the ultimate allowable bioburden at launch and the required effectiveness of DHMR to maintain compliance with NASA regulation and international treaty.

B.2.9.3   Nuclear Safety

The Europa Orbiter Mission concept requires the use of nuclear energy sources for electrical power and heating. The radioactive material used for this purpose is potentially hazardous to humans and the environment unless precautions are taken for its safe deployment. The following circumstances are of concern:

- Handling: People would be in the vicinity while nuclear sources (ASRGs or RHUs) are being constructed, transported, and installed on the spacecraft.
- Launch: In the event of a catastrophic LV failure, the spacecraft with its nuclear components would be potentially subject to explosion, fire, impact, or the heat and forces of immediate reentry.
- Injection: If injection into interplanetary flight is not achieved, the spacecraft may be left in an Earth orbit that could decay to reentry after some time, thus exposing nuclear components to reentry conditions.
- Earth Flyby: If unplanned trajectory errors cause the spacecraft to reenter Earth's atmosphere, nuclear components would be exposed to reentry conditions.

Safety from nuclear hazards in each of these circumstances is essential.

The National Environmental Policy Act of 1969 (NEPA) specifies measures intended to mitigate these concerns. [This is enough ID for a public law—no need to put it in the References.]Project compliance with NEPA is mandatory and is described in more detail below.

B.2.9.3.1   NEPA Compliance

Environmental review requirements would be satisfied by the completion of a mission-specific Environmental Impact Statement (EIS) for the Europa Orbiter Mission. In accordance with the requirements of NPR 7120.5D, NPR 7120.5E (pending) and NPR 8580.1(NASA 2007, 2012), the Record

of Decision (ROD) for this EIS would be finalized prior to or concurrent with project PDR.

The Europa Orbiter Mission Launch Approval Engineering Plan (LAEP) is completed no later than the Mission Definition Review (MDR). This plan describes the approach for satisfying NASA's NEPA requirements for the mission, and the approach for complying with the nuclear safety launch approval process described in Presidential Directive/National Security Council Memorandum #25 (PD/NSC-25) (1977) and satisfying the nuclear safety requirements of NPR 8715.3 (NASA 2010b). The LAEP provides a description of responsibilities, data sources, schedule, and an overall summary plan for preparing the following:

- A mission-specific environmental review document and supporting nuclear safety risk-assessment efforts
- LV and flight system/mission design data requirements to support nuclear risk assessment and safety analyses in compliance with the requirements of NPR 8715.3 (NASA 2010b) and the PD/NSC-25 nuclear safety launch approval process
- Support of launch site radiological contingency planning efforts
- Earth swing-by analysis
- Risk communication activities and products pertaining to the NEPA process, nuclear safety, and planetary protection aspects of the project.

It is anticipated that NASA HQ would initiate the Europa Orbiter Mission NEPA compliance document development as soon as a clear definition of the baseline plan and option space has been formulated. The Department of Energy (DOE) provides a nuclear risk assessment to support the environmental review document, based upon a representative set of environments and accident scenarios compiled by the KSC Launch Services Program working with JPL. This deliverable might be modeled after the approach used for the MSL EIS.

DOE provides a Nuclear Safety Analysis Report (SAR) based upon NASA-provided mission-specific launch system and flight system data to support the PD/NSC-25 compliance effort. The SAR is delivered to an ad hoc Interagency Nuclear Safety Review Panel (INSRP) organized for the Europa Orbiter Mission. This INSRP reviews the SAR's methodology and conclusions and prepares a Safety Evaluation Report (SER). Both the SER and the SAR are then provided by NASA to the Environmental Protection Agency, Department of Defense, and DOE for agency review. Following agency review of the documents and resolution of any outstanding issues, NASA, as the sponsoring agency, would submit a request for launch approval to the Director of the Office of Science and Technology Policy (OSTP). The OSTP Director reviews the request for nuclear safety launch approval and can either approve the launch or defer the decision to the President.

As part of broader nuclear safety considerations, the Europa Orbiter Mission would adopt ATLO, spacecraft, trajectory (e.g., for sufficiently high orbit at launch, and for Earth flybys), and operations requirements that satisfy the nuclear safety requirements of NPR 8715.3 (NASA 2010b).

Development of coordinated launch site radiological contingency response plans for NASA launches is the responsibility of the launch site Radiation Protection Officer. Comprehensive radiological contingency response plans, compliant with the National Response Framework and appropriate annexes, would be developed and put in place prior to launch as required by NPR 8715.2 and NPR 8715.3 (NASA 2009a, 2010b). The Europa Orbiter Mission would support the development of plans for on-orbit contingency actions to complement these ground-based response plans.

A project-specific Risk Communication Plan would be completed no later than the MDR. The Risk Communication Plan details the rationale, proactive strategy, process, and products of communicating risk-related aspects of the project, including nuclear safety and planetary protection. The communication strategy and process would comply with the approach and requirements outlined in the Office of Space Science Risk Communication Plan for Deep Space Missions (JPL D-16993, 1999).

B.3 Programmatics

B.3.1 Management Approach

The management approach draws upon extensive experience from Galileo and Cassini. It follows NPR 7120.5E and incorporates NASA lessons learned.

The project approach includes a work breakdown structure (WBS), technical management processes conducted by veteran systems engineers, and integrated schedule/cost/risk planning and management. The project will take advantage of existing infrastructure for planning, acquisition, compliance with the National Environmental Policy Act (NEPA), compliance with export control regulations (including International Traffic in Arms Regulations), independent technical authority (as called for in NPR 7120.5E), mission assurance, ISO 9001 compliance, and earned value management (EVM).

The Europa Orbiter Mission employs JPL's integrated project controls solutions to manage and control costs. Skilled business and project control professionals are deployed to projects, utilizing state of the art tools and executing processes that support the project cost, schedule, and risk management requirements. Key attributes of the project controls solution are as follows:

- The Business Manager, project focal point on all business management issues, and the project control staff lead

project planners and managers in application of the most effective and efficient implementation of project control processes.
- Mature and successfully demonstrated cost and schedule tools are employed.
- Cost and schedule data are tied directly to work scope.
- "Early warning" metrics are provided monthly to key decision makers. Metrics include 1) cost and schedule variances based on the cost value of work performed and 2) critical-path and slack analysis derived from fully integrated end-to-end network schedules. Each end-item deliverable is scheduled with slack to a fixed receivable. Erosion of this slack value is tracked weekly and reported monthly.
- An integrated business management approach is applied to all system and instrument providers. This approach includes relative performance measurement data integrated into the total project database for a comprehensive understanding of project cost and schedule dynamics.
- Risk management processes are integrated with the liens management process for full knowledge of project reserve status. Early risk identification is maintained as a potential threat to project reserves. Reserve utilization decisions are made with the knowledge of risks and risk mitigation, project performance issues, and increases in scope.

JPL flight projects that have used this integrated project controls approach include Juno, Grail, MSL, and Phoenix.

Requirements for project controls evolve throughout the project life cycle. Pre–Phase A and Phase A will require less support than phases B, C, and D. During Phase B, the project controls capability is established at full strength to establish all the appropriate data-

bases and gate products required for a successful Confirmation Review. During phases C and D, the project controls will be fully functioning with recurring performance measurement analysis and cost and schedule tracking reports. During phases E and F, the project controls function reduces to minimal levels.

B.3.2   WBS

The Europa Orbiter Mission Work Breakdown Structure (WBS) is structured to enable effective cost, schedule and management integration. The WBS is derived from JPL's Standard Flight Project WBS Version 5 and is fully compliant with NPR 7120.5E. This WBS is a product-oriented hierarchical division of the hardware, software, services, and data required to produce end products. It is structured according to modular design of the spacecraft, and reflects the way the work would be implemented, and the way in which project costs, schedule, technical and risk data are to be accumulated, summarized, and reported.

The top-level WBS is shown Figures B.3.2-1 and B.3.2-2.

B.3.3   Schedule

A top-level schedule and implementation flow is shown in Figure B.3.3-1. The phase durations draw on experience from previous outer planet missions and are conservative. A bottom-up, WBS-based integrated schedule would be generated during Pre–Phase A.

B.3.3.1   Pre–Phase A

Up to and including this report, many alternative concept studies have been conducted. Those studies form the basis of an assessment of alternatives that have resulted in the current mission concept and its readiness to complete Pre–Phase A. To complete Pre-Phase A, a pre-project team would be formed to refine the baseline mission concept and implementation plan to align with programmatic goals and objectives. This refinement, along with interactions with NASA and other potential stakeholders, will result in further definition of the mission concept and draft project-level requirements.

The Pre–Phase A activities include completion of Pre–Phase A Gate Products specified in NPR 7120.5D and the forthcoming revision NPR 7120.5E (NASA 2007, NASA 2012 (pending)), preparation of a Project Information Package (PIP) in support of NASA's development of an AO for instrument acquisition, and a Mission Concept Review leading to Key Decision Point (KDP) A. In addition to those activities required for transition to Phase A, the team will identify additional planning, advanced development, and risk-reduction tasks that could provide a prudent and cost-effective approach to early reduction of cost and schedule risk and have the potential to reduce the estimated cost of the mission. Primary activities include reducing the radiation and planetary protection risks associated with instrument and spacecraft development.

B.3.3.2   Phases A–F

The Phase A–F schedule reflects the total project scope of work as discrete and measurable tasks and milestones that are time-phased through the use of task durations, interdependencies, and date constraints. To ensure low risk, the schedule includes slack for all tasks.

The Project Manager controls the project schedule, with support from a Project Schedule Analyst. An Integrated Master Schedule identifies key milestones, major reviews, and receivables/deliverables (Rec/Dels). Schedule reserves included in the schedule for the November 2021 launch opportunity meet or exceed JPL DP requirements (schedule reserves of 1 month per year for Phases A through D, with schedule reserves of 1 week per month for activities at the launch site [JPL 2010a]). The project uses an integrated cost/schedule system in Phase B to fully implement an EVM baseline in Phases C, D, and E. Inputs are supplied to NASA's Cost Analysis Data Requirement (CADRe) support contractor for reporting at major reviews. Schedule and cost
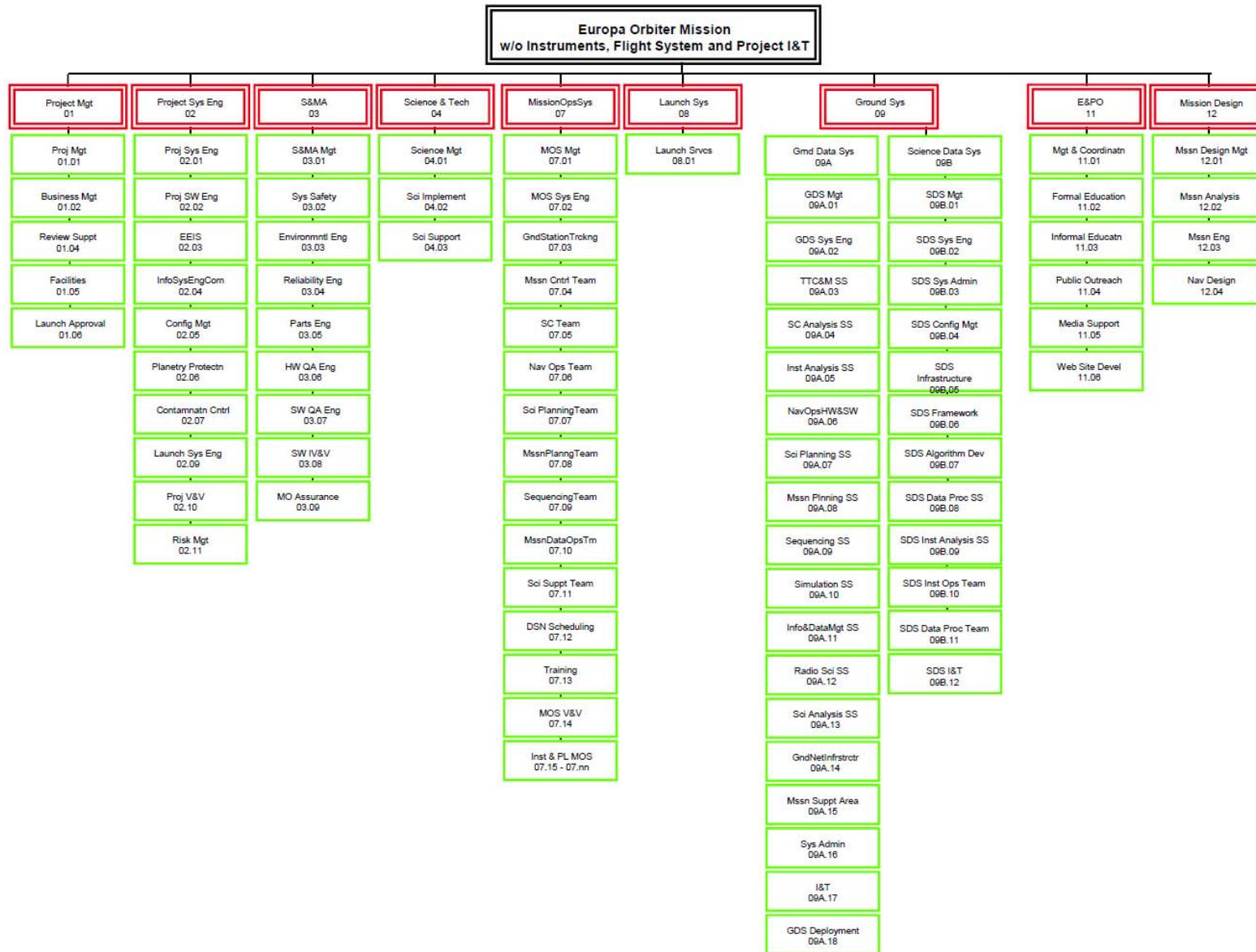
Figure B.3.2-1. Orbiter Mission Work Breakdown Structure
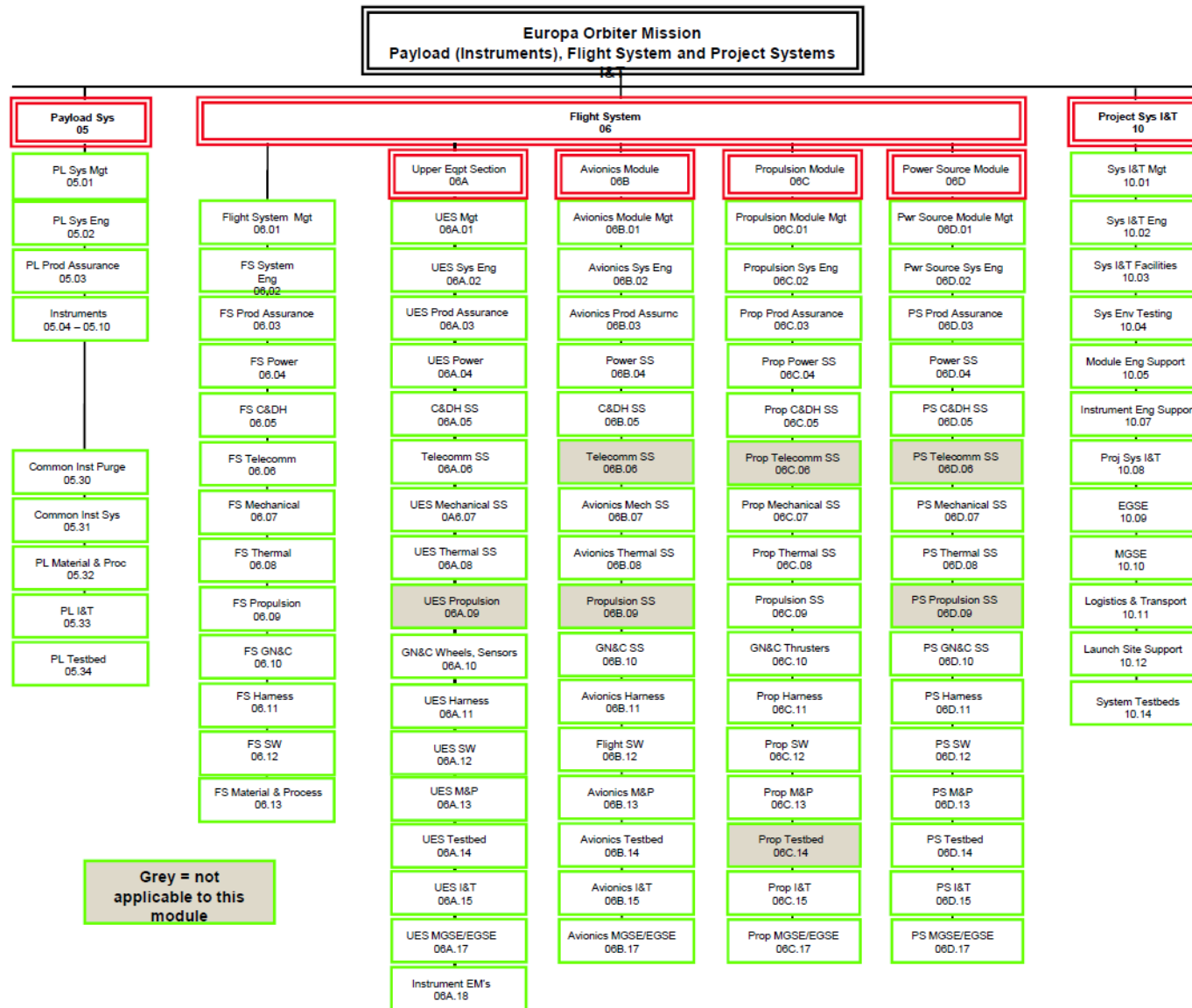
Figure B.3.2-2. Orbiter Mission Work Breakdown Structure: Payload, Flight Systems, I&T.
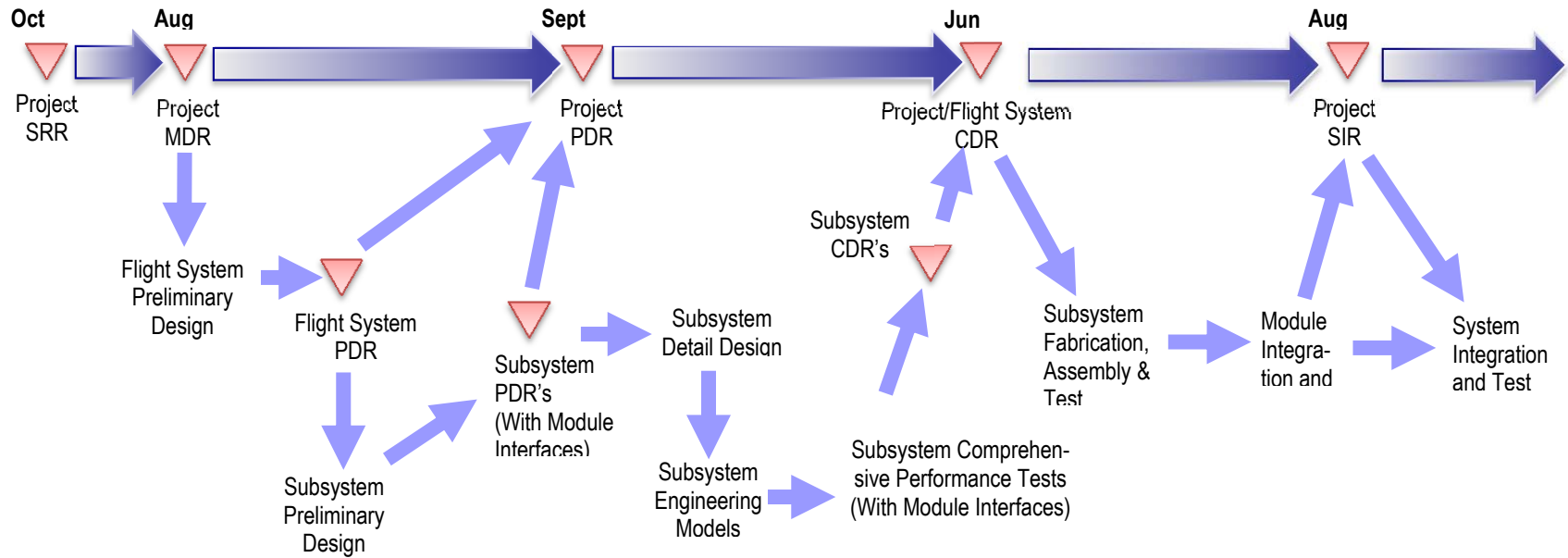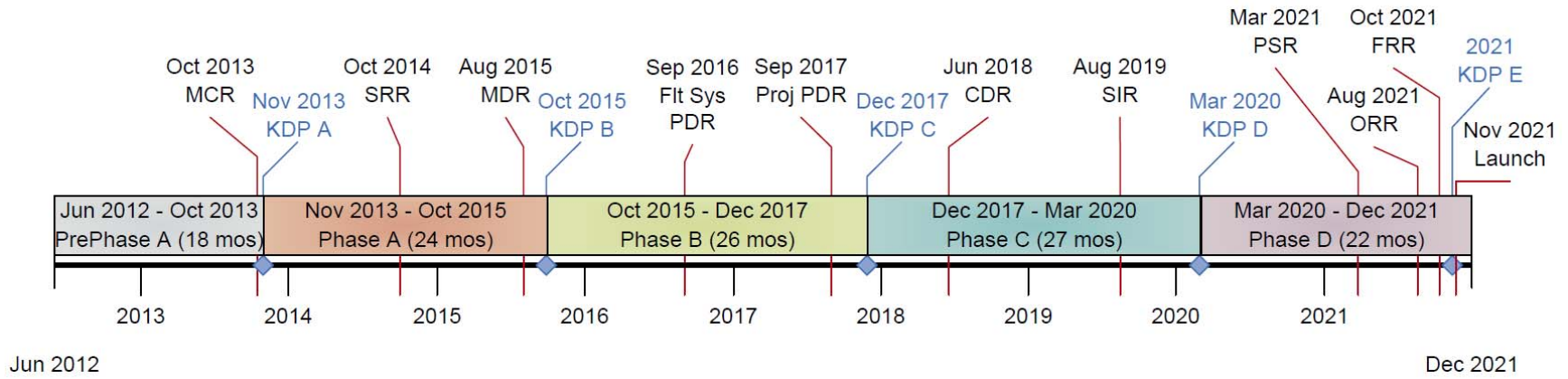
Figure B.3.3-1. Top-level schedule and Implementation Flow for the Europa Orbiter Mission.

estimates at completion (EACs) are prepared at regular intervals as part of the EVM process. Major project review milestones (not all shown) are consistent with NPR 7120.5D (NASA 2007) and will be reviewed for compliance with NPR 7120.5E (NASA 2012 [pending]).

B.3.3.3   Phases A–B

The length of phases A and B (24 months for A, 26 months for B) is driven by the need to mature the mission architecture in advance of selecting instruments in response to an AO and need to develop the selected instruments to adequate maturity before PDR. In Phase A, the primary tasks are completing the Gate Products required and facilitating the selection of the science instruments. The 8-month period between instrument selection and the system Mission Definition Review (MDR) allows instrument designers to work directly with the project personnel on issues related to accommodation, requirements, radiation, and planetary protection. The schedule is front-loaded with a long Phase A to give adequate time to define requirements early in the mission development life cycle.

B.3.3.4   Phases C–D

The length of phases C and D (27 months for C, 22 months D) is primarily driven by the schedule to bring the flight system to launch readiness. Phase C is longer than typical due to the added time required to implement the radiation and planetary-protection requirement-mitigation aspects of the design. The long Phase C also allows for a lower staff-level profile, which keeps the mission cost profile flat. Phase D was developed using the Cassini model of ATLO and includes 1.5 months to perform the system-level dry-heat sterilization.

A trailblazer activity is scheduled to occur at the launch facility in Phase D to ensure that the spacecraft design is compatible with the launch vehicle and facility limitations at the launch site for transporting and loading of the ASRGs. This activity starts at a very low level in Phase B and continues with increasing activity until the approach to ASRG installation is validated in Phase D. The trailblazer activity is also used to dry-run the system-level dry-heat sterilization activities that will take place in a thermal vacuum chamber at KSC.

B.3.3.5   Phases E–F

Phase E (9.5 years) is driven by the interplanetary trajectory and science requirements at Europa. Phase F (6 months) is structured to carry out the end-of-mission scenario and to complete data analysis and archiving.

B.3.4   Risk and Mitigation Plan

The main risks and their mitigation approaches are understood.

The primary challenges of a mission to Europa are Jupiter's radiation environment, planetary protection, trajectory management for numerous consecutive Jovian tour flybys, and the large distance from the Sun and Earth. Driving technical risks are

1. Advanced Stirling radioisotope generator (ASRG) development
2. Performance in a radiation environment
3. Instrument development
4. Planetary protection

B.3.4.1   ASRG

NASA is developing the ASRG as the long-term solution for reducing the plutonium requirements for future planetary missions. Any problems with the development and validation of the ASRG could have a serious impact on the Europa Orbiter Mission, since it is baselining a radioisotope power system. ASRG development and qualification risks could have high consequences and are outside the control of the Europa Orbiter Mission project. The ASRGs are a new development, and the likelihood of problems is not known; however, successful development of new radioisotope thermoelectric generators can be difficult. Risks to the mission associated with this development can be mitigated if well-defined

and stable ASRG characteristics are known early in Phase A to allow the system designers to adequately incorporate them into the spacecraft system. However, if these characteristics are not known and stable early in Phase A, late design changes and impacts on mass, power, cost, and schedule are likely. The Europa Power Source Module concept allows for later ASRG delivery, thereby diminishing some of the development risk, as does the Europa Study Team's close work with NASA to clearly delineate the mission requirements on the ASRGs. Mitigation of these risks also requires that the project work closely with the Program Executive at NASA Headquarters for the ASRG Development Program to ensure that the technology is flight-qualified with completed life tests, no later than Phase B. A robust ground-test program is essential to migrating the ASRG risks. The NASA ASRG development efforts are currently underway (see Section B.2.7.5.2).

B.3.4.2   Performance in a radiation environment

The radiation environment to which the Europa Orbiter Mission hardware would be exposed, and its accumulated effects by end of mission, are significant. Radiation effects expected in the mission are TID effects and SEE in electronic components, displacement damage (DD) effects in components and materials, noise effects in detectors, and surface and internal charging (IC). The primary risk considered here is the likelihood that premature component failure or compromised performance could have a serious impact on spacecraft functionality if the radiation problem is not addressed appropriately. Sensors for instruments used for pointing and navigation and in science instruments are particularly sensitive to radiation effects, primarily due to noise and displacement effects. Test techniques used to verify component suitability might over-predict component hardness due to inadequate accounting for radiation rate or source type effects that are negligible at lower

doses. Also, unanticipated failure mechanisms might be present or might become important at high doses or at high DD levels that are not of concern for missions conducted at nominal total-dose exposures. The measures described here reduce both the likelihood and the consequences of such impacts, with designs for this radiation environment robust beyond the level normally accomplished for spaceflight design. The Europa Orbiter Mission design concept uses an approach similar to that taken by Juno, using an electronics vault to shield the electronic components to a mission dose of 150 krad, thereby reducing the likelihood of radiation-related problems while increasing the likelihood of parts availability. There has been significant effort exerted by experts to mitigate this risk over the past decade. In 2007, the Europa Study Team convened several review teams to assess the particular risks in each area. The results of the reviews were presented in Appendix C of the 2007 Europa Explorer Mission Study report (Clark et al. 2007). As a result of those reviews, a Risk Mitigation Plan: Radiation and Planetary Protection (Yan 2007, outlined in Clark et al. 2007) was further developed and executed to make strategic investments related to reducing even further the likelihood of component failure and degradation, and the related radiation risk. Results of this work were reported in the 2008 JEO final report (Clark et al. 2008). An expanded systems engineering approach focuses on graceful degradation and reduces the consequences of any component failures in electronic parts.

B.3.4.3   Instrument Development

Instrument development and delivery will undoubtedly be on the critical path, as has historically been the case. Only four instruments are needed to fulfill the Europa Orbiter Mission science requirements. An Approved Parts and Materials List (APML), addressing planetary protection and radiation constraints, will be available in time for the instrument AO. In addition, design guidelines will be incorporated into the AO. This facilitates mat-

uration of instrument concepts prior to selection. The instruments in the model payload are all based on mature technologies, and if deployed on a mission in the inner solar system, would represent low risk. For a Europa mission though, radiation can be expected to have a detrimental impact on instrument performance. If such problems cannot be resolved satisfactorily, the science objectives of the mission would not be met. Therefore, instruments will be selected as early as possible in Phase A, and early funding will be made available in order to alleviate development risks. In addition, the project will assign instrument interface engineers to work with each instrument provider to ensure that the instrument meets interface requirements and the spacecraft accommodates specific instrument needs.

To reduce the likelihood that the instruments fall short of their desired specifications or run into resource and schedule problems due to radiation issues, typical interface engineering support will be augmented for each instrument with personnel experienced in the area of radiation design. Design guidelines will be generated for the instrument teams to describe radiation constraints and to provide recommendations for design issues, and for parts and material selection. Development of a knowledge base for potential instrument providers has already begun. Four instrument workshops were held to engage the instrument provider community in a dialogue on needs and potential driving requirements for a mission to Europa. Information regarding radiation and planetary protection requirements was disseminated. The Europa Orbiter Mission development schedule provides abundant time plus reserves after selection for instrument developers and the project to work through and understand the particular design implications for each instrument of radiation and planetary protection. The project schedule also allows ample time for the instruments to be developed and delivered to system test. In

addition, the modular spacecraft approach, early local testing with spacecraft emulators, and a straightforward instrument interface allow instruments to be integrated last in the system integration process, if necessary.

B.3.4.4   Planetary Protection

The planetary protection requirements for a mission to Europa are significant and can drive mission design, schedule, and cost. The final fate of the Europa Orbiter Mission, impacting on the Europan surface, means that the mission will be classified as at least Category III under current Committee on Space Research (COSPAR) and NASA policy (COSPAR 2002). If prelaunch cleanliness levels are not met, expenditure of cost and schedule reserves might be required to address contamination problems late in the process to prevent contamination of Europa. This risk is cross-cutting and is mitigated in part by a review added in Phase B to confirm the approach and assess implementation. This risk is also mitigated by the previous Europa Study activities. The approach to planetary protection compliance for the Europa Orbiter Mission concept, at this time is 1) prelaunch DHMR to control bioburden for those areas not irradiated in-flight and 2) in-flight microbial reduction via radiation prior to Europa orbit insertion. The prelaunch method is to perform a full system DHMR as one of the last steps in the ATLO process at KSC. A chamber has been identified at KSC that is capable of performing DHMR, though specific details will need to be worked during Phase A. A pathfinder activity is planned as a dress rehearsal to resolve any procedural challenges. Compilation of the Europa Orbiter Mission APML will address compliance of materials with the DHMR process.

B.3.5   Cost

B.3.5.1   Cost Summary

The Total Mission Cost for the Europa Orbiter Mission concept is estimated at $1.6B to $1.7B FY15, *excluding the launch vehicle, which is costed separately*. The mission base-

line comprises an Orbiter spacecraft carrying four instruments—Laser Altimeter (LA), Mapping Camera (MC), Magnetometer (MAG), and Langmuir Probe (LP)—that will spend one month taking geophysical measurements of Europa from orbit. The Europa Orbiter Mission enables investigators to characterize the extent of the Europan ocean and investigate Europa's habitability for life.

Table B.3.5-1 summarizes the Europa Orbiter Mission cost estimate at WBS level 2.

The Total Mission Cost is broken down into $1.4B for the Phase-A through -D development period and $0.25B for operations during Phases E and F. The Europa Orbiter Mission holds 37% in cost reserves that is broken down into 40% for Phases A, B, C, and D, and 20% for Phases E and F.

The estimated cost is based on the implementation approach described in Section B.2, which includes the following key features in the baseline plan:

- Redundant flight system with selected cross-strapping
- No new technologies requiring extraordinary development
- Simple, repeated, algorithm-driven observations capable of achieving all of the science goals
- Experienced providers of key systems and subsystems

B.3.5.2   Cost Estimating Methodology

To estimate the cost for the Europa Orbiter Mission concept, JPL used their institutional cost estimation process applicable for the design maturity of a concept study in early formulation. This process focuses on using parametric cost models, analogies, and other non-grassroots estimating techniques, which provide the following advantages:

- Provide rapid turnaround of extensive trade studies

Table B.3.5-1. Europa Orbiter cost summary by WBS (FY15 $M).

WBS Element	PRICE-H	SEER
01 Proj Mgmt	55	54
02 Project System Engineering	45	43
03 Safety & Mission Assurance	49	47
04 Science	64	64
05 Payload System	75	75
06 Spacecraft System	507	482
ASRG	200	200
07 Mission Operations System	161	161
08 Launch System	-	-
09 Ground Data System	39	39
10 Proj Sys I&T	51	43
11 Education and Public Outreach	10	10
12 Mission Design	21	20
Subtotal (FY15$M)	**1,276**	**1,238**
Reserves	386	371
Total (FY15$M)	**1,661**	**1,609**

- Enable design-to-cost to narrow the trade space and define a baseline concept
- Establish reasonable upper and lower bounds around a point estimate

A cost estimation process begins with the Europa Study Team developing a Technical Data Package (TDP) that describes the science requirements, technical design, mission architecture, and project schedule. Next, all work is organized, defined, and estimated according to the NASA standard WBS. The Europa Study Team then tailors the WBS as needed for cost estimation and planning.

The institutional business organization uses the TDP and WBS to develop the cost estimate by applying estimating methods and techniques appropriate for each WBS element, based on the maturity of design and manufacturing requirements, availability of relevant historical information, and degree of similarity to prior missions. For the Europa Orbiter Mission, the tools and methods used include the following:

- Calibration of commercial, off-the-shelf (COTS) tools PRICE-H and

SEER to Juno, the most relevant JPL planetary mission

- Use of the NASA Instrument Cost Model (NICM) for the notional payload, tailored for the Europa environment
- Use of the NASA Space Operations & Cost Model (SOCM) for Phases E and F
- Wrap factors based on analogous historical planetary missions for Project Management, Project Systems Engineering, Safety and Mission Assurance, and Mission Design

The Europa Study Team's estimate is a compilation of these multiple techniques. The Europa Study team then vets the integrated cost rollup and detailed basis of estimate (BOE), and reviews the results for consistency and reasonableness with the mission design, WBS, and NASA requirements to ensure that technical and schedule characteristics are accurately captured and a consistent cost-risk posture is assumed.

To validate the resulting proposed cost, the Europa Study Team used Team X to independently cost the baseline concept with the JPL Institutional Cost Models (ICMs): 33 integrated, WBS-Level-2 through -4 models built by JPL line organizations to emulate their grassroots approach. The Europa Study Team also contracted with the Aerospace Corporation to perform an Independent Cost Estimate (ICE) and Cost and Technical Evaluation (CATE.) The Aerospace results are discussed in Section B.4.5.

The Europa Study Team then used an S-curve cost risk analysis to validate and bound the cost reserves. The reserves substantiation is discussed in Section B.3.5.7.

B.3.5.3   Basis of Estimate

The integrated Europa Orbiter Mission cost estimate is based on the science and mission implementation approach described in Section B.2. In addition, the Master Equipment

List (MEL) provided the key inputs for mass, quantities, and the quantification of electronics versus structures that are needed to run the parametric tools. The cost estimating methodologies and assumptions used to develop the Europa Orbiter Mission cost estimate are summarized in Table B.3.5-2.

B.3.5.4   Instrument Cost Estimates

The NASA Instrument Cost Model (NICM) system model with an augmentation to account for radiation and planetary protection was used to estimate instrument costs. Each notional instrument was characterized for performance establishing instrument type, aggregate power estimates, and subsystem level mass. Table B.3.5-3 shows the input parameters used for each instrument for the NICM system model.

B.3.5.4.1   NICM Adjustments

NICM outputs at the 70 percentile were reported in FY15$. This reference cost estimate was then augmented for radiation and planetary protection. The NICM model does not

Table B.3.5-2. Cost estimation methodology.

WBS Element	Methodology
01 Project Management	Historical wrap factor based on analogous historical planetary missions. Estimate was augmented by $15M to account for Nuclear Launch Safety Approval (NLSA) and National Environmental Policy Act (NEPA) costs associated with usage of the advanced Stirling radioisotope generators (ASRGs).
02 Project Sys Engineering	Historical wrap factor based on analogous historical planetary missions.
03 Safety & Msn Assurance	Historical wrap factor based on analogous historical planetary missions.
04 Science	Expert-based estimate from the science team based on mission class, schedule, and the number and complexity of instruments. Cost estimate captures the level of effort for a Project Scientist, two Deputy Project Scientists, the Science Team, and participating scientists, with additional workforce requirements for Phases C and D, based on the size of the team, the number of meetings with the team, and the products required from this group. For Phases E and F, the cost estimate also assumes a science team for each instrument, with the estimated level of effort based on existing instrument teams supporting current mission, and on the number of months in hibernation, cruise, and science operations.
05 Payload System	Historical wrap factor for Payload Management, Systems Engineering, and Product Assurance based on analogous historical planetary missions.
	Instrument costs developed using the NASA Instrument Cost Model (NICM), Version 5.0. The 70% confidence-level estimate was selected as a conservative point estimate for each notional instrument. Instrument costs are then augmented for radiation shielding, detector radiation redesign, and planetary protection for any DHMR material properties issues. For payload radiation shielding, the cost was estimated separately using PRICE-H and SEER, and the cost is included under WBS 06 Spacecraft System. For planetary protection a flat fee was then added to each instrument, based on instrument complexity. For radiation redesign, an additional fee of $2M was assessed per detector.
06 Spacecraft System	Historical wrap factor for Flight System Management, Systems Engineering, and Product Assurance based on analogous historical planetary missions.
	Spacecraft hardware costs estimated using PRICE-H and SEER calibrated to Juno at the subsystem level. Juno selected as an analogous mission for the calibration due to the operation of the flight system in a comparable radiation environment. Software costs estimated using a wrap factor of 10% on the hardware cost.
	ASRG cost provided by NASA Headquarters in the Europa Study Statement of Work, dated October 4, 2011 (NASA 2011). Estimate includes four ASRGs at $50M each (FY15$).
07 Mission Ops System	Team X estimate based on historical data for a Class A mission for Phases A-D; SOCM estimate for Phases E-F
08 Launch System	Launch Vehicle costs, including nuclear processing costs, are not included and will be provided by NASA Headquarters as directed in the Europa Study Statement of Work.
09 Ground Data System	Team X estimate based on historical data for a Class A mission for Phases A-D; SOCM estimate for Phases E-F
10 Project Systems I&T	PRICE-H and SEER estimate calibrated to Juno.
11 Education & Public Outreach	1.0% wrap factor on the total mission cost excluding the launch system (WBS 08), ASRG, and DSN tracking costs. Based on the percentage prescribed in the recent AOs for Discovery 2010 and New Frontiers 2009 (NASA 2010a, 2009c).
12 Mission Design	Historical wrap factor based on analogous historical planetary missions.
Reserves	40% for Phases A–D and 20% for Phases E–F on the total mission cost excluding the launch system (WBS 08), ASRG, and DSN tracking costs. These percentages were based on historical experience with recent planetary missions.

Table B.3.5-3. NICM System Model Inputs for Baseline.

Instrument Name	Langmuir Probe (LP)	Laser Altimiter (LA)	Magnetometer (MAG)	Mapping Camera (MC)
Remote Sensing or In-Situ?	Remote Sensing	Remote Sensing	Remote Sensing	Remote Sensing
Environment	Planetary	Planetary	Planetary	Planetary
Remote Sensing Instrument Type	Particles	Optical	Fields	Optical
Total Mass (kg)	2.7	5.5	3.3	2.5
Max Power (W)	2.3	15	4	6
Design Life (months)	108	108	108	108
Number of Detectors	0	0	0	1

Table B.3.5-4. Instrument Cost Estimation Process.

Master Instrument Costing Matrix	Instrument Cost (excluding radiation shielding) (A)	Detector Radiation Design Costs (B)	Planetary Protection Fee (C)	Total Instrument Cost	Radiation Shielding Cost – Included in WBS 06
Instrument X	NICM 70th percentile estimate	$2M per detector	Based on complexity	A+B+C	Estimated in PRICE-H/SEER

Table B.3.5-5. Instrument Cost Estimation Details (FY15$M).

Instrument	Acronym	NICM 70% Cost	Detector Radiation Design Costs	Planetary Protection Fee	TOTAL INSTRUMENT COST
Laser Altimeter	LA	28.8	0.0	1.4	30.2
Langmuir Probe	LP	7.1	0.0	0.1	7.1
Mapping Camera	MC	14.3	2.0	0.7	17.1
Magnetometer	MAG	10.9	0.0	0.3	11.2
TOTAL		**61.1**	**2.0**	**2.6**	**65.6**

have parameters or characteristics sufficient to model planetary protection requirements or radiation environments. A flat fee for Planetary Protection was added to each instrument, based on instrument complexity. An estimate for the number of electronic boards and detectors was made for each instrument, and an additional fee of $2M was assessed per detector for radiation redesign costs. The instrument radiation shielding masses were estimated separately in PRICE-H and SEER, and are included in WBS 06 spacecraft costs under Payload Radiation Shielding. Table B.3.5-4 summarizes the instrument cost estimation process.

B.3.5.4.2   NICM Estimate

Table B.3.5-5 provides the final NICM system cost estimate including all adjustments for radiation and planetary protection.

B.3.5.5   Spacecraft Hardware Costs

The Europa Orbiter Mission spacecraft hardware costs were estimated using PRICE-H and SEER, calibrated to Juno. The Orbiter spacecraft is most closely analogous to the Juno spacecraft. Configuration, avionics subsystems, radiation environment, mission complexity and design lifetime match closely to the corresponding aspects of the Juno mission.

B.3.5.5.1.1   PRICE-H and SEER Cost Estimates

The Spacecraft System costs generated for PRICE-H and SEER are shown in Table B.3.5-6. The Spacecraft System is bookkept in in WBS 06. The Payload Radiation Shielding is captured as part of the Mechanical Subsystem and the costs are bookkept under WBS 06.07b. The RPS System was estimated at a cost of $50M per ASRG unit as directed by NASA HQ, and included in WBS 06, separate from the Spacecraft System costs. The I&T

Table B.3.5-6. PRICE-H and SEER Cost Estimates for the Europa Orbiter Mission. (FY15$M).

Spacecraft System	PRICE-H	SEER
06 Spacecraft System		
06.04 Spacecraft Power SS	50	68
06.05 Spacecraft C&DH SS	37	27
06.06 Spacecraft Telecom SS	93	54
06.07 Spacecraft Mechanical SS	54	46
06.07a Radiation Shielding	9	9
06.07b Payload Radiation Shielding	2	1
06.08 Spacecraft Thermal SS	10	10
06.09 Spacecraft Propulsion SS	41	60
06.10 Spacecraft GN&C SS	51	56
06.11 Spacecraft Harness SS	6	6
06.12 Spacecraft Flight SW	35	34
06C RPS System	**200**	**200**
10 I&T	**51**	**43**

costs are kept in WBS 10. Spacecraft flight software was estimated as a 10% wrap factor based on hardware cost, which is a high-level rule of thumb derived from JPL's historical software cost data.

B.3.5.6   Phase E and F Cost Estimates

The NASA Space Operations Cost Model (SOCM) was used to estimate operations costs in Phases E and F. The Europa Study science team provided an expert-based estimate for WBS 04 Science based on schedule and the number and complexity of instruments. The Europa Orbiter Mission Phase E and F Cost Estimate are shown in Table B.3.5-7.

B.3.5.7   Estimate Reasonableness (Validation)

A JPL Team X cost session was used to assess the reasonableness of the parametrically derived PRICE-H and SEER-based Flight System (WBS 06) and Project Systems I&T (WBS 10) estimates and associated wraps. In addition, Aerospace Corporation independently ran an Independent Cost Estimate (ICE) and Cost and Technical Evaluation (CATE). Aerospace Corporation found the project cost estimate to be reasonable and found no cost or schedule threats. The results of the Team X cost session and Aerospace Corporation analysis are presented in Table B.3.5-8 along with

Table B.3.5-7. Phase E and F Cost Estimate for the Europa Orbiter Mission. (FY15$M).

WBS Element	Phase E & F Cost
01 Project Management	7
02 Project Systems Engineering	7
03 Safety & Mission Assurance	7
04 Science	38
05 Payload	0
06 Spacecraft	0
07 Mission Operations	119
08 Launch System	0
09 Ground Data Systems	12
10 Project System Integration & Test	0
11 Education & Public Outreach	2
SUBTOTAL	**193**
DSN Tracking	15
20% Reserves (excluding DSN)	39
TOTAL	**246**

Table B.3.5-8. Comparison of Team X, and Aerospace Corporation cost estimates. (FY15$B).

	Team X	Aerospace ICE	Aerospace CATE
Total FY15$B)	**1.5**	**1.7**	**1.8**

the PRICE- and SEER-based project estimates for comparison. The Aerospace CATE report is located in Appendix B.4.5.

B.3.5.8   Cost-Risk Assessment and Reserve Strategy

The Europa Study Team conservatively applied project-level reserves of 40% for Phases A–D and 20% for Phases E and F on all elements except for Launch Services, ASRGs, and DSN tracking. These reserve levels are more conservative than the reserve guidelines set forward in JPL Flight Project Practices, Rev. 8 (JPL 2010b).

The Europa Orbiter Mission cost risk and uncertainty assessment is a natural extension of the cost modeling discussed in Sections B.3.5.1-7, and is consistent with standard practice at NASA and JPL. This assessment considers the wide band of uncertainty that typically accompanies missions at early phases of development, as well as the technical risk and uncertainties of the Europa Orbiter Mission as
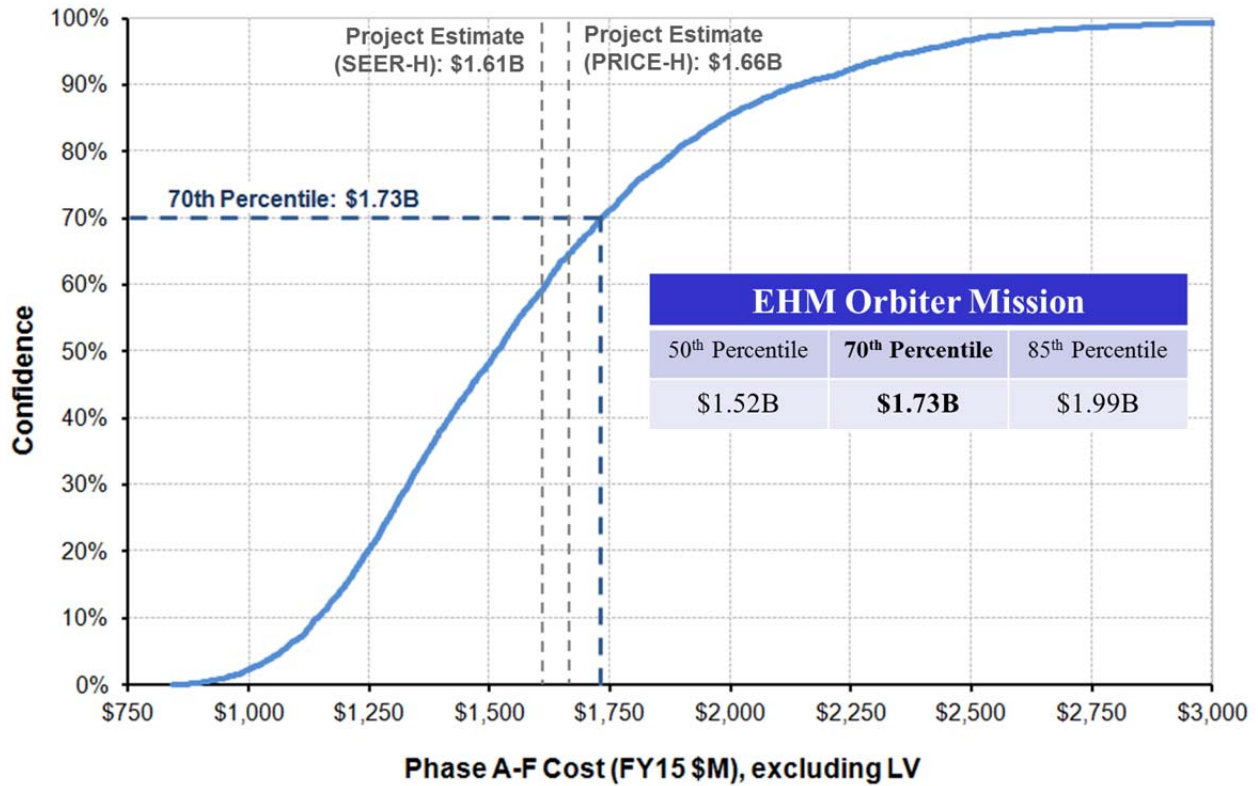
Figure B.3.5-1. Europa Orbiter Mission cost estimate S-curve analysis.

understood at this time and as experienced on prior competed and directed missions (e.g. Juno, MRO, MSL).

The primary technique utilized for this assessment is an S-Curve. This provides a statistically-based distribution of total project cost around the project's point estimate based on the cost models used in this analysis and the historical JPL data to which they are calibrated. Equivalently, this technique provides a probabilistic estimate of total project cost based on variability and uncertainties in the model-based estimates.

An S-curve analysis was performed on the study cost estimate, and demonstrated a 70th-percentile cost estimate of $1.73B (FY15$) (Figure B.3.5-1). Comparing the Europa Study Team estimate (including cost reserves) to the S-Curve indicates that the Europa Study Team estimate of $1.6B to $1.7B is at approximately 65th-percentile. To be at 70th-percentile, the Europa Study Team would need to increase reserves by ~$70M to ~$120M, resulting in a reserve position of 45% overall (Phase A-F).

B.4 Appendices

B.4.1 References

Anderson, J.D., Schubert, G., Jacobson, R.A., Lau, E.L., Moore, W.B., et al., 1998. Europa's differentiated internal structure: Inferences from four Galileo encounters. Science 281, 2019–2022.

Becker, H., Miyahira, T., Johnston, A., 2003. The influence of structural characteristics on the response of silicon avalanche photodiodes to proton irradiation, IEEE Trans. Nucl. Sci. 50(6), 1974–1981.

Bierhaus, E.B., Zahnle, K., Chapman, C.R., 2009. Europa's crater distributions and surface ages. In: Pappalardo, R.T., McKinnon, W.B., Khurana, K.K. (Eds.), Europa, U. Arizona Press, Tucson, 161–180.

Billings, S.E., Kattenhorn, S.A., 2005. The great thickness debate: Ice shell thickness models for Europa and comparisons with estimates based on flexure at ridges. Icarus 177, 397–412.

Bills, B.G., 2005. Free and forced obliquities of the Galilean satellites of Jupiter. Icarus 175, 233–247.

Bills, B.G., Nimmo, F., 2008. Forced obliquity and moment of inertia of Titan. Icarus 196, 293–297.

Bills, B.G., Lemoine, F.G., 1995. Gravitational and topography isotropy of the Earth, Moon, Mars, and Venus. J. Geophys. Res. 100, 26,275–26,295.

Bills, B.G., Nimmo, F., Karatekin, Ö., Van Hoolst, T., Rambaux, N., et al., 2009. Rotational dynamics of Europa. In: Pappalardo, R.T., McKinnon, W.B., Khurana, K.K. (Eds.), Europa, U. Arizona Press, Tucson, 119–136.

Boldt, J., et al., 2008. Assessment of radiation effects on detectors and key optical components. JPL D-48256.

Carr, M.H., Belton, M.J.S., Chapman, C.R., Davies, M.E.., Geissler, R., Greenberg, R., McEwen, A.S., Tufts, B.R., Greeley, R., Sullivan, R., Head, J.W., Pappalardo, R.T., Klaasen, K.P., Johnson, T.V., Kaufman, J., Senske, D., Moore, J., Neukum, G., Schubert, G., Burns, J.A., Thomas, P., Veverka, J., 1998. Evidence for a subsurface ocean on Europa. Nature 391, 363–365.

Cavanaugh, J., Smith, J., Sun, X., Bartels, S., Bartels, A., Ramos-Izquierdo, L., Krebs, D., McGarry, J., Trunzo, R., Novo-Gradac, A., Britt, J., Karsh, J., Katz, R., Lukemire, A., Szymkiewicz, R., Berry, D., Swinski, J., Neumann, G., Zuber, M., Smith, D., 2007. The Mercury Laser Altimeter instrument for the MESSENGER mission. Space Sci. Rev. 131, 451–479.

Clark, K., 2008. EJSM Europa Orbiter Mission Design and Architecture (presentation slides). Outer Planets Flagship Mission Instrument Workshop, June 3, 2008.

Clark, K., et al., 2007. Europa Explorer Mission Study: Final Report, JPL D-41283.

Clark, K., et al., 2008. Jupiter Europa Orbiter Mission Study 2008 Final Report, JPL D-48279.

Clark, K., et. al., 2009. Europa Jupiter System Mission Joint Summary Report, January 16, 2009.

Cole, T., Boies, M., El-Dinary, A., Cheng, A., 1997. The Near-Earth Asteroid Rendezvous Laser Altimeter. Space Sci. Rev. 82, 217–253.

Collins, G., Nimmo, F., 2009. Chaotic terrain on Europa. In: Pappalardo, R.T., McKinnon, W.B., Khurana, K.K. (Eds.), Europa, U. Arizona Press, Tucson, 259–282.

Committee on Space Research, 2002. COSPAR Planetary Protection Policy, as amended March 2005). <http://www.cosparhq.org/scistr/PPPolicy.htm>.

Comstock, R.L., Bills, B.G., 2003. A solar system survey of forced librations in longitude. J. Geophys. Res. 108, doi: 10.1029/ 2003JE002100.

Constable, S., Constable, C., 2004. Observing geomagnetic induction in magnetic satellite measurements and associated implications for mantle conductivity. Geochemistry, Geophysics, Geosystems 5, doi: 10.1029/ 2003GC000634.

Doggett, T., Greeley, R., Figueredo, P., Tanaka, K., Weiser, S., 2009. Geologic stratigraphy and evolution of Europa's surface. In: Pappalardo, R.T., McKinnon, W.B., Khurana, K.K. (Eds.), Europa, U. Arizona Press, Tucson, 137–160.

Dyal P. and Parkin C. W. (1973) Global electromagnetic induction in the moon and planets. Phys. Earth Planet. Inter., 7, 251–265.

Figueredo, P.H., Greely, R., 2004. Resurfacing history of Europa from pole-to-pole geological mapping. Icarus 167, 287–312.

Geissler, P.E., Greenberg, R., Hoppa, G., McEwen, A., Tufts, R., Phillips, C., Clark, B., Ockert-Bell, M., Helfenstein, P., Burns, J., Veverka, J., Sullivan, R., Greeley, R., Pappalardo, R. T., Head, J. W., Belton, M. J. S., Denk, T., 1998. Evolution of lineaments on Europa: Clues from Galileo multispectral imaging observations. Icarus 135, 107–126, doi: 10.1006/icar.1998.5980.

Greeley, R., Chyba, C.F., Head, J.W. III, McCord, T.B., McKinnon, W.B., Pappalardo, R.T., Figueredo, P., 2004. Geology of Europa. In: Bagenal, F., Dowling, T.E., McKinnon, W.B. (Eds.), Jupiter: The Planet, Satellites, and Magnetosphere, Cambridge U. Press, Cambridge, U.K., 329–362.

Greenberg, R., G.V. Hoppa, B.R. Tufts, P. Geissler, J. Riley, and S. Kadel, 1999. Chaos on Europa. Icarus 141, 263–286.

Hand, K.P. and C.F. Chyba 2007. Empirical constraints on the salinity of the europan ocean and implications for a thin ice shell. Icarus 189, 424–438.

Hand, K.P., C.F. Chyba, J.C. Priscu, R.W. Carlson, and K.H. Nealson 2009. Astrobiology and the potential for life on Europa. Europa (R.T. Pappalardo, W.B. McKinnon, and K.K. Khurana, Eds.), Univ. of Arizona Press, Tucson , 589–630.

Head, J.W., Pappalardo, R.T., 1999. Brine mobilization during lithospheric heating on Europa: Implications for formation of chaos terrain, lenticula texture, and color variations. J. Geophys. Res., Planets 104, 27143–27155.

Henschel, H., Köhn, O., Schmidt, H., Bawirzanski, E., Landers, A., 1994. Optical fibres for high radiation dose environments. IEEE Trans. Nucl. Sci. 41(3), 510–516.

Hoppa, G.V., et al. 1999. Formation of cycloidal features on Europa. Science 285, 1899–1902.

Hussman, H., Spohn, T., 2004. Thermal-orbital evolution of Io and Europa. Icarus 171, 391–410.

Jet Propulsion Laboratory, 2009. JPL Standard Flight Project Work Breakdown Structure Template, Rev. 5, JPL Rules! DocID 59533, March 18, 2009.

Jet Propulsion Laboratory, 2010a. Design, Verification/Validation and Ops Principles for Flight Systems (Design Principles), Rev. 4, JPL Rules! DocID 43913, September 20, 2010.

Jet Propulsion Laboratory, 2010b. Flight Project Practices, Rev. 8, JPL Rules! DocID 58032, October 6, 2010.

Johnston, A., 2001. Proton displacement damage in light-emitting and laser diodes. IEEE Trans. Nucl. Sci. 48(5), 1713–1720.

Kattenhorn, S.A., Hurford, T., 2009. Tectonics of Europa. In: Pappalardo, R.T., McKinnon, W.B., Khurana, K.K. (Eds.), Europa, U. Arizona Press, Tucson, 199–236.

Khurana, K.K., M. Kivelson, D. Stevenson, G. Schubert, C. Russell et al. 1998. Induced magnetic fields as evidence for subsurface oceans in Europa and Callisto. Nature 395, 777–780.

Khurana, K.K., M.G. Kivelson, and C. T. Russell, 2002. Searching for Liquid Water in Europa by Using Surface Observatories. Astrobiology 2, 93-103.

Khurana, K.K., M.G. Kivelson, K.P. Hand, and C.T. Russell 2009. Electromagnetic induction from Europa's ocean and the deep interior, Europa (R.T. Pappalardo, W.B. McKinnon, and K.K. Khurana, Eds.), Univ. of Arizona Press, Tucson, 571–588.

Kivelson, M.G., K.K. Khurana, C.T. Russell, M. Volwerk, R.J. Walker et al. 2000. Galileo magnetometer measurements: A stronger case for a subsurface ocean at Europa. Science 289, 1340–1343.

Klaasen, K., Clary, M., Janesick, J., 1984. Charge-coupled device television camera for NASA's Galileo mission to Jupiter. Optical Engineering 23, 334–342.

Konopliv, A.S., C.F. Yoder, E.M. Standish, D-N. Yuan, and W.L. Sjogren 2006. A global solution for the Mars static and seasonal gravity, Mars orientation, Phobos and Deimos masses, and Mars ephemeris. Icarus 182, 23–50.

Kwok, J., Prockter, L., Senske, D., Jones, C., 2007. Jupiter System Observer Mission Study: Final Report, JPL D-41284.

Lock, R., 2008. EJSM Europa Orbiter Science Scenarios (presentation slides). Outer Planets Flagship Mission Instrument Workshop, June 3, 2008.

Lock, R., 2010. Concept of Operations (presentation slides), Jupiter Europa Orbiter Internal Mission Concept Review, June 7–9, 2010.

Ludwinski, J., 1997. Galileo Mission Planning Office Closeout (Lessons Learned), JPL IOM 311.1/98/01, January 19, 1997.

Luthcke, S.B., C. Carabajal, and D. Rowlands 2002. Enhanced geolocation of spaceborne laser altimeter surface returns: Parameter calibration from the simultaneous reduction of altimeter range and navigation tracking data. J. Geodynamics 34, 447–475.

Luthcke, S.B., D. Rowlands, T. Williams, and M. Sirota 2005. Reduction of ICES at systematic geolocation errors and the impact on ice sheet elevation change detection. Geophys. Res. Lett. 32, L21S05.

Luttrell, K. and D. Sandwell 2006. Strength of the lithosphere of the Galilean satellites. Icarus 183, 159–167.

Moore, J.M., Asphaug, E., Belton, M., Bierhaus, B., Breneman, H., et al. 2001. Impact features on Europa: Results of the Galileo Europa Mission (GEM). Icarus 151, 93–111.

Moore, J.M., Black, G., Buratti, B., Phillips, C.B., Spencer, J., Sullivan, R., 2009. Surface properties, regolith, and landscape degradation. In: Pappalardo, R.T., McKinnon, W.B., Khurana, K.K. (Eds.), Europa, U. Arizona Press, Tucson, 369–380.

Moore, W.B. and G. Schubert 2000. The tidal response of Europa. Icarus 147, 317–319.

NASA, 2005. NASA Procedural Requirements (NPR) 8020.12B. Planetary Protection Provisions for Robotic Extraterrestrial Missions. NASA, Washington, DB.

NASA, 2007. NASA Program and Project Management Processes and Requirements, NASA Procedural Requirements (NPR) 7120.5D, March 6, 2007. NASA, Washington, DC.

NASA, 2010a. Discovery 2010 Announcement of Opportunity, NNH10ZDA007O, June 7, 2010.

NASA, 2010b. NASA Emergency Preparedness Plan Procedural Requirement, NPR 8715.3, December 16, 2010. NASA, Washington, DC.

NASA, 2011. Europa Study Statement of Work, October 4, 2011. NASA, Washington, DC.

Neumann, G.A. D. Rowlands, F. Lemoine, D. Smith, and M. Zuber 2001. Crossover analysis of Mars Orbiter Laser altimeter data. J. Geophys. Res. 106, 23,753–23,768.

Newhall, X. X. and J. C. Williams 1997. Dynamics and astrometry of natural and artificial celestial bodies: proceedings of IAU Colloquium 165, Poznan, Poland, July 1-5, 1996 / edited by I.M. Wytrzyszczak, J.H. Lieske, R.A. Feldman. Dordrecht; Boston : Kluwer Academic Publishers, QB1 I56 no.165, p. 21.

Nimmo, F. and M. Manga 2009. Geodynamics of Europa's icy shell. Europa (R.T. Pappalardo, W.B. McKinnon, and K.K. Khurana, Eds.), Univ. of Arizona Press, Tucson, 381–404.

Nimmo, F., Giese, B., Pappalardo, R.T., 2003. Estimates of Europa's ice shell thickness from elastically supported topography. Geophys. Res. Lett. 30, 1233.

O'Brien, H., Brown, P., Beek, T., Carr, C., Cupido, E., Oddy, T., 2007. A radiation tolerant digital fluxgate magnetometer. Meas. Sci. Technol.18, 3645–3650.

Ojakangas, G.W., D.J. Stevenson 1989. Thermal state of an ice shell on Europa. Icarus 81, 220–241.

Paczkowski, B., et al., 2008. Outer Planets Flagship Mission Science Operations Concept Study Report, JPL D–46870. June 2008.

Pappalardo, R.T., et al., 1998. Geological evidence for solid-state convection in Europa's ice shell. Nature 391, 365.

Pappalardo, R.T., Head, J.W., Greeley, R., Sullivan, R.J., Pilcher, C., et al., 1999. Does Europa have a subsurface ocean? Evaluation of the geological evidence. J. Geophys. Res. 104, 24,015–24,056. [Move other authors over to Lander chapter.]

Parkinson, W. D., 1983. *Introduction to Geomagnetism.* Scottish Academic Press, Edinburgh, 433 pp.

Peale, S.J., 1976. Orbital resonances in the solar system. Ann. Rev. Astron. Astrophys. 14, 215–246.

Prockter, L.M., Head, J.W., Pappalardo, R.T., Sullivan, R.J., Clifton, A.E., Giese, B., Wagner, R., Neukum, G., 2002. Morphology of Europan bands at high resolution: A mid-ocean ridge-type rift mechanism, J. Geophys. Res. 107, 4-1–4-28. doi:10.1029/2000JE001458.

Prockter, L.M., Pappalardo, R.J., 2000. Folds on Europa: Implications for crustal cycling and accommodation of extension. Science 289, 941–943.

Prockter, L.M., Patterson, G.W., 2009. Morphology and evolution of Europa's ridges and bands. In: Pappalardo, R.T., McKinnon, W.B., Khurana, K.K. (Eds.), Europa, U. Arizona Press, Tucson, 237–258.

Rasmussen, R., 2009. System architecture for JEO (presentation slides), EJSM Instrument Workshop, July 15–17, 2009.

Riley, J., Hoppa, G.V., Greenberg, R. Tufts, B.R., Geissler, P., 2000. Distribution of chaotic terrain on Europa. J. Geophys. Res. 105, 22,599–22,616.

Rose, T., Hopkins, M., Fields, R., 1995. Characterization and control of gamma and proton radiation effects on the performance of Nd:YAG and ND:YLF Lasers. IEEE J. Quantum Electron. 31(9), 1593–1602. doi: 10.1109/3.406369.

Rowlands, D.D., D. Pavlis, F. Lemoine, G. Neumann, and S. Luthcke 1999. The use of laser altimetry in the orbit and attitude determination of Mars Global Surveyor. Geophys. Res. Lett. 26, 1191–1194.

Sarid, A.R., R. Greenberg, G.V. Hoppa, T.A. Hurford, B.R. Tufts et al. 2002. Polar wander and surface convergence of Europa's ice shell: Evidence from a survey of strike-slip displacement. Icarus 158, 24–41.

Schenk, P. 2009. Slope characteristics of Europa: Constraints for landers and radar sounding. Geophy. Res. Lett. 36, L15204.

Schenk, P., Pappalardo, R., 2004. Topographic variations in chaos on Europa: Implications for diapiric formation. Geophys. Res. Lett. 31, L16703 1–5.

Schenk, P.M., Chapman, C.R., Zahnle, K., Moore, J.M., 2004. Ages and interiors: The cratering record of the Galilean satellites. In: Bagenal, F., Dowling, T.E., McKinnon, W.B. (Eds.), Jupiter: The Planet, Satellites, and Magnetosphere, Cambridge U. Press, Cambridge, U.K., 427–457.

Schenk, P.M., Turtle, E.P., 2009. Europa's impact craters: Probes of the icy shell. In: Pappalardo, R.T., McKinnon, W.B., Khurana, K.K. (Eds.), Europa, U. Arizona Press, Tucson, 181–198.

Schilling, N., F.M. Neubauer, and J. Saur, J. 2007. Time-varying interaction of Europa with the Jovian magnetosphere: Constraints on the Conductivity of Europa's subsurface ocean. Icarus 192, 41–55.

Schmidt, B.E., Blankenship, D.D., Patterson, G.W., Schenk, P.M., 2011. Active formation of "chaos terrain" over shallow subsurface water on Europa. Nature 479, 502–505. doi: 10.1038/nature10608.

Schubert, G., F. Sohl, and H. Hussmann 2009. Interior of Europa. Europa (R.T. Pappalardo, W.B. McKinnon, and K.K. Khurana, Eds.), Univ. of Arizona Press, Tucson, 353–368.

Seas, A., Li, S., Stephen, M., Novo-Gradac, A-M., Kashem, N., Vasilyev, A., Troupaki, E., Chen, S., Rosanova, A., 2007. Development and vacuum life test of a diode-pumped Cr:Nd:YAG laser (heritage laser) for space applications, Conference on Lasers and Electro-Optics. doi: 10.1109/CLEO.2007.4452342.

Sotin, C., G. Tobie, J. Wahr, and W.B. McKinnon 2009. Tides and tidal heating on Europa. Europa (R.T. Pappalardo, W.B. McKinnon, and K.K. Khurana, Eds.), Univ. of Arizona Press, Tucson, 85–118.

Space Studies Board, 2000. Preventing the Forward-Contamination of Europa. National Academy Press, Washington, DB.

Space Studies Board, 2003. New Frontiers in the Solar System: An Integrated Exploration Strategy 2003–2013. The National Academies Press, Washington, DC.

Space Studies Board, 2011. Visions and Voyages for Planetary Science in the Decade 2013–2022. The National Academies Press, Washington, DC.

Sullivan, R., Greeley, R., Homan, K., Klemaszewski, J., Belton, M.J.S, Carr, M.H., Chapman, C.R., Tufts, R., Head, J.W. III, Pappalardo, R., Moore, J., Thomas, P., and the Galileo Imaging Team, 1998. Episodic plate separation and fracture infill on the surface of Europa. Nature 391, 371–373.

Tsang, T., Radeka, V., 1995. Electro-optical modulators in particle detectors. Rev. Sci. Instrum. 66(7), 3844–3854.

Tufts, B.R., Greenberg, R., Hoppa, G., Geissler, P., 2000. Lithospheric dilation on Europa. Icarus 146, 75–97.

Tyler, R.H., S. Maus, and H. Luhr 2003. Satellite observations of magnetic fields due to ocean tidal flow. Science 299, 239–241.

Valavanoglou, A., Oberst, M., Magnes, W., Hauer, H., Neubauer, H., Baumjohann, W., Falkner, P., 2007. Magnetometer front-end ASIC (MFA). Geophys. Res. Abstr. 9, 3645–3650.

Wahlund, J.-E., Blomberg, L.G., Morooka, M., Cumnock, J.A., Andre´, M., Eriksson, A.I., Kurth, W.S., Gurnett, D.A., Bale, S.D., 2005. Science opportunities with a double Langmuir probe and electric field experiment for JIMO. Adv. Space Res. 36, 2110–2119.

Wahr, J.M., M. Zuber, D. Smith, and J. Lunine 2006. Tides on Europa, and the thickness of Europa's icy shell. J. Geophys. Res. 111, doi: 10.1029/2006JE002729.

Ward, W.R. 1975. Past orientation of the lunar spin axis. Science 189, 377–379.

Wu, X.P., Bar-Sever, Y.E., Folkner, W.M., Williams, J.G., Zumberge, J.F., 2001. Probing Europa's hidden ocean from tidal effects on orbital dynamics. Geophys. Res. Lett. 28, 2245–2248.

Wu, X.P., Y. Bar-Sever, W. Folkner, J. Williams, and J. Zumberge 2001. Probing Europa's hidden ocean from tidal effects on orbital dynamics. Geophys. Res. Lett. 28, 2245–2248.

Yoder, C.F. and S. Peale 1981. Tidal variations of Earth rotation. J. Geophys. Res. 86, 881–891.

Zahnle, K., Dones, L., Levison, H.F., 1998. Cratering rates in the Galilean satellites. Icarus 136, 202–222.

Zahnle, K., Schenk, P., Levison, H., Dones, L., 2003. Cratering rates in the outer solar system. Icarus 163, 263–289.

Zimmer, C., K.K. Khurana, and M. Kivelson 2000. Subsurface oceans on Europa and Callisto: Constraints from Galileo magnetometer observations. Icarus 147, 329–347.

Zombeck, M.V, 1982. Handbook of Space Astronomy and Astrophysics. Cambridge U. Press, Cambridge, U.K.

Zuber, M.T., D. Smith, S. Solomon, D. Muhleman, J. Head 1992. The Mars Observer Laser Altimeter investigation. J. Geophys. Res. 97, 7781–7797.

B.4.2   Acronyms and Abbreviations

ΔV	delta velocity, delta-V
3D	three-dimensional
A	ampere
A	approach
A/D	analog to digital
ABSL	
AC	alternating current
ACS	attitude control subsystem
ACU	ASRG controller unit
ADC	analog-to-digital converter
AFT	allowable flight temperature
Ah	ampere-hour
anti-jovian	
AO	Announcement of Opportunity
APL	Applied Physics Laboratory
APML	Approved Parts and Materials List
APS	active pixel sensor
ASC	Advanced Stirling converter
ASIC	application-specific integrated circuit
ASRG	Advanced Stirling Radioisotope Generator
ATK/PSI	
ATLO	assembly, test, and launch operations
B	baseline
BIU	Bus Interface Unit
BOM	beginning of mission
BTE	bench-test equipment
C&DH	command and data handling/ command and data handling subsystem

C_3	injection energy per unit mass ($V\infty2$), km2/s2 (also C3)
CAD	computer-aided design
CADRe	Cost Analysis Data Requirement
CATE	Cost and Technical Evaluation
CBE	current best estimate
CCD	charge-coupled device
CCSDS	Consultative Committee for Space Data Systems
CDR	Critical Design Review
CEM	channel electron multiplier
CFDP	CCSDS File Delivery Protocol
CG	center of gravity
CM	center of mass
CMMI	Capability Maturity Model Integration
CMOS	complementary metal-oxide semiconductor
COSPAR	Committee on Space Research
COT	crank over the top
CPT	comprehensive performance test
CRAM	chalcogenide random-access memory
CRISM	Compact Reconnaissance Imaging Spectrometer for Mars
CU	cleanup
DC	direct current
DC/DC	direct current to direct current
DD	displacement damage
DDD	displacement damage dose

DHMR	dry-heat microbial reduction	FPPs	Flight Project Practices
DOD	depth of discharge	FS	flight system
DOE	Department of Energy	FSW	flight software
DPs	Design Principles	FSWTB	flight software testbed
DSM	deep-space maneuver	FWHM	full width at half maximum
DSN	Deep Space Network	G/T	gain to equivalent noise temperature
DTM	developmental test model		
DWG	Detector Working Group	GDS	Ground Data System
EEE	electrical, electronic, and electromechanical	GHA	generator housing assembly
		GM	product of gravitational constant and mass
EFM	Europa Flyby Mission		
EGA	Earth gravity assist	GN&C	guidance, navigation, and control
EHM	Europa Habitibility Mission		
EHS	electrical heater source	GN&C	guidance, navigation, and control
EIRP	effective isoloated radiated power		
		GPHS	General Purpose Heat Source
EIRP	Environmental Incident Response Plan?	GRAIL	Gravity Recovery and Interior Laboratory
EIS	Environmental Impact Statement	GSE	ground-support equipment
		H/W	hardware
EJSM	Europa Jupiter System Mission	HCIPE	High-Capability Instrument for Planetary Exploration
EM	engineering model	HEPA	high-efficiency particulate air
EMI	electromagnetic interference	HGA	high-gain antenna
EOI	Europa Orbit Insertion	HQ	NASA Headquarters
EOM	end of mission	HS	heat source
ES	Europa Study	HY	RF hybrid
ESA	European Space Agency	I&T	integration and test
ESD	electrostatic discharge	I/O	input/output
ETL	Export Technical Liaison	IC	internal charging
EVEE	Earth-Venus-Earth-Earth	ICD	Interface Control Document
FMECA	failure modes, effects, and criticality analysis	ICE	Independent Cost Estimate
		ICM	Institutional Cost Model
FOV	field of view	ID	identification/identifier

ID	inner diameter	M3	Moon Mineralogy Mapper
IFOV	3.2.2, p 2	MAG	Magnetometer
IFOV	instantaneous field of view	MARCI	Mars Color Imager
IMU	inertial measurement unit	MARSIS	Mars Advanced Radar for Subsurface and Ionosphere Sounding
INMS	Ion and Neutral Mass Spectrometer		
INSRP	Interagency Nuclear Safety Review Panel	MC	Mapping Camera
		MCP	microchannel plate
IOM	interoffice memorandum	MCR	Mission Concept Review
IP	interplanetary		
IPR	Ice-Penetrating Radar	MDIS	Mercury Dual Imaging System
IR	infrared	MDR	Mission Definition Review
ITAR	International Traffic in Arms Regulations	MEL	Master Equipment List
		MER	Mars Exploration Rover
I-V	current-voltage	MESSENGER	Mercury Surface, Space Environment, Geochemistry, and Ranging
JEO	Jupiter Europa Orbiter		
JOI	Jupiter Orbit Insertion		
JPL	Jet Propulsion Laboratory	MEV	maximum expected value
K&D	key and driving	MGA	medium-gain antenna
KSC	Kennedy Space Center	MIC	Mars Imaging Camera
L1, L2	Level-1, Level-2, etc.	MLI	multilayer insulation
LAEP	Launch Approval Engineering Plan	MMM	Moon Mineralogy Mapper
		MMRTG	multimission radioisotope thermoelectric generator
LAT	limited angle torque		
LCE	Launch Control Equipment	MOLA	Mars Orbiter Laser Altimeter
LEV	lowest expected value	MPSS	multimission power switch slice
LGA	low-gain antenna		
LORRI	Long-Range Reconnaissance Imager	MRO	Mars Reconnaissance Orbiter
		MSL	Mars Science Laboratory
LP	Langmuir Probe	MSTB	Mission System Testbed
LST	local solar time	MTIB	minimum torque impulse bit
LVA	launch vehicle adapter	MVIC	Multispectral Visible Imaging Camera
LVDS	Low-voltage differential signaling		
		NASA	National Aeronautics and Space Administration

NEPA	National Environmental Policy Act		PJR	perijove raise
NICM	NASA Instrument Cost Model		PMD	propellant-management device
NIMS	Near-Infrared Mapping Spectrometer		PMSR	Project Mission System Review
NLS	NASA Launch Services		PoL	point of load
NLSA	Nuclear Launch Safety Approval		PRA	probablilistic risk assessment
NR	nonresonant, nonres		PRA	Project Resource Analyst
NSI	NASA Standard Initiator		PRICE-H	Parametric Review of Information for Costing and Evaluation—Hardware
NTO	nitrogen tetroxide		PSA	Project Schedule Analyst
O&C	Operations & Checkout		RAD750	radiation-hardened microprocessor
OD	orbit determination			
OPAG	Outer Planets Assessment Group		ram	direction of forward velocity vector
ORT	operations readiness test		RAM	random-access memory
OSTP	Office of Science and Technology Policy		RCS	reaction-control subsystem
			RDE	Real-Time Development Environment
OTS	off the shelf			
P	preliminary		RDF	radiation design factor
P/L	payload		RDM	radiation design margin
P/N	part number		RF	radio frequency
PBC	power bus controller		RHU	radioisotope heater unit
PCA	pressurant-control assembly		Rj	jovian radii
PCU	power converter unit		ROD	Record of Decision
PDE	propulsion drive electronics		ROIC	readout integrated circuit
PDR	Preliminary Design Review		ROSINA	Rosetta Orbiter Spectrometer for Ion and Neutral Analysis
PEL	Power Equipment List			
PFC	pyro-firing card		RTG	radioisotope thermoelectric generator
PHSF	Payload Hazardous Service Facility			
			RTOF	reflectron time-of-flight
PI	Principal Investigator		RWA	reaction wheel assembly
PIA	propellant-isolation assembly		S/N	signal-to-noise ratio
			S/S	subsystem
PIP	Project Information Package		SAF	Spacecraft Assembly Facility

SAR	Safety Analysis Report		TCM	trajectory correction maneuver
SDS	shunt driver slice		TDP	Technical Data Package
SDST	small deep-space transponder		TI	Topographical Imager
SDT	Science Definition Team		TID	total ionizing dose
SDU	shunt dissipater unit		TOF	time of flight
SEE	single-event effect		TRL	technology readiness level
SEER	System Evaluation and Estimation of Resources		TVC	thrust vector control
			TWTA	traveling-wave tube amplifier
SEL	single-event latchup		U	update
SEMP	Systems Engineering Management Plan		UES	Upper Equipment Section
			V	volt, velocity, vector
SER	Safety Evaluation Report		V&V	verification and validation
set point			VEE	Venus-Earth-Earth
SEU	single-event upset		VEEGA	Venus-Earth-Earth gravity assist
SHARAD	Shallow Radar			
SMAP	Soil Moisture Active Passive		VIMS	Visual and Infrared Mapping Spectrometer
SNR	signal-to-noise ratio			
SQRT	mean radiation signal per pixel		VRHU	variable radioisotope heating unit
SRAM	static random-access memory			
SRR	System Requirements Review		W	watts
SRU	stellar reference unit		We	watts electrical
SS	subsystem		Wt	watts thermal
SSE	Spacecraft Support Equipment		WBS	work breakdown structure
SSI	solid-state imager		WSTS	workstation testset
SSPA	solid-state power amplifier		WTS	waveguide transfer switch
SSR	solid-state recorder			
STV	Solar Thermal Vacuum			
SWIRS	Shortwave Infrared Spectrometer			
SysML	Systems Modeling Language			
TAYF	test as you fly			
TB	testbed			
TCA	thruster cluster assembly			

B.4.3   Master Equipment List

Master Equipment List (MEL) removed for compliance with export-control (ITAR) regulations.
Available upon request."

B.4.4   *Europa Orbiter Mission Senior Review Board Report*

STANFORD
AERONAUTICS &
ASTRONAUTICS

DURAND BUILDING, 496 LOMITA MALL
STANFORD, CA 94305-4035
http://aa.stanford.edu
(650) 723-3317, fax: (650) 723-0279

Dr. Firouz Naderi   December 1, 2011
Solar System Exploration Directorate
JPL
Pasadena, CA

Dear Dr. Naderi

The recent Planetary Decadal Survey determined that the Europa Jupiter Science Mission (EJSM) had compelling science but was not affordable based on an independent cost estimate of $4.8B provided to the National Research Council by The Aerospace Corporation. The Decadal Survey recommended that the mission be descoped to significantly reduce cost. In response, the Europa Jupiter System Mission (EJSM) was separated into two elements (i.e., Orbiter and Flyby) and focused solely on Europa science. Subsequently, NASA directed that a soft lander be added to the options under consideration.

As requested by JPL and consistent with the direction from NASA HQs, a Review Board was created to assess the viability of the three mission options to be provided to NASA HQ. These options were to focus on Europa only and develop Orbiter, Flyby (multiple) and Lander concepts, identifying the lowest achievable cost with a target value of ≈$1.5B for each concept, not including launch vehicle. It was recognized by the Board that at a ≈ 70% reduction in cost from the original EJSM concept any new mission design and corresponding science content would be dramatically different and go far beyond the usual meaning of a simple "descope".

In the charge to the Board, it was emphasized that the Board's responsibility was to conduct an "existence proof" evaluation of a pre-pre Phase A concept. In addition, each project was to be evaluated independently, not as one element of a program series.

The Board listed below was assembled and on November 15, convened at JPL to review the Orbiter and Flyby mission designs.

Scott Hubbard	Chair – NASA Ret.
Orlando Figeroa	NASA Ret. (via telephone)
Mark Saunders	NASA Ret.
Dave Nichols	JPL Div. 31
Jeff Srinivasan	JPL Div. 33
Barry Goldstein	JPL Div. 34
Cindy Kahn	JPL Div. 35
Rosaly Lopes	JPL Div. 32

Gentry Lee　　　　JPL 4X Chief Engineer
Will Devereux　　　APL
Douglas Eng　　　　APL

To assist the Board in assessing the concepts, members of the JPL staff provided presentations and responded to many questions. This entire effort was applauded by all of the members of the Board and contributed to a most successful meeting.

The high level Europa Review Board conclusions can be summarized in a few statements:
- The overall approach to spacecraft modularity and radiation shielding was unanimously lauded as a creative approach to reducing technical risk and cost. No engineering "showstoppers" were identified.
- Both the Orbiter and Flyby mission concepts satisfied the "existence proof" test as missions that met Europa science requirements, could be conducted within the cost constraints provided and have substantial margins.
  o However, several Board members expressed a strong opinion that a "science per dollar" criterion such as applied by the Decadal Survey would find the Flyby mission to yield much greater benefits than the Orbiter Project.
- The Board was unanimous in identifying two technical risks that impact both mission concepts:
  o The Advanced Stirling Radioisotope Generator (ASRG) has been selected as a critical enabling technology. The Board recommends that the study teams thoroughly familiarize themselves with the development status, schedule and performance of the current version of the ASRG and identify any potential modifications from the Discovery version for Europa. In addition, availability of ^{238}Pu stock and ASRG performance elicited concerns from the Board. In particular, there was a recommendation that much more data be collected on ASRG response to the space mission environment, *e.g.,* microphonics and performance under loads.
  o While the "nested" approach to radiation shielding clearly mitigated the risk to the spacecraft and instrument electronics, the detectors will be exposed to the space environment. The Board found that early assessment and investment must be provided to ensure proper sensor performance.
- Consistent with the above statement, a Board consensus emerged that if either of these mission concepts moves ahead, particular attention must be paid to the Announcement of Opportunity (AO) for the science investigations so that the AO enables a simple approach and clearly specifies the PI-mission interface in critical areas such as total detector dose.

Detailed Considerations:
In the charter distributed to the Board prior to the review, we were asked to consider the following criteria:
- Ability of the mission to satisfy the Science Objectives
- Mission design approach
- Robustness of the mission and system architectures

2

– Robustness of mission and system margins; compliance with JPL design principles.
– Proposed scope, including available options, is consistent with funding target value to complete the mission
– Cost risk Project planning risks, including design, environment mitigation plans, integration and test plans, schedule and margins.

Within this overall review framework the following more specific comments were noted where at least two or more Board members addressed similar issues:

Science and Mission Design:
• During the science presentations, there were numerous questions about the changes from the original EJSM instrument suite and experiment goals. Following a request from the Board, Dr. Pappalardo gave a summary of science traceability. A number of the Board members suggested that more work be done by the SDT to clearly define the relationship of a given mission concept to the Decadal Survey.
• The Orbiter mission is challenging in that the science campaign occurs in the last 30 days of the mission and after significant radiation exposure. The Flyby mission has a much slower accumulation of total dose. This distinction needs to be sharpened.

Robustness and Margins:
• Systems margins presented for power, mass, and data were substantial, and of course have implications for launch vehicle requirements and cost. There was considerable discussion and some disagreement about whether maintaining such large technical margins may inappropriately drive the costs at this stage of maturity. A majority of the Board concluded that a conservative approach was appropriate at this point in the life cycle, particularly with the uncertainty in the launch vehicle capabilities a decade or more away from now.

Cost and Cost Risk:
• A majority of the Board appeared satisfied that the two study teams had produced credible cost estimates using a variety of tools and approaches. While the Flyby mission was slightly higher than the $1.5B FY15 target, both projects were deemed to be "in the ballpark". There was a minority opinion that expressed concern over an inconsistency in trends between two parametric tools. Clearly, ongoing cost evaluation and the Aerospace CATE are needed to track these concepts.

Schedule:
• The Study leader (Gavin) noted at the beginning of the review that detailed schedules would not be available. While the Board accepted this limitation as a necessary element of an "existence proof" review, there was clear concern about whether the schedule supported the hardware development as proposed. At subsequent reviews more explicit schedule data is required in order to understand the risks involved.

On behalf of the entire Board, I wish to express again our congratulations to the JPL team in the high quality of the studies. We look forward to the Lander review early in 2012.

3

Sincerely,

Prof. G. Scott Hubbard
Chair, Europa Mission Review Board
Cc: Board members, Tom Gavin

B.4.5   Aerospace Independent Orbiter Concept CATE: Cost and Technical Evaluation

(see next page)

Europa Habitability Mission: Orbiter Concept CATE: Cost and Technical Evaluation

April 24, 2012

Randy Persinger[1], Robert Kellogg[2], Mark Barrera[3]
[1]Advanced Studies and Analysis Directorate, NASA Programs Division
[2]Space Architecture Department, Systems Engineering Division
[3]Vehicle Concepts Department, Systems Engineering Division

Prepared for:

Jet Propulsion Laboratory
4800 Oak Grove Drive
Pasadena, CA 91109

Contract No. 1393581

Authorized by: Civil and Commercial Operations

.

AEROSPACE
Assuring Space Mission Success

Europa Habitability Mission: Orbiter Concept CATE: Cost and Technical Evaluation

Approved by:

Matthew J. Hart, Principal Director
Advanced Studies and Analysis Directorate
Ground Enterprise
NASA Programs Division
Civil and Commercial Operations

Acknowledgments

Contents

Figures

Tables

1. Purpose

The Aerospace Corporation was tasked in November 2011 to participate as an independent party to review three separate, but related, Europa Habitability Mission (EHM) concepts under study by the Jet Propulsion Laboratory (JPL) to visit Europa in the continuing search for life in our solar system. The three concepts were being studied by JPL in the context of guidance provided by the National Research Council (NRC) Planetary Decadal Survey report released to the public in March 2011. In this report, a mission to the Jupiter/Europa system was rated very high with regard to science importance to the United States in the next decade. However, based on the expected high cost of the baseline reference mission evaluated by the NRC Planetary Decadal Steering Committee, the guidance was to descope the reference mission and significantly reduce mission cost while providing sufficient scientific investigation capability considered to be of paramount importance over the next decade. Aerospace, having participated as the NRC Cost and Technical Evaluation (CATE) contractor in the cost, technical, and schedule risk assessment of the planetary concepts evaluated by the Planetary Steering Committee, was a logical choice to independently evaluate the three updated EHM concepts with the same CATE techniques and processes. The three separate EHM mission concepts evaluated were: Orbiter, Flyby and Lander. This report presents the cost, technical, and schedule risk assessment for the **EHM Orbiter Mission** using the CATE process originally established by the NRC.

The key parameters of the EHM Orbiter Mission can be found in Figure 1.

Europa Habitability Mission Orbiter

Europa Orbiter

Scientific Objectives:
- Explore Europa to investigate its habitability
- Key science themes cited:
  - *Characterize the extent of the Europan* **ocean** *and its relation to the deeper interior*
  - *Understand the formation of surface* **geology**
    - Including sites of recent or current activity
    - Characterize high science interest localities

Key Parameters:
- Model Payload (4 instruments)
  - *Ocean: Laser Altimeter, (Radio Science – Telecomm Subsystem)*
  - *Geology: Mapping Camera*
  - *Particles and Fields: Langmuir Probe, Magnetometer*
- 4 Advanced Stirling Radioisotope Generators (ASRGs)
- Launch Mass: 3748 kg
- Launch Date: 2021 (on Atlas V 551)
- Orbit: 100 km Europa orbit + ~ 15 Gravity Assist flybys before EOI (no planned science during cruise/flybys)
- Radiation Environment: 1.1 Mrad TID (100 mil Al Si) cruise + 400 krad TID (100 mil Al Si) Europa orbit
- Disposal Location: Europa

Key Challenges:
- Mission Requirements Growth
  - *Unexploited science opportunities*
  - *Unexploited capacity*
- ASRG Development
  - *Performance and life qualification*
  - *Impact of ASRG-induced jitter on system*
- Radiation Environment
  - *Impact to external hardware and sensitive detectors*
  - *Fail operational software fault management*
- Planetary Protection
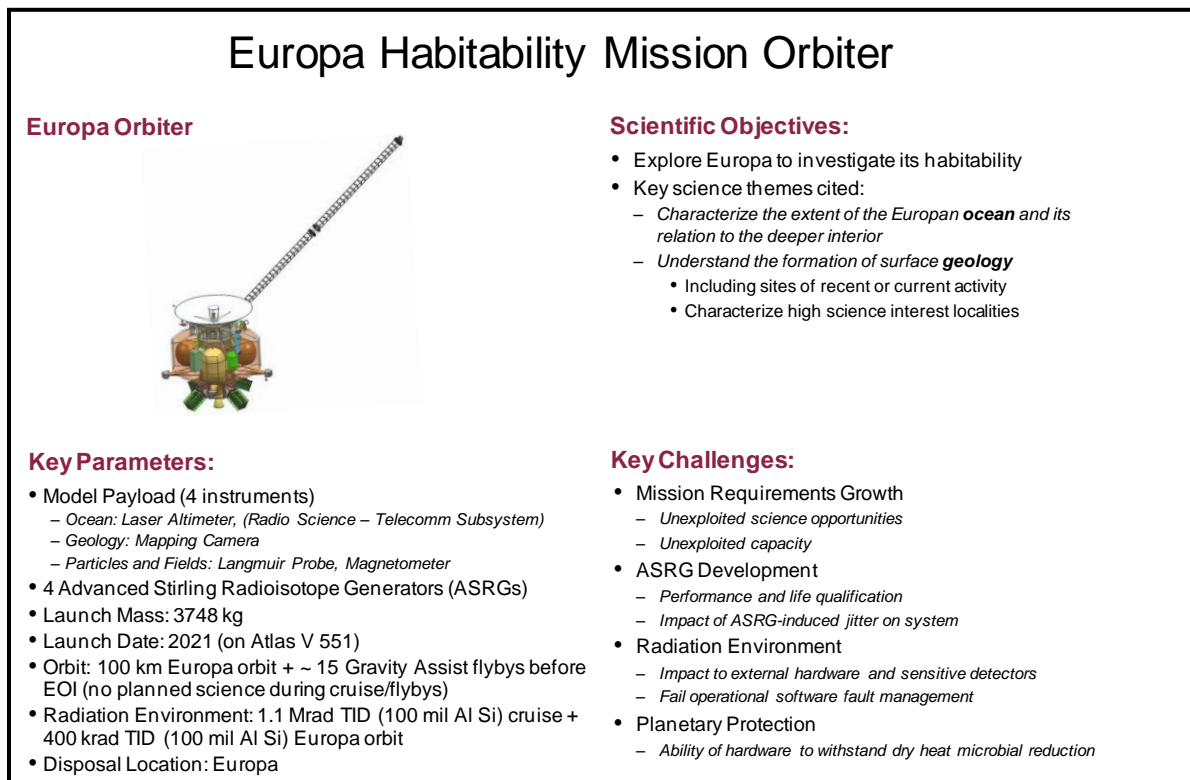 - *Ability of hardware to withstand dry heat microbial reduction*

Figure 1.   EHM Orbiter Mission Concept Overview

2. Executive Summary

The EHM Orbiter concept was found to have a Medium technical risk and is well designed for an orbiter mission to Europa. Mass and power margins are robust, and the design incorporates modularity with well-defined interfaces. Technology development is mainly related to engineering implementation; however, concern does exist with the technology development of the radioisotope power source (ASRGs) currently under development by NASA. An additional concern is the selection of hardware that is tolerant to the dry heat microbial reduction process planned to ensure satisfaction of Planetary Protection requirements. The impact of radiation for this mission is also a concern but has been mitigated by compartmentalization and the modular design, as well as the mission design.

The CATE cost estimate for the EHM Orbiter concept is $1.8B in FY15 dollars excluding launch services. The EHM Orbiter CATE, estimate excluding launch services, is compared to the Project's cost estimate in Figure 2. Including a launch service cost of $272M, consistent with CATE estimates for the Planetary Decadal Survey Steering Committee, the CATE estimate including launch services is $2.0B. The cost estimate for four ASRGs is assumed to be $200M based on guidance provided by NASA. The cost risk associated with the ASRG technology development required for the EHM mission concepts has not been included in the CATE cost estimate, nor have the associated schedule risk to the project and technical risk to the flight system.

The project schedule of 73 months is considered to be realistic with the independent estimate being 75 months. The concept's use of modularity provides the opportunity to focus and minimize risk through parallel development paths.
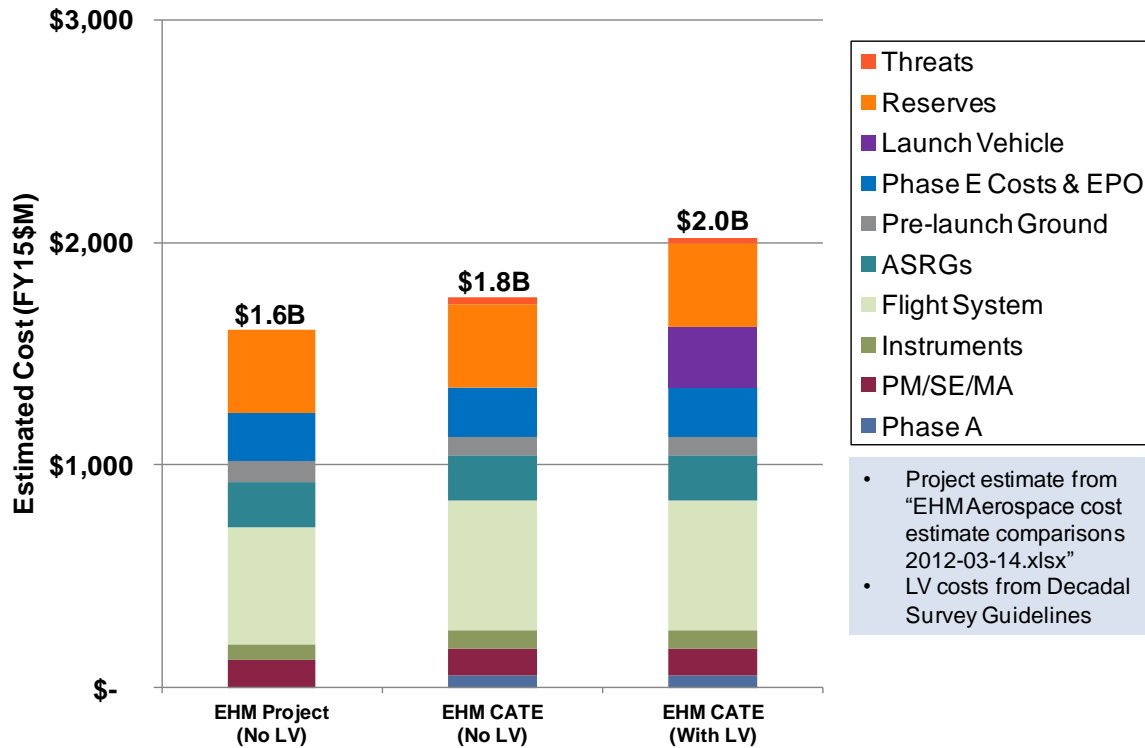

Figure 2.   Europa Orbiter Cost Estimates

3

3. CATE Background

The NRC Astro2010 Decadal Survey Steering Committee established the CATE process in June 2009. The CATE process was then used for three NRC Decadal Surveys: Astro2010, Planetary, and Heliophysics. Previous NRC Decadal Surveys had underestimated the costs associated with the recommended science priorities. The NRC and others recognized that mission costs were being under estimated, so the US Congress mandated that an independent contractor be utilized to provide more realistic cost, technical and schedule risk assessment directly to the decadal steering committees for consideration and evaluation in executing their charter. Select portions of the Planetary Decadal report, *Vision and Voyages*, from Appendix C are provided below to summarize the CATE process. It is important to note that the CATE process is intended to inform future NASA Science Mission Directorate (SMD) budget decisions, not to decide if a specific concept meets a cost target or to decide if a specific mission concept should be selected for flight versus another mission. Because the CATE process is used for future budgetary decisions, it incorporates potential cost threats that may occur in the future based on concept maturity at the time of evaluation.

The CATE process focuses on cost and schedule risk assessment, but limited technical evaluation is also required to categorize concept maturity, technology development, and the potential impact that insufficient margins and contingency (mass and power) may have on schedule or cost.

Vision and Voyages, Planetary Decadal Report, Appendix C: *The objective of the CATE process is to perform a cost and technical risk analysis for a set of concepts that may have a broad range of maturity, and to ensure that the analysis is consistent, fair, and informed by historical data. Typically, a concept evaluated using the CATE process is early in its life cycle and therefore likely to undergo significant subsequent design changes. Historically, such changes have resulted in cost growth. Therefore, a robust process is required that fairly treats a concept of low maturity relative to one that has undergone several iterations and review. CATEs take into account several components of risk assessment.*

The primary goal of the CATE cost appraisal is to provide independent estimates (in fiscal year [FY] 2015 dollars) that can be used to prioritize various concepts within the context of the expected NASA budgetary constraints for the coming decade. ... To be consistent for all concepts, the CATE cost process allows an increase in cost resulting from increased contingency mass and power, increased schedule, increased required launch vehicle capability, and other cost threats depending on the concept maturity and specific risk assessment of a particular concept. ... All cost appraisals for the CATE process are probabilistic in nature and are based on the NASA historical record and documented project life-cycle growth studies.

The evaluation of technical risk and maturity in the CATE process focuses on the identification of the technical risks most important to achieving the required mission performance and stated science objectives. The assessment is limited to top-level technical maturity and risk discussions. Deviations from the current state of the art as well as system complexity, operational complexity, and integration concerns associated with the use of heritage components are identified. Technical maturity and the need for specific technology development, including readiness levels of key technologies and hardware, are evaluated. ... The CATE technical evaluation is limited to high-level technical risks that potentially impact schedule and cost. The CATE process places no cost cap on mission concepts, and hence risk as a function of cost is not considered. Concept maturity and technical risk are evaluated in terms of the ability of a concept to meet performance goals within proposed launch dates with adequate mass, power, and performance margins.

To aid in the assessment of concept risk, independent schedule estimates are incorporated as part of the CATE cost estimate.

4. Technical Evaluation

The EHM Orbiter technical risk rating is Medium. The mission will require medium new development, mostly in the engineering implementation. Radioisotope, or ASRG, power source qualification, radiation mitigation for external hardware, software fault management, bake stable treatment of detectors for planetary protection, and qualification of the AMBR 890 N (HiPAT) engine will be some of the key challenges associated with this mission. Mass margins are high, with an average mass contingency of 64% for the bus and 88% for the instruments. Power margins and battery depth of discharge are adequate assuming four ASRGs. The concept design is within the capability of the Atlas V 551 and 541 launch vehicles, with greater than 10% launch mass margin. The radiation environment contributes to Medium operational risk. The proposed "fail operational" approach to fault management of radiation upsets also contributes to this risk. An additional concern is the development of hardware to withstand Planetary Protection measures, given the vehicle will be disposed of on the surface of Europa.

The top technical risks associated with the EHM Orbiter Mission are:

1. **Mission Requirements Growth** to utilize additional capacity
2. **Advanced Stirling Radioisotope Generator (ASRGs)** development impact
3. Survival of flight system in **Radiation Environment**
4. Development of hardware to withstand **Planetary Protection** methods

These top risks are discussed below. Figure 3 illustrates some key aspects of the EHM Orbiter concept.
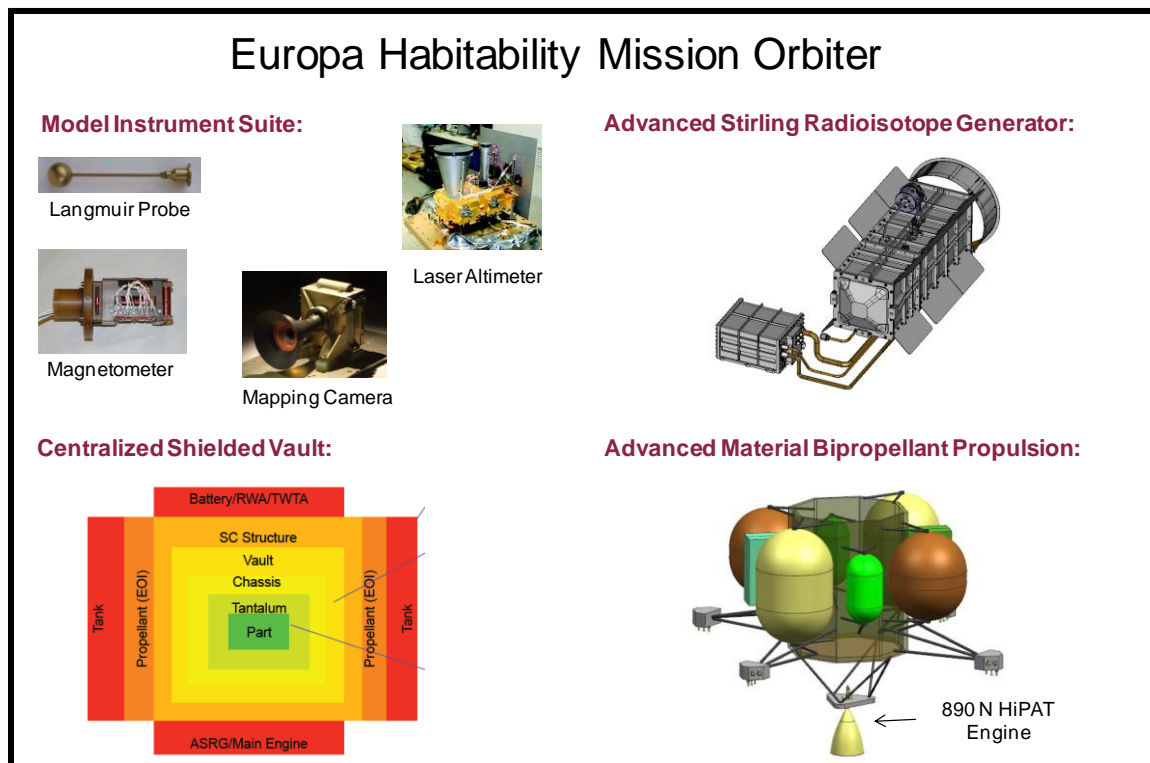

Figure 3.   EHM Orbiter Mission Concept Features

7

Mission Requirements Growth

The anticipated high mass margins for the EHM Orbiter mission have the benefit of mitigating the risk of unplanned mass growth; however, they also offer a temptation to increase the science payload from the current focused concept, which may impact the overall complexity and cost of the mission. As illustrated in Figure 4, the proposed concept has a launch mass margin of greater than 10% on Atlas V 541 and 551. This margin already considers the best-estimate mass as well as an average 64% mass growth contingency for the bus and 88% mass growth contingency for the instruments. Since the mass margins are high, there is a concern that instrument providers may wish to utilize excess capacity. Competitively chosen instruments may have higher mass or complexity than the model instruments for the EHM concept. Also, there is a concern that instrument types from the EHM Flyby concept may be added to the Orbiter mission. Neither of these potential scenarios was included in the CATE cost estimate.
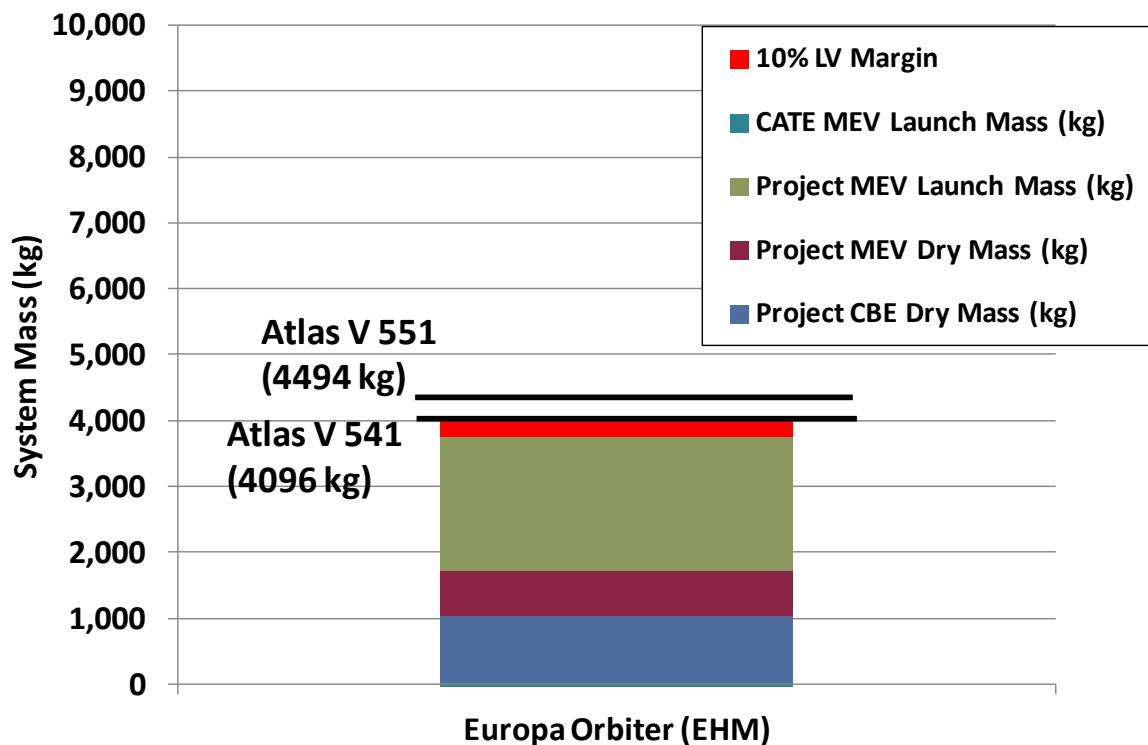
Figure 4.   EHM Orbiter Launch Mass Margin

Power margins during normal operations are acceptable assuming 4 ASRG power, as shown in Figure 5. There are small differences in the expected maximum battery depth of discharge due to differences in power growth allowances in CATE estimates versus project estimates; however, all estimated power margins are within acceptable limits. Battery depth-of-discharge is held to 28% or lower in the worst case (at either telecom or Jupiter orbit insertion).

Advanced Stirling Radioisotope Generator (ASRGs)

Uncertainty associated with technology development for the ASRGs contributes to risk of design changes and schedule delays for the project. The ASRG is currently estimated at TRL 5 and is part of an ongoing development effort. Results from the ground based testing program may possibly lead to changes in the ASRG interface to the spacecraft. Items that are of particular concern include the contribution of jitter from the ASRGs to the Mapping Camera and Laser Altimeter as well as the

Power Growth Contingency

Project: 67% load power contingency (payload and bus)

CATE: 80% load power contingency for payload and 50% for bus

Maximum Battery DOD

Project: 28% during JOI

CATE: 17% during JOI

Figure 5.   EHM Orbiter Power Margin

impact of electromagnetic interference (EMI). Also, there is concern that the ASRG may not provide the expected power for the mission environment. If the ASRGs provide less power than expected, then either a fifth ASRG may need to be considered or a modification to mission operations may be necessary. No additions to the CATE cost or schedule estimates were made based on possible delays in ASRG development.
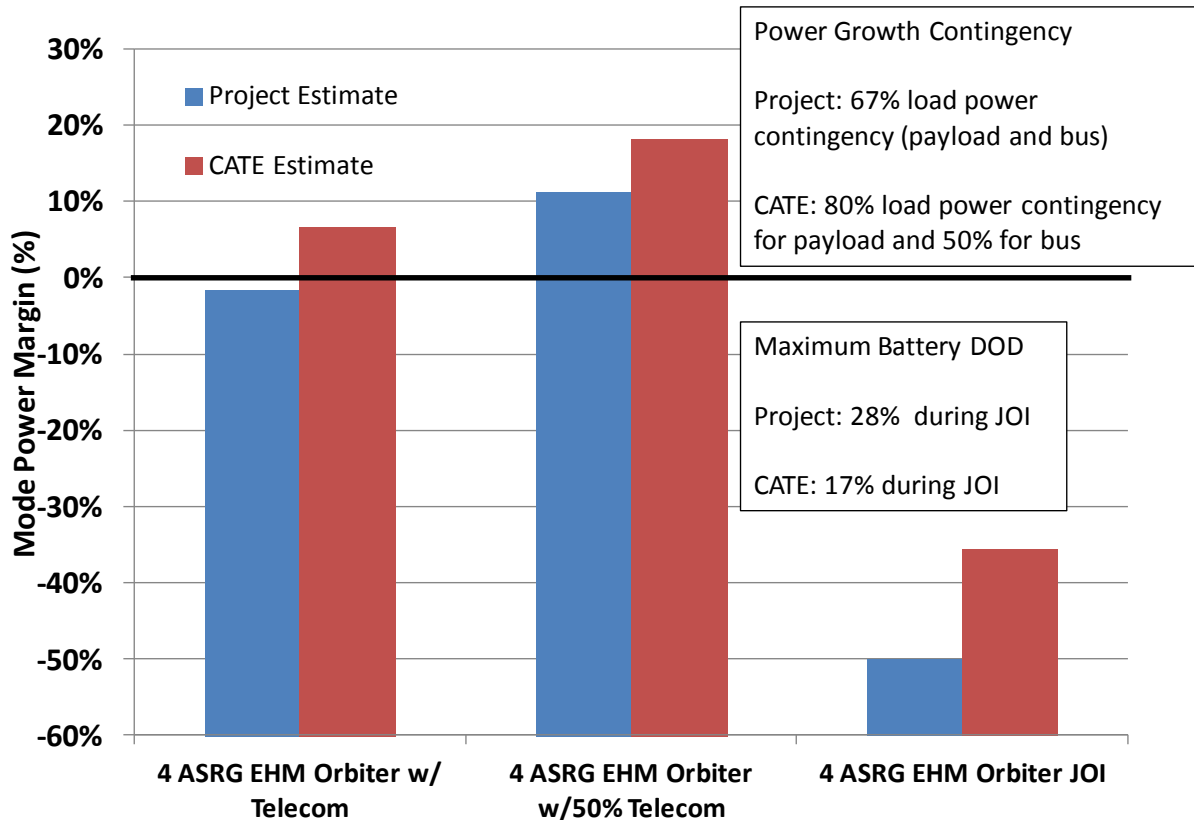
Radiation Environment

The radiation environment for the EHM Orbiter mission contributes to uncertainty in mass, cost, and schedule. Hardware that is external to the radiation vault, particularly exposed sensor heads, will require qualification for the mission radiation environment. Delays in radiation qualification of sensor detectors or optics may adversely impact project cost and schedule. Hardware that is internal to the radiation vault may need to be assessed for compatibility (EMI and thermal) within the common enclosure. Additional systems engineering effort is anticipated for successful integration of electronics within the common radiation vault. In order to maintain operations through radiation upsets, the EHM Orbiter mission proposes a "fail operational" software fault management approach. While this approach may help to maintain operations pacing, it will require a more complete understanding of hardware failure modes than a "fail safe" approach. Some delays in fault management software are anticipated as the hardware implementation matures. The impact to the CATE cost estimate was considered by using the Juno mission as a cost analogy and adding a 5% multiplier to the bus and camera estimates for radiation issues.

Planetary Protection

The EHM Orbiter is intended for disposal on the surface of Europa and as a result is subject to Planetary Protection requirements. These requirements will place a stringent limit on spores on surfaces, in joints, and in the bulk of nonmetallic materials. Currently, the project plans to use dry heat microbial reduction to meet these requirements and possibly other means if necessary. Hardware used on the EHM Orbiter must be tolerant to the high heat (~110°C-125°C) microbial reduction process or other processes as needed. These requirements will constrain hardware selection and may result in adverse impacts to cost and schedule. In order to ensure satisfaction of Planetary Protection requirements, the project will need to implement a compliance effort throughout the system development. In order to account for instrument and bus planetary protection, a 5% multiplying factor was used in the cost estimate.

Technology Development

Technology development items for the EHM Orbiter mission include development of the ASRG, radiation-hardened detectors for the Europa mission environment, and qualification of the AMBR 890 N (HiPAT) engine. The ASRG is currently estimated at TRL 5 based on DoE engineering unit testing with further testing by NASA Glenn Research Center. Further life testing is anticipated as well as a modified housing design. Additional development of radiation hardened detectors is anticipated to advance beyond TRL 5-6. The current level of maturity depends on the selected manufacturers and their proposed manufacturing techniques for hardending of CCD and CMOS type detectors. The AMBR engine is currently estimated at TRL 6, based on unit level environmental and performance testing, although additional performance and life testing is ongoing.

5. Cost and Schedule Evaluation

Figure 6 illustrates the CATE cost estimating approach in the form of a flow diagram. The initial focus is to estimate, with multiple analogies and cost models, the concept hardware such as instruments and spacecraft bus. Following the estimation of other cost elements based on historical data, a probabilistic cost-risk analysis is employed to estimate appropriate cost reserves. To ensure consistency for all concepts, the cost estimates are updated with information from the technical team with regard to mass and power contingencies and potentially required additional launch vehicle capacity. Using independent schedule estimates, costs are adjusted using appropriate burn rates to properly reflect the impact of schedule delays or multiple work shifts to ensure meeting a launch date. Finally, the results are integrated, cross-checked with other independent cost and schedule estimating capabilities, and verified for consistency.

Figure 6. CATE Cost Estimating Process

Hardware Cost Estimates

The hardware cost elements estimated for the Europa Orbiter concept are the spacecraft bus and the four instruments. Multiple estimates are developed for each of these elements. Both parametric cost models and analogy-based estimates are used. Figure 7 illustrates the analogy-based estimating process, which uses a cost estimating relationship (CER) to adjust the actual costs of past missions. By using the actual costs of past missions, unique attributes of those missions or performing organizations, which are similar to the mission being estimated, can be captured. This can provide insight that is different from most parametric cost models, which are based more on an "industry average" approach.

For the spacecraft bus, a total of five estimates were developed using the NASA and Air Force Cost Model (NAFCOM), the PRICE-H cost model and analogy-based estimates using Juno, Cassini, and Mars Reconnaissance Orbiter (MRO). The final CATE estimate is an average of these five estimates. The results of these estimates are depicted in Figure 8. The cost estimates shown include the spacecraft hardware, Project Management and Systems Engineering at the bus level, as well as bus

$$\text{Estimate} = \text{Actual analogy cost} \times \text{CER (new)/CER (analogy)}$$

Figure 7.   Analogy-Based Estimating Process

Figure 8.   Orbiter Bus Cost Estimates

and system-level integration and test. ASRG costs are not included in these estimates. As can be seen, there is reasonable agreement between the CATE ($582M) and Project ($523M) cost estimate for the spacecraft bus or flight system.

For the Orbiter instruments, the cost estimates are based on either two or three parametric cost models and three to five analogy-based estimates. The parametric models used for the Orbiter instruments include the NASA Instrument Cost Model (NICM), The Multivariate Instrument Cost Model (MICM), and the Space-based Optical System Cost Model (SOSCM). The results for the instruments are depicted in Figures 9 to 12. In addition to the individual instrument estimates, the total payload

12
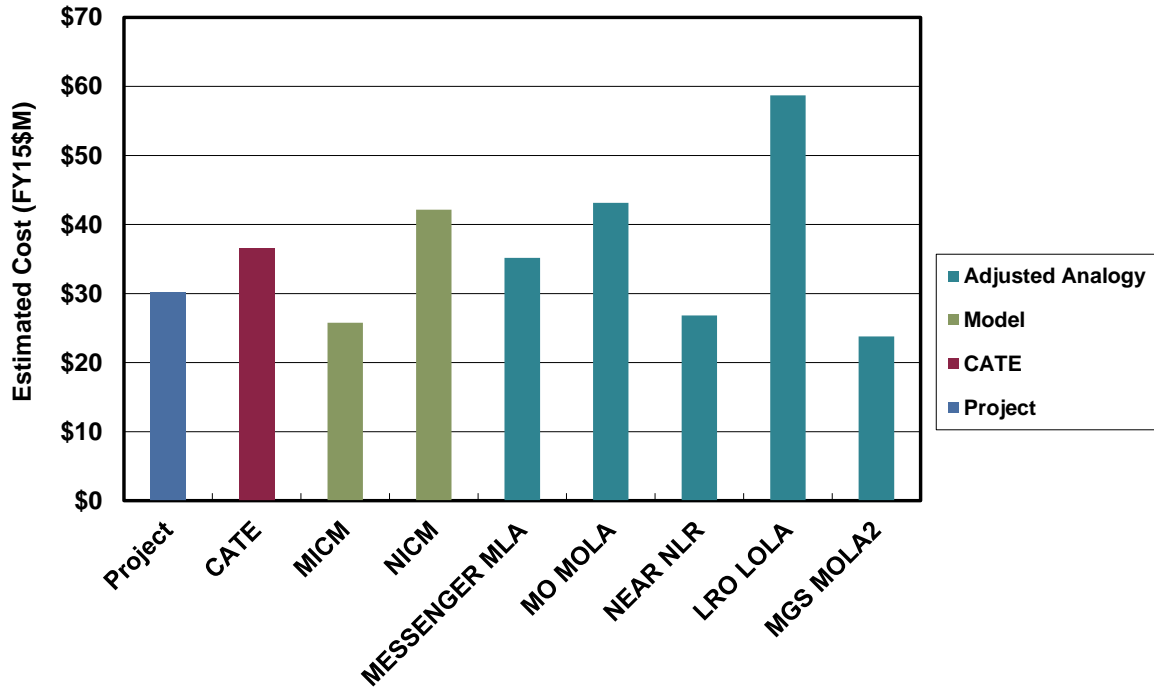
Figure 9.   Orbiter Laser Altimeter Cost Estimates
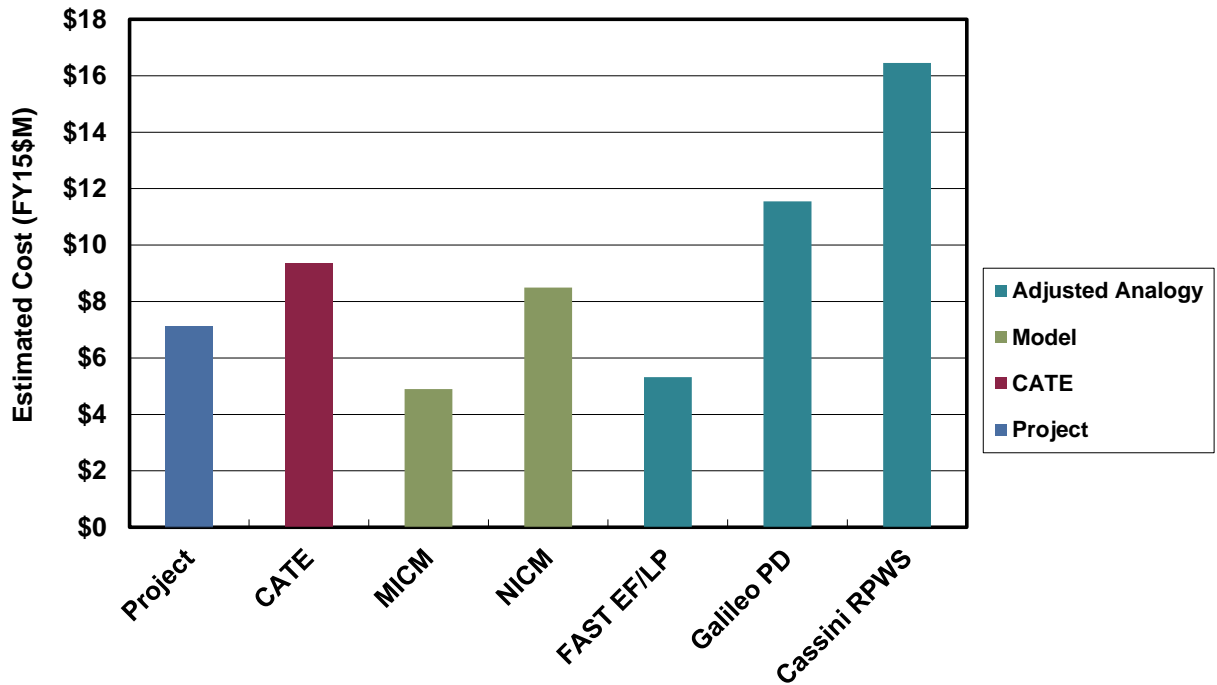
Figure 10. Orbiter Langmuir Probe Cost Estimates
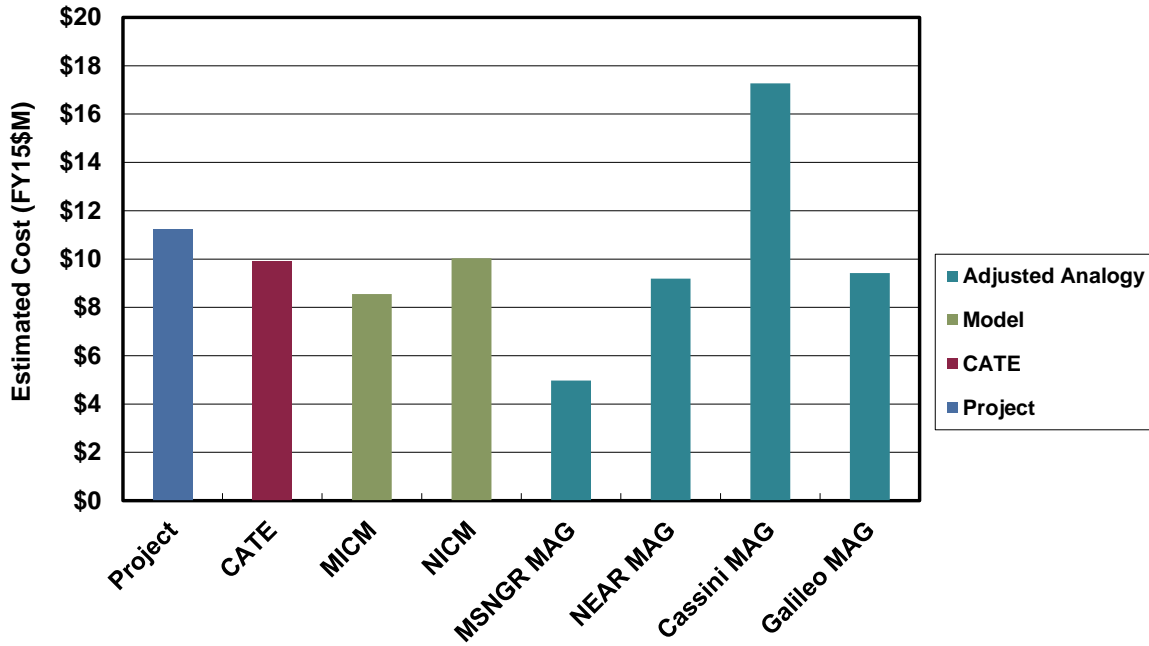
Figure 11. Orbiter Magnetometer Cost Estimates
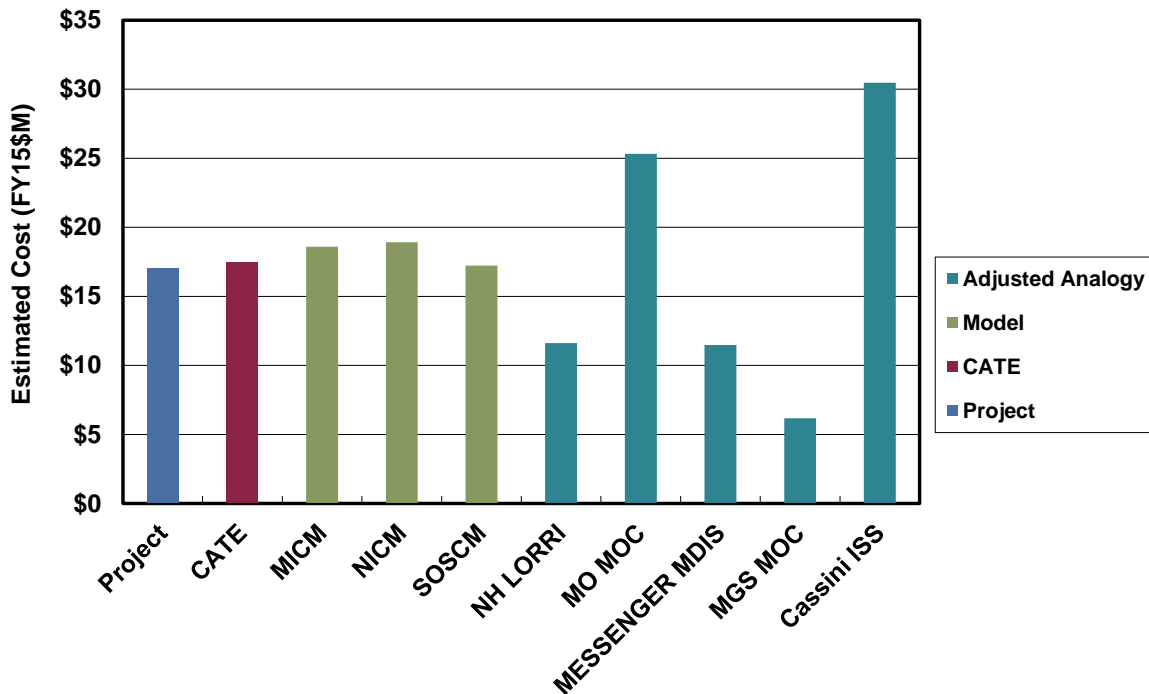
Figure 12. Orbiter Mapping Camera Cost Estimates

estimates include an estimate of the payload-level Project Management and Systems Engineering. For the total payload, there is good agreement between the CATE ($81M) and Project ($75M) cost estimates, as shown in Figure 13.
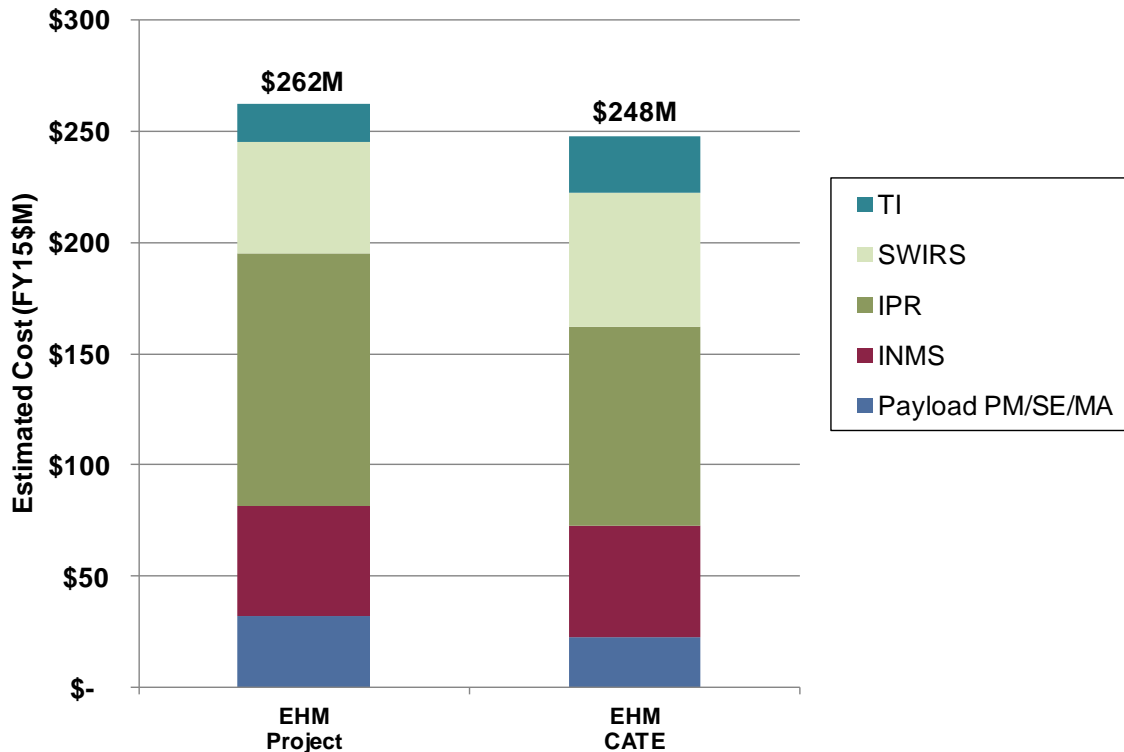
14

Figure 13. Total Payload Cost Comparison

Other Cost Elements

Other cost elements estimated for the EHM Orbiter concept include project-level Project Management, Systems Engineering, and Mission Assurance, pre-launch Science and Ground System Development, Pre-Phase A/Phase A, Phase E, and Education and Public Outreach (EPO). Other cost elements included in the total cost estimated, but not independently estimated, are the ASRGs and launch vehicle.

Project Management, Systems Engineering, and Mission Assurance were estimated as a single total (PM/SE/MA) using "wrap factors" based on similar historical projects. The historical missions used for the Orbiter PM/SE/MA estimate are Cassini, Juno, MER, and Mars Exploration Rover (MRO). The "wrap factors" are calculated as a percentage of hardware costs for the historical missions. These percentages are then applied to the estimated hardware cost of the Orbiter concept. Specifically, the average percentage wrap factor is applied to the total of the average estimate for each hardware element.

Pre-launch Science and Ground System Development estimate is similarly developed using wrap factors based on historical missions. The historical missions used are Cassini, Juno, MER, and MRO.

Pre-Phase A/Phase A costs are estimated using a rule of thumb of 1.5% of the Phase B-D development costs per year of Pre-Phase A/Phase A. For the EHM Orbiter concept, the total duration used was 40 months starting in June 2012 and ending in October 2015. This is actually earlier than the Phase A end date shown on the project schedule (Figure 14). However, significant activities are planned to start in October 2015. These activities have historically been a part of Phase B, so an adjusted Phase B start date is used for all schedule-related analyses.

15
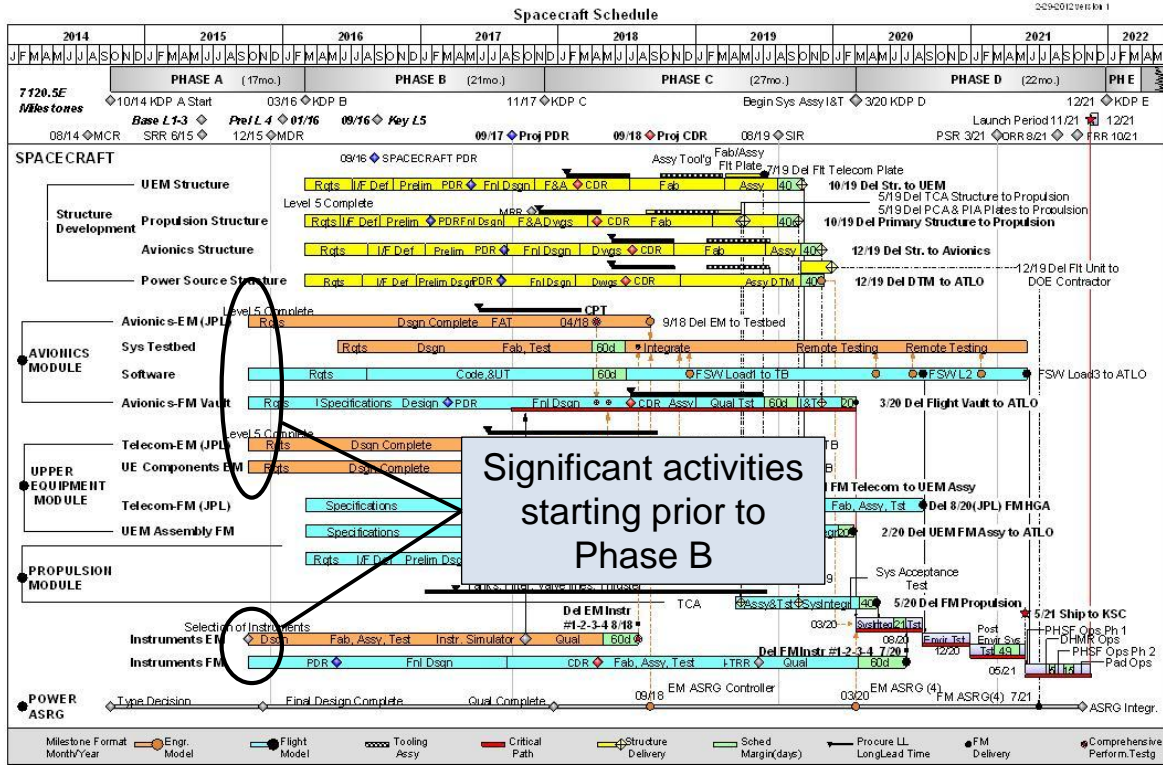
Figure 14. Europa Orbiter Planned Development Schedule

Phase E costs were estimated using annual spend rates from similar historical projects. Because of the potentially different staffing required during cruise and encounter, these phases were estimated separately using historical rates appropriate for the respective phase. For the cruise phase, annual rates from MESSENGER, Juno, and New Horizons cruise phases were used. For the encounter phase, annual rates from MRO and the predicted annual rate from Juno encounter phases were used.

EPO costs are estimated as 1% of total project costs excluding launch vehicle.

For the ASRGs, the project estimate of $50M each, supplied by NASA HQ, was used in the CATE estimate. For the Atlas V 551 launch vehicle, a $272M estimate from the Planetary Decadal Survey was assumed for consistency.

Cost Reserves

Cost reserves are estimated using a process illustrated in Figure 15. For each Work Breakdown Structure (WBS) element, a triangular distribution of possible costs is developed. The cost values for the triangle are derived from the range of cost estimates as illustrated in the bus and instrument figures above. The lowest of the multiple estimates is used as the low value of the triangular distribution. The average of the multiple estimates is used as the mode or most-likely value of the triangular distribution. The high value of the triangular distribution starts with the highest of the multiple estimates but then adds an additional Design Maturity Factor. The DMF is a multiplier based on the maturity of the proposed design and the experience of the team. This factor helps ensure that the high value of the distribution truly represents a worst case.

Once the triangular distributions are developed for each WBS element, they are statistically combined to produce a total cost probability distribution. This distribution is typically plotted as a cumulative

Figure 15. Cost Reserve Estimate Process Overview

distribution, which takes the familiar "S-curve" shape. The difference between the 70th percentile value from this curve and the sum of the most-likely estimates is the cost reserves estimate.

Mass and Power Contingency Threat

The mass and power contingency threat is a concept that was developed to support the CATE estimates, initially for the Astro2010 Decadal Survey, then later applied to the Planetary Science and Heliophysics Decadal Surveys. The motivation was to provide a methodology to account for the design evolution that has historically occurred from early conceptual design through development and launch. In order to assign a cost to these design changes, historical mass and power growth data was examined. This data showed values that were well above the typical guidelines of roughly 30% at Phase B start. Because data prior to Phase B start was sparse, the available data was extrapolated back to early conceptual phases.

Figure 16 shows an example of the data used for the mass and power contingency threats. This plot shows payload mass growth data for seven historical planetary missions. The red line is the average of this historical mission data. The black line is the CATE contingency that is used for the threat calculation.

To estimate the threat cost, the project-proposed mass and power contingencies (used in the hardware estimates described above) are replaced with the CATE contingencies. The estimates, including reserves, are then recalculated and the difference between this result and the result using project contingencies is recorded as the mass and power contingency threat.

For most projects, the CATE contingencies are well above the contingency values assumed in the proposed concept. However, the Europa Orbiter concept already carried significant contingencies, so the estimated contingency threat was insignificant ($15M). Table 1 is a summary of the mass properties provided for the CATE assessment.

17
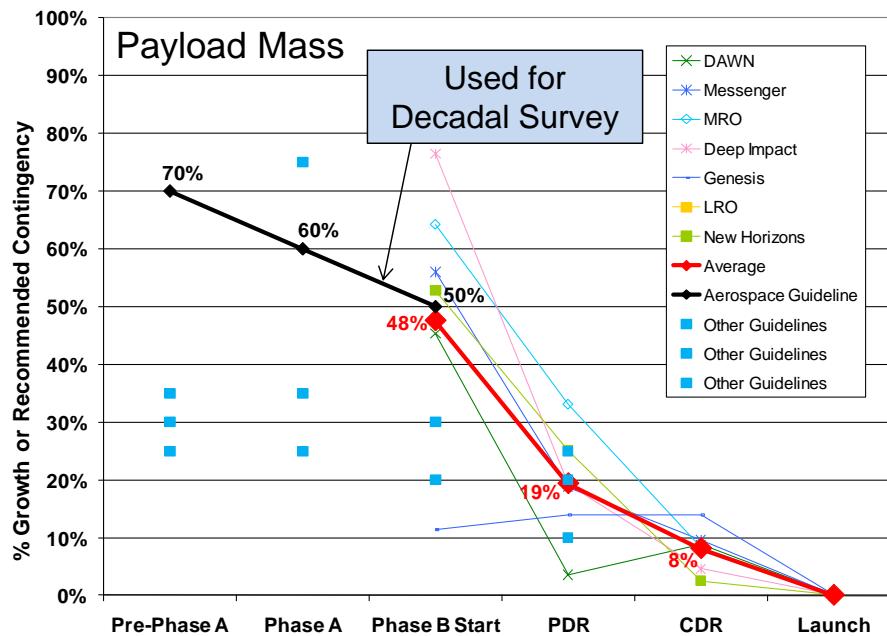
Figure 16. Contingency Values Used For Threat Estimates

Table 1. Europa Orbiter Mass Properties

	Project CBE (kg)	Project Cont. (%)	Project MEV (kg)	CATE Cont. (%)	CATE MEV (kg)
Orbiter Flight System Total	**1033.4**	**63%**	**1685.7**	**51%**	**1555.9**
Orbiter Payload Total	**29.1**	**76%**	**51.4**	**70%**	**49.5**
Instrument Chassis	2.0	63%	3.3	70%	3.4
Laser Altimeter	4.4	88%	8.2	70%	7.4
Langmuir Probe	2.2	88%	4.1	70%	3.7
Magnetometer	2.7	88%	5.0	70%	4.5
Mapping Camera	2.0	88%	3.8	70%	3.4
Payload Shielding	15.9	70%	27.1	70%	27.1
Orbiter Bus Total	**1004.2**	**63%**	**1634.3**	**50%**	**1506.4**
C&DH	12.0	63%	19.5	50%	18.0
GN&C	31.5	44%	45.2	50%	47.2
Harness	56.0	88%	105.0	50%	84.0
Mechanical	436.2	59%	694.3	50%	654.2
Power (w/o ASRGs)	41.5	34%	55.4	50%	62.2
ASRGs (4)	102.4	88%	192.0	50%	153.6
Propulsion	153.7	57%	241.6	50%	230.6
Telecom	60.9	71%	103.8	50%	91.3
Thermal	35.0	63%	56.9	50%	52.5
Bus Shielding	75.2	60%	120.6	50%	112.8

Schedule Threat

The base cost estimate described above uses the project-proposed development schedule. Historically, project schedule estimates have proven to be optimistic. As part of the CATE process, a probabilistic

18

Independent Schedule Estimate (ISE) is developed. If the 70th percentile duration from the ISE is longer than project schedule, then a schedule threat is added.

Figure 17 illustrates the ISE process. The ISE is based on actual schedule durations from similar, historical missions. The duration of each schedule phase is treated as a triangular distribution, which can be statistically combined to yield a probability distribution of total project development time. The triangular distribution of durations for each phase is derived from the actual phase durations from the historical missions. The lowest duration is used as the low end of the triangular distribution, the average duration is used as the mode or most-likely value, and the highest historical value is used as the high value of the triangular distribution.

Figure 17. Independent Schedule Estimate Process Overview

Figure 18 compares the actual Phase B-D duration of the four analogous missions used in the ISE with the proposed Europa Orbiter Phase B-D duration. Figure 19 shows the results of the ISE as a cumulative probability distribution or S-curve. The 70th percentile ISE value is 75 months while the Europa Orbiter proposed value is 73 months (after adjusting the effective Phase B start date as described above). Figure 20 is a breakdown of the results by project phase. While the overall durations agree quite well, the 70th percentile historical duration for the CDR to start of spacecraft I&T phase is significantly longer than the project value. Although this difference does not contribute to the CATE cost estimate, the plan for this phase should be examined to ensure its adequacy.

The difference between the 70th percentile value and the proposed project duration is then converted to a cost threat using a burn rate based on the project budget without reserves or launch vehicle. For Europa Orbiter, the roughly two months' difference is multiplied by a burn rate of roughly $7M per month to yield a schedule threat of $17M.

19
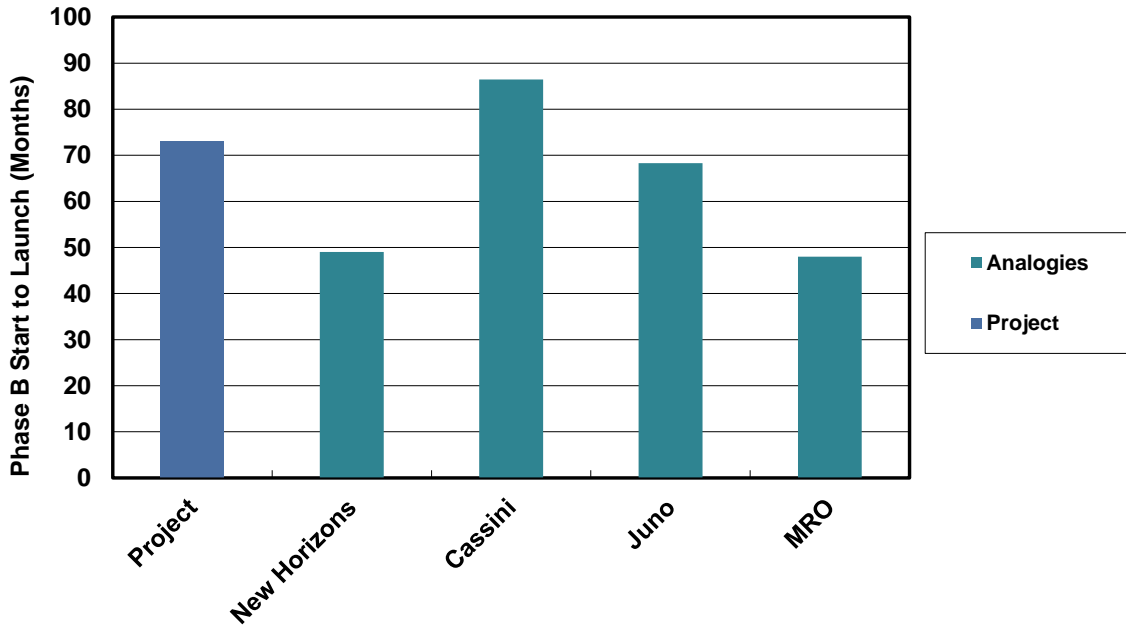
Figure 18. Analogous Mission Development Time Comparison
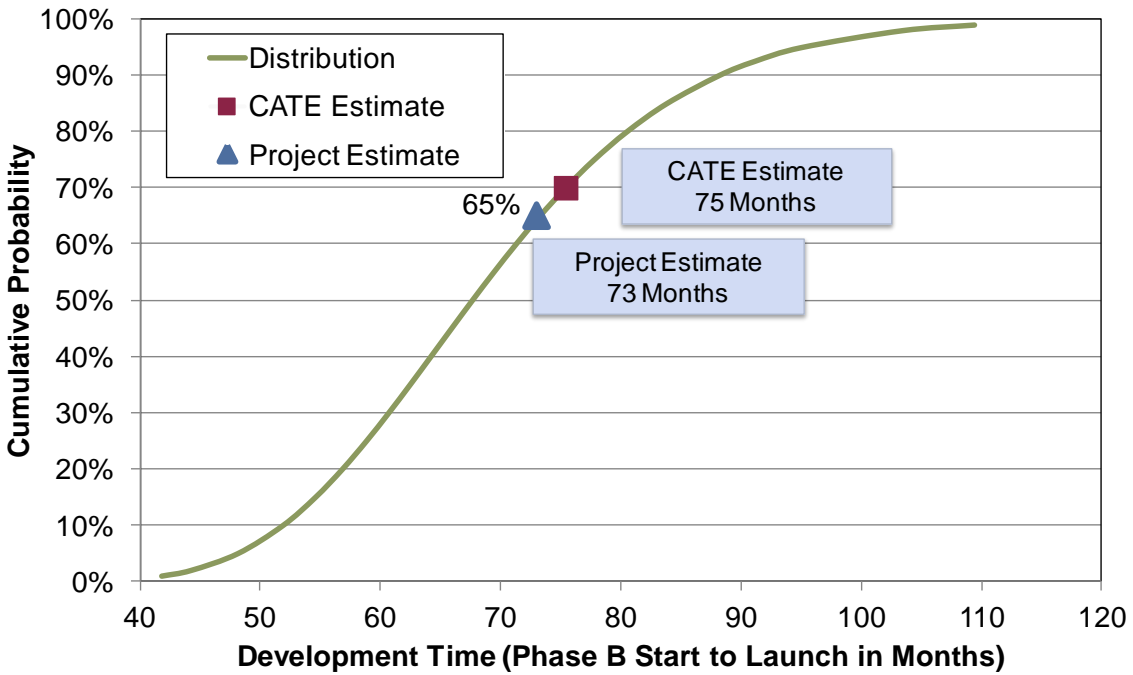
Figure 19. Europa Orbiter ISE S-Curve
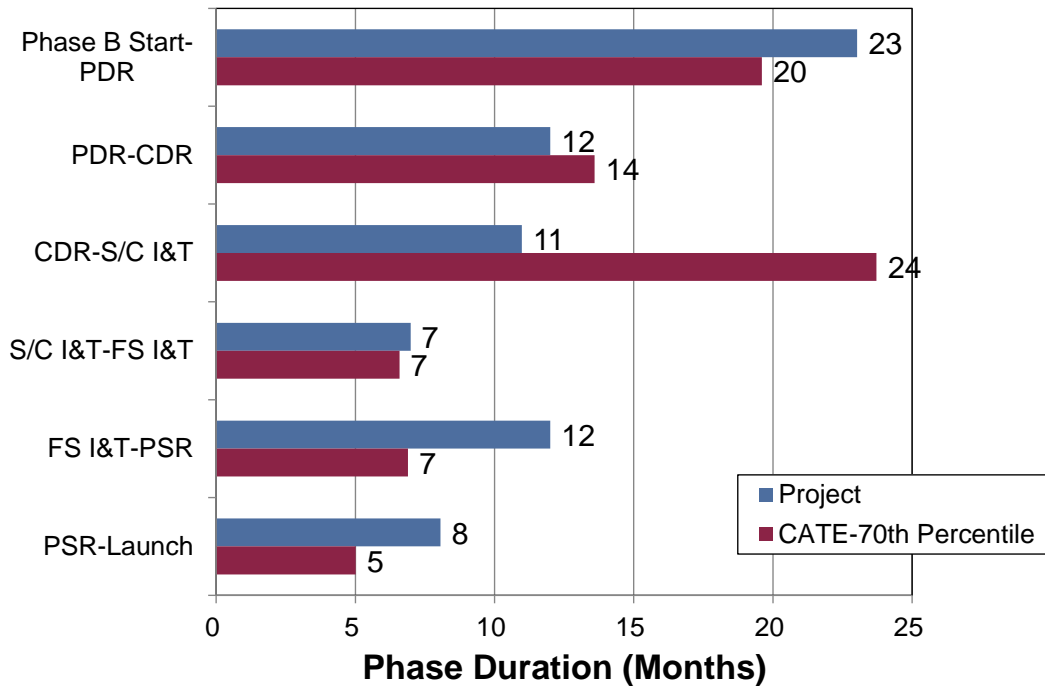
Figure 20. Europa Orbiter Analogous Mission Phase Comparison

Results

Table 2 presents the final CATE cost results compared to the current Europa team cost estimate. The agreement between the two estimates is quite close in all WBS elements. Figures 21 and 22 present the same data in graphical form.

Table 2.   Europa Orbiter Cost Estimate Comparison (FY15$M)

WBS Element	Project Estimate	CATE Estimate	Basis of CATE Estimate
Pre-Phase A, Phase A	incl. below	$ 54	1.5% of Dev cost per year for 40 months
Mission PM/SE/MA	$ 123	$ 125	Percentage of HW based on Cassini, Juno, MRO, MER + NEPA
Instruments	$ 75	$ 81	MICM, NICM, SOCM and analogies to planetary instruments
Flight System	$ 523	$ 582	NAFCOM11, PRICE, Juno, MRO, Cassini
ASRGs	$ 200	$ 200	Project Value for 4 ASRGs
Pre-launch Ground and Science	$ 99	$ 85	Percentage of HW based on Cassini, Juno, MRO, MER
Phase E and EPO	$ 216	$ 225	Based on annual rates from MESSENGER, NH, Juno, MRO
Total Reserves	$ 370	$ 369	70% from cost risk analysis
Mission Cost Before Threats	**$ 1,606**	**$ 1,719**	
Schedule Threats		$ 17	2 months at Phase D burn rate ($7M/month scaled from JEO)
Mass and Power Contingency Threats		$ 15	Based on 2/14 MEL
LV Threats		$ -	Adequate margins on Atlas V 551
Mission Cost With Threats	**$ 1,606**	**$ 1,751**	
Launch Vehicle/Services	$ 272	$ 272	Atlas V551 cost from DS guidelines + nuclear processing
Total Mission Cost With Threats	**$ 1,878**	**$ 2,023**	
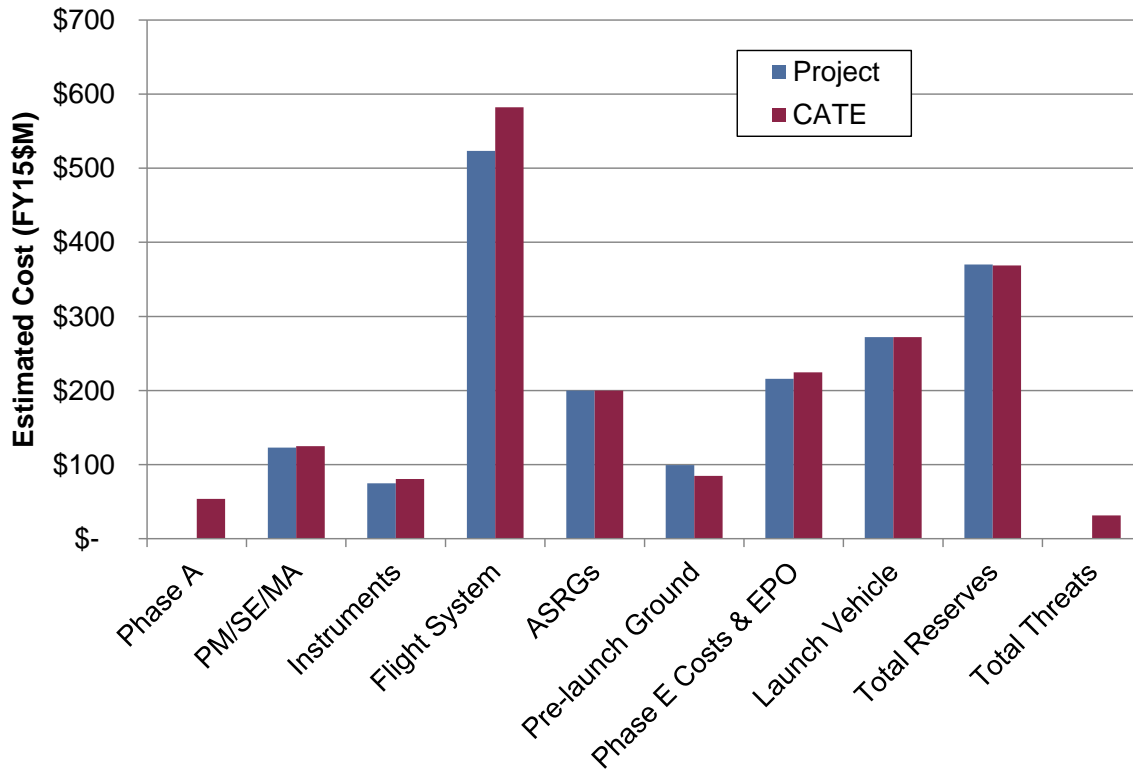
Figure 21. Europa Orbiter Key Cost Element Comparison
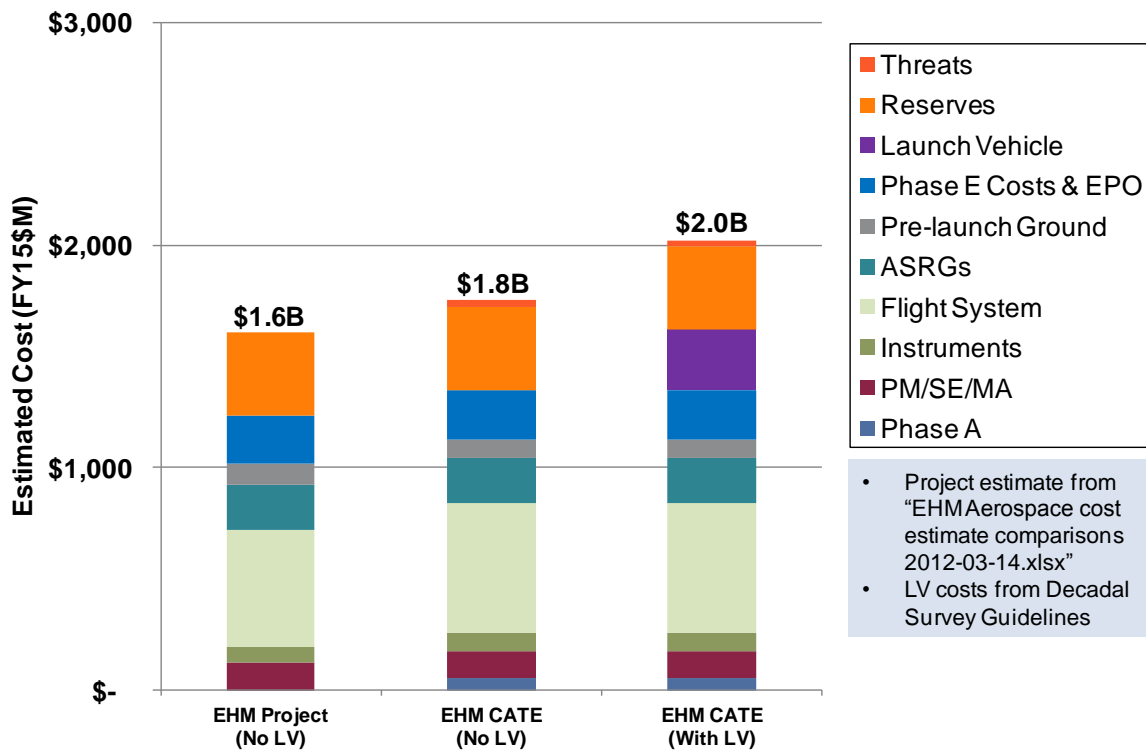
Figure 22. Europa Orbiter Cost Estimates

22

Complexity-Based Risk Assessment (CoBRA)

As a cross-check of the CATE results, the Complexity-Based Risk Assessment (CoBRA) process was also applied to the Europa Orbiter concept. The CoBRA process uses technical and programmatic parameters from the conceptual design to calculate a complexity value for the design. This is done by ranking each of the individual parameters against a database of historical space missions. The calculated complexity values for the historical missions are plotted against development cost and schedule. The missions are classified as successful, partially successful, failed, or yet to be determined. A best-fit line is drawn through the successful missions, and the estimated cost and schedule of the Europa Orbiter concept can be compared to missions of similar complexity. Figures 23 and 24 show the CoBRA cost and schedule analysis results. Both the project and CATE cost estimates are slightly above the green trend line, which is in family with successful past missions of this complexity. Both the project and CATE schedule estimates are below the green trend line but above the blue trend line, which is drawn through successful missions that had a planetary launch window constraint. Again, this result adds confidence that the Europa Orbiter schedule estimates are in family with comparable successful missions.
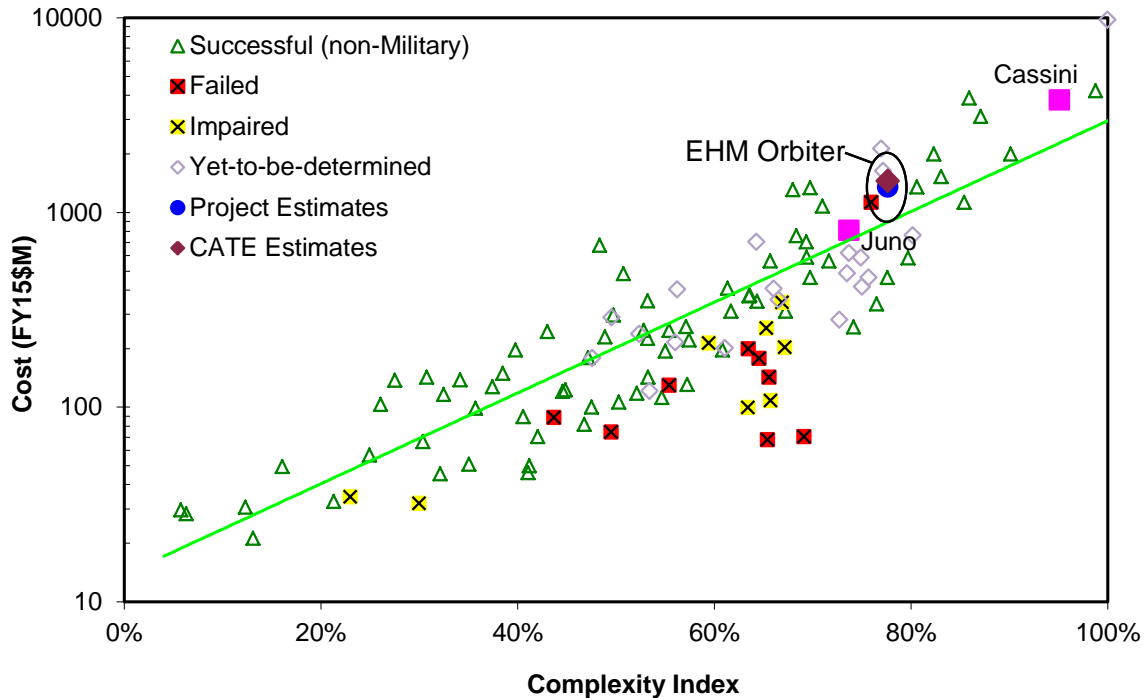
Figure 23. Complexity-Based Risk Assessment Cost Analysis
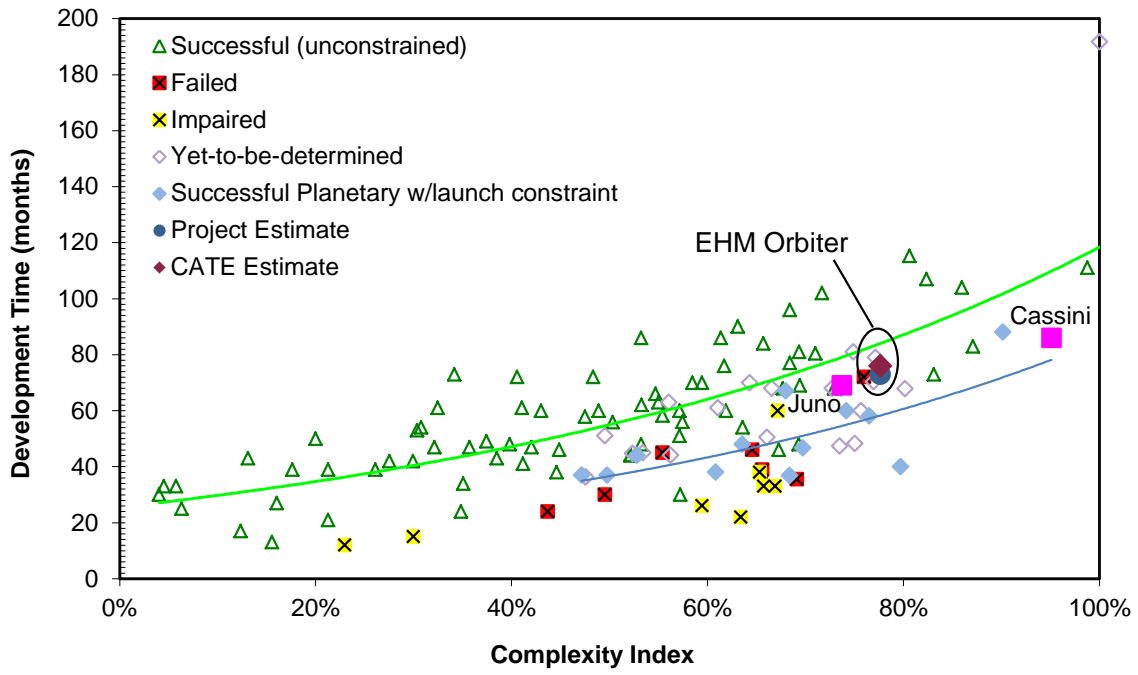
Figure 24. Complexity-Based Risk Assessment Schedule Analysis

National Aeronautics and Space Administration

EUROPA STUDY 2012 REPORT
EUROPA MULTIPLE FLYBY MISSION

Europa Study Team, 1 May 2012, JPL D-71990
Task Order NMO711062 Outer Planets Flagship Mission

Cover art Michael Carroll

Europa Study Final Report—Multiple-Flyby

Contents

The cost information contained in this document is of budgetary and planning nature and is intended for informational purposes only. It does not constitute a commitment on the part of JPL and/or Caltech.

C.   MULTIPLE-FLYBY MISSION

The Flyby Mission would explore Europa to investigate its habitability, delivering cost-effective, low-risk science.

Executive Summary

Background

The 2011 Planetary Science Decadal Survey recommended an immediate effort to find major cost reductions for the Jupiter Europa Orbiter (JEO) concept. To that end, NASA Headquarters appointed a Science Definition Team (SDT) and directed the Europa Study Team, guided by the SDT, to redefine a set of minimal science missions to Europa. The cost target was $2.25B ($FY15, excluding launch vehicle) and additional guidelines were levied, as described In Section A. Independent cost and technical review was to be performed on all study results. These studies, independent reviews, and all deliverables were delivered to NASA Headquarters on May 1, 2012.

One of these mission concepts, a Europa Multiple-Flyby Mission, is well suited to addressing the chemistry and energy themes of Europa exploration. It would involve a spacecraft in wide orbit around Jupiter that makes many close passes by Europa, each flying over a different region for broad coverage (see Foldout C-2 [FO C-2]). This concept, as detailed below, represents the combined effort since April 2011 of the SDT and a technical team from the Jet Propulsion Laboratory (JPL) and Johns Hopkins University's Applied Physics Laboratory (APL).

Science Objectives

Europa is a potentially habitable world and is likely to be geologically and chemically active today. Many well-defined and focused science questions regarding past and present habitability may be addressed by exploring Europa.

The 2003 Planetary Decadal Survey, "New Horizons in the Solar System" (Space Studies Board 2003) and 2011 Planetary Decadal Survey, "Vision and Voyages" (Space Studies
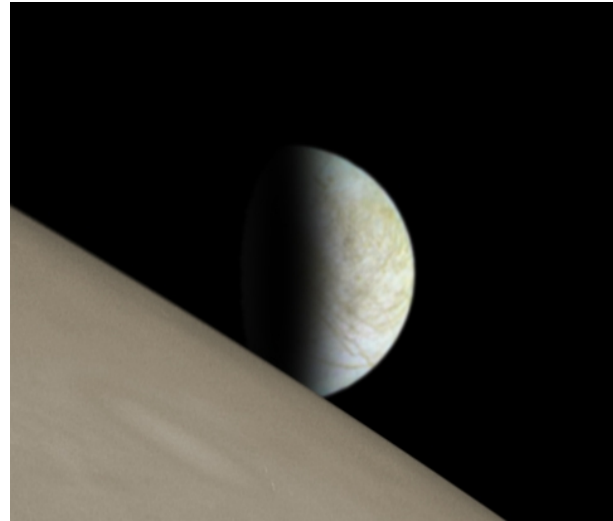
Figure C-1. Europa over the horizon of its parent planet, Jupiter.

Board 2011) both emphasize the importance of Europa exploration as "the first step in understanding the potential of the outer solar system as an abode for life" (Space Studies Board 2011, p. 1). The 2011 Decadal Survey discusses the likelihood of contemporary habitats with the necessary conditions for life, stressing the inherent motivation for "a Europa mission with the goal of confirming the presence of an interior ocean, characterizing the satellite's ice shell, and understanding its geological history" (Space Studies Board 2011, pp. 1–2). Thus, the goal adopted for the current Europa studies is to "Explore Europa to investigate its habitability", which recognizes the significance of Europa's astrobiological potential. "Habitability" includes characterizing any water within and beneath Europa's ice shell, investigating the chemistry of the surface and ocean, and evaluating geological processes that may permit Europa's ocean to possess the chemical energy necessary for life. Understanding Europa's habitability is intimately tied to understanding the three "ingredients" for life: water, chemistry, and energy.

Rationale for Multiple-Flyby Science

Science observations that address chemistry and energy themes can be accomplished via a spacecraft that orbits Jupiter and focuses on

remote measurements accomplished via multiple close flybys of Europa. Such a mission—investigating subsurface dielectric horizons, surface constituents, atmospheric constituents, and targeted landforms—would be directly responsive to the Decadal Survey's recommendation for reduced Europa science, and would be an excellent platform from which to investigate Europa's potential as a habitable environment. Comprehensive remote sensing campaigns capable of addressing regional and global investigations tend to produce considerable data. The short-flyby, long-orbit periodicity of a flyby mission design is well suited to this type of campaign.

Complete traceability of chemistry and energy science to a plausible Flyby Mission implementation is compiled and contained in this report. This is summarized in a Traceability Matrix (FO C-1), which provides specific prioritized objectives, investigations, and example measurements, each directed toward the overarching goal to "Explore Europa to investigate its habitability." These are described further in the narrative.

In addition, notional instruments are provided as a proof of concept to demonstrate that these investigations, objectives, and goals could be realistically addressed. The model payload contains an Ice-Penetrating Radar (IPR), Shortwave Infrared Spectrometer (SWIRS), Ion and Neutral Mass Spectrometer (INMS), and Topographical Imager (TI). However, these examples are not meant to be exclusive of other measurements and instruments that might be able to meet the scientific objectives in other ways. NASA will ultimately select the payload through a formal Announcement of Opportunity (AO) process.

Architecture Implementation

The Multiple-Flyby Mission architecture described here is well suited to satisfying the science objectives in a cost-effective, lowest-risk manner. A trajectory has been identified that provides globally distributed regional coverage

of the Europan surface through a series of flybys. Once the flyby campaign begins, Europa is encountered every 7 to 21 days. This approach allows for high-data-rate science collection followed by days of playback time, while greater mass margins afforded by foregoing Europa orbit insertion enable shielding to a lower radiation dose. This mission architecture is well suited to Europa Multiple-Flyby Mission instruments, which are heavy, require significant operating power, and generate considerable data. On each flyby, science data is collected for approximately one hour, leaving the remainder of the 7 to 21 days between Europa encounters for science data return and battery recharging. Science operations for the flybys are repetitive, which leads to lower cost mission operations.

The conceptual flight system (Figure C-2) uses a modular architecture, which facilitates the implementation, assembly, and testing of the system. This is facilitated further by the approach to Europa planetary protection requirements, which are met through system-level dry-heat microbial reduction in a thermal-vacuum chamber late in the integration process at the launch site. The chosen instru-
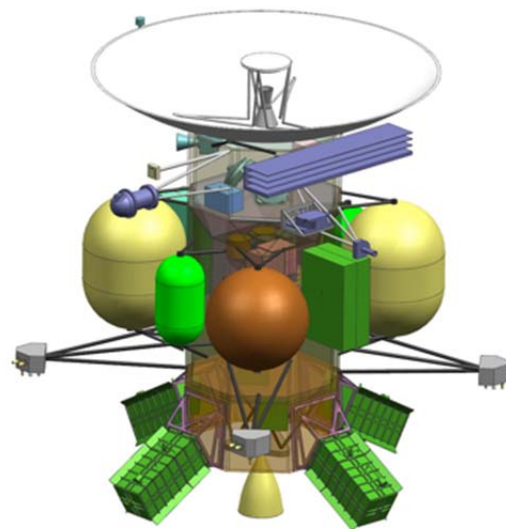
Figure C-2. The Europa Multiple-Flyby Mission flight system provides a robust platform to collect, store, and transmit a high volume of science data.

ment interfaces and other accommodations also allow for delivery late into the system level integration and tests, providing program flexibility.

The flight system is 3-axis-stabilized for precise instrument pointing, and avoids solar pointing constraints by using four Advanced Stirling Radioisotope Generators (ASRGs) for power. An innovative propulsion system accommodation for an internal, Juno-style electronics vault and a nested shielding strategy provides significant protection from the radiation environment, allowing the use of 300-krad-tolerant parts.

Technical margins for the mission design concept are robust, with 48% mass margin, and 40% power margin and 80% downlink margin during science operations.

Schedule and Cost

A top-level development schedule is shown in Figure C-3. Phase durations draw on experience from previous outer planets missions and are conservative. This schedule would facilitate front-loading of requirements development, provide significant time during instrument development to understand the actual design implications for radiation and planetary protection, and offer a flatter than typical mission funding profile.

The Flyby Mission study applied a hybrid costing methodology that includes institutional cost models, the NASA Instrument Cost Model (NICM), percentage wrap factors, expert-based opinion, and JPL's Team X cost estimates. An S-curve analysis performed on the

study cost estimates resulted in a $2.0B ($FY15, excluding launch vehicle) 70th-percentile cost estimate. In addition, the Aerospace Corporation performed an Independent Cost Estimate (ICE) and a Cost And Technical Evaluation (CATE) and found no cost or schedule threats, as opposed to the 2011 Decadal Survey conclusion.

Summary

A Multiple-Flyby Mission concept meets the challenge from NASA and the Decadal Survey for a reduced scope Europa mission relative to JEO, yet still has exceptional science merit. Study results are in compliance with NASA Headquarters' direction and guidelines. The mission design concept is conservative, has large margins, and meets the NASA cost target of ~$2.25B ($FY15, excluding launch vehicle). The Europa Multiple-Flyby Mission was presented to the Outer Planets Assessment Group (OPAG) in October 2011, and the feedback from the community was extremely positive. An independent technical review of the Europa Multiple-Flyby Mission concept was conducted, chaired by Scott Hubbard. The key findings were:

- The overall approach to modularity and radiation shielding was universally lauded as a creative approach to reducing technical risk and cost;
- No engineering "showstoppers" were identified;
- The Flyby concept satisfied the "existence proof" test as a mission that met Europa
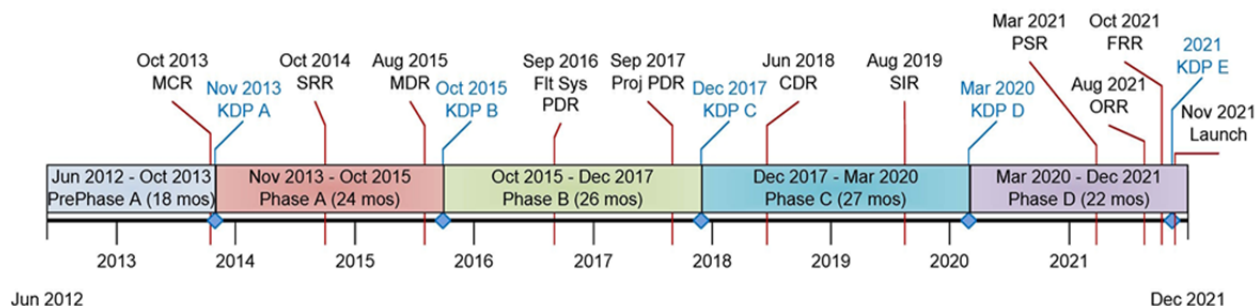
Figure C-3. Top-level development schedule with conservative durations provides appropriate time to address radiation and planetary protection challenges.

science requirements, could be conducted within the cost constraints provided and has substantial margins;

- Two technical risks were identified: ASRG and radiation mitigation for instrument detectors.

The detailed findings of this technical review are shown in Section C.4.5.

C.1 Science of the Multiple-Flyby Mission

C.1.1 Flyby Science

Europa is a potentially habitable world that is likely to be geologically and chemically active today. As outlined below, there are many well-defined and focused science questions to be addressed by exploring Europa. The 2003 Planetary Decadal Survey, *New Horizons in the Solar System,* and the 2011 Planetary Decadal Survey, *Vision and Voyages,* both emphasize the importance of Europa exploration (Space Studies Board 2003, 2011). These Decadal Surveys discuss Europa's relevance to understanding issues of habitability in the solar system, stressing this as the inherent motivation for Europa exploration.

"Because of this ocean's potential suitability for life, Europa is one of the most important targets in all of planetary science" (Space Studies Board 2011).

Understanding Europa's habitability is intimately tied to understanding the three "ingredients" for life: water, chemistry, and energy (Section A of this report). A Jupiter-orbiting spacecraft that makes many flybys of Europa would be an excellent platform from which to conduct remote sensing measurements to investigate Europa's ice shell, composition, and geology, and thus the three ingredients for life. Remote sensing investigations tend to be resource-intensive, in terms of data volume and data rate drivers, and in the mass and power of necessary instruments. Such needs are readily accommodated by a multiple-flyby mission implementation. In this section, we discuss the

science background of a multiple-flyby mission that concentrates on remote sensing to address Europa's habitability.

C.1.1.1 Ice Shell

To assess Europa's habitability, it is necessary to see how the ingredients for life might be brought together in this environment. This includes unraveling the dynamic processes that connect Europa's underlying ocean to the surface of its ice shell. Therefore, a detailed understanding of the internal structure of the Europa's ice (Figure C.1.1-1) is essential. Probing the third dimension of the shell is key to understanding the distribution of subsurface water both within and beneath the ice shell. Understanding the processes of ice–ocean exchange would indicate whether surface oxidants can be transported to Europa's ocean, providing the chemical nutrients for life. Moreover, if ocean material can be transported back to Europa's surface, then we could confidently understand the chemistry of the ocean by examining the composition of surface and atmospheric materials. Therefore, exploration of Europa's ice shell is pertinent to all three ingredients for life: water, chemistry, and energy.

Remaining questions to be addressed about Europa's ice shell include the following:

- Is Europa's ice shell thin and thermally conductive, or thick and convecting?
- Are surface oxidants transported from the surface into the ocean (providing chemical energy to the ocean) and vice-versa (allowing us to understand ocean chemistry through surface observations), and if so, what are the transport processes?
- What are the three-dimensional characteristics of Europa's geological structures, and do they enable surface–ocean communication?
- Are there liquid water bodies within Europa's ice shell?
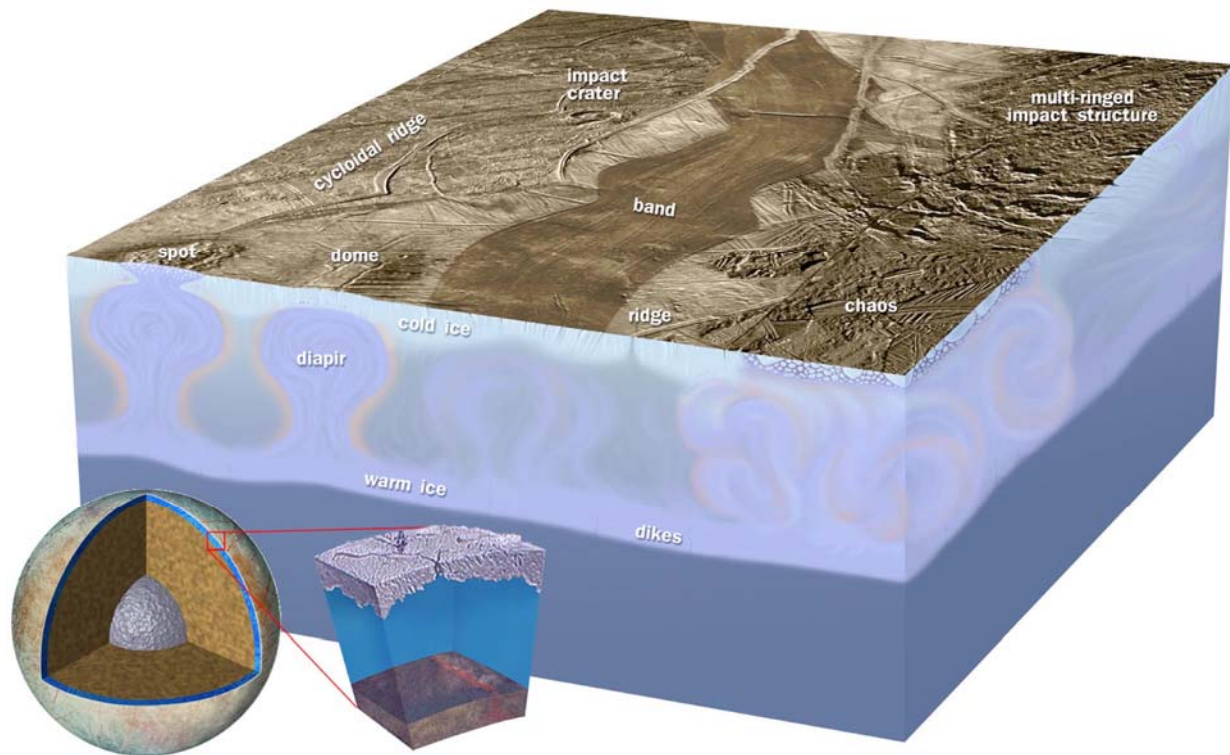
Figure C.1.1-1. Diagram of Europa's ice shell above a global-scale ocean, showing possible ice-shell processes leading to thermal, compositional, and structural horizons. Hypothesized convective diapirs (domed upwellings at the front of the block diagram) could cause thermal perturbations and partial melting in the overlying rigid ice. Tectonic faulting driven by tidal stresses (upper surface) could result in fault damage and frictional heating. Impact structures (back right) are expected to have central refrozen melt pools and to be surrounded by ejecta.

The thickness of Europa's ice shell is an important question left unanswered by the Galileo mission. While the total depth of Europa's H_2O-rich outer shell—ice over liquid water—is believed to be approximately 100 kilometers, the current thickness of the ice shell is unknown, with estimates ranging from relatively thin (a few kilometers) to relatively thick (tens of kilometers) (Billings and Kattenhorn 2005). Depending on thickness and other factors, a number of different processes may be at work shaping this shell and its dynamics. These include episodes of thickening and thinning, thermal and geological processing, and exogenic processes. For instance, geological processes have clearly altered and deformed the surface and transported material horizontally and vertically within the shell, while exogenic processes such as cratering and regolith formation have influenced the surface

and deeper structure. Determining the ice-shell thickness is of fundamental astrobiological significance: It constrains answers to questions about how much tidal heat the satellite is generating; whether the silicate interior exhibits high heat production or not; and to what extent the ocean and near-surface ice are likely to exchange material.

Just as a geologist on Earth uses structural information to understand the dynamics of the Earth's crust, three-dimensional electromagnetic sounding of the ice shell—with the potential to find water within the ice shell, identify the ice-ocean interface of Europa, and measure the ice shell thickness—would reveal the processes connecting the surface to the ocean. Dielectric losses in very cold ice are low, yet highly sensitive to increasing temperature, water, and impurity content; therefore, much could be learned through remote elec-

tromagnetic sounding of the ice shell. This is especially true when subsurface profiling is coupled to observations of the topography and morphology of surface landforms and placed in the context of both surface composition and subsurface density distribution. Because of Jupiter's strong radio emissions and the unknown size of volume scatterers within Europa's ice shell, the range of sounding frequencies must be carefully matched to the science objectives.

C.1.1.1.1   Thermal Processing

Regardless of the properties of the shell or the overall mechanism of heat transport, the uppermost several kilometers of the ice shell are cold and stiff. The thickness of this conductive "lid" is set by the total amount of heat that must be transported. Thus, a measurement of the thickness of the cold and brittle part of the shell is a powerful constraint on the heat production in the interior. The lower, convecting part of the shell (if it exists) is likely to be much cleaner because regions with impurities should have experienced melting at some point during convective circulation, and melt would segregate downward efficiently, extracting impurities (Pappalardo and Barr 2004). Thermal processing might have altered the internal structure of the shell through convection or local melting, potentially creating huge "lakes" within the ice shell (Schmidt et al. 2011).

Convective instabilities can also result in thermal variations in the outer part of the shell, including rising diapirs of warm ice, which might be associated with features at the surface of Europa (lenticulae and chaos), with scales ranging from ~1–100 km. If warm, relatively pure ice diapirs from the interior approach the surface, they might be far from the pure-ice melting point, but above the eutectic point[1] of some material trapped in the shallow portions of the ice shell, potentially creating regions of melting (Schmit et al. 2011). Other

---

[1]   The eutectic point is the reduced melting temperature of substances when they are mixed.

sources of local heating such as friction on faults might also lead to local melting (Gaidos and Nimmo 2000).

The ability to perform electromagnetic sounding through Europa's ice shell is essential to understanding its thermal processing. Detection of water lenses would require a vertical resolution of at least a few tens of meters. High horizontal resolution (a few hundred meters) is required to avoid scale-related biases.

C.1.1.1.2   Ice–Ocean Exchange

Europa's ice shell has likely experienced one or more phases of thickening and thinning over time (Hussmann and Spohn 2004, Moore and Hussmann 2009). This would likely lead to significant structural horizons from contrasts in ice-crystal fabric and composition.

Similarly, melting to form lenticulae and chaos on Europa's surface (Greenberg et al. 1999, Schmidt et al. 2011) implies that ice would accrete beneath the melt feature after it forms. This process would result in a sharp boundary between old ice and deeper accreted ice. The amount of accreted ice would be directly related to the time since melting occurred and could be compared with the amount expected, based on the inferred surface age.

Testing these hypotheses would require measuring the depth of interfaces to a resolution of a few hundred meters and horizontal resolutions of a fraction of any lid thickness, i.e., a kilometer or so.

C.1.1.1.3   Surface and Subsurface Structure

Europa represents a unique tectonic regime in the solar system, and the processes controlling the distribution of strain in Europa's ice shell are uncertain. Tectonic structures could range from low-angle extensional fractures to near-vertical strike-slip features. These would produce structures associated primarily with the faulting process itself through formation of pervasively fractured ice and zones of deformational melt, injection of water, or preferred orientation of crystal fabric. Some faults might

show local alteration of preexisting structure, including fluid inclusions, or by juxtaposition of dissimilar regions through motion on the fault.

There are many outstanding questions regarding tectonic features. A measurement of their depth and association with thermal anomalies or melt inclusions would strongly constrain models of their origins. In particular, correlation of subsurface structure with surface properties (length, position in the stratigraphic sequence, height, and width of the ridges) would test hypotheses for the mechanisms that form the fractures and support the ridges. The observation of melt along ridges could make these features highly desirable targets for future *in situ* missions.

Dilational bands observed on Europa might be particularly important for understanding material-exchange processes. If the analogy with terrestrial spreading centers (Prockter et al. 2002) is accurate, the material in the band is newly supplied from below and might have a distinct structure.

Thus, the origin of band material can be constrained by sounding the subsurface. Bands and ridges typically have widths of several kilometers. Horizontal sounding resolutions of several hundred meters would be required to discriminate processes. The ability to image structures sloping more than a few degrees is also needed. Additionally, tens of meters of vertical resolution would be required to image any near-surface melt inclusions.

The impact process should also represent a profound disturbance of the local structure of the shell, yet few large impact sites are apparent. An outstanding mystery on Europa is the process by which these craters are erased from the surface. It is possible though that Europa's *sub*-surface records events that have penetrated the entire thickness of the shell. Around the impact site, the ice would have been fractured and heated, and some melt generated; the surface directly around the impact would be bur-

ied with a blanket of ejecta; and relaxation of the crater would have created a zone of deformation that could include both radial and circumferential faulting. These processes all create subsurface structures that might be probed by sounding. Thus, it might be possible to find the subsurface signature of impacts that are no longer evident at the surface, which would place constraints on the resurfacing processes that operate at Europa.

Three types of structural horizons are expected to be derived from impact: the former surface buried beneath an ejecta blanket, solidified melts in the impact structure itself, and impact-related fractures. Vertical resolutions on the scales of a few tens to hundreds of meters would be required to identify ejecta blankets and frozen melt pools. Detection of at least the edges of steep interfaces would aid in the identification of radial dikes, buried crater walls, and circumferential fractures.

C.1.1.2   Composition

Characterizing the surface organic and inorganic composition and chemistry provides fundamental information about Europa's history and evolution, the properties and habitability of the subsurface and ocean, its interaction with the surface, and the role of exogenic processes. Surface materials might be ancient, derived through time from the ocean and altered by radiation, or they might be exogenic in origin.

Current understanding of Europa's bulk density and of solar and stellar composition suggests the presence of both water and silicates. It is likely that the differentiation of Europa resulted in mixing of water with the silicates and carbonaceous materials that formed the moon, resulting in chemical alteration and redistribution. Interior transport processes would then have brought a variety of materials from the interior first into the ocean and from there up to the surface.

Much of what is known about Europa's composition comes from spectroscopic observa-

tions in the visible to near-infrared. Earth-based telescopic observations and data from the Voyager and Galileo spacecraft (see reviews by Alexander et al. 2009 and Carlson et al. 2009) show that the surface of Europa is primarily water ice in both crystalline and amorphous forms.

The barrage of high-energy particles from Jupiter's magnetosphere also leaves an imprint on the surface composition that provides clues to this environment, further complicating the formation, evolution, and modification of the surface.

Finally, surface materials could be incorporated into the subsurface and react with the ocean, or could be sputtered from the surface to form Europa's tenuous atmosphere.

C.1.1.2.1   Icy and Non-Icy Composition

Compositional information from Earth-based telescopic observations and data from the Voyager and Galileo spacecraft (e.g., Kuiper 1957, Moroz 1965, Clark and McCord 1980, Dalton 2000, McCord 2000, Spencer et al. 2005, Alexander et al. 2009) show that the surface of Europa is composed primarily of water ice in both crystalline and amorphous forms (Pilcher et al. 1972, Clark and McCord 1980, Hansen and McCord 2004).

The dark, non-icy materials that make up much of the rest of Europa's surface are of extreme interest for unraveling Europa's geological history; determining their composition is the key to understanding their origin. The spatial distribution and context of these materials at geologically relevant scales allows the processes that have formed the surface and the connection between the surface and the interior to be understood. This link provides important constraints on the nature of the interior, the potential habitability of subsurface liquid water environments, and the processes and time scales through which interior materials are transported to the surface. Compositional variations in surface materials might reflect age differences indicative of recent activity,
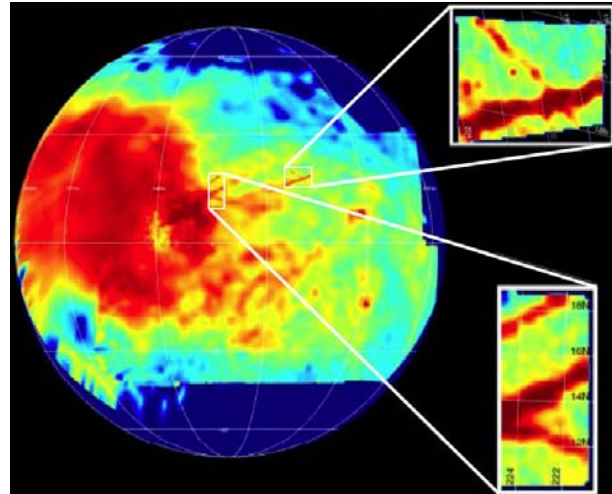
Figure C.1.1-2. The distribution of hydrated materials on Europa (red) reaches its maximum near the apex of the trailing hemisphere, where impinging radiation flux is highest, and is associated with geologically disrupted terrains and triple bands (insets).

and the discovery of active vents or plumes would show current activity.

The non-ice components are known to include carbon dioxide (CO_2), sulfur dioxide (SO_2), hydrogen peroxide (H_2O_2) and molecular oxygen (O_2), based on comparison of measured spectra with laboratory studies of the relevant compounds (Lane et al. 1981; Noll et al. 1995; Smythe et al. 1998; Carlson 1999, 2001; Carlson et al. 1999a, b; Spencer and Calvin 2002; Hansen and McCord 2008). Spectral observations from the Galileo Near-Infrared Mapping Spectrometer (NIMS) reveal disrupted dark and chaotic terrains on Europa with distorted and asymmetric absorption features indicative of water bound in non-ice hydrates. Hydrated materials observed in regions of surface disruption (Figure C.1.1-2) have been suggested to be magnesium and sodium sulfate minerals (Figure C.1.1-3) that originate from subsurface ocean brines (McCord et al. 1998a, 1998b, 1999). Alternatively, these materials might be sulfuric acid hydrates created by 1) radiolysis[2] of sulfur from Io, 2) processing of endogenic

---

[2]   Radiolysis is chemical decomposition by ionizing radiation.
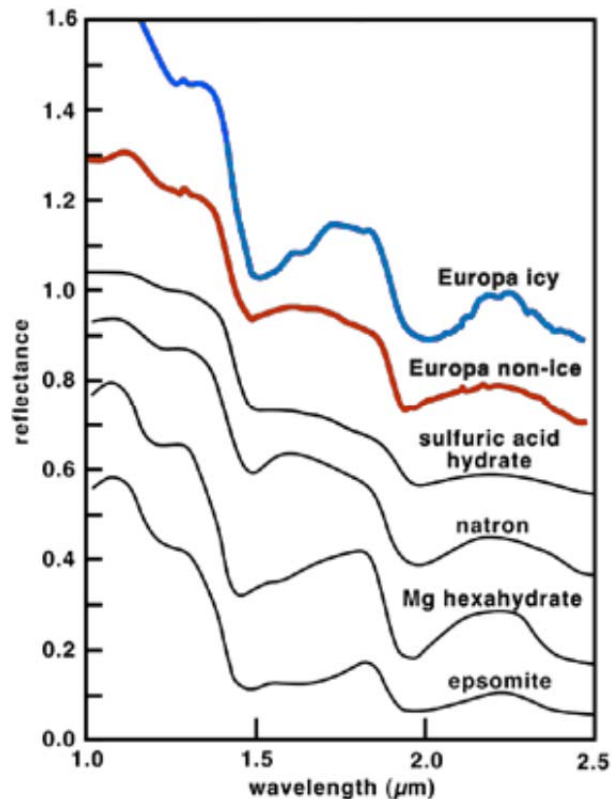
Figure C.1.1-3. Reflectance spectra of hydrated materials on Europa. Candidate materials for Europa's non-ice component include sulfuric acid hydrate ($H_2SO_4 \cdot nH_2O$) and various hydrated sulfate and carbonate salts (McCord et al. 1999, 2002).

SO_2, and/or 3) extrusion of ocean-derived sulfates (Carlson et al. 1999b, 2002, 2005). It is also possible that these surfaces are a combination of both hydrated sulfate salts and hydrated sulfuric acid (Dalton 2000; McCord et al. 2001a, b, 2002; Carlson et al. 2005; Orlando et al. 2005; Dalton et al. 2005), as suggested by linear spectral mixture analyses of disrupted terrains (Dalton 2007). An important objective for Europa science is to resolve the compositions and origins of these hydrated materials.

Material in the space surrounding Europa also provides compositional clues. Brown and Hill (1996) first reported a cloud of sodium around Europa, and Brown (2001) detected a cloud of potassium and reported that the Na/K ratio suggested that endogenic sputtering produced these materials.

A broad suite of additional compounds is predicted for Europa based on observations of other icy satellites, as well as from experimental studies of irradiated ices, theoretical simulations, and geochemical and cosmochemical arguments. Organic molecular groups, such as CH and CN, have been found on the other icy Galilean satellites (McCord et al. 1997, 1998b), and their presence or absence on Europa is important to understanding Europa's potential habitability. Other possible compounds that might be embedded in the ice and detectable by high-resolution spectroscopy include H_2S, OCS, O_3, HCHO, H_2CO_3, SO_3, $MgSO_4$, H_2SO_4, H_3O^+, $NaSO_4$, HCOOH, CH_3OH, CH_3COOH, and more complex species (Moore 1984; Delitsky and Lane 1997, 1998; Moore and Hudson 1998; Moore et al. 2003; Brunetto et al. 2005).

As molecules become more complex, however, their radiation cross-section also increases and they are more susceptible to alteration by radiation. Radiolysis and photolysis could alter the original surface materials and produce many highly oxidized species that react with other non-ice materials to form a wide array of compounds. Given the extreme radiation environment of Europa, complex organic molecules are not expected in older deposits or in those exposed to higher levels of irradiation (Johnson and Quickenden 1997, Cooper et al. 2001). However, diagnostic molecular fragments and key carbon, nitrogen, and sulfur products might survive in some locales. Regions of lesser radiation (i.e., the leading hemisphere) and sites of recent or current activity would be the most likely places to seek evidence of organic or derived products.

Improved spectral observations at significantly higher spectral and spatial resolution than is presently available, together with detailed laboratory analyses under the appropriate temperature and radiation environment, are needed to fully understand Europa's surface chemistry. These data would provide major improvements in the identification of original and

derived compounds and of the radiation environment and reaction pathways that create and destroy them.

C.1.1.2.2   Isotopic Constraints

The varying degree of preference for lighter isotopes in many physical and chemical processes is expected to lead to mass fractionation effects that should be evident in isotopic ratios. Ratios of D/H, $^{13}C/^{12}C$, $^{15}N/^{14}N$, $^{18}O/^{17}O/^{16}O$, $^{34}S/^{32}S$, and $^{40}Ar/^{36}Ar$, and comparison among them, could provide insights into geological, chemical, and possible biological processes, such as planetary formation, interior transport, surface evolution, radiolysis, atmospheric escape, and metabolic pathways.

The determination of isotopic ratios would provide a powerful indicator of several planetary processes. Exchange rates among the Earth's oceans, crust, mantle, and atmosphere are closely linked to ratios of radiogenic noble gas isotopes; these isotope ratios have also been used at Venus and Mars to better understand the evolution of their volatile reservoirs. In satellite systems around large gaseous planets such as Jupiter and Saturn, questions about the presence, extent, and composition of a primordial circumplanetary disk surrounding the host protoplanet could be addressed by comparing isotope ratios measured at different satellites in the system with those measured in the host planet's atmosphere.

Endogenic processes on Europa might have measurable effects on isotope compositions. Moreover, the exogenic processes of sublimation and sputtering should also cause isotopic fractionation. Differences in solubilities and clathrate dissociation pressures would cause materials and isotopes of interest to freeze or become enclathrated into Europa's ice shell in different proportions than found in the aqueous solution of the ocean. Such differences might be evident from comparison of the predominant ice-rich background terrain on Europa's surface with cracks, chaos regions, and other features rich in non-icy material, which might have been deposited directly from the ocean.

C.1.1.2.3   Relationship of Composition to Processes

Galileo's instruments were designed to study surface compositions at regional scales. The association of hydrated and reddish materials with certain geologic terrains, revealed by Galileo, suggests an endogenic source for the emplaced materials, although these might since have been altered by radiolysis. Many surface features with compositionally distinct materials were formed by tectonic processes, suggesting that the associated materials are derived from the subsurface. Major open questions include the links between surface composition and that of the underlying ocean and rocky interior (Fanale et al. 1999, Kargel et al. 2000, McKinnon and Zolensky 2003), and the relative significance of radiolytic processing (Johnson and Quickenden 1997; Cooper et al. 2001; Carlson et al. 2002, 2005; Grundy 2007). For example, compositional variations associated with surface features such as chaos suggest that material might be derived from an ocean source, either directly through melting or eruptions, or indirectly through processes such as diapirism (McCord et al. 1998b, 1999; Fanale et al. 1999; Orlando et al. 2005).

One of the critical limitations of the Galileo NIMS experiment was the low spatial resolution of the high-quality spectra and the limited spatial coverage due to failure of the spacecraft's high-gain antenna. The spectra used to identify hydrated materials were typically averaged from areas ~75 km by 75 km (McCord et al. 1998b, Carlson et al. 1999b) (although a few higher-resolution "postage stamp" data sets were obtained and analyzed). This typical footprint is shown in Figure C.1.1-4, illustrating the tremendous mixing of surface terrain types that occurs within an area of this extent; less than 10% of the NIMS footprint contains materials associated with ridges, bands, or fractures. In order to isolate and identify the young, non-ice materials associated with these
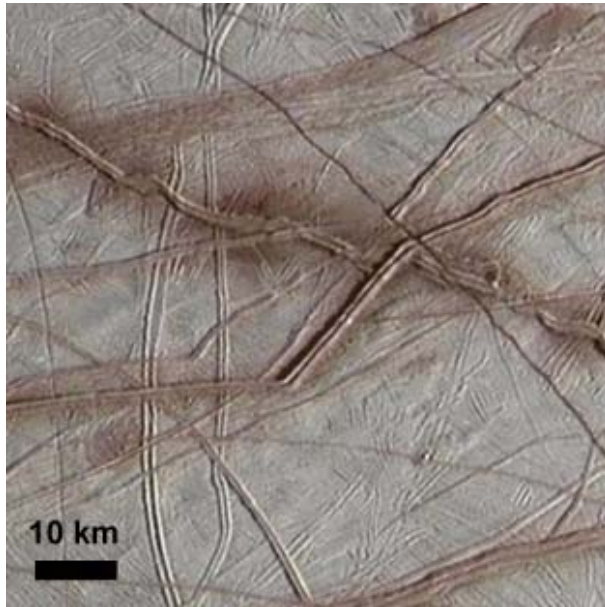
Figure C.1.1-4. This portion of a Galileo image is the size of a typical Galileo NIMS footprint, demonstrating how NIMS sampled multiple terrain types in each spectrum.

structures, and look for spectral variations within geological structures, future observations must be able to resolve the non-ice materials to better than 100-m scales.

In addition to compositional differences associated with recent geological activity, compositional changes related to exposure age also provide evidence for sites of recent or current activity. The composition of even the icy parts of Europa is variable in space and time. Polar fine-grained deposits suggest frosts formed from ice sputtered or sublimated from other areas (Clark et al. 1983, Dalton 2000, Hansen and McCord 2004). Equatorial ice regions are more amorphous than crystalline, perhaps due to radiation damage. Venting or transient gaseous activity on Europa would indicate present-day surface activity.

Exogenic processes are also a key part of Europa's composition story, but much remains unknown about the chemistry and sources of the materials being implanted. Magnetic field measurements by Galileo of ion-cyclotron waves in the wake of Europa provide evidence of sputtered and recently ionized Cl, O_2, SO_2

and Na ions (Volwerk et al. 2001). Medium energy ions (tens to hundreds of keV) deposit energy in the topmost few tens of microns; heavier ions, such as oxygen and sulfur ions, have an even shorter depth of penetration, while MeV electrons could penetrate and affect the ice to a depth of more than 1 m (Paranicas et al. 2002, and references therein, Paranicas et al. 2009). The energy of these particles breaks bonds to sputter water molecules, molecular oxygen, and any impurities within the ice (Cheng et al. 1986), producing the observed atmosphere and contributing to the erosion of surface features.

A major question is the exogenic versus endogenic origin of volatiles, such as CO_2, and their behavior in time and space. CO_2 was reported on the surfaces of Callisto and Ganymede (McCord et al. 1998b), with hints of SO_2 (Smythe et al. 1998) and H_2O_2 (Carlson et al. 1999a). Recent analyses of the NIMS spectra indicate a concentration of CO_2 and other non-ice compounds on the anti-Jovian and trailing sides of Europa (Hansen and McCord 2008), suggesting an endogenic origin. Radiolysis of CO_2 and H_2O ices is expected to produce additional compounds (Moore 1984; Delitsky and Lane 1997, 1998; Brunetto et al. 2005). Determining the presence and source of organic molecular compounds, such as CH and CN groups detected by IR spectroscopy at Callisto and Ganymede (McCord et al. 1997, 1998b) and tentatively identified on Phoebe (Clark et al. 2005), would be important to evaluating the astrobiological potential of Europa, especially if there is demonstrable association with the ocean.

Some surface constituents result directly from exogenic sources. For example, sulfur from Io is transported by the magnetosphere and is implanted into Europa's ice. Once there it could form new molecules and might create some of the dark components on the surface. It is important to separate surface materials formed by implantation from those that are endogenic, and this could be done by quantitative analy-

sis. For example, the detected Na/K ratio is supportive of an endogenic origin—and perhaps an ocean source—for sodium and potassium (Brown 2001, Johnson et al. 2002, McCord et al. 2002, Orlando et al. 2005).

Spatial variations could also help separate exogenic and endogenic processes. For example, comparison of spectra of disrupted terrain on the leading and trailing hemispheres, which encounter far different radiolytic fluxes, would help to isolate the effects of the radiation environment and unravel endogenic and exogenic chemical processes that led Europa to its present state (Shirley et al. 2010).

Regardless of origin, surface composition results from combinations of all these processes, and materials emplaced at the surface are subsequently processed by radiation to produce the observed composition (Dalton 2000). For example, material derived from the ocean could be a mixture of dominantly Mg and Na salts. Na sulfates would be more vulnerable to radiative disassociation, producing sulfuric acid (H_2SO_4) (Dalton 2000, 2007; McCord et al. 2001b, 2002; Orlando et al. 2005). Such a mixture would allow for both indigenous salts and sulfuric acid, and could account for the origin of Na and K around Europa.

Some key outstanding questions to be addressed regarding Europa's composition include the following:

- Are there endogenic organic materials on Europa's surface?
- Is chemical material from depth carried to the surface?
- Is irradiation the principal cause of alteration of Europa's surface materials through time?
- Do materials formed from ion implantation play a major role in Europa's surface chemistry?

C.1.1.2.4   Geology

By understanding Europa's varied and complex geology (Figure C.1.1-5), we can deci-pher the moon's past and present processes, along with implications for habitability. By such understanding we can also gather clues about geological processes on other icy satellites with similar surface features, such as Miranda, Triton, and Enceladus.

The relative youth of Europa's surface (60 million years on average) (Schenk et al., 2004) compared to most other solar system bodies is inherently linked to the ocean and the effects of gravitational tides, which trigger processes that include cracking of the ice shell, resurfacing, and possibly a release of materials from the interior. Clues to these and other processes are provided by spectacular surface features, such as linear fractures and ridges, chaotic terrain, and impact craters.

C.1.1.2.5   Linear Features

Europa's unusual surface is dominated by tectonic features in the form of linear ridges, bands, and fractures. The class of linear features includes simple troughs and scarps (e.g., Figure C.1.1-5g), double ridges separated by a trough, and intertwining ridge-complexes. Whether these represent different processes or stages of the same process is unknown. Ridges are the most common feature type on Europa and appear to have formed throughout the satellite's visible history (Figure C.1.1-5j and l). They range from 0.1 to >500 km long, are as wide as 2 km, and could be several hundred meters high. Cycloidal ridges are similar to double ridges, but form chains of linked arcs.

Most models of linear feature formation involve fracturing in response to processes within the ice shell (Greeley et al. 2004, Kattenhorn and Hurford 2009, Prockter and Patterson 2009). Some models suggest that liquid oceanic material or warm mobile subsurface ice squeezes through fractures to form the ridge, while others suggest that ridges form by frictional heating and possibly melting along the fracture shear zone. Thus, ridges might represent regions of material exchange between the surface, ice shell, and ocean, providing a
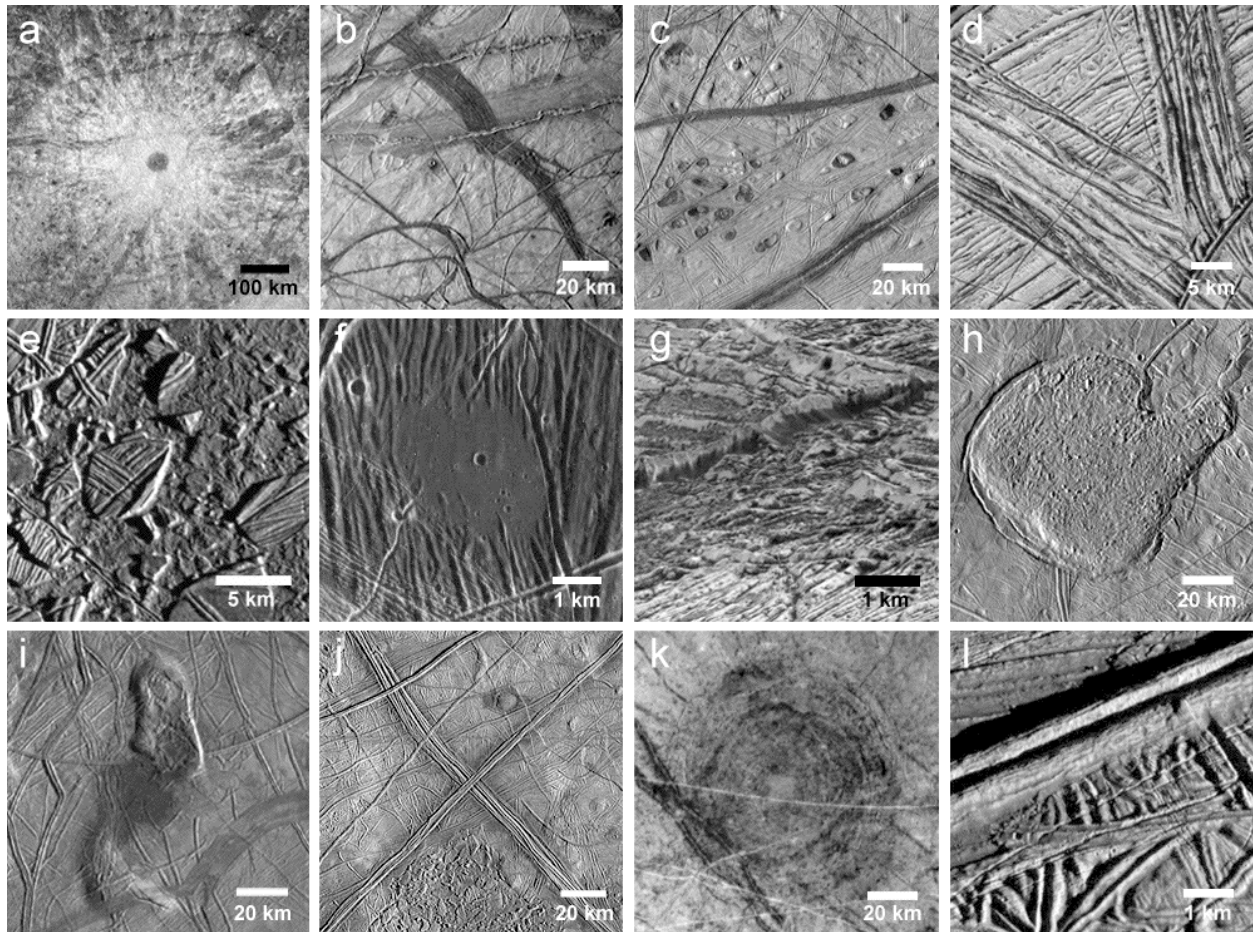
Figure C.1.1-5. Europa is a geological wonderland, with a wide variety of surface features. Many appear to be unique to this icy moon. While much was learned from Galileo, it is still not understood how many of these features form, or their implications for Europa's evolution. Shown here are (a) the impact crater Pwyll, the youngest large crater on Europa; (b) pull-apart bands; (c) lenticulae; (d) pull-apart band at high resolution; (e) Conamara Chaos; (f) dark plains material in a topographic low, (g) very high-resolution image of a cliff, showing evidence of mass wasting; (h) Murias Chaos, a cryovolcanic feature which appears to have flowed a short distance across the surface; (i) The Castalia Macula region, in which the northernmost dome contains chaos and is ~900 m high; (j) regional view of two very large ridge complexes in the Conamara region; (k) Tyre impact feature, showing multiple rings; and (l) one of Europa's ubiquitous ridges, at high resolution.

means for surface oxidants to enter the ocean. Some features, such as cycloidal ridges, appear to arise as a direct result of Europa's tidal cycle (Hoppa et al. 1999).

Bands reflect fracturing and lithospheric separation, much like sea-floor spreading on Earth, and most display bilateral symmetry (e.g., Sullivan et al. 1998) (Figure C.1.1-5b and d). Their surfaces vary from relatively smooth to heavily fractured. The youngest bands tend to be dark, while older bands are bright, suggest-

ing that they brighten with time. Geometric reconstruction of bands suggests that a spreading model is appropriate, indicating extension in these areas and possible contact with the ocean (Tufts et al. 2000, Prockter et al. 2002).

The accommodation of extensional features remains a significant outstanding question regarding Europa's geology. A small number of contractional folds were found on the surface (Prockter and Pappalardo 2000) and some sites of apparent convergence within bands have been suggested (Sarid et al. 2002), but these

are insufficient to accommodate the extension documented across Europa's surface. Some models suggest that ridges and local folds could reflect such contraction, but the present lack of global images, topographic information, and knowledge of subsurface structure precludes testing these ideas.

Fractures are narrow (from hundreds of meters to the ~10 m limit of image resolution) and some exceed 1,000 km in length. Some fractures cut across nearly all surface features, indicating that the ice shell is subject to deformation on the most recent timescales. The youngest ridges and fractures could be active today in response to tidal flexing. Subsurface sounding and surface thermal mapping could help identify zones of warm ice coinciding with current or recent activity. Young ridges might be places where there has been material exchange between the ocean and the surface, and would be prime targets as potentially habitable niches.

C.1.1.2.6   Chaotic Terrain

Europa's surface has been disrupted to form regions of chaotic terrain. Disrupted terrain may appear in the form of irregularly shaped, generally larger (tens to hundreds of kilometers) chaos zones (Figure C.1.1-5j), or smaller terrain (10-15 km) subcircular regions known as lenticulae (Collins and Nimmo 2009). Lenticulae include pits, spots of dark material, and domes where the surface is upwarped and commonly broken (Figure C.1.1-5c and f). Chaos is generally characterized by fractured plates of ice that have been shifted into new positions within a background matrix (Figure C.1.1-5e). Much like a jigsaw puzzle, many plates could be fit back together, and some ice blocks appear to have disaggregated and "foundered" into the surrounding finer-textured matrix (Spaun et al. 1998). Some chaos areas stand higher than the surrounding terrain (Figure C.1.1-5h and i).

Pappalardo et al. (1998, 1999) argued that chaos features are typically ~10 km across and

possibly formed by upwelling of compositionally or thermally buoyant ice diapirs through the ice shell. In such a case, their size distribution would imply an ice shell thickness of at least 10 to 20 km at the time of formation. Models of chaos formation suggest whole or partial melting of the ice shell, perhaps enhanced by local pockets of brine (Head and Pappalardo 1999). Downward and upward doming forms have been interpreted to correlate with recently formed chaos regions, each created through subsurface brine mobilization and subsequent freezing as occurs in Antarctic ice. Based on this model, at least one chaotic region, Thera Macula, might have been actively forming at the time of observations by the Galileo mission (Schmidt et al. 2011).

An alternative model suggests that there is no dominant size distribution and that lenticulae are small members of chaos (Greenberg et al. 1999), formed through either direct material exchange (through melting) or indirect exchange (through convection) between the ocean and surface (e.g., Carr et al. 1998a). Thus, global mapping of the size distribution of these features could address their origin.

Chaos features are stratigraphically young (Figueredo and Greeley 2004), possibly indicating a geologically recent increase in internal heating in Europa. Chaos and lenticulae commonly have associated dark, reddish zones thought to be material derived from the subsurface, possibly from the ocean. However, these and related models are poorly constrained, because the total energy partitioning within Europa is not known, nor are details of the composition of non-ice components. Subsurface sounding, surface imaging, and topographic mapping (e.g., Schenk and Pappalardo 2004) are required to understand the formation of chaotic terrain, and its implications for habitability.

C.1.1.2.7   Impact Features

Only 24 impact craters ≥10 km have been identified on Europa (Schenk et al. 2004), re-

flecting the youth of the surface. This is remarkable in comparison to Earth's Moon, which is only slightly larger but far more heavily cratered. The youngest crater on Europa is thought to be the 24 km-diameter Pwyll, (Figure C.1.1-5a) which still retains its bright rays, and likely formed less than 5 million years ago (Zahnle et al. 1998, Bierhaus et al. 2009). Complete global imaging would provide a full crater inventory, allowing a more comprehensive determination of the age of Europa's surface, and helping to identify the very youngest areas.

Crater morphology and topography provide insight into ice layer thickness at the time of the impact. Morphologies vary from bowl-shaped depressions with crisp rims, to shallow depressions with smaller depth-to-diameter ratios. Craters up to 25–30 km in diameter have morphologies consistent with formation in a warm but solid ice shell, while the two largest impacts (Tyre [Figure C.1.1-5k] and Callanish) might have punched through brittle ice about 20 km deep into a liquid zone (Moore et al. 2001, Schenk et al. 2004, Schenk and E.P. Turtle 2009).

C.1.1.2.8   *Geological History*

Determining the geological histories of planetary surfaces requires identifying and mapping surface units and structures and placing them into a time-sequence. In the absence of absolute ages derived from isotopic measurements of rocks, planetary surface ages are commonly assessed from impact crater distributions, with more heavily cratered regions reflecting greater ages. The paucity of impact craters on Europa limits this technique. Thus, superposition (i.e., younger materials burying older materials) and cross-cutting relations are used to assess sequences of formation (Figueredo and Greeley 2004, Doggett et al. 2009). Unfortunately, only 10% of Europa has been imaged at a resolution sufficient to understand temporal relationships among surface features; for most of Europa, imaging data is both incom-

plete and disconnected from region to region, making the global surface history difficult to decipher.

Where images of sufficient resolution exist (i.e., better than 200 m/pixel), it appears that the style of deformation has evolved through time from ridge and band formation to chaotic terrain (Greeley et al. 2004), although there are areas of the surface where this sequence is less certain (e.g., Riley et al. 2000). The mechanism for the change in geological style is uncertain, but a plausible mechanism for the change is one in which Europa's ocean is slowly cooling and freezing out as the ice above it is thickening. Once the ice shell reaches a critical thickness, solid-state convection might be initiated, allowing diapiric material to be convected toward the surface. A thickening ice shell could be related to a waning intensity of geological activity.

Given the relative youth of Europa's surface, such a fundamental change in style might seem unlikely over the last ~1% of the satellite's history, and its activity over the rest of its ~4.5-billion-year existence could only be speculated. Four possible scenarios have been proposed (Figure C.1.1-6):

(a) Europa resurfaces itself in a steady-state and relatively constant, but patchy style;

(b) Europa is at a unique time in its history, having undergone a recent major resurfacing event;

(c) Global resurfacing is episodic or sporadic;

(d) Europa's surface is actually much older than current cratering models suggest (Zahnle et al. 2003).

From the standpoint of the dynamical evolution of the Galilean satellite system, there is good reason to believe that Europa's surface evolution could be cyclical. If so, Europa could experience cyclical variations in its orbital characteristics and tidal heating on time-
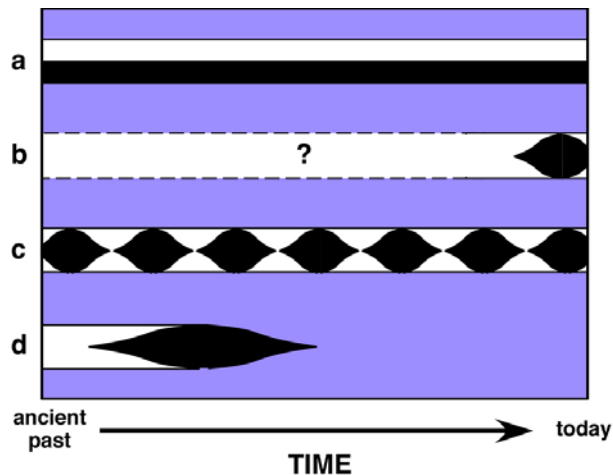
Figure C.1.1-6. Possible evolutionary scenarios for Europa's surface: (a) steady-state, relatively constant resurfacing; (b) unique time in history with recent major resurfacing event; (c) episodic or sporadic global resurfacing; (d) surface older than cratering models suggest. Geological mapping of imaging data would help to distinguish among these models. After Pappalardo et al. (1999).

scales of perhaps 100 million years (Hussman and Spohn 2004).

Global monochrome and color imaging, coupled with topography and subsurface sounding, would enable these evolutionary models to be tested. Europa's surface features generally brighten and become less red through time, so albedo and color could serve as a proxy for age (Geissler et al. 1998, Moore et al. 2009). Quantitative topographic data (Schenk and Pappalardo 2004) could provide information on the origin of geologic features and might show trends with age. Profiles across ridges, bands, and various chaotic terrains would aid in constraining their modes of origin. Moreover, flexural signatures are expected to be indicative of local elastic lithosphere thickness at the time of their formation, and might provide evidence of topographic relaxation (e.g., Nimmo et al. 2003, Billings and Kattenhorn 2005).

Some remaining outstanding questions related to Europa's geology include the following:

- Do Europa's ridges, bands, chaos, and/or multiringed structures require the presence of near-surface liquid water to form?
- Where are Europa's youngest regions?
- Is current geological activity sufficiently intense that heat flow from Europa's interior is measurable at the surface?

C.1.2 Flyby Traceability Matrix

Understanding planetary processes and habitability are key drivers for Europa exploration. Thus, the goal adopted for the Europa Multiple-Flyby Mission concept is to

Explore Europa to investigate its habitability.

The phrase "investigate its habitability" recognizes the significance of Europa's astrobiological potential. As discussed in Section A, "habitability" includes characterizing any water within and beneath Europa's ice shell, investigating the chemistry of the surface and ocean, and evaluating geological processes that might permit Europa's ocean to possess the chemical energy necessary for life.

The Europa Multiple-Flyby Mission objectives flow from the key science issues outlined in Section A.3. These objectives represent a key subset of Europa science best accomplished by a Europa Multiple-Flyby Mission. These objectives are categorized in priority order as

- I. Europa's Ice Shell: Characterize the ice shell and any subsurface water, including their heterogeneity, and the nature of surface-ice–ocean exchange.
- C. Europa's Composition: Understand the habitability of Europa's ocean through composition and chemistry.
- G. Europa's Geology: Understand the formation of surface features, including sites of recent or current activity, and characterize high science interest localities.

The complete traceability from goal to objectives to investigations, and then to example measurements and the notional instruments

that could accomplish them, is compiled in Foldout C-1 (FO C-1). These example measurements and the notional instruments that could accomplish them are provided as a proof of concept, to demonstrate the types of measurements that could address the goal, objectives, and investigations. These measurements and notional instruments are in no way meant to be exclusive of other measurements and instruments that might be able to address the objectives and investigations in other ways.

The traceability matrix (FO C-1), with its overarching goal to "explore Europa to investigate its habitability," provides specific objectives (listed in priority order), along with specific investigations (listed in priority order within each objective). The example measurements that could address each investigation are also listed in priority order for each investigation. Each objective and its investigations are described in Sections C.1.2.1 through C.1.2.4 below, along with the corresponding example measurements that could address them. The right-hand columns of the traceability matrix provide an assessment regarding which of the three themes (water, chemistry, and energy) each investigation addresses.

C.1.2.1 Europa's Ice Shell

C.1.2.1.1   Investigation I.1: Characterize the distribution of any shallow subsurface water and the structure of the icy shell.

The subsurface signatures from near-global Ice-Penetrating Radar (IPR) surveys at high depth resolution, combined with surface topography of similar vertical resolution, would identify regions of possible ongoing or relatively recent upwelling of liquid water or brines. Orbital subsurface profiling of the top 3 km of Europa's ice shell should be feasible (Chyba 1998, Moore 2000) and is recommended at frequencies slightly above the upper end of Jupiter's radio noise spectrum (i.e., about 60 MHz) to establish the geometry of various thermal, compositional, and structural horizons to a depth resolution of about 10 m

(requiring a bandwidth of about 10 MHz). This high-resolution search for shallow water would produce data analogous to that of the Shallow Subsurface Radar (SHARAD) instrument onboard the Mars Reconnaissance Orbiter (Figure C.1.2-1).
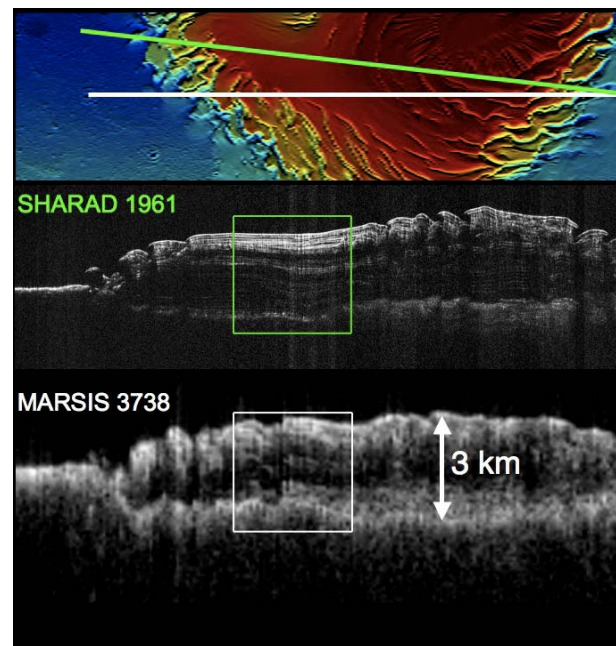
Figure C.1.2-1. Orbital subsurface profiling of Mars north polar cap. These nearly co-linear profiles across the Mars North Polar Cap (Mars Orbiter Laser Altimeter data at top left) demonstrate the value of the complementary perspectives provided by the high-center-frequency and high-bandwidth profiling of the SHARAD instrument (20 MHz and 10 MHz, respectively), and the low-center-frequency and low-bandwidth profiling of the Mars Advanced Radar for Subsurface and Ionosphere Sounding (MARSIS) (5 MHz and 1 MHz, respectively). In particular, note the clarity of shallow horizons revealed by SHARAD (detail at top right) and the prominence of deep interfaces revealed in the MARSIS results (detail at bottom right). The value of a multifrequency approach to subsurface profiling on Europa would be significantly enhanced in the presence of strong volume scattering. (MARSIS data courtesy of Picardi, Plaut, and the MARSIS Team; SHARAD data courtesy of Seu, Phillips, and the SHARAD Team.)

Goal	Objective	Investigation	Measurement	Model Instrument	Mission Constraints/Requirements	Water	Chemistry	Energy
Explore Europa to investigate its habitability	I. Ice Shell Characterize the ice shell and any subsurface water, including their heterogeneity, and the nature of surface-ice-ocean exchange.	I.1 Characterize the distribution of any shallow subsurface water and the structure of the icy shell.	I.1a Identify and regionally characterize subsurface thermal or compositional horizons and structures related to the current or recent presence of water or brine. Obtain pairs of intersecting profiles of subsurface dielectric horizons and structures at depths of 100 meters to 3 km at 10-meter vertical resolution, with estimations of subsurface dielectric properties and the density of buried scatterers.	Ice-Penetrating Radar (IPR) with altimeter mode	(1) Globally distributed regions: 6 equatorial panels (±30 deg Lat) and 4 panels at each pole (±60 deg in Lat); total of 14 panels. (2) Low-altitude flyby along a groundtrack achieving 800-km segments within each panel at altitude <400 km, at <6 km/s, and with 25- to 100-km closest approach. Two 800-km groundtrack segments in each sub-Jovian panel and at least three 800-km groundtracks in anti-Jovian panels. Each groundtrack shall also intersect another groundtrack (intersection may be outside the panel of interest); a single radar pass of sufficient length and geometry may satisfy groundtrack and intersection requirements in adjacent panels. (3) Radar groundtrack begins below ~1000-km altitude. (4) Tracks of 1/12 Europa's circumference in length co-located with a nadir-pointed altimetric profile with absolute height accuracy of 10 m. (5) *Floor:* (1) & (2) satisfied in 8 of 14 of the panels, including both anti- and sub-Jovian equatorial panels; *Baseline:* (1) & (2) satisfied in 11 of 14 panels; one groundtrack intersection within each panel, if possible.	✔		✔
			I.1b Topography on the order of 250-m horizontal scale and better than or equal to 20-m vertical resolution and accuracy extending to 50 km on either side of subsurface profiles.	Topographical Imager (TI) and Ice-Penetrating Radar (IPR) with altimeter mode	(1) Globally distributed regions: 6 equatorial panels (±30 deg Lat) and 4 panels at each pole (±60 deg in Lat); total of 14 panels. (2) Low-altitude flyby along a groundtrack achieving 800-km segments within each panel at altitude <400 km, at <6 km/s, and with 25- to 100-km closest approach. Two 800-km groundtrack segments in each sub-Jovian panel and at least three 800-km groundtracks in anti-Jovian panels. Each groundtrack shall also intersect another groundtrack (intersection may be outside the panel of interest); a single radar pass of sufficient length and geometry may satisfy groundtrack and intersection requirements in adjacent panels. (3) Radar groundtrack begins below 1000-km altitude with altimetry mode. (4) Tracks of 1/12 Europa's circumference in length, co-located with a nadir-pointed altimetric profile with absolute height accuracy of 10 m. Stereo imaging: (5) The cross-track angular width (FOV) should be sufficient to provide stereo imaging of the radar sounder groundtrack. (6) Acceptable range for stereo imaging is incidence angles of ~20 to 80°. To the extent possible, imaging should be at solar incidence angles greater than 45°. Ideally, the incidence angle would be 70°. Ice-Penetrating Radar: (7) *Floor:* (1) & (2) satisfied in 8 of 14 of the panels, including both anti- and sub-Jovian equatorial panels; *Baseline:* (1) & (2) satisfied in 11 of 14 panels; one groundtrack intersection within each panel, if possible.	✔		✔
		I.2 Search for an ice-ocean interface.	I.2a Identify deep thermal, compositional, or structural horizons by obtaining globally distributed regional profiles of subsurface dielectric horizons and structures at depths of 1- to 30-km at 100-m vertical resolution.	Ice-Penetrating Radar (IPR) with altimeter mode	(1) Globally distributed regions: 6 equatorial panels (+/-30 deg Lat) and 4 panels at each pole (60 deg in Lat); total of 14 panels. (2) Low-altitude flyby along a groundtrack achieving ~1600-km segments within each panel at altitude <1000 km, at <6 km/s, and with 25- to 100-km closest approach. Each groundtrack shall also intersect another groundtrack (intersection may be outside the panel of interest); a single radar pass of sufficient length and geometry may satisfy groundtrack and intersection requirements in adjacent panels. (3) Radar groundtrack begins below 1000-km altitude with altimetry mode. (4) Tracks of 1/6 of Europa's circumference in length co-located with a nadir-pointed altimetric profile with absolute height accuracy of 10 m. (5) *Floor:* (1) & (2) satisfied in 8 of 14 of the panels, thus including both anti- and sub-Jovian equatorial panels; *Baseline:* (1) & (2) satisfied in 11 of 14 of panels, including polar and equatorial anti-Jovian panels.	✔		✔

☐ Floor
▨ Baseline only

Water: Water in its liquid form as pertaining to habitability as an oxidizer and medium for the transport of chemical constituents.
Energy: Energy that supports and fosters a means for potential metabolism to be established and sustained.
Chemistry: The constituents that foster and sustain the processes and environment for metabolic activity.

Goal	Objective	Investigation	Measurement	Model Instrument	Mission Constraints/Requirements	Water	Chemistry	Energy
Explore Europa to investigate its habitability	I. Ice Shell Characterize the ice shell and any subsurface water, including their heterogeneity, and the nature of surface-ice-ocean exchange.	I.2 Search for an ice-ocean interface.	I.2b Topography on the order of 250-m horizontal scale and better than or equal to 20-m vertical resolution and accuracy extending to 50 km on either side of subsurface profiles.	Topographical Imager (TI) and Ice-Penetrating Radar (IPR) with altimeter mode	(1) Globally distributed regions: 6 equatorial panels (±30 deg Lat) and 4 panels at each pole (±60 deg in Lat); total of 14 panels. (2) Low-altitude flyby along a groundtrack achieving ~1600-km segments within each panel at altitude <1000 km, at <6 km/s, and with 25- to 100-km closest approach. Each groundtrack shall also intersect another groundtrack (intersection may be outside the panel of interest); a single radar pass of sufficient length and geometry may satisfy groundtrack and intersection requirements in adjacent panels. (3) Radar groundtrack begins below 1000-km altitude with altimetry mode. (4) Tracks of 1/6 of Europa's circumference in length co-located with a nadir-pointed altimetric profile with absolute height accuracy of 10 m. Stereo Imaging: (5) The cross-track angular width (FOV) should be sufficient to provide stereo imaging of the radar sounder groundtrack. (6) Acceptable range for stereo imaging is incidence angles of ~20 to 80°. To the extent possible, imaging should be at solar incidence angles greater than 45°. Ideally, the incidence angle would be 70°. Ice-Penetrating Radar: (7) _Floor:_ (1) & (2) satisfied in 8 of 14 of the panels, thus including both anti- and sub-Jovian equatorial panels; _Baseline:_ (1) & (2) satisfied in 11 of 14 of panels including polar and equatorial anti-Jovian panels.	✔		✔
		I.3 Correlate surface features and sub-surface structure to investigate processes governing material exchange among the surface, ice shell, and ocean.	I.3a Identification and regional characterization of subsurface dielectric horizons and structures, at depths 1- to 30-km at 100-m vertical resolution and depths of 100-m to 3-km at 10-m vertical resolution, by obtaining intersecting subsurface profiles distributed over a variety of surface features.	Ice-Penetrating Radar (IPR) with altimeter mode	(1) Globally distributed regions: 6 equatorial panels (±30 deg Lat) and 4 panels at each pole (±60 deg in Lat); total of 14 panels. (2) Low-altitude flyby along a groundtrack achieving 800-km segments within each panel at altitude <400 km, at <6 km/s, and with 25- to 100-km closest approach. Two 800-km groundtrack segments in each sub-Jovian panel and three 800-km groundtracks in anti-Jovian panels. Each groundtrack shall also intersect another groundtrack (intersection may be outside the panel of interest); a single radar pass of sufficient length and geometry may satisfy groundtrack and intersection requirements in adjacent panels. (3) Radar groundtrack begins below ~1000-km altitude. (4) Tracks of 1/12 Europa's circumference in length co-located with a nadir-pointed altimetric profile with absolute height accuracy of 10 m. (5) _Floor:_ (1) & (2) satisfied in 8 of 14 of the panels, including both anti- and sub-Jovian equatorial panels; _Baseline:_ (1) & (2) satisfied in 11 of 14 panels; one groundtrack intersection within each panel, if possible.	✔	✔	✔
			I.3b Measure surface reflectance from 850-5000 nm with 10-nm resolution n <2500 nm and 20 nm from 2500-5000 nm. Targeted observations of ~100 representative landforms at 300-m/pixel sampling over a wide range of latitudes and longitudes.	Shortwave Infra-red Spectrometer (SWIRS)	(1) Ability to target specific geologic locations that are globally distributed (6 equatorial panels (±30 deg Lat) and 4 panels at each pole (±60 deg in Lat); total of 14 panels). (2) Low-altitude flyby along a groundtrack within each panel at altitude <1000 km, at ≤6 km/s, and with 25- to 100-km closest approach. Ability to collect data at different locations along each groundtrack to sample desired landforms. (3) Observations on the leading and trailing hemisphere are required in addition to at least one high-latitude pass. (4) Solar incidence angles at the equator of less than 45° (local true solar time between 9:00 to 15:00) [Note: Illumination requirements for the SWIRS have a higher priority than those for the Topographical Imager]. (5) Ability of spacecraft to smoothly scan over the surface to build up spectral image cube. (6) Spacecraft stability: Less than 1/2 IFOV over the integration time. (7) Regional scale (300 m/pixel) observations: _Floor:_ Sampling in 8 of the 14 panels; _Baseline:_ Sampling in 11 of 14 panels.	✔	✔	✔

Floor
Baseline only

Water: Water in its liquid form as pertaining to habitability as an oxidizer and medium for the transport of chemical constituents.
Energy: Energy that supports and fosters a means for potential metabolism to be established and sustained.
Chemistry: The constituents that foster and sustain the processes and environment for metabolic activity.

Goal	Objective		Investigation	Measurement		Model Instrument	Mission Constraints/Requirements	Water	Chemistry	Energy
Explore Europa to investigate its habitability	I. Ice Shell	Characterize the ice shell and any subsurface water, including their heterogeneity, and the nature of surface-ice-ocean exchange.	I.3 Correlate surface features and sub-surface structure to investigate processes governing material exchange among the surface, ice shell, and ocean.	I.3c	Topography on the order of 250-m horizontal scale and better than or equal to 20-m vertical resolution and accuracy extending to 50 km on either side of subsurface profiles.	Topographical Imager (TI) an Ice-Penetrating Radar (IPR) with altimeter mode	(1) Globally distributed regions: 6 equatorial panels (±30 deg Lat) and 4 panels at each pole (±60 deg in Lat); total of 14 panels. (2) Low-altitude flyby along a groundtrack achieving 800-km segments within each panel at altitude <400 km, at <6 km/s, and with 25- to 100-km closest approach. Two 800-km groundtrack segments in each sub-Jovian panel and three 800-km groundtracks in anti-Jovian panels. Each groundtrack shall also intersect another groundtrack (intersection may be outside the panel of interest); a single radar pass of sufficient length and geometry may satisfy groundtrack and intersection requirements in adjacent panels. (3) Radar groundtrack begins below 1000-km altitude with altimetry mode. (4) Tracks of 1/12 Europa's circumference in length co-located with a nadir-pointed altimetric profile with absolute height accuracy of 10 m. Stereo Imaging: (5) Stereo imaging: The cross-track angular width (FOV) should be sufficient to provide stereo imaging of the radar sounder groundtrack. (6) Acceptable range for stereo imaging is incidence angles of ~20 to 80°. To the extent possible, imaging should be at solar incidence angles greater than 45°. Ideally the incidence angle would be 70°. Ice-Penetrating Radar: (7) *Floor:* (1) & (2) satisfied in 8 of 14 of the panels including both anti- and sub-Jovian equatorial panels; *Baseline:* (1) & (2) satisfied in 11 of 14 panels; one groundtrack intersection within each panel if possible.	✔	✔	✔
			I.4 Characterize regional and global heat flow variations.	I.4a	Identify and map subsurface thermal horizons by obtaining profiles of subsurface dielectric horizons at depths of 1- to 30-km at 10- to 100-m vertical resolution.	Ice-Penetrating Radar (IPR)	(1) Globally distributed regions: 6 equatorial panels (±30 deg Lat) and 4 panels at each pole (±60 deg in Lat); total of 14 panels. (2) Low-altitude flyby along a groundtrack achieving 800-km segments within each panel at altitude <400 km, at <6 km/s, and with 25- to 100-km closest approach. Two 800-km groundtrack segments in each sub-Jovian panel and three 800-km groundtracks in anti-Jovian panels. Each groundtrack shall also intersect another groundtrack (intersection may be outside the panel of interest); a single radar pass of sufficient length and geometry may satisfy groundtrack and intersection requirements in adjacent panels. (3) Radar groundtrack begins below ~1000-km altitude. (4) Tracks of 1/12 Europa's circumference in length co-located with a nadir-pointed altimetric profile with absolute height accuracy of 10 m. (5) *Floor:* (1) & (2) satisfied in 8 of 14 of the panels including both anti- and sub-Jovian equatorial panels; *Baseline:* (1) & (2) satisfied in 11 of 14 of panels with one groundtrack intersection within each panel if possible.	✔		✔
	C. Composition	Understand the habitability of Europa's ocean through composition and chemistry.	C.1 Characterize the composition and chemistry of the Europa ocean as expressed on the surface and in the atmosphere.	C.1a	Measure surface reflectance from 850-5000 nm with 10-nm resolution n <2500 nm and 20 nm from 2500-5000 nm. Targeted observations of ~100 representative landforms at regional-scales (300-m/pixel sampling) over a wide range of latitudes and longitudes.	Shortwave Infrared Spectrometer (SWIRS)	(1) Ability to target specific geologic locations that are globally distributed: 6 equatorial panels (±30 deg Lat) and 4 panels at each pole (±60 deg in Lat); total of 14 panels. (2) Low-altitude flyby along a groundtrack within each panel at altitude <1000 km, at ≤6 km/s, and with 25- to 100-km closest approach. Ability to collect data at different locations along the groundtrack to sample desired landforms. (3) Observations on the leading and trailing hemisphere are required in addition to at least one high-latitude pass. (4) Solar incidence angles at the equator of less than 45° (local true solar time between 9:00 to 15:00) [Note: Illumination requirements for the SWIRS have a higher priority than those for the Topographical Imager]. (5) Ability of spacecraft to smoothly scan over the surface to build up spectral image cube. (6) Spacecraft stability: Less than 1/2 IFOV over the integration time. (7) Regional scale (300 m/pixel) observations: *Floor:* Sampling in 8 of the 14 panels; *Baseline:* Sampling in 11 of 14 panels.	✔	✔	
				C.1b	Characterize the composition of sputtered surface products over a mass range better than 300 daltons, mass resolution better than 500, with sensitivity of at least 10 particles cm^{-3}.	Ion and Neutral Mass Spectrometer (INMS)	(1) Flyby Velocity of <7 km/s, with slower speeds desirable. (2) Flight altitudes of <200 km, with lower altitude passes desired (as low as 25 km).	✔	✔	

☐ Floor
▨ Baseline only

Water: Water in its liquid form as pertaining to habitability as an oxidizer and medium for the transport of chemical constituents.
Energy: Energy that supports and fosters a means for potential metabolism to be established and sustained.
Chemistry: The constituents that foster and sustain the processes and environment for metabolic activity.

Goal	Objective	Investigation	Measurement	Model Instrument	Mission Constraints/Requirements	Water	Chemistry	Energy
Explore Europa to investigate its habitability	C. Composition	Understand the habitability of Europa's ocean through composition and chemistry.	C.2 Determine the role of Jupiter's radiation environment in processing materials on Europa.	C.2a Measure surface reflectance from 850-5000 nm with 10-nm resolution n <2500 nm and 20 nm from 2500-5000 nm. Targeted observations of ~100 representative landforms at regional-scales (300-m/pixel sampling) over a wide range of latitudes and longitudes.	Shortwave Infra-red Spectrometer (SWIRS)	(1) Ability to target specific geologic locations that are globally distributed: 6 equatorial panels (±30 deg Lat) and 4 panels at each pole (±60 deg in Lat); total of 14 panels. (2) Low-altitude flyby along a groundtrack within each panel at altitude <1000 km, at ≤6 km/s, and with 25- to 100-km closest approach. Ability to collect data at different locations along the groundtrack to sample desired landforms. (3) Observations on the leading and trailing hemisphere are required in addition to at least one high-latitude pass. (4) Solar incidence angles at the equator of less than 45° (local true solar time between 9:00 to 15:00) [Note: Illumination requirements for the SWIRS have a higher priority than those for the Topographical Imager]. (5) Ability of spacecraft to smoothly scan over the surface to build up spectral image cube. (6) Spacecraft stability: Less than 1/2 IFOV over the integration time. (7) Regional scale (300 m/pixel) observations: _Floor:_ Sampling in 8 of the 14 panels; _Baseline:_ Sampling in 11 of 14 panels.		✔	✔
				C.2b Characterize the composition of sputtered surface products over a mass range better than 300 daltons, mass resolution better than 500, with sensitivity of at least 10 particles cm^{-3}.	Ion and Neutral Mass Spectrometer (INMS)	(1) Flyby Velocity of <7 km/s, with slower speeds desirable. (2) Flight altitudes of <200 km, with lower altitude passes desired (as low as 25 km).		✔	✔
			C.3 Characterize the chemical and compositional pathways in Europa's ocean.	C.3a Measure surface reflectance from 850-5000 nm with 10-nm resolution <2500 nm and 20 nm from 2500-5000 nm. Targeted observations of ~100 representative landforms at 300-m/pixel sampling and global-scale coverage with a spatial sampling better than or equal to 10 km/pixel.	Shortwave Infra-red Spectrometer (SWIRS)	(1) Ability to target specific geologic locations that are globally distributed: 6 equatorial panels (±30 deg Lat) and 4 panels at each pole (±60 eg in Lat); total of 14 panels. (2) Low-altitude flyby along a groundtrack within each panel at altitude <1000 km, at ≤6 km/s, and with 25- to 100-km closest approach. Ability to collect data at different locations along the groundtrack to sample desired landforms. (3) Observations on the leading and trailing hemisphere are required in addition to at least one high-latitude pass. (4) Global-scale coverage with a spatial sampling better than or equal to 10 km/pixel that samples 70% of the surface at local true solar times (LTST) between 9:00 and 15:00 and at ~5 to 10° intervals in latitude and longitude. (5) Solar incidence angles at the equator of less than 45° (local true solar time between 9:00 to 15:00) [Note: Illumination requirements for the SWIRS have a higher priority than those for the Topographical Imager]. (6) Ability of spacecraft to smoothly scan over the surface to build up spectral image cube. (7) Spacecraft stability: Less than 1/2 IFOV over the integration time. (8) Regional scale (300 m/pixel) observations: _Floor:_ Sampling in 8 of the 14 panels; _Baseline:_ Sampling in 11 of 14 panels.	✔	✔	
				C.3b Characterize the composition of sputtered surface products over a mass range better than 300 daltons, mass resolution better than 500, with sensitivity of at least 10 particles cm^{-3}.	Ion and Neutral Mass Spectrometer (INMS)	(1) Flyby Velocity of <7 km/s, with slower speeds desirable. (2) Flight altitudes of <200 km, with lower altitude passes desired (as low as 25 km).	✔	✔	
				C.3c Correlate surface composition with geologic features through mapping at resolution of better than or equal to 100 m/pixel for locations measured spectroscopy.	Topographical Imager (TI) (stereo)	(1) Acceptable range for stereo imaging is incidence angles of ~20° to 80°. To the extent possible, imaging should be at solar incidence angles greater than 45°. Ideally, the incidence angle would be 70°. (2) The cross-track angular width (FOV) should be sufficient to cover the effective cross-track width of the radar sounder.	✔	✔	

☐ Floor
▨ Baseline only

Water: Water in its liquid form as pertaining to habitability as an oxidizer and medium for the transport of chemical constituents.
Energy: Energy that supports and fosters a means for potential metabolism to be established and sustained.
Chemistry: The constituents that foster and sustain the processes and environment for metabolic activity.

Goal		Objective	Investigation	Measurement	Model Instrument	Mission Constraints/Requirements	Water	Chemistry	Energy
Explore Europa to investigate its habitability	G. Geology	Understand the formation of surface features, including sites of recent or current activity, and characterize high science interest localities.	G.1 Determine sites of most recent geological activity, and characterize localities of high science interest.	G.1a Characterize selected targets at ~20 m/pixel and characterize their topography at better than 50-m horizontal scale and better than or equal to 10-meter vertical resolution and accuracy.	Topographical Imager (TI) (stereo), Ion and Neutral Mass Spectrometer (INMS)	(1) Acceptable range for stereo imaging is incidence angles of ~20° to 80°. To the extent possible, imaging should be at solar incidence angles greater than 45°. Ideally, the incidence angle would be 70°. (2) The cross-track angular width (FOV) should be sufficient to cover the effective cross-track width of the radar sounder. (3) Flyby Velocity of <7 km/s, with slower speeds desirable. (4) Flight altitudes of <200 km, with lower altitude passes desired (as low as 25 km).	✔		✔

☐ Floor
▨ Baseline only

Water: Water in its liquid form as pertaining to habitability as an oxidizer and medium for the transport of chemical constituents.
Energy: Energy that supports and fosters a means for potential metabolism to be established and sustained.
Chemistry: The constituents that foster and sustain the processes and environment for metabolic activity.

This profiling should be done in conjunction with colocated stereo imaging and a radar altimeter that could be used to register photogrammetric topography to vertical resolution of better than 20 m, permitting surface clutter effects to be removed from the radar data. Stereo imaging is susceptible to relative errors, and stereo vertical accuracy might vary across a scene. However, significantly higher vertical resolutions could be extracted using photoclinometry that is controlled by stereo imaging and radar altimetry data. By tying this high-horizontal-resolution relief to the high absolute vertical resolution of a radar altimeter, we could generate improved digital elevation models, which could be used to model and subtract radar clutter. Ultimately, shallow subsurface profiles should sample regions that are globally distributed across Europa's surface.

C.1.2.1.2   Investigation I.2: Search for an ice–ocean interface.

Subsurface signatures from lower-resolution but more deeply penetrating radar surveys might reveal the ice–ocean interface, which could be validated over a region by carefully correlating ice thickness and surface topography. An unequivocally thin ice shell, even within a limited region, would have significant implications for understanding direct exchange between the ocean and the overlying ice. Similarly, the detection of deep subsurface interfaces in these surveys and the presence or absence of shallower interfaces above them would test hypotheses regarding the convective upwelling of deep, ductile ice into the cold, brittle shell, implying indirect exchange with any ocean. Additional orbital profiling of the subsurface of Europa to depths of 30 km with a vertical resolution of about 100 m would establish the geometry of any deeper geophysical interfaces such as an ice–ocean interface.

Although warm ice is very attenuating to radar (Chyba et al. 1998), thick ice in a regime of steady-state thermal conduction could be sounded on Europa to depths of 25 to 40 km if

it is essentially free of impurities (Moore 2000). Although impurities are almost certainly present, the non-steady-state convective thermal regime could generate "windows" of very cold downwelling material within the ice shell, allowing local penetration to great depth (McKinnon 2005). Moreover, while the presence of meter-scale voids within the ice shell would confound sounding measurements at higher frequencies (>15 MHz) (Eluszkiewicz 2004), the presence of such large voids is probably unrealistic (Lee et al. 2005).

Deep ocean searches would produce data analogous to those of the Mars Advanced Radar for Subsurface and Ionosphere Sounding (MARSIS) instrument on the Mars Express spacecraft (Figure C.1.2-1). This profiling should establish the geometry of any deeper geophysical interfaces that might correspond to an ice–ocean boundary, to a vertical resolution of about 100 m (requiring a bandwidth of about 1 MHz).

Frequencies significantly less sensitive to any volume scattering that might be present in the shallow subsurface profiling detailed above (i.e., about 9 MHz) should be used on the anti-Jovian side of Europa, which is substantially shadowed from Jupiter's radio emissions. This low-frequency, low-resolution profiling should be complemented by high-frequency, low-resolution profiling over Europa's sub-Jovian surface (where Jupiter's radio noise is an issue for low-frequency sounding). Combined, the deep, low-resolution profiling should sample regions that are globally distributed across Europa's surface. Profiling should be performed along with colocated stereo imaging and radar altimetry of better than 100 m topographic resolution, permitting surface clutter effects to be removed from the radar data.

C.1.2.1.3   *Investigation I.3: Correlate surface features and subsurface structure to investigate processes governing material exchange among the surface, ice shell, and ocean.*

Targeted radar observations would lead to understanding the processes controlling the distribution of any shallow subsurface water and either the direct or indirect exchange of materials between the ice shell and its underlying ocean. Similarly, differences in the physical and compositional properties of the near-surface ice might arise due to age differences, tectonic deformation, mass wasting, or impact gardening. Knowledge of surface properties gained from spectroscopy and high-resolution image and topographic data would be essential for integrated interpretation of subsurface structure, and for understanding liquid water or ductile ice within Europa's ice shell.

Because of the complex geometries expected for subsurface structures, subsurface radar images should be obtained along profiles in globally distributed regions across Europa, either to a depth of 3 km for high-resolution imaging or to a depth of 30 km for lower-resolution imaging of deeper features, in conjunction with colocated topographic data.

C.1.2.1.4   *Investigation I.4: Characterize regional and global heat-flow variations.*

The thermal structure of the shell (apart from local heat sources) is set by the transport of heat from the interior. Regardless of the properties of the shell or the overall mechanism of heat transport, the uppermost few kilometers at least are cold and stiff. The thickness of this "lid" is set by the total amount of heat that must be transported; thus, a measurement of the thickness of the cold and brittle part of the shell would provide a constraint on the heat production in the interior.

For a thin ice shell, the ice–ocean interface would form a significant dielectric horizon at the base of the thermally conductive layer. However, if warm pure-ice diapirs from the interior of a thicker convective shell approach the surface, they might be different from the pure-ice melting point and above the eutectic of many substances; this could create regions of melting within the rigid shell above them as the temperature increases above a diapir. Any dielectric horizon associated with such melt regions would also provide a good measurement of the thickness of the cold lid. Global radar profiles of the subsurface thermal horizons to depths of 30 km at a vertical resolution of 100 m would enable characterization of regional and global heat-flow variations in Europa's ice shell.

The key outstanding questions relating to Europa's ice shell (Table C.1.2-1) can be related to and addressed by the Objective I investigations described above, as summarized in FO C-1.

C.1.2.2   Europa's Composition

Surface composition forms the linkages that enable understanding of Europa's potential habitability in the context of geologic process-

Table C.1.2-1. Hypothesis tests to address selected key questions regarding Europa's ice shell.

	Example Hypothesis Questions	Example Hypothesis Tests
I.1	Is Europa's ice shell very thin and conductive or thick and convecting?	Sound Europa's ice shell for a strong water reflector at shallow depth, or to observe a gradual absorption of the signal with depth, which might reveal diapiric structures.
I.2	Is there fluid transport from the ocean to the near-surface or surface, and vice versa?	Sound Europa's ice at shallow and greater depths for liquid water, and correlate to surface morphology, compositional, and thermal data.
I.3	What are the three-dimensional characteristics of Europa's geological structures?	Combine ice-penetrating radar and topographic measurements with high-resolution imaging to investigate the 3D structure of geological features.
I.4	Are there regional variations in the thickness of Europa's thermally conductive layer?	Sound Europa's ice shell to map dielectric horizons in globally distributed regions.

es. Composition is also a probe of the interior and records the evolution of the surface under the influence of internal and external processes. Investigations regarding Europa's chemistry and composition require synergistic, coordinated observations of targeted geological features, along with stereo imaging and radar sounding.

There are two basic approaches to determining the composition of Europa's surface: Materials could be measured on the surface using remote optical spectroscopy, or the surface composition could be inferred by measuring materials sputtered or ejected from the surface into an atmosphere. Optical measurements of the surface could determine the composition and distribution of materials at geologically relevant scales (tens to hundreds of meters). However, the spectroscopy of solids is complicated by the physical properties of the material (e.g., grain size and temperature), and by material mixing, and high-quality spectra of specific surface units are required to identify minor components. Materials with strong, narrow, isolated absorption features could be accurately identified with detection limits of ~1%, and much greater sensitivity (~0.1%) could be achieved for strongly absorbing components intimately mixed with a less-absorbing component such as water ice. Materials with broad, shallow features might have detection limits of ≥10%, and their identification might be limited to the mineral or functional group of material present (e.g., phyllosilicates). Some materials (e.g., NaCl) are optically inactive through much of the visible and infrared and are difficult to detect remotely. In addition, the surface composition can be inferred from measurements of daughter products that have been derived from the surface by sputtering and radiation-induced chemistry.

Before discussing the specific investigations for the objective related to Europa's composition, we first explore the techniques of infrared spectroscopy to understand surface composi-

tion, and ion and neutral spectroscopy to understand atmospheric composition.

Surface Composition through Infrared Spectroscopy

A well-established means to map surface composition at the spatial scales relevant to geologic processes is through infrared imaging spectroscopy. Data obtained by the Galileo NIMS for Europa and observations by the Cassini Visual and Infrared Mapping Spectrometer (VIMS) of the Saturnian system demonstrate the existence of a wealth of spectral features throughout the near-infrared spectral range (e.g., McCord et al. 1998b; Carlson et al. 1999a, b; Clark et al. 2005; Cruikshank et al. 2007).

Of the materials studied thus far in the laboratory, the hydrated sulfates appear to most closely reproduce the asymmetric and distorted H_2O spectral features observed at Europa. In these compounds, hydration shells around anions and/or cations contain water molecules in various configurations, held in place by hydrogen bonds. Each configuration corresponds to a particular vibrational state, resulting in complex spectral behavior that is diagnostic of composition. These bands become particularly pronounced at temperatures below 150 K as the reduced intermolecular coupling causes the individual absorptions that make up these spectral features to become more discrete (Crowley 1991; Dalton and Clark 1998; Carlson et al. 1999b, 2005; McCord et al. 2001a, 2002; Orlando et al. 2005; Dalton et al. 2003, 2005; Dalton 2000, 2007). As a result, the spectra of low-temperature materials provide highly diagnostic, narrow features ranging from 10 to 50 nm wide (Figure C.1.2-2).

Cryogenic spectra for all of the hydrated sulfates and brines in Figure C.1.2-2 display the diagnostic absorption features near 1.0, 1.25, 1.5, and 2.0 μm that are endemic to water-bearing compounds. These features generally align with those in water ice and with the features observed in the Europa spectrum. Other
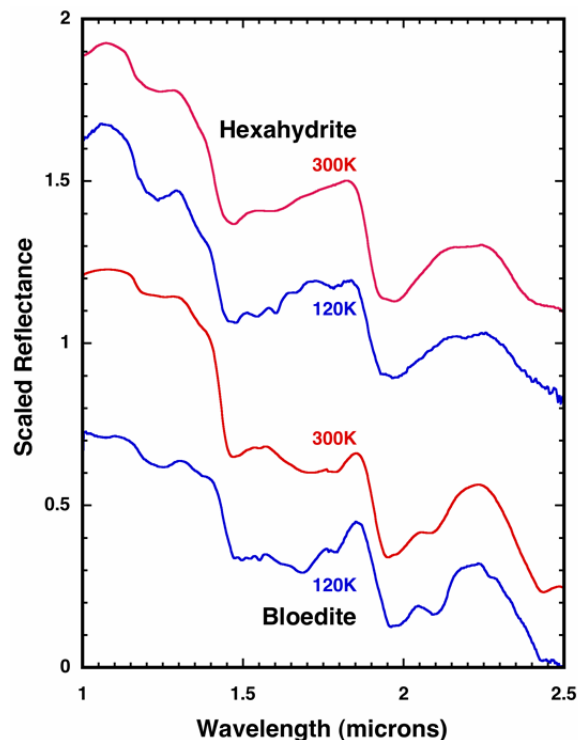
Figure C.1.2-2. Reflectance spectra of two hydrated salts at room temperature and at 120 K, as expected at the surface of Europa. The fine spectral structure apparent at high (~5 nm) spectral resolution could be exploited to discriminate between hydrates. From Dalton et al. (2003).

spectral features arising from the presence of water occur in many of the spectra, including features of moderate strength near 1.65, 1.8, and 2.2 µm (Figure C.1.2-3). An additional absorption common to the hydrates at 1.35 µm arises from the combination of low-frequency lattice modes with the asymmetric O-H stretching mode (Hunt et al. 1971a, b; Crowley 1991; Dalton and Clark 1999). Although weak, this feature is usually present in hydrates and has been used to place upper limits on abundances of hydrates in prior studies (Dalton and Clark 1999, Dalton 2000, Dalton et al. 2003).

Cassini VIMS observations of Phoebe provide additional examples of the wealth of information available in infrared spectra. Clark et al. (2005) reported 27 individual spectral features, indicating a complex surface containing a rich array of ices including H_2O and CO_2,

and organic species including CN-bearing ices. The 3- to 5-µm portion of the Phoebe spectrum includes absorptions tentatively interpreted as nitrile and hydrocarbon compounds. This spectral range is useful for detecting numerous organic and inorganic species anticipated at Europa (Figures C.1.2-3 and C.1.2-4).

Unexpectedly, the diagnostic spectral features of hydrated minerals are not seen in high-spectral-resolution 1.45- to 1.75-µm Keck telescopic spectra collected from regions of dark terrain on Europa that are several hundred kilometers in extent, suggesting that hydrated
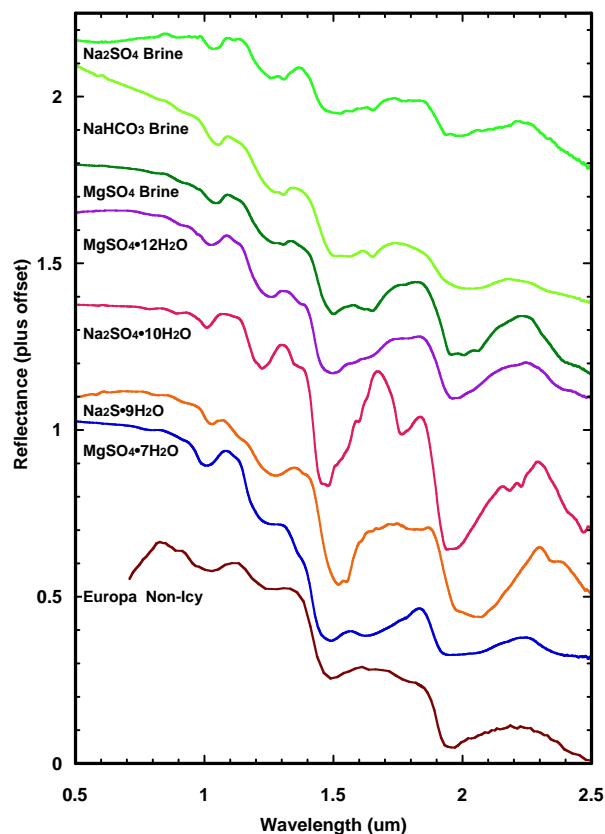
Figure C.1.2-3. Cryogenic reflectance spectra of hydrated sulfates and brines, compared to Europa. Spectra of epsomite ($MgSO_4 \cdot 7H_2O$), hexahydrite ($MgSO_4 \cdot 6H_2O$) and bloedite ($Na_2Mg(SO_4)_2 \cdot 4H_2O$) were measured at 100, 120, and 120 K, respectively (Dalton 2000, 2003). Spectra of sodium sulfide nonahydrate ($Na_2S \cdot 9H_2O$); mirabilite ($Na_2SO_4 \cdot 10H_2O$); magnesium sulfate dodecahydrate ($MgSO_4 \cdot 12H_2O$); and $MgSO_4$, $NaHCO_3$, and Na_2SO_4 brines were measured at 100 K (Dalton et al. 2005).

Figure C.1.2-4. Notional reflectance spectra for ice-rich regions (blue curves) and ice-poor regions (red curves) on Europa (based on observations of compounds observed on other Jovian and Saturnian satellites) at 10 nm spectral resolution in the 1–5 μm (1000–5000 nm) spectral range. A variety of materials and molecules have been identified or inferred from the Galileo results. The spectra shown here are composites to illustrate the types and variety of features found or expected. The detailed spectral structure observed in hydrates at high spectral resolution (e.g., Figure C.1.2-2, Figure C.1.2-3) is not fully represented here. The 2.8–5 μm range spectra are scaled by 20 compared to the shorter-wavelength range. Figure courtesy Diana Blaney.

materials might be noncrystalline (glassy) because of radiation damage or flash-freezing (Spencer et al. 2006)

Although these regions of Europa are dominated by dark materials, ice-rich materials probably occur within the observed area, and significant spatial mixing and dilution of the spectra of the optically active species might occur. It is also possible that the various hydrated species are mixed in such proportions that their diagnostic features overlap. It is expected that there would be smaller regions (perhaps the youngest ones) on Europa in which diagnostic spectral features could be found if observed at higher spatial resolution. An excellent example of the importance of spatial resolution is observed for Martian dark-region spectra, in which telescopic spectra in

both the thermal and short-wave infrared (e.g., Bell 1992, Moersch et al. 1997) did not reveal the mineralogical components until high-spatial-resolution spectra were acquired from orbit (e.g., Christensen et al. 2001, Bibring et al. 2005, Ehlmann et al. 2008, Mustard et al. 2008).

Laboratory studies have shown that at Europa's surface temperature, anticipated materials—in particular hydrates—exhibit fine structure, with the full width at half maximum (FWHM) of spectral features ranging from 7 to 50 μm (Carlson et al. 1999b, 2005; Dalton 2000; Dalton et al. 2003; Orlando et al. 2005). Analysis shows that to detect materials in relatively low abundance, or in mixtures with dark materials, signal-to-noise ratio (S/N) > 128 is desirable in the wavelength range 0.85 to 2.6

µm, and S/N > 32 is desirable in the wavelength range 2.6 to 5.0 µm (Figure C.1.2-5). An ideal spectral resolution of 2 nm per channel would be sufficient to identify all features observed in laboratory hydrates thus far (Dalton et al. 2003, Dalton et al. 2005). This would ensure multiple channels across each known feature of interest. However, at Jupiter's distance from the Sun, the reflected near-infrared radiance limits the achievable spectral resolution for high-spatial-resolution mapping. The S/N performance is further complicated by the severe radiation noise effects at Europa's orbit.

The spatial resolution required for compositional mapping is determined by the scale of critical landforms such as bands, lenticulae, chaos, and craters. Europa displays albedo and morphological heterogeneity at scales of ~100 m, suggesting that compositional variations also exist at this scale. However, the composition of these features remains unknown because Galileo NIMS observations are averages of light reflected from large areas containing both icy and "non-icy" terrain units (e.g., McCord et al. 1999, Fanale et al. 1999). Spectra of adjacent regions within an instrument field of view combine to produce an average spectrum, with spectral features from all the materials. However, these composite spectra have potential overlap of spectral features and reduced spectral contrast relative to the spectra of the individual surface units. Because spectral mixing and reduced contrast will decrease detectability, it is desirable to resolve regions of uniform composition in order to map distinct surface units. While these in turn might be mixtures, spatially resolving dark terrains that have fewer components and are free of the strong and complex absorption features of water-ice would greatly facilitate identification of the non-ice materials. For reasonable statistical sampling, it is also desirable to have multiple pixels within a given surface unit. Adjacent measurements could then be compared with each other and averaged together to improve the signal and reduce noise.

Galileo images of Europa suggest geologically recent formation ages for ridges, chaos, and other features. The images also show abundant evidence for much younger materials exposed by mass wasting of faces and scarps (Sullivan
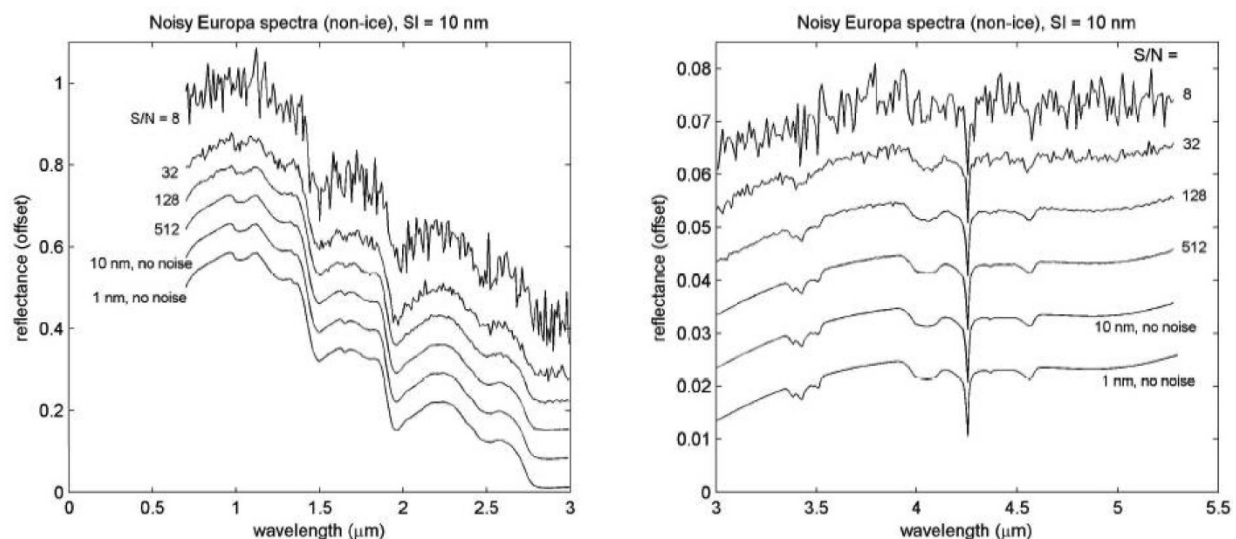
Figure C.1.2-5. Infrared reflectance spectra for a range of signal-to-noise ratios (S/Ns) show that to detect absorption bands of materials in relatively low abundance, or in mixtures with dark materials, S/N >128 is desirable in the shorter-wavelength range 0.85–2.6 µm, and S/N >32 is desirable in the longer-wavelength range 2.6–5.0 µm (Tom McCord, personal communication). The model payload's Shortwave Infrared Spectrometer would achieve S/N ~18 with 1 row of target 100 at 5 µm (TMC 8), 18 at 5 µm (TMC 1).

et al. 1999). These postformational modification processes have likely affected many surfaces, potentially exposing fresh materials that are less altered than their surroundings. Spectroscopy at a resolution better than 300 m would isolate these surfaces and provide an opportunity to determine the composition of primary materials. Additional important compositional information could come from an Ion and Neutral Mass Spectrometer (INMS), which could measure sputtered materials. Integration of results from spectroscopic analysis and *in situ* INMS measurements would be key to identifying the non-ice materials on Europa's surface.

In summary, the multiple spectral features and fine (10 to 50 nm) structure of materials of interest in the 1 to ≥ 5 µm range in low-temperature spectra are sufficiently unique to allow these materials to be identified even in mixtures of only 5 to 10 weight percent (Dalton 2007, Hand 2007). The ability to fully resolve these features through high-spectral, high-spatial resolution observations would permit determination of the relative abundances of astrobiologically relevant materials on the surface of Europa.

Atmospheric Composition through Ion and Neutral Mass Spectrometry

Europa's composition is expressed in its sputtered atmosphere, with ties to the subsurface ocean and habitability. An INMS would provide a sensitive means to measure ions and neutrals present in Europa's atmosphere that are derived from the surface by sputtering, outgassing, and sublimation, considerably aiding

identification of surface materials. Europa's tenuous atmosphere, first postulated in the 1970s, has four observed components: O (Hall et al. 1995, 1998) near the surface, Na and K in the region from ~3.5 to 50 R_E (Brown and Hill 1996, Brown 2001, Leblanc et al. 2002, Leblanc et al. 2005), and H_2 in Europa's co-orbiting gas torus (Smyth and Marconi 2006). Robust plasma bombardment of Europa's surface is expected to produce many other components (e.g., Johnson et al. 1998). To date there have been few measurements of the Europan atmosphere, so models must be relied upon to infer its vertical structure, and especially the abundances of species other than those already detected (O, Na, and K).

Major volatiles would be easily detectable using current INMS technology. Figure C.1.2-6 shows one such model of Europa's atmosphere (Smyth and Marconi 2006), with sensitivity of
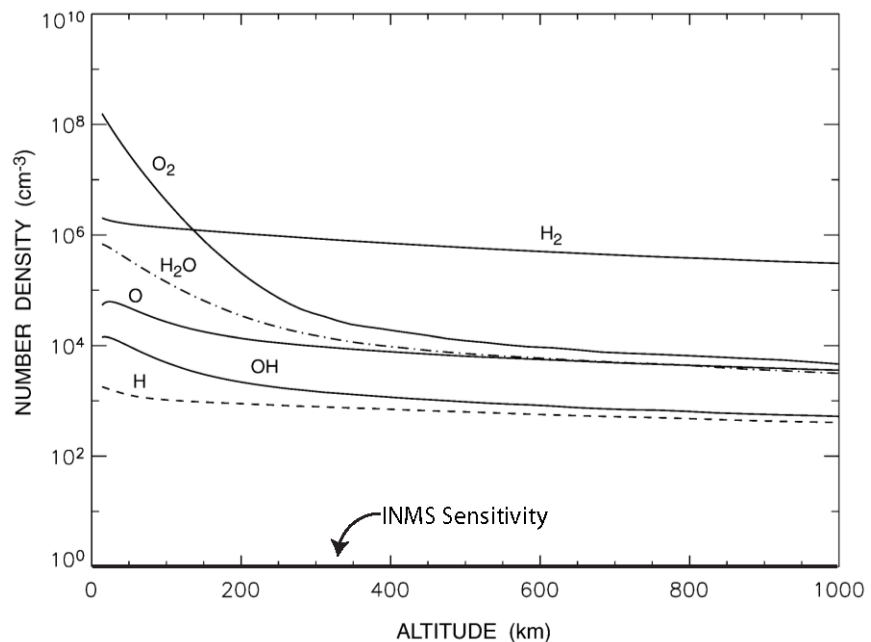
Figure C.1.2-6. Vertical distribution of the modeled abundance, globally averaged density of potential atmospheric components. The O_2 rate was set to reproduce the 135.6-nm O brightness of 37 ±15 Rayleigh observation of Hall et al. (1995). Sublimation was taken into account but is unimportant except in the subsolar region. In both simulations, the ejecta energy distributions discussed in the text were used for H_2O and O_2, and thermalization of returning H_2 and O_2 in the regolith is assumed. From Smyth and Marconi (2006).
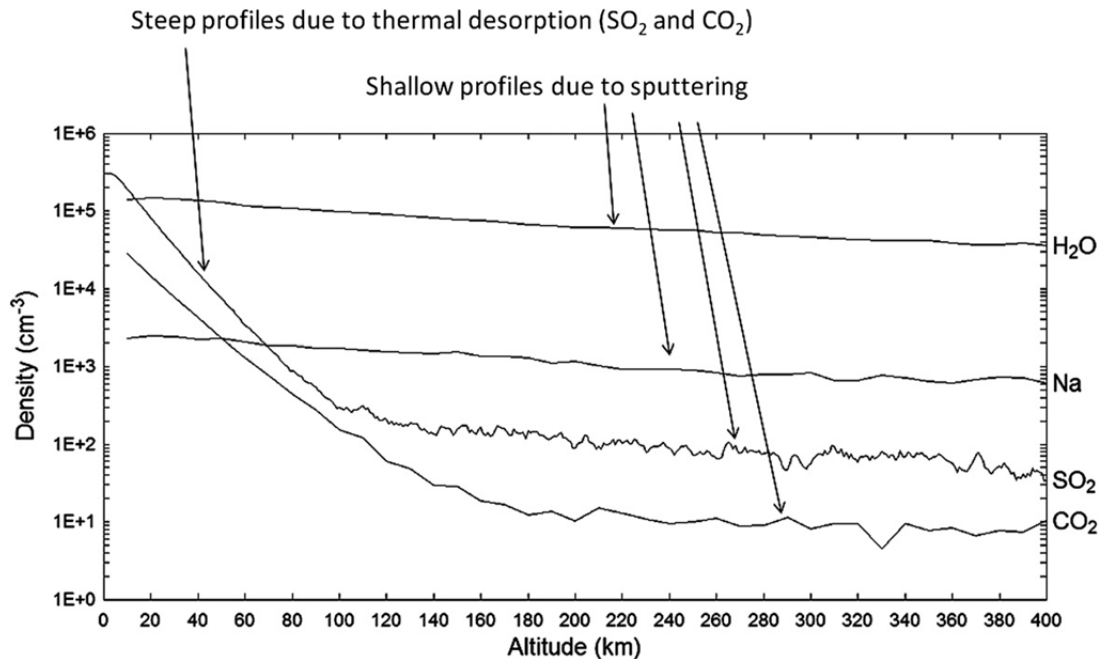
Figure C.1.2-7. Neutral density vs. altitude for selected species and cases. Shallow profiles decay much faster than $1/r^2$. At 100 km, a mass detection threshold of greater than 100 cm^{-3} is needed to characterize key volatiles. SO$_2$ and CO$_2$ abundances increase dramatically approaching the surface within about 150 km. From Cassidy et al (2009).

1 cm^{-3} for a model Flyby INMS superimposed.

Trace materials detected from surface spectroscopy (SO$_2$, CO$_2$) should be readily detectable using INMS (Johnson et al. 2004). Further characterization of hydrate and associated dark materials could be accomplished for comparison to remote-sensing observations of the surface. For example, Mg should be present in the atmosphere if MgSO$_4$, expected to dominate Europa's ocean composition, is present at the surface. Atmospheric emission measurements for Na and K have confirmed a surface source (Johnson et al. 2002, LeBlanc et al. 2002), with some evidence that the Na and K originate specifically from dark regions (LeBlanc et al. 2005, Cassidy et al. 2008). However, these have not yet been detected in surface spectral measurements.

Vented material or materials from flows that are emplaced on the surface are rapidly degraded by the incident radiation. This degradation process also produces sputtered products that could be detected and interpreted. Figure C.1.2-7 shows how sputtered atmospheric

density is predicted to rapidly increase approaching Europa's surface. The composition of Europa's atmospheric CO^2, as shown in Table C.1.2-2, from Cassidy et al. (2009) sets the model INMS detection threshold of 1 cm^{-3}. From 100 km approach distance SO$_2$, Na, and H$_2$O would be far above the model INMS performance of 1 cm^{-3}.

Ionospheric model results, shown in Figure C.1.2-8, are expected to be within INMS detection limits, indicated by the black line. From this analysis it is apparent that an INMS could detect vapor from an active vent, sublimation from a warm region, sputter products during the degradation process, and ions that are in all of these processes.

Another important contribution from an INMS, although not a scientific priority for the

Table C.1.2-2. Calculated global-average densities of sputtered Europa surface materials at 100 km.

Species	Predicted Densities @ 100 km
Na	60–1600 cm^{-3}
CO$_2$	36–193 cm^{-3}
SO$_2$	110–600 cm^{-3}
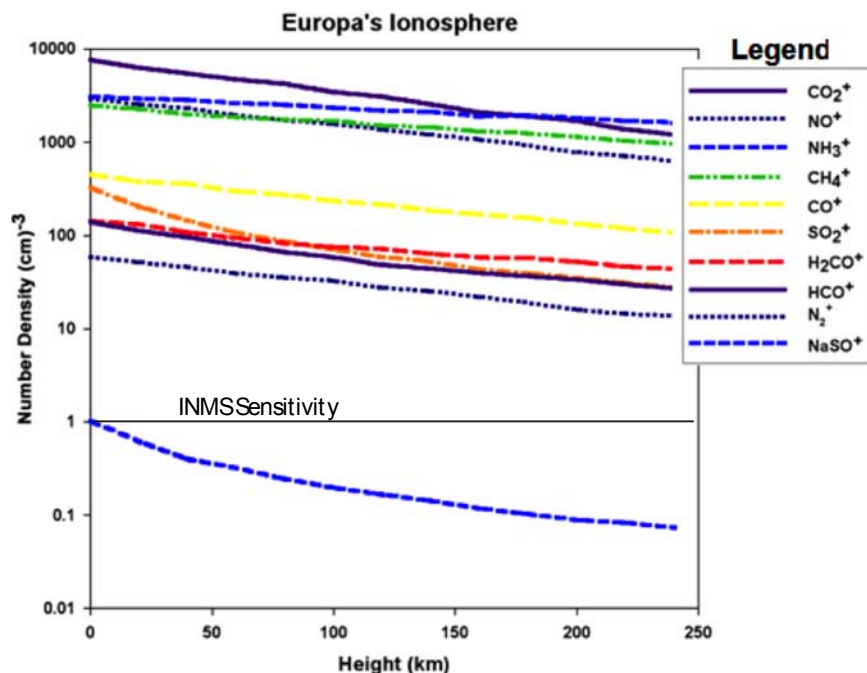
Figure C.1.2-8. Ionosphere densities vs. altitude, determined as discussed in Johnson et al. (1998) for molecules sputtered from the Europa's surface based on suggested surface materials. All densities, except those of $NaSO^+$ exceed the detection limit (1 cm^{-3}; Y-axis) of the model Ion and Neutral Mass Spectrometer.

Trace organics would also be sputtered with the ice from the surface. Based on estimates by Cassidy et al. (2009) shown in Figure C.1.2-9, these would be detectable if sputtered from materials concentrated by geological processes at the surface, such as concentration and subsequent segregation of brine and organics (e.g., Schmidt et al. 2011).

C.1.2.2.1   Investigation C.1: Characterize the composition and chemistry of the Europa ocean as expressed on the surface and in the atmosphere.

The first-priority investigation for Europa's surface composition and chemistry is to identify the surface organic and inorganic constituents, with emphasis on materials relevant to Europa's habitability, and to map their distribution and association with geologic features. The search for organic materials, including compounds with CH, CO, CC, and CN, is especially relevant to understanding Europa's potential habitability. Moreover, identifying specific salts and/or acids might constrain the composition, physical environment, and origin of Europa's ocean (Kargel et al. 2000, McKinnon and Zolensky 2003, Zolotov and Kargel 2009). Additional compounds of interest include species that could be detected at UV wavelengths, such as

current mission, would be the ability to measure isotopic ratios. Variations in the $^{17}O/^{16}O$ and $^{18}O/^{16}O$ ratios in water vapor are the most useful system for distinguishing different planetary materials (Table C.1.2-3).

For example, it has been argued that two gaseous reservoirs, one terrestrial and one ^{16}O rich, are required to explain O-isotopic variations in meteorites. The terrestrial fractionation line is due to mass fractionation of the O isotopes in terrestrial materials, and the carbonaceous chondrite fractionation line represents mixing between different components. Obtaining similar isotope information for Europa would provide important constraints on the origin of water ice in the Galilean satellites. Based on other observations in the solar system, rare isotopes of oxygen are ~10^4 less abundant than their more common counterparts, which is still within the model instrument sensitivity of 1 cm^{-3}.

Table C.1.2-3. Water vapor components, including isotopes, in Europa's atmosphere expected to be measurable by an INMS (from Cassidy et al. 2009).

Species	Mass	Expected density (cm^{-3}) at 100 km
H2	2.01	10–6
O2	31.99	4×106 to 107
O	15.9	3×104 to 105
H2O	18.0	104 to 2×105
OH	17.0	100 to 9×10^4
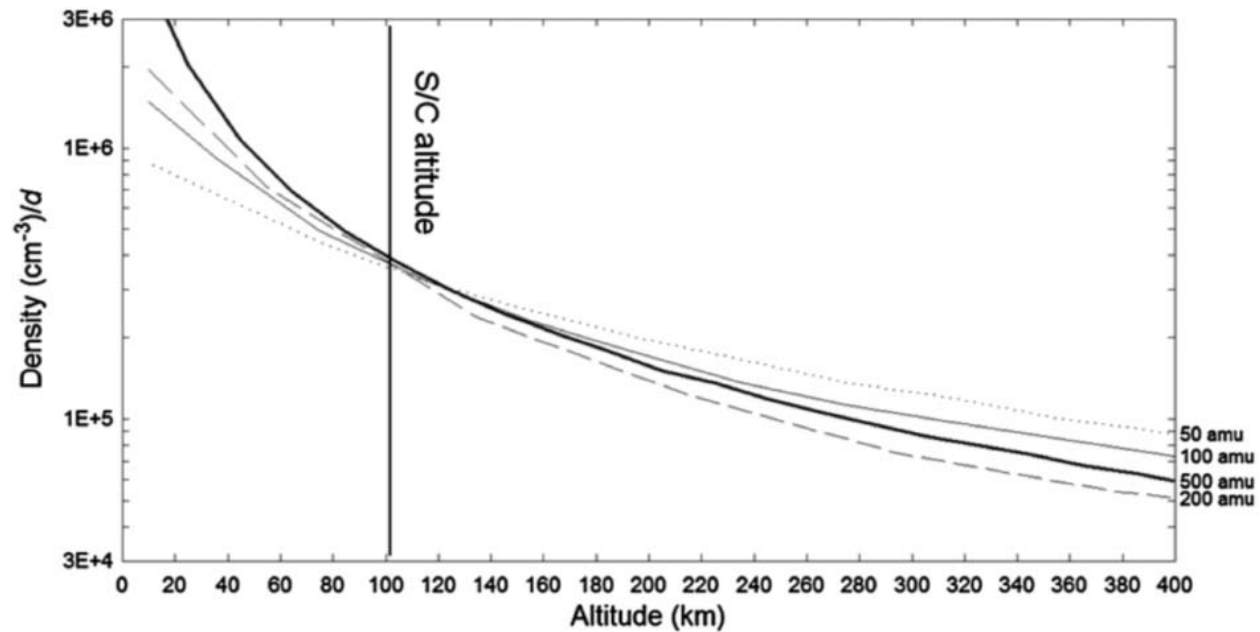
Figure C.1.2-9. Density vs. altitude for refractory molecules of different masses. The density of a given atmospheric species with a number fraction d in the surface is given by multiplying the plotted density by the number fraction, allowing estimates of minimum detectable surface concentration at the spacecraft (S/C) altitude. The different species happen to have similar densities at 100 km. From Cassidy et al. (2009).

water ice (crystalline and amorphous phases), products of irradiation (e.g., H_2O_2), compounds formed by implantation of sulfur and other ions, and other as yet unknown materials.

A spectral sampling of ~10 nm through the visible and near-IR wavelengths of 0.85 to ~2.5 μm and of ~20 nm from ~2.5 to ≥5 μm would provide the required S/N while maximizing spectral separability (Figures C.1.2-2, C.1.2-3, and C.1.2-4) (Dalton et al. 2003, Dalton 2007). Global observations (10 km/pixel) would be augmented with high-resolution observations having better than 300-m/pixel spatial resolution in order to resolve small geologic features, map compositional variations, and search for locations with distinctive compositions. High spectral resolution, coupled with high spatial resolution that could permit sampling of distinct compositional units at 100-m scales, would allow identification and quantification of the contributions of hydrated salts, sulfuric acid, sulfur polymers, CO_2, organics,

and other compounds anticipated at the surface of Europa.

INMS observations would be performed to determine the composition of sputtered products. Such measurements should be made at a mass range better than 300 daltons, with a mass resolution (m/Δm) of greater than 500, and with sensitivity better than 10 particles/cm^3. Low-altitude measurements (<100 km) are highly desirable in sampling denser portions of Europa's atmosphere.

C.1.2.2.2   Investigation C.2: Determine the role of Jupiter's radiation environment in processing materials on Europa.

In order to understand the surface composition, it is important to determine separately the effects of weathering by photons, neutral and charged particles, and micrometeoroids. In particular, radiolytic processes might alter the chemical signature over time, complicating efforts to understand the original composition of the surface. Assessing these relationships requires a detailed sampling of the surface with infrared spectroscopy, using global and

targeted observations. Efforts to separate the primary and alteration surface composition would be aided by the acquisition of high-spatial-resolution spectra on both leading and trailing hemispheres, in which younger, less altered materials might be exposed by magmatic, tectonic, or mass-wasting processes.

In addition, an INMS would provide a highly sensitive means to directly measure species sputtered off the surface, which might include organic fragments. A nonuniform atmosphere is anticipated, and its structure could be examined with INMS measurements.

C.1.2.2.3   *Investigation C.3: Characterize the chemical and compositional pathways in Europa's Ocean.*

In order to relate composition to geological processes, especially material exchange with the interior, composition interpretations need to be considered in the context of geophysical and morphological measurements. The suite of observation types discussed above provides a means to understand the three-dimensional structure of the near-surface crust and its relation to surface material units and processes of exchange between the interior and the surface. Specifically, compositional maps should be compared to detections of subsurface dielectric horizons obtained using Ice-Penetrating Radar, and to morphology and topography derived from stereo imaging. In addition, understanding tectonic and volcanic processes as manifested in structures and outcrops and their relation to surface materials will lead to a greater understanding of interactions between the ocean and the surface.

The key outstanding questions relating to Europa composition can be addressed by the Objective C investigations described above, as summarized in Table C.1.2-4.

C.1.2.3   Europa's Geology

Europa's landforms are enigmatic, and a wide variety of hypotheses have been offered for their formation. Characterization of sites of most recent geological activity is especially significant for understanding the formation of surface features, including whether and how liquid water is involved in their formation. Moreover, the formation processes of surface landforms is important to how material is transported between the surface and the subsurface, and thus to whether and how surface oxidants could be transported to the ocean, providing chemical energy for life. In these ways, geology is directly pertinent to the potential habitability of Europa.

C.1.2.3.1   *Investigation G.1: Determine sites of most recent geological activity, and characterize localities of high science interest.*

Europa's incessant tidal activity leads to speculation that some landforms might be actively forming today and are the most likely locations for near-surface liquid (see Section C.1.2.1). The most promising regions for current activity are regions of chaos in which thermally or compositionally buoyant diapirs rise to the surface, or cracks that have recently formed in response to tidal stresses. Low-albedo smooth plains associated with some chaotic terrains might be composed of subsurface materials, such as brines, that have been emplaced onto the surface (Collins and Nimmo 2009, Schmidt et al. 2011). These

Table C.1.2-4. Hypothesis tests to address selected key questions regarding Europa's composition.

	Example Hypothesis Questions	Example Hypothesis Tests
C.1	Are there endogenic organic materials on Europa's surface?	Examine surface and sputtered materials for absorptions and masses consistent with organic materials, and correlate distributions to likely endogenic materials.
C.2	Is irradiation the principal cause of alteration of Europa's surface materials through time?	Determine the suite of compounds observable on Europa's surface, correlating to the local radiation environment and to the relative age of associated surface features.
C.3	Is chemical material from depth carried to the surface?	Determine whether hydrates and other minerals that might be indicative of a subsurface ocean are concentrated in specific geologic features, and correlate with evidence for subsurface liquid water at these locations.

plains might therefore represent sites of high scientific interest. Recently or currently active regions are expected to best illustrate the processes involved in the formation of some surface structures, showing pristine morphologies and distinct geologic relationships, and perhaps exhibiting associated plume activity such as that seen on Enceladus.

Determining the relative ages of Europa's surface features allows the evolution of the surface to be unraveled. Indication of relative age comes from the stratigraphy, derived from crosscutting and embayment relationships, and the relative density of small impact craters. These relationships enable a history to be assembled within local regions, for global extrapolation.

Of primary importance is the detailed characterization of surface features—especially their distribution, morphologies, and topography—at local to regional scales, to understand the processes by which they formed. Galileo images demonstrate that high-resolution data of a few tens of pixels is excellent for investigating the detailed formation and evolution of surface features such as bands, ridges, chaos, and impact features. Yet less than 0.05% of the surface was imaged at scales of 50 m/pixel or better, leading to only tantalizing and ambiguous glimpses of how these features formed (e.g., Figure C.1.2-2). Stereo imaging of the surface was extremely scarce, but the topographic models derived from it have contributed greatly to understanding how Europa's surface features formed. For example, digital terrain models (DTMs) of chaos regions suggest that these regions form from diapiric upwelling of material from below (e.g., Schenk and Pappalardo 2004, Prockter and Schenk 2005, Collins and Nimmo 2009), aided by brines in the subsurface (Schmidt et al. 2011). High-resolution Galileo images of Europa (Figure C.1.2-10) show abundant evidence for very young materials exposed by mass wasting of faces and scarps (Sullivan et al. 1999).
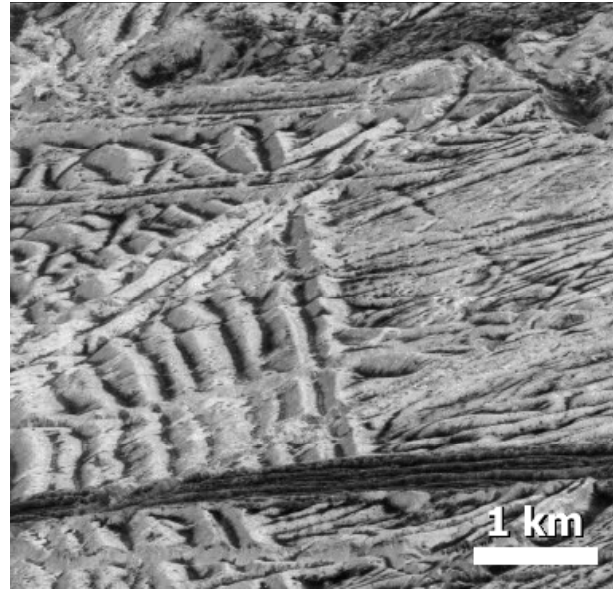
Figure C.1.2-10. Galileo Solid-State Imager image of ridged plains on Europa at 6 m/pixel horizontal resolution. The lineae in the central portion of the image have central troughs with deposits of dark material ~100 m wide, but with bright, presumably icy ridges and walls close by.

These postformational modification processes have likely affected many surfaces, potentially exposing fresh materials that are less altered than their surroundings. Topographical imaging of different feature types at several locations distributed across Europa's surface would allow detailed characterization of sites of high scientific interest, and would enable evaluation of sites of expected current or recent activity. Topographical mapping through stereo images acquired at regional scales can permit construction of digital elevation models with vertical resolution of ~10 m and horizontal resolution of 50 m, which would greatly aid morphologic characterization and geological interpretation of all known feature types on Europa. Images that are correlated with subsurface sounding measurements would allow the subsurface structure of geological landforms to be related to their surface expression, and the third dimension of these features to be fully characterized for the first time. Models of topography will also aid in the interpretation of compositional data.

Table C.1.2-5. Hypothesis test to address selected key questions regarding Europa's geology.

	Example Hypothesis Question	Example Hypothesis Test
G.1	Where are the youngest regions on Europa and how old are they?	Use stereo imaging and sputter measurements to determine the freshest, uncompensated surfaces, and potential locations of plumes.

The key outstanding questions relating to Europa geology (Table C.1.2-5) can be addressed by the Objective G investigation described above, as summarized in FO C-1.

C.1.3   Science Instrument Complement

The Europa Multiple-Flyby Mission focuses on measurements that can be taken over multiple flybys.

C.1.3.1   Mission Goal Relation to Core Measurements and Instrumentation

The overarching goal of the flyby mission would be to determine the habitability of Europa. As such, the recommended scientific measurements and scientific payload follow objectives (Section C.1.1) of characterizing the ice shell and any subsurface water (including the distribution of subsurface water and searching for an ice-ocean interface), understanding ocean habitability though composition and chemistry (as expressed on the surface and in the atmosphere), and addressing the surface geology (geological history and processes, including high science interest localities). In this way, the payload links tightly with the three science themes that relate to Water, Chemistry, and Energy. Particular to Europa, the presence of a subsurface ocean, the overall structure and thickness of the ice shell and the exchange of material between the subsurface (ice shell and ocean) and the surface layer over time, followed by the physical evolution of the surface, leads to a complex story of Europa habitability. Unraveling this story requires an integrated package of instruments that work ideally and effectively in coordination. The Flyby Mission offers unique abilities to observe the surface and address the goal of understanding Europa's habitability.

The recommended science measurements and payload utilize the strengths of each archetypal

instrument and technique to address key questions:

- Where is there subsurface water within Europa, and what are the mechanisms of surface-ice ocean exchange?
- What does surface composition and chemistry imply about the habitability of Europa's ocean?
- How do Europa's surface features form, and what are the characteristics of sites of recent or current activity?

C.1.3.2   Integration of Instrument Categories

Coordination and integration of observations and measurements acquired by different instruments is central to determining Europa's habitability. Spatially or temporally coordinated observations greatly enhance the scientific value of the mission. For example, obtaining clear insight into processes of material exchange at Europa requires various types of measurements working in concert. Understanding composition benefits from measuring chemical clues from both the surface and atmosphere. We can learn the most about the potentially active surface regions through complementary imaging and atmospheric analyses. In this way the suite of instruments integrates to address the broader questions of habitability in a way that cannot be accomplished by any instrument alone.

C.1.3.3   Instrument Payload

The choice of instruments for the scientific payload is driven by the need for specific types of measurements that trace from the overarching goal of Europa's habitability, as detailed in the Europa Multiple-Flyby Mission traceability matrix (FO C-1). These measurements are designed to focus on characterization of the Chemistry and Energy themes for Europa, but they also do an excellent job in addressing Water within Europa. These fundamental

Table C.1.3-1. Baseline and floor scientific instruments of the model payload. INMS (shaded) is additional to floor.

Model Instrument	Key Science Investigations and Measurements
Ice-Penetrating Radar (IPR)	Sounding of subsurface dielectric horizons to probe for water.
Shortwave Infrared Spectrometer (SWIRS)	Surface composition and chemistry through reflection spectroscopy.
Topographical Imager (TI)	Landform characterization and stereo topography.
Ion and Neutral Mass Spectrometer (INMS)	Atmospheric composition and chemistry through mass spectrometry.

measurements drive the recommendation of model instruments. These concentrate on remote sensing (Ice-Penetrating Radar, infrared spectroscopy, and high-resolution stereo imaging) along with in situ measurement of the atmospheric composition (by means of an ion and neutral mass spectrometer).

The baseline model payload of instruments is divided into three principal categories, as summarized in Table C.1.3-1. The first category, defining the science floor (unshaded in Table C.1.3-1), consists of those instruments fundamental to the mission objectives, without which the mission is not worth flying. The second category consists of a single additional scientific instrument which would greatly contribute to the scientific return of the mission, and thus is included in the baseline model payload, but which is not considered part of the floor payload: it could be descoped from the model payload if not accommodatable (shaded in Table C.1.3-1).

These model instruments work in concert to fully realize the value of data collected. For example, The Ice-Penetrating Radar (IPR) would be used to sound dielectric horizons within Europa's ice shell to search for liquid water. Simultaneously, the Topographical Imager (TI) would obtain stereo images that put the IPR observations into geological context and which provide topographic information necessary to process the IPR data. The Shortwave Infrared Spectrometer (SWIRS) and Ion and Neutral Mass Spectrometer (INMS) would work together in complemen-

tary ways to determine composition and chemistry through surface (SWIRS) and atmospheric (INMS) measurements. The Topographical Imager (TI) could be used to identify areas that are geologically young or active through stratigraphic relationships and by searching for surface changes, while the INMS could be used to search for unusual density and composition of the atmospheric components that might indicate currently active plumes. The combined investigations achievable from a Flyby Mission would fundamentally advance the state of knowledge and understanding of the habitability of Europa.

C.1.3.4   Potential Europa Ocean Science from a Flyby Mission

Three additional instruments were considered by the SDT as potentially attractive to enhance the scientific return of a Europa Multiple-Flyby Mission by addressing ocean science (Table C.1.3-2). However, these were not included in the baseline model payload because the Orbiter Mission would be the more appropriate platform for the associated measurements. If a Flyby Mission were chosen for Europa, then these valuable instruments might be considered in developing the optimal payload for a Flyby mission, to address a portion of the ocean science.

The science of the Europa Orbiter Mission concept (Section B) includes investigation of the deep interior structure of Europa by examining changes in the gravitational and magnetic fields of Europa, which are induced by rotational and orbital motions of Europa about Ju-

Table C.1.3-2. Potential enhanced instruments, not included in baseline model payload.

Model Instrument	Key Science Investigations and Measurements
Radio Subsystem (RS)	Gravitational tides and static gravity field to detect an interior ocean.
Magnetometer (MAG)	Magnetic measurements to derive ocean thickness and bulk salinity.
Langmuir Probe (LP)	Plasma correction for magnetic measurements.

piter. In both cases, the imposed fields (gravitational or magnetic) are well known, and the phase and amplitude of the response are diagnostic of Europa's internal structure. In the Orbiter Mission design, the spacecraft would be in a (nearly) circular and (nearly) polar orbit, and would make essentially continuous measurements of the magnetic and gravitational fields. In both cases, it is anticipated that these fields have static and time-dependent components. The primary interest here is in the time-dependent parts of the fields, as they are more diagnostic of deep interior structure. As an orbiting spacecraft moves through a gravitational or magnetic field of a body like Europa, the signal at the spacecraft will have time variations, even if the body-fixed field is constant. Separating the static and temporally varying components of the fields requires sufficient spatial and temporal coverage for the measurements, to recover a reasonably high fidelity spherical harmonic model.

Conducting similar investigations from the Flyby Mission can be done, but it places constraints on the encounter geometry. First we consider the gravitational investigation. The principal cause of time variations in the gravitational field is that Europa moving around Jupiter in a slightly eccentric orbit. As a result, the gravitational field of Jupiter, at the position of Europa, varies with orbital position. The deformation of Europa by the imposed tidal potential from Jupiter produces an additional gravitation potential with the same spatio-temporal pattern as the imposed field. The scaling factor, which relates the induced field to the imposed field, is known as the tidal Love number. It is large for a fluid body and small for an elastic solid. The desire is to determine the tidal Love number accurately enough to test the hypothesis of a global internal ocean, through precise measurements of the Doppler shift of the spacecraft's Radio Subsystem.

In order to measure the tidal changes in Europa's gravitational field, the flyby encounter geometry needs to allow one or more locations on Europa to be visited repeatedly, at different phases of Europa's motion around Jupiter. That is largely because the tidal-induced changes in gravity are small compared to the static gravity field spatial variations. A recent analysis (Park et al. 2011) has shown that an orbit tour with three dozen Europa encounters can yield uncertainties in the degree-2 tidal Love number of 0.045 for X-band radio tracking data, and 0.009 for Ka-band. The latter value is sufficient to infer the presence of an ocean. The implication for a Europa Multiple-Flyby Mission, to meet this level of performance would be: use of Ka-band tracking, and having a steerable antenna, so that Doppler tracking can be performed during times of Europa close approach.

The magnetic induction experiment aims to characterize the salinity and thickness of Europa's ocean by measuring the induction signature of Europa at multiple frequencies. Similar to the tidal gravity experiment, determining magnetic induction requires repeat measurements at the same location on Europa, at different times in Europa's orbit around Jupiter. The magnitude and phase of the induced magnetic field are related to those of the imposed field, and the relationship between them is a measure of electrical conductivity variations within the interior. A salty water ocean would have a very different conductivity than ice or silicate rock (Khurana et al. 1998).

A major difference between the gravity and magnetic induction experiments is that the magnetometer measures the vector field, whereas the Doppler shift in gravity tracking data only delivers the projection of the spacecraft velocity onto the line-of-site to Earth. Another difference is that the magnetic field at Europa has a more complex temporal variation. There is an effect due to Europa's orbital motion around Jupiter (85.2 hour period) and another due to Jupiter's rotation (11.2 hour period), among others. A partially compensating difference from tidal gravity is that any

permanent magnetic dipole field of Europa is expected to be small compared to the time-varying induced field, so there is not magnetic requirement on sampling the same location at different phases of the forcing periods.

We have not performed detailed simulations of magnetic induction experiments at Europa from a flyby geometry, but it seems that similarity in measurement requirements to the tidal gravity investigation suggests that it could potentially be done. The implications for the mission would be to carry a magnetometer deployed on a boom, to include a Langmuir probe or plasma instrument to permit corrections of plasma effects, and to reasonably control magnetic cleanliness of the spacecraft.

The ability to resolve tidal gravity and magnetic induction effects increase significantly with increasing number of flyby encounters. The actual increase in knowledge, per flyby, is a complicated function of the tempo and spatial pattern of encounters.

A currently unresolved challenge is how to accommodate the spatiotemporal sampling requirements of tidal gravity, magnetic induction, and the remote sensing investigations of the flyby spacecraft.

C.2   Multiple-Flyby Mission Concept

C.2.1   Mission Overview

The Multiple-Flyby Mission deploys a robust spacecraft with four science instruments into the Jovian system to perform repeated close flybys of Europa.

C.2.1.1   Flyby Study Scope and Driving Requirements

The purpose of the 2011 Europa Multiple-Flyby Mission study was to determine the existence of a feasible, cost effective, scientifically compelling mission concept. In order to be determined feasible, the mission had to have the following qualities:

- Accommodate the measurements and model payload elements delineated in the Science Traceability Matrix.

- Launch in the 2018-2024 timeframe w/ annual backup opportunities
- Use existing Atlas V 551 launch vehicle capability or smaller
- Utilize ASRGs (no limit on number, but strong desire to minimize ^{238}Pu usage)
- Mission Duration < 10 years, launch to EOM
- Use existing aerospace 300-krad radiation hardened parts
- Optimize design for cost (looking for the lowest cost possible while achieving baseline science)
- Maintain robust technical margins to support cost commitment

The study team's strategy in investigating this concept was to develop a well-defined, well-documented architecture description early in the mission life cycle. From that architecture space, lighter, more compact design solutions were favored to reduce shielding and overall system mass. Hardware procurement, implementation, and integration were simplified by using a modular design. Mission operation costs were reduced through best practice system robustness and fault tolerance capabilities to allow for extended periods of minimally monitored operations during the long interplanetary cruise and through repetitive operation for Europa science. Radiation dose at the part level was reduced to currently existing aerospace part tolerances. Specifically, the part total dose was reduced to levels demonstrated by geosynchronous and medium earth orbit satellites components.

These strategies, together, contribute to an overall reduction in mission cost while maintaining a compelling, high reliability mission.

C.2.1.2   Flyby Mission Concept Overview

The flyby mission concept centers around deploying a spacecraft into the Jovian system to perform repeated close flybys of the Jovian moon Europa to collect information on ice shell thickness, composition, and surface geo-

morphology. The science payload consists of four instruments: a Shortwave Infrared Spectrometer (SWIRS), an Ice-Penetrating Radar (IPR), a Topographical Imager (TI), and an Ion and Neutral Mass Spectrometer (INMS). Except for calibration and maintenance, these instruments are operated only during Europa flybys.

The nominal flyby mission performs 32 flybys of Europa at altitudes varying from 2700 km to 25 km. In the course of performing these flybys, the mission would also fly by the Jovian moons Ganymede and Callisto, although these flybys are solely to shape the orbit and are not driving science priorities.

The nominal Flyby mission launches from Cape Canaveral Air Force Station in November 2021 and spend 6.5 years traveling in solar orbit to Jupiter. During this time, the mission performs gravity assist flybys, first of Venus and then two of Earth, before swinging out to Jupiter. All terrestrial body flybys have a closest approach altitude greater than 500 km.

Jupiter orbit insertion would occur in April 2028 when the vehicle performs a nearly 2-hour main engine burn to impart a 900 m/s velocity change on the spacecraft. This maneuver places the spacecraft in an initial 200-day Jovian orbit. An additional burn at apojove raises the perijove altitude. The spacecraft then performs four Ganymede flybys over the course of three months to reduce orbital energy and align the trajectory with Europa.

The Europa flyby campaign is comprised of four segments each designed to provide good coverage of a wide region on Europa with consistent lighting conditions. The first segment concentrates on the anti-Jovian hemisphere with seven flybys (Europa is tidally locked with Jupiter, so the side of the moon that faces toward or "sub-Jovian" and away or "anti-Jovian" never changes). Flyby closest approach altitudes range from 730 km to 25 km and cover latitudes from 80N to 80S.

During each flyby, a preset sequence of science observations would be executed. For any given flyby, the science team will have the opportunity to adjust some targeting and instrument performance parameters in advance, but the bulk of the sequence will execute unchanged for all Europa flybys. At approximately 60,000 km, the SWIRS instrument will begin a low-resolution global scan. This scanning is done via a "nodding" spacecraft pointing profile that is repeated for each encounter. At 2,000 km, the SWIRS instrument will switch to a targeted high-resolution scan mode. During these high-resolution scans the spacecraft is nadir-pointed. At 1,000 km the IPR, TI, and INMS power up, stabilize and perform calibration activities. The IP pass occurs from 400-km inbound altitude to 400-km outbound altitude during which TI and INMS data are acquired continuously. The spacecraft is nadir-pointed and the INMS is aligned near the ram direction. The SWIRS instrument, passive during the ±400 km closest approach, then conducts additional high- and low-resolution scans as the spacecraft moves away from Europa.

The Europa flyby campaign continues through three more segments, the second also concentrating on the anti-Jovian side of Europa under different lighting conditions, and providing calibrating cross tracks for better interpretation of IPR data. The third and fourth segments concentrate on the sub-Jovian hemisphere providing comprehensive coverage of the other half of the moon.

Once the nominal mission has been completed, depending on consumable reserves and system reliability assessments, the flyby mission could continue to execute Europa flybys during an extended mission. However, the intent in this concept is to decommission the spacecraft via targeted Ganymede impact before consumable resources are fully depleted or system robustness has been compromised by radiation exposure.

C.2.1.3   Flyby Mission Elements

The flyby mission system would be composed of a flight system and a ground system. The ground system is responsible for planning, testing, transmitting, and monitoring all command sequences executed by the flight system, collecting and distributing the acquired science observation data, monitoring the flight systems health, and planning and executing any anomaly recovery activities required to maintain system health and mission robustness.

The flight system is composed of a modularly designed spacecraft with a vertical stack of three main modules: Avionics, Propulsion, and Power Source.

The Avionics Module hosts the bulk of the flight systems powered elements including the central computers, power conditioning and distribution electronics, radios, and mass memory. These units are housed in a vault structure that provides significant radiation shielding. The Upper Equipment Section (UES) of the Avionics Module hosts the batteries, reaction wheels, star-trackers as well as all of the science payload elements. Sensitive payload electronics are housed in a separate vault in the UES to increase flexibility during integration and test.

The Propulsion Module supports the fuel, oxidizer, and pressurant tanks, as well as the pressurant control assembly panel and the propellant isolation assembly panel. Four thruster clusters supported by tripod booms at the base of the Propulsion Module each contain four 1-lb reaction control system thrusters and one 20-lb thrust vector control thruster. The main engine is mounted to a baseplate suspended from the bottom of the Propulsion Module main structure.

The Power Source Module is composed of a ring and four vibration isolation systems, which each support an Advanced Stirling Radioisotope Generator (ASRG). The control units for the ASRGs are mounted directly to the Power Source Module's main ring struc-

ture. The launch vehicle adapter sits at the base of the Power Source Module's primary ring structure.

C.2.1.4   Flyby Mission Architecture Overview

Architecturally, the flight system's modular design offers several advantages and efficiencies. First, the Avionics Module is designed to place radiation sensitive components in a central vault structure. Centralization of sensitive components takes advantage of significant self-shielding benefits that are further enhanced by the vault structure. Late in the integration flow, the Avionics Module is stacked onto the Propulsion Module placing the avionics vault in the core of the spacecraft; surrounded on all sides by the Propulsion Module's structure and propellant tanks (the propellant itself does not provide significant additional shielding, since most of it expended during JOI and PJR). In this way, dedicated, single purpose radiation shielding mass is minimized while still providing an internal vault radiation environment comparable to the doses received by the electronics of geosynchronous satellites after a 20-year mission.

Additionally, the central vault avionics configuration allows waste avionics heat to be applied directly to warming the propellant. This configuration is so efficient that preliminary analysis indicates supplemental electrical heaters will not need to be used on the propellant tanks. There is sufficient heat collected from the avionics to keep the propellant above 15°C for the life of the mission.

Finally, the modular design allows for a flexible procurement, integration, and testing strategy, where each module is assembled and tested separately with schedule margin. Delays or problems on one module do not perturb the testing schedules of the other modules.

C.2.2   Model Payload

Proof of concept payload demonstrates feasibility of obtaining compelling science.

C.2.2.1   Payload

Instrument concepts and techniques that meet the mission objectives will be selected via NASA's Announcement of Opportunity (AO) process. Notional instruments and instrument capabilities presented within this report are not meant to prejudge AO solicitation outcome. Rather, this Europa Multiple-Flyby Mission model payload is used to deduce suitable engineering aspects of the mission and spacecraft design concept, including operational scenarios that could obtain the data necessary to meet the science objectives.

In addition, model payload instruments were defined well enough to demonstrate a plausible approach to meeting the measurement objectives, performing in the radiation environment, and meeting the planetary protection requirements. Therefore, instrument descriptions are provided here only to show proof of concept. Heritage or similarities discussed here refer only to instrument techniques and basic design approaches, and do not imply that specific implementations are fully viable in their detail. Physical and electrical modifications of any previous instrument designs would be necessary for them to function within the unique environmental context of this mission. Such

modifications are allowed for in the resource estimates. Instrument mass estimates assume performance only from currently available detectors.

The model payload selected for the Europa Multiple-Flyby Mission consists of a set of remote-sensing instruments and an *in situ* instrument. Instrument representatives on the Science Definition Team (SDT) (or identified by SDT members) were consulted extensively to understand the drivers for each notional instrument. Table C.2.2-1 presents the estimated resource demands of each instrument and for the total planning payload; Table C.2.2-2 summarizes the instruments and their capabilities. A more detailed mass estimate for each instrument is included in the Master Equipment List (MEL) (Section C.4.3) as input for the NASA Instrument Cost Model (NICM).

C.2.2.1.1   Payload Accommodation

All of the remote-sensing instruments in the model payload point in the nadir direction when flying by Europa, as shown in Figure C.2.2-1. Because the SDT analysis indicates that nominal nadir (or near-nadir) pointing of the remote-sensing instruments meets the science objectives, no spacecraft-provided scan platform is baselined. Individual instruments that need rapid scan systems for target tracking or target motion compensation are assumed to provide such a system as an inte-

Table C.2.2-1. Europa Multiple-Flyby Mission model payload resource characteristics.

Instrument	Acronym	Unshielded Mass (kg)	Shielding Mass (kg)	Total Mass (kg)	Operating Power (W)	Data Volume (Gb)/flyby	Telemetry Interface	Pointing
Ice-Penetrating Radar	IPR	28.0	5.0	33.0	55	25.2	SpaceWire	Nadir
Shortwave Infrared Spectrometer	SWIRS	11.6	9.1	20.7	19.1	1.3	SpaceWire	Nadir ± 45°
Ion and Neutral Mass Spectrometer	INMS	14.0	10.1	24.1	32.5	.002	SpaceWire	Ram
Topographical Imager	TI	2.5	4.5	7.0	5.9	3.1	SpaceWire	Nadir
TOTAL ALL INSTRUMENTS		**56.1**	**28.7**	**84.8**	**112.5**	**29.6**		
TOTAL ALL INSTRUMENTS + 30% contingency				**110.2**	**146.3**			

Table C.2.2-2. Europa Multiple-Flyby Mission model payload resource characteristics and accommodations.

Instrument	Characteristics	Similar Instruments	
Ice-Penetrating Radar (IPR)	**Dual-Mode Radar Sounder** **Shallow Mode**: 60 MHz with 10-MHz bandwidth **Vertical Depth:** ~3 km **Vertical Resolution:** 10 m **Deep Mode:** 9 MHz with 1-MHz bandwidth **Vertical Depth:** ~30 km **Vertical Resolution:** 100 m	Mars Express Mars Advanced Radar for Subsurface and Ionosphere Sounding (MARSIS) MRO Shallow Radar (SHARAD)	
Shortwave Infrared Spectrometer (SWIRS)	**Pushbroom Spectrometer** **Detector:** HgCdTe **Spectral Range:** 850 nm–5 μm **Spectral Resolution:** 10 nm **Spatial Resolution:** 300 m @ 2000 km **FOV:** 4.2 deg cross-track **IFOV:** 150 μrad	Chandrayaan Moon Mineralogy Mapper (M3)	
Ion and Neutral Mass Spectrometer (INMS)	**Reflectron Time-of-Flight Mass Spectrometer** **Mass Range:** 1 to 300 daltons **Mass Resolution:** >500 (m/Δm) **Sensitivity:** 10 particles/cm^3 **FOV:** 60 degrees	Rosetta Rosetta Orbiter Spectrometer for Ion and Neutral Analysis (ROSINA) reflectron time-of-flight (RTOF) spectrometer Cassini Ion and Neutral Mass Spectrometer (INMS)	
Topographical Imager (TI)	**Panchromatic Stereo Pushbroom Imager** **Detector:** CMOS or CCD line arrays **Detector size:** 4096 pixels wide **Spatial Resolution:** 25 m from 100 km (@ C/A) **FOV:** 58 deg **IFOV:** 250 μrad	MRO Mars Color Imager (MARCI) MESSENGER Mercury Dual Imaging System (MDIS) New Horizons Multi-spectral Visible Imaging Camera (MVIC)	

gral part of the instrument. Presently, for instance, one instrument in the model payload, the SWIRS, uses an along-track scan mirror in order to perform target motion compensation to increase the signal to noise. Slower scanning is accommodated by the spacecraft. For instance, the spacecraft will perform slewing at long range from Europa in order for the SWIRS to perform global low-resolution mapping.
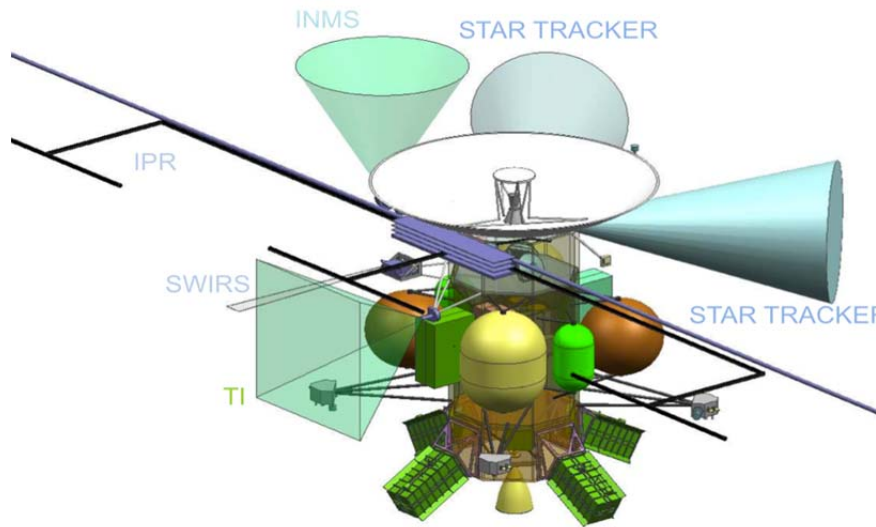
Figure C.2.2-1. Notional model payload accommodation and fields of view.

The Europa Multiple-Flyby Mission data acquisition strategy involves rapid data collection into onboard storage over a short period of time (a few hours) near each flyby, followed by an extended period (many days), during which the data are downlinked to the ground. The capacity of the spacecraft solid-state recorder (SSR) (see Section C.2.4.1.3) is sized to accommodate the expected data volume from each flyby (see Table C.2.2-1) plus contingency. All of the instruments, other than IPR, perform data compression before sending the data to the SSR. IPR, with the highest instantaneous data rate, records raw data on the SSR, which is subsequently reduced before downlink. The notional model payload approach is to assume the data system architecture with SpaceWire interfaces baselined for all of the instruments.

The instrument electronics are currently baselined to be accommodated with each instrument, shielded separately. However, the spacecraft concept accommodates an additional science chassis that can house all of the payload electronics, as well as perform some of the data reduction for IPR. This approach results in a conservative mass estimate, adding further margin in radiation shielding. Further trades need to be conducted on the benefits of a separate science chassis and its functionality. Since the presented model payload is notional, the payload trade will be re-evaluated once the flight instruments are selected.

Adequate mounting area is available for the remote-sensing instruments on nadir-facing areas of the UES (see Figure C.2.2-1). Moreover, the Topographical Imager (TI) and SWIRS are mounted on brackets to ensure clear fields of regard for both instruments. The *in situ* instrument, the Ion and Neutral Mass Spectrometer (INMS), is pointing in the ram direction and is located next to the high-gain antenna (HGA). Note that the HGA is placed well clear of the INMS wide field of view. Instrument mounting and accommodation needs are summarized in Table C.2.2-1.

The science payload is expected to contain instruments with detectors requiring cooling to as low as 80 K for proper operation while dissipating perhaps 300 mW of heat. Cooling to this level would be accomplished via passive radiators, mounted so their view is directed away from the Sun and away from Europa to the extent necessary.

The remote-sensing instruments require spacecraft pointing control to better than or equal to 1 mrad, stability to 30 µrad/s, and reconstruction to 0.15 mrad. Pointing performance is driven by SWIRS, which has a 150 µrad pixel field of view and requires exposure times of up to 1 s, enabled by use of a scan mirror.

C.2.2.1.2   *Radiation and Planetary Protection*

The severe radiation environment at Europa presents significant challenges for the science instruments, as does the need to meet the planetary protection requirements outlined in Sec-

tion C.2.6.2. Payload radiation challenges have been addressed through a combination of generous shielding and radiation-hardened parts, while also identifying viable candidate technologies, such as detectors (as discussed below), for the notional instruments.

Detector Working Group

A thorough study of both radiation effects and the impact of planetary protection protocols on detectors were conducted for the 2008 Jupiter Europa Orbiter (JEO) study by a Detector Working Group (DWG) (Boldt et al. 2008). The DWG developed a methodology for determining the required radiation shielding for successful instrument operation in the transient radiation environment at Europa, assessed degradation of detectors due to total ionizing dose and displacement damage effects, and assessed the compatibility of candidate detectors with the planetary protection protocols. Because the radiation and planetary protection challenges for a Europa Multiple-Flyby Mission would be quite similar in nature and magnitude to those of JEO, the DWG conclusions apply here as well without alteration.

The DWG concluded that the radiation and planetary protection challenges facing the model payload for a Europa mission are well understood. The question of detector survivability and science data quality was not considered to be a significant risk, provided appropriate shielding is allocated to reduce cumulative total ionizing dose (TID), displacement damage dose (DDD), and instantaneous electron and proton flux at the detector.. Specific activities have been identified to support early education of potential instrument providers in the complexity of meeting radiation and planetary protection requirements. A series of instrument workshops was also completed as part of the Europa Study. The Flyby Mission instrument detectors are a subset of those studied by the JEO DWG.

Payload Shielding Architecture

The mission radiation design point for the Flyby Mission is 2.01 Mrad behind an equivalent of 100 mil of aluminum shielding, as shown in Section C.2.3. Designs are required to tolerate twice this (a radiation design factor [RDF] of 2). Therefore, sensors and supporting electronics require significant radiation shielding. The most mass-efficient approach to providing radiation shielding is to centrally locate as much of the instrument electronics as possible deep in the interior of the spacecraft, minimizing the electronics that must be co-located with the sensor portion of the instrument. Besides utilizing a structurally nested configuration that exploits surrounding passive mass (such as propellant tanks) for self-shielding, this approach uses the large mass margins available from the flyby concept to maximize dedicated radiation shielding as well, thus providing a large reduction in radiation dose to the electronics.

Planetary Protection Protocols

The approach to planetary protection compliance for the Europa Multiple-Flyby Mission concept is presented in full in Section C.2.6.2 and can be summarized as follows:

- In-flight microbial reduction of exterior elements via radiation prior to completion of the orbit energy pump-down phase
- Prelaunch microbial reduction to control the bioburden for areas not irradiated in flight

The preferred prelaunch method is dry heat microbial reduction (DHMR). Our plan is to perform DHMR on the entire spacecraft upon completion of assembly. Current planetary protection protocols include a time vs. temperature profile ranging from 125°C for 5 hours to 110°C for 50 hours.

Planetary protection guidelines would be generated and disseminated to potential instrument providers early, allowing providers to adequately address planetary protection issues

during the instrument selection and design process. A mid-Phase B Payload Planetary Protection Review is baselined so that issues and mitigation strategies can be identified and addressed. Instrument-specific planetary protection concerns are addressed in subsequent sections. The Flyby Mission would dispose of the spacecraft at Ganymede. During Phase A and B the potential of following a Juno-like planetary protection approach would be explored, with the objective of showing that the probability of successfully disposing on Ganymede meets NASA requirements without DHMR.

C.2.2.2   Model Instrument Descriptions

C.2.2.2.1   *Ice-Penetrating Radar*

The notional Ice-Penetrating Radar (IPR) is a dual-frequency sounder (nominally 9 MHz with 1-MHz bandwidth, and 60 MHz with 10-MHz bandwidth). The higher-frequency band is designed to provide high spatial resolution (footprint and depth) for studying the subsurface above 3-km depth at high (10-m) vertical resolution. The low-frequency band, which can penetrate much deeper, is designed to search for the ice/ocean interface on Europa or the hypothesized transition between brittle and ductile ice in the deep subsurface at a depth of up to 30 km (and a vertical resolution of 100 m). This band mitigates the risks posed by the unknown subsurface structure, both in terms of unknown attenuation due to volumetric scattering in the shallow subsurface and thermal/compositional boundaries that may be characterized by brine pockets. Additionally, the low-frequency band is less affected by surface roughness, which can attenuate the reflected echo and add clutter noise.

Because the low-frequency band is vulnerable to Jupiter noise when operating on the sub-Jovian side of the moon, it is necessary to increase the radiated power as compared with spaceflight hardware currently deployed for subsurface studies of Mars. Jupiter noise should not impair radar performance on the anti-Jovian side of Europa. It should also be

noted that Jupiter noise is expected to be intermittent, even on the sub-Jovian side.

The IPR is similar to the Mars Advanced Radar for Subsurface and Ionosphere Sounding (MARSIS) instrument on Mars Express and the Shallow Radar (SHARAD) instrument on the Mars Reconnaissance Orbiter (MRO). The notional Ice-Penetrating Radar baselined for Europa Multiple-Flyby Mission is tailored to satisfy the science requirements identified in Section C.1. It requires simultaneous cross-track surface topography coverage of the radar swath via stereo imaging from the TI in order to support data interpretation through modeling of off-nadir signal clutter. The Europa Multiple-Flyby Mission design concept provides sufficient flybys to meet the requirements for globally distributed intersecting and adjacent swaths at <400 km altitude.

Instrument Description

The notional IPR uses a dual antenna system with a nadir-pointed 60-MHz dipole array, and a backing element that also serves as a dipole antenna for the 9-MHz system. Because this instrument is a depth sounder operating at relatively low frequencies and using a dipole antenna, the FOV is very wide and there are no strict pointing requirements. A 15-m dipole similar to those used by MARSIS and SHARAD is baselined (shown deployed in Figure C.2.2-1, and stowed in Table C.2.2-2). Deployment releases the folded antenna elements in the nadir direction and is planned for early in the mission.

A conceptual physical block diagram of the IPR is shown in Figure C.2.2-2. The transmitters and matching network are located close to the antenna array. The receivers, digital electronics, and power supply are located remotely, in the Avionics Module.

The IPR has essentially only one operating mode, where the radar performs both shallow and deep sounding of Europa's surface. This mode is a raw data mode, in which a burst of unprocessed data is collected below 400 km
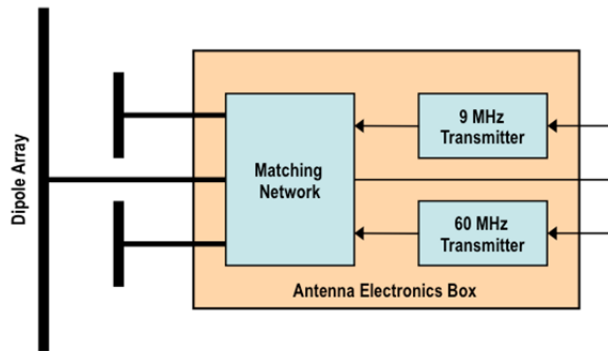
Figure C.2.2-2. Block diagram of the notional Ice-Penetrating Radar.

altitudes during the flyby. The radar is capable of bursts of raw data at a number of preselected rates up to a peak of ~130 Mbps. Due to the high data rate, the radar employs onboard processing elsewhere in the system to reduce the total data volume from the flyby to a manageable 25.2 Gbits. Processing will include range compression, presumming, Doppler filtering, data averaging, and resampling as needed to reduce output data volume.

Radiation Effects

Space-qualifiable parts that are radiation-hardened to 1 Mrad are currently available for use in the IPR transmitter and matching network. 5 kg of radiation shielding mass is allocated to protect this hardware, which is located adjacent to the dipole array. The rest of the IPR electronics are located in the UES of the Avionics Module, which provides shielding sufficient for parts tolerant to 300 krad or less (see Table C.2.6-7).

Planetary Protection

All of the IPR electronics can be prepared for planetary protection using dry heat microbial reduction. The deployed dipole array will be treated via radiation in flight.

Resource Estimates

The mass estimate for the IPR includes 6 kg for a stiffened 15-m dipole and 3 kg for a 5-m dipole array based on scaling from existing MARSIS and SHARAD designs. A mass es-

timate of 8 kg for the transmitter/matching network is derived from previous work performed under the High-Capability Instrument for Planetary Exploration (HCIPE) program with an additional 5 kg allocated for radiation shielding mass. Harness and antenna feeds are estimated at 3 kg, while remote digital electronics (including 4 receivers) are estimated at 8 kg, resulting in a total mass estimate for the IPR of 33 kg.

The power estimate for IPR is 55 W, driven by the use of both frequencies simultaneously.

C.2.2.2.2   Shortwave Infrared Spectrometer

The notional Shortwave Infrared Spectrometer (SWIRS) is a pushbroom spectrometer with a single-axis along-track scan mirror system for motion compensation. Functionality is similar to that of the Moon Mineralogy Mapper (M3) developed for the Chandrayaan-1 mission, shown in Table C.2.2-2.

Two primary modes of operation are defined for SWIRS. Inbound and outbound global-scale scans are obtained at ~10 km/pixel resolution, and inbound and outbound high-resolution scans are obtained at <300 m/pixel. The global scans are accomplished using a combination of spacecraft slews and internal scan mirror motion, while the high-resolution scans use the scan mirror as the spacecraft maintains a nadir orientation.

SWIRS is tailored to meet the science drivers identified in Section C.1.

- 150-μrad IFOV spatial resolution from 0.85 to 5.0 μm
- 10-nm spectral resolution from 0.85 to 5.0 μm
- S/N >100 from 0.85 to 5.0 μm (with target-motion compensation of up to 8 lines)

Instrument Description

The notional SWIRS consists of a single reflective telescope with a beam splitter feeding a grating spectrometer and detector. This op-

tics design concept yields an instrument IFOV of 150 µrad.

The notional detectors are 640×480 HgCdTe arrays, as used previously by M3 and by MRO's Compact Reconnaissance Imaging Spectrometer for Mars (CRISM). The wavelength cutoff is adjusted to 5 µm, as dictated by the science drivers. Extensive radiation shielding will be required to minimize transient radiation noise in the HgCdTe detector elements. This effectively mitigates concerns over total dose effects on these detectors. The use of 480 cross-track pixels results in a 4.2° instrument FOV. Spectral resolution of 10 nm from 0.85 to 5.0 µm requires the use of 420 columns on the detector.

To achieve the required S/N at long wavelengths in the high-resolution targeted mode, target motion compensation is added via an along-track scan mirror that enables extended exposure times. S/N can also be improved by a selectable combination of spatial and spectral binning, similar to that implemented by MRO CRISM.

Preliminary SWIRS performance analysis has been completed assuming the pixel performance characteristics (quantum efficiency, well depth, 27-µm pixel size) of the Teledyne TMC6604a HgCdTe image sensor. Low surface reflectance at Europa at 5 µm limits system performance and drives the need for target motion compensation in the targeted mode. Assuming a 180-mm-focal-length telescope with 72-mm aperture (*f*/2.5), a 2:1 focal reducer, an optical efficiency of 75%, a grating efficiency of 66% at long wavelengths, 80% detector quantum efficiency, and 2% surface reflectance at long wavelengths, ~990 signal-electrons per pixel would be collected at 5 µm per 120-ms exposure (2.5 km/s ground-track rate at 300 m/pixel, no target motion compensation). Assuming 100 electrons of read noise from the TMC6604a detector produces an S/N of 10. Applying target motion compensation via the scan mirror to allow 960-ms exposures,

~7,900 signal-electrons are collected, resulting in an estimated S/N of 60 at 5 µm. Due to increased solar flux, the S/N at 4 µm improves to ~100 and at 2.6 µm reaches ~210. The S/N values estimated for targeted mode and mapping mode do not include noise due to transient radiation noise in the HgCdTe detectors. Many data binning and/or editing options exist for data reduction in the mapping mode to achieve data volume allocation of 1.5 Gb per flyby.

A conceptual physical block diagram of the notional SWIRS is shown in Figure C.2.2-3. Consistent with the payload architecture described in Section C.2.2.1.2, minimal electronics are packaged at the focal plane with the detector, with most of the SWIRS electronics housed in the UES of the Avionics Module, which provides an environment shielded sufficiently for use of parts tolerant to a 300 krad or less total dose.

The scan mirror motor, with ~±45° range, is assumed to be a limited angle torque (LAT) motor with no internal electronic components. Scan mirror position sensing is assumed to be via a multispeed resolver or Inductosyn, also with no internal electronic components.

Motor drive and position sensing interface electronics and the SWIRS low-voltage power supply make up one of three electronics boards in the SWIRS electronics unit. The second board contains detector interface logic, pixel processing, and data compression. The third board contains the system controller and a SpaceWire interface to the spacecraft. These functions are implemented in radiation-hardened ASICs that use external radiation-hardened static RAM (currently available as 16-Mb devices) for temporary buffering of incoming spectrometer data, performing pipelined pixel processing, storing data compression intermediate products, and buffering incoming and outgoing SpaceWire command and telemetry data.
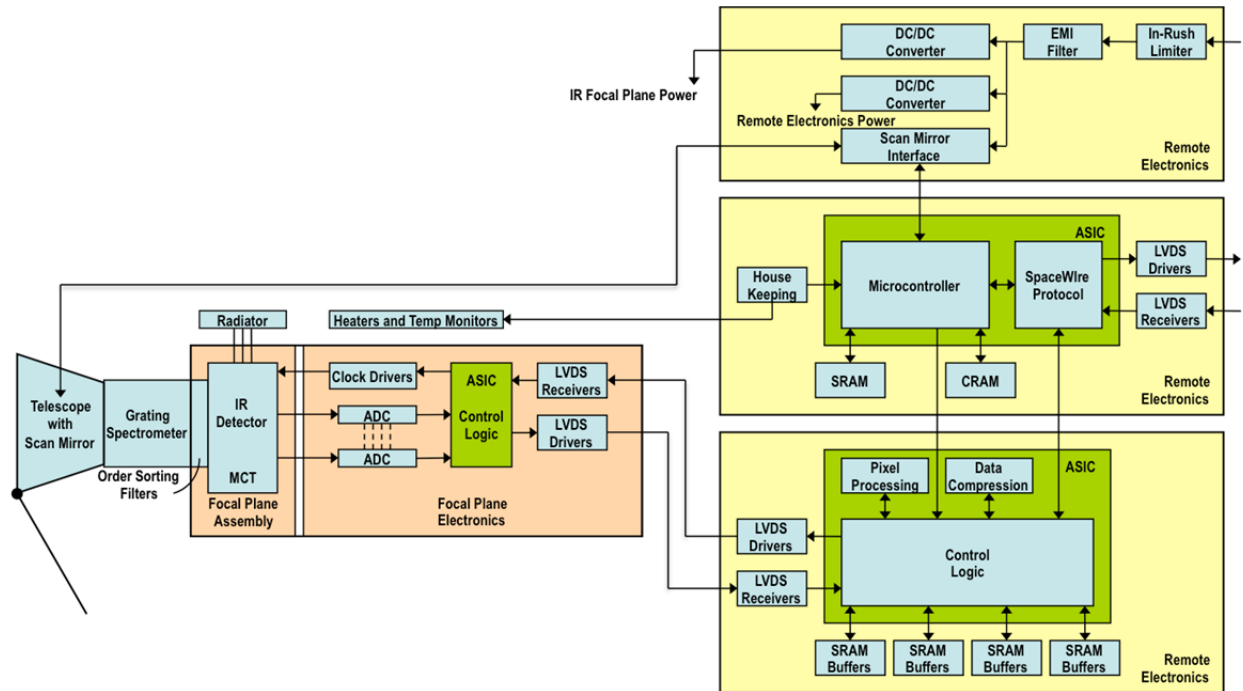
Figure C.2.2-3. Block diagram of the notional SWIRS.

Data compression is assumed to be wavelet based with commandable degrees of compression. Wavelet data compression algorithms developed for the Mercury Surface, Space Environment, Geochemistry, and Ranging (MESSENGER) mission have been tested using CRISM flight data and assuming onboard subtraction of a dark image (requiring ~8 Mb of SRAM) to remove fixed-pattern noise prior to compression. Results of this testing show acceptable noise levels with a 3:1 compression ratio.

A passive thermal design is baselined for SWIRS with a desired detector temperature of ~80 K. Accommodation of this radiator is discussed in Section C.2.2.1.1.

Radiation Effects and Shielding

While longer exposure times obtained through the use of target motion compensation can be used to increase the S/N, longer exposure times also increase the vulnerability to noise induced by background radiation. With 1 cm of Ta shielding, an estimated 4.3×10^5 electrons/cm^2/s and 50 protons/cm^2/s would reach the HgCdTe detectors through the shield while

in orbit at Europa (see Section C.2.2.1.2). Assuming 27-μm pixels and 154-ms exposure times, an estimated 45% of all pixels would be struck by an incident electron during an integration period. Each incident electron is estimated to deposit an average of 12,000 signal-electrons in the HgCdTe detector (per Boldt et al. 2008), while ~990 signal-electrons due to optical input are estimated at 5 μm for 120-ms exposures. Clearly, the SWIRS detectors will require additional radiation shielding. With 2 cm of Ta shielding, approximately 15% of SWIRS pixels would be struck during a 120-ms exposure. With 3 cm of Ta shielding, that rate is reduced to approximately 4%. For the notional SWIRS, a 3-cm Ta shield is assumed

The detector radiation shield is estimated at 4.6 kg with a notional configuration providing front-side detector shielding from the 2008 JEO study shown in Figure C.2.2-4. Shielding of the detector electronics, assumed to require an 8×8×2-cm interior volume, with 0.4 cm of Ta (100-krad components) is estimated at 1.30 kg each.
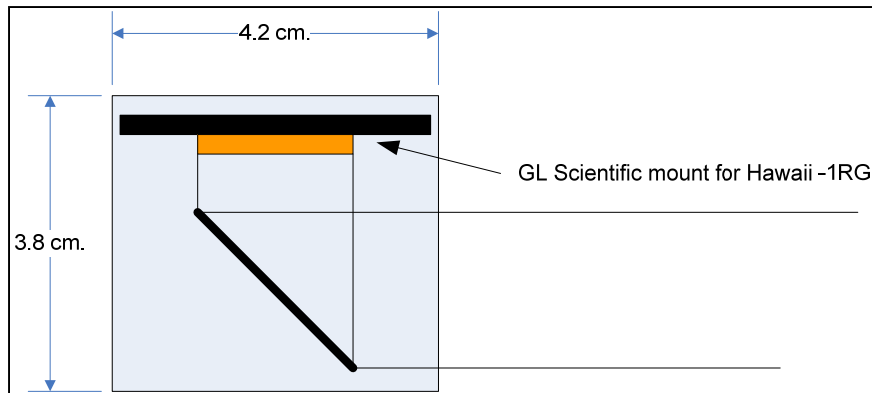
Figure C.2.2-4. Nominal SWIRS detector radiation shielding.

Transient radiation noise suppression in near-IR focal planes has seen considerable development effort due to its potential benefit to military systems. Various filtering approaches have been considered (Parish 1989) and some have been demonstrated within the readout integrated circuits (ROICs) underlining the HgCdTe detector elements. The Sensor Hardening Technology Program successfully implemented gamma noise suppression circuitry, including optical pulse suppression, within a ROIC using the BAE Systems 0.8-μm radiation-hardened complementary metal-oxide semiconductor (CMOS) process (Hairston et al. 2006). Transient suppression was achieved by dividing each image integration period into sub-frames using a Compact Signal Averager within each pixel to monitor each sub-frame and suppress outliers prior to charge integration within the ROIC. This technique is most effective in suppressing large transient events, and its overall effectiveness depends upon the pulse height distribution of the transient noise reaching the detector through the radiation shielding. While a factor-of-50 pulse suppression was achieved in the cited reference, the actual performance of such a system in the Europa environment is unknown at this time. Nonetheless, this approach looks promising. This technology suggests a possible radiation noise mitigation approach to be employed by SWIRS, but its implementation is not assumed for this report.

Planetary Protection

Planetary protection concerns would ideally be met for SWIRS through dry-heat microbial reduction, but survivability of the HgCdTe detector elements using the currently defined Europa Study planetary protection protocol is in question. A new "bake-stable" process has recently been developed that produces HgCdTe focal plane arrays that can be baked at 90ºC to 100ºC for extended periods or 110ºC for 24 hours. While this proprietary process has not yet been applied to the science-grade devices typically used for planetary space missions, it is thought that the bake-stable process can be applied to any HgCdTe focal plane array (James Beletic, Teledyne Imaging Sensors, private communication). A risk-reduction effort to fully quantify the performance impact of high-temperature bake-out on HgCdTe detector elements at the temperatures called for by the Europa Multiple-Flyby Mission planetary protection protocol is required. Alternatively, the SWIRS could be designed for removal of the focal plane during system DHMR, with a different microbial reduction technique performed on it.

Resource Estimates

The mass estimate for the notional SWIRS is based on an M3 system with scan mirror. The total mass estimate for SWIRS is 20.7 kg, of which 9.1 kg is radiation shielding.

Power dissipation for the notional SWIRS is estimated at 19.1 W, based on a bottoms-up estimate using M3 data.

The data volume estimate for the notional SWIRS in targeted mode is based on output of 480 cross-track pixels by 420 spectral pixels with 12 bits per pixel and a nominal 3:1 data compression ratio. Various combinations of spectral binning, spectral editing, spatial bin-

ning, and spatial editing can be used to reduce the compressed output data volume.

C.2.2.2.3   Ion and Neutral Mass Spectrometer

The notional INMS would determine the elemental, isotopic, and molecular composition of Europa's atmosphere and ionosphere during close flybys. Performing a role similar to that of the Cassini INMS, the Europa Multiple-Flyby Mission INMS concept has been adapted from the more recent design of the Reflectron Time-Of-Flight (RTOF) Rosetta Orbiter Spectrometer for Ion and Neutral Analysis (ROSINA). The Cassini and Rosetta spectrometers are both shown in Table C.2.2-2.

Due to the nature of Europa flybys, the SDT concluded that the INMS for the Flyby Mission requires greater sensitivity in a shorter integration time to achieve the science objectives than the heritage instruments offer. Research with potential INMS providers showed solutions for the Flyby Mission that could be tailored to the uniqueness of each INMS approach (quadrupole mass spectrometer vs. time-of-flight system, etc.). The notional model INMS represent a conservative merger of all of the solutions, considering resource needs. Therefore, while the INMS baselined for the Europa Multiple-Flyby Mission should satisfy the science drivers identified in Section C.1 (and listed below), the model instrument design concept has not been specified in as much detail as for other instruments.

The INMS is required to characterize the composition of sputtered products from energetic particle bombardment of Europa's surface, to include positive ions and neutral particles, with the following parameters:

- Mass range: up to 300 Da
- Mass resolution: $\Delta M/M \geq 500$
- Sensitivity: 10 particles/cm^3

Instrument Description

The notional INMS collects exospheric ions and gases and forwards them to sensors that

determine their mass and mass-to-charge ratios. A clear 60º×60º FOV envelope in the spacecraft ram direction has been accommodated in the spacecraft configuration (see Figure C.2.2-1). Detectors of choice (either microchannel plate [MCP] or channel electron multipliers [CEMs]) detect the ion bunches, and their output is sampled by the instrument's data acquisition system. High-speed memory captures this output for postprocessing.

For the purposes of this study, it was assumed that the INMS data acquisition systems could be relocated from the sensor assembly to a separate electronics unit to make most efficient use of radiation shielding mass.

Radiation Effects and Shielding

There are two main areas of concern for radiation effects on the notional INMS: the high-speed data acquisition systems and detectors. The front end, consisting of mechanical parts at high voltage, would not be sensitive to radiation.

High-speed data acquisition systems on heritage instruments use analog-to-digital converters (ADCs) and high-speed memory. Existing ADCs from multiple sources are hardened to 300 krad and provide satisfactory 12-bit resolution at speeds of ≥ 20 MHz. Modern radiation-hardened memory offers access times as low as 20 ns with radiation hardness of up to 1 Mrad.

Transient radiation effects on the INMS detectors are mitigated by the extremely short duration of the burst of data acquisition produced when an ion bunch is released towards the detector. With 0.6 cm of Ta shielding, an estimated 8.7×10^5 electrons/cm^2/s and 50 protons/cm^2/s would reach the detectors through the shield during flyby of Europa (see Section C.2.2.1.2). As an example, for a notional 18-mm-diameter detector (similar to the ROSINA RTOF MCP), a 1-ns digitization window, and a worst-case assumption that each incident electron or proton generates an MCP output, ~0.2% of A/D samples will be

corrupted by background radiation. This represents a tolerable noise floor in a multisampled mass spectra. Given the small size of the detectors, only ~100 g of radiation shielding is required; however, a total of 1.1 kg of shielding has been allocated.

Electronics remaining in the notional INMS sensor unit (including front-end electronics, pulsers, and high-voltage power supplies) are assumed to be hardened to 1 Mrad, requiring a 0.2-cm Ta radiation shield and 2 kg of shielding mass.

Planetary Protection

Planetary protection concerns will be met for INMS through dry heat microbial reduction. The bare unpowered MCPs and CEMs can tolerate high-temperature soaks, but the drivers on the bake-out of the front end assembly and mass analyzer will need to be further investigated. The proposed INMS front-end assembly should tolerate up to 150°C bake-out temperatures.

Resource Estimates

The mass estimate for the notional INMS is derived by a conservative merging of inputs from the instrument community. The resulting mass estimate for the INMS sensor assembly is 24.1 kg. Of that mass, 10.5 kg is allocated to the sensor and an additional 3.1 kg to the sensor shielding. Two electronics boards in the science electronics unit (2.5 kg total) are assumed with additional shielding of 7.0 kg, and with 1 kg of harness mass allocated due to instrument partitioning. The notional INMS telemetry rate is estimated at 2 kbps, and power dissipation is estimated at 33 W.

C.2.2.2.4   Topographical Imager

The TI provides stereo imaging of Europa landforms to fulfill geology objectives, and it assists in removal of IPR clutter noise from off-nadir surface topography. The TI has basic functionality similar to that of the MRO Mars Color Imager (MARCI) instrument shown in Table C.2.2-2 and is tailored to satisfy the following science measurement requirements identified in Section C.1:

- High-resolution panchromatic imagery of Europa during flybys:
  – Along-track stereo
  – 58° cross-track coverage
  – 250-µrad IFOV
  – Concurrent operation with the IPR

Instrument Description

The notional TI has a 0.25-mrad IFOV to produce a 25-m pixel footprint from a 100-km distance. Use of a 4096-pixel-wide image sensor results in an instrument FOV of ~58° full angle. A detector operating in pushbroom mode is baselined. A focal-plane detector, either dual charge-coupled devices (CCDs) or a CMOS active pixel sensor (APS) with multiple elements on a single substrate (similar to that developed by e2v Technologies for the New Horizons Multispectral Visible Imaging Camera [MVIC]) provides the along-track stereo image separation required. While future instrument proposers have a choice of available detectors, the higher radiation tolerance of CMOS APS devices and continued improvements in their performance for scientific applications (Janesick et al. 2008) make them the nominal detector choice for a notional TI.

Preliminary TI performance analysis has been completed using the pixel characteristics (quantum efficiency, 13-µm pixel size, 100k e-well depth) of the e2v CCD47-20BT image sensor used by the New Horizons Long-Range Reconnaissance Imager (LORRI) instrument as an example of the performance expected from the TI sensor. Assuming a 52-mm-focal-length telescope with 13-mm aperture (*f*/4), an optical efficiency of 85%, an average detector quantum efficiency of 60%, and a surface reflectance of 20% at Europa, approximately 4.36×10^4 electrons per pixel are collected during the maximum exposure time of 5.5 ms. The required TI pixel readout rate (for 25-m resolution at 100 km with nominal ground speed of 4500 m/s) for a 4096-pixel line array

is 810 kHz, smaller than LORRI's readout rate of 1.2 MHz and its measured 20-electron system read noise. However, if the TI needs to take images at 25-km passes as well (though it is not a driving requirement), then the readout rate increases to 2.9 MHz, with corresponding increase of electron noise to ~30 electrons. Therefore, for the notional TI calculations, a 20-electron read noise is assumed. Coupled with photon noise and barring background radiation noise, the estimated panchromatic S/N is ~315. The driving cases for TI are the flybys at 25 km. However, even then, the S/N exceeds 200.

A conceptual physical block diagram for the TI is provided in Figure C.2.2-5. Consistent with the instrument architecture described in Section C.2.2.1.2, minimal electronics are packaged at the focal plane with the detector. The signal chain shown in the focal plane electronics contains elements required for a CCD image sensor (clock drivers, correlated double sampler, A/D conversion) that either are not necessary or are typically implemented within a CMOS APS device. A highly integrated CMOS APS device is an ideal solution for the Europa Multiple-Flyby Mission TI, as it minimizes components at the focal plane that require radiation shielding.

The camera processor board contains camera interface logic, image data compression and a SpaceWire command and telemetry interface to the spacecraft. A single, radiation-hardened ASIC with 3:1 nominal wavelet-based data compression is assumed. A second electronics board provides DC/DC power conversion.

The TI detector is cooled by a passive, Sun-protected radiator. A detector-annealing heater is baselined as a means to mitigate radiation damage.

Radiation Effects and Shielding

To protect the TI image sensor from total dose, displacement damage, and transient radiation noise, radiation shielding with 1 cm of Ta is baselined, comparable to shielding used by the Galileo Solid State Imager (SSI). The Europa Multiple-Flyby Mission radiation dose depth curve indicates a ~17.6 krad total dose behind 1 cm of Ta shielding. With a required RDF of 2, this allows use of detectors tolerant of 35.2 krad. While a CMOS APS device is favored for the notional Europa Multiple-Flyby Mission TI, this dose level allows a choice of silicon device technologies including CMOS APS, P-channel CCD, and arguably N-channel CCD.

Shielding mass of 4.5 kg is allocated for a 1-cm Ta, 5×5×4-cm enclosure. This is slightly larger than that shown in Figure C.2.2-6, which was designed to house a STAR1000-based CMOS APS and its interface electronics. The slight increase in dimensions allows for additional circuitry required for a CCD-based focal plane or additional electronics required by a multioutput CMOS APS device.

Background radiation noise is mitigated by the very short exposure times employed by TI.
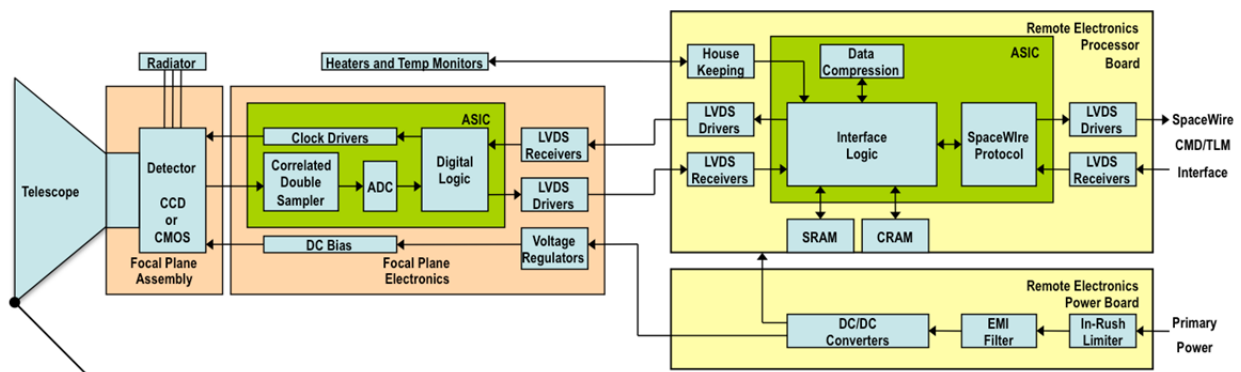
Figure C.2.2-5. Block diagram of the notional Topographical Imager
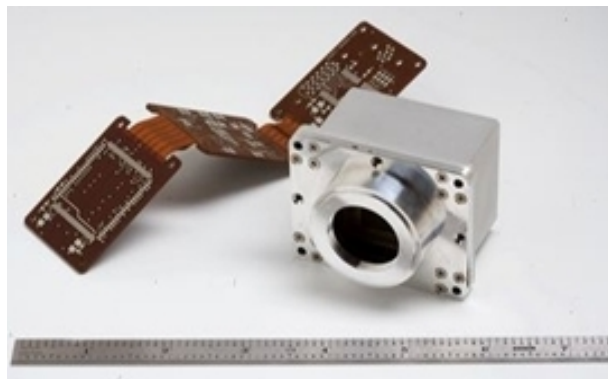
Figure C.2.2-6. Miniature focal plane assembly for a STAR1000 CMOS APS indicative of the TI focal plane electronics.

With 1 cm of Ta shielding, an estimated 4.3×10^5 particles/cm^2/s would reach the detector through the shielding (see Section C.2.2.1.2). Assuming 13-µm pixels and 5.5-ms exposure times, it is estimated that ~0.4% of all pixels would be struck by an incident electron during the integration period, which is a tolerable level. For a typical silicon image sensor, each incident electron can be expected to generate an average of 2,000 signal-electrons in the detector (per Boldt et al. 2008). With the assumption that the signal-electrons generated by the incident particles are concentrated on a single pixel, the method of calculating S/N adopted for the Galileo SSI camera can be employed (Klaasen et al. 1984). Based on empirical data, radiation-induced noise was approximated at 35×SQRT (mean radiation signal per pixel). For a 0.4% hit rate and 2,000 electrons per hit, the radiation-induced noise would contribute ~100 electrons to the TI S/N calculation. This reduces the TI S/N to 300 from 315.

The TI electronics present no significant radiation concerns beyond those particular to the detector; use of parts tolerant to 100 krad is assumed.

Planetary Protection

Planetary protection concerns for TI can be met through dry-heat microbial reduction. Temperature effects on optical materials, the adhesives used in optical mounts, and the image sensor will require thorough testing early in instrument development.

Resource Estimates

The TI mass estimate of 7.0 kg (including 4.5 kg of shielding mass) is derived from similarity to the New Horizons LORRI instrument and assumed values for harness mass and separate electronics unit. Power dissipation is estimated at 5.9 W during image acquisition and is driven by pixel rate, data compression, and the high-speed SpaceWire interface.

For pushbroom operation at a range of 100-km orbit for a typical flyby, the TI line period is 5.5 ms. Assuming 14 bits/pixel, one 70-line stereo image is 8 Mb. Data volume from a typical flyby is estimated at 3.1 Gb, compressed 3:1, assuming ~1,100 images per flyby that can be allocated by the science team to meet the science objectives.

C.2.3 Mission Design

A fully integrated proof-of-concept trajectory has been developed for a compelling Europa Multiple-Flyby Mission that efficiently accomplishes high-quality scientific observations and measurements.

The trajectory design goal for this Europa Multiple-Flyby Mission study was to establish the existence and feasibility of a flyby-only Europa mission that meets the SDT observation and measurement requirements, as outlined in the traceability matrix (FO C-1). The focus for this study was to maximize IPR, TI, SWIRS and INMS coverage while minimizing total ionizing dose[3] (TID), mission duration, and ΔV.

Current Europa Multiple-Flyby Mission concept needs are presently satisfied by the capabilities of an Atlas V 551 launched from Cape Canaveral Air Force Station on a Venus-Earth-Earth gravity assist (VEEGA) interplanetary trajectory. In this concept, after a cruise of

---

[3] Total ionizing dose Si behind a 100-mil Al, spherical shell.

6.37 years, the spacecraft will fly by Ganymede just prior to performing Jupiter Orbit Insertion (JOI) via a large main engine maneuver. The spacecraft will then perform four additional Ganymede gravity assists over 11 months to lower its orbital energy with respect to Jupiter and set up the correct flyby conditions (lighting and relative velocity) at Europa. The spacecraft will then embark on an 18-month Europa science campaign. The first part of the science campaign will focus on Europa's then day lit anti-Jovian hemisphere (Figure C.2.3-1). After the first phase, six Europa and three Ganymede flybys will be used to place the subsequent Europa flybys on the opposite side of Jupiter where the sub-Jovian hemisphere of Europa will then be day lit. These Europa flybys, constituting the second phase of the science campaign, will focus on Europa's sub-Jovian hemisphere. Finally, the mission will culminate with spacecraft disposal via Ganymede impact. FO C-2 depicts a summary of the mission design concept.

For a discussion of data acquisition scenarios, data return strategies, and communication strategies, see Section C.2.1.
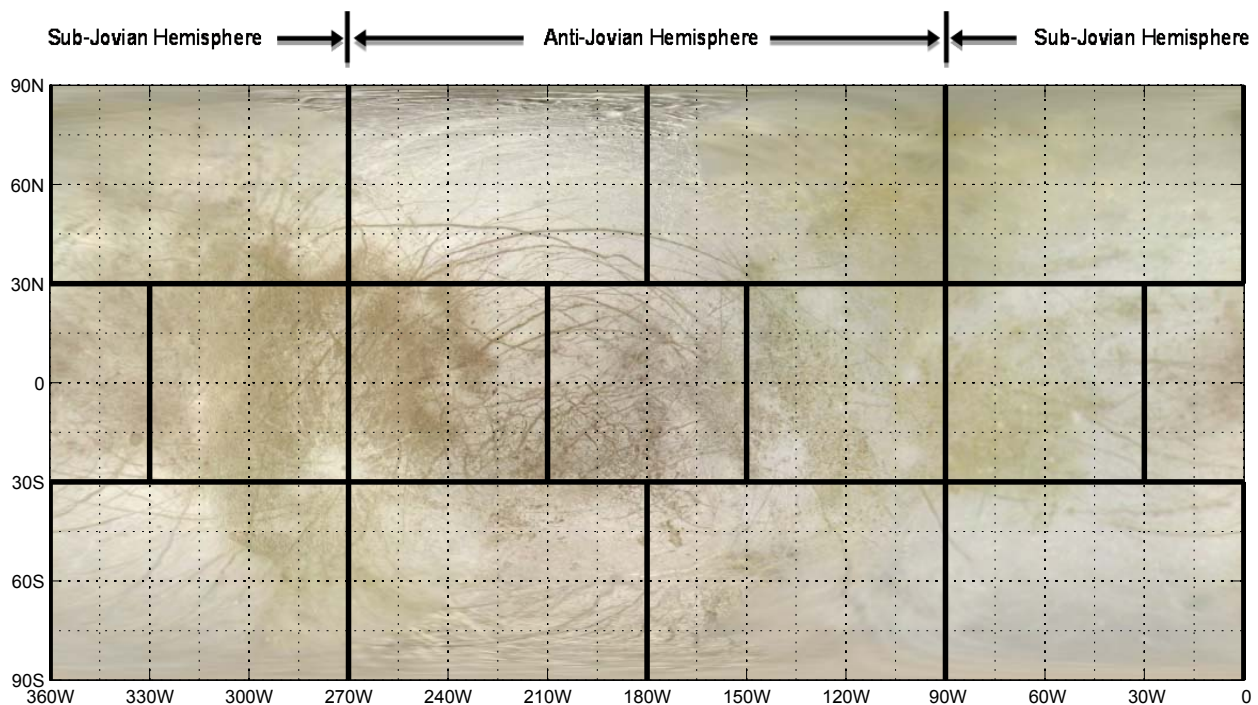
Figure C.2.3-1. Europa Mercator projection map including the 14 sectors defined by the SDT used to assess global coverage. In addition, since Europa is tidally locked, the same hemispheres (and associated sectors) always face towards (sub-Jovian) or away (anti-Jovian) from Jupiter.

Europa Multiple-Flyby Mission Design: Multiple-Flyby Approach to Explore Europa and Investigate Its Habitability

A) Interplanetary Phase: VEEGA Trajectory (6.37 years)

VGA (5/14/22)
EGA-1 (10/24/23)
EGA-2 (10/24/25)
Launch (11/21/21)
JOI (4/4/28)
Jupiter's Orbit
Sun

B) Pre-JOI Ganymede Flyby
(Reduces JOI ΔV by ~400 m/s)

Ganymede Gravity Assist (500 km altitude)
JOI (1-hr burn)
Sun

Satellite positions plotted at time of Ganymede gravity assist

C) Tour Phase (2.3 years)

Delivery Phases

Interplanetary Trajectory

Science Phases

Pump Down
COT-1 (Anti-Jovian Hem.)
Non-Res
COT-2 (Anti-Jovian Hem.)
Change Lighting Conditions 180º
COT-3 (Sub-Jovian Hem.)
Non-Res
COT-4 (Sub-Jovian Hem.)

Sun

Phase names, orbits, ground tracks, and encounter markers are jointly color coded

COT-1 | COT-2 | Change Lighting Conditions 180° | COT-3 | COT-4

INTERPLANETARY

2021	2022	2023	2024	2025
Launch	VGA	EGA-1		EGA-2

JOVIAN TOUR

2028	2029	2030

JOI

Key Parameters	Value
Launch Vehicle	Atlas V 551
Earth to Jupiter Trajectory	VEEGA
Earth Launch Period	11/15/21 to 12/05/21
C3 (Max), R.A., Dec.	15 km^2/s^2, 334.5°, 11.7°
Jupiter Arrival Date	4/4/2028
Jupiter Arrival V-infinity	5.6 km/s (maximum)
JOI Earth Range	4.52 AU
JOI Periapsis Altitude	12.8 R$_j$
Jupiter Capture Orbit Period	206 days
Tour	4/3/28–8/25/30 (2.4 yrs.)
Europa Science	2/25/29–8/6/30 (1.5 yrs.)
Ganymede/Europa Flybys	8/34
TID (behind 100 mil Al SS)	2.06 Mrad
Spacecraft disposal	Ganymede Impact

Radiation dose TID behind 100 mil Al SS (Mrad)

Non-res (I/O)
Non-res (O/I)
COT-1
COT-2
Change lighting conditions 180°
COT-3
COT-4
Europa encounters
E5
E13
E19
E27
E36 E41
Disposal

Pump down
Ganymede encounters
G0
G1 G2 G3 G4
G24-G26

C.2.3.1   Mission Overview and Phase Definitions

General descriptions of each mission phase and related activities are summarized in Table C.2.3-1.

Table C.2.3-1. Mission phase definitions and descriptions.

Phase	Subphase	Activity	Start–End
Interplanetary	Launch and Early Operations	Begins with the launch countdown, launch, initial acquisition by the DSN, checkout and deployment of all major flight-system sub-systems, and a moderate maneuver to clean up trajectory errors from launch vehicle injection.	Nov./Dec. 2021 + 30 days
	Cruise	Science instrument calibrations, Venus and Earth gravity-assist flyby operations, annual spacecraft health checks, trajectory correction maneuvers, and operations readiness tests (ORTs).	Jan. 2021–Oct. 2027
	Jupiter Approach	Training, and ORTs for all mission elements in preparation for JOI and Jovian tour. This phase includes the Ganymede (G0) flyby ~12 hours before JOI and ends with completion of JOI.	Oct. 2027–Apr. 2028
Pump-down		Reduces energy relative to Jupiter via four Ganymede gravity assists. The sequence of four outbound Ganymede flybys (G1–G4) following the inbound G0 flyby sets up the encounter geometry for the first Europa science phase such that an acceptable velocity relative to Europa is achieved and the anti-Jovian hemisphere is well illuminated.	Apr-2028–Feb. 2029 (11 months)
Europa Anti-Jovian Hemisphere Coverage	COT-1	A seven Europa-flyby crank-over-the-top (COT) sequence is used to systematically cover Europa's anti-Jovian hemisphere. Places groundtrack in all seven anti-Jovian hemisphere sectors. All Europa flybys occur at the ascending node. COT-1 sequence changes the flybys from outbound to inbound.	Feb. 2029–Jul. 2029 (4.7 months)
	Nonresonant Transfer	Inbound-to-outbound Europa nonresonant transfer to get back to outbound flybys such that another COT sequence can be implemented to cover the anti-Jovian hemisphere.	Jul. 2029–Aug. 2029 (0.5 months)
	COT-2	A five Europa-flyby COT sequence is used to systematically cross all COT-1 groundtracks to fulfill the IPR/TI requirements for *all* anti-Jovian hemisphere sectors. All flybys occur at the descending node. COT-2 changes the flybys from outbound to inbound.	Aug. 2029–Oct. 2029 (2.4 months)
Change Lighting Conditions	Pump-down, Crank-up	Reduces spacecraft orbit period and increases inclination to set up correct geometry for Europa-to-Ganymede pi-transfer.	Oct. 2029–Jan. 2030 (3.5 months)
	Pi-Transfers	Includes a Europa-to-Ganymede pi-transfer, a Ganymede pi-transfer (placing periapsis on the opposite side of Jupiter), and finally a Ganymede-to-Europa pi-transfer that places the subsequent Europa flybys approximately 180° from the location of the Europa flybys in COT-2.	Jan. 2030–Feb. 2030 (0.6 months)
Europa Sub-Jovian Hemisphere Coverage	COT-3	Eight Europa flybys are used to increase spacecraft orbit period while also cranking over the top to cover the sub-Jovian hemisphere. All Europa flybys occur at the descending node. COT-3 changes the flybys from inbound to outbound.	Feb. 2030–Jun. 2030 (3.7 months)
	Nonresonant Transfer	Outbound-to-inbound Europa flyby nonresonant transfer to get back to inbound flybys such that another COT sequence can be implemented to cover the sub-Jovian hemisphere.	Jun. 2030 (0.3 months)
	COT-4	A six Europa-flyby COT sequence is used to systematically cross the COT-3 groundtracks to fulfill the IPR/TI requirements for 6 of the 7 sub-Jovian hemisphere sectors. All flybys occur at the ascending node.	Jun. 2030–Aug. 2030 (2.4 months)
Spacecraft Disposal		Baseline strategy: Ganymede impactor (although many options exist—see Section C.2.3.9).	Aug. 2030

C.2.3.2   Launch Vehicle and Launch Period

An Atlas V 551 would launch the spacecraft with a maximum C_3 of 15.0 km^2/s^2 during a 21-day launch period opening on November 15, 2021. The optimal launch date within the launch period is November 21, 2021 (Figure C.2.3-2). The date of Jupiter arrival is held fixed throughout the launch period, incurring only a negligible penalty, while simplifying the design of the tour in the Jovian system. Launch vehicle and launch period parameters are shown on FO C-2. Launch vehicle performance is taken as that specified in the NASA Launch Services (NLS)-II Contract, which includes, in particular, a performance degradation of 15.2 kg/yr for launches occurring after 2015. The spacecraft propellant tanks are sized for maximum propellant, given the trajectory and launch vehicle capability, and are assumed to be fully loaded. The flight system is designed to launch on any given day in the launch period without reconfiguration or modification.

C.2.3.3   Interplanetary Trajectory

The baseline interplanetary trajectory used for the Europa Multiple-Flyby Mission is a VEEGA (FO C-2 and Table C.2.3-2). Cruise navigation will use Doppler and range observations from the Deep Space Network (DSN). The deep-space maneuver (DSM) ΔV required on the optimal day of the launch period is zero, but is about 80 m/s at the start of the launch period and reaches its highest level of 100 m/s
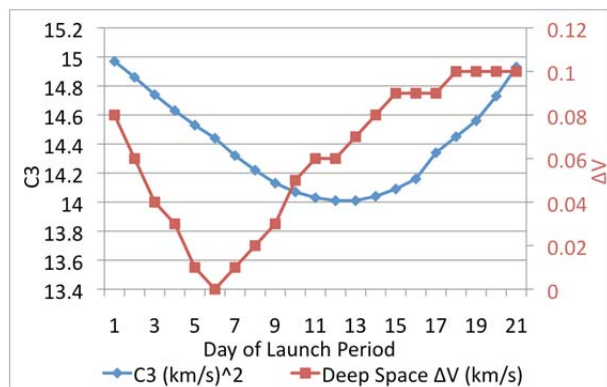
Figure C.2.3-2. Baseline interplanetary launch period

Table C.2.3-2. Baseline VEEGA interplanetary trajectory (for optimal launch date).

Event	Date	V∞ or ΔV (km/s)	Flyby Alt. (km)
Launch	21 Nov 2021	3.77	-
Venus	14 May 2022	6.62	3184
Earth	24 Oct 2023	12.07	11764
Earth	24 Oct 2025	12.05	3336
G0	03 Apr 2028	7.37	500
JOI	04 Apr 2028	0.858	12.8 R_J

on the last day. The DSM occurs near aphelion on the Earth-Earth leg of the trajectory.

The interplanetary trajectory design will comply with all required National Environmental Policy Act (NEPA) assessments and safety analyses (see Section C.2.6). An aim-point-biasing strategy will be used for the Earth flybys.

The nominal flyby altitudes of Venus and Earth do not vary significantly over the launch period and are relatively high, as seen in Table C.2.3-2. For comparison, Cassini flew by Earth at an altitude of 1,166 km, and Galileo at altitudes of 960 and 304 km.

A 500-km Ganymede flyby will be performed approximately 12 hours before JOI, thereby saving about 400 m/s of ΔV (compared to the case of no Ganymede flyby). The JOI maneuver will last about 2 hours and occur at perijove at a range of 12.8 R_J (i.e., in the less intense outer regions of the radiation belts). Gravity losses are negligible due to the small angle subtended by the burn-arc. This also permits a far less complicated contingency strategy for this critical event.

C.2.3.4   Backup Interplanetary Trajectories

Many backup interplanetary trajectory options are available, offering launch opportunities every calendar year. The results of a comprehensive search of all 1-, 2-, 3-, and 4-gravity-assist trajectories are shown in Figure C.2.3-3. The best candidates from the search are shown in Table C.2.3-3, which includes launch period effects.
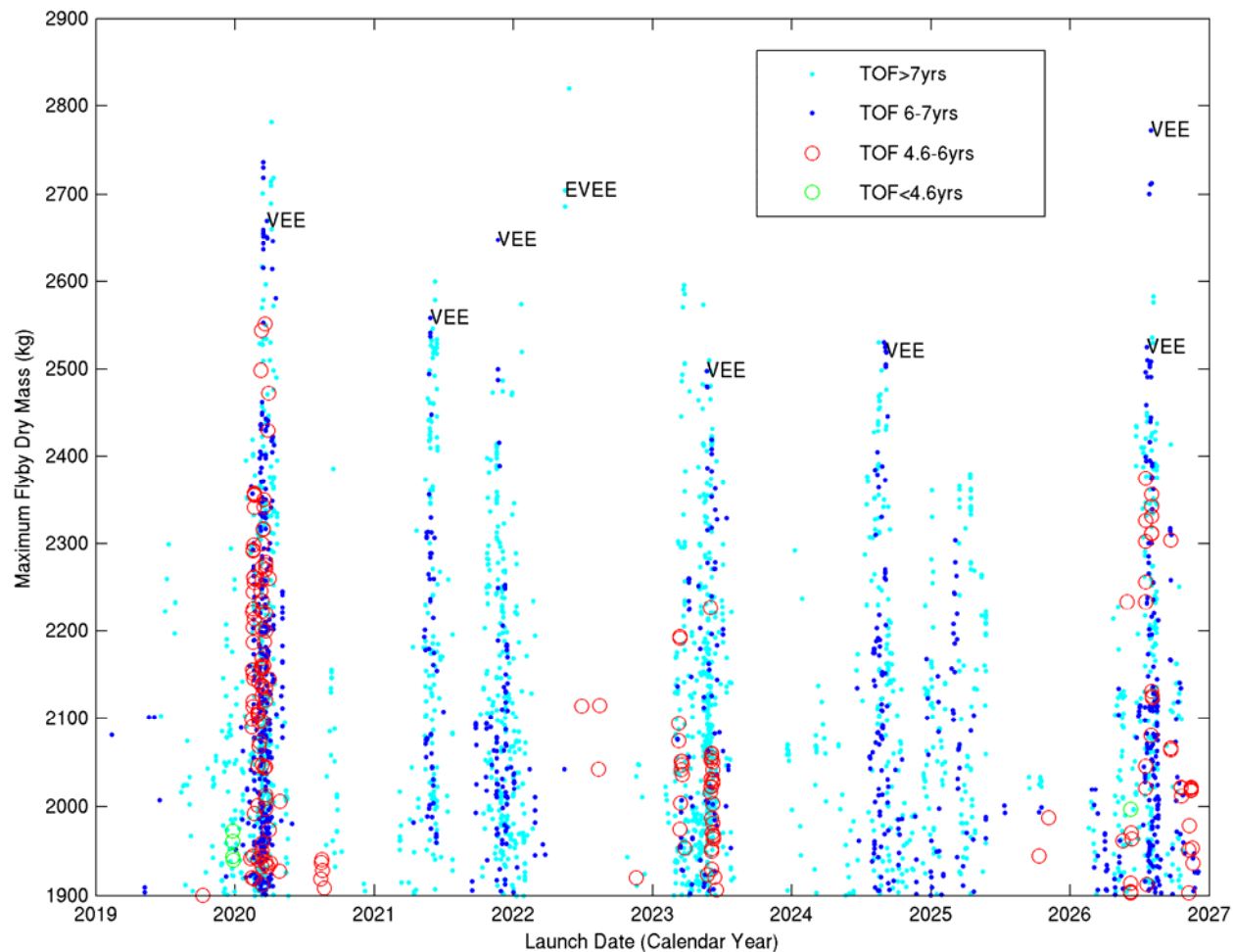
Figure C.2.3-3. Interplanetary trajectory options.

Table C.2.3-3. Short list of interplanetary trajectories, including launch period effects. Baseline trajectory is in bold; subsequent trajectories represent viable backup opportunities.

Launch Date	Flyby Path	TOF to JOI (yrs.)	C_3 (km2/s2)	Atlas V 551 Capability (kg)	Max Prop Mass (MEV DV) (kg)	Max Dry Mass (kg)	Prop for CBE Dry Mass (kg)
25 Mar 2020	VEE	6.03	15.6	4456	1739	2717	864
27 May 2021	VEE	6.87	14.5	4541	1938	2603	1005
21 Nov 2021	**VEE**	**6.37**	**15.0**	**4494**	**1846**	**2648**	**898**
15 May 2022	EVEE	7.22	10.2	4935	2182	2753	1070
23 May 2023	VEE	6.18	16.4	4339	1797	2542	955
03 Sep 2024	VEE	6.71	13.8	4562	1998	2564	1052
01 Aug 2026	VEE	6.94	10.0	4893	2112	2781	1026
21 Jul 2026	VEE	6.15	15.2	4400	1831	2569	962

The table shows, for each trajectory, the optimal launch date of the launch period, the flight time to Jupiter, the expected maximum C_3 over the launch period, the launch vehicle capability at maximum C_3 for the indicated launch year (NLS-II contract), the propellant required for flying the mission (assuming the full launch vehicle capability is used), the maximum dry mass (i.e., the difference between the two preceding numbers), and the propellant required to fly the mission assuming the CBE value for the dry mass. In all cases, the MEV (maximum expected value) ΔV from Table C.2.3-5 is used.

It is worth noting that two types of commonly considered trajectories do not appear in the short list of Europa Multiple-Flyby Mission interplanetary trajectories because of their relatively poor mass performance. The first type is the ΔV-Earth gravity assist (ΔV-EGA), which is a V_∞ leveraging type of trajectory involving a large maneuver near aphelion before the Earth flyby. For the ΔV-EGA, the maximum dry mass that can be delivered in the years 2019–2027 is about 1,650 kg (about 1,000 kg less than the "Max Dry Mass" numbers in the short list, Table C.2.3-3). The required C_3 is in the range 25–30 km^2/s^2, and the flight time is typically 4–5 years, corresponding to a 2:1 ΔV-EGA (4.5 years for the maximum-dry-mass case). The second type is the Venus-Earth Gravity Assist (VEGA), involving a large maneuver after the Venus flyby. For flight times of around 4.4 yrs., the maximum dry mass for the VEGA is about 1,740 kg. For flight times around 5.4 yrs., approaching the VEEGA flight times, the maximum dry mass becomes about 2,190 kg. Thus,

these two trajectory types significantly underperform in terms of delivered mass compared to the typical VEEGA trajectory. To save some flight time, these trajectory types may be considered in later phases of the mission design, once the vehicle mass is better characterized, assuming it does not grow significantly from current levels.

C.2.3.5   Jovian Tour (11-F5 Trajectory)

The current baseline Jupiter tour for the Europa Multiple-Flyby Mission is a fully integrated trajectory (i.e., flight-level fidelity, no approximations made), and one of many tours developed for this study. The baseline tour, referred to as 11-F5, begins after JOI and consists of 34 Europa and 9 Ganymede flybys over the course of 2.4 years, reaches a maximum Jovicentric inclination of 15º, has a deterministic ΔV of 157 m/s (post–PJR [perijove raise maneuver]), and has a TID of about 2 Mrad. This proof-of-concept trajectory employs a novel combination of mission design techniques to successfully fulfill a set of SDT-defined scientific objectives (see FO C-1) including global Ice-Penetrating Radar (IPR), Topographic Imager (TI), and Shortwave Infrared Spectrometer (SWIRS) observations, and Ion and Neutral Mass Spectrometer (INMS) *in situ* measurements. Navigational constraints concerning superior conjunctions of Jupiter, which occur every 13 months and require a several-day hiatus in spacecraft commanding, were not considered but are easily accommodated and will be included during Phase A. The 11-F5 trajectory can be broken into five distinct phases, each detailed in Table C.2.3-4 and depicted in FO C-2.

Table C.2.3-4. Detailed 11-F5 flyby and maneuver summary.

Phase	Flyby/ Maneuver	In/ Out	Date	Altitude (km)	B-Plane Ang (deg)	V-Infinity (km/s)	Inc. (deg)	Peri. (R_J)	Apo. (R_J)	m	n	Period (days)	TOF (days)	Total TOF (months)
Jupiter Approach	**Ganymede0**	I	**03-Apr-2028 14:56:45**	**500**	**0.1**	**7.382**	**5.17**	**12.96**	**-**	**N**	**R**	**-**	**202.1**	**0.00**
	JOI		*04-Apr-2028 03:30:08*	ΔV =	*857 m/s*		*4.97*	*12.78*	*268.5*	*-*	*-*	*205.7*	*0.5*	
	PJR		*13-Jul-2028 14:52:13*	ΔV =	*114 m/s*		*4.95*	*13.6*	*264.5*	*-*	*-*	*202.6*	*100.5*	
Pump-down	**Ganymede1**	O	**22-Oct-2028 16:52:57**	**100**	**-171.1**	**6.34**	**4.6**	**11.99**	**97.73**	**7**	**1**	**50.09**	**50.1**	**6.74**
	CU-Man-G1		*25-Oct-2028 17:51:55*	ΔV =	*0 m/s*								*3.0*	
	Apo-Man-G1		*16-Nov-2028 02:26:26*	ΔV =	*0.427 m/s*								*21.4*	
	Ganymede2	O	**11-Dec-2028 19:05:43**	**100**	**-136.4**	**6.42**	**1.54**	**11.16**	**64.37**	**4**	**1**	**28.61**	**28.6**	**8.41**
	Apo-Man-G2		*25-Dec-2028 08:31:15*	ΔV =	*4.821 m/s*								*13.6*	
	Ganymede3	O	**09-Jan-2029 09:42:57**	**3496.3**	**-175.5**	**6.37**	**1.37**	**10.63**	**51.74**	**3**	**1**	**21.46**	**21.5**	**9.36**
	CU-Man-G3		*12-Jan-2029 11:40:03*	ΔV =	*0 m/s*								*3.1*	
	Apo-Man-G3		*19-Jan-2029 07:59:00*	ΔV =	*0 m/s*								*6.8*	
	Ganymede4	O	**30-Jan-2029 20:52:12**	**172.9**	**191.1**	**6.40**	**0.45**	**9.33**	**36.18**	**N**	**R**	**13.37**	**25.9**	**10.07**
	CU-Man-G4		*02-Feb-2029 22:47:42*	ΔV =	*0 m/s*								*3.1*	
	Apo-Man-G4		*05-Feb-2029 15:05:55*	ΔV =	*0 m/s*								*2.7*	
Europa Anti-Jovian Hemisphere Coverage — COT-1	**Europa5**	O	**25-Feb-2029 17:45:14**	**724.3**	**104.6**	**3.84**	**2.32**	**9.27**	**34.04**	**7**	**2**	**12.43**	**24.9**	**10.94**
	CU-Man-E5		*10-Mar-2029 02:14:25*	ΔV =	*0 m/s*								*12.4*	
	Apo-Man-E5		*16-Mar-2029 06:24:12*	ΔV =	*7.375 m/s*								*6.2*	
	Europa6	O	**22-Mar-2029 14:52:04**	**100**	**25**	**3.92**	**3.33**	**9.42**	**37.93**	**4**	**1**	**14.20**	**14.2**	**11.77**
	CU-Man-E6		*25-Mar-2029 14:59:58*	ΔV =	*9.125 m/s*								*3.0*	
	Apo-Man-E6		*29-Mar-2029 15:26:54*	ΔV =	*0 m/s*								*4.0*	
	Europa7	O	**05-Apr-2029 19:35:07**	**100**	**73.6**	**3.92**	**5.98**	**9.45**	**33.89**	**7**	**2**	**12.43**	**24.9**	**12.24**
	CU-Man-E7		*18-Apr-2029 04:34:59*	ΔV =	*0 m/s*								*12.4*	
	Apo-Man-E7		*24-Apr-2029 09:45:13*	ΔV =	*1.216 m/s*								*6.2*	
	Europa8	O	**30-Apr-2029 16:28:04**	**100**	**-18.1**	**3.94**	**5.01**	**9.50**	**37.86**	**4**	**1**	**14.20**	**14.2**	**13.07**
	CU-Man-E8		*03-May-2029 16:38:07*	ΔV =	*0 m/s*								*3.0*	
	Apo-Man-E8		*07-May-2029 18:50:08*	ΔV =	*2.201 m/s*								*4.1*	
	Europa9	I	**14-May-2029 20:58:09**	**100**	**24.1**	**3.93**	**6.03**	**9.48**	**33.86**	**7**	**2**	**12.43**	**24.9**	**13.54**
	CU-Man-E9		*27-May-2029 08:55:17*	ΔV =	*0 m/s*								*12.5*	
	Apo-Man-E9		*02-Jun-2029 14:05:16*	ΔV =	*1.951 m/s*								*6.2*	
	Europa10	I	**08-Jun-2029 17:51:49**	**25**	**-72.3**	**3.92**	**3.27**	**9.42**	**37.92**	**4**	**1**	**14.20**	**14.2**	**14.37**
	CU-Man-E10		*11-Jun-2029 18:15:35*	ΔV =	*1.439 m/s*								*3.0*	
	Apo-Man-E10		*15-Jun-2029 22:22:27*	ΔV =	*0 m/s*								*4.2*	
	Europa11	I	**22-Jun-2029 22:24:10**	**100**	**-25**	**3.93**	**2.05**	**9.29**	**33.94**	**7**	**2**	**12.43**	**24.9**	**14.84**
	CU-Man-E11		*25-Jun-2029 23:12:45*	ΔV =	*0 m/s*								*3.0*	
	Apo-Man-E11		*11-Jul-2029 17:51:19*	ΔV =	*11.635 m/s*								*15.8*	

Phase	Flyby/ Maneuver	In/ Out	Date	Altitude (km)	B-Plane Ang (deg)	V-Infinity (km/s)	Inc. (deg)	Peri. (R_J)	Apo. (R_J)	m	n	Period (days)	TOF (days)	Total TOF (months)
	Europa12	I	17-Jul-2029 19:10:35	100	-124.6	3.90	0.34	9.34	38.12	N	R	14.25	14.4	15.67
Nonresonant	CU-Man-E12		20-Jul-2029 19:24:29	ΔV =	0 m/s								3.0	
	Apo-Man-E12		25-Jul-2029 01:26:55	ΔV =	3.976 m/s								4.3	
	Europa13	O	01-Aug-2029 05:25:51	100	-74.2	3.81	3.11	9.39	37.98	4	1	14.20	14.2	16.15
	CU-Man-E13		04-Aug-2029 06:49:40	ΔV =	0 m/s								3.1	
	Apo-Man-E13		08-Aug-2029 07:27:23	ΔV =	2.142 m/s								4.0	
	Europa14	O	15-Aug-2029 10:30:01	100	-36.1	3.82	4.72	9.42	37.96	4	1	14.20	14.2	16.63
	CU-Man-E14		18-Aug-2029 11:44:29	ΔV =	0 m/s								3.1	
COT-2	Apo-Man-E14		22-Aug-2029 13:31:02	ΔV =	2.498 m/s								4.1	
	Europa15	I	29-Aug-2029 15:32:40	100	1.4	3.82	4.55	9.37	38	4	1	14.20	14.2	17.10
	CU-Man-E15		01-Sep-2029 16:39:17	ΔV =	0 m/s								3.0	
	Apo-Man-E15		05-Sep-2029 19:49:51	ΔV =	1.045 m/s								4.1	
	Europa16	I	12-Sep-2029 20:33:20	25	40.9	3.81	2.58	9.31	38.07	4	1	14.20	14.2	17.57
	CU-Man-E16		15-Sep-2029 21:32:51	ΔV =	0 m/s								3.0	
	Apo-Man-E16		20-Sep-2029 01:53:29	ΔV =	4.581 m/s								4.2	
	Europa17	I	27-Sep-2029 01:34:33	25	82.1	3.80	0.72	9.27	38.09	4	1	14.20	14.2	18.05
	CU-Man-E17		30-Sep-2029 01:29:00	ΔV =	0 m/s								3.0	
	Apo-Man-E17		04-Oct-2029 06:05:15	ΔV =	2.908 m/s								4.2	
	Europa18	I	11-Oct-2029 06:13:06	100	74.2	3.82	3.36	9.22	34.12	7	2	12.43	24.8	18.52
	CU-Man-E18		14-Oct-2029 06:21:55	ΔV =	0 m/s								17.2	
	Apo-Man-E18		30-Oct-2029 00:14:13	ΔV =	5.847 m/s								15.7	
	Europa19	I	05-Nov-2029 02:34:07	100	92.4	3.85	6.17	9.17	29.92	3	1	10.65	10.6	19.35
	CU-Man-E19		08-Nov-2029 03:53:46	ΔV =	2.465 m/s								3.1	
	Apo-Man-E19		10-Nov-2029 13:54:09	ΔV =	0 m/s								2.4	
Pump-down, Crank-up	Europa20	I	15-Nov-2029 18:02:04	100	97.7	3.85	8.73	9.22	25.39	5	2	8.88	17.7	19.70
	CU-Man-E20		18-Nov-2029 19:32:54	ΔV =	0 m/s								3.1	
	Apo-Man-E20		28-Nov-2029 13:38:02	ΔV =	6.345 m/s								9.8	
	Europa21	I	03-Dec-2029 11:56:44	100	92.9	3.87	11.09	9.23	20.6	2	1	7.10	7.1	20.30
	Apo-Man-E21		05-Dec-2029 16:04:02	ΔV =	2.68 m/s								2.2	
	Europa22	I	10-Dec-2029 14:14:08	100	109.1	3.88	12.87	9.28	17.15	5	3	5.92	17.7	20.53
	CU-Man-E22		22-Dec-2029 11:06:26	ΔV =	0 m/s								11.9	
	Apo-Man-E22		25-Dec-2029 10:07:17	ΔV =	2.082 m/s								3.0	
	Europa23	I	28-Dec-2029 08:03:48	805.1	117.6	3.89	13.87	8.27	14.03	N	R	5.22	28.7	21.12
	CU-Man-E23		07-Jan-2030 20:29:36	ΔV =	0 m/s								10.5	
Pi-transfers	Apo-Man-E23		10-Jan-2030 11:09:44	ΔV =	0 m/s								2.6	
	Ganymede24	O	26-Jan-2030 00:58:15	1346.7	-88.3	2.78	14.86	13.91	13.99	pi-tran		7.15	3.5	22.08

Left rotated labels: "Europa Anti-Jovian Hemisphere Coverage" (upper section), "Change Lighting Conditions" (lower section)

Phase	Flyby/ Maneu-ver	In/Out	Date	Altitude (km)	B-Plane Ang (deg)	V-Infinity (km/s)	Inc. (deg)	Peri. (RJ)	Apo. (RJ)	m	n	Period (days)	TOF (days)	Total TOF (months)
	CU-Man-G24		27-Jan-2030 13:36:44	ΔV =	0 m/s								1.5	
	Ganymede25	O	29-Jan-2030 13:39:45	123.1	-2.7	2.79	11.93	12.64	17.3	1	1	7.11	7.1	22.20
	Apo-Man-G25		31-Jan-2030 14:18:35	ΔV =	0 m/s								2.0	
	Ganymede26	O	05-Feb-2030 16:18:38	1584.7	-157.6	2.75	10.2	9.06	15.75	N	R	5.39	8.5	22.44
	Apo-Man-G26		06-Feb-2030 11:27:15	ΔV =	0 m/s								0.8	
	Europa27(e)	I	14-Feb-2030 04:41:04	100	-144.6	3.51	10.81	9.35	17.07	5	3	5.92	17.7	22.72
	CU-Man-E27		20-Feb-2030 08:02:04	ΔV =	0 m/s								6.1	
	Apo-Man-E27		01-Mar-2030 05:07:30	ΔV =	2.338 m/s								8.9	
	Europa28(e)	I	03-Mar-2030 22:40:57	100	166.1	3.50	9.63	9.43	20.41	2	1	7.10	7.1	23.31
	CU-Man-E28		07-Mar-2030 00:20:31	ΔV =	1.92 m/s								3.1	
	Apo-Man-E28		08-Mar-2030 01:48:52	ΔV =	0 m/s								1.1	
	Europa29(e)	I	11-Mar-2030 01:00:39	100	122.8	3.50	7.26	9.45	25.18	5	2	8.88	17.7	23.55
	CU-Man-E29		19-Mar-2030 22:37:34	ΔV =	0 m/s								8.9	
	Apo-Man-E29		23-Mar-2030 19:59:29	ΔV =	9.779 m/s								3.9	
	Europa30(e)	I	28-Mar-2030 18:58:34	100	112.4	3.50	4.52	9.42	29.67	3	1	10.65	10.6	24.14
	CU-Man-E30		31-Mar-2030 19:59:29	ΔV =	0 m/s								3.0	
	Apo-Man-E30		03-Apr-2030 03:11:29	ΔV =	1.912 m/s								2.3	
	Europa31	O	08-Apr-2030 09:47:49	100	-135.6	3.48	6.56	9.39	25.25	5	2	8.88	17.8	24.49
	CU-Man-E31		17-Apr-2030 06:36:22	ΔV =	0 m/s								8.9	
	Apo-Man-E31		21-Apr-2030 05:49:06	ΔV =	5.931 m/s								4.0	
	Europa32	O	26-Apr-2030 04:12:11	100	89	3.50	3.51	9.38	29.71	3	1	10.65	10.6	25.09
	CU-Man-E32		29-Apr-2030 05:49:06	ΔV =	7.373 m/s								3.1	
	Apo-Man-E32		01-May-2030 12:25:55	ΔV =	0 m/s								2.3	
	Europa33	O	06-May-2030 19:02:35	25	-162.5	3.44	4.4	9.28	25.36	5	2	8.88	17.8	25.44
	CU-Man-E33		15-May-2030 15:19:14	ΔV =	0 m/s								8.8	
	Apo-Man-E33		19-May-2030 15:38:43	ΔV =	11.098 m/s								4.0	
	Europa34	O	24-May-2030 13:26:26	601.8	45	3.47	2.52	9.34	29.78	3	1	10.65	10.6	26.03
	CU-Man-E34		27-May-2030 14:22:34	ΔV =	0 m/s								3.0	
	Apo-Man-E34		29-May-2030 19:18:54	ΔV =	10.07 m/s								2.2	
	Europa35	O	04-Jun-2030 04:55:10	100	113.6	3.49	0.47	9.32	29.66	N	R	10.58	10.3	26.39
	CU-Man-E35		07-Jun-2030 06:03:39	ΔV =	0 m/s								3.0	
	Apo-Man-E35		09-Jun-2030 10:10:59	ΔV =	13.642 m/s								2.2	
	Europa36	I	14-Jun-2030 13:13:38	100	111.6	3.48	3.47	9.31	29.79	3	1	10.65	10.7	26.73
	CU-Man-E36		17-Jun-2030 13:50:22	ΔV =	0 m/s								3.0	
	Apo-Man-E36		20-Jun-2030 00:31:43	ΔV =	3.714 m/s								2.4	

Phases (left column labels): Europa Sub-Jovian Hemisphere Coverage; COT-3 Pump-up, Crank-down; Europa Sub-Jovian Hemisphere Coverage; Nonresonant; COT-4

Phase	Flyby/ Maneuver	In/Out	Date	Altitude (km)	B-Plane Ang (deg)	V-Infinity (km/s)	Inc. (deg)	Peri. (R_J)	Apo. (R_J)	m	n	Period (days)	TOF (days)	Total TOF (months)
	Europa37	I	**25-Jun-2030 04:56:31**	100	144	3.46	5.2	9.37	29.74	3	1	10.65	10.6	27.09
	CU-Man-E37		28-Jun-2030 05:31:29	ΔV =	0 m/s								3.0	
	Apo-Man-E37		30-Jun-2030 14:47:53	ΔV =	9.232 m/s								2.4	
	Europa38	I	**05-Jul-2030 20:10:39**	100	175.1	3.49	5.26	9.36	29.75	3	1	10.65	10.7	27.44
	CU-Man-E38		08-Jul-2030 21:12:34	ΔV =	0 m/s								3.0	
	Apo-Man-E38		11-Jul-2030 04:40:04	ΔV =	2.909 m/s								2.3	
	Europa39	O	**16-Jul-2030 11:54:32**	100	-147.6	3.49	3.52	9.33	29.76	3	1	10.65	10.6	27.80
	CU-Man-E39		19-Jul-2030 12:53:40	ΔV =	0 m/s								3.0	
	Apo-Man-E39		21-Jul-2030 18:49:52	ΔV =	0.656 m/s								2.2	
	Europa40	O	**27-Jul-2030 02:56:52**	25	-113.3	3.42	0.43	9.29	29.77	3	1	10.65	10.6	28.15
	CU-Man-E40		30-Jul-2030 04:33:56	ΔV =	0 m/s								3.1	
	Apo-Man-E40		01-Aug-2030 09:55:21	ΔV =	0 m/s								2.2	
	Europa41	O	**06-Aug-2030 16:56:23**	2661.5	-157.5	3.31	0.19	9.12	28.08	N	R	9.89	18.6	28.50
	CU-Man-E41		09-Aug-2030 20:13:52	ΔV =	0 m/s								3.1	
	Apo-Man-E41		11-Aug-2030 16:26:24	ΔV =	0 m/s								1.8	
Impact	**Ganymede42**	I	**25-Aug-2030 06:48:55**	100	17.8	5.77	-	-	-	-	-	-	-	29.12

B-plane = B-plane angle relative to the satellite's mean equator of epoch; V-infinity = Hyperbolic excess velocity; In/Out = inbound (I) or outbound (O) flyby; Inc., Peri., Apo., and Period = Spacecraft central body mean equator inclination, perijove, apojove, and period after the encounter; m = Integer number of gravity-assist body orbits; n = Integer number of spacecraft orbits (NR=nonresonant transfer);TOF = time of flight; CU-Man = Postflyby cleanup maneuver; Apo-Man = Orbit shaping maneuver typically done near apojove; e = Flyby in eclipse.

C.2.3.5.1   Jupiter Orbit Insertion and Energy Pump-Down

The purpose of the first mission phase is threefold: 1) insert into orbit around Jupiter, 2) reduce the spacecraft's energy relative to Jupiter, and 3) orient the spacecraft orbit such that the first set of Europa flybys has near-optimal relative velocity and lighting conditions for IPR, TI, and SWIRS observations (Figure C.2.3-4).

On the initial approach to Jupiter, the spacecraft will execute an inbound[4] Ganymede gravity assist just prior to JOI. JOI, an 857-m/s maneuver, straddles the 12.8-Jovian-radii (R_J) perijove and puts the spacecraft into a 206-day period orbit. Near apojove of this first orbit, another large maneuver (PJR) is necessary to counter solar perturbations induced as a result of the spacecraft's large distance from Jupiter and to target an outbound[5] Ganymede flyby. Four additional Ganymede flybys are then used to further pump-down the spacecraft's energy relative to Jupiter in order to reach the required hyperbolic excess velocity (V_∞) for the first Europa science campaign.

Lastly, since Europa is tidally locked (i.e., the prime meridian always faces towards Jupiter), the terrain illuminated by the Sun is simply a function of where Europa is in its orbit. By implementing a nonresonant G0–G1 transfer followed by three outbound resonant transfers, we can rotate the spacecraft's line of nodes clockwise such that the first set of Europa flybys will occur very near the Sun–Jupiter line (and hence Europa's anti-Jovian hemisphere will be well lit). This is necessary since visible wavelength stereo imaging must be done in unison with IPR measurements.
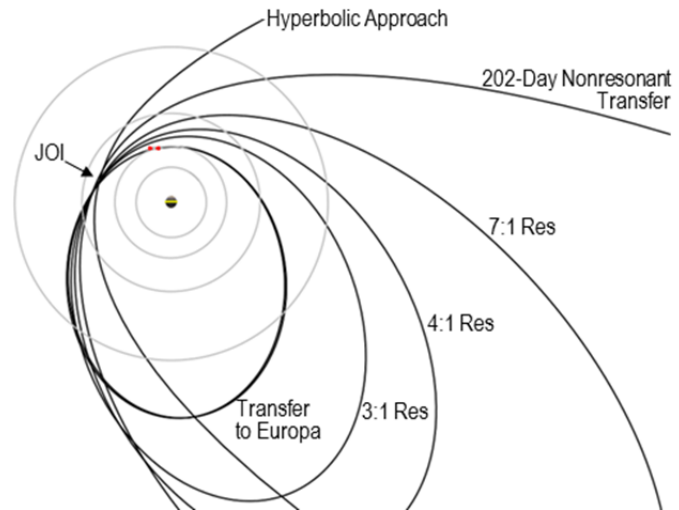

Figure C.2.3-4. View from Jupiter's north pole (Sun-fixed, towards top) of the pump-down phase of the 11-F5 trajectory. Black: spacecraft orbit; Gray: orbits of the four Galilean satellites.

C.2.3.5.2   Crank-over-the-Top

The mission design technique used to systematically cover a specific hemisphere of Europa is referred to as a crank-over-the-top (COT) sequence. This technique entails starting from an equatorial orbit, cranking the inclination up to the maximum[6] (i_{max}) and then returning it to the equatorial plane via a set of resonant transfers. When starting from an inbound flyby, the COT sequence changes the flybys to outbound (transition occurs after i_{max} is reached, hence the term "over-the-top"), and vice versa when starting with outbound flybys. COT sequences starting from inbound flybys render coverage of the sub-Jovian hemisphere; COT sequences starting from outbound flybys cover the anti-Jovian hemisphere. The number of flybys—hence the density of groundtracks—for a given COT sequence is a function of spacecraft orbit period and its V_∞ relative to the gravity-assist body. Specifically,

- For a given period: The number of flybys increases/decreases as V_∞ increases/decreases.

---

[4]   Inbound flyby: Flyby that occurs prior to Jupiter perijove (180º<spacecraft true anomaly<360º)

[5]   Outbound flyby: Flyby that occurs after Jupiter perijove (0º<spacecraft true anomaly<180º)

[6]   Maximum inclination is a function of spacecraft period and the V_∞ relative to the gravity assist body.
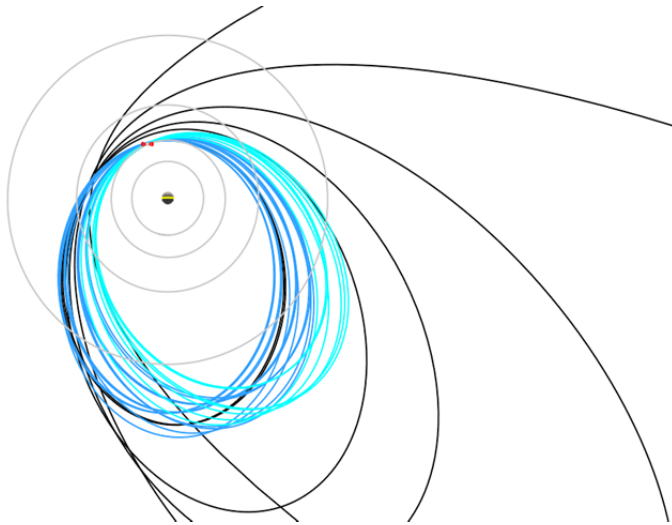
Figure C.2.3-5. View from Jupiter's north pole (Sun-fixed, towards top) of the anti-Jovian hemisphere coverage mission phase. Black: pump-down; blue: COT-1; cyan: COT-2; gray: orbits of the four Galilean satellites.

- For a given V_∞: The number of flybys increases/decreases as the spacecraft period decreases/increases.

Lastly, if the same period resonant transfers are used throughout a COT sequence (i.e., only cranking, no pumping), all closest approaches will lie very near the prime or 180º meridians (i.e., longitudinally 90º away from gravity-assist body's velocity vector). If different period resonant transfers are used during a COT sequence (i.e., cranking and pumping), the closest approach can be placed away from the prime or 180º meridians.

C.2.3.5.3   *Europa Science Campaign, Part I: Europa Anti-Jovian Hemisphere Coverage*

The first Europa science campaign focuses on Europa's anti-Jovian hemisphere (Figure C.2.3-5). This was done since it was more efficient (time, TID, and ΔV) to reach the proper lighting conditions–required by TI and SWIRS observations–on the anti-Jovian hemisphere given the Jupiter arrival conditions of the interplanetary trajectory. This strategy was also preferred by the SDT since IPR measure-

ments performed on Europa's anti-Jovian hemisphere yield a much higher S/N[7].

To meet the science coverage requirements but also minimize the number of Europa flybys (and hence TID), the first COT sequence (COT-1) uses a combination of 4:1 (T=14.3 days) and 7:2 (T=12.4 days) resonant transfers with a V_∞ of approximately[8] 3.9 km/s. While alternating between the two resonances takes more time and leads to a higher TID (7:2 resonance has two perijove passages between Europa flybys), compared to using only 4:1 resonant transfers, it results in the closest approaches being pulled away from the 180º meridian enough to place a large portion of the groundtrack in the equatorial leading and trailing sectors (Figure C.2.3-6), as required for science coverage.

Once COT-1 is complete (which has changed the Europa flybys from outbound to inbound), a nonresonant Europa transfer is used to get back to an outbound flyby such that another COT sequence can be implemented to cover the anti-Jovian hemisphere of Europa. This nonresonant transfer also changes the local solar time (LST) of the Europa flybys by approximately half an hour (counter-clockwise away from the Sun–Jupiter line).

All flybys in COT-1 occur at the ascending node. COT-2 (using strictly 4:1 resonant transfers) instead cranks in the opposite direction, placing the flybys at the descending node. This results in the COT-2 groundtracks intersecting the COT-1 sequence groundtracks (instead of running nearly parallel), hence fulfilling the IPR requirements in all seven anti-Jovian hemisphere sectors to have groundtracks with intersections (Figure C.2.3-7).

---

[7] Jupiter is a radio source in the operating spectrum of the IPR instrument. Hence, IPR measurements done on the hemisphere of Europa shielded from Jupiter render a higher S/N.

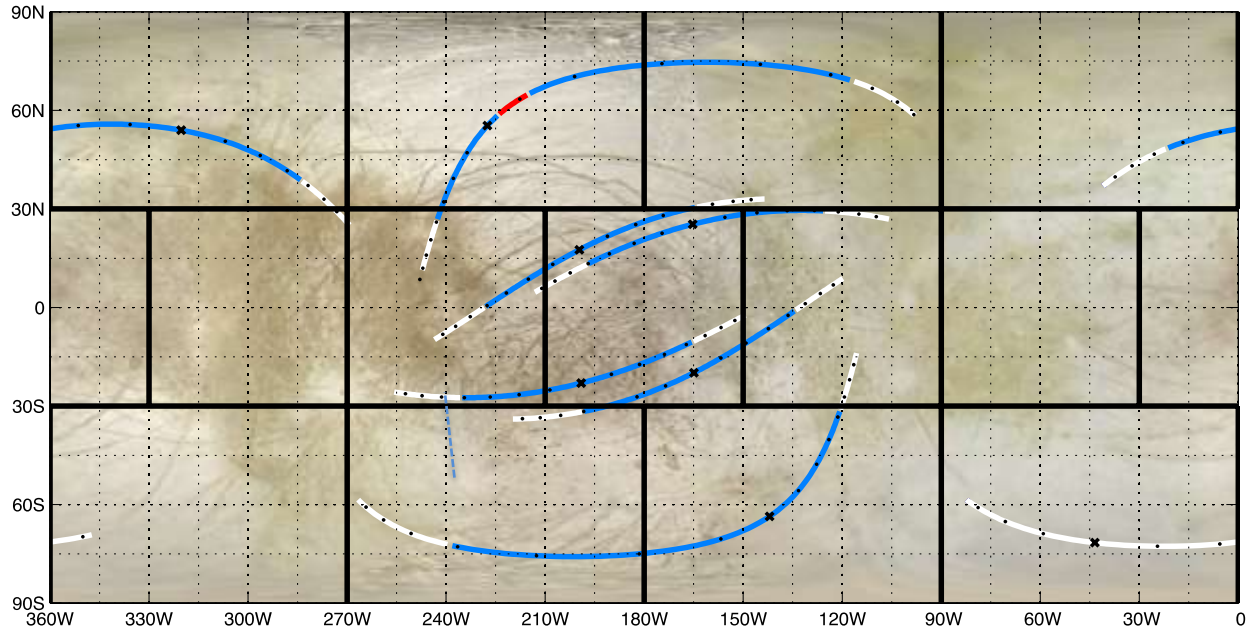[8] Variations in V_∞ occur due to Europa's eccentricity and apsidal precession.

Figure C.2.3-6. Europa nadir groundtrack for COT-1. Closest approach is marked with an "x" and numbered in accordance with Table C.2.3-4. Red: 0<alt≤25 km; blue: 25<alt<400 km; white: 400<alt<1,000 km.
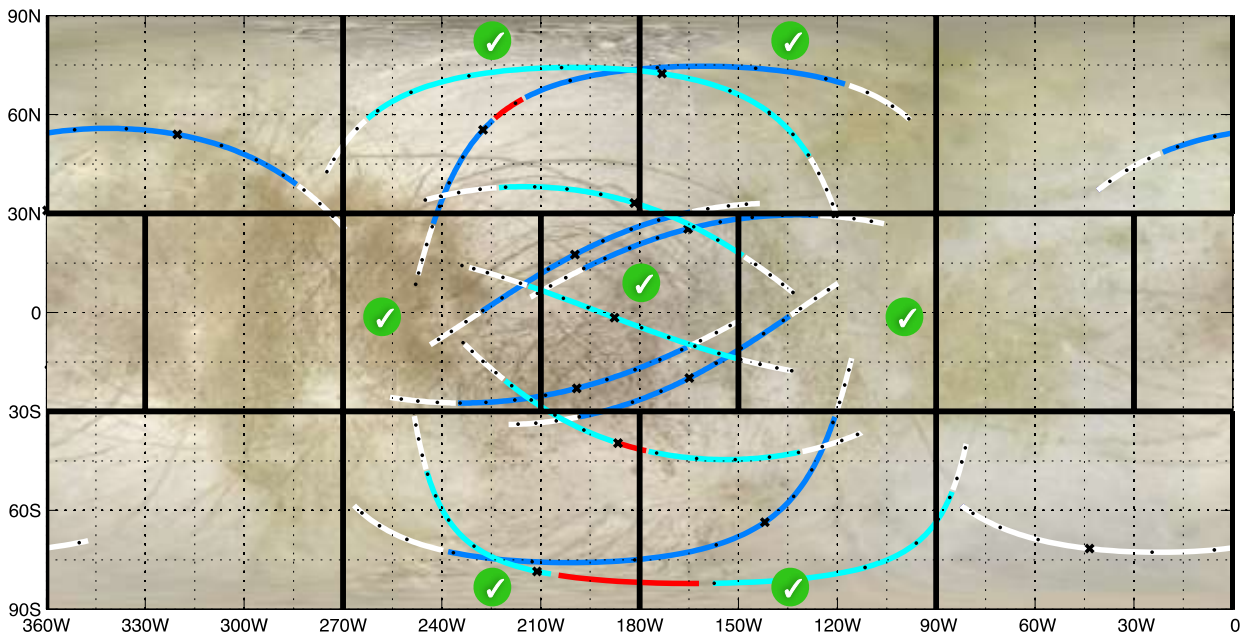

Figure C.2.3-7. Europa nadir groundtrack plot with COT-1 and COT-2. Green check marks indicate IPR requirements are met in specified sector. Closest approach is marked with an "x" and numbered in accordance with Table C.2.3-4. Red: 0<alt≤25 km; blue (COT-1) and cyan (COT-2): 25<alt<400 km; white: 400<alt<1,000 km.

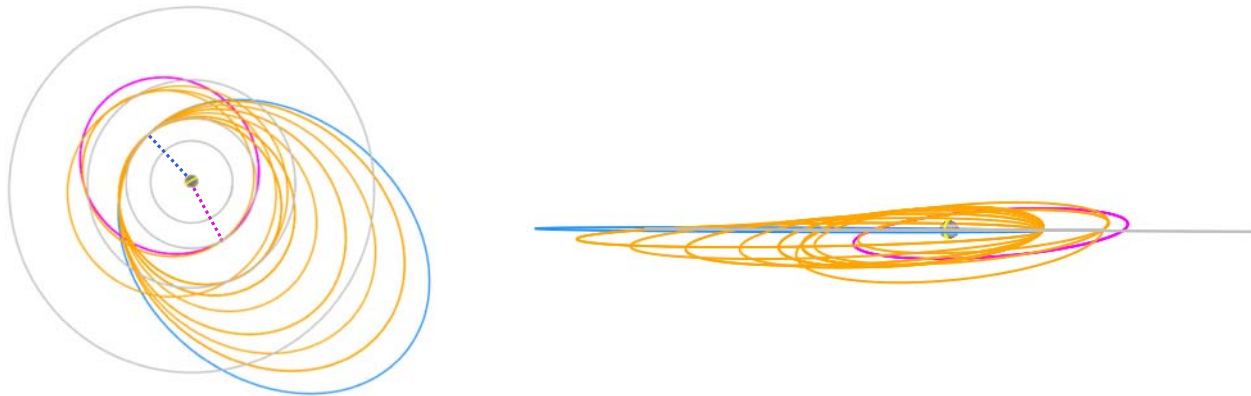**Figure C.2.3-8.** "Switch-flip" method used to change the Europa lighting conditions by ~180º. Dashed lines indicate locations of the Europa flybys before (blue) and after (magenta) the switch-flip. Blue: Last COT-2 orbit; orange: switch-flip sequence; magenta: first COT-3 orbit. <u>Left</u>: View from Jupiter's north pole (Sun-fixed, towards top). <u>Right</u>: View from Jupiter's equatorial plane, north pole towards top of the page.

C.2.3.5.4   Lighting Condition Change

Again, since visible wavelength stereo imaging must be done in unison with IPR measurements, it's necessary to change the observation lighting conditions by 180º prior to taking IPR data on Europa's sub-Jovian hemisphere. That is, the location of the Europa flybys needs to be moved to the opposite side of Jupiter so that Europa's sub-Jovian hemisphere is well lit. Three different strategies can be implemented to accomplish this, using

1. Primarily nonresonant Callisto and/or Ganymede transfers
2. Only nonresonant Europa transfers
3. A "switch-flip" (Europa-to-Ganymede pi-transfer[9] → Ganymede pi-transfer → Ganymede-to-Europa pi-transfer)

Each has its advantage. Option 1 will have the longest time of flight (TOF) but the lowest TID since perijove will be above Europa's orbit radius the majority of the time. Option 2 will have the highest TID but will stay at Europa the entire time providing opportunities for continuous Europa observations over a wide range of geometries. Option 3 provides by far

the fastest way to get from one side of Jupiter to the other, but does have a fairly high TID (although not as high as Option 2).

For this study, the switch-flip option was employed due to its time efficiency (Figure C.2.3-8). The detailed sequence of events includes first cranking up the inclination and pumping down the orbit period to set up the correct geometry for a Europa-to-Ganymede transfer. A Ganymede pi-transfer is then executed (3.5-day TOF), followed by a 1:1 resonant Ganymede transfer that cranks down the inclination and sets up the Ganymede-to-Europa pi-transfer. The result: All subsequent Europa flybys are located ~180º away from the last Europa flyby in COT-2.

It should be noted that either Option 1 or 2 could instead be seamlessly added to the end of the 11-F5 COT-2 sequence.

*C.2.3.5.5   Europa Science Campaign, Part II:
Europa Sub-Jovian Hemisphere
Coverage*

The second Europa science campaign focuses on Europa's sub-Jovian hemisphere. Immediately following the Ganymede-to-Europa transfer, Europa flybys are used to pump-up the orbit and crank-over-the-top. Like COT-1, the goal of COT-3 is to minimize the number of flybys while still providing adequate coverage for science. However, since the V_∞ is

---

[9]   A nonresonant transfer (typically inclined) in which two successive flybys are separated by 180º (or pi-radians) in true anomaly (i.e., flybys occur on the opposite sides Jupiter).

~3.5 km/s (instead of 3.9 km/s in COT-1), the COT-3 sequence must alternate between 3:1 (T=10.7 days) and 5:2 (T=8.8 days) resonant transfers to accomplish this. Lastly the first four Europa flybys in COT-3 (Europa27 [E27] to Europa30 [E30]), are in Jupiter's shadow; hence no stereo imaging can be performed in unison with IPR measurement (see Figure C.2.3-9).

Once COT-3 is complete, a nonresonant Europa transfer is used to get back to an inbound flyby such that another COT sequence can be implemented to cover Europa's sub-Jovian hemisphere. This nonresonant transfer also changes the LST of the Europa flybys by approximately one hour (clockwise away from the Sun–Jupiter line).

Finally, COT-4 cranks in the opposite direction from COT-3 (i.e., switches the node at the Europa flybys from descending to ascending) with 3:1 resonant transfers to intersect the COT-3 sequence groundtracks, fulfilling the IPR requirements in six of the seven sub-Jovian hemisphere sectors (Figure C.2.3-10).

At the conclusion of COT-4, 13 of the 14 sectors have been covered sufficiently to meet the observational and measurement requirements of all four instruments on board as defined by the SDT (Figure C.2.3-10).

C.2.3.6   Navigational Feasibility

The 11-F5 trajectory (Figure C.2.3-11) is a proof-of-concept trajectory establishing the potential for a Europa Multiple-Flyby Mission that accomplishes high-quality scientific observations and measurements to significantly advance our knowledge of one of the most scientifically intriguing targets in our solar system. To prove we can—with a very high level of confidence—navigate the 11-F5 trajectory (or something similar) in the Jupiter system would require a high-fidelity covariance analysis, a task beyond the scope of the study. However, we can make a preliminary assessment of the 11-F5 trajectory by analyzing key mission events and comparing them to Cassini,

the most complicated gravity-assist trajectory ever flown.

Due to the distance from Earth of deep space missions, the spatial and temporal proximity of key/critical events (i.e., operational intensity) are among the most important factors in determining operational feasibility. In terms of navigation, analysis can be focused on two types of events, targeted flybys and propulsive maneuvers.

C.2.3.6.1   Targeted Flybys

A sufficient amount of time is required between successive targeted flybys to accurately determine the spacecraft's orbit after the first flyby, as well as design, uplink, and perform a series of maneuvers to target the subsequent flyby. This places a lower bound on the TOF between targeted encounters.

The delivery accuracy for a given targeted flyby is primarily a function of the spacecraft trajectory uncertainties, as well as the ephemeris uncertainties of the bodies in the system the spacecraft resides in (especially the targeted flyby body). The delivery accuracy for a given flyby directly affects the ΔV costs (i.e., how much propellant is requires to cleanup flyby misses) and the minimum allowable flyby altitude of a body (probability of impact must be nil after the last maneuver to target the flyby has been executed). As the spacecraft and system uncertainties decrease–as knowledge of the system is gained via radiometric tracking data–so too does the minimum TOF between targeted flybys and the minimum flyby altitude. As such, the 11-F5 trajectory adheres to a two-prong strategy:

1) Temporally ratchet down minimum flyby altitudes (paying particular attention to the first encounter of each body).
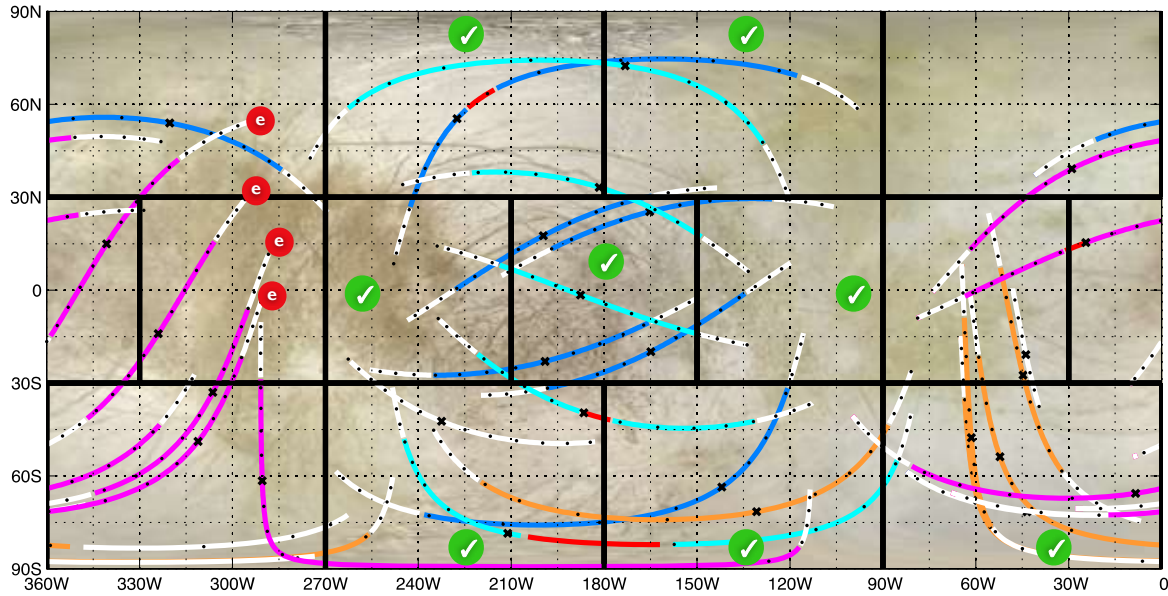
2) Slowly decrease the average TOF between flybys.

Figure C.2.3-9. Europa nadir groundtrack plot for COT-1 through COT-3. Green check marks indicate IPR requirements are met in specified sector. Red circles with "e" indicate flybys in eclipse. Closest approach is marked with an "x" and numbered in accordance with Table C.2.3-4. Red: 0<alt≤25 km; blue (COT-1), cyan (COT-2), orange (change lighting), and magenta (COT-3): 25<alt<400 km; white: 400<alt<1,000 km.
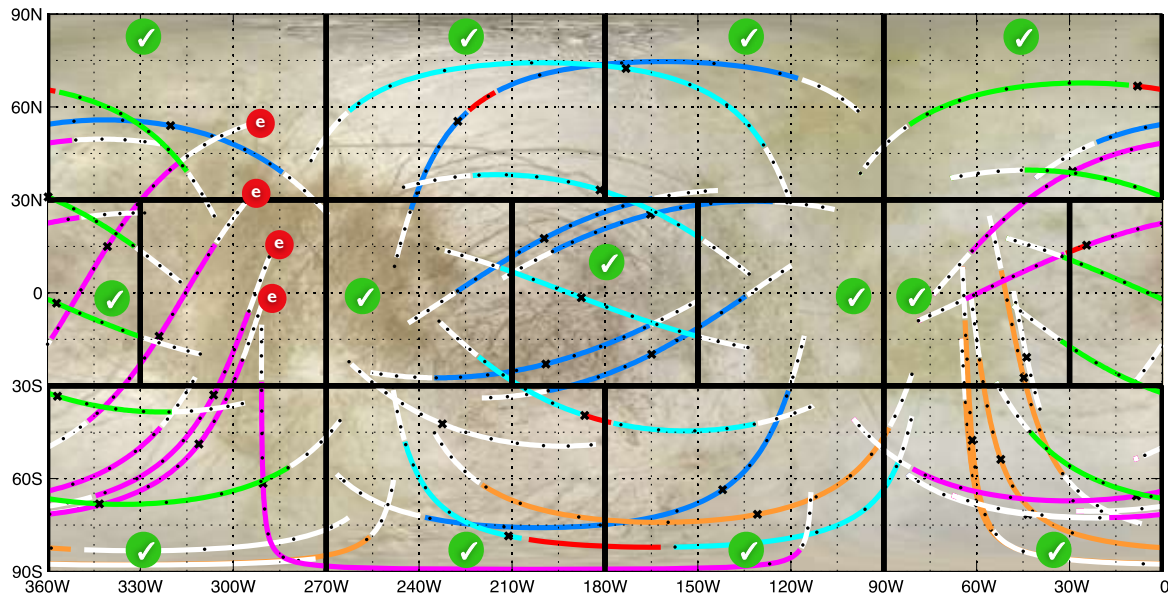

Figure C.2.3-10. Europa nadir groundtrack plot for entire 11-F5 baseline trajectory. Green check marks indicate IPR requirements are met in specified sector. Red circles with "e" indicate flybys in eclipse. Closest approach is marked with an "x" and numbered in accordance with Table C.2.3-4. Red: 0<alt≤25 km; blue (COT-1), cyan (COT-2), orange (switch-flip), magenta (COT-3), and green (COT-4): 25<alt<400 km; white: 400<alt<1,000 km.
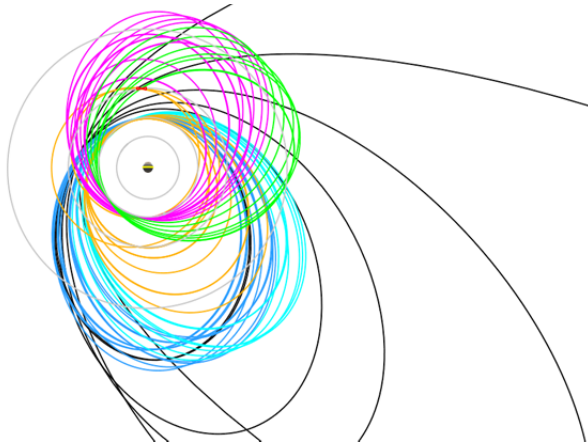
Figure C.2.3-11. View from Jupiter's north pole (Sun-fixed, towards top) of the 11-F5 baseline trajectory. Black: pump-down; blue: COT-1; cyan: COT-2; orange: switch-flip; magenta: COT-3; green COT-4; gray: orbits of the four Galilean satellites.

The first portion of the strategy is implemented by targeting the first Ganymede and Europa flybys to altitudes (500 and 724 km, respectively, as in Table C.2.3-4). These are relatively high when compared to minimum flyby altitudes executed by Galileo. Subsequent flybys of each body decrease uncertainties, and hence allow lower flybys to be carried out. Notice that all 25 km Europa flybys (done to maximize the quality of INMS measurements) will be performed at the end of COT sequences, where numerous 100 km flybys will have been completed and Europa's ephemeris will have become well known (at the particular LST the COT sequence occurs at). Lastly, it should be noted that since Ganymede and Europa are in a 2:4 orbital resonance, the first five Ganymede flybys (G0-G4) will provide knowledge of Europa's dynamics, thereby decreasing Europa's ephemeris uncertainties prior to the first Europa flyby.

The second portion of the strategy will be implemented by beginning with alternating 4:1 (TOF=14.2 days) and 7:2 (TOF=24.88 day) resonant transfers in the first COT sequence (COT-1). This oscillation in resonance transfers lessens the navigation intensity by interleaving longer-TOF multirevolution resonant transfers between each shorter 4:1 resonant transfer, and results in a mean TOF/encounter equal to 19.5 days.

With decreased Europa ephemeris uncertainties, a 14.4-day non-resonant transfer will be followed by COT-2, consisting of five back-to-back 4:1 resonant transfers, translating to a mean TOF/encounter of 14.2 days.

The pump-down and pi-transfer phases of the tour continue the downward average TOF/encounter trend, namely a decrease to 14 days. Of notable interest is the 3.5-day Ganymede-to-Ganymede pi-transfer. This transfer was implemented to minimize total tour TOF and is believed to be navigationally feasible based on the ballistic nature of the transfer (i.e., no deterministic maneuvers) and the high altitude of the first Ganymede flyby (G24, 1,346 km), which will decrease the ΔV sensitivity of a flyby miss. The later characteristic will minimize the magnitude of the G24 cleanup maneuver, which is important since there will only be time for a single maneuver. For comparison, Cassini successfully executed an 8-day Titan pi-transfer in 2009. This transfer was also designed to be ballistic; in operations a single maneuver was executed with a magnitude of 0.75 m/s. If however the current baseline 3.5-day Ganymede pi-transfer is ultimately deemed too aggressive, a 3-, 5-, or 7-pi-transfer (i.e., TOFs of 10.5, 14, or 17.5 days, respectively) could be utilized instead.

COT-3 and COT-4 will proceed to further reduce the TOF/encounter, with values of 13.75 and 11.95, respectively. The former will use the same alternating resonance strategy as COT-1 (only this time with 3:1 [TOF=10.65 days] and 5:2 [TOF=25.44 days] resonances), and the latter will implement five back-to-back 3:1 resonant transfers.

As a reference, Cassini performed nine back-to-back 1:1 resonant transfers with Titan (15.9-day TOF) under much more dynamic

Table C.2.3-5. 11-F5 flyby ΔV summary.

Activity	CBE ΔV (m/s)	MEV ΔV (m/s)	Comments
Launch Injection Cleanup	20	20	Estimate to correct injection errors from launch vehicle.
Earth Bias ΔV	50	50	Needed for final correction of deliberate aim-point bias away from the Earth. ~25 m/s per Earth flyby. May be performed separately or integrated with other TCMs.
Deep Space Maneuver (DSM)	0–100	150	Maneuver on Earth-Earth leg near aphelion. Baseline launch period variation goes from 0 m/s up to 100 m/s.
Interplanetary Statistical & ΔV Cleanup	50	50	Multiple small maneuvers.
JOI at 12.8 R_J, 500-km G0 Flyby	857	900	200-day initial orbit.
Perijove Raise Maneuver	114	135	Counteracts solar perturbations, targets G1 flyby.
Tour Deterministic ΔV	157	200	Used primarily for targeting many resonant transfers.
Tour Statistical ΔV	63	170	~5 m/s per flyby for first 20 flybys, then 3 m/s for last 22 flybys (conservative). Rounded up. Expected average per-flyby values: 1.5 m/s per flyby
TOTALS	**1311***	**1675**	

*Assumes maximum DSM value

conditions (12–63º inclination and much closer central body periapses) and higher ΔV loads[10].

C.2.3.6.2   Maneuvers

Throughout a mission's lifetime, numerous deterministic maneuvers are required to shape the trajectory, and numerous statistical maneuvers are necessary to correct trajectory errors due to a number of sources. In the case of the 11-F5 trajectory, maneuver locations were generally placed 3 days after each flyby to cleanup any flyby errors, and near apoJove to target the subsequent flyby (where timing permitted). Due to time constraints associated with this study, the maneuvers have not yet been placed for optimal navigation robustness (i.e., provide time for apoJove backup maneuver locations prior to the targeted flyby). However, all transfers in the 11-F5 trajectory have, at most, only one maneuver with a deterministic component. In addition, the trajectory has very comfortable ΔV margins. These facts make future adjustments to maneuver locations of no foreseeable concern (based on extensive design experience on Cassini's prime and two extended missions).

C.2.3.6.3   Overall Flexibility

The proposed 11-F5-like trajectory will push the envelope of navigational complexity, but will do so in a very strategic manner. However, if future analysis reveals any portion of the trajectory is navigationally infeasible, or stresses the system in other ways, such as fault recovery time, many trajectory design options exist. As previously mentioned, phasing orbits can be inserted to lengthen the 3.5-day-TOF transfer, and other "lighting condition change" options can be implemented, whether it's the alternate options detailed in Section C.2.3.5.4 or a different switch-flip sequence to obtain a higher V_∞ at Europa, so the COT-3 and COT-4 sequences maintain a high average TOF between flybys.

C.2.3.7   Mission ΔV

Table C.2.3-5 summarizes both the estimated current best estimate (CBE) and maximum expected value (MEV) for the total ΔV needed to execute the Europa Multiple-Flyby mission. The two totals are comprised of both computed values (DSM, JOI, PJR and the tour's deterministic ΔV) and estimated values (launch injection cleanup, Earth bias ΔV, interplanetary statistical ΔV and tour's statistical ΔV).

---

[10] Cassini's average ΔV budget was ~100 m/s per year during the Prime and Equinox missions.

The 11-F5 trajectory is a fully integrated trajectory from launch to end of mission in a high-fidelity force model including *n*-body perturbations. As such, high confidence can be placed on all computed ΔV components.

Statistical ΔV estimates are ultimately computed via a high-fidelity covariance analysis in unison with Monte Carlo simulations. Because this analysis is outside the scope of the Europa Study, the statistical ΔVs for this report were estimates based on previous operational experience with Cassini and Galileo.

See the Mass Margin Summary (Section C.2.4.7.1) for calculations of propellant loading based on ΔV and thruster usage.

C.2.3.8   Potential Extended Mission(s)

Given a healthy Europa Multiple-Flyby Mission spacecraft with demonstrable radiation margin at the end of the prime mission (and the necessary authorization, of course), a variety of different extended missions are possible from an orbital mechanics point of view. They include, but are not limited to

- Higher density core science observations (i.e., cover greater variety of terrain with higher frequency)
- New Europa campaigns:
  – Gravity/tides investigation
  – Regional mapping of the leading and trailing hemispheres
- Regional global-coverage missions at Ganymede, Callisto, or both
- Europa, Ganymede or Callisto orbit (if sufficient propellant is available)

C.2.3.9   Spacecraft Disposal

Planetary protection may require that, before control of the spacecraft is lost, action is taken to minimize the probability of biological contamination of Jupiter's moon Europa resulting from spacecraft impact. To preclude Europa impact, the study team chose Ganymede impact as the baseline spacecraft disposal scenario. This disposal scenario was chosen simply

because it was the transfer with the lowest TOF (post Europa-41) that resulted in impact.

Many additional potential spacecraft disposal options exist that avoid collision with Europa, including (but not limited to) the following:

- Jovian system impacting trajectories:
  – Jupiter (via short- or long-period orbits, the latter using solar perturbations)
  – Io, Ganymede, or Callisto
- Long-term Jupiter-centered orbits:
  – Circular orbit between Ganymede and Callisto
  – Eccentric orbit outside of Callisto
- Jupiter system escape:
  – Heliocentric orbit
  – Saturn flyby, impactor, or potentially even capture
  – Icy-giant flyby or impactor
  – Trojan asteroid flyby or impactor

While theoretically all of these options are possible, numerical verification would need to be carried out to prove the existence (particularly the gas- and icy-giant flyby/impact trajectories) and quantify the TOF and associated ΔV costs of each.

C.2.4   *Flight System Design and Development*

The flyby flight system is a highly capable spacecraft tailored to the flyby science objectives of agile pointing, large data storage, and large data transmission.

C.2.4.1   Flight System Overview

The Europa Multiple-Flyby Mission flight system (FS) concept, pictured in Figure C.2.4-1, is a three-axis-stabilized spacecraft with three distinct modules arranged along the Z (vertical) axis from top to bottom.

The Avionics Module is dominated by the 3-meter high-gain antenna (HGA) on top of the UES along the +Z axis. This module also includes the science payload consisting of four instruments mounted beneath the HGA. Avionics and instrument electronics are carried in

an internal radiation vault descending into the core.

The Propulsion Module lies centrally, surrounding the electronics vault, with the main rocket engine at the bottom, directed along the –Z axis. Tanks and the outrigger-mounted control thruster are at mid-span.

The ASRGs for power generation are mounted symmetrically about the main engine as part of the Power Source Module, which also includes the launch adapter.

These three modules are discussed in more detail below.

Instruments

The FS is configured to support the notional model payload described above, consisting of the following science instruments:

- Topographical Imager (TI)
- Shortwave Infrared Spectrometer (SWIRS)
- Ice-Penetrating Radar (IPR)
- Ion and Neutral Mass Spectrometer (INMS)

The TI, SWIRS, and IPR are coboresighted and configured for nadir-pointing during the close flyby of Europa. The INMS is configured to nominally point in the velocity vector direction during the flyby, roughly perpendicular to the nadir direction.

Attitude Control

The flyby spacecraft is three-axis-stabilized in all phases of flight. Stabilization is achieved through the use of inertial measurement and star measurement for attitude determination and thrusters or reaction wheels for attitude control.

Data Handling

During each flyby over 32 Gbits of data are generated by the instruments and engineering subsystems. This data can be stored multiple times in a large, redundant, solid-state data recorder (256 Gbits in total; 128 Gbits per card) that is part of the Command and Data

Handling Subsystem (C&DH). Concepts for data integrity using the excess storage capability will be studied during Phase A.

Power

The proposed power source for this spacecraft is four ASRGs. The power system is sized to accommodate one failure (mechanical or electrical) of an ASRG. Excess power is stored in the 59-A-hr lithium-ion battery or dumped as heat through a thermal shunt. For mission activities that are not power-positive, a positive energy margin is obtained by using the battery, which has been sized accordingly.

Thermal

To minimize the power demand of the spacecraft (because we desire to minimize the number of ASRGs), the spacecraft was designed to minimize the use of electrical heaters. To achieve this goal, the heat from spacecraft electronics is captured inside a thermal shroud surrounding the midsection. This allows the propellant to be kept near room temperature without the need for supplemental electrical heaters. The concept also includes 30 radioisotope heater units (RHUs) and/or variable RHUs (VRHUs), which will be used in select locations (e.g., thruster cluster assemblies) to minimize the need for electrical heaters.

Communications

The Communications Subsystem is designed to support the high volume of science data to be transmitted back to Earth after each flyby. This system consists of X-band downlink for low-data-rate telemetry, and Ka-band downlink using a 3-meter HGA for high-data-rate telemetry (including the science data collected during the flyby). X-band uplink is used for commands.

Propulsion

The Propulsion Subsystem must support attitude control, momentum management, trajectory correction, and Jupiter Orbit Insertion (JOI). To achieve these requirements the Pro-

pulsion Subsystem is a dual-mode, bipropellant architecture. The fuel, oxidizer, pressurant tanks, and supporting structure are distributed around the core of the spacecraft to provide radiation shielding to the internal electronics. During Phase A, a risk assessment will be performed on potential micrometeoroid damage to the tanks; if necessary, the thermal shroud can be upgraded with standoff Whipple bumper shields. The tanks are sized for maximum propellant for spacecraft on the Atlas 551 and can support up to 1.68 km/s of ΔV. The actuators consist of one 458-N main engine, four thrust vector control (TVC) thrusters, and sixteen attitude-control thrusters (eight primary, eight redundant) arranged in four clusters, each thruster cluster assembly (TCA) containing four attitude-control thrusters and one TVC thruster.

Redundancy

The spacecraft uses a redundancy philosophy similar to that of Cassini and comparable systems, where most active elements are redundant, with selected cross-strapping, and where the instruments are single-string. The main engine and TVC are also single-string; these single-string elements will undergo a risk assessment in Phase A to determine if the risk is acceptable. There is sufficient mass margin to accommodate dual redundancy here, if appropriate.

Radiation

This mission has a very demanding total ionizing dose (2.01 Mrad behind an equivalent of 100 mil Al Si), mostly from electrons). To support the use of standard aerospace EEE parts, we have employed a multilayered radiation shielding approach as part of the spacecraft design concept. Most of the spacecraft electronics are housed in a radiation vault (similar to that on the Juno spacecraft); this vault is also located inside the spacecraft to benefit from shielding provided by other spacecraft elements, such as the batteries, structure, and tanks. Inside the vault the end of

mission TID environment is 150 krad , with boards nearer the center encountering even less. Electronics will be tolerant to at least 300 krads, for a radiation design factor of 2 or better.

C.2.4.1.1   *Flight System Configuration*

The engineering configuration of the spacecraft concept is shown in Figure C.2.4-1. On the left side of the figure is the CAD model without the thermal shroud and with instruments stowed. On the right side of the figure is a cross-sectional view.

Avionics Module

The 3-meter HGA is at the top of the Avionics Module. Co-located on this structure is the medium-gain antenna (MGA) and one of three low-gain antennas (LGAs). Below the HGA is the UES. This holds the instruments, reaction wheels, and star-trackers. At the bottom of the Avionics Module is the avionics vault. Inside the vault is a majority of the spacecraft avionics, which is nested within the Propulsion Module to maximize the radiation shielding from the tanks, structure, and propellant. The Avionics Module attaches to the Propulsion Module. The equipment in the vault is accessible throughout integration and testing of the Avionics Module, while the equipment in the UES is accessible throughout integration and testing of the spacecraft as a whole. After spacecraft integration, a demate operation from the Propulsion Module will enable access to the vault.

Propulsion Module

The Propulsion Module is an integrated structure with all the tanks (fuel, oxidizer, pressurant), plumbing, pressurization control assembly (valves, filters, sensors, etc.), propellant isolation assembly (valves, filters, sensors, etc.), the thrusters mounted on four thruster clusters, and main engine mounted at the bottom of the module.
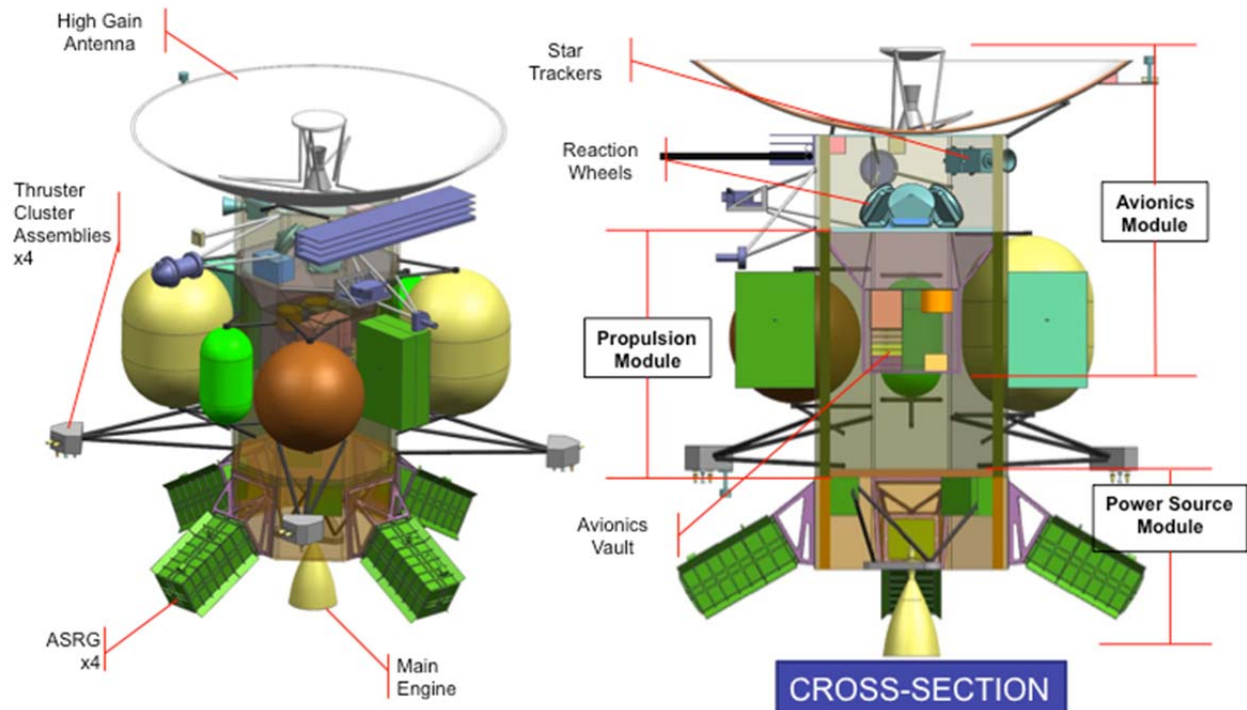
Figure C.2.4-1. The modular configuration shown provides maximum radiation shielding for the electronics (thermal shroud is not shown).

Power Source Module

The Power Source Module is an integrated structure with the launch vehicle adapter and ASRGs. The ASRG consists of the power sources, mounted externally, and their control electronics, located further inboard.

Thermal Shroud and Shading

The thermal shroud covers most of the spacecraft including parts of all three modules. Figure C.2.4-2 shows the spacecraft (with the 15-m IPR antenna deployed) enveloped by the thermal shroud, shown semi-transparently around the midsection. The bottom view shows how the HGA and thermal shroud protect the spacecraft from the high solar flux during the Venus flyby portion of the interplanetary cruise. Besides the HGA, the few elements exposed to the solar flux are the LGA, thruster clusters, and INMS (with cover). These elements can tolerate heating during the flyby without shading.

C.2.4.1.2   System Block Diagram

Figure C.2.4-3 shows the system block diagram for the flyby spacecraft. The top box is the Avionics Module. The middle box is the Propulsion Module. The bottom box is the Power Source Module. Note items like electrical heaters and temperature sensors are distributed across all the modules. The legend shows the key interface types between elements.

Note that some of the boxes in the block diagram (e.g., C&DH) do not show redundancy because they are internally redundant in configurations not yet determined.

C.2.4.1.3   Flight System Key Requirements

Table C.2.4-1 shows the key drivers on the FS from the science measurements. Two bands of measurement data from the IPR must be captured and processed. During the 15 minutes of data collection per flyby, nadir-pointing and low pointing jitter is required from GN&C.
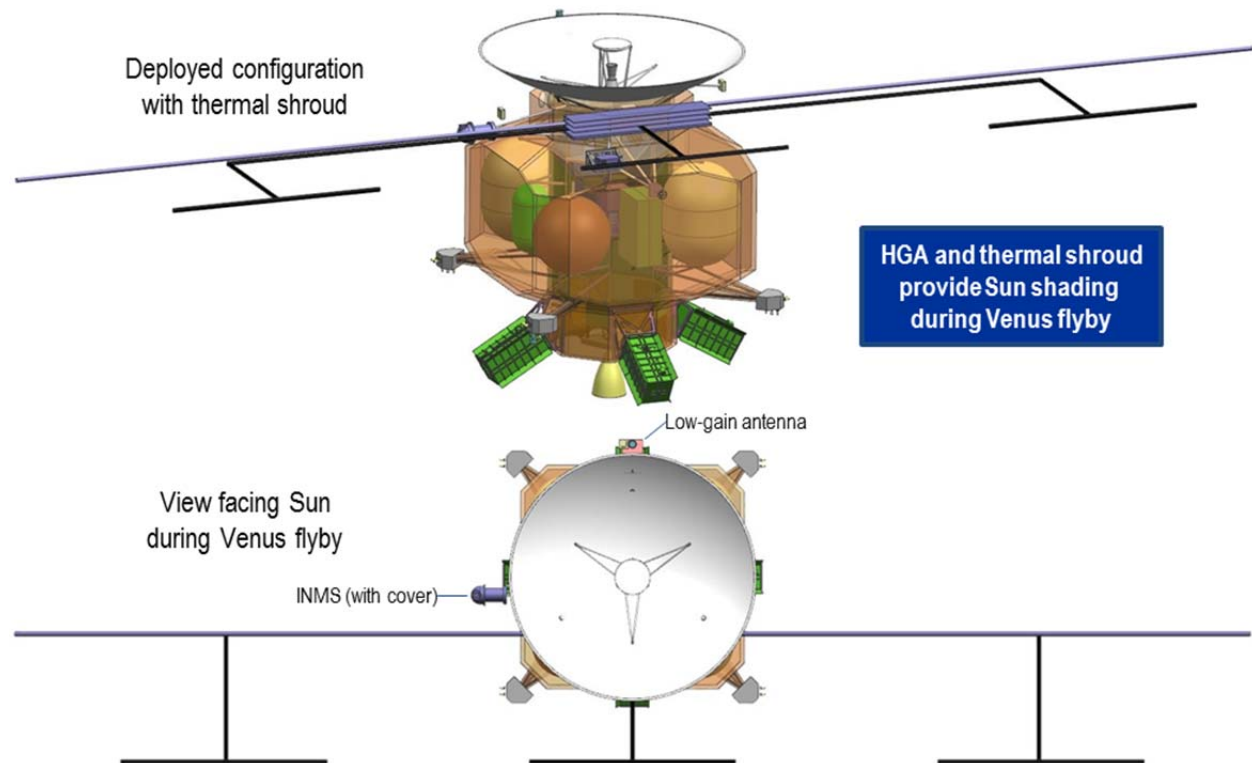
Figure C.2.4-2. The flight system provides thermal balance throughout all mission phases.

The 25 Gbit collected per Europa flyby is a driver on the solid-state recorder (SSR) size. It also drives sizing of the Telecom Subsystem for Ka-band downlink of the radar data. The need to process the radar data after collection but before downlinking drives the throughput capacity of the onboard computer. The 15-meter IPR antenna is required is stowed to fit within the launch vehicle faring at launch, and is deployed after separation from the launch vehicle.

Image resolution of the TI drives low pointing jitter capability from GN&C during nadir-pointing. Stereo imagery during the flyby adds several gigabits of science data and is a driver on the SSR size. The imager must be aligned with the IPR, and it needs a contamination cover that can be deployed after launch.

SWIRS is also aligned with the IPR and TI. Its integration time drives target motion compensation and pointing jitter drivers on GN&C. Its data volume over a 10-hour flyby is several Gbits, driving the SSR size. Finally, its thermal radiator needs an unobstructed view of space during operation.

The INMS aperture must be aligned to the velocity vector during the Europa flyby. It also needs a contamination cover that can be deployed after the Venus flyby.

All brackets, struts, secondary structures, and mechanisms are mechanically grounded to the primary structure. Loads for these appendages are determined using the Atlas V mass acceleration curve.

The power demand of IPR, SWIRS and INMS together forms one of the sizing cases for the battery (JOI is the other)

Table C.2.4-2 shows the key drivers that flow down to the FS from the mission design.

The Venus flyby is a driver for the spacecraft thermal design. This has been addressed by configuring the spacecraft such that the HGA and a thermal shroud can shade the rest of the vehicle.
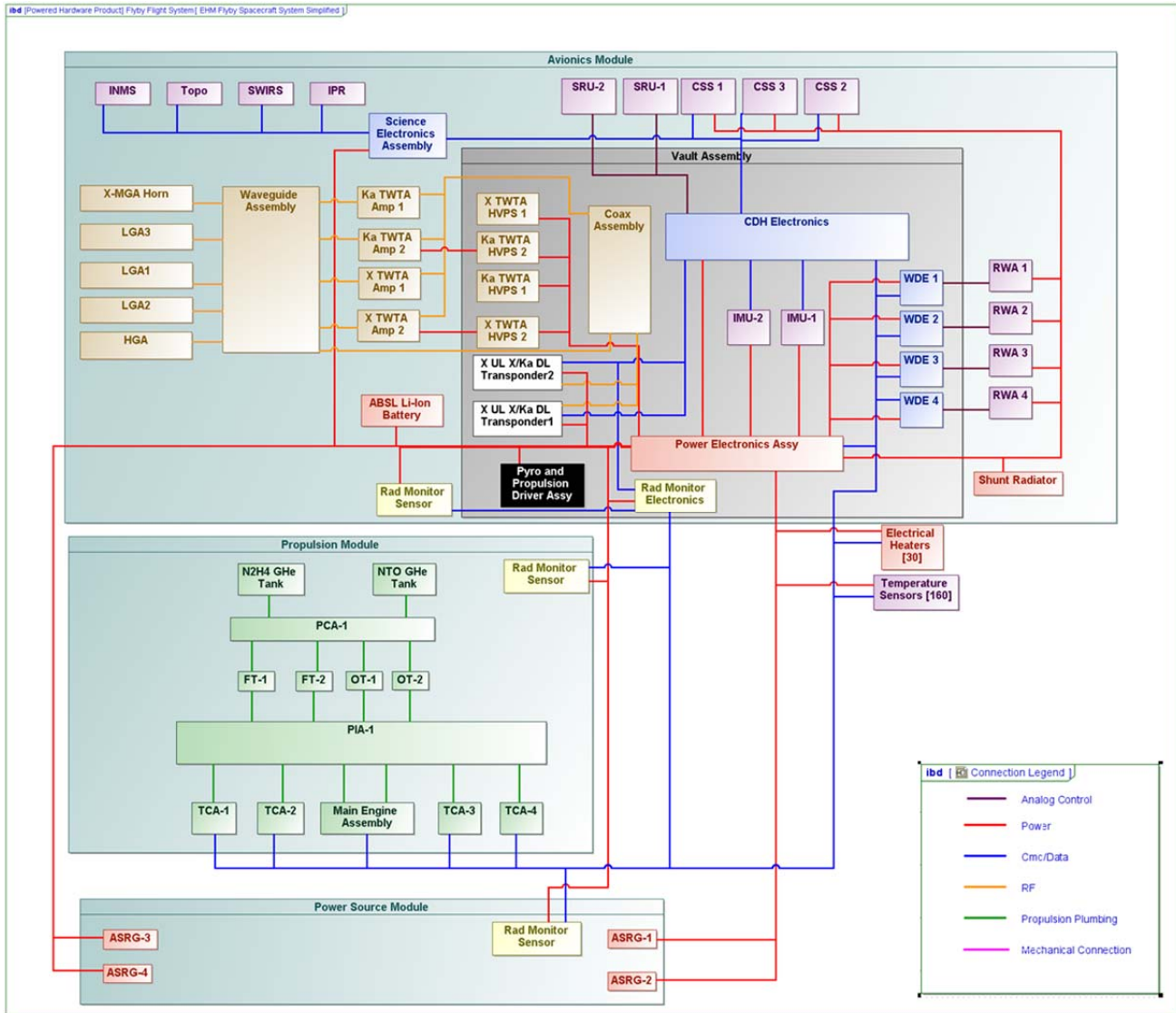
Figure C.2.4-3. The system block diagram shows the simple interfaces among modules on the spacecraft.

During inner solar system cruise, while the HGA must be pointed at the Sun for shading, geometric constraints on telecommunication has been addressed with an X-band system for uplink and downlink using 4-pi steradian coverage from the LGAs.

During the outer-solar-system cruise, commanding and telemetry are accommodated with an X-band system for uplink and downlink using an MGA.

At all times in the outer solar system, cold conditions drive the thermal design of the spacecraft. To minimize electrical heater power demand, internal heating from the electronics is captured within the thermal shroud to keep the spacecraft equipment within allowable flight temperatures. External elements will require electrical heaters or VRHUs. Even so, outer cruise safe mode is currently the sizing case for the number of ASRGs.

JOI is a fully autonomous critical event that requires robust system fault management. A cross-strapped dual-string architecture allows failures to be isolated so that recovery can occur on the backup hardware.

Table C.2.4-1. The spacecraft driving requirements from the science measurements appear to be feasible and consistent, and have been vetted through several Science Definition Team meetings.

Sci. Measure	Requirement	GN&C	Telecom	Power	C&DH	Prop	Thermal	Mech
IPR	Capture & process 2 bands of radar data	Nadir pt	Telecom Ka down	Battery sizing	• Solid-state recorder • Through-put			Antenna de-ploy
TI	Image resolution	• Nadir pt • Jitter						
	Stereo imagery				Solid-state recorder			
	Accommodation							• Align with IPR • Cover
SWIRS	Image resolution, 1/2 IFOV over integration time	• Jitter						
	Data volume				Solid-state recorder			
	Accommodation			Battery sizing				Radiator view of space
INMS	Accommodation			Battery sizing				• Align to RAM • Cover

Table C.2.4-2. Flight system design elements flow down from the mission design driving requirements.

Msn Design	Reqt.	System	GN&C	Telecom	Power	C&DH	Prop	Thermal	Mech
Venus Flyby	Thermal control							Shade with HGA & shroud	
Inner-Solar-System Cruise	Command & telemetry			Xup/ Xdown with LGA					
	Earth fly-bys with ASRG	Fault man-agement							
Outer-Solar-System Cruise	Command & telemetry		Sun-sensors	Xup/ Xdown with MGA					
Outer-Solar-System Cruise/ Europa Flybys	Thermal control				# of ASRGs			Thermal shroud/ RHU/ VRHU	
JOI	Critical event	Fault man-agement	Dual-string/ hot-sparing	Dual-string/ hot-sparing	Dual-string/ hot-sparing	Dual-string/ hot-sparing	TVC size Engine size		
TCM	Navigation			Doppler					
Europa Flybys	Attitude control		Reaction wheel siz-ing						
	Radiation	Fault man-agement	<300-krad parts	<300-krad parts	<300-krad parts	<300-krad parts			Vault & config

However, most fault toler-ance complexity will be driven by the need to react cautiously to any type of disruption, suspending ac-tivity temporarily if need-ed, yet regaining control and resuming the orbit in-sertion with appropriate burncorrections for the in-terruption. This sort of ca-pability is well established, as demonstrated several times throughout the solar system, including with GLL at Jupiter. JOI is pres-ently the driving mode for battery sizing due to the long JOI burn of roughly 2 hours.The mis-sion has several trajectory correction maneu-vers (TCMs), both deterministic and statistical. The onboard communication system must support Doppler tracking to enable adequate navigation reconstruction of these maneuvers on the ground.

Attitude maneuvers during Europa flyby drive the sizing of reaction wheels. Radiation is also worst around flybys, driving fault-protection requirements on the ability to recover and con-tinue science activities after a radiation-induced events (SEU, SEL, etc.). Radiation also drives the shielding design on the vehicle and the selection of EEE parts.

C.2.4.2   Structures and Mechanisms

The overall configuration of the spacecraft (Figure C.2.4-1) comprises the Avionics Mod-ule at the top, followed by the Propulsion Module and the Power Source Module at the bottom. The primary structure of these mod-ules (Figure C.2.4-4) consists of these three commensurate octagonal segments, stacked vertically and joined mechanically to one an-other only via a simple octagonal ring inter-face. Each structure segment is based on an aluminum forging machined from the outside. Aluminum was chosen because it provides the
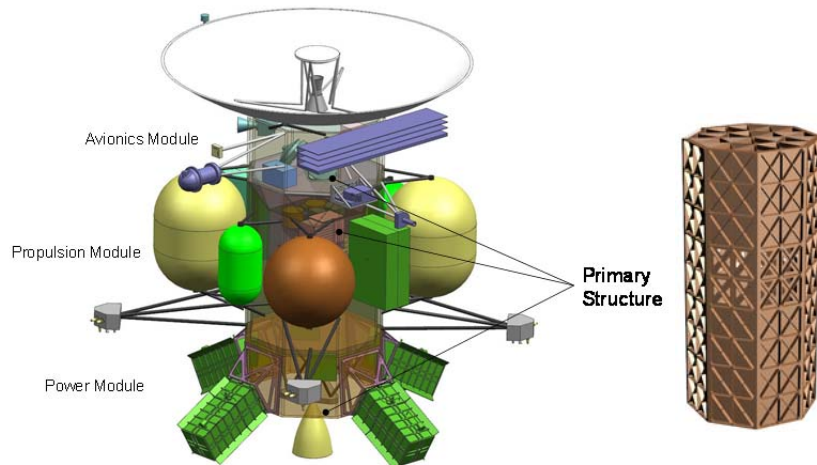

Figure C.2.4-4. Flyby primary structure.

best balance among weight, strength, stiffness, and radiation-shielding. After machining, deep stiffening ribs and a vertical wall remain. This provides for a lightweight, high-strength, and stiff structure. When all three modules are stacked, they form a superstructure that is able the meet the Atlas V launch vehicle's load and frequency requirements.

The predominant mechanism on the Europa Multiple-Flyby Mission spacecraft is the Ice-Penetrating Radar (IPR) antenna boom. Fig-ure C.2.4-5 shows the stowed IPR antenna, and Figure C.2.4-6 shows the deployed IPR antenna.

The structures and mechanism in this concept require no new technology. Design approaches from past missions (like Cassini) can be adapted to address all of the structural and functional requirements for the Europa Multi-ple-Flyby Mission spacecraft. In addition, the overall numbers of mechanisms, consisting
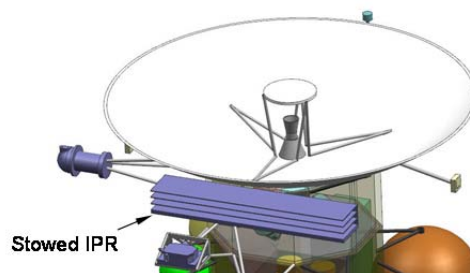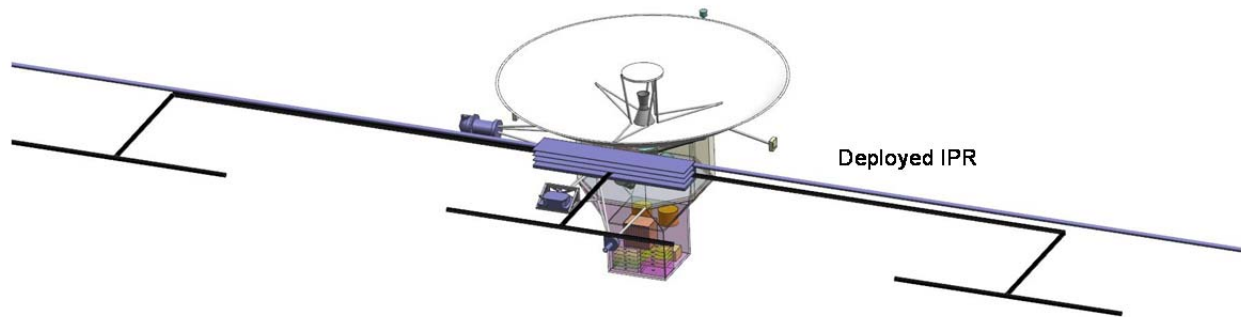

Figure C.2.4-5. IPR stowed.

Figure C.2.4-6. IPR deployed.

mainly of small deployed items, such as covers, were minimized to reduce technical risk, cost, and schedule.

C.2.4.2.1   Key Mechanical Requirements

- First mode fundamental frequency: 8 Hz
- Primary structure lateral launch acceleration: 2 G
- Atlas V mass acceleration curve for appendages
- Isolation of the spacecraft to 20 Hz from a single Stirling converter failure at 102 Hz

C.2.4.3   Thermal Control

The thermal design concept uses, to the fullest extent practicable, waste heat, insulation, and louvers to control temperatures. This approach consumes little to no operational heater power, is low-mass, and has a flight-proven heritage.

C.2.4.3.1   Key Thermal Requirements

- Maintain the propulsion system and battery within allowable flight temperature (AFT) ranges (typically 15°C to 50°C and 10°C to 25°C, respectively).
- Maintain all instruments within the AFT limits.
- Accommodate the variation in environmental heat loads

from the Sun and Venus at 0.7 AU to Jupiter shadow at 5.5 AU (i.e., 2.0 to 0.03 Earth Suns).
- Tolerate limited transient off-Sun exposure (typically about an hour) at less than 1 AU during fault conditions or trajectory maneuvers.
- Minimize replacement heater power during outer solar system cruise and Jupiter operations.

C.2.4.3.2   Thermal Design

Figures C.2.4-7 and C.2.4-8 show the primary thermal components on the spacecraft. A lightweight thermal shroud surrounds the propulsion tanks and associated plumbing. Consisting of multilayered insulation (MLI) supported by a latticework, this shroud creates a
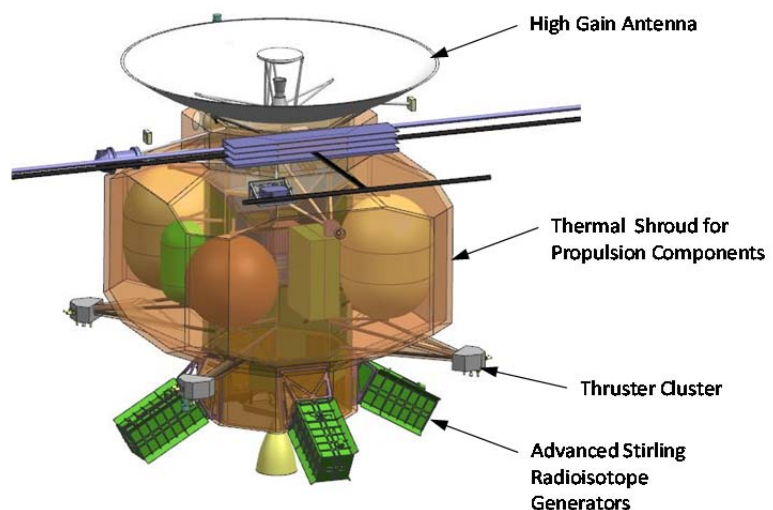

Figure C.2.4-7. Flyby spacecraft with thermal shroud surrounding propulsion tanks.
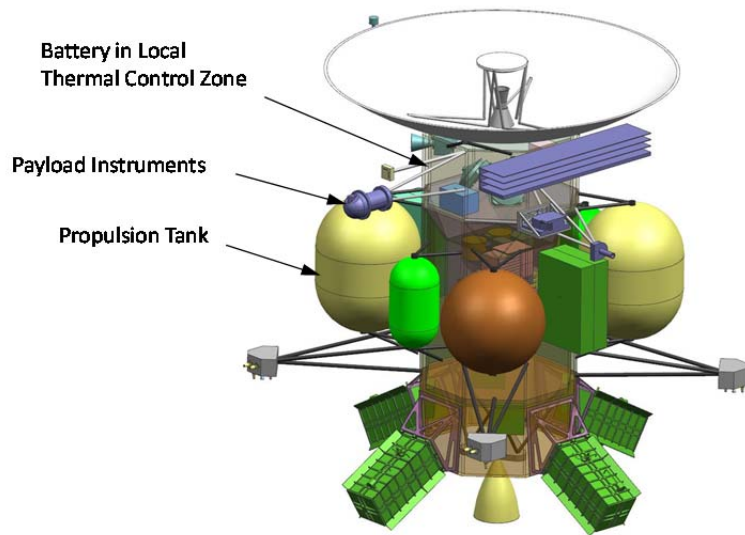
Figure C.2.4-8. Flyby spacecraft with thermal shroud removed.

radiative cavity around the tanks. A clearance of 100 mm between the propulsion components and shroud provides adequate view factors for radiation.

Waste heat from the avionics vault and advanced Stirling radioisotope generator (ASRG) electronics radiates into the cavity and warms the propulsion system. Openings in the primary structure allow heat to radiate from the vault onto the tanks and into the cavity.

A temperature-regulation system is necessary to accommodate the wide variation in environmental loads and internal dissipations. Accordingly, louvers over external radiators on both ends of the spacecraft regulate the cavity temperature to maintain acceptable vault and propulsion temperatures. Heat from the vault and ASRG electronics warms the shroud in the cold case, while louvers on the mounting structure reject excess heat to space in the hot case, thereby producing acceptable temperatures on the propulsion system and vault in all conditions.

This system of waste heat and louvers requires no additional electrical heaters for normal operation. With an MLI external area of 26 m^2 and a nominal effective thermal emissivity of 0.01, acceptable tank temperatures occur with a 200-W heat flow. During the mission, 216 W

to 416 W is available from the avionics vault and ASRG electronics. Hence, the heat balance is always positive. Fault conditions, where the avionics may be off and waste heat is low, are a factor in deciding the partitioning and placement of shunt radiators and replacement heaters. Survival operation will be studied in Phase A.

There are no driving temperature-stability requirements or temperature-gradient-control requirements; therefore louvers are adequate for overall temperature control.

The high-gain antenna (HGA) performs an important thermal-control function, shading the spacecraft from the Sun during the hot conditions of the inner solar system, especially near Venus. During this period, the spacecraft is oriented such that the HGA faces the Sun. This orientation preserves the heat balance on the thermal shroud and louvers. To tolerate a temporary disruption in attitude control under these thermal conditions, a hybrid MLI layup with five external layers of embossed Kapton protects against high exterior temperatures. Off-Sun illumination and the impact on temperatures will be studied during Phase A.

A separate thermal-control zone, with a dedicated radiator and louver, controls the temperature of the battery. This is accomplished by piggybacking the battery to structure in the Avionics Module's UES, but biased colder using a dedicated radiator.

Variable radioisotope heating units (VRHUs) control the temperature of the thruster clusters. Local heating from the VRHUs is required due to the remote location of the thrusters. Each VHRU consists of two to three individual RHUs mounted in a rotating cylinder. One half of the cylinder is painted white while the other half is insulated. A bimetallic spring positions the cylinder to radiate heat into the thruster

cluster when the cluster is cold, or out to space when the cluster is warm. There are four VHRUs per thruster cluster with a total of ten individual RHUs per cluster. Four thruster clusters yield a total of sixteen VHRUs and 40 individual RHUs. This design tolerates a failure mode where one VHRU is stuck fully open or fully closed.

Thermal control must be individually customized for each instrument via local radiators and heaters, orientation to thermal sources like the Sun, and control of the surrounding thermal context on the spacecraft. Addressing these issues in more detail for the model payload will be an important task during Phase A, and then again, once instruments are chosen.

Great care is also necessary, as in any thermal-control system, where thermal performance is affected by workmanship. The effective emissivity of MLI is a notable example. For the Europa Multiple-Flyby, this risk is mitigated by conservative design and by test. Margin in the active louver system provides tolerance for hardware variations. Also, thermal development tests of the louvers and critical areas of MLI reduce risk to acceptable levels.

C.2.4.3.3   Heritage

The thermal design concept for the Europa Multiple-Flyby Mission follows that of Cassini. In the Cassini design, the propulsion system was enclosed in a shroud that formed a radiative cavity. Heat for the Cassini shroud came from radioisotope thermoelectric generators (RTGs), whereas on the Europa Multiple-Flyby Mission spacecraft the heat comes from the avionics vault, the power shunt radiator, and the ASRG electronics. VRHUs control the temperature of the thruster clusters on Cassini, as planned for the Europa Multiple-Flyby Mission. HGA shading protected the Cassini spacecraft from solar loading at Venus and will do the same for the Europa Multiple-Flyby Mission. Other thermal hardware, such as louvers, heaters, MLI, and platinum resistance thermometers, also have good heritage

based on the flight experience of prior JPL missions.

C.2.4.3.4   Thermal Assessment of the Propulsion System

Thermal radiation from the Vault into the thermal enclosure provides passive temperature control for the propulsion tanks and lines, an approach similar to that used on Cassini. Three environmental conditions test the soundness of this approach.

Inner cruise takes the spacecraft near Venus. In this 0.7-AU hot condition, the high-gain antenna shades the spacecraft and prevents overheating. The internal heat dissipation is 290W, while the net heat loss from the thermal enclosure is 150W. Side-facing louvers reject the remainder of the heat, Figure C.2.4-9.

In the cold science mode, the internal heat dissipation drops to 216W while the heat loss off of the thermal enclosure increases to 200W. Sixteen watts remains to be rejected by the lower louver. The upper louver is closed, Figure C.2.4-10.

Power levels change again for orbit insertion and trajectory correction maneuvers. In this
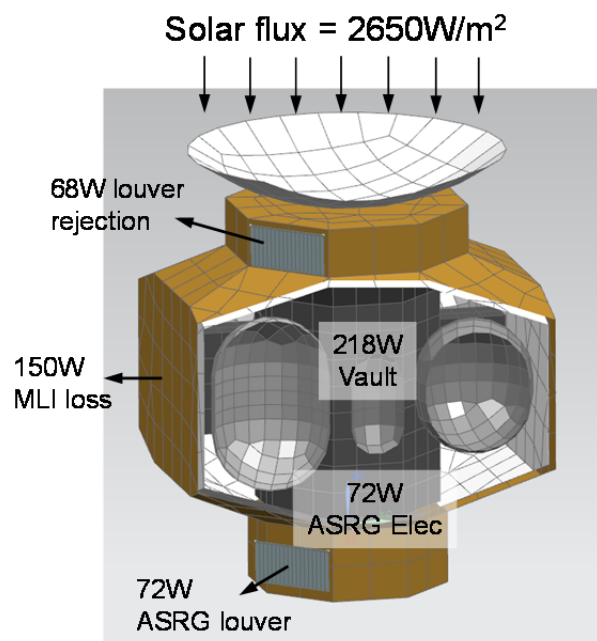

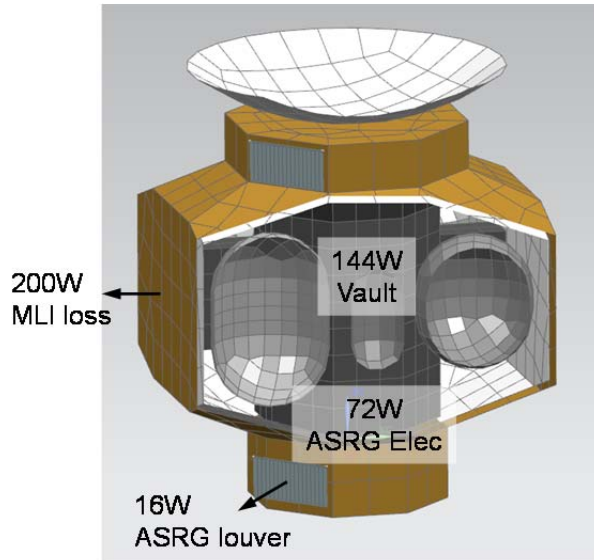**Figure C.2.4-9.** Heat balance for inner cruise.

Figure C.2.4-10. Heat balance for Flyby science.
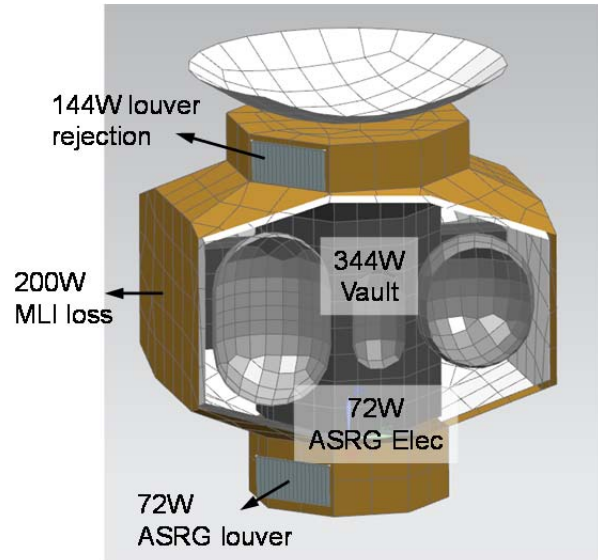
Figure C.2.4-11. Heat balance for orbit insertion and trajectory correction maneuvers.
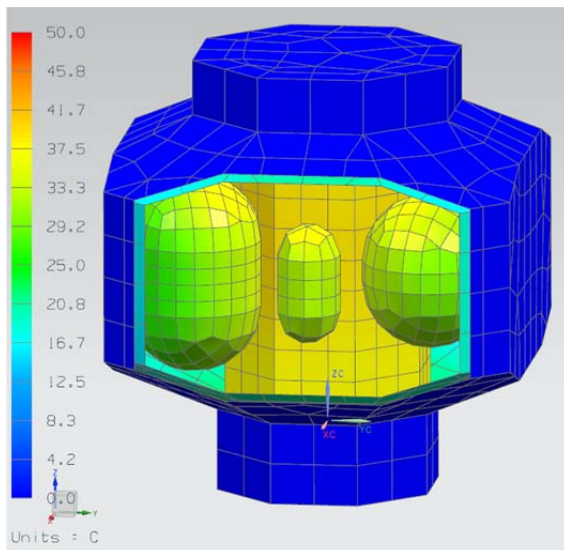
Figure C.2.4-12. Tank temperatures.
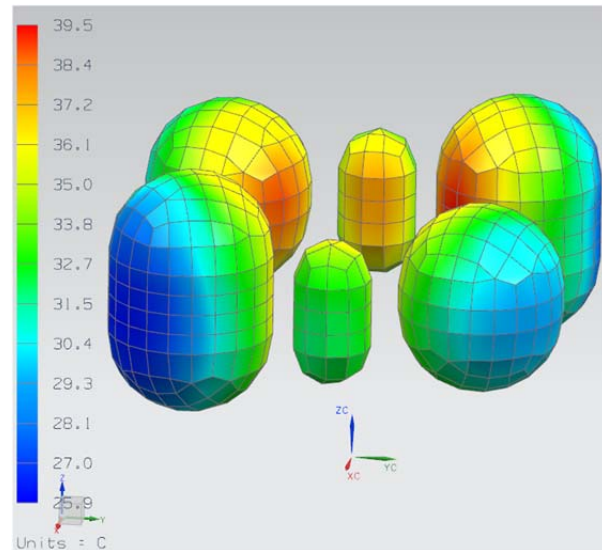
Figure C.2.4-13. Predicted tank temperatures, showing only the tanks.

high-power condition, 200W still leaks through the thermal enclosure, but the vault dissipates 344W. Both the upper and lower louvers participate in rejecting the balance of the heat and regulating the temperature, Figure C.2.4-11.

At Jupiter, in the worst-case cold condition, thermal equilibrium occurs with a heat flow of 200W from the inner structure to the insulation of the shroud. An initial thermal analysis for this case shows that the propulsion tanks remain within 25°C to 40°C, in compliance with their AFTs, without direct heating or active control. Figures C.2.4-12 and C.2.4-13 show predictions of the tank temperatures.

C.2.4.4   Propulsion Module

C.2.4.4.1   Propulsion

This Propulsion Subsystem, specifically designed for a long-life outer-planet mission, would provide the impulse and reliability necessary to meet the needs of the Europa Multiple-Flyby Mission.

The Europa Multiple-Flyby Mission spacecraft Propulsion Subsystem is a dual-mode bipropellant system. The propellants are hydrazine (N_2H_4) and nitrogen tetroxide (NTO). The hydrazine fuel and nitrogen tetroxide oxidizer are used by the bipropellant main engine, and the hydrazine fuel alone is used by the monopropellant Reaction-Control Subsystem (RCS) thrusters and thrust vector control (TVC) thrusters. Figure C.2.4-14 shows a schematic of the Propulsion Subsystem.

Driving Requirements

The requirements that drive the design of the Propulsion Subsystem are typical of those for outer-planet missions, with the possible exception of the requirement to configure the system to take advantage of the Propulsion Subsystem mass to provide radiation shielding for the

electronics. The key driving requirements for the Propulsion Module are to

1. Provide ΔV for maneuvers, including Jupiter Orbit Insertion (JOI).
2. Provide thrust vector control during main engine operation.
3. Provide for attitude control when the spacecraft is not using reaction wheels.
4. Provide for reaction wheel momentum unloading.
5. Configure the Propulsion Module to provide a substantial augmentation to radiation shielding of the spacecraft electronics.
6. Provide the central structure connecting the Power Source and Avionics Modules.
7. Support the thermal control concept with its shroud and internal radiative cavity.

Propulsion Module Configuration

Figure C.2.4-15 shows that the Propulsion Module configuration is based on a core octagonal structure with the propellant tanks, pressurant tanks, and component plates
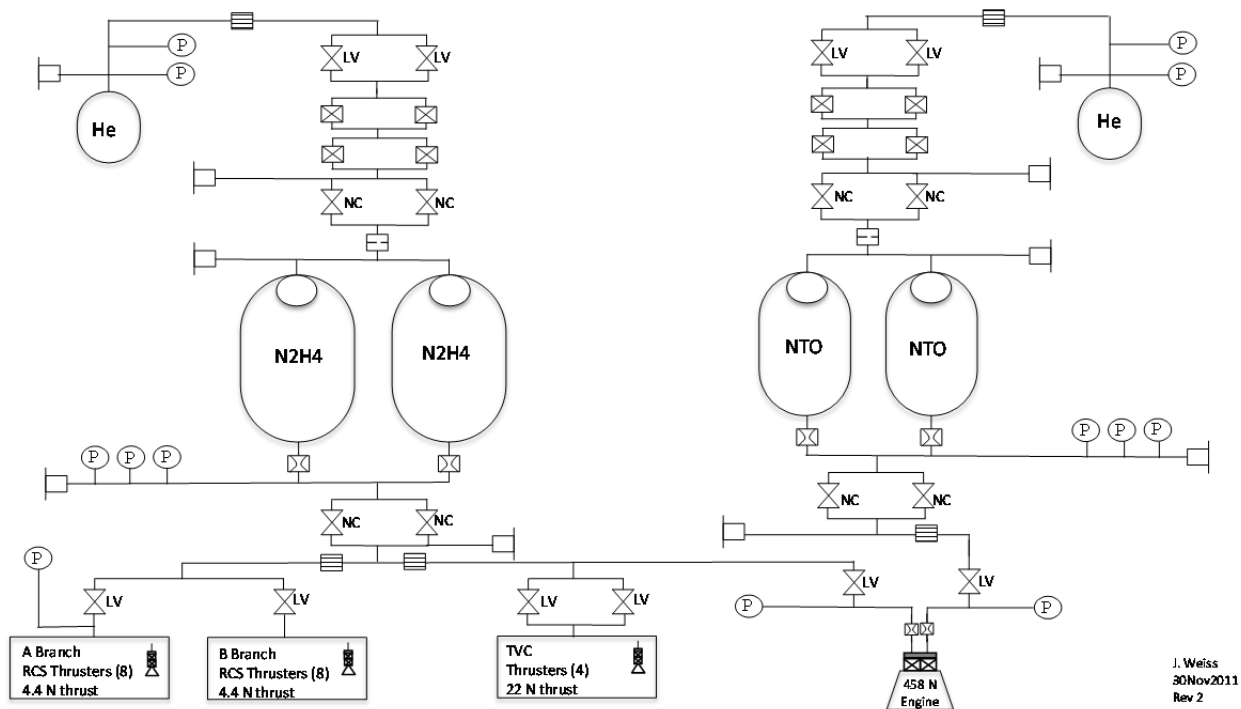

Figure C.2.4-14. Dual-mode, bipropellant Propulsion Subsystem schematic.
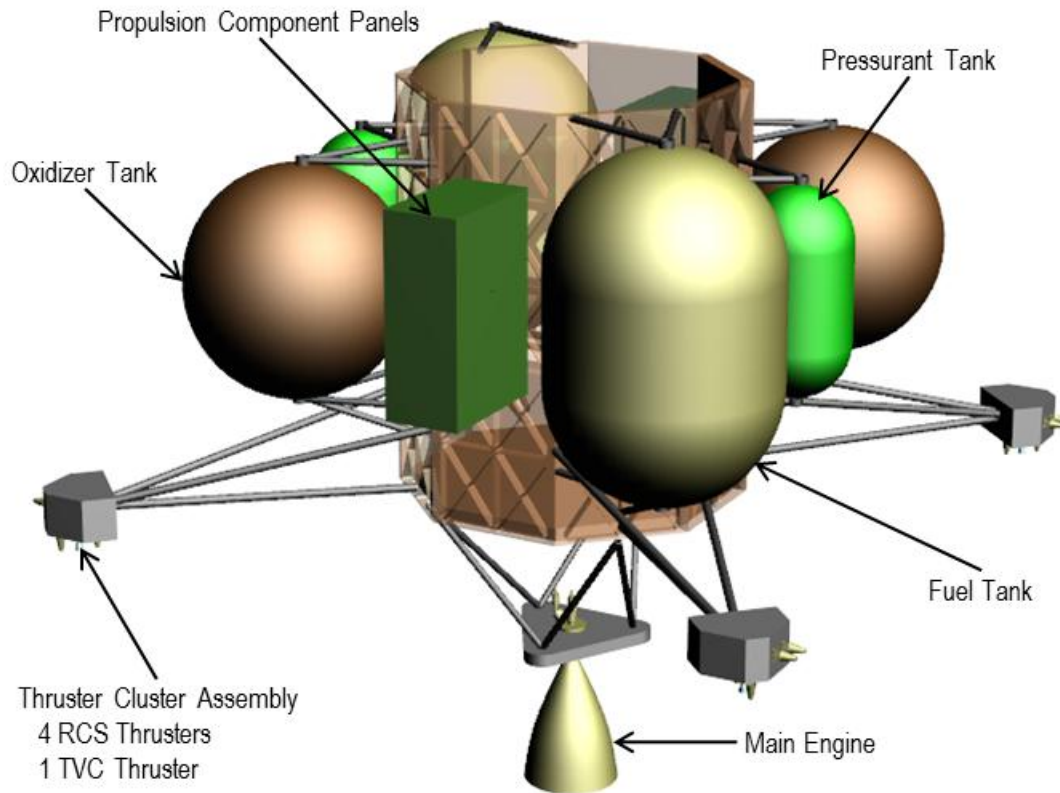
Figure C.2.4-15. Propulsion Module configuration.

mounted on the exterior sides of the octagonal structure. This configuration is driven by the necessity to maximize the radiation shielding for the spacecraft electronics, mounted on the Avionics Module and located internal to the Propulsion Module core structure. Mounting the tanks and the propulsion components on the external sides of the core structure provides additional shielding for the spacecraft electronics mounted internal to the vehicle.

Note that the propulsion components' plates are mounted perpendicular to the core structure (see Figure C.2.4-15). This is done because there is insufficient space to mount the component plates in a more traditional fashion (i.e., parallel) without increasing the length or diameter of the Propulsion Module. It was decided not to mount the component plates to an interior wall of the Propulsion Module because of limited accessibility during ATLO.

A single main engine, mounted using struts at the bottom of the Propulsion Module and protruding through the Power Source Module, provides for primary ΔV. The RCS and TVC thrusters are mounted on four thruster cluster assemblies (TCAs), which in turn are mounted on struts extending away from the spacecraft. This configuration is very similar to that of the Cassini RCS. Each TCA contains four RCS thrusters (two primary and two redundant) and a single TVC thruster. The RCS thrusters are block-redundant, in that there are two strings of eight thrusters. Each string of eight thrusters is isolated by a single latch valve and can perform all required functions. The second string is a backup. The RCS thruster configuration provides for coupled thrust about the Z-axis (roll) and uncoupled thrust in pitch and yaw, identical to the Cassini configuration. The spacecraft can be turned to align this axis with the reaction wheel momentum vector in order to minimize ΔV during momentum manage-

ment. Both the main engine and TVC thrusters are single-string in the present concept. This decision will be reassessed in Phase A.

Propulsion System Design

Engines and Thrusters. The baselined main engine for the Flyby spacecraft is the Ampac LEROS 1c (or equivalent). This is nominally a 458-N (103-lbf) engine. It operates at a nominal mixture ratio of 0.85 and has a minimum specific impulse of 324 seconds. This engine has been qualified for flight and has flown on numerous spacecraft. However, the engine will likely require a delta qualification test program for use on the Europa Multiple-Flyby Mission spacecraft. Although the total qualified throughput well exceeds the demands of the Europa Multiple-Flyby Mission, the tested single-burn duration of 60 minutes is insufficient. The Flyby Mission, as currently planned, requires a JOI maneuver on the order of 122 minutes. The vendor has indicated that they believe the risk of this delta qualification test to be very low.

It should be noted that the engine chamber interior wall is coated with R512E disilicide, which could be subject to micrometeoroid damage. The actual risk of failure and time to failure caused by damage is unknown, and likely indeterminate. The presented concept does not include an engine cover but the design does not preclude its addition. This would be reevaluated during Phase A.

The TVC thruster currently assumed for the flyby spacecraft is the Aerojet MR-106 thruster (or equivalent), providing approximately 22 N (5 lbf) of thrust. A preliminary analysis has been performed showing that this thruster provides adequate control authority for the vehicle during main engine operation, given different deployment configurations, but with assumptions on balanced propellant flow. Explicit measures to ensure propellant balance will be studied in Phase A. For now, ballast mass is included in the mass budget to keep the dry system center of mass near the sym-

metry axis of the tanks. The RCS thruster currently assumed is the Aerojet MR-111 thruster (or equivalent), providing approximately 4.4 N (1 lbf) of thrust. Both thrusters are qualified for flight and have high heritage.

Pressurization System. The baselined pressurization system allows for independent pressurization and regulation of the oxidizer and fuel tanks. Rather than using a traditional mechanical regulator, this system uses a set of four solenoid valves configured to be parallel and series-redundant (i.e., for a minimum of single fault tolerance), allowing for electronic regulation using pressure transducer feedback. Flight software would provide closed-loop control using pressure transducers measuring tank pressure. In the present concept, three pressure transducers would be polled to protect from a transducer failure scenario (though further study is required during Phase A to consider common mode issues). There are several advantages of this system over a more traditional pressurization system using mechanical regulators, especially for long-duration outer-planet missions:

1. Separate pressurization and regulation of the oxidizer and fuel tanks eliminates the risk of propellant vapor mixing in the pressurization system. It also eliminates the need for numerous check valves and pyro-valve isolation, reducing dry mass.
2. Elimination of the mechanical pressure regulator reduces the risk of regulator leakage. The series-redundant solenoid valves are less susceptible to leakage than are mechanical regulators.
3. The design allows for active control of oxidizer and fuel tank pressures. This is advantageous because the oxidizer-to-fuel mixture ratio can be adjusted during the mission. It allows for more accurate control of mixture ratio, which in turn reduces residual propellant.

The schematic in Figure C.2.4-14 shows that the quad-redundant solenoid valves are isolat-

ed above by parallel redundant, high-pressure latch valves and below by parallel redundant, normally closed pyro valves. The pyro valves would remain closed until first use of the regulating solenoid valves is required.

Systems similar in concept to this have been used in the past on other spacecraft (e.g., MiTEx Upper Stage, Clementine, GeoLite, and Orbital Express).

Propellant and Pressurant Tanks. The propellant tanks are sized for a total propellant load of 1,872 kg. This assumes the maximum launch capability of the 21 November 2021 launch window, providing a ΔV of 1.52 km/s. Table C.2.4-3 shows the rack-up of propellant, including residual and ACS propellant. The hydrazine tanks are about 130 cm high by 90 cm in diameter (6% ullage), and the oxidizer tanks are 90-cm diameter spheres. The oxidizer tanks are significantly oversized for the current propellant load. These dimensions are based on available tanks. The tanks are oversized for these mission drivers; sizing will be revisited in Phase A.

The pressurant tanks are essentially off-the-shelf tanks and significantly oversized for the current propellant load. The pressurant tank sizing will be optimized as the design matures.

Propellant Isolation. The propellant tanks are isolated from the thrusters using parallel redundant, normally closed pyro valves and low-pressure latch valves. This design concept provides sufficient mechanical inhibits to meet

KSC launch safety requirements.

Careful design of the propellant tank surface-tension propellant-management devices (PMDs) and the venturis downstream of the tanks will be necessary in order to prevent propellant transfer between the two tanks, or preferential draw of propellant from one tank. It may also be necessary to take more positive measures to prevent propellant transfer, such as the addition of latch valves to isolate the propellant tanks from each other when not in use and to regulate differential flow. Further detailed analyses will be required before this design concept can be finalized.

Heritage

The majority of the components used in the flyby propulsion system are flight qualified and considered off-the-shelf. This includes the RCS thrusters, TVC thrusters, service valves, pressure transducers (except for required shielding), filters, and solenoid and latch valves. As discussed above, the baselined main engine is also flight-qualified and has flown before. However, it will likely require a delta qualification test to qualify the single-burn duration for JOI. Regarding the propellant tanks, it is the intent to size them based on a heritage design that makes use of qualified hemisphere forgings. The current design concept makes use of an 89.15-cm (35.1-in.) tank, but will likely require a change in length of the cylindrical section. In addition, a new PMD for the oxidizer and fuel tanks will need to be designed and integrated. Hence, the propellant tanks will likely require a new qualification test program. A similar approach has been taken with the pressurant tanks, using a qualified design that best meets the requirements for the Europa Multiple-Flyby Mission.

The pressurization system, which makes use of electronic regulation, will need to go through a program that develops and qualifies it as an integrated system, including the propulsion hardware, controller, and flight software.

Table C.2.4-3. Maximum propellant load case for Flyby spacecraft propellant tank sizing.

Required Propellant	Mass (kg)
Propellant load for 1.52 km/s ΔV	1711
Hydrazine (MR=0.85)	925
NTO	786
Hydrazine for TVC	75
Allocation of ACS propellant (N_2H_4)	40
Hydrazine residual/hold up (2.5%)	26
NTO residual/hold up (2.5%)	20
Total hydrazine	1066
Total NTO	806
Total Propellant Load	**1872**

C.2.4.4.2   *Propulsion Module Structure*

The Propulsion Module (Figure C.2.4-15) supports the fuel tanks, TVC and RCS thrusters, propellant-isolation assembly (PIA), pressurant-control assembly (PCA), and main engine. The propulsion fuel tanks are supported by bipod and tripod combinations and are attached to the primary structure. The main engine is attached at the bottom and extends through and below the Power Source Module. Four thruster clusters are supported at the ends of four tripods sized for adequate control authority and minimal plume impingement. The PIA and PCA are attached together, back to back and parallel to each other. The PIA/PCA assembly is in turn attached to the Propulsion Module's primary structure.

The Propulsion Module's primary structure has triangular holes in the wall at the location where the warm avionics has a radial view to the propulsion tanks. These holes allow for a direct radiation path to the tanks. In this region, the primary structure's wall thickness is increased to compensate for the holes. The necessary radiation shielding is still maintained due to the position of the tanks and the thickness of the vault.

C.2.4.5   Power Source Module

The Power Source Module (Figure C.2.4-16) would include four ASRGs, the launch vehicle adapter, the main engine thermal shroud, and structure to support these items and carry the Propulsion and Avionics Modules above. Each ASRG provides a power and command interface to the Avionics Module. Electrically heated units will be used during system integration and test, after which the Power Source Module will be demated and return for fueled ASRG integration. The Power Source Module will then be delivered directly to the launch site for reintegration (Section C.2.4.8). The thermal dissipation of the ASRGs inside the primary structure contributes to the overall thermal input inside the thermal shroud of the spacecraft. The main engine assembly of the Propulsion Module goes through the center of the Power Source Module with a thermal shroud protecting against the heat of the engine.

C.2.4.5.1   *Power Source*

The power source would be the combined contribution of four ASRGs. Its power interface to the rest of the system is through a single industry-standard power bus with a 22 to 34-V range defined at the load interface with the Power Source Module. The power bus is a direct energy transfer architecture, with the power source output connected to the Power Subsystem in the Avionics Module. The Power Subsystem provides power bus voltage regulation, not the Power Source Module.
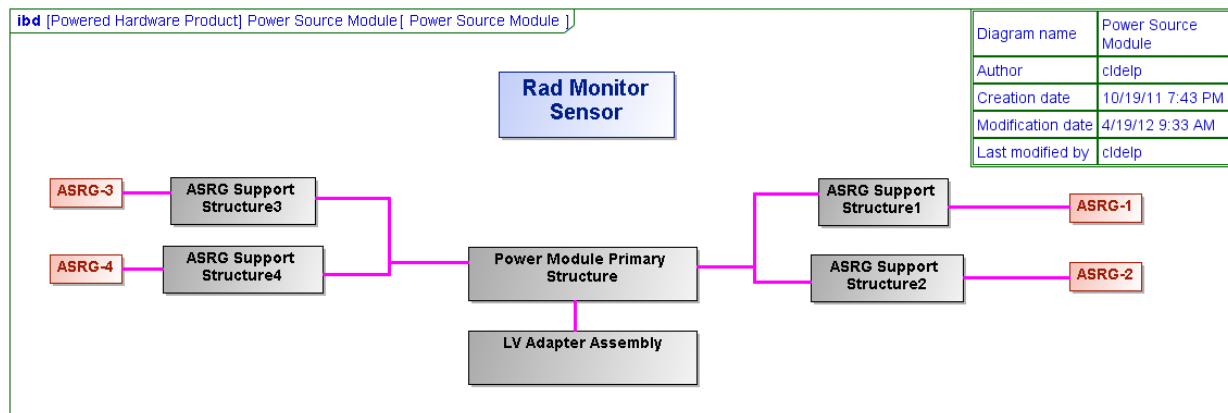

Figure C.2.4-16. Power Source Module block diagram.

Power Source Driving Requirements

The key drivers for the power source are to

1. Provide 392 W at EOM, assuming a single Stirling engine failure in one ASRG.
2. Provide constant power over the nominal power bus voltage operating range of 22 to 34 V as defined at the power source output.
3. Tolerate a power bus overvoltage up to 40 V for an indefinite period of time.
4. Provide diminished but positive power to the power bus if the voltage drops to less than 22 V in order to support recovery from a bus overload.

C.2.4.5.2   ASRG

ASRG Functional Description

Each ASRG (Figure C.2.4-17) consists of two General-Purpose Heat Source (GPHS) mod-ules, two ASRG Stirling converters (ASCs), a generator housing assembly (GHA), a shunt dissipater unit (SDU), an ASC controller unit (ACU), and associated internal cables.

The GPHS contains plutonium dioxide fuel pellets and is designed to meet all safety and handling requirements. The GPHS produces from 244 W to 258 W at encapsulation when the fuel mixture is set in the pellet and placed in the module. From the point of encapsulation, the GPHS thermal output will degrade with the radioactive decay rate of plutonium-238, which is approximately 0.8% per year. It has been assumed that the average GPHS encapsulation will be 3 years before launch.

The ASC converts the thermal energy from the GPHS to AC electrical current using a piston and linear alternator. The ACU rectifies the AC power to DC power and provides it to the power bus with a constant power I-V curve
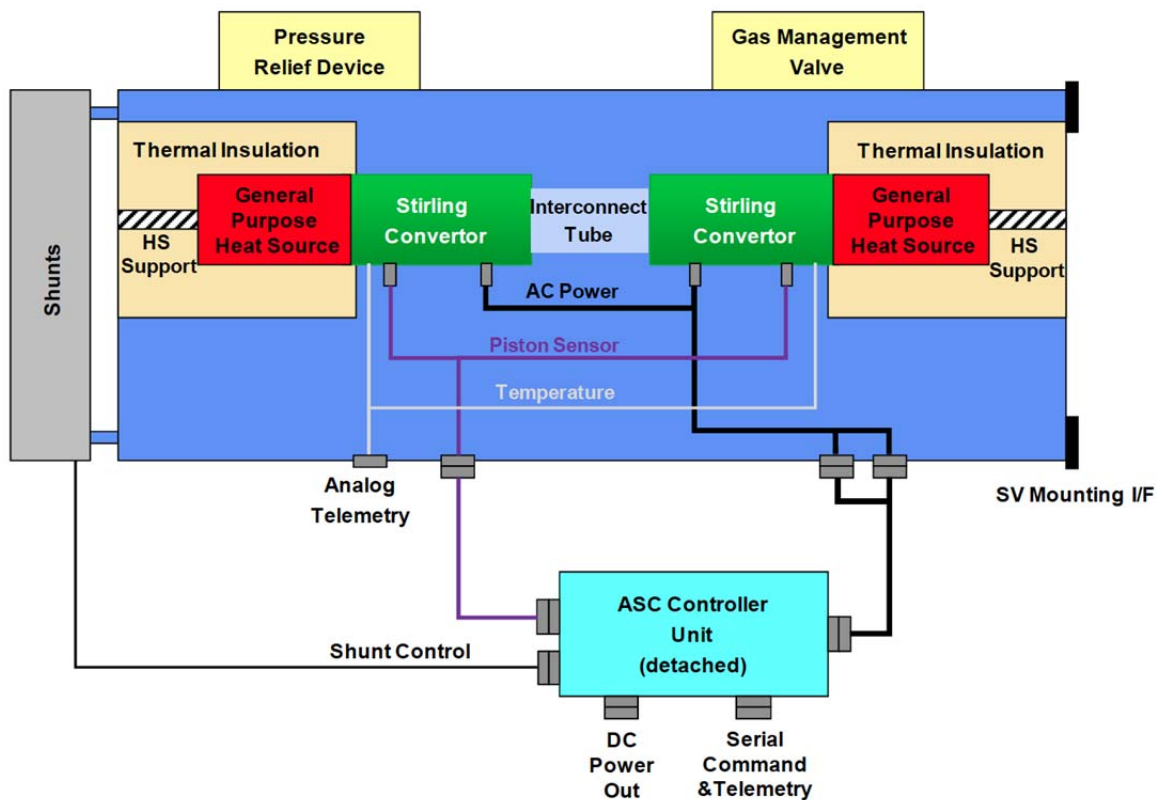

Figure C.2.4-17. This ASRG block diagram includes all functional elements that make up the ASRG, including the detached controller that provides the electrical interface with the spacecraft.

over the power bus voltage range controlled by the spacecraft. The constant power I-V curve allows for more than one ASRG to be connected to the same power bus and share the power.

The ASRG protects itself if the bus voltage goes outside of the specified range of 22–34 V at the ASRG output. The ACU disengages the output from the power bus and shunts the power to the attached radiator if the bus voltage exceeds 35 V ±1 V. The internal ASRG shunt regulator is independent of the Power Subsystem shunt regulator used to regulate the power bus voltage. The ASRG shunt radiator is on the outboard end of the GHA and is used during flight only for the off-nominal bus voltage. The power system maintains the bus voltage range at less than 34 V at the ASRG interface to prevent disengagement. The ASRG reengages once the bus voltage drops back into the safe range. The ASRG provides a current limited to 3.5 A if the bus voltage drops below 22 V, enabling the system to recover by charging the battery.

The ACU is detached from the GHA (Figure C.2.4-18) and mounted on the inside of the Power Source Module primary structure.

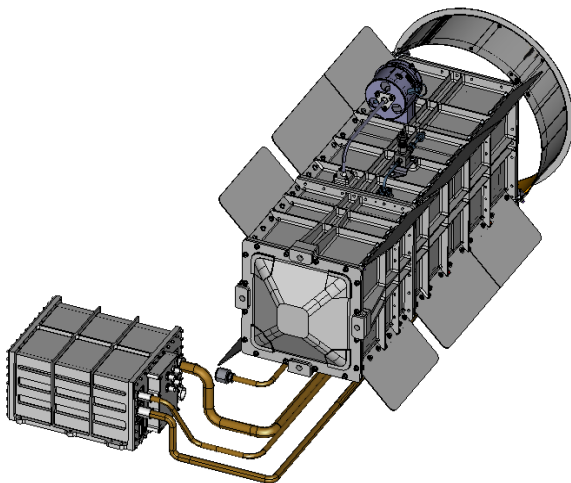The ACU is single-fault-tolerant with an N+1 internal voting architecture and two 1553 data

Figure C.2.4-18. ASRG CAD model shows the detached controller with cabling and outboard shunt radiator.
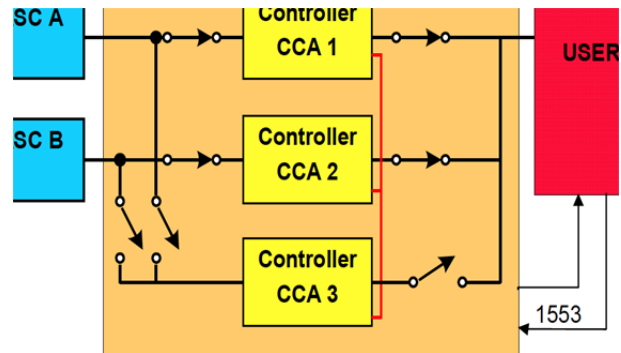
Figure C.2.4-19. ASC controller unit block diagram shows the spare controller # 3 to which the internal fault management switches with the detection of a failure.

bus interfaces (Figure C.2.4-19). The ACU needs to be within 1.8 meters (by cable length) due to impedance constraints from the controller. The ACU also needs to be greater than 1 meter away (by geometric distance) to tolerate self-generated radiation levels.

The ACU has internal fault management to switch automatically to the spare controller board with the detection of a fault. Additional shielding mass was allocated to the ASRGs so that the ACU would be shielded to 50 krad with a radiation design factor of 2 at the component level, including radiation from the ASRG as well as from the environment.

ASRG Performance

ASRG output power is a function of time and environment. The power graphs below show the predicted power output of the four ASRGs, with degradation due to natural decay of the plutonium dioxide fuel as a function of the time from encapsulation, and assuming each GHA has a direct view to space after launch (Figure C.2.4-20). Three graphs are shown. The graph for total power CBE (current best estimate) assumes the nominal specified GPHS thermal output of 250 W at encapsulation. The graph for total power specification is from the ASRG user guide with a BOM power at 130 W, assuming a failure of one single Stirling converter shortly after launch, and 1% degradation per year. The graph for lowest expected value (LEV) assumes the minimum

Figure C.2.4-20. The Europa Study Team uses conservative ASRG performance that includes end-of-life output and takes into account the failure of one Stirling engine.

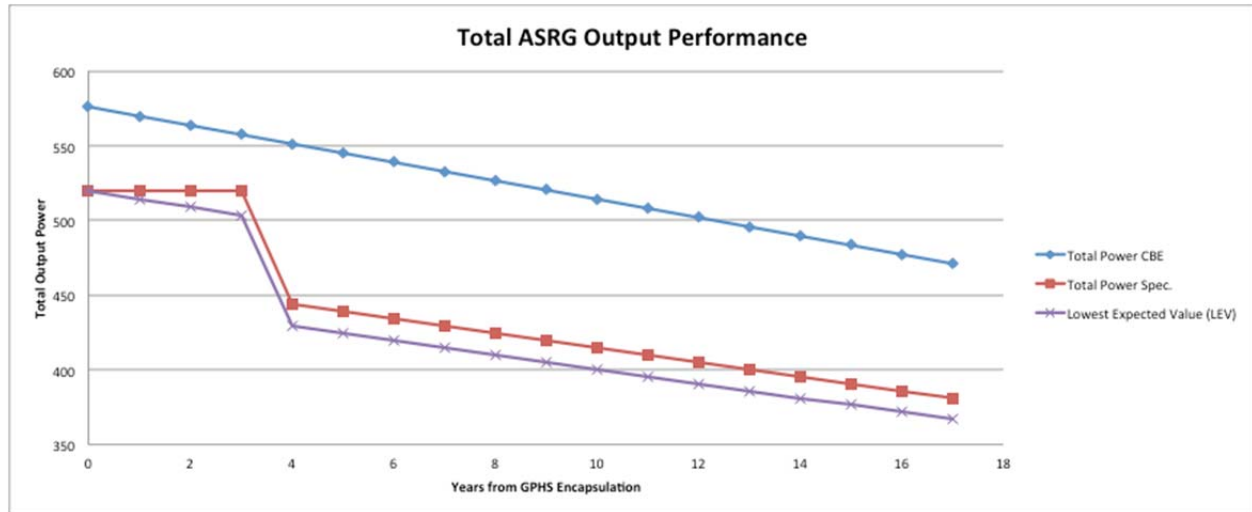specified GPHS thermal output of 244 W at encapsulation, 1% degradation per year, and failure of a single Stirling converter shortly after launch. The LEV graph has been assumed for the Europa Multiple-Flyby Mission concept. The main difference between this and the Department of Energy (DOE) specification is that the 1% degradation per year is presumed in the LEV case to begin 3 years prior to launch at the average GPHS encapsulation date. With a Europa Multiple-Flyby Mission duration at 12 years, at least 392 W is expected at EOM.

The curve above assumes a direct view to space with a sink temperature equivalent to 4 K. The power output graph below shows the degradation as the sink temperature increases due to the environment (Figure C.2.4-21).

The spacecraft configuration uses the high-gain antenna and thermal blanket envelope to shade the ASRGs from the Sun within 1 AU. For the changing environment of launch, inner cruise, and Venus gravity assist, a commands are sent to the ASRGs to adjust an internal operational set point to make sure the ASRGs are safe from over-temperature which would impact the output power. This operation is independent of the power bus voltage set points

controlled by the spacecraft. The spacecraft has adequate power margin for such environmentally impacted mission phases.

C.2.4.5.3   Power Source Module Structure/LVA

The four ASRGs would reside on the Power Source Module (Figure C.2.4-22). The Propulsion Module's main engine assembly passes through the center of but does not directly attach to the Power Source Module's primary structure.

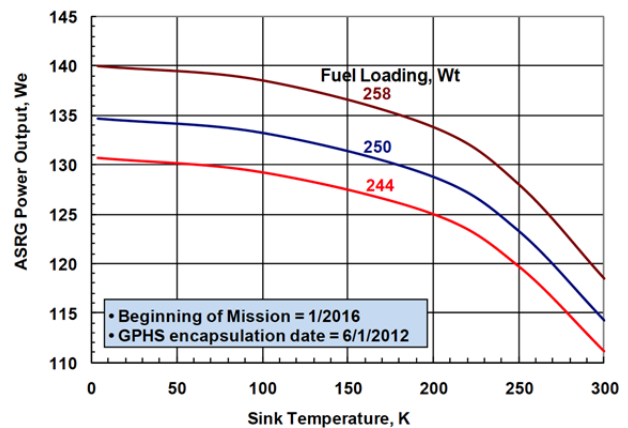Each ASRG has two opposing advanced Stirling converters (ASCs). To counter vibration,

Figure C.2.4-21. ASRG output power vs. sink temperature shows that depending on the environment the output power will degrade. The ASRG power output power will depend on the view to space.
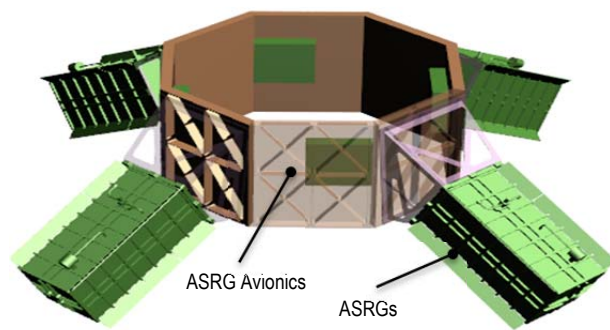
Figure C.2.4-22. ASRGs and their avionics on the Power Source Module.

they are paired in an opposing configuration and tuned through active control by the ACU. As long as both ASCs are working, the ACU controls the phase to reduce the vibration. If an ASC fails, the mechanical interface must dampen or counter the resulting vibration from operating a single ASC.

In the present concept, compression spring assemblies are assumed, oriented parallel to the long axis of the ASRG. These can be tuned to couple poorly with the ASC's frequency of 102 Hz, while still ensuring margin against launch accelerations. However, other ways to accomplish isolation have been identified. These would need to be studied in detail during Phase A.

Because the Power Source Module is the bottom-most module, it experiences the largest moment loads during launch. This will require its primary structure to have a slightly greater wall thickness than the Propulsion and Avionics Modules.

At the bottom of the Power Source Module is the launch vehicle adapter (LVA, Figure C.2.4-23). The LVA provides for a

transition between the octagonal geometry of the upper Power Source Module structure and the circular Marmon clamp separation interface.

C.2.4.6   Avionics Module

The Avionics Module concept results in radiation shielding that enables the use of standard aerospace industry radiation tolerant parts.

Avionics Module Overview

The Avionics Module described below includes the following subsystems:

- Telecom
- Power
- Guidance, Navigation, and Control
- Command and Data Handling
- Software
- Structure, along with instrument accommodation

Besides supporting instruments and the mission design, some of the unique design objectives for the Avionics Module have been as follows:

- Modular design for parallel I&T with Propulsion and Power Source Modules
- Avionics vault to shield a majority of the spacecraft electronics
- Enabling of late integration of instruments
- Simple interfaces with Propulsion and

Figure C.2.4-23. Launch vehicle adapter.
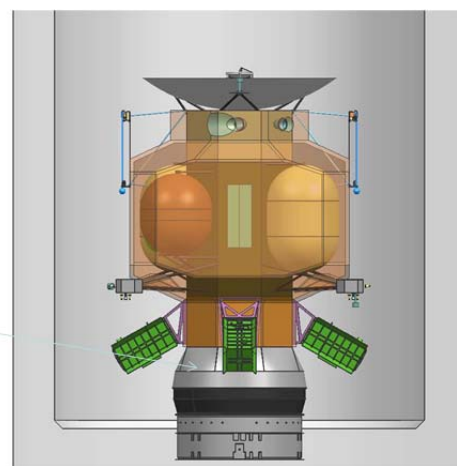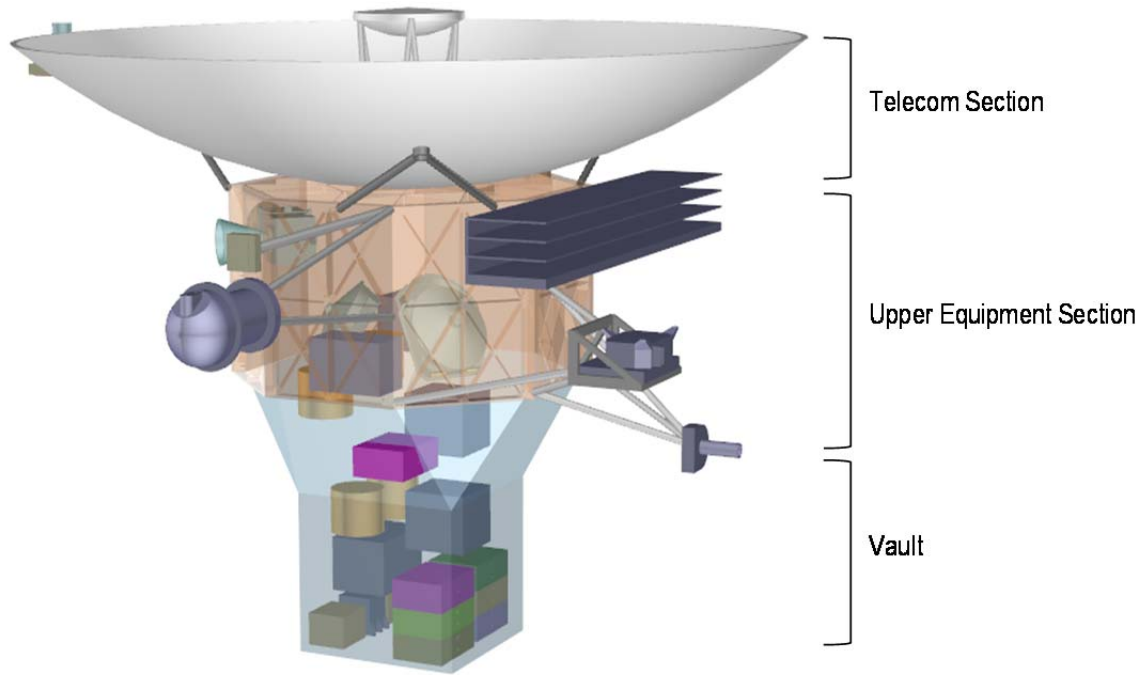
Figure C.2.4-24. The three assemblies of the Avionics Module (telecom, Upper Equipment Section, and Avionics Vault Section) are configured for simple interfaces to enable parallel integration and test.

Power Source Modules

Figure C.2.4-24 shows the configuration of the Avionics Module. It consists primarily of three separate entities: the Telecom Section, the UES, and the Avionics Vault Section.

Figure C.2.4-25 shows the system block diagram of the Avionics Module. The red inter-

faces are DC power; the blue interfaces are data; and the gold interfaces are RF.

Inside the avionics vault are the C&DH electronics (this box is internally redundant), four-for-three reaction wheel electronics(RWE), internally redundant power electronics, internally redundant pyro/propulsion drive elec-
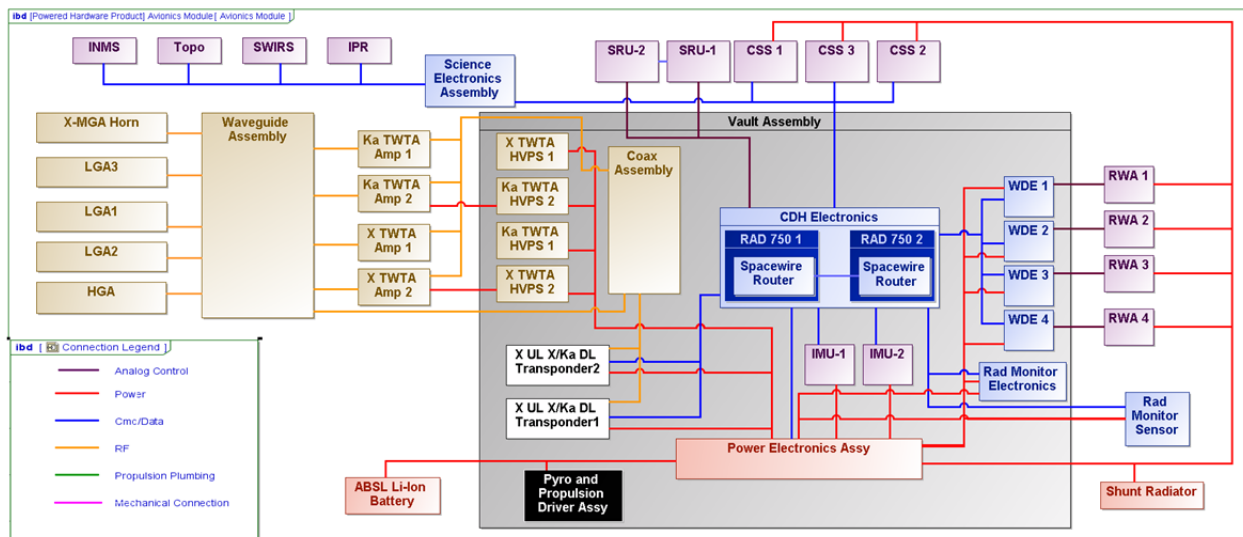
Figure C.2.4-25. A majority of the spacecraft electronics protected in the avionics vault.

tronics, block-redundant IMUs, and block-redundant small deep-space transponders (SDSTs). In the UES are the instruments (TI, SWIRS, IPR, and INMS) and instrument electronics. Also in the UES are the following GN&C components: four-for-three reaction wheel mechanical assemblies (RWA), block-redundant Sun-sensors, and block-redundant SRUs. All the elements outside the vault are individually shielded for total-dose radiation. In the case of instrument and star-tracker detectors, the shielding also mitigates the effect of the electron flux, which is likely to drive shielding mass. The Power Subsystem components outside the vault are the shunt radiator, and battery (both internally redundant). The Telecom Section houses the following components: the TWTAs, coax, waveguide, switches, and antennas configured in a single-fault-tolerant configuration for Ka-band and X-band communication.

C.2.4.6.1   Telecom Subsystem

The Telecom Subsystem performs a dual role for the spacecraft: two-way communications with Earth and Earth-to-spacecraft ranging and Doppler to support navigation.

Driving Requirements

There are a number of drivers for the subsystem. It must accept uplinked commands through all postlaunch mission phases, as well as transmit engineering telemetry and science data to Earth. Key data rates required are

- Engineering telemetry: ~2 kbps
- Uplink commanding: ~1 kbps
- Safe mode commanding: ~7.8 bps
- Safe mode telemetry: ~10 bps
- Science data return: ~112 kbps

Implicit in the above is communications with the Deep Space Network (DSN) 34-m subnet for routine communications and the 70-m subnet (or equivalent) for emergency/safe mode communications.

Subsystem Features

The implementation of the Telecom Subsystem includes X-band uplink and downlink capabilities as well as a Ka-band downlink. Ka-band downlink enables the mission to meet science data volume drivers concurrently with stringent drivers for DC power. While the downlink data volume drivers could be met with X-band alone (assuming a much more powerful X-band TWTA), a trade study between available DC power and science data volume return informed the selection of a more DC-power-efficient architecture for high-rate science data. A similar trade study was undertaken for the Dawn mission. For Dawn, however, more DC power was available, thus enabling a higher DC/RF power X-band downlink for science data; no Ka-band downlink was required. For the Europa Multiple-Flyby Mission, by contrast, the use of Ka-band for high-rate science downlink directly lowers the number of ASRGs required to meet mission objectives.

The Telecom Subsystem features a 3-m-diameter X/Ka-band high-gain antenna (HGA), three LGAs, an MGA with dual polarizations, redundant 35-W (RF power) Ka-band TWTAs, redundant 20-W (RF power) X-band TWTAs, redundant SDSTs, and a complement of microwave waveguide and coax elements. The SDSTs are X-band uplink and downlink capable as well as being Ka-band downlink capable. There is no capability for Ka-band uplink.

The Telecom Subsystem is also expected to be single-fault-tolerant. This drives The Telecom Subsystem architecture to include redundant transponders (small deep-space transponders [SDSTs]), redundant X-band and Ka-band traveling-wave tube amplifiers (TWTAs), a waveguide transfer switch (WTS) network to support cross-strapping, as well as a set of low- and medium-gain antennas. One X-band low-gain antenna (LGA) and the medium-gain antenna (MGA) are tolerant of a single WTS failure. Even though there is a single High
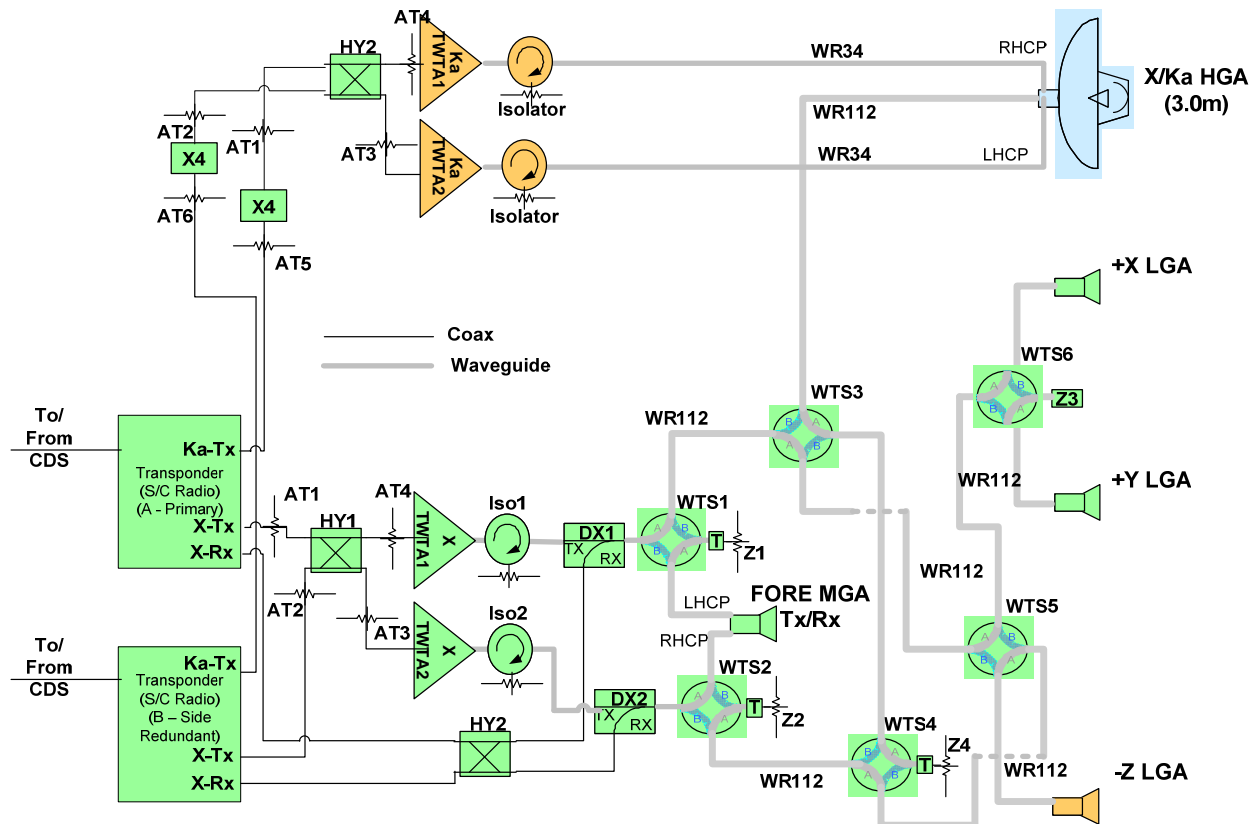
Figure C.2.4-26. The Telecom Subsystem provides robust fault-tolerance through a simplified architecture that minimizes potential for single-point failures.

Gain Antenna (HGA), the HGA features the capability of two downlink polarizations for fault tolerance to a single failure in the Telecom Subsystem's transmitter/receiver hardware chain.

Block Diagram

The equipment configuration shown in the Telecom Subsystem block diagram (Figure C.2.4-26) is based upon many years of deep-space communications heritage. For example, the -Z LGA is fault-tolerant to a single WTS failure in order to provide fault-tolerance for communications during the inner-cruise portion of the mission when the spacecraft uses it's HGA as a sunshield. The LGA configuration enables communications through all cruise periods out to approximately 2 to 3 AU from Earth after which the MGA takes over the safe-mode and general cruise communications. Ka-band downlink redundancy is provided through the use of redundant hardware chains and downlink antenna polarizations. This simplified architecture promotes a more robust system fault-tolerance than could be achieved with the inclusion of an additional WTS to switch between the redundant downlink TWTAs. Similarly, for the X-band uplink, an RF hybrid is used (HY2) in place of a WTS. This alone eliminates a potential single-point failure in the critical X-band uplink path. Similarly the MGA has dual polarizations that enable single-fault-tolerant safe-mode communications at Europa. Overall the Telecom Subsystem presents a robust, fault tolerant, and low risk posture for the mission.

Equipment Heritage

Telecom hardware heritage comes from a number of previous missions. The HGA will be similar to the Juno HGA. It will be redesigned for higher gain by scaling up Juno's
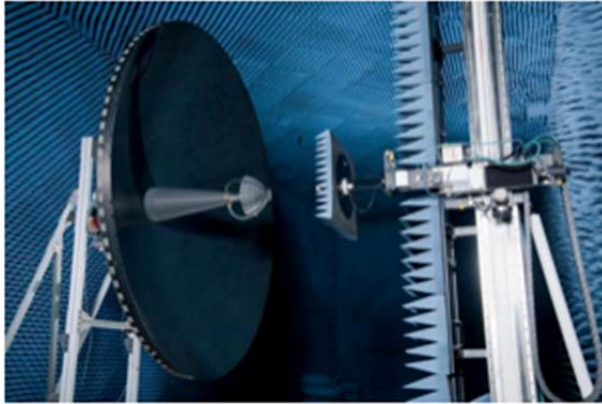
Figure C.2-27. Juno's 2.5-m HGA (X/Ka-band) provides the basis for the Europa HGA.

2.5 m in diameter to 3 m. The Europa Multiple-Flyby Mission's HGA will leverage technology developed for the Juno HGA reflector (Figure C.2.4-27) to meet the surface-tolerance requirements for precision Ka-band pointing and efficiency. The Juno HGA optics will be redesigned to improve Ka-band performance for the Europa Multiple-Flyby Mission's high-rate downlink communications needs.

The TWTAs have heritage from multiple JPL missions: Juno, Dawn, and MRO (X-band) and Kepler (Ka-band). A good example here is the X-band TWTA for the Dawn mission, shown in Figure C.2.4-28. We propose to leverage a long history of downlink TWTAs designed specifically for the requirements of deep-space missions.
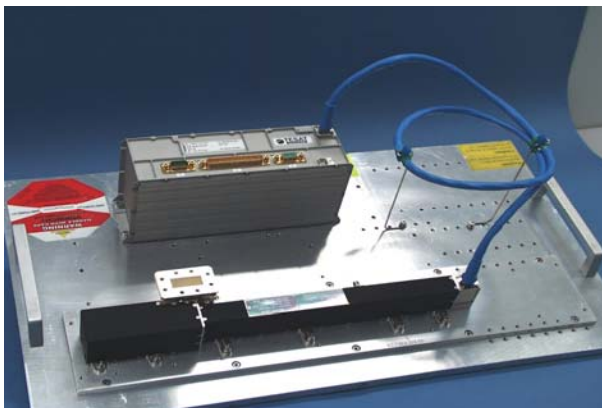
Figure C.2.4-28. Candidate X-band TWTA (flown on MRO, MSL, and Dawn).

Figure C.2.4-29. The SDST product line provides the mission-critical communications link to Earth.

We propose to use the SDST, a very mature product, to provide the mission-critical uplink and downlink functions. The SDSTs have heritage from Juno (X/X/Ka-bands), Dawn (X-band), MRO (X/X/Ka-bands), MSL (X-band), Kepler (X/X/Ka-bands), and others. A candidate SDST, flown recently on the Dawn mission, is shown in Figure C.2.4-29. Due to the extensive heritage inherent in the SDST product line, the use of the SDST lowers the overall residual mission risk.

Characteristics and Sizing

The average Telecom Subsystem downlink data rate must be at least 112 kbps during Europa science operations. The telecom link budget is designed to meet this with the parameters shown in Table C.2.4-4. We've sized the Telecom Subsystem to have a worst case bit rate of 112 kbps. This yields a nominal average bit rate of 134 kbps.

The HGA is body-fixed to the spacecraft and requires a ≤1-mrad pointing accuracy to meet communications throughput requirements. We've taken a conservative approach with the telecom link by requiring 3 dB margin minimum and by making conservative estimates of individual contributors to the link. Parameters such as RF losses in the downlink path, DSN station performance due to low station elevations, link degradation at low Sun–Earth pointing (SEP) angles and Jupiter's hot-body noise

Table C.2.4-4. Telecom link budget inputs.

Parameter	Required Capability	Notes
Throughput Rate (worst case)	112 kbps	Average = 1.2 × worst case= 134 kbps
TWTA RF Power	35 W (Ka), 20 W (X)	2× for Power Dissipation
HGA Diameter	3.0 m	Body fixed HGA, 60% efficiency
HGA Pointing Error	≤1.0 mrad	Reaction-wheel control
DSN Weather	90% cumulative dist.	
Canberra Elevation	20°	Worst-case, fixed
Earth S/C Range	6.5 AU	Average mission design
Hot Body Noise	16 K	About 0.6 dB loss
Turbo Coding	Rate=1/6, 8920-bit frame	
TWTA to HGA Losses	2 dB	Conservative estimate
Link Margin	3 dB	Per Institutional guidelines
SEP Angle	20°	Worst-case assumption
Operational Configuration	X-band up, Ka-band down	X-band downlink for safe mode & cruise
Gravity Science Doppler	None	
Hardware Configuration	X-band up, X/Ka-band down 3 LGAs, MGA, HGA, TWTAs	Possible X-band SSPA in lieu of TWTA

at Ka-Band are all taken into account. Overall, we propose very conservative and robust X-band and Ka-band communications links.

The LGA complement provides full 4π-steradian coverage; this enables command uplink at any spacecraft attitude unless the line-of-sight to Earth is blocked, which occurs only for brief episodes. Spacecraft communications during the inner cruise portion of the mission (<1 AU solar distance) use a single-fault-tolerant LGA (-Z LGA). The distances to Jupiter, however, prevent LGA communications at the required safe mode rates. To meet safe mode communications rate requirements in this situation, a body-fixed MGA with an approximate full-cone beamwidth of 20 deg, pointed at the sun using the spacecraft sun sensors, is used. All high-rate communications are performed through the HGA. Turbo coding at rate = 1/6 is also part of the baseline communications architecture.

C.2.4.6.2 Power

The Flyby Power Subsystem electronics and energy storage provide the power bus regulation and distribute power from the ASRGs and battery to the loads.

Power Driving Requirements

1. Be single-fault-tolerant

2. Provide energy storage to level the mission load profile
3. Provide power bus regulation
4. Provide battery charge control
5. Accept power from the ASRGs
6. Distribute power to the loads
7. Actuate valves
8. Fire pyro events

Power Subsystem Description

The Power Subsystem electronics regulates the power bus, directly connected to the ASRGs, and distributes power to the loads on the spacecraft. The Power Subsystem provides rechargeable energy storage to cover the transient load profiles of the different Flyby Mission scenarios. It is single-fault-tolerant, using a combination of block-redundancy with cross-strapping and some majority-voted functions. It provides valve-drive and pyro-firing functions with range and mission safety inhibits for hazardous functions.

The Power Subsystem consists of a Li-ion battery, a shunt radiator, a shunt driver slice (SDS), two multimission power switch slices (MPSSs), two power bus controllers (PBCs), two power converter units (PCUs), two pyro-firing cards (PFCs), and four propulsion drive electronics slices (PDEs) (Figure C.2.4-30).
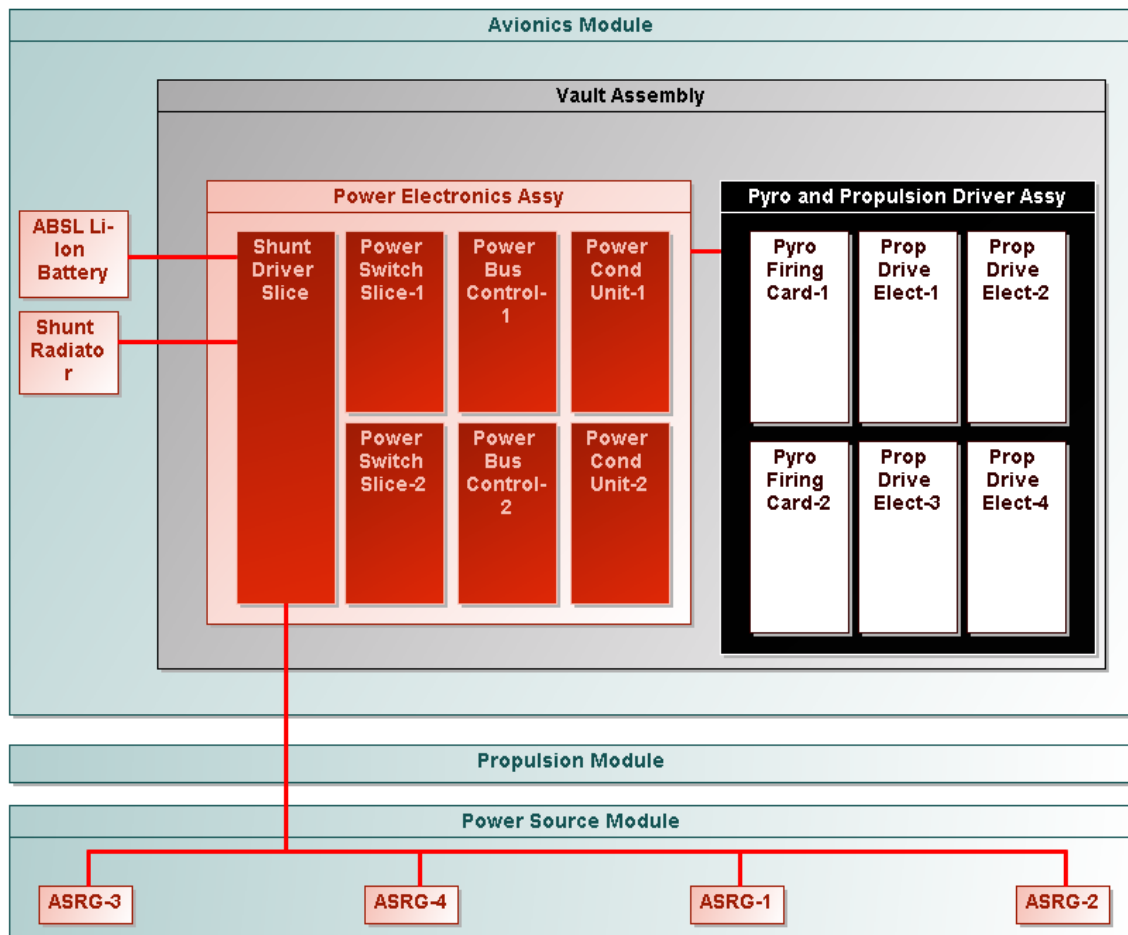
Figure C.2.4-30. The power electronics are shielded inside the vault.

Power Control

The PBC slices provide the SpaceWire command interface to C&DH. The PBC provides a low-power serial data bus to all of the other power electronics slices. It converts commands from the C&DH via the SpaceWire interface and distributes them to other slices through a low-power serial data bus. The PBC collects Power Subsystem telemetry and makes it available to C&DH via the SpaceWire interface.

The PBC contains control algorithms for regulating the power bus by commanding shunt switches in a shunt regulator. The ASRG power source has a constant power I-V curve over a power bus voltage range of 22 to 34 V at the ASRG output. The control function senses the current in the battery and adds or subtracts shunt current to limit the battery charge current to C/5 (full Charge in 5 hours). The PBC commands discrete shunt driver switches in the SDS that drive power to the shunt radiator to control the power bus. The current regulation will taper to 0 current at the voltage set point correlating to the desired state of charge. We are using 32.8 V as the 100% state of charge for the selected Li-Ion battery technology. The PBC has several commanded set points to set the battery at the desired state of charge.
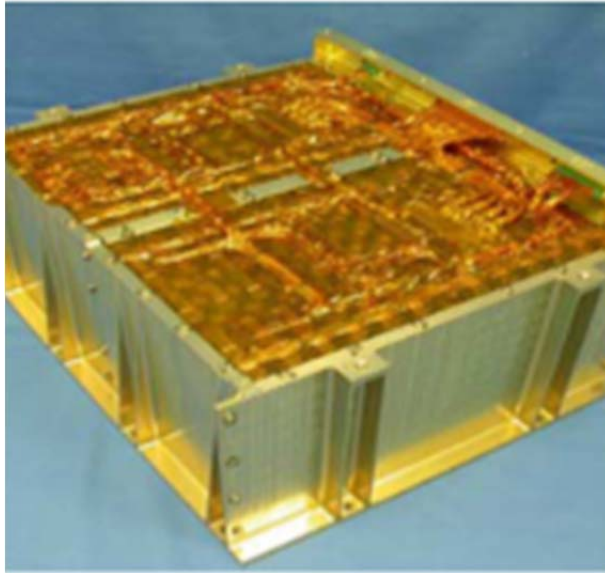
Figure C.2.4-31. Small-cell ABSL reference battery is the same size as the SMAP battery configured with 8 cells in series and 52 strings in parallel.

The energy storage technology assumed for this study is based upon the characteristics of the small-cell ABSL Li-ion battery used on the Soil Moisture Active Passive (SMAP) mission (Figure C.2.4-31). The battery is configured with eight cells in series to get the desired bus voltage operating range, and 52 cells in parallel to get the desired 59 Ah of energy storage at the beginning of life. The battery has a capacity of 40 Ah at EOM after a single-string failure, including degradation for life, discharge rate, and operating temperature. The reference scenario that defines the energy storage needed for the Europa Multiple-Flyby Mission is the 2-hour JOI maneuver, which requires 13 Ah at 10°C with a 6.5-A discharge rate. JPL Design Principles allow for a 70% depth of discharge (DOD), making a 19-Ah battery adequate for the Flyby Mission (JPL 2010a).

The small-cell battery approach does not implement individual cell monitoring and balancing due to the matched cell behavior; however, a trade between the large cell with cell balancing and the small cell needs to be studied.

Power Distribution

The power distribution function is a combination of centralized power switches in the MPSS and distributed power switches on the primary side of each PCU. This combination enables the system to optimize the mass of the cabling by using centralized switches for heater buses and other loads that do not require a PCU and distributed switches for each PCU, reducing point-to-point cabling for the major subsystems. A slice packaging approach enables the addition of centralized power switches without affecting the mechanical footprint and cabling and without modifications to a chassis or backplane. Growth in the command and telemetry interface is handled by the addition of addresses on the serial bus implemented in cabling. The thermal interface scales with the mechanical footprint.

Independent high- and low-side switches prevent any single failure from resulting in a stuck-on load and permit the resolution of load shorts to chassis. Commanding is cross-strapped to the power switches through each PBC, such that no single failure will prevent the commanding of any power switch. Each set of load switches is part of the load fault-containment region, regardless of the centralized or distributed location of the switch.

Power Conversion

The power conversion function for each electronic assembly uses a distributed point of load (POL) architecture (Figure C.2.4-32), where appropriate. This approach has a single isolated power converter on the PCU board, providing an intermediate power bus voltage that is distributed to each subassembly in the assembly. Where this is used (e.g., C&DH), the front end of each subassembly can cross-strap the intermediate power bus and provide on and off capability with fault management to enable low-power operating modes and improve fault-containment regions. The primary side power switch is controlled by the Power Subsystem, and the POL regulators are command-
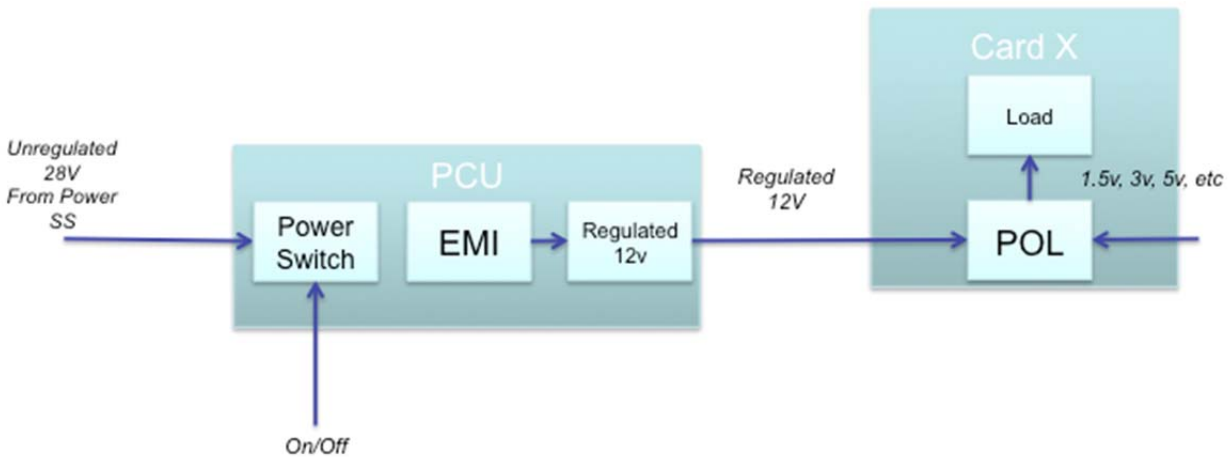
Figure C.2.4-32. POL power conversion architecture shows the primary power bus interface with distributed switch controlled by the Power Subsystem. The distributed POL converters are controlled by the local assembly.

ed by the assembly. In electronic assemblies where POL switching is not needed, primary side power switching would still be used.

PCUs in other subsystems would not be part of the Power Subsystem, but the PCU design would be a common delivery from the Power Subsystem to other subsystems/payloads, both to minimize cost through commonality and to ensure the greatest integrity of the overall system power architecture.

Pyro Firing and Valve Drive

Pyro-firing and valve-drive functions are provided by a set of centralized power switches in the Power Subsystem electronics commanded by C&DH via the PBC. The PFCs are fail-safe off, with two cards providing block-redundancy. Each PFC fires up to 32 NASA Standard Initiators (NSIs) from a protected load power bus that provides all of the safety inhibits required for launch. The PFC controls the current into each NSI, with the ability to fire six events simultaneously.

The PDE actuates valves for the main engine and the ACS thrusters. The PDE also actuates propulsion latch and solenoid valves and switches power from the protected load bus with necessary safety inhibits in place. The PDE is fail-safe off with single-fault-tolerance provided by a block-redundant set.

Power Subsystem Heritage

This Power Subsystem concept uses the same architecture as SMAP, and many of the slice designs are the same. The power bus control algorithm is the same as used on SMAP, as is the slice packaging design and designs for the PFC and PDE. The MPSS is the high-side and low-side variant of the design used on SMAP. The PBC has a new command interface, but the control of the shunt regulator is the same as for SMAP. The ABSL battery is the same design as used on SMAP, and the cell technology has flight heritage with Kepler.

C.2.4.6.3   Guidance, Navigation, and Control

The GN&C Subsystem provides an agile pointing platform for science data collection and a stable platform for science telemetry transmission.

The Europa Multiple-Flyby Mission GN&C Subsystem provides three-axis attitude control through all mission phases after separation from the launch vehicle in order to meet science and engineering pointing needs for instruments, antennas, radiators, shades, and so on. All pointed elements (except the SWIRS mirror for image integration) are body-fixed, so pointing is via spacecraft orientation. GN&C also detumbles the spacecraft after separation, controls ΔV maneuvers and performs momentum management. During JOI or

larger TCMs, when the fixed main engine is used, GN&C provides thrust vector control using dedicated TVC thrusters mounted on the thruster clusters.

At flyby ranges greater than 1,000 km, the spacecraft points at areas of interest for SWIRS images. During flyby maneuvers with ranges less than 1,000 km, the spacecraft is pointed to nadir to enable science instrument data collection; after each flyby, the spacecraft points the HGA towards Earth to downlink the science data.

The C&DH Subsystem hosts GN&C software, which is developed in a GN&C design and simulation environment.

GN&C hardware consists of reaction wheels, inertial measurement units (IMUs), sun sensors and stellar reference units (SRUs). Four reaction wheels and block redundant IMUs and SRUs provide single fault tolerance. The reaction wheel, IMU, and SRU electronics are heavily shielded from radiation, allowing the use of standard space products. The SRU head with detector is shielded to reduce the electron/proton flux so that <4th-magnitude stars can be tracked. Analysis of attitude determination capabilities in the Europa environment demonstrated pointing knowledge capability exceeding the requirements driven by HGA pointing with Ka-band.

As on Cassini, the location over time of the spacecraft and of pointing targets will be stored on board, enabling ephemeris-based tracking, including target relative pointing profiles and motion compensation, as necessary. Cassini demonstrated that this improves performance and reduces operations complexity. The use of thrusters for thrust vector control eliminates the development cost and complexity for a gimbaled engine and reduces the number of unique interfaces on the vehicle. When the redundancy of the main engine is revisited in Phase A, this configuration would be subject to change, including possibly the need for gimbals.

Table C.2.4-5. The GN&C Subsystem design provides an agile platform with precise pointing control.

Item	Value	Sizing
Reaction Wheel Momentum	12 Nm	Handle flyby maneuvers
Attitude-Control Thruster Size	4.45 N	Minimum torque impulse bit for deadband control during cruise/safe mode
TVC Thruster Size	22 N	TVC control for CM offset
Ka-Pointing	1 mrad	Support HGA link budget at required data rate with 3 dB of margin
X-Pointing	112 mrad	MGA communication while Sun-pointing
Ti Jitter	25 μrad/ 3.5 ms	
IPR Jitter	5 cm/32 s	Assumes 15-m IPR antenna

Table C.2.4-5 shows the key characteristics of the GN&C Subsystem. The reaction wheel sizing is driven not by environmental momentum accumulation but by the flyby maneuver. The momentum sizing of 12 Nms was based on vehicle inertias and the maximum flyby rate, with 100% margin for unknowns. The torque sizing of 95 mNm was based on vehicle inertias and maximum acceleration during the flyby, with 100% margin for unknowns (on top of the torque required to overcome losses inside the wheel). Figure C.2.4-33 shows the thruster configuration.

Given a thruster moment arm of approximately 2 meters, the attitude-control thruster sizing of 4.45 N is to provide a sufficiently small minimum torque impulse for deadband attitude
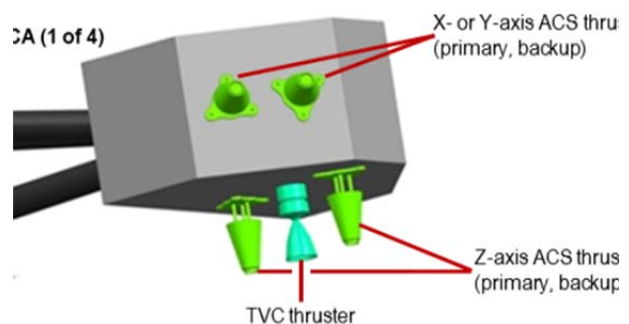
Figure C.2.4-33. The thruster configuration leverages the proven Cassini approach.

control during interplanetary cruise (or safe mode). The TVC thruster sizing of 22 N is provides sufficient control authority for up to a 9-centimeter shift of the vehicle center of mass (CM) during the mission. Ballast mass is included in the MEL (Section C.4.3) to provide initial center of mass alignment. Methods of controlling CM offset from propellant migration will be studied in Phase A.

The 1 mrad Ka-pointing control requirement is a radial, three-sigma number derived from the telecom link analysis. The X band pointing for safe mode is 112 mrad, based on a beam width that allows Sun-pointing with Sun-sensors while still communicating with Earth from Europa. The TI jitter is 25 microradians over the exposure time of the camera of 3.5 milliseconds. The IPR jitter is based on keeping the antenna beam aligned with the orbit normal such that there is no more than a 5 centimeter deflection off that line at the ends of the 15 meter boom over 32 seconds. The capability of the concept will be assessed when more details about spacecraft flexible-body effects and propellant slosh are modeled.

Figure C.2.4-34 shows the block diagram of the GN&C Subsystem. At the center of the subsystem is the FSW that resides in the RAD750 processor in the C&DH electronics. For Sun-pointing modes of operation, the knowledge of the Sun vector with respect to the vehicle reference frame is provided by three Sun-sensors distributed on the Avionics Module to provide near 4π-steradian coverage. If there are any gaps in the coverage a spiral scan attitude maneuver can quickly bring the Sun into a sensor's FOV. For precise attitude determination a combination of inertial measurements corrected by stellar updates is provided by the IMUs in the avionics vault and shielded SRUs outside the vault.

For precision attitude control, three of four reaction wheels are used; accumulated angular momentum from external torque is eliminated, as needed, by the attitude-control thrusters. The reaction wheel drive electronics (RWE) are in the avionics vault while the mechanical assembly (RWA) is outside the vault. For less precise attitude control during cruise or during safe mode, the attitude-control thrusters can be used. Note that using the Cassini configuration for thrusters uncouples forces and torque in
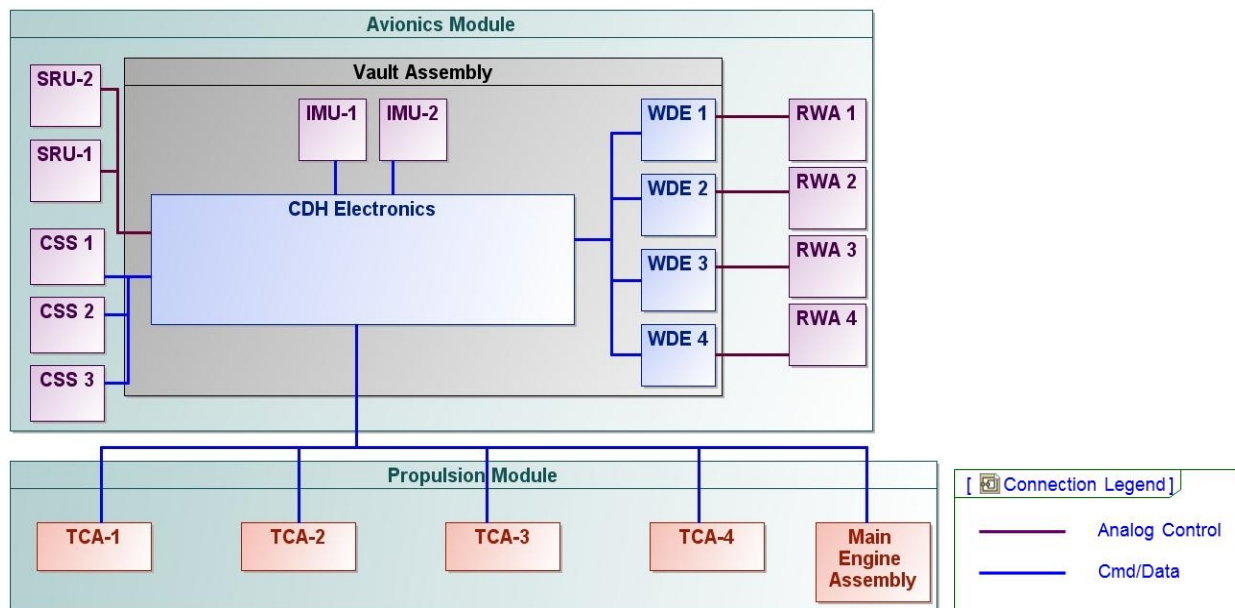
Figure C.2.4-34. The GN&C Subsystem is redundant and cross-strapped to provide robust fault-tolerance to radiation events.

Table C.2.4-6. GN&C hardware items, and approach to deal with radiation.

Item	Radiation Approach
Reaction Wheel	Sensitive wheel-drive electronics in avionics vault Mechanical assembly radiation-hard by design
Sun-Sensor	Radiation-hard by design
Stellar Reference Unit	Shielding for flux and total dose
Inertial Measurement Unit	In avionics vault

Figure C.2.4-35. The RAD750 provides high heritage for both the C&DH electronics and FSW designs.

roll, but not in pitch or yaw. For attitude control during TCM or JOI (when the main engine is fired), the TVC thrusters are used for pitch and yaw control while the attitude-control thrusters are used for roll control.

The GN&C architecture is cross-strapped such that any SRU can be used with any IMU to provide the attitude information to any computer. Attitude control can be accomplished with any three of four reaction wheels or with any set of eight block-redundant thrusters.

Given the radiation shielding provided by the rest of the spacecraft, the GN&C Subsystem can use standard space GN&C products with high TRL. Table C.2.4-6 shows the GN&C hardware items, and the approach to deal with radiation.

C.2.4.6.4 Command and Data Handling Subsystem

The C&DH provides a cross-strapped and redundant radiation-hard platform to support the data storage and processing needs of flyby science.

The Europa Multiple-Flyby Mission C&DH is the control center for most activities on the spacecraft, including nominal command sequencing; general system operation; GN&C, propulsion, and thermal control algorithms; and fault management. Both science and engineering data are also gathered, stored, and processed in C&DH for telemetry.

Several additional key requirements drive the C&DH, as follows. The design must be single-fault-tolerant and cross-strapped. It must be able to fail operational during single-event ef-

fects in the high-radiation environment of the Jovian system, and should allow easy swapping of redundant subassemblies to enable rapid transition of control after a fault. A RAD750 single-board computer (see Figure C.2.4-35) was selected to leverage the processor's flight heritage and radiation-hardness, and JPL's software architecture heritage. Onboard data storage is sized to accommodate multiple copies of the flyby science data. Concepts for data integrity using this redundant storage capacity will be investigated in Phase A.

The C&DH electronics occupies a single box that is internally redundant. Given the use of SpaceWire (see Figure C.2.4-36) as the primary interface, there is no need for a backplane or motherboard within the box; this increases the C&DH box reliability and simplifies packaging. A standard-size chassis of a 6U × 220 mm cards was selected to enable the use of heritage single-board computers and provide sufficient board area for the I/O and memory cards.

Time broadcast and synchronization are part of the SpaceWire standard so no external timing
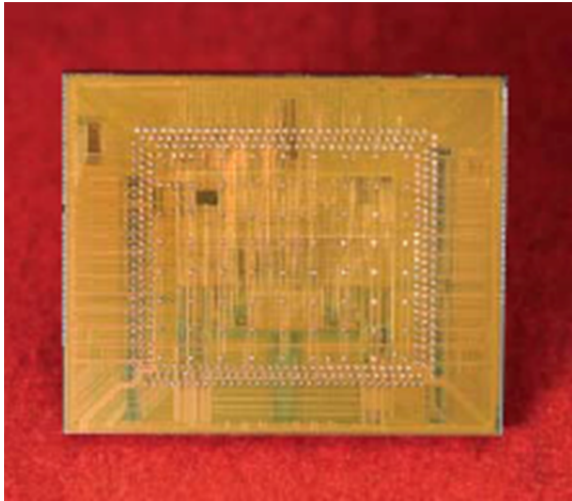
Figure C.2.4-36. The SpaceWire interface chip is radiation-hard and provides a high-speed standard interface to the cards in the C&DH.

network is required. Remote I/O units handle all the low-level interfaces such as analog and discrete measurements, and serial I/O; they also provide the Telecom Subsystem interface, critical relay commanding, and processor swap functions. I/O is multiplexed through an enhanced SpaceWire interface that can support programmable I/O functions. I/O circuits are standard designs from other JPL spacecraft.

The solid-state recorder provides 128 Gbit of storage using Flash memories. Although Flash memories are commercial parts, recent testing shows several radiation-tolerant options. A

radiation characterization risk-mitigation activity in Phase A will identify the best part, followed by a lifetime buy for the project. The memories are interfaced to the spacecraft through a SpaceWire interface with embedded processor that will allow it to behave as "network-attached" storage: Reading from and writing to this recorder doesn't require involvement of the RAD750, freeing this processor for other functions, such as IPR data processing. The power-conditioning unit (PCU) takes in unregulated 28 V off the power bus, provides EMI filtering, and converts it to a regulated 12 V that is distributed to each card in the box. The PCU on/off switch is controlled by the Power Subsystem. The local card on/off is software controlled via the processor and commands issued via the remote I/O.

A physical block diagram of C&DH is shown in Figure C.2.4-37. This shows the cards in the C&DH box. The box is internally redundant and cross-strapped (both data and power). SpaceWire supports multiple topologies (e.g., star or daisy chain). The box consists of two RAD750 single-board computers with SpaceWire router, two mass memory cards, two remote I/O cards, and two PCUs. The mass memory card interfaces to the single board computer via SpaceWire. The remote I/O cards interfaces to the single-board computer via SpaceWire.

The C&DH electronics does not require any new technologies. The RAD750 single-board computer with SpaceWire is an off-the-shelf product. The SpaceWire interface chip is an off-the-shelf product. The I/O circuits, power supply, and mass memory have analogs on previous projects. The 6U × 220 mm packaging standard has been qualified and used on previous projects.

C.2.4.6.5   Software

Highly reliable software for mission-critical applications is essential for this long-life mission. The flight software (FSW) baseline extends JPL's long heritage in FSW architecture development, and will be implemented in accordance with JPL requirements for NASA Class B (non–human-space-rated) software development. JPL has established a set of institutional software development and acquisition policies and practices as well as design principles that apply to mission-critical and mission-support software. These practices conform to NASA Software Engineering Requirements, NPR 7150.2 (NASA 2009b) and are an integral part of the JPL Design Principles (DPs) and Flight Project Practices (FPPs) (JPL 2010a, b). All Europa Multiple-Flyby

Mission FSW will be developed in accordance with JPL institutional policies and practices for deep space missions, including JPL's Software Development Requirements (JPL 2010c), which address all Capability Maturity Model Integration (CMMI) process areas up to maturity level 3. Software identified as safety-critical will comply with safety-critical requirements, regardless of software classification. Software safety-criticality assessment, planning, and management will be performed for all software, including new, acquired, inherited, and legacy software and for supporting software tools. Software is identified and documented as safety-critical or not safety-critical based upon a hazard analysis conducted prior to start of development activities.

Key functions allocated to software include system command and control, health and safety management, attitude and ΔV control (such as maintaining concurrent HGA Earth pointing during telecom sessions, or instrument surface tracking during science operations), science data collection and processing, onboard data management, and reliable delivery using Consultative Committee for Space Data Systems (CCSDS) File Delivery Protocol (CFDP).
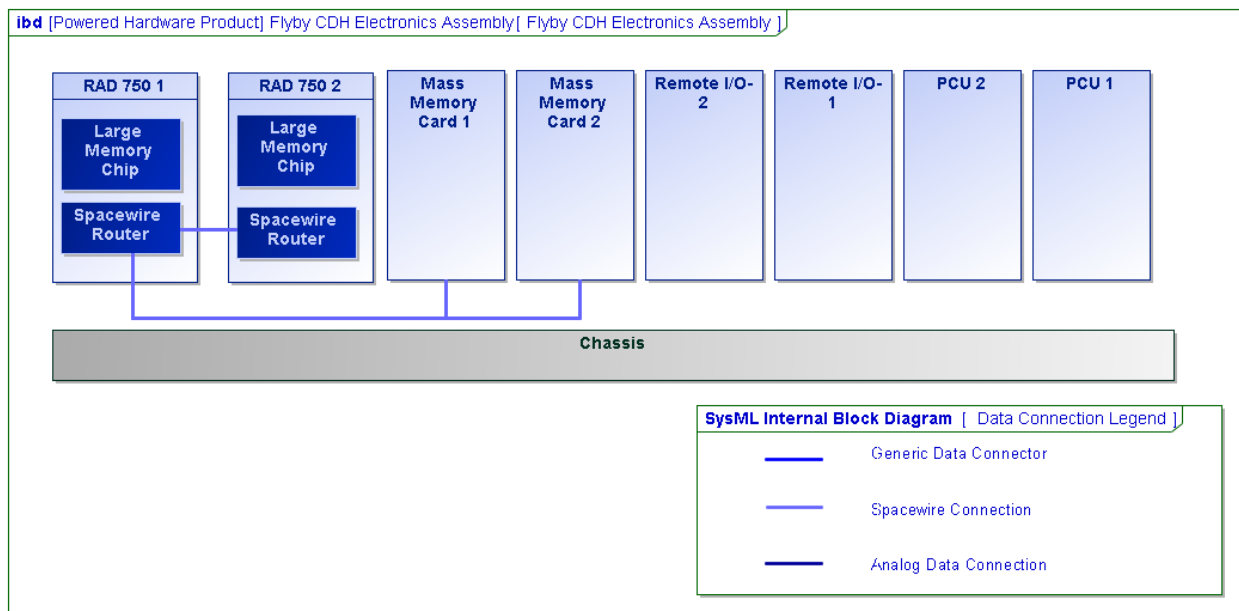
Figure C.2.4-37. The C&DH is redundant and cross-strapped to provide robust fault-tolerance.

Onboard ephemeris-based pointing and the use of CFDP help to simplify operations and thus reduce long-term operations costs. None of these capabilities are new technology, and significant algorithm and architecture heritage is available from Cassini, MSL, SMAP, MESSENGER, and other missions.

Flight software has a key role in system fault management. Critical activities are expected to include postlaunch separation, detumble, and acquisition, Jupiter orbit insertion, and possibly a moderate number of propulsive maneuvers needed to achieve the planned sequence of flybys. Although the flyby sequences are expected to be less complex than comparable Cassini or Galileo flybys, due to having fewer instruments and no articulation, they repeat at a more demanding rate than experienced in previous missions, and occur in the hostile radiation environment around Jupiter and Europa. Moreover, coverage objectives require most of the flybys to complete with minimal disruption. For this reason the FSW coordinates a system fault-management approach, consistent with current best practices, aimed at protecting essential resources, but trying to maintain scheduled operations using automatic fault responses such as resetting devices, switching to redundant devices, or selectively trimming subsets of planned activities.

The FSW is organized in a layered architecture, as shown in Figure C.2.4-38.

The Platform Abstraction layer interfaces directly with the hardware. This layer contains drivers that provide control, and data abstractions to the device-manager and services layers. The drivers communicate with the hardware using the device-specific syntax and protocol, allowing higher layers of software to interact with these devices using system-standard communication protocols and message formats. Notably, the use of industry-standard SpaceWire as a common hardware communications medium reduces the number of different device types that must be supported, with commensurate reductions in software system complexity. Furthermore, the ability of SpaceWire interface devices to buffer data and perform other control functions in hardware (as demonstrated by MESSENGER) is expected to further reduce the complexity and time-criticality of the FSW implementation.

Figure C.2.4-38. Flight software benefits from appropriate reuse and evolution within a layered architecture.

The Platform Abstraction layer also encapsulates the real-time operating system, device drivers, and all interprocess communications, leveraging flight heritage with the RAD750 platform and all JPL missions since Pathfinder. The commercial operating system provides real-time task scheduling, memory management, and interfaces to I/O devices immediately associated with the processor board.

The Behaviors layer includes software elements that perform closed-loop control around specific system behaviors. These behaviors are typically responsible for the management of one or more hardware devices or subsystems, as well as integrated behaviors associated with them, such as attitude control. Closed-loop behaviors also incorporate fault detection and localized fault management capabilities.

Behavior coordination is provided in a separate Coordination layer that can sequence and coordinate the control of underlying behaviors. This layer is also responsible for coordinating any fault responses at a system level.

The MetaControl layer provides services for initializing and supervising reliable operation of the rest of the software and computing system and for supporting external commanding and configuration (such as changing system behavior from the ground).

Instrument-embedded software is developed by instrument providers and tested locally using a spacecraft simulator (see Testbed Approach). It is delivered with the instruments. Some engineering devices may also include embedded software. All other software is developed in-house.

C.2.4.6.6   Structure

The Avionics Module (Figure C.2.4-24) supports the majority of the avionics, batteries, science instruments, star-trackers, Sun-sensors, and reaction wheels. Its vault houses and shields most of the avionics components and extends below the Avionics Module's mechanical interface with the Propulsion Module. This configuration optimizes radiation-shielding by making use of the existing structure in all directions: From the top the octagonal primary structure, reaction wheel mechanical assemblies, and batteries provide shielding; from the sides the primary structure, tanks, and thermal enclosure provide shielding; and from the bottom the Power Source Module's primary structure and the Propulsion Module's main engine assembly provide shielding, complementing the vault's thick walls. Waste heat from the avionics is allowed to radiate out from the vault into an enveloping thermal shroud to help maintain the propulsion tanks at their required temperatures.

The topmost part of the Avionics Module, called the Upper Equipment Section (UES), is also octagonal. The vault is box-shaped. The structure that connects the UES of the Avionics Module to the vault is composed of machined stringers riveted to sheet-metal panels. An octagonal ring is riveted to the top of the module, and a square interface ring is riveted to the bottom.

The vault consists of six machined panels that are riveted together, with access panels integrated to allow for installation and removal of the avionics.

The batteries and reaction wheels reside inside the UES of the Avionics Module.

Instrument Accommodation Structures

The INMS, TI, SWIRS, and IPR are all mounted to the Avionics Module's primary structure, as shown in Figure C.2.4-39. Each instrument has been positioned to accommodate the required aperture and radiator fields of view to support its science function.

Thermal Section Structures

The thermal enclosure consists of blankets made from aluminized Kapton, aluminized Mylar, and Dacron net separators, supported by a lightweight, carbon-fiber tubular frame.

C.2.4.7   Technical Budgets

Three primary technical margins are addressed here: mass, power/energy, and data balance.

Other key technical margins are covered elsewhere in this report: Radiation tolerance margin is treated in Section C.2.6.1.
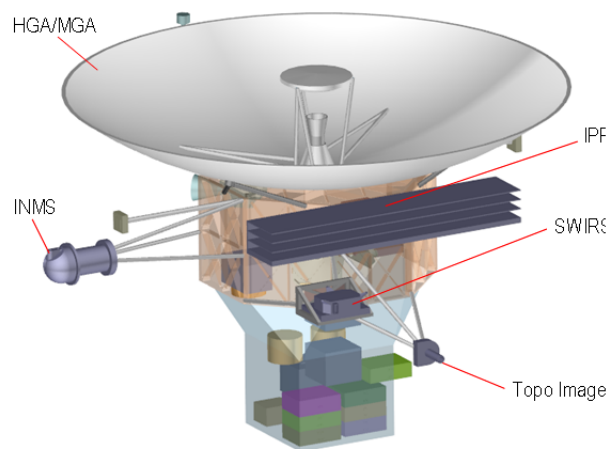
Figure C.2.4-39. Avionics Module primary structure.

The approach to technical resources in this study has been to model what is well understood, and then include conservative margin based on past experience to account for items not known well enough to model.

To minimize cost and schedule risk, we have striven to achieve high levels of technical margin wherever possible.

C.2.4.7.1   MEL and Mass Margins

Mass margin follows the definitions and conventions specified in the JPL Design Principles, Section 6.3.2 (JPL 2010a). The earliest milestone at which the Design Principles specify a mass margin, however, is the Project Mission System Review (PMSR), when at least 30% is required. In consideration of the fact that the Europa Multiple-Flyby Mission concept is in a study phase, we have set a more conservative policy of ≥40% mass margin for this report. This is consistent with the expected evolution of JPL's institutional guidance. The method of calculating the Design Principles margin is shown in Table C.2.4-7.

The dry mass current best estimate (CBE) includes tanks sized to carry the maximum propellant load, plus radiation shielding, and the launch vehicle adapter (LVA). Each of these is discussed in more detail below.

Use of "Max Propellant"

The Design Principles explicitly require that the propellant load assumed for the margin calculation be that amount of propellant needed to provide the required ΔV for the maximum possible launch mass on that launch vehicle (LV), given ΔV requirements for the

chosen trajectory. In addition, the dry mass of the propellant tanks reflects tanks sized for this maximum propellant load. This approach gives an accurate reading of the overall dry mass margin, *assuming* that the flight system grows

Table C.2.4-7. Europa Multiple-Flyby Mission mass margin.

Flyby Mass Margin			
T. Bayer 24 Apr 2012	LAUNCH		
Flyby Model - Final Report Update	Flight System Mass, kg		
	CBE	Cont.*	MEV
Ion & Neutral Mass Spectrometer	24	50%	36
Ice Penetrating Radar	33	50%	50
ShortWave IR Spectrometer	21	50%	31
Topographical Imager	7	50%	11
Payload	**85**	**50%**	**127**
Power	59	21%	72
C&DH	39	30%	51
Telecom	98	29%	126
Structures	529	27%	673
Thermal Control	44	30%	57
Propulsion	175	28%	224
GN&C	68	23%	84
Harness	70	50%	105
Radiation Monitor	8	30%	10
ASRGs (4)	174	45%	252
Spacecraft	**1264**	**31%**	**1655**
Flight System Total Dry	**1349**	**32%**	**1782**	**Max Prop**
Bipropellant	860		1277	1711
TVC Monopropellant	75		75	75
ACS Monopropellant	40		40	40
Pressurant	6		6	6
Residual and Holdup	24		35	46
Propellant	**1005**		**1432**	**1877**
Flight System Total Wet	**2354**		**3214**	
Capability (21-Nov-21 VEEGA)	Atlas V 551:		**4494**	
System Margins			
JPL DVP (Capability - Max Prop - CBE Dry) / (Capability - Max Prop)			48%
Total payload shielding	48	42%	68
Total spacecraft shielding	170	29%	220
LV adapter	89	25%	111

*Using ANSI/AIAA Guide G-020-1992, "Estimating and Budgeting Weight and Power Contingencies for Spacecraft Systems", applied at the component level.

to the maximum launchable mass.

Specifically, in Table C.2.4-7, propellant mass is computed from the ΔV required for the 21 November 2021 Venus-Earth-Earth gravity assist (VEEGA) trajectory. The CBE propellant is computed using the CBE dry mass and CBE ΔV. The maximum expected value (MEV) propellant is computed using the MEV dry mass and the MEV ΔV. The max propellant is computed using the maximum possible dry mass and the CBE ΔV.

Radiation Shielding

The mass model tracks the amount of shielding necessary to protect each piece of sensitive electronics. This mass is accounted for at the appropriate level of assembly (card, box, or module), and shown as a payload and engineering total in Table C.2.4-7.

Launch Vehicle Adapter

A standard Atlas LVA is assumed. The mass shown in Table C.2.4-7 includes both the part that remains with the spacecraft and the part that remains with the Centaur upper stage but is considered by launch services as "payload mass" for the purpose of LV performance. Delta-V calculations carry only the part that remains with the spacecraft.

This margin calculation adds "growth contingency" mass to the CBE masses to arrive at an MEV mass and the propellant required for that mass. It then compares this value to the LV capability. For determination of contingency factors, the Europa Study Team has used the ANSI/AIAA Guide G-020-1992 (American National Standards Institute 1992), applied at the component level. This specifies the *minimum* contingency factor based on project phase and component sizing and maturity, and

allows a higher factor where the project deems it appropriate. The guideline is generally consistent with traditional JPL practice, but provides a more rigorous grounding through its use of historical data.

As can be seen in Table C.2.4-7, the Europa Multiple-Flyby Mission has excellent mass margins. A more detailed mass breakdown can be found in the MEL (Section C.4.3).

C.2.4.7.2   PEL and Power/Energy Margins

The Power Equipment List (PEL) contains the CBE power needs for power loads in various modes, with a contingency for maturity. Europa Multiple-Flyby Mission power modes are based on the mission scenarios described previously (see Section C.2.1.2). The policy established for Europa Multiple-Flyby Mission policy has been to maintain 40% of the power source capability after an ASRG single failure as power margin on the load for all mission power modes. Each mission mode is assessed against this policy. Transient modes are assessed with power margin on the load included, and using the JPL Design Principles depth of discharge (DOD) guidelines for actual battery capacity, assuming a single failure. Others are steady state (S/S). Summary results of the mission mode power analysis are shown in Table C.2.4-8.

The PEL provides the CBE capability of the power source and its LEV for each mission mode. The power source estimate takes into account degraded performance of the ASRG during launch due to the environmental conditions inside the shroud. The LEV of the ASRG assumes a failed Stirling converter after launch, effectively producing the power of 3.45 ASRGs.

Table C.2.4-8. Europa Multiple-Flyby Mission power analysis compares the power source capability to the estimated load for all phases of the mission. There are two mission modes that rely on the battery, and the DOD is displayed.

Mission Phase	Flyby Power Analysis							
	ASRG Power, W		Flight System Power, W				Stdy State or Transi-ent?	Max Bat DOD, %
	CBE	LEV	CBE	Cont.	MEV	Margin %		
Launch	426	334	113	19%	135	66%		
Inner Cruise	535	420	224	24%	279	47%	S/S	
Inner Cruise (Safe)	535	420	245	23%	302	42%	S/S	
Outer Cruise	514	403	177	23%	217	56%	S/S	
Outer Cruse (Safe)	514	403	245	23%	302	39%	S/S	
Orbit Insertion/TCM	505	403	355	24%	438	40%	Transient	32%
Flyby Science (all instruments)	498	391	264	27%	391	40%	Transient	2
Flybys Science (without IPR)	498	391	207	25%	258	47%	S/S	
Telecom Downlink	498	391	224	27%	284	43%	S/S	

The PEL reports for each load a CBE, a contingency to cover estimated growth based on maturity, and a maximum expected value (MEV), which includes transient loads. Each identified power mode is covered in the PEL, along with a summation of all of the loads that are on in that mode. The mission mode total is compared to the power source capability for the same mission mode, with the power margin calculated per the JPL Design Principles approach of (Capability − CBE) / Capability (JPL 2010a). The transient modes are modeled to estimate the battery DOD with the actual battery capacity.

One mission mode that needs some investigation is the outer Cruise Safe Mode, in which the power margin is slightly below the Europa Multiple-Flyby Mission policy at 39%. This is a steady-state mode that cannot rely on the battery, so sizing adjustments will be analyzed in Phase A to comply with the mission policy margin.

The two transient modes in the PEL are Orbit Insertion /TCM and Flyby Science (all instruments). Orbit insertion is presently the driving mode for battery sizing due to the long JOI burn of roughly 2 hours. However, this is based on very conservative assumptions regarding backup strategies that will be revisited in Phase A. Under such assumptions, the load profile and battery DOD are shown in Figure C.2.4-40, given a battery capacity estimated to be 40 Ah with a 6.5-A discharge at 10°C near EOM.

The JPL Design Principles allow for a 70% DOD for events such as orbit insertion that involve less than 100 cycles (JPL 2010a).

The other transient mode is the Flyby Science (all instruments) mode, in which the different instruments are turned on, depending on the distance range from Europa. The system is power-positive until the Ice-Penetrating Radar (IPR) is turned on for 16 minutes near closest approach to Europa (see Figure C.2.4-41).

We presently have only 2% DOD for this Flyby Science mode. The JPL Design Principles allow 60% DOD for less than 5,000 cycles (JPL 2010a).

Because both transient modes presently possess generous margins, there may be an opportunity to adjust the size of the battery to reduce mass, if necessary.
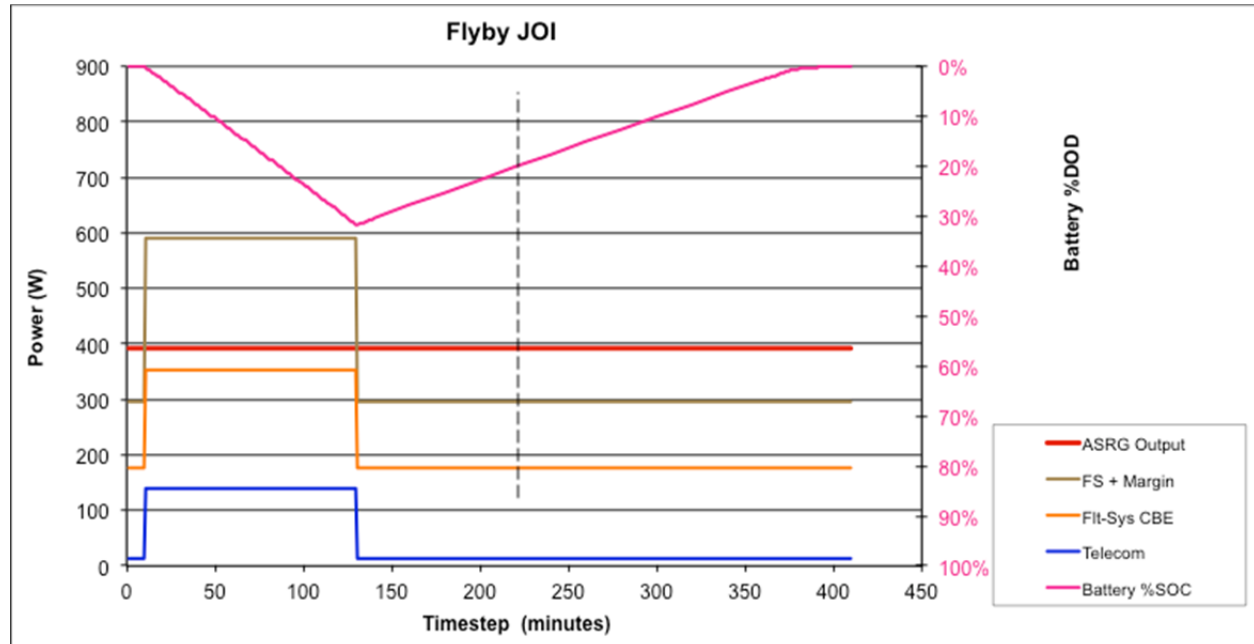
Figure C.2.4-40. Flyby JOI power analysis shows a 2-hour discharge of the battery using the Europa Study policy of 40% margin on the load profile.
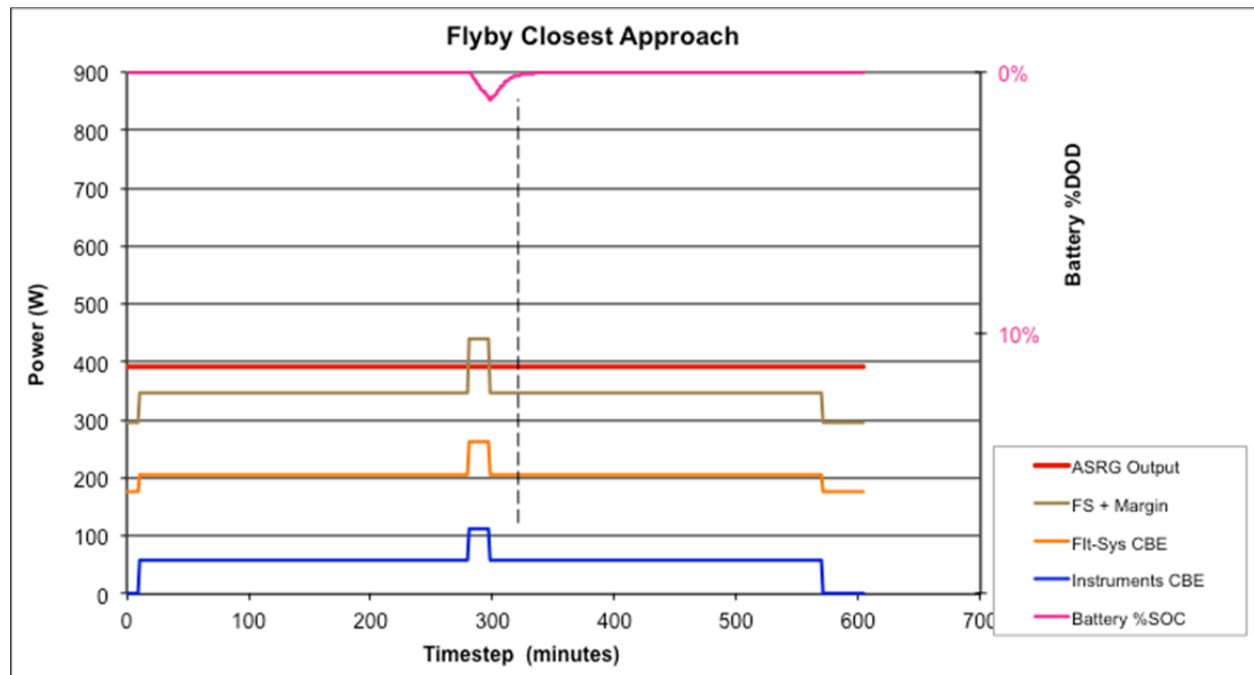

Figure C.2.4-41. Flyby science mode power profile shows that the system is power-negative only when the IPR is on for 16 minutes of each flyby.

C.2.4.7.3   Data Balance

Mission data balance is driven by the science objectives described in Section C.2.1, and the corresponding operations strategy described in Section C.2.5. This science scenario is viewed as the driving case for data collection rates because this is the only time the science instruments are operated, and because all must be operated concurrently when under 1,000 km in altitude. Each flyby is nearly identical, so the concept is to use essentially the same sequence of science observations each time, resulting in about the same data volume each time, as well. The notional instruments have a small number of operating modes where data output rate changes significantly. Operating modes for the nominal scenario are assumed to be producing data at the maximum expected rates.

The majority of orbits in the present mission concept have a 4:1 resonance with the period of Europa's orbit, so a 4-Eurosol period is used as the nominal repeat cycle for science operations to determine the time available for downlink. Each cycle begins with about 10 hours of science observations during the closest approach to Europa, producing about 32 Gbit of stored. The observation phase is followed immediately by a short battery-recharge period and then data playback during the ascending petal of the orbit. During this period, data is transmitted on Ka-band to maximize downlink throughput. Ground tracking is provided using 34-m DSN stations operating alternate 8-hour passes until the data from the flyby is recovered (this provides the option of inserting additional station passes to recover

from a missed pass). Additional downlink time is available during the descending petal of the orbit to recover any data missed during the first playback.

256 Gbit of solid-state data storage is provided by the C&DH Subsystem to provide redundant storage for the data from a single flyby, and/or data from an additional flyby to accommodate missed passes or other downlink interruptions (e.g., from weather). This strategy also accommodates the small number of flybys in transitional orbits that may have less downlink time between them, requiring downlink over subsequent orbits.

Downlink margins are shown in Table C.2.4-9. The 32 Gbit of accumulated data include the quantities of science data shown plus engineering data collected at 2 kbps. Downlink capacity is computed using the Ka link budget described in Section C.2.4.6.1, computed for a worst-case range of 6.5 AU, and DSN elevation angle of 20 degrees, and then multiplied by a factor of 1.2, based on the 2008 JEO analysis, to account for the ability to step downlink bit rates over each pass to maximize the throughput. Note that the telecom link budget already includes some margin for weather, and the downlink strategy described here includes additional margin in the form of time available to use different or alternate DSN stations if one station is disabled due to failure or weather.

Stored data is managed as products (files) in the onboard store; CFDP is used to ensure reliable transport of this data to the ground. At the

Table C.2.4-9. Data balance and margin.

	IPR	TI	SWIRS	INMS	Total/Flyby
Raw Data Rate (kbps)	28000	10258	116	2	
On-time per flybys (min)	15	15	554	15	
Compression Factor	1	3	3	1	
Effective Output Rate (kbps)	28000	3419	47	2	
Average Data Per Flyby (Gbit)	**25.2**	**3.1**	**1.3**	**0.002**	**32 Gbit**
Average Downlink Rate (kbps)					134 kbps
Downlink Time Required (hr)					66.3 hr
Downlink Time Available (hr)					326.8 hr
Downlink Margin					**80%**

average rate of 134 kbps data accumulates on the ground at a rate of about 3.8 Gbit/pass, or about 5.8B Gbit/day. Over the course of 27 science flybys, the mission accumulates a total of about 1 Tb of data. Because the rates given in Table C.2.4-9 are computed assuming worst-case conditions, the actual downlink rates could be higher for some flybys, requiring slightly more time to recover the data. Maximum downlink rates have yet to be determined.

C.2.4.8   Module Development, Integration, and Test

The modular approach for the spacecraft allows parallel testing before delivery to system integration and test at a higher level of integration than was possible for previous spacecraft.

The spacecraft would be comprised of the Avionics Module, the Propulsion Module, and the Power Source Module.

Development of the spacecraft modules begins with the design and fabrication of a developmental test model (DTM) of the spacecraft structure. The DTM is populated with appropriate mass mockups as required to properly represent the mass properties of the spacecraft. After assembly, a full set of structure qualification tests is be performed, including static loads, modal survey and pyro-shock testing. The DTM is also be used later as a "trailblazer" to ensure that all facilities (such as the launch site and LV) and mechanical ground support equipment (MGSE) characteristics are compatible. Because the DTM components are built to the same drawings as flight, elements of the DTM could also be used as surrogates for the flight structure, if required.

As the DTM program progresses, the flight model (FM) structural components are fabricated and delivered to the module teams (Avionics Module, Propulsion Module and Power Source Module) for integration with active components and secondary structure, and for module-level testing, including environments, prior to the start of system integration and test. 2 months of schedule margin is allocated for

the structure deliveries to the Module Development Teams, and a minimum of 1.5 months schedule margin is allocated for the delivery of the tested flight modules for system integration. Since the Avionics Module is the most complex functionally, 3.5 months of margin are allocated in recognition of its schedule criticality to System Integration and Test.

The module concept adopted for the spacecraft permits testing, both functional and environmental, to be performed with flight cabling and flight structure at a higher level of integration prior to delivery than has been performed on similar previous missions, such as Cassini. Development of more highly integrated modules allows more parallel path testing, reducing the number of interfaces that need to be verified at the system level, compared to a project like Cassini, where individual components and subsystems were delivered and integrated during System Integration and Test.

The major deliveries to system integration are the Avionics Module (consisting of the UES with science instruments (see below), the avionics vault and its contents, and the telecom assembly), the Propulsion Module (with tanks, other propulsion components, and harnessing), and the Power Source Module. The Power Source Module is populated with advanced Stirling radioisotope generators (ASRG) that are electrically heated to permit realistic testing and evaluation of the end-to-end power delivery system for the spacecraft. Emulations of other modules at electrical interfaces will be used to support module-level integration in each case.

All module deliveries are planned to occur at the start of System Integration and Test to maximize flexibility. The UES is initially delivered with Engineering-Model (EM) Science Instruments. The Flight Model (FM) science instruments are delivered later as shown in the System Integration and Test flow, permitting any interface or performance issues to be resolved before the flight deliveries.

C.2.4.8.1   Testbed Approach

Consistent with longstanding practice, the Europa Multiple-Flyby Mission has adopted a system integration approach that is supported by an additional set of software and hardware testbeds, enabling early and thorough integration of key hardware and software interfaces prior to ATLO. This development and validation approach begins with scenario development during formulation and design, and progresses incrementally to system validation using an ever-growing battery of regression tests that verify and validate system architecture as it is designed and developed. Figure C.2.4-42 depicts the proposed testbeds described in the following paragraphs.

Since science instruments are likely to be developed externally, instrument developers must be provided with a testbed environment that includes an emulator for engineering subsystems (hardware and software) that simulates the power, data, and control interfaces with which the instrument must integrate. This ensures that all interface issues have been resolved prior to delivery, thereby helping to keep the ATLO work focused on system integration and on the concerns that can be verified only in an assembled system context. Similar subsystem assembly testbeds are provided for early integration testing of major subsystems (telecom, propulsion, power, etc.).
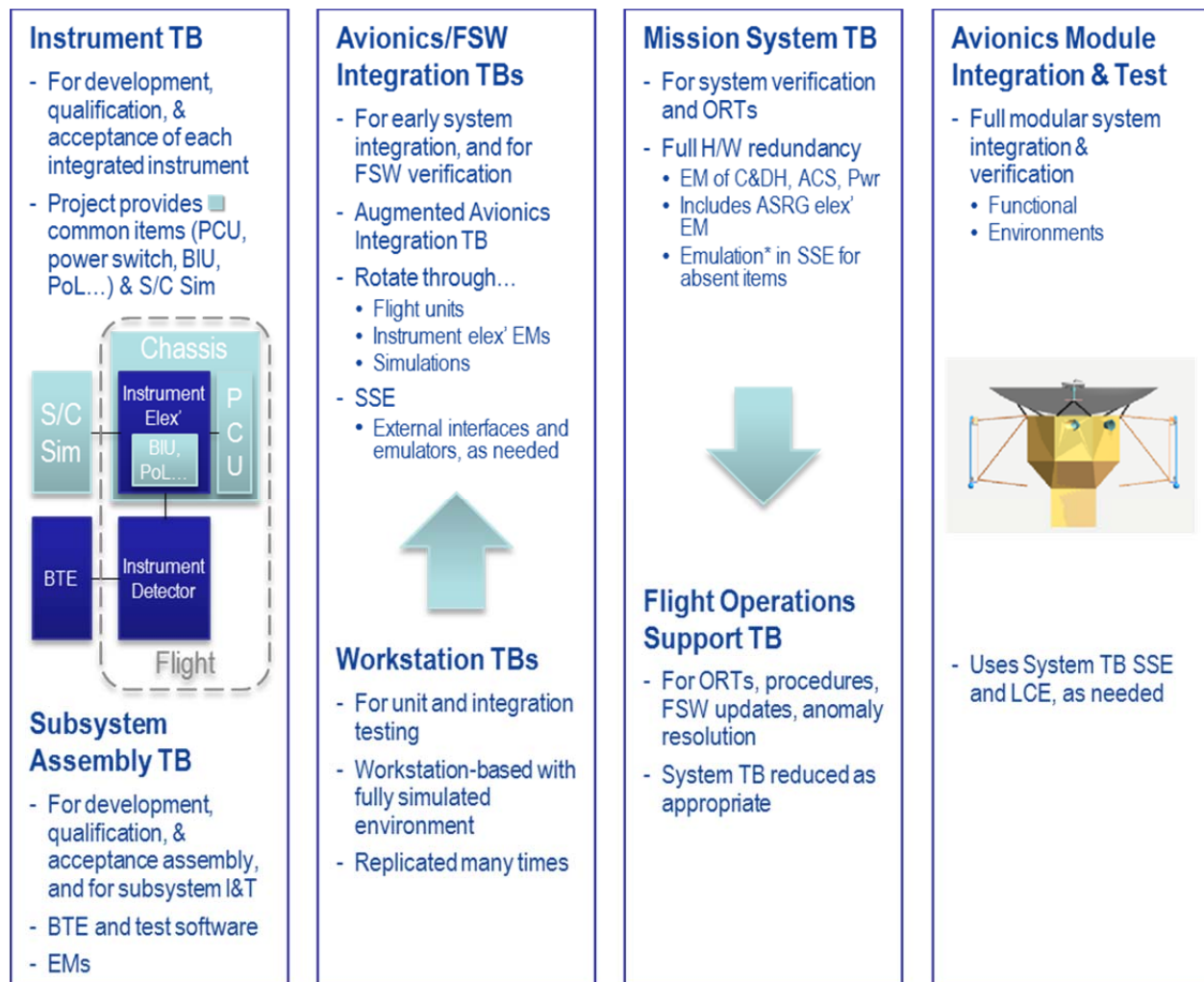

Figure C.2.4-42. System integration testbeds.

A high-fidelity model-based simulation capability (known as the workstation test set [WSTS] on MSL and SMAP) is baselined for FSW development test and verification. This includes but is not limited to fault management development and test, attitude control system-level verification and validation (V&V), and mission activity development and test; so several groups will exploit this capability, which can be replicated cheaply as often as necessary. The software simulation of hardware must be of sufficient fidelity to allow seamless migration of FSW and test cases from simulation to hardware-in-the-loop testbeds. This capability is important and necessary because certain software services are needed to support the instrument testbeds and the testing and integration of devices. Therefore, emphasis will be placed during hardware testing on validating simulation model fidelity.

The first workstation-based spacecraft simulator version will be available in time to support development of the first FSW release, and will progress with expanded capability, as needed to support testing of subsequent FSW builds. It will be available on all software developers', systems engineers', and testers' workstations. Capabilities will include closed-loop spacecraft behaviors operating in both nominal and off-nominal modes. These simulators are built to allow for interchangeability between software models and hardware engineering models (EMs) later in the "hardware-in-the-loop" testbeds in a manner that is transparent to the FSW and to test scripts, at least at the interface level. This enables use of the same test scripts whenever the testbed models are interchanged with EMs or hardware emulators.

In addition to the simulation capability described above, the Europa Multiple-Flyby Mission would have three system testbeds. The first two are the Avionics/FSW integration testbeds, which are similarly configured with single-string avionics. These support the development and test of ground support equipment (GSE) hardware and software, the devel-

opment and validation of test scripts, and the maturation of databases, such as command and telemetry dictionaries. First on line is the Real-Time Development Environment (RDE), which is dedicated to GSE hardware and software development and test. The next instance of this testbed, the Flight Software Testbeds (FSWTBs), becomes available later in the development process to allow V&V to proceed in parallel with FSW development. The third system testbed is the Mission System Testbed (MSTB), a full redundant, high-fidelity testbed dedicated to system V&V, FSW fault management tests, mission system tests, and AT-LO support.

These system testbeds include the C&DH, GN&C, Power, Telecom, and Harness subsystems, as well as Ground Data System (GDS) hardware and software. The EM versions of all flight system engineering subsystems and instruments will pass through these testbeds for integration and interface verification. No flight units are required to pass through the testbeds unless there are major modifications from the EM. However, the testbeds can support flight hardware integrations, if needed. The V&V simulation environment can offload the hardware-in-the-loop testbeds and use the EM integration effort to help evaluate model fidelity. The simulation environment interfaces and procedures are compatible with those of the hardware testbeds. These testbeds are also used to train test analysts to support system testing, as well as to support ATLO procedure development and anomaly investigation. All FSW versions are verified on the system testbeds prior to being loaded onto the flight system during ATLO or flight operations. The flight system testbed transitions to operational use for this purpose after launch.

C.2.4.8.2   *System Integration and Test*

The conservatively derived system integration and test program is based on actual durations from the Cassini project. Launch operations durations are based on actuals from the MSL project along with operations unique to the Europa Multiple-Flyby Mission.

The System Integration and Test (SI&T) Phase, described graphically in Figure C.2.4-43, begins with the delivery of the flight Avionics Module components, Propulsion Module, and Power Source Module for system integration. The Avionics Module components, consisting of the telecom assembly, UES (with EM science instruments) and the Avionics Vault, is integrated initially using extender cables. These permit access to circuits for integration and troubleshooting, as well as for connection of direct access equipment needed for closed-loop operation of the Attitude Control Subsystem during mission scenario and comprehensive performance testing. During integration, interface signal characteristics are measured and recorded for comparison with requirements.

Even though traditional EMC/EMI system engineering methods will be employed during development, the early integration of the Telecom Subsystem permits monitoring of spectral characteristics as other hardware is added to the system for detection and identification of any interfering spurious signals. A thorough telecom functional test is included in the flow to establish baseline performance while operating with the rest of the Avionics Module.

The Propulsion Module is electrically integrated through extender cables next in the flow to demonstrate signal characteristics to propulsion valves and thrusters, and to perform an initial verification of proper phasing. The design of the extender cables and the layout of the modules in the test facility address cable length issues, as appropriate. Phasing of propulsion components (as well as G&C components) is repeated after spacecraft stacking to remove any influence of the extender cables.

Finally, the Power Source Module is electrically integrated through extender cables. Plans call for fully functional ASRGs that are electrically heated and can be used to verify end-to-end performance, as well as to verify integration procedures that will be used for the flight ASRG integration at KSC.

A Deep Space Network (DSN) compatibility test is performed at this point (with the DSN compatibility test trailer) followed by an Engineering Baseline Comprehensive Performance Test (CPT). This and other configuration-dependent baseline tests are performed throughout the ATLO program in order to detect performance changes resulting from either trending or environments.

A series of fault management tests is performed to establish correct operation of the fault management system software in conjunction with associated hardware detections and responses.

The first mission scenario test is the launch sequence test, executed both nominally and with selected fault and off-nominal conditions. Subsequently, a trajectory correction maneuver test (including orbit insertion) is performed in both nominal and off nominal conditions. Other capabilities of the spacecraft to support required operational modes, science observations, and other noncritical mission scenarios will be incorporated in CPT(s) rather than in specific scenario tests so that spacecraft capabilities are fully established, rather than merely performing point-design mission scenario verifications. Since all operations described above are first-time events, one-month schedule margin is included at this point to prevent any delay to the science instrument integration.

At this point, any outstanding science instruments are delivered and integrated into the Avionics Module, replacing their EMs that have been serving as surrogates throughout system testing.
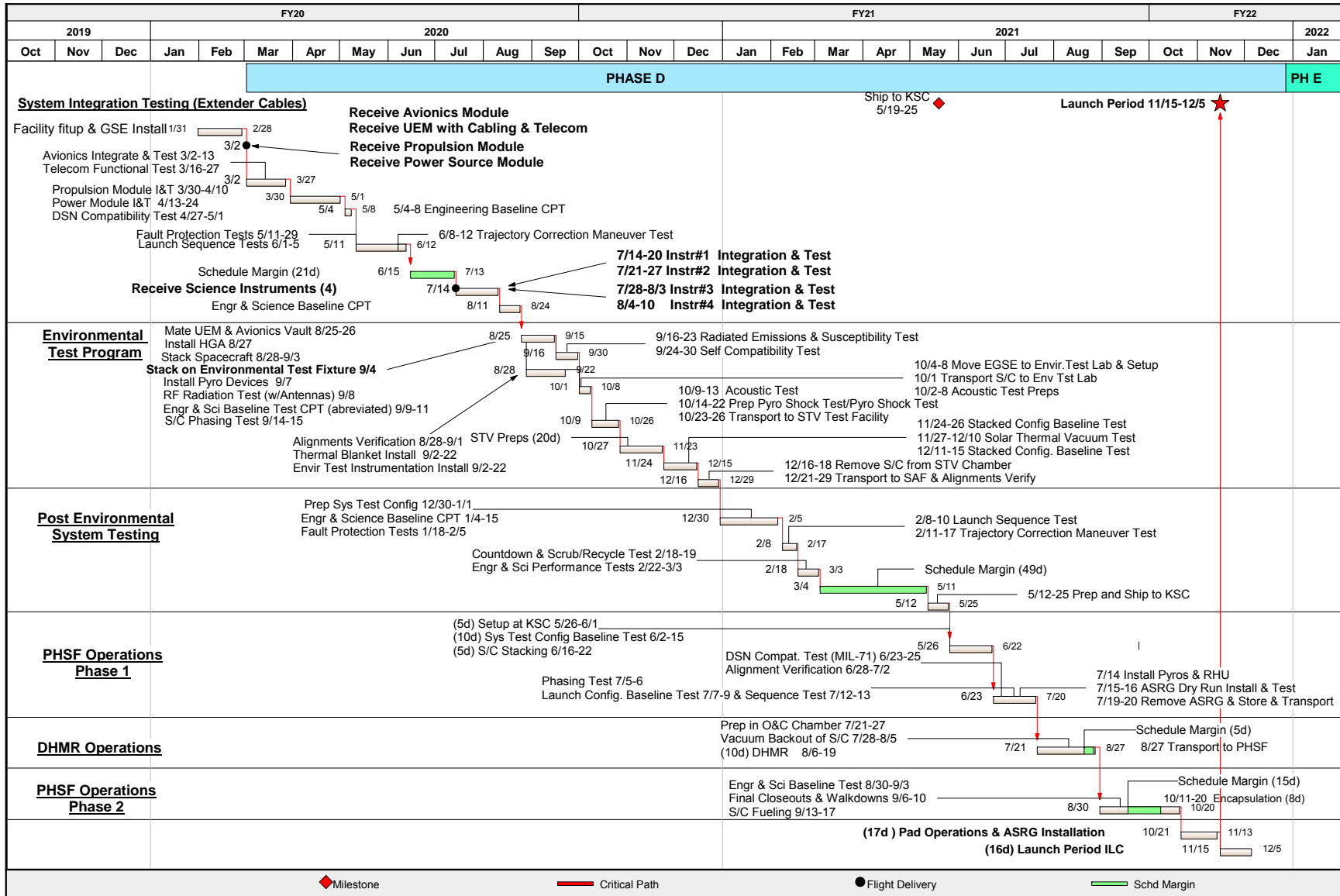
Figure C.2.4-43. The comprehensive ATLO program is based on as-run durations from Cassini and MSL plus JPL-required schedule margins.

An Engineering and Science CPT follows integration, with all spacecraft components present to establish the performance of the spacecraft before reconfiguration for environmental test.The environmental test program starts with the mechanical and electrical integration of the UES, avionics vault and the telecommunications assembly to complete the Avionics Module. Stacking of the Propulsion Module, Power Source Module, and Avionics Module to each other, stacking the spacecraft on the Launch Vehicle Adapter (provided by the Launch Service) and the installation of pyro devices needed for pyro-shock testing. An Abbreviated Baseline CPT is performed, as well as an RF radiation test using the flight antennas, and a phasing test to demonstrate proper phasing without extender cables. This is the first time the spacecraft is in a flight-like electrical and mechanical configuration.

Radiated emissions and radiated susceptibility tests are then performed, as well as a self-compatibility test. This is followed by an alignment verification to establish pre–environmental alignment data. Thermal blankets (including the thermal shroud) and environmental test instrumentation are installed after the spacecraft is stacked.

The spacecraft is then transported to the Environmental Test Lab (ETL), where acoustics tests and pyro-shock tests are performed. The pyro-shock test also verifies the LV separation mechanical interfaces.

The spacecraft is then moved to the 25-foot Space Simulator, where a baseline test is performed to verify configuration and performance prior to starting solar thermal-vacuum (STV) tests. The STV test is primarily a verification of worst-case hot and cold performance, as well as selected thermal balance conditions. Additional tests (such as science instrument modes that require vacuum conditions) are performed during thermal transitions, if they are not otherwise required for the worst-case thermal tests that verify margins required by

JPL Design Principles and Flight Project Practices (JPL 2010a, b).

After STV test, the spacecraft is transported back to the Spacecraft Assembly Facility (SAF), where post–environmental alignment verifications are performed, followed by de-stacking to a system test configuration. The Engineering and Science CPT is repeated for post–environmental performance verification. Launch sequence tests, trajectory correction maneuver tests, countdown and scrub/recycle tests, and engineering and science performance tests are performed prior to shipment to KSC. Two months of schedule margin are included at this point to protect the ship date and KSC operations. Shipment to KSC is performed at the module level because of the large size of the stacked spacecraft and to permit access to direct access signals for the final comprehensive performance testing at KSC.

After arrival at the KSC Payload Hazardous Servicing Facility (PHSF), the spacecraft modules, interconnected with extender cables, are put through a System Test Configuration Baseline CPT to reestablish the health of all spacecraft systems. Spacecraft stacking is then performed, followed by a DSN Compatibility Test with MIL-71, alignment re-verification, and a final Phasing Test using the launch version of flight software. A Launch Configuration Baseline Test is performed, followed by a Launch Sequence Test from prelaunch through early cruise. Flight pyrotechnic devices (excluding those for spacecraft separation) are installed. A dry-run installation of the flight ASRG(s) is performed as well. After the flight ASRG(s) are removed and secured, the spacecraft is transported to the KSC Operations and Checkout (O&C) facility for dry heat microbial reduction (DHMR). ASRG fueling is performed during this time in a separate facility. The descriptions of operations with the ASRG assume that they can be handled in similar fashion to the MMRTG used on Mars Science Laboratory (MSL). These operations will be

refined as the ASRG requirements and development proceed.

At the O&C the spacecraft is installed in an existing thermal chamber in the O&C high bay. Vacuum bakeout of the spacecraft is performed, followed by backfill to an appropriate convective atmospheric environment for heating (either nitrogen or filtered air at the preference of the Planetary Protection Engineer). Spacecraft temperatures are elevated and verified, at which point the DHMR operation is conducted. Because of uncertainty in the durations of each of these operations, five days of schedule margin are allocated at this point. Over one month of schedule is allocated to the end-to-end DHMR operation. The spacecraft is then transported back to the PHSF. Conservative planetary protection handling is planned beyond this point, consistent with a spacecraft that could impact Europa.

At the PHSF, a baseline test is performed to confirm the status of all spacecraft systems after DHMR. Since the ASRG(s) would not be present, the spacecraft will be powered by ground support equipment power supplies. Final spacecraft closeouts and walk-down inspections are performed, followed by propellant and pressurant loading of the Propulsion Module. Three weeks of schedule margin are included at this point to protect the date of delivery to the LV for integrated operations.

At this point, the spacecraft is ready for integrated operations with the LV, including mating to the flight LVA, encapsulation with the fairing, transport to the launch pad, and fueled ASRG installation for flight, countdown, and launch.

Durations for most of the spacecraft test operations (including setup, reconfiguration, preps, and transportation) are based on actual "as-executed" durations from Cassini. Cassini was used as a reference because its ATLO plan was executed without any holiday work, or any work on a holiday weekend, minimal Saturday work, and a nominal five-day-per-week, single-shift operation. Integrated operations with the LV are based on actuals from MSL, which had similar operations with the same/similar LV and integration of an MMRTG. These estimates have been informed by MSL complications of MMRTG installation inside the MSL aeroshell and implementation of required cooling systems. Cooling may not be required for the Europa Multiple-Flyby Mission, given the characteristics of ASRGs.

The ATLO flow described above has not been optimized to incorporate opportunities for parallel operations, except in the case of preparations for environmental testing, where such operations are customary. The flow described also includes the 20% schedule margin at JPL, and one day per week schedule margin at KSC, as required by the JPL Design Principles (JPL 2010a).

C.2.5   Mission Operations Concepts

Repetitive activities, centralized operations and focus on Europa science enables realization of efficient, low-cost operations.

Europa and its vicinity pose a challenging and hazardous environment for operating any science mission. Based on the cost-reduction mandate from the decadal survey for 2013–2022 (Space Studies Board 2011), and hand-in-hand with the design of the Europa Multiple-Flyby Mission and spacecraft, the operations strategies described herein have been developed principally to achieve the intended Europa science described in Section C.1 at the lowest feasible cost, yet while minimizing mission risk in this environment. Therefore, the central guiding theme of Europa Multiple-Flyby Mission operations has been to deliver the spacecraft to Europa safe and fully capable of conducting science observations, consisting of remote and in situ measurements that can be accomplished best via multiple flybys.

Europa science is the driver of mission architecture. No tangential activities have been allowed to drive the design of the operations systems and concepts. All design decisions—

be they for the spacecraft or operations—are studied, often with the applications of models and/or scenarios, to measure the cost, performance, and risk across all phases of the project, including operations.

Operations development has drawn much wisdom from the many NASA-wide studies of Europa exploration from as early as 1997. In addition, two key studies in 2008 were conducted to capture relevant operations lessons learned from past and present missions, incorporating members from JPL, APL, and NASA Ames (Paczkowski et al. 2008, Lock 2008). These studies focused in particular on flight and ground system capabilities needed to simplify science operations, on early integrated development of flight and ground concepts to ensure appropriate implementation, and on postlaunch activities and development to ensure practiced functional capabilities and simplified operations. All of these operations assessments, from the many studies and from scenario work of highly experienced engineers, emphasize early consideration of operability issues in the system architecture and design. All system trades (spacecraft, operations, science, etc.) are treated as collective mission trades to work toward the best cost/risk for the overall mission, rather than optimizing a single element and unknowingly adding significant cost/risk to another.

C.2.5.1   Operations Concept—Science Phase

The Europa Multiple-Flyby Mission science phase described in Section C.2.3 begins after the pumpdown phase of the in-orbit trajectory and is achieved via 34 flybys of Europa, spaced over 18 months of Jupiter orbit. These occur over a total of 55 orbits at flyby spacings that vary typically from 11 to 25 days (there is also one 7-day encounter-to-encounter leg). Each flyby has a unique geometry, and the altitudes do vary across the mission; however, simple, repeated observations flowing from one conceptual design are capable of delivering all of the science goals. The Europa en-
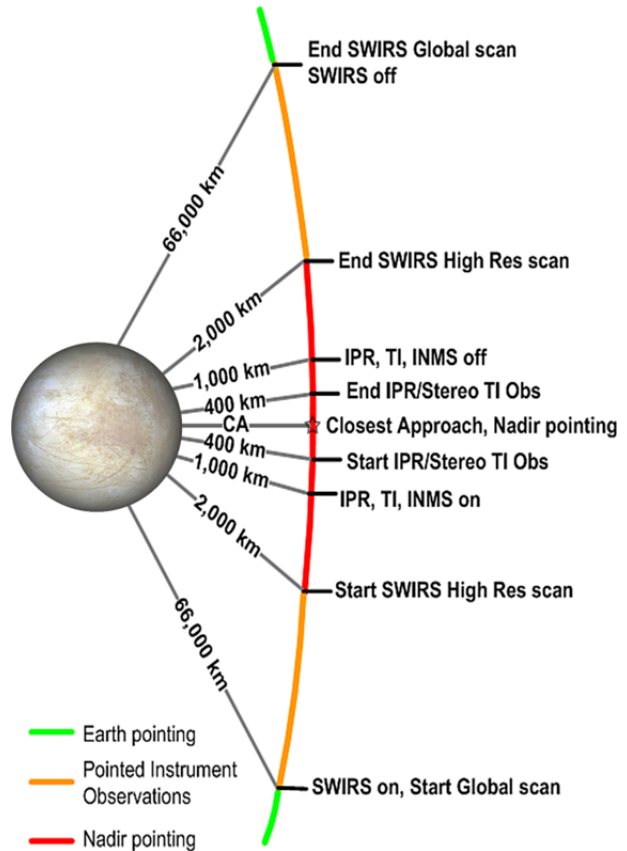
Figure C.2.5-1. Europa encounter concept—Multiple-Flyby Mission.

counter template (i.e., one conceptual design for all encounters) is shown in Figure C.2.5-1. This sequence of activities is described in Section C.2.1.

Operating durations for the various instruments are shown in Table C.2.5-1.

Away from the science flybys, orbit operations are shown in a rudimentary fashion in Fig-

Table C.2.5-1. Instrument on times per flyby.

Altitude Range (km)	Time at Altitude (minutes)	Instrument On Time (minutes)			
		IPR	TI	SWIRS	INMS
66,000 to 2,000	265			265	
2,000 to 1,000	5			5	
1,000 to 400	4	4	4	4	4
400 to CA	4	4	4	4	4
CA to 400	4	4	4	4	4
400 to 1,000	4	4	4	4	4
1,000 to 2,000	5			5	
2,000 to 6,000	265			265	
Total Minutes	554	15	15	554	15
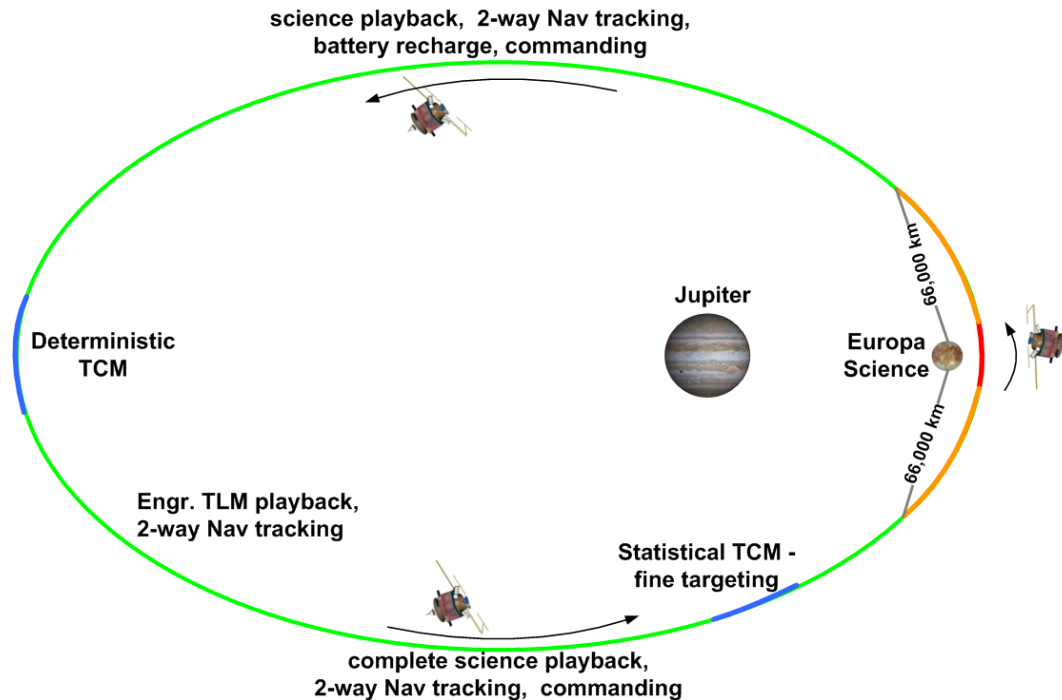
Figure C.2.5-2. Orbit concept—Multiple-Flyby Mission (not to scale).

ure C.2.5-2. The flyby concept permits a store-and-forward data-return strategy via at least daily DSN passes between science operations, and it also exploits battery use for short intervals with ample time for recharging between science operations. In addition, because science observations and data collection occur at different time, instruments can be fixed on the spacecraft body. During the downlink and re-charging interval, the spacecraft is Earth-pointed (except for trajectory correction maneuvers), with science playback, engineering telemetry, and two-way navigation during DSN passes scheduled at least daily. The data balance described in Section C.2.4.7 allows for reasonable DSN tracking and healthy data volume margin in returning each encounter's science observations.

This data collection and pointing profile is quite similar in nature for each flyby. Mainly, the geometry and timing change. Therefore, given nominal operation, these observations can be laid down algorithmically with the same approach for each encounter. No negotiation for resources or case-by-case optimiza-

tion is necessary. Simple, repeated operations are sufficient to accomplish this. The instruments are on during each science flyby, and off otherwise. All flybys follow a single science profile of activities. There is no optimization per flyby, and the sharing of pointing is clearly defined and needs no negotiations. Maneuvers occur every few days; and other than maneuvers and encounters, activity intensity is low, with continuous, simply sequenced background activities.

The Europa Multiple-Flyby Mission design concept, along with the groundtrack geometry, has been described in Section C.2.3. Combined with the operations approach described above, the instrument coverage of Europa's surface that can be achieved as shown in Figures C.2.5-3 through C.2.5-6. These coverage profiles meet the science goals described in Section C.1. Each figure is shown as an equirectangular projection of Europa's surface. The center of the figure (longitude 180°) is anti-Jovian, whereas the edges (longitude 0/360°) are sub-Jovian. Europa's north pole is at the top.
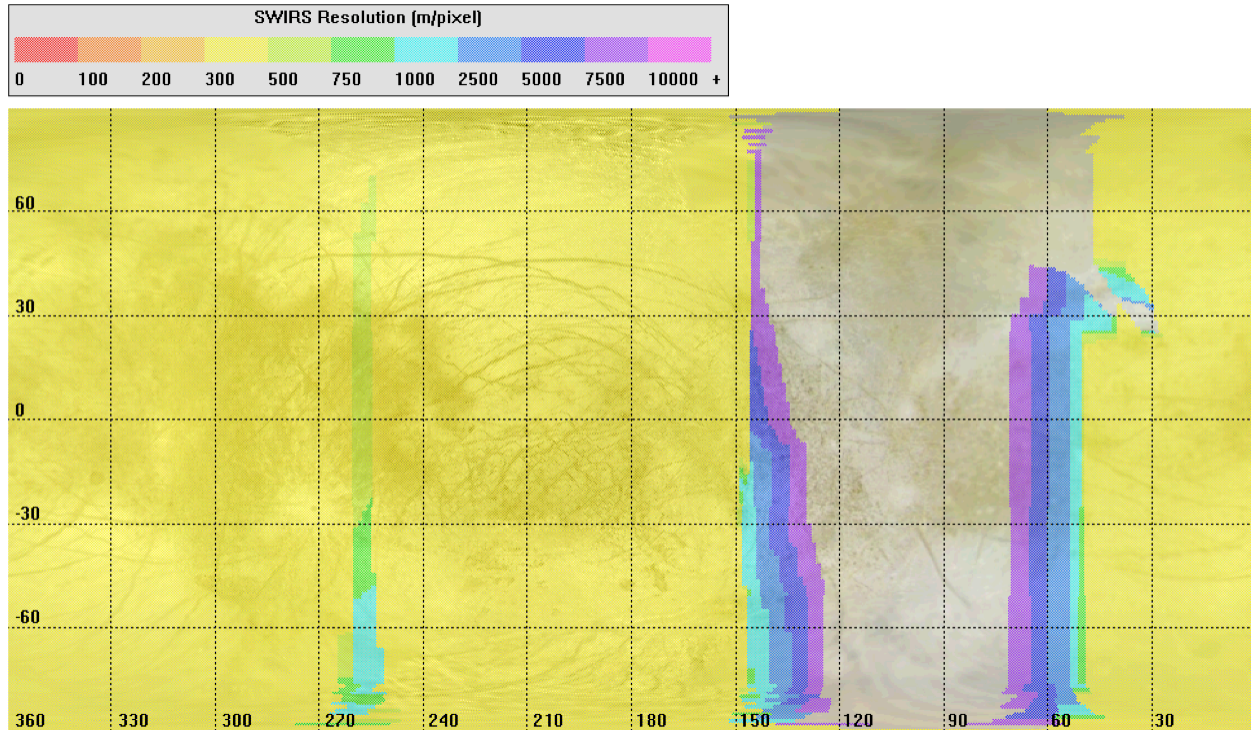
Figure C.2.5-3. SWIRS low-resolution coverage (66,000 km to 2,000 km altitude).
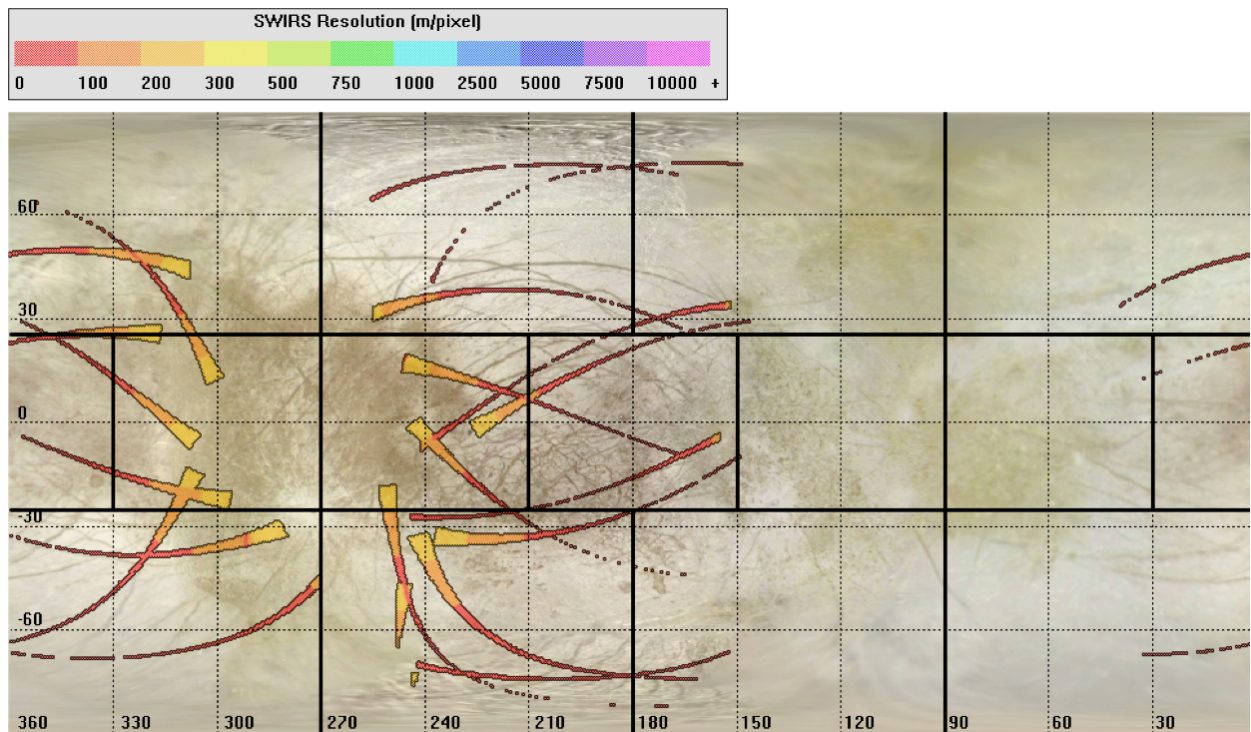
Figure C.2.5-4. SWIRS high-resolution coverage (under 2,000 km altitude).
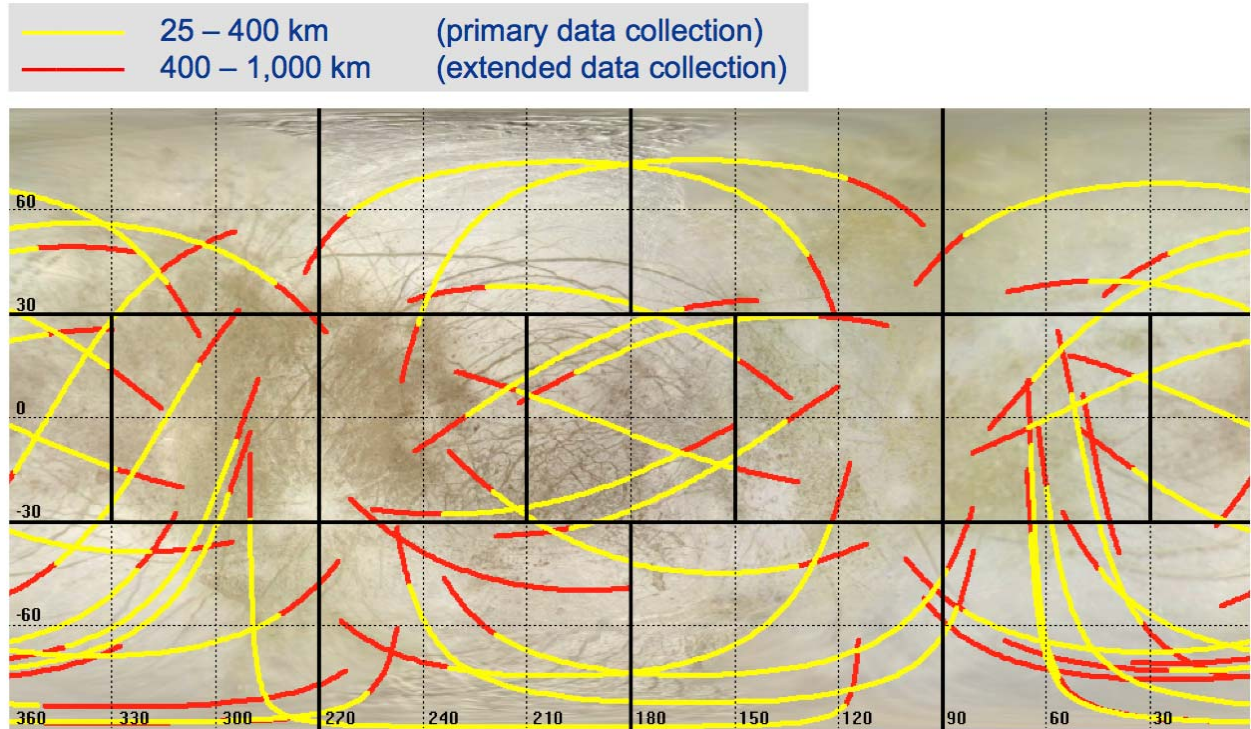
Figure C.2.5-5. IPR ground coverage.
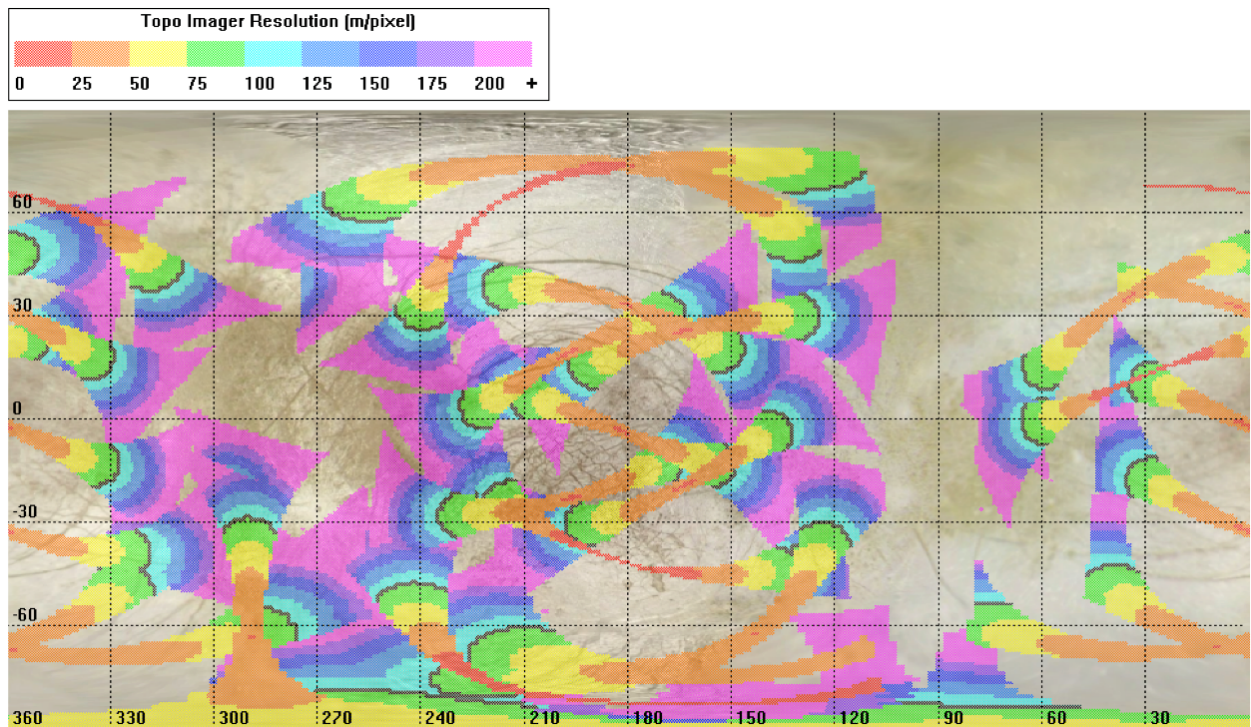
Figure C.2.5-6. TI instrument coverage.

C.2.5.2 Interplanetary and Jupiter Cruise

After launch, mission focus is on the checkout, characterization, and deployment of all flight systems. In the first few weeks of cruise, DSN coverage is nearly continuous, driven to some extent by real-time commanding for schedule flexibility. Once postlaunch configuration and checkouts are complete, the mission transitions to interplanetary cruise.

Interplanetary cruise is quiescent, save for elevated activity required for gravity assists and maneuvers. The spacecraft is minimally operated, with basic telemetry expected only once per week; however, 24-hour coverage is expected around maneuvers, and daily to continuous tracking is expected prior to gravity assists, particularly for nuclear safety prior to gravity assists involving Earth. In between gravity assists, the project focuses efforts on development and improvement of operations processes and tools for Europa encounters, as well as science team meetings to refine the Europa template of operations. After JOI, instrument characterization and checkout resume, and operations readiness tests (ORTs) and instrument calibrations are conducted prior to the first Europa encounter.

C.2.5.3 Development Supporting Europa Operations

As mentioned at the beginning of Section C.2.5, early consideration of operability issues in the system architecture and design is of great importance. The Europa Multiple-Flyby Mission plans significant operations scenario development during Phases A-D. Science operations will be a strong element of the prelaunch flight systems engineering. Science operations scenarios will be developed early and at a level of detail that permits flight system design choices to be assessed thoroughly. Operations and ground system architecture, requirements, models, and software will be developed to a level sufficient to support prelaunch development and flight system trade studies. Science planning tools will be devel-

oped such that they can be used to evaluate the ground and flight system requirements and capabilities. Based on these preparations, refinements can then be made much more confidently in cruise and throughout the mission to this unified ground and flight system architecture and its software requirements.

Modeling will be conducted to simulate representative operations in deep space, including Europa flyby operations. The ATLO phase includes testing of at least one representative operational sequence to be used during Europa encounters. These efforts, though they add early cost, should bring net savings to the project over all life cycle phases because they make possible more efficient operations, and uncover problems at a time when something can be done to mitigate them.

Opportunities for process improvement are built into the schedule after launch. A long cruise period presents some challenges, among them the risks of personnel attrition and ground system obsolescence. However, the varying level of intensity—lower between gravity assists, for example—also offers opportunities to improve processes, software, IT infrastructure, and operations concepts and the science template for Europa observations. A Europa Flyby Mission project would aim to fill the "bathtubs" between major events in cruise with periods of further development and training. The project would strategically defer some operations development until after launch. Doing so has several advantages. First, it obviates the need to staff the project up for major cruise events and down afterwards. Second, it allows the project to take advantage of improvements in technology as they become available and to work with a flight team more likely to be present during later operations than is the flight team in place at launch. Third, it affords the flight team opportunities to contribute to the design of the operations system, improving staff skill and possibly retention as team members choose to remain with the project in part to see their efforts bear fruit in Jupiter orbit. Finally, it ensures that the

operations team on the line during orbital operations is deeply familiar with the system, such that disruptions from faults or radiation issues can be handled in an expeditious, reliable, and expert manner.

Staffing levels should remain at approximately the late Phase D workforce level through launch and initial checkouts, after which it can drop to a more sustainable cruise staffing level. Cruise staffing should be relatively flat thereafter, with a moderate increase in development staff in the later portion of interplanetary cruise. Because the navigation team must be fully capable for JOI, they would staff up to Jupiter cruise/Europa flyby levels no later than six months before JOI. Spacecraft system and subsystem support needed to support navigation and maneuvering would also be added at this time. Other operations teams would staff up at around JOI to test final processes, the science template, and software, with the first ORTs for Europa beginning 1 to 2 months thereafter.

C.2.6   Systems Engineering

Through key investments in infrastructure, engineering products, and team-building, the Europa Study Team is well positioned to move into pre-project formulation.

This section outlines the overall systems engineering approach and plan. The subsections that follow address three specific systems engineering challenges: radiation, planetary protection, and nuclear safety.

In general the Europa Multiple-Flyby Mission can be said to have the following technical and programmatic characteristics:

- Technical:
  – Functioning in the presence of radiation flux, SEEs, radiation damage to parts and materials
  – Satisfying planetary protection of the Europan ocean, as well as of Ganymede and Callisto, from delivered bioburden
  – Lifetime and reliability over a long mission

  – Maintaining conservative resource margins
  – Integrating a suite of competitively selected science instruments from a diverse field of providers
  – Integrating radioisotope power sources
  – Contrasting thermal environments at Venus flyby and Jupiter
  – Critical orbit insertion at Jupiter
  – Intense science operations schedule at Europa after years of unhurried cruise
  – Keeping a 10-year-plus "corporate memory" of the requirements, detailed design, and the rationales for design choices
- Programmatic:
  – Succeeding in a cost- and cost-profile-constrained environment
  – Coordinating the efforts of a large, diverse engineering team
  – Integrated the project and design with competitively selected instruments
  – Accommodating development and maturation issues of the radioisotope power sources
  – Multi-institution and potential multinational partnerships (JPL, APL, PIs)

To help address these concerns, the following overarching systems engineering objectives have been set for formulation:

- By System Requirements Review (SRR), produce a Baseline System Specification (L1-L3 Baseline; L4 Preliminary; L5 Key and Driving), a committed systems engineering schedule and cost profile, and a committed mission architecture.
- By Preliminary Design Review (PDR), produce a released set of procurement specifications, a fully developed preliminary design, and a committed project schedule and cost.

Institutional project and line management is uniformly committed to making major strides in systems engineering, supporting and enforcing the following approach:

- Exercise rigorous engineering discipline. Expect engineering rationale to be documented as complete and logical chains of thought, and in appropriate tools (Mathematica/Maple not Power-Point; IOMs not emails)
- Make use of emerging new systems engineering capabilities as appropriate, including system modeling language standards and tooling, model integration and exchange standards and tooling, and Web-based report generation.
- Starting from the beginning, build persistent and evolvable artifacts.
- Starting from the beginning, build a core team of systems engineers who can faithfully promulgate the architecture later as the project grows.
- Proactively align with forthcoming NPR 7120.5E (NASA 2012).
- Emphasize architecture and design space exploration through MCR. An architectural approach keeps the team properly focused on the "why," and design space keeps us properly focused on the concept rather than a point design. In this endeavor, trusted models and analytical tools are essential investments.
- Make decisions by a process that is explicitly guided by Architecture, is timely and responsive, is transparent to all stakeholders, and includes balanced consideration of multiple experienced viewpoints.

The Europa Multiple-Flyby Mission is well positioned to move into preproject formulation. The Europa Study Team has made key investments in infrastructure, engineering artifacts, and team-building, as described below:

- Infrastructure has been under development for the long term. Already set up and in initial use are a collaborative Systems Modeling Language (SysML) environment (MagicDraw/Teamwork Server), a collaborative architecture development environment (Architecture Framework Tool), the project document repository (DocuShare), and the project workflow management system (JIRA).
- Key plans and processes are in place. Key parts of the architecture description are in preliminary form, as outlined in this report. The core of a system model is established.
- Our team processes and practices are maturing. Cost estimates, some technical margin estimates, and mechanical configuration changes have been improved over past practice.

From this strong starting point, a plan that achieves robust maturity at SRR and PDR has been constructed. The sketch of this plan, expressed as key artifacts per life-cycle phase through PDR, is shown in tables C.2.6-1 through C.2.6-4. In these tables the changes from one table to the next are shown in **bold blue font**, and the parentheticals following the artifact names denote required maturity levels:

(A):   Approach is defined, and possibly a sketch of the artifact.
(K&D):   Key and Driving cases are identified and covered.
(P):   Preliminary. A full version for review and discussion leading to a baseline version.
(B):   Baseline. The artifact is under configuration control.
(U):   Update.

After PDR, systems engineering focus changes from development to implementation: managing the change-control process while maintaining architectural integrity, implementing I&T and V&V programs, and preparing for flight operations.

Table C.2.6-1. Present maturity of systems engineering artifacts.

At Tech Review	Systems Engineering Plan: Key Artifacts per Life-Cycle Phase Artifact Type						
	Plan	Scenario	Model	Analysis & Sim	Report	Spec	
Program (L1)						L1 Rqmts (K&D)	
Project (L2)	Arch Dev Plan (P) SEMP (A) Model Mgt Plan (A)	Driving Mission (K&D)	Trajectory (P) Science Margin (A) Data Margin (P) FS Radiation (P)	Delta-V/Prop (P) Science Margin (A) Data Margin (P) FS Radiation Life (P)	Concept Report (P) Msn Arch Descr (P) Ops Concept (A) Tech Assessment (A) Eng Dev Assess (A) Top Risks (A)	L2 Rqmts (A) Env Definition (A)	
System (L3)		Flight Sys Ops (K&D)	FS Functional (P) FS Physical (P) FS Shielding (P) FS Power (P) FS Static Mech (P) FS Thermal (P) FS Telecom Link (P) FS Attitude Ctrl (P)	FS Mass Margin (P) FS Shield Mass (P) FS Pwr Margin (P) FS Mass Props (P) FS Therm Balance (P) FS Link Margin (P) FS Pntg Margin (P)		L3 Rqmts (A)	
Subsystem (L4)			Power (K&D) Thermal (K&D) Propulsion (K&D) Telecom (K&D) Avionics (K&D) Structure (K&D)	Power Bus Sim (P) Therm Balance (P) JOI Perf (A) EIRP, G/T (P) C&DH Throughput (A) LV Static Envel (P)			
Component (L5)			Radiation Effects (P) DHMR Effects (P)	Component Life (P) Parts/Matl Issues (P)	Approved Parts (A) Approved Matls (A)		

Left margin label: **SCOPE**

Right margin legend (bottom to top): (A) Approach   (K&D) Key & Driving   (P) Preliminary   (B) Baseline   (U) Update   **Blue = Change**

Table C.2.6-2. Maturity of systems engineering artifacts at MCR.

At MCR (SCOPE)	Systems Engineering Plan: Key Artifacts per Life-Cycle Phase — Artifact Type					
	Plan	**Scenario**	**Model**	**Analysis & Sim**	**Report**	**Spec**
Program (L1)						L1 Rqmts **(P)**
Project (L2)	Arch Dev Plan **(B)** SEMP **(P)** Model Mgt Plan **(P)** **Integr Plan (A)** **V&V Plan (A)**	Driving Mission **(P)**	Trajectory **(B)** Science Margin **(B)** Data Margin **(B)** FS Radiation **(B)**	Delta-V/Prop (P) Science Margin **(P)** Data Margin (P) FS Radiation Life (P) **Rqmt Traceability (P)**	Concept Report **(B)** Msn Arch Descr (P) Ops Concept **(P)** Tech Assessment **(P)** Eng Dev Assess **(P)** Top Risks **(P)**	L2 Rqmts **(P)** Env Definition **(P)** **External ICDs (K&D)** **Intersystem ICDs (K&D)** **S/C–P/L ICD (K&D)**
System (L3)		Flight Sys Ops **(P)**	FS Functional (P) FS Physical (P) FS Shielding (P) FS Power (P) FS Static Mech (P) FS Thermal (P) FS Telecom Link (P) FS Attitude Ctrl (P) **FS Behavior (P)** **FS Fault Contnmt (P)**	FS Mass Margin (P) FS Shield Mass (P) FS Pwr Margin (P) FS Mass Props (P) FS Therm Balance (P) FS Link Margin (P) FS Pntg Margin (P)		L3 Rqmts **(K&D)** **Intra-FS ICDs (K&D)**
Subsystem (L4)			Power **(P)** Thermal **(P)** Propulsion **(P)** Telecom **(P)** Avionics **(P)** Structure **(P)**	Power Bus Sim (P) Therm Balance (P) JOI Perf **(P)** EIRP, G/T (P) C&DH Throughput **(P)** LV Static Envel (P)		
Component (L5)			Radiation Effects (P) DHMR Effects (P)	Component Life (P) Parts/Matl Issues (P)	Approved Parts **(P)** Approved Matls **(P)**	

Legend (right margin): **Blue = Change**, (U) Update, (B) Baseline, (P) Preliminary, (K&D) Key & Driving, (A) Approach

Table C.2.6-3. Maturity of systems engineering artifacts at SRR.

At SRR	Systems Engineering Plan: Key Artifacts per Life-Cycle Phase Artifact Type						
	Plan	Scenario	Model	Analysis & Sim	Report	Spec	
Program (L1)						L1 Rqmts (B)	
Project (L2)	Arch Dev Plan (U) SEMP (B) Model Mgt Plan (B) Integr Plan (P) V&V Plan (P) **S/W Mgt Plan (P)**	**Mission Plan (K&D)**	Trajectory (U) Science Margin (U) Data Margin (U) FS Radiation (U)	Delta-V/Prop (B) Science Margin (B) Data Margin (B) FS Radiation Life (B) Rqmt Traceability (B)	Concept Report (U) Msn Arch Descr (B) Ops Concept (B) Tech Assessment (B) Eng Dev Assess (B) Top Risks (B) **Instrument AO PIP (B)**	L2 Rqmts (B) Env Definition (B) External ICDs (B) Intersystem ICDs (P) S/C-P/L ICD (P)	
System (L3)		Flight Sys Ops (B)	FS Functional (B) FS Physical (B) FS Shielding (B) FS Power (B) FS Static Mech (B) FS Thermal (B) FS Telecom Link (B) FS Attitude Ctrl (B) FS Behavior (B) FS Fault Contnmt (B)	FS Mass Margin (P) FS Shield Mass (P) FS Pwr Margin (P) FS Mass Props (P) FS Therm Balance (P) FS Link Margin (P) FS Pntg Margin (P) **FS PRA (A)** **FS Func FMECA (A)** **FS TAYF Exceptions (A)**	**Ground Sys Arch (P)** **Payload Arch (P)**	L3 Rqmts (B) Intra-FS ICDs (P) **Procurement Specs (P)**	
Subsystem (L4)			Power (B) Thermal (B) Propulsion (B) Telecom (B) Avionics (B) Structures (B)	Power Bus Sim (P) Therm Balance (P) JOI Perf (P) EIRP, G/T (P) C&DH Throughput (P) LV Static Envel (P)		**L4 Rqmts (P)** **Intrasubsystem ICDs (P)**	
Component (L5)			Radiation Effects (B) DHMR Effects (B)	Component Life (P) Parts/Matl Issues (P)	Approved Parts (P) Approved Matls (P)		

Left axis: SCOPE
Right axis: Blue = Change (U) Update (B) Baseline (P) Preliminary (K&D) Key & Driving (A) Approach

Table C.2.6-4. Maturity of systems engineering artifacts at PDR.

At PDR (SCOPE)	Systems Engineering Plan: Key Artifacts per Life-Cycle Phase — Artifact Type						Legend
	Plan	Scenario	Model	Analysis & Sim	Report	Spec	
Program (L1)						L1 Rqmts (B)	**Blue = Change**
Project (L2)	Arch Dev Plan (B) SEMP **(U)** Model Mgt Plan **(U)** Integr Plan **(B)** V&V Plan **(B)** S/W Mgt Plan **(B)**	Mission Plan **(P)**	Trajectory (U) Science Margin (U) Data Margin (U) FS Radiation (U)	Delta-V/Prop **(U)** Science Margin **(U)** Data Margin **(U)** FS Radiation Life **(U)** Rqmt Traceability **(U)** **Mission Fault Tree (P)**	Concept Report (U) Msn Arch Descr **(U)** Ops Concept **(U)** Tech Assessment **(U)** Eng Dev Assess **(U)** Top Risks **(U)** Instrument AO PIP (B)	L2 Rqmts (B) Env Definition (B) External ICDs (B) Intersystem ICDs **(B)** S/C–P/L ICD **(B)**	(U) Update
System (L3)		Flight Sys Ops **(U)**	FS Functional (B) FS Physical (B) FS Shielding (B) FS Power (B) FS Static Mech (B) FS Thermal (B) FS Telecom Link (B) FS Attitude Ctrl (B) FS Behavior (B) FS Fault Contnmt (B)	FS Mass Margin **(B)** FS Shield Mass **(B)** FS Pwr Margin **(B)** FS Mass Props **(B)** FS Therm Balance **(B)** FS Link Margin **(B)** FS Pntg Margin **(B)** FS PRA **(P)** FS Func FMECA **(P)** FS TAYF Exceptions **(P)**	Ground Sys Arch **(B)** Payload Arch **(B)**	L3 Rqmts **(B)** Intra-FS ICDs **(B)** Procurement Specs **(B)**	(B) Baseline
Subsystem (L4)			Power (B) Thermal (B) Propulsion (B) Telecom (B) Avionics (B) Structures (B)	Power Bus Sim **(B)** Therm Balance **(B)** JOI Perf **(B)** EIRP, G/T **(B)** C&DH Throughput **(B)** LV Static Envel **(B)**	**Subsys Des Desc (P)** **P/L Design Desc (P)**	L4 Rqmts **(B)** Intrasubsystem ICDs **(B)**	(P) Preliminary
Component (L5)			Radiation Effects (B) DHMR Effects (B)	Component Life **(B)** Parts/Mat Issues **(B)**	Approved Parts **(B)** Approved Matls **(B)**	**L5 Rqmts (P)**	(K&D) Key & Driving (A) Approach

C.2.6.1   Radiation

The effects of radiation on the spacecraft are mitigated by the efficient use of inherent shielding provided by the spacecraft itself and additional dedicated shield mass, combined with radiation-tolerant materials and electronics.

The Europa Multiple-Flyby Mission spacecraft would be exposed to both naturally occurring and self-generated radiation from launch to the end of the mission. The self-generated radiation, composed of neutrons and gamma rays, is produced from the Advanced Stirling Radioisotope Generators (ASRGs). The naturally occurring radiation encountered during the cruise phase between launch and Jupiter Orbit Insertion (JOI) consists of solar flare protons. Between JOI and the end of the mission, the spacecraft is exposed to protons, electrons, and heavy ions trapped in the Jovian magnetosphere. In addition, there is a background of galactic cosmic rays throughout the entire mission.

The radiation encountered during the mission can affect onboard electronics, thermal control materials, surface coatings, and other nonmetallic items by depositing energy that can disrupt the properties of these materials. Cumulative damage in electronics can through ionization, called total ionizing dose (TID), or displacement of atoms in the crystalline lattice, called displacement damage dose (DDD). The expected accumulated TID from launch to end of mission as a function of effective aluminum shielding thickness is shown in Table C.2.6-5.

Radiation can also cause noise in science instrument and star-tracker detectors due to the intense proton and electron flux encountered in the Jovian system. Peak electron and proton fluxes for the mission are shown in Table C.2.6-6.

The selection of electronic parts with respect to their radiation tolerance and reliability in the Europa radiation environment will be achieved through a combination testing and analysis. The minimum acceptable total ioniz-

Table C.2.6-5. Expected Flyby Mission accumulated total ionizing dose as a function of shield thickness.

Aluminum Thickness (mil)	Total Ionizing Dose (krad Si)				
	Electron	Photon	Proton	ASRG	Total
100	1960	7.0	46.6	1.3	2010
200	893	7.9	10.9	1.3	913
400	341	8.9	1.9	1.3	353
600	178	9.5	0.8	1.3	189
800	107	9.9	0.5	1.3	118
1000	70.5	10.0	0.4	1.3	81.1
1200	48.9	10.0	0.3	1.3	60.4
1400	35.2	9.8	0.2	1.3	46.5
1600	25.9	9.6	0.2	1.3	37.0

ing dose hardness of electronic devices will be 100 kilorad. The minimum single-event-effects (SEE) hardness will be documented in a Parts Program Requirements (PPR) document. A combination of radiation testing (TID, DDD, and SEE) of electronic devices and buying vendor guaranteed radiation hardened parts that meet the minimum TID and SEE requirements will ensure that robust electronics will be used in spacecraft and instrument electronics. Radiation testing will be done at industry-standard high-dose-rates and at low-dose-rate for electronic devices types that are susceptible to Enhanced Low Dose Rate Sensitivity (ELDRS) effects (primarily bipolar devices). Electronic part parameter degradation observed during radiation testing will be documented and used as input into the spacecraft and instrument electronics end of mission worst-case analysis (WCA). Electronic devices that do not meet the minimum TID and SEU hardness requirements will not be used within the spacecraft electronics or instruments unless approved by a requirements waiver.

The guidelines for selecting nonmetallic mate-

Table C.2.6-6. Expected Flyby Mission peak electron and proton flux.

Particle Energy (MeV)	Flux (#>Energy cm^{-2} sec^{-1})	
	Electron	Proton
10	1.7 E6	1.5 E5
20	4.8 E5	3.2 E4
30	2.2 E5	8.7 E3
50	7.9 E4	8.6 E2
100	1.8 E4	2.0 E1

rials for radiation susceptibility and reliability have been documented by Willis (2011). Detailed evaluations will be performed for these materials after exposure to end-of-mission radiation environment to ensure end of life performance requirements are met. Radiation testing will be performed for materials which do not have available radiation data.

The Europa Multiple-Flyby mission will develop an Approved Parts and Materials List (APML) for the purpose of identifying standard parts approved for flight equipment developed under the project's cognizance. The APML will be populated with EEE parts and materials, as well as many critical parts such as sensors, detectors, power converters, FPGAs, and non-volatile memories. Each entry will be accompanied with a Worst Case Datasheet (WCD) and application notes describing proper use of the part at selected radiation levels. Dissemination of this information early in the design process is critical to enable the spacecraft electronics and instrument providers to adequately design for the radiation environment.

Every approved part listed on the APML will meet the reliability, quality, and radiation requirements specified in the PPR. The APML will be updated as new radiation data become available. Parts not listed as approved on the APML are defined as non-standard parts and will require a Nonstandard Parts Approval Request (NSPAR) for use in the Europa Multiple-Flyby mission. All non-standard parts will be reviewed, screened, and qualified to the requirements of PPR.

Every part on the APML will be approved by the Parts Control Board (PCB). The PCB recommends and approves parts for inclusion in the APML. Criteria will be based on absolute need, the number of subsystems requiring the part, qualification status, TID, Single Event Effects (SEE), and procurement specification review. Mission designers should use standard parts to the maximum extent possible so that

they can reduce the radiation testing and qualification expenditure to the minimum.

Radiation-induced effects on instrument detectors and other key instrument components ultimately impact the quality and quantity of the mission science return and the reliability of engineering sensor data critical to flight operations. High-energy particles found within the Europa environment will produce increased transient detector noise as well as long-term degradation of detector performance and even potential failure of the device. Transient radiation effects are produced when an ionizing particle traverses the active detector volume and creates charges that are clocked out during readout. Radiation-induced noise can potentially swamp the science signal, especially in the infrared wavebands where low solar flux and low surface reflectivity result in a relative low signal. Both TID and DDD effects produce long-term permanent degradation in detector performance characteristics. This includes a decrease in the ability of the detector to generate signal charge or to transfer that charge from the photo active region to the readout circuitry; shifts in gate threshold voltages; increases in dark current and dark current non-uniformities, and the production of high-dark-current pixels (hot pixels or spikes). It is important to identify and understand both the transient and permanent performance degradation effects in order to plan early for appropriate hardware and operations risk mitigation to insure mission success and high-quality science returns.

A JEO Detector Working Group (DWG) was formed in FY08 to evaluate the detector and laser components required by the planning payload and stellar reference unit. The DWG participants included experienced instrument, detector, and radiation environment experts from APL and JPL. For each technology required for the payload, the DWG (i) reviewed the available radiation literature and test results, (ii) estimated the radiation environment incident on the component behind its shield,

and (iii) assessed the total dose survivability (both TID and DDD) and radiation-induced transient noise effects during peak flux periods. The assessment included the following technologies: visible detectors, mid-infrared and thermal detectors, micro-channel plates and photomultipliers, avalanche photodiodes, and laser-related components (pump diode laser, solid-state laser, fiber optics).

The DWG assessment, reported in Boldt (2008), concluded that the radiation challenges facing the JEO notional payload and SRU detectors and laser components are well understood. With the recommended shielding allocations, the total dose survivability of these components is not considered to be a significant risk. In many cases, the shielding allocation was driven by the need to reduce radiation-induced transient noise effects in order to meet science and engineering performance requirements. For these technologies—notably mid-infrared detectors, avalanche photodiode detectors, and visible detectors for star-tracking—the extensive shielding (up to 3-cm-thick Ta) for transient noise reduction effectively mitigates all concern over total dose degradation. For the remaining technologies, more modest shielding thicknesses (0.3–1.0 cm Ta, depending upon the specific technology) were judged to be sufficient to reduce the total dose exposure and transient noise impact to levels that could be further reduced with known mitigation techniques (detector design, detector operational parameters, algorithmic approaches and system-level mitigations). The DWG conclusions reached for the JEO are applicable for the science detectors and the SRU onboard the Europa Multiple-Flyby mission.

A rigorous "test-as-you-fly" policy with respect to detector radiation testing, including irradiation with flight-representative species and energies for TID, DDD, and transient testing, will be adopted for the Europa Multiple-Flyby mission.

The Jovian electron environment also causes dielectric materials and ungrounded metals to collect charge, both on spacecraft external surfaces and within the spacecraft. This can cause damaging or disruptive transient voltages and currents in the spacecraft when an electrostatic discharge (ESD) event occurs.

Surface charging effects are mitigated by limiting the differential charging of external materials. This is accomplished by using materials that have surface coatings and treatments that allow the accumulated charges to bleed to spacecraft ground. A significant number of such surface materials have been used extensively in severe charging environments for spacecraft with long lifetimes (typically geo-synchronous communications spacecraft, but also Juno, GLL, and others) and are usable for the Europa Multiple-Flyby Mission. These materials include

- Carbon-loaded Kapton thermal blankets
- Indium-tin-oxide-coated gold Kapton thermal blankets
- Germanium-coated, carbon-loaded Kapton thermal blankets
- Electrostatic-conductive white paint
- Electrostatic-conductive black paint
- Composite materials
- Metallic materials

When surface discharge does occur, the voltage and current transients are mitigated by shielding around harness lines and using interface electronic devices that can tolerate the energy from ESD-induced transients that couple into the harness center conductors.

Internal ESD is controlled by shielding to reduce the electron flux present at dielectric materials within the spacecraft (typically circuit boards) and by limiting the amount of ungrounded metal (ungrounded harness conductors, connector pins, device radiation shields, part packages, etc.). The shielding required to reduce the TID to acceptable levels for the Europa Multiple-Flyby Mission is more than suf-

ficient to reduce the electron flux to levels that preclude discharge events to circuit boards. Grounding of radiation shields, part packages, harness conductors, and connector pins through ESD bleed wires or conductive coatings limits the ungrounded metals to small areas that cannot store enough energy to cause damaging discharges to electronic devices.

This surface and internal charging methodology has been used extensively in a severe charging environment for spacecraft with long lifetimes and was used specifically on the Juno project.

The spacecraft's exposure to radiation is attenuated to acceptable levels by providing shielding between the external environment and the sensitive materials and electronic parts in the spacecraft. Most of the spacecraft electronics are placed in a shielded vault. Payload electronics and sensor heads external to the vault have shielding tailored for their design and location on the spacecraft. Science instrument detector shielding to suppress radiation-induced background noise and permanent damage effects is achieved through a combination of instrument-level shielding for detector support electronics and internal high-Z (high-atomic-number) material shielding for the detector devices.

Efficient use of dedicated shield mass is achieved through a nested shield design concept, shown in Figure C.2.6-1. Spacecraft structure and placement of the Propulsion Subsystem hardware (fuel tanks, oxidizer tanks, helium pressurant tanks, and propellant that remains in the tanks after JOI) provide significant collateral shielding to the electronics packaged within the vault. The vault's wall thickness and material composition, 7.3-mm-thick aluminum, further limit the Flyby Mission TID to 150 krad for the enclosed electronics. Localized shielding at the assembly level then reduces the Flyby Mission TID even more, from 150 krad to 50 krad at the device level for all electronics.
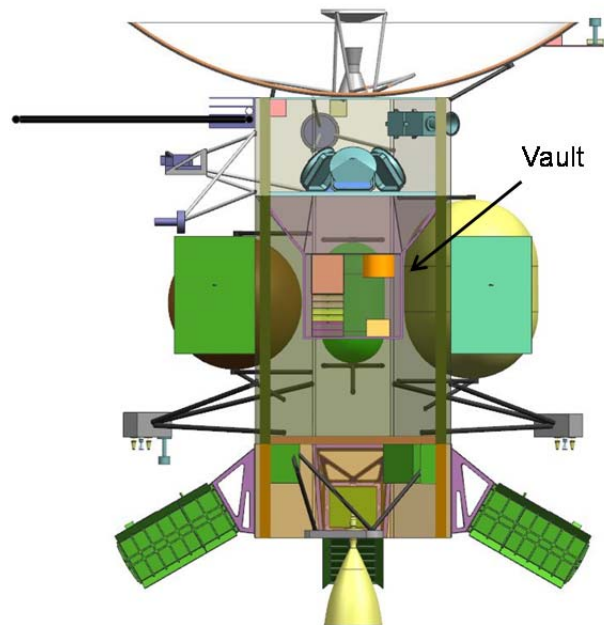
Figure C.2.6-1. Flyby Mission electronics are shielded by the spacecraft structure, propulsion tanks, and a dedicated electronics vault.

The dedicated shield mass for the Europa Multiple-Flyby Mission is a total of 218 kg, as shown in Table C.2.6-7. The shield mass was calculated based on a detailed radiation transport analysis that takes into account the spacecraft configuration shown in Figure C.2.6-1, material composition and thickness of the spacecraft structural elements and propulsion tanks, and the locations of electronic units and science instruments. Analysts used the following process:

1. Generate spacecraft element configuration and locations from a CAD model.
2. Explicitly calculate the shielding effectiveness of materials used in spacecraft structure, propulsion tanks, electronics unit chassis, dedicated vault, and added electronics assembly shielding based on material composition, density, and location using the NOVICE radiation transport code. The NOVICE code results have been correlated against a ray tracing code shielding code FASTRAD that is used by Aerospace contractors in both European and the United

States. For this analysis, the propulsion tanks are modeled as empty tanks.

3. To minimize the cost and risk of assuming electronic parts with higher radiation tolerance, assume all spacecraft electronics use 100-krad-tolerant electronic parts.

4. Understand science instrument front-end electronics co-located with detectors to have radiation tolerances that are instrument-specific (see Section C.2.2).

5. Through adjustments to assembly-level shielding mass, shield all spacecraft electronics assemblies to a TID of 50 krad or less at end of mission (i.e., to account for environmental uncertainty, they are given a radiation design factor [RDF] greater than or equal to 2 at the end of the mission).

6. Shield science instrument front-end electronics to have a minimum RDF of 2 for TID at the end of the mission.

7. To minimize cost, use aluminum shielding for all spacecraft electronics except science instrument and star-tracker detectors.

8. To minimize the radiation-induced noise at each detector location, shield science instrument and star-tracker detectors using high-Z materials (such as tantalum) (see Section C.2.2).

9. At the individual assembly level, to allow the use of off-the-shelf electronics without modification, wrap shielding around each assembly rather than integrating it into the assembly chassis.

10. Model circuit boards within the electronic assemblies as unpopulated boards. (Modeling component layouts on boards will be performed as the project progresses into Phase B. Including component layout in the radiation transport model will further reduce TID at the device level.)

Significant opportunities to reduce the dedicated shield mass have been identified although they have remained unexercised at this time. These opportunities include the following:

1. Change electronics unit placement within the vault to better protect units with lower-TID-capable electronic parts.

2. Place electronics cards within units to provide the lowest local TID at the part level.

3. Use a more efficient shield material than aluminum.

4. Add detail to the radiation transport model by including populated boards and individual device shielding.

5. Integrate the shielding into the electronics chassis.

6. Use multiple-material layered shielding, which is known to improve shielding efficiency.

The shield masses in Table C.2.6-7 have been incorporated into the spacecraft MEL (Section C.4.3).

Table C.2.6-7. Calculated shield masses to reduce the mission TID to 50 krad within each assembly.

Item	Shield Mass (kg)
Vault Structure	51.9
C&DH Subsystem	5.9
Power Subsystem	12.6
MIMU (2)	10.1
SDST (2)	6.1
WDE (4 slices)	4.4
Ka HVPS (2)	6.8
X HVPS (2)	6.0
ASRG (4)	45.9
Star-Tracker (2)	16.8
Pressure Transducer (10)	3.9
Science Electronics	21.8
INMS	10.1
Ice-Penetrating Radar	5.0
Topographic Imager	1.5
SWIRS	9.1
Flyby Spacecraft Total	218

C.2.6.2   Planetary Protection

NASA Planetary Protection policy (NPR 8020.12C [NASA 2005]) specifies requirements for limiting forward contamination in accordance with Article IX of the 1967 Outer Space Treaty. As Europa is a body of extreme interest to the astrobiological community as a possible location for the emergence of extra-terrestrial life, contamination of Europa with Earth-derived biology must be carefully avoided.

The mission's plan for responding to planetary protection requirements is to perform Dry Heat Microbial Reduction (DHMR) on as much of the spacecraft as possible, as late in the integration flow as possible. DHMR involves raising the bulk temperature of the spacecraft above the survival threshold for microbes and their spores. For materials contamination reasons, this bake out is typically done in vacuum or inert gas (nitrogen). To the extent possible, all spacecraft components will be designed to accommodate late integration DHMR without disassembly or recalibration. However, components or instrumentation unable to comply with DHMR requirements may be removed and sterilized through other means.

The extent to which DHMR sterilization and subsequent recontamination must reduce the spacecraft bioburden before liftoff is greatly influenced by the expected impact of post-launch sterilization processes and contamination probabilities. These include:

a) Probability of organism survival during interplanetary cruise
b) Probability of organism survival in the Jovian radiation environment
c) Probability of impacting Europa
d) Probability of organism survival on the surface of Europa before subsurface transfer
e) The duration required for transport to the Europan subsurface
f) Organism survival and proliferation after subsurface transfer

Each of these factors will be carefully examined to determine the ultimate allowable bioburden at launch and the required effectiveness of DHMR to maintain compliance with NASA regulation and international treaty.

C.2.6.3   Nuclear Safety

Missions to the outer solar system generally require the use of nuclear energy sources for electrical power and heating. The radioactive material used for this purpose is potentially hazardous to humans and the environment unless precautions are taken for its safe deployment. The following circumstances are of concern:

- Handling: People will be in the vicinity while nuclear sources (ASRGs or RHUs) are being constructed, transported, and installed on the spacecraft.
- Launch: In the event of a catastrophic LV failure, the spacecraft with its nuclear components is potentially subject to explosion, fire, impact, or the heat and forces of immediate reentry.
- Injection: If injection into interplanetary flight is not achieved, the spacecraft may be left in an Earth orbit that could decay to reentry after some time, thus exposing nuclear components to reentry conditions.
- Earth Flyby: If unplanned trajectory errors cause the spacecraft to reenter Earth's atmosphere, nuclear components would be exposed to reentry conditions.

Safety from nuclear hazards in each of these circumstances is essential.

The National Environmental Policy Act of 1969 (NEPA) specifies measures intended to address these concerns. Project compliance with NEPA is mandatory and is described in more detail below.

C.2.6.3.1   NEPA Compliance

Environmental review requirements will be satisfied by the completion of a mission-

specific Environmental Impact Statement (EIS) for the Europa Multiple-Flyby Mission. In accordance with the requirements of NPR 7120.5D, NPR 7120.5E and NPR 8580.1 (pending) (NASA 2007, 2012), the Record of Decision (ROD) for this EIS is finalized prior to or concurrent with project PDR.

The Europa Multiple-Flyby Mission Launch Approval Engineering Plan (LAEP) is completed no later than the Mission Definition Review (MDR). This plan describes the approach for satisfying NASA's NEPA requirements for the mission, and the approach for complying with the nuclear safety launch approval process described in Presidential Directive/National Security Council Memorandum #25 (PD/NSC-25) (1977) and satisfying the nuclear safety requirements of NPR 8715.3 (NASA 2010b). The LAEP provides a description of responsibilities, data sources, schedule, and an overall summary plan for preparing the following:

- A mission-specific environmental review document and supporting nuclear safety risk-assessment efforts
- LV and flight system/mission design data requirements to support nuclear risk assessment and safety analyses in compliance with the requirements of NPR 8715.3 (NASA 2010b) and the PD/NSC-25 nuclear safety launch approval process
- Support of launch site radiological contingency planning efforts
- Earth swing-by analysis
- Risk communication activities and products pertaining to the NEPA process, nuclear safety, and planetary protection aspects of the project.

It is anticipated that NASA HQ would initiate the Europa Multiple-Flyby Mission NEPA compliance document development as soon as a clear definition of the baseline plan and option space has been formulated. The Department of Energy (DOE) provides a nuclear risk assessment to support the environmental review document, based upon a representative set of environments and accident scenarios compiled by the KSC Launch Services Program working with JPL. This deliverable might be modeled after the approach used for the MSL EIS.

DOE provides a Nuclear Safety Analysis Report (SAR) based upon NASA-provided mission-specific launch system and flight system data to support the PD/NSC-25 compliance effort. The SAR is delivered to an ad hoc Interagency Nuclear Safety Review Panel (INSRP) organized for the Europa Multiple-Flyby Mission. This INSRP reviews the SAR's methodology and conclusions and prepares a Safety Evaluation Report (SER). Both the SER and the SAR are then provided by NASA to the Environmental Protection Agency, Department of Defense, and DOE for agency review. Following agency review of the documents and resolution of any outstanding issues, NASA, as the sponsoring agency, would submit a request for launch approval to the Director of the Office of Science and Technology Policy (OSTP). The OSTP Director reviews the request for nuclear safety launch approval and can either approve the launch or defer the decision to the President.

As part of broader nuclear safety considerations, the Europa Multiple-Flyby Mission would adopt requirements for ATLO, spacecraft design, trajectory design (e.g., for sufficiently high orbit at launch, and for Earth flybys), and operations that satisfy the nuclear safety requirements of NPR 8715.3 (NASA 2010b).

Development of coordinated launch site radiological contingency response plans for NASA launches is the responsibility of the launch site Radiation Protection Officer. Comprehensive radiological contingency response plans, compliant with the National Response Framework and appropriate annexes, is developed and put in place prior to launch as required by NPR 8715.2 and NPR 8715.3 (NASA 2009a,

2010b). The Europa Multiple-Flyby Mission would support the development of plans for on-orbit contingency actions to complement these ground-based response plans.

A project-specific Risk Communication Plan would be completed no later than the MDR. The Risk Communication Plan details the rationale, proactive strategy, process, and products of communicating risk aspects of the project, including nuclear safety and planetary protection. The communication strategy and process would comply with the approach and requirements outlined in the Office of Space Science Risk Communication Plan for Deep Space Missions (JPL D-16993).

C.3   Multiple-Flyby Programmatics

C.3.1   Management Approach

The management approach for the Europa Multiple-Flyby Mission draws upon extensive experience from Galileo and Cassini. It follows NPR 7120.5E and incorporates NASA lessons learned.

The project approach includes a conventional Work Breakdown Structure (WBS), technical management processes conducted by veteran systems engineers, and integrated schedule/cost/risk planning and management. The project will take advantage of existing infrastructure for planning, acquisition, compliance with the National Environmental Policy Act (NEPA), compliance with export control regulations (including International Traffic in Arms Regulations and Export Administration Regulations), independent technical authority (as called for in NPR 7120.5E [NASA 2012]), mission assurance, ISO 9001 compliance, and earned value management (EVM).

The Europa Multiple-Flyby Mission employs JPL's integrated project controls solutions to manage and control costs. Skilled business and project control professionals are deployed to projects, utilizing state of the art tools and executing processes that support the project cost, schedule, and risk management requirements.

Key attributes of the project controls solution are as follows:

- The Business Manager, project focal point on all business management issues, and the project control staff lead project planners and managers in application of effective and efficient implementation of project control processes.
- Mature and successfully demonstrated cost and schedule tools are employed.
- Cost and schedule data are tied directly to work scope.
- "Early warning" metrics are provided monthly to key decision makers. Metrics include 1) cost and schedule variances based on the cost value of work performed and 2) critical-path and slack analysis derived from fully integrated end-to-end network schedules. Each end-item deliverable is scheduled with slack to a fixed receivable. Erosion of this slack value is tracked weekly and reported monthly.
- An integrated business management approach is applied to all system and instrument providers. This approach includes relative performance measurement data integrated into the total project database for a comprehensive understanding of project cost and schedule dynamics.
- Risk management processes are integrated with the liens management process for full knowledge of project reserve status. Early risk identification is emphasized, with each risk tracked as a potential threat to project reserves. Reserve utilization decisions are made with the knowledge of risks and risk mitigation, project performance issues, and increases in scope.

JPL flight projects that have used this integrated project controls approach include Juno, GRAIL, MSL, and Phoenix.

Requirements for project controls evolve throughout the project life cycle. Pre–Phase A and Phase A will require less support than phases B, C, and D. During Phase B, the project controls capability is established at full strength to establish all the appropriate databases and gate products required for a successful Confirmation Review. During phases C and D, full application of project controls will continue, with recurring performance measurement analysis and cost and schedule tracking reports. During phases E and F, the project controls function is reduced to lower levels commensurate with the scale of postlaunch activities.

C.3.2   WBS

The Europa Multiple-Flyby Mission Work Breakdown Structure (WBS) is structured to enable effective cost, schedule and management integration.

The WBS is derived from JPL's Standard Flight Project WBS Version 5 (JPL 2009) and is fully compliant with NPR 7120.5E. This WBS is a product-oriented hierarchical division of the hardware, software, services, and data required to produce end products. It is structured according to modular design of the spacecraft, and reflects the way the work would be implemented, and the way in which project costs, schedule, technical and risk data are to be accumulated, summarized, and reported.

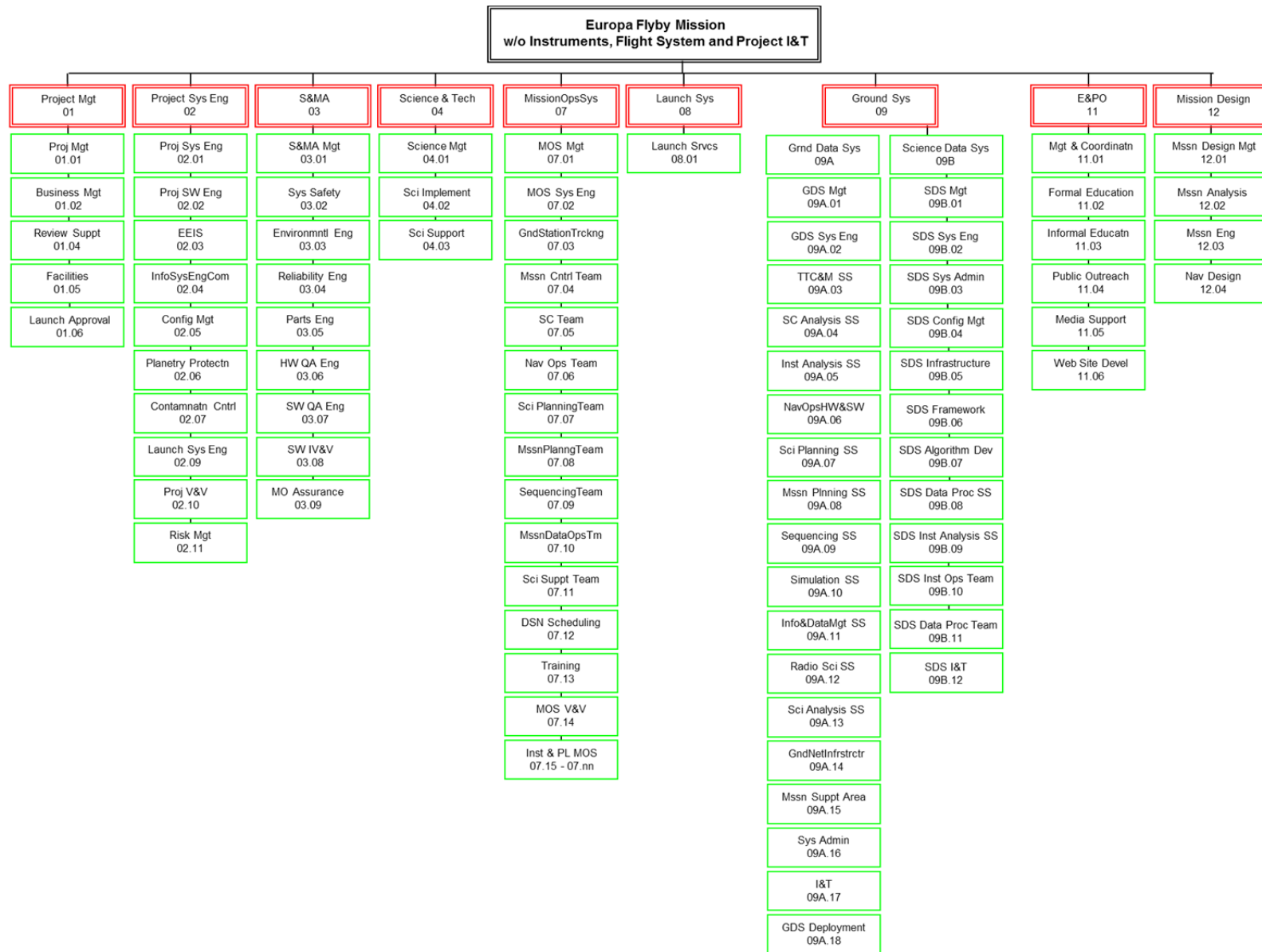The top-level WBS is shown Figures C.3.2-1 and C.3.2-2.

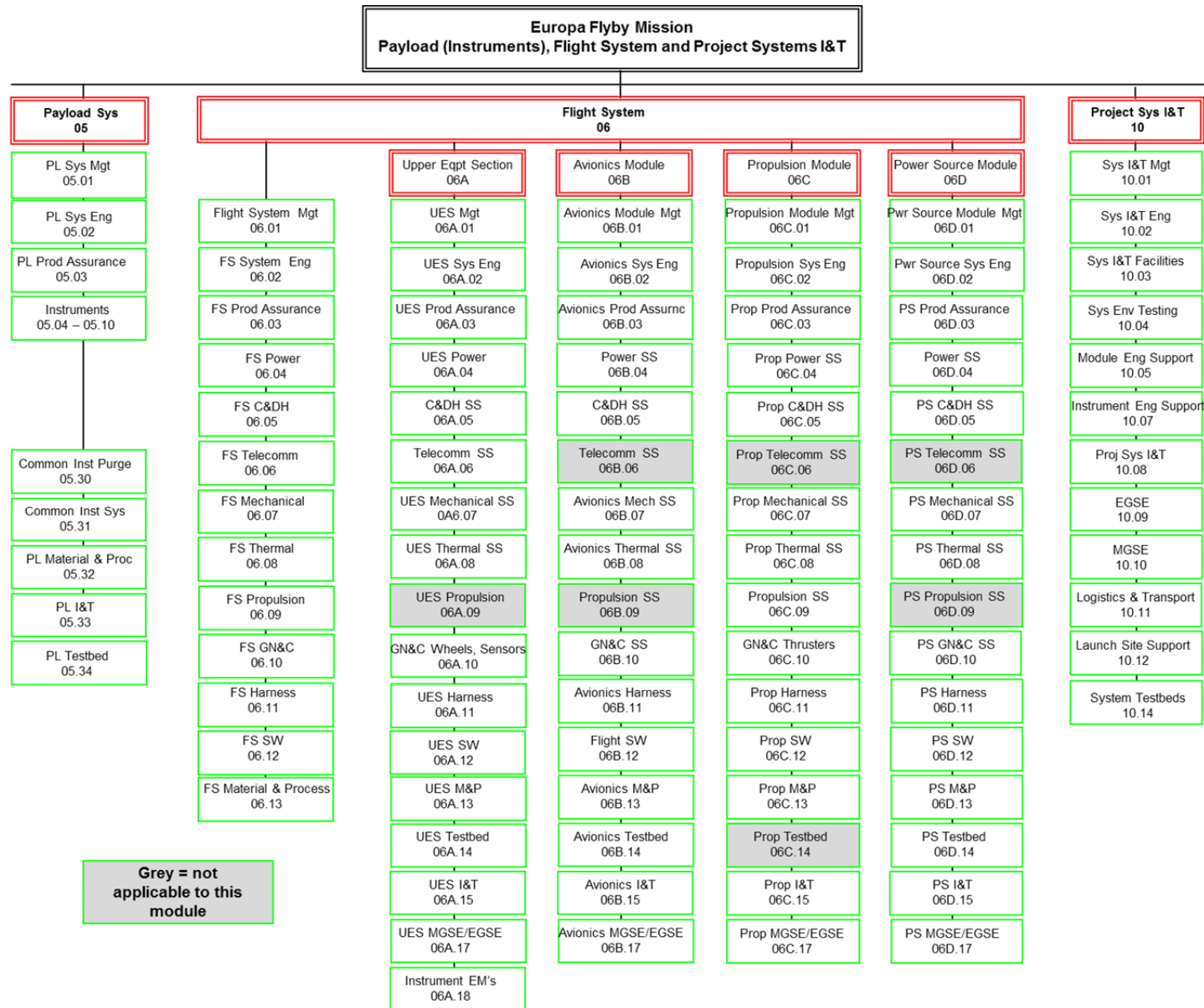**Figure C.3.2-1.** Europa Multiple-Flyby Mission concept work breakdown structure.

Figure C.3.2-2. Europa Multiple-Flyby Mission work breakdown structure: Payload, Flight Systems, I&T.

C.3.3   Schedule

The low-risk schedule is informed by previous outer planet missions.

A top-level schedule with implementation flow is shown in Figure C.3.3-1. The phase durations draw on experience from previous outer planet missions and are conservative. A bottom-up, WBS-based integrated schedule will be generated during Pre–Phase A.

C.3.3.1   Pre–Phase A

In preparation for this report, many alternative concept studies have been conducted. Should the Flyby concept be carried forward to Pre–Phase A, a preproject team will be formed to refine the baseline mission concept and implementation plan to align with programmatic goals and objectives. This refinement, along with interactions with NASA and other stakeholders, will result in further definition of the mission concept and draft project-level requirements.

Pre–Phase A activities include completion of NPR 7120.5D-specified Pre–Phase A Gate Products (NASA 2007), preparation of a Project Information Package (PIP) in support of NASA's development of an Announcement of Opportunity (AO) for instrument acquisition, and a Mission Concept Review leading to Key Decision Point (KDP) A. In addition to those activities required for transition to Phase A, the team will identify additional planning, advanced development, and risk-reduction tasks that could provide a prudent and cost-effective approach to early reduction of cost and schedule risk and have the potential to reduce the estimated cost of the mission. Primary activities include reducing the radiation and planetary-protection risks associated with instrument and spacecraft development.

C.3.3.2   Phases A–F

The Phase A–F schedule reflects the total project scope of work as discrete and measurable tasks and milestones that are time-phased through the use of task durations, interdepend-

encies, and date constraints. To ensure low risk, the schedule includes margin for all tasks.

The Project Manager controls the project schedule, with support from a Project Schedule Analyst. An Integrated Master Schedule identifies key milestones, major reviews, and receivables/deliverables (Rec/Dels). Schedule reserves for the November 2021 launch opportunity meet or exceed JPL Design Principles (DPs) requirements (schedule reserves of 1 month per year for phases A through D, with schedule reserves of 1 week per month for activities at the launch site) (JPL 2010a). The project utilizes an integrated cost/schedule system in Phase B, in order to fully implement an EVM baseline in phases C, D, and E. Inputs are supplied to NASA's Cost Analysis Data Requirement (CADRe) support contractor for reporting at major reviews. Schedule and cost estimates at completion (EACs) are prepared at regular intervals as part of the EVM process. Major project review milestones (not all shown) are consistent with NPR 7120.5D (NASA 2007).

C.3.3.3   Phases A–B

The length of phases A and B (24 months for A, 26 months for B) is primarily driven by the schedule to select the instruments in response to the AO and advance the selected instruments to the PDR level of maturity. In Phase A the primary tasks are completing the Gate Products required and facilitating the selection of the science instruments. The 8-month period between instrument selection and the system Mission Definition Review (MDR) allows instrument designers to work directly with the project personnel on issues related to accommodation, requirements, radiation, and planetary protection. The schedule is front-loaded with a long Phase A to give adequate time to define requirements early in the mission development life cycle. A basic approach to meeting the planetary protection requirements has been outlined and agreed to by the Planetary Protection Officer at NASA Headquarters.
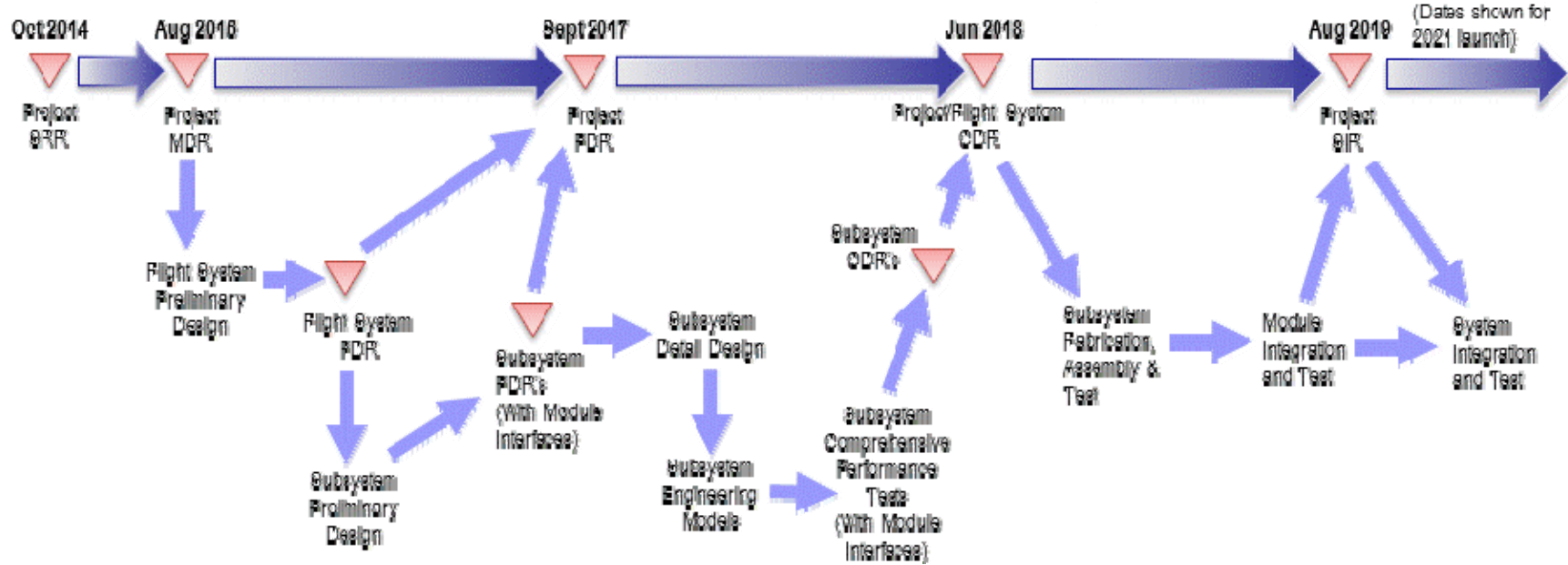
Figure C.3.3-1. Project implementation flow.

During Phase B it is anticipated that there will be a review of the detailed implementation approach, including any major outstanding issues related to mission design, flight system design, or operations concepts. This review might ultimately be combined with the Project PDR if it is effective to do so.

C.3.3.4   Phases C–D

The length of phases C and D (27 months for C, 22 months for D) is primarily driven by the schedule to bring the flight system to launch readiness. Phase C is longer than typical due to the added time required to implement the radiation and planetary-protection aspects of the design. The long Phase C also allows for a lower staff-level profile, which keeps the mission cost profile flatter. Phase D was developed using the Cassini model of ATLO and includes 1.5 months to perform the system-level DHMR.

A trailblazer activity is scheduled to occur at the launch facility in Phase D to ensure that the spacecraft design is compatible with the launch vehicle and facility limitations at the launch site for transporting and loading of the ASRGs. This activity starts at a very low level in Phase B and continues with increasing activity until the approach to ASRG installation is validated in Phase D. The trailblazer activity is also be used to dry-run the system-level DHMR activities that will take place in a thermal-vacuum chamber at KSC.

C.3.3.5   Phases E–F

Phase E (9.5 years) is driven by the interplanetary trajectory and science requirements at Europa. Phase F (6 months) is structured to carry out the end-of-mission disposal scenario and to complete data analysis and archiving.

C.3.4   Risk and Mitigation Plan

The main risks and their mitigation approaches are understood.

The primary challenges of a mission to Europa are Jupiter's radiation environment, planetary protection, trajectory management for numer-

ous consecutive flybys, and the large distance from the Sun and Earth. Driving technical risks are

1. Advanced Stirling radioisotope generator (ASRG) development
2. Performance in a radiation environment
3. Instrument development
4. Planetary protection

C.3.4.1   ASRG

NASA is developing the ASRG as the long-term solution for reducing the plutonium requirements for future planetary missions. Any problems with the development and validation of the ASRG could have a serious impact on the Europa Multiple-Flyby Mission, since it is baselining a radioisotope power system. ASRG development and qualification risks have high consequences and are outside the control of the Europa Multiple-Flyby Mission project. The ASRGs are a new development, and the likelihood of problems is not known; however, successful development of new radioisotope thermoelectric generators can be difficult. Risks to the mission associated with this development can be mitigated if well-defined and stable ASRG characteristics are known early in Phase A to allow the system designers to adequately incorporate them into the spacecraft system. However, if these characteristics are not known and stable early in Phase A, late design changes and impacts on mass, power, cost, and schedule are likely. The Europa Power Source Module concept allows for later ASRG delivery, thereby diminishing some of the development risk, as does the Europa Study Team's close work with NASA to clearly delineate the mission requirements on the ASRGs. Mitigation of these risks also requires that the project work closely with the Program Executive at NASA Headquarters for the ASRG Development Program to ensure that the technology is flight-qualified with completed life tests, no later than Phase B. A robust ground-test program is essential to migrating the ASRG risks. The NASA ASRG

development efforts are currently underway (see Section C.2.4.6).

C.3.4.2   Performance in a radiation environment

The radiation environment to which the Europa Multiple-Flyby Mission hardware would be exposed, and its accumulated effects by end of mission are significant. Radiation effects expected in the mission are TID effects and SEE in electronic components, displacement damage (DD) effects in components and materials, noise effects in detectors, and surface and internal charging (IC). The primary risk considered here is the likelihood that premature component failure or compromised performance could have a serious impact on spacecraft functionality if the radiation problem is not addressed appropriately. Sensors for instruments used for pointing and navigation and in science instruments are particularly sensitive to radiation effects, primarily due to noise and displacement effects. Test techniques used to verify component suitability might over-predict component hardness due to inadequate accounting for radiation rate or source type effects that are negligible at lower doses. Also, unanticipated failure mechanisms might be present or might become important at high doses or at high DD levels that are not of concern for missions conducted at nominal total-dose exposures. The measures described here reduce both the likelihood and the consequences of such impacts, with designs for this radiation environment robust beyond the level normally accomplished for spaceflight design. The Europa Multiple-Flyby Mission design concept uses an approach similar to that taken by Juno, using an electronics vault to shield the electronic components to a mission dose of 150 krad, thereby reducing the likelihood of radiation-related problems while increasing the likelihood of parts availability. There has been significant effort exerted by experts to mitigate this risk over the past decade. In 2007, the Europa Study Team convened several review teams to assess the particular risks in each ar-

ea. The results of the reviews were presented in Appendix C of the 2007 Europa Explorer Mission Study report (Clark et al. 2007). As a result of those reviews, a Risk Mitigation Plan: Radiation and Planetary Protection (Yan 2007, outlined in Clark et al. 2007) was further developed and executed to make strategic investments related to reducing even further the likelihood of component failure and degradation, and the related radiation risk. Results of this work were reported in the 2008 JEO final report (Clark et al. 2008). An expanded systems engineering approach focuses on graceful degradation and reduces the consequences of any component failures in electronic parts.

C.3.4.3   Instrument Development

Instrument development and delivery will undoubtedly be on the critical path, as has historically been the case. Only four instruments are needed to fulfill the Europa Multiple-Flyby Mission science requirements. An Approved Parts and Materials List (APML), addressing planetary protection and radiation constraints, will be available in time for the instrument AO. In addition, design guidelines will be incorporated into the AO. This facilitates maturation of instrument concepts prior to selection. The instruments in the model payload are all based on mature technologies, and if deployed on a mission in the inner solar system, would represent low risk. For a Europa mission though, radiation can be expected to have a detrimental impact on instrument performance. If such problems cannot be resolved satisfactorily, the science objectives of the mission would not be met. Therefore, instruments will be selected as early as possible in Phase A, and early funding will be made available in order to alleviate development risks. In addition, the project will assign instrument interface engineers to work with each instrument provider to ensure that the instrument meets interface requirements and the spacecraft accommodates specific instrument needs.

To reduce the likelihood that the instruments fall short of their desired specifications or run into resource and schedule problems due to radiation issues, typical interface engineering support will be augmented for each instrument with personnel experienced in the area of radiation design. Design guidelines will be generated for the instrument teams to describe radiation constraints and to provide recommendations for design issues, and for parts and material selection. Development of a knowledge base for potential instrument providers has already begun. Four instrument workshops were held to engage the instrument provider community in a dialogue on needs and potential driving requirements for a mission to Europa. Information regarding radiation and planetary protection requirements was disseminated. The Europa Multiple-Flyby Mission development schedule provides abundant time plus reserves after selection for instrument developers and the project to work through and understand the particular design implications for each instrument of radiation and planetary protection. The project schedule also allows ample time for the instruments to be developed and delivered to system test. In addition, the modular spacecraft approach, early local testing with spacecraft emulators, and a straightforward instrument interface allow instruments to be integrated last in the ATLO integration process, if necessary.

C.3.4.4   Planetary Protection

The planetary protection requirements for a mission to Europa are significant and can drive mission design, schedule, and cost. The final fate of the Europa Multiple-Flyby Mission, impacting on the Ganymede surface, means that the mission will be classified as Category III under current Committee on Space Research (COSPAR) and NASA policy (COSPAR 2002). If prelaunch cleanliness levels are not met, expenditure of cost and schedule reserves might be required to address contamination problems late in the process to prevent contamination of Europa. This risk is cross-cutting and is mitigated in part by a review added in Phase B to confirm the approach and assess implementation. This risk is also mitigated by the previous Europa Study activities. The approach to planetary protection compliance for the Europa Multiple-Flyby Mission concept, at this time is 1) prelaunch DHMR to control bioburden for those areas not irradiated in-flight and 2) in-flight microbial reduction via radiation prior to the first Europa flybys. The prelaunch method is to perform a full system DHMR as one of the last steps in the ATLO process at KSC. A chamber has been identified at KSC that is capable of performing DHMR, though specific details will need to be worked during Phase A. A pathfinder activity is planned as a dress rehearsal to resolve any procedural challenges. Compilation of the Europa Multiple-Flyby Mission APML will address compliance of materials with the DHMR process.

C.3.5   Cost

The Flyby Mission cost is well-understood and thoroughly validated.

C.3.5.1   Cost Summary

The Total Mission Cost for the Europa Multiple-Flyby Mission concept is estimated at $1.9B to $2.0B FY15, *excluding the launch vehicle, which is costed separately*. The mission baseline comprises a flyby spacecraft carrying four instruments—Ice-Penetrating Radar (IPR), Shortwave Infrared Spectrometer (SWIRS), Ion And Neutral Mass Spectrometer (INMS), and Topographical Imager (TI)—that would spend 18 months taking remote measurements of Europa via multiple flybys. The Europa Multiple-Flyby Mission enables investigators to understand the chemistry of this moon and investigate its habitability for life.

Table C.3.5-1 summarizes the mission cost estimate at WBS level 2.

The total mission cost is broken down into $1.6 to $1.7B for the Phase-A through -D development period and $0.3B for operations during Phases E and F. The Europa Multiple-

Table C.3.5-1. Europa Multiple-Flyby Mission cost summary by WBS (FY15 $M).

WBS Element	PRICE-H	SEER
01 Proj Mgmt	62	60
02 Project System Engineering	52	50
03 Safety & Mission Assurance	57	55
04 Science	71	71
05 Payload System	262	262
06 Spacecraft System	489	468
ASRG	200	200
07 Mission Operations System	171	171
08 Launch System	—	—
09 Ground Data System	39	39
10 Proj Sys I&T	48	42
11 Education & Public Outreach	13	12
12 Mission Design	25	24
Subtotal (FY15$M)	**1,489**	**1,456**
Reserves	467	454
Total (FY15$M)	**1,956**	**1,911**

Flyby Mission holds 37% in cost reserves that is broken down into 40% for Phases A, B, C, and D, and 20% for Phases E and F.

The estimated cost is based on the implementation approach described in Section C.2, which includes the following key features in the baseline plan:

- Redundant flight system with selected cross-strapping
- No new technologies requiring extraordinary development
- Simple, repeated, algorithm-driven observations capable of achieving all of the science goals
- Experienced providers of key systems and subsystems

C.3.5.2 Cost Estimating Methodology

To estimate the cost for the Europa Multiple-Flyby Mission concept, JPL used their institutional cost-estimation process applicable for the design maturity of a concept study in early formulation. This process focuses on using parametric cost models, analogies, and other non-grassroots estimating techniques, which provide the following advantages:

- Provide rapid turnaround of extensive trade studies

- Enable design-to-cost to narrow the trade space and define a baseline concept
- Establish reasonable upper and lower bounds around a point estimate

A cost-estimation process begins with the Europa Study Team developing a Technical Data Package (TDP) that describes the science requirements, technical design, mission architecture, and project schedule. Next, all work is organized, defined, and estimated according to the NASA standard WBS. The Europa Study Team then tailors the WBS as needed for cost estimation and planning.

The institutional business organization uses the TDP and WBS to develop the cost estimate by applying estimating methods and techniques appropriate for each WBS element, based on the maturity of design and manufacturing requirements, availability of relevant historical information, and degree of similarity to prior missions. For the Europa Multiple-Flyby Mission, the tools and methods used include the following:

- Calibration of commercial, off-the-shelf (COTS) tools PRICE-H and SEER to Juno, the most relevant JPL planetary mission
- Use of the NASA Instrument Cost Model (NICM) for the notional payload, tailored for the Europa environment
- Use of the NASA Space Operations & Cost Model (SOCM) for Phases E and F
- Wrap factors based on analogous historical planetary missions for Project Management, Project Systems Engineering, Safety and Mission Assurance, and Mission Design

The Europa Study Team's estimate is a compilation of these multiple techniques. The Europa Study team then vets the integrated cost rollup and detailed basis of estimate (BOE), and reviews the results for consistency and

reasonableness with the mission design, WBS, and NASA requirements to ensure that technical and schedule characteristics are accurately captured and a consistent cost-risk posture is assumed.

To validate the resulting proposed cost, the Europa Study Team used Team X to independently cost the baseline concept with the JPL Institutional Cost Models (ICMs): 33 integrated, WBS-Level-2 through -4 models built by JPL line organizations to emulate their grassroots approach. The Europa Study Team also contracted with the Aerospace Corporation to perform an Independent Cost Estimate (ICE) and Cost and Technical Evaluation (CATE.) The Team X and Aerospace results are discussed in Section C.3.5.7.

The Europa Study Team then used an S-curve cost risk analysis to validate and bound the cost reserves. The reserves substantiation is discussed in Section C.3.5.8.

C.3.5.3   Basis of Estimate

The integrated Europa Multiple-Flyby Mission cost estimate is based on the science and mission implementation approach described in Section C.2. In addition, the MEL (Section C.4.3) provided the key inputs for mass, quantities, and the quantification of electronics versus structures that are needed to run the parametric tools. The cost estimating methodologies and assumptions used to develop the Europa Multiple-Flyby Mission cost estimate are summarized in Table C.3.5-2.

C.3.5.4   Instrument Cost Estimates

The NASA Instrument Cost Model (NICM) system model with an augmentation to account for radiation and planetary protection was used to estimate instrument costs. Each notional instrument was characterized for performance establishing instrument type, aggregate power estimates, and subsystem-level mass. Table C.3.5-3 shows the input parameters used for each instrument for the NICM system model.

C.3.5.4.1   NICM Adjustments

NICM outputs at the 70 percentile were reported in FY15$. This reference cost estimate was then augmented for radiation and planetary protection. The NICM model does not have parameters or characteristics sufficient to model planetary protection requirements or radiation environments. A flat fee for Planetary Protection was added to each instrument, based on instrument complexity. An estimate for the number of electronic boards and detectors was made for each instrument, and an additional fee of $2M was assessed per detector for radiation redesign costs. The instrument radiation shielding masses were estimated separately in PRICE-H and SEER, and are included in WBS 06 spacecraft costs under Payload Radiation Shielding. Table C.3.5-4 summarizes the instrument cost-estimation process.

C.3.5.4.2   NICM Estimate

Table C.3.5-5 provides the final NICM system cost estimate, including all adjustments for radiation and planetary protection.

C.3.5.5   Spacecraft Hardware Costs

The Europa Multiple-Flyby Mission spacecraft hardware costs were estimated using PRICE-H and SEER, calibrated to Juno. The Flyby spacecraft is most closely analogous to the Juno spacecraft. Configuration, avionics subsystems, radiation environment, mission complexity, and design lifetime match closely to the corresponding aspects of the Juno mission.

Table C.3.5-2. Cost-estimation methodology.

WBS Element	Methodology
01 Project Management	Historical wrap factor based on analogous historical planetary missions. Estimate was augmented by $15M to account for Nuclear Launch Safety Approval (NLSA) and National Environmental Policy Act (NEPA) costs associated with usage of the advanced Stirling radioisotope generators (ASRGs).
02 Project Sys Engineering	Historical wrap factor based on analogous historical planetary missions.
03 Safety & Msn Assurance	Historical wrap factor based on analogous historical planetary missions.
04 Science	Expert-based estimate from the science team based on mission class, schedule, and the number and complexity of instruments. Cost estimate captures the level of effort for a Project Scientist, two Deputy Project Scientists, the Science Team, and participating scientists, with additional workforce requirements for Phases C and D, based on the size of the team, the number of meetings with the team, and the products required from this group. For Phases E and F, the cost estimate also assumes a science team for each instrument, with the estimated level of effort based on existing instrument teams supporting current mission, and on the number of months in hibernation, cruise, and science operations.
05 Payload System	Historical wrap factor for Payload Management, Systems Engineering, and Product Assurance based on analogous historical planetary missions.
	Instrument costs developed using the NASA Instrument Cost Model (NICM), Version 5.0. The 70% confidence-level estimate was selected as a conservative point estimate for each notional instrument. Instrument costs are then augmented for radiation shielding, detector radiation redesign, and planetary protection for any DHMR material properties issues. For payload radiation shielding, the cost was estimated separately using PRICE-H and SEER, and the cost is included under WBS 06 Spacecraft System. For planetary protection a flat fee was then added to each instrument, based on instrument complexity. For radiation redesign, an additional fee of $2M was assessed per detector.
06 Spacecraft System	Historical wrap factor for Flight System Management, Systems Engineering, and Product Assurance based on analogous historical planetary missions.
	Spacecraft hardware costs estimated using PRICE-H and SEER calibrated to Juno at the subsystem level. Juno selected as an analogous mission for the calibration due to the operation of the flight system in a comparable radiation environment. Software costs estimated using a wrap factor of 10% on the hardware cost.
	ASRG cost provided by NASA Headquarters in the Europa Study Statement of Work, dated October 4, 2011 (NASA 2011). Estimate includes four ASRGs at $50M each (FY15$).
07 Mission Ops System	Team X estimate based on historical data for a Class A mission for Phases A-D; SOCM estimate for Phases E-F
08 Launch System	Launch Vehicle costs, including nuclear processing costs, are not included and will be provided by NASA Headquarters as directed in the Europa Study Statement of Work.
09 Ground Data System	Team X estimate based on historical data for a Class A mission for Phases A-D; SOCM estimate for Phases E-F
10 Project Systems I&T	PRICE-H and SEER estimate calibrated to Juno.
11 Education & Public Outreach	1.0% wrap factor on the total mission cost excluding the launch system (WBS 08), ASRG, and DSN tracking costs. Based on the percentage prescribed in the recent AOs for Discovery 2010 and New Frontiers 2009 (NASA 2010a, 2009c).
12 Mission Design	Historical wrap factor based on analogous historical planetary missions.
Reserves	40% for Phases A–D and 20% for Phases E–F on the total mission cost excluding the launch system (WBS 08), ASRG, and DSN tracking costs. These percentages were based on historical experience with recent planetary missions.

Table C.3.5-3. Inputs for NICM cost estimation.

Instrument Name	Ice-Penetrating Radar (IPR)	Shortwave Infrared Spectrometer (SWIRS)	Ion and Neutral Mass Spectrometer (INMS)	Topographic Imager (TI)
Remote Sensing or In-Situ?	Remote Sensing	Remote Sensing	Remote Sensing	Remote Sensing
Remote Sensing Instrument Type	Active	Optical	Particles	Optical
Mission Destination	Planetary	Planetary	Planetary	Planetary
Total Mass (kg)	28	12	14	3
Max Power (W)	55	19	33	6
Design Life (months)	108	108	108	108
Max Data Rate (kbps)	300	N/A	N/A	N/A
TRL	5	N/A	N/A	N/A
Number of Detectors	0	1	0	1

Table C.3.5-4. Instrument cost-estimation process.

Master Instrument Costing Matrix	Instrument Cost (Excluding Radiation Shielding) (A)	Detector Radiation Design Costs (B)	Planetary Protection Fee (C)	TOTAL INSTRUMENT COST	Radiation Shielding Cost— Included in WBS 06
Instrument X	NICM 70th percentile estimate	$2M per detector	Based on complexity	A+B+C	Estimated in PRICE-H/SEER

Table C.3.5-5. Instrument cost-estimation details (FY15$M).

Instrument	Acronym	NICM 70% Cost	Detector Radiation Design Costs	Planetary Protection Fee	TOTAL INSTRUMENT COST
Ice-Penetrating Radar	IPR	109.9	0.0	3.3	113.2
Shortwave Infrared Spectrometer	SWIRS	43.8	2.0	4.4	50.2
Topographic Imager	TI	14.3	2.0	0.7	17.0
Ion and Neutral Mass Spectrometer	INMS	47.9	0.0	1.4	49.4
TOTAL		**216.0**	**4.0**	**9.8**	**229.9**

PRICE-H and SEER Cost Estimates

The Spacecraft System costs generated for PRICE-H and SEER are shown in Table C.3.5-6. The Spacecraft System comprises the Carrier System and the Lander System in WBS 06. The Payload Radiation Shielding is captured as part of the Lander System and the costs are bookkept under WBS 06B.07. The RPS was estimated at a cost of $50M per ASRG unit as directed by NASA HQ, and included in WBS 06, separate from the Carrier System and Lander System costs. The I&T costs are kept in WBS 10. Spacecraft flight software was estimated as a 10% wrap factor based on hardware cost, which is a high-level rule of thumb derived from JPL's historical software cost data.

Table C.3.5-6. PRICE-H and SEER cost estimates for the Europa Multiple-Flyby Mission. (FY15$M)

Spacecraft System	PRICE-H	SEER
06 Spacecraft System		
06.04 Spacecraft Power SS	50	68
06.05 Spacecraft C&DH SS	37	27
06.06 Spacecraft Telecom SS	83	48
06.07 Spacecraft Mechanical SS	52	44
06.07a Radiation Shielding	11	11
06.07b Payload Radiation Shielding	3	2
06.08 Spacecraft Thermal SS	10	10
06.09 Spacecraft Propulsion SS	38	54
06.10 Spacecraft GN&C SS	51	56
06.11 Spacecraft Harness SS	6	6
06.12 Spacecraft Flight SW	34	33
06C RPS System	**200**	**200**
10 I&T	**48**	**42**

Table C.3.5-7. Phase E and F cost estimate for the Europa Multiple-Flyby Mission (FY15$M).

WBS Element	Phase E & F Costs
01 Project Management	7
02 Project Systems Engineering	7
03 Safety & Mission Assurance	7
04 Science	46
05 Payload	0
06 Spacecraft	0
07 Mission Operations	124
08 Launch System	0
09 Ground Data Systems	12
10 Project System Integration & Test	0
11 Education & Public Outreach	2
SUBTOTAL	**204**
DSN Tracking	19
20% Reserves (excluding DSN)	41
TOTAL	**264**

C.3.5.6   Phase E and F Cost Estimates

The NASA Space Operations Cost Model (SOCM) was used to estimate operations costs in Phases E and F. The Europa Study science team provided an expert-based estimate for WBS 04 Science based on schedule and the number and complexity of instruments. The Europa Multiple-Flyby Mission Phase E and F cost estimate is shown in Table C.3.5-7.

C.3.5.7   Estimate Reasonableness (Validation)

A JPL Team X cost session was used to assess the reasonableness of the parametrically derived PRICE-H and SEER-based Flight System (WBS 06) and Project Systems I&T (WBS 10) estimates and associated wraps. In addition, Aerospace Corporation independently ran an Independent Cost Estimate (ICE) and Cost and Technical Evaluation (CATE). The results of the Team X cost session and Aerospace Corporation analysis are presented in Table C.3.5-8 along with the PRICE- and SEER-based project estimates for comparison.

C.3.5.8   Cost-Risk Assessment and

Reserve Strategy

The Europa Study Team conservatively applied project-level reserves of 40% for Phases A–D and 20% for Phases E and F on all elements except for Launch Services, ASRGs, and DSN tracking. These reserve levels are more conservative than the reserve guidelines set forward in JPL Flight Project Practices, Rev. 8 (JPL 2010b).

The Europa Multiple-Flyby Mission cost risk and uncertainty assessment is a natural extension of the cost modeling discussed in Section C.3.5.1, and is consistent with standard practice at NASA and JPL. This assessment considers the wide band of uncertainty that typically accompanies missions at early phases of development, as well as the technical risk and uncertainties of the Europa Lander Mission as understood at this time and as experienced on prior competed and directed missions (e.g., Juno, MRO, MSL).

The primary technique used for this assessment is an S-Curve. This provides a statistically-based distribution of total project cost around the project's point estimate based on the cost models used in this analysis and the historical JPL data to which they are calibrated. Equivalently, this technique provides a probabilistic estimate of total project cost based on variability and uncertainties in the model-based estimates. An S-curve analysis was performed on the study cost estimate, and demonstrated a 70th-percentile cost estimate of $1.98B ($FY15, excluding launch vehicle) (Figure C.3.5-1). Comparing the Europa Study Team estimate (including cost reserves) to the S-Curve indicates that the Europa Study Team estimate of $1.9B to $2.0B is at approximately the 68th-percentile. To be at 70th-percentile, the Europa Study Team would need to increase reserves by ~$25M to ~$70M, resulting in a

Table C.3.5-8. Comparison of Europa Study cost estimates with Team X and Aerospace Corporation cost estimates..

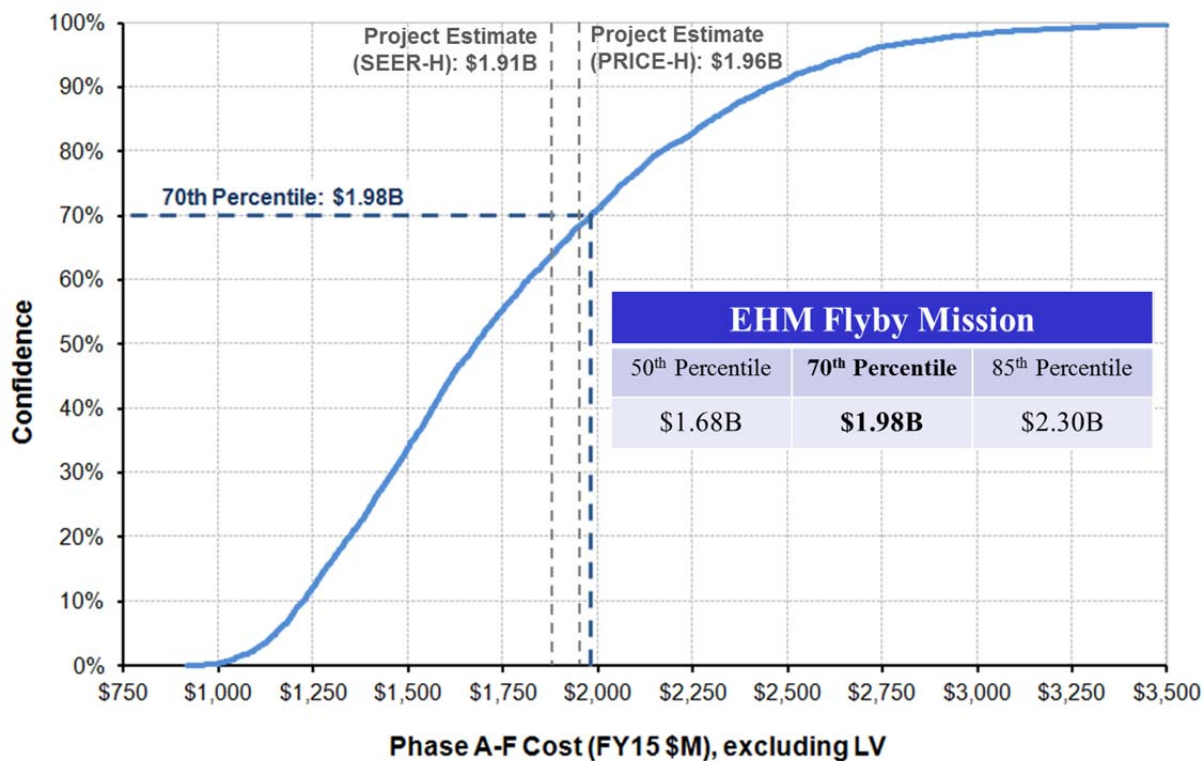| WBS Element	PRICE	SEER	Team X	Aerospace ICE	Aerospace CATE
Total (FY15$B)	2.0	1.9	1.7	2.1	2.1

Figure C.3.5-1. Europa Multiple-Flyby Mission cost estimate S-curve analysis.

reserve position of 40% overall (Phases A–F).

C.4 Multiple-Flyby Mission Appendices

C.4.1 References

Alexander, C., Carlson, R., Consolmagno, G., Greeley, R., Morrison, D. 2009. The exploration history of Europa. In: Pappalardo, R.T., McKinnon, W.B., Khurana, K.K. (Eds.), Europa, U. Arizona Press, Tucson, 3–26.

American National Standards Institute, 1992. ANSI/AIAA Guide G-020-1992, Estimating and Budgeting Weight and Power Contingencies for Spacecraft Systems. American Institute of Aeronautics and Astronautics, Washington, DC.

Bell, J.F., 1992. Charge-coupled device imaging spectroscopy of Mars 2: Results and implications for Martian ferric mineralogy. Icarus 100, 575–597.

Bibring, J., Langevin, Y., Gendrin, A., Gondet, B., Poulet, F., Berthe, M., Soufflot, A., Arvidson, R., Mangold, N., Mustard, J., et al., 2005. Mars surface diversity as revealed by the OMEGA/Mars express observations. Science 307, 1576–1581.

Bierhaus, E.B., Zahnle, K., Chapman, C.R., 2009. Europa's crater distributions and surface ages. In: Pappalardo, R.T., McKinnon, W.B., Khurana, K.K. (Eds.), Europa, U. Arizona Press, Tucson, 161–180.

Billings, S.E., Kattenhorn, S.A., 2005. The great thickness debate: Ice shell thickness models for Europa and comparisons with estimates based on flexure at ridges. Icarus 177, 397–412.

Boldt, J., et al., 2008. Assessment of radiation effects on detectors and key optical components. JPL D-48256.

Brown, M.E., 2001. Potassium in Europa's atmosphere. Icarus 151, 190–195.

Brown, M.E., Hill, R.E., 1996. Discovery of an extended sodium atmosphere around Europa. Nature 380, 229–231.

Brunetto, R., et al., 2005. Reflectance and transmittance spectra (2.2–2.4 μm) of ion irradiated frozen methanol. Icarus 175, 226–232.

Carlson, R.W., 1999. A tenuous carbon dioxide atmosphere on Jupiter's moon Callisto. Science 283, 820–821.

Carlson, R.W., 2001. Spatial distribution of carbon dioxide, hydrogen peroxide, and sulfuric acid on Europa. Bull. Am. Astron. Soc. 33, 1125.

Carlson, R.W., et al., 1999a. Hydrogen peroxide on the surface of Europa. Science 283, 2062–2064.

Carlson, R.W., Johnson, R.E., Anderson, M.S., 1999b. Sulfuric acid on Europa and the radiolytic sulfur cycle. Science 286, 97–99.

Carlson, R.W., et al., 2002. Sulfuric acid production on Europa: The radiolysis of sulfur in water ice. Icarus 157, 456–463.

Carlson, R.W., et al., 2005. Distribution of hydrated sulfuric acid on Europa. Icarus 177, 461–471.

Carr, M.H., Belton, M.J.S., Chapman, C.R., Davies, M.E.., Geissler, R., Greenberg, R., McEwen, A.S., Tufts, B.R., Greeley, R., Sullivan, R., Head, J.W., Pappalardo, R.T., Klaasen, K.P., Johnson, T.V., Kaufman, J., Senske, D., Moore, J., Neukum, G., Schubert, G., Burns, J.A., Thomas, P., Veverka, J., 1998. Evidence for a subsurface ocean on Europa. Nature 391, 363–365.

Cassidy, T., Johnson, R., Geissler, P., Leblanc, F., 2008. Simulation of Na D emission near Europa during eclipse. J. Geophys. Res. 113, doi: 10.1029/2007 JE002955.

Cassidy, T.A., Johnson, R.E., Tucker, O.J., 2009. Trace constituents of Europa's atmosphere. Icarus 201, 182–190.

Cheng, K.S., et al., 1986. Energetic radiation from rapidly spinning pulsars: 1. Outer magnetosphere gaps. Astrophys. J. 300, 500–521.

Christensen, P.R., et al., 2001. Mars Global Surveyor thermal emission spectrometer experiment: Investigation description and surface science results. J. Geophys. Res. 106, 23,823–23,871.

Chyba, C.F., Ostro, S.J., Edwards, B.C., 1998. Radar detectability of a subsurface ocean on Europa. Icarus 134, 292–302.

Clark, K., et al., 2007. Europa Explorer Mission Study: Final Report, JPL D-41283.

Clark, K., et al., 2008. Jupiter Europa Orbiter Mission Study 2008 Final Report, JPL D-48279.

Clark, R.N., McCord, T.B., 1980. The Galilean satellites: New near-infrared spectral reflectance measurements (0.65–25 μm) and a 0.325–5 μm summary. Icarus 41, 323–339.

Clark, R.N., Fanale, F., Zent, A., 1983. Frost grain size metamorphism: Implications for remote sensing of planetary surfaces. Icarus 56, 233–245.

Clark, R.N., et al., 2005. Compositional maps of Saturn's moon Phoebe from imaging spectroscopy. Nature 435, 66–69.

Collins, G., Nimmo, F., 2009. Chaotic terrain on Europa. In: Pappalardo, R.T., McKinnon, W.B., Khurana, K.K. (Eds.), Europa, U. Arizona Press, Tucson, 259–282.

Cooper, J.F., et al., 2001. Energetic ion and electron irradiation of the icy Galilean satellites. Icarus 149, 133–159.

Committee on Space Research, 2002. COSPAR Planetary Protection Policy, as amended March 2005). <http://www.cosparhq.org/scistr/PPPolicy.htm>.

Crowley, J.K., 1991. Visible and near-infrared (0.4–2.5μm) reflectance spectra of playa evaporite minerals. J. Geophys. Res. 96, 16,231–16,240.

Cruikshank, D.P., et al., 2007. Surface composition of Hyperion. Nature 448, 54–56.

Dalton, J.B., 2000. Constraints on the surface composition of Jupiter's moon Europa based on laboratory and spacecraft data. Ph.D. dissertation, Univ. of Colorado, Boulder.

Dalton, J.B., 2007a. Linear mixture modeling of Europa's non-ice material using cryogenic laboratory spectroscopy. Geophys. Res. Lett. 34, 21,205.

Dalton, J.B., 2007b. Modeling Europa's surface composition with cryogenic sulfate hydrates. LPI Contributions 1357, 36–37.

Dalton, J.B., Clark, R.N., 1998. Laboratory spectra of Europa candidate materials at cryogenic temperatures. Bull. Am. Astron. Soc. 30, 1081.

Dalton, J.B., Clark, R.N., 1999. Observational constraints on Europa's surface composition from Galileo NIMS data. Proc. Lunar Planet. Sci. Conf. XXX, 2064.

Dalton, J.B., Mogul, R., Kagawa, H., Chan, S., Jamieson, C., 2003. Near-infrared detection of potential evidence for microscopic organisms on Europa. Astrobiology 3, 505–529.

Dalton, J.B., et al., 2005. Spectral comparison of heavily hydrated salts to disrupted terrains on Europa. Icarus 177, 472–490.

Dawson, S., 1999, Office of Space Science Risk Communication Plan for Planetary and Deep Space Missions, JPL D-16993.

Delitsky, M.L., Lane, A.L., 1997. Chemical schemes for surface modification of icy satellites: A road map. J. Geophys. Res. 102, 16,385–16,390.

Delitsky, M.L., Lane, A.L., 1998. Ice chemistry on the Galilean satellites. J. Geophys. Res. 103, 31,391–31,403.

Doggett, T., Greeley, R., Figueredo, P., Tanaka, K., Weiser, S., 2009. Geologic stratigraphy and evolution of Europa's surface. In: Pappalardo, R.T., McKinnon, W.B., Khurana, K.K. (Eds.), Europa, U. Arizona Press, Tucson, 137–160.

Ehlmann, B., Mustard, J., Fassett, C., Schon, S., Head, J. III, Des Marais, D., Grant, J., Murchie, S., 2008. Clay minerals in delta deposits and organic preservation potential on Mars. Nature Geoscience 1, 355.

Eluszkiewicz, J., 2004. Dim prospects for radar detection of Europa's ocean. Icarus 170, 234–236.

Fanale, F.P., et al., 1999. Galileo's multi-instrument spectral view of Europa's surface composition. Icarus 139, 179–188.

Figueredo, P.H., Greely, R., 2004. Resurfacing history of Europa from pole-to-pole geological mapping. Icarus 167, 287–312.

Figueredo, P.H., Greeley, R., 2004. Resurfacing history of Europa from pole-to-pole geological mapping. Icarus 167, 287–312.

Gaidos, E., Nimmo, F., 2000. Tectonics and water on Europa. Nature 405, 637.

Geissler, P.E., Greenberg, R., Hoppa, G., McEwen, A., Tufts, R., Phillips, C., Clark, B., Ockert-Bell, M., Helfenstein, P., Burns, J., Veverka, J., Sullivan, R., Greeley, R., Pappalardo, R. T., Head, J. W., Belton, M. J. S., Denk, T., 1998. Evolution of lineaments on Europa: Clues from Galileo multispectral imaging observations. Icarus 135, 107–126, doi: 10.1006/icar.1998.5980.

Greeley, R., Chyba, C.F., Head, J.W. III, McCord, T.B., McKinnon, W.B., Pappalardo, R.T., Figueredo, P., 2004. Geology of Europa. In: Bagenal, F., Dowling, T.E., McKinnon, W.B. (Eds.), Jupiter: The Planet, Satellites, and Magnetosphere, Cambridge U. Press, Cambridge, U.K., 329–362.

Greenberg, R., G.V. Hoppa, B.R. Tufts, P. Geissler, J. Riley, and S. Kadel, 1999. Chaos on Europa. Icarus 141, 263–286.

Grundy, W., Buratti, B., Cheng, A., Emery, J., Lunsford, A., McKinnon, W., Moore, J., Newman, S., Olkin, C., Reuter, D., et al., 2007. New horizons mapping of Europa and Ganymede. Science 318, 234.

Hairston, A., Stobie, J., Tinkler, R., 2006. Advanced readout integrated circuit signal processing, Infrared Technology and Applications XXXII. Proc. SPIE. 6206, Part 2: 62062Z.

Hall, D.T., Strobel, D.F., Feldman, P.D., McGrath, M.A., Weaver, H.A., 1995. Detection of an oxygen atmosphere on Jupiter's moon Europa. Nature 373, 677–679.

Hall, D.T., Feldman, P.D., McGrath, M.A., Strobel, D.F., 1998. The far-ultraviolet oxygen airglow of Europa and Ganymede. Astrophys. J. 499, 475–481.

Hand, K.P., 2007. On the physics and chemistry of the ice shell and sub-surface ocean of Europa. Ph.D. dissertation, Stanford U.

Hansen, G., McCord, T.B., 2004. Amorphous and crystalline ice on the Galilean satellites: A balance between thermal and radiolytic processes. J. Geophys. Res. 109, doi: 10.1029/2003JE002149.

Hansen, G., McCord, T.B., 2008. Widespread CO_2 and other non-ice compounds on the anti-Jovian and trailing sides of Europa from Galileo/NIMS observations. Geophys. Res. Lett. 35, L01202.

Head, J.W., Pappalardo, R.T., 1999. Brine mobilization during lithospheric heating on Europa: Implications for formation of chaos terrain, lenticula texture, and color variations. J. Geophys. Res., Planets 104, 27143–27155.

Hoppa, G.V., et al. 1999. Formation of cycloidal features on Europa. Science 285, 1899–1902.

Hunt, G.R., Salisbury, J.W., Lenhoff, C.J., 1971a. Visible and near-infrared spectra of minerals and rocks. III. Oxides and hydroxides. Mod. Geol. 2, 195–205.

Hunt, G.R., Salisbury, J.W., Lenhoff, C.J., 1971b. Visible and near-infrared spectra of minerals and rocks. IV. Sulphides and sulphates. Mod. Geol. 3, 1–14.

Hussman, H., Spohn, T., 2004. Thermal-orbital evolution of Io and Europa. Icarus 171, 391–410.

Janesick, J., Elliott, T., Tower, J., 2008. CMOS detectors: Scientific monolithic CMOS imagers come of age. Laser Focus World 44:7, 68. <http://www.laserfocusworld.com/display_article/332970/12/none/none/Feat/CMOS-Detectors:-Scientificmonolithic-CMOS-imagers-come-of-ag>

Johnson, R.E., Quickenden, T.I., 1997. Radiolysis and photolysis of low-temperature ice. J. Geophys. Res. 102, 10,985–10,996.

Johnson, R.E., Killen, R.M., Waite, J.H., Lewis, W.S., 1998. Europa's surface composition and sputter-produced iono–sphere. Geophys. Res. Lett. 25, 3257–3260.

Johnson, R.E., Leblanc, F., Yakshinskiy, B.V., Madey, T.E., 2002. Energy distributions for desorption of sodium and potassium from ice: The Na/K ratio at Europa. Icarus 156, 136–142.

Johnson, R.E., R.W. Carlson, J.F. Cooper, C. Paranicas, M.H. Moore, and M. Wong 2004. Radiation effects on the surfaces of the galilean satellites. In: Bagenal, F., Dowling, T.E., McKinnon, W.B. (Eds.), Jupiter: The Planet, Satellites, and Magnetosphere, Cambridge U. Press, Cambridge, U.K., 485–512.

Jet Propulstion Laboratory, 2005. Risk Communication Plan for Planetary and Deep Space Missions, Rev. 2, JPL Rules! DocID 61272, August 30, 2005.

Jet Propulsion Laboratory, 2009. JPL Standard Flight Project Work Breakdown Structure Template, Rev. 5, JPL Rules! DocID 59533, March 18, 2009.

Jet Propulsion Laboratory, 2010a. Design, Verification/Validation and Ops Principles for Flight Systems (Design Principles), Rev. 4, JPL Rules! DocID 43913, September 20, 2010.

Jet Propulsion Laboratory, 2010b. Flight Project Practices, Rev. 8, JPL Rules! DocID 58032, October 6, 2010.

Jet Propulsion Laboratory, 2010c. Software Development (Requirement), Rev. 8, JPL Rules! DocID 23713, September 20, 2010.

Kargel, J., et al., 2000. Europa's Crust and Ocean: Origin, Composition, and the Prospects for Life, Icarus 148, no. 1: 226-265.

Kattenhorn, S.A., Hurford, T., 2009. Tectonics of Europa. In: Pappalardo, R.T., McKinnon, W.B., Khurana, K.K. (Eds.), Europa, U. Arizona Press, Tucson, 199–236.

Khurana, K.K., et al., 1998. Induced magnetic fields as evidence for subsurface oceans in Europa and Callisto. Nature 395, 777–780.

Klaasen, K., Clary, M., Janesick, J., 1984. Charge-coupled device television camera for NASA's Galileo mission to Jupiter. Optical Engineering 23, 334–342.

Kuiper, G.P., 1957. Infrared observations of planets and satellites. Astro. J. 62, 295.

Kwok, J., Prockter, L., Senske, D., Jones, C., 2007. Jupiter System Observer Mission Study: Final Report, JPL D-41284.

Lane, A.L., et al., 1981. Evidence for sulphur implantation in Europa's UV absorption band. Nature 292, 38–39.

Leblanc, F., Johnson, R.E., Brown, M.E., 2002. Europa's sodium atmosphere: An ocean source? Icarus 159, 132–144.

Leblanc, F., et al., 2005. Origins of Europa Na cloud and torus. Icarus 178, 367–385.

Lee, S., Pappalardo, R.T., Makris, N.C., 2005. Mechanics of tidally driven fractures in Europa's ice shell. Icarus 177, 367–379.

Lock, R., 2008. EJSM Europa Orbiter Science Scenarios (presentation slides). Outer Planets Flagship Mission Instrument Workshop, June 3, 2008.

Lock, R., 2010. Concept of Operations (presentation slides), Jupiter Europa Orbiter Internal Mission Concept Review, June 7–9, 2010.

Lockheed Martin, 2011. ASRG User Interface Control Document. Lockheed Martin Contract No. DE-AC07-00SF22191, Specification #912IC002085, Rev. A, June 2011.

Ludwinski, J., 1997. Galileo Mission Planning Office Closeout (Lessons Learned), JPL IOM 311.1/98/01, January 19, 1997.

Ludwinski, J., 1997. Galileo Mission Planning Office Closeout (Lessons Learned), JPL IOM 311.1/98/01, January 19, 1997.

McCord, T.B., 2000. Surface composition reveals icy Galilean satellites' past. Eos Trans. Am. Geophys. Union 81, 209.

McCord, T.B., et al., 1997. Organics and other molecules in the surfaces of Callisto and Ganymede. Science 278, 271–275.

McCord, T.B., et al., 1998a. Salts on Europa's surface detected by Galileo's near infrared mapping spectrometer. Science 280, 1242.

McCord, T.B., et al., 1998b. Non-water-ice constituents in the surface material of the icy Galilean satellites from the Galileo near-infrared mapping spectrometer investigation. J. Geophys. Res. 103, 8603–8626.

McCord, T.B., et al., 1999. Hydrated salt minerals on Europa's surface from the Galileo near-infrared mapping spectrometer (NIMS) investigation. J. Geophys. Res. 104, 11,827–11,851.

McCord, T.B., Hansen, G.B., Hibbitts, C.A., 2001a. Hydrated salt minerals on Ganymede's surface: Evidence of an ocean below. Science 292, 1523–1525.

McCord, T.B., et al., 2001b. Thermal and radiation stability of the hydrated salt minerals epsomite, mirabilite, and natron under Europa environmental conditions. J. Geophys. Res. 106, 3311–3320.

McCord, T.B., et al., 2002. Brines exposed to Europa surface conditions. J. Geophys. Res. 107, 4-1–4-6.

McKinnon, W.B., 2005. Radar sounding of convecting ice shells in the presence of convection: Application to Europa, Ganymede, and Callisto. LPI Workshop on Radar Investigations of Planetary and Terrestrial Environments, Feb. 7–10, 2005, Houston, Texas, abstract no. 6039.

McKinnon, W.B., Zolensky, M.E., 2003. Sulfate content of Europa's ocean and shell: Evolutionary considerations and some geological and astrobiological implications. Astrobiology 3, 879–897.

Moersch, J., Bell, J. III, Carter, L., Hayward, T., Nicholson, P., Squyres, S., Van Cleve, J., 1997. What happened to Cerberus? Telescopically observed thermophysical properties of the Martian surface. Mars Telescopic Observations Workshop II, Lunar and Planetary Science Technical Report 97-03, 26.

Moore, J.M., 2000. Models of radar absorption in Europan ice. Icarus 147, 292–300.

Moore, J.M., et al. 2001. Impact features on Europa: Results of the Galileo Europa Mission (GEM). Icarus 151, 93–111.

Moore, J.M., Black, G., Buratti, B., Phillips, C.B., Spencer, J., Sullivan, R., 2009. Surface properties, regolith, and landscape degradation. In: Pappalardo, R.T., McKinnon, W.B., Khurana, K.K. (Eds.), Europa, U. Arizona Press, Tucson, 329–352.

Moore, M.H., 1984. Studies of proton-irradiated SO_2 at low-temperatures—Implications for Io. Icarus 59, 114–128.

Moore, M.H., Hudson, R. L., 1998. Infrared study of ion-irradiated water-ice mixtures with hydrocarbons relevant to comets. Icarus 135, 518–527.

Moore, M.H., Hudson, R.L., Ferrante, R.F., 2003. Radiation products in processed ices relevant to Edgeworth-Kuiper-belt objects. Earth Moon Planets 92, 291–306.

Moore, W.B., Hussmann, H., 2009. Thermal evolution of Europa's silicate interior. In: Pappalardo, R.T., McKinnon, W.B., Khurana, K.K. (Eds.), Europa, U. Arizona Press, Tucson, 369–380.

Moroz, V.I., 1965. Infrared spectrophotometry of the Moon and the Galilean satellites of Jupiter. Soviet Astro. 9, 999.

Mustard, J., Murchie, S. Pelkey, S. Ehlmann, B. Milliken, R. Grant, J. Bibring, J. Poulet, F. Bishop, J. Dobrea, E., et al., 2008. Hydrated silicate minerals on Mars observed by the Mars Reconnaissance Orbiter CRISM instrument. Nature 454, 305.

NASA, 2005. Planetary Protection Provisions for Robotic Extraterrestrial Missions. NASA Procedural Requirements (NPR) 8020.12C. NASA, Washington, DC.

NASA, 2007. NASA Program and Project Management Processes and Requirements, NASA Procedural Requirements (NPR) 7120.5D, March 6, 2007. NASA, Washington, DC.

NASA, 2009a. NASA Emergency Preparedness Plan Procedural Requirement, NPR 8715.2, January 9, 2009. NASA, Washington, DC.

NASA, 2009b. NASA Software Engineering Requirements, NPR 7150.2, November 19, 2009. NASA, Washington, DC.

NASA, 2009c. New Frontiers 2009 Announcement of Opportunity, NNH09ZDA007O, April 20, 2009.

NASA, 2010a. Discovery 2010 Announcement of Opportunity, NNH10ZDA007O, June 7, 2010.

NASA, 2010b. NASA Emergency Preparedness Plan Procedural Requirement, NPR 8715.3, December 16, 2010. NASA, Washington, DC.

NASA, 2011. Europa Study Statement of Work, October 4, 2011. NASA, Washington, DC.

NASA, 2012. NASA Program and Project Management Processes and Requirements, NPR 7120.5E, (anticipated) June 2012. NASA, Washington, DC.

Nimmo, F., Giese, B., Pappalardo, R.T., 2003. Estimates of Europa's ice shell thickness from elastically supported topography. Geophys. Res. Lett. 30, 1233.

Noll, K.S., Weaver, H.A., Gonnella, A.M., 1995. The albedo spectrum of Europa from 2200 to 3300. J. Geophys. Res. 100, 19,057–19,060.

Orlando, T.M., et al., 2005. The chemical nature of Europa surface material and the relation to a sub-surface ocean. Icarus 177, 528–533.

Paczkowski, B., et al., 2008. Outer Planets Flagship Mission Science Operations Concept Study Report, JPL D–46870. June 2008.

Pappalardo, R.T., Barr, A.C., 2004. Origin of domes on Europa: The role of thermally induced compositional buoyancy. Geophys. Res. Lett. 31, L01701.

Pappalardo, R.T., et al. 1998. Geological evidence for solid-state convection in Europa's ice shell. Nature 391, 365.

Pappalardo, R.T., et al. 1999. Does Europa have a subsurface ocean? Evaluation of the geological evidence. J. Geophys. Res. 104, 24,015–24,056.

Paranicas, C., Mauk, B., Ratliff, J., Cohen, C., Johnson, R., 2002. The ion environment near Europa and its role in surface energetics. Geophys. Res. Lett. 29, 18–1.

Paranicas, C., Cooper, J.F., Garrett, H.B., Johnson, R.E., Sturner, S.J., 2009. Europa's radiation environment and its effects on the surface. In: Pappalardo, R.T., McKinnon, W.B., Khurana, K.K. (Eds.), Europa, U. Arizona Press, Tucson, 529–544.

Parish, A., 1989. Development of algorithms for on-focal plane gamma circumvention and time delay integration. Twenty-Third Asilomar Conference on Signals, Systems, and Computers.

Park, R.S., et al., 2011. Detecting tides and gravity at Europa from multiple close flybys. Geophys. Res. Lett. 38, L24202.

Pilcher, C.B., Ridgway, S.T., McCord, T.B., 1972. Galilean satellites. J. Geophys. Res. 103, 31,391–31,403.

Presidential Directive/National Security Council Memorandum #25 (PD/NSC-25), Scientific or Technological Experiments with Possible Large-Scale Adverse Environmental Effects and Launch of Nuclear Systems into Space, December 14, 1977.

Prockter, L.M., Pappalardo, R.J., 2000. Folds on Europa: Implications for crustal cycling and accommodation of extension. Science 289, 941–943.

Prockter, L.M., Schenk, P., 2005. Origin and evolution of Castalia Macula, an anomalous young depression on Europa, Icarus, 177, no. 2: 305-326

Prockter, L.M., Patterson, G.W., 2009. Morphology and evolution of Europa's ridges and bands. In: Pappalardo, R.T., McKinnon, W.B., Khurana, K.K. (Eds.), Europa, U. Arizona Press, Tucson, 237–258.

Prockter, L.M., Head, J.W., Pappalardo, R.T., Sullivan, R.J., Clifton, A.E., Giese, B., Wagner, R., Neukum, G., 2002. Morphology of Europan bands at high resolution: A mid-ocean ridge-type rift mechanism, J. Geophys. Res. 107, 4-1–4-28. doi:10.1029/2000JE001458.

Rasmussen, R., 2009. System architecture for JEO (presentation slides), EJSM Instrument Workshop, July 15–17, 2009.

Riley, J., Hoppa, G.V., Greenberg, R. Tufts, B.R., Geissler, P., 2000. Distribution of chaotic terrain on Europa. J. Geophys. Res. 105, 22,599–22,616.

Sarid, A.R., Greenberg, R., Hoppa, G.V., Hurford, T.A., Tufts, B.R., Geissler, P., 2002. Polar wander and surface convergence of Europa's ice shell: Evidence from a survey of strike-slip displacement. Icarus 158, 24–41.

Schenk, P., Pappalardo, R., 2004. Topographic variations in chaos on Europa: Implications for diapiric formation. Geophys. Res. Lett. 31, L16703 1–5.

Schenk, P.M., Turtle, E.P., 2009. Europa's impact craters: Probes of the icy shell. In: Pappalardo, R.T., McKinnon, W.B., Khurana, K.K. (Eds.), Europa, U. Arizona Press, Tucson, 181–198.

Schenk, P.M., Chapman, C.R., Zahnle, K., Moore, J.M., 2004. Ages and interiors: The cratering record of the Galilean satellites. In: Bagenal, F., Dowling, T.E., McKinnon, W.B. (Eds.), Jupiter: The Planet, Satellites, and Magnetosphere, Cambridge U. Press, Cambridge, U.K., 427–457.

Schmidt, B.E., Blankenship, D.D., Patterson, G.W., Schenk, P.M., 2011. Active formation of ''chaos terrain'' over shallow subsurface water on Europa. Nature 479, 502–505.

Shirley, J.H., Dalton, J.B. III, Prockter, L.M., Kamp, L.W., 2010. Europa's ridged plains and smooth low albedo plains: Distinctive compositions and compositional gradients at the leading side–trailing side boundary. Icarus 210, 358–384.

Smyth, W.H., Marconi, M.L., 2006. Europa's atmosphere, gas tori, and magnetospheric implications. Icarus 181, 510–526.

Smythe, W.D., et al. 1998. Galileo NIMS measurements of the absorption bands at 4.03 and 4.25 microns in distant observations of Europa. Amer. Astronom. Soc. 30, 1448.

Space Studies Board, 2000. Preventing the Forward-Contamination of Europa. National Academy Press, Washington, DC.

Space Studies Board, 2003. New Frontiers in the Solar System: An Integrated Exploration Strategy 2003–2013. The National Academies Press, Washington, DC.

Space Studies Board, 2011. Visions and Voyages for Planetary Science in the Decade 2013–2022. The National Academies Press, Washington, DC.

Spaun, N.A., Head, J.W., Collins, G.C., Prockter, L.M., Pappalardo, R. T., 1998. Conamara Chaos Region, Europa: Reconstruction of mobile polygonal ice blocks. Geophys. Res. Lett. 25, 4277–4280.

Spencer, J.R., Calvin, W.M., 2002. Condensed O_2 on Europa and Callisto. Astron. J. 124, 3400–3403.

Spencer, J.R., et al., 2005. Mid-infrared detection of large longitudinal asymmetries in Io's SO_2 atmosphere. Icarus 176, 283–304.

Spencer, J.R., Pearl, J.C., Segura, M., Flasar, F.M., Mamoutkine, A., Romani, P., Buratti, B.J., Hendrix, A.R., Spilker, L.J., Lopes, R.M.C., 2006. Cassini encounters Enceladus: Background and the discovery of a south polar hot spot. Science 311, 1401–1405.

Sullivan, R., Greeley, R., Homan, K., Klemaszewski, J., Belton, M.J.S, Carr, M.H., Chapman, C.R., Tufts, R., Head, J.W. III, Pappalardo, R., Moore, J., Thomas, P., and the Galileo Imaging Team, 1998. Episodic plate separation and fracture infill on the surface of Europa. Nature 391, 371–373.

Sullivan, R., Moore, J., Pappalardo, R., 1999. Mass-wasting and slope evolution on Europa, Lunar Planet. Sci. 30, Abstract #1747, Lunar and Planetary Institute, Houston (CD-ROM).

Tufts, B.R., Greenberg, R., Hoppa, G., Geissler, P., 2000. Lithospheric dilation on Europa. Icarus 146, 75–97.

Volwerk, M., et al. 2001. Wave activity in Europa's wake: Implications for ion pickup. J. Geophys. Res. 106, 26,033–26,048.

Willis, P.B., 2011. Materials Survivability and Selection for Nuclear Powered Missions. JPL D-34098.

Yan, T.-Y., 2007. Risk Mitigation Plan: Radiation and Planetary Protection. JPL D-47928.

Zahnle, K., Dones, L., Levison, H.F., 1998. Cratering rates in the Galilean satellites. Icarus 136, 202–222.

Zahnle, K., Schenk, P., Levison, H., Dones, L., 2003. Cratering rates in the outer solar system. Icarus 163, 263–289.

Zolotov, M.Y., Kargel, J.S., 2009. On the chemical composition of Europa's icy shell, ocean, and underlying rocks. In: Pappalardo, R.T., McKinnon, W.B., Khurana, K.K. (Eds.), Europa, U. Arizona Press, Tucson, 431–458.

Zombeck, M.V, 1982. Handbook of Space Astronomy and Astrophysics. Cambridge U. Press, Cambridge, U.K.

C.4.2   Acronyms and Abbreviations

ΔV	delta velocity, delta-V
3D	three-dimensional
A	ampere
A	approach
A/D	analog to digital
ABSL	ABSL Power Solutions Ltd. used to be AEA Battery Systems, Ltd., where AEA stood for Atomic Energy Authority (a privatized branch of the U.K. AEA)
AC	alternating current
ACS	Attitude Control Subsystem
ACU	ASRG controller unit
ADC	analog-to-digital converter
AFT	allowable flight temperature
Ah	ampere-hour
AO	Announcement of Opportunity
APL	Applied Physics Laboratory
APML	Approved Parts and Materials List
APS	active pixel sensor
ASC	Advanced Stirling converter
ASIC	application-specific integrated circuit
ASRG	Advanced Stirling Radioisotope Generator
ATK/PSI	
ATLO	assembly, test, and launch operations
B	baseline
BIU	bus interface unit
BOM	beginning of mission

BTE	bench-test equipment
C&DH	Command and Data Handling Subsystem
C_3	injection energy per unit mass (V∞2), km2/s2 (also C3)
CAD	computer-aided design
CADRe	Cost Analysis Data Requirement
CATE	Cost and Technical Evaluation
CBE	current best estimate
CCD	charge-coupled device
CCSDS	Consultative Committee for Space Data Systems
CDR	Critical Design Review
CEM	channel electron multiplier
CFDP	CCSDS File Delivery Protocol
CG	center of gravity
CM	center of mass
CMMI	Capability Maturity Model Integration
CMOS	complementary metal-oxide semiconductor
COSPAR	Committee on Space Research
COT	crank over the top
CPT	comprehensive performance test
CRAM	chalcogenide random-access memory
CRISM	Compact Reconnaissance Imaging Spectrometer for Mars
CU	cleanup

DC	direct current		ETL	Export Technical Liaison
DC/DC	direct current to direct current		EVEE	Earth-Venus-Earth-Earth
DD	displacement damage		FMECA	failure modes, effects, and criticality analysis
DDD	displacement damage dose		FO	Foldout
DHMR	dry-heat microbial reduction		FOV	field of view
DOD	depth of discharge		FPPs	Flight Project Practices
DOE	Department of Energy		FS	flight system
DPs	Design Principles		FSW	flight software
DSM	deep-space maneuver		FSWTB	flight software testbed
DSN	Deep Space Network		FWHM	full width at half maximum
DTM	developmental test model		G/T	gain to equivalent noise temperature
DWG	Detector Working Group		GDS	Ground Data System
EEE	electrical, electronic, and electromechanical		GHA	generator housing assembly
EFM	Europa Multiple-Flyby Mission		GM	product of gravitational constant and mass
EGA	Earth gravity assist		GN&C	guidance, navigation, and control
EHS	electrical heater source		GPHS	General-Purpose Heat Source
EIRP	effective isotropic radiated power		GRAIL	Gravity Recovery and Interior Laboratory
EIS	Environmental Impact Statement		GSE	ground-support equipment
EJSM	Europa Jupiter System Mission		H/W	hardware
ELDRS	enhanced low-dose-rate sensitivity		HCIPE	High-Capability Instrument for Planetary Exploration
EM	engineering model		HEPA	high-efficiency particulate air
EMI	electromagnetic interference		HGA	high-gain antenna
EOI	Europa Orbit Insertion		HQ	NASA Headquarters
EOM	end of mission		HY	RF hybrid
ES	Europa Study		I&T	integration and test
ESA	European Space Agency		I/O	input/output
ESD	electrostatic discharge		IC	internal charging

ICD	Interface Control Document	MARSIS	Mars Advanced Radar for Subsurface and Ionosphere Sounding
ICE	Independent Cost Estimate	MCP	microchannel plate
ICM	Institutional Cost Model	MCR	Mission Concept Review
ID	identification/identifier	MDIS	Mercury Dual Imaging System
ID	inner diameter	MDR	Mission Definition Review
IFOV	instantaneous field of view	MEL	Master Equipment List
IMU	inertial measurement unit	MER	Mars Exploration Rover
INMS	Ion and Neutral Mass Spectrometer	MESSENGER	Mercury Surface, Space Environment, Geochemistry, and Ranging
IOM	interoffice memorandum		
IPR	Ice-Penetrating Radar	MEV	maximum expected value
IR	infrared	MGA	medium-gain antenna
ITAR	International Traffic in Arms Regulations	MLI	multilayer insulation
		MMM	Moon Mineralogy Mapper
I-V	current-voltage	MMRTG	multimission radioisotope thermoelectric generator
JEO	Jupiter Europa Orbiter		
JOI	Jupiter Orbit Insertion	MOLA	Mars Orbiter Laser Altimeter
JPL	Jet Propulsion Laboratory	MPSS	multimission power switch slice
K&D	key and driving		
KSC	Kennedy Space Center	MRO	Mars Reconnaissance Orbiter
L1, L2	Level-1, Level-2, etc.	MSL	Mars Science Laboratory
LAEP	Launch Approval Engineering Plan	MSTB	Mission System Testbed
		MTIB	minimum torque impulse bit
LAT	limited angle torque	MVIC	Multispectral Visible Imaging Camera
LCE	launch control equipment		
LEV	lowest expected value	NASA	National Aeronautics and Space Administration
LGA	low-gain antenna		
LORRI	Long-Range Reconnaissance Imager	NEPA	National Environmental Policy Act
LST	local solar time	NICM	NASA Instrument Cost Model
LVA	launch vehicle adapter		
M3	Moon Mineralogy Mapper	NIMS	Near-Infrared Mapping Spectrometer
MARCI	Mars Color Imager		

NLS	NASA Launch Services		PoL	point of load
NLSA	Nuclear Launch Safety Approval		PRA	probablilistic risk assessment
NR	nonresonant, nonres		PRA	Project Resource Analyst
NSI	NASA Standard Initiator		PRICE-H	Parametric Review of Information for Costing and Evaluation—Hardware
NTO	nitrogen tetroxide			
O&C	operations and checkout		PSA	Project Schedule Analyst
OD	orbit determination		RAD750	radiation-hardened microprocessor
OPAG	Outer Planets Assessment Group		RAM	random-access memory
ORT	operations readiness test		RCS	Reaction-Control Subsystem
OSTP	Office of Science and Technology Policy		RDE	Real-Time Development Environment
OTS	off the shelf		RDF	radiation design factor
P	preliminary		RF	radio frequency
P/L	payload		RHU	radioisotope heater unit
P/N	part number		R_J	Jovian radii
PBC	power bus controller		ROD	Record of Decision
PCA	pressurant-control assembly		ROIC	readout integrated circuit
PCU	power converter unit		ROSINA	Rosetta Orbiter Spectrometer for Ion and Neutral Analysis
PDE	propulsion drive electronics			
PDR	Preliminary Design Review		RS	Radio Subsystem
PEL	Power Equipment List		RTG	radioisotope thermoelectric generator
PFC	pyro-firing card			
PHSF	Payload Hazardous Service Facility		RTOF	reflectron time-of-flight
			RWA	reaction wheel assembly (wheel and housing)
PI	Principal Investigator			
PIA	propellant-isolation assembly		RWE	reaction wheel electronics (same as WDE)
PIP	Project Information Package			
PJR	perijove raise maneuver		S/N	signal-to-noise ratio
PMD	propellant-management device		S/S	steady state
			SAF	Spacecraft Assembly Facility
PMSR	Project Mission System Review		SAR	Safety Analysis Report
			SDS	shunt driver slice
			SDST	small deep-space transponder

SDT	Science Definition Team		TCM	trajectory correction maneuver
SDU	shunt dissipater unit		TDP	Technical Data Package
SEE	single-event effect		TI	Topographical Imager
SEER	System Evaluation and Estimation of Resources		TID	total ionizing dose
SEL	single-event latchup		TOF	time of flight
SEMP	Systems Engineering Management Plan		TRL	technology readiness level
SER	Safety Evaluation Report		TVC	thrust vector control
set point			TWTA	traveling-wave tube amplifier
SEU	single-event upset		U	update
SHARAD	Shallow Radar		UES	Upper Equipment Section
SMAP	Soil Moisture Active Passive		V	volt, velocity, vector
SNR	signal-to-noise ratio		V&V	verification and validation
SQRT	mean radiation signal per pixel		VEE	Venus-Earth-Earth
SRAM	static random-access memory		VEEGA	Venus-Earth-Earth gravity assist
SRR	System Requirements Review		VIMS	Visual and Infrared Mapping Spectrometer
SRU	stellar reference unit		VRHU	variable radioisotope heating unit
SS	subsystem		W	watts
SSE	spacecraft support equipment		W_e	watts electrical
SSI	solid-state imager		W_t	watts thermal
SSPA	solid-state power amplifier		WBS	work breakdown structure
SSR	solid-state recorder		WDE	Wheel drive electronics (same as RWE)
STV	solar thermal-vacuum		WSTS	workstation testset
SWIRS	Shortwave Infrared Spectrometer		WTS	waveguide transfer switch
SysML	Systems Modeling Language			
TAYF	test as you fly			
TB	testbed			
TCA	thruster cluster assembly			

C.4.3   *Master Equipment List*

Master Equipment List (MEL) removed for compliance with export-control (ITAR) regulations. Available upon request.

C.4.4   Aerospace Corporation Independent Cost Estimate

AEROSPACE REPORT NO.
ATR-2012(5583)-4

Europa Habitability Mission: Flyby Concept
CATE: Cost and Technical Evaluation

April 24, 2012

Randy Persinger[1], Robert Kellogg[2], Mark Barrera[3]
[1]Advanced Studies and Analysis Directorate, NASA Programs Division
[2]Space Architecture Department, Systems Engineering Division
[3]Vehicle Concepts Department, Systems Engineering Division

Prepared for:

Jet Propulsion Laboratory
4800 Oak Grove Drive
Pasadena, CA 91109

Contract No. 1393581

Authorized by: Civil and Commercial Operations

PUBLIC RELEASE IS AUTHORIZED.

AEROSPACE
Assuring Space Mission Success

Europa Habitability Mission: Flyby Concept
CATE: Cost and Technical Evaluation

April 24, 2012

Randy Persinger[1], Robert Kellogg[2], Mark Barrera[3]
[1]Advanced Studies and Analysis Directorate, NASA Programs Division
[2]Space Architecture Department, Systems Engineering Division
[3]Vehicle Concepts Department, Systems Engineering Division

Prepared for:

Jet Propulsion Laboratory
4800 Oak Grove Drive
Pasadena, CA 91109

Contract No. 1393581

Authorized by: Civil and Commercial Operations

PUBLIC RELEASE IS AUTHORIZED.

Europa Habitability Mission: Flyby Concept
CATE: Cost and Technical Evaluation

April 24, 2012

Randy Persinger[1], Robert Kellogg[2], Mark Barrera[3]
[1]Advanced Studies and Analysis Directorate, NASA Programs Division
[2]Space Architecture Department, Systems Engineering Division
[3]Vehicle Concepts Department, Systems Engineering Division

Prepared for:

Jet Propulsion Laboratory
4800 Oak Grove Drive
Pasadena, CA 91109

Contract No. 1393581

Authorized by: Civil and Commercial Operations

AEROSPACE
Assuring Space Mission Success

Europa Habitability Mission: Flyby Concept
CATE: Cost and Technical Evaluation

Approved by:

Matthew J. Hart, Principal Director
Advanced Studies and Analysis Directorate
Ground Enterprise
NASA Programs Division
Civil and Commercial Operations

SL0084(1, 4320, 31, GN)

ii

Acknowledgments

The following individuals are recognized for their contributions as authors, reviewers, and editors of the Cost and Technical Evaluation (CATE) for the Europa Habitability Mission: Flyby concept.

David Bearden
Ray Nakagawa
Anh Tu
Mark Cowdin
Gary North

iii

iv

Contents

v

Figures

Tables

1. Purpose

The Aerospace Corporation was tasked in November 2011 to participate as an independent party to review three separate, but related, Europa Habitability Mission (EHM) concepts under study by the Jet Propulsion Laboratory (JPL) to visit Europa in the continuing search for life in our solar system. The three concepts were being studied by JPL in the context of guidance provided by the National Research Council (NRC) Planetary Decadal Survey report released to the public in March 2011. In this report, a mission to the Jupiter/Europa system was rated very high with regard to science importance to the United States in the next decade. However, based on the expected high cost of the baseline reference mission evaluated by the NRC Planetary Decadal Steering Committee, the guidance was to descope the reference mission and significantly reduce mission cost while providing sufficient scientific investigation capability considered to be of paramount importance over the next decade. Aerospace, having participated as the NRC Cost and Technical Evaluation (CATE) contractor in the cost, technical, and schedule risk assessment of the planetary concepts evaluated by the Planetary Steering Committee, was a logical choice to independently evaluate the three updated EHM concepts with the same CATE techniques and processes. The three separate EHM mission concepts evaluated were: Orbiter, Flyby, and Lander. This report presents the cost, technical, and schedule risk assessment for the **EHM Flyby Mission** using the CATE process originally established by the NRC.

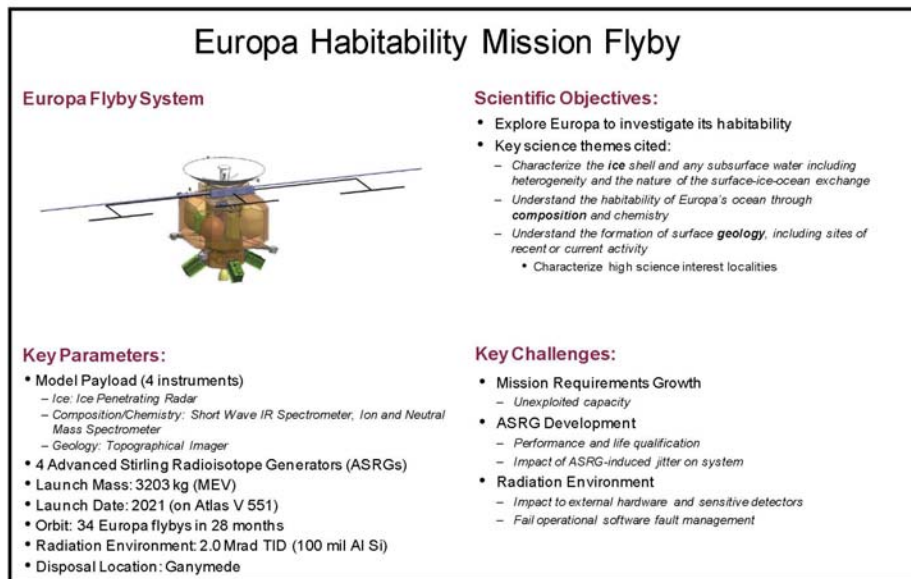The key parameters of the EHM Flyby Mission can be found in Figure 1.

Europa Habitability Mission Flyby

Europa Flyby System

Scientific Objectives:
- Explore Europa to investigate its habitability
- Key science themes cited:
  - Characterize the *ice* shell and any subsurface water including heterogeneity and the nature of the surface-ice-ocean exchange
  - Understand the habitability of Europa's ocean through *composition* and chemistry
  - Understand the formation of surface *geology*, including sites of recent or current activity
    - Characterize high science interest localities

Key Parameters:
- Model Payload (4 instruments)
  - Ice: Ice Penetrating Radar
  - Composition/Chemistry: Short Wave IR Spectrometer, Ion and Neutral Mass Spectrometer
  - Geology: Topographical Imager
- 4 Advanced Stirling Radioisotope Generators (ASRGs)
- Launch Mass: 3203 kg (MEV)
- Launch Date: 2021 (on Atlas V 551)
- Orbit: 34 Europa flybys in 28 months
- Radiation Environment: 2.0 Mrad TID (100 mil Al Si)
- Disposal Location: Ganymede

Key Challenges:
- Mission Requirements Growth
  - Unexploited capacity
- ASRG Development
  - Performance and life qualification
  - Impact of ASRG-induced jitter on system
- Radiation Environment
  - Impact to external hardware and sensitive detectors
  - Fail operational software fault management

Figure 1.   EHM Flyby Mission Concept Overview

1

2

2. Executive Summary

The EHM Flyby concept was found to have a Medium-Low technical risk and is well designed for a flyby mission to Europa. Mass and power margins are robust, and the design incorporates modularity with well-defined interfaces. Technology development is mainly related to engineering implementation; however, concern does exist with the technology development of the radioisotope power source (ASRGs) currently under development by NASA. The impact of radiation for this mission is also a concern but has been mitigated by compartmentalization and modular design as well as the mission design.

The CATE cost estimate for the EHM Flyby concept is $2.1B in FY15 dollars excluding launch services. The EHM Flyby CATE, excluding launch services, is compared to the Project's cost estimate in Figure 2. Including a launch service cost of $272M, consistent with CATE estimates for the Planetary Decadal Survey Steering Committee, the CATE estimate including launch services is $2.4B. The cost estimate for four ASRGs is assumed to be $200M based on guidance provided by NASA. The cost risk associated with the ASRG technology development required for the EHM mission concepts has not been included in the CATE cost estimate, nor have the associated schedule risk to the project and technical risk to the flight system.

The project schedule of 73 months is considered to be realistic, with the independent estimate being 75 months. The concept's use of modularity provides the opportunity to focus and minimize risk through parallel development paths.
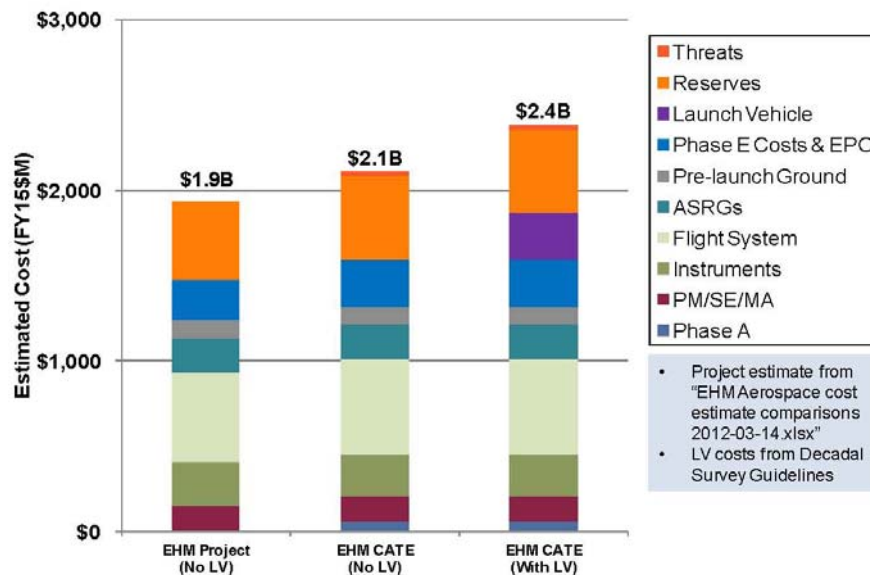

Figure 2.   Europa Flyby Cost Estimates

3

4

3. CATE Background

The NRC Astro2010 Decadal Survey Steering Committee established the CATE process in June 2009. The CATE process was then used for three NRC Decadal Surveys: Astro2010, Planetary, and Heliophysics. Previous NRC Decadal Surveys had underestimated the costs associated with the recommended science priorities. The NRC and others recognized that mission costs were being underestimated, so the U.S. Congress mandated that an independent contractor be utilized to provide more realistic cost, technical, and schedule risk assessment directly to the decadal steering committees for consideration and evaluation in executing their charter. Select portions of the Planetary Decadal report, *Vision and Voyages,* from Appendix C are provided below to summarize the CATE process. It is important to note that the CATE process is intended to inform future NASA Science Mission Directorate (SMD) budget decisions, not to decide if a specific concept meets a cost target or to decide if a specific mission concept should be selected for flight versus another mission. Because the CATE process is used for future budgetary decisions, it incorporates potential cost threats that may occur in the future based on concept maturity at the time of evaluation.

The CATE process focuses on cost and schedule risk assessment, but limited technical evaluation is also required to categorize concept maturity, technology development, and the potential impact that insufficient margins and contingency (mass and power) may have on schedule or cost.

Vision and Voyages, Planetary Decadal Report, Appendix C: The objective of the CATE process is to perform a cost and technical risk analysis for a set of concepts that may have a broad range of maturity, and to ensure that the analysis is consistent, fair, and informed by historical data. Typically, a concept evaluated using the CATE process is early in its life cycle and therefore likely to undergo significant subsequent design changes. Historically, such changes have resulted in cost growth. Therefore, a robust process is required that fairly treats a concept of low maturity relative to one that has undergone several iterations and review. CATEs take into account several components of risk assessment.

The primary goal of the CATE cost appraisal is to provide independent estimates (in fiscal year [FY] 2015 dollars) that can be used to prioritize various concepts within the context of the expected NASA budgetary constraints for the coming decade. ... To be consistent for all concepts, the CATE cost process allows an increase in cost resulting from increased contingency mass and power, increased schedule, increased required launch vehicle capability, and other cost threats depending on the concept maturity and specific risk assessment of a particular concept. ... All cost appraisals for the CATE process are probabilistic in nature and are based on the NASA historical record and documented project life-cycle growth studies.

The evaluation of technical risk and maturity in the CATE process focuses on the identification of the technical risks most important to achieving the required mission performance and stated science objectives. The assessment is limited to top-level technical maturity and risk discussions. Deviations from the current state of the art as well as system complexity, operational complexity, and integration concerns associated with the use of heritage components are identified. Technical maturity and the need for specific technology development, including readiness levels of key technologies and hardware, are evaluated. ... The CATE technical evaluation is limited to high-level technical risks that potentially impact schedule and cost. The CATE process places no cost cap on mission concepts, and hence risk as a function of cost is not considered. Concept maturity and technical risk are evaluated in terms of the ability of a concept to meet performance goals within proposed launch dates with adequate mass, power, and performance margins.

To aid in the assessment of concept risk, independent schedule estimates are incorporated as part of the CATE cost estimate.

5

6

4. Technical Evaluation

The EHM Flyby technical risk rating is Medium-Low. The mission will require medium new development, mostly in the engineering implementation. Radioisotope, or ASRG, power source qualification, radiation mitigation for external hardware, and software fault management will be some of the key challenges associated with this mission. Mass margins are high, with an average mass contingency of 63% for the bus and 88% for the instruments. Power margins and battery depth of discharge are adequate assuming four ASRGs. The concept design is within the capability of the Atlas V 551, 541, and 531 launch vehicles with greater than 10% launch mass margin. The radiation environment contributes to Medium-Low operational risk. The proposed "fail operational" approach to fault management of radiation upsets also contributes to this risk, although adequate time is available to address faults between flybys.

The top technical risks associated with the EHM Flyby Mission are:

1. **Mission Requirements Growth** to utilize additional capacity
2. **Advanced Stirling Radioisotope Generator (ASRGs)** development impact
3. Survival of flight system in **Radiation Environment**

These top risks are discussed below. Figure 3 illustrates some key aspects of the EHM Flyby concept.
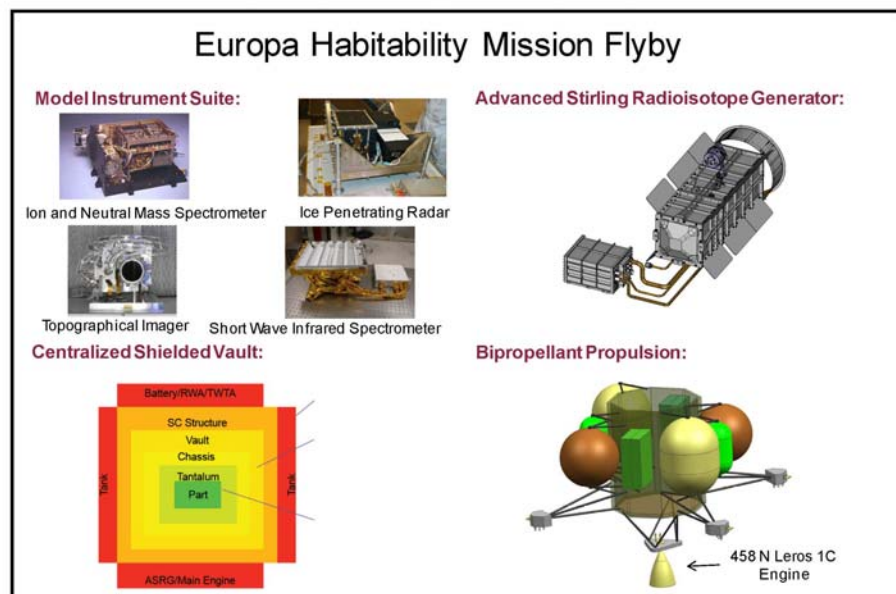

Figure 3.   EHM Flyby Mission Concept Features

Mission Requirements Growth

The anticipated high mass margins for the EHM Flyby mission have the benefit of mitigating the risk of unplanned mass growth however, they also offer a temptation to increase the science payload from the current focused concept, which may impact the overall complexity and cost of the mission. As

7

illustrated in Figure 4, the proposed concept has a launch mass margin of greater than 10% on Atlas V 531 and above. This margin already considers the best-estimate mass as well as an average 63% mass growth contingency for the bus and 88% mass growth contingency for the instruments. Since the mass margins are high, there is a concern that instrument providers may wish to utilize excess capacity. There is a concern that competitively chosen instruments may have higher mass or complexity than the model instruments for the EHM concept. Also, there is a concern that instrument types from the EHM Orbiter concept may be added to the Flyby mission. Neither of these potential scenarios were included in the CATE cost estimate.
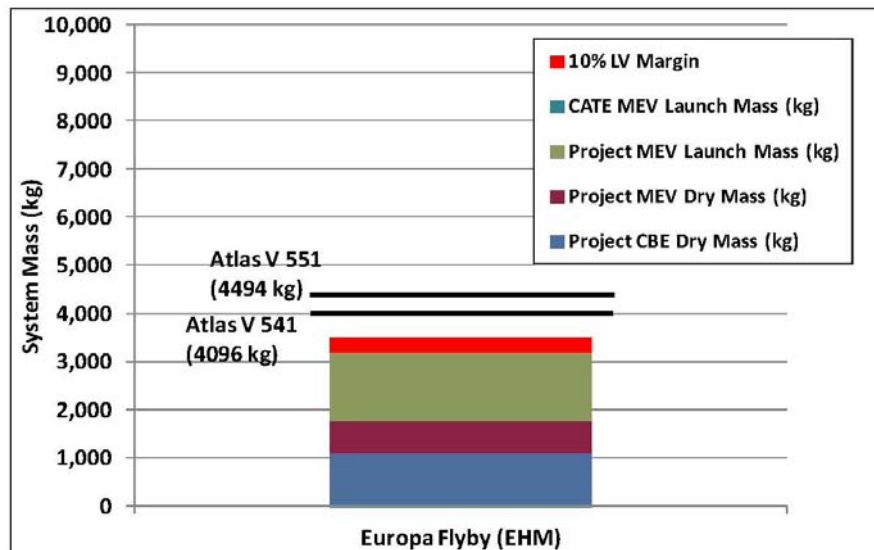
Figure 4.   EHM Flyby Launch Mass Margin

Power margins during normal operations are acceptable assuming 4 ASRG power, as shown in Figure 5. There are small differences in the expected maximum battery depth of discharge due to differences in power growth allowances in CATE estimates versus project estimates; however, all estimated power margins are within acceptable limits. Battery depth-of-discharge is held to 35% or lower in the worst case (at Jupiter orbit insertion) and is much lower during the remaining mission phases.

Advanced Stirling Radioisotope Generator (ASRGs)

Uncertainty associated with technology development for the ASRGs contributes to risk of design changes and schedule delays for the project. The ASRG is currently estimated at TRL 5 and is part of an ongoing development effort. Results from the ground based testing program may possibly lead to changes in the ASRG interface to the spacecraft. Items that are of particular concern include the contribution of jitter from the ASRGs to the Topographic Imager and SWIR Spectrometer as well as the impact of electromagnetic interference (EMI). Also, there is concern that the ASRG may not provide the expected power for the mission environment. If the ASRGs provide less power than expected, then either a fifth ASRG may need to be considered or a modification to mission operations may be necessary. No additions to the CATE cost or schedule estimates were made based on possible delays in ASRG development.
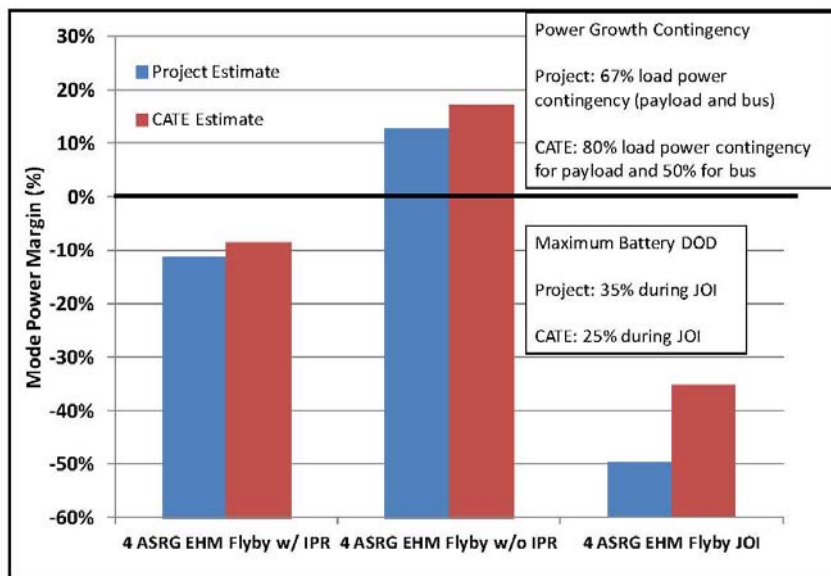
8

Figure 5.   EHM Flyby Power Margin

Radiation Environment

The radiation environment for the EHM Flyby mission contributes to uncertainty in mass, cost, and schedule. Hardware that is external to the radiation vault, particularly exposed sensor heads, will require qualification for the mission radiation environment. Delays in radiation qualification of sensor detectors or optics may adversely impact project cost and schedule. Hardware that is internal to the radiation vault may need to be assessed for compatibility (EMI and thermal) within the common enclosure. Additional systems engineering effort is anticipated for successful integration of electronics within the common radiation vault. In order to maintain operations through radiation upsets, the EHM Flyby mission proposes a "fail operational" software fault management approach. While this approach may help to maintain operations pacing, it will require a more complete understanding of hardware failure modes than a "fail safe" approach. Some delays in fault management software are anticipated as the hardware implementation matures. The impact to the CATE cost estimate was considered by using the Juno mission as a cost analogy and adding a 5% multiplier to the bus and camera estimates for radiation issues.

Technology Development

Technology development items for the EHM Flyby mission include development of the ASRG and radiation-hardened detectors for the Europa mission environment. The ASRG is currently estimated at TRL 5 based on DoE engineering unit testing, with further testing by NASA Glenn Research Center. Further life testing is anticipated as well as a modified housing design. Additional development of radiation-hardened detectors is anticipated to advance beyond TRL 5-6. The current level of maturity depends on the selected manufacturers and their proposed manufacturing techniques for hardening of CCD and CMOS type detectors.

9

10

5. Cost and Schedule Evaluation

Figure 6 illustrates the CATE cost estimating approach in the form of a flow diagram. The initial focus is to estimate, with multiple analogies and cost models, the concept hardware such as instruments and spacecraft bus. Following the estimation of other cost elements based on historical data, a probabilistic cost-risk analysis is employed to estimate appropriate cost reserves. To ensure consistency for all concepts, the cost estimates are updated with information from the technical team with regard to mass and power contingencies, and potentially required additional launch vehicle capacity. Using independent schedule estimates, costs are adjusted using appropriate burn rates to properly reflect the impact of schedule delays or multiple work shifts to ensure meeting a launch date. Finally, the results are integrated, cross-checked with other independent cost and schedule estimating capabilities, and verified for consistency.
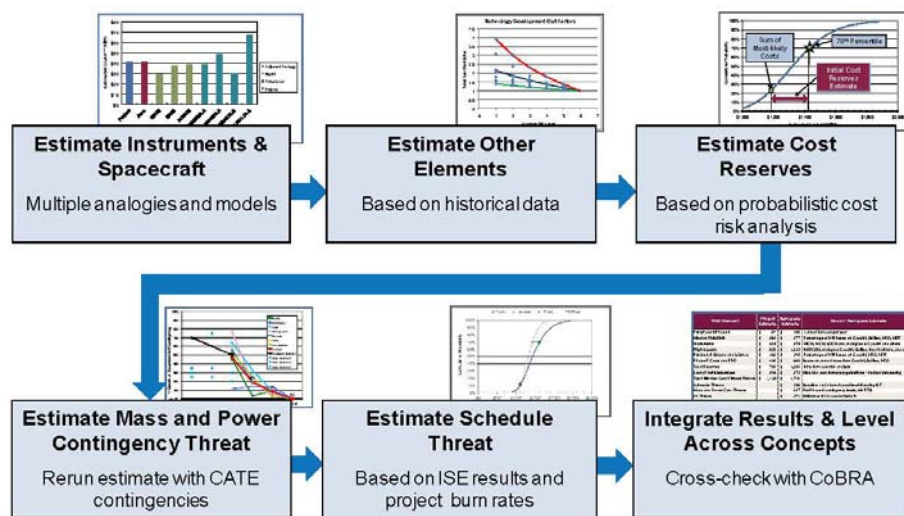

Figure 6.   CATE Cost Estimating Process

Hardware Cost Estimates

The hardware cost elements estimated for the Europa Flyby concept are the spacecraft bus and the four instruments. Multiple estimates are developed for each of these elements. Both parametric cost models and analogy-based estimates are used. Figure 7 illustrates the analogy-based estimating process, which uses a cost estimating relationship (CER) to adjust the actual costs of past missions. By using the actual costs of past missions, unique attributes of those missions or performing organizations, which are similar to the mission being estimated, can be captured. This can provide insight that is different from most parametric cost models, which are based more on an "industry average" approach.

For the spacecraft bus, a total of five estimates were developed using the NASA and Air Force Cost Model (NAFCOM), the PRICE-H cost model and analogy-based estimates using Juno, Cassini, and Mars Reconnaissance Orbiter (MRO). The final CATE estimate is an average of these five estimates. The results of these estimates are depicted in Figure 8. The cost estimates shown include the spacecraft hardware, Project Management and Systems Engineering at the bus level, as well as bus
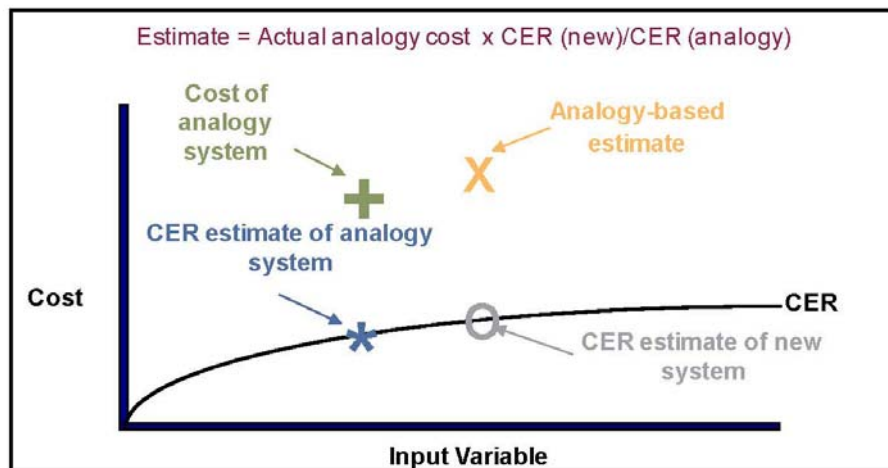
11

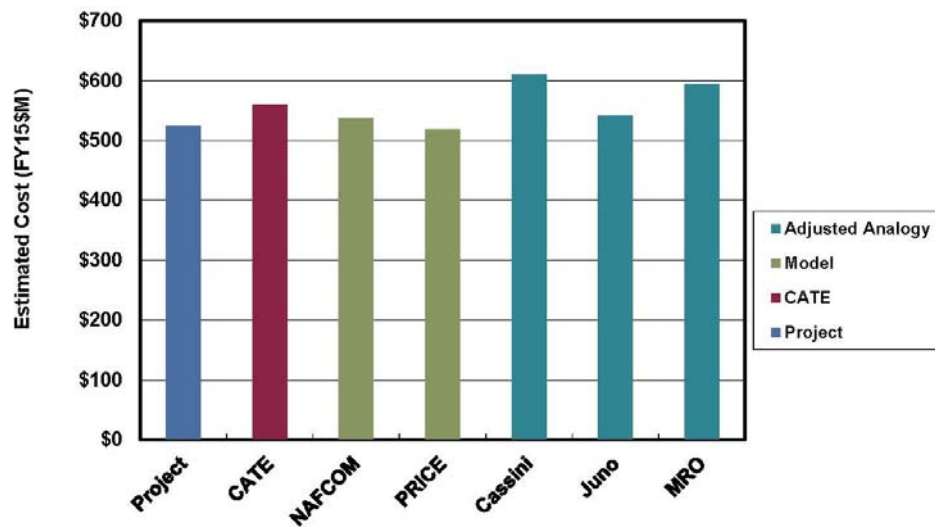Figure 7.   Analogy-based Estimating Process

Figure 8.   Flyby Bus Cost Estimates

and system-level integration and test. ASRG costs are not included in these estimates. As can be seen, there is good agreement between the CATE ($560M) and Project ($524M) cost estimate for the spacecraft bus or flight system.

For the Flyby instruments, the cost estimates are based on either two or three parametric cost models and either two or three analogy-based estimates. The parametric models used for the Flyby

12

instruments include the NASA Instrument Cost Model (NICM), The Multivariate Instrument Cost Model (MICM), and the Space-based Optical System Cost Model (SOSCM). The results for the instruments are depicted in Figures 9 to 12. In addition to the individual instrument estimates, the total payload estimates include an estimate of the payload-level Project Management and Systems Engineering. For the total payload, there is good agreement between the CATE ($248M) and Project ($262M) cost estimates, as shown in Figure 13.
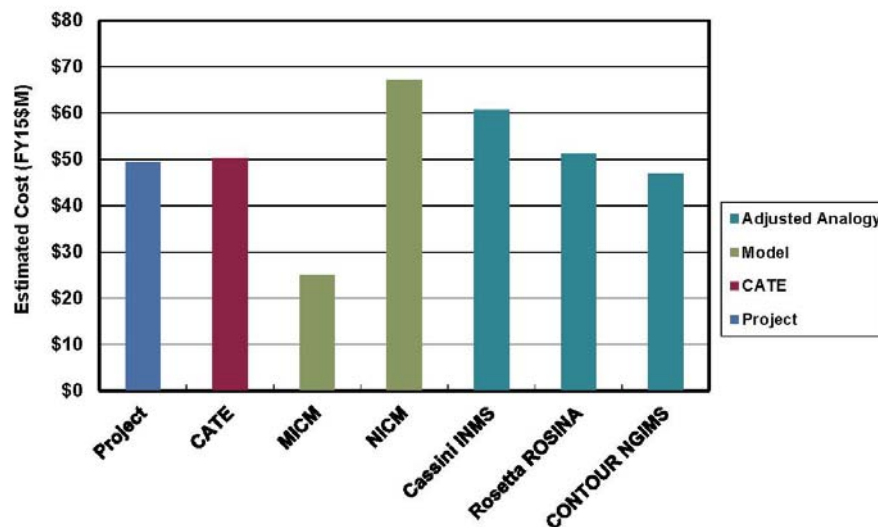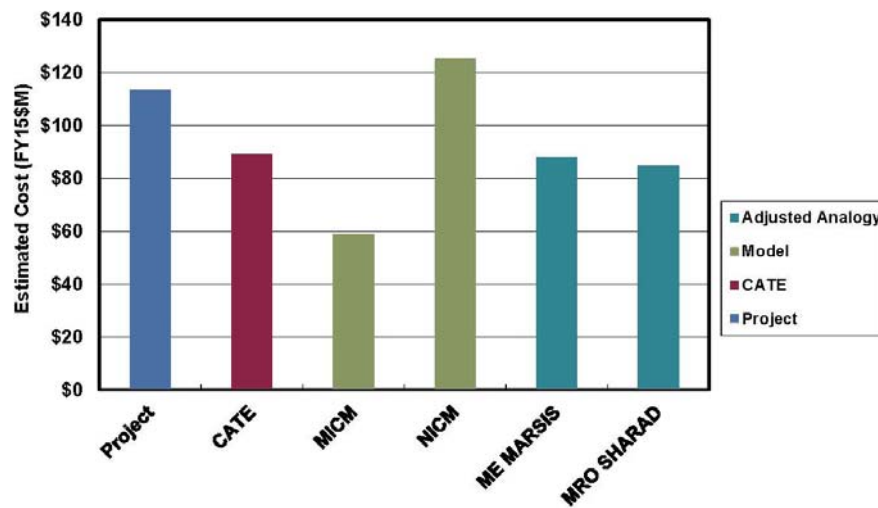

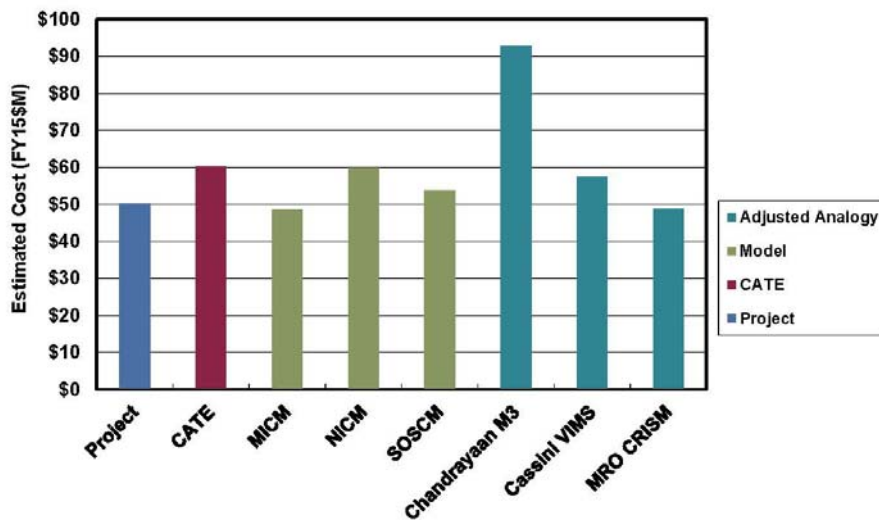Figure 9. Flyby INMS Cost Estimates

Figure 10. Flyby IPR Cost Estimates

13

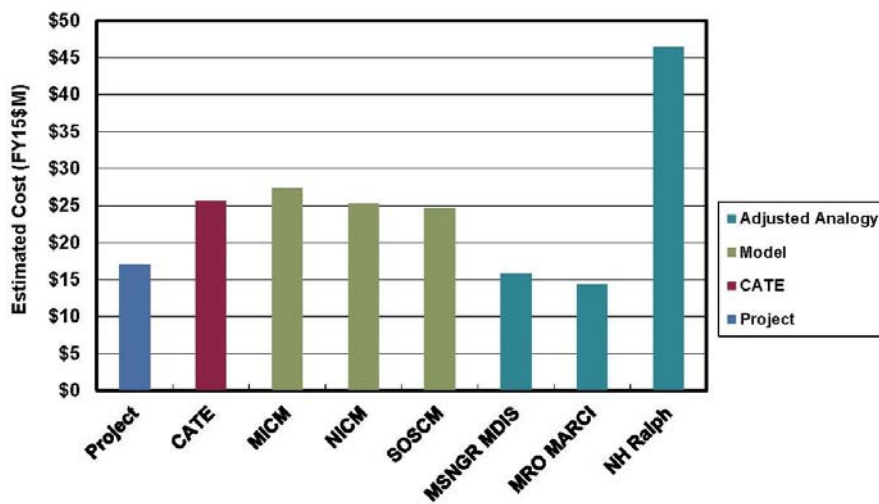Figure 11. Flyby SWIRS Cost Estimates

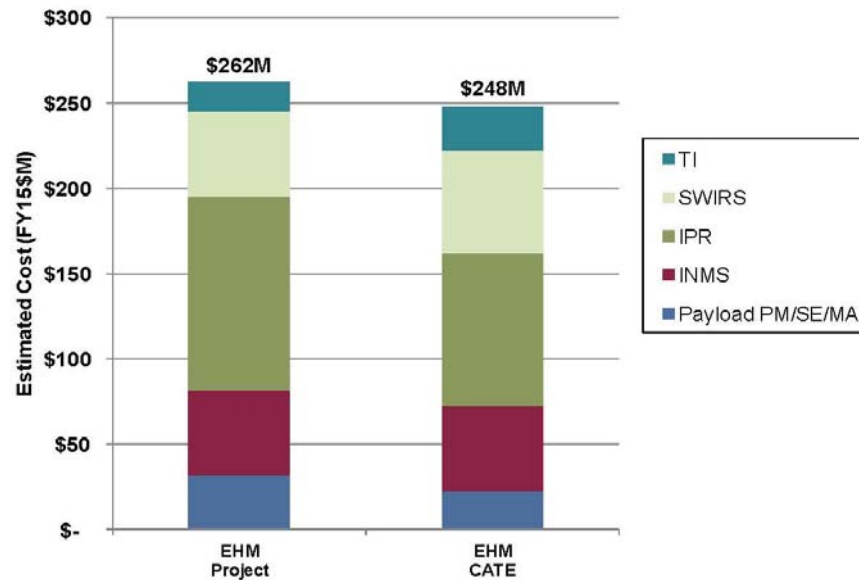Figure 12. Flyby TI Cost Estimates

14

Figure 13. Total Payload Cost Comparison

Other Cost Elements

Other cost elements estimated for the EHM Flyby concept include project-level Project Management, Systems Engineering, and Mission Assurance, pre-launch Science and Ground System Development, Pre-Phase A/Phase A, Phase E, and Education and Public Outreach (EPO). Other cost elements included in the total cost estimate, but not independently estimated, are the ASRGs and launch vehicle.

Project Management, Systems Engineering, and Mission Assurance were estimated as a single total (PM/SE/MA) using "wrap factors" based on similar historical projects. The historical missions used for the Flyby PM/SE/MA estimate are Cassini, Juno, Mars Exploration Rover (MER), and MRO. The "wrap factors" are calculated as a percentage of hardware costs for the historical missions. These percentages are then applied to the estimated hardware cost of the Flyby concept. Specifically, the average percentage wrap factor is applied to the total of the average estimate for each hardware element.

Pre-launch Science and Ground System Development estimate is similarly developed using wrap factors based on historical missions. The historical missions used are Cassini, Juno, MER, and MRO.

Pre-Phase A/Phase A costs are estimated using a rule of thumb of 1.5% of the Phase B-D development costs per year of Pre-Phase A/Phase A. For the EHM Flyby concept, the total duration used was 40 months starting in June 2012 and ending in October 2015. This is actually earlier than the Phase A end date shown on the project schedule (Figure 14). However, significant activities are planned to start in October 2015. These activities have historically been a part of Phase B, so an adjusted Phase B start date is used for all schedule-related analyses.
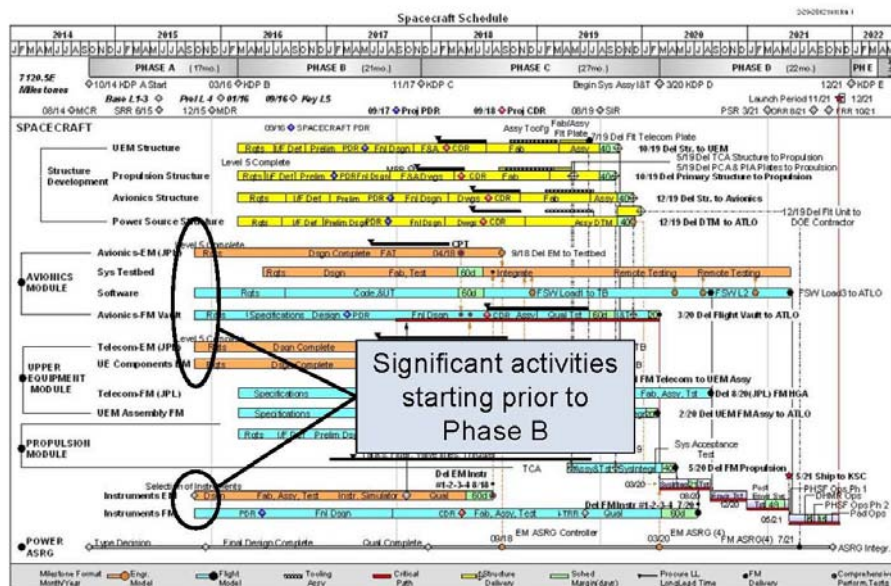
15

Figure 14. Europa Flyby Planned Development Schedule

Phase E costs were estimated using annual spend rates from similar historical projects. Because of the potentially different staffing required during cruise and encounter, these phases were estimated separately using historical rates appropriate for the respective phase. For the cruise phase, annual rates from MESSENGER, Juno, and New Horizons cruise phases were used. For the encounter phase, annual rates from MRO and the predicted annual rate from Juno encounter phases were used.

EPO costs were estimated as 1% of total project costs excluding launch vehicle.

For the ASRGs, the project estimate of $50M each, supplied by NASA HQ, was used in the CATE estimate. For the Atlas V 551 launch vehicle, a $272M estimate from the Planetary Decadal Survey was assumed for consistency.

Cost Reserves

Cost reserves are estimated using a process illustrated in Figure 15. For each Work Breakdown Structure (WBS) element, a triangular distribution of possible costs is developed. The cost values for the triangle are derived from the range of cost estimates as illustrated in the bus and instrument figures above. The lowest of the multiple estimates is used as the low value of the triangular distribution. The average of the multiple estimates is used as the mode or most-likely value of the triangular distribution. The high value of the triangular distribution starts with the highest of the multiple estimates but then adds an additional Design Maturity Factor (DMF). The DMF is a multiplier based on the maturity of the proposed design and the experience of the team. This factor helps ensure that the high value of the distribution truly represents a worst case.

Once the triangular distributions are developed for each WBS element, they are statistically combined to produce a total cost probability distribution. This distribution is typically plotted as a cumulative
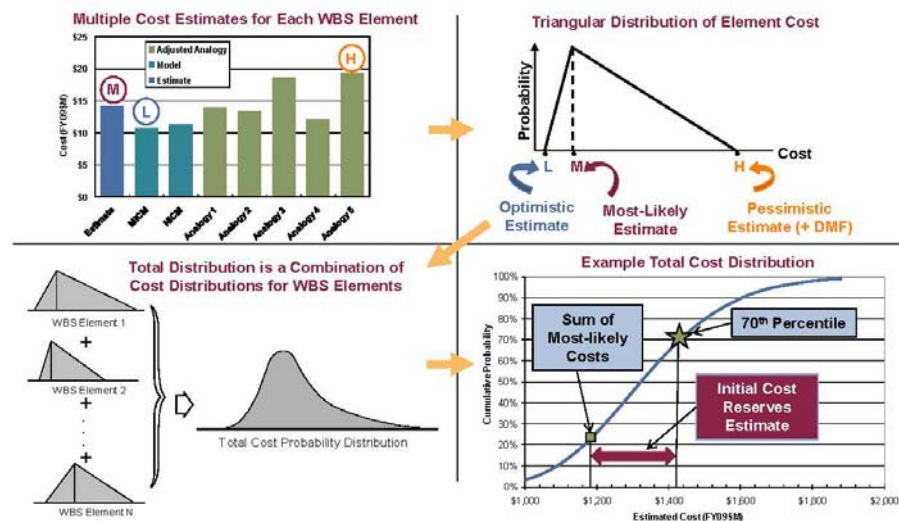
16

Figure 15. Cost Reserve Estimate Process Overview

distribution, which takes the familiar "S-curve" shape. The difference between the 70th percentile value from this curve and the sum of the most-likely estimates is the cost reserves estimate.

Mass and Power Contingency Threat

The mass and power contingency threat is a concept that was developed to support the CATE estimates, initially for the Astro2010 Decadal Survey, then later applied to the Planetary Science and Heliophysics Decadal Surveys. The motivation was to provide a methodology to account for the design evolution that has historically occurred from early conceptual design through development and launch. In order to assign a cost to these design changes, historical mass and power growth data was examined. This data showed values that were well above the typical guidelines of roughly 30% at Phase B start. Because data prior to Phase B start was sparse, the available data was extrapolated back to early conceptual phases.

Figure 16 shows an example of the data used for the mass and power contingency threats. This plot shows payload mass growth data for seven historical planetary missions. The red line is the average of this historical mission data. The black line is the CATE contingency that is used for the threat calculation.

To estimate the threat cost, the project-proposed mass and power contingencies (used in the hardware estimates described above) are replaced with the CATE contingencies. The estimates, including reserves, are then recalculated and the difference between this result and the result using project contingencies is recorded as the mass and power contingency threat.

For most projects, the CATE contingencies are well above the contingency values assumed in the proposed concept. However, the Europa Flyby concept already carried significant contingencies, so the estimated contingency threat was insignificant ($9M). Table 1 is a summary of the mass properties provided for the CATE assessment.
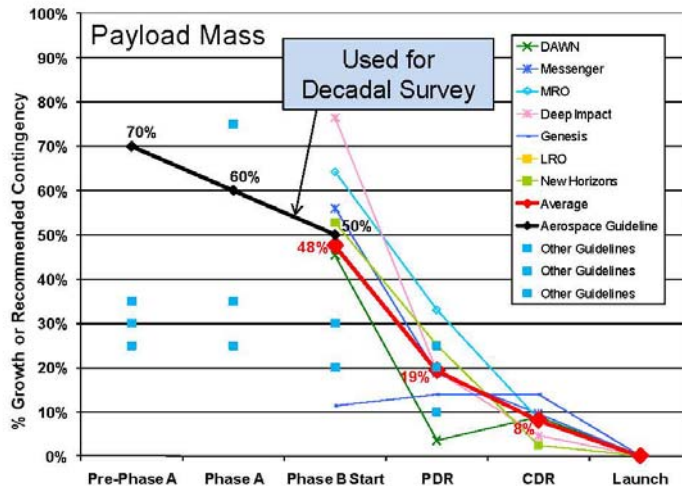
17

Figure 16. Contingency Values Used for Threat Estimates

Table 1.   Europa Flyby Mass Properties

	Project CBE (kg)	Project Cont. (%)	Project MEV (kg)	CATE Cont. (%)	CATE MEV (kg)
Flyby Flight System Total	1079.9	65%	1778.1	52%	1636.9
Flyby Payload Total	**85.3**	**82%**	**155.6**	**70%**	**145.0**
Instrument Chassis	2.0	63%	3.3	70%	3.4
INMS	11.2	88%	21.0	70%	19.0
IPR	22.4	88%	42.0	70%	38.1
SWRS	9.3	88%	17.4	70%	15.8
TI	1.9	88%	3.5	70%	3.2
Payload Shielding	38.5	77%	68.4	70%	65.5
Flyby Bus Total	**994.6**	**63%**	**1622.5**	**50%**	**1491.9**
C&DH	12.0	63%	19.5	50%	18.0
GN&C	29.4	54%	45.2	50%	44.1
Harness	56.0	88%	105.0	50%	84.0
Mechanical	423.3	59%	673.4	50%	634.9
Power (w/o ASRGs)	41.5	34%	55.4	50%	62.2
ASRGs (4)	102.4	88%	192.0	50%	153.6
Propulsion	136.4	61%	219.2	50%	204.6
Telecom	63.8	63%	103.8	50%	95.8
Thermal	35.0	63%	56.9	50%	52.5
Bus Shielding	94.8	60%	152.1	50%	142.3

Schedule Threat

The base cost estimate described above uses the project-proposed development schedule. Historically, project schedule estimates have proven to be optimistic. As part of the CATE process, a probabilistic Independent Schedule Estimate (ISE) is developed. If the 70th percentile duration from the ISE is longer than project schedule, then a schedule threat is added.

Figure 17 illustrates the ISE process. The ISE is based on actual schedule durations from similar, historical missions. The duration of each schedule phase is treated as a triangular distribution, which
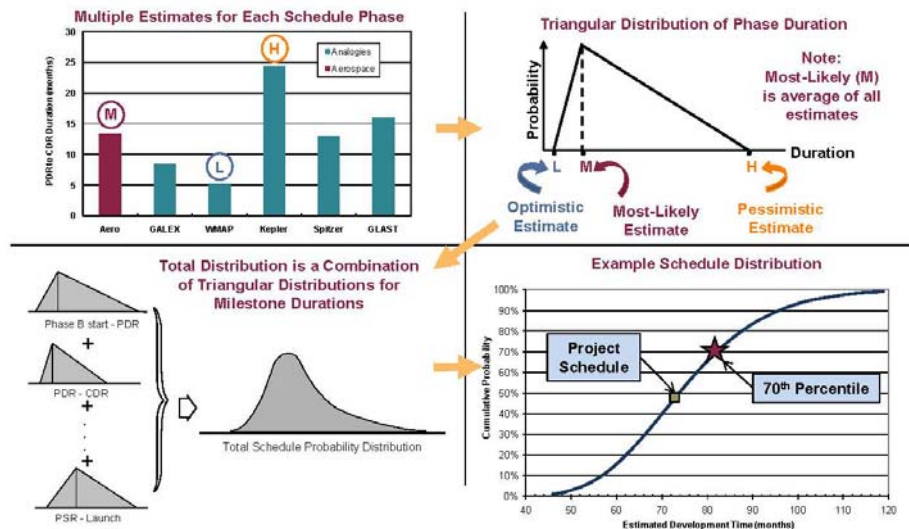
18

Figure 17. Independent Schedule Estimate Process Overview

can be statistically combined to yield a probability distribution of total project development time. The triangular distribution of durations for each phase is derived from the actual phase durations from the historical missions. The lowest duration is used as the low end of the triangular distribution, the average duration is used as the mode or most-likely value, and the highest historical value is used as the high value of the triangular distribution.

Figure 18 compares the actual Phase B-D duration of the four analogous missions used in the ISE with the proposed Europa Flyby Phase B-D duration. Figure 19 shows the results of the ISE as a cumulative probability distribution or S-curve. The 70th percentile ISE value is 75 months while the Europa Flyby proposed value is 73 months (after adjusting the effective Phase B start date as described above). Figure 20 is a breakdown of the results by project phase. While the overall durations agree quite well, the 70th percentile historical duration for the CDR to start of spacecraft I&T phase is significantly longer than the project value. Although this difference does not contribute to the CATE cost estimate, the plan for this phase should be examined to ensure its adequacy.

The difference between the 70th percentile value and the proposed project duration is then converted to a cost threat using a burn rate based on the project budget without reserves or launch vehicle. For Europa Flyby, the roughly two months' difference is multiplied by a burn rate of roughly $7M per month to yield a schedule threat of $17M.

Results

Table 2 presents the final CATE cost results compared to the current Europa team cost estimate. The agreement between the two estimates is quite close in all WBS elements. Figures 21 and 22 present the same data in graphical form.
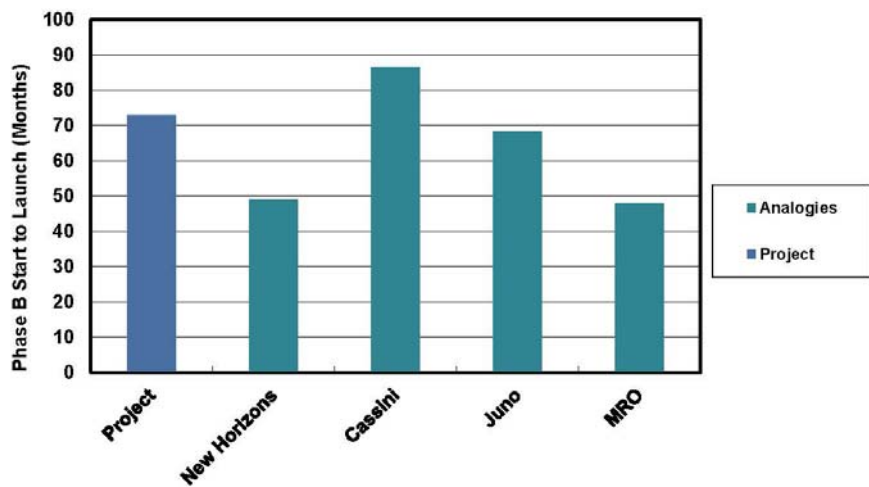
19

Figure 18. Analogous Mission Development Time Comparison
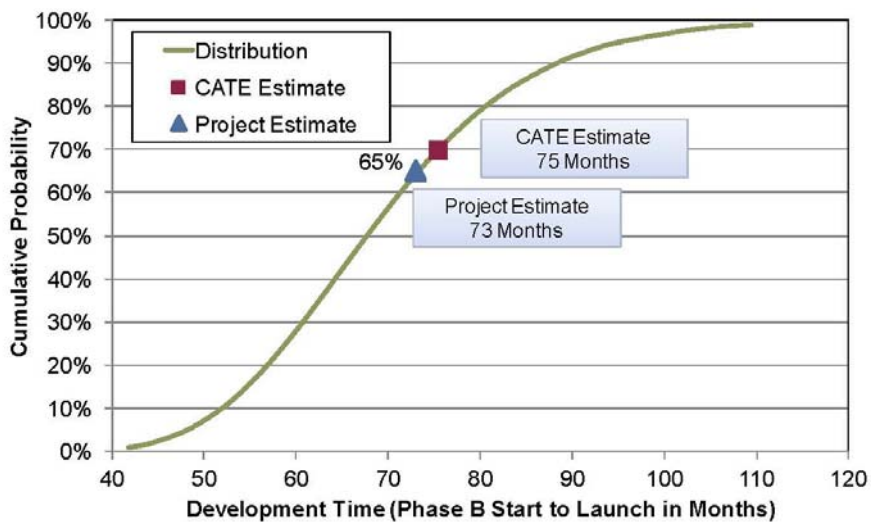

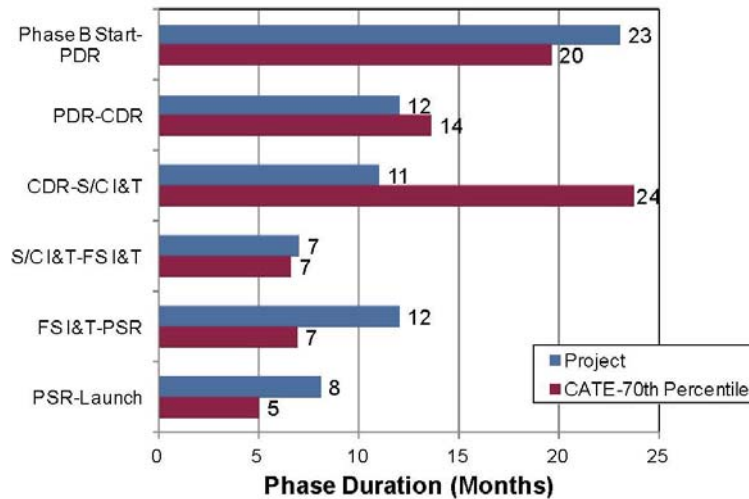Figure 19. Europa Flyby ISE S-curve

20

Figure 20. Europa Flyby Analogous Mission Phase Comparison

Table 2.　Europa Flyby Cost Estimate Comparison (FY15$M)

WBS Element	Project Estimate	CATE Estimate	Basis of Aerospace Estimate
Pre-Phase A, Phase A	incl. below	$　　63	1.5% of Dev cost per year for 40 months
Mission PM/SE/MA	$　　148	$　　143	Percentage of HW based on Cassini, Juno, MRO, MER + NEPA
Instruments	$　　262	$　　248	MICM, NICM, SOCM and analogies to planetary instruments
Flight System	$　　524	$　　560	NAFCOM11, PRICE, Juno, MRO, Cassini
ASRGs	$　　200	$　　200	Project Value for 4 ASRGs
Pre-launch Ground and Science	$　　105	$　　103	Percentage of HW based on Cassini, Juno, MRO, MER
Phase E and EPO	$　　234	$　　280	Based on annual rates from MESSENGER, NH, Juno, MRO
Total Reserves	$　　461	$　　488	70% from cost risk analysis
Mission Cost Before Threats	**$　1,934**	**$　2,085**	
Schedule Threats		$　　17	2 months at Phase D burn rate ($7M/month scaled from JEO)
Mass and Power Contingency Threats		$　　9	Based on 2/14 MEL
LV Threats		$　　-	Adequate margins on Atlas V 551
Mission Cost With Threats	**$　1,934**	**$　2,111**	
Launch Vehicle/Services	$　　272	$　　272	Atlas V 551 cost from DS guidelines + nuclear processing
Total Mission Cost With Threats	**$　2,206**	**$　2,383**	

Complexity-Based Risk Assessment (CoBRA)

As a cross-check of the CATE results, the Complexity-Based Risk Assessment (CoBRA) process was also applied to the Europa Flyby concept. The CoBRA process uses technical and programmatic parameters from the conceptual design to calculate a complexity value for the design. This is done by ranking each of the individual parameters against a database of historical space missions. The calculated complexity values for the historical missions are plotted against development cost and schedule. The missions are classified as successful, partially successful, failed, or yet to be determined. A best fit line is drawn through the successful missions, and the estimated cost and schedule of the Europa Flyby concept can be compared to missions of similar complexity. Figures 23 and 24 show the CoBRA cost and schedule analysis results. Both the project and CATE cost estimates are slightly above the green trend line, which is in family with successful past missions of this complexity. Both the project and CATE schedule estimates are below the green trend line but above the blue trend line, which is drawn through successful missions that had a planetary launch window constraint. Again, this result adds confidence that the Europa Flyby schedule estimates are in family with comparable successful missions.
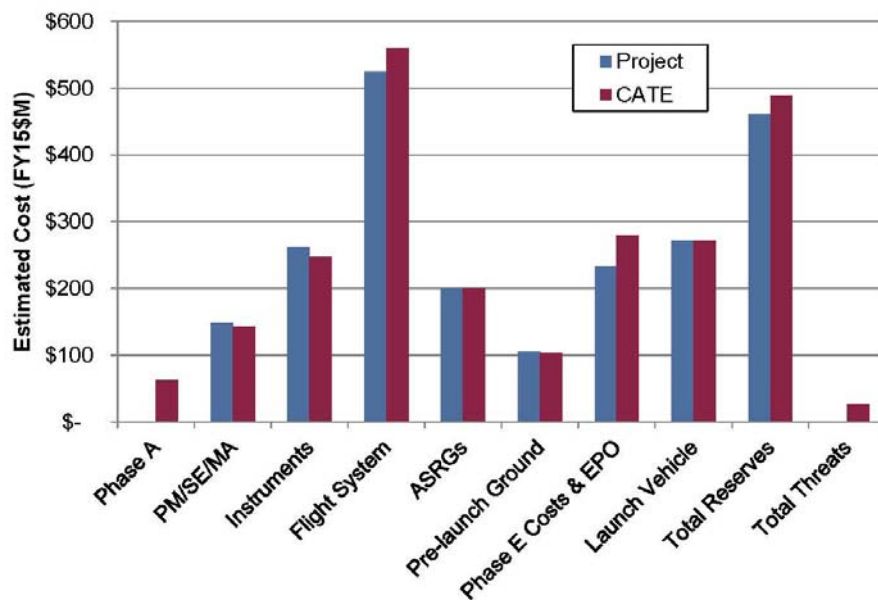
21

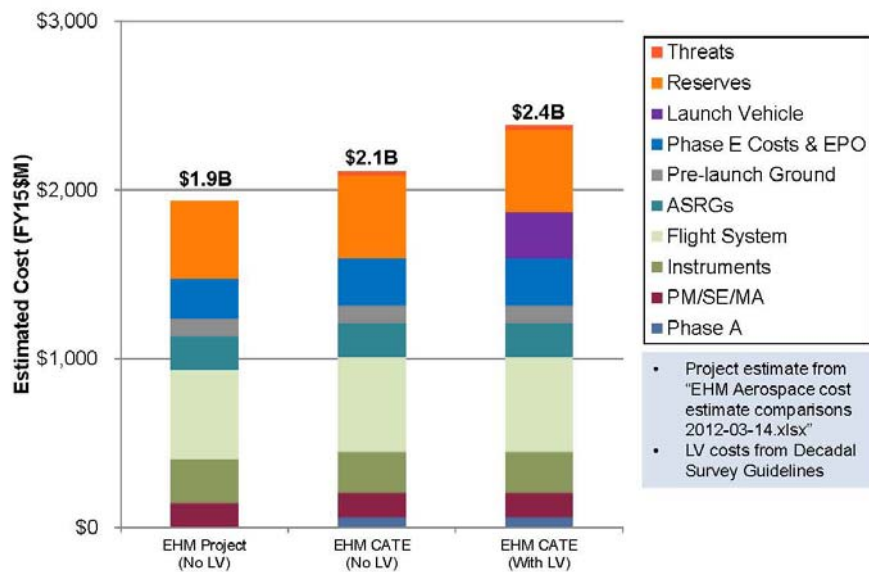Figure 21. Europa Flyby Key Cost Element Comparison
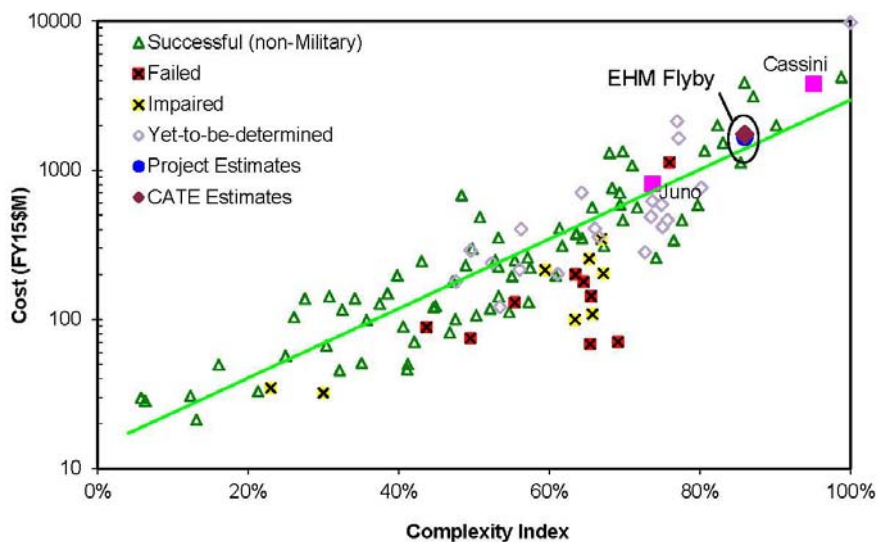

Figure 22. Europa Flyby Cost Estimates

22

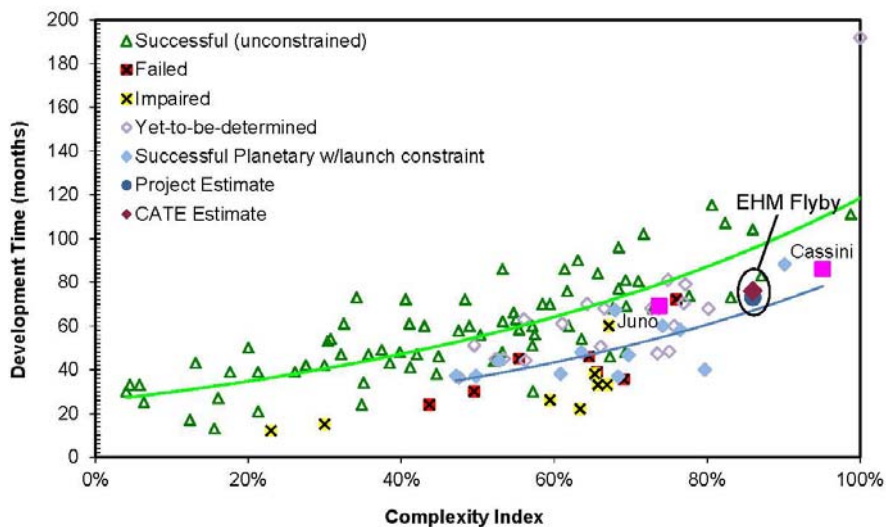Figure 23. Complexity-Based Risk Assessment Cost Analysis

Figure 24. Complexity-Based Risk Assessment Schedule Analysis

23

24

C.4.5   NASA Review Board Report

STANFORD
AERONAUTICS &
ASTRONAUTICS

DURAND BUILDING, 496 LOMITA MALL
STANFORD, CA 94305-4035
http://aa.stanford.edu
(650) 723-3317, fax: (650) 723-0279

Dr. Firouz Naderi   December 1, 2011
Solar System Exploration Directorate
JPL
Pasadena, CA

Dear Dr. Naderi

The recent Planetary Decadal Survey determined that the Europa Jupiter Science Mission
(EJSM) had compelling science but was not affordable based on an independent cost
estimate of $4.8B provided to the National Research Council by The Aerospace
Corporation. The Decadal Survey recommended that the mission be descoped to
significantly reduce cost. In response, the Europa Jupiter System Mission (EJSM) was
separated into two elements (i.e., Orbiter and Flyby) and focused solely on Europa
science. Subsequently, NASA directed that a soft lander be added to the options under
consideration.

As requested by JPL and consistent with the direction from NASA HQs, a Review Board
was created to assess the viability of the three mission options to be provided to NASA
HQ. These options were to focus on Europa only and develop Orbiter, Flyby (multiple)
and Lander concepts, identifying the lowest achievable cost with a target value of ≈$1.5B
for each concept, not including launch vehicle. It was recognized by the Board that at a ≈
70% reduction in cost from the original EJSM concept any new mission design and
corresponding science content would be dramatically different and go far beyond the
usual meaning of a simple "descope".

In the charge to the Board, it was emphasized that the Board's responsibility was to
conduct an "existence proof" evaluation of a pre-pre Phase A concept. In addition, each
project was to be evaluated independently, not as one element of a program series.

The Board listed below was assembled and on November 15, convened at JPL to review
the Orbiter and Flyby mission designs.

Scott Hubbard	Chair – NASA Ret.
Orlando Figeroa	NASA Ret. (via telephone)
Mark Saunders	NASA Ret.
Dave Nichols	JPL Div. 31
Jeff Srinivasan	JPL Div. 33
Barry Goldstein	JPL Div. 34
Cindy Kahn	JPL Div. 35
Rosaly Lopes	JPL Div. 32

1

Gentry Lee   JPL 4X Chief Engineer
Will Devereux   APL
Douglas Eng   APL

To assist the Board in assessing the concepts, members of the JPL staff provided presentations and responded to many questions. This entire effort was applauded by all of the members of the Board and contributed to a most successful meeting.

The high level Europa Review Board conclusions can be summarized in a few statements:
- The overall approach to spacecraft modularity and radiation shielding was unanimously lauded as a creative approach to reducing technical risk and cost. No engineering "showstoppers" were identified.
- Both the Orbiter and Flyby mission concepts satisfied the "existence proof" test as missions that met Europa science requirements, could be conducted within the cost constraints provided and have substantial margins.
    o However, several Board members expressed a strong opinion that a "science per dollar" criterion such as applied by the Decadal Survey would find the Flyby mission to yield much greater benefits than the Orbiter Project.
- The Board was unanimous in identifying two technical risks that impact both mission concepts:
    o The Advanced Stirling Radioisotope Generator (ASRG) has been selected as a critical enabling technology. The Board recommends that the study teams thoroughly familiarize themselves with the development status, schedule and performance of the current version of the ASRG and identify any potential modifications from the Discovery version for Europa. In addition, availability of ^{238}Pu stock and ASRG performance elicited concerns from the Board. In particular, there was a recommendation that much more data be collected on ASRG response to the space mission environment, *e.g.,* microphonics and performance under loads.
    o While the "nested" approach to radiation shielding clearly mitigated the risk to the spacecraft and instrument electronics, the detectors will be exposed to the space environment. The Board found that early assessment and investment must be provided to ensure proper sensor performance.
- Consistent with the above statement, a Board consensus emerged that if either of these mission concepts moves ahead, particular attention must be paid to the Announcement of Opportunity (AO) for the science investigations so that the AO enables a simple approach and clearly specifies the PI-mission interface in critical areas such as total detector dose.

Detailed Considerations:
In the charter distributed to the Board prior to the review, we were asked to consider the following criteria:
- Ability of the mission to satisfy the Science Objectives
- Mission design approach
- Robustness of the mission and system architectures

2

– Robustness of mission and system margins; compliance with JPL design principles.
– Proposed scope, including available options, is consistent with funding target value to complete the mission
– Cost risk Project planning risks, including design, environment mitigation plans, integration and test plans, schedule and margins.

Within this overall review framework the following more specific comments were noted where at least two or more Board members addressed similar issues:

Science and Mission Design:
• During the science presentations, there were numerous questions about the changes from the original EJSM instrument suite and experiment goals. Following a request from the Board, Dr. Pappalardo gave a summary of science traceability. A number of the Board members suggested that more work be done by the SDT to clearly define the relationship of a given mission concept to the Decadal Survey.
• The Orbiter mission is challenging in that the science campaign occurs in the last 30 days of the mission and after significant radiation exposure. The Flyby mission has a much slower accumulation of total dose. This distinction needs to be sharpened.

Robustness and Margins:
• Systems margins presented for power, mass, and data were substantial, and of course have implications for launch vehicle requirements and cost. There was considerable discussion and some disagreement about whether maintaining such large technical margins may inappropriately drive the costs at this stage of maturity. A majority of the Board concluded that a conservative approach was appropriate at this point in the life cycle, particularly with the uncertainty in the launch vehicle capabilities a decade or more away from now.

Cost and Cost Risk:
• A majority of the Board appeared satisfied that the two study teams had produced credible cost estimates using a variety of tools and approaches. While the Flyby mission was slightly higher than the $1.5B FY15 target, both projects were deemed to be "in the ballpark". There was a minority opinion that expressed concern over an inconsistency in trends between two parametric tools. Clearly, ongoing cost evaluation and the Aerospace CATE are needed to track these concepts.

Schedule:
• The Study leader (Gavin) noted at the beginning of the review that detailed schedules would not be available. While the Board accepted this limitation as a necessary element of an "existence proof" review, there was clear concern about whether the schedule supported the hardware development as proposed. At subsequent reviews more explicit schedule data is required in order to understand the risks involved.

On behalf of the entire Board, I wish to express again our congratulations to the JPL team in the high quality of the studies. We look forward to the Lander review early in 2012.

3

Sincerely,

Prof. G. Scott Hubbard
Chair, Europa Mission Review Board
Cc: Board members, Tom Gavin

4

National Aeronautics and Space Administration

EUROPA STUDY 2012 REPORT
EUROPA LANDER MISSION

Europa Study Team, 1 May 2012, JPL D-71990
Task Order NMO711062 Outer Planets Flagship Mission

Cover art Michael Carroll

Europa Study 2012 Report—Lander

Table of Contents

The cost information contained in this document is of budgetary and planning nature and is intended for informational purposes only. It does not constitute a commitment on the part of JPL and/or Caltech.

D. LANDER MISSION

The Europa Lander Mission is an exciting mission that would be the first to explore the Europa surface to investigate its habitability.

Executive Summary

Europa is a potentially habitable world and is likely to be geologically and chemically active today. Many well-defined and focused science questions might be addressed by exploring Europa (Figure D-1).

The 2003 Planetary Decadal Survey, "New Horizons in the Solar System," and 2011 Planetary Decadal Survey, "Vision and Voyages" (Space Studies Board 2003, 2011), both emphasize the importance of Europa exploration as "the first step in understanding the potential of the outer solar system as an abode for life" (Space Studies Board 2011, p. 1). The 2011 Decadal Survey discusses the likelihood of contemporary habitats with the necessary conditions for life, stressing the inherent motivation for "a Europa mission with the goal of confirming the presence of an interior ocean, characterizing the satellite's ice shell, and
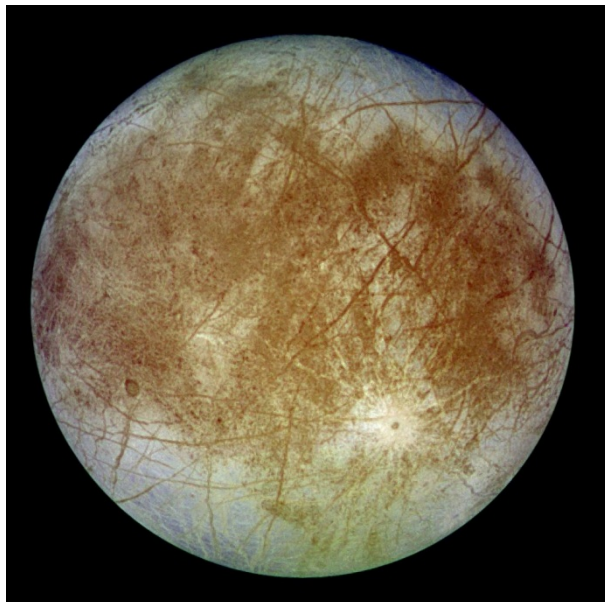
Figure D-1. Europa: a world of rock, ice, and water the size of the Earth's Moon. The 2011 Planetary Decadal Survey identifies exploration of Europa as "the first step in understanding the potential of the outer solar system as an abode for life" (Space Studies Board 2011, p. 1).

understanding its geological history" (Space Studies Board 2011, pp. 1–2).

Understanding Europa's habitability is intimately tied to understanding the three "ingredients" for life: water, chemistry, and energy. These astrobiological themes can be well addressed by a landed mission to Europa. Measurements obtained from Europa's surface could allow for direct analysis of the satellite's chemistry and mineralogy through *in situ* investigations and measurements that are not possible to achieve remotely: A properly equipped Lander could allow for sampling beneath the radiation processed uppermost portion of Europa's icy shell, providing insights about its native composition and implications for life. A Lander is an excellent platform from which to perform geophysical measurements to probe Europa's ice shell and subsurface ocean. A landed mission could permit detailed analyses of local surface geology. Within this report, we discuss the science to be achieved, the data types that are needed, and the means by which they can be acquired. The Europa Lander Mission concept is directly responsive to the Decadal Survey's recommendations for Europa science.

Lander Science Objectives

As outlined in the science section of this report, multiple well-defined and focused science questions will be addressed by exploring Europa to understand the potential for life in the outer solar system. Interrelated physical processes and habitability are key drivers for Europa exploration. Thus, the goal adopted for the Europa Lander Mission concept is to:

Explore Europa to investigate its habitability.

This goal implies understanding processes, origin, and evolution. These include testing the numerous scientific issues described above. "Investigate its habitability" recognizes the significance of Europa's astrobiological potential. "Habitability" includes investigating the composition of Europa's surface materials,

confirming the existence and determining the characteristics of water within and below Europa's icy shell, and evaluating the processes that have affected Europa. A Europa Lander could provide direct assessment of Europa's habitability and ocean composition while addressing physical processes at a local scale. Four candidate sites outside of the trailing-side high-radiation zone were suggested by the Europa Science Definition Team, with Thera or Thrace appearing to be the most attractive (Figure D-2). The sites suggested in the report were to guide the study; a rigorous science site selection process would be followed during the project execution.

The Europa Lander Mission objectives flow from the science issues discussed in this report. These objectives represent a key subset of Europa science that can be well accomplished by a landed Europa mission. These objectives are categorized in priority order as:

C. Europa's Composition: *Understand the habitability of Europa's ocean through composition and chemistry*.

O. Europa's Ocean and Ice Shell: *Characterize the local thickness, heterogeneity, and dynamics of any ice and water layers*.

G. Europa's Geology: *Characterize a locality of high scientific interest to understand the formation and evolution of the surface at local scales*.

The complete traceability to example measurements and the model instruments that could accomplish them is compiled and contained in this report. The example measurements and the notional instruments are provided as a proof of concept to demonstrate the types of measurements that could address the investigations, objectives, and goals. These are not meant to be exclusive of other measurements and instruments that might be able to address the investigations and objectives in other ways. The planning payload selected for the Europa Lander study consists of a notional set

Figure D-2. Thera Macula may be a region of active chaos formation above a large liquid water lens. Topographic data indicates that Thera is low-lying, suggesting subsurface water today. Galileo image at 220-m/pixel resolution.

of instruments including a Mass Spectrometer (MS), Magnetometer (MAG), Multiband Seismometer Package (MBS), Site Imaging System (SIS), Raman Spectrometer (RS), and a Microscopic Imager (MI). NASA will ultimately select the payload through a formal Announcement of Opportunity (AO) process.

The traceability matrix in Foldout D-1 (FO D-1) maps the Europa Lander Mission objectives (in priority order) to specific investigations (in priority order within each objective) to address the overarching mission goal. Specific measurements for each investigation are listed (in priority order within each investigation). The Lander objectives and investigations are discussed in detail in Sections D.2.1 through D.2.4.

Architecture Implementation

The Lander Mission architecture described here is well suited to satisfying the science objectives in a single mission and using tech-

nologies currently in development. It is designed to meet the baseline science objectives.

The spacecraft would be launched on a Delta IV Heavy on a Venus-Earth-Earth gravity assist (VEEGA) trajectory taking 6.4 years to get to Jupiter. After Jupiter Orbit Insertion (JOI), the spacecraft energy is reduced so that EOI can occur 1.4 years later while accumulating only 125 kilorads of radiation through a unique mission design. This enables longer mission duration at Europa for the Lander.

The Europa Lander Mission would be launched as an integrated spacecraft consisting of Carrier and Lander elements. The integrated spacecraft, pictured in Figure D-3, has the Lander on the +Z axis attached to the Carrier on the –Z axis. The Lander's deployable components are stowed until after landing on Europa. The integrated spacecraft would use power from the Carrier Advanced Stirling
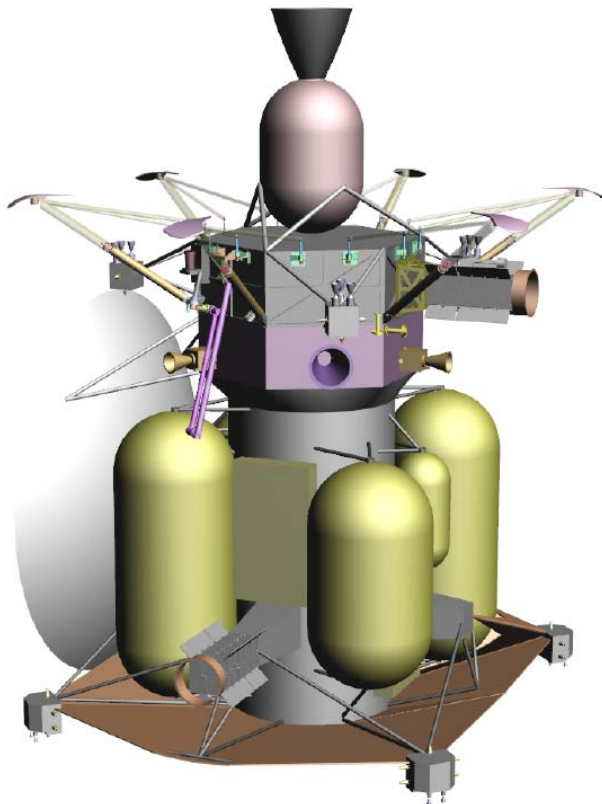
Figure D-3. The integrated spacecraft with Carrier and Lander elements provides reconnaissance, safe landing, and in-situ science in a single mission.

Radioisotope Generators (ASRGs) and Lander ASRGs. The Carrier has two distinct modules oriented about the Z axis from top to bottom and is dominated by the 3-meter high-gain antenna (HGA) on the side of the Propulsion Module along the +Y axis; the main rocket engine is located on the -Z axis; the Propulsion Module tanks and the outrigger-mounted control thruster engines are located at midspan; and the ASRGs for power-generation are mounted symmetrically about the main engine (ME) at the base of the Propulsion Module. After Europa Orbit Insertion (EOI), the integrated spacecraft will perform reconnaissance imaging of the potential landing sites. Ground-based analysis will aid in the site-certification process. Precision landing is required for safety (not science) with the Lander configured for pinpoint landing. After 30 days in orbit, the Lander will be released and a deorbit burn performed via a solid-rocket motor (SRM) followed by a powered terminal descent to touchdown using monopropellant thrusters. Onboard navigation uses a high-precision inertial reference unit augmented by terrain-relative navigation (TRN) using descent imaging to determine location and reachable sites. Onboard guidance calculates and updates the thrust profile in real time to divert to a top-priority reachable site. A hazard-avoidance system will ensure that the Lander is set down in acceptable surface conditions.

Once on the surface, the Lander (Figure D-4) would spend the rest of the mission lifetime acquiring science data and transmitting it to the Carrier. Should the Carrier fail before end of mission (EOM), data can be transmitted directly to Earth from the Lander. As a minimum, all of the floor science data can be transmitted in this mode. The surface operations are divided into four main phases: Checkout and Commission Phase, Context Acquisition Phase, Sampling Phase, and Continuous Monitoring Phase. Landed operations will be completed and data transmitted to Earth within a month. Science measurement
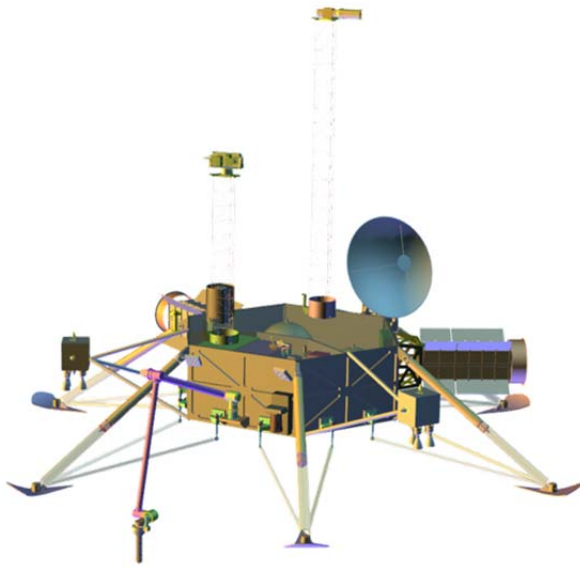
Figure D-4. The Lander (surface configuration) provides a reliable platform for completing the baseline science objectives

requirements are fully met with this mission design and operations concept. The Lander is expected to continue to operate after the baseline one-month of science, so an extended mission is possible. Technical margins for the Lander are reasonable, with 29% mass margin, 40% power margin, and large data transmission margins using the Carrier in a store-and-forward mode. The Carrier has 28% mass margin and 40% power margin.

Schedule and Cost

A top-level development schedule is shown in Figure D-5. Phase durations draw on experience from previous outer planets missions and are conservative. This schedule would facili-

tate front-loading of requirements development, provide significant time during instrument development to understand the actual design implications for radiation and planetary protection, and offer a flatter-than-typical mission funding profile.

The Lander Mission study applied a hybrid costing methodology that includes institutional cost models, the NASA Instrument Cost Model (NICM), percentage wrap factors, expert-based opinion, and JPL's Team X estimates. An S-curve analysis performed on the study cost estimates resulted in a \$2.8 (FY15\$), 70th-percentile cost estimate. In addition, the Aerospace Corporation performed an independent cost analysis and found a 70th-percentile cost of \$3.0B (FY15\$).

Technical Review

An independent technical review board, chaired by Professor Scott Hubbard, reviewed the Europa Lander Mission concept. The key findings are (paraphrased) that a soft-lander with the science return specified would greatly advance the knowledge of Europa habitability, but that the concept did not meet the "approximately \$1.5B (without launch vehicle)" cost criterion because of the risk inherent in performing reconnaissance and safe landing in one mission. The board recommended investment in a technology program and the use of a precursor mission for landing site reconnaissance to retire the landing risks. The detailed findings of this technical review are provided in Section D.4.8.
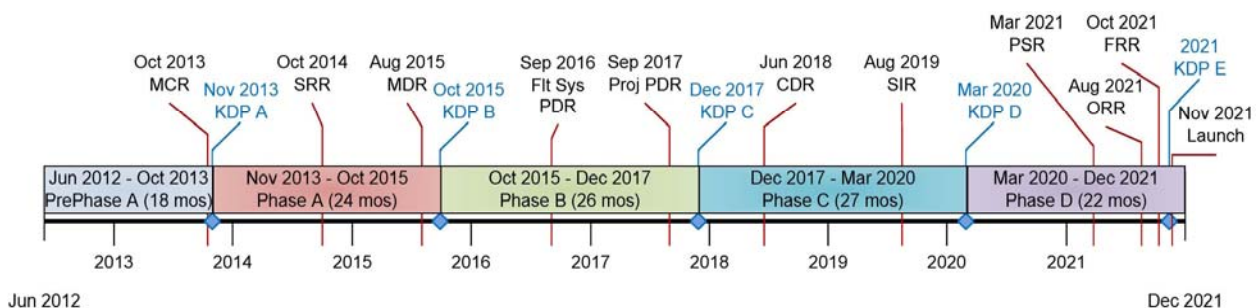
Figure D-5. Top-level development schedule with conservative durations provides appropriate time to address radiation and planetary protection challenges.

Summary

A Lander Mission concept falls short in meeting the challenge from NASA and the Decadal Survey for a reduced-scope Europa mission relative to JEO, yet still has exceptional science merit. Study results are in compliance with NASA Headquarters direction and guidelines. The mission design concept is conservative and has good margins. The science and technical overview of the Lander Mission concept were presented at open meeting of OPAG on March 29, 2012. OPAG viewed the lander science as exciting science; however, the concept was considered infeasible in the short term due the cost magnitude and the need for technology maturation.

D.1   Science of the Lander Mission

D.1.1   Lander Science

Landing on Europa provides valuable science on a world that is potentially habitable.

Europa is a potentially habitable world. As outlined below, there are many well-defined and focused science questions to be addressed by exploring Europa. Both the 2003 Planetary Decadal Survey, *New Horizons in the Solar System,* and the 2011 Planetary Decadal Survey, *Vision and Voyages,* emphasize the importance of Europa exploration (Space Studies Board 2003, 2011). Both Decadal Surveys discuss Europa's relevance to understanding issues of habitability in the solar system, stressing this as the inherent motivation for Europa exploration. For example:

> *"Because of this ocean's potential suitability for life, Europa is one of the most important targets in all of planetary science."* (Space Studies Board 2011)

Understanding Europa's habitability is intimately tied to understanding the three "ingredients" for life: water, chemistry, and energy (see Section A of this report). These astrobiological themes can be well addressed by a landed mission to Europa. Measurements obtained from Europa's surface could allow for direct analysis of the satellite's chemistry

and mineralogy through *in situ* investigations and measurements that are not possible to achieve remotely: A properly equipped Lander could allow for sampling beneath the radiation processed uppermost portion of Europa's icy shell, providing insights about its native composition and implications for life. A Lander is an excellent platform from which to perform geophysical measurements to probe Europa's ice shell and subsurface ocean. A landed mission could permit detailed analyses of local surface geology. In this section, we discuss the science background most relevant to a Europa Lander Mission, which addresses Europa's habitability through analyses of the satellite's composition, ocean and ice shell, and geology.

D.1.1.1   Habitability of Europa

The habitability of an environment is dependent on the concurrent availability of three "ingredients" that, along with a suitably clement physicochemical environment, are necessary for life as we know it:

1. A solvent capable of supporting complex biochemistry. For terrestrial life, the presence of liquid water at a chemical activity[1] of about 0.65 or greater is an absolute requirement.
2. A source of energy with which to create and maintain the complex molecules, structures, and pathways on which life depends. Life on Earth is known to use chemical and visible to near-infrared light energy, and is thought to have discrete minimum requirements for both flux and Gibbs energy (Hoehler 2004).
3. Raw materials for biosynthesis. All life on Earth requires the elements C, H, N, O, P, and S, and also variously requires

---

[1] The chemical activity of water—or water activity—is a measure of the availability of water, which for open surface water is simply the water fugacity. For an ocean saturated with sea salt the water activity would be about 0.72 or higher (Siegel, 1979; Marion et al., 2003).

many "micronutrients" (typically, transition metals) (Wackett et al. 2004).

These ingredients must be available within the context of physicochemical (environmental) conditions that allow for the assembly, stability, and function or interaction of complex structures and molecules. Life on Earth maintains activity over temperatures from below -20 to over 120°C; pH from approximately 0 to 13; salinities from fresh to halite saturation; and pressures to at least 150 MPa, and possibly much greater (see, e.g., Committee on the Limits of Organic Life in Planetary Systems 2007). Electromagnetic or particle radiation capable of breaking biomolecular bonds can also limit habitability.

In assessing the astrobiological potential of Europa, the requirements for habitability as defined by life on Earth provide a useful framework in which to place our current understanding of Europa as a potentially habitable world, and elucidate key areas for advancing this understanding by Lander-enabled science.

D.1.1.1.1　Water on Europa

The presence of a global subsurface ocean of liquid water has driven decades-long interest in Europa's potential as an abode of life. Evidence for a contemporary global liquid water ocean on Europa is compelling, both empirically (Khurana et al. 1998, Carr et al. 1998) and on theoretical grounds (Cassen et al. 1979, Squyres et al. 1983). A subsurface ocean is consistent with Europa's broad range of geological features (Greeley et al. 2004), and formation of Europa's cycloid-shaped features require the action of significant diurnal tides produced by orbital eccentricity along with the effects spin pole obliquity, suggesting an ocean at the time of their formation (Hoppa et al. 1999, Hurford et al. 2009). Thermal modeling predicts an ocean beneath an ice shell of a few, to a few tens of kilometers thickness, depending on the tidal heating rates in the ice shell and rocky mantle (Ojakangas and Ste-

venson 1989, Moore and Hussman 2009). Europa's global ocean may have persisted since the origin of the Jovian system (Cassen et al. 1982).

While the availability of liquid water is perhaps the best resolved aspect of Europan habitability; nonetheless, there remain areas where this understanding can be improved. Determining the volume and depth of the ocean would provide important additional constraints on the chemical evolution of the ocean—e.g., water-to-rock ratios and pressure-temperature constraints for thermodynamic and kinetic models of silicate-water interactions. Furthermore, determining the spatial distribution of liquid water within the ice shell (e.g., Schmidt et al. 2011), if any, would inform the possibility for transiently habitable regions beyond the ocean that could differ substantially in several aspects of their suitability for life.

D.1.1.1.2　Energy on Europa

Possible sources of energy for life on Europa have been identified, but considerable uncertainty exists as to whether, or at what rate, such energy is made available in the ocean. Spectroscopy of Europa's surface reveals the presence of a variety of oxidized species (e.g., O_2, H_2O_2, CO_2, SO_2, SO_4) thought to result from radiation processing of the ice, a hypothesis supported by laboratory experiments (Carlson et al. 1999a, b; Carlson et al. 2009). Interaction of liquid water with mafic or ultramafic rocks, such as might occur at the base of the Europan ocean, is expected to generate reduced species including hydrogen and, depending on the chemical composition of ocean fluids and the pressure and temperature of interaction, reduced forms of carbon (methane), sulfur (hydrogen sulfide), and nitrogen (ammonia) (McCollom 1999, Zolotov and Shock 2004, Vance et al. 2007). Life on Earth is capable of catalyzing the reaction of a variety of combinations of the surface oxidants observed on Europa with hypothetical subsurface reductants, and coupling the liberated

chemical energy to growth (Chyba 2000, Hand et al. 2007). Thus, the surface and subsurface environments of Europa may constitute, in essence, a battery—stored chemical energy that could conceivably support life.

Biological potential depends critically on the rate at which energy can be accessed. Growth rate and the amount of standing biomass that can be supported scale with energy flux, and some fluxes may simply be too low to support life. In this regard, several critical questions remain concerning the extent to which Europa's "battery" exists and is tapped and replenished:

1. Delivery of reduced species to the ocean depends on the extent and nature of reactions between water and rock. The inferred range of salinity of the ocean (Hand and Chyba 2007) suggests that extensive reactions with silicates has affected its bulk properties, but the duration (including present occurrence), temperature, and other critical aspects of such reactions remain to be constrained (e.g., McKinnon and Zolensky 2003). Thus, the strength and present availability of the reduced endmember is unclear.

2. While it is clear from theory and observation that oxidants exist in the surface ice (with abundance constrained), it is not clear whether or how fast these oxidants may be delivered to the ocean. Resurfacing on time scales less than 100 Ma is implied by crater counts and surface morphology (Zahnle et al. 2008), but it is not clear how this may translate to mechanisms or rates of delivery of surface oxidants to the ocean (Hand et al. 2007, Greenberg et al. 2010). Understanding Europa's geology through landing site reconnaissance and detailed landing site characterization (Section D.1.4) would help us infer the ways that Europa's ocean dynamics help or hinder the bringing to-

gether of interior reductants and surface oxidants (Vance and Goodman 2009).

3. Beyond constraints imposed on biology by total energy flux, the mode of delivery may also be critically important. For example, focused delivery of reduced fluids into an oxidized ocean (as with Earth's hydrothermal vents) would carry considerably different biological potential than diffusely distributed delivery of oxidants, e.g., by melting of foundered surface ice, into a reduced ocean.

While limitations clearly exist in the capability to observe, characterize, and constrain the delivery of energy to the Europan ocean, this is perhaps the most critical area for advancement in our understanding of the past and present habitability of this world.

D.1.1.1.3 *Elemental Raw Materials in Europa's Ocean*

Qualitatively, the assumed chondritic origin of Europa (Kargel et al. 2000) combined with exogenous delivery of materials (Pierazzo and Chyba 2002) should have provided Europa with the range of elements that are essential for Earth-like life. Hydrothermal activity, if present, would mobilize these elements from the silicate mantle and deliver them to the ocean. In quantitative terms, elemental availability at biologically meaningful levels would further depend on a variety of constraints, including the water-rock ratio in aqueous alteration of chondritic material (this is particularly important in light of the large water volume hypothesized for the Europan ocean) and pH-Eh conditions that can markedly affect speciation of many elements into soluble versus insoluble forms. Beyond the bulk constraint imposed by bounds on ocean salinity (Hand and Chyba 2007), these factors are essentially unknown.

D.1.1.1.4　The Physicochemical Context of Europa's Ocean

Modeling and empirical constraints suggest that temperature, pressure, pH, and salinity within the ocean likely fall within the limits known to be tolerated by extant terrestrial life (Nealson 1997; Zolotov and Shock 2001, 2004; Marion et al. 2003; Committee on the Limits of Organic Life in Planetary Systems 2007; Hand et al. 2009). It should be borne in mind that the ability of life on Earth to tolerate such broad-ranging conditions derives from physical compartmentalization (e.g., cell membranes) and a capability to invest energy into biomolecular repair or maintenance of internal conditions that differ from those outside the organism. Hence, the range of conditions tolerated by extant life may be narrowed if the available energy flux is low. Moreover, the range of conditions conducive to origin of life chemistry is not well understood, and may be narrower still. For example, it has been argued that life's emergence on Earth may have required relatively fresh water to sustain model cell membrane materials (Monnard et al. 2002) and thus that the high end of possible salinities for Europa's ocean may be limiting to the emergence of life (Hand and Chyba 2007). That arguments favoring saline environments have also been made (Spitzer and Poolman 2009) serves to underscore the uncertainty associated with origin of life chemistry even on Earth. Thus, while caution is always warranted in extrapolating a discussion of habitability from extant to emerging life, no aspect of the physics and chemistry of the Europan ocean, as presently understood, would appear to disallow biology.

Our current scientific understanding is that, qualitatively, Europa is likely habitable today and likely has been habitable for much of the history of the solar system. Further observation, particularly as enabled by landed science, will allow for advancement from qualitative to quantitative assessment of Europa's biological potential. Investigations that constrain inputs

of energy and chemical evolution in the ocean would be particularly important in this regard.

Finally, though hypothesis-driven science is well-served by measurements that can help constrain Europa's habitability, the importance of discovery-driven science should not be disregarded in the astrobiological exploration of Europa. Observation of plausibly prebiotic compounds, or complex organic molecules or structures consistent with biological origins, would greatly advance NASA's goal of determining whether or not life does exist beyond Earth (Des Marais et al. 2008, Space Studies Board 2011).

D.1.1.2　Composition Science Background

Europa's surface and near-surface composition (both inorganic and organic) provide a window into the habitability of its ocean. While not a direct match to the ocean, surface and near-surface composition will provide evidence from compounds directly incorporated into the ice shell from the ocean or that result from crustal formation processes such as fractional crystallization of salt-rich brines (Zolotov and Shock 2001). Europa's ice also records the history of exogenous materials delivered through impacts and dust, particularly material from neighboring Io (Zahnle et al. 2008, Carlson et al. 2009). Modification from the barrage of high-energy particles from Jupiter's magnetosphere complicates efforts to understand Europa's surface and the ocean beneath, but provides insight into the production of oxidants (Hand et al. 2007, Carlson et al 2009).

D.1.1.2.1　Icy and Non-Icy Composition

Much of what is known about Europa's composition comes from spectroscopic observations in the visible to near-infrared. Earth-based telescopic observations and data from the Voyager and Galileo spacecraft (see reviews by Alexander et al. 2009 and Carlson et al. 2009) show that the surface of Europa is primarily water ice in both crystalline and amorphous forms.

Dark, non-icy materials that mottle the rest of Europa's surface are linked to Europa's geological history, and determining their composition is key to understanding their origin. Non-icy components include carbon dioxide (CO_2), sulfur dioxide (SO_2), hydrogen peroxide (H_2O_2), and molecular oxygen (O_2), based on comparison of measured spectra with laboratory studies of the relevant compounds (Lane et al. 1981; Noll et al. 1995; Smythe et al. 1998; Carlson 1999, 2001; Carlson et al. 1999a, b; Spencer and Calvin 2002; Hansen and McCord 2008). Spectral observations from the Galileo Near-Infrared Mapping Spectrometer (NIMS) reveal disrupted dark and chaotic terrains on Europa with distorted and asymmetric absorption features indicative of water bound in non-ice hydrates. Hydrated materials observed in regions of surface disruption have been interpreted as magnesium and sodium sulfate minerals that originate from subsurface ocean brines (McCord et al. 1998a, 1998b, 1999). Alternatively, these might be sulfuric acid hydrates created by radiolysis of sulfur from Io (Carlson et al. 1999b, 2002, 2005; Strazzula 2011) or a combination of hydrated salts and hydrated sulfuric acid (Dalton 2000; McCord et al. 2001a, b, 2002; Carlson et al. 2005; Orlando et al. 2005; Dalton et al. 2005, 2007) (Figure D.1.1-1). A main objective for Europa science is to resolve the compositions and origins of these hydrated materials.

A broad suite of additional compounds is predicted for Europa based on observations of other icy satellites, as well as from experimental studies of irradiated ices, theoretical simulations, and geochemical and cosmochemical arguments. Organic molecular groups, such as CH and CN, have been identified on the other icy Galilean satellites (McCord et al. 1997, 1998b), and their presence or absence on Europa is important to understanding Europa's potential habitability. Other possible naturally occurring compounds that might be embedded in the ice and detectable by spectroscopic methods include H_2S,

OCS, O_3, $HCHO$, H_2CO_3, SO_3, $MgSO_4$, H_2SO_4, H_3O^+, $NaSO_4$, $HCOOH$, CH_3OH, CH_3COOH, and more complex species (Moore 1984; Delitsky and Lane 1997, 1998; Hudson and Moore 1998; Moore et al. 2003; Brunetto et al. 2005).

D.1.1.2.2   *Organic Molecules*

The possible presence of abiogenic organic molecules on Europa has implications for the moon's ability to support life, and also for understanding the distribution of such materials in the solar system. These organic molecules are important as indicators for habitability.
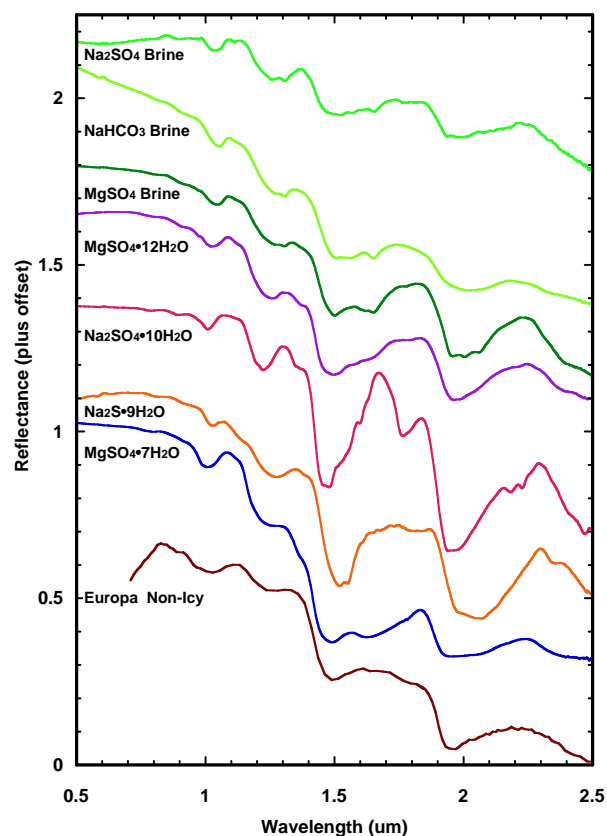
Figure D.1.1-1. Cryogenic reflectance spectra of hydrated sulfates and brines, compared to Europa. Spectra of epsomite ($MgSO_4 \cdot 7H_2O$), hexahydrite ($MgSO_4 \cdot 6H_2O$) and bloedite ($Na_2Mg(SO_4)2 \cdot 4H_2O$) were measured at 100, 120, and 120 K, respectively (Dalton 2000, 2003). Spectra of sodium sulfide nonahydrate ($Na_2S \cdot 9H_2O$); mirabilite ($Na_2SO_4 \cdot 10H_2O$); magnesium sulfate dodecahydrate ($MgSO_4 \cdot 12H_2O$); and $MgSO_4$, $NaHCO_3$, and Na_2SO_4 brines were measured at 100 K (Dalton et al. 2005).

However, a key element of evaluating habitability is knowledge of environmental factors that may be conducive or hostile to the production and preservation of organic molecules either from biotic or abiotic sources. On Mars, for instance, nondetection of organics in the Viking biological experiments led to the understanding that the combination of high ultraviolet flux and an oxidant-rich soil acts to rapidly break down organic material, and prompted a dimming in optimism toward the habitability of Mars (e.g., Klein 1979). Recent insights from the Phoenix Lander—namely the discovery of highly oxidizing perchlorate salts (Hecht et al. 2009)—have led to a reinterpretation of the Viking experiments and to the realization that the design of the experiments may have caused the destruction of sampled organic materials prior to processing for detection (Navarro–Gonzáles et al. 2010).

Additionally, the distribution and types of organic molecules found in an environment can be an indicator of life. For instance, a single complex organic molecule may not be diagnostic of life, but a distribution of molecules could provide intriguing evidence for selective processes that are unlike abiotic catalysis (Hand et al. 2010).

The abundance of organic molecules (complex or otherwise) on Europa is currently unknown.

The potential range of abundances can be estimated by comparison with terrestrial analogs (Hand et al. 2009). As shown in Table D.1.1-1, diverse environments may have abundances that vary by many orders of magnitude. As with salts, secondary processes may also play a role in concentrating organics (e.g., in sublimation lags) on Europa's surface. The total amount of organics in Europa's ice shell that are derived from the ocean would be dependent on the total dissolved organic compounds concentration at the ice-ocean interface. Even on Earth the abundance of material can be highly variable depending on the productivity of the system (see Table D.1.2-1). Therefore, it is critical that sensitivity to low levels of individual compounds be part of any investigation of Europa's organic composition.

More complex molecules have larger radiation cross-sections, so they are more susceptible to alteration by radiation. Radiolysis and photolysis probably alter the original surface materials and produce highly oxidized species that react with other non-ice materials, forming a wide array of compounds. Given the intense radiation environment of Europa, complex organic molecules are not expected in older deposits or in those exposed to higher levels of irradiation (Johnson and Quickenden 1997, Cooper et al. 2001). However, diagnostic molecular fragments and key carbon, nitrogen,

Table D.1.1-1. Abundances of cells in terrestrial environments.

Location	Abundance in Surface (cells/ml)[*]	Abundance in Surface (g cells / kg Water)[†]	Mass Fraction Cells	Mass Fraction of Glycine[#]
Ocean Surface (Low)	5000	1.20E-06	1.20E-09	4.8E-11
Ocean Surface (High)	500000	1.20E-04	1.20E-07	4.8E-09
Ocean Deep Basins (High)	10000	2.30E-06	2.30E-09	9.2E-11
Hydrothermal Vents (Low)	100000	2.30E-05	2.30E-08	9.2E-10
Hydrothermal Vents (High)	1.00E+09	2.30E-01	2.30E-04	9.2E-06
Vostok Accretion Ice (High)	260	6.00E-08	6.00E-11	2.4E-12
Vostok Water (Estimate)	150	3.45E-08	3.45E-11	1.4E-12

[*]Hand et al. 2009 (Table 3).

[†]Assumes no concentration mechanisms. After Hand et al (2009), using 2.3×10^{-13} g/cell value (Madigan et al 2003).

[#]Assumes same ratio as in *E.coli*. Using the mass ratio of glycine/cellglycine/cell mass in McCollom and Amend (2005), comparable to results from Glavin et al. (2001), in which organic content is taken as 200 µg/g based on average for materials from sample containing *E. Coli* in the amount of 10^{10} cells/g. Specific molecules and amounts are: aspartic acid (187), glutamic acid (310), serine (117), glycine (298), alanine (222), and valine (102), representing 70% of the total inventory of amino acids and about 9% of the cells' mass.

and sulfur products might survive in regions of lesser radiation (e.g., the leading hemisphere [Section D.1.4.2]) and sites of recent or current activity. Additionally, materials in the shallow subsurface are also protected from the bulk of this exogenic processing.

D.1.1.2.3   Salts

The salt composition of Europa's surface is a primary measure of the underlying ocean's composition and habitability (Zolotov and Shock 2004). As with organic materials, the processes of radiation, exogenous mixing, and diagenetic alteration acts on salts and their precursor fluids. Dissolved materials are expected to enter Europa's ocean through reactions between the ocean water and the underlying rocks (e.g., Kargel et al. 2000, Zolotov and Shock 2001, McKinnon and Zolensky 2003); the composition of Europa's ocean depends on the composition of the rocks and input fluids, as well as the temperatures, pressures and durations of water-rock reactions. Predictions based on assuming that the rocks have the same bulk composition as CV chondrites (e.g., Zolotov and Shock 2001, Marion et al. 2003) indicate that the ocean on Europa would be enriched in sulfate relative to the Earth's ocean, and depleted in sodium, chloride, and potassium. Magnesium and calcium are predicted to be at similar abundances. Much depends on the assumptions made in these models. Differences in rock composition, water-rock ratio, and in the efficiency of elemental extraction can cause large differences in the composition of resulting ocean fluids (e.g., Zolotov and Shock 2001).

A major reason that surface salts would differ from the underlying ocean composition is fractional crystallization during freezing and ascent of fluids from the ocean to the surface. As an example, for the predicted composition mentioned above, a series of salts would form as ocean water began to freeze on its ascent to the surface of the ice. As ice forms it incorporates very little in the way of solutes from the water, causing concentrations in the coexisting

brine to increase. Theoretical models (Zolotov and Shock 2001) indicate the order of precipitation of salts from the brine as temperature drops would be gypsum ($CaSO_4•2H_2O$), mirabolite ($Na_2SO_4•10H_2O$), magnesium sulfate ($MgSO_4•10H_2O$), sylvite (KCl), and hydrohalite ($NaCl•H_2O$). Magnesium sulfate is predicted to be the most abundant salt from the fractional freezing process, followed by mirabolite and gypsum. Sylvite would be more abundant than hydrohalite, but both would be 1 to 2 orders of magnitude less abundant than the sulfates. Again, differences in the composition of the underlying ocean could cause major changes in the order and abundance of salts formed, as could differences between the actual freezing process and the process modeled by the calculations.

Warm ice will sublimate at Europa's surface (Spencer 1987, Moore et al.1999), leading to lag deposits of salts. This will enhance the ability of a landed mission to detect salts. Many of the salts predicted to form initially through fractional freezing are extensively hydrated. Once exposed to surface conditions these hydrated salts can incrementally dehydrate, and dehydration through sublimation would drive changes in salt mineralogy (Zolotov and Shock 2001). So, the sublimation process that concentrates salts at the surface also alters the hydration state of those salts. The details of the effects of sublimation depend on relative stabilities of hydrated salts as the partial pressure of H_2O changes in the salt lag deposits, and the temperature at which the sublimation occurs. In addition, at an individual sample location, salts may have formed predominantly through fractional freezing of ocean water, or they may also have formed through freezing of residual brines generated by the fractional freezing process. The major consequence of these differences will be found in the proportion of sulfate salts relative to chloride salts. Gradients between surface and subsurface samples could be used to refine the mineralogy where differences in hydration

state may have been preserved in the subsurface. In addition to recombination of ions due to changes in hydration state of salt deposits thermal processing of Europa's near-surface may also lead to characteristic recombination of ions (Loeffler and Hudson 2011).

D.1.1.2.4 Exogenic Processes

Exogenic processes are a key part of Europa's composition story, but much remains to be learned about the types and sources of materials being implanted. Some surface constituents result directly from exogenic sources. For example, sulfur from Io is transported by the magnetosphere and is implanted into Europa's ice. Ejecta from impacts on Io are predicted to reach Europa's surface in substantial amounts in the form of olivine, the presumed bulk composition of Io (Zahnle et al. 2008). Micrometeorites also should be an important contributor of organic and nonorganic compounds (Pierazzo and Chyba 2002, Johnson et al. 2004, review by Carlson et al 2009 and references therein).Thus, compositional variations

with depth could help separate exogenic and endogenic material and associated processes. For example, comparison of the composition of a surface and subsurface sample could allow for the identification of gradients related to variations in radiation penetration and gardening depth, thus helping to unravel the chemical processes that led Europa to its present state.

Magnetic field measurements by Galileo of ion-cyclotron waves in the wake of Europa provide evidence of sputtered and recently ionized Cl, O_2, SO_2, and Na ions (Volwerk et al. 2001). Medium-energy ions (tens to hundreds of keV) deposit energy in the topmost few tens of microns; heavier ions, such as oxygen and sulfur ions, have an even shorter depths of penetration; while MeV electrons could penetrate and affect the ice to a depth of more than 1 m (Paranicas et al. 2002, 2009 and references therein, Figure D.1.1-2). The energy of these particles breaks bonds to sputter water molecules, molecular oxygen, and any
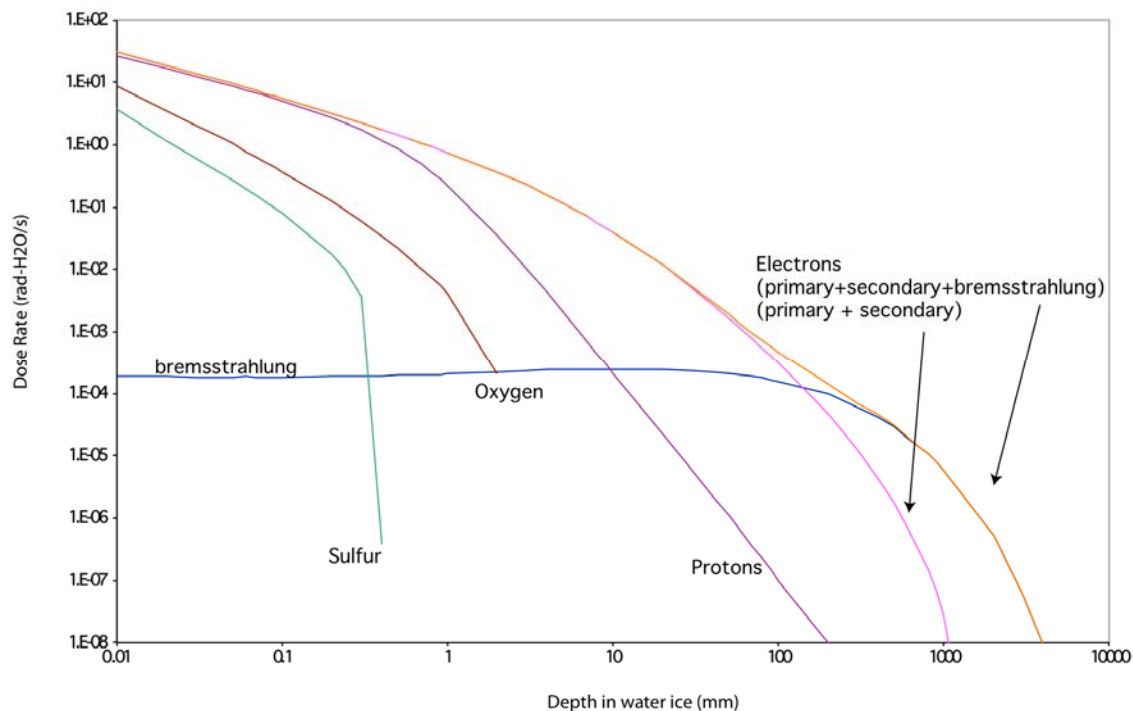

Figure D.1.1-2. Assessed surface-averaged dose rates, in rad/s per molecule of water as a function of depth, for electrons, protons, oxygen, and sulfur in the vicinity of the trailing hemisphere equator. From Paranicas et al. (2009).

impurities within the ice (Cheng et al. 1986), producing the observed atmosphere and contributing to the erosion of surface features. Recent work (Patterson et al. 2012) shows that for protected locations on the surface, penetration depths are expected to be only 1–3 cm (Section D.1.4.2). This would lead to a shallow near surface that has been processed, and far more pristine materials slightly deeper (10-20 cm) that would have experienced little radiation processing.

As electrons bombard Europa's surface and slow down, they produce bremsstrahlung photons. It has been shown that these particles can penetrate up to a meter into Europa's surface (Paranicas et al. 2009). However, the number of bremsstrahlung photons produced decreases with the energy of the electrons, as does the range of possible photon energies (Agostinelli et al. 2003, Allison et al. 2006). In other words, the depth of penetration for such particles is related to the energy of the electron that produced them. This implies that, while the lower latitudes of Europa's trailing hemisphere will be radiolytically processed to depths of about 1 m (Paranicas et al. 2009), the leading hemisphere of the satellite and higher latitude regions of the trailing hemisphere will only be affected to depths in the micron to centimeter range (Patterson et al. 2012).

Sulfur is the dominant material exported from Io to Europa, but a substantial mass of erupted olivine is anticipated as well (Zahnle et al. 2008), with an additional contribution transferred from Io as ejecta from cometary impacts (Alvarellos et al. 2008). Interplanetary dust particles and cometary materials may contain a host of organic and inorganic constituents. For example, the primitive chondritic Tagish Lake meteorite (Brown et al. 2000) was found to contain more than a characteristic array of elements representative of the early solar system's composition; it also contains mono- and dicarboxylic acids, dicarboximides, pyridine carboxylic acids, a sulfonic acid, and both aliphatic and aromatic hydrocarbons (Piz-

zarello et al. 2001). Silicates in particular would be a strong marker for an exogenic origin of materials on Europa because their solubility is low in Europa's ocean, even in models that quench the ocean's composition at a relatively high temperature (Zolotov and Kargel 2009). The possibility for exogenous organics and their irradiated byproducts on Europa's surface underscores the need for compositional measurements both close to the surface and at some depth below.

Johnson et al. (2004) calculated that the globally averaged micrometeoroid flux for Europa, Ganymede, and Callisto is $\sim1.5\times10^{-16}$ g cm^{-2} s^{-1}, which amounts to a total of ~45 g s^{-1} of chondritic material to Europa's surface. For a chondritic composition of ~6% sulfur and 3.4 to 24% carbon (Lodders 2003), this leads to $\sim2\times10^{-3}$ g cm^{-2} sulfur and $\sim1\times10^{-3}$ to 7×10^{-3} g cm^{-2} carbon accumulated on Europa's surface per one thousand years. In other words, over relatively short geological time-scales, carbon concentrations from exogenous delivery could reach the parts-per-million level for the upper centimeter of Europa's surface. As a result, it is important that a surface science investigation seeking to distinguish exogenous from endogenous organic chemistry target a young surface, collect samples from beneath the surface, and be able to characterize the structure and complexity of organics in any samples collected (Hand et al. 2009, 2010).

D.1.1.3   Ocean and Ice Shell Science Background

The habitability of Europa cannot be decoupled from processes associated with the evolution of its ice shell. Values of several key parameters are still quite uncertain, including the thickness of Europa's ice shell, the depth of the ocean, and the degree to which the surface is in communication with the subsurface (e.g., Cassen et al. 1978; Squyres et al. 1983; Carr et al. 1998; Kivelson et al. 1999, 2000; Pappalardo et al. 1999; Greenberg et al. 1999; Figueredo and Greeley 2002).

The strongest constraint on the existence and extent of Europa's ocean comes from Galileo's magnetometer investigations, which measured Europa's induced magnetic field. Results imply a global conducting layer, consistent with a salty ocean, within about 50 km of the surface (Khurana et al. 1999; Kivelson et al. 1999, 2000; Zimmer et al. 2000). The details of this signature depend upon the depth of the ocean, the thickness of the ice shell, and the salinity of the ocean (e.g., Zimmer et al. 2000, Hand and Chyba 2007). Magnetometers can also be utilized to discern local sources, in addition to global fields, on landed or orbital platforms (e.g., Dyal et al. 1970, Acuna et al.1999, Hood et al. 1997, Hood et al. 2005, Khurana et al. 2007). However, Galileo magnetometer measurements lacked both spatial and temporal resolution to detect whether a small intrinsic signature might exist.

Because Europa's measured magnetic field is induced by the 9.925-hr rotation of Jupiter's magnetic field, the signal at Europa is time-varying with two dominant periods. The shorter period is 11.23 hours, which is the beat period between Europa's orbital motion and Jupiter's rotation. The longer period (85.228 hours) is just that of Europa's orbital motion about Jupiter, in a slightly eccentric path. Thus, the magnetic field of Europa can be utilized to study oceanic processes as well as the deep interior, with a long baseline of observations across several Jovian rotations.

Central to the debate about ice and ocean thickness is the geomorphology of the surface, including ridges, bands, and chaos terrains (Section D.1.4). Of these, chaos terrains in particular (Section D.1.4.1) have been central to these issues, as the terrain possibly represents regions of material exchange between the surface and the ocean (Collins and Nimmo 2009, Schmidt et al. 2011). Because such exchange is critical to the habitability of Europa (Section D.1.1), a dedicated Lander mission must address and test hypotheses regarding ice shell thickness, ocean depth, and the mecha-

nisms for exchange between the surface and subsurface.

To address these hypotheses, observations must be made that sample the region surrounding the Lander. The best sources of energy for these observations are the seismic waves generated by cracking within Europa's ice shell. Geophysical models of Europa indicate that any ice shell beyond a thickness of ~15 km must transfer heat through thermal convection of a mobile ice layer underlying a shallow brittle layer (e.g., McKinnon 1999; Tobie 2003; Showman 2004; Mitri and Showman 2008; Showman and Han 2005, 2010) or diapirism by which localized ice plumes rise through the ice shell (Rathbun et al. 1998, Pappalardo et al. 1998, Pappalardo and Barr 2002, Sotin et al. 2002). These are consistent with observations of the morphology of Europa's surface (e.g., Pappalardo et al. 1998, Figueredo and Greeley 2002) and of its impact craters (Schenk 2002). However, observations of cycloids and other surface features have been used to argue for a much thinner shell (e.g., Carr et al. 1998, Greenberg et al. 1999, Hoppa et al. 1999).

Cycloidal ridges are composed of chains of arcuate cusp ridge segments joined at acute angles, possibly indicative of progressive opening in the presence of a changing stress field as might be cause by diurnal tides called "tidal-walking" (e.g., Hoppa et al. 1999). However, tail-crack propagation initiated by diurnal forcing but occurring over much longer time periods (Marshall and Kattenhorn 2005) may explain these features as well. In particular, tail-crack propagation provides a good observational fit to inverted and paired cycloids (e.g., Marshall and Kattenhorn 2005). Nonetheless, cracking, ridge formation and chaos formation would be appreciably different in a thin shell than from a thick shell, and thus should be testable utilizing both seismic measurements.

Both melt-through of a "thin" (less than 10 km) ice shell (e.g., Carr et al. 1998, Green-

berg et al. 1999, O'Brien et al. 2002), and disruption of a thick shell (greater than 10 km) by diapirism (Rathbun et al. 1998, Pappalardo et al. 1998, Pappalardo and Barr 2002, Sotin et al. 2002) or convective upwellings (e.g., McKinnon 1999, Tobie 2003, Showman 2004) have been suggested as the mechanisms that may form chaos terrains. Both models can produce the appearance of floating icebergs within some of the terrain; however, both suffer difficulty reproducing the topography of chaos terrain (Collins et al. 2000, Collins and Nimmo 2009). In such scenarios, the survival of ascending warm plumes of ice into the shallow subsurface might cause localized partial melting of salty ice or focusing of tidal energy within the plume (e.g., Pappalardo and Head 1999, Nimmo and Giese 2000, Sotin et al. 2002, Mitri and Showman 2008).

A recent model for chaos formation based upon the collapse of the ice lid above large, liquid water lenses formed near the brittle-ductile transition in a thick ice shell has been suggested to account for the formation of chaos terrains above melt water formed within the ice, and implies that some regions are active today (Schmidt et al. 2011). Thus, independent of the model assumed, chaos terrains are likely sites of exchange of material between Europa's surface, the ice shell and ocean, as well as significant tectonic activity, making them astrobiologically relevant for further study and sources of seismic activity by which to test ice shell hypotheses.

On Earth, seismological techniques are useful for understanding both the flow dynamics of ice sheets (e.g., Neave and Savage 1970, Blankenship et. al. 1986, Alley et al. 1986, Blankenship et al. 1987, Anandakrishnan and Alley 1997, Winberry et al. 2009) and the dynamics and properties of floating ice shelves (e.g., Johnson and Smith 1997, Lambrect et al. 2007, McMahon and Lackie 2006, Bassis et al. 2005, Brajanovski 2006). Dynamic ice processes provide a range of seismic energy sources that allow characterization of both the source process and the ice properties between the source and receiver. Thus, seismic sources and techniques are of interest for the landed exploration of Europa (Kovach and Chyba 2001, Chyba 2001, Lee et al. 2003, Cammarano et al. 2006).

Trapped waves known as Love waves have been suggested as useful for diagnosing ice shell thickness (Kovach and Chyba 2001, Chyba 2001). However, Lee et al. (2003) have shown that these waves, which are trapped within the shell, have diagnostic power only at distances that are large compared to the ice shell thickness. For an ice shell from a few to tens of kilometers thick, both Love and Rayleigh waves require powerful sources at known and large (>100 km) distances that are likely beyond the discrimination capabilities of a single landed receiver.

Body waves can be used to accomplish echosounding based on comparing primary "compressional" (P) and secondary "shear" (S) wave arrivals, along with their reflections (PP and SS) and P-S wave conversions at a variety of interfaces (Figure D.1.1-3). Figure D.1.1-4 shows various signal characteristics for direct, reflected and converted waves traversing

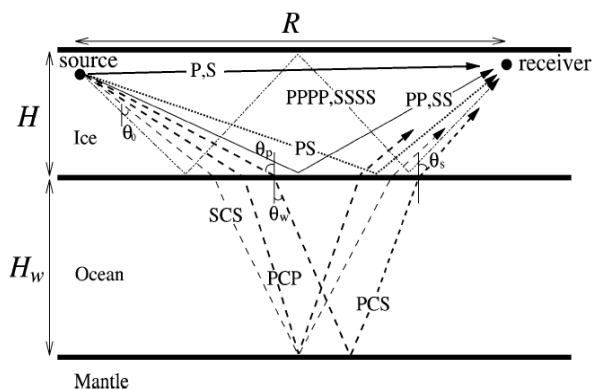**Figure D.1.1-3.** Ray paths of compressional (P) and shear (S) waves through the ice shell and acoustic (C) waves through the ocean. PP, PS, SS waves are single reflections from the ice-water interface, while PCP, PCS, and SCS waves are single reflections from the water-mantle interface. Letters are added consecutively when it reflects from or transmits through an interface. From Lee et al. (2003).
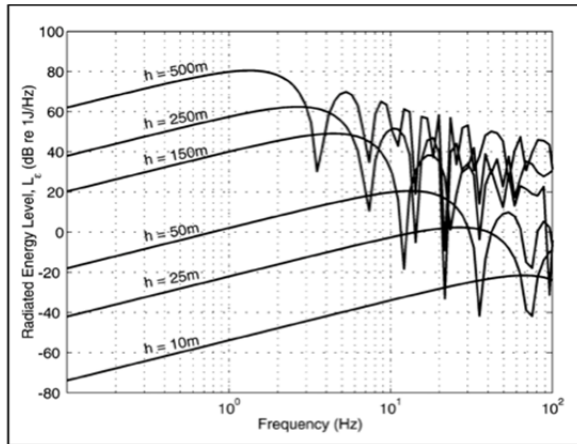
Figure D.1.1-4. Cracking events and their detectability by seismic techniques (reproduced from Lee et al 2003). Left: Frequency of energy radiated by cracks of depth h. Right: Particle velocities for direct waves (P and S) and waves reflected (PP and SS) and converted (PS, PPSS and PSSS) at the ice-ocean interface within a 20-km ice shell at 50 km range for crack depth h = 250 m.
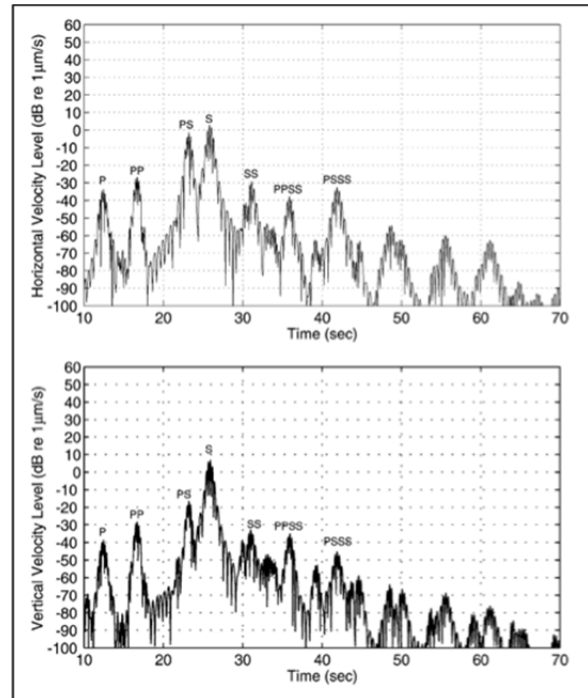
Europa's ice shell for source to receiver offset of 50 km, generated by a surface crack with a rupture depths of 250 m. This illustrates that body waves are particularly useful for studies of Europa's ice shell and underlying ocean (Lee et al. 2003).

In order to design a seismic experiment on the surface of Europa, we need some knowledge of likely source and noise characteristics. Current models are not well constrained, and thus lead to a wide range of predicted source and noise parameters. Sources of seismic energy in Europa's ice shell have been assumed to be associated with fracture events from the near surface or the ice-ocean interface (Lee et al. 2003, Kovach and Chyba 2001, Chyba 2001, Cammarano et al. 2006). These analyses generally assume crack propagation at ridges or cycloids to be the dominant source of seismic waves, and the initial work assumed that ridges and cycloidal cusps form as a release of energy within one tidal cycle (one Eurosol), akin to the tidal-walking model of cycloid formation (Hoppa et al. 1999).

Under this assumption, the ambient background noise from the formation of geograph-

ically distributed cracks of varying size is sufficiently high that only 100-250m cracking events would be energetic enough events to detect above the background (Lee et al. 2003). Alternatively, the build up of stress over several diurnal cycles may be required to permit crack propagation (e.g., Marshall and Kattenhorn 2005). Thus the estimates of the rate of large events generating body waves of sufficient energy to sound the full ice shell (either thick or thin) and ocean advanced by Lee et al. 2003 and others are likely to be an overestimation by one to a few orders of magnitude. However, it is also true that the corresponding background seismic noise will also be much lower if cracks propagate slower or form less frequently. The ambient noise decreases by ~20 dB for two-orders of magnitude lower source rates, implying that even at 50km source-receiver range, 100-m deep cracking events will be of sufficient energy for both the ice-ocean interface and ocean floor to be detected above the noise, and 50 m cracks may also be detectable. Thus regardless of crack source frequency, seismic techniques offer robust characterization of the ice shell and ocean.

The rupture and refreeze of ice above liquid lenses (e.g., Schmidt et al. 2011) could provide an additional source of seismic events to be quantified if the Lander is located nearby (within tens of kilometers). Energetic seismic waves could be used to diagnose the thickness of a water lens and the ice shell above and below using body wave analyses, akin to the 5-km and 20-km ice shell scenarios envisioned by Lee et al. (2003).

Ultimately, the greatest unknowns for bounding our knowledge of the exchange processes that modulate the potential habitability of Europa are the nature of ice-ocean exchange, which results in up-welling of any material from the ocean into the shell and the downwelling of the near-surface materials. In the context of the geophysical models described above, the following major questions should be addressed by landed ocean and ice shell science investigations:

i. How deep is the ocean and how does it interact with the overlying ice to supply upwelling material and receive downwelling material?

ii. Do shallow liquid bodies exist within the ice shell, and if so, how do they communicate with the surface, and with the ocean below?

iii. Is surface-ocean exchange active today?

iv. Is geological activity coupled to the tidal cycle?

D.1.1.4 Geology Science Background

Europa has a varied and complex geology (Figure D.1.1-5), the principal expression of the moon's past and present processes. The potential habitability of Europa is intimately tied to the satellite's geological evolution. A better knowledge of Europa's geology also allows us to gather clues about geological processes on other icy satellites, such as Miranda, Triton, and Enceladus.

The relative youth of Europa's surface is inherently linked to the ocean and the effects of gravitational tides, which trigger processes that include cracking of the ice shell, resurfacing, and possibly release of materials from the interior (e.g., Pappalardo et al. 1999, Doggett et al. 2009, Schmidt et al. 2011). Clues to these and other processes are provided by spectacular surface features such as chaotic terrain, lenticulae, smooth plains, impact craters, and linear fractures and ridges.

D.1.1.4.1 Chaotic Terrain, Lenticulae, and Smooth Plains

Of particular interest to assessing Europa's habitability is access to material from the ocean that has recently been transported to the surface. Probably the prime candidate terrain type where such material might be found is chaotic terrain.

Europa's surface has been disrupted to form regions of chaotic terrain, as subcircular features termed lenticulae, and irregularly shaped, generally larger chaos zones (Collins and Nimmo 2009). Lenticulae include pits, spots of dark material, and domes where the surface is upwarped and commonly broken (Figure D.1.1-5c and f). Chaos is generally characterized by fractured plates of ice that have been shifted into new positions within a background matrix (Figure D.1.1-5e). Much like a jigsaw puzzle, many plates could be fit back together, and some ice blocks appear to have disaggregated and "foundered" into the surrounding finer-textured matrix (Spaun et al. 1998). Some chaos areas stand higher than the surrounding terrain (Figure D.1.1-5h and i).

Pappalardo et al. (1998a, 1999) argued that chaos features possibly formed by upwelling of compositionally or thermally buoyant ice diapirs through the ice shell. In such a case, onset of convection would imply an ice shell thickness of at least 10–20 km at the time of formation. Models of chaos formation suggest whole or partial melting of the ice shell, perhaps enhanced by local pockets of brine (Head and Pappalardo 1999). Downward and upward doming forms have been interpreted to corre-
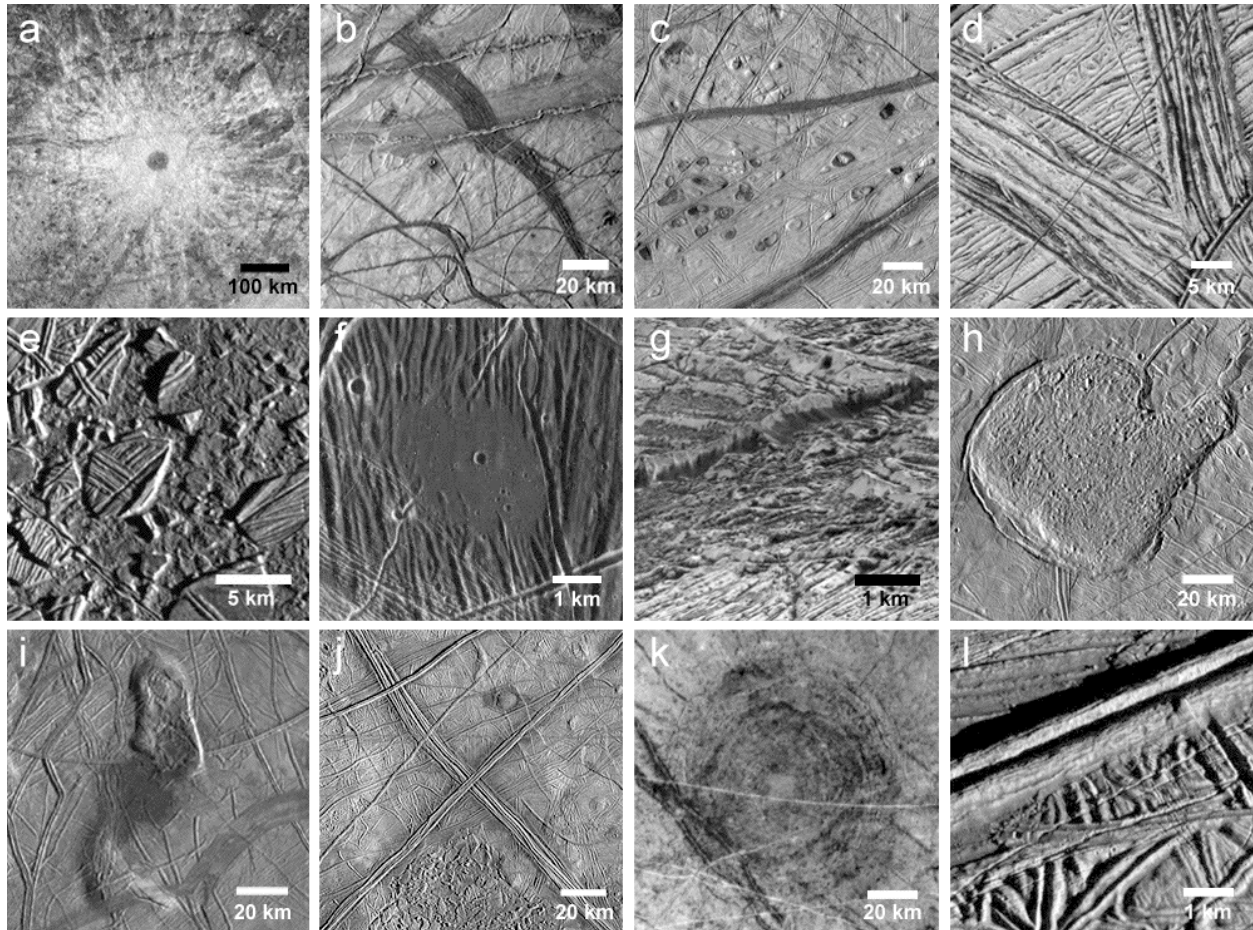
Figure D.1.1-5. Europa is a geological wonderland, with a wide variety of surface features. While much was learned from Galileo observations, it is still not understood how most of these features form, or their implications for Europa's evolution. Shown here are (a) the impact crater Pwyll, the youngest large crater on Europa; (b) pull-apart bands; (c) lenticulae; (d) ridge complexes at high resolution; (e) Conamara Chaos; (f) dark plains material in a topographic low, (g) very high-resolution image of a cliff, showing evidence of mass wasting; (h) Murias Chaos, a cryovolcanic feature which appears to have flowed a short distance across the surface; (i) The Castalia Macula region, in which the northernmost dome contains chaos and is ~900 m high; (j) regional view of two very large ridge complexes in the Conamara region; (k) Tyre impact feature, showing multiple rings; and (l) one of Europa's ubiquitous ridges, at high resolution.

late with recently formed chaos regions created through subsurface brine mobilization, and through subsequent freezing, respectively; based on this model, at least one chaotic region, Thera Macula, might be actively forming today (Schmidt et al. 2011). An alternative model suggests that chaotic terrain formed through direct material exchange (by melting) between the ocean and surface (Carr et al. 1998a, Greenberg et al. 1999).

Chaos features are stratigraphically young (Figueredo and Greeley 2004), possibly indicating a geologically recent increase in internal heating in Europa. Chaos and lenticulae commonly are dark and reddish, thought to be material derived from the subsurface ocean. Schmidt et al (2011) concluded that chaos terrains form above liquid water lenses perched within the ice shell as shallow as 3 km, proposing that ice–water interactions and freeze-out give rise to the diverse morphologies and topography of chaos terrains.

Figure D.1.1-6. Thera Macula may be a region of active chaos formation above a large liquid water lens. Topographic data indicates that Thera is low-lying, suggesting subsurface water today. Galileo image at 220 m/pixel resolution.

They suggest that the sunken topography of Thera Macula indicates that Europa is actively resurfacing over a lens comparable in volume to the Great Lakes in North America (Figure D.1.1-6).

There are small (few kilometers wide) occurrences of smooth level, commonly dark, plains (Figure D.1.1-5f) that may be associated with chaos and lenticulae. These features are plausibly explained by the release of low-viscosity fluid at the surface (Fagents 2003). Typically, these features consist of smooth, low albedo surfaces which occupy topographic lows, may embay surrounding ridged terrain, are apparently confined by topographic features such as ridges, and can exhibit lobate morphology (Greeley et al. 2000). Galileo color images show that low-albedo surfaces tend to be reddish-brown (Clark et al. 1998, Geissler et al. 1998). These units may be associated with small or large-scale disruptions of the surface and range in size from a few to 10s of kilome-

ters. For example, Figure D.1.1-5f shows a small, smooth, low-albedo pond-like feature lying in a depression in ridged plains near 6°N, 327°W. This feature has been interpreted as a small-volume (0.5 km^3) fluid effusion (Head et al. 1999).

D.1.1.4.2   Impact Features

A large, recent impact event could potentially transport material from the ocean to the surface, and *vice versa*. Hence, such sites could be potential locations for *in situ* sampling of ocean-derived material. Only 24 impact craters ≥10 km have been identified on Europa (Schenk et al. 2004), reflecting the youth of the surface. This is remarkable in comparison to Earth's Moon, which is only slightly larger than Europa but far more heavily cratered. The youngest Europan crater is thought to be the 24-km-diameter Pwyll, (Figure D.1.1-5a) which still retains its bright rays, and likely formed less than 5 Myr ago (Zahnle et al. 1998, Bierhaus et al. 2009).

Crater morphology and topography provide insight into ice layer thickness at the time of the impact. Morphologies vary from bowl-shaped depressions with crisp rims, to shallow depressions with smaller depth-to-diameter ratios. Craters up to 25–30 km in diameter have morphologies consistent with formation in a warm but solid ice shell, while the two largest impacts (Tyre [Figure D.1.1-5k] and Callanish) might have punched through brittle ice about 20 km deep into a liquid zone (Moore et al. 1998, 2001; Schenk et al. 2004; Schenk and Turtle 2009).

D.1.1.4.3   Linear Features

Europa's unusual surface is dominated by tectonic features in the form of linear ridges, bands, and fractures. The class of linear features includes simple troughs and scarps (e.g., Figure D.1.1-5g), double ridges separated by an axial trough, and intertwining ridge complexes. Whether these represent different processes or stages of the same process is uncertain. Ridges are the most common fea-

ture type on Europa and appear to have formed throughout the satellite's visible history (Figure D.1.1-5j and l). They range from 0.1 to >500 km long, are as wide as 2 km, and can be several hundred meters high. Cycloidal ridges are similar to double ridges, but form chains of linked arcs as viewed from above.

Most models for the formation of Europa's linear features involve fracturing in response to processes within the ice shell (Greeley et al. 2004, Kattenhorn and Hurford 2009, Prockter and Patterson 2009). Some models suggest that liquid oceanic material or warm mobile subsurface ice squeezes through fractures to form a ridge, while others suggest that ridges

form by frictional heating and possibly melting along a shear zone. Thus, ridges might represent regions of material exchange between the surface, ice shell, and ocean, providing a means for surface oxidants to enter the ocean.

Bands reflect fracturing and lithospheric separation, potentially like sea-floor spreading on Earth, and most display bilateral symmetry (e.g., Sullivan et al. 1998) (Figure D.1.1-5b and d). Their surfaces vary from relatively smooth to heavily fractured. The youngest bands tend to be dark, while older bands are bright, suggesting that they brighten with time. Geometric reconstruction of bands suggests a spreading model, indicating extension in these areas and possible contact with the ocean (Tufts et al. 2000, Prockter et al. 2002).

Fractures are narrow (from hundreds of meters to the ~10 m limit of Galileo image resolution) and some exceed 1000 km in length. Some fractures cut across nearly all surface features, indicating that the ice shell is subject to deformation on the most recent timescales. The youngest ridges and fractures could be active today in response to tidal flexing. Young ridges might be places where there has been material exchange between the ocean and the surface.

D.1.1.4.4　Small Scale Features

The greatest uncertainty facing *in situ* investigations on Europa's surface is the lack of knowledge as to the nature of the landscape at scales smaller than a decameter (Figure D.1.1-7). This uncertainty has both substantial scientific and engineering-operational
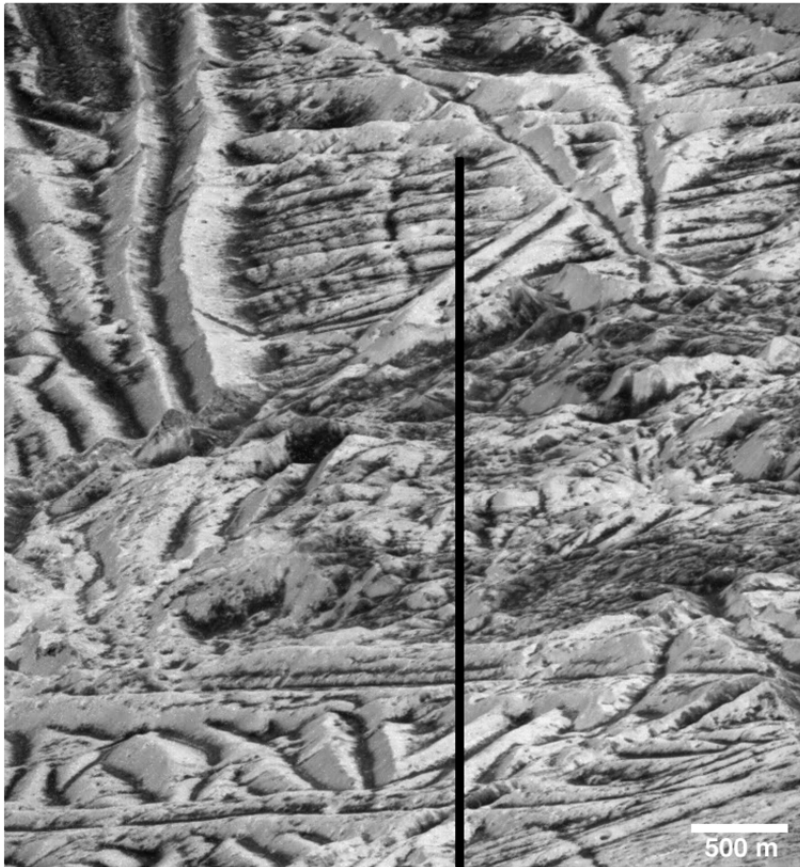
Figure D.1.1-7. Europa's surface at the highest resolution available. This oblique image was acquired by Galileo at 6 m/pixel in the horizontal direction. The image is not reprojected, but is presented as it was taken by the spacecraft, as if one were looking out of an aircraft window from 600 km above Europa's surface. Ridged regions are in the foreground and background here, with chaotic terrain in between. The darker areas appear smooth in context imaging at regional (~200 m) resolution.

implications (Section D.2.8.2). Many potential high-science-interest targets, such as chaos terrain, have a substantial chance of extreme roughness at the decameter to decimeter scales. The processes potentially responsible for these roughness elements are uncertain, but candidates are: mass-wasting occurring both during and after ice or water emplacement; sublimation erosion and local ice segregation; textures formed by freezing and chemical exsolution; and perhaps to a lesser extent impact gardening and sputtering.

D.1.2   Lander Science Traceability Matrix

The Lander Science Traceability matrix contents show a rigorous flow-down of science goals and objectives to instrument and mission requirements

As outlined in Section D.1, multiple well-defined and focused science questions will be addressed by exploring Europa to understand the potential for life in the outer solar system. Interrelated physical processes and habitability are key drivers for Europa exploration. Thus, the goal adopted for the Europa Lander Mission concept is to

Explore Europa to investigate its habitability.

This goal implies understanding processes, origin, and evolution. These include testing the numerous scientific issues described above. "Investigate its habitability" recognizes the significance of Europa's astrobiological potential. "Habitability" includes investigating the composition of Europa's surface materials, confirming the existence and determining the characteristics of water within and below Europa's icy shell, and evaluating the processes that have affected Europa. A Europa Lander could provide direct assessment of Europa's habitability and ocean composition while addressing physical processes at a local scale.

The Europa Lander Mission objectives flow from the science issues outlined in Section D.1. These objectives represent a key subset of Europa science that can be well accomplished by a landed Europa mission.

These objectives are categorized in priority order as:

C. Europa's Composition: *Understand the habitability of Europa's ocean through composition and chemistry.*

O. Europa's Ocean and Ice Shell: *Characterize the local thickness, heterogeneity, and dynamics of any ice and water layers.*

G. Europa's Geology: *Characterize a locality of high scientific interest to understand the formation and evolution of the surface at local scales.*

The traceability matrix, compiled in FO D-1, maps the Lander objectives (in priority order) to specific investigations (in priority order within each objective) to address the overarching mission goal. Specific measurements for each investigation are listed (in priority order within each investigation). The Lander objectives and investigations are discussed in detail in Sections D.1.2.1–D.1.2.4.

D.1.2.1   Habitability: Implications for Science Traceability

A landed suite of instruments offers unique and valuable possibilities to advance our understanding of the biological potential of Europa. Investigations that take full advantage of the potential for high-resolution imaging, physical contact with the surface, and direct compositional measurements on surface and subsurface samples would maximize the astrobiology science yield of a Lander mission.

D.1.2.1.1   Implications of Composition

An ability to broadly characterize the composition of samples directly acquired from the surface and shallow subsurface of Europa would provide quantitative metrics and insight from which to assess the habitability of this world. Such capability also offers inherent "discovery potential" with respect to molecules or structures that could be consistent with biological origins.

Goal	Objective	Investigation	Measurement	Model Instrument	Mission Constraints/Requirements	Notional Mission Type	Water	Chemistry	Energy
Explore Europa to investigate its habitability	C. Composition	Understand the habitability of Europa's ocean through composition and chemistry.	C.1 Characterize surface and near-surface chemistry, including complex organic chemistry to constrain ocean composition and understand the endogenic processes from which it evolves.	C.1a Measure organic content (including complex organics) of surface (0.5-2 cm depth) and near-surface (5-10 cm depth) materials to as low as 1 ppb concentration.	Mass Spectrometer (MS), Raman Spectrometer (RS)	(1) Maintain the sample at a temperature to prevent melting (<198K); to preserve O_2, CO and CO_2, the sample needs to be maintained at a temperature lower than 150K. (2) Mass Spectrometer with capability for filtration, thermally evolved gas analysis, and organic separation. (3) Raman spectra of collected samples (lower sensitivity to organics than Mass Spectrometer). (4) *Baseline:* Mass Spectrometer and Raman measurements of two samples from different depths; Raman and Mass Spectrometer to measure the same sample. *Floor:* Mass Spectrometer measurements of samples acquired from two depths. Europa Sampling System: Two samples of ~1 cc each. Obtain a minimum of one sample from 0.5-2 cm depth, and one from 5-10 cm depth. Samples are not required to be from the same location. Contamination control of spacecraft organics in the sample analysis chain of < 1 ppb.	Lander		✔	✔
				C.1b Measure mineralogy and volatile content of surface (0.5-2 cm depth) and near-surface (5-10 cm depth) materials to as low as 0.1 Wt %.	Mass Spectrometer (MS), Raman Spectrometer (RS)	(1) Ability to collect Raman spectra of samples from two depths; Raman spectra of any sample collected for analytical analysis; analytical analysis with protocols compatible with measuring trapped volatiles and volatiles evolved from salts. (2) Maintain the sample at a temperature to prevent melting (<198K); to preserve O_2, CO and CO_2, the sample needs to be maintained at a temperature lower than 150K. (3) Mass Spectrometer capability for filtration and thermally evolved gas analysis (less specificity in inorganic mineralogy than Raman). (4) *Baseline*: Mass Spectrometer and Raman measurements of two samples from different depths; Raman and Mass Spectrometer to measure the same sample. *Floor*: Mass Spectrometer measurements of samples acquired from two depths; Europa Sampling System: Two samples of ~1 cc each. Obtain a minimum of one sample from 0.5-2 cm depth, and one from 5-10 cm depth. Samples are not required to be from the same location. Contamination control in the sample analysis chain of volatile and detectable inorganic compounds at < 1 ppm.	Lander		✔	✔
		C.2 Characterize surface and near-surface chemistry, including complex organic chemistry to constrain the exogenic processes and material fluxes that affect ocean composition.		C.2a Measure organic content (including complex organics) of surface (0.5-2 cm depth) and near-surface (5-10 cm depth) materials to as low as 1 ppb concentration.	Mass Spectrometer (MS)	(1) Maintain the sample at a temperature to prevent melting (<198K); to preserve O_2, CO and CO_2, the sample needs to be maintained at a temperature lower than 150K. (2) Mass Spectrometer with capability for filtration, thermally evolved gas analysis, and organic separation. (3) Raman spectra of collected samples (lower sensitivity to organics than Mass Spectrometer). (4) *Baseline:* Mass Spectrometer and Raman measurements of two samples from different depths; Raman and Mass Spectrometer to measure the same sample. *Floor:* Mass Spectrometer measurements of samples acquired from two depths. Europa Sampling System: Two samples of ~1 cc each. Obtain a minimum of one sample from 0.5-2 cm depth, and one from 5-10 cm depth. Samples are not required to be from the same location. Contamination control of spacecraft organics in the sample analysis chain of < 1 ppb.	Lander		✔	✔
				C.2b Measure mineralogy and volatile content of the surface (0.5-2 cm depth) and near-surface (5-10 cm depth) materials to as low as 0.1 Wt %, including exogenous and processed constituents.	Mass Spectrometer (MS), Raman Spectrometer (RS	(1) Ability to collect Raman spectra of samples from two depths; Raman spectra of any sample collected for analytical analysis; analytical analysis with protocols compatible with measuring trapped volatiles and volatiles evolved from salts. (2) Maintain the sample at a temperature to prevent melting (<198K); to preserve O_2, CO and CO_2, the sample needs to be maintained at a temperature lower than 150K. (3) Mass Spectrometer capability for filtration and thermally evolved gas analysis (less specificity in inorganic mineralogy than Raman). (4) *Baseline*: Mass Spectrometer and Raman measurements of two samples from different depths; Raman and Mass Spectrometer to measure the same sample. *Floor*: Mass Spectrometer measurements of samples acquired from two depths; Europa Sampling System: Two samples of ~1 cc each. Obtain a minimum of one sample from 0.5-2 cm depth, and one from 5-10 cm depth. Samples are not required to be from the same location. Contamination control in the sample analysis chain of volatile and detectable inorganic compounds at < 1 ppm.	Lander		✔	✔

☐ Floor
▨ Baseline only

Water: Water in its liquid form as pertaining to habitability as an oxidizer and medium for the transport of chemical constituents.
Energy: Energy that supports and fosters a means for potential metabolism to be established and sustained.
Chemistry: The constituents that foster and sustain the processes and environment for metabolic activity.

Explore Europa to investigate its habitability

C. Composition

Understand the habitability of Europa's ocean through composition and chemistry.

Sub-objective	Measurement	Instrument	Requirements	Platform			
C.3 Constrain the context of compositional measurements.	C.3a Image sampling area prior to sample collection to provide local and site specific context.	Reconnaissance Imager (RI), Site Imaging System (SIS)	(1) Provide local-scale context of the landing area, both before and after landing along with detailed coverage of the work area from which the samples will be acquired.	Carrier & Lander	✔	✔	✔
	C.3b Image collected samples at better than 100 microns.	Microscopic Imager (MI)	(1) Imager and target need to be located in close proximity. (2) Prefer sample to be as undisturbed as possible.	Lander	✔	✔	✔

O. Ocean and Ice Shell

Characterize the local thickness, heterogeneity, and dynamics of any ice and water layers.

Sub-objective	Measurement	Instrument	Requirements	Platform			
O.1 Constrain the thickness and salinity of Europa's ocean.	O.1a Distinguish between ice and water via determining conductivity as a function of depth by producing time-ordered magnetic field vectors (3-axis vector) over a bandwidth of 0 to 16 Hz with a sensitivity of 0.03 nT.	Magnetometer (MAG)	(1) Continuous operations while on the surface; *Baseline*, 9 Eurosols; *Floor*, 3 Eurosols. (2) Orientation of 0.25°, 3 sigma single axis relative to MAG mounting interface. (3) Knowledge of attitude (reconstruction) of 0.5° to 1° relative to a Europa coordinate system. (4) Sampling at 16 samples per second with signal averaging to 4 samples per second to remove potential 6Hz proton cyclotron frequency.	Lander	✔	✔	
	O.1b Measure the thickness of the ocean by observing reflecting body waves (and possibly surface waves) over multiple bands (0.1-50 Hz and 125-250 Hz).	Multiband Seismometer Package (MBS)	(1) Deploy at least three sensors with three components of motion (*Baseline* and *Floor*) with at least several meters separation. (2) Good contact with surface (e.g. deploy sensors to the surface via lander legs). (3) Sensor orientation on each footpad: two-degree orientation accuracy of each sensor, and positional accuracy of 5-10 cm in x-y-z space. (4) Acquire 180-second single-element low-band intervals with a range sensitivity for sources of up to 50 km, triggered by a six-second three-element high-band interval to obtain azimuthal sensitivity of +/-22.5 degrees. (5) The ASRG signal/drill operation/antenna movement/camera operations will be seen by the seismometer and will need to be both isolated and filtered out; an ASRG center frequency of 102 Hz is assumed. (6) Once deployed, continuous operations, *Baseline*, 9 Eurosols; *Floor*, 3 Eurosols. (7) Low-bandpass frequency of 100 mHz (low end) to 50 Hz; High-bandpass frequency of 125 Hz to 250 Hz (i.e., greater than 2 x ASRG center frequency). (8) Return of acquired data: *Baseline*: Triggered data recording, 180 sec low-pass record from a single sensor with a 6 sec 3-sensor high-pass header; 2 per Eurosol for 9 Eurosols; *Floor*: Triggered data recording, 180 sec low-pass record from a single sensor with a 6 sec 3-sensor high-pass header; 1 per Eurosol for 3 Eurosols.		✔	✔	
O.2 Constrain the thickness of ice and the thickness of any water layers in the region.	O.2a Determine the depth to local water sources (e.g. lakes) through measurement of time-ordered B field vectors (3-axis vector) over a bandwidth of 0 to 16 Hz with a sensitivity of 0.03 nT.	Magnetometer (MAG)	(1) Continuous operations while on the surface; *Baseline*, 9 Eurosols; *Floor*, 3 Eurosols. (2) Orientation of 0.25°, 3 sigma single axis relative to MAG mounting interface. (3) Knowledge of attitude (reconstruction) of 0.5° to 1° relative to a Europa coordinate system. (4) Sampling at 16 samples per second with signal averaging to 4 samples per second to remove potential 6Hz proton cyclotron frequency.	Lander	✔		
O.2 Constrain the thickness of ice and the thickness of any water layers in the region.	O.2b Measure the thickness of the ice shell and any subsurface water lenses by observing body waves (and possibly surface waves) over multiple bands (0.1-50 Hz and 125-250 Hz).	Multiband Seismometer Package (MBS)	(1) Deploy at least three sensors with three components of motion (*Baseline* and *Floor*) with at least several meters separation. (2) Good contact with surface (e.g. deploy sensors to the surface via lander legs). (3) Sensor orientation on each footpad: two-degree orientation accuracy of each sensor, and positional accuracy of 5-10 cm in x-y-z space. (4) Acquire 60-second single-element low-band intervals with a range sensitivity for sources of up to 50 km, triggered by a six-second three-element high-band interval to obtain azimuthal sensitivity of +/-22.5 degrees. (5) The ASRG signal/drill operation/antenna movement/camera operations will be seen by the seismometer and will need to be both isolated and filtered out; an ASRG center frequency of 102 Hz is assumed. (6) Once deployed, continuous operations, *Baseline*, 9 Eurosols; *Floor*, 3 Eurosols. (7) Low-bandpass frequency of 100 mHz (low end) to 50 Hz; High-bandpass frequency of 125 Hz to 250 Hz (i.e., greater than 2 x ASRG center frequency). (8) *Baseline*: Triggered data recording, 60 sec low-pass record from a single sensor with a 6 sec 3-sensor high-pass header; 24 per Eurosol for 9 Eurosols; *Floor*: Triggered data recording, 60 sec low-pass record from a single sensor with a 6 sec 3-sensor high-pass header; 12 per Eurosol for 3 Eurosols.	Lander	✔		

Legend:
- ☐ Floor
- ▨ Baseline only

Water: Water in its liquid form as pertaining to habitability as an oxidizer and medium for the transport of chemical constituents.
Energy: Energy that supports and fosters a means for potential metabolism to be established and sustained.
Chemistry: The constituents that foster and sustain the processes and environment for metabolic activity.

Explore Europa to investigate its habitability	**O. Ocean and Ice Shell**	Characterize the local thickness, heterogeneity, and dynamics of any ice and water layers.	O.3 Search for local heterogeneity of the ice and any subsurface water.	O.3a Locate cracks and characterize the intervening porosity distribution and any associated brine infill (both horizontal and vertical), and their correlation with surface features and subsurface water by observing reflected and refracted body waves (and possibly surface waves) over multiple bands (0.1-50 Hz and 125-250 Hz).	Multiband Seismometer Package (MBS)	(1) Deploy at least three sensors with three components of motion (*Baseline* and *Floor*) with at least several meters separation. (2) Good contact with surface (e.g. deploy sensors to the surface via lander legs). (3) Sensor orientation on each footpad: two-degree orientation accuracy of each sensor, and positional accuracy of 5-10 cm in x-y-z space. (4) Acquire 60- and 180-second single-element low-band intervals with a range sensitivity for sources of up to 50 km, triggered by a six-second three-element high-band interval to obtain azimuthal sensitivity of +/-22.5 degrees. (5) The ASRG signal/drill operation/antenna movement/camera operations will be seen by the seismometer and will need to be both isolated and filtered out; an ASRG center frequency of 102 Hz is assumed. (6) Once deployed, continuous operations, *Baseline*, 9 Eurosols; *Floor*, 3 Eurosols. (7) Low-bandpass frequency of 100 mHz (low end) to 50 Hz; High-bandpass frequency of 125 Hz to 250 Hz (i.e., greater than 2 x ASRG center frequency). (8) *Baseline*: (a) Triggered data recording, 60 sec low-pass record from a single sensor with a 6 sec 3-sensor high-pass header; 24 per Eurosol for 9 Eurosols; (b) Triggered data recording, 180 sec low-pass record from a single sensor with a 6 sec 3-sensor high-pass header; 2 per Eurosol for 9 Eurosols; (c) Daily seismic event catalog, e.g. events triggered on horizontal energy, vertical energy, decay rate and/or azimuth; up to 12 per hour (1000 per Eurosol); *Floor*: (a) Triggered data recording, 60 sec low-pass record from a single sensor with a 6 sec 3-sensor high-pass header; 12 per Eurosol for 3 Eurosols; (b) Triggered data recording, 180 sec low-pass record from a single sensor with a 6 sec 3-sensor high-pass header; 1 per Eurosol for 3 Eurosols; (c) Daily seismic event catalog, e.g., events triggered on horizontal energy, vertical energy, decay rate and/or azimuth; up to 6 per hour (500 per Eurosol).	Lander	✔	✔	
			O.4 Characterize Europa's seismic activity and its variation over the tidal cycle.	O.4a Measure the frequency of energy release by identifying and cataloging body wave events and evaluating any associated surface wave energy from select events using observations made over multiple bands (0.1-50 Hz and 125-250 Hz).	Multiband Seismometer Package (MBS)	(1) Deploy at least three sensors with three components of motion (*Baseline* and *Floor*) with at least several meters separation. (2) Good contact with surface (e.g. deploy sensors to the surface via lander legs). (3) Sensor orientation on each footpad: two-degree orientation accuracy of each sensor, and positional accuracy of 5-10 cm in x-y-z space. (4) Acquire 60- and 180-second single-element low-band intervals with a range sensitivity for sources of up to 50 km, triggered by a six-second three-element high-band interval to obtain azimuthal sensitivity of +/-22.5 degrees. (5) The ASRG signal/ drill operation/ antenna movement/ camera operations will be seen by the seismometer and will need to be both isolated and filtered out; an ASRG center frequency of 102 Hz is assumed. (6) Once deployed the seismometers will be taking data continuously, *Baseline*, 9 Eurosols; *Floor*, 3 Eurosols. (7) Low-bandpass frequency of 100 mHz (low end) to 50 Hz ; High-bandpass frequency of 125 Hz to 250 Hz (i.e. greater than 2 x ASRG center frequency). (8) *Baseline*: (a) Triggered data recording, 60 sec low-pass record from a single sensor with a 6 sec 3-sensor high-pass header; 24 per Eurosol for 9 Eurosols; (b) Triggered data recording, 180 sec low-pass record from a single sensor with a 6 sec 3-sensor high-pass header; 2 per Eurosol for 9 Eurosols; (c) Daily seismic event catalog, e.g. events triggered on horizontal energy, vertical energy, decay rate and/or azimuth; up to 12 per hour (1000 per Eurosol); *Floor*: (a) Triggered data recording, 60 sec low-pass record from a single sensor with a 6 sec 3-sensor high-pass header; 12 per Eurosol for 3 Eurosols; (b) Triggered data recording, 180 sec low-pass record from a single sensor with a 6 sec 3-sensor high-pass header; 1 per Eurosol for 3 Eurosols; (c) Daily seismic event catalog, e.g., events triggered on horizontal energy, vertical energy, decay rate and/or azimuth; up to 6 per hour (500 per Eurosol).	Lander	✔		✔

☐ Floor
▓ Baseline only

Water: Water in its liquid form as pertaining to habitability as an oxidizer and medium for the transport of chemical constituents.
Energy: Energy that supports and fosters a means for potential metabolism to be established and sustained.
Chemistry: The constituents that foster and sustain the processes and environment for metabolic activity.

Explore Europa to investigate its habitability	G. Geology	Characterize a locality of high scientific interest to understand the formation and evolution of the surface at local scales.	G.1 Constrain the processes that exchange material between the surface, near-surface, and subsurface	G.1a Panoramic stereo images at 1 mm/pixel at 3 m distance in at least 3 filters (RGB), but prefer 968-nm, 756-nm and 560-nm filters with a SNR: >100:1.	Site Imaging System (SIS)	(1) Cameras mounted 0.3 m apart, on a ~ 1.5 m high mast. (2) 2-axis gimbal to be able to look from the edge of lander up to horizon and down to the sampling region. (3) Ability to correlate frames (filters) with Reconnaissance imager data. (4) Data acquisition and return: *Baseline* imaging: ACQUIRE 1st Priority 1 downlink --Foot pads, 6 images at 6:1 compression --Horizon, 2 images at 6:1 compression --Sun, 1 image 6:1 compression --Near field regolith (thruster pit and adjacent regolith) 2 frames, stereo (1 eye color), 8 images 3:1 compression ACQUIRE 2nd Priority 2 downlink --Site panorama, N frames, 360 deg, lander to horizon, single eye, monochromatic, 6:1 compression --Far field regolith (surface outside disrupted zone), 2 frames, stereo, 1 eye color, 3:1 compression, 8 images Priority 3 downlink --Site panorama, color full resolution, single eye, 3:1 compression Priority 4 downlink --Stereo part of site panorama, other eye, no color, 3:1 compression ACQUIRE 3rd Priority 5 downlink --Photometry, color, single eye, selected locations, repeat at different times of day, 3:1 compression --Change detection (mass wasting, frost, sublimation) selected locations, 3:1 location, as mission allows. *Floor* imaging: Downlink of Priority 1 and 2 data from Acquisitions 1 and 2.	Lander	✔	✔	✔
				G.1b Image landing site at resolutions ranging from 250 m/pixel (monochromatic) down to 20 cm/pixel at increments of no greater than a factor of 2. Site imaging in RGB filters, but prefer 968-nm, 756-nm and 560-nm filters.	Reconnaissance Imager (RI) & Site Imaging System (SIS)	(1) Reconnaissance imaging of landing site both prior and after landing. (2) Ability to correlate reconnaissance imaging frames with SIS data.		✔	✔	✔
				G.1c Characterize ice grains and non-ice materials within the sample down to plate scales of ~10 microns/pixel to understand sample heterogeneity, ice history (ice morphology, inclusions), and context of non-ice materials	Microscopic Imager (MI)	(1) Imager and target need to be located in close proximity. (2) Prefer sample to be as undisturbed as possible.	Lander	✔	✔	✔

☐ Floor
▨ Baseline only

Water: Water in its liquid form as pertaining to habitability as an oxidizer and medium for the transport of chemical constituents.
Energy: Energy that supports and fosters a means for potential metabolism to be established and sustained.
Chemistry: The constituents that foster and sustain the processes and environment for metabolic activity.

Explore Europa to investigate its habitability	G. Geology	Characterize a locality of high scientific interest to understand the formation and evolution of the surface at local scales.	G.2 Constrain the processes and rates by which the surface materials (regolith and bedrock) form and evolve over time.	G.2a Panoramic stereo images at 1 mm/pixel at 3 m distance in at least 3 filters (RGB), but prefer 968-nm, 756-nm and 560-nm filters with a SNR: >100:1.	Site Imaging System (SIS)	(1) Cameras mounted 0.3 m apart, on a ~ 1.5 m high mast. (2) 2-axis gimbal to be able to look from the edge of lander up to horizon and down to the sampling region. (3) Ability to correlate frames (filters) with Reconnaissance imager data. (4) Data acquisition and return: _Baseline_ imaging: ACQUIRE 1st Priority 1 downlink --Foot pads, 6 images at 6:1 compression --Horizon, 2 images at 6:1 compression --Sun, 1 image 6:1 compression --Near field regolith (thruster pit and adjacent regolith) 2 frames, stereo (1 eye color), 8 images 3:1 compression ACQUIRE 2nd Priority 2 downlink --Site panorama, N frames, 360 deg, lander to horizon, single eye, monochromatic, 6:1 compression --Far field regolith (surface outside disrupted zone), 2 frames, stereo, 1 eye color, 3:1 compression, 8 images Priority 3 downlink --Site panorama, color full resolution, single eye, 3:1 compression Priority 4 downlink --Stereo part of site panorama, other eye, no color, 3:1 compression ACQUIRE 3rd Priority 5 downlink --Photometry, color, single eye, selected locations, repeat at different times of day, 3:1 compression --Change detection (mass wasting, frost, sublimation) selected locations, 3:1 location, as mission allows. _Floor_ imaging: Downlink of Priority 1 and 2 data from Acquisitions 1 and 2.	Lander	✔	✔	✔
				G.2b Image landing site at resolutions ranging from 250 m/pixel (monochromatic) down to 20 cm/pixel at increments of no greater than a factor of 2. Site imaging in RGB filters, but prefer 968-nm, 756-nm and 560-nm filters.	Reconnaissance Imager (RI) & Site Imaging System (SIS)	(1) Reconnaissance imaging of landing site both prior and after landing. (2) Ability to correlate reconnaissance imaging frames with SIS data.	Carrier & Lander	✔	✔	✔
				G.2c Characterize ice grains and non-ice materials within the sample down to plate scales of ~10 microns/pixel to understand sample heterogeneity, ice history (ice morphology, inclusions), and context of non-ice materials	Microscopic Imager (MI)	(1) Imager and target need to be located in close proximity. (2) Prefer sample to be as undisturbed as possible.	Lander	✔	✔	✔

☐ Floor
▨ Baseline only

Water: Water in its liquid form as pertaining to habitability as an oxidizer and medium for the transport of chemical constituents.
Energy: Energy that supports and fosters a means for potential metabolism to be established and sustained.
Chemistry: The constituents that foster and sustain the processes and environment for metabolic activity.

Explore Europa to investigate its habitability	G. Geology	Characterize a locality of high scientific interest to understand the formation and evolution of the surface at local scales.	G.3 Understand the regional and local context of the landing site.	G.3a Panoramic stereo images at 1 mm/pixel at 3 m distance in at least 3 filters (RGB), but prefer 968-nm, 756-nm and 560-nm filters with a SNR: >100:1.	Site Imaging System (SIS)	(1) Cameras mounted 0.3 m apart, on a ~ 1.5 m high mast. (2) 2-axis gimbal to be able to look from the edge of lander up to horizon and down to the sampling region. (3) Ability to correlate frames (filters) with Reconnaissance imager data. (4) Data acquisition and return: *Baseline* imaging: ACQUIRE 1st Priority 1 downlink --Foot pads, 6 images at 6:1 compression --Horizon, 2 images at 6:1 compression --Sun, 1 image 6:1 compression --Near field regolith (thruster pit and adjacent regolith) 2 frames, stereo (1 eye color), 8 images 3:1 compression ACQUIRE 2nd Priority 2 downlink --Site panorama, N frames, 360 deg, lander to horizon, single eye, monochromatic, 6:1 compression --Far field regolith (surface outside disrupted zone), 2 frames, stereo, 1 eye color, 3:1 compression, 8 images Priority 3 downlink --Site panorama, color full resolution, single eye, 3:1 compression Priority 4 downlink --Stereo part of site panorama, other eye, no color, 3:1 compression ACQUIRE 3rd Priority 5 downlink --Photometry, color, single eye, selected locations, repeat at different times of day, 3:1 compression --Change detection (mass wasting, frost, sublimation) selected locations, 3:1 location, as mission allows. *Floor* imaging: Downlink of Priority 1 and 2 data from Acquisitions 1 and 2.		✔	✔	✔
				G.3b Image landing site at resolutions ranging from 250 m/pixel (monochromatic) down to 20 cm/pixel at increments of no greater than a factor of 2. Site imaging in RGB filters, but prefer 968-nm, 756-nm and 560-nm filters.	Reconnaissance Imager (RI) & Site Imaging System (SIS)	(1) Reconnaissance imaging of landing site both prior and after landing. (2) Ability to correlate reconnaissance imaging frames with Site Imaging System data.	Carrier & Lander	✔	✔	✔
			G.4 Constrain the physical properties of the surface and near-surface at the landing site to provide context for the sample.	G.4a Image landing site at resolutions ranging from 250 m/pixel (monochromatic) down to 20 cm/pixel at increments of no greater than a factor of 2. Site imaging in RGB filters, but prefer 968-nm, 756-nm and 560-nm filters.	Reconnaissance Imager (RI) & Site Imaging System (SIS)	(1) Reconnaissance imaging of landing site both prior and after landing. (2) Ability to correlate reconnaissance imaging frames with Site Imaging System data.	Carrier & Lander		✔	
				G.4b Characterize ice grains and non-ice materials within the sample down to plate scales of ~10 microns/pixel.	Microscopic Imager (MI)	(1) Imager and target need to be located in close proximity. (2) Prefer sample to be as undisturbed as possible.	Lander		✔	
				G.4d Determine mechanical properties of sampled surface.	Europa Sampling System	(1) Well-calibrated motor current engineering data to determine torques and forces to infer physical properties of the surface material.	Lander		✔	

	Floor
	Baseline only

Water: Water in its liquid form as pertaining to habitability as an oxidizer and medium for the transport of chemical constituents.
Energy: Energy that supports and fosters a means for potential metabolism to be established and sustained.
Chemistry: The constituents that foster and sustain the processes and environment for metabolic activity.

Characterization of both organic and inorganic composition would provide complementary information about the habitability of the ocean. Inorganic composition would provide a snap-shot of ocean chemical evolution as driven by the interaction of the hydrosphere and litho-sphere, along with inputs of exogenic material. Such information can provide not only a bulk measure of the extent of evolution (e.g., the extent of hydrous alteration of the lithosphere), but could also help to distinguish among dif-fering modes and models of ocean chemical evolution. Inorganic composition can also reflect availability of bioessential elements and, potentially, ocean redox and pH. These factors bear directly on the energy flux and physicochemical environmental aspects of habitability. Organic composition would re-flect a combination of initial inventory, endo-genic synthesis, and exogenic inputs, and could provide a direct and independent meas-ure of whether organics (and, as a subset, prebiotic or biological molecules) are stable under present Europan ocean conditions. Broad-based organic compositional measure-ments also offer discovery potential for prebi-otic or possibly biogenic molecules that is unique to landed science.

To the extent that the ocean and ice shell exchange material (see below), both ocean and surface composition can be expected to reflect a combination of endogenic and exogenic processes and inputs. Deconvolving these inputs to the greatest extent possible will be important for acquiring an accurate picture of ocean composition and, by characterizing the purely exogenic end-member, inferring endo-genic processes.

D.1.2.1.2   Implications of Ocean and Ice Shell

A Lander offers potential to understand the bulk properties of the ocean and a unique capability, afforded by direct contact with the surface, to understand the regional structure of the ice. Measurements of ocean salinity and thickness (and by extrapolation, volume) can place first order constraints on material inputs

to the ocean. With a defined ocean volume, salinity provides a bulk measure of the amount of material that has been processed through water-rock reaction, and thereby imposes a key boundary condition for models of ocean chemical evolution and the endogenic contri-bution to energy flux. Local to regional char-acterization of ice shell structure would pro-vide a direct complement to this information. Specifically, an understanding of the internal structure of the ice—including cracks, phase transitions, and near-surface water bodies—would, in combination with surface geomor-phology (Section D.1.2.4), provide insight into mechanisms of mass transport and ocean-ice exchange. These processes bear critically on understanding the energy flux contribution to the biological potential of Europa. Identifica-tion of discrete near-surface water bodies (e.g., lakes within the ice shell) would open a new avenue in consideration of Europan astrobiol-ogy—pockets of potential transient habitability that could differ from the global ocean with respect to the "ingredients for life" and their modes of material exchange with the accessi-ble surface.

D.1.2.1.3   Implications of Geology

A capability for high-resolution imaging and remote sensing on scales ranging from region-al to microscopic, as is possible only with a landed mission, bears on several key aspects of astrobiology science on Europa. Detailed study of geomorphology from imaging across a continuum of scales from planetary to local will be important for constraining processes of mass transport and ocean-ice exchange. Un-derstanding the mechanisms and rate of such exchange bears directly on the question of energy flux to the ocean, and is thus among the most critical areas for advancement of astrobi-ology science on Europa. Such imaging can also characterize the external processes that shape surface geomorphology and thus, in combination with an understanding of ocean-ice exchange, help to constrain exogenic in-puts to the ocean. Finally, numerous studies on

Earth, as well as recent experience with landed science on Mars, have shown that the ability to interpret compositional measurements is significantly enhanced by (and sometimes requires) a detailed understanding of the geological context of acquired samples. In addition to the importance of understanding samples in the context of both mass transport processes and exogenic effects (as above), it would also be valuable to understand the microscopic context of the samples. Specifically, for example, assessment of ice crystal morphology and whether inclusions are present would be important for understanding how compositional information is preserved or modified by the processes that transport ocean materials to the surface.

D.1.2.2   Composition Traceability

Assessing Europa's composition is critical to understanding the potential habitability of the satellite. Such measurements can be well achieved by direct *in situ* analyses of surface materials. The highest-priority objective of the Europa Lander Mission is to

> *Understand the habitability of Europa's ocean through composition and chemistry.* From this objective flow the two chief composition investigations, each of which has two associated measurement recommendations:

> *Investigation C.1: Characterize surface and near-surface chemistry, including complex organic chemistry to constrain ocean composition and understand the endogenic processes from which it evolves.*
> – Measure organic content (including complex organics) of surface (0.5– 2 cm depth) and near-surface (5– 10 cm depth) materials to as low as 1 ppb concentration.
> – Measure mineralogy and volatile content of surface (0.5–2 cm depth) and near-surface (5–10 cm depth) materials to as low as 0.1 wt%.

> *Investigation C.2: Characterize surface and near-surface chemistry, including*

complex organic chemistry to constrain the exogenic processes and material fluxes that affect ocean composition.
> – Measure organic content (including complex organics) of surface (0.5– 2 cm depth) and near-surface (5– 10 cm depth) materials to as low as 1 ppb concentration.
> – Measure mineralogy and volatile content of the surface (0.5–2 cm depth) and near-surface (5–10 cm depth) materials to as low as 0.1 wt%, including exogenous and processed constituents.

A third investigation is dedicated to understanding the context of the samples:

> *Investigation C.3: Constrain the context of compositional measurements.*
> – Image sampling area prior to sample collection to provide local and site specific context.
> – Image collected samples at resolution of better than 100 microns/pixel.

Measuring composition in situ does not *directly* determine the origin of the material, e.g., from meteorites vs. from Europa's ocean. Such interpretation must come from analysis of the data compared with expected chemical correlations and distributions, and in the context of data from other instruments. The composition investigations cannot be made independently, but rather must be performed in an integrated manner.

Composition measurement requirements thus are formulated for identifying and quantifying relevant compounds and understanding the context in which they were deposited.

D.1.2.2.1   Separating Endogenic and Exogenic Materials

As discussed in Section D.1.2, accessing Europa's ocean composition directly is not possible, but we can learn much about its potential habitability from understanding the salt content and the presence and abundance of
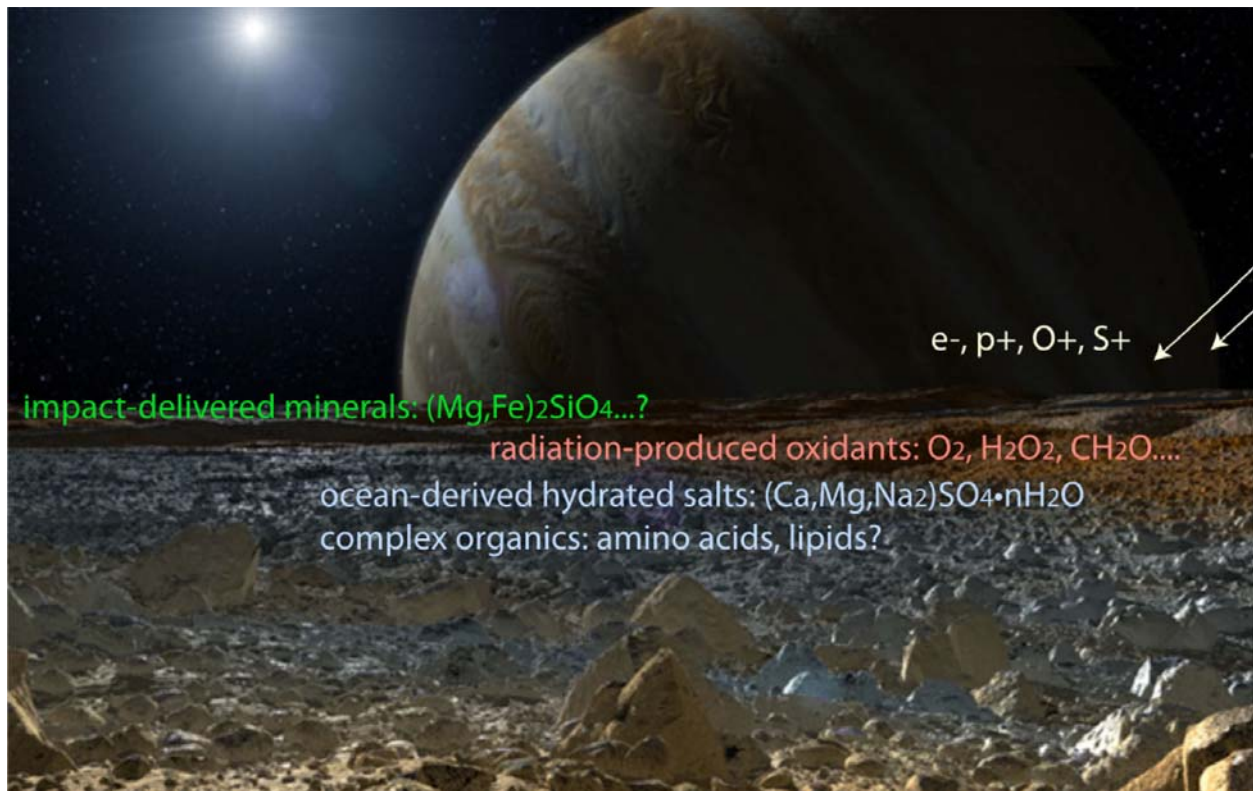
Figure D.1.2-1. Europa's surface composition is derived from a mixture of processes, which must be unraveled to understand the ocean below.

organics. The overall process is complicated by exogenic processing of the surface by radiation alteration of material and ion and micrometeorite implantation (Figure D.1.2-1); the surface and near-surface provide a witness plate to the all these processes.

Key to unraveling endogenic and exogenic materials is taking advantage of the different exogenic processing histories of surface and subsurface materials. Materials at the surface are more highly altered and gardened by radiation, while subsurface material compositions may be more strongly controlled by the ocean chemistry. The surface should be sampled from the first 0.5–2 cm to ensure that radiation effects are captured.

Landing on the surface of Europa will substantially alter the topmost layer both mechanically and chemically. Based on testing and experience from past landed missions (e.g., Plemmons et al. 2008, Mehta et al. 2011, Metzgar et al. 2011), hydrazine thrusters would significantly alter the topmost layer of the surface. Expected effects include the mobilization of unconsolidated material, thermal erosion of ice-rich material, and the chemical addition of thruster exhaust compounds dominated by ammonia (hydrazine-by product) plus small amounts of contaminants in the hydrazine including water and organics. The spacecraft itself may be a source of outgassed and mobile volatiles and organics. Total spacecraft contamination should be at or below the sensitivity requirements of the instrumentation: 1 ppb for complex organic contaminants and below 1 ppm for inorganic contaminants. A sample that meets the contamination requirement from a shallow depth (0.5–2 cm) is desired to understand implantation effects.

In order to understand Europa's endogenic composition, i.e., the composition most closely representing the ocean, a second sample should be selected from below the radiation-processed surface layer. Landing site selection

requirements (Section D.4.2) of young materials and a relatively low radiation environment imply that this second sample does not need to be selected from great depth. Depth of 5-10 cm should put the material below the radiation-damaged zone (e.g., Patterson et al. 2012). Thus, two samples are deemed sufficient for compositional measurements, and all relevant compositional measurements should be made on each of the two samples.

Because evolved volatiles are to be studied, heating of the sample above the maximum diurnal temperature of the sample is to be avoided during acquisition and handling. This also prevents melting, which would combine exogenic and endogenic materials, making interpretation of the data difficult or impossible. To preserve volatiles in the ice (e.g., O_2, CO, CO_2), the sample bulk temperature should be less than 150 K, close to expected peak daytime heating temperature. Ideally the entire sample should not see temperatures above 150 K. However, the prime science results involve the relative abundances of species, so it is acceptable that only portions of a sample are heated. If diurnal temperatures are to be exceeded, the temperature limit for melting is lower than 273 K, as salts will lower the eutectic melt temperature. Sulfuric acid hydrate has the lowest eutectic melting temperature of the materials expected to be present on Europa, at 198.6 K (McCarthy et al. 2007).

D.1.2.2.2   *Compositional Measurements*

Two key categories of measurement emerge from the compositional science investigations. The first is measurement of organic content, and the second is measurement of mineralogy and volatile content.

The low expected abundance of organics based on terrestrial systems (Table D.1.1-1) suggests that organic measurements will require high sensitivity relative to present technological capabilities. Assuming that the organic content of Europa is similar to biologically rich waters leads to setting limits for confident detection of organic species at about 1 ppb. This sensitivity levies a spacecraft contamination control requirement of less than 1 ppb organic material in the sample transfer chain.

Non-icy materials on Europa are believed to be present at less than 1 wt% to tens of wt%, depending on the species (Table D.1.2-1). Recent work mapping the distribution of ice and salts (Shirley et al. 2010) shows that even on large spatial scales the composition can be highly variable. The mineralogical structures of sampled materials may be temperature dependent, so they should be measured with minimal thermal processing. To prevent salts and other soluble materials from combining, melting should be avoided. Nonorganic spacecraft contaminants should be controlled to less than 1 ppm.

While a variety of instruments could potentially make these measurements (see Section D.1.2.2.2.4), the Europa Lander study used a combination of a Mass Spectrometer and a Raman Spectrometer. The MS was

Table D.1.2-1. Observed inorganic materials and their abundances on Europa.

Compound	(Species)	Formula	Measured Range	Reference
Water Ice		H_2O	0–100%	Carlson et al. 2009 and references therein, Shirley et al. 2010
Hydrogen Peroxide		H_2O_2	0.1%	Carlson et al. 2009 and references therein
Sulfur Dioxide		SO_2	0.2%–4%	Carlson et al. 2009 and references therein
Sulfuric Acid Hydrate		$H_2SO_{4^*}$	18–30%	Shirley et al. 2010
Mg-Sulfate Brine		Mg, SO_4 in solution	0–30%	Shirley et al. 2010
Hydrate Salts			18–65%	Shirley et al. 2010
Hydrated $MgSO_4$	Bloedite		0–27%	Shirley et al. 2010
Hydrated $MgSO_4$	Mirabilite		7–20%	Shirley et al. 2010
Hydrated $MgSO_4$	Hexihydrite		5–20%	Shirley et al. 2010

optimized to detect low-level organics, while the RS focused on salt mineralogy and ice/volatile chemistry. To be able to fully interpret the measurements, mass spectrometry and Raman spectroscopy measurements must be made on the same sample. Details of the measurement approach are provided below.

D.1.2.2.3   Mass Spectrometer

The key method of measuring the organics on the Europa Lander model payload is mass spectrometry. Mass spectrometers have been used on numerous spacecraft missions, including Cassini, Phoenix, and MSL-Curiosity, for their ability to undertake broad surveys of organic materials and detect organics in low abundances (~1 ppb). This instrument is part of the mission floor. As a floor instrument, it is also required to address minimum measurements of salt mineralogy and volatiles if the second composition instrument for mineralogy (Raman Section D.1.2.2.2) cannot be accommodated, or as a backup in case of failure. The instrument requires a macroscopic (several gram) sample of consolidated or loosely consolidated ice matrix material, which is transferred to an oven for thermal processing. Monitoring of background and escaping volatiles (e.g., CH_4, CO, CO_2) begins immediately at ambient conditions in the hermetically sealed oven, with the sampled pressure controlled via a gas split. The majority of the water ice is then sublimated away. In order to preserve the salt mineralogy, and to avoid mixing dissolved Europa salts with implanted ions (e.g., H^+, Na^+), care must be taken not to melt the sample (i.e., the pressure is kept low). Once water ice is baked out, the sample is slowly heated to 400° C. The sample gas is split with part going directly into the mass spectrometer and the other part being diverted to a low-temperature organic trap and then to a gas chromatograph in order to detect organics at low abundances ~1 ppb. Continued heating of the sample, up to 1200°C, leads to the breakdown of salts, such as sulfates (e.g., gypsum) and other mineral species. Measure-

ment of the volatiles released and the temperature of release can constrain the salt mineralogy. An example evolved gas profile of three selected species (H_2O, SO_2, and CO_2) from a mixture of calcite $CaCO_3$ and melanterite $FeSO_4$ $7H_2O$, used to calibrate the Sample Analysis at Mars (SAM) mass spectrometer, is shown in Figure D.1.2-2a. The onset, peak position, and width of such temperature profiles are diagnostic of the particular mineral phases, and a full mass spectrum (Figure D.1.2-2b) is associated with each point in the temperature ramp, permitting identification of breakdown products of organic materials.

Raman Spectrometer

The secondary technique for determining composition is one that measures compositional structure (mineralogy) directly. The SDT chose Raman spectroscopy as best meeting this requirement. In Raman spectroscopy, laser light is focused on a sample and inelastically scattered. The shift in the wavelength of the scattered laser light due to vibrations in mineral structure is diagnostic of the material being probed. An infrared laser was selected as optimal for Raman at Europa's surface, because there is minimal unwanted mineral fluorescence in that range, and because visible wavelength lasers can destroy organics. Raman has the additional advantage that it is nondestructive to the sample and therefore can look at the same sample that is then measured in another way (e.g., a mass spectrometer), providing complementarity and simplifying the sampling requirements and sample transfer train.

Raman spectroscopy can measure both the salt and volatile content of materials near the landing site. On Earth, Raman spectra of ice cores are used to study their volatile content (e.g., Pauler et al. 1996, Iizuka et al. 2008, Fall et al. 2011). The nondestructive nature of the technique makes it ideal for studying mineral phases that are unstable to increase in temperature. Raman can also be used to investigate salt mineralogy, addressing such issues as the
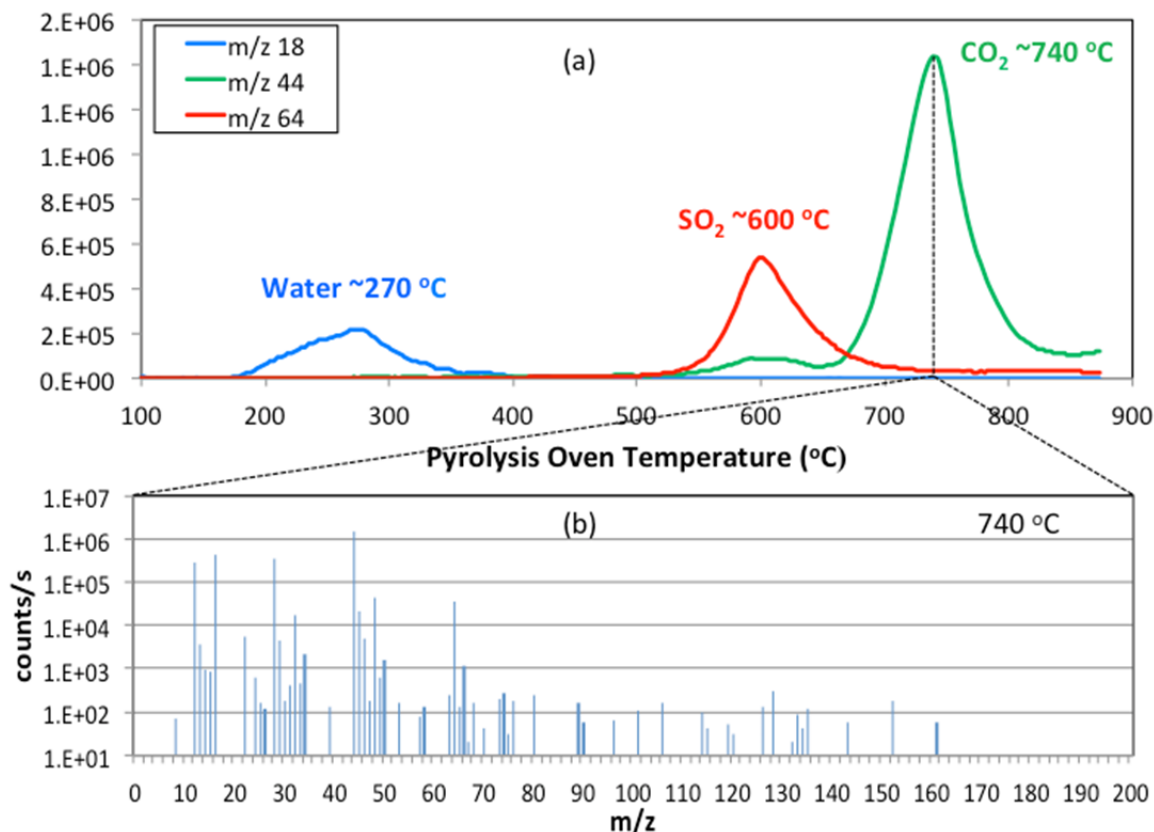
Figure D.1.2-2. Evolved gas analysis of selected volatile compounds coupled with highly sensitive mass spectrometry enables organic and mineralogical analysis of solid samples. (a) Evolution of water and sulfur dioxide from melanterite and carbon dioxide from calcite are diagnostic signatures. The full mass spectrum (b) at the calcite breakdown temperature shows the dominant release of CO_2 and its fragments, and residual sulfate breakdown, along with alkane fragments indicating trace levels of hydrocarbons in the background.

nature of salt mineralogy cations and the hydration state. As can be seen from the suite of sulfates minerals in Figure D.1.2-3, Raman spectra are highly sensitive and thus diagnostic of variation in the structure of minerals due to the inclusion of water in the matrix (Chaban et al. 2002, Wang et al. 2003, Chio et al. 2007).

Sample Context

The need to distinguish between exogenic and endogenic processes on Europa means that sample context is critical to the interpretation of results. At the spatial scale of the only sample collected, there is no certain information about Europa. For instance, a sample from a lag deposit created by sublimation would have a very different concentration of materials than a more ice-rich sample, which

Figure D.1.2-3. Example Raman spectra of Mg, K, Na, and Ca sulfates assembled from spectra in the RRUFF database (Downs 2006).

could influence the interpretation of habitability.

The primary method for deriving sample context is imaging. Context comes in two forms: geologic context and sampling context.

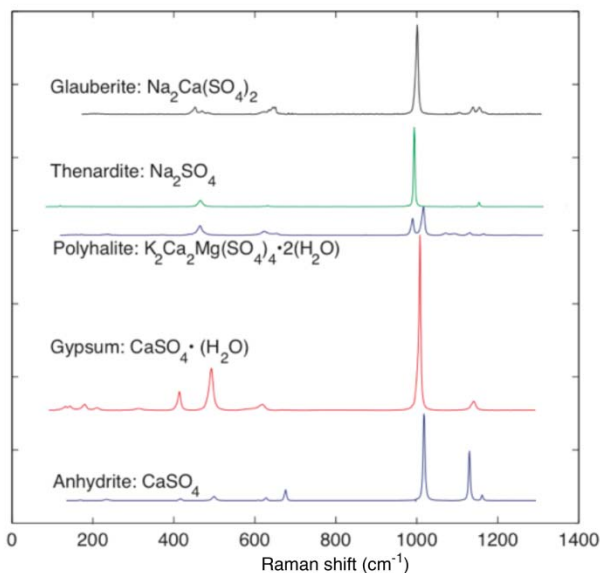Geologic context includes processes that created the landforms from which composition is measured. For instance, landing on the ejecta blanket of a small crater might imply material is from a greater depth beneath the surface. A chaotic feature or landform related to exposure of ocean material to the surface would be expected to contain a higher proportion of salts, and possibly also of organic materials. Landing on the leading hemisphere would imply a lower concentration of irradiated materials created by electron impacts from particles corotating with Jupiter's magnetic field. Understanding the history of the surface is essential in tracing the derived compositions back to the ocean. In order to accomplish this we require the sampling site to be imaged at <0.5 mm per pixel prior to sampling. Also, imaging the site after sampling would enable us to understand more about the sample collection process, for example by exposing albedo and morphological variation associated with depth.

Sampling context is primarily a microscopic measurement at spatial scales from 10 to 50 μm per pixel to look at the degree of homogeneity. Solid inclusions, for instance, might suggest the presence of impact-delivered solids or diagenesis of brines and ice grains prior to cooling of emplaced materials. While an intact sample would preserve structural relationships between elements, an estimate of sample heterogeneity can be made with a fragmented sample.

D.1.2.2.4   *Other Measurement Approaches*

Many different and complementary technologies are available that might be employed to evaluate Europa's surface composition. The suite of technologies for compositional analysis adopted by the Europa SDT is one of many possible options for addressing the composition objective of the Lander concept.

The model payload was chosen upon assessment of cost, feasibility, and risk. Otherwise available techniques include tunable laser absorption, X-ray diffraction, UV and infrared spectroscopy, and gas and high-pressure liquid chromatography. A brief assessment of these alternatives is provided in Table D.1.2-2, including brief explanation of why they were not chosen for the model payload.

D.1.2.3   Ocean and Ice Shell Traceability

Geophysical techniques to probe Europa's ocean and ice shell are well-suited to a Europa Lander. A significant objective for the Europa Lander Mission is to

> *Characterize the local thickness, heterogeneity, and dynamics of any ice and water layers of the ice shell.*

This leads to the four specific investigations described next.

D.1.2.3.1   *Investigation I.1: Constrain the thickness and salinity of Europa's ocean.*

Magnetic fields interact with conducting matter at length scales ranging from atomic to galactic. Magnetic fields are produced when electrical charges flow and produce currents in response to electric potential differences between two regions. Many planets generate their own stable internal magnetic fields, in metallic cores or inner shells, through dynamos powered by convection from internal heat or gravitational settling of the interior. Still others have induced magnetic fields, which arise through interactions between externally imposed magnetic fields and their interiors. The imposed magnetic field causes a current to flow in a conductive layer of the planet, inducing a magnetic field equal in magnitude and opposite in direction to the imposed field. This secondary field is readily measured by a MAG located outside the conductor.

Galileo observations of Europa demonstrated that it possesses an induced magnetic field

Table D.1.2-2. Alternative techniques for assessing composition from a Europa Lander.

	Type	Measurement: Pros	Assessment: Cons	Model Instruments	References
Chromatography	High Pressure Liquid, Ion Exchange, Ion Microprobe, Differential Mobility, Gas	Fatty acids and complex organic molecules, separation of inorganics for detection by a mass spectrometer	HPLC requires melting of sample and pressure greater than 30 MPa; as a plus-up, a GC might serve as a front end for the MS	HPLC- chip/DMS MSL/SAM GCMS	Coy et al. 2011, Mahaffy 2008
Spectroscopy	Infrared	Mapping of materials around the landing site, complementarity with Galileo NIMS	Not as capable as a Raman instrument; could be included in a proposed Pan Cam as a plus-up	Galileo NIMS, Cassini VIMS	Mahaffy 2008, Brown et al. 2004
	Ultraviolet	Mapping of organics around the landing site	Not as compound specific for organics as mass spectrometer, lower detection limit.	Cassini UVIS	Esposito et al. 2004
	X-Ray Diffraction	Bulk inorganic composition	Definitive mineralogy; more complex sample handling and a separate sample from the mass spec	MSL/CheMin XRD	Bish et al. 2007
Spectrometry	Tunable Laser	Unambiguous absolute and isotopic make-up of low-mass molecules	High mass, power, and complexity; insufficient for heavy organics	MSL/SAM TLS	Mahaffy 2008

caused by its interactions with Jupiter (e.g., Khurana et al. 1998; Kivelson et al. 1999, 2000). Europa's induced field arises from the primary alternating magnetic field of Jupiter, because its rotation and magnetic dipole axes are not aligned. Europa's field must arise from interactions with a near-surface conductive layer (Khurana et al 1998, Kivelson et al. 2000), and is most consistent with induction within a salty subsurface ocean. The measured signal was shown to remain in phase with the primary field of Jovian origin (Kivelson et al. 2000), thus unambiguously proving that the perturbation signal is a response to Jupiter's field. While no intrinsic magnetic field was observed in the flybys by Galileo (Kivelson et al. 2000), an upper limit of 25 nT for a possible intrinsic component was derived (Schilling et al. 2004). Thus a MAG may be used both to characterize the ocean of Europa, and also possibly its deeper interior.

Modeling of the measured induction signal, although clearly indicative of a Europan ocean, suffers from nonuniqueness in the derived parameters because of the limited data. Individual flyby measurements, such as those obtained by the Galileo spacecraft, suffer from both temporal and geometric constraints, and that inhibits separation of higher order field components. This is usually dealt with by assuming that the inducing signal is composed of a single frequency, corresponding to the synodic rotation period of Jupiter.

Geometric information from several flybys has been used to reconstruct some aspects of the field, but observations of how the field evolves in time, in response to external forcing or any internal source, were beyond the scope of Galileo's mission architecture. Unfortunately, single frequency data cannot be inverted to determine independently both the ocean thickness and the conductivity. Nevertheless, the

single frequency analysis of Zimmer et al. (2000) reveals that the ocean must have a conductivity of at least 0.06 S/m. Recently, Schilling et al. (2004) determined that the ratio of induction field to primary field is 0.96 ±0.3, leading Hand and Chyba (2007) to infer that the ice shell is <15 km thick and the ocean water conductivity >6 S/m.

Clear delineation of an internal intrinsic field on Europa will require measurements of the magnetic field in situ over many Jovian rotations and Eurosols. In order to determine the ocean thickness and conductivity, magnetic sounding of the ocean at multiple frequencies is required. The depth to which an electromagnetic wave penetrates is inversely proportional to the square root of its frequency. Thus, longer period waves sound to larger depths and could provide information on the thickness of the ocean, and sufficiently long periods could even probe conductivity of the silicate mantle, and possible metallic core. Electromagnetic sounding at multiple frequencies is routinely used to study Earth's mantle and core from surface magnetic data (Parkinson 1983). Recently, Constable and Constable (2004) demonstrated that data from orbit can be used for electromagnetic induction sounding at multiple frequencies.

Multiple low-frequency variations are present at Europa. The dominant timescale over which Europa experiences magnetic variations is at 11 hours, Jupiter's synodic rotation period, and has an amplitude of 200-250 nT (Zimmer, Khurana, and Kivelson, 2001). The second period, at 85.2 hours, occurs as Europa's eccentric orbit moves the moon closer to and farther from the planet, which varies the near-moon magnetic field by about 15 nT. The third variation is due to other magnetospheric effects and does not have a regular periodicity. Russell et al. (2001) found that the field strength in the Jovian inner magnetosphere varied by about 30 nT over the course of the Galileo mission and could regularly change by 10 nT, comparable to the eccentricity-driven

variation, between successive passes through the region.

Over a broad range of the relevant parameter space (ocean thickness and conductivity), the induction responses of Europa at the two dominant frequencies (those of its orbital period and Jupiter's rotation) will intersect (Figure D.1.2-4). In that range, the ocean thickness and conductivity may be determined uniquely. In order to sound the ocean at these two frequencies, continuous data are required from low altitude over a long duration of observations; at least one month (8 Eurosols)
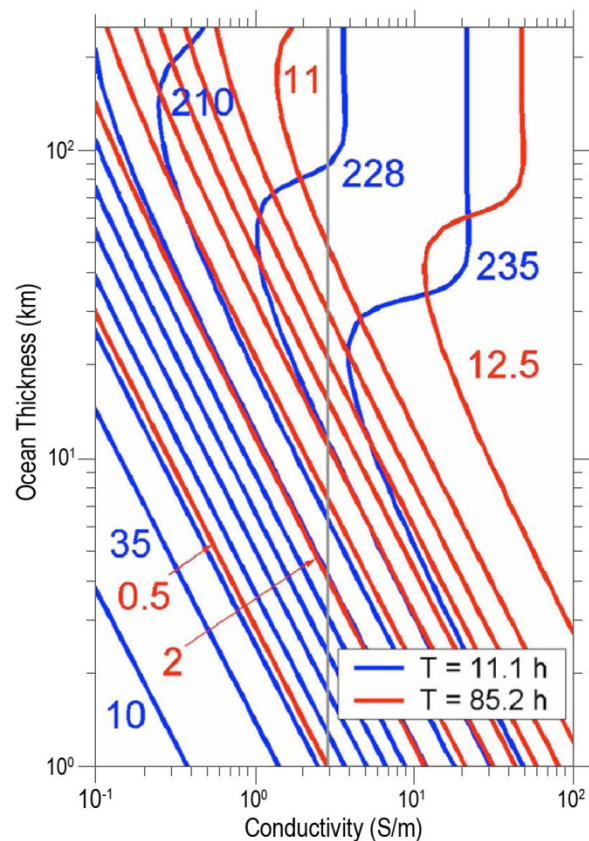
Figure D.1.2-4. Contours of the induced magnetic field (in nT) generated at the surface of Europa, predicted at Jupiter's synodic rotation period of 11.1 hr (blue) and at Europa's orbital period of 85.2 hr (red), as a function of ocean thickness and ocean conductivity. For relatively large values of ocean thickness and conductivity, the predicted induction curves intersect, permitting ocean thickness and conductivity to be uniquely determined from orbital measurements. (From Khurana et al. [2002].)

is preferred. A longer observation time would also better enable the removal of any variations noted by Russell et al. (2001) from the eccentricity-generated periodicity.

The periods and magnitudes of expected variations in the magnetic field and plasma environment dictate the MAG specifications. The short-term magnetospheric and orbital variations in the magnetic field strength are 10 and 15 nT, respectively. The orbital variation alone would create a signal at the Lander of less than 7 nT. In the worst case, if the magnetospheric field varies such that the 15 nT is reduced to a difference of 5 nT over Europa's orbit due to interference between orbit-derived and variations and those inherent to the Jovian system, the magnitude of the expected contribution to the induced field would be a minimum of 2.5 nT. Observational precision of 0.03 nT would allow the MAG to measure about one percent of this minimum signal and thus still accurately quantify Europa's induced response to the orbital variation.

During passes through Europa's wake, Volwerk et al. (2001) found magnetic field variations, with 20 nT peak-to-peak amplitude and frequencies below 0.2 Hz, that were associated with the ionization of heavy molecules, like O_2. Although these observations were made downstream of Europa, the Galileo spacecraft was about three Europa radii away and could not determine whether waves were observed closer to the moon. If a MAG samples at a frequency comparable to plasma waves such as these, significant aliasing issues would affect the search for induction signals. The observed waves could, for instance, dwarf any 82.5 hour signal. Protons, a product of the moon's water-ice surface, would generate the highest-frequency waves that would affect the proposed analysis. In the ~400 nT field at Europa, the proton-generated waves would occur at frequencies between 6 and 7 Hz. The minimum sampling rate to avoid aliasing issues is twice that frequency, thus sampling over a bandwidth of at least 16 Hz is recom-

mended. To reduce data volumes, onboard averaging of the data by a factor of two to four could be employed.

Inversion of multifrequency magnetic field observations, as described above, is a well-established means of estimating ice shell thickness and conductivity of any underlying water body. Independent constraints on these inversions will significantly improve confidence in their critical salinity–thickness results. In addition, the relationship of the landed observation platform to water bodies other than the ocean that are below it or adjacent to it will complicate simple magnetic inversions for the vertical conductivity profile and possibly lead to significant uncertainties in thickness/conductivity estimates.

In order to address the ambiguities inherent with a single observational type, seismic sounding of the ocean, in parallel with magnetospheric observations, is recommended. As described above and in detail for the investigations below (and shown in Figure D.1.2-5), seismic events (likely fracturing of the ice) within the ice shell provide a source of compressional (P) and shear (S) body waves that can be transmitted through the ice–ocean interface, reflect off the silicate interior, and reach the receiver with a characteristic travel time in the range of 110–160 seconds (Lee et al. 2003). Constraints on ocean thickness can be obtained via detection and recording of seismic body waves, with both travel times and, some indication of the azimuth and inclination from which these waves are arriving. This seismic estimate of ocean thickness will be highly complementary to magnetic induction investigations and allow improved constraints on the salinity of Europa's ocean.

D.1.2.3.2   Investigation I.2: Constrain the thickness of ice and the thickness of any local water layers in the region.

As stated in Section D.1.3, knowledge of the thickness of Europa's ice shell is critical if we are to test dynamic hypotheses that bound both the nature and rate of exchange of materials

Figure D.1.2-5. Observation design for detecting seismic events on Europa. Time-range plots for a (top) 20-km ice shell model and a (bottom) 5-km ice shell model. Colors indicate the horizontal velocity level in both panels. Note that for both models the ice-water interface reflections occur within 60 seconds, while the water-mantle interface reflections occur within 180 seconds, leading to the recommended data recording approach. (From Lee et al. [2003].)

between Europa's surface and ocean. Similarly, knowledge of the thickness of any subsurface water bodies ("lenses") and their overlying ice lids would be important for establishing estimates of the rate of potential large-scale mixing between the surface and subsurface including both the water lens itself and ultimately the ocean below. In addition, explicit knowledge of the interaction of the ocean and the overlying ice is important for establishing the relative significance of upwelling and downwelling processes and their potential link to water inside the ice shell.

The geophysical measurements required to constrain thickness of ice layers over either subsurface water lenses or the ocean itself are

well known: much has been written about potential seismic investigation of Europa's ice shell using both reflected body waves (Section D.1.3, Lee et al. 2003, Figure D.1.2-5) and Love waves trapped within the floating ice shell (Kovachs and Chyba 2001). In much of this literature the emphasis has been on establishing the thickness of the ice shell over the ocean. In some cases the long-period Rayleigh waves from excitement of the surface boundary by rupture below it have been advocated for inferring the thermal state of the underlying silicate mantle (Cammarano et al. 2006, Panning et al. 2006). As discussed in Section D.1.3, both Love and Rayleigh waves are problematic for ice and ocean studies at Europa from a single landed site, because of the

requirements for long receiver-source separation and known source locations. Thus, seismic sounding via body waves is the preferred technique (Lee et al. 2003).

From the terrestrial perspective, natural seismicity associated with ice dynamics has been used to establish the depth to sources both adjacent to and below an observation site (e.g., Blankenship et al. 1987; see Figure D.1.2-6). These studies are particularly powerful because of the reasonably well-known elastic behavior of both primary compressional (P)
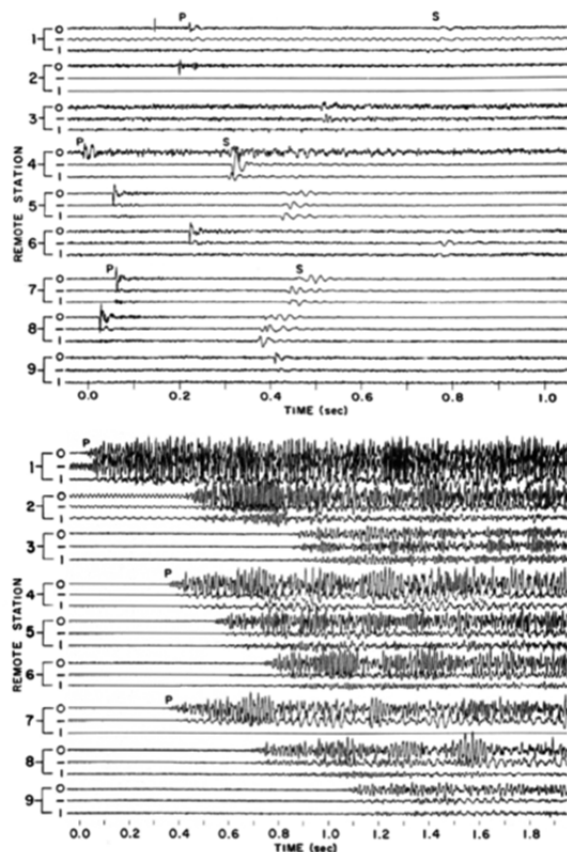

Figure D.1.2-6. Examples of seismograms indicating the detection of P and S waves from ice microseismic events (reproduced from Blankenship et al. [1987]). At top, detections from a thrust event at the base of ice stream B, West Antarctica. Cracking events on Europa are expected to have similar return structure. At bottom, events from shallow crevassing along the margins of Ice Stream B. Events occurring inside chaos matrix material or heavily crevassed areas of Europa's surface are likely to suffer from such clutter due to the complex scattering environment.

and secondary shear (S) waves as a function of density and temperature in ice (Robin 1958, Bentley 1964, Roethlisburger 1972), although ice can be significantly anisotropic.

For this study, with its emphasis on Europa's habitability, seismic studies are recommended using both refracted and reflected body waves to sample the ice shell and any subsurface water as well as the underlying ocean. The range to ice shell fracture events can be determined from direct observations of P and S waves for sources within a range of about 50 km to the Lander (Figure D.1.1-4 and Figure D.1.2-5). In order to determine the ice shell thickness as well as the depth and thickness of any subsurface water lenses, observations must be recorded over the characteristic travel times of these reflected waves. In order to detect waves reflected off the ice-ocean interface, we recommend collecting seismic records of about 60 second duration over a frequency band of 0.1 to 50 Hz, whenever an event above an appropriate threshold is detected. Observations should occur over a time scale of at least 9 Eurosols (~1 month), considering the likelihood that several cracking events should occur over that period to ~250 m depth, which would be expected to sound the full thickness of a ~20-km ice shell, and could sound the ocean depth as well if the background noise is sufficiently quiet (Lee et al. 2003).

Correlating seismic events with particular surface features and local geology requires knowledge of the direction from which seismic energy is propagating. In addition, the magnetic induction measurements described above for establishing the depth of the ocean are sensitive to a range of local electromagnetically conductive brine-rich targets such as water layers and lenses. Because of this, any seismic investigation must be focused not only on decreasing the uncertainty of the ocean salinity inversions (Section D.2.3.1) but also extending these inversions to understanding the thickness and conductivity of any intra-ice water lenses.

This will require assessing whether any detected body waves have arrived from adjacent to or beneath the observation platform, and from which direction, which emphasizes the need for some azimuthal sensitivity as well as the ability to discriminate sources with near vertical inclinations. Azimuthal sensitivity requirements are not trivial since any near surface vertical velocity gradient will render azimuths from incident compressional wave displacements (or transverse or vertically polarized shear waves) as highly uncertain. At least three, three-component sensors are required, with good surface contact, with a baseline distance of at least several meters between them, and with knowledge of their positions and orientations.

Because cold ice is only moderately attenuating (Kohnen 1974), an alternative means for establishing azimuth is through the detection of energy from arrivals of sufficiently high frequency content over intervals long enough (i.e., several seconds) to be statistically phase correlative (i.e., more than one sample offset) for direct waves across a small array that is roughly the dimension of the Lander footprint (several meters between footpads or about one to two milliseconds of travel time for P and S direct arrivals, respectively). Coupling these coarse (about 45° for 200 Hz arrivals) azimuthal estimates with those inferred from displacements is likely to be especially powerful for projecting body wave arrivals back to their source using P and S wave travel time differences. Given the broad frequency spectrum for tensile cracking of moderate dimension (i.e., 10s to 100s of meters [Lee et al. 2003 and Figure D.1.1-4]) this should be achievable. Most predictions of contemporary Europa activity (e.g., Schmidt et al. 2011) imply that these sources should be numerous in Europa's ice.

Identifying the location of seismic sources at Europa using direct body wave arrivals is essential to using any succeeding near-vertical reflection to infer either the thickness of the shell (Lee et al. 2003) or intra-ice water lenses and associated ice lids.

D.1.2.3.3 *Investigation I.3: Search for local heterogeneity of the ice and any shallow subsurface water.*

As a potential indicator of Europa's habitability, the detection of porous ice, water-saturated ice, or any hydraulic connectivity between subsurface water bodies is of prime importance. The velocity of body waves in ice depends upon both temperature and porosity, with about two m/s of slowing for P waves for each one degree of warming (Kohnen 1974) and a P wave velocity decreased by about half for an increase in porosity of about 30-40% (Blankenship 1989, Van den Broeke et al. 2008). In addition, the presence of water in any porous granular medium can have an intense impact on the ratio of P to S wave velocity, indicative of both porosity and effective pressure (e.g., Blankenship et al. 1986). Because of this, knowledge of both the mode and azimuth of incident body waves can be a powerful indicator of both horizontal and vertical heterogeneity in Europa's ice shell, making both porosity and water within the ice matrix potentially detectable.

For example, the balance between seismic velocity decrease as the ice temperature increases with depth and the velocity increase as porosity decreases with depth is likely to give rise to a pervasive waveguide at a depth where the two effects yield the highest velocity. This is a well-established phenomenon for terrestrial ice masses and a powerful scenario for inverting for vertical velocity structure (Grant and West 1965), particularly of any Europa near-surface megaregolith. Similarly, significant deviations in the P and S travel time ratios for reflected or refracted waves traversing water-saturated ice can be a direct indicator of relative water content both vertically and horizontally.

Seismic waves generated at the ice-ocean interface are expected to have a lower frequency content than those originating from

shallower sources associated with water lenses. In this ice-ocean interface case, any small array optimized for azimuthal sensitivity would act as a single detector with some capacity for establishing the limits for any body-wave arrivals from below. Once determined to be sufficiently vertical, the P to S wave travel-time differences of these arrivals can be used to establish the thickness of the total ice shell (Section D.1.3), with an uncertainty governed only by the unknown temperature structure of the shell (Lee et al. 2003). As discussed above, this independent determination of shell thickness can be used to increase the conductivity resolution of the magnetic inversions.

D.1.2.3.4 *Investigation I.4: Characterize Europa's seismic activity and its variation over the tidal cycle.*

It is hypothesized that Europa exhibits tidally-driven temporal variation in seismic activity associated with surface crack evolution, (e.g., Greenberg et al. 1998, Hoppa et al. 1999). Similarly, the significant lateral and vertical heterogeneity of any active regions such as chaos should result in spatial variation of source distribution and frequency resulting from Europa's hypothesized tidal stresses. The ability to record and return to Earth in their entirety enough seismic records to statistically characterize this activity across the full width of the source spectrum is not really necessary to answer the question of tidal drivers for ice shell strain release. Continuous monitoring of seismic activity (in two bands) with return of selected events chosen through carefully designed trigger algorithms would yield a very comprehensive event catalog for each of these algorithms that can be utilized to establish the tidal correlation across a very broad source spectrum. Inclusion of event azimuth and inclination, and P to S time estimates, will allow these correlations to be spatially targeted to accommodate significant expected lateral heterogeneity.

D.1.2.4 Geology Traceability

Europa's geological landforms are enigmatic, and a wide variety of hypotheses have been offered for their formation. Characterization of sites of most recent geological activity is especially significant for understanding the formation of surface features, including whether and how liquid water is involved in their formation. Moreover, the formation processes of surface landforms is important to understanding how material is transported between the surface and the subsurface, and thus to understanding whether and how surface oxidants could be transported to the ocean, potentially providing chemical energy for life, and how oceanic material can be transported to the surface. In these ways, geology is directly pertinent to the potential habitability of Europa.

Thus, an objective of the Europa Lander Mission is to characterize the processes responsible for fine-scale (decameter and smaller) geological features at the selected landing site, especially those features that reveal the details of material recently derived from the ocean:

> *Characterize a locality of high scientific interest to understand the formation and evolution of the surface at local scales.*

From this objective flow three key investigations, described next.

D.1.2.4.1 *Investigation G.1: Constrain the processes that exchange material between the surface, near-surface, and subsurface.*

Europa's incessant tidal activity leads to consideration that some landforms might be actively forming today and are the most likely locations for near-surface water. The most promising regions for current activity are regions of chaos, or cracks that have recently formed in response to tidal stresses. Low-albedo smooth plains associated with some chaotic terrains might be composed of subsurface materials, such as brines, that have been emplaced onto the surface (Collins and Nimmo 2009, Schmidt et al. 2011). These recently active regions might therefore repre-

sent sites of high scientific interest. Recently or currently active regions are expected to best illustrate the processes involved in the formation of some surface landforms, showing pristine morphologies and distinct geological relationships, and perhaps exhibiting associated plume activity analogous to that seen on Enceladus (Spitale and Porco 2009).

High-resolution Galileo images of Europa (e.g., Figure D.1.1-5g and Figure D.1.1-7) show abundant evidence for very young materials exposed by mass wasting of faces and scarps (Sullivan et al. 1999). These postformational modification processes have likely affected many surfaces to expose fresh materials that are less altered than their surroundings. Given the decameter/pixel limit of the best resolution existing images of Europa, it will be essential to have higher resolution images of the landing site from above (either obtained from orbital reconnaissance, or else from a descent imager), to place *in situ* measurements into their geological context and to relate landforms of the types currently recognized from orbital images (Figure D.1.1-5) to features and materials of high science interest to be studied *in situ* from a Lander. Moreover, *in situ* images should be obtained down to the scale of millimeters/pixel and in stereo, in order to constrain formation processes of local landforms and small-scale features.

In order to accomplish a comprehensive survey of the landscape around the Lander, it will be necessary to obtain panoramic stereo images at 1 mm/pixel from 3 m distance in at least three filters (RGB). The MER rover mast cameras (Pancam), for instance, have 1 mm/pixel resolution in the near field and in stereo, which approximates the 20-20 vision of a field geologist. Panoramic coverage is necessary because planetary landscapes are heterogeneous on a variety of scales. Moreover, many processes only reveal themselves at the smallest scales, from the statistics derived from particle shapes, sizes, and distributions. The scene around the Lander should be in

stereo to ensure that the true shapes and sizes of local features can be unambiguously characterized. Likewise three-color imaging allows unambiguous discrimination of composition variations in the area, as distinguished from merely textural variations. This is especially critical in mapping the ice versus non-ice components of local materials.

D.1.2.4.2   *Investigation G.2: Constrain the processes and rates by which the surface materials (regolith and bedrock) form and evolve over time.*

Following surface emplacement (e.g., tectonism or volcanism), progressive modification processes have likely affected many surfaces (e.g., from sublimation and mass wasting), potentially exposing fresh materials that are less altered than their surroundings. Unambiguous characterization of landforms to understand surface processes at a local scale requires millimeter-scale imaging resolution, like the MER Pancam. A minimum of three colors is necessary to differentiate compositional variation (e.g., ice from non-ice) from shading effects at these resolutions. It is valuable to be able to characterize ice grains and non-ice materials within the sample to understand sample heterogeneity, ice history (ice morphology, inclusions), and the context of non-ice materials (size, shape, and texture). It will be necessary to characterize particle size, sintering, and thickness variations at landing site scales (decameter to submillimeter) to understand history and evolution of the regolith. This can be achieved by imaging samples of surface and subsurface materials at resolutions of better than 50 microns. These requirements are based on terrestrial, Mars Exploration Rover, and Phoenix experience.

D.1.2.4.3   *Investigation G.3: Understand the regional and local context of the landing site.*

Of primary importance is the detailed characterization of surface features—especially their distribution, morphologies, textures, local slopes and shapes, and associated embedded or

loose fine-grained components—at a variety of scales—to understand the processes by which they formed. The measurement requirements needed to accomplish this investigation, and the rationale for these measurements, are as those that constrain geological processes (Section D.1.2.4.1). Identifying the landing site from orbit following a successful landing will be especially important to understanding the geological context of *in situ* panoramic images, as has been the case for the suite of lunar and Martian landers and rovers.

D.1.2.4.4　Investigation G.4: Constrain the physical properties of the surface and near-surface at the landing site to provide context for the sample.

As part of the assessment of compositional heterogeneity of the local environment around the Lander at millimeter scales, it is valuable to characterize ice grains and non-ice materials within samples through microscopic imaging to understand sample heterogeneity, ice history (morphology and inclusions), and the context of non-ice materials.

Part of this characterization requires an understanding of the physical properties of local terrain, including information on porosity, density, and cohesion of the samples and the local environment. This information can come from engineering data associated with the landing system as it touches down, and from motor currents of the sampling system which provide information on torques and forces associated with contacting the surface. Much knowledge was gained about the physical properties of the Martian from similar approaches (e.g., Moore et al. 1982).

The probably fine-scale heterogeneity of the surface within the sampling arm workspace requires that this work space be thoroughly characterized from Lander imaging, that is to say, at ~1 mm/pixel, in stereo, and in at least three colors. This will allow sample spots to be identified and prioritized, based on the likelihood that size, shape, color, texture, etc. will indicate where the best ocean-derived material

can be analyzed following landing. A microscope with a resolution of ~10 μm/pixel would permit the recognition of compositional variation of materials within the samples analyzed by the RS and MS.

D.1.3　*Science Instrument Complement*

The model payload offers a unique set of abilities to sample and observe the surface of Europa.

D.1.3.1　Mission Goal Relation to Core Measurements and Instrumentation

The overarching goal of a landed mission is to determine the habitability of Europa. As such, the recommended scientific measurements and scientific payload follow familiar astrobiological themes (Section D.1.1) of examining the organic chemical composition (building blocks of life), the presence of liquid water (the occurrence and extent of a subsurface ocean), and the environmental history (ocean history, exchange of material between the subsurface ocean and the sampled surface, lifetime of surface materials, etc.). In this way, the payload links tightly with the three science objectives that relate to composition, ocean and ice, and geology. In particular to Europa, the exchange of material between the subsurface (ice shell and ocean) and the near-surface layer over time, followed by the physical and chemical evolution of the surface, leads to a complex story of Europa habitability. Unraveling this story required an integrated package of instruments that work ideally and effectively in coordination. A landed mission offers unique abilities to sample and observe the surface and unambiguously address the goal of understanding Europa's habitability.

Thus, the recommended science measurements and payload utilize the strengths of each archetypal instrument and technique to address key questions:

- The composition of ocean water, through active *in situ* chemical analysis of cryo-volcanically extruded or tectonically uplifted frozen water.

- The depth and salinity of the ocean, ice shell thickness and structure, and pathways by which ocean water may exchange with the surface, through passive sensing achievable by a landed platform.
- The geological signatures of surface-ocean exchange of materials and the surface history through imagery at a range of scales from meters to millimeters.

D.1.3.2   Integration of Instrument Categories

Coordination and integration of observations and measurements acquired by different instruments is central to determining Europa's habitability. Spatially or temporally coordinated observations greatly enhance the scientific value of the mission. For example, interpreting *in situ* surface composition as representing the composition of the sub-ice ocean requires knowledge of sample context, heterogeneity of ice and non-ice components, the geological history of the sample, and independent estimates the bulk salinity of the ocean. Understanding the geological history of the landing site reaches beyond panoramic imaging, requiring knowledge of the proximity of water, as well as regional surface and ice shell structure such as faults and fractures as pathways for the exchange of water with the surface. Interpreting the environmental conditions and habitability within the ocean requires combining observations of the depth distribution of water and ice with measurements of organic

and inorganic compounds dissolved within ocean-derived material that presently survives on the surface. In this way the suite of instruments integrates to address the broader questions of habitability in a way that cannot be accomplished by each instrument alone.

D.1.3.3   Instrument Payload

The choice of instruments for the baseline scientific payload is driven by the need for specific types of measurements that trace from the overarching goal of Europa's habitability, as detailed in the Europa Lander traceability matrix (FO D-1). These measurements focus on areas of the organic and inorganic composition of Europa's surface and near-surface materials, the scale of the ocean and thickness of the overlying ice shell, and the history of active exchange between the subsurface ocean and the observed surface. These fundamental measurements drive the recommendation of model instruments. These include direct measurements (such as composition or ocean bulk salinity), along with indirect measurements (such as context imaging or sample heterogeneity) that are needed to best interpret the direct measurements.

The baseline model payload of instruments is thus divided into three principal categories, as summarized in Tables D.1.3-1 and D.1.3-2. The first category, defining the science floor (unshaded in Table D.1.3-1), consists of those instruments fundamental to the mission objectives. The second category consists of additional scientific instruments that would greatly

Table D.1.3-1. Baseline and floor scientific instruments of the model payload.

Model Instrument	Key Science Investigations and Measurements
Mass Spectrometer (MS)	Surface and near-surface chemistry (especially organic content) to understand endogenic and exogenic processes and ocean composition.
Raman Spectrometer (RS)	Surface and near-surface chemistry (especially mineralogy) to understand endogenic and exogenic processes and ocean composition.
Magnetometer (MAG)	Ocean thickness and bulk salinity; depth to local water layers.
Multiband Seismometer Package (MBS)	Thickness of ice and local water layers; local ice-water heterogeneity; seismic activity and variation over tidal cycle.
Site Imaging System (SIS)	Context of compositional measurements; material exchange processes; surface formation and evolution; landing site context.
Microscopic Imager (MI)	Context of compositional measurements; ice and non-ice grain characterization.

Note: Floor science instruments are unshaded; additional science instruments of the baseline payload are shaded.

Table D.1.3-2. Engineering equipment providing science measurements.

Model Instrument	Key Science Investigations and Measurements
Reconnaissance Camera (RC)	Geological, regional, and local context of Lander on the surface.
Europa Sampling System (ESS)	Sample acquisition and delivery; cohesion and structure of surface materials.

contribute to the scientific return of the mission, and thus are included in the baseline model payload, but that are not considered part of the floor payload. They could be descoped from the model payload if they cannot be accommodated (shaded in Table D.1.3-1).

D.1.3.4 Engineering Equipment Providing Science Measurements

The RC on the Carrier and the ESS on the Lander contribute critically to the fundamental scientific objectives, and are otherwise needed for engineering a successful mission. This equipment (Table D.1.3-2) is needed to determine where the Lander will safely land and to deliver samples to the science payload. Data from this equipment has core scientific value; the two hardware items are listed here because they are central to meeting the science objectives of the mission.

The Reconnaissance Camera (RC) system, located on the Carrier element, is required for scouting safe landing sites, and along with its post-landing orbital images, provides critical data for geolocation of the Lander to place it in proper geological context for interpretation of in situ compositional, seismic, and site imaging data. The Europa Sampling System (ESS) is needed to mechanically obtain and deliver samples for scientific analyses. In addition, engineering performance data (such as motor currents and encoder positions) is important to understanding the physical structure of the surface layer sampled for scientific interpretation.

D.1.3.5 Coordinated Investigations with Multiple Instruments

Post-landing imaging data from the RC is used to place the landing site into global and regional context so that the proximity to major faults, ridges, and other structures can be compared with seismic data. Post-landing *in situ* imaging data, both from the Site Imaging System (SIS) and Microscopic Imager (MI), will provide context for ESS sampling and interpretation of sample heterogeneity and will aid interpretation of the geological history of samples and of how representative these compositional samples are of the overall region. The combination of Multiband Seismometer Package (MBS) and Magnetometer (MAG) data will allow for a robust characterization of the ice shell and the ocean. The combination of inorganic composition from the Mass Spectrometer (MS) and Raman Spectrometer (RS) along with ocean bulk salinity (MAG) will allow for interpretation of salt species concentration in the ocean, as well as how liquid water freezes and segregates these dissolved salt ions during ascent to the surface. The MS and RS will also work together to characterize organic content of the surface and shallow subsurface.

The two instruments included in the baseline model payload but not in the floor—the Raman Spectrometer and Microscopic Imager—provide important observations for the overarching mission objectives. The RS would provide inorganic compositional and mineralogical information that would be linked to ocean salinity and the evolution of brines and fluid inclusions during transmission of water from the ocean to the surface. The MI would provide information about the structure and potential heterogeneity of the collected sample, to constrain the origin of non-water-ice compositional components as inclusions, coating, or meteoric contamination. Details of these instruments and measurement objectives are discussed above (Sections D.1.2.2.2, D.1.2.2.3, and D.1.1.4.4). If these instruments were descoped, loss of their observations would degrade the integrated scientific value

of the mission, but the remaining floor instruments would still address the most fundamental questions pertinent to the habitability of Europa.

D.1.3.6 Additional Instrument Considerations

Two additional instruments were regarded by the SDT as very attractive to enhance the scientific return of the mission, but they were not deemed necessary to meet the fundamental scientific objectives (Table D.1.3-3). These are in addition to the several candidate techniques and instruments considered by the SDT for deriving compositional information (Table D.1.2-2).

A Thermal Radiometer would provide surface temperature measurements from observations of the emitted thermal infrared radiation from different areas around the landing site. Such measurements would provide ground truth for existing Earth-based and past spacecraft remote-sensing measurements of Europa's seasonal and diurnal temperature cycles. Such observations could be used in a variety of ways to constrain the structural properties of the regolith in the vicinity of the Lander (such as particle size, porosity, density, ice-grain sintering) through derivation of the thermal inertia of the surface layer (e.g., Spencer et al. 1999, Rathbun et al. 2010; see also Mellon et al. 2008 for discussion of thermal inertia). These measurements could also be used to assess subsurface structure such as the thickness of the regolith or changes in cohesion with depth. Knowledge of the regolith structure would place additional constraints on the rate of formation, ablation, and gardening of surface materials being chemically analyzed. The potential heterogeneity or homogeneity of the landing-site surface materials relative to the sample site, and how this material represents

the regional and global surface of Europa, could be further constrained by such measurements.

A Charged Particle Detector would provide measurements of the local radiation environment at the landing site, knowledge of which at present is extrapolated from space-based measurements. The history of radiation damage and alteration of surface materials affects the interpretation of surface versus subsurface composition (Section D.1.2.4). However, a charged particle detector could only provide observations at the time of surface operations, so these observations could only provide a partly representative sample of a radiation environment that is spatially and temporally variable (Mauk et al. 1999).

D.1.3.7 Sampling Strategy

As outlined in Section D.1.2.2.1, a key objective of a landed mission is to obtain and analyze samples of the surface ice to determine the organic and inorganic content of ocean water, which either extruded onto the surface and froze or was mechanically/tectonically driven to the surface. However, the radiation environment at the surface of Europa is harsh and these non-ice molecules residing at or very near the surface are continually bombarded with high energy electrons and heavy ions (Johnson et al. 2009, Paranicas et al. 2009). Over time, the composition of the surface ice is modified by fragmenting and sputtering larger molecules, and by emplacement of ions from space such as sulfur (Carlson et al. 2009). Thus, samples acquired from the very surface will not compositionally represent the ocean. Depending on the type and geographic location, this radiation damage is expected to reach depths of several centimeters (Patterson et al. 2012), and obtaining samples from as deep as 10 cm becomes necessary. Additionally, obtaining a near-surface sample (from 0.5–2 cm

Table D.1.3-3. Potential enhanced instruments, not included in baseline model payload.

Model Instrument	Key Science Investigations and Measurements
Thermal Radiometer	Surface temperature and characterization of regolith physical structure.
Charged Particle Detector	Characterization of surface radiation environment.

depth) and a deeper sample (5–10 cm depth) would provide an *in situ* assessment of the effects of radiation on ice composition. Therefore, the recommended strategy is to drill into the surface up to a depth of 10 cm, obtaining samples from at least two different depths.

D.1.4   Landing Sites

Landing sites on chaotic terrain are recommended to characterize Europa's habitability. Thera Macula is the primary landing site used in this concept study.

D.1.4.1   Science Requirements for Landing Sites

Landing on Europa for the first time represents a considerable challenge that can only be met by careful consideration of the scientific requirements and engineering constraints involved. This section concentrates on the scientific issues involved, and is complementary to Section D.2.8.2, which concentrates on the engineering issues associated with landing operations. In order to investigate Europa's astrobiological potential, it is important to understand the chemistry of its subsurface ocean, the structure of its icy shell, and the ice shell's formation and transport processes. Because the thickness of the ice shell precludes direct sampling of the ocean, the surface must be sampled at regions that are expected to provide "windows" to the subsurface. These regions are prioritized on criteria including surface concentration of non-ice materials and evidence that materials were transported from the subsurface (e.g., Figueredo et al. 2003, Ivanov et al. 2011). One critical consideration is how these materials have been affected by Europa's radiation environment, given that radiolysis of surface materials presents a significant obstacle to preserving potential biosignatures (Hand et al. 2009 and references therein).

The scientific objectives described in Sections D.1.1-D.1.3 can be best met by carefully choosing landing sites that meet a specific set of criteria. These sites have been determined

by considering the requirements of each Europa Lander science objective, and by selecting candidate sites that meet all the required criteria without subjecting a landed spacecraft to undue risk. We here describe how each of the scientific objectives flows into the selection of a landing site, and present some potential candidate sites.

D.1.4.1.1   Composition Considerations

The highest priority objective for a landed mission to Europa is to understand the habitability of the ocean through composition and chemistry. This involves characterizing the surface and near-surface chemistry to (1) constrain the ocean composition and understand the endogenic processes from which it evolves, (2) constrain the effects of exogenic processes, such as sputtering and radiolysis, and (3) understand the context of the compositional measurements. Spectral measurements have shown that low-albedo, disrupted areas on Europa's surface are comprised of non-ice components including hydrated materials (Section D.1.2.1). An important objective for Europa science is to resolve the compositions and origins of these hydrated materials and additional compounds; thus, these dark, disrupted areas are key areas of interest for compositional measurements. To choose the best locations for compositional measurements, however, other factors must be taken into account, including the likely genesis of the features, their relative age, degree of radiolytic weathering, and whether or not they have exchanged material with the subsurface.

The composition of Europa's surface and near-surface materials is expected to vary with the amount of exposure to Jupiter's radiation environment (Cooper et al. 2001, Johnson et al. 2004, Paranicas et al. 2009, Patterson et al. 2012). The lower latitudes of Europa's trailing hemisphere will be radiolytically processed to depths of at least several centimeters and, considering the effects of bremsstrahlung photons, may be processed at up to meter depths (Section D.4.2). However, the leading

hemisphere of the satellite, and higher latitude regions of the trailing hemisphere, may only be affected to depths in the micron to centimeter range. Although the average age of the surface is relatively young (~60 Ma, Schenk et al. 2004), stratigraphic mapping has shown that Europa's landforms are of different relative age (e.g., Greeley et al. 2004), and certain classes of feature—specifically chaos features—appear to be among the youngest landforms on the surface (Prockter et al. 2002, Figueredo and Greeley 2004, Doggett et al. 2009) so are probably less radiolytically processed. Revealed by cross-cutting relationships, most geological features appear to have a low albedo when newly formed, then to gradually brighten with age, ultimately reaching a relatively uniform high-albedo brightness (Geissler et al. 1998). Although the exact mechanism for this process is not well understood, it is likely related to radiation processing and/or the deposition of frost (e.g., Geissler et al. 1998). This brightening correlates with relative age, such that the youngest features on the surface are typically the darkest, while intermediate-aged features appear to be gray, and the oldest features are bright and largely indistinguishable in brightness from each other (e.g., Prockter et al. 2002). Shirley et al. (2010) used spectral data from the Galileo NIMS instrument to show that there is a distinct gradient in composition across the leading-trailing hemisphere boundary, verifying suspicions that the composition of surface units is altered by radiation processing (Carlson et al. 2009 and references within). Thus, the best compositional targets for a landed mission are the youngest, least radiation-processed materials, which also tend to be the lowest in albedo.

A second requirement to meet the compositional objective is to seek areas in which subsurface material (which may be derived from the ocean) has been exchanged with the surface in recent geological times. Studies of pull-apart bands suggest that they formed when Europa's lithosphere may have been thinner and more mobile (Section D.1.4.4). Bands also have shallower topographic slopes than other Europan landforms (Schenk 2009). Although they are clearly regions in which subsurface material has been brought to the surface, and therefore might appear to be good potential landing sites, they are generally older than chaos terrain (Figueredo and Greeley 2004, Doggett et al. 2009), and many are of intermediate albedo, also suggesting they are not particularly youthful.

Ridges (Section D.1.4.4) are ubiquitous on Europa, and appear to have formed throughout its history. Many ridges crosscut bands and chaos, so are thought to be quite young (e.g., Kattenhorn and Hurford 2009 and references therein). However, they are not ideal landing sites, because the mechanism of ridge formation is not well understood and it is not known whether the surface and subsurface exchange material at ridges. It is likely that the ridge margins are composed of crushed ice formed through tectonic or volcanic mechanisms. Many ridges have dark material associated with their margins (e.g., Belton et al. 1996), which may be of interest to compositional studies, but given the uncertainties about their genesis, it is difficult to make a case for ridges as candidate landing sites.

Chaos regions and smooth plains deposits within lenticulae (Section D.1.4.1) appear to have generally disrupted and/or embayed the preexisting terrain, implying that they are relatively young, and that they at least partially consist of material that has been brought up from the subsurface (Carr et al. 1998, Pappalardo et al. 1998). Thought to have formed from diapiric upwellings (e.g., Collins and Nimmo, 2010 and references therein), these features may have entrained subsurface material, and the briny deposits associated with chaos may represent subsurface ocean water or lenses of water (Schmidt et al. 2011). Thus chaos regions, especially those associated with

smooth, dark plains deposits, are of particular interest for compositional measurements.

D.1.4.1.2   *Ocean and Ice Shell Considerations*

The geophysics objective for a landed mission is to characterize the local thickness, heterogeneity, and dynamics of any ice and water layers of the ice shell. This characterization involves (1) investigating the heterogeneity and thickness of ice and water within Europa's shell, (2) determining the ocean salinity and thickness, and (3) characterizing how the satellite's seismic activity varies over its tidal cycle. To meet these objectives, a landed payload must be positioned such that it can detect signals from seismic sources, determine the conductivity of ice and constrain the salinity of subsurface water bodies.

Europa's surface is disrupted by tectonic features and chaos over most of the imaged regions (e.g., Doggett et al. 2009), and models of tidal straining predict that significant stresses and concomitant cracking should occur

across the globe (e.g., Greenberg et al. 1998). Figure D.1.4-1 illustrates the maximum tension predicted across Europa's globe during its diurnal tidal cycle, illustrating that every point on the surface experiences significant tidal stress at some time during Europa's 3.55-day orbital period. This ubiquity means that seismic measurements can be made from essentially anywhere on the surface and it is likely that good results will be returned. Ideally, a seismometer would be positioned within a few 10s of kilometers of a feature of interest, such as around the margin of a chaos region, in order to best characterize seismic effects from that region. We estimate the range to ice shell fracture events can be determined from direct observations of P and S waves for sources within a range of about 50 km from a Lander (Figure D.1.1-3 and Figure D.1.2-5).

The magnetic induction experiment recommended to characterize Europa's ocean is relatively insensitive to Lander location. We note that if there were a very high-conductivity
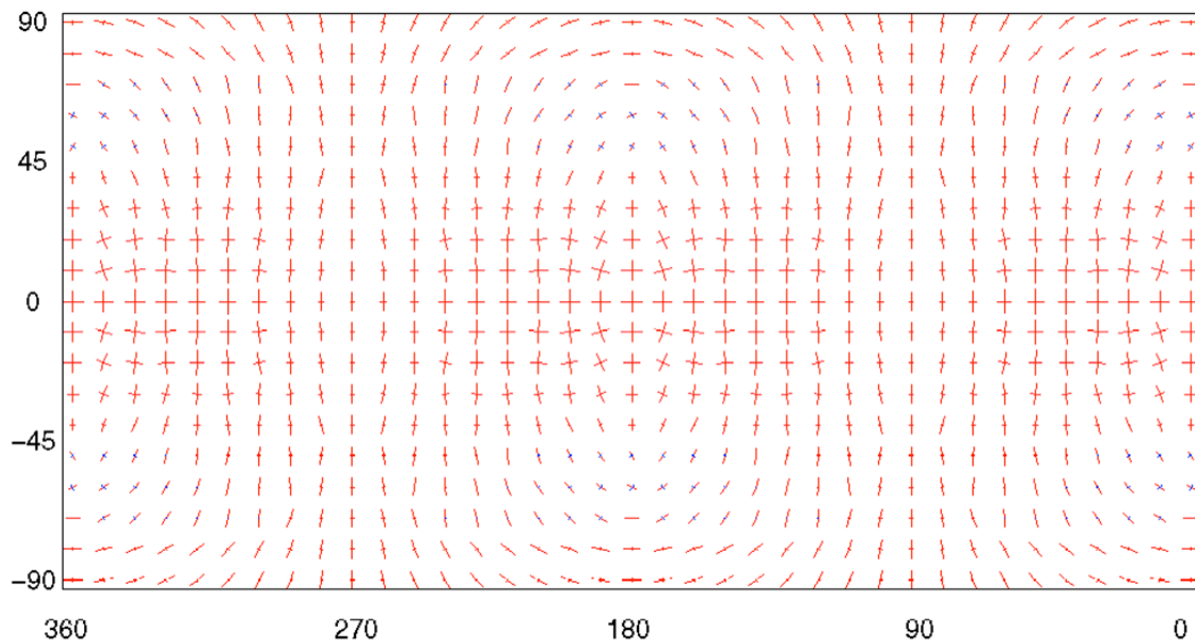

Figure D.1.4-1. Maximum tensile principal stresses over Europa's surface during the course of the satellite's orbit. At each point, magnitude (red tensile, blue compressive) and orientation of stress vectors are shown for the point in the diurnal tidal cycle when tensile stress is maximized at that point. Maximum magnitude is about 100 kPa. This map illustrates that the entire surface experiences significant diurnal tidal stress at some point during Europa's 3.55-day tidal cycle. (Z. Crawford and R. Pappalardo, pers. comm.)

layer within the ice shell (e.g., a saturated brine lens) immediately below the Lander, such would dominate the higher-frequency (11.2-hr) response, but should not significantly affect the lower-frequency (85.2-hr) response.

D.1.4.1.3   *Geology Considerations*

The primary geological objective for a Europa Lander involves characterizing a locality of high scientific interest in order to understand how the surface has formed and evolved at local scales. This involves characterizing the surface to (1) constrain the processes that exchange material between the surface and subsurface, (2) constrain the processes and rates by which surface materials form and evolve over time, and (3) understand the regional and local context of the landing site, and (4) constrain the physical properties of the surface and near-surface at the landing site. Some of these observations are essential for understanding the geological context of any samples and being able to fully interpret measurements from the surface. Although many exchange processes are regional in scale and are best characterized from an orbital or flyby platform, studies of local processes can yield abundant information about the history and evolution of Europa's landforms and the extent to which Europa's regolith is processed. The mechanical properties of a surface can be investigated, and ice grains and non-ice materials can be imaged to complement compositional measurements. Nearby landforms can be imaged to understand their slopes, regolith characteristics, and erosion and formation processes.

None of these measurements needs to be made at a specific location on the surface; the scale of the Lander is so much smaller than the scale of any known landforms on Europa that is it probable that only the local Lander-scale characteristics of the surface can be investigated. Investigation of regolith processes might yield more information in older terrains, where the surface has been modified by micrometeor-

ite bombardment and radiolytic processing over longer timescales.

D.1.4.2   Characteristics of Potential Landing Sites

In order to meet the scientific requirements, the candidate landing sites need to meet certain criteria that cannot be mutually exclusive. In considering the composition objective, inferences about relative age suggest that the most compositionally interesting (darkest) features are also the youngest and probably least radiolytically processed; therefore, it is desirable to conduct compositional measurements in such regions. Regions of older (brightened) materials could be targeted, but this would necessitate the sampling of materials from below the radiation-processed layer (tens of centimeters below the surface [Section D.1.4.1]), which would place additional constraints on the Lander.

Therefore, candidate landing sites have been selected in regions of lower radiation, primarily outside lower latitudes of the trailing hemisphere (Figure D.1.4-2). In order to meet the compositional requirement to sample material that has been most recently derived from the interior, Europa's chaos regions provide the most likely targets, on the basis of their young age and inferred formation mechanism. Furthermore, several of the margins of chaos regions are associated with dark, relatively flat plains material that has embayed its surroundings. These places appear to be frozen fluid that has extruded from the subsurface, so are attractive candidate landing sites. Recent work by Schmidt et al. (2011) suggests that Thera Macula, a large chaos region in Europa's southern hemisphere, may be actively forming today; thus, Thera Macula is a promising candidate landing site (Figure D.1.4-2).

The geophysical measurements can be made almost anywhere on the surface, but ideally are acquired close to a region that is potentially active and has interesting subsurface structure. For this reason, a seismic instrument would
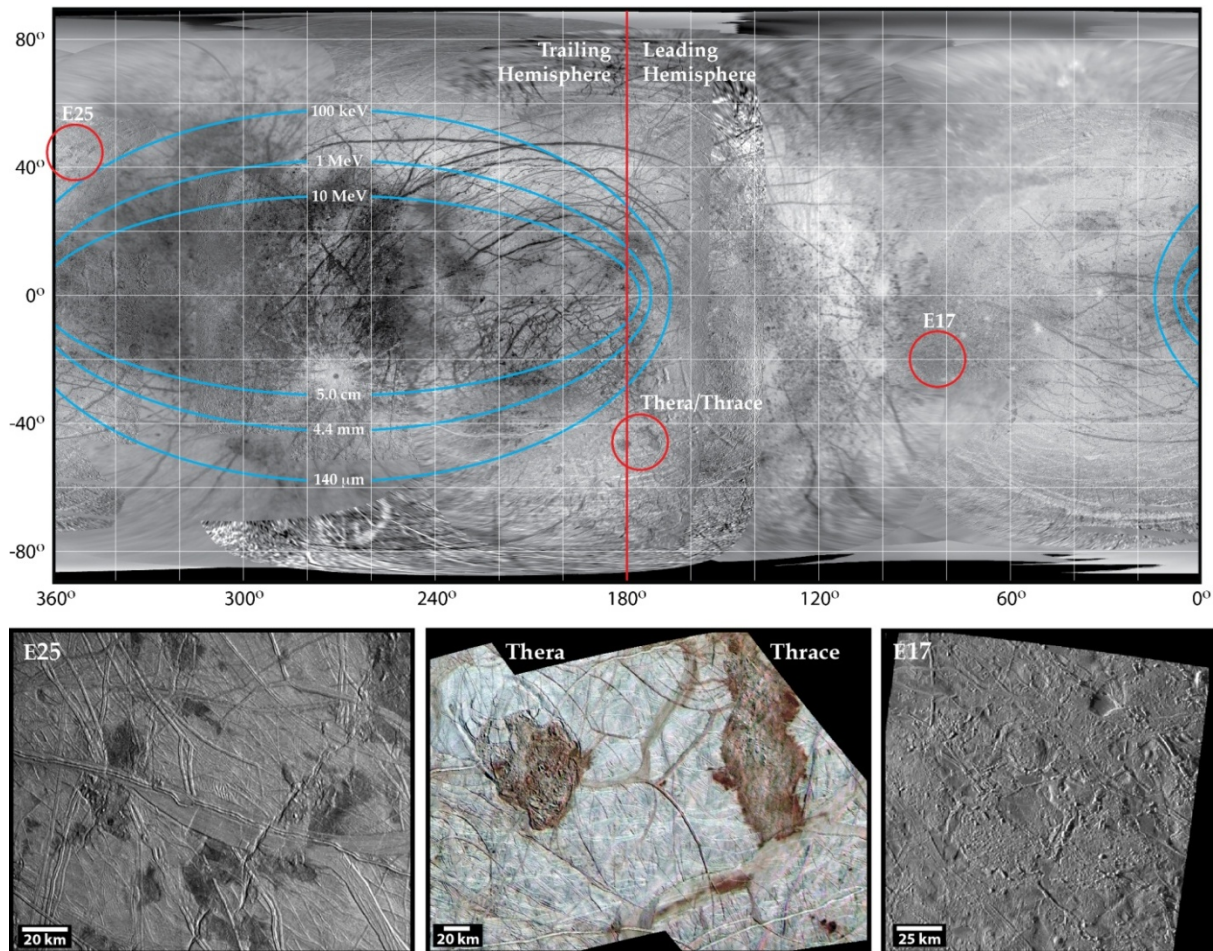
Figure D.1.4-2. Candidate landing sites on Europa. Top: Blue contours show radiation intensity on Europa's surface, as labeled with the geographic extent to which electrons of a given energy affect the surface and how deeply they penetrate (excluding the effects of secondary particles) (from Patterson et al. [2012] and C. Paranicas pers. comm.). Candidate landing sites are indicated by red circles on the global map, and shown in regional scale images at bottom. Left: Dark plains associated with chaos in the Galileo "E25" region. Center: The chaos terrains Thera and Thrace Maculae. Right: Dark chaotic terrain in the Galileo "E17" regional mosaic. Each candidate site satisfies the criteria of low-albedo, youthful material that appears to have originated from the subsurface, and is outside the most intense radiation regions on the satellite. Thera and Thrace Maculae present very attractive targets for exploration on the basis of their low albedo, relatively young age (they have disrupted the preexisting terrain), and likely endogenic origin. It has been suggested that water may exist beneath Thera Macula today.

best be situated within a few tens of kilometers from the edge of a tectonically active landform.

For the geological objective for a Europa Lander, there is no preferred region on the surface, although for studies of regolith processes, older terrains are preferred. However, it is expected that useful scientific data could be collected anywhere on the surface, and the geology objective is of lower priority than the

composition or geophysics objectives, so geology does not drive the selection of a landing site.

In light of the science objectives determined for characterizing Europa's habitability, candidate landing sites on or near chaotic terrain are deemed to be the most likely to yield fruitful results. Several candidate landing sites have been selected on the basis of the criteria described above, and are shown in Fig-

ure D.1.4-2. Our primary landing site is Thera Macula, which has a low albedo, relatively young age (it has disrupted the preexisting terrain), and likely endogenic origin; it has been suggested that water may exist beneath Thera Macula today (Schmidt et al. 2011).

D.1.4.3 Requirements for Orbital Reconnaissance of Potential Landing Sites

The highest resolution images of Europa's surface currently available are the handful acquired by the Galileo spacecraft with resolutions that range from 6-12 m/pixel. These show a surface that is rough down to the pixel level, containing fractures, slopes, and scarps. Most daunting are plates and matrix material resulting from chaos formation (Figure D.1.1-5e and Figure D.1.1-6), although these are scientifically very attractive places to explore. Imaging with resolution of 4 m/pixel of very young and active terrain on Saturn's satellite Enceladus—in a portion of Enceladus that resembles Europa's surface at comparable (tens of meters) resolution—reveals a landscape with many large ice boulders down to the resolution limit (Figure D.1.4-3).

It is impossible to be certain of the character of Europa's surface at Lander scales without additional orbital reconnaissance data. Based on existing slope data (Schenk 2009) at larger scales (Figure D.1.4-4), we can expect that Europa's surface will continue to be rough, even in places that appear smooth at larger scale (10s to 100s m/pixel).

The primary objective for orbital reconnaissance of a landing site would be to ensure safe landing. It is expected that several candidate landing sites, such as Thera Macula, would be chosen prior to arrival at

Europa, using existing Galileo data. These several sites would all be deemed scientifically acceptable, and that acceptability would be confirmed by orbital reconnaissance imaging. Then the landing site that is deemed the best combination of safety for landing and science potential would be chosen. While orbital reconnaissance of a landing site would provide useful scientific information, there are enough unknowns about Europa's composition, ice shell, and geology, that such reconnaissance is a requirement for engineering safety rather than for scientific analysis of potential landing sites. To pick the landing site on Europa that would truly yield the maximum scientific return, precursor observations would be needed, including months of reconnaissance prior to selecting a scientifically optimized landing site.
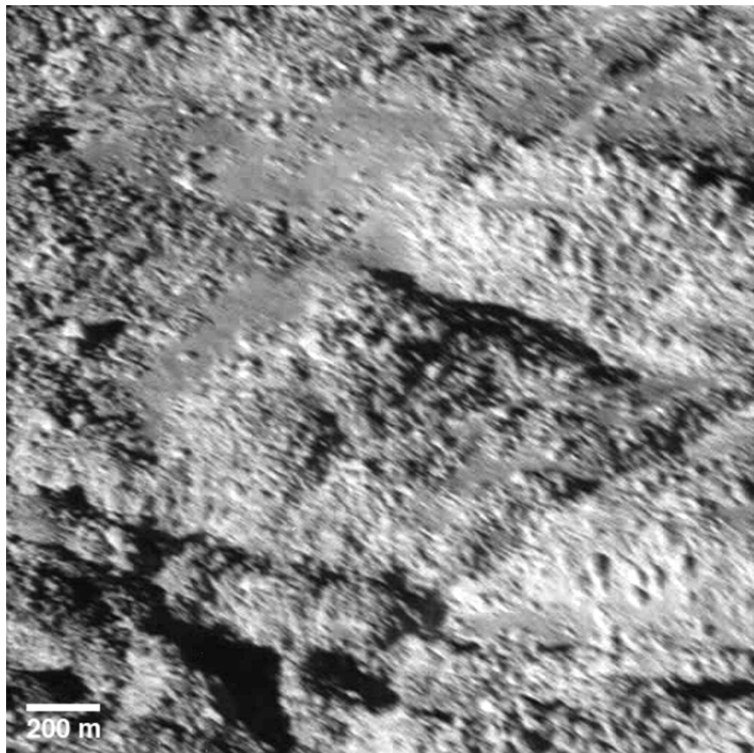

Figure D.1.4-3. At the highest resolution obtained by Cassini at Enceladus (4 m/pixel), that satellite's active "tiger stripe" region near the south pole is strewn with boulders 10s of m across, along with some intervening smooth patches. Spacecraft motion has caused minor smearing of the image. (PIA06252, NASA/JPL/SSI.) A Lander would fit within a single pixel of this image.
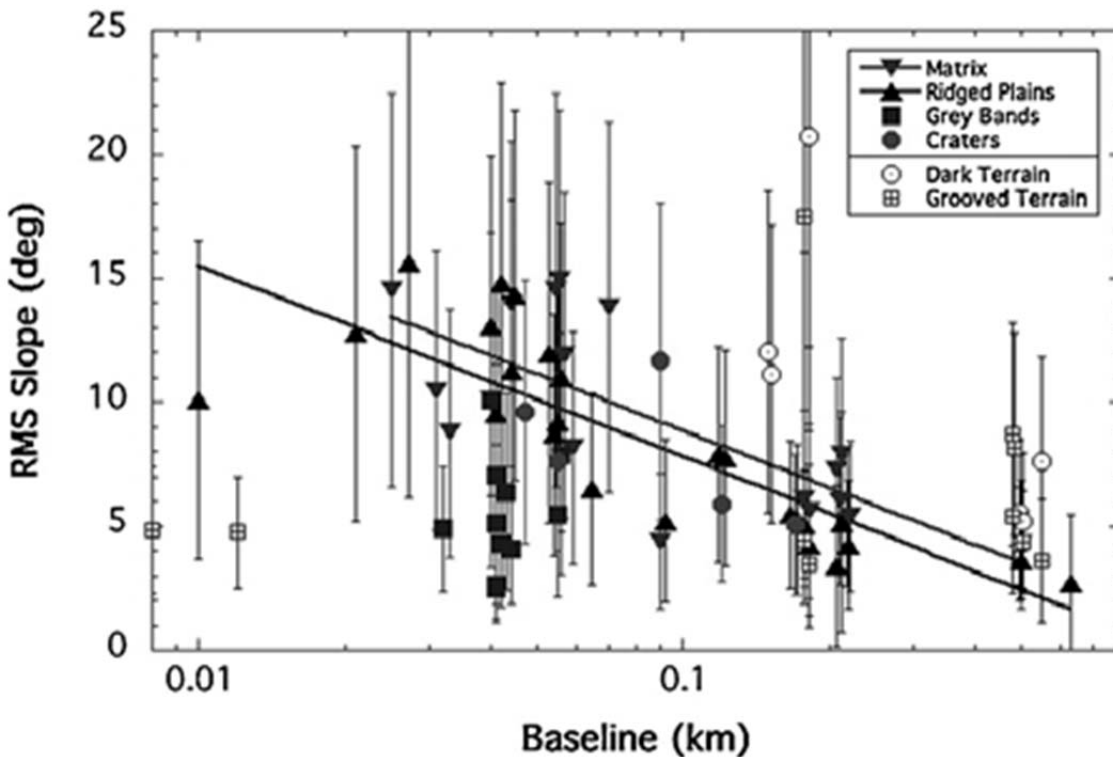
Figure D.1.4-4. RMS slope distributions for four major terrain types on Europa as a function of length scale. Standard deviations for RMS values (shown as error bars) indicate a high degree of slope variability at any given site. The major exceptions are pull-apart bands (squares), which have low slopes and low variability at observed scales. Also shown are available high-resolution data for dark and bright terrains on Ganymede (open symbols). Lines are least-squares fits through Europa matrix and ridged plains data, which suggest RMS slopes of ~20° if extrapolated linearly to ~1 m scale. (From Schenk 2009.)

D.2   Lander Mission Concept

D.2.1   Mission Overview

The Europa Lander provides the ability to meet the baseline science objectives in a single mission, without the need of any precursor missions.

D.2.1.1   Lander Study Scope and Concept Design Drivers

The purpose of the 2011 Europa Lander Mission study was to determine the existence of a feasible, cost-effective, scientifically compelling mission concept. In order to be determined feasible, the mission had to have the following qualities:

- Provide a high probability of landing success (>95%) without any precursor missions

- Accommodate the measurements and model payload elements delineated in the Science Traceability Matrix

- Launch in the 2018–2024 time frame with annual backup opportunity

- Use existing Delta IV Heavy launch vehicle (LV) or smaller

- Utilize ASRGs. No limit on number, but strong desire to minimize ^{238}Pu usage

- Mission duration <10 years from launch to EOM

- Use existing aerospace <300-krad radiation-hardened parts

- Focus on keeping radiation total ionizing dose (TID) low for the Lander because the shielding mass affects the wet mass of the Lander AND is also reflected in the wet mass of the Carrier

- Optimize design for cost, looking for the lowest cost possible while achieving baseline science
- Maintain robust technical margins to support cost commitment

The Europa Study Team's strategy in investigating this concept was to develop a well-defined, well-documented architecture description early in the mission life cycle. From that architecture space, lighter, more compact design solutions were favored to reduce shielding and overall system mass. Hardware procurement, implementation, and integration were simplified through a modular design. Mission operation costs were reduced by increasing system robustness and fault tolerance to allow for extended periods of minimally monitored operations during the long interplanetary cruise. Radiation dose at the part level was reduced to currently existing aerospace part tolerances. Specifically, the part total dose was reduced to levels demonstrated by geosynchronous and medium earth orbit satellite components.

D.2.1.2   Lander Mission Concept Overview

The Lander Mission concept centers on deploying a single, robust, highly capable, radiation-tolerant Lander to the surface of Jupiter's moon Europa to perform in-situ investigation of surface and near-surface composition and chemistry, seismographic study of local and regional ice thickness and dynamics, high-resolution imagery of landing site and sampling workspace morphology, and investigation of local magnetic field dynamics. These investigations will be performed during a 30-day science campaign from a single location on the surface of Europa. The landing site will be selected from several candidates identified before launch and narrowed to one site after an on-orbit landing site reconnaissance campaign and site selection process determines the optimal site for safe Lander deployment within one month of entering Europa orbit.

The Lander Mission launches from Cape Canaveral Air Force Station in November 2021 and spends 6.5 years travelling in solar orbit to Jupiter. During this time, the mission performs gravity-assist flybys, a flyby of Venus first, then two flybys of Earth, before swinging out to Jupiter. All terrestrial body flybys have altitudes greater than 500 km, required for a spacecraft carrying radioactive materials, to protect against the unlikely event of an impact.

JOI occurs in April 2028 when the vehicle performs a nearly 2-hour main engine (ME) burn to impart a 900-m/s velocity change on the spacecraft. This maneuver places the spacecraft in an initial 200-day Jovian orbit. An additional burn at apojove raises the perijove altitude and reduces the orbital period. The spacecraft then performs eleven gravity-assist flybys of Ganymede and Callisto over the course of eighteen months to reduce orbital energy and align the trajectory with Europa.

EOI and circularization of the orbit are performed using a three-burn sequence over two Europa orbits. The first burn of ~800 m/s places the spacecraft into a 200 × 7000–km, 10 a.m.–node near-polar orbit. A second burn of ~100 m/s performs a plane change to adjust the equatorial crossing node to 7:30 a.m. local solar time. A final periapsis burn circularizes the orbit to its final 200 × 200–km, 7:30 a.m. near-polar specification required for reconnaissance imagery collection. This unique mission design keeps the total dose radiation accumulation to 125 krad (100 mil Al) before EOI.

One-half-meter-per-pixel high-resolution imagery is taken in 10 × 10–km swaths for each of the candidate science sites in the first three days after arrival. This data is downlinked to the ground for automated processing, surface rectification, and hazard detection analysis. Processed imagery is provided to an expert science team for interpretation and final site selection. Concurrently, terrain-relative navigation (TRN) maps are produced from the

reconnaissance imagery. Once a final landing site is selected, the TRN map for that site is uploaded to the spacecraft.

Lander deployment is initiated by lowering the spacecraft to a 5×200–km orbit aligned with the landing site. The Lander is deployed by the Carrier at the appropriate time and position to begin its descent. A STAR-30E SRM is fired to eliminate the majority of the Lander's orbital velocity. After the SRM burn it is jettisoned. A deorbit cleanup maneuver is performed using monopropellant thrusters. Imagery is acquired early in the descent to locate the Lander's position on the previously uploaded TRN map. A divert maneuver of up to 3 km is performed to correct any deorbit performance deviations and ensure precision landing site targeting. Descent thrusters provide constant deceleration during the majority of the descent. Approximately 300 m from touchdown, the hazard detection and avoidance system images the ground to determine if any unsafe obstacles exist at the landing site. A divert maneuver of up to 50 m is performed to finalize Lander targeting to a safe location. Soft touchdown occurs at less than 0.5 m/s (about 1 mph) to minimize the chance of tip-over.

Once the Lander is safely on the surface, a 30-day science campaign begins with safing the propulsion system, establishing communications with the Carrier element (now in a 200×200–km near-polar orbit), deploying the HGA, and establishing communications with Earth. Initial landing site imagery is taken of the footpads and sent to the Carrier element for relay to the ground. Ground commands initiate deployment of the SIS, MAG, and ESS. Detailed imagery of the sample acquisition workspace is collected, the MAG is set to collect data, and the seismometers are set to collect narrow-band data on threshold-crossing seismic events. Ground commands initiate ice sample acquisition at a selected location using a rotary percussive coring drill at the end of a five-degree-of freedom (DOF) arm. A sample

will be collected from 0.5–2 cm below the surface and delivered to a sample port on the top of the Lander. The MI and RS examine the sample before it is heated and ingested by the MS. Another sample will be acquired from 5–10 cm below the surface and examined in a similar manner using a second sample port. Finally, comprehensive stereo imagery of the landing site is collected using multiple filters.

D.2.1.3   Lander Mission Elements

The Europa Lander Mission would be accomplished with a launch vehicle, a spacecraft, and a ground system. The ground system is responsible for planning, testing, transmitting, and monitoring all command sequences executed by the spacecraft, monitoring the spacecraft's health and planning, and executing any anomaly recovery activities required to maintain system health and mission robustness.

The spacecraft is composed of a Carrier element and a Lander element. The Carrier element provides all support functions to the Lander before Lander separation, performs all predeployment propulsive maneuvers, and collects reconnaissance site imagery. After separation, the Carrier element serves as a high-bandwidth communications relay between the Earth and the Lander. The Lander is powered off for the majority of the cruise to Europa. A passive thermal system maintains allowable nonoperation temperatures for the Lander avionics and deorbit SRM. Excess power from the Lander's two ASRGs is available to the Carrier before Lander deployment via separable harness connections.

The Carrier element employs a modular design with two main modules: the Avionics Module and the Propulsion Module.

The Avionics Module hosts the bulk of the Carrier's powered elements, including the computers, power conditioning and distribution electronics, radios, and mass memory. These units are housed in a vault structure that provides significant radiation shielding. The upper section of the Avionics Module is called

the Upper Equipment Section (UES) and hosts the batteries, reaction wheels, star-trackers, RC, and Lander support structure.

The Propulsion Module supports the fuel, oxidizer, and pressurant tanks as well as the pressurant control assembly and the propellant isolation assembly. Four thruster clusters supported by tripod booms at the base of the Propulsion Module each contain four 1-N reaction-control-system thrusters and two 40-N thrust-vector-control (TVC) thrusters. The ME is mounted to a baseplate suspended from the bottom of the Propulsion Module main structure. Two ASRGs are mounted to the base of the Propulsion Module primary structure. Mounted to the side of the Propulsion Module is the 3-m HGA used for communication to the Earth.

The Lander is a compact, integrated spacecraft capable of performing deorbit, descent, and landing (DDL), followed by surface science. The Lander performs attitude determination and control after separation, executing the deorbit burn and divert maneuvers, collecting and processing TRN and hazard-avoidance imagery, to enable a soft touchdown. After touchdown the Lander communicates to the Carrier element (or directly to Earth) and executes the science investigations on the surface. Two ASRGs would be mounted to the outside of the Lander body to provide power for avionics, heating, and science instrumentation.

D.2.1.4 Lander Mission Architecture Overview

The Lander mission was architected to reduce the total radiation dose incurred on critical flight elements while maintaining reasonable mass margin on the Lander element. Creative mission design eliminated the accumulation of any appreciable radiation dose until very late in the approach to Europa. Significant radiation exposure occurs during the 30-day orbital reconnaissance phase of the mission, but it is possible that radiation shielding could be

reduced if the Lander avionics remain powered off. For this study, it is assumed that the Lander must take the entire total dose of radiation. This assertion will be the subject of rigorous future investigation. Once on the surface, the Lander radiation dose is greatly reduced by the selection of a low-radiation-flux landing site and hemispherical shielding provided by proximity to the moon.

The unknown surface terrain on Europa at Lander scales drove the architecture to deploy all means feasibly available to ensure a precision landing on safe terrain. These means include predeployment orbital reconnaissance, precision deorbit maneuver execution using high-resolution inertial measurement, TRN with significant divert capability, low-altitude hazard avoidance, altimetry-guided soft landing, high-stability pallet landing system with crushable energy attenuation, and access to an oversized sample acquisition workspace with an agile sample-collection system. Although some of these technologies require development, it was the opinion of the Europa Study Team that all of these techniques were required to ensure a safe landing and completion of the primary science objectives in a single mission (no precursor reconnaissance missions were assumed in this study).

D.2.1.5 Lander Mission Technology Development and Risk Mitigation

A single Lander Mission to Europa (with no precursor) to meet the science objectives requires some technology development. Table D.2.1-1 summarizes the technology development activity required.

D.2.2 Payload

The Europa Lander model payload leverages heritage designs to achieve the measurements necessary to characterize Europa's habitability.

Instrument concepts and techniques that meet the mission objectives will be selected via NASA's AO process. Notional instruments and instrument capabilities presented here are not meant to prejudge AO solicitation out-

TableD.2.1-1. Technology development for the Europa Lander Mission enables safe landing and high-quality science in a single mission.

Item	Current State	Why Needed
MBS	MEMS seismometers have not been qualified or flown in a space environment.	Required to meet floor science objectives.
RS	No Raman has flown in space.	Required to meet baseline science objectives.
ESS	End-effector design for Europa surface and temperature control.	Required to meet floor science objectives
ASRG	In development, but has not flown.	Solar power not feasible; other RTG designs not available.
TRN	In development under Mars Program and Human Program.	Pin point landing required to meet Ps >95%.
HD	In development under Mars Program and Human Program.	Required to detect hazards to meet Ps >95%.

come; rather this Europa Lander Mission model payload is used to deduce suitable engineering aspects of the mission and spacecraft design concept, including operational scenarios that could obtain the data necessary to meet the science objectives. In addition, model payload instruments were defined well enough to demonstrate a plausible approach to (1) meeting the measurement objectives, (2) performing in the radiation environment, and (3) meeting the planetary protection requirements. Therefore, instrument descriptions are provided here only to show proof of concept. Heritage or similarities discussed here refer only to instrument techniques and basic design approaches. Physical and electrical modifications of any previous instrument designs would be necessary for them to function within the unique environmental context of this mission. Such modifications are accounted for in the mass and cost estimates. Instrument mass estimates assume performance only from currently available detectors. Advanced developments have been included in the cost estimates, but their projected performance improvements have not been assumed in these performance calculations.
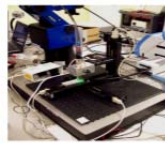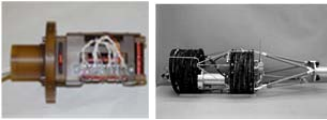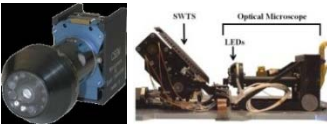
The model planning payload selected for the Europa Lander study consists of a set of remote-sensing instruments and *in situ* instruments. Instrument representatives on the SDT (or identified by SDT members) were consulted extensively to understand the requirements for each notional instrument. Table D.2.2-1 shows the estimated resource requirements for each instrument and for the total planning payload. Table D.2.2-2 summarizes the instruments and their capabilities.

The RC is an engineering camera that is accommodated on the Carrier and is used for conducting the reconnaissance campaign prior to landing. The camera requirements for selecting and certifying the landing site were derived by SDT representatives and are accommodated in the shown design.

Table D.2.2-1. Model payload resources are accommodated with margin by the Carrier and Lander elements.

Instrument	Unshielded Mass (kg)	Shielding Mass (kg)	Total Mass (kg)	Operating Power (W)	Data Rate	Telemetry Interface	# Boards
Mass Spectrometer (MS)	14.8	3	17.8	30	3.1 kbps	RS-422	6
Raman Spectrometer (RS)	6.5	2	8.5	30	1.6 kbps	RS-422	4
Multiband Seismometer Package (MBS)	5.8	2.7	8.5	4.6	72 kbps	RS-422	4
Magnetometer (MAG)	2.2	0	2.2	4.0	1.8 kbps	RS-422	2
Site Imaging System (SIS)	2.8	3.0	5.8	4.0	1.2 Mbps	SpaceWire	2
Microscopic Imager (MI)	2.3	1.5	3.8	10	1.2 Mbps	SpaceWire	2
Science Chassis	9.5	12.5	22.5				
TOTAL ALL INSTRUMENTS (w/o Science Chassis)	**34.2**	**12.2**	**46.4**	**82.6**	**3.8 Mbps**		**20**
Reconnaissance Camera (RC)	33.4	1.6	35	38	706 Mbps	SpaceWire	2

Table D.2.2-2. The model payload characteristics are grounded by heritage analogs.

Instrument	Characteristics	Similar Instruments	
Mass Spectrometer (MS)	Quadrupole mass spectrometer, with gas chromatography, evolved gas analysis and pyrolyis capabilities Mass range: 2 to 550 Da Mass resolution: 1 Da over full range Dynamic range: >1 x 10^8 over full range Limit of detection: <1 ppbw of 1-fluoronapthalene in calcite/silica 0.05 cm^3 pyrolysed sample	Huygens GCMS MSL SAM Rosetta COSAC	
Raman Spectrometer (RS)	Raman infrared line spectrometer Spectral range: 900 nm–1.5 μm Resolution: <7 cm^{-1} Peak accuracy: <2 cm^{-1} Laser wavelength: 976 nm Detector: InGaAs	New development; some similarity to ExoMars RS and MMRS	
Multiband Seismometer Package (MBS)	Six 3-axis MEMS seismometers Frequency range: 0.1 to 75 Hz (low-pass), 125-250 Hz (high-pass), notched at ASRG frequency (103 Hz) Noise: <5 x 10^{-8} m s^{-2} $(Hz)^{-0.5}$ @ 10 Hz	New development; some similarity to ExoMars SP sensors and COTS seismometers	
Magnetometer (MAG)	3-axis fluxgate magnetometer Boom: 2 m Dynamic range: 1024 nT Sensitivity: 0.03 nT Nominal sampling rate: 16 Hz	MASSENGER MAG Galileo MAG	
Site Imaging System (SIS)	Dual stereo color imagers FOV/IFOV: 16 degrees/ 0.3 mrad Filters: 8 F#: f/20 Maximum frame rate: 0.1 Hz Detector size: 1024 x 1024 pixels SNR: 100 for 50-ms panchromatic exposure; 5-s 30-nm bandpass violet filter exposure Illumination: Worksite visible LEDs Mechanisms: Gimballed platform, 1.0-m mast	MER Pancam	
Microscopic Imager (MI)	Wide-angle close-focus camera FOV: 25 degrees Filters: RGB Bayer filter Detector size: 1024 × 1024 pixels SNR: >200 Illumination of the sample: White light/ UV Mechanisms: Autofocus	MSL MAHLI Phoenix MECA Microscope MER Microscopic Imager Beagle 2 Microscope	
Reconnaissance Camera (RC)	Engineering pushbroom panchromatic narrow-angle camera FOV/IFOV: 3 degrees/2.5 µrad F#: f/10 Detector Size: 12288 × 128 pixels SNR: >100 TDI: 21 stages	MRO HiRise Camera	

D.2.2.1   Payload Accommodation

Adequate instrument mounting area is available for the science payload on the Lander top deck and also below the top deck (see FO D-2). The SIS minimizes obstructions in its field of view (FOV) by being mounted on a 1.0-m mast and a gimbaled platform on top of the Lander deck. The MAG is mounted on a 2-m boom. The MBS sensors are mounted on the Lander legs. The sample analysis instruments are mounted below the top deck looking at the MS ovens through a mirror/prism assembly. The HGA is deployed so as to be clear of instrument fields of view. Instrument mounting and accommodation requirements are summarized in Table D.2.2-2.

The science payload is expected to contain instruments with detectors requiring cooling to as low as 160 K for proper operation while dissipating up to 600 mW of heat. Cooling will be accomplished with passive radiators, mounted so their view is directed away from the Sun (this is achieved by rotating the Lander appropriately during descent). The impact on instrument thermal design and/or operational constraints imposed by the thermal perturbations caused by Jupiter in the FOV of radiators will be addressed during Phase A.

The RC requires Carrier pointing control to better than or equal to 1 mrad, stability to 100 µrad/s and reconstruction to 3 µrad/s, and is mounted in the UES of the Carrier element with a clear FOV.

The storage capacity of the spacecraft solid state recorder (SSR) (see Section D.2.5.8) exceeds the payload requirements. The notional model payload block diagram shown in FO D-2 assumes a data system architecture with RS-422 interfaces for low-data-rate instruments (MAG, MS, RS, and MBS), and SpaceWire interfaces for high-data-rate instruments, such as SIS & MI.

D.2.2.2   Radiation and Planetary Protection

The severe radiation environment at Europa presents significant challenges for the science instruments. These challenges have been addressed with a notional payload architecture that efficiently implements radiation shielding and EEE parts selection, and by leveraging work achieved by the JEO Detector Working Group (DWG). The DWG developed a methodology for determining the required radiation shielding for successful instrument operation in the severe transient radiation environment at Europa, assessed degradation of detectors due to total dose and displacement damage (DD) effects, and assessed the compatibility of candidate detectors with the planetary protection protocols. To enable the use of 100-krad EEE parts (radiation design factor [RDF] =2), the science electronics chassis is designed such that the equivalent TID environment inside the chassis is 50 krad. Because the radiation and planetary protection challenges for a Europa Flyby Mission would be quite similar in nature and magnitude to those of JEO, the DWG conclusions apply here as well without alteration.

D.2.2.2.1   *Detector Working Group*

The DWG, established as part of JEO study, was charged with assessing the existence of a feasible pathway for photonic detector technologies required by the JEO model payload. This work is directly applicable to Europa Lander Mission. The DWG included experienced instrument, detector, and radiation environment experts from the Applied Physics Laboratory (APL) and JPL. The DWG used an empirical approach to determine worst-case estimates of the effects of electrons and protons incident on detectors. This information was used to assess the performance potential of existing detector technologies subjected to the EOM total dose. Additionally, the impact of radiation-induced transient noise in each detector technology was evaluated for radiation flux levels encountered during Europa orbit. Finally, the tolerance of each detector technol-

ogy to dry-heat microbial reduction (DHMR) for planetary protection was evaluated.

The DWG concluded that the radiation and planetary protection challenges facing the model payload are well understood. The question of detector survivability and science data quality is not considered to be a significant risk provided appropriate shielding is allocated to reduce cumulative TID, displacement damage dose (DDD), and instantaneous electron and proton flux at the detector, and early mitigation approaches are implemented. Radiation shielding allocations and the impact of radiation-induced transient noise on science data quality are presented for each instrument of the model payload in subsequent sections of this report. The full DWG assessment report may be found under separate cover (Boldt et al. 2008). Specific activities to support early education of potential instrument providers to the complexity of meeting radiation and planetary protection requirements have been identified. For the Europa Lander, the scope of the payload and the radiation dose are much smaller than for JEO; moreover, all but two technologies used (MBS, RS) have been examined during the JEO study. For MBS and RS, a radiation testing campaign and a technology development plan are recommended as part of Phase A.

D.2.2.2.2   Payload Shielding Architecture

The Lander radiation design point is 520 krad behind 100 mils of aluminum shielding without design margin as described in Section D.2.9.1. Therefore, sensors and supporting electronics require significant shielding. The most mass-efficient approach to providing radiation shielding is to centrally locate as much of the instrument electronics as possible, minimizing the electronics that must be colocated with the sensor portion of the instrument. The model payload design presented here assumes instrument partitioning in this manner, as shown in FO D-2, and includes a science electronics chassis implemented using the industry standard 6U Compact PCI form-

factor. Space for twenty redundant electronics boards is baselined, with radiation shielding sufficient to allow use of components hardened to 100 krad or above without additional spot shielding. The total radiation shielding mass for the science electronics chassis is estimated to be 12.5 kg. Internal partitioning of the science electronics is baselined to provide electrical isolation between instruments and to mitigate electromagnetic interference (EMI). Louvers will provide thermal control of the science electronics chassis in the same manner used for the spacecraft avionics systems.

D.2.2.2.3   Detector Radiation Noise Methodology

The impact of radiation-induced transient noise on detectors was analyzed by estimating the number of high-energy electrons and protons penetrating the radiation shield and assessing their effect on the detector material. The flux of incident electrons reaching the detector for different radiation shielding thicknesses T can be estimating by applying the cutoff energy E determined from $E(\text{MeV}) = [T (g/\text{cm}^2) + 0.106]/0.53$ (Zombeck 1982) to the external integral electron flux. For 1 cm of Ta shielding, an estimated 4.3×10^5 electrons/cm^2 s would reach the detector while in orbit at Europa. The flux of incident protons reaching the detector can be estimated by applying a 100-MeV cutoff energy to the external integral proton flux. For 1 cm of Ta shielding, about 50 protons/cm^2 s would reach the detector while in orbit at Europa. During the reconnaissance phase of the mission (in Europa orbit), the RC is shielded against these peak fluxes. The Lander instrument detectors can be annealed before landing on Europa. Once on the surface of Europa, for 1 cm Ta shielding, an estimated 7.0×10^3 electrons/cm^2 s and <50 protons/cm^2 s would reach the detectors. The predominance of electrons in the Jovian environment is the determining factor for the detector radiation shielding analysis presented in subsequent sections.

D.2.2.2.4   *Planetary Protection Protocols*

The approach to planetary protection compliance for the Europa Lander Mission is presented in full in Section D.2.9.3 and can be summarized as follows:

- Prelaunch microbial reduction to control the bioburden for areas not cleaned by radiation in flight
- In-flight microbial reduction of exterior elements via radiation prior to EOI.

The preferred prelaunch method is DHMR. Current planetary protection protocols include a system-level DHMR with time vs. temperature profile ranging from 125°C for 5 hours to 110°C for 50 hours. It is anticipated that in some cases contamination control bake-out parameters can be modified to allow bioburden reduction credit. During assembly, test and launch operations (ATLO) it is assumed that cleanliness will be maintained (as for the Mars Exploration Rovers and the Mars Science Laboratory) to ensure that surface spore density does not exceed 300 spores/m^2, so that remaining surface spore bioburden will be reduced via radiation during flight. To support cleaning operations during ATLO, high-efficiency particulate air (HEPA) filters and instrument aperture covers with biobarriers are baselined.

Planetary protection guidelines will be generated and disseminated to potential instrument providers early, allowing providers to adequately address planetary protection issues during the instrument selection process. A mid-Phase B Payload Planetary Protection Review is baselined so that issues and mitigation strategies can be identified and addressed. Instrument-specific planetary protection concerns are addressed in subsequent sections.

D.2.2.2.5   *Samples*

The baseline science requirement calls for only two samples. The concept shown in this section meets this requirement exactly; the ESS and instruments do not define the limit, but currently the oven door closure is a one-time opportunity, and there are no provisions for cleaning the ESS between sampling. There will be a trade study in Phase A on increasing the number of samples.

D.2.2.3   Model Instrument Descriptions

D.2.2.3.1   *Mass Spectrometer (MS)*

The notional Mass Spectrometer is a quadrupole instrument that is capable of performing evolved gas analysis (EGA), pyrolysis, and gas chromatography (GC). The MS design adopted for the Europa Lander is based on the Huygens GCMS and MSL SAM, with the oven design from the Rosetta COSAC (see Figure D.2.2-1). The mass spectrometer is a key instrument in determining the composition of the Europa's surface and near surface by measuring the composition of two samples delivered to it by arm retrieved from 0.5–2 cm and 5–10 cm below the surface. It will analyze the samples, retrieving abundances of organics (as low as 1 ppb) and inorganics (as low as 1 ppm).
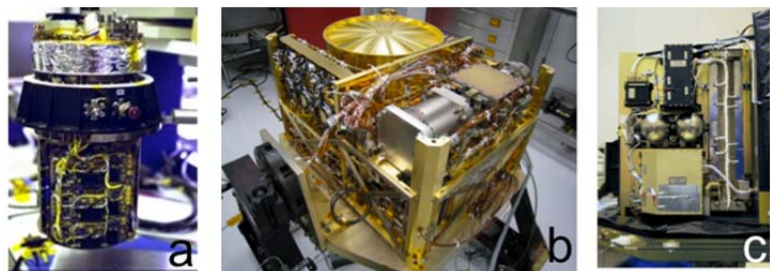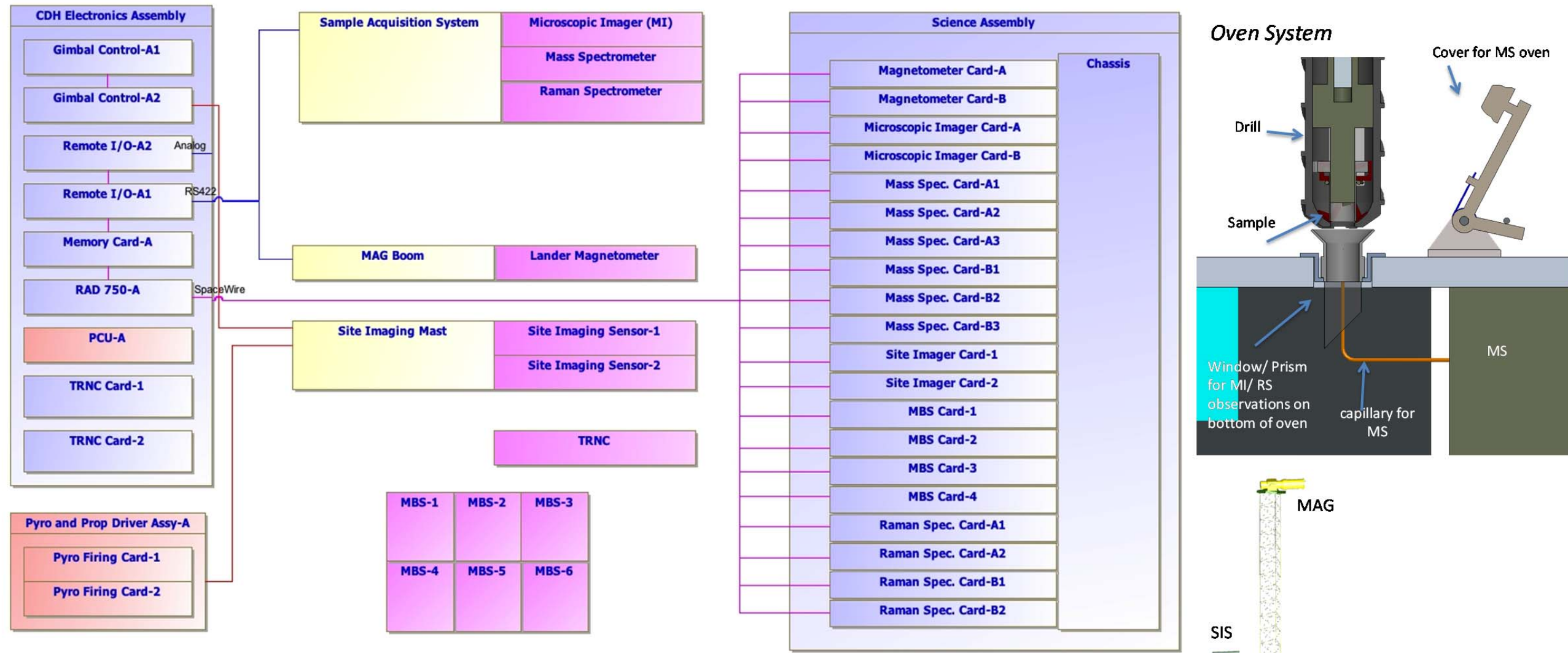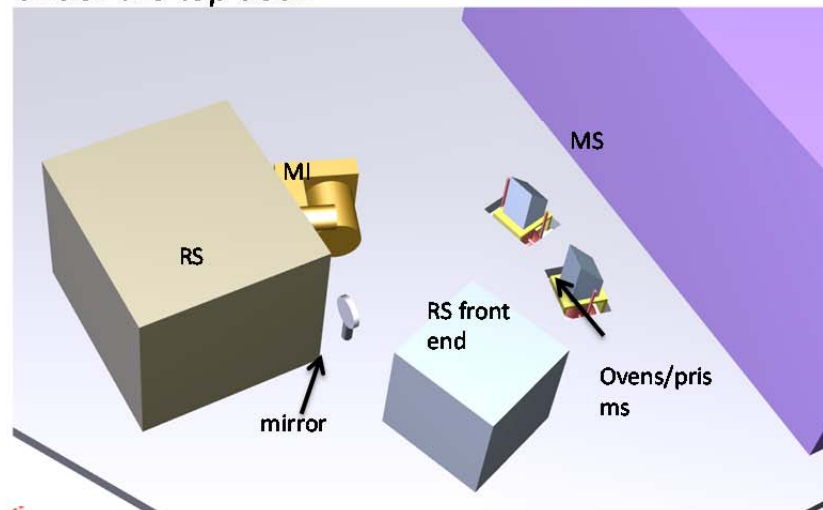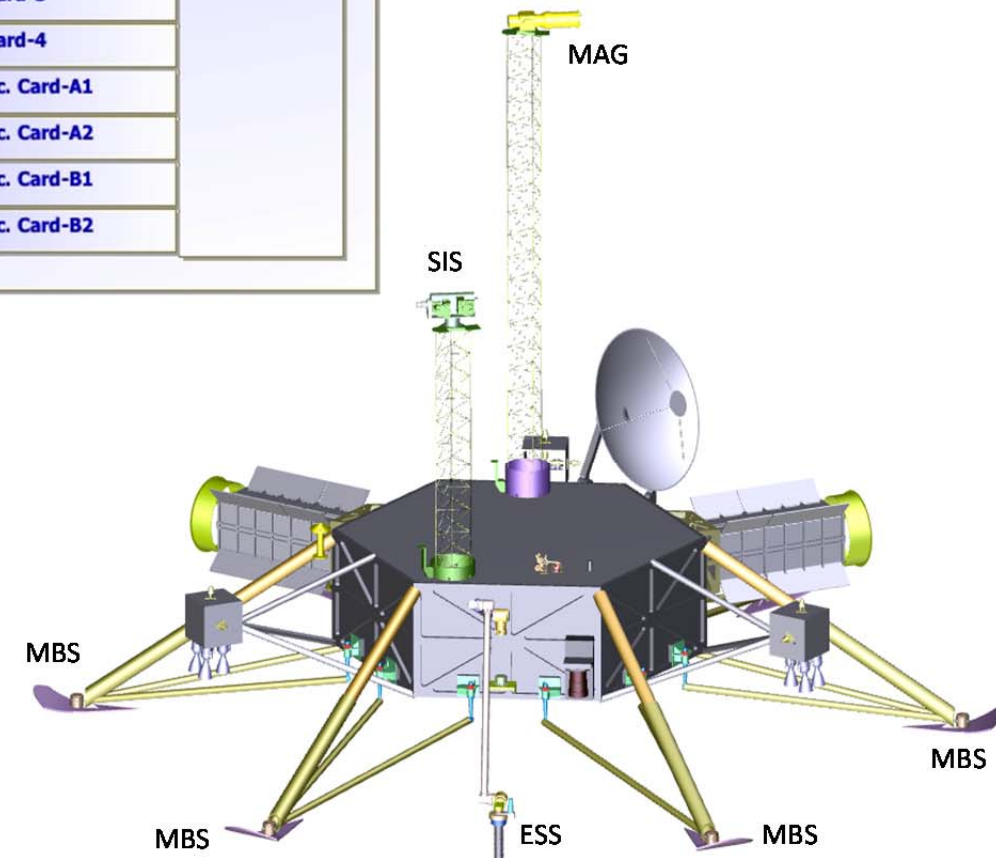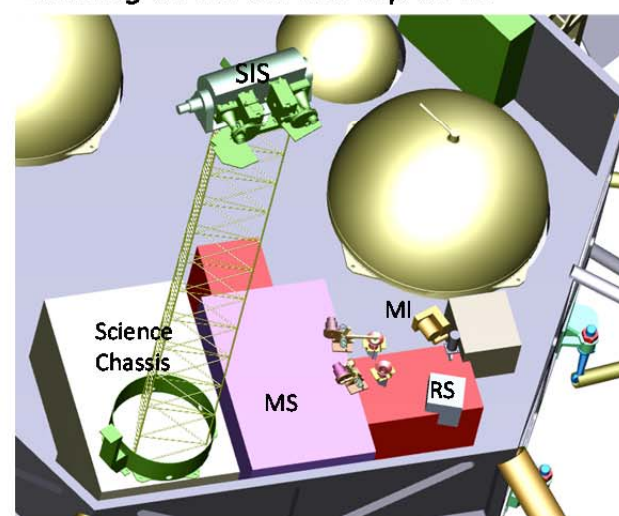

Figure D.2.2-1. Huygens GCMS (a), MSL SAM (b), and Rosetta COSAC (c) analogues to the Europa Lander Mission MS.

CDH Electronics Assembly
- Gimbal Control-A1
- Gimbal Control-A2
- Remote I/O-A2 — Analog
- Remote I/O-A1 — RS422
- Memory Card-A
- RAD 750-A — SpaceWire
- PCU-A
- TRNC Card-1
- TRNC Card-2

Pyro and Prop Driver Assy-A
- Pyro Firing Card-1
- Pyro Firing Card-2

Sample Acquisition System
- Microscopic Imager (MI)
- Mass Spectrometer
- Raman Spectrometer

MAG Boom — Lander Magnetometer

Site Imaging Mast
- Site Imaging Sensor-1
- Site Imaging Sensor-2

TRNC

MBS-1 | MBS-2 | MBS-3
MBS-4 | MBS-5 | MBS-6

Science Assembly — Chassis
- Magnetometer Card-A
- Magnetometer Card-B
- Microscopic Imager Card-A
- Microscopic Imager Card-B
- Mass Spec. Card-A1
- Mass Spec. Card-A2
- Mass Spec. Card-A3
- Mass Spec. Card-B1
- Mass Spec. Card-B2
- Mass Spec. Card-B3
- Site Imager Card-1
- Site Imager Card-2
- MBS Card-1
- MBS Card-2
- MBS Card-3
- MBS Card-4
- Raman Spec. Card-A1
- Raman Spec. Card-A2
- Raman Spec. Card-B1
- Raman Spec. Card-B2

Oven System

Cover for MS oven
Drill
Sample
Window/ Prism for MI/ RS observations on bottom of oven
capillary for MS
MS

MAG
SIS
MBS
MBS
MBS
ESS
MBS

Under the top deck

MI
MS
RS
RS front end
Ovens/prisms
mirror

Looking down on the top deck

SIS
MI
Science Chassis
MS
RS

Instrument Description

The notional MS uses a quadrupole mass analyzer technique in conjunction with evolved gas analysis, pyrolysis, and gas chromatography. The mass range of interest for the MS is from 2 to 550 Da, with unit resolution and $>1 \times 10^8$ dynamic range over the full mass range with <1 ppb sensitivity for organics and less than <1 ppm sensitivity for inorganics. The limit of detection will be tested by analyzing <1 ppbw of 1-fluoronaphthalene in a 0.05 cm^3 calcite/silica pyrolysed sample. The instrument comprises of four major components, described in the following sections: the ovens, the gas chromatograph (GC), the mass spectrometer and the main electronics. Additional plumbing and filters are also described.

The samples will be delivered into the ovens shown in Figure D.2.2-2, which are then closed, heated, and the evolved gaseous species are transferred to the MS and GC. Depending on the stage of the analysis, gases are trapped on a valved hydrocarbon trap for subsequent GC analysis (see Section D.2.8.2.2), or partially exhausted (e.g., during the water sublimation). The two ovens made of platinum are baselined, for heating from 200°C to 1100°C by resistive platinum
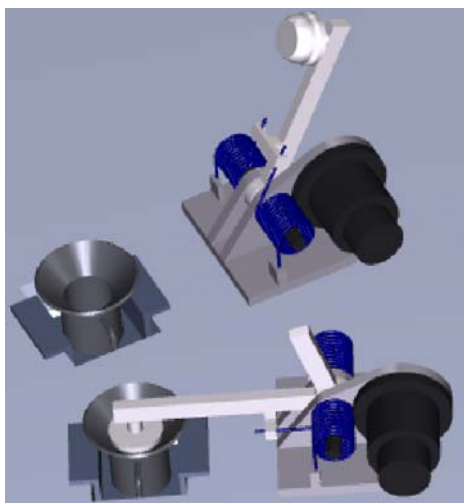

Figure D.2.2-2. The MS oven design concept is based on Rosetta COSAC. The door is spring-loaded and actuated by a pinpuller, resulting in simple and reliable actuation.

wires coiled around the oven, based on Rosetta COSAC (Goesmann et al. 2006) Thermocouples monitor the temperature rise. The ovens contain a diamond window and a prism on the bottom of the oven for sample inspection by the RS and MI prior to the MS analysis. The ovens are connected controlled by the electronics board accommodated in the science chassis, and to the MS ion source via base frit plumbed to a very low conductance leak. A spring-loaded pin-puller activated oven door is baselined, with a zirconia plug located at the lever end to provide good seal (see Figure D.2.2-2). The ovens are oversized to accommodate the sample deposition by the arm and to ensure that the sample is fully deposited into the oven, assuming the arm accuracy and position capabilities described in Section D.2.5.11. However, it is recognized that this operation is of utmost concern based on Phoenix Thermal and Evolved Gas Analyzer (TEGA) experience, and thus the ovens should be prototyped and tested with arm prototype early in the project.

The quadrupole mass spectrometer is a similar design to MSL SAM, with a smaller radio frequency voltage supply and minimal subset of the gas pumping system hardware (no pumps), simplifying the MS electronics (no pump controller needed). The gas from the ovens or from the GC is ionized by an ion source using electron impact ionization. The ion beam, generated by the ion sources, is pushed through quadrupole rods, which are excited by radio frequency and direct current potentials, creating a dynamic electric field, and transmitting only ions of a chosen charge-to-mass ratio. Scanning the radio frequency scans the mass range, because of the inverse relationship between the two. Voltage can be scanned as well, but requires more power dissipation. The selected ion beams are then focused on secondary electron multiplier ion detectors. The choice of the detectors is driven by the radiation requirements, and robust Channel Electron Multiplier (CEM) technolo-

gy is baselined. The ion sources are sealed to maintain interior sterility and cleanliness prior to landing, and a one-time pyroelectric break-off cover is baselined.

The GC is used to separate, identify and quantify the components of a mixture of volatile molecules. The gas from the hydrocarbon trap is introduced into a Carrier gas stream, which flows continuously into gas chromatograph columns (long capillary tubes with a filter). Ideally, each component in the gas elutes from the column at a different time and is detected in the quadrupole mass analyzer. Helium is selected as a Carrier gas due to its chemical inertness and expected low abundance at Europa.

Consistent with the instrument architecture described in Section D.2.2.2.1, minimal electronics are packaged with the detector. This approach is a departure from a typical MS practice where the RF supply is located close to the detector to minimize the RF noise. Instead, the HVPS and the RF supply are located on one of the three 6U cPCI cards allocated to the mass spectrometer in the main electronics chassis. The other cards accommodate data processing, including a processor, a PROM, an EEPROM, a SRAM, and additional controllers. The control logics are realized by field-programmable gate arrays (FPGAs)—controlling, in addition, the pyrolytic unit, high voltages, the ion source, the door, the DC/DC converters, MS spectrum accumulation, and main activities of the GC unit, including heater, valve, injector switching, and data registration.

The MS can be operated in various modes, including the band scan, unit scan (1 Da), and fine scan (0.1 Da), allowing flexibility for zeroing in on mass range of interest, while keeping the data rate manageable. Each mass channel has a 27-ms dwell time and a 3-ms channel switch, which allows scanning of all of the mass range in ~17 s. Multiple scans of preprogrammed ranges and broad searches for signal are accommodated within this design.

Since this instrument achieves some of the critical science on the Lander, redundancy is achieved by providing redundant electron ionization source filaments, and ion detectors, and redundant electronics, which are accommodated in the science chassis.

Radiation Effects and Shielding

Other than the detector in the quadrupole mass analyzer and the main electronics, which are accommodated in the science chassis, the MS design is relatively robust to radiation and presents no issues in meeting the Europa Lander radiation requirements. With the use of parts tolerant to 100 krad and more, and allocated shielding, the main electronics have no significant radiation concerns. The CEM detectors are resilient to the TID; however, they do see increased background noise due to radiation. Further study is needed to determine the shielding provided by the instrument packaging and its location on the Lander deck.

Resource Estimates

The mass estimate for the MS is based on the scaled-down version of the MSL SAM. The instrument assembly, which consists of ovens, plumbing, the quadrupole mass spectrometer, the gas chromatograph, the hydrocarbon trap and the ionization source is 10.3 kg. The estimated mass of six 6U cPCI boards (three redundant) is 4.5 kg, for a total unshielded mass of 14.8 kg. The shielding for the detector and readout electronics is estimated at 3 kg, for a shielded total of 17.8 kg. The MS operational power is 30 W, with a peak of 50 W. The data rate is estimated at 3.1 kbps.

Planetary Protection

Planetary protection concerns for MS will be met through system DHMR. Moreover, MS system hardware would be maintained under full bioburden mitigation protocol through flight I&T with QMS baked to greater than 250°C under purge prior to pinchoff and controlled GSE flight environment simulator. With proper selection of materials, and im-
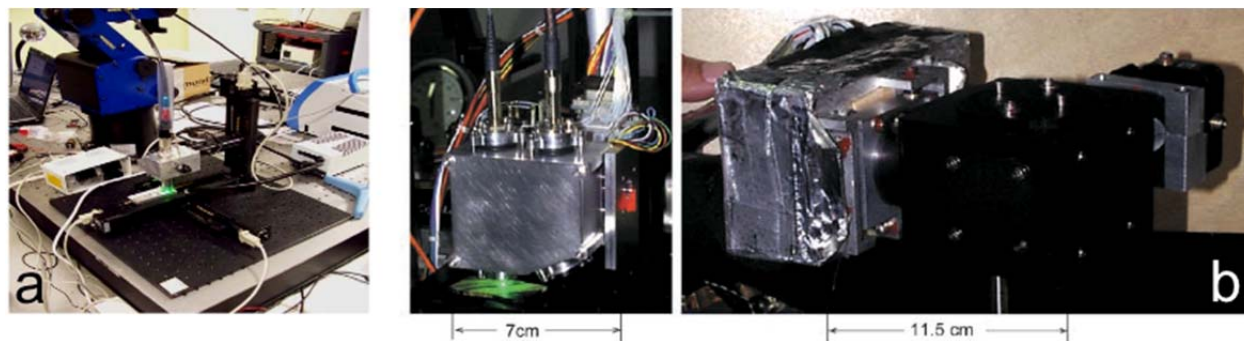
Figure D.2.2-3. ExoMars RLS (a) and MMRS (b) Raman spectrometer prototypes.

plementing lessons learned from Phoenix TEGA and MSL SAM, no issues are expected.

D.2.2.3.2 Raman Spectrometer (RS)

The Raman Spectrometer will help characterize the surface and near-surface chemistry, including complex organic chemistry to constrain the ocean composition. It will also provide complementary measurements to the MS. While the Raman technique is frequently used in laboratories on Earth, no Raman has ever flown in space. Therefore, the notional Raman Spectrometer described here is based on the new developments for ExoMars RLS (Rull et al. 2011) and MMRS (Wang et al. 2003) prototypes (see Figure D.2.2-3), with changes to obtain the measurements to satisfy Europa Lander science objectives described in Section D.1:

Characterize the surface and near-surface chemistry by:

- Measuring mineralogy and volatile content of the surface and near-surface materials on two samples retrieved from 0.5–2 and 5–10 cm below the surface to as low as 0.1 wt%
- Providing complementary measurements to the MS of organics from the two samples described above

Instrument Description

The notional Raman Spectrometer contains three units: the optical head (including the laser and focusing optics), the spectrometer, and the electronics (accommodated in the science chassis). The optical head is connected to the spectrometer by fiber optics. All three units are located below the top deck of the Lander, with the optical head looking at the sample in the MS oven via a prism/ mirror assembly. Another approach is to use two optical fibers coupled to the oven window, and an internal mirror to switch between the two samples. Both (mirror and fiber) configurations can be accommodated, and it is up to the individual instrument providers to decide on the best solution. In the two-fiber scenario, the laser light is focused on the sample via a fiber with optics (e.g., GRIN lens) coupled to the oven prism, and it is then scattered due to the vibrations in the mineral structure into the "return" fiber that sends it to a collimator, then to a holographic grating in the spectrometer. The grating disperses the light through focusing optics onto a fixed detector array, where the Raman spectrum is registered. The electronics unit includes the DC/DC power converters and data processing capability.

The chosen continuous excitation wavelength at 976 nm is provided by a diode laser. Both heritage instruments (RLS and MMRS) use a 532-nm laser, which has the advantage of a higher signal-to-noise ratio (SNR) (scattering intensity varies as 1/wavelength[4]). However, for the 532-nm laser design, unwanted mineral fluorescence signal must be suppressed and the laser can destroy organics. The 976-nm choice avoids both of these issues, however a detector that extends out into the infrared (900–1500 nm) must be used to detect these Raman

shifts (0–3100 cm^{-1}), and longer integration times are baselined to achieve good signal to noise ratio. An Indium Gallium Arsenide (InGaAs) photodiode detector array is baselined, with a size of 1024 × 1 pixels, giving a resolution of 4 cm^{-1}, better than the requirement of 7 cm^{-1}. Because the detector wavelength does not extend past 1.5 μm, the thermoelectric cooler is not needed (the detector Quantum Efficiency at room temperature starts decreasing dramatically past 1.6 μm). The peak accuracy for the spectra is required to be less than 2 cm^{-1}. Further investigations of the SNR must be conducted to understand the trade space for the laser irradiance and spot size.

Traditionally, the Raman spectrometers place tight requirements on positioning of the front end next to the sample. An autofocusing mechanism approach on RLS and a passive approach on MMRS exist that allow flexibility within a 5- to 7-mm range. This flexibility is taken into account in the oven design presented in the MS section.

Radiation Effects and Shielding

Fiber optics for MMRS were tested to 104 krad, and have shown no degradation. Little information was found for the penetrating electron and proton fluxes that the detector and fibers will experience while at Europa's surface, as well as ASRG generated neutron effects. However, dark current increase by a few orders of magnitude has been observed in InGaAs detectors due to proton and neutron DD. Therefore, a rigorous modeling and testing approach is needed to prove that the RS in its current configuration will meet Lander requirements. The front end electronics will have to be analyzed and tested to Lander TID levels. The electronics are located in the science chassis, and will be shielded to allow usage of 100-krad parts.

Resource Estimates

The mass estimate of the RS is based on the mass of RLS and MMRS prototypes. The front end allocation for laser and optics is 1 kg. The spectrometer mass is allocated 2 kg, with harness and cables adding up to another 0.5 kg. With the masses of four (two for redundancy) 6U cPCI boards for the electronics, the total unshielded mass for RS is 6.5 kg. Even though the upper deck is going to provide some shielding to the RS, an additional 2 kg are allocated for the shielding of the spectrometer, for the total shielded mass of 8.5 kg. The operational power of the spectrometer is estimated at 30 W. Data rate is based on assuming a 10-second spectrum collection time for the total of integration time of 5 minutes, and 300 bps of housekeeping data, for an average data rate of 1.6 kbps.

Planetary Protection

Planetary protection concerns for RS will be met through system DHMR. With proper selection of materials for the diode laser and fiber optics (if used), no issues are expected.

D.2.2.3.3　Multiband Seismometer Package (MBS)

The notional MBS characterizes Europa's seismic activity and its variation over the tidal cycle by operating at Europa for one month, and constrains the thickness of ice and water layers in the region. It also searches for local heterogeneity of the ice and any subsurface water. Seismometers have not been flown to other planets since Viking (Anderson et al. 1977). The MBS baselined for Europa Lander is tailored to satisfy the following science requirements identified in Section D.1:

- Low-bandpass frequency of 100 mHz (low) to 50 Hz; high-bandpass frequency of 125 Hz to 250 Hz
- Sensor orientation on each footpad: two-degree orientation accuracy of each sensor, and positional accuracy of 5–10 cm in x-y-z space
- Sensitivity $<5 \times 10^{-8}$ m s^{-2} (Hz)$^{-0.5}$ @ 10 Hz

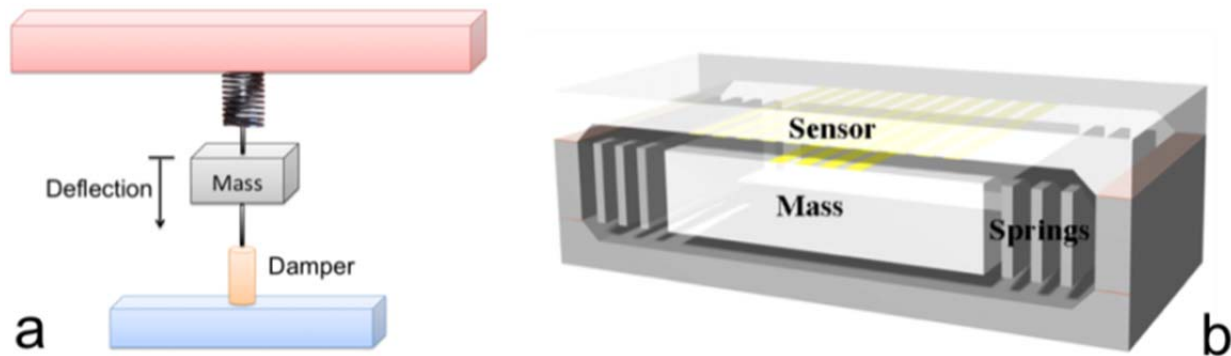Since the Europa Lander Mission requirements are well beyond what was expected of Viking

Figure D.2.2-4. Illustration of seismometer principle (a) and one of the methods of accomplishing it in a MEMS seismometer (b) (Pike and Kumar 2007).

on Mars, the seismology experiment is considered a new development.

Instrument Description

The notional MBS implementation consists of six 3-axis microelectromechanical system (MEMS) seismometers located on the legs of the Lander. The seismometers require good coupling to the ground, and it is expected that at least three of the Lander legs will be placed on the ground. The data from all of the seismometers is recorded at first to understand which legs have good coupling, but only the data from the well-coupled legs will be downlinked to Earth. Mounting the seismometers in a 3-axis configuration and spread out among six Lander legs, allows for sensing the directionality of the source and determining the type of the seismic wave.

The fundamental goal of the seismometer is to measure the movement of the planetary surface, which is usually accomplished by recording the extent of the motion of the instrument chassis (resting in the ground) with respect to a seismic mass that stays fixed over a relevant period (the period being determined by the seismic mass and the restoring force that may be applied, e.g., a pendulum or a spring) (see Figure D.2.2-4). The bigger the mass, the more sensitive it is in the low-frequency domain. For MEMS seismometers, the masses are in the milligram range. For these seismometers, the thermomechanical noise, caused by Brownian motion and spring imperfections, dominates over electronics noise, raising the noise floor. Therefore, while many companies have been developing MEMS seismometers since the early 1990s, no current MEMS device exists that meets both the frequency range needed for the Europa seismometers and the sensitivity requirements. The closest available analogues are shown in Figure D.2.2-5.

The ExoMars Short Period sensors (a) that are currently in development have a shorter frequency response than what is needed for Europa (0.1–50 Hz). The Silicon Designs INC (b) produces low noise analog accelerometers
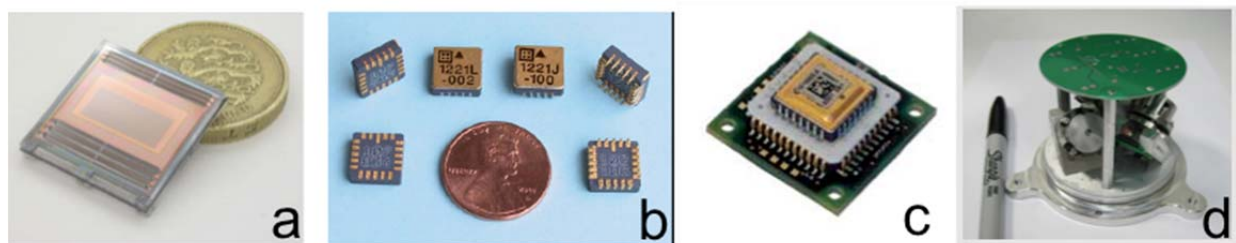

Figure D.2.2-5. ExoMars Short Period Sensors (a) and COTS solutions from Silicon Designs INC ES-1221 (b), Colibrys SF1600S (c), and Silicon Audio GeoLight (d).

in the right frequency range, however the sensitivity is three orders of magnitude lower that what is needed. Colibrys SF3000L sensor (c) operates in a 0.1–1000 Hz, and has noise of 1×10^{-6} m s^{-2} (Hz)$^{-0.5}$ @ 10 Hz (about one order of magnitude higher than required). Since the Colibrys sensor was the closest available analogue, and though it did not meet the requirements, it was used as an estimate for the resources for the model instrument with an added power supply. In these accelerometers, the most common method of mass position detection is capacitive, where a proof mass is sandwiched between two capacitive plates. The capacitance is a weak sensing mechanism and force (for feedback control), which necessitates small masses (mg) and small distances (microns). However, this approach is less useful for larger masses that are needed to achieve the sensitivity required for Europa. The Department of Energy (DOE) has been investing heavily into development of seismometers with larger masses (0.25–2 grams), noncapacitive mass position sensing (inductive, optical, fluidic), and feedback control. Kinemetrics, Symphony Acoustics, Sandia National Labs, and Silicon Audio (shown in d) have all been developing new sensors that are lower noise, and close to the target bandwidth (Merchant 2009). Over the next 5 years, there is strong potential for at least one of the DOE R&D MEMS seismometer projects to reach a point of being used in space applications. Nevertheless, these seismometers will still have to be space-qualified, and tested in the relevant Europa environment. In particular, none of the MEMS seismometers have been tested at the low temperatures expected at Europa.

Additional challenges to accomplishing a good seismometer measurement include operation in conjunctions with ASRGs, and other spurious triggers such as drill and camera operations, and the antenna movement. Moreover, thermal blanket popping and venting from the propellant tanks caused spurious signals in a high

frequency band during the Apollo investigations (Lorenz 2011). One approach is to notch the bandwidth around the ASRG 102-Hz operating frequency.

It is also planned to time-tag mechanism operations and any other potentially noisy events on the Lander so that these can be edited or filtered out of the data. The orientation of the sensors with respect to vertical direction must be adequately characterized, since the component of gravity along a misaligned axis can be a very strong perturbation. It is possible to carry leveling screws or other mechanisms to adjust accordingly; however, additional investigation is required of the maximum tilt angles.

Radiation Effects and Shielding

While silicon and metals generally do not show mechanical degradation in radiation at the TIDs expected for the Lander, capacitive MEMS devices, such as Colibrys seismometers, have been reported to fail at doses of a few kilorads (Oudea et al. 2009). Primarily, they fail due to radiation-induced trapped charge in dielectrics. Geometry changes, shielding of the exposed dielectric with conductors and changing of the dielectric material to one with lower trap density are all approaches to mitigate the dielectric charging (Shea 2003). Investigation of piezoresistive MEMS approaches could also lead to mitigation of the radiation risk.

Resource Estimates

The mass estimate for the MBS Package is based on the current mass of a Colibrys SF1600S sensor and preamp board (7 g) with three sensors packed in a unit similar to that shown for Silicon Audio GeoLight, with brackets and internal harness (@ 113 g/m of cable), for a total mass of 0.4 kg per sensor head unit. The six units together with masses of four (two for redundancy) 6U cPCI boards give total of 5.8 kg unshielded mass. Shielding is allocated another 0.4 kg per sensor, for the total of 8.5 kg for all of MBS. The power is based on Colibrys SF1600S typical consump-

tion per 1-axis sensor of 180 mW, for the total of 4.6 W. The data rate is based on the baseline data acquisition sequence (see Section D.1), and averages out to 0.2 kbps.

Planetary Protection

Planetary protection concerns for MBS will be met through system DHMR. As part of the space qualification, the sensors will be routinely heated to 125°C. Potential issues include coefficient of thermal expansion mismatches, so additional testing of the MEMS devices would be needed at these temperatures.

D.2.2.3.4   Magnetometer (MAG)

The notional MAG measures the magnetic field at Europa with sufficient sensitivity to resolve the induction signal generated in Europa's ocean as a response to Jupiter's magnetic field. Operation at Europa's surface for a month allows sounding at multiple frequencies to determine ocean thickness and conductivity. Performing a role similar to that of the Galileo magnetometer, the notional MAG is adapted from more recent designs, such as the MESSENGER magnetometer (see Table D.2.2-2), and from ongoing developments in ASIC design for highly integrated magnetometer electronics. The MAG baselined for Europa Lander is tailored to satisfy the following science requirements identified in Section D.1:

- Characterize the magnetic environment at Europa to determine the induction response from the ocean:
  - Measurement rate: 16 samples/s, with signal averaging to 4 samples/s to remove potential 6 Hz proton cyclotron frequency
  - Measurement sensitivity: better than 0.3 nT

Instrument Description

The notional MAG contains one sensor located on a 2-m boom on top of the Lander deck. The ex-

pected magnetic field range over the full Europa Lander Mission is 0–500 nT. To achieve the required sensitivity, a magnetic cleanliness program is required to limit the magnetic field of the Lander at the 2-m point of the boom to <0.25 nT, with variation of <0.03 nT. An analysis of the impact of using ASRGs as the Lander power source still needs to be performed to verify that this level of EMI could be achieved with a 2-m boom.

The notional MAG sensors use three orthogonally mounted ring-core fluxgate sensors and are based on the MESSENGER MAG sensor assembly shown in Figure D.2.2-6. The sensors are excited by an AC signal that is also used to synchronously detect the signals from the fluxgate sensors. In an analog fluxgate magnetometer, the output from each synchronous detector is applied to an integrator, which supplies the feedback current used to null the field seen by the sensor. The output of the integrator is directly proportional to the component of the magnetic field along each orthogonal axis and is sampled by a high-bit-count A/D converter. In a digital fluxgate magnetometer, the output from each synchronous detector is applied to an integrator whose output is digitized by an A/D converter. All subsequent filtering is done in the digital domain, and feedback to null the field seen by the sensor is generated by a D/A converter.

Digital fluxgate magnetometers capable of meeting the Europa Lander science requirements have been demonstrated (O'Brien et al. 2007), and substantial progress has been made in developing a magnetometer front-end ASIC (MFA) that incorporates a complete magne-
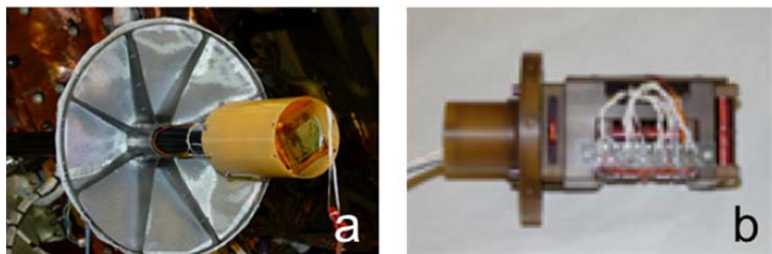

Figure D.2.2-6. MESSENGER MAG on boom (a), sensor assembly (b).

tometer signal chain, including synchronous detection, high-bit-count ΣΔ A/D converters, digital filtering, ΣΔ D/A converters for sensor feedback, and basic output data formatting into a single device (Valavanoglou et al. 2007, Magnes et al. 2008). The current versions of MFA show no degradation in performance up to TID of 170 krad, so with shielding the Lander requirements can be met. This approach is baselined for the notional MAG.

A conceptual physical block diagram of the notional MAG is shown in Figure D.2.2-7. A single 6U cPCI electronics board located in the science electronics chassis contains ASICs for magnetometer signal processing, spacecraft interface electronics, and a low-voltage power supply.

Fluxgate sensors suffer from small drifts in their zero levels that require periodic calibration. During the cruise phase, calibrations can be achieved even though a sensor is stowed. Mostly it will be detecting spacecraft fields. We will test on the ground in the same configuration; then during the cruise we can look at the evolution of the signal over time, and characterize some of the drift. Once the spacecraft is landed, since the surface lifetime is only ~1 month total, the drift in zero level is not expected to be significant.

Radiation Effects and Shielding

Fluxgate magnetometer sensors contain no active electrical parts and, with proper selec-

tion of materials, present no issues in meeting the Europa Lander radiation requirements. The notional MAG electronics are located in the science electronics chassis, which provides radiation shielding sufficient for components hardened to 100 krad.

Resource Estimates

The mass estimate for the notional MAG is based on the as-built mass of the MESSENGER MAG sensor (250 g), the as-built mass per unit length of the MESSENGER MAG harness (113 g/m), and the estimated mass of two 6U cPCI boards. The total mass estimate for MAG is 2.2 kg. MAG power dissipation is estimated at 4 W based on scaling measured performance of the MESSENGER MAG. The MAG telemetry rate is estimated at 1.8 kbps based on scaling of the MESSENGER MAG telemetry rate for a higher sampling rate (32 Hz max), exceeding the requirement of 16 Hz.

Planetary Protection

Planetary protection concerns for MAG will be met through system DHMR. With proper selection of materials for the MAG sensor, no issues are expected.

D.2.2.3.5   Site Imaging System (SIS)

The notional SIS consists of a pair of wide-angle cameras with basic functionality similar to that of the MER Pancam instrument (Bell et al. 2003) shown in Table D.2.2-2. The SIS imager will be used after landing on Europa to
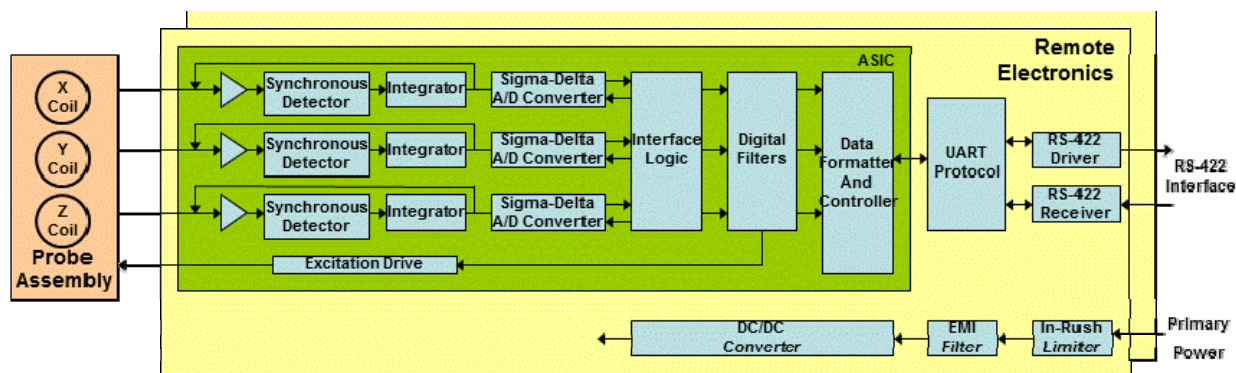

Figure D.2.2-7. Block diagram of the notional Magnetometer locates redundant remote electronics in a radiation-shielded enclosure.

provide stereo landform mapping of the landing site from near the Lander to the horizon to search for evidence of surface/subsurface material exchange and to constrain the processes and rates by which the surface materials form and evolve over time. The SIS will also be used to help understand the local context of the landing site, in particular the sample acquisition location. The SIS baselined for Europa Lander is tailored to satisfy the following science measurement requirements identified in Section D.1:

- Resolution of 1 mm/pixel at 3 m distance.
- Three color filters.
- SNR >100:1.

Instrument Description

Meeting the stated resolution requirements for the SIS implies an IFOV of 0.3 mrad. The 1024×1024–pixel image sensor then results in an instrument FOV of ~16°× 16° full angle. A compact wide-angle refractive telescope similar to that of the MER Pancam is baselined. The two cameras are mounted on a gimbaled platform atop a mast extending ~1.0 m above the Lander top deck (Figure D.2.2-8). The gimbals will allow the cameras to be pointed over an azimuth range of 360° and an elevation range of ±90° with respect to the plane of the Lander deck. The cameras will be separated by about 0.3 m with their boresights slightly toed in to provide stereo convergence. A full 360° panorama from directly below the Lander to the horizon can be covered with about 150 FOVs. The focal planes are radiation-shielded. A Pancam-like filter wheel houses at least three color filters (Figure D.2.2-9). The optics are protected until after landing by one-time deployable covers.

Preliminary SIS performance analysis has been completed using the pixel characteristics (quantum efficiency, 13-μm pixel size, 100-Ke$^-$ well depth) of the e2v CCD47-20BT image sensor used by the New Horizons

LORRI instrument as *an example* of the performance expected from the SIS image sensor. The measured LORRI system readout noise of 20 electrons was assumed, although the LORRI pixel readout rate is considerably higher than that required for SIS (1.2 MHz vs. ~100 kHz). Nominal selections for the color filters are:

- Band #1: 540-580 nm
- Band #2: 730-790 nm
- Band #3: 900-1000 nm.

Using the wavelength-dependent quantum efficiency of the CCD47-20BT (*example only*), assuming f/20 optics (like Pancam) and surface reflectance of 20%, SIS will yield SNR = 200 for an exposure time of about 0.5 s in Band #1 and Band #2 and for an exposure time of about 1 s in Band #3. Longer exposure times could be used with little impact since the scene is essentially static. A maximum frame

Figure D.2.2-8. The MER Pancam mounted on a two-axis-gimbaled platform atop a 1.5-m-tall mast provides a good analog for the Europa Lander SIS.
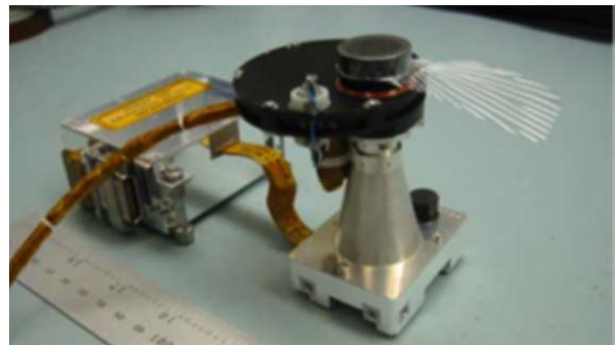

Figure D.2.2-9. Each SIS camera will include a color filter wheel similar to that shown on the front of this single MER Pancam camera.

rate of 0.1 Hz would be more than adequate allowing a full one-color, one-eye panorama to be acquired in less than 30 minutes. There is no need to operate more than one camera of the pair at a time.

A conceptual physical block diagram of the SIS is given in Figure D.2.2-10.

Consistent with the instrument architecture described in Section D.2.2.2.1, minimal electronics are packaged at the focal planes with the detectors. The signal chain shown in the focal plane electronics contains elements required for a CCD image sensor (clock drivers, correlated double sampler, A/D conversion) that either are unnecessary or are typically implemented within a CMOS APS device. A highly integrated CMOS APS device is an ideal solution, as it minimizes components at the focal plane that require radiation shielding.

A passive thermal design is baselined for the SIS with a side-facing radiator used for detector cooling. Detector anneal heaters are base-

lined to mitigate radiation damage.

Each SIS camera is baselined with one electronics board (6U cPCI format) housed remotely in the science electronics chassis. The board provides DC/DC power conversion for both the camera and the electronics board itself. Camera interface logic, image data compression, and a SpaceWire interface to the spacecraft are contained in a single ASIC. Data compression is assumed to be wavelet based, with commandable degrees of compression. Radiation-hardened static RAM (currently available as 16-Mb devices) is included for buffering incoming imager data, data compression intermediate products, and incoming and outgoing SpaceWire command and telemetry data.

Radiation Effects and Shielding

To protect the SIS image sensors from total dose, DD, and transient radiation noise, radiation shielding with 1 cm of Ta, comparable to that used by the Galileo SSI, is baselined. The
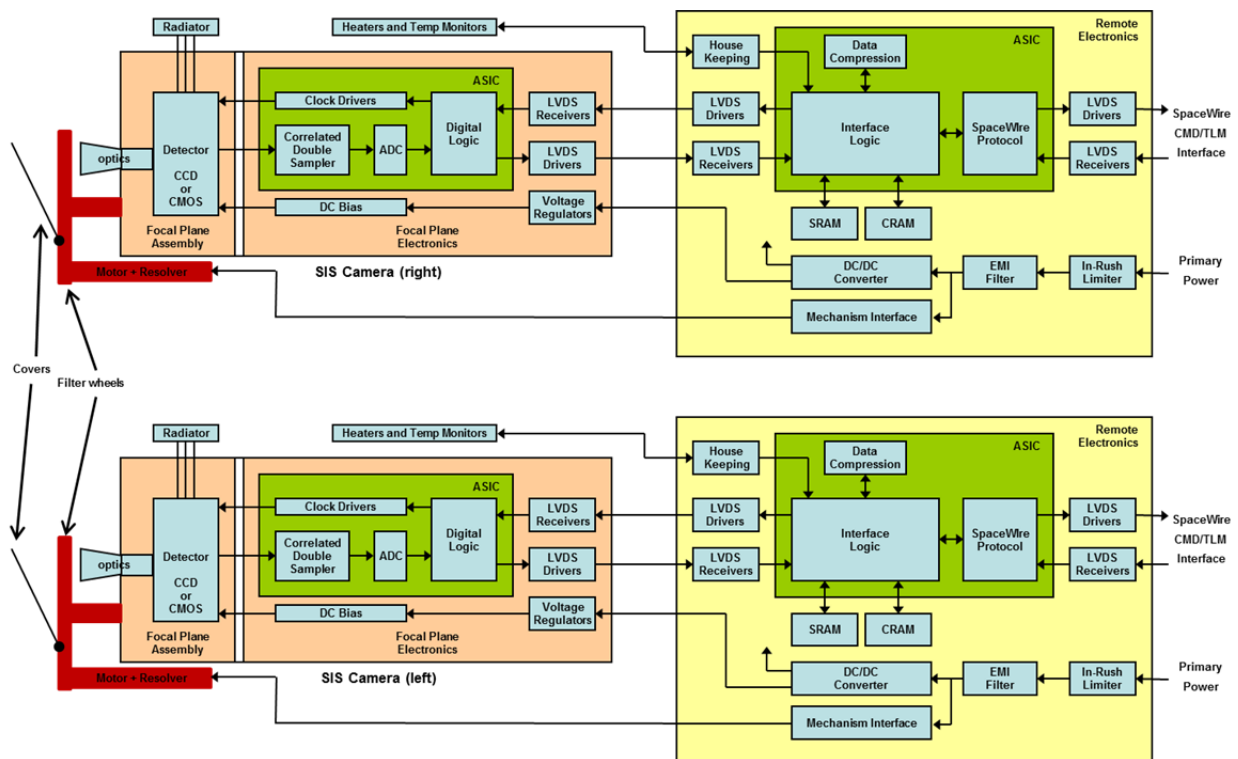

Figure D.2.2-10. Block diagram of the notional Site Imaging System features fully redundant cameras and locates remote electronics in a radiation-shielded enclosure.

Europa Lander Mission radiation dose depth curve indicates a ~6 krad total dose behind 1 cm of Ta shielding, which, assuming a required design margin of 2, allows use of detectors tolerant of 12 krad. While a CMOS APS device is favored for the notional Europa Lander SIS due to its potential for high radiation tolerance, this dose level allows a choice of silicon device technologies, including CMOS APS, P-channel CCD, and (arguably) N-channel CCD. Shielding mass of 1.5 kg is allocated for a 1-cm Ta, $5 \times 3 \times 4$–cm enclosure similar to that shown in Figure D.2.2-11, which is designed to house a STAR1000-based CMOS APS and its interface electronics.
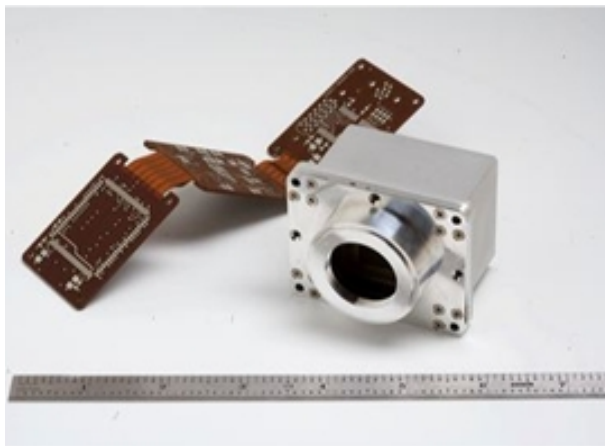

Figure D.2.2-11. Ample radiation shielding encloses a miniature focal plane assembly for a STAR1000 CMOS APS.

The impact of radiation background noise on the SIS has been analyzed by estimating the number of high-energy electrons and protons penetrating the 1-cm Ta shield and assessing their effect on the silicon detector. An estimated 7000 electrons/cm^2·s would reach the detector through 1 cm of Ta shielding when on the surface of Europa (see Section D.2.2.2.4). For a typical silicon image sensor, each incident electron can be expected to generate an average of 2000 signal electrons in the detector (per Boldt et al. 2008). Assuming 13-µm pixels and a maximum exposure plus readout time of 1 s for the notional SIS, a "hit rate" of 1.2% of pixels per integration time is expected

on the surface of Europa. With the assumption that the signal-electrons generated by the incident particles are concentrated on a single pixel, the method of calculating the SNR adopted for the Galileo SSI camera can be employed (Klaasen et al. 1984). Based on empirical data, the radiation-induced noise was approximated as 35×SQRT (mean radiation signal per pixel). For a 1.2% hit rate and 2000 electrons per hit, the radiation-induced noise would contribute 170 electrons to the SIS SNR calculation if the radiation noise were uniformly distributed across the array. This noise would reduce the average SIS SNR to ~150 (~90 for the 950-nm band). However, since >95% of the pixels would be unaffected by radiation-induced signal, they would retain their normal SNR value, while a small minority of pixels would have severely reduced SNR (~20), most of which can be repaired during ground processing. The number of incident protons reaching the detector through the 1-cm Ta shield can be estimated using the external integral 100-MeV flux level at Europa. The expected 50 protons/cm^2 s, when combined with 13-µm pixels and a maximum 1-s exposure plus readout time, result in a hit rate of 0.0085% of pixels per integration time on the surface of Europa. While the proton is expected to cause a strong signal (~10,000 signal-electrons) in a pixel or pixel group at the impact site, the low number of occurrences, <100 per 1-Mpixel image, and the strong signal are expected to have no significant impact on Europa science after ground-based postprocessing to remove artifacts.

The SIS electronics present no significant radiation concerns beyond those particular to the detector, and use of parts tolerant to 100 krad is assumed. Total dose and DD effects on optical materials can be mitigated through use of a combination of fused silica and radiation-hardened glasses. In a system with refractive optics, the optics itself acts as a "forward shield" for the image sensor, with the

remainder of the image sensor surrounded by radiation shielding material.

Resource Estimates

Mass estimates for the SIS (2.8 kg for each camera including 1.5 kg of radiation shielding) are derived from similarity to the camera subassemblies of MER Pancam and from assumed values for the harness mass and the 6U cPCI electronics boards. Power estimates for SIS (4 W per camera) are based on measured values of the MESSENGER MDIS camera subassemblies and New Horizons LORRI electronics. The volume of the sensor head of each camera is estimated to be $15 \times 9 \times 7$ cm.

The SIS detectors will be read out quickly (<1 s) to an internal frame buffer to minimize the image susceptibility to radiation noise. Since SIS will be imaging only static scenes, the instrument data readout rates to the Lander data system can be relatively modest. Assuming 12 bits/pixel encoding and a frame transfer time to the spacecraft of 10 s, the SIS uncompressed data rate across the interface is 1.2 Mbps, and the compressed data rate (with compression factor of 3 assumed) is 0.4 Mbps.

Planetary Protection

Planetary protection concerns for the SIS will be met through system DHMR. Temperature effects on optical materials, optical mounts and the image sensor will be a key aspect of the component and material selection process.

D.2.2.3.6   Microscopic Imager (MI)

The notional Microscopic Imager (MI) consists of a wide-angle, close-focused camera with basic functionality similar to that of the Beagle 2 (Thomas et al. 2004) and Phoenix MECA (http://phoenix.lpl.arizona.edu/science_meca.php) microscopes, the MER Microscopic Imager (Herkenhoff et al. 2003), and the MSL Mars Hand Lens Imager (MAHLI; http://msl-scicorner.jpl.nasa.gov/Instruments/MAHLI/) instruments shown in Figure D.2.2-12.
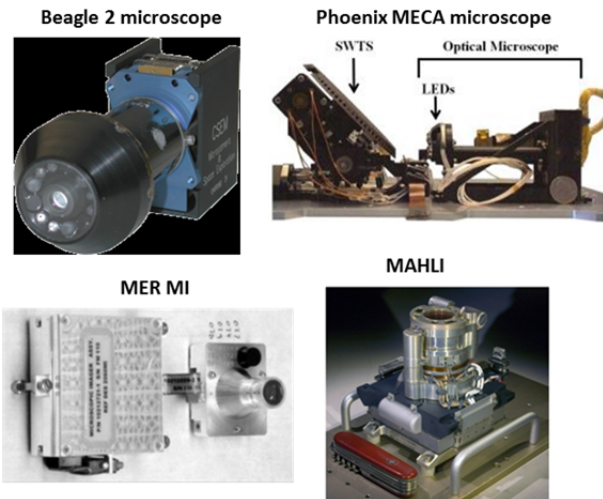

Figure D.2.2-12. Previously flown microscopes provide good analogs for the Europa Microscopic Imager.

The MI imager will be used after landing on Europa to provide high-resolution images of the collected samples from the surface and near subsurface of Europa in order to support the interpretation of the compositional measurements. The MI images will characterize the ice grains and non-ice materials within the samples to understand their heterogeneity, ice history, and context. The MI baselined for Europa Lander is tailored to satisfy the following science measurement requirements identified in Section D.1:

- Resolution of ~10 µm/pixel
- Focus adjustment for variable sample distances
- SNR >100:1.

Instrument Description

Meeting the stated resolution requirements for the MI over a sample area of 1x1 cm implies use of a 1024×1024–pixel image sensor. The placement of the MI relative to the sample location is not specifically prescribed, but a working distance of 2 cm would imply a FOV of 28° and an IFOV of ~500 µrad, while a working distance of 18 cm (the current design placement) would imply a FOV of ~3° and an IFOV of ~50 µrad. The optics will need to have a depth of field of at least 1.6 mm and to have

adjustable focus to ensure being able to bring portions of the sample at varying distances from the MI into sharp focus. A set of white-light LEDs is included to illuminate the samples. Although not in the current baseline, the addition of an RGB Bayer filter superimposed over the detector would provide color imaging capability with little impact. The optics are protected until after landing by one-time deployable covers.

MI SNR performance will depend on a number of yet undetermined variables such as the number and brightness of the LEDs, the actual working distance of the microscope, the detector pixel size and quantum efficiency, etc. However, analogy with the MAHLI and Beagle 2 instruments suggests that with white-light LED illumination, SNR of 100 can be obtained for exposure times of <1 s.

A conceptual physical block diagram of the MI is given in Figure D.2.2-13.

Consistent with the instrument architecture described in Section D.2.2.2.1, minimal electronics are packaged at the focal plane with the detector. The signal chain shown in the focal plane electronics contains elements required for a CCD image sensor (clock drivers, correlated double sampler, A/D conversion) that either are unnecessary or are typically implemented within a CMOS APS device. A highly integrated CMOS APS device is an ideal solution, as it minimizes components at the focal plane that require radiation shielding.

A passive thermal design is baselined for the MI with a radiator mounted to the outer side of the Lander used for detector cooling. Detector anneal heaters are baselined to mitigate radiation damage.

The MI camera is baselined with redundant electronics. Dual-focal-plane electronics are colocated with the single detector. Redundant remote electronics boards (6U cPCI format) are housed in the science electronics chassis. The remote board provides DC/DC power conversion for both the camera and the electronics board itself. Camera interface logic, image data compression, and a SpaceWire interface to the spacecraft are contained in a single ASIC. Data compression is assumed to be wavelet based, with commandable degrees of compression. Radiation-hardened static RAM (currently available as 16-Mb devices) is included for buffering incoming imager data, data compression intermediate products, and incoming and outgoing SpaceWire command and telemetry data.

Radiation Effects and Shielding

To protect the MI image sensor from total dose, DD, and transient radiation noise, radiation shielding with 1 cm of Ta, comparable to that used by the Galileo SSI, is baselined. The Europa Lander Mission radiation dose depth curve indicates a ~6-krad total dose behind 1 cm of Ta shielding, which, assuming a re-

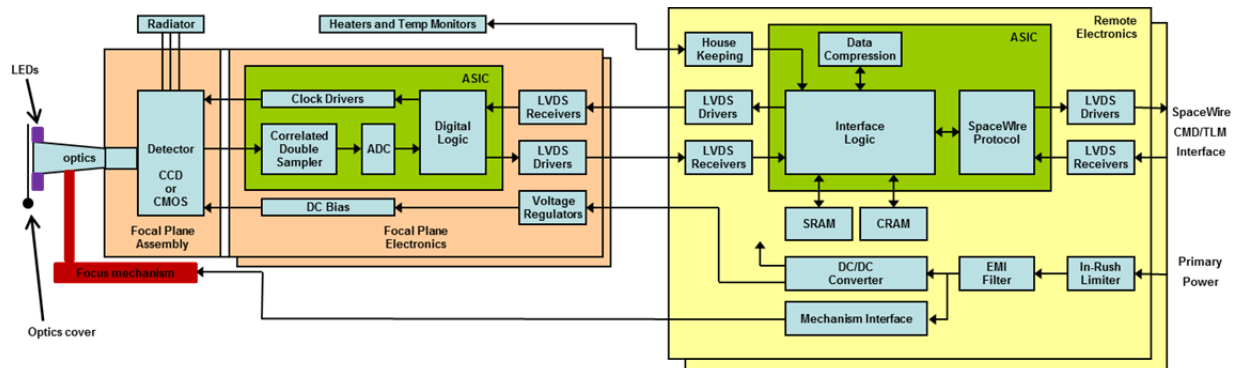**Figure D.2.2-13.** Block diagram of the notional Microscopic Imager features focusing optics and LED illuminators and locates redundant focal plane electronics near the detector and redundant remote electronics in a radiation-shielded enclosure.

quired design margin of 2, allows use of detectors tolerant of 12 krad. While a CMOS APS device is favored for the notional Europa Lander MI due to its potential for high radiation tolerance, this dose level allows a choice of silicon device technologies, including CMOS APS, P-channel CCD, and (arguably) N-channel CCD. Shielding mass of 1.5 kg is allocated for a 1-cm Ta, $5 \times 3 \times 4$–cm enclosure similar to that shown in Figure D.2.2-11.

The impact of radiation background noise on the MI has been analyzed by estimating the number of high-energy electrons and protons penetrating the 1-cm Ta shield and assessing their effect on the silicon detector. The hit rate and radiation-induced noise will be the same as for the SIS cameras. This noise would reduce an average MI SNR of 100 to ~50. However, since >95% of the pixels would be unaffected by radiation-induced signal, they would retain their normal SNR value, while a small minority of pixels would have severely reduced SNR (~20), most of which can be repaired during ground processing. The number of incident protons reaching the detector through the 1-cm Ta shield can be estimated using the external integral 100-MeV flux level at Europa. The effects of incident energetic protons will also be the same as for SIS and will not have any significant impact on MI science.

The MI electronics present no significant radiation concerns beyond those particular to the detector, and use of parts tolerant to 100 krad is assumed. Total dose and DD effects on optical materials can be mitigated through use of a combination of fused silica and radiation-hardened glasses. In a system with refractive optics, the optics itself acts as a "forward shield" for the image sensor, with the remainder of the image sensor surrounded by radiation shielding material.

Resource Estimates

Mass estimates for the MI (3.75 kg including 1.5 kg of radiation shielding) are derived from similarity to the camera subassemblies of the Beagle 2 and MER microscopes and from assumed values for the harness mass and the 6U cPCI electronics boards. The power estimate for MI (10 W) is based on measured values of the MER MI and MSL MAHLI microscopes and includes average power for the LEDs and focus mechanism. The volume of the MI sensor head is estimated to be $15 \times 9 \times 7$ cm.

The MI detector will be readout quickly (<1 s) to an internal frame buffer to minimize the image susceptibility to radiation noise. Since MI will be imaging only static scenes, the instrument data readout rates to the Lander data system can be relatively modest. Assuming 12 bits/pixel encoding and a frame transfer time to the spacecraft of 10 s, the SIS uncompressed data rate across the interface is 1.2 Mbps, and the compressed data rate (with compression factor of 3 assumed) is 0.4 Mbps.

Planetary Protection

Planetary protection concerns for the MI will be met through system DHMR. Temperature effects on optical materials, optical mounts and the image sensor will be a key aspect of the component and material selection process.

D.2.2.3.7　　Reconnaissance Camera (RC)

D.2.2.3.8　　Instrument Requirements

The notional Reconnaissance Camera (RC) consists of a narrow-angle camera with basic functionality similar to that of the MRO HiRISE instrument (McEwen, et al. 2003) shown in Figure D.2.2-14. The RC will be carried on the Carrier element and used to capture high-resolution imagery of the candidate landing sites from Europa orbit prior to deployment of the Lander. These images will be used to select and certify as safe for landing the final targeted landing site. The RC will also capture imagery of the actual landing site location after landing to provide local and site-specific context for the landed measurements to satisfy the science requirements identified in Section D.1.

Figure D.2.2-14. The HiRISE instrument inside a clean room tent at Ball Aerospace and Technology Corporation in Boulder, Colorado; this is a good analog for the Europa Lander Mission RC

The RC baselined for the Europa Carrier is tailored to satisfy the following measurement requirements as discussed further in Section D.2.8.2.1:

- Resolution of 0.5 m/pixel from a 200-km orbital altitude
- Coverage of a ≥10-km-wide swath from a 200-km orbital altitude
- SNR >100:1.

Instrument Description

Meeting the stated resolution requirements for the RC implies an IFOV of 2.5 µrad. For a typical imaging detector pixel size of 10 × 10 µm, an optics focal length of ~4 m is required with an aperture of ~0.4 m. The swath width requires an image with at least 20,000 pixels across. The FOV must be ~3°, which can be accomplished with a reflective telescope. The ground speed of 1.3 km/s means that the nadir point moves by one pixel

in ~380 µsec. The SNR requires an integration time of about 8 msec. So some type of image motion compensation is required to achieve the SNR required without smearing the image by more than one pixel. The very large detector array size and optical telescope coupled with the need for image motion compensation suggests that a pushbroom imager is the best solution.

An example detector that will meet the imaging requirements is the Fairchild CCD10121 device, which has a 12288 × 128–pixel array format. This device has 8.75-µm pixels, so the telescope focal length is 3.5 m. Two of these devices are end-butted in the focal plane to provide the required cross-track swath width. The along-track dimension of the array permits use of time-delay integration (TDI) to perform the image motion compensation. The pixel charge packets are shifted along the CCD columns at precisely the rate required to com-

pensate for ground motion so as to build up integration time without image smearing. Approximately 21 stages of TDI are required to achieve a SNR of 100 assuming use of f/10 optics, which provide a good match between the diffraction limited point-spread function and the pixel size. Higher SNR can be achieved by accumulating signal over more than 21 stages. The instrument is assumed to be mounted to view in the nadir direction. A spacecraft roll will be required to point the FOV off to the side to capture targets that are not positioned right on the ground track. The RC collects photons over a broad panchromatic bandpass and does not include any color imaging capability. The optics are protected during launch and cruise by a one-time deployable cover.

A conceptual physical block diagram of the RC is given in Figure D.2.2-15.

Consistent with the instrument architecture described in Section D.2.2.2.1, minimal electronics are packaged at the focal plane with the detectors. The electronics are fully redundant with dual strings controlling each of the two end-butted detectors. If one string should fail,

the other string can continue to operate while covering only half the normal swath width.

A passive thermal design is baselined for the RC with an anti-Sun side-facing radiator used for detector cooling. Detector anneal heaters are baselined to mitigate radiation damage.

Each RC electronics string is baselined with one electronics board (6U cPCI format) housed remotely in the science electronics chassis. The board provides DC/DC power conversion for both the camera and the electronics board itself. Camera interface logic, image data compression, and a SpaceWire interface to the spacecraft are contained in a single ASIC. Data compression is assumed to be wavelet based, with commandable degrees of compression. Radiation-hardened static RAM (currently available as 16-Mb devices) is included for buffering incoming imager data, data compression intermediate products, and incoming and outgoing SpaceWire command and telemetry data.

Radiation Effects and Shielding

To protect the RC image sensors from total dose, DD, and transient radiation noise, radiation shielding with 1 cm of Ta, comparable to
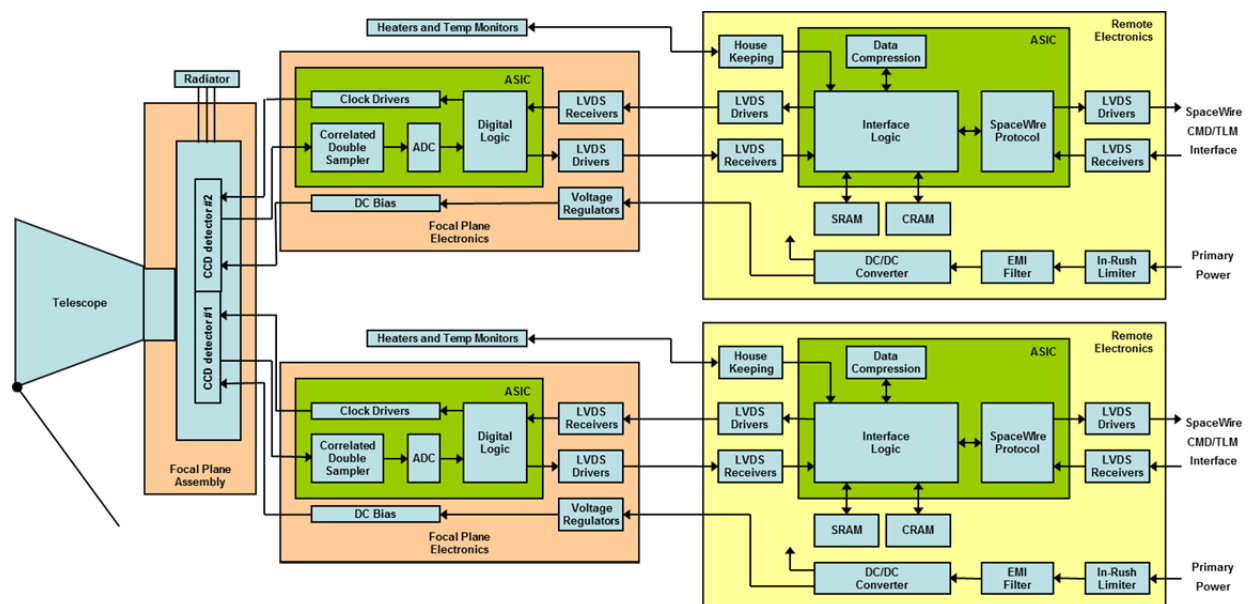

Figure D.2.2-15. Block diagram of the notional Reconnaissance Camera features fully redundant electronics for each of the two end-butted detectors and locates remote electronics in a radiation-shielded enclosure.

that used by the Galileo SSI, is baselined. The Europa Carrier mission radiation dose depth curve indicates a ~7.5-krad total dose behind 1 cm of Ta shielding, which, assuming a required design margin of 2, allows use of detectors tolerant of 15 krad. Shielding mass of 1.6 kg is allocated for a 1-cm Ta, $12 \times 2 \times 2$–cm enclosure.

The impact of radiation background noise on the RC has been analyzed by estimating the number of high-energy electrons and protons penetrating the 1-cm Ta shield and assessing their effect on the silicon detector. An estimated 4.3×10^5 electrons/cm^2 s would reach the detector through 1 cm of Ta shielding when in orbit about Europa (see Section D.2.2.2.4). For a typical silicon image sensor, each incident electron can be expected to generate an average of 2000 signal electrons in the detector (per Boldt et al. 2008). Assuming 8.75-µm pixels and a maximum exposure plus readout time of 8 ms for the notional RC, a "hit rate" of 0.3% of pixels per integration time is expected in orbit at Europa. With the assumption that the signal-electrons generated by the incident particles are concentrated on a single pixel, the method of calculating the SNR adopted for the Galileo SSI camera can be employed (Klaasen et al. 1984). Based on empirical data, the radiation-induced noise was approximated as $35 \times$ SQRT (mean radiation signal per pixel). For a 0.3% hit rate and 2000 electrons per hit, the radiation-induced noise would contribute 80 electrons to the RC SNR calculation if the radiation noise were uniformly distributed across the array. This noise would reduce the average RC SNR to ~80. However, since >98% of the pixels would be unaffected by radiation-induced signal, they would retain their normal SNR value, while a small minority of pixels would have severely reduced SNR (~10), most of which can be repaired during ground processing. The number of incident protons reaching the detector through the 1-cm Ta shield can be estimated using the external integral 100-MeV flux level

at Europa. The expected 50 protons/cm^2·s, when combined with 8.75-µm pixels and a maximum 8-ms exposure plus readout time, result in a hit rate of 3×10^{-7} of pixels per integration time in orbit about Europa. While the proton is expected to cause a strong signal (~10,000 signal-electrons) in a pixel or pixel group at the impact site, the low number of occurrences, <150 per 20000×20000-pixel image, and the strong signal are expected to have no significant impact on Europa site-certification imaging or science after ground-based postprocessing to remove artifacts.

The RC electronics present no significant radiation concerns beyond those particular to the detector, and use of parts tolerant to 100 krad is assumed. Total dose and DD effects on optical materials can be mitigated through use of a combination of fused silica and radiation-hardened glasses. In a system with refractive optics, the optics itself acts as a "forward shield" for the image sensor, with the remainder of the image sensor surrounded by radiation shielding material.

Resource Estimates

Mass estimates for the RC (35 kg including 1.6 kg of radiation shielding) are derived from similarity to the HiRISE mass, scaling for the difference in telescope aperture, and from assumed values for the harness mass and the 6U cPCI electronics boards. Power estimates for RC (38 W while imaging, 20 W standby) are based on measured values of the HiRISE camera adjusted downward by reducing the electrical power used to maintain uniform telescope temperatures. The reduction in electrical power is justified by assuming that relative to the HiRISE design we (1) use improved insulation on the secondary mirror and spider legs, (2) use a VRHU to radiatively heat the primary mirror, and (3) reduce the telescope operating temperature to 0°C instead of 20°C. The volume of the detector head of each camera is estimated to be $15 \times 9 \times 7$ cm. The optics aperture is 36 cm in diameter; the tele-

scope barrel is about 1 m long excluding a sunshade. The sunshade might extend another 0.3 m.

The RC detectors will be readout extremely rapidly (~350 Mbps from each detector) to keep up with the pushbroom imaging rate (10,000 pixels from each detector every 380 μsec with 12-bit encoding). A single 10 × 10-km swath will require a data volume of 4.8 Gb uncompressed. The baseline RC concept does not include sufficient data storage volume or processing capability to store and compress this volume of data. Therefore, RC will require that its data interface to the Carrier data system be able to support a total rate of at least 700 Mbps. The Carrier data system will be expected to store and compress the RC data for subsequent downlink to Earth.

The RC will require pointing control to ≤5 mrad, absolute pointing knowledge of ≤1 mrad, and relative pointing knowledge to ≤3 μrad within any 1-second interval. Pointing must be stable to ≤100 μrad/s. High-frequency (>50 Hz) pointing jitter at the RC mounting interface must not exceed 2 μrad in peak-to-peak amplitude.

Planetary Protection

Planetary protection concerns for the RC will be met through system DHMR. Temperature effects on optical materials, optical mounts and the image sensor will be a key aspect of the component and material selection process.

D.2.3   Mission Design

A robust mission design is developed that meets the high-ΔV challenges of landing and operating a high-value payload on the surface of Europa.
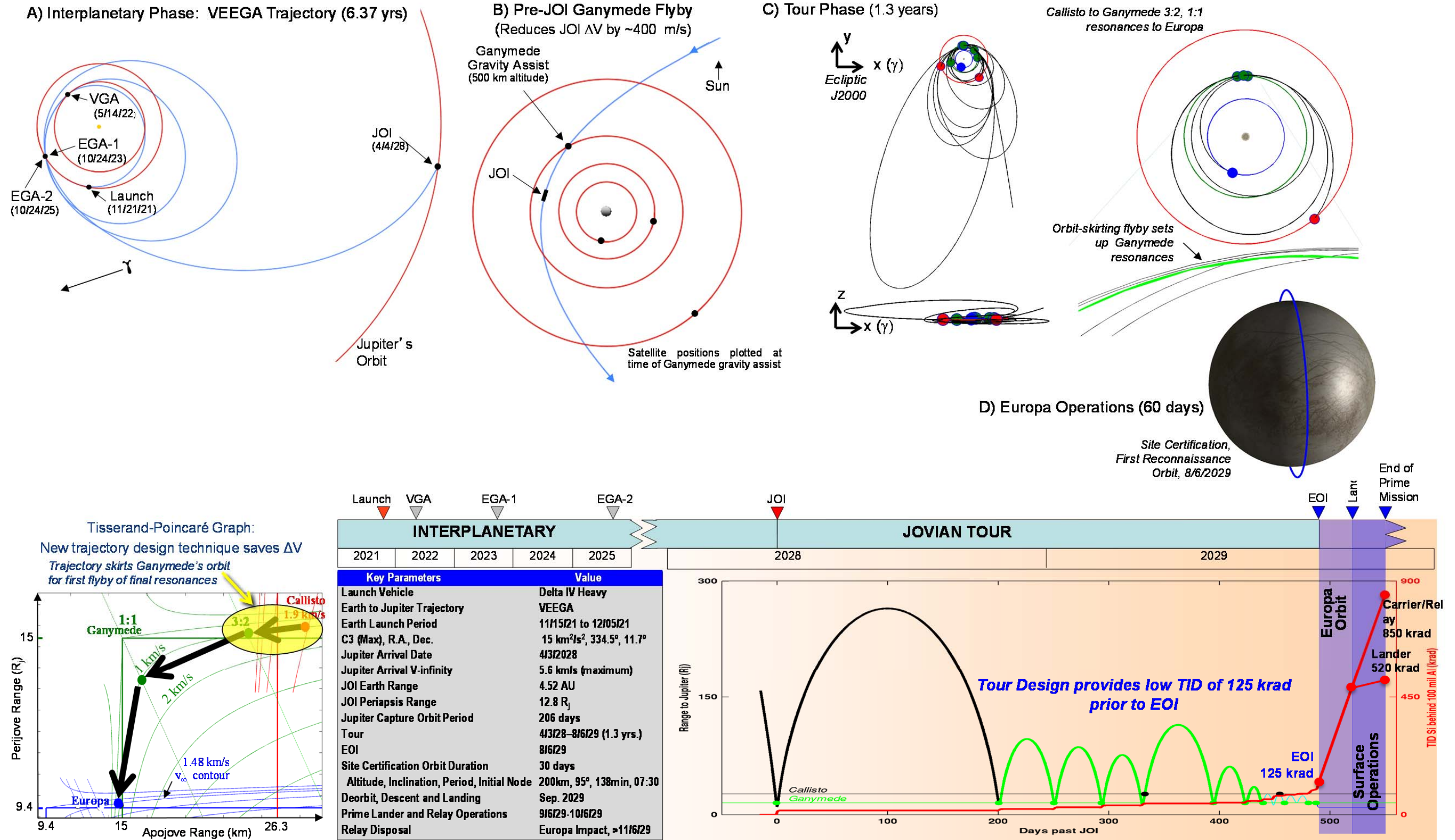
The trajectory design goal for this mission study was to show the feasibility of a Europa Lander Mission that meets the SDT *in-situ* observation and measurement requirements as outlined in the traceability matrix (FO D-1). The focus for this study was to deliver, with low risk, a sufficiently massive payload onto the surface of Europa so as to accommodate

the necessary science instruments while minimizing flight time and TID[2].

The Europa Lander Mission concept needs are satisfied by the capabilities of a Delta IV Heavy launched from Cape Canaveral Air Force Station on a VEEGA interplanetary trajectory. In this concept, after a cruise of 6.37 years, the spacecraft will fly by Ganymede just prior to performing JOI via a large main-engine maneuver. The spacecraft will then perform additional Ganymede and Callisto flybys over about 1.5 years to lower its energy with respect to Europa, at which point an EOI burn and circularization sequence is performed. The spacecraft is placed into a near-polar, near-circular 200-km-altitude orbit, with a 7:30-a.m. node, which provides optimal lighting for performing reconnaissance of the surface at sub-meter resolution. After 30 days in this site-certification orbit, periapsis is lowered to 5 km, where the Lander is released to perform its 1.4 km/s deorbit burn and landing sequence. After separation, the Carrier returns to the 200-km circular orbit to perform data-relay functions and to take images of the Lander. The Carrier remains in orbit for a nominal mission of 30 days, after which, if left uncontrolled, the Carrier will impact Europa due to natural orbit periapsis decay over the course of two to three months. FO D-3 depicts a summary of the mission design concept.

---

[2]   Total ionizing dose Si behind a 100-mil Al, spherical shell.

Europa Lander Mission Design: Low-Radiation Approach to Perform *in situ* measurements on Europa to Investigate its Habitability

A) Interplanetary Phase: VEEGA Trajectory (6.37 yrs)

VGA (5/14/22)
EGA-1 (10/24/23)
EGA-2 (10/24/25)
Launch (11/21/21)

B) Pre-JOI Ganymede Flyby
(Reduces JOI ΔV by ~400 m/s)

Ganymede Gravity Assist (500 km altitude)

JOI (4/4/28)

JOI

Sun

Jupiter's Orbit

Satellite positions plotted at time of Ganymede gravity assist

C) Tour Phase (1.3 years)

Callisto to Ganymede 3:2, 1:1 resonances to Europa

y
x (γ)
Ecliptic J2000

z
x (γ)

Orbit-skirting flyby sets up Ganymede resonances

D) Europa Operations (60 days)

Site Certification, First Reconnaissance Orbit, 8/6/2029

Tisserand-Poincaré Graph:
New trajectory design technique saves ΔV

Trajectory skirts Ganymede's orbit for first flyby of final resonances

Callisto 1.9 km/s
1:1 Ganymede
3:2
1 km/s
2 km/s
1.48 km/s v_∞ contour
Europa

Perijove Range (R_j): 15, 9.4
Apojove Range (km): 9.4, 15, 26.3

Launch	VGA	EGA-1	EGA-2		JOI			EOI	Land	End of Prime Mission

INTERPLANETARY					JOVIAN TOUR					
2021	2022	2023	2024	2025	2028			2029		

Key Parameters	Value
Launch Vehicle	Delta IV Heavy
Earth to Jupiter Trajectory	VEEGA
Earth Launch Period	11/15/21 to 12/05/21
C3 (Max), R.A., Dec.	15 km²/s², 334.5°, 11.7°
Jupiter Arrival Date	4/3/2028
Jupiter Arrival V-infinity	5.6 km/s (maximum)
JOI Earth Range	4.52 AU
JOI Periapsis Range	12.8 R_j
Jupiter Capture Orbit Period	206 days
Tour	4/3/28–8/6/29 (1.3 yrs.)
EOI	8/6/29
Site Certification Orbit Duration	30 days
Altitude, Inclination, Period, Initial Node	200km, 95°, 138min, 07:30
Deorbit, Descent and Landing	Sep. 2029
Prime Lander and Relay Operations	9/6/29-10/6/29
Relay Disposal	Europa Impact, >11/6/29

Range to Jupiter (Rj): 300, 150, 0

Tour Design provides low TID of 125 krad prior to EOI

Callisto
Ganymede

EOI 125 krad

Europa Orbit

Carrier/Relay 850 krad
Lander 520 krad

Surface Operations

TID Si behind 100 mil Al (krad): 900, 450, 0

Days past JOI: 0, 100, 200, 300, 400, 500

D.2.3.1 Mission Overview and Phase Definitions

The general descriptions of each mission phase and the related activities are summarized in Table D.2.3-1.

D.2.3.2 Launch Vehicle and Launch Period

A Delta IV Heavy will launch the spacecraft with a maximum C_3 of 15.0 km^2/s^2 during a 21-day launch period opening on November 15, 2021. The optimal launch date within the launch period is November 21, 2021 (Figure D.2.3-1). The date of Jupiter arrival is held fixed throughout the launch period, incurring only a negligible penalty while simplifying the design of the tour in the Jovian system. The launch vehicle and launch period parameters are shown on FO D-3. The launch vehicle performance is taken as that specified in the NASA Launch Services (NLS)-I Contract. There is assumed to be no launch-date-dependent performance degradation. The spacecraft propellant tanks will be loaded up to the launch vehicle capability. The spacecraft is designed to launch on any given day in the launch period without reconfiguration or modification.

D.2.3.3 Interplanetary Trajectory

The baseline trajectory used for the Europa
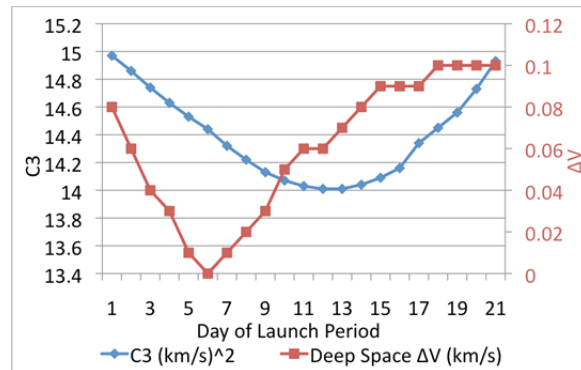
Figure D.2.3-1. The mission design supports a robust 20-day launch period.

Table D.2.3-1. Mission phase definitions and descriptions.

Phase	Subphase	Activity	Start–End
Interplanetary	Launch and Early Operations	Begins with the launch countdown, launch, initial acquisition by the DSN, checkout and deployment of all major flight-system subsystems, and a moderate maneuver to clean up trajectory errors from launch vehicle injection.	Nov./Dec. 2021 + 30 days
	Cruise	Science instrument calibrations, Venus and Earth gravity-assist flyby operations, annual spacecraft health checks, trajectory correction maneuvers, and operations readiness tests (ORTs).	Jan. 2021–Oct. 2027
	Jupiter Approach	Training, and ORTs for all mission elements in preparation for JOI and Jovian cruise. This phase includes the Ganymede (G0) flyby ~12 hours before JOI and ends with completion of JOI.	Oct. 2027–Apr. 2028
Pumpdown		Reduces energy relative to Jupiter via nine Ganymede gravity assists and two Callisto gravity assists. Ends with an orbit-skirting Hohmann transfer from Ganymede to Europa.	Apr. 2028–Aug. 2029 (16 months)
	EOI Sequence	Accomplished by three burns to reduce gravity losses and make any remaining plane changes efficiently.	Aug. 2029 (2.4 months)
Site Certification		200-km near-polar circular orbit, perform reconnaissance of the candidate landing areas and select one	Aug-Sept 2029 (1 month)
Lander Release		Periapsis dropped to 5 km, Lander released, performs deorbit burn and executes landing sequence. Carrier returns to 200-km polar orbit as a UHF relay.	Sept 2029
Science Operations		Lander performs science measurements, data transmitted to Earth via Carrier, or via DTE as a backup.	Sept-Oct 2029 (1 month)
Carrier Disposal		Natural periapsis decay and surface impact after Carrier resources are exhausted. Targeted impact is possible if commanded while Carrier still healthy	Nov-Dec. 2029 (nominal Carrier surface impact)
Lander End of Mission		Lander operates on surface as long as resources permit after nominal mission.	Nov 2029 or later.

Lander Mission is a VEEGA (FO D-3 and Table D.2.3-2). Cruise navigation will use Doppler and range observations from the Deep Space Network (DSN). The deep-space maneuver (DSM) ΔV required on the optimal day of the launch period is zero, but is about 80 m/s at the start of the launch period and reaches its highest level of 100 m/s on the last day. The DSM occurs on the Earth-Venus leg of the trajectory. The interplanetary trajectory design will comply with all required National Environmental Policy Act (NEPA) assessment and safety analysis (see Section D.2.6). An aim-point-biasing strategy will be used for the Earth flybys. The nominal flyby altitudes of Venus and Earth do not vary significantly over the launch period and are relatively high, as seen in Table D.2.3-2. For comparison with other missions that carried RTGs, Cassini flew by Earth at an altitude of 1166 km, and Galileo at altitudes of 960 and 304 km.

A 500-km flyby is performed at Ganymede about 12 hours before JOI, thereby saving about 400 m/s of ΔV (compared to the case of no Ganymede flyby). The JOI maneuver lasts about 2 hours and occurs at perijove at a range of 12.8 Rj, which is in the less intense, outer regions of the radiation belts. Gravity losses are negligible due to the small angle subtended by the burn-arc. This also permits a far less complicated contingency strategy for this critical event.

D.2.3.4 Backup Interplanetary Trajectories

Many trajectory options are available, offering a launch opportunity every calendar year through 2024. The results of a comprehensive

Table D.2.3-2. Baseline VEEGA interplanetary trajectory (for optimal launch date) enable the mission capabilities with an existing Delta IV Heavy LV.

Event	Date	V∞ or ΔV (km/s)	Flyby Alt. (km)
Launch	21 Nov 2021	3.77	-
Venus	14 May 2022	6.62	3184
Earth	24 Oct 2023	12.07	11764
Earth	20 Oct 2025	12.05	3336
G0	03 Apr 2028	7.37	500
JOI	04 Apr 2028	0.858	12.8 Rj

search of all 1-, 2-, 3-, and 4-gravity-assist trajectories are shown in Figure D.2.3-2. The best candidates from the search are shown in Table D.2.3-3, which includes launch period effects. The table shows, for each trajectory, the optimal launch date of the launch period, the flight time to Jupiter, the expected maximum C_3 over the launch period, the launch vehicle capability at maximum C_3 for the indicated launch year (NLS-I contract), the propellant required for flying the mission (assuming the full launch vehicle capability is used), the maximum dry mass (i.e., the difference between the two preceding numbers), and
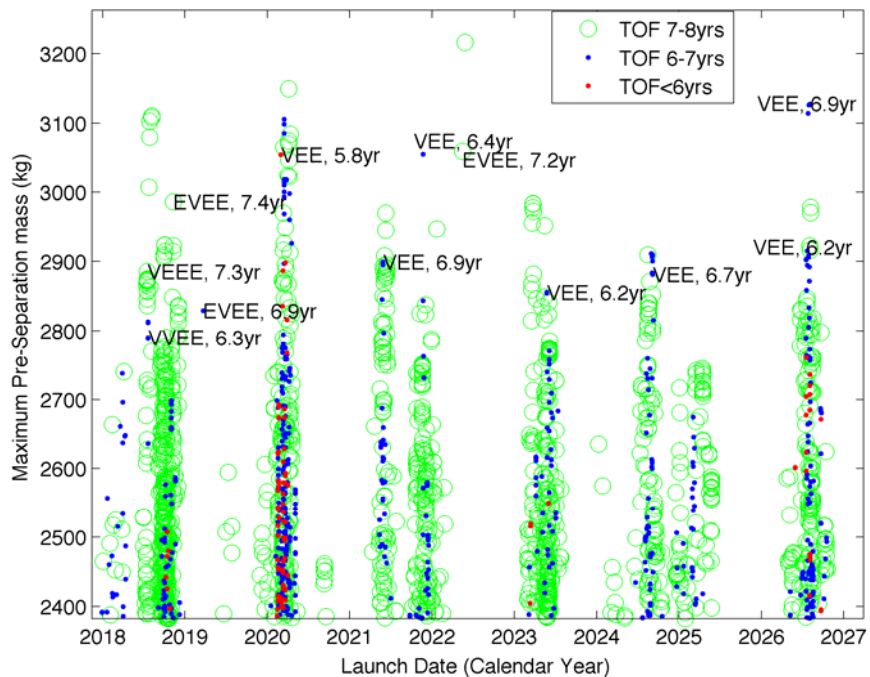

Figure D.2.3-2. Interplanetary trajectory options demonstrate that we can have an annual backup launch opportunity.

Table D.2.3-3. Short list of interplanetary trajectories, including launch period effects. Study trajectory is highlighted in yellow; other listed trajectories represent viable backup opportunities.

Launch Date	Path	TOF to JOI (yr)	C_3 (km²/s²)	Delta-IV Heavy Capability (kg)	Max. Prop. Mass, Carrier Vehicle (kg)	Max. Preseparation Mass (kg)	Carrier Vehicle Prop. Mass for CBE Vehicles (kg)
Nov-2018	EVEE	7.37	3.82	8721	5735	2986	3888
Mar-2019	EVEE	6.91	10.52	7733	4904	2829	3508
Feb-2020	VEE	6.03	15.6	7410	4355	3055	2885
May-2021	VEE	6.87	14.5	7176	4276	2900	2985
Nov-2021	VEE	6.36	15.0	7105	4049	3056	2733
May-2022	EVEE	7.22	10.2	7779	4719	3059	3122
May-2023	VEE	6.18	16.4	6914	4058	2856	2876
Sep-2024	VEE	6.71	13.8	7272	4390	2882	3084
Jul-2026	VEE	6.15	15.2	7082	4166	2916	2892
Aug-2026	VEE	6.94	10.0	7804	4677	3127	3027

the propellant required to fly the mission assuming the current best estimate (CBE) value for the dry mass. In all cases, the CBE ΔV from Table D.2.3-5 is used.

It is worth noting that two types of commonly considered trajectories do not appear in the short list of Europa Lander Mission trajectories because of their relatively poor mass performance. The first type is the ΔV-Earth gravity assist (ΔV-EGA), which is a V_∞ leveraging type of trajectory involving a large maneuver near aphelion before the first Earth flyby). For the ΔV-EGA, the maximum dry mass that can be delivered in the years 2019–2027 is about 1650 kg (about 1000 kg less than the "Max Preseparation Mass" numbers in the short list, Table D.2.3-3). The required C_3 is in the range 25–30 km²/s², and the flight time is typically 4–5 years, corresponding to a 2:1 ΔV-EGA (4.5 years for the maximum-dry-mass case). The second type is the Venus-Earth Gravity Assist (VEGA), involving a large maneuver after the Venus flyby. For flight times of around 4.4 yr, the maximum dry mass for the VEGA is about 1740 kg. For flight times around 5.4 yr, approaching the VEEGA flight times, the maximum dry mass becomes about 2190 kg. Thus, these two trajectory types significantly underperform in terms of delivered mass compared to the typical VEEGA trajectory.

D.2.3.5   Jovian Tour 12-L01

It is desired to keep the TID as low as possible during the Jovian tour so to avoid having to carry extra shielding mass for the Lander (landed mass affects both the Lander wet mass AND the Carrier wet mass); To meet this low-TID goal, the Jovian pumpdown tour uses gravity assists of only Ganymede and Callisto, which are just outside the main radiation belts, and it maintains periapsis as high as possible, near Ganymede's orbit, before approaching Europa. EOI is performed after a Hohmann-type transfer from Ganymede. To reduce EOI below the two-body Hohmann value, multi-body gravitational effects are used in the final Ganymede gravity assist sequence—the spacecraft's orbit essentially skirts Ganymede's and Europa's, rather than intersecting them. The approximate trade-offs between ΔV, flight time and TID are outlined in in Table D.2.3-4. Jupiter cruise has a TID of 125 krad up to EOI.

After JOI and a perijove raise maneuver (PJR), the Jovian cruise starts with three resonant Ganymede flybys which greatly reduce the orbital period and energy. The first Callisto flyby, C-4, raises periapsis while not greatly affecting orbital energy. Three more Ganymede flybys are again used for energy reduction, followed by C-8 for periapsis raising. There follow the last three flybys of the tour, G-9 through G-11, involving resonances of 3:2

Table D.2.3-4. Approximate trade-offs between Flight-time, deterministic ΔV, and TID (Si behind 100 mil Al, spherical shell) for various types of tours. The study approach is highlighted in yellow. This approach minimizes the mass of the Lander and makes this mission possible.

Flight Time (yr)	ΔV (km/s)	TID (Mrad)	Type of Tour
		JOI-to-EOI, Inclusive	
0	>5.5	~0	No JOI, direct insertion to Europa orbit from interplanetary trajectory
0.25	4	~0	Callisto gravity assists and V-infinity leveraging
0.5	3	~0	Further Callisto gravity assists and V-infinity leveraging
1	2.5	0.1–0.5	Callisto and Ganymede gravity assists (no endgame)
1.5	1.5	0.8–1.2	Callisto, Ganymede, and Europa gravity assists (4:3, 6:5 endgame)
2.5	1.3	1.7	Callisto, Ganymede, Europa and Io gravity assists

and 1:1 (spacecraft-to-Ganymede revolutions between flybys). The 3:2 resonance has a small deterministic ΔV of 17 m/s at apoapsis of the second spacecraft revolution. The maneuver raises periapsis to just above Ganymede's orbit, reducing TID while still coming close enough to Ganymede for a gravity assist at G-10. The G-10 flyby sets up a 1:1 resonance leading to G-11, which then puts the spacecraft on a transfer to Europa. The transfer is Hohmann-like, but has even lower V-infinity at Europa than a traditional Hohmann because multibody effects are exploited. Details of tour 12L-01, which is a fully integrated, high precision trajectory with n-body gravitational models, are presented in Table D.2.3-5 and in FO D-3.

The Europa-approach geometry of 12L-01 leaves a roughly 10-deg plane change to be done to obtain the desired 7:30 a.m. node for the site-certification orbit. The ΔV required for this plane change would likely be eliminated in future designs by correcting the phasing early in the tour (i.e., incurring little or no TID penalty). Thus, the ΔV allocated for the tour and EOI in this design is conservative—it is at the upper end of the range expected. There is considerable flexibility in the tour design, both early in the tour and later, where different resonance sequences can be employed.

The navigation strategy and statistical ΔV are based on experience with Galileo and Cassini, because a full-blown navigation study with precise maneuver locations and covariances is

Table D.2.3-5. Flybys of 12L-01. Maneuvers are impulsive.

Event		Date (ET)	ΔV (km/s)	v∞ (km/s)	Altitude (km)	In/Out
Ganymede	0	2028 APR 03 06:23:42		9.218	500	In
JOI		2028 APR 03 16:48:10	0.839			
PJR		2028 JUN 26 17:48:59	0.162			
Ganymede	1	2028 OCT 21 06:22:24		5.698	294	In
Ganymede	2	2028 DEC 10 08:31:35		5.629	185	In
Ganymede	3	2029 JAN 22 06:48:18		5.595	109	In
Callisto	4	2029 MAR 02 13:49:54		6.314	200	Out
Ganymede	5	2029 MAY 03 11:41:02		3.806	205	In
Ganymede	6	2029 JUN 01 01:59:33		3.814	559	In
Ganymede	7	2029 JUN 17 10:33:28		3.715	2170	Out
Callisto	8	2029 JUL 02 15:23:51		1.816	2879	In
Ganymede	9	2029 JUL 06 20:19:05		1.489	15818	In
DSM		2029 JUL 12 00:14:13	0.017			
Ganymede	10	2029 JUL 28 10:32:00		1.347	581	In
Ganymede	11	2029 AUG 04 09:29:41		1.396	3970	In
Europa Arrival		2029 AUG 06 15:37:13		1.485	200	

beyond the scope of this study. The main uncertainties early in the tour are the satellite ephemerides. The maneuver execution errors and perturbing ΔVs are much less significant by comparison, except perhaps for the large JOI and EOI burns. Thus, up to three statistical maneuvers are envisioned per orbit around Jupiter: about three days after a flyby, near apoapsis, and about three days before a flyby. For the 2-day G11-Europa leg, the navigation schedule becomes tighter, having a single TCM, with one backup opportunity. Especially since G-11 is a high-altitude flyby, this schedule should not pose any issues. A cleanup maneuver will be done a few days after JOI to counteract errors both from the 500-km G0 flyby and from JOI itself. Similarly, EOI will have a cleanup maneuver done about 6 to 12 hours after the final EOI burn to give sufficient time for ground-based orbit determination (OD). Two-way Doppler and range are assumed for OD, with optical navigation considered a "nice-to-have."

After the G0 flyby, Ganymede's ephemeris uncertainties will be significantly reduced for the next flyby which occurs roughly in the same place in Ganymede's orbit. G2 further reduces the uncertainties and also contributes to ephemeris knowledge for Europa and Callisto, since the satellites are in resonance with each other.

D.2.3.6   Europa Orbit Insertion, Site-Certification Orbit

Reconnaissance and site certification will be done from orbit for one month prior to landing. In this way, the least hazardous landing sites can be chosen from within the areas of interest. After consultation with imaging scientists, the reconnaissance orbit was chosen to

have a 7:30 a.m. node (roughly the midpoint of a ±10-degree permissible range), a polar inclination and an altitude of 200 km. The polar inclination allows coverage of all latitudes and provides more flexibility in the delivery of the Lander.

A three-burn EOI and circularization maneuver strategy was developed as shown in Table D.2.3-6. Such a sequence has several advantages over a one-burn scheme. First, the gravity losses are reduced from approximately 25% to 11% overall; second, adjustments to the orbit plane can be made much more cheaply by maneuvering on the distant apoapsis of the first orbit; third, the burn durations are shorter. The option to perform a lower-gravity-loss EOI using an SRM was examined, but was found to offer only marginal mass advantage, if any, due to the lower specific impulse. The second burn of the sequence will likely be much smaller in future designs, perhaps on the order of meters per second, because the phasing for the approach geometry can likely be achieved earlier in the tour at no ΔV expense.

The EOI burn puts the spacecraft into a roughly 12-hour orbit. The plane-change maneuver occurs near apoapsis of the second orbit (to provide enough time for ground-in-the-loop commanding), based on IMU updates and a ground-based OD update, although it would be possible to delay the maneuver for several orbits if warranted for navigational purposes (the only drawback would be the extra TID). The final maneuver circularizes the orbit and is followed by cleanup maneuvers after ground-based OD.

Weekly orbit maintenance maneuvers are sufficient to control the growth of the eccen-

Table D.2.3-6. The three-burn approach to EOI and circularization minimizes gravity losses.

Activity	Orbit	Finite Burn ΔV (m/s)	Gravity Loss (%)	Burn Arc (deg)	Burn Duration (min)
EOI	200 × 7000 km, 10:00 a.m. node	787	16	107	57
Plane Change	200 × 7000 km, 7:30 a.m. node	100	0	0	6
Circularization	200 × 200 km, 7:30 a.m. node	396	2	67	24

tricity, which occurs mainly due to Jupiter's gravity, and will fine-tune the orbit period for obtaining specific ground tracks. The total ΔV needed for maintenance for a month is only 5 m/s. The maneuver frequency and magnitude can be reduced further still if the orbital eccentricity vector is properly set once the main gravity harmonics of Europa are estimated. The TID for the one-month site-certification orbit is about 360 krad, a figure which accounts for the shielding effect of Europa.

D.2.3.7　Lander Separation

Once a landing site is selected (pinpoint landing is assumed), the Carrier and Lander combined spacecraft will lower its periapsis to 5 km using a 40-m/s burn. Note that in Phase A we will trade this decision with just having the Lander separate and lower its periapsis. The integrated spacecraft will remain in the 200 × 5–km orbit to allow time for ground-based OD to determine the orbit period more accurately. Since timing uncertainties are the main contributor to the pre-deorbit landing error ellipse, this OD serves to shrink the error ellipse by more than half. After a navigation update and go-ahead from the ground, the Lander and Carrier will separate by means of a spring release that imparts a small ΔV. The Lander then performs a deorbit maneuver of about 1.44 km/s on an SRM that uses mono-propellant TVC and burns for about 50 s. The uncertainty in the burn duration is about 5% and is a significant factor in the size of the error ellipse. The impulse uncertainty is only about 0.5%. The 5% burn-duration uncertainty also means that the TVC translational ΔV uncertainty is also approximately 5%. All together, the 3-sigma error ellipse, before the SRM burn, is estimated at about 3 × 6 km (minor-by-major axes), a size which will be refined in future studies. About 30 m/s of residual velocity are deliberately left to make it easier for the descent profile to correct for a 3-sigma under-burn on the SRM and to assist in avoiding a collision between the Lander and the spent SRM. The 5-km altitude of deorbit

and the 30 m/s residual ΔV were chosen based on preliminary analyses that indicated feasibility. These numbers will be refined in future studies as ΔV is traded between the SRM and the descent profile and as the error ellipse estimate is improved.

The orbital period before the periapsis-lowering maneuver is refined so as to place the ground track over the landing site at the time of the SRM burn. A cross-track bias can also be employed to avoid collision with the jettisoned SRM casing.

The Lander deorbit, descent, and landing (DDL) is a short event lasting less than 5 minutes; the geometry between the Carrier and Lander during this event supports the use of UHF relay between the two elements. The Lander will telemeter critical DDL data to the Carrier; in parallel the X-band direct-to-Earth (DTE) system on the Lander will issue tones to also communicate DDL state/event information.

D.2.3.8　Deorbit, Descent, and Landing Operations

Currently the single greatest challenge presented by landing on Europa is the unknown characterization of the Europa surface environment at the scale of the Lander. The DDL concept is therefore designed to mitigate this surface knowledge risk by providing as much sensed surface information as possible both before and during the landing event. A strategy of prelanding reconnaissance combined with terrain relative navigation (TRN) and hazard detection (HD) is designed to increase the probability for a successful landing within the constraints of the mission. Figure D.2.3-3 illustrates the landing hazard risk mitigation strategy. Prior to landing, a reconnaissance campaign will image the science areas of interest at 0.5-m/pixel resolution in a 10 × 10–km area (outlined in blue). Within this area, a ground team will identify hazardous and safe areas and designate a target landing site that minimizes local hazards. The red landing
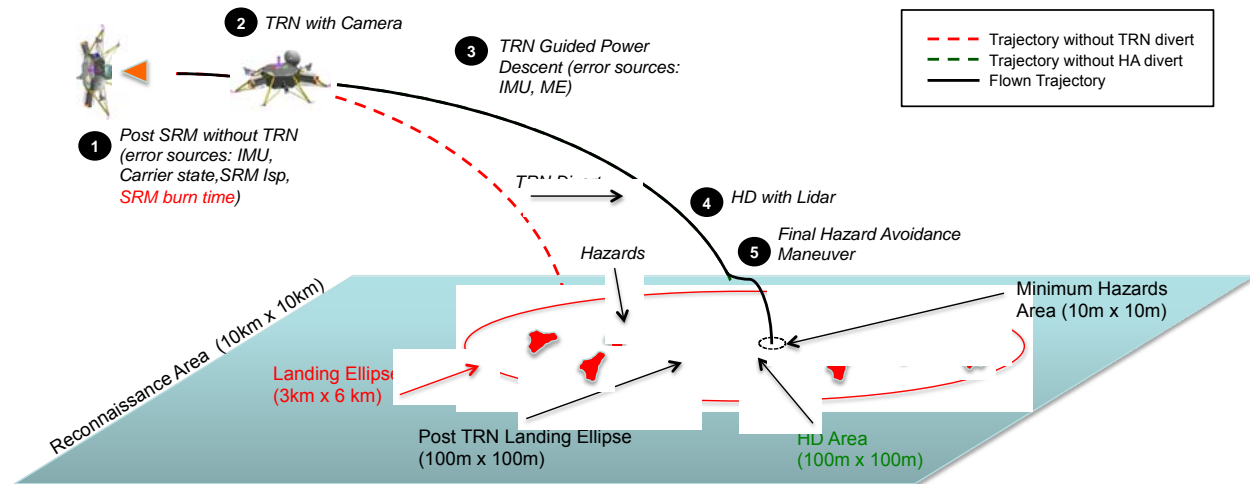
Figure D.2.3-3. Landing strategy to mitigate landing terrain hazards.

ellipse in Figure D.2.3-3 is centered on this designated landing site, and the 3 × 6–km size of the ellipse represents the uncertainty in landing location prior to deorbiting. After deorbit, TRN provides continuous updates to the Lander position using descent camera imagery taken at 1 Hz, and a 3-km divert capability provides the Lander the ability to maneuver to within 50 m of the center of the pinpoint landing ellipse (the green area), to the designated landing site. Note that multiple pinpoint-landing targets can be included, and the system will select the nearest opportunity. During final descent, an onboard HD system detects any local hazards not detected by reconnaissance and the Lander has the capability to maneuver to an identified safest landing area within the 100 × 100–m green HD area. In this way, risk from local landing hazards is mitigated. A more detailed discussion of this strategy follows in the sections below. The timeline charts presented below are meant to represent a concept; more detailed study of the timeline is required in Phase A.

It is recognized that there may be other concepts for landing on rough terrain that would require less knowledge of the landing site and allow for a large landing ellipse or require less reconnaissance by the carrier. This will be the subject of a trade study to be completed in Phase A.

D.2.3.8.1 Reconnaissance and Landing Preparation

Built into the landing strategy is a prelanding reconnaissance campaign carried out by the Carrier via a high-resolution, 0.5-m/pixel imager while in a 200 × 200–km orbit. As shown in Figure D.2.3-4, the reconnaissance of four previously identified prospective science areas begins 30 days prior to DDL. Over the course of one Eurosol, a 10 × 10–km image is captured of each landing area. The images are downlinked to a landing site selection team that processes the images, generating data products used by the team to identify safest landing sites within the landing areas. Once a landing site is chosen, a terrain map is generated and uplinked to the spacecraft as a key element in the TRN system used during landing. The process of capturing images, processing data, identifying a target landing site and uplinking a TRN map occurs over a 30-day window.

While the landing site selection team is processing images, the spacecraft operations team is performing Lander checkouts that begin the process of landing preparation. At 24 hours before deorbit, the ME and SRM heaters are turned on, and spacecraft status is downlinked to the ground. Once the checkouts are complete, at 5.3 hours prior to the deorbit SRM
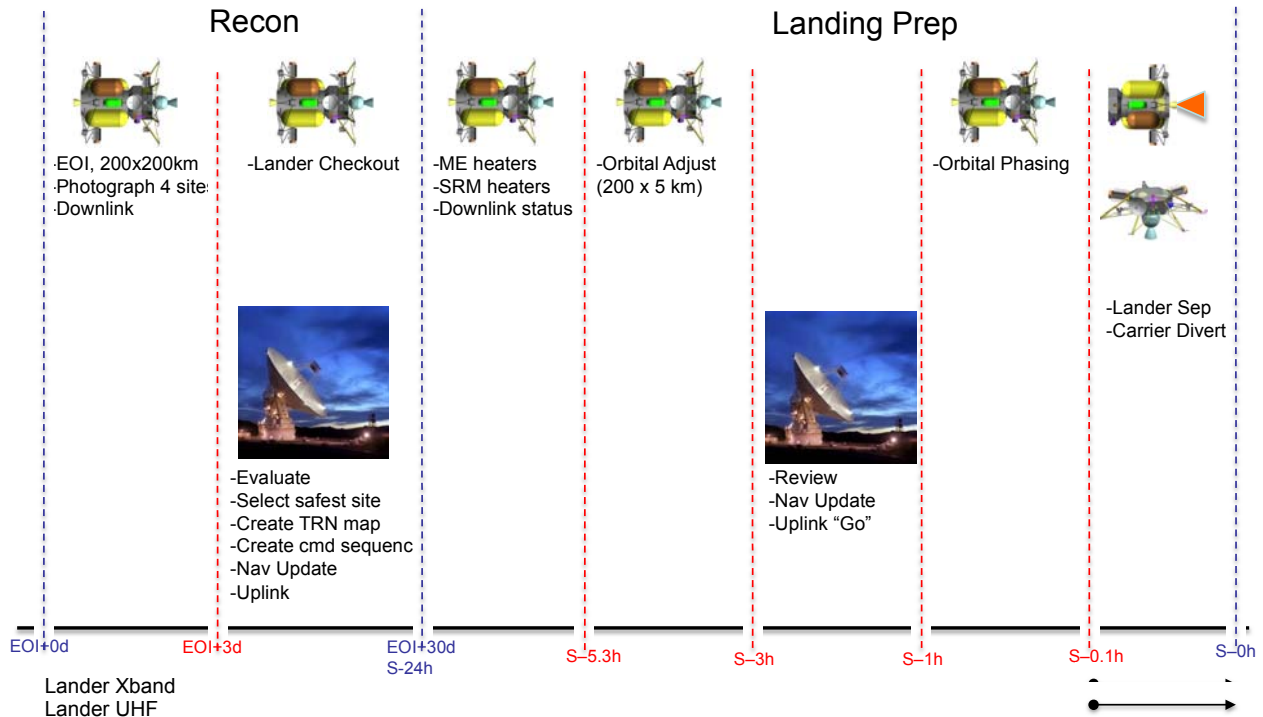
Figure D.2.3-4. Reconnaissance and landing prep timeline provide the ground team with time to make a safe landing site selection.

burn, the spacecraft performs an orbital adjustment, lowering its periapsis and positioning itself in a 200 × 5–km orbit, shown at S-5.3h in Figure D.2.3-4. At 3 hours before deorbit, spacecraft status is reviewed, an updated navigation state is generated, and at 1 hour before entry, the navigation state is uplinked to the spacecraft along with a final "go" to proceed with deorbit burn. Prior to deorbit, landing prep completes with a final phasing maneuver to place the spacecraft on a final approach to the deorbit point, followed by separation of the Lander from the Carrier element.

D.2.3.8.2   Deorbit, Descent and Landing

DDL delivers the Europa Lander from a 5-km altitude to the surface of Europa via a number of maneuvers, as outlined in Figure D.2.3-5. The sequence begins with a deorbit burn, is followed by a free-fall segment and concludes with powered descent that delivers the Lander to a touchdown on Europa's surface minutes after the start of the sequence. During DDL,

primary communications with the ground is provided by a UHF link to the Carrier element, which records and then sends the data back to Earth. Additionally, the Lander X-band DTE LGA will be transmitting status semaphores or tones, providing a secondary communication link, as shown at the bottom of Figure D.2.3-5.

D.2.3.8.3   Deorbit Burn

The DDL sequence of events begins with the deorbit burn. The deorbit burn is executed by the SRM which provides a ΔV of 1.4 km/s, nulling vertical velocity to 0 m/s while deliberately leaving a residual horizontal velocity of 30 m/s to 100 m/s at an altitude of 5 km. During the deorbit burn, attitude control in the pitch, yaw, and roll axes is accomplished using the nine MR-107 descent thrusters via TVC. The variability in descent thruster activity during the deorbit burn contributes significantly to the 30 m/s to 100-m/s residual velocity range (uncertainty) at the end of the deorbit burn. The uncertainty in Lander position following the deorbit burn is 6 km in downrange.
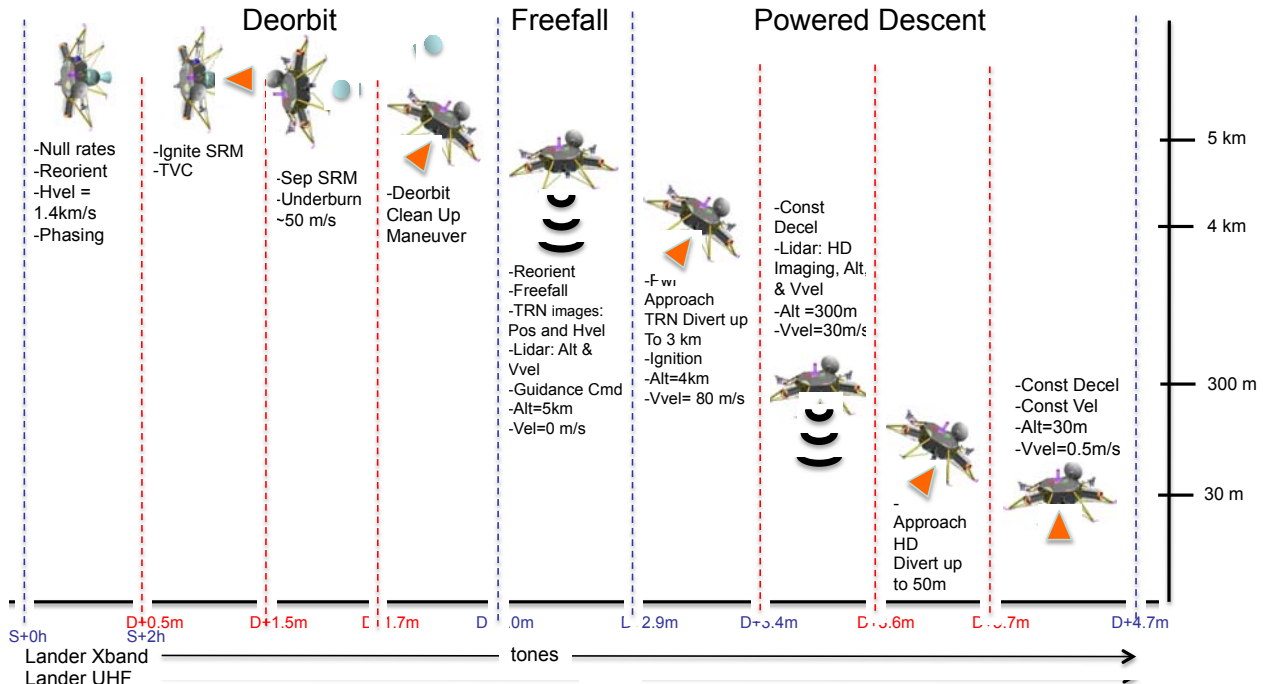
Figure D.2.3-5. Deorbit, descent, and landing events use precision landing technologies to achieve high probability of landing success.

This corresponds to the 3 × 6–km ellipse shown in Figure D.2.3-3.

D.2.3.8.4   Free Fall

Upon the completion of the deorbit burn, the SRM is separated from the Lander and, partly due to the designed residual horizontal velocity, will impact at least 1 km from the Lander touchdown location. Section D.3.8.7 (Future

Work) outlines a lateral divert strategy currently under study that promises a more efficient method of gaining separation from the SRM. Following SRM separation, the Lander executes a free fall. Approximately 2 minutes into the DDL sequence, the Lander attitude is reoriented to point the onboard descent imager and HD flash LIDAR to the surface, after which the descent imager begins capturing images, and collection of altimetry measurements begins at 20Hz using the HD LIDAR in altimetry mode. Descent images are matched to the onboard TRN map at 1Hz. Locations of matched image in the map, measurements of altitude and altitude rate from the LIDAR, and IMU data are input to an onboard estimation

filter which continuously updates the lander's position and velocity relative to the targeted landing site. Using the updated Lander position and velocity state from the filter, the Lander computes an optimized trajectory terminating at the landing site. The Lander has sufficient propellant to divert a horizontal distance of up to 3 km guaranteeing the target landing site is reachable given the position uncertainty following the deorbit burn.

D.2.3.8.5   Powered Descent

With an optimized trajectory computed, powered descent begins nominally at approximately 4 km above the Europan surface with a vertical velocity accumulated during free fall of approximately 80 m/s. Powered descent is accomplished with nine MR-107 engines, each having a maximum thrust capability of 270 N. During powered descent, effective thrust is varied from 15% to 90% via pulse-width modulation; the additional 10% is reserved for attitude control. The optimized trajectory flown by the Lander is computed to provide the necessary divert distance, bringing the

Lander to the local proximity of the landing site at an altitude above the surface of 300 m.

During powered descent, smaller terrain features become visible, and the appearance of the surface in the descent images can begin to diverge from its appearance in the onboard map. At some point in descent, TRN transitions to matching features in descent images taken 0.1 second apart, instead of matching images to the onboard map. Tracking of features is used to compute the change in position between images, and this information is input to the filter, which continues to update position and velocity to touchdown. During powered descent, the thrust profile required to effect either the TRN or HD diverts could require significantly off-nadir attitudes for short periods of time. During this time, descent images could include terrain outside the onboard map. Onboard software will be capable of discarding or cropping images that are unusable for this reason. In addition, powered descent guidance incorporates the capability to impose attitude constraints to ensure a sufficient number of usable images for TRN and HD.

At 300 m altitude, with the Lander nearly over the target landing site, the HD phase of DDL begins. Active HD is initiated using a flash LIDAR that is able to detect surface hazards as small as 3 m wide and 1 m tall/deep, and slopes 25° and larger. Using an onboard algorithm, the Lander selects the safest 10 × 10–m touchdown zone within its final 50-m horizontal divert capability and computes a thrust profile to take it to this final target. This divert brings the Lander to a point 30 m altitude directly over the 10 × 10–m target touchdown site. The final 30 m of descent is performed at a constant vertical descent velocity of 0.5 m/s, and touchdown nominally occurs with a vertical velocity of 0.5 m/s and a horizontal velocity no greater than 0.25 m/s. In this final phase of descent, the Lander will be rotated so that radiators and worksite are placed in a preferred orientation with respect to the Sun.

D.2.3.8.6　　Landing Surface Environment and Lander Design

The purpose of the DDL phase is to bring the velocity of the Lander to an acceptably low value to enable a safe, low-velocity touchdown in the surface environment of Europa. Without a current measure of the environment on the scale of the Lander, a "challenge" environment was crafted to provide a bounding case against which to measure the Lander capability. Figure D.2.3-6 illustrates the challenge environment. It was crafted to generate a post-landing tilt on the Lander no greater than 50°. As Figure D.2.3-6 shows, the challenge environment is a combination of a ground slope of 25° and a rock or icy object of height of 1.5 m. Assuming a 4 m Lander base length and a landing orientation with one Lander leg atop the 1.5 m height object, the object adds an additional 22° effective slope, bringing the total Lander tilt to 47° relative to the local horizontal.

Maximum 47° effective landing surface angle
- Maximum 25° slope plus
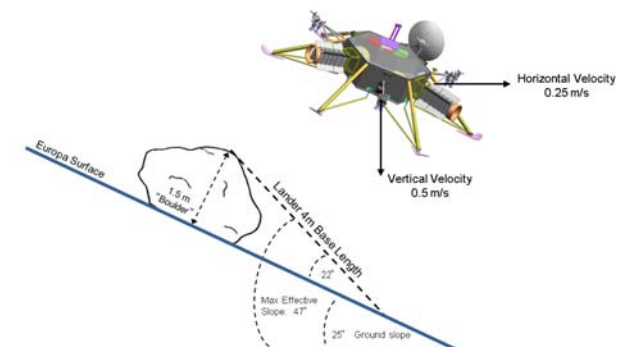- Maximum 1.5 m high boulder OR 1.5 m deep crater

Figure D.2.3-6. Europa mission challenge surface environment is used to establish a robust landing system concept.

In response to this surface environment, the Lander has a number of design attributes that maximize the ability of the Lander to execute a successful touchdown. As mentioned in Section D.2.3.8.5, there are nine 270-N terminal descent thrusters to control velocity and attitude. The Lander structure is of a pallet design providing a wide base area and low center of

gravity. This concept provides excellent tip-over stability. The wide base area of the Lander is created by six outrigger legs that also provide energy absorption. The outrigger legs are a low mass design solution to creating a wide base area. The combination of these attributes provides a design that is assessed to be appropriate for at least some fraction of accessible Europan terrain.

D.2.3.8.7   Future Work

The Europa Study Team has identified near-term work to further refine the concept design of DDL, minimize the propellant load, and characterize the Lander capability. Additional design work for powered descent has yielded a promising trajectory strategy with further work needed to mature the design. Additionally, a touchdown dynamics analysis using the Adams multibody dynamics simulation tool is planned for Phase-A.

Refinement of Powered Descent Strategy

Ongoing powered descent design work has yielded a new, very promising powered descent divert strategy that provides robust separation of the Lander touchdown point and the SRM ground impact point. This separation is achieved by planning a cross-range component into the powered descent divert maneuver.

Initial analysis of the strategy has generated the two trajectory plots shown in Figure D.2.3-7. The first plot shows the trajectory in three dimensions, and the second is a ground track plot. In both plots, the SRM ground track is shown as a red dashed line. As can be seen in the plots, by designing in a cross-track maneuver at least as large as the semi-minor axis of the 6×3–km initial landing ellipse, the Lander touchdown point and SRM

ground impact point will reliably be separated by at least 1.5 km. The strategy requires a deorbit trajectory bias of 1.5 km to place the SRM impact ellipse in the required location relative to the desired landing site. Current analysis shows a propellant mass of 102 kg is required for a powered descent divert of greatest distance, exceeding the current monopropellant allocation of 95 kg. Further analysis is planned to mature the strategy.

Adams Touchdown Analysis

Previous pallet Lander concepts, including an early design of the Mars Science Laboratory (MSL) Lander and the Surface and Atmosphere Geochemical Explorer (SAGE) Lander concept for Venus, used the Adams multibody dynamics simulation tool to provide initial characterizations of landing dynamics. The Europa Study Team is planning a similar near-term initial assessment. The tool provides the capability to model the Lander as a multibody object and assess dynamic and structural responses to terrain slopes and rocks under expected touchdown velocity and attitude states. Figure D.2.3-8 shows an Adams visualization output from a previous pallet Lander concept with a rock represented by a partially buried, green spherical object. The sloping line represents the ground. The analysis planned by
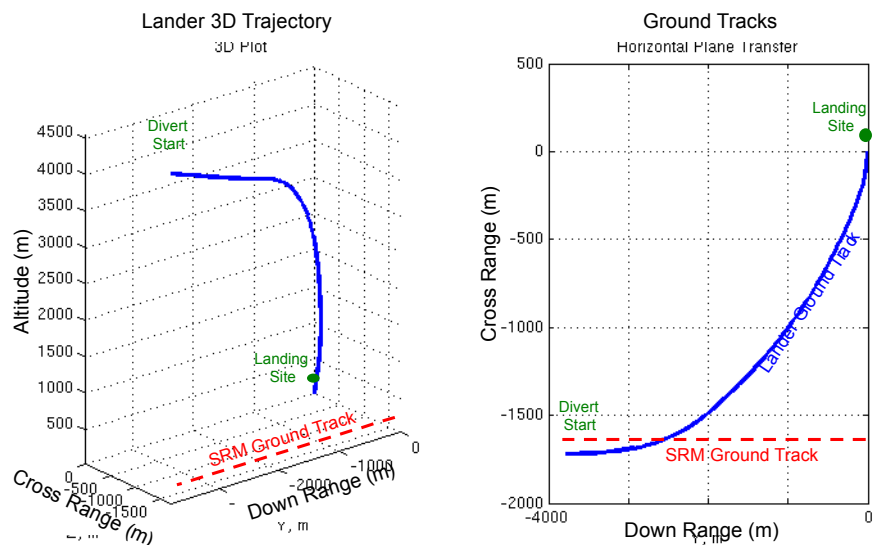

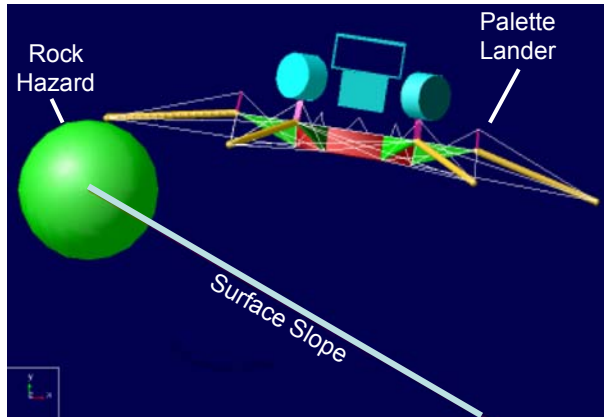**Figure D.2.3-7**. Powered descent with cross-range divert maneuver.

Figure D.2.3-8. Previous pallet lander landing dynamics analysis in Adams, similar to planned Europa Lander analysis, will mitigate risk with the landing system design

the Europa Study Team will provide a more detailed assessment of the Lander touchdown performance capability against the challenge surface environment represented in Figure D.2.3-6.

D.2.3.9 Relay Operations and Landing Site Context Imaging

After Lander separation, the Carrier returns to a 200-km circular orbit, by means of a 40 m/s periapsis burn. Now acting as a relay, the orbiting craft will have two sets of flyovers over the Lander per Eurosol—one set in sunlight and one in darkness. In addition to relay operations, the Carrier, using the RC, will take pictures of the actual landing site to provide context for the science team. The Carrier will perform weekly orbit maintenance, totaling 10 m/s for one month of operations. The larger ΔV budget (as compared to the site-certification orbit) reflects the expected tighter requirements on the orbit to optimize the relay capability.

D.2.3.10 Carrier Disposal

Without active maintenance, low, circular orbits above about 40 degrees inclination will naturally impact the surface of Europa due to eccentricity growth. Starting in the relay orbit, it would take at least two months for an uncontrolled spacecraft to impact Europa. Thus, if the Carrier becomes nonfunctional, it will

eventually impact the surface of Europa at a random location. Alternatively, it may be decided after the prime mission to set a still-functioning Carrier on a deliberate impact course with a specific spot on the surface. There would not be sufficient propellant remaining at the end of the prime mission to enable the Carrier to escape from Europa. Thus, impact with Europa is the ultimate fate of the Carrier.

Near the end of mission, before the Lander fails, the Carrier could be intentionally crashed onto Europa to provide a seismic input for the seismometers. Arguably, the most scientifically important seismometer measurements made on the Moon by the ALSEP packages were when the S-IV B stages were intentionally crashed onto the Moon, and the Moon would ring afterward for quite some time.

D.2.3.11 Lander Mission ΔV

Table D.2.3-7 summarizes both the CBE and maximum estimated value (MEV) for the total ΔV needed to execute the Carrier and relay functions of the Europa Lander Mission. The two totals are comprised of both computed values (DSM, JOI, PRM and the tour's deterministic ΔV) and estimated values (launch injection cleanup, Earth bias ΔV, statistical ΔV, orbit maintenance ΔV). Table D.2.3-8 summarizes the Lander ΔV.

Table D.2.3-8. The Lander ΔV enables precision landing on any ground-selected safe landing site.

Activity	Engine	ΔV	Duration
Deorbit Burn (30 m/s residual velocity)	SRM & TVC	1440 m/s	50 s
Deorbit Cleanup	Monoprop	7 m/s	
Descent Profile	Monoprop	320 m/s	

Details on the descent profile can be found in Section D.2.3.7.

Table D.2.3-7. Interplanetary trajectory, tour 12-L01, site-certification, and relay orbits ΔV summary.

Activity	Alloc. (m/s)	Point Design	Comments
Launch Injection Cleanup	20	20	Estimate to correct injection errors from launch vehicle.
Earth Bias DV	50	50	Needed for final correction of deliberate aim-point bias away from the Earth. ~25m/s/E-flyby. May be performed separately or integrated with other TCMs.
Deep Space Maneuver	100	150	Maneuver on Earth-Earth leg near aphelion. Baseline launch period variation goes from 0m/s up to 100 m/s.
IP Statistical & ΔV Cleanup	50	50	Multiple small maneuvers.
JOI at 12.8 R_J, 500-km G0 flyby	880	900	200-day initial orbit. Includes 3% for cleanup & minimal gravity losses.
Perijove Raise	162	180	Counteracts solar perturbations, targets G1 flyby.
Pump-Down Phase Statistical	36	80	~8 m/s per flyby (conservative) (11 flybys). Expected average per flyby: ~3 m/s.
Pump-Down Deterministic	17	30	Multiple maneuvers
EOI ΔV, Impulsive	1068	1168	Two burns, MEV value gives more flexibility in arrival conditions. 200 × 200 km
EOI ΔV Gravity Loss	85	93	<~8% for MEV mass case and 890N engine
EOI Cleanup	21	23	~2% of EOI, probably multiple maneuvers
Orbit Plane Change	100	100	Arrival geometry gives an offset in desired plane.
Orbit Maintenance	15	15	5 for 30-day reconnaissance orbit, 10 for 30-day relay orbit (tighter tolerances needed)
Periapse Lower/Raise	80	80	40m/s to lower stack to 200 × 5 km, 40 m/s to return Carrier to 200 × 200 km
TOTAL	**2685**	**2870**	

D.2.4 Integrated Spacecraft and Carrier Element

The integrated spacecraft concept, consisting of a Carrier element and Lander element, is a highly capable system tailored to the objectives of landing site reconnaissance, safe Lander deployment, and Lander telecom relay.

D.2.4.1 Integrated Spacecraft Overview

The integrated spacecraft, pictured in Figure D.2.4-1, has the Lander on the +Z axis attached to the Carrier, which is on the –Z axis. The Carrier element controls the integrated spacecraft from launch through separation of the Lander. The integrated spacecraft uses power from the Carrier ASRGs and Lander ASRGs. A sunshield at the –Z axis protects the integrated spacecraft during Venus flyby.

Section D.2.4 will discuss the integrated spacecraft and also the Carrier element; the Lander element will be covered in Section D.2.5.

The following nomenclature is used throughout the report:

- Integrated spacecraft or spacecraft: The Lander and Carrier together.
- Carrier or Carrier element: The Carrier portion of the integrated spacecraft. It controls the integrated spacecraft from launch though Lander separation. After Lander separation, the Carrier performs the telecom relay function.
- Propulsion Module: A module of the Carrier element with propulsion, telecom, ASRGs, and LV adapter.
- Avionics Module: A module of the Carrier element with C&DH electronics, power electronics, and GN&C equipment.
- Vault: The portion of the Avionics Module that contains the majority of the Carrier electronics. By design the vault provides a huge amount of radiation shielding.
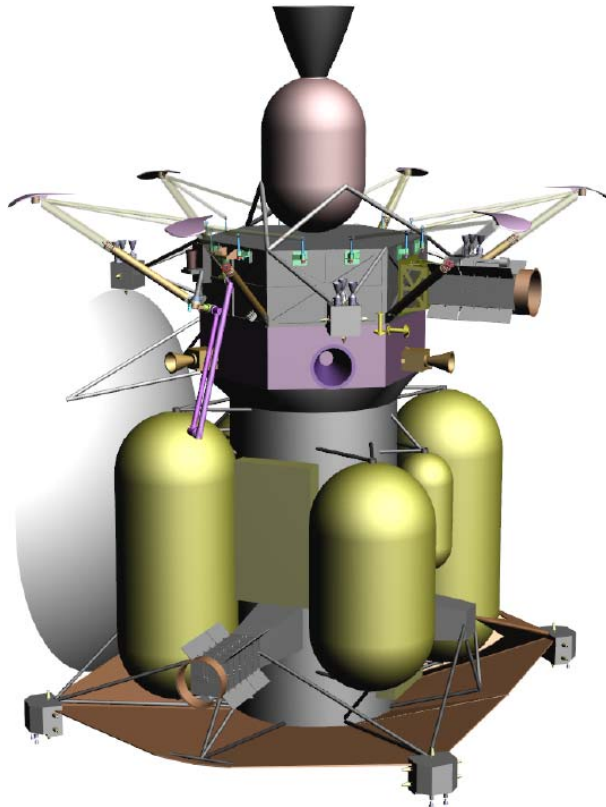
Figure D.2.4-1. The integrated spacecraft (shown here without its thermal shroud) provides a robust platform to get the Lander into Europa orbit safely.
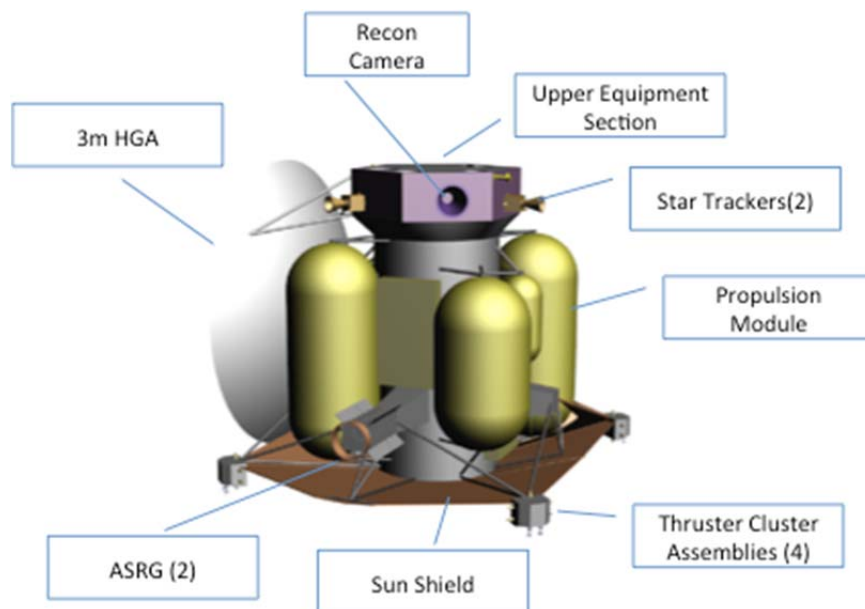

Figure D.2.4-2. The Carrier (shown here without thermal shroud or Lander) provides a modular design approach to enable parallel development and simplified integration.

- Upper Equipment Section (UES): The

portion of the Avionics Module that contains equipment not easily housed in the vault (e.g., the RC).

- Lander or Lander element: The landed portion of the integrated spacecraft. It performs the surface science.

D.2.4.2   Carrier Element Overview

The Carrier element, pictured alone in Figure D.2.4-2, has two distinct modules oriented about the Z axis from top to bottom and is dominated by the 3-meter HGA on the side of the Propulsion Module along the +Y axis; the main rocket engine on the –Z axis; the Propulsion Module tanks and the outrigger-mounted control thruster engines at mid-span; and the ASRGs for power-generation mounted symmetrically about the ME at the base of the Propulsion Module. The two modules are discussed in more detail below. The Carrier accommodates the Lander on the +Z axis; beneath the Lander on the UES are the RC and the UHF relay antenna.

Lander Support from the Carrier

The Carrier is configured to support the Lander in the following way:

- Data interface to provide TRN maps and state updates prior to separation
- Separation elements for the Lander
- Landing site RC to generate images for site selection and TRN maps
- UHF antenna for Lander command and data relay

The camera and UHF antenna are configured for nadir pointing by the Carrier.

Attitude Control

The Carrier element is

three-axis-stabilized in all phases of flight. Stabilization is achieved through the use of inertial measurement and star measurement for attitude determination and thrusters or reaction wheels for attitude control.

Data Handling

During the mission there are two sources of data that must be stored; before Lander release the RC will take images that will be stored then downlinked over time. After Lander release, the Carrier will act as a relay for Lander data. These data can be stored multiple times in a large, redundant, solid-state data recorder (6.4 Gbit per card) that is part of the Command and Data Handling (C&DH) Subsystem. Concepts for data integrity using the excess storage capability will be studied during Phase A.

Power

The power source for the integrated spacecraft is from four ASRGs (two on the Carrier and two on the Lander). After Lander separation the Carrier can perform its mission with two ASRGs. The power system is sized to accommodate one failure (mechanical or electrical) of an ASRG. Excess power is stored in the 30-A-hr lithium-ion battery or dumped as heat through a thermal shunt. For mission activities that are not power-positive, a positive energy margin is obtained by using the battery, which has been sized accordingly.

Thermal

To minimize the power demand of the spacecraft (because we desire to minimize the number of ASRGs), the spacecraft was designed to minimize the use of electrical heaters. To achieve this goal, the heat from spacecraft electronics is captured inside a thermal shroud surrounding the Propulsion Module. This concept allows the propellant to be kept near room temperature without the need for supplemental electrical heaters. The concept also includes 30 radioisotope heater units (RHUs) and variable RHUs (VRHUs) that will be used in select locations (e.g., thruster cluster assem-

blies) to minimize the need for electrical heaters. A sunshield at the –Z end of the spacecraft provides shading during the Venus flyby.

Communications

The Communications Subsystem is designed to support the high volume of data to be transmitted back to Earth after each reconnaissance pass or Lander relay pass. This system consists of X-band uplink for commands, X-band downlink for low-data-rate telemetry, and Ka-band downlink using a 3-meter HGA for high-data-rate telemetry.

Propulsion

The Propulsion Subsystem must support attitude control, momentum management, trajectory correction, JOI, EOI, and orbit changes at Europa. To achieve these requirements the Propulsion Subsystem employs a dual-mode, bipropellant architecture. The fuel, oxidizer, and pressurant tanks are distributed around the core of the spacecraft to provide radiation shielding to the internal electronics. During Phase A, a risk assessment will be performed on potential micrometeoroid damage to the tanks; if necessary, the thermal shroud can be upgraded with standoff Whipple/bumper shields. The tanks are sized for the maximum possible propellant load for the spacecraft launched on the Delta IV Heavy and can support up to 2.9 km/s of ΔV. The actuators consist of one 890-N ME, eight TVC thrusters, and 16 (eight primary, eight redundant) attitude-control thrusters; each thruster cluster assembly (TCA) contains four attitude-control thrusters and two TVC thrusters.

Redundancy

The spacecraft uses a redundancy philosophy similar to that of Cassini in that the Carrier is redundant with selected cross-strapping. The structure, ME, and TVC, however, are single-string; these elements will undergo a risk assessment in Phase A to determine if the risk is acceptable. There is sufficient mass margin to accommodate dual redundancy here if appropriate.

Radiation

This mission has demanding TID (0.85 Mrad behind 100 mil Al) requirements; to support the use of standard aerospace EEE parts, we have employed a multilayered radiation shielding approach as part of the spacecraft design concept. Most of the spacecraft electronics are housed in a radiation vault (similar to that on the Juno spacecraft); this vault is also located inside the spacecraft to benefit from shielding provided by other spacecraft elements such as the batteries, structure, tanks, and ASRGs. Inside the vault the EOM TID environment is reduced to 50 krad with boards nearer the center encountering even less. Electronics will be tolerant to at least 100 krad for an radiation design factor of 2 or better.

D.2.4.2.1   Carrier Configuration

The cross-sectional view of the Carrier element is shown in Figure D.2.4-3.

Avionics Module

At the top of the Carrier is the UES. This section holds the RC, reaction wheels, and star-trackers. At the bottom of the Avionics Module is the radiation vault; inside the vault is a majority of the spacecraft avionics. The Avionics Module is mounted to the Propulsion Module. The equipment in the UES is accessible throughout spacecraft ATLO; the equipment in the vault is accessible throughout the Avionics Module ATLO. After spacecraft integration, a demate operation from the Propulsion Module will enable access to the vault.

Propulsion Module

The Propulsion Module contains the fuel tanks, oxidizer tanks, and pres-

surant tanks as shown in Figure D.2.4-2. At the bottom of the Propulsion Module is the ME and four thruster clusters holding the attitude-control thrusters; these are supported on booms to maximize the moment arm for attitude control and to reduce plume impingement. The 3-meter HGA is mounted to the side of the Propulsion Module. Collocated on this structure is the medium-gain antenna (MGA) and one of three low-gain antennas (LGAs). At the base of the Propulsion Module are the two ASRGs and the launch vehicle adapter (LVA).

Figure D.2.4-4 shows the Carrier with the Lander and the thermal shroud (which is not part of any module, though supported by them). The view on the left shows how the thermal shroud insulates the spacecraft during the cold phases of the mission. The view on the right shows how the sunshield protects the spacecraft from the high solar flux during Venus flyby portion of the interplanetary cruise. The few elements exposed to the solar flux are the LGA, thruster clusters, RC light shades and star-tracker light shades. These
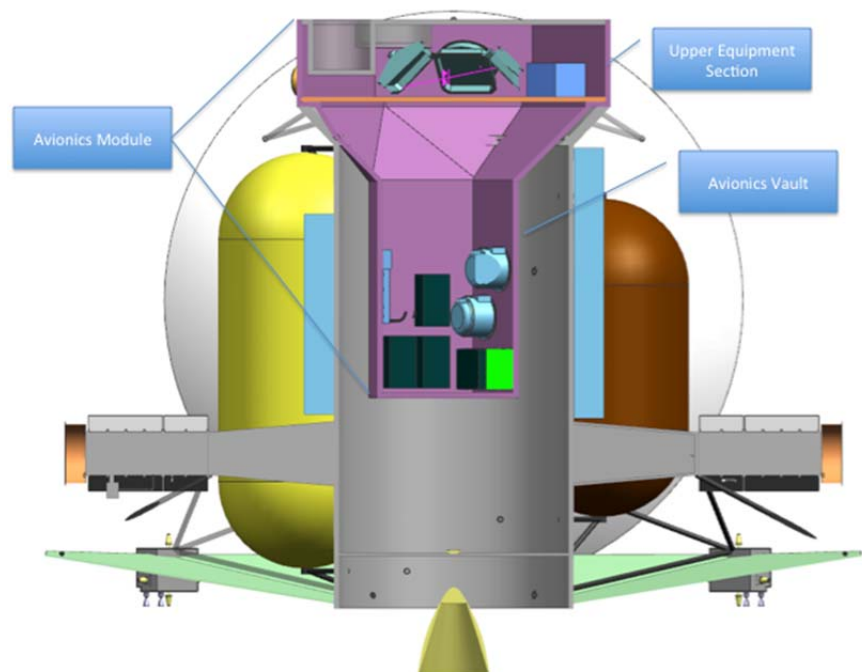

Figure D.2.4-3. The modular configuration of the Carrier element provides maximum radiation shielding for the electronics (thermal shroud not shown).
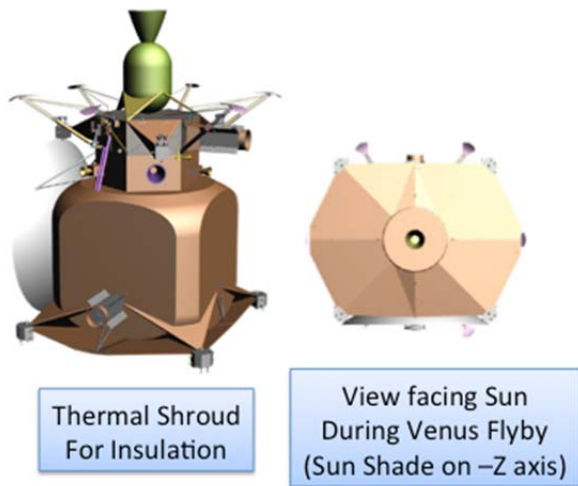
Figure D.2.4-4. The integrated spacecraft provides thermal balance throughout all mission phases.**.**

three elements can tolerate heating during the flyby without shading.

D.2.4.2.2   Carrier Block Diagram

Figure D.2.4-5 shows the system block diagram for the Carrier element. The left box is the Avionics Module. The right box is the Propulsion Module. The thermal shroud and

some other components are shown as distributed among the modules.

The Avionics Module holds the majority of the spacecraft avionics. Inside the vault are the C&DH electronics, power electronics, pyro/propulsion drive electronics, inertial measurement units (IMUs), wheel drive electronics (WDE), and universal space transponders (USTs). In the UES is the RC and the following GN&C components: RWAs , Sun-sensors, and stellar reference units (SRUs). The Power Subsystem components outside the vault are the shunt radiator and battery. The Telecom Subsystem components outside the vault are the travelling-wave tube amplifiers (TWTAs), coax, waveguide, switches, and antennas.

The Propulsion Module is an integrated structure containing the tanks (fuel, oxidizer, pressurant), plumbing, pressurization control assembly (valves, filters, sensors, etc.), propellant isolation assembly (valves, filters, sensors, etc.), thrusters, and ME. The Propulsion Module also supports the LVA and ASRGs. The ASRG consists of the power sources and the
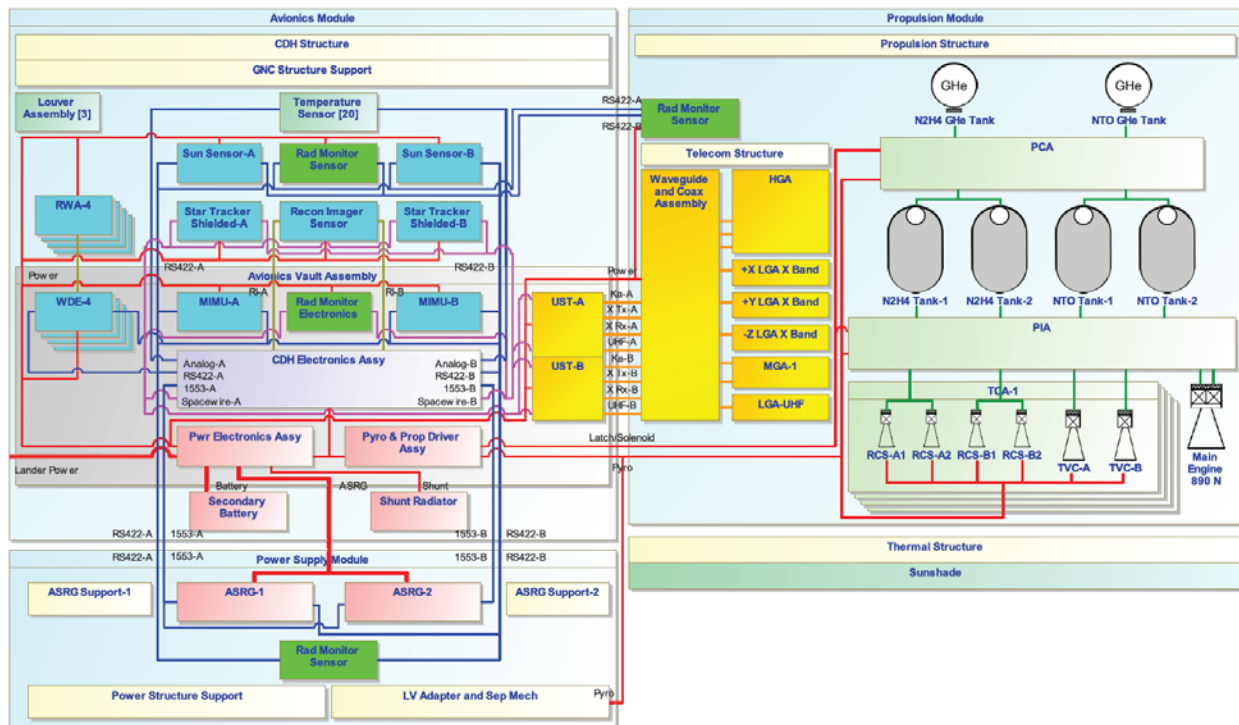
Figure D.2.4-5. The Carrier element block diagram shows the simple interfaces among modules.

control electronics. Some of the boxes (e.g., C&DH) do not show block-redundancy because they are internally redundant.

D.2.4.2.3   Carrier Design Drivers

Table D.2.4-1 shows the design drivers that flow down to the Carrier from the mission design.

The Venus flyby is a driver for the spacecraft thermal design and results in an approach where the spacecraft points the Sun-shade (-Z axis) towards the Sun to shade the vehicle.

During inner solar system cruise, there are two key drivers on the Carrier design. Commanding and telemetry during this phase require an X-band system for uplink and downlink using 4-pi steradian coverage from the LGAs. This type of telecom approach is needed since the spacecraft cannot always point the fixed HGA to Earth because of thermal constraints.

During the outer-solar-system cruise, commanding and telemetry require an X-band system for uplink and downlink using an MGA.

During the outer-solar-system cruise and Jupiter cruise phase, the cold conditions drive the thermal design of the spacecraft. To minimize electrical heater power demand, internal heating from the electronics is captured within the thermal shroud to keep the spacecraft equipment within allowable flight temperatures. External elements will require electrical heaters or VRHUs.

JOI and EOI are fully autonomous critical events that require robust system fault management. A cross-strapped, dual-string architecture allows failures to be isolated so that recovery can occur on the backup hardware. However, most fault-tolerance complexity will be driven by the need to react cautiously to any type of disruption, suspending activity temporarily if needed, yet regaining control and resuming the orbit insertion with appropriate burn corrections for the interruption. This sort of capability is well established, as

demonstrated several times throughout the solar system, including with Galileo at Jupiter.

Since the mission has several trajectory correction maneuvers (TCMs), both deterministic and statistical, the onboard communication system must support Doppler tracking to enable navigation on the ground.

The Jupiter cruise and Europa orbit phases result in a large cumulative radiation total dose of approximately 0.85 Mrad (behind 100 mil Al); this radiation level drives the fault-management requirements to recover and continue science activities after a radiation event (single-event upset [SEU], single-event latchup [SEL], etc.). It also drives the shielding design on the vehicle and the EEE parts selection.

The need for a priori landing site reconnaissance drives several requirements on the spacecraft. To support the RC the pointing stability needs to be very good; the large amount of data collected requires on board storage and the use of Ka-band to downlink the data. The Lander separation drives the need for separation mechanism on the Carrier. The relay function of the Carrier drives the need for data storage in the C&DH, Ka-band to downlink the data, and UHF to receive the Lander data.

D.2.4.3   Structures and Mechanisms—Integrated Spacecraft and Carrier Element

D.2.4.3.1   Key Design Drivers

Launch vehicle minimum first-mode structural frequency requirements for the integrated spacecraft launch configuration:

- Fixed-boundary condition first-mode lateral frequency ≥8 Hz
- Fixed-boundary first-mode axial frequency ≥30 Hz

Table D.2.4-1. The Carrier incorporates design elements that flow down from the mission design driving requirements.

Mission Design	Requirement	System	GN&C	Telecom	Power	C&DH	Prop	Thermal	Mech
Venus flyby	Thermal control							Thermal shade	
Inner solar system cruise	Command & telemetry			X-up/ X-dn with LGA					
	Earth flybys with ASRG	Fault management							
Outer solar system cruise, Jupiter cruise, Europa	Command & telemetry		Sun-sensors	X-up/ X-dn with HGA					
	Thermal control							Thermal shroud/ RHU/VRHU	
JOI/EOI	Critical event	Fault management	Dual-string/ hot sparing	Dual-string/ hot sparing	Dual-string/ hot sparing	Dual-string/ hot sparing	TVC + ME size		
TCM, Europa orbit maintenance	Navigation			Doppler					
Jupiter cruise + Europa orbit	Radiation	Fault management	<300-krad parts	<300-krad parts	<300-krad parts	<300-krad parts			Vault & config
Landing site reconnaissance	High-res imaging & high-volume D/L		Pointing Stability	Ka-down		High data throughput			
Lander separation	Critical event	Fault management							Pyro
Lander relay	Forward/return UHF link			Ka-down UHF-up/dn	Limited to 2 ASRGs	High data throughput			

The Carrier will survive all applicable load cases:

- Random vibration
- Acoustic
- Carrier ME burn
- Separation of the Lander

The Carrier separation mechanism will be designed so that there is no recontact during Lander separation. The separation mechanism will provide a sufficient ΔV to the Lander.

Integrated Spacecraft Configuration

The integrated spacecraft is mounted on the launch vehicle's Marmon clamp via a JPL-supplied LVA cone. The Lander is mounted, with its topside down, to the top of the Carrier with six separation nuts. Attached to the bottom of the Lander is an SRM, which is used during Lander descent. This SRM is also

attached with six separation nuts and is jettisoned during descent. Figure D.2.4-6 shows the integrated spacecraft primary structure and secondary structure in launch configuration.

The overall configuration starts with the Lander on top, followed by the Carrier's Avionics Module, then the Carrier's Propulsion Module. The primary structure of each is based on an aluminum forging that is machined from the outside. After machining, deep stiffening ribs and a floor wall remain. This approach provides for a lightweight, high-strength, and stiff structure that also serves a dual purpose as radiation shielding. When Carrier and Lander are stacked they form a superstructure that is able the meet the Delta IV Heavy launch vehicle's loads and frequency requirements.

All propulsion tanks are supported by com-

- Forged to approximate dimensions and machined
- No new technology required
- Can be broken up into smaller sections as required
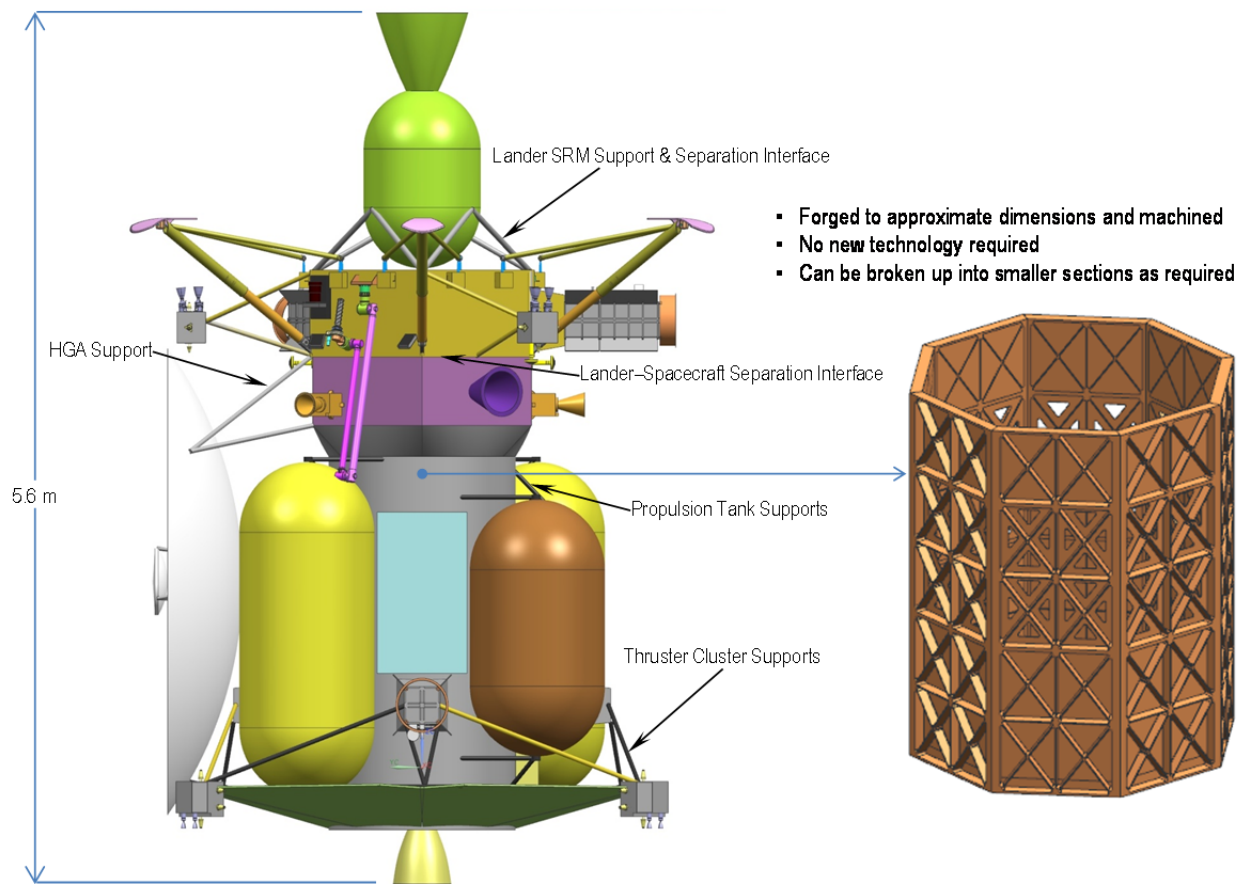
Figure D.2.4-6. Carrier primary structure and secondary supports leverage heritage design techniques.

bined bipod and tripod strut systems. The thruster clusters are supported by tripod strut assemblies.

All brackets, struts, secondary structures, and mechanisms are mechanically grounded to the primary structure. Loads for these appendages are determined using Delta IV Heavy mass acceleration curve (MAC).

D.2.4.3.2   Sizing Analysis

A Carrier primary structure driving-load-case lateral-bending analysis was performed to determine size and thickness for estimating mass. The MAC for the Delta IV Heavy launch vehicle was used to size the secondary structure.

D.2.4.3.3   Equipment Heritage

Europa Carrier structures and mechanisms require no new technology development and are typical with other recent flight missions.

D.2.4.4   Thermal Design

The Carrier thermal design uses, to the fullest extent practicable, waste heat, insulation, and louvers to control temperatures. This approach consumes little to no electrical heater power, is low-mass, and has a flight-proven heritage.

D.2.4.4.1   Key Design Drivers

- Maintain the propulsion system and battery within allowable flight temperature (AFT) ranges of 15°C to 50°C and 4°C to 32°C, respectively.
- Maintain the avionics within an AFT range of -40°C to 50°C.
- Maintain the RC within its AFT limits.
- Accommodate the variation in environmental heat loads from Venus at 0.7 AU to Jupiter at 5.2 AU (i.e., 2.0 to 0.04 Earth Suns).
- Tolerate limited transient off-Sun exposure at less than 1 AU during fault conditions or trajectory maneuvers.
- Minimize replacement heater power at outer cruise and Jupiter.

Figures D.2.4-7 and D.2.4-8 show the primary thermal components of the Carrier. A lightweight thermal shroud surrounds the propulsion tanks and associated plumbing. Consisting of multilayered insulation (MLI) supported by a latticework, this shroud creates a radiative cavity around the tanks. A clearance of 100 mm between the propulsion components and shroud provides adequate view factors for radiation.

Waste heat from the vault and ASRG electronics radiates into the cavity and warms the propulsion system. Openings in the primary structure allow heat to radiate from the vault onto the tanks and into the cavity.

A temperature-regulation system accommodates the variation in environmental loads and internal dissipations. Louvers over external radiators regulate the structure to 40°C producing acceptable vault and propulsion temperatures. Heat from the vault and ASRG electronics, coupled with louvers on the mounting structure, warms the shroud in the cold case and rejects excess heat to space in the hot case, producing acceptable temperatures on the propulsion system and vault.

This system of waste heat and louvers requires no additional electrical heaters for normal operation. With an MLI external area of 26 m^2 and a nominal effective emittance of 0.01, acceptable tank temperatures occur with a 200-W heat flow. During the mission, 260 W is dissipated by the vault and ASRG electronics. Hence, the heat balance is always positive. Survival operation will be studied in Phase A.
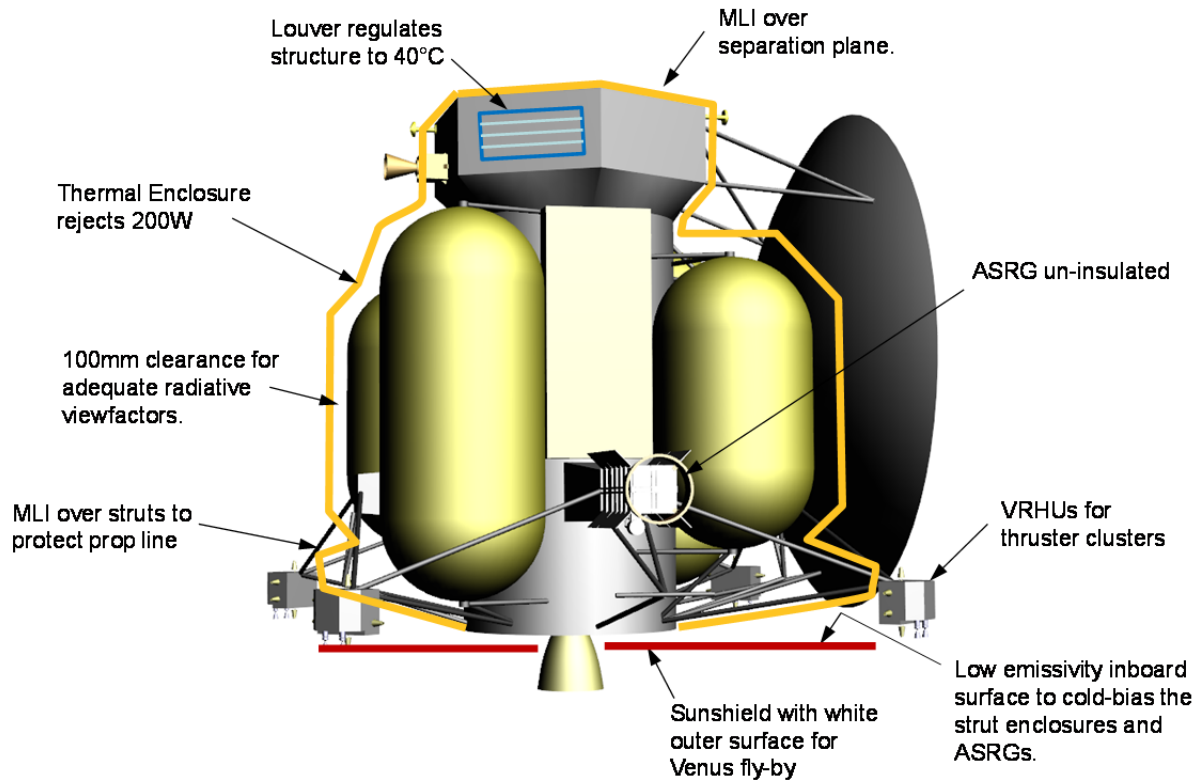
Figure D.2.4-7. Carrier with thermal shroud surrounding propulsion tanks provides thermal control from 0.6 AU (Venus) to 5.5 AU (Jupiter).
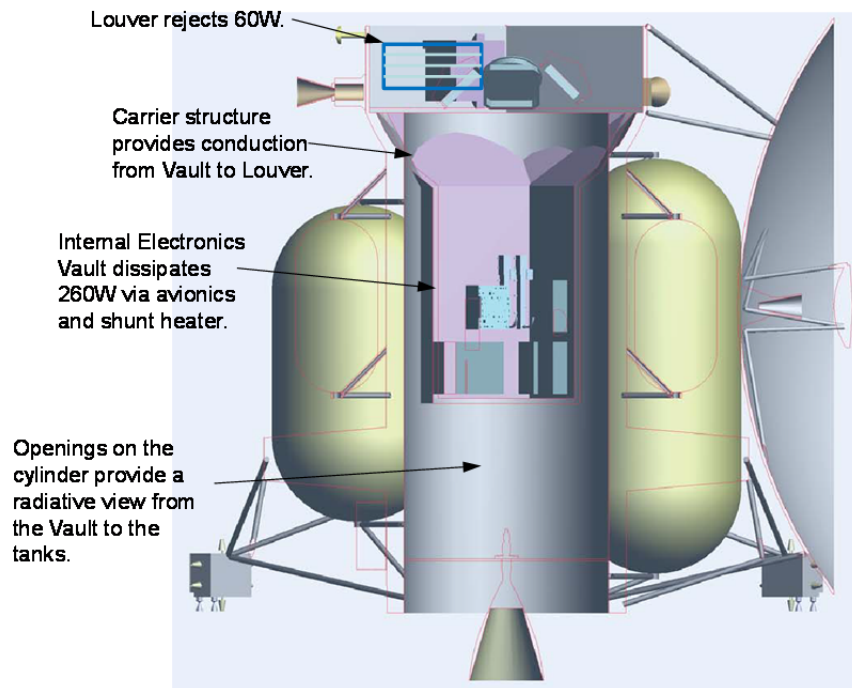

Figure D.2.4-8. Carrier thermal design keeps the propellant warm while not requiring any electrical heaters.

A sunshield protects the Carrier from the high solar loading near Venus. Shading by the sunshield preserves the heat balance on the thermal shroud and louvers. The sunshield features a low emissivity inner surface and clearance to the thermal enclosure. This arrangement cools the thermal enclosure, ASRGs, and propulsion strut enclosures during high solar loading near Venus. If necessary to tolerate a loss-of-attitude fault at Venus, a hybrid MLI layup with five external layers of embossed Kapton will tolerate high exterior MLI temperatures. Off-Sun illumination and the impact on temperatures will be studied during Phase A of the project.

A separate thermal-control zone with a dedicated radiator and louver controls the temperature of the battery. This control is accomplished by piggy-backing the battery to a structure in common with the propulsion system, but biased colder using a dedicated radiator.

Variable radioisotope heating units (VRHUs) control the temperature of the thruster clusters. Local heating from the VRHUs is required due to the remote location of the thrusters. Each VRHU consists of two to three individual RHUs mounted in a rotating cylinder. One half of the cylinder is painted white while the other half is insulated. A bimetallic spring positions the cylinder to radiate heat into the thruster cluster when the cluster is cold, or out to space when the cluster is warm. There are four VRHUs per thruster cluster with a total of ten individual RHUs per cluster. Four thruster clusters yield a total of sixteen VRHUs and 40 individual RHUs. This design tolerates a failure mode where one VRHU is stuck fully open or fully closed. Insulation and low conductance attachments minimize heat transfer to the Lander. Instrument thermal control is individually customized via local radiators and heaters to maintain acceptable temperatures.

Risk exists, as in any thermal-control system, where thermal performance is affected by workmanship. The effective emissivity of MLI

is a notable example. For the Carrier, this risk is mitigated by design and by test. Margin in the active louver system provides tolerance for hardware variations. Also, thermal development tests of the louvers and critical areas of MLI reduce risk to acceptable levels.

D.2.4.4.2   Heritage

The thermal design for the Carrier follows that of Cassini. In the Cassini design, the propulsion system was enclosed in a shroud that formed a radiative cavity. Heat for the Cassini shroud came from radioisotope thermoelectric generators (RTGs), whereas on the Carrier the heat comes from the vault and the ASRG electronics. VRHUs control the temperature of the thruster clusters for both the Cassini spacecraft and the Europa Lander Mission Carrier. HGA shading protected the Cassini spacecraft from solar loading at Venus whereas a sunshield protects the Europa Lander Mission Carrier. Other thermal hardware, such as louvers, heaters, MLI, and platinum resistance thermometers, also have good heritage based on the flight experience of prior JPL missions.

D.2.4.4.3   Assessment of Propulsion Tanks and Lines

Passive thermal control of the propulsion tanks and adjacent lines is by radiation into the thermal cavity. This approach is used on Cassini. At Jupiter, in the worst-case cold condition, thermal equilibrium occurs with a heat flow of 200 W from the inner structure into the cavity and out through the insulation. An initial thermal analysis shows that the propulsion tanks remain within 25°C to 40°C, in compliance with their AFTs, without direct heating or active control. Figure D.2.4-9 shows predictions of the tank temperatures.

D.2.4.5   Carrier Propulsion Module

This Propulsion Module, specifically designed for long-life outer-planet missions, will provide the impulse and reliability necessary to meet the needs of the Europa Lander Mission Carrier element.
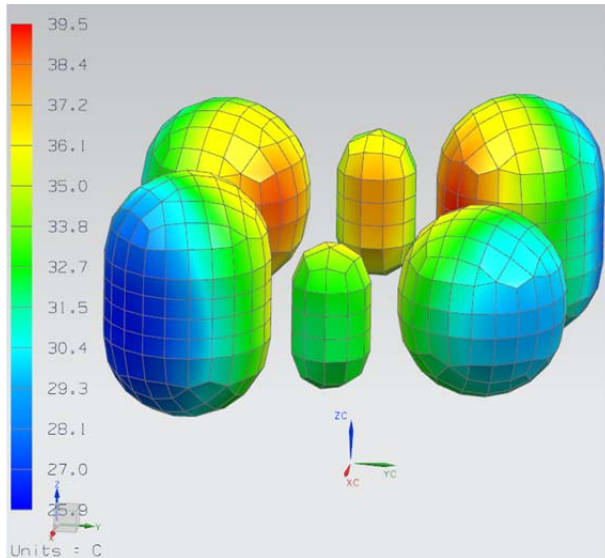
Figure D.2.4-9. Predicted tank temperatures, showing only the tanks. Propellant is kept warm without supplemental electrical heating.

D.2.4.5.1   Propulsion

The Carrier element Propulsion Subsystem is a dual-mode bipropellant system. The propellants are hydrazine (N_2H_4) and nitrogen tetroxide (NTO). The hydrazine fuel and nitrogen tetroxide oxidizer are used by the bipropellant ME, and the hydrazine fuel alone is used by the monopropellant Reaction-Control Subsystem (RCS) thrusters and TVC thrusters. Figure D.2.4-10 shows a schematic of the Propulsion Subsystem.

Design Drivers

The requirements that drive the design of the Propulsion Subsystem are typical of those for outer-planet missions, with the possible exception of the requirement to configure the system to take advantage of the Propulsion Subsystem mass to provide radiation shielding to sensitive electronics. The key driving requirements for the Propulsion Subsystem are to

1. Provide ΔV for maneuvers, including JOI and EOI.
2. Provide thrust vector control (TVC) during ME operation.

3. Provide for attitude control when the spacecraft is not using reaction wheels.
4. Provide for reaction wheel momentum unloading.
5. Configure the system to augment radiation shielding of the spacecraft electronics.

Propulsion Module Configuration

Figure D.2.4-11 shows that the Propulsion Module configuration is based on a cylindrical core structure with the propellant tanks, pressurant tanks, and component plates mounted on the exterior sides of the core structure. This configuration is driven by the necessity to maximize the radiation shielding for the spacecraft electronics, mounted on the Avionics Module and located internal to the Propulsion Module core structure. By mounting the tanks and the propulsion components on the external sides of the core structure, additional shielding is provided for the spacecraft electronics, which are mounted internal to the core structure. Note that the propulsion components' plates are mounted perpendicular to the core structure (see Figure D.2.4.5-2). This mounting configuration is used because there is insufficient real estate to mount the component plates in a more traditional fashion (i.e., parallel) without increasing the length or
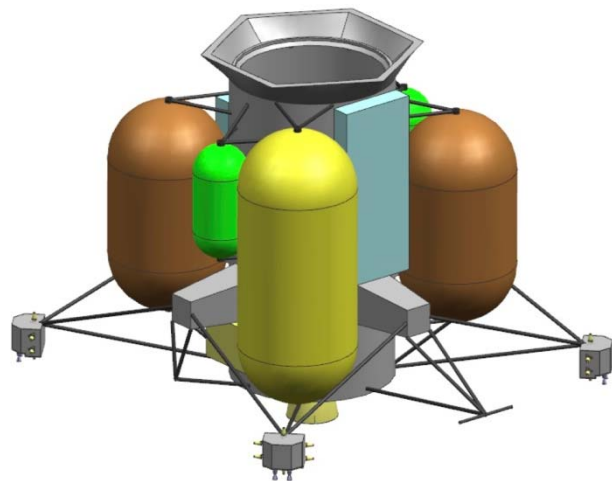

Figure D.2.4-11. Propulsion Module configuration enables parallel development and simplified spacecraft integration & test.**.**
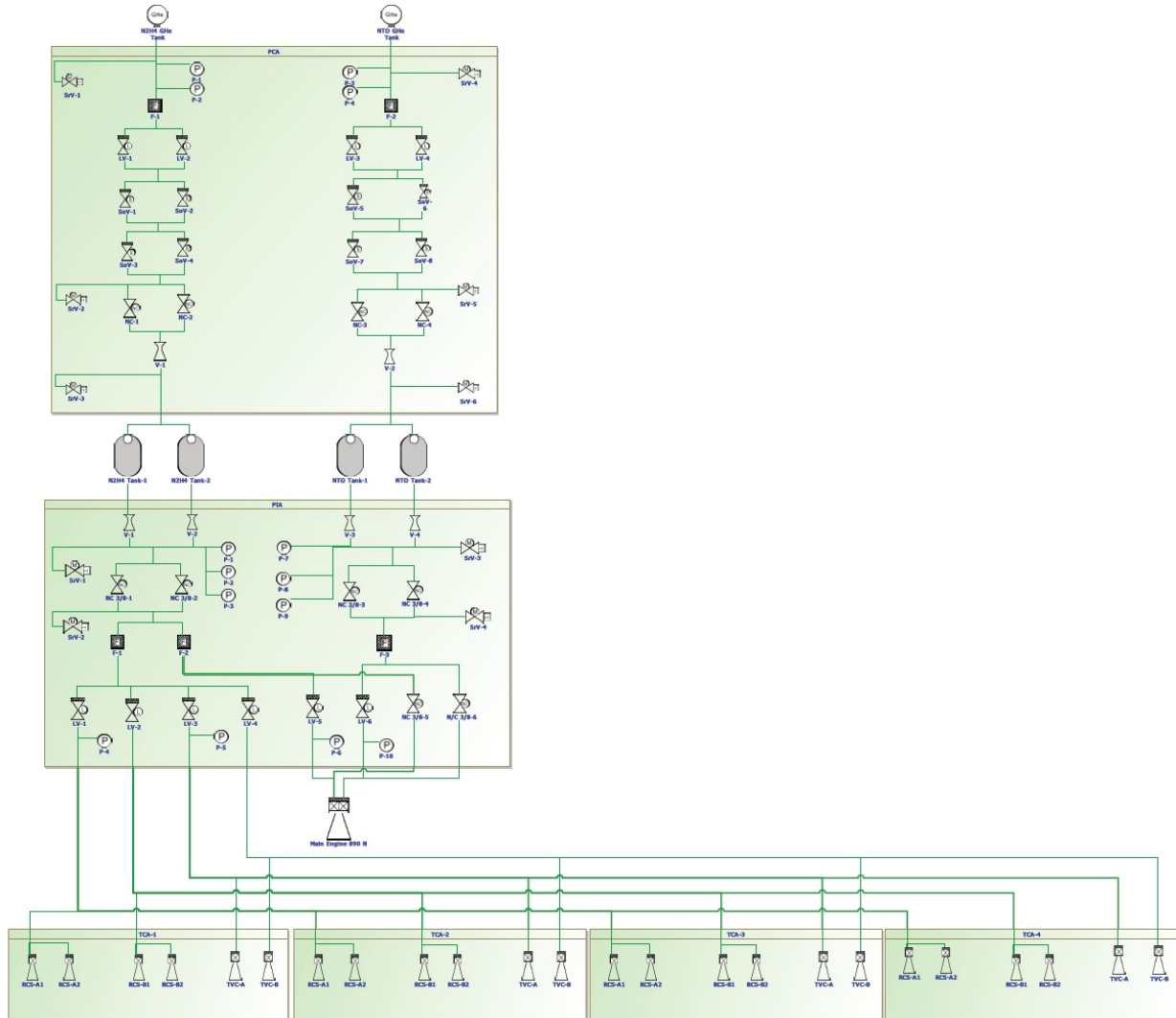
Figure D.2.4-10. Dual-mode, bipropellant Propulsion Subsystem design operates after one failure.

diameter of the Propulsion Module. It was decided not to mount the component plates to an interior wall of the Propulsion Module because of limited accessibility during ATLO.

A single ME, mounted using struts at the bottom of the Propulsion Module and protruding through the Power Source Module, provides for primary ΔV. The RCS and TVC thrusters are mounted on four TCAs, which in turn are mounted on struts extending away from the spacecraft. This configuration is very similar to that of the Cassini RCS. Each TCA contains four RCS thrusters (two primary and two redundant) and a pair of TVC thrusters (one primary and one redundant). The RCS

thrusters are block-redundant, in that there are two strings of eight thrusters. Each string of eight thrusters is isolated by a single latch valve. The RCS thruster configuration provides for coupled thrust about the Z-axis (roll) and uncoupled thrust in pitch and yaw, identical to the Cassini configuration. The spacecraft can be turned to align this axis with the reaction wheel momentum vector in order to minimize ΔV during momentum management. The ME is currently envisioned to be single-string, as has been the case for many previous planetary missions (Galileo, Odyssey, Messenger, etc.). This risk posture will be revisited in Phase A.

Propulsion System Design

Engines and Thrusters. The baselined ME for the Carrier is the Aerojet R-42DM. This engine nominally provides 890 N of thrust. It operates at a nominal mixture ratio of 1.0 and has a minimum specific impulse of 324 seconds. This engine has been development tested and brought to a technology readiness level (TRL) of 6, but has not been qualified for flight. The engine will require a qualification test program for use on the Carrier.

It should be noted that the engine chamber interior wall is coated with a thin layer of iridium, which is required to protect the rhenium chamber from oxidation and which could be subject to micrometeoroid damage. The actual risk of failure and time to failure caused by damage is unknown, and likely indeterminate. The design includes an engine cover, similar in design to the cover used by the Juno spacecraft. The decision to use the engine cover will be revisited during Phase A.

The TVC thruster currently assumed for the Carrier is the Aerojet MR-106 thruster (or equivalent), providing approximately 40 N of thrust. A preliminary analysis has been performed showing that this thruster provides adequate control authority for the vehicle during main engine operation, given different deployment configurations, but with assumptions on balanced propellant flow. Explicit measures to ensure propellant balance will be studied in Phase A. For now, ballast mass is included in the mass budget to keep the dry system center of mass near the symmetry axis of the tanks. The RCS thruster currently assumed is the Aerojet MR-111C thruster (or equivalent), providing approximately 4.45 N of thrust. Both thrusters are qualified for flight and have high heritage.

Pressurization System. The baselined pressurization system allows for independent pressurization and regulation of the oxidizer and fuel tanks. Rather than using a traditional mechanical regulator, this system uses a set of four solenoid valves configured to be parallel and series-redundant (i.e., for a minimum of single-fault tolerance), allowing for electronic regulation using pressure transducer feedback. Flight software would provide closed-loop control using pressure transducers measuring tank pressure. In the present concept, three pressure transducers would be polled to protect from a transducer failure scenario (though further study is required during Phase A to consider common mode issues). There are several advantages of this system over a more traditional pressurization system using mechanical regulators, especially for long-duration outer-planet missions:

1. Separate pressurization and regulation of the oxidizer and fuel tanks eliminates the risk of propellant vapor mixing in the pressurization system. This concept also eliminates the need for numerous check valves and pyrovalves for vapor isolation, reducing dry mass.
2. Elimination of the mechanical pressure regulator significantly reduces the risk of regulator leakage. The series-redundant solenoid valves are much less susceptible to leakage than are mechanical regulators.
3. The design allows for active control of the oxidizer and fuel tank pressures. This capability is advantageous because the oxidizer-to-fuel mixture ratio can be adjusted during the mission. This adjustability allows for more accurate control of mixture ratio, which in turn allows a reduction of the propellant reserves required to account for mixture ratio uncertainties.

The schematic in Figure D.2.4-5 shows that the quad-redundant solenoid valves are isolated above by parallel redundant, high-pressure latch valves and below by parallel redundant, normally closed pyrovalves. The pyrovalves would remain closed until first use of the regulating solenoid valves is required.

Systems similar in concept to this have been used in the past on other spacecraft (e.g., MiTEx Upper Stage, Clementine, GeoLite, and Orbital Express).

Propellant and Pressurant Tanks. The propellant tanks are sized for a total propellant load of 4302 kg. Table D.2.4-2 shows the rack-up of propellant, including residual and ACS propellant. Cylindrical tanks 89.15 cm in diameter were selected to allow the use of existing forging designs used to manufacture the ATK P/N 80399 (or equivalent) propellant tank. Two tanks are used for fuel and two tanks are used for oxidizer. The propellant tank designs will maintain a minimum ullage volume of six percent and will require a unique Propellant Management Device (PMD) design. The PMD must be designed to ensure that the fuel and oxidizer loads are evenly distributed between the tanks in zero G by use of surface tension effects. Furthermore, the PMDs must be designed with bubble points high enough that the first tank to drain will not allow helium pressurant to enter the propellant feed system. This requirement also places constraints on the allowable pressure drops in the portions of the fuel and oxidizer feed system between the tank outlets and the portions of the feed system common to both tanks.

The pressurant tanks are essentially off-the-shelf tanks and have not been optimized for the current propellant load. The pressurant tank sizing will be optimized as the design matures.

Propellant Isolation. The propellant tanks are

isolated from the thrusters using parallel redundant, normally closed pyrovalves and low-pressure latch valves. The design provides sufficient mechanical inhibits to meet KSC launch safety requirements.

Careful design of the venturis downstream of the tanks will be necessary in order to limit preferential draw of propellant from one tank during maneuvers. As previously discussed, the propellant tank PMDs will be designed to maintain even distribution of the propellant in zero G and to prevent gas ingestion when one tank empties. It may be necessary to take more positive measures to prevent propellant transfer, such as the addition of latch valves to control which propellant tank is drawn from during maneuvers, but this complexity is highly undesirable. Further detailed analyses will be required before this design concept can be finalized.

Heritage

The majority of the components used in the Carrier propulsion system is flight-qualified and considered off-the-shelf, including the RCS thrusters, TVC thrusters, service valves, pressure transducers, filters, and latch valves. As discussed above, the baselined ME has not been previously qualified or flown, and this risk is recommended for early retirement by conducting a qualification test earlier in the program than might otherwise have been considered. Regarding the propellant tanks, it is the study team's intent to size them based on a heritage design that makes use of qualified hemisphere forgings. The current design makes use of an 89.15-cm-diameter tank, but will likely require a change in length of the cylindrical section as well as the new PMD design discussed above. The propellant tanks will therefore require a new qualification test program. The study team is taking a heritage approach to the pressurant tanks, using a qualified design that best meets the requirements for the Europa Lander Mission.

Table D.2.4-2. Conservative sizing of propellant tanks: Maximum propellant load case is utilized.

Required Propellant	Mass (kg)
Propellant load for ΔV	4057
Hydrazine for TVC	100
Allocation of ACS propellant (N_2H_4)	40
Residual andHhold up (2.5%)	105
Total Propellant Load	**4302**
Pressurant	6
Total Loaded Fluids	4308

The pressurization system, which makes use of electronic regulation, will need to go through a program that develops and qualifies it as an integrated system, including the propulsion hardware, controller, and flight software.

D.2.4.5.2   Propulsion Module Structure

The Propulsion Module (Figure D.2.4-11) supports the propellant and pressurant tanks, attitude-control thrusters, propellant-isolation assembly (PIA), pressurant-control assembly (PCA), and ME. The propulsion tanks are supported by bipod and tripod combinations and are attached to the primary structure. The ME is attached at the bottom and extends through and below the Power Source Module. Four GN&C thruster clusters are supported at the ends of four tripods sized for adequate control authority and minimal plume impingement. The PIA and PCA are attached together, back to back and parallel to each other. The PIA/PCA assembly is in turn attached to the Propulsion Module's primary structure.

The Propulsion Module's primary structure has triangular holes in the wall at the location where the warm avionics have a radial view to the propulsion tanks. These holes allow for a direct radiation path to the tanks. In this region, the primary structure's wall thickness is increased to compensate for the holes. The necessary radiation shielding is still maintained due to the position of the tanks and the vault's wall thickness.

In addition to supporting the propulsion hardware, the Propulsion Module structure provides mechanical mounting provisions for the HGA and ASRGs, and provides the interface to the LVA. A cylindrical aluminum skin-and-stringer construction similar to that used on the Cassini Propulsion Module is envisioned.

D.2.4.5.3   ASRG

ASRG Functional Description

The Carrier power source is an Advanced Stirling Radioisotope Generator (ASRG). The ASRG provides power to an industry standard defined 22 to 36-V power bus. The power bus architecture is a direct energy transfer architecture, with the power source output connected to the Power Subsystem in the Avionics Module. The Power Subsystem electronics provides the power bus voltage regulation.

Power Source Design Drivers

The key driving requirements for the power sources after Lander separation are:

1. Provide 166 W at EOM, assuming a single Stirling engine failure in one ASRG.
2. Provide a constant power over the nominal power bus voltage operating range of 22 to 34 V as defined at the power source output.
3. Survive with a power bus voltage over the 34 V and less than 40 V for an indefinite period of time.
4. Provide a diminished power for the power bus voltage less than 22 V to support a bus overload recovery.

The power source is the combined contribution of two ASRGs for the Carrier (after Lander separation).

For the integrated spacecraft (Carrier and Lander) the power source is the combined contribution of two ASRGs on the Carrier and two ASRGs on the Lander. During that stage of the mission the only change to the requirements is:

1. Provide 396 W at EOM assuming a single Stirling engine failure in one ASRG.

Each ASRG (Figure D.2.4-12) consists of two General-Purpose Heat Source (GPHS) modules, two ASRG Stirling converters (ASCs), a generator housing assembly (GHA), a shunt dissipater unit (SDU), associated cables, and an ASC controller unit (ACU).

The GPHS contains plutonium dioxide fuel pellets and is designed to meet all safety and handling requirements. The GPHS produces
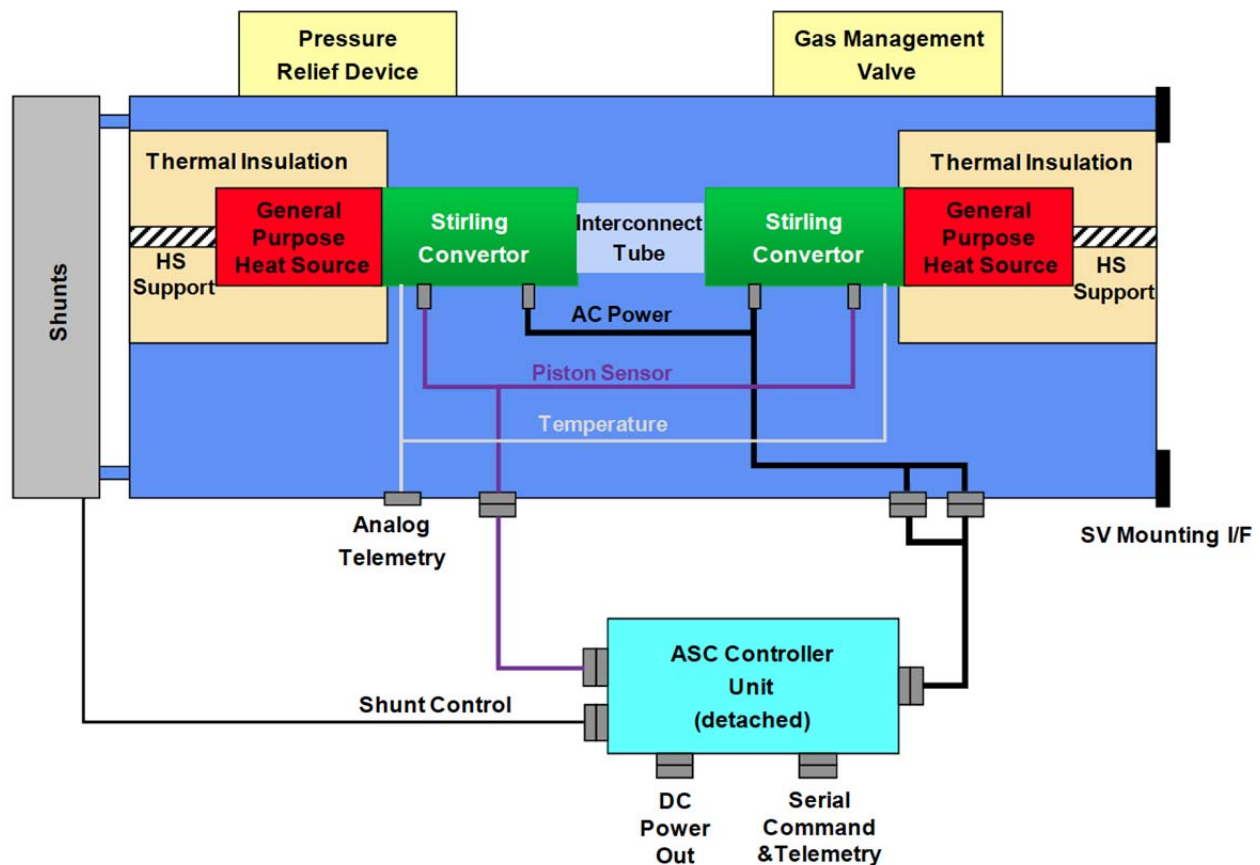
Figure D.2.4-12. This ASRG block diagram includes all functional elements that make up the ASRG, including the detached controller that provides the electrical interface with the spacecraft.

from 244 Watts thermal (W_t) to 258 W_t at encapsulation when the fuel mixture is set in the pellet and placed in the module. From the point of encapsulation, the GPHS thermal output degrades with the radioactive decay rate of plutonium-238, which is approximately 0.8% per year. It has been assumed that the average GPHS encapsulation will be 3 years before launch.

The ASC converts the thermal energy from the GPHS to AC electrical current using a piston and linear alternator. The ACU rectifies the AC power to DC power and provides it to the power bus with a constant power I-V curve over the power bus voltage range controlled by the spacecraft. The constant power I-V curve allows for more than one ASRG to be con-

nected to the same power bus and share the power.

The ASRG protects itself if the bus voltage goes outside of the specified range of 22–34 V at the ASRG output. The ACU disengages the output from the power bus and shunts the power to the attached radiator if the bus voltage exceeds 35 V ±1 V. The internal ASRG shunt regulator is independent of the Power Subsystem shunt regulator used to regulate the power bus voltage. The ASRG shunt radiator is on the outboard end of the GHA and is used only for the off-nominal bus voltage. The power system maintains the bus voltage range at less than 34 V at the ASRG interface to prevent the disengagement. The ASRG reengages once the bus voltage drops back into the range. The ASRG provides a current limited to 3.5 A if the bus voltage drops below 22 V,

enabling the system to recover by charging the battery.

The ACU is detached from the GHA (Figure D.2.4-13) and mounted on the inside of the Power Source Module primary structure.

The ACU is single-fault-tolerant with an N+1 internal voting architecture and two 1553 data bus interfaces (Figure D.2.4-14). The ACU needs to be within 3 meters (by cable length) due to impedance constraints from the controller. The ACU also needs to be greater than 1 meter away (by geometric distance) to tolerate self-generated radiation levels.

The ACU has internal fault managment to switch automatically to the spare controller board with the detection of a fault. The ACU is shielded to 50 krad with an RDF of 2 at the component level, including radiation from the ASRG as well as from the environment.

ASRG Performance

The ASRG output power is a function of time and environment. The power graphs below show power output of the four ASRGs that includes the Carrier and Lander combined source, with degradation due to GPHS decay as a function of the time from encapsulation,

3
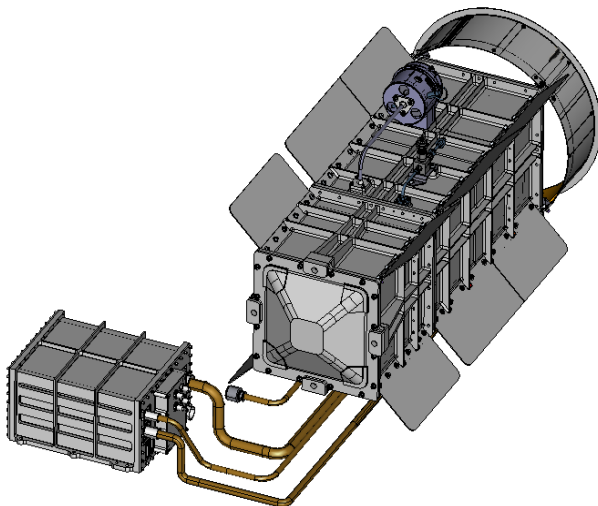
Figure D.2.4-13. ASRG CAD model shows the detached controller with cabling and outboard shunt radiator.
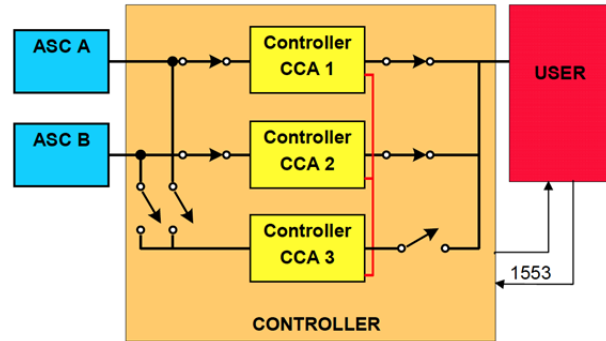
Figure D.2.4-14. ASC controller unit block diagram shows the spare controller # 3 to which the internal fault management switches with the detection of a failure.

and assuming each GHA has a direct view to space (Figure D.2.4-15) after launch. For a single ASRG, the total power CBE is with the nominal specified GPHS thermal output of 250 W_t at encapsulation. The total power specification is from the ASRG user guide with a beginning-of-mission (BOM) power at 130 W, failure of a single Stirling converter shortly after launch, and 1% degradation per year. The lowest expected value (LEV) is with the minimum specified GPHS thermal output at 244 W_t at encapsulation, 1% degradation per year, and failure of a single Stirling converter after launch. The main difference between the Department of Energy (DOE) specification and the Europa Study Team's LEV is that we start the 1% degradation per year 3 years prior to launch (assumption) at the average GPHS encapsulation date. With the duration from encapsulation to EOM at 11 years, for the integrated spacecraft prior to Lander separation we expect at least 396 W at EOM (from four ASRGs with one Stirling engine failure). For the Carrier element after Lander separation we expect at least 166 W at EOM for two ASRGs with one Stirling engine failure.

The curve above assumes a direct view to space with a sink temperature equivalent to 4 K. The power output graph below shows the degradation as the sink temperature increases due to the environment (Figure D.2.4-16).
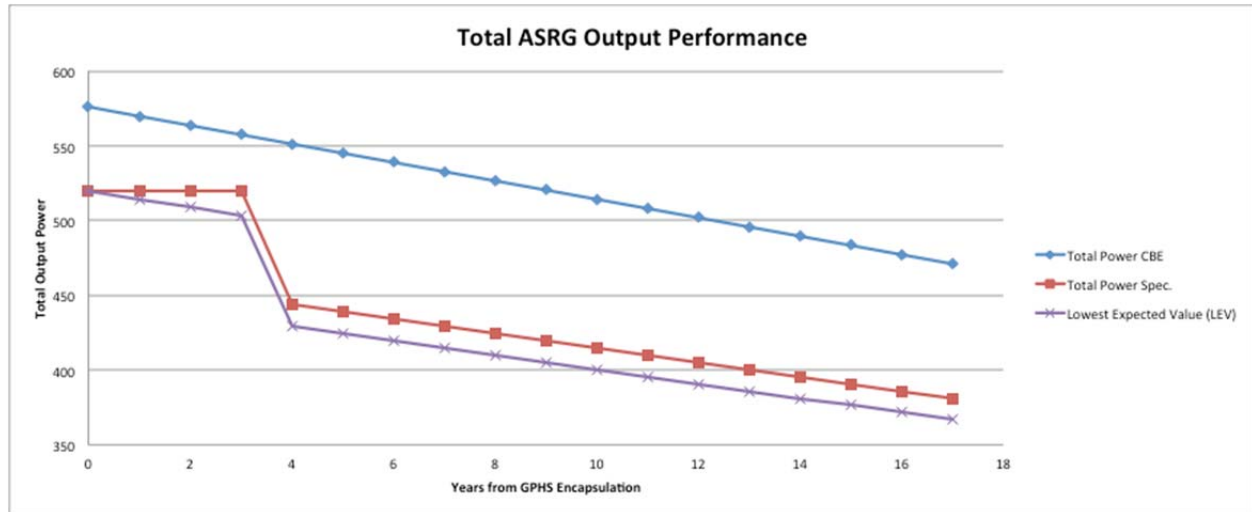
Figure D.2.4-15. Conservative assumptions were used for estimating the ASRG power output at EOM. From the comparison of the ASRG output CBE to the specification and the LEV with a failure after launch, the LEV degrades performance from GPHS encapsulation; however, the specification defines BOM after launch and degrades from that point on.

The spacecraft configuration uses the HGA and thermal blanket envelope to shade the ASRGs from the Sun within 1 AU. For the changing environment of launch, inner cruise, and Venus gravity assist, a command is sent to the ASRG to adjust the internal operational set point to make sure the ASRG is safe from over temperature which will impact the output power. This operation is independent of the power bus voltage set points controlled by the
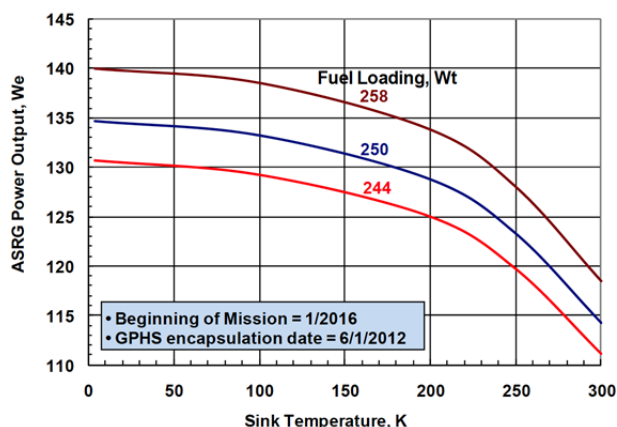
Figure D.2.4-16. The spacecraft design maximizes the ASRGs' view of cold space to maximize power output. ASRG output power vs. sink temperature shows that depending on the environment the output power will degrade.

spacecraft. The spacecraft has adequate power margin for the expected environmentally impacted mission phases. The operation of the ASRG is covered in the ASRG Users Guide (Lockheed Martin 2011).

The ASRGs have two opposing advanced Stirling converters (ASCs). To counter vibration, they are paired in an opposing configuration and tuned through active control by the ACU. As long as both ASCs are working, the ACU controls the phase to reduce the vibration. If an ASC fails, the mechanical interface must dampen or counter the resulting vibration from operating a single ASC.

In the present concept, compression spring assemblies are assumed, oriented parallel to the long axis of the ASRG. These can be tuned to couple poorly with the ASC's frequency of 102 Hz, while still ensuring margin against launch accelerations. However, other ways to accomplish isolation have been identified. These would need to be studied in detail during Phase A.

In Phase A we will examine in more detail the stand-alone testing, handling, and installation of the ASRG on the spacecraft, including

spacecraft accommodation through launch before the unit has a direct view of space.

D.2.4.6   Avionics Module

The Avionics Module concept results in radiation shielding that enables the use of standard aerospace industry radiation-tolerant parts.

Avionics Module Overview

The key design goals for the Avionics Module are

- Modular design for parallel I&T with Propulsion Module and Lander
- Radiation vault to shield a majority of the spacecraft electronics
- Simple interfaces with Propulsion Module and Lander

Figure D.2.4-17 shows the configuration of the Avionics Module. It consists primarily of two separate entities: the UES and the radiation vault, or simply, just the vault.

Figure D.2.4-18 shows the system block diagram of the Avionics Module. The red interfaces are 28-V power; the olive/magenta interfaces are data; and the gold interfaces are RF.

Inside the vault are the C&DH electronics (this box is internally redundant), WDE, power electronics (this box is internally redundant), pyro/propulsion drive electronics (this box is internally redundant), two block-redundant IMUs, and two block-redundant USTs. In the UES are the RC and shielded camera electronics. Also in the UES are the following GN&C components: RWAs, Sun-sensors, and SRUs.
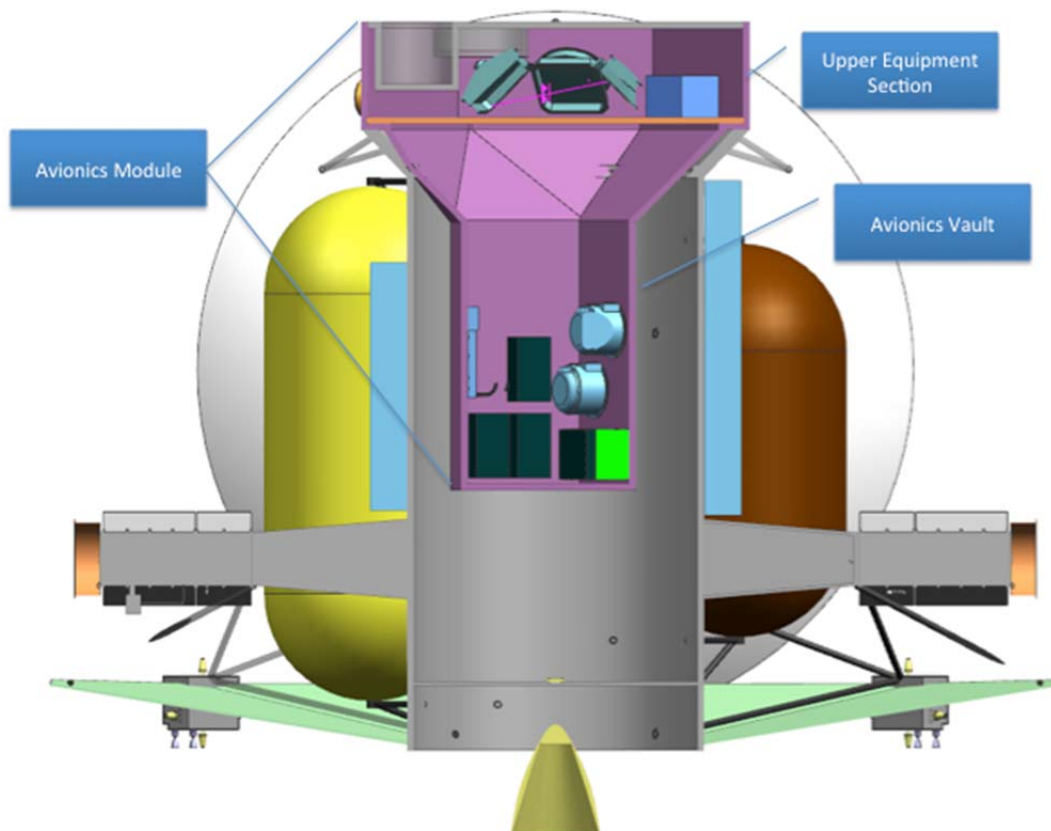

Figure D.2.4-17. The two assemblies of the Avionics Module (UES and radiation vault) are configured for simple interfaces to enable parallel integration and test.
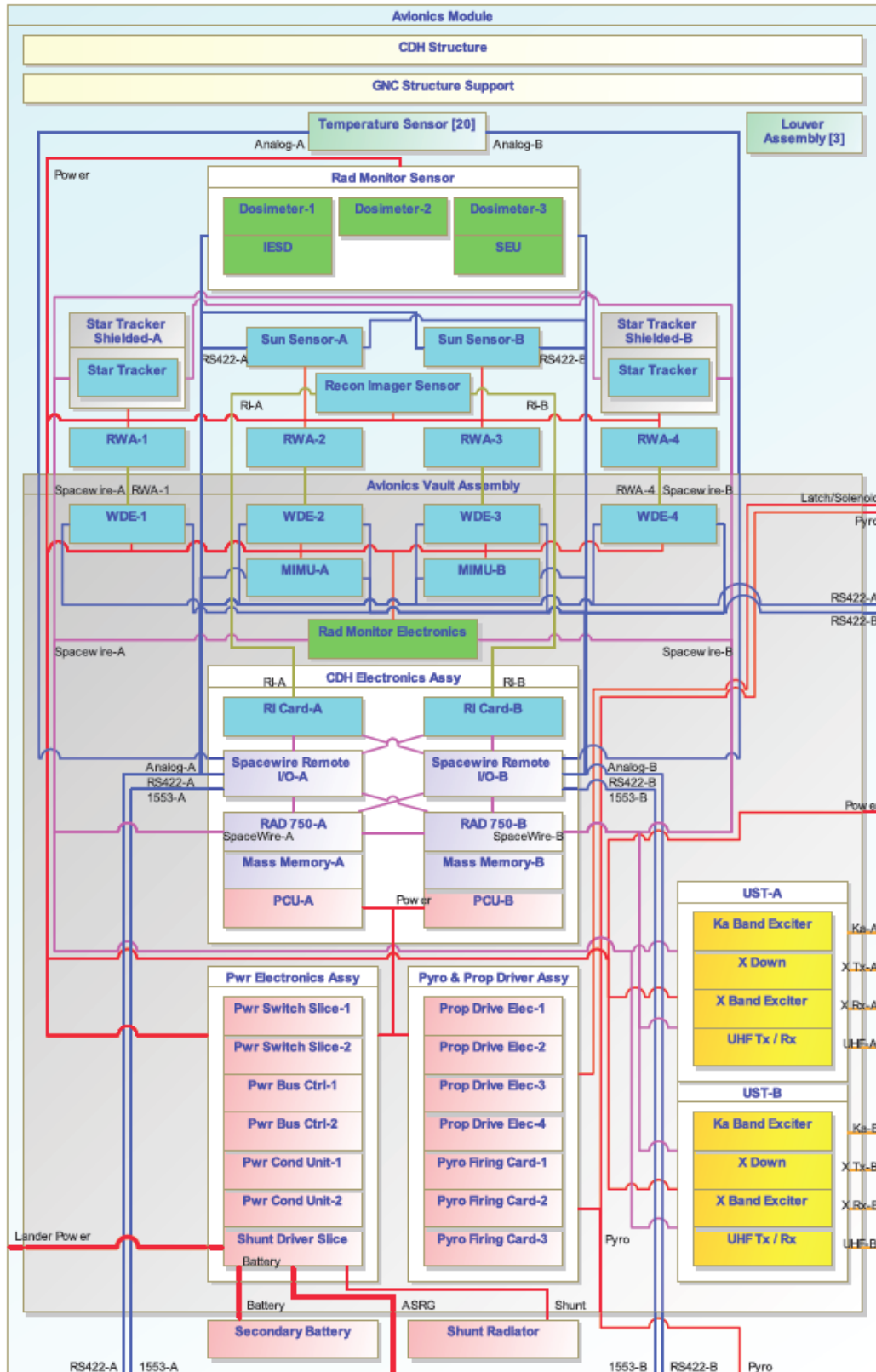
Figure D.2.4-18. A majority of the spacecraft electronics is protected in the radiation vault.

All the elements outside the vault are individually shielded for total-dose radiation; in the case of camera and star-tracker detectors, the shielding also mitigates the effect of the electron flux. The Power Subsystem components outside the vault are the shunt radiator, battery (internally redundant), and ASRG control electronics. The Telecom Subsystem components outside the vault are the TWTAs, coax, waveguide, switches, and antennas configured in a single-fault-tolerant configuration for Ka-band and X-band communication.

D.2.4.6.1　Telecom Subsystem

The Telecom Subsystem performs a triple role for the Carrier:

a) Two-way communications with Earth,
b) Earth-to-Carrier Doppler and ranging to support navigation and precision OD
c) Relay communications with the Europa Lander

Design Drivers

There are a number of driving requirements for the subsystem. It must accept uplinked commands through all postlaunch mission phases as well as send to Earth engineering telemetry and science data. Key X-band data rates required through the DSN 34-m subnet are

- Engineering telemetry: ~2 kbps
- Uplink commanding: ~1 kbps
- Safe mode commanding: ~7.8 bps
- Safe mode telemetry: ~10 bps
- Science and landing site engineering data return: ~75 kbps (thruster pointing)/129 kbps (reaction wheel pointing)
- Doppler 0.1 mm/s for precision OD
- Single-fault tolerance
- Lander + Carrier data minimum volume: 12.6 Gbit (Lander 4.6 Gbit; Carrier 8 Gbit)
- Total mission capacity via X-band link: 83 Gbit

Implicit in these requirements is communications with the Deep Space Network (DSN)

34-m subnet for routine communications and the 70-m subnet (or arrayed 34-m antenna) for emergency/safe mode communications.

For relay communications with the Lander, the driving requirements are

- Science and engineering telemetry: multiple hundreds of kilobytes per second (multiple factors affect this)
- Forward Link commanding: ~75 kbps (thruster pointing)/129 kbps (reaction wheel pointing)
- Baseline Science Return: 4.6 Gbit (mission total)
- Total Relay Capacity: 33 Gbit (30° elevation case)
- Delay Tolerant Networking (DTN)
- Adaptive Data Rate (ADR) capability

Subsystem Features

The implementation of the Telecom Subsystem includes X-band uplink and downlink capabilities as well as a Ka-band downlink. Ka-band downlink enables the mission to meet relay data volume requirements concurrently with stringent requirements for DC power. While the downlink data volume requirements could be met with X-band alone (assuming a much more powerful X-band TWTA), a trade study between available DC power and science data volume return informed the selection of a more DC-power-efficient architecture for high-rate science data. For the Europa Lander Mission, the use of Ka-band for high-rate science downlink directly lowers the number of ASRGs required to meet mission objectives.

The Telecom Subsystem features a 3-m-diameter X/Ka-band HGA, three LGAs, an MGA with dual polarizations, redundant 35-W (RF power) Ka-band TWTAs, redundant 20-W (RF power) X-band TWTAs, redundant USTs, and a complement of microwave waveguide and coax elements. The USTs are X-band uplink and downlink capable as well as being Ka-band downlink capable. There is no capability for Ka-band uplink. Additionally, the

USTs are UHF-capable for relay operations with the Lander.

The Telecom Subsystem is also required to be single-fault-tolerant. This requirement drives the Telecom Subsystem architecture to include redundant transponders (the UST), redundant X-band and Ka-band TWTAs), a complex waveguide transfer switch (WTS) network, and a set of LGAs and MGAs. One X-band LGA and the MGA are tolerant of a single WTS failure. Even though there is a single HGA, the HGA features the capability of two downlink polarizations for fault-tolerance to a single failure in the Telecom Subsystem's transmitter/receiver hardware chain. Additionally, the UST provides a redundant UHF relay capability through a UHF up/down slice.

Block Diagram

As shown in the Telecom Subsystem block diagram (Figure D.2.4-19), the equipment configuration is based upon many years of deep-space communications heritage. For example, the -Z LGA is fault-tolerant to a single WTS failure; this concept provides a robust fault-tolerance posture for communications during the inner-cruise portion of the mission when the spacecraft is required to use its HGA as a sunshield. The LGA configuration enables communications through all cruise periods out to approximately 2 to 3 AU from Earth after which the MGA takes over the safe-mode and general cruise communications. Ka-band downlink redundancy is provided through the use of redundant hardware chains and downlink antenna polarizations. This simplified architecture promotes a more robust system fault-tolerance than could be achieved with the inclusion of an additional WTS to switch between the redundant downlink TWTAs. Similarly, for the X-band uplink an RF hybrid is used (HY2) in place of a WTS. This choice alone eliminates a potential single-point failure in the critical X-band uplink path. Similarly, the MGA has dual polarizations that enable single-fault-tolerant safe-mode communications at Europa. UHF relay communications is through a UHF slice
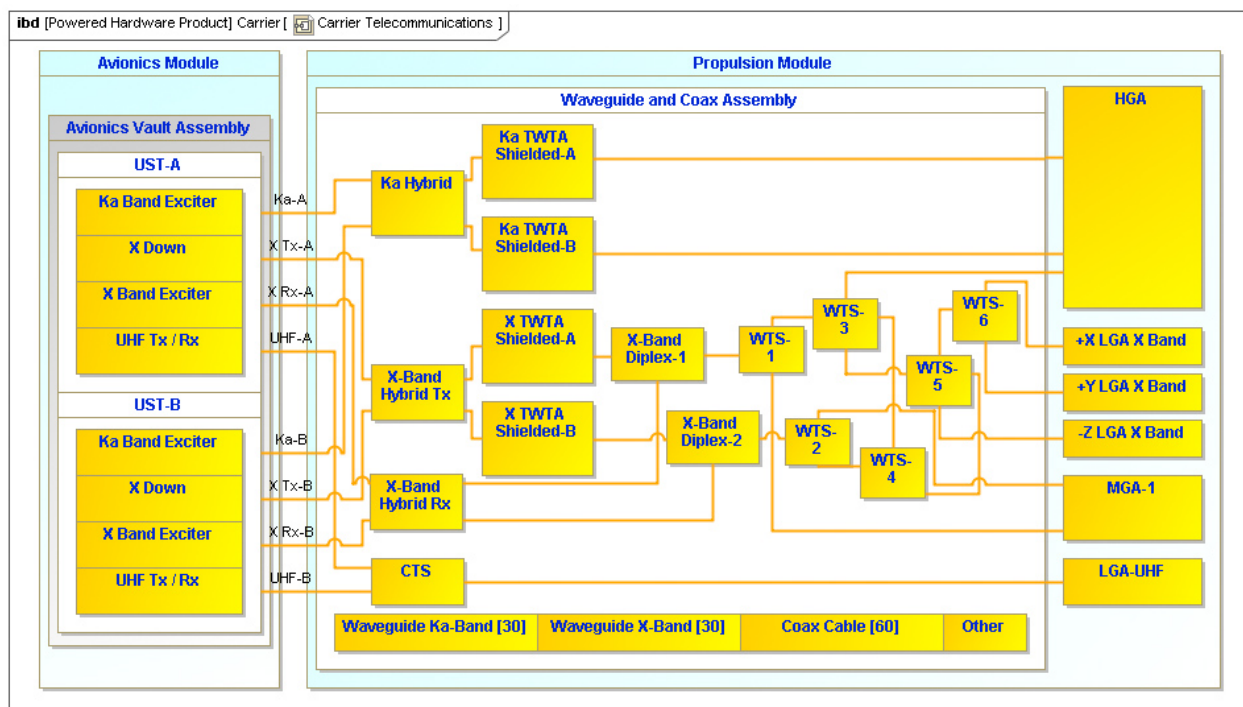

Figure D.2.4-19. The Telecom Subsystem provides robust fault-tolerance through a simplified architecture that minimizes potential for single-point failures.

within the UST. A single UHF Helix LGA provides the relay communications path. Common to the X/Ka/UHF links is the digital baseband processing module (DBPM). The DBPM is the same digital backend used on the Lander UST thus providing maximum relay compatibility. Overall the Telecom Subsystem presents a robust fault-tolerant and low-risk posture for the mission.

Equipment Heritage

Hardware heritage comes from a number of previous missions. The HGA will be similar to the Juno HGA, but scaled up from Juno's 2.5-m-diameter HGA to 3 m. The Europa Lander Mission's HGA will leverage technology developed for the Juno HGA reflector (Figure D.2.4-20) to meet the surface-tolerance requirements for precision Ka-band pointing and efficiency.
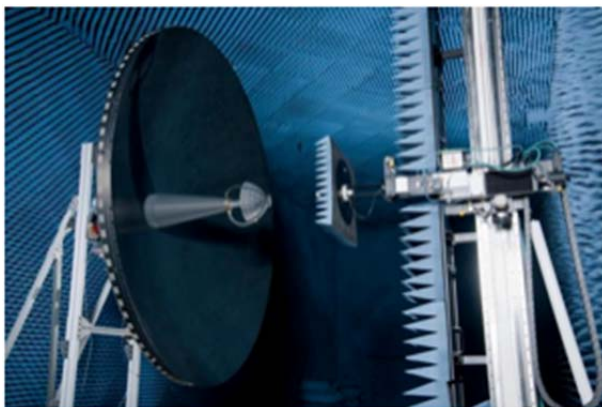
Figure D.2.4-20. Juno's 3-m HGA (X/Ka-band) provides the basis for the Europa HGA.

The Juno HGA optics will be redesigned to improve Ka-band performance for the Europa Carrier's high-rate downlink communications requirements.

The TWTAs have heritage from multiple JPL missions: Juno, Dawn, and MRO (X-band) and Kepler (Ka-band). A good example here is the X-band TWTA for the Dawn mission, shown in Figure D.2.4-21. We propose to leverage a long history of downlink TWTAs designed specifically for the requirements of deep-space missions.
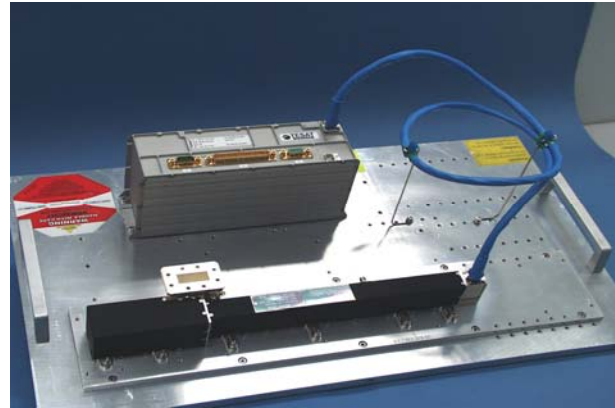

Figure D.2.4-21. Candidate X-band TWTA (flown on MRO, MSL, and Dawn).

We propose to use universal space transponders (USTs) to provide the mission-critical uplink and downlink function. The USTs have heritage from the Electra Payloads onboard MRO and MSL (Figure D.2.4-22), as well as years of experience with deep space communications hardware in the Small Deep Space Transponder. The UST acts as the relay agent between the DSN and the Europa Lander.

For UHF relay communications, redundant USTs each can deliver UHF communications through a coaxial transfer switch (CTS) to a single UHF helix antenna. The UHF antenna would be similar if not identical to those flown on MRO, Odyssey, or MSL. This antenna is fixed to the spacecraft body and can be either nadir pointed (no spacecraft target slew) or target pointed at the Lander (spacecraft slew during relay communications passes). Target pointing can yield a modest increase in relay throughput; determinations for operations concepts such as this are made in mission Phase B.

Characteristics and Sizing

The Telecom Subsystem downlink data rate must be at least 75 kbps during relay operations. The telecom link budget is designed to meet this requirement with the parameters shown in Table D.2.4-3.

Figure D.2.4-22. The Electra Payload, as shown on MRO, provides the basis for UST Relay Communications for the Europa Lander..

The HGA is body-fixed to the spacecraft and requires a ≤1.7-mrad pointing accuracy to meet communications throughput requirements post–Lander separation. The 1.7-mrad pointing requirement is met through thruster control; reaction wheels are not required. Prior to Lander separation, with reaction wheel control the link throughput rate can be increased to approximately 129 kbps. This supports the reconnaissance downlink requirements.

We've taken a conservative approach with the telecom link by requiring 3 dB margin minimum and by making conservative estimates of individual contributors to the link. Parameters such as RF losses in the downlink path, DSN station performance due to low station elevations, link degradation at low Sun–Earth pointing (SEP) angles and Jupiter's hot-body noise at Ka-band are all taken into account. Overall, we propose very conservative and robust X-band and Ka-band communications links.

The LGA complement provides full 4π-steradian coverage; this configuration

Table D.2.4-3. Conservative margins utilized to size Carrier X-band Telecom Subsystem.

Parameter	Required Capability	Notes
Throughput Rate (worst case)	75 /129 kbps	Average = 1.2 × worst case relay requirement/ reconnaissance requirement
OD Residual Doppler	≤0.1 mm/s @ 60-second integration	Met with Two-Way Coherent Mode
TWTA RF Power	35 W (Ka), 20 W (X)	2× for Power Dissipation
HGA Diameter	3.0 m	Body-fixed HGA, 60% efficiency
HGA Pointing Error	≤1.7 /1.0 mrad	Thruster control (post–Lander separation)/reaction wheel control (pre–Lander separation)
DSN Weather	90% cumulative dist.	
Canberra Elevation	20°	Worst-case, fixed
Earth S/C Range	6.5 AU	Maximum mission design
Hot Body Noise	16 K	About 0.6 dB loss
Turbo Coding	Rate=1/6, 8920-bit frame	
TWTA to HGA Losses	2 dB	Conservative estimate
Link Margin	3 dB	Per Institutional guidelines
SEP Angle	20°	Worst-case assumption
Operational Configuration	X-band up, Ka-band down	X-band downlink for safe mode, cruise Ka-band for Science/Eng Tlm return at Europa X-band uplink for all uplink & forward-link UHF relay ops
Hardware Configuration	X-band up, X/Ka-band down 3 LGAs, MGA, HGA, TWTAs	

enables command uplink at any spacecraft attitude unless the line of sight to Earth is blocked, which occurs only for brief episodes. Spacecraft communications during the inner cruise portion of the mission (<1 AU solar distance) use a single-fault-tolerant LGA (-Z LGA). The distances to Jupiter, however, prevent LGA communications at the required safe mode rates. To meet safe mode communications rate requirements, an MGA is needed. All high-rate communications are performed through the HGA. Turbo coding at rate = 1/6 is also part of the baseline communications architecture.

D.2.4.6.2　Power—Integrated Spacecraft and Carrier Element

The Carrier Power Subsystem electronics and energy storage provide the power bus regulation and distribute power to the loads. The Power Subsystem operates in two configurations throughout the mission.

The first configuration is the combination of Carrier and the Lander. This configuration is used for all mission phases until the Lander separation in Europa orbit. The Carrier Power Subsystem will work with the Lander Power Subsystem to provide power bus regulation across the interface of the two elements. The power bus is connected between the two elements through a set of power switches that enable the power buses to be connected together before separation. The switches are on each side of the separation connectors to protect each power bus after the separation when the cables are cut.

The second configuration is the Carrier alone without the power from the Lander. The Carrier Power Subsystem operates with half of the power to support the post-separation operation. Post-separation is the defining case for sizing of the power source and energy storage with a one-time deep discharge to capture an image of the landing site.

Power Driving Requirements for Pre- and Pos-Separation

1. Be single-fault-tolerant.
2. Provide energy storage to level the mission load.
3. Provide power bus regulation in Carrier-plus-Lander and Carrier-only configuration.
4. Provide battery charge control.
5. Accept power from the ASRGs.
6. Distribute power to the loads.
7. Actuate valves.
8. Fire pyro events.

Power Subsystem Description

The Power Subsystem electronics regulate the power bus, directly connected to the ASRGs, and distributes power to the loads on the spacecraft. The Power Subsystem will provide energy storage to cover the transient load profiles of the different mission scenarios. It is single-fault-tolerant, using a combination of block-redundancy with cross-strapping and some majority-voted functions. It provides the valve-drive and pyro-firing functions with range and mission safety inhibits for the hazardous functions.

In the combined Carrier and Lander configuration, the Power Subsystem is designed to operate with two independent power bus controllers on the same power bus by regulating the current into each battery with a gradual taper enabling both controllers to be active at the same time without cross-regulation issues.

The Power Subsystem consists of a Li-ion battery, a shunt radiator, a shunt driver slice (SDS), two multimission power switch slices (MPSSs), two power bus controllers (PBCs), two power converter units (PCUs), two pyro-firing cards (PFCs), and four propulsion drive electronics slices (PDEs) (Figure D.2.4-23).

Power Control

The PBC slices provide the SpaceWire command interface to C&DH. The PBC provides a low-power serial data bus to all of the other power electronics slices. It converts the com-
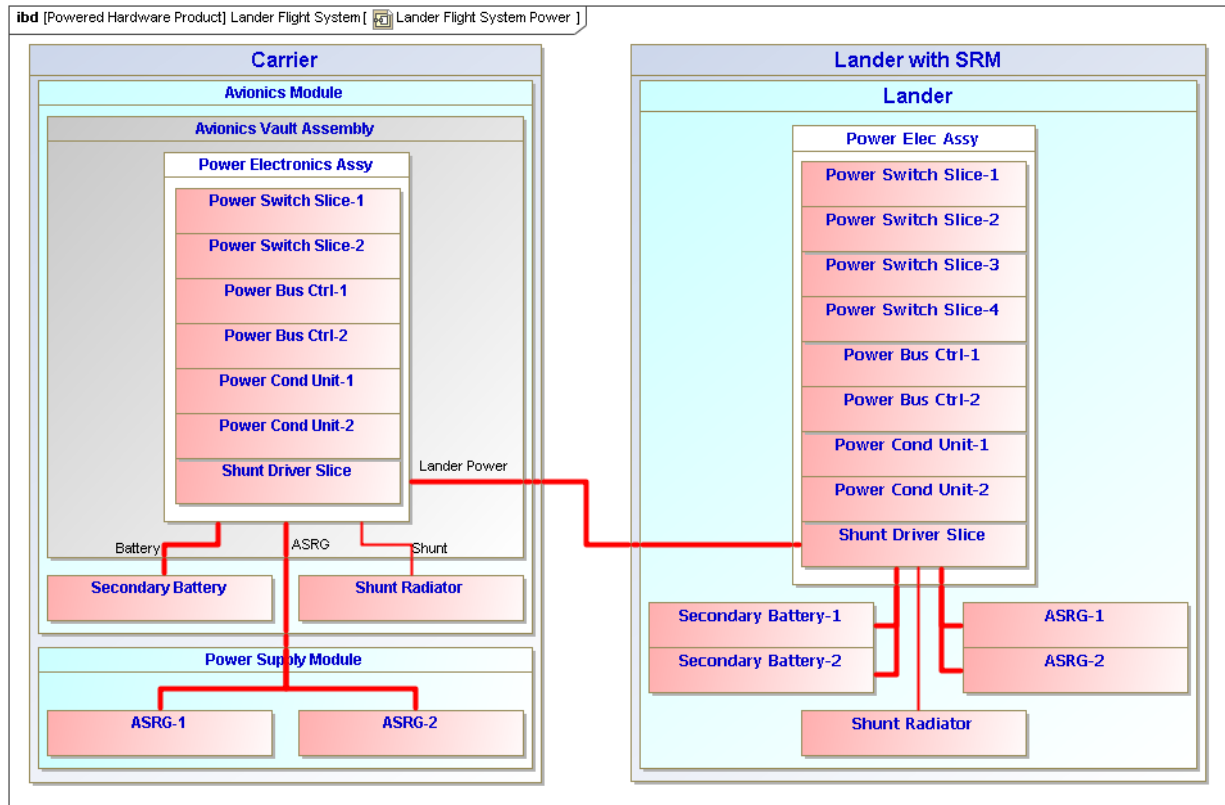
Figure D.2.4-23. The integrated spacecraft utilizes Lander ASRG power to help it perform the reconnaissance mission; this minimizes the number of ASRGs needed for the mission.

mands from C&DH via the SpaceWire interface and distributes them to other slices through the low-power serial data bus. The PBC collects the Power Subsystem telemetry and makes it available to C&DH via the SpaceWire interface.

The PBC contains the control algorithms for regulating the power bus by commanding the shunt switches in a shunt regulator. The ASRG power source has a constant power I-V curve over a power bus voltage range of 22 to 34 V at the ASRG output. The control function senses the current in the battery and adds or subtracts shunt current to limit the battery-charge current based on the actual capacity. The PBC commands discrete shunt driver switches in the SDS that drive power to the shunt radiator to control the power bus. The current regulation will taper to 0 current at the voltage set point correlating to the desired

state of charge. We are using 32.8 V as the 100% state of charge for the selected Li-Ion battery technology. The PBC has several commanded set points to set the battery at the desired state of charge. By regulating the current into the battery with a taper charge, it enables the two power bus controllers to share the control of the bus at the same time without an interaction that would cause the bus to oscillate.

Each SDS is sized to shunt the full power source capability of both the Carrier and the Lander. The SDS has the capability to switch in two secondary batteries or any combination of secondary and primary batteries. The SDS can apply a load to depassivate a primary battery if used on one of the interfaces. The SDS is single fault tolerant with a combination of block-redundant functions and majority voted interfaces.

The energy storage technology assumed for this study is based upon the characteristics of the small-cell ABSL Li-ion technology used on the Soil Moisture Active Passive (SMAP) mission (Figure D.2.4-24). The battery is configured with eight cells in series to get the desired bus voltage operating range, and 26 cells in parallel to get the desired 30 Ah of energy storage at the beginning of life. We have an actual capacity of 20 Ah at EOM after a single-string failure, including degradation for life, discharge rate, and operating temperature. The reference scenario that defines the energy storage for the Carrier is post-separation, with the camera taking pictures of the landing site, which requires a total of 40 Ah at 10°C with a 2.7-A discharge rate for 12 hours. The combination of a primary battery of 20 Ahr with a 20 Ahr secondary covers this one time deep discharge of the camera operation. The JPL Design Principles (DPs) allow for a 70% depth of discharge (DOD), making a 30-Ah battery BOL with 30 Ahr primary adequate for the post-separation Carrier (JPL 2010a). So there is an opportunity to reduce the size of the secondary battery in the Carrier by increasing the size of the primary battery to reduce mass. The secondary battery
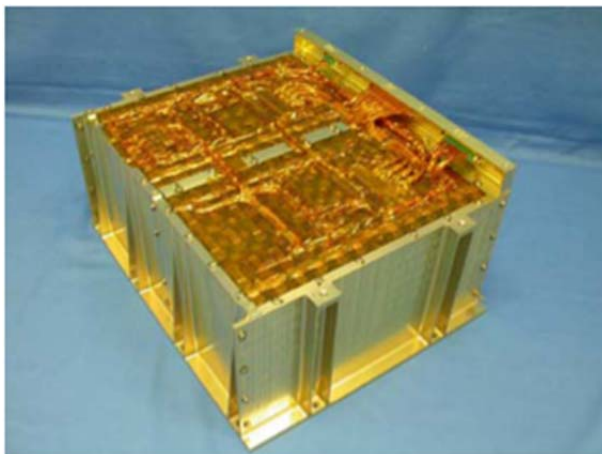

Figure D.2.4-24. Small-cell ABSL reference battery is similar to the SMAP battery configured with 8 cells in series and 26 strings in parallel (Model No. 8S26P). The Carrier actual capacity is 30 Ahr BOL and 20 Ahr at the EOL.

only sees a DOD of 10% after the camera operation.

The small-cell battery approach does not implement individual cell monitoring and balancing due to the matched cell behavior; however, a trade between the large cell with cell balancing and the small cell needs to be studied for this lifetime and operating conditions. The size of the secondary battery can be reduced by an increase in the primary battery to reduce mass. This will be studied in more detail during Phase A.

Power Distribution

The power distribution function is a combination of centralized power switches in the MPSS and distributed power switches on the primary side of each PCU. This combination enables the system to optimize the mass of the cabling by using centralized switches for heater buses and other loads that do not require a PCU and distributed switches for each PCU, reducing the point-to-point cabling for the major subsystems. The slice packaging approach enables the addition of centralized power switches while impacting only the mechanical footprint and cabling without modifications to a chassis or backplane. The command and telemetry interface is handled by the addition of addresses on the serial bus implemented in cabling. The thermal interface scales with the mechanical footprint.

Independent high- and low-side switches prevent any single failure from resulting in a stuck-on load and permit the resolution of load shorts to the chassis. Commanding is cross-strapped to the power switches through each PBC such that no single failure will prevent the commanding of any power switch. Each set of load switches is part of the load fault-containment region regardless of the location as a centralized or distributed switch.

Power Conversion

The power conversion function for each electronic assembly uses a distributed point-of-

load (POL) architecture (Figure D.2.4-25) where appropriate. This approach has a single isolated power converter on the PCU board, providing an intermediate power bus voltage that is distributed to each subassembly in the assembly. Where this is used (e.g., in C&DH), the front end of each subassembly can cross-strap the intermediate power bus and provide on and off capability with fault management to enable low-power operating modes and im-prove subsystem fault-containment regions. The primary side power switch is controlled by the Power Subsystem, and the POL regula-tors are commanded by the assembly. In elec-tronic assemblies where POL switching is not needed, primary-side power switching would still be used.

PCUs in other subsystems would not be part of the Power Subsystem, but the PCU design would be a common delivery from the Power Subsystem to other subsystems, both to mini-mize cost through commonality and to ensure the greatest integrity of the overall system power architecture.

Pyro Firing and Valve Drive

The pyro-firing and valve-drive functions are provided by a set of centralized power switch-es in the Power Subsystem electronics com-manded by C&DH via the PBC. The PFCs are fail-safe off, with two cards providing the block-redundancy. Each PFC fires 39 NASA Standard Initiators (NSIs) from a protected load power bus that provides all of the safety inhibits required for launch. The PFC controls the current into each NSI, with an overall capability to fire three simultaneous events from each card and a total capability of six simultaneous events with both A and B sides.

The PDE actuates the valves for the ME and the ACS thrusters. The PDE switches power from the protected load bus with the necessary safety inhibits in place. The PDE is fail-safe off with the single-fault-tolerance provided by a block-redundant set. Each PDE is capable of actuating 16 valves. The ME thrusters require an actuate-and-hold function requiring two valve drivers per interface.

Power Subsystem Heritage

The Power Subsystem uses the same architec-ture as SMAP, and many of the slice designs are the same. The power bus control algorithm is the same as used on SMAP, as is the slice packaging design and designs for the PFC and PDE. The MPSS is the high-side and low-side variant of the design used on SMAP. The PBC has a new command interface, but the control of the shunt regulator is the same as for SMAP solar array switching. The ABSL battery is the
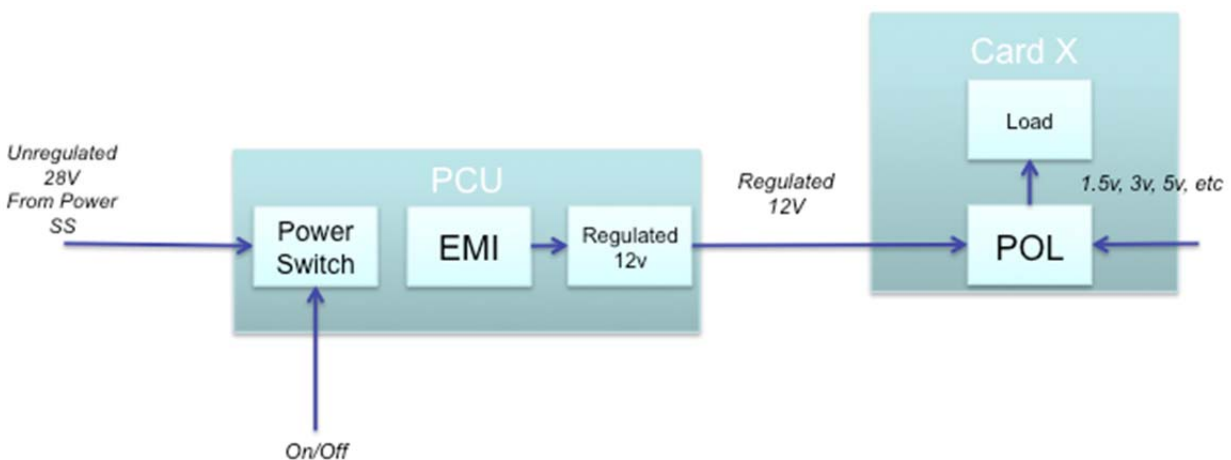

Figure D.2.4-25. Distributed power switching and POL converters reduce harness mass and increase power conversion efficiency. POL power conversion architecture shows the primary power bus interface with distributed switch controlled by the Power Subsystem. The distributed POL converters are controlled by the local assembly.

same design as used on SMAP, and the cell technology has flight heritage with Kepler and many European missions.

D.2.4.6.3 Carrier Guidance, Navigation, and Control Subsystem

The Carrier GN&C Subsystem provides a stable platform for reconnaissance and relay telemetry transmission and reconnaissance imaging.

The GN&C Subsystem provides three-axis attitude control through all mission phases to meet the reconnaissance and engineering pointing needs. All elements are body-fixed, so reconnaissance and telecom pointing is via spacecraft pointing. During TCMs, JOI or EOI, when the fixed ME is used, the GN&C provides TVC using dedicated TVC thrusters mounted on the thruster clusters. Once in Europa orbit the spacecraft will provide a stable nadir point platform for reconnaissance. After Lander release the spacecraft will nadir point the UHF antenna. For both phases of the mission in Europa orbit the spacecraft provides a precision pointing platform for Ka-band downlink via the HGA.

Table D.2.4-4 shows the key features and benefits of the GN&C architecture. The C&DH Subsystem hosts the FSW, including all of the GN&C software. Using the heritage approach common to all recent JPL spacecraft, the GN&C software is delivered in C-code developed from the GN&C design and simulation environment. The WDE, IMU, and SRU are heavily shielded from radiation, allowing the use of standard space products. The SRU

head with detector is shielded to reduce the electron/proton flux so that <4th-magnitude stars can be tracked. The Europa Study team analyzed attitude determination capabilities in the Europa environment and demonstrated attitude knowledge capability exceeding the requirements for the attitude knowledge contribution of the HGA pointing and reconnaissance. All known targets will be stored on board, enabling ephemeris-based tracking. Based on Cassini lessons learned, this approach reduces operations complexity. Finally, the use of thrusters for TVC reduces the development cost for a gimbaled engine and reduces the number of unique interfaces on the vehicle. The trade for gimbal vs. nongimbal engine will be addressed in Phase A.

Table D.2.4-5 shows the key characteristics of the GN&C Subsystem. The reaction wheel sizing of 45 Nm is driven by gravity gradient momentum accumulation at Europa. The sizing was based on vehicle inertias and the gravity gradient secular momentum accumulation between desaturation with 100% margin for unknowns. Figure D.2.4-26 shows the

Table D.2.4-4. The GN&C Subsystem features help reduce development and operations cost.

Feature	Benefit
C&DH hosts GN&C FSW and provides interface to sensor/actuators	Allows autocode direct from GN&C design
Spacecraft radiation shielding	Enables use of off-the-shelf GN&C H/W
Star-tracker radiation-shielded for flux	Tracks to 4.0-magnitude stars; meets pointing knowledge
Ephemeris-based pointing	Reduces operations overhead
Thruster-based TVC	Lower cost, fewer unique interfaces

Table D.2.4-5. The GN&C Subsystem design provides precise pointing control.

| Item	Value	Sizing
Reaction Wheel Momentum	45 Nm	Handle momentum accumulation from gravity gradient torques in Europa orbit
Attitude-Control Thruster Size	4.45 N	Minimum torque impulse bit for deadband control during cruise/relay/safe mode
TVC Thruster Size	40 N	TVC control for CM offset
Ka-Pointing	1 mrad	Support HGA link budget at required data rate with 3 dB of margin
X-Pointing	112 mrad	MGA communication while Sun-pointing
Recon Pointing Knowledge	1 mrad	Image tie back to Europa coordinate system
Recon knowledge drift	3 μrad/s	Image reconstruction—small geometric distortion (offset between image lines)
Recon stability	100 μrad/s	Clear map hazard assessment
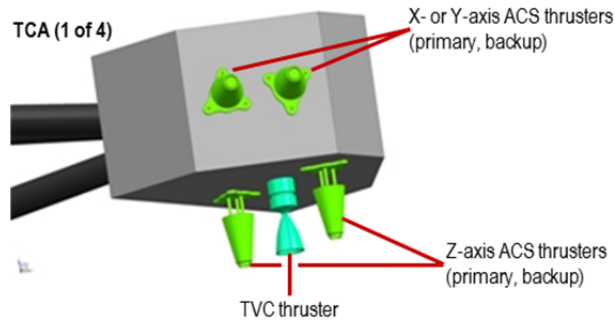
Figure D.2.4-26. The Carrier thruster configuration leverages the proven Cassini approach.

thruster configuration. The attitude-control thruster sizing of 4.45 N is to provide a sufficiently small minimum torque impulse for deadband attitude control during interplanetary cruise, relay operations, or safe mode. The TVC thruster sizing of 40 N is to provide sufficient control authority for up to a 9-centimeter shift of the vehicle center of mass (CM) during the mission. This shift is more than was experienced during Cassini flight (an estimated maximum shift of 7 centimeters). Ballast mass is also included in the MEL (Section D.4.3) to provide initial CM/center of gravity (CG) alignment. For attitude control and TVC, a thruster moment arm of approxi-

mately 2 meters is used. Methods of controlling CM offset from propellant migration will be studied in Phase A.

The 1-mrad Ka-pointing control requirement is a radial, three-sigma number derived from the telecom link analysis. The X-band pointing for safe mode is 112 mrad, based on a beam width that allows Sun-pointing with Sun-sensors while still communicating with Earth from Europa. The reconnaissance pointing knowledge is 1 mrad to ensure that the images are adequately tied back to the Europa coordinate system. The reconnaissance pointing knowledge can drift no more than 3 µrad/s to ensure that there are only small geometric distortions between consecutive image lines (to support image reconstruction). The stability of the spacecraft is 100 µrad/s to ensure clear images for hazard assessment. The capability of the concept will be assessed when more details about spacecraft flexible-body effects and propellant slosh are modeled.

Figure D.2.4-27 shows the block diagram of the GN&C Subsystem. At the center of the subsystem is the FSW that resides in the
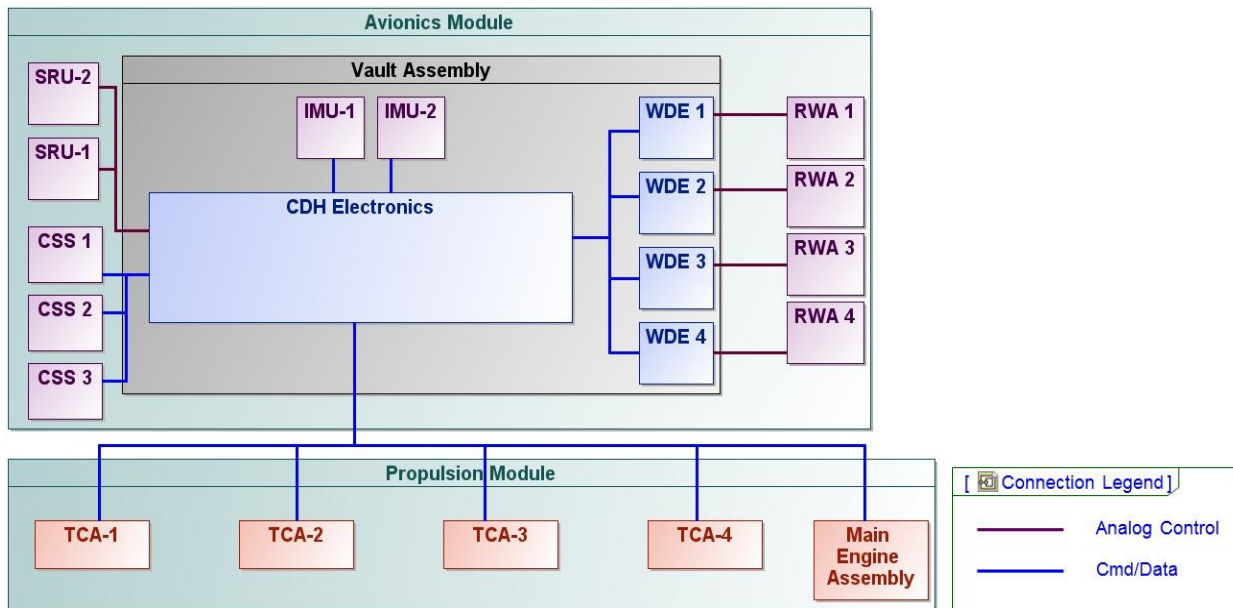

Figure D.2.4-27. The GN&C Subsystem is redundant and cross-strapped to provide robust fault-tolerance to radiation events.

RAD750 processor in the C&DH electronics. For Sun-pointing modes of operation, the Sun vector with respect to the vehicle reference frame is provided by the three Sun-sensors distributed on the Avionics Module to provide near-4π-steradian coverage. If there are any gaps in the coverage a spiral scan attitude maneuver can quickly bring the Sun into a sensor's FOV. For precise attitude determination a combination of inertial measurements corrected by stellar updates is provided by the IMUs in the vault and shielded SRUs outside the vault. SRU detector anneal heaters are baselined to mitigate radiation DD.

For precision attitude control during reconnaissance, three of four RWs are used; these are desaturated as needed by the attitude-control thrusters. The WDE is in the vault while the mechanical assembly is outside the vault. For less precise attitude control during cruise, relay, or safe mode, the attitude-control thrusters can be used. Note that using the Cassini configuration for thrusters uncouples forces and torque in pitch and yaw, but not in roll. For attitude control during TCM, JOI, or EOI (when the ME is fired), the TVC thrusters are used for pitch and yaw control while the attitude-control thrusters are used for roll control.

The architecture is cross-strapped such that any SRU can be used with any IMU to provide the attitude information to any computer. Attitude control can be accomplished with any three of four RWs or with any set of eight block-redundant thrusters.

Given the radiation shielding provided by the spacecraft, the GN&C Subsystem can use standard space GN&C products with high TRL. Table D.2.4-6 shows the GN&C hardware items, suppliers with high-TRL products, and the approach to deal with radiation.

Table D.2.4-6. The radiation-hardening approach enables the use of heritage GN&C hardware.

Item	Supplier(s)	Radiation Approach
Reaction Wheels	Collins	Sensitive wheel-drive electronics in vault
	Honeywell	Mechanical assembly radiation-hard by design
Sun-Sensor	Adcole	Radiation-hard by design
Stellar Reference Unit	Sodern	Shielding for flux and total dose
	Ball	
	SELEX Galileo	
Inertial Measurement Unit	Honeywell	In the vault
	Northrop Grumman	

D.2.4.6.4   *Carrier Command and Data Handling Subsystem*

The Carrier C&DH provides a cross-strapped and redundant radiation-hard platform to support the data storage and processing needs of Carrier reconnaissance and relay functions.

The Europa Lander Mission C&DH is the control center for most activities on the spacecraft, including nominal command sequencing; general system operation; GN&C, propulsion, and thermal control algorithms; and fault management.

The functional requirements and goals of the C&DH are as follows. The design should be single-fault-tolerant and cross-strapped to enable the C&DH to fail operational during single-event effects in the high-radiation environment of the Jovian system. The design should allow swapping to enable rapid transition of control during a fault. A RAD750 single-board computer (see Figure D.2.4-28) was selected to leverage the processor flight heritage, radiation-hardness, and JPL's software architecture heritage. The onboard data storage accommodates multiple copies of the Carrier reconnaissance and relay data; Phase A will look at concepts for data integrity using the excess storage capability

The C&DH electronics occupies a single box that is internally redundant. Given the use of SpaceWire (see Figure D.2.4-29) as the primary interface, there is no need for a backplane or
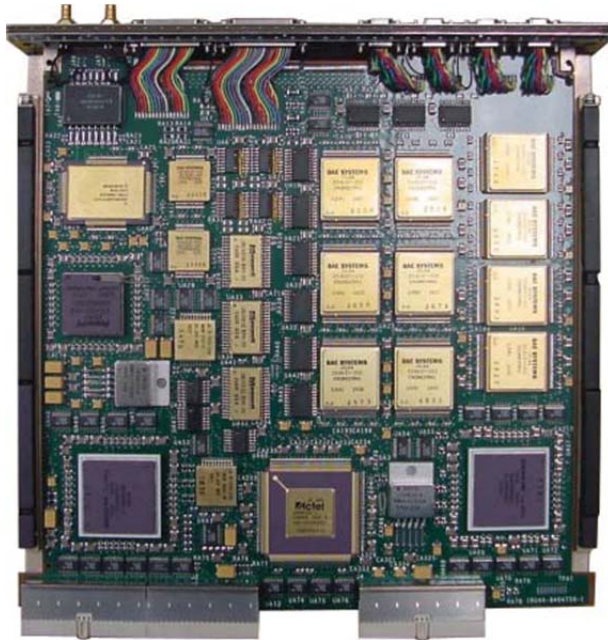
Figure D.2.4-28. The RAD750 provides high heritage for both the C&DH electronics and FSW designs.

Figure D.2.4-29. The SpaceWire interface chip is radiation-hard and provides a high-speed standard interface to the cards in the C&DH.

motherboard within the box to increase the C&DH box reliability and simplifies packaging.

A standard-size chassis of a 6 U × 220 mm cards was selected to enable the use of heritage single-board computers and provide sufficient board area for the I/O and memory cards. Time broadcast and synchronization are part of the SpaceWire standard, so no external timing network is required. The remote I/O handles all the low-level interfaces such as analogs, discretes, and serial I/O; it also provides the telecom interface, critical relay commanding, and processor swap functions. The I/O is multiplexed through the SpaceWire interface chip; this radiation-hard chip includes an embedded processor to accommodate programmable I/O functions. The I/O circuits are standard designs from other JPL spacecraft. The RC card is described in Section D.2.2.2.

The solid-state recorder provides greater than 6.4 Gbit of storage using Flash memories; although the Flash memories are commercial parts, recent parts testing shows several radiation-tolerant options. A radiation characteriza-
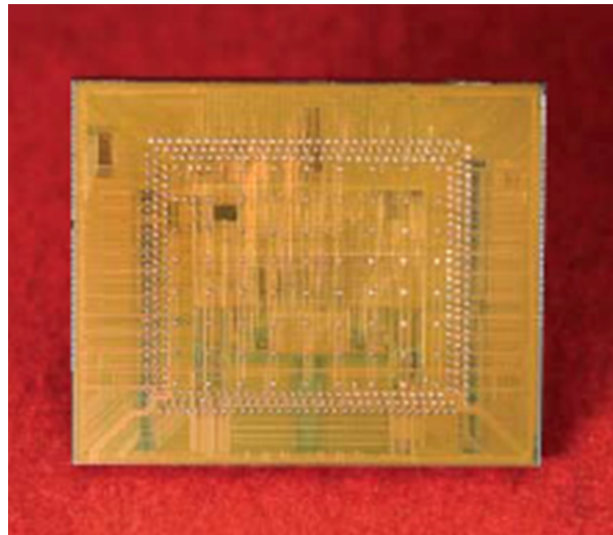
tion risk-mitigation activity in Phase A will identify the best part, followed by a lifetime buy for the project. The memories are interfaced to the spacecraft through a SpaceWire interface chip; this chip includes an embedded processor that will make this device behave as "network-attached" storage: Reading/writing to this recorder doesn't require the RAD750.

The power-conditioning unit (PCU) takes in unregulated 28 V off the power bus, provides EMI filtering, and converts it to a regulated 12 V that is distributed to each card in the box. The PCU on/off switch is controlled by the Power Subsystem. The local card on/off is software controlled via the processor and commands issued via the remote I/O.

The physical block diagram is shown in Figure D.2.4-30. This figure shows the cards in the C&DH box. The box is internally redundant and cross-strapped (both data and power). SpaceWire supports multiple topologies (e.g., star or daisy chain). The box consists of two RAD750 single-board computers with SpaceWire router, two mass memory cards, two remote I/O cards, two RC electronics cards, and two PCUs. The mass memory card interfaces to the single-board computer via Space-
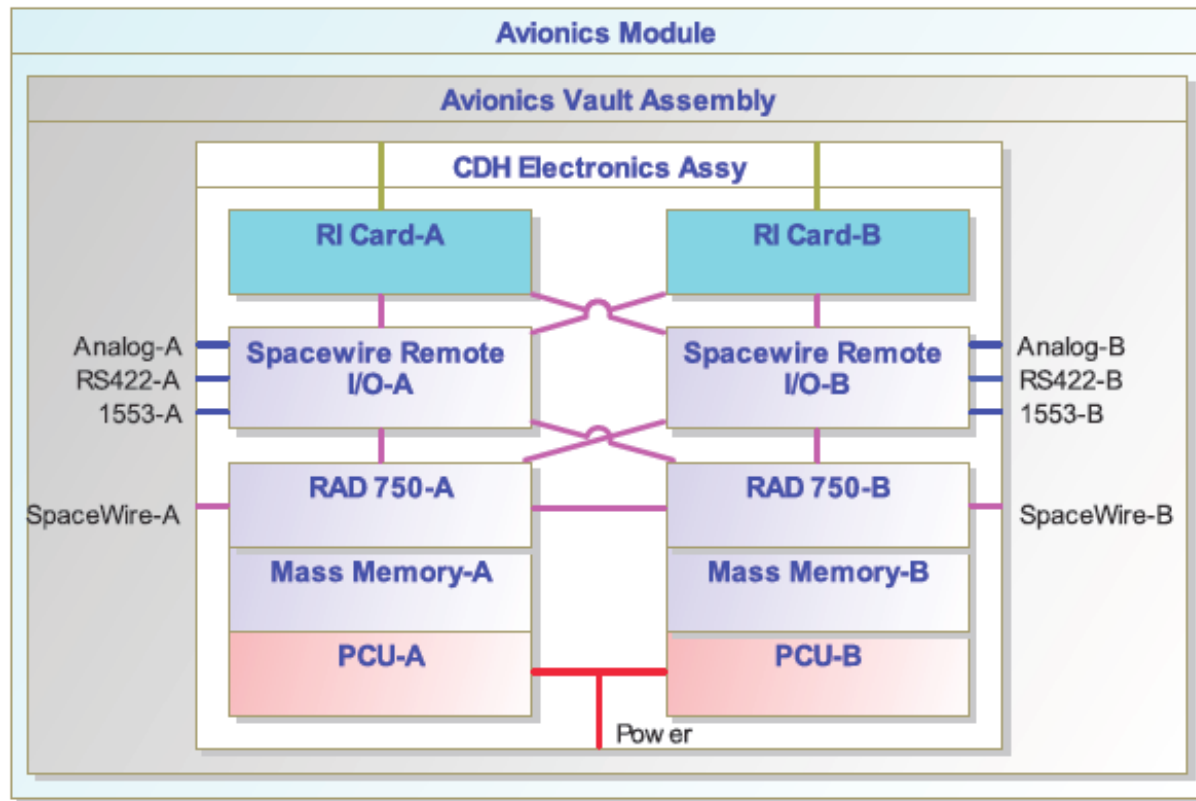
Figure D.2.4-30. The C&DH is redundant and cross-strapped to provide robust fault-tolerance.

Wire. The remote I/O cards interface to the single-board computer via SpaceWire. The topology of the SpaceWire network will be established during Phase A to optimize throughput and fault-tolerance.

The C&DH electronics do not require any new technologies. The RAD750 single-board computer with SpaceWire is an off-the-shelf product. The SpaceWire interface chip is an off-the-shelf product. The I/O circuits, power supply, and mass memory have analogs on previous projects. The 6 U × 220–m packaging standard has been qualified and used on previous projects.

D.2.4.6.5   *Software—Integrated Spacecraft*

Highly reliable software for mission-critical applications is essential for this long-life mission. The flight software (FSW) baseline extends JPL's long heritage in FSW architecture development, and is implemented in accordance with JPL requirements for NASA

Class B (non–human-space-rated) software development. JPL has established a set of institutional software development and acquisition policies and practices as well as design principles that apply to mission-critical and mission-support software. These practices conform to NASA Software Engineering Requirements, NPR 7150.2 (NASA 2009b) and are an integral part of the JPL Design Principles (DPs) and Flight Project Practices (FPPs) (JPL 2010a, b). All Europa Lander Mission FSW will be developed in accordance with JPL institutional policies and practices for deep space missions, including JPL's Software Development Requirements (JPL 2010c), which address all Capability Maturity Model Integration (CMMI) process areas up to maturity level 3. Software identified as safety-critical will comply with safety-critical requirements, regardless of software classification. Software safety-criticality assessment, planning, and management will be performed

for all software, including new, acquired, inherited, and legacy software and for supporting software tools. Software is identified and documented as safety-critical or not safety-critical based upon a hazard analysis conducted prior to the start of development activities.

Key functions allocated to software include system command and control, health and safety management, attitude control (maintaining concurrent HGA Earth pointing during telecom sessions, or instrument surface tracking during landing site imaging operations), onboard data management, reliable data delivery using Consultative Committee for Space Data Systems (CCSDS) File Delivery Protocol (CFDP), and TVC during critical propulsion maneuvers. Onboard ephemeris-based pointing and the use of CFDP help to simplify operations and thus reduce long-term operations costs. None of these capabilities are seen as new technology, and significant algorithm and architecture heritage is available from Cassini, MSL, SMAP, MESSENGER, and other missions.

Critical control activities managed by software are expected to include postlaunch separation, detumble, acquisition, Jupiter and Europa orbit insertions, and relay communications. Data relay behaviors and protocols have been developed and proved in the Mars program, and much of that technology can be inherited as reusable software.

Flight software also has a key role in system fault management. This mission concept includes a number of time-critical activities, including orbit insertions, critical maneuvers, and DDL, where the physics of motion through space constrains the time in which the activity must be completed without mission-limiting consequences. For this reason the FSW coordinates a system fault-management approach, consistent with current best practices, aimed at protecting essential resources, but trying to maintain scheduled operations using automatic fault responses such as resetting devices, switching to redundant devices, or

selectively trimming subsets of planned activities.

The FSW is organized in a layered architecture, as shown in Figure D.2.4-31. The Carrier and Lander elements each have separate flight computers with distinct flight software systems. However, they do share a common architecture that is consistent with current best practices and may enable some common development. The specific contents of some of the functional elements will differ between systems. So, for example, the Propulsion Subsystem control on each element will be customized to the particular set of propulsion hardware carried on that element.

The platform abstraction layer interfaces directly with the hardware. This layer contains drivers that provide control and data abstractions to the device-manager and services layers. The drivers communicate with the hardware using the device-specific syntax and protocol, allowing higher layers of software to interact with these devices using system-standard communication protocols and message formats. Notably, the use of industry-standard SpaceWire as a common hardware communications medium reduces the number of different device types that must be supported, with commensurate reductions in software system complexity. Furthermore, the ability of SpaceWire interface devices to buffer data and perform other control functions in hardware (as demonstrated by MESSENGER) is expected to further reduce the complexity and time-criticality of the FSW implementation.

The platform-abstraction layer also encapsulates the real-time operating system, device drivers, and all interprocess communications, leveraging flight heritage with the RAD750 platform and all JPL missions since Pathfinder. The commercial operating system provides real-time task scheduling, memory management, and interfaces to I/O devices immediately associated with the processor board.
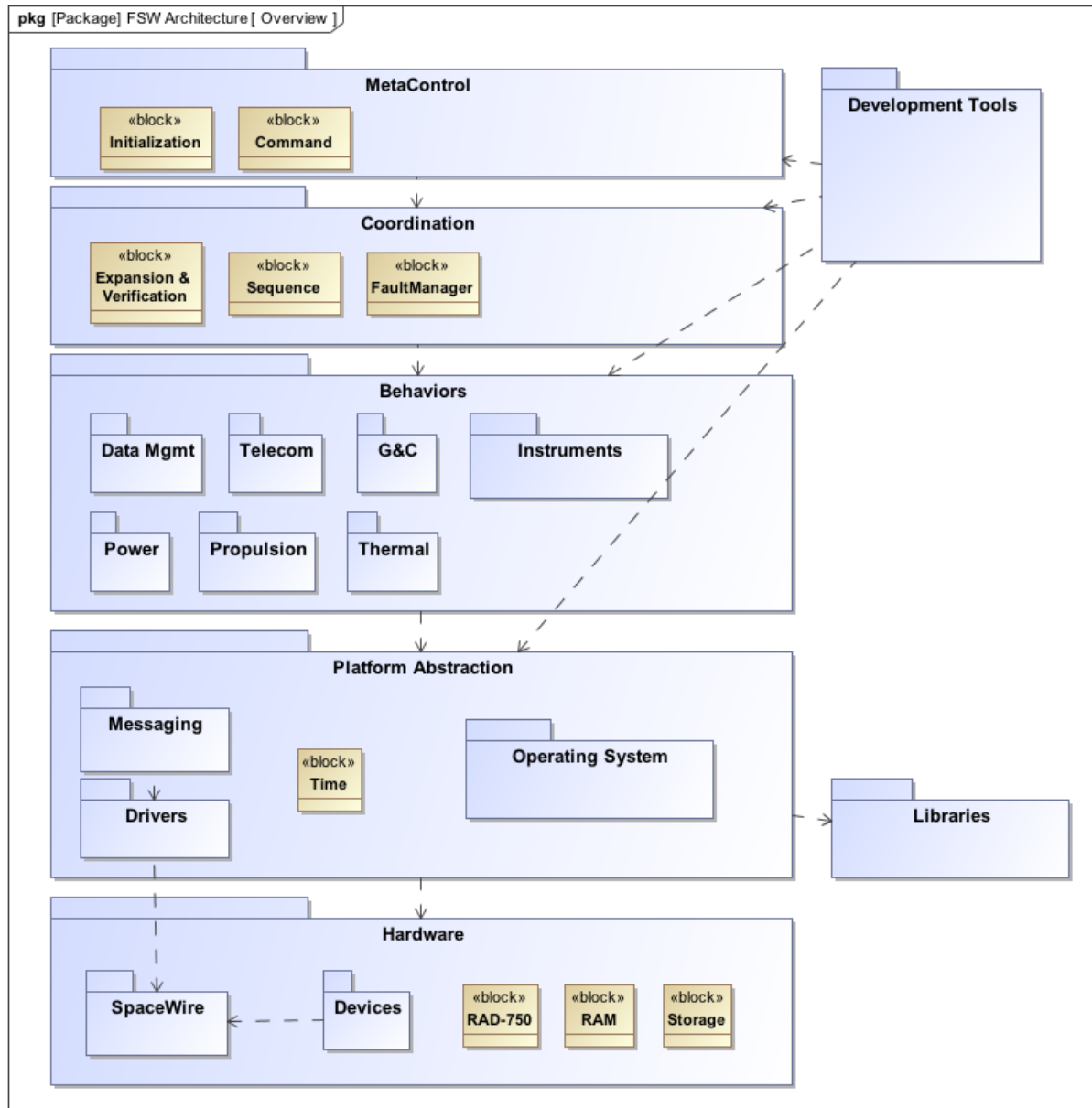
Figure D.2.4-31. Carrier and Lander share the same layered flight software architecture.

The behaviors layer includes software elements that perform closed-loop control around specific system behaviors. These behaviors are typically responsible for the management of one or more hardware devices or subsystems. Closed-loop behaviors incorporate fault-detection and localized fault-management capabilities.

On the Carrier element the guidance and control (G&C) module would include a behavior

for maintaining the HGA pointed to Earth, pointing the camera to nadir, and other attitude-control behaviors needed to support propulsive maneuvers and orbit insertions. This module would also need to be able to adjust to the changed mass and balance properties of the Carrier after separating from the Lander.

Both elements would include the same data-management software to manage the store-

and-forward flow of data from Lander to Carrier and then to Earth. CFDP would be used to manage the data flow from Lander to Earth via the Carrier, including most replay management.

Behavior coordination is provided in a separate coordination layer that can sequence and coordinate the control of underlying behaviors. This layer is also responsible for coordinating any fault responses at a system level. The metacontrol layer provides services for initializing and supervising reliable operation of the rest of the system and supporting commanding (changing system behavior from the ground).

The Carrier element has no science instruments, but it does have the RC, which requires management by flight software. This package replaces the instruments group shown in Table D.2.2-2. This package is developed in-house along with the camera hardware.

D.2.5   Lander Element

The Lander concept is a highly capable spacecraft element tailored to provide a safe landing and meet the science objectives.

D.2.5.1   Lander Overview

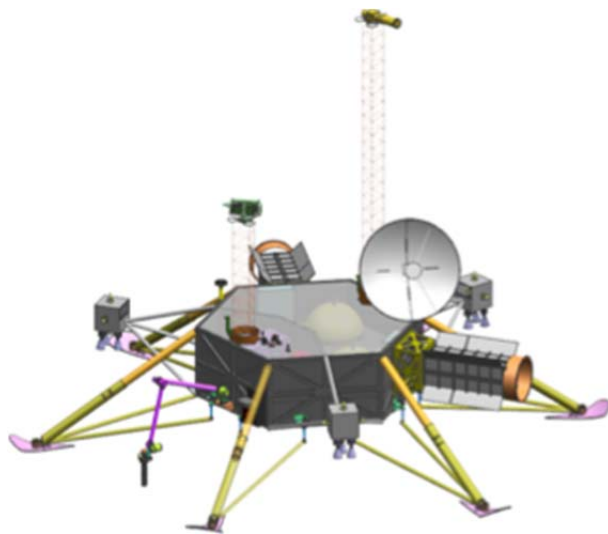The Lander, pictured in Figure D.2.5-1, has a central hexagonal body that holds the propel-

Figure D.2.5-1. The Lander provides a robust platform to collect and analyze samples, image the landing site, perform magnetometry and perform seismometry.

lant tanks, avionics, and sample analyzing instruments. External to the body on the top deck are the SIS on its 1-meter mast, the MAG on its 2-meter mast, and the DTE HGA/MGA. On the side of the body, there are three TCAs, two ASRGs, the sampling arm, and six landing legs with seismometers on each footpad.

Instruments

The Lander is configured to support the following science instruments:

- Mass Spectrometer (MS)
- Magnetometer (MAG)—this is deployed
- Multiband Seismometer (MBS)—six, one on each footpad
- Site Imaging System (SIS)—this is deployed
- Raman Spectrometer (RS)
- Microscopic Imager (MI)

The sampling system provides samples to the MS, RS, and MI.

Attitude Control

The Lander is three-axis-stabilized in all phases of flight. Stabilization is achieved through the use of inertial measurement and thrusters for attitude control. TRN using a descent camera and onboard map is the basis for powered descent guidance commands for pinpoint landing. HD LIDAR is used near landing to detect hazards, select the safest reachable landing site, and command a hazard-avoidance divert maneuver.

Data Handling

During the surface phase, the instruments and spacecraft generate over 4.6 Gbit of data. Data can be stored between relay telecom passes in a redundant, solid-state data recorder (3.5 Gbit per card) that is part of the Command and Data Handling Subsystem (C&DH). Concepts for data integrity using the excess storage capability will be studied during Phase A.

Power

The power source for the Lander is two ASRGs. The power system is sized to accommodate one failure (mechanical or electrical) of an ASRG. Excess power is stored in the 60-A-hr lithium-ion battery or dumped as heat through a thermal shunt. For mission durations that are not power-positive, a positive energy margin is obtained by using the battery.

Thermal

To minimize the power demand of the Lander (because we desire to minimize the number of ASRGs), the Lander was designed to minimize the use of electrical heaters. To achieve this goal, the heat from electronics with a combination of excess ASRG energy (dumped to the thermal shunt) is captured inside the Lander body during the cold phases of the mission. This approach allows the propellant to be kept near room temperature without the need for supplemental electrical heaters. The concept includes multiple radioisotope heater units (RHUs) and/or variable RHUs (VRHUs) that will be used in select locations (e.g., TCAs) to minimize the need for electrical heaters.

Communications

The Communications Subsystem is designed to support the needs of DDL and the transmission of science data back to Earth. This system consists of a UHF relay to the orbiting Carrier as the primary telecom approach with a back-up Telecom Subsystem consisting of a 0.75-m X-band HGA. During DDL the UHF relays EDL telemetry to the Carrier and the X-band LGA sends DDL states to Earth via RF carrier tones.

Propulsion

The Propulsion Subsystem must support attitude control, deorbit, and descent. To achieve these requirements the subsystem consists of an SRM for deorbit and a hydrazine, monopropellant system for attitude control, TVC, and descent control. The fuel and pressurant tanks are inside the Lander body. The SRM is sized for an under-burn so that it does not

impact near the landing site. The tanks are sized for maximum propellant for the Lander allocation from the Carrier and can support up to a 3-km divert maneuver. The subsystem consists of one Star30E-class SRM, nine landing thrusters, and 12 (six primary, six redundant) attitude-control thrusters; each TCA contains four attitude-control thrusters and three landing thrusters.

Redundancy

The Lander uses a redundancy philosophy similar to that of Cassini; the Lander is redundant with selected cross-strapping. The instruments electronics are redundant but the detectors are single-string. The structure and SRM are single-string; these single-string elements will undergo a risk assessment in Phase A to determine if the risk is acceptable.

Radiation

This mission has a demanding total dose requirement (0.5 Mrad behind 100 mil Al). To support the use of standard aerospace EEE parts, we have included tailored radiation shields for sensitive components. Unlike the Carrier element, the Lander does not employ a vault to shield its electronics. The Lander avionics electronics and science instrument electronics are shielded from TID at the assembly level. Inside the shields the environment is 50 krad; this allows 100-krad parts to be used (RDF=2).

D.2.5.1.1   Lander Configuration

Two configurations of the Lander are shown in Figure D.2.5-2. On the left side of the figure is the Lander as configured for deorbit; on the right side of the figure is the Lander as configured for surface operations with all elements deployed.

Deorbit Configuration

After separation from the Carrier, the Lander is fully fueled with hydrazine for descent control and includes an SRM for deorbit. After the deorbit burn is complete the SRM is separated from the Lander. The three thruster
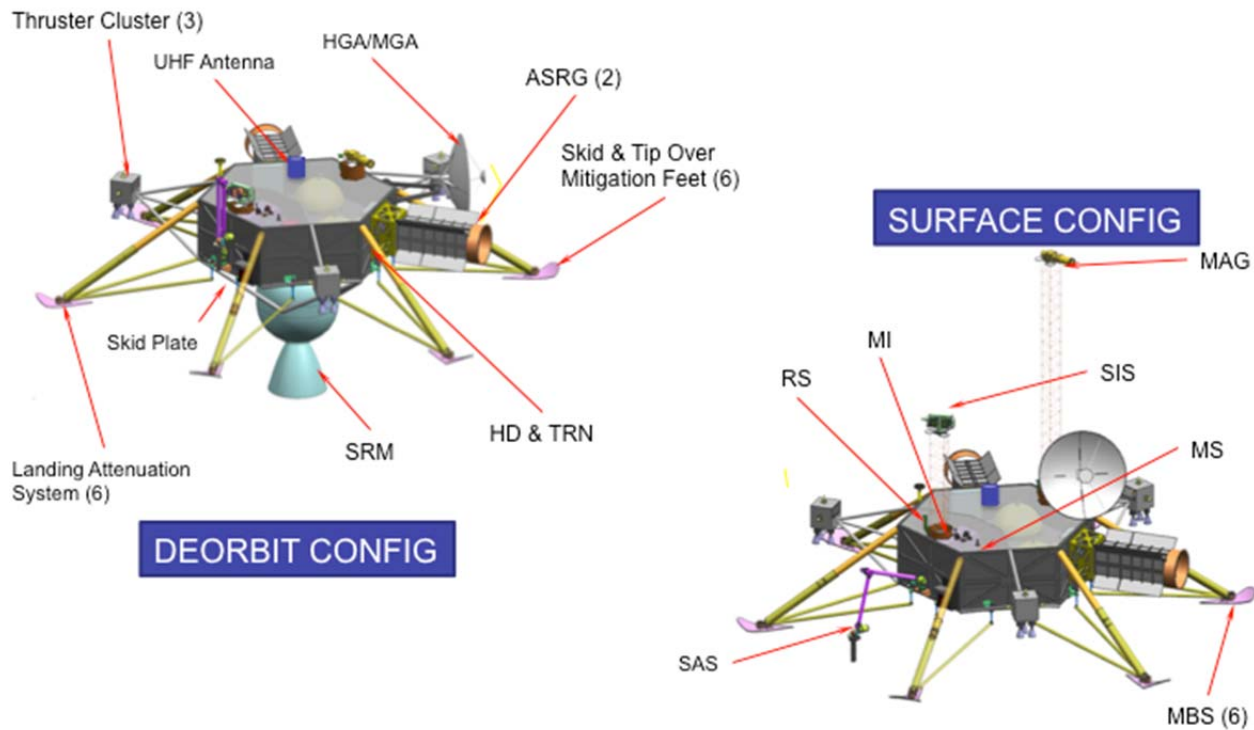
Figure D.2.5-2. The deorbit configuration of the Lander shows the key components for a safe landing; the surface configuration of the Lander shows the highly capable science platform.

clusters hold the ACS thrusters and descent thrusters. The UHF antenna is on the top deck along with the X-band LGA; these are used for communication during DDL. The HGA, MGA, sampling arm, and instruments remain stowed. The two ASRGs provide power and are situated opposite the instruments and avionics to provide mass balance. The six landing legs and feet are distributed symmetrically around the hexagonal body. The "wheel base" of the legs is over 4 meters. The clearance under the body is 0.5 meter.

Surface Configuration

Once on the surface, the instruments—HGA, MGA, and sampling arm—are deployed. The MAG is deployed on a 2-meter boom; the SIS is deployed on a 1-meter boom. The MS, MI, and RS are internal to the hexagonal body but placed so that the sampling system can provide samples to these instruments. The seismometers are on each leg although only three are needed for science. There are certain landing

site topographies where only three legs will rest on the surface.

D.2.5.1.2 System Block Diagram

Figure D.2.5-3 shows the system block diagram for the Lander. The red interfaces are power, the blue/purple interfaces are data, the green interfaces are propellant plumbing, the orange interfaces show pyro/prop control, and the brown are RF interfaces. The Lander provides robustness to faults and failures by provide primary and backup capabilities for most systems. The elements are cross-strapped to enable a higher probability of mission success in the high radiation environment.

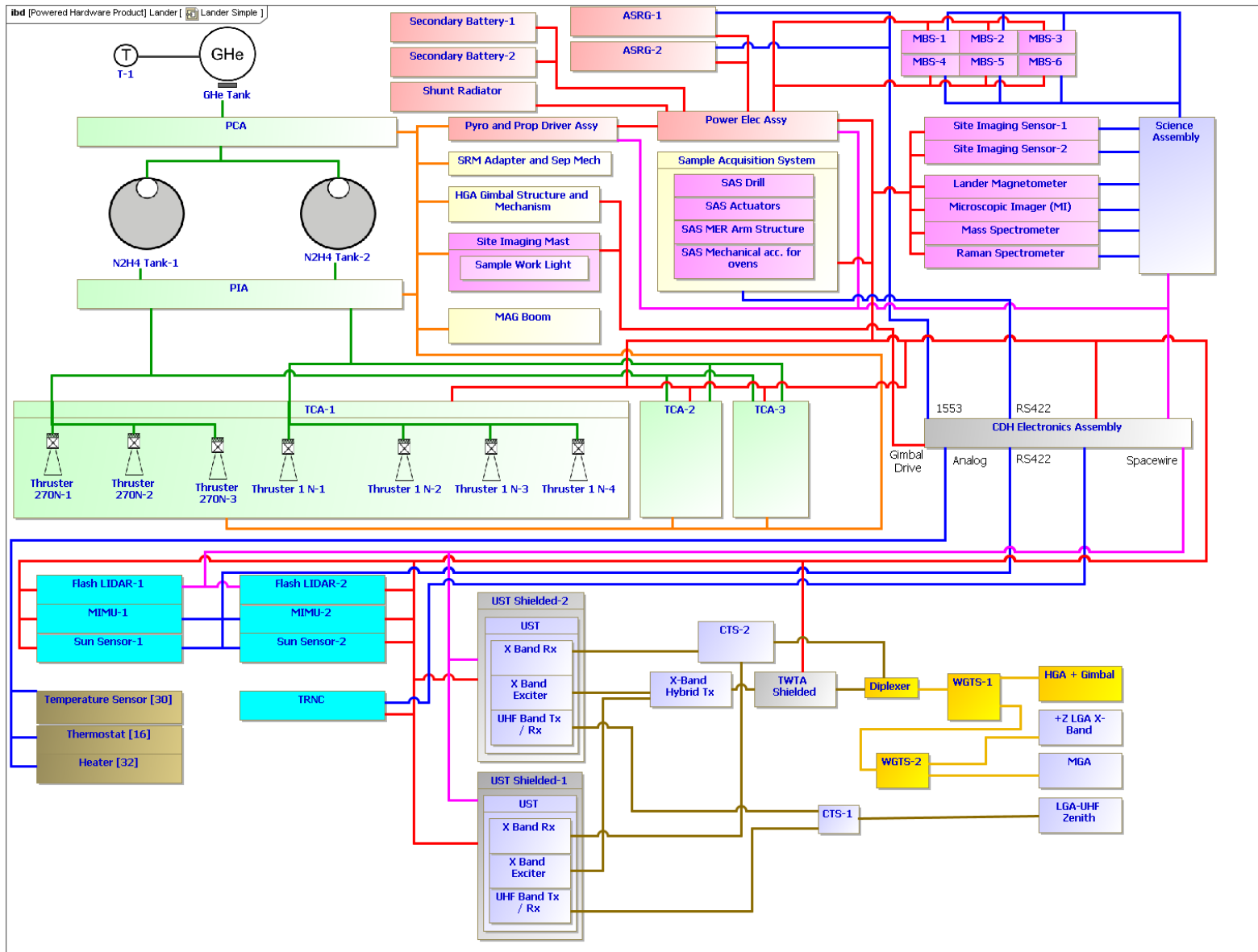Note that some of the boxes (e.g., C&DH) do not show redundancy because they are internally redundant.

Figure D.2.5-3. The system block diagram demonstrates the Lander's robustness through redundancy.

D.2.5.1.3   Lander Design Drivers

Table D.2.5-1 shows the design drivers that flow down to the Lander from the science measurements.

The MS and RS require samples from two depth ranges: 0.5–2 cm and 5–10 cm below the surface. Collecting these samples requires a sampling arm and drill that must keep the sample below 150 K. To provide the ability to sample anywhere in the work area the GN&C requires a stereo image of the worksite, which is processed on the ground to create a DEM. Trajectories are calculated to the desired sampling site and then are uplinked to the sampling arm. In the situation where shadows are present, the Lander provides worksite lighting. The complexity and flexibility needs of a sampling system require processor-based software control. Once a sample is taken, the same sampling arm moves the sample to the input ports of these instruments. To avoid inadvertent contamination of the sample, the system uses DHMR prior to launch.

To support magnetometry measurements, the Lander must be designed to be magnetically "clean," and the MAG must be deployed away from the spacecraft body.

The SIS and MI images are the drivers for data storage: We need a UHF relay to transmit the large volume of data in a timely manner. The SIS also requires a two-axis gimbal to provide the panoramic images and the images of the worksite.

Table D.2.5-2 shows the design drivers that flow down to the Lander from the mission design. Deorbiting from the 200×5–km orbit requires 1.4 km/s of ΔV, which is obtained by using an SRM.

The descent and landing function drives three key features of the Lander design. After separation from the Carrier the Lander may have to wait up to 2 hours prior to deorbiting; this delay is a driver on the battery sizing. The requirement for terrain-relative navigation (TRN) and hazard avoidance results in the use of a camera-based TRN scheme and Flash LIDAR hazard detection. TRN and HD require processor based control and large memory to store images. The divert capability required is a driver in the amount of ΔV required from the monopropellant system.

Table D.2.5-1. The Lander design drivers from the science measurements are mature and have been vetted through several Science Definition Team meetings.

Sci Measure	Requirement	GN&C	Telecom	Power	C&DH	Prop	Thermal	Mech
Mass & Raman Spectro-meter	Sample from 2 cm and 10 cm	SIS to create DEM & trajecto-ries		Worksite lighting	Proc-based control		Sample @<150 K	Arm & drill
	Sample transfer						Sample @<150 K	Arm
	Cleanliness							DHMR
Magneto-metry	Provide magnetically clean Lander	EMI	EMI	EMI	EMI			Deploy on boom
Cameras	SIS data & visibility		UHF relay		Data storage			Deploy; gimbal system
	MI Data & Visibility		UHF relay		Data storage			
Seismometry	Low vibration & good surface contact & thermal isolation						Thermal isolation	ASRG isolation & on each leg

Table D.2.5-2. The Lander incorporates design elements that flow down from the mission design driving requirements.

Msn Des	Requirement	System	GN&C	Telecom	Power	C&DH	Prop	Thermal	Mech
Deorbit	Provide 1.4 km/s ΔV						SRM		
Descent & Landing	2-hour phasing prior to landing				Sizes battery				
	Hazard Detection & Avoidance		HD with Flash LIDAR/TRN with Camera System			Proc-based Memory	Divert ΔV		
	Landing on undetected surface features		Slow to <0.5 m/s vertical & 0.25 m/s horiz						Landing system
Europa Surface	DTE Command & Telemetry		Sun sensors	Xup/ Xdown with HGA & MGA					
	Planetary Protection		DHMR	DHMR	DHMR	DHMR		DHMR	DHMR
	Thermal control							RHU/ ASRG	
Jupiter Cruise + Europa Surface	Radiation TD & Electron Flux	Fault Recovery	<300-krad parts	<300-krad parts	<300krad parts	<300-krad parts			Shielding

Landing on undetected surface features is a driver on the landing system mechanical design; it reduces tip-over and skidding and absorbs landing energy to protect the remainder of the spacecraft. The GN&C will slow the Lander to minimize landing energy to acceptable levels.

To support safe mode and contingency modes of operation after landing, the Telecom Subsystem has a DTE capability using X-band through the HGA. In the event that all state information is lost onboard the Lander; the Sun-sensors can be used to point the MGA for communication.

Because all elements of the integrated spacecraft will end up on the surface of Europa, planetary protection is a driving requirement. All elements will be capable of undergoing a system-level DHMR.

The cold surface conditions drive the thermal design of the Lander. To minimize electrical heater power demand, internal heating from the electronics and excess ASRG electrical energy are captured within the Lander body to keep the spacecraft equipment within allowable flight temperatures. External elements will require electrical heaters or VRHUs.

A large radiation total dose of approximately 0.5 Mrad (behind 100 mil Al) is accumulated during this mission; this dose drives the shielding design on the Lander and the EEE parts selection. Radiation tolerance also drives fault-management requirements to recover and continue science activities after a radiation event (SEU, SEL, etc.).

D.2.5.2   Instrument Accommodations

D.2.5.2.1   *Magnetometer and SIS Camera Boom Deployment*

Both the Magnetometer and SIS camera booms are based on a passive self-deploying design. Figure D.2.5-4 shows the booms in the deployed state. This design makes use of the mast's own stored strain energy to drive the deployment. The mast is stowed by coiling and compressing it axially. In the stowed position a lanyard retains the mast. A second lanyard is
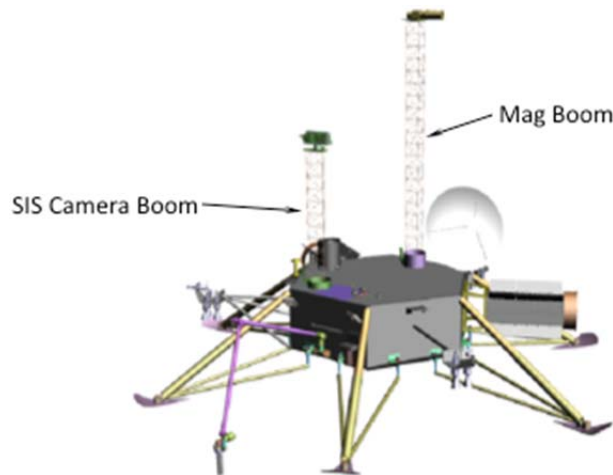
Figure D.2.5-4. A passive deployment scheme provides reliable deployment of the SIS and MAG.

Figure D.2.5-5. The ESS reliably delivers the sample to the instruments.

attached to the top of the mast and to an eddy-current damper rate-limiter. The damper is attached to the Lander's primary structure. The eddy-current damper acts to reduce the impact loads at the end of deployment. A pyro cutter cuts the retaining lanyard, and the boom slowly extends to its maximum length.

D.2.5.2.2 ESS and Oven Accessibility

The ESS drill system has a full range of motion that allows it to both drill core samples from the required depths and deliver those samples to the ovens. The ovens are located behind the drill and on the top surface of the Lander deck. There are no obstructions in the path of the drill arm that would interfere with its articulation.

Figure D.2.5-4 shows the Lander with the drill tip on the surface. Figure D.2.5-5 shows the position of the drill mechanism required to deliver the sample to the oven. Figure D.2.5-6 is a close-up of the oven showing the conical interface surface that the tip of the drill would engage prior to inserting the sample into the oven.

D.2.5.2.3 Lander SIS Camera FOVs

The SIS cameras' FOVs are shown in Figure D.2.5-7. Prior to deployment the SIS camera FOVs are not obstructed. This device and
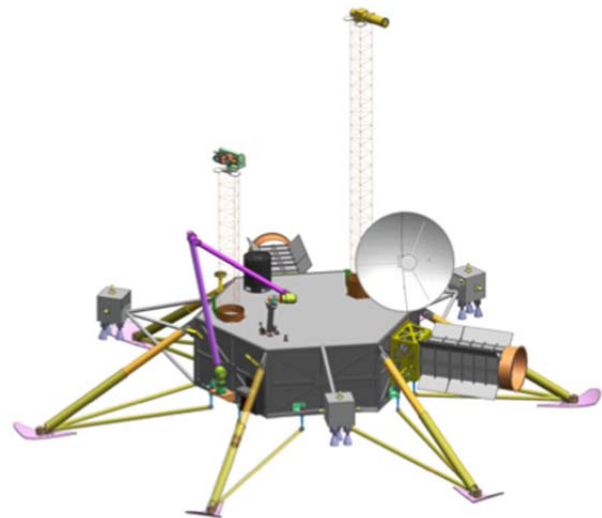
method of deployment have been used on other successful missions.

D.2.5.2.4 SIS Camera Radiator

Each of the two SIS cameras has a 25-cm^2 radiator mounted horizontally with the face up relative to the Lander coordinate system. These radiators are required in order to maintain the cameras' detectors at their operational temperature. The radiators are made of alumi-
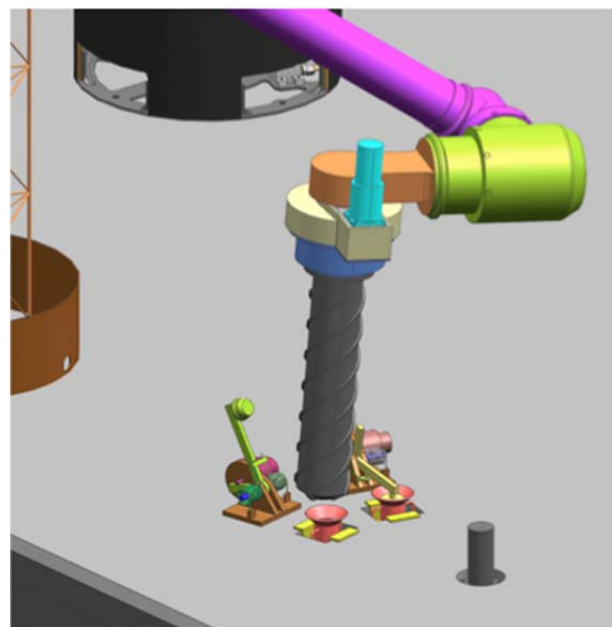

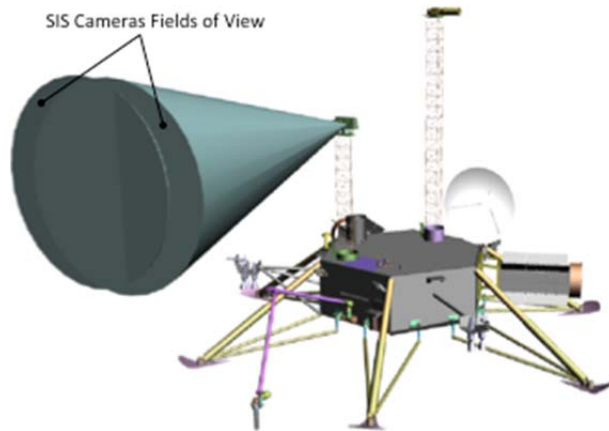**Figure D.2.5-6.** Close-up of ESS delivering a sample to the oven ports.

Figure D.2.5-7. The SIS FOVs provide stereo coverage from a height similar to that of a standing person viewing the surface.

num and are bolted directly to the camera's housing. Figure D.2.5-8 shows direction of the face of the radiators.

D.2.5.3 Structures and Mechanisms

D.2.5.3.1 Driving Mechanical Requirements

All structures are designed to survive all applicable load cases:

- Random vibration
- Acoustic
- Carrier liquid burn
- Lander SRM Burn
- Landing impact

Thermal:

- Meet all applicable functional requirements over the operating temperature range
- Survive nonoperational temperature range
- Accommodate temperature control hardware:
  - Thermal enclosure
  - Lander and SRM blankets systems divided by the separation planes
  - Heaters, thruster cluster RHUs and thermostats

Separation:

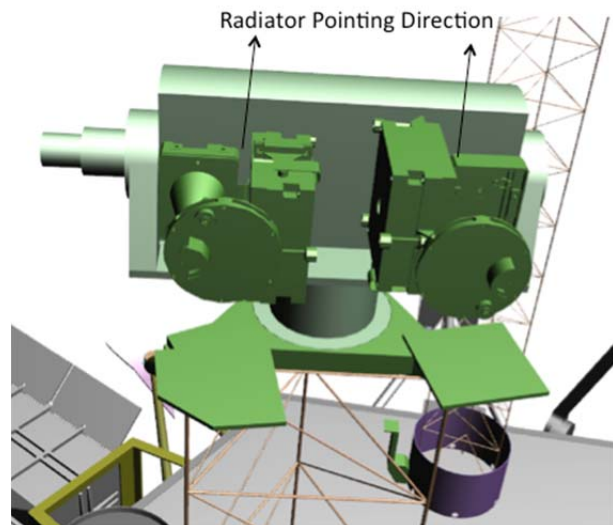- No recontact during Lander separation

Figure D.2.5-8. The SIS radiators will be managed by gimballing to passively control the temperature of the cameras.

- Lander must separate from spacecraft with a ΔV sufficient to prevent recontact

Landing:

- Lander must land without tip-over

Drilling:

- Lander must be able to react to maximum drilling loads with a factor of safety of 3.0

D.2.5.3.2 Features

Lander Configuration

The Lander has six energy-absorbing legs. Its footprint is 4 meters wide. The Lander's primary structure is a machined hexagonal forging. The thruster clusters are attached to the primary structure with tripod strut systems. The Lander's primary structure is based on an aluminum forging that is machined from the outside. After machining, deep stiffening ribs and a floor wall remain. This approach provides for a lightweight, high-strength, and stiff structure that also serves a dual purpose as radiation shielding.

All brackets, struts, secondary structures, and mechanisms are mechanically grounded to the

primary structure. Loads for these appendages are determined using the Delta IV Heavy mass acceleration curve (MAC).

The legs have an integrated crushable energy-absorbing mechanism. As part of the energy-absorbing feature there is a preload compression spring that removes the backlash after landing impact.

The Lander has no radiation-shielding vault, as the Carrier has. For the Lander, shielding is addressed at the avionics chassis level, local and integral to the item that requires the shielding.

The Lander's HGA is mounted on two-axis gimbals, as shown in Figure D.2.5-9. Although the HGA is adjacent to the MAG boom, the two-axis gimbals allow for articulation of the HGA in order to track the Earth and not interfere with the MAG boom. The HGA gimbal geometry allows for pointing reorientation to compensate for Lander attitude after landing. The HGA gimbal actuators do not require launch locks. By taking advantage of the actuator's high gear ratio, these gimbals can tolerate launch accelerations without failure or being back-driven.
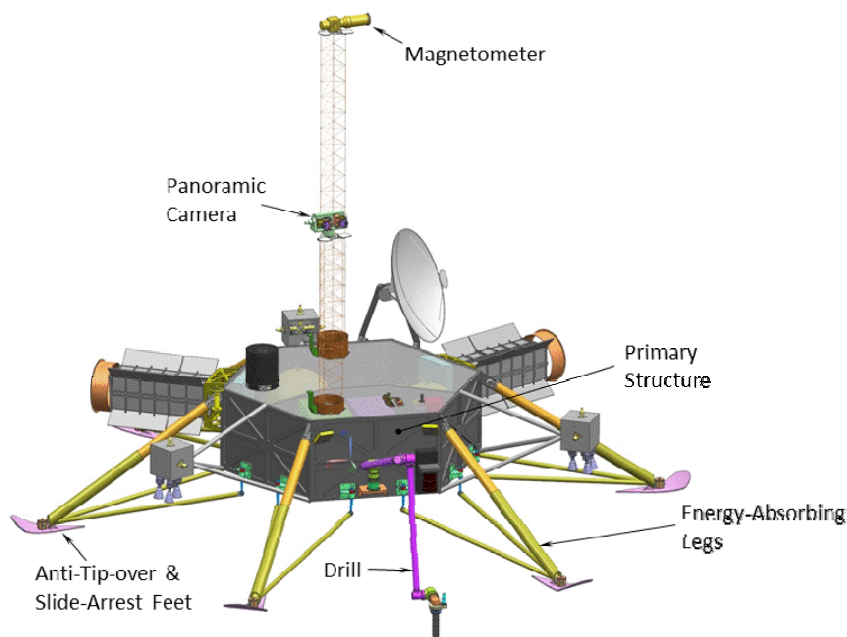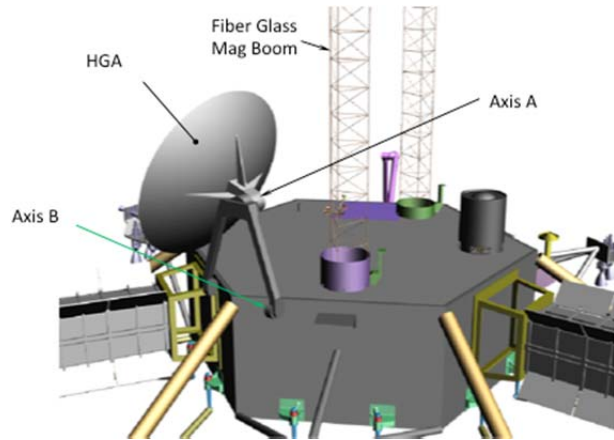

Figure D.2.5-9. The two-axis gimbals allow HGA/MGA communication from the landing sites in any Lander orientation.

The isometric view of the Lander is in Figure D.2.5-10. Figures D.2.5-11 and D.2.5-12 show top and side view dimensions for scale, respectively.

D.2.5.3.3   Schematic/Block Diagram

The Lander block diagram is shown in Figure D.2.5-3.

D.2.5.3.4   Sizing Analysis

A tip-over analysis was performed to determine the Lander's sensitivity to the number and size of energy-absorbing legs.

The MAC for the Delta IV Heavy launch vehicle was used to size the secondary structure.

D.2.5.3.5   Equipment Heritage

Europa Lander structures and mechanisms require no new technology development. Most applicable flight missions have used similar technologies.

D.2.5.4   Lander Thermal Control

The Lander thermal design uses, to the fullest extent

Figure D.2.5-10. Isometric view of operational Lander.

practicable, waste heat, insulation, and louvers to control temperatures. This approach consumes little to no operational heater power, is low mass, and has a flight-proven heritage.

D.2.5.4.1 Key Thermal Requirements

- Maintain the mono-propellant system and SRM within allowable flight temperature (AFT) ranges of 15°C to 50°C and 4°C to 32°C respectively.
- Maintain the battery within an AFT range of 10°C to 35°C.
- Maintain the avionics within an AFT range of -40°C to 50°C.
- Maintain all instruments within their Allowable Flight Temperatures.
- Accommodate the variation in environmental heat loads from Venus at 0.7 AU to Jupiter at 5.2 AU (2.0 to 0.04 Earth Suns).
- Minimize replacement heater power at outer cruise and on the surface of Europa.

Figure D.2.5-11. Top view of operational Lander.
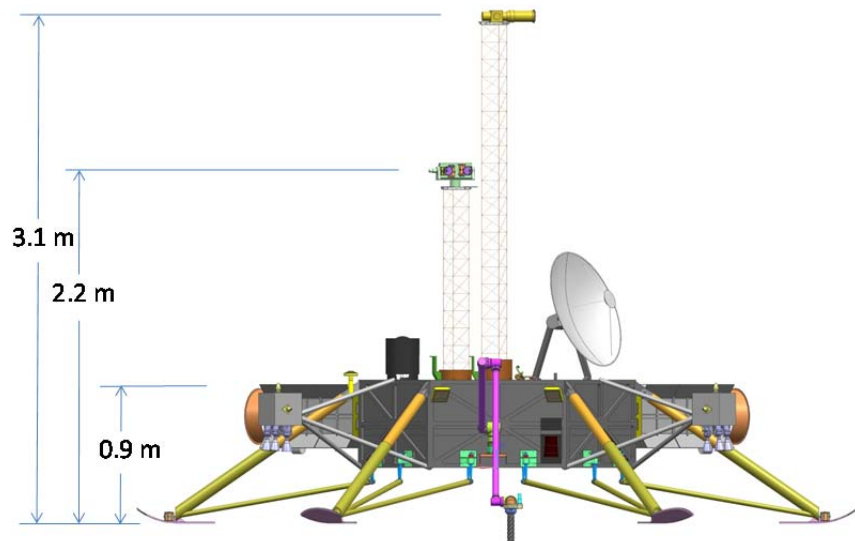
Figure D.2.5-12. Side view of operational Lander.

D.2.5.4.2 Thermal Design

Figure D.2.5-13 shows the primary thermal components of the Lander. The thermal-control system for the Lander features slightly oversized radiators to bias the system cold and louvers to regulate the hardware to the desired temperatures. The louvers effectively trim the radiator areas to produce acceptable temperatures.

Plain radiators reject approximately half of the waste heat. Louvers reject the remaining heat and regulate the Lander sides to 20°C, near the lower propulsion AFT. Conduction through the structure limits internal temperatures to 45°C, near the upper propulsion AFT. Areas

Figure D.2.5-13. The Lander design leverages electronics heat dissipation and VRHUs to minimize the electrical heating needs.

not dedicated to radiators and louvers are covered by multilayered insulation, including the Lander top, bottom, sides, and thruster cluster struts. High temperature stability is not required, nor are small temperature gradients. Louvers are adequate for overall temperature control.
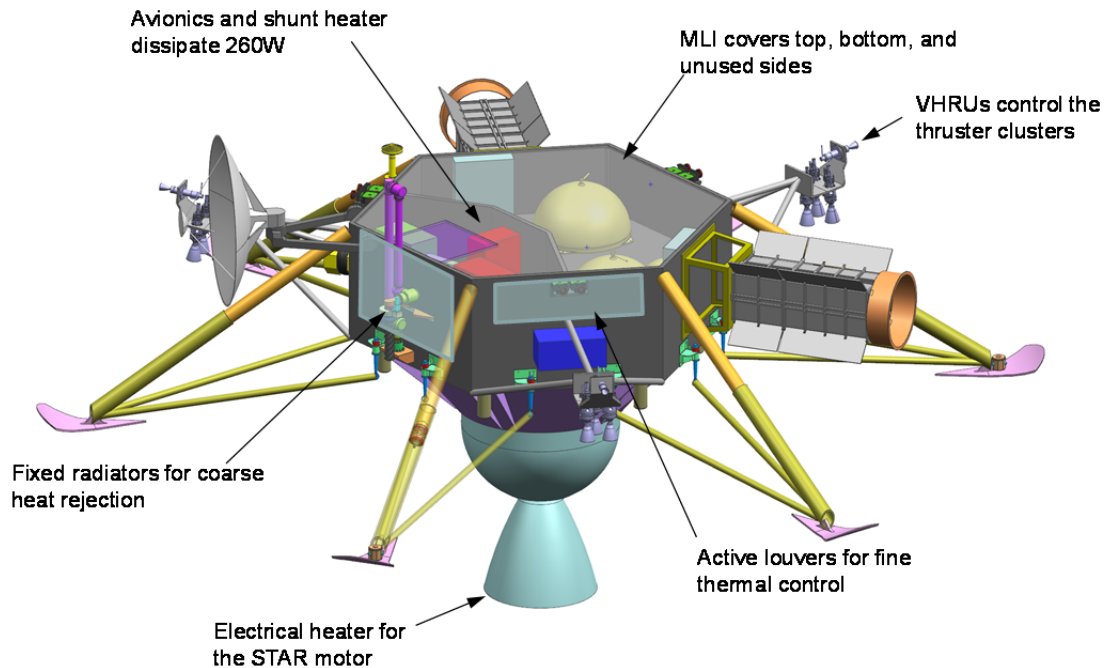
Two ASRGs, at 130 W each of electrical energy, produce a total of 260 W. This power is delivered either as electrical input to the avionics or as a load on the shunt heaters. By colocating the avionics and shunt heaters, the location of power and magnitude of power dissipation remain roughly constant.

Thermal control must be individually customized for each instrument via local radiators and heaters, orientation to thermal sources like the Sun, and control of the surrounding thermal context on the spacecraft. Addressing these issues in more detail for the model payload will be an important task during Phase A, and then again, once instruments are chosen.

The battery is mounted in a separate thermal zone with a dedicated louver because of the smaller AFT range. This mounting is accom-

plished by piggy-backing the battery to structure common with the propulsion system, but biased colder with a dedicated radiator.

Thermal control of the internal propulsion tanks and lines is a direct benefit of the radiator and louver design. No additional heaters are required for the internal propulsion components.

Due to its external location, RHUs and electrical heaters are required for the Star motor. RHUs make up a portion of the required power, leading to a cold biased motor. Software controlled electrical heaters trim the motor to its allowable temperatures. This system is single fault tolerant.

A thermal shroud over the struts that support the thruster clusters protects the lines from the Lander body to the thruster clusters. Heat radiating from the large, inboard end warms the strut cavity.

Variable radioisotope heating units (VRHUs) control the temperature of the thruster clusters. Local heating from the VRHUs is required due to the remote location of the thrusters. Each VRHU consists of two to three individual

RHUs mounted in a rotating cylinder. One half of the cylinder is painted white while the other half is insulated. A bimetallic spring positions the cylinder to radiate heat into the thruster cluster when the cluster is cold, or out to space when the cluster is warm. There are four VRHUs per thruster cluster with a total of ten individual RHUs per cluster. Three thruster clusters yield a total of twelve VRHUs and 30 individual RHUs. This design tolerates a failure mode where one VRHU is stuck fully open or fully closed.

To tolerate a loss-of-attitude fault at Venus, a hybrid MLI layup with five external layers of embossed Kapton protects against high exterior temperatures. Off-Sun illumination and the impact on temperatures will be studied during Phase A of the program.

D.2.5.5   Lander Propulsion

The Lander Propulsion Subsystem provides for deorbit and a controlled soft landing on the surface of Europa.

A block diagram of the Lander Propulsion Subsystem is shown in Figure D.2.5-14; Table D.2.5-3 describes key design characteristics. The Lander propulsion approach makes use of an ATK Star 30E SRM to provide the bulk of the ΔV for descent from Europa orbit. A monopropellant hydrazine propulsion system is used to complete the deorbit and carry out a soft landing. The monopropellant architecture comes from Phoenix heritage. In Phase A of the project we will perform a trade study of this hydrazine approach with a bipropellant approach.

The monopropellant hydrazine system provides TVC during the SRM burn using nine MR-107S 270-N thrusters. These descent thrusters are mounted on three clusters with three engines per cluster. Two of the thrusters on each cluster are canted slightly to produce a moment about the vehicle roll axis. The SRM propellant load will be selected such that the minimum horizontal velocity at SRM burnout is approximately 30 m/s. This under-burn allows the monopropellant system to be used for final deceleration of the vehicle so that recontact with the SRM is precluded.

Twelve Aerojet MR-103 (or equivalent) 1-N thrusters are used to provide three-axis attitude control between the time of separation from the Carrier element and SRM ignition. The thrusters are mounted four per cluster such that control moments can be produced about all spacecraft axes with minimal unbalanced impulse to perturb the orbit prior to SRM ignition. This attitude-control function will be performed in a blowdown mode (i.e., prior to activating the pressurization system) to minimize the mission's exposure to potential regulator leakage.

Immediately prior to separation from the Carrier, the Lander propulsion feed system will be filled down to the thruster valves by firing normally closed pyrovalve NC-1, which allows the lines to be filled from Tank 1 only. A flow-restriction orifice OR-1 is used to limit the water hammer pressures induced when the previously evacuated lines are filled. OR-1 is also sized such that the twelve 1-N thrusters can be operated to maintain attitude control prior to firing of the SRM. This prevents potential propellant transfer between the two propellant tanks during this period of zero gravity. Immediately prior to SRM ignition, the pyrovalves NC-1, -3, -4, and -5 are fired to allow flow from both propellant tanks to the twelve 270-N thrusters used for TVC during the solid burn and terminal descent.

Table D.2.5-3. The Lander Propulsion Subsystem uses heritage components to mitigate risk.

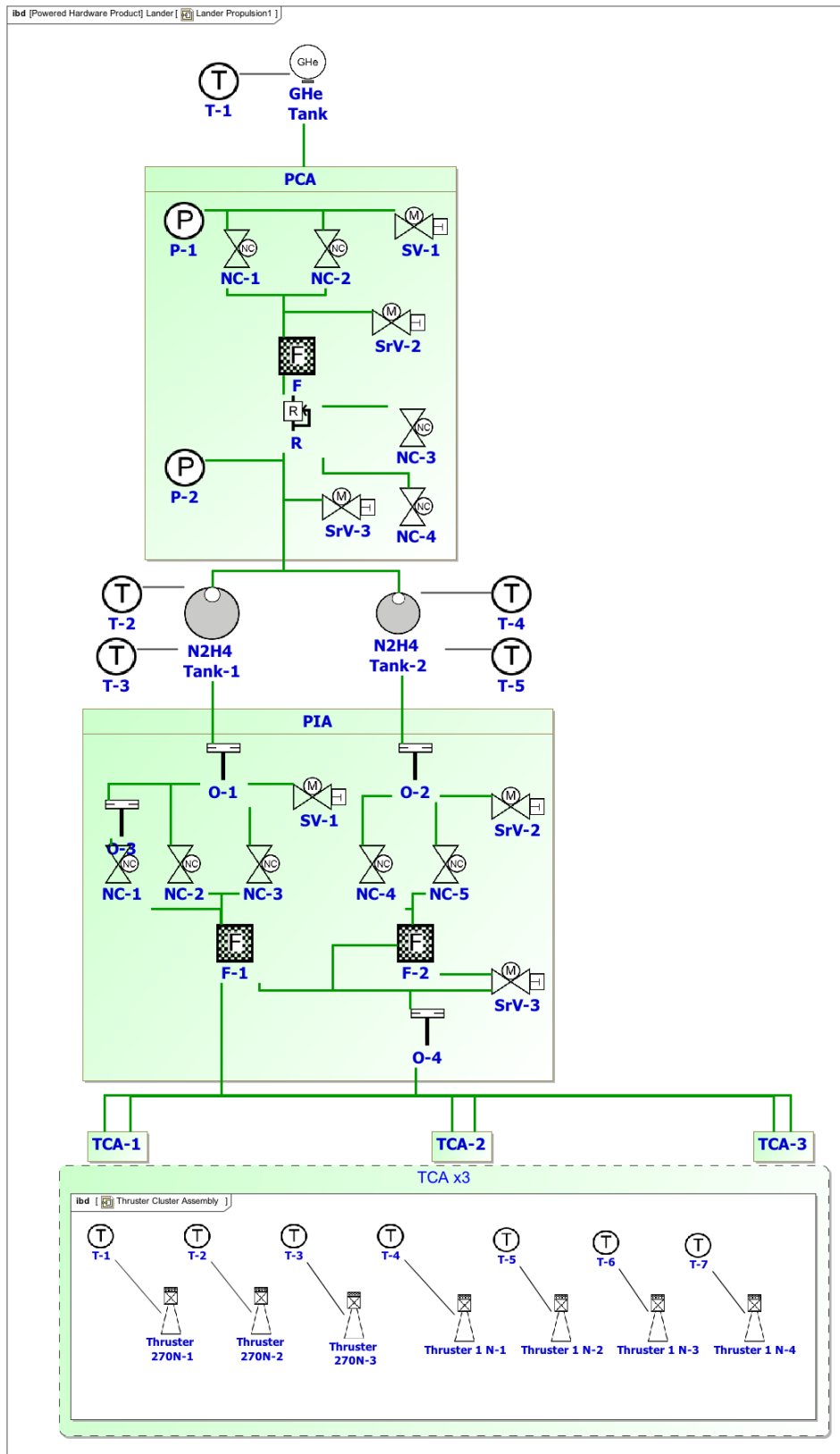| Propulsion Types	SRM (TAR 30E) Monopropellant hydrazine
Engines and Thrust Levels	SRM (35 kN average thrust) MR-107S (270-N thrust) MR-103 (1-N thrust)
Specific Impulse	SRM: 290.4 (effective) MR-107S (230 s) MR-103 (230 s)
Propellant Allocation	SRM: 631 kg max; monorop: 95 kg

Figure D.2.5.5-14. The Lander Propulsion Subsystem utilizes Phoenix architecture to enable a soft landing.

Fired in a Phoenix-style pulse-width-modulated throttling scheme, the 270-N thrusters provide controlled final descent following SRM separation. In this approach, all nine thrusters are fired at the start of each control period (approximately 100 ms) with the duration of each thruster pulse selected to produce the desired average thrust and to allow for control of pitch, yaw, and roll.

Allowing for the response time of the thrusters and the need to control attitude the average thrust can be varied over the range of approximately 365 N (15%) to 2200 N (90%). These descent thrusters are mounted on three clusters with three engines per cluster. Two of the thrusters on each cluster are canted slightly to produce a moment about the vehicle roll axis.

The hydrazine system relies entirely on off-the-shelf propulsion components, except for the CONAX pyrovalves, which will undergo delta-qualification using a stainless steel primer chamber assembly (PCA). Using pyro-isolation valves and single-seat thruster valves provide the required three mechanical inhibits (the pyrovalve providing two seals at two shear surfaces) against propellant leakage. SRM burn control and final descent will be performed in a pressure-regulated mode using the same series-redundant regulator design successfully flown on Phoenix. Two propellant tanks (approximately 53 cm in diameter) are equipped with elastomeric diaphragms to minimize slosh. The tank design may be based on the ATK P/N 80273-3 propellant tank. The Aerojet MR-107S has demonstrated 20-ms minimum response time, providing sufficient control for pulsed SRM control and final decent maneuvers.

The Star 30E SRM is a flight-proven design first flown in 1988. The mission will fly the motor for 7.8 years before it used. There is risk with duration this long, but there is data from at least two sources for long-duration exposure of SRM propellant. The solid propellant used in the motor has demonstrated in-space storage of 15 months on the Magellan mission (in a Star 48B SRM), and in excess of 5 years on the Long-Duration Exposure Facility (LDEF) with no evidence of performance degradation or changes in propellant structural properties. Starting in Phase A, a risk-mitigation effort will address the risk with long exposure and radiation exposure.

D.2.5.6 Lander Power/ASRG

The Lander Power Subsystem includes two ASRGs and 60 Ahr of secondary battery. The ASRGs are the same as described in the Section D.2.4.5.3. The Lander provides power to the Carrier in the combined configuration for all of the mission phases prior to separation. After separation the Lander operates for two hours in orbit prior to the descent and landing. Post-separation through landing is the defining case for energy storage.

The Lander Power Subsystem electronics are the same design as used on the Carrier with an increase in the number of MPSSs and MPDEs to increase the switch count and number of valve drivers.

The Lander Power Subsystem provides power to the Carrier in the combined configuration. After separation, the Lander provides the power bus regulation and distributes the power to the Lander loads. The Power Subsystem electronics provides switches in series to the Carrier interface to protect the power bus after separation.

D.2.5.6.1 *Power Driving Requirements for Pre- and Post-Separation*

1. Be single-fault-tolerant.
2. Provide energy storage for the mission load.
3. Provide power bus regulation in Carrier-and-Lander combination and Lander-only configuration.
4. Provide battery-charge control.
5. Distribute power to the loads.
6. Actuate valves.
7. Fire pyro events.

D.2.5.6.2   Power Subsystem Description

The Lander Power Subsystem electronics regulates the power bus and distributes power to the loads using the same architecture as defined in Section D.2.4.5.2. They are single-fault-tolerant, using a combination of block-redundancy with cross-strapped interfaces and some majority-voted functions. They provide the valve-drive and pyro-firing functions with range and mission safety inhibits for the hazardous functions.

In the combined Carrier and Lander configuration, the Power Subsystem is designed to operate with two independent power bus controllers on the same power bus by regulating the current into each battery with a gradual taper enabling both controllers to be active at the same time without cross-regulation issues.

In the post-separation operation, the Lander Power Subsystem provides energy for a two-hour orbit prior to descent and landing. This scenario is the defining case for energy storage. An opportunity exists where one secondary battery can be changed to a primary battery to cover the post-separation mode and maintain a 70% DOD for the DTE baseline science scenario. This will be studied in Phase A.

The Power Subsystem consists of two ABSL Li-ion batteries, a shunt radiator, an SDS, four PSSs, two PBCs, two PCUs, four PFCs, and four PDEs (Figure D.2.5-15).

D.2.5.6.3   Power Control

The PBC and SDS are the same designs as used on the Carrier with single-fault-tolerant capability to regulate the power bus with all four ASRGs in the combined configuration. The SDS provides an independent interface to each battery maintaining the current control into each battery.

The Lander uses two small-cell ABSL Li-ion batteries identical to the battery used on the Carrier as described in Section D.2.4.5.2. Each battery has a capability of 20 Ah at EOM after a single-string failure, including degradation for life, discharge rate, and operating temperature. The reference scenario that defines the
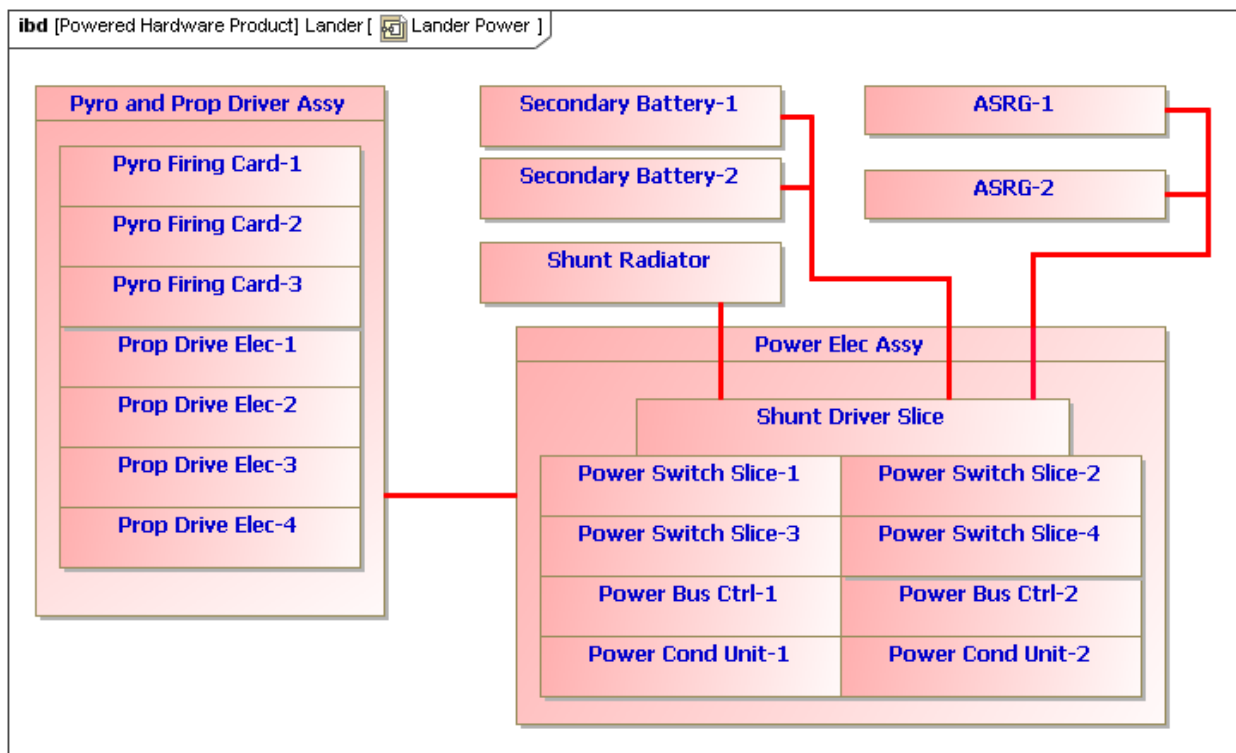
Figure D.2.5-15. The Lander Power Subsystem block diagrams show that the subsystem is single-fault-tolerant.

energy storage for the Lander is the 2-hour post-separation to deorbit burn (this is sized conservatively; it could be as little as 5 minutes), which requires 51 Ah at 10°C with a 15-A discharge rate. The JPL DPs allow for a 70% DOD, making a 51-Ahr EOL battery adequate for the post-separation Lander (JPL 2010a) for any combination of primary and secondary battery. So there is an opportunity to reduce the size of the secondary battery by adding a primary battery to cover the post-separation mode.

D.2.5.6.4 Power Distribution

The power distribution architecture is the same combination of centralized power switches in the MPSS and distributed power switches on the primary side of each PCU as used on the Carrier. This combination enables the system to optimize the mass of the cabling by using centralized switches for heater buses and other loads that do not require a PCU and distributed switches for each PCU, reducing the point-to-point cabling to reduce the mass in the Lander.

Independent high- and low-side switches prevent any single failure from resulting in a stuck-on load. Commanding is cross-strapped to the power switches through each PBC such that no single failure will prevent the commanding of any power switch. Each set of load switches is part of the load fault-containment region regardless of the location as a centralized or distributed switch.

D.2.5.6.5 Power Conversion

The power conversion architecture for each subsystem is the same as for the Carrier using a distributed point-of-load (POL) approach. The approach has a single isolated power converter on the PCU board, providing an intermediate power bus voltage that is distributed to each subassembly in the subsystem. The front end of each subassembly can cross-strap the intermediate power bus and provide on and off capability with fault management to enable low-power operating modes and improve subsystem fault-containment regions.

The primary side power switch is controlled by the Power Subsystem, and the POL regulators are commanded by the subsystem.

D.2.5.6.6 Pyro Firing and Valve Drive

The pyro-firing and valve-drive functions are provided by a set of centralized power switches in the Power Subsystem electronics commanded by C&DH via the PBC. The PFCs are fail-safe off, with two cards providing the block-redundancy. Each PFC fires 39 NASA Standard Initiators (NSIs) from a protected load power bus that provides all of the safety inhibits required for launch. The PFC controls the current into each NSI, with an overall capability to fire six simultaneous events.

The PDE actuates the valves for the ME and the ACS thrusters. The PDE also switches power from the protected load bus with the necessary safety inhibits in place. The PDE is fail-safe off with the single-fault-tolerance provided by a block-redundant set.

D.2.5.6.7 Power Subsystem Heritage

The Lander Power Subsystem uses the same architecture as the Carrier and is based on heritage from SMAP. The power bus control algorithm is the same for both the Carrier and Lander.

D.2.5.7 Lander Telecom Subsystem

The Telecom Subsystem performs a single role for the Lander: two-way communications with Earth. This function is accomplished though through two independent routes: first, DTE communications via an X-band low-rate link, and second, relay communications through the Carrier element. Each link has a very specific set of roles as discussed below.

D.2.5.7.1 Design Drivers

There are a number of driving requirements for the subsystem. It must accept uplinked commands through all postlaunch mission phases as well as send to Earth engineering telemetry and science data. Design drivers are:

- DTE (via 70-m equivalent):

– Science and engineering telemetry: ~9 kbps
– Uplink commanding: ~1 kbps
– Safe mode commanding: ~7.8 bps
– Safe mode telemetry: ~10 bps
– Floor Science Return: 1.3 Gbit (mission total)
– Total DTE Capacity: 7.8 Gbit (30° elevation case)
– Semaphore communications during DDL
– Delay-tolerant networking (DTN)
- Relay communications via Carrier element:
   – Science and engineering telemetry: multiple hundreds of kbps (multiple factors affect this)
   – Forward link commanding: ~100 kbps
   – Baseline science return: 4.6 Gbit (mission total)
   – Total relay capacity: 33 Gbit (30° elevation case)
   – DTN
   – ADR capability

For the DTE link, implicit in these requirements is communications with the DSN 70-meter-equivalent station(s). In order to achieve these requirements, communications must be through either a 70-m station itself or through an arrayed set of four 34-m stations that, when combined, meet the throughput capabilities of a single 70-m station.

There are no driving requirements for Doppler navigation; however, Doppler tracking through the UHF relay link can improve Lander positional knowledge accuracy.

The Telecom Subsystem is also required to be single-fault-tolerant. Single-fault-tolerance is achieved through the use of block-redundant USTs and frequency diversity (UHF and X-band). The X-band link hardware complement (antennas, power amplifier, and microwave hardware) and UHF hardware (antennas and switching hardware) are all single-string.

D.2.5.7.2 *Subsystem Features*

The implementation of the Telecom Subsystem includes X-band uplink and downlink capabilities for DTE communications as well as a UHF relay communications link through the Carrier element. Since there will be extended periods when the Lander does not have communications with Earth, the Telecom Subsystem is configured as a store-and-forward architecture complete with DTN capabilities. This architecture enables both science data and engineering data to be stored locally on the Lander and forwarded when a communications link, either via X-band DTE or UHF relay, is available.

The prime component within the Telecom Subsystem is the UST. The UST is a derivation of the Electra Relay Communications Payload currently flying aboard the Mars Reconnaissance Orbiter (MRO). MRO Electra is strictly a UHF-capable radio at TRL-9. UST is, however, currently in the design phase to add on both an X-band up/downlink capability and a Ka-band downlink capability. As of the writing of this report, UST is at TRL-4, with elements, capabilities, and numerous features having already been demonstrated through TRL-9 with the Electra payloads on both MRO and the MSL. For the Europa Lander Mission, we propose to fly fully redundant USTs to achieve full single-fault-tolerance. The Lander version of the UST will contain an X-band uplink/downlink slice as well as a UHF slice. No Ka-band capability is envisioned. The prime UST is powered on all the time while the redundant UST is kept in cold (powered-off) standby condition.

The UHF slice of the UST contains all the equipment necessary for relay communications, including a UHF power amplifier (~10 watts RF), low-noise amplifier, and RF up/down converters.

The X-band slice of the UST contains all the equipment necessary for DTE communications with Earth via X-band, including the RF

up/down converters and other RF electronics. Power amplification is achieved through the use of a stand-alone TWTA. Additional external hardware includes WTSs, a 0.75-m two-axis steerable antenna for high-rate (~9-kbps) communications to Earth as well as an LGA/MGA antenna suite for communications during DDL and safe mode. This implementation configuration enables communications in the event the Carrier element is not available for relay communications. Further this implementation enables the Lander state to be communicated to Earth through the use of semaphores throughout the entire DDL mission phase.

Within the UST, the digital baseband processing module (DBPM) is shared by both the X-band hardware and the UHF hardware, which handles all the necessary data manipulation (framing, formatting, scheduling, etc.) as well as the necessary link protocols (Proximity-1 for relay and the relevant CCSDS protocols for DTE). Included in the DBPM is a mass memory module for storing science data as well as engineering data in preparation for transmission back to Earth.

The UHF relay link is the prime communications path during landed operations. It also provides backup communications during DDL should the Carrier element be in view during DDL. Relay communications take place anytime the Carrier element is above the local Lander horizon. The communications link is sized to and designed for a 30° minimum elevation mask but can communicate with the Carrier down to a 0° elevation should it be available. This capability is achieved through the use of a low-gain helix antenna similar to what is used on both MRO and MSL. Further this antenna enables relay communications to the Carrier should the Lander land on a local slope or with one or more landing feet on a rock (resulting in a tilted Lander). This architecture has been successfully proven on both the Mars Explorer Rovers (MER) as well as MSL.

D.2.5.7.3   *Block Diagram*

As shown in the Telecom Subsystem block diagram (Figure D.2.5-16), the equipment configuration is based upon many years of both deep-space and relay communications heritage. There is an X-band portion dedicated to DTE communications as well as a UHF portion dedicated to relay.

X-band communications is enabled through one of three antennas. During DDL, the X-band link sends semaphore communications through the LGA. This ensures a robust understanding of the Lander state during the critical DDL mission phase. Upon landing, data communications can take place at a low rate through the MGA or a higher rate through the steerable 0.75-m dish antenna. Further the MGA enables safe mode communications should the Lander lose its understanding of the Earth's location; the MGA is simply pointed at the Sun, and the Earth will fall within its beamwidth. Switching between the antennas is accomplished through the use of WTSs. Power amplification is through the use of a TWTA.

For the UHF link, the UHF helix antenna is switched between the two USTs via a CTS. The UHF antenna is fixed to the Lander body and is pointed nominally at zenith. The beamwidth of the UHF antenna is broad enough (between 120° and >180°) that if the Lander lands on a local slope, communications is still achievable with the Carrier element.

Overall, the use of the dual-frequency architecture results in a robust communications link. Should communications between the Carrier element and the Lander be lost (for whatever reason), the DTE link provides the capability for the floor science mission. Both DTE and relay communications architectures have been proven through multiple Mars missions such as MRO, MER, and soon MSL.

D.2.5.7.4   *Equipment Heritage*

Hardware heritage comes from a number of previous missions. The HGA will be similar to the Kepler's 0.85-m-diameter HGA (Fig-
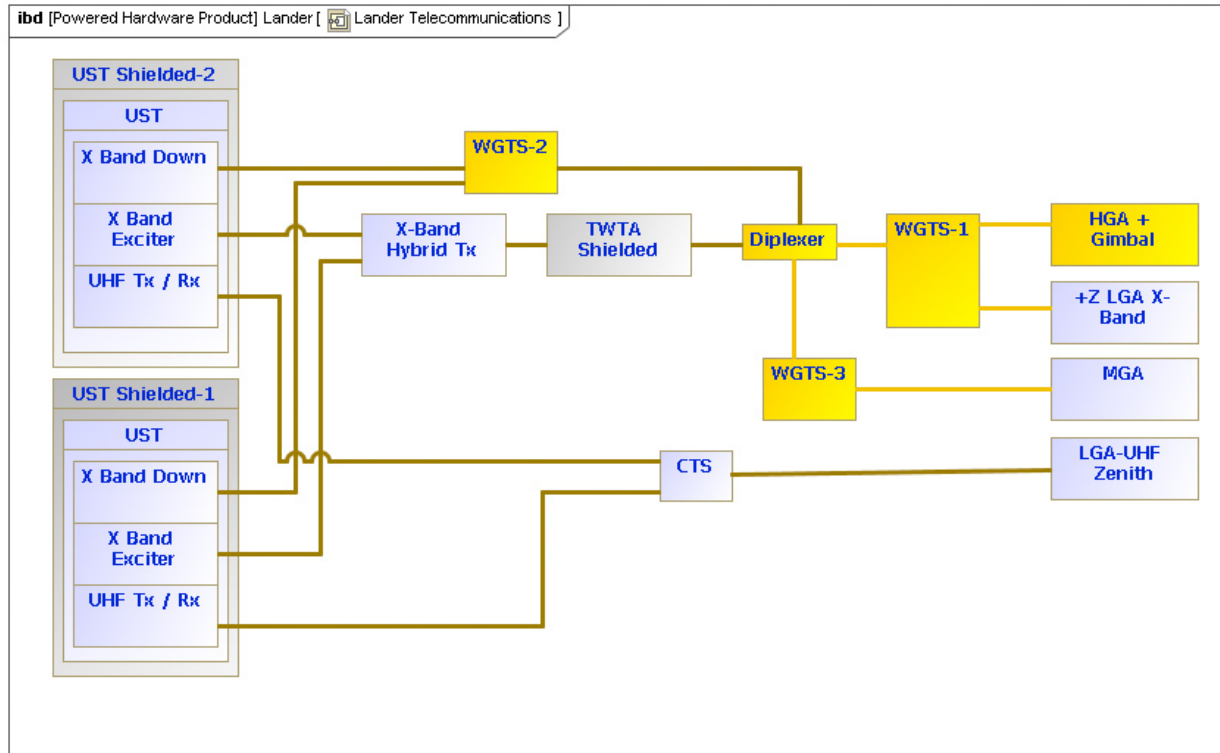
Figure D.2.5-16. The Telecom Subsystem provides robust fault-tolerance through a simplified architecture that minimizes potential for single-point failures.

ure D.2.5-17). Kepler's design solely used Ka-band but can easily be converted to an X-band-only configuration.

The TWTAs have heritage from multiple JPL missions: Juno, Dawn, and MRO (X-band). A good example here is the X-band TWTA for the Dawn mission, shown in Figure D.2.5-18. The Europa Lander Mission will leverage a long history of downlink TWTAs designed specifically for the requirements of deep-space missions.
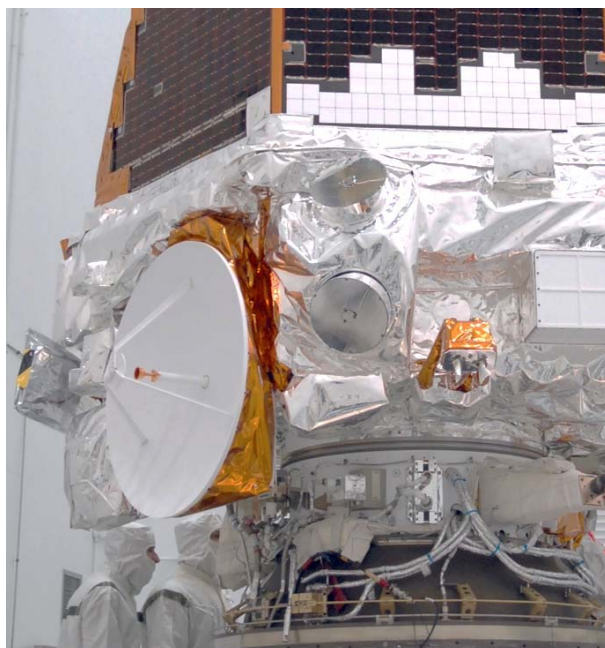
Figure D.2.5-17. Kepler's 0.85-m HGA provides the basis for the Europa Lander Mission HGA.

Figure D.2.5-18. Candidate X-band TWTA (flown on MRO, MSL, and Dawn).

Figure D.2.5-19. The Electra payload, as shown on MRO, provides the basis for UST relay communications for the Europa Lander Mission.

USTs, which provide the mission-critical uplink and downlink function, have heritage from the Electra payloads onboard MRO and MSL as well as years of experience with deep-space communications hardware in the Small Deep Space Transponder (Figure D.2.5-19).
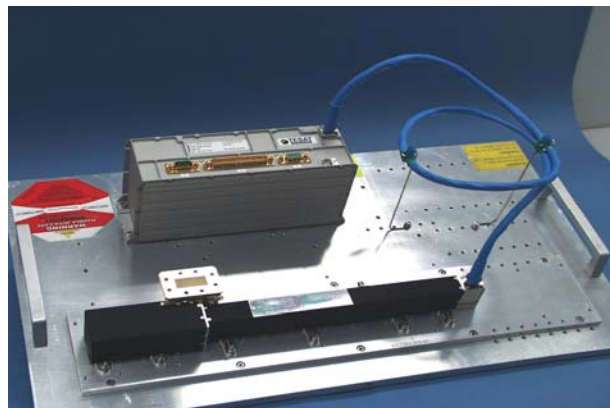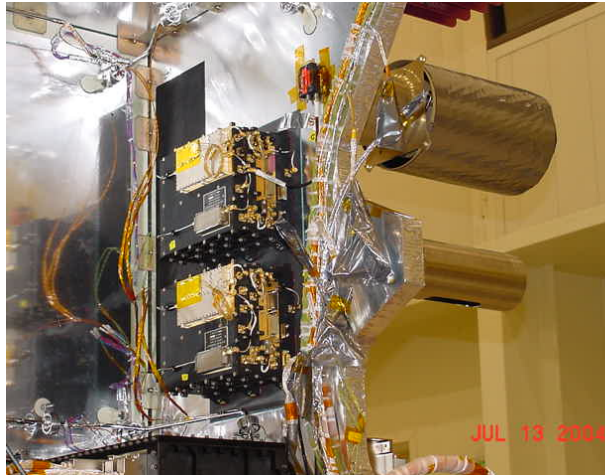
D.2.5.7.5　Characteristics and Sizing

The Telecom Subsystem downlink data rate is configured to meet a minimum 3.7 Gb/Eurosol with an elevation mask of 30° during nominal relay operations with the Carrier element in a 200-km circular orbit, as shown in Figure D.2.5-20.

We've taken a conservative approach with the telecom link by requiring 3 dB margin minimum and by making conservative estimates of individual contributors to the link (Table D.2.5-4). Parameters such as RF losses in the downlink path, DSN station performance due to low station elevations, link degradation at low Sun–Earth pointing (SEP) angles are all taken into account.

Overall, we propose a very conservative and robust X-band communications link.

The LGA provides only 2π-steradian coverage; this view enables command uplink as well as semaphores for downlink state status at very specific spacecraft attitudes. The distances to Jupiter, however, prevent LGA communications at the required safe mode rates. To meet safe mode communications rate requirements, an MGA is needed. All high-rate communications are performed through the HGA. Turbo coding at rate = 1/6 is also part of the baseline communications architecture.

D.2.5.8　Lander Guidance, Navigation, and Control

The Lander GN&C Subsystem provides the capability for pinpoint landing on Europa's surface to maximize the probability of landing success.

The GN&C Subsystem provides three-axis attitude control through DDL and actuator control during surface operations. During DDL the Lander provides three-axis control via thrusters. Small ACS thrusters (1 N) are used after Carrier separation and before the SRM is ignited. After SRM ignition, the large thrusters (270 N) provide attitude control; they are also used after SRM burnout for attitude and descent control to the surface. State information is transferred from the Carrier prior to separa-

10 degree Elevation Mask

Orbit (km)	Passes/ES	Duration/ES	Data/ES (Gb)	Energy
50x50	5	20 min	1.8	0.05J/kbit
100x100	8	53 min	4.1	0.054J/kbit
200x200	12	133 min	7.9	0.07J/kbit
300x300	14	220 min	10.5	0.09 J/kbit

30 degree Elevation Mask

Orbit (km)	Passes/ES	Duration/ES	Data/ES (Gb)	Energy
50x50	2	2.9 min	0.36	0.05J/kbit
100x100	3	10.7 min	1.2	0.054J/kbit
200x200	6	36.2 min	3.7	0.07J/kbit
300x300	8	66.5 min	6.1	0.09 J/kbit

Target Orbit

Figure D.2.5-20. The Telecommunications Subsystem X-band DTE link is sized to meet the floor mission with margin.

Table D.2.5-4. Telecom X-band is conservatively sized with good link margins.

Parameter	Required Capability	Notes
Throughput Rate (worst case)	9 kbps	At 5.5 AU from Earth
TWTA RF Power	25 W (X)	2× for Power Dissipation
HGA Diameter	0.75m	Body fixed HGA, 60% efficiency
HGA Pointing Error	≤1.0°	Set by Earth pointing knowledge
DSN Station Capability	70-m equivalent	Can be 4 × 34-m antennas arrayed
DSN Weather	90% cumulative dist.	
DSN Station Elevation	20°	Worst-case, fixed
Earth S/C Range	5.5 AU	Average mission design
Turbo Coding	Rate=1/6	Short frame
TWTA to HGA Losses	2 dB	Conservative estimate
Link Margin	3 dB	Per Institutional guidelines
SEP Angle	20°	Worst-case assumption
Operational Configuration	X-band up, X-band down	X-band DTE as backup to relay
Operational Configuration	DDL: Semaphores through LGA After landing: Telemetry through HGA Safe mode: Telemetry through MGA	All Lander mission phases covered through DTE
Hardware Configuration	X-band up, X/X-band down 1 each LGA, MGA, HGA, TWTA, WTSs	Possible X-band SSPA in lieu of TWTA

tion and is propagated by the IMUs; pinpoint landing guidance is accomplished through TRN and hazard detection near touchdown is accomplished through an onboard LIDAR. Section D.2.3.4 describes the operations concept for DDL.

On the surface, the GN&C will control the HGA/MGA for DTE communication. It also controls the SIS for collecting science imaging and site imaging for sampling. Finally, GN&C controls the five-DOF sampling system with ground based trajectories based from DEMs created from the SIS images.

Table D.2.5-5 shows the key features and benefits of the Lander GN&C architecture. The C&DH Subsystem hosts the FSW, including all of the GN&C software. Using the heritage approach common to all recent JPL spacecraft, the GN&C software is delivered in C-code developed from the GN&C design and simulation environment. The IMUs, TRN cameras, and LIDARs are heavily shielded from radiation (total dose and electron flux), allowing the use of standard space products. TRN camera detector and LIDAR detector anneal heaters are baselined to mitigate radiation DD. The shielded TRN camera takes

images and matches those to an onboard map of the landing area to calculate a guidance command to the desired pinpoint landing zone (100m x 100m). The shielded LIDAR is used at the end of descent to detect small hazards; the GN&C FSW then calculates and commands a divert to the safest landing spot. Sun

Table D.2.5-5. The GN&C Subsystem provides TRN guidance and LIDAR hazard detection to enable a safe pin-point landing.

Feature	Benefit
C&DH hosts GN&C FSW and provides interface to sensor/actuators	Allows autocode direct from GN&C design
Spacecraft radiation shielding	Enables use of off-the-shelf GN&C H/W
TRN camera radiation shielded for electron flux	Meets requirements for pinpoint landing with TRN
TRN guidance	Provide ability to land on any 100 m x 100m landing site selected for scientific interest and safety
LIDAR radiation shielded for electron flux	Meets requirements for hazard detection to allow hazard avoidance maneuvers
LIDAR hazard detection	Provides ability to divert to safest 10m x 10m landing zone in the 100m x 100m landing site.
Sun pointed MGA	Allow DTE communication without any state knowledge

sensors combined with a wide FOV MGA enable communication to Earth in the event that the Lander does not have any state information.

Table D.2.5-6 shows the key characteristics of the GN&C Subsystem. Figure D.2.5-21 shows the thruster configuration. The attitude-control thruster sizing of 1 N is to provide a sufficiently small minimum torque impulse for deadband attitude control after Carrier separation and before DDL begins. The TVC thruster sizing of 270 N is to provide sufficient control authority for up to a 2-centimeter shift of the vehicle center of mass (CM) during the SRM burn; these same thrusters also provide the necessary thrust-to-weight ratio for descent and landing. Ballast mass is also included in the MEL (Section D.2.3.4) to provide initial CM/center of gravity (CG) alignment. For attitude control and TVC, a thruster moment arm of approximately 2 meters is used.

The 10-mrad X-band HGA pointing requirement is a radial, three-sigma number derived
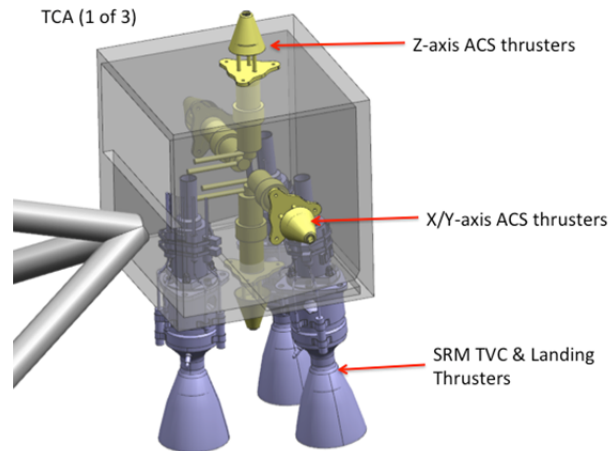

Figure D.2.5-21. The Lander thruster configuration leverages the proven Phoenix Lander approach.

from the telecom link analysis; this link supports the floor science data transmission requirements. The X-band MGA pointing requirement for safe mode is 174 mrad, based on a beam width that allows Sun-pointing with Sun-sensors while still communicating with Earth from Europa. The horizontal and vertical velocity control (0.25 and 0.5 m/s respectively) meets the requirements for not damaging the Lander or tipping over when applied to the "challenge" landing case (Section D.2.3.4). The HD feature resolution of 3m wide by 1m relief is required to detect hazards not located by the reconnaissance image processing and allows a divert to a safe landing site. The HD slope detection of 25 degrees or greater is required to detect hazard not located by the reconnaissance image processing and allows a divert to a safe landing site.

Figure D.2.5-22 shows the block diagram of the GN&C Subsystem. The subsystem is single-fault-tolerant. At its center is the FSW that resides in the dual RAD750 processor in the C&DH electronics. The TRN camera head is cross-strapped to redundant TRN control electronics. The dual HD LIDAR is interfaced to redundant TRN control electronics. For Sun-pointing of the MGA, the Sun vector with respect to the vehicle reference frame is pro-

Table D.2.5-6. The GN&C Subsystem design provides safe deorbit, descent, and landing.

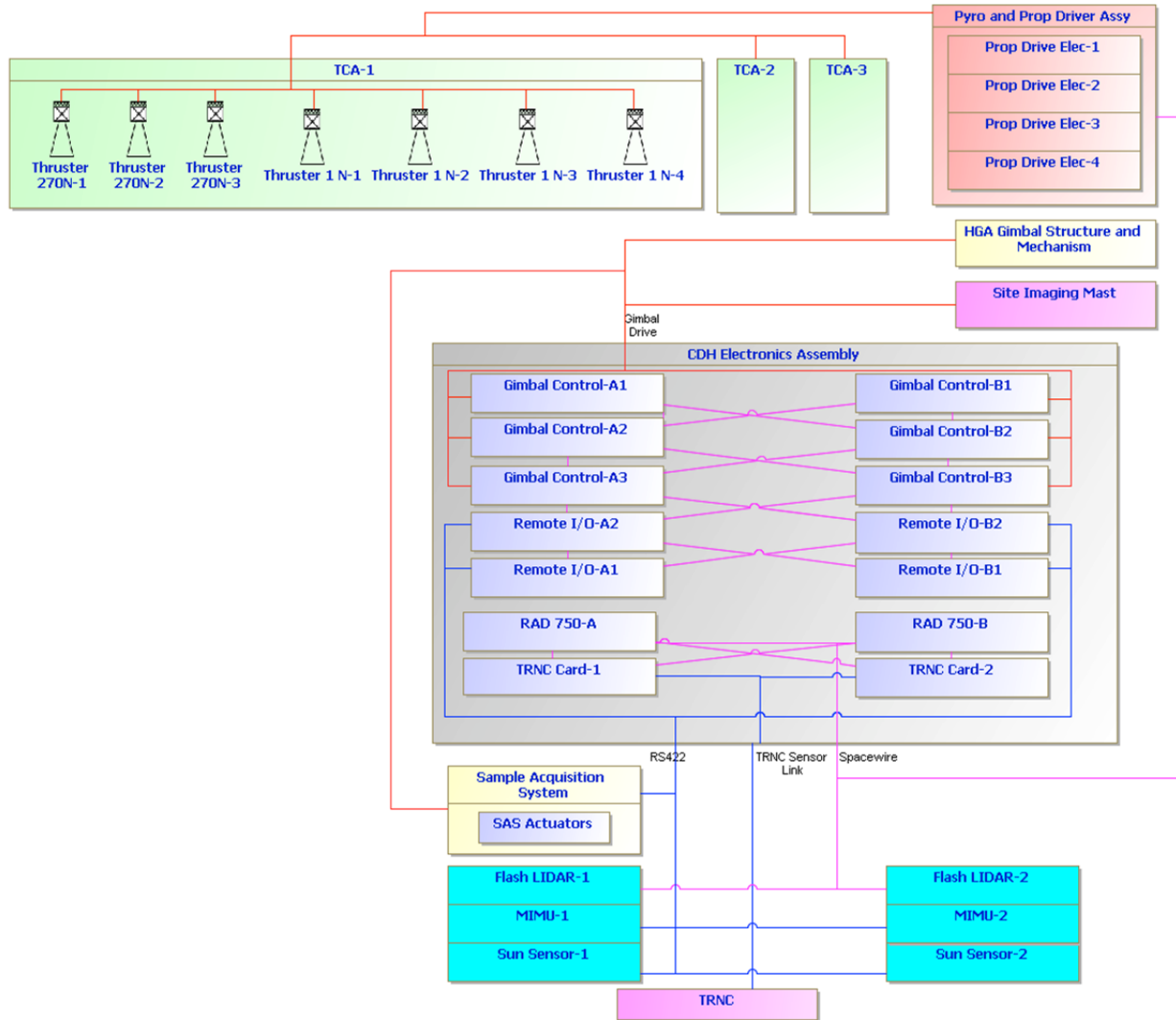| Item	Value	Sizing
Attitude-Control Thruster Size	1 N	Minimum torque impulse bit for deadband control after Carrier separation
Landing/TVC thruster	270 N	Thrust to weight for landing & SRM TVC command authority
X-band DTE HGA pointing	10 mrad	Support HGA link budget at required data rate with 3 dB of margin
X-band DTE MGA pointing	174 mrad	MGA communication while Sun-pointing
Horizontal Velocity Control	0.25 m/s	Necessary to prevent tip-over on challenge case landing site
Vertical Velocity Control	0.50 m/s	Necessary to prevent tip-over and structural damage on challenge case landing site
HD Feature Resolution	3m wide x 1m relief	Necessary to prevent tip-over and structural damage on challenge case landing site
Slope detection	>25 degrees	Necessary to prevent tip-over and structural damage on challenge case landing site

Figure D.2.5-22. The GN&C Subsystem is redundant and cross-strapped to provide robust fault-tolerance to radiation events.

vided by the three Sun-sensors distributed on the Lander to provide 2π-steradian coverage (this function is needed only on the surface of Europa). Before Lander separation the high precision state of the vehicle is transferred to the GN&C FSW; this state is propagated during DDL by either of the dual, navigation-grade IMUs.

For fine attitude control, after Carrier separation but before SRM ignition, the GN&C will use the small, 1-N thrusters. For high authority attitude control and descent control the GN&C will use the large, 270-N thrusters. The redundant motor drive electronics reside in the

C&DH; the GN&C software provides closed outer loop control of the SIS two-axis gimbals, DTE antenna two-axis gimbals, and the five-DOF sampling arm. The architecture is cross-strapped such that any sensor/actuator can be connected to any processor.

Given the radiation shielding provided by the spacecraft, the GN&C Subsystem can use standard space GN&C products with high TRL. Table D.2.5-7 shows the GN&C hardware items, suppliers with high-TRL products, and the approach to deal with radiation.

Table D.2.5-7. The radiation-hardening approach enables the use of heritage GN&C hardware.

Item	Supplier(s)	Radiation Approach
Sun-Sensor	Adcole	Radiation-hard by design
TRN Camera	JPL	Shielded for total dose and electron flux
HD LIDAR	ACS	Shielded for total dose and electron flux
Inertial Measurement Unit	Honeywell Northrop Grumman	Shielded for total dose

Terrain-Relative Navigation (TRN)

TRN compares images taken during descent to an onboard map to locate the Lander within the local terrain frame, as shown in Figure D.2.5-23. The map is constructed from images taken from orbit during the reconnaissance phase, and is uplinked to the Lander prior to descent.

Descent images are compared to the map through a two stage TRN process. In the first stage (TRN matching) a large image patch is extracted from the descent image and then warped to a grid aligned with the map coordinate frame using the best available states from an onboard estimation filter for altitude and attitude. The patch is correlated with the map using frequency domain techniques. The map is cropped using the position estimate from NAV to minimize the correlation processing time. The location of the matched patch in the map provides a position estimate. This process is repeated on a sequence of images at 1 Hz, and if the position estimates agree with each other, then a position lock has been achieved.

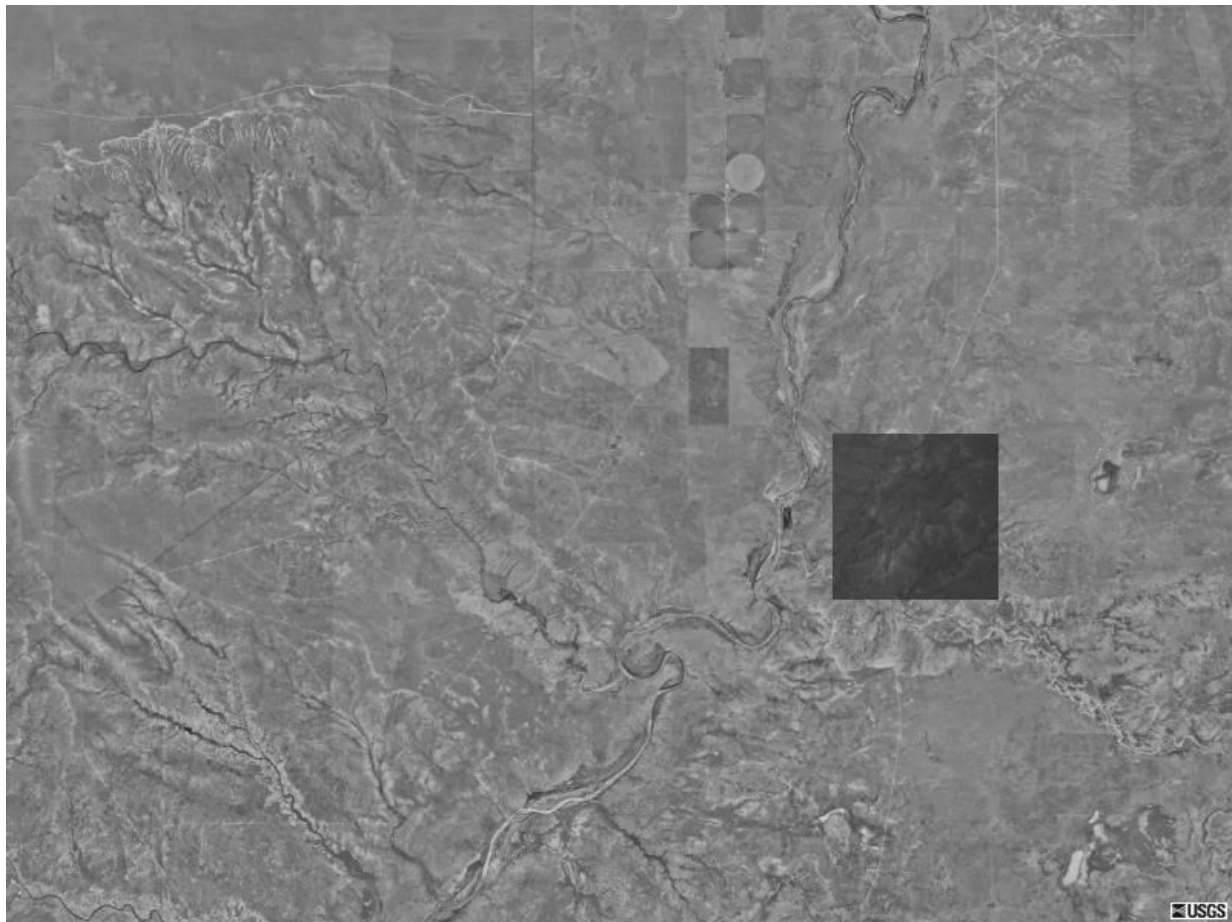Once a position lock has been achieved the second TRN stage (TRN tracking) begins.

Figure D.2.5-23. TRN enables safe, pinpoint landing. TRN correlates descent image (darker) with onboard map constructed from orbital imagery (example from Earth-based flight test).

Every second, a descent image is warped to the map frame. A feature selector is applied to the warped image and feature locations are extracted. These feature patches are correlated with the map. The match locations are converted to map landmarks (3D landmark positions in the map and 2D bearing angles in the image). The mapped landmarks are compared to each other to identify outliers. After outliers are rejected, landmarks are passed to an estimation filter. Also input to the filter is LIDAR range measurements.

After the altimeter measurement is solid and images are being taken, the velocity estimation phase begins and continues to the ground. VEL uses similar processing to the second stage of TRN, but the matching is between two descent images taken at 10 Hz (0.1 second apart) apart instead of between a pair of descent images and the reference map. The two images are warped to the map frame using the altitude and attitude estimates from the filter when the images were captured. The feature selector is applied to the first image, and then the selected features are correlated with windows from the second descent image. The feature tracks and the range measurement from the first image are input to a module that computes the change in position (vertical and horizontal) between the images. This change in position is provided as input to the filter. These velocity estimates continue all the way to touchdown.

The filter uses the above measurements to update Lander position, attitude, and velocity.

Once the filter has converged on a solid Lander position and velocity estimate, estimates are passed back to NAV on the Lander. The TRN process continues until the Lander signals that ignition has occurred.

The best available position and velocity estimates from the filter are used during free-fall by powered descent guidance (PDG) to generate a ΔV-optimal trajectory and thrust profile to the target. Prior to DDL, attitude, speed, and "glide slope" constraints can be specified as input to PDG. PDG also has a "fuel-limited targeting" mode that it can use in the unlikely event that onboard computation shows that the trajectory to the target requires more propellant than is available. In this mode, PDG retargets to the closest point to the intended target within fuel range.

Hazard Detection and Avoidance

The Lander uses a 3D flash LIDAR for hazard detection (HD). This LIDAR has a detector array in which each element is capable of independently sensing time of flight of returning photons. Each "flash" of the laser produces a "range image" with a point for each detector element. Transforming the range image into the terrain frame produces a 3D digital elevation map of terrain that is used to detect hazards (Figure D.2.5-24).

Hazard detection begins once the spacecraft indicates that near-vertical descent has started and the spacecraft is below ~250 m (the LIDAR's maximum range). The LIDAR is reconfigured to the wide illumination mode for
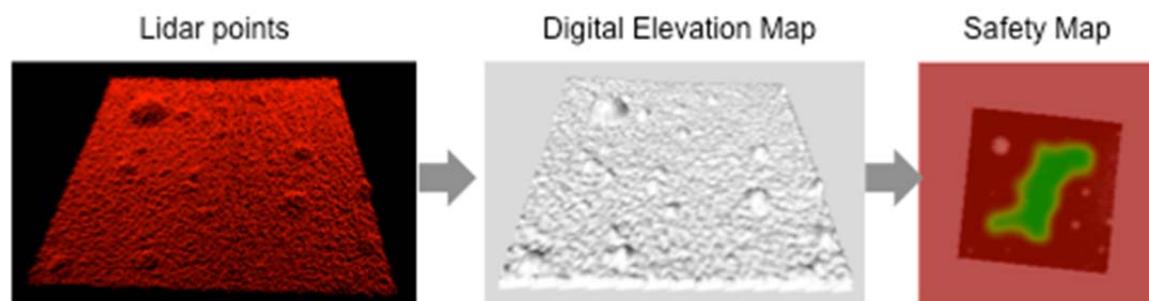

Figure D.2.5-24. Range image from the HD flash LIDAR converted to a digital elevation map, from which a safety map is created and safe landing site selected.

HD, and two flash LIDAR range images are taken. The range images are processed to identify hazards within the LIDAR FOV, and the safest reachable site is selected. The coordinates of the new target site are passed to the spacecraft, and PDG calculates a new trajectory to divert to the new target. During all of vertical descent, including the HD phase, LIDAR data is being processed to measure range, albeit with the wider coverage of the HD range image.

D.2.5.9 Lander Command and Data Handling Subsystem

The Lander C&DH provides a cross-strapped and redundant radiation-hard platform to support the data storage and processing needs of Lander science.

The functional requirements and goals of the C&DH are as follows. The design should be single-fault-tolerant and cross-strapped to enable the C&DH to fail operational during single-event effects in the high-radiation environment at Europa. The design should allow swapping to enable rapid transition of control during a fault. A RAD750 single-board computer (see Figure D.2.5-25) was selected to leverage the processor flight heritage, radia-

tion-hardness, and JPL's software architecture heritage. Onboard data storage will accommodate multiple copies of the Lander science data; Phase A will consider concepts for data integrity using the excess storage capability.

The C&DH electronics box is a single box that is internally redundant. The electronics chassis is the radiation shield for the electronics. The material and thickness will provide an equivalent TID environment of 50 krad. Given the use of SpaceWire (see Figure D.2.5-26) as the primary interface, there is no need for a backplane or motherboard within the box to increase the C&DH box reliability.

A standard-size chassis of 6 U × 220–mm cards was selected to enable the use of heritage single-board computers and provide sufficient board area for the I/O and memory cards. Time broadcast and synchronization are part of the SpaceWire standard, so no external timing network is required. The remote I/O handles all the low-level interfaces such as analogs, discretes, and serial I/O; it also provides the telecom interface, critical relay commanding, and processor swap functions. The I/O is multiplexed through the SpaceWire interface chip. This radiation-hard chip includes an
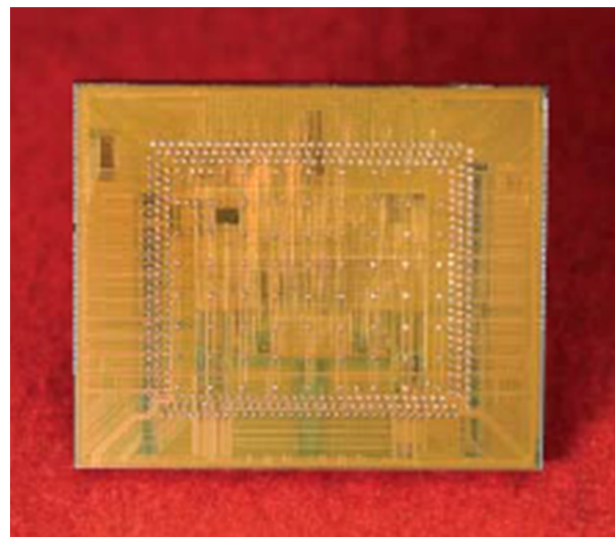

Figure D.2.5-25. The RAD750 provides high heritage for both the C&DH electronics and FSW designs.

Figure D.2.5-26. The SpaceWire interface chip is radiation-hard and provides a high-speed standard interface to the cards in the C&DH.

embedded processor to accommodate programmable I/O functions. The I/O circuits are standard designs from other JPL spacecraft.

Motor drive cards drive the Lander HGA two-axis gimbal, SIS two-axis gimbal, and ESS (five-DOF arm and end-effector). The drive card controls the motor inner loops and communicates to the processor over SpaceWire for outer-loop control. The motor drive circuits are standard designs from other JPL spacecraft.

The solid-state recorder provides >1.7 Gbit of storage using Flash memories. Although the Flash memories are commercial parts, recent parts-testing shows several radiation-tolerant options. A radiation characterization risk-mitigation activity in Phase A will identify the best part, followed by a lifetime buy for the project. The memories are interfaced to the spacecraft through a SpaceWire interface chip. This chip includes an embedded processor that

will make this device behave as "network-attached" storage: Reading/writing to this recorder doesn't require the RAD750. The power-conditioning unit (PCU) takes in unregulated 28 V off the power bus, provides EMI filtering, and converts it to a regulated 12 V that is distributed to each card in the box. The PCU on/off switch is controlled by the Power Subsystem. The local card on/off is software controlled via the processor and commands issued via the remote I/O.

The system block diagram is shown in Figure D.2.5-27. This figure shows the cards in the C&DH box. The box is internally redundant and cross-strapped (both data and power). SpaceWire supports multiple topologies (e.g., star or daisy chain). The box consists of two RAD750 single-board computers with SpaceWire router, two mass memory cards, four remote I/O cards, six motor drive cards, and
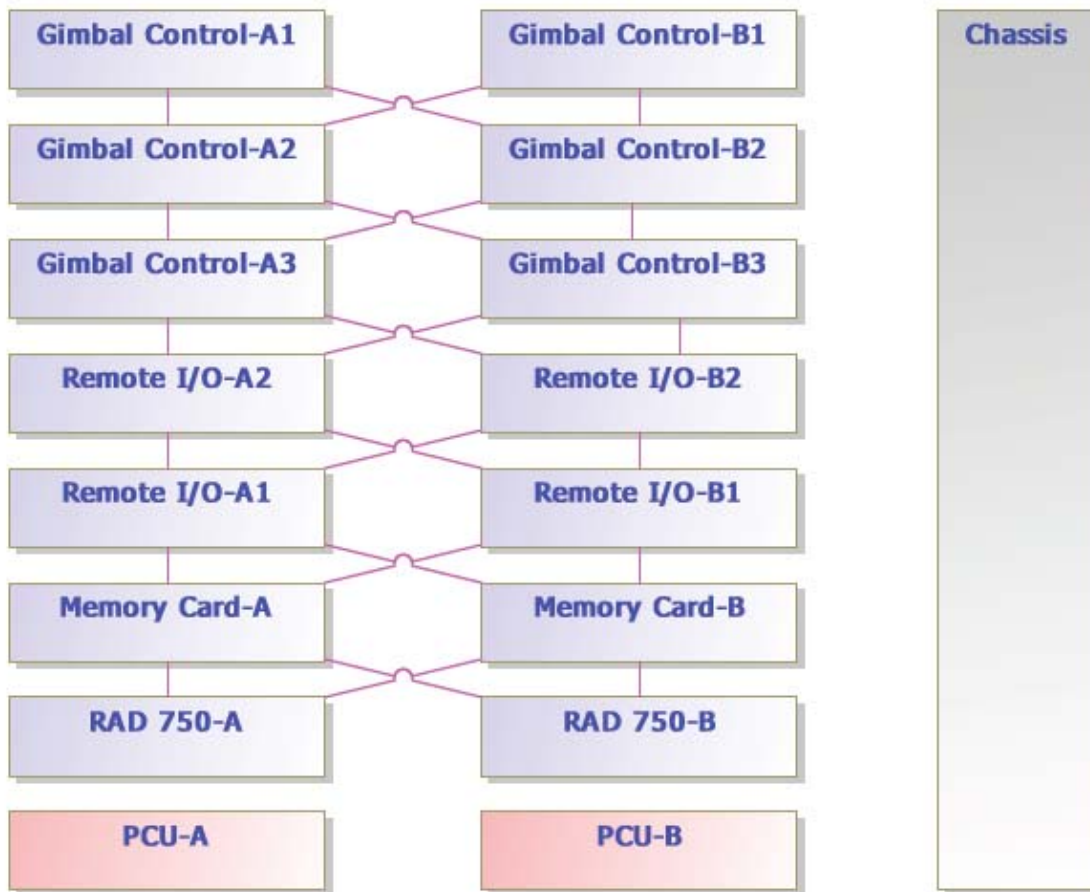

Figure D.2.5-27. The C&DH is redundant and cross-strapped to provide robust fault-tolerance.

two PCUs. The mass memory card interfaces to the single board computer via SpaceWire. The remote I/O cards and motor drive cards interface to the single-board computer via SpaceWire.

The C&DH electronics do not require any new technologies. The RAD750 single-board computer with SpaceWire is an off-the-shelf product. The SpaceWire interface chip is an off-the-shelf product. The I/O circuits, motor drive, power supply, and mass memory have analogs on previous projects. The 6 U × 220 m packaging standard has been qualified and used on previous projects. During Phase A a trade study will be commissioned to look at the benefits of replacing the centralized motor control cards with distributed motor control.

D.2.5.10 Software—Lander

Flight software for the Lander is designed and developed under all of the same constraints and policies as for the Carrier as described in Section D.2.4.5.5.

Distinct flight software functions allocated to the Lander flight software include system command and control, health and safety management, attitude and propulsion control during DDL, science data collection, onboard data management, and reliable data delivery using CFDP. None of these capabilities are seen as new technology, and significant algorithm and architecture heritage is available from Cassini, MSL, SMAP, MESSENGER, and other missions. Science-related functions include the operation of each of the science instruments on the surface, and control of the sample acquisition system to collect and deliver surface samples to the instruments.

Critical activities managed by software are expected to include DDL, science sampling and data collection, and data relay. Because Europa has no significant atmosphere, the descent and landing guidance would be akin to landing on Earth's Moon. Targeted landing technology developed by MSL and the Constellation program could be leveraged here.

Data-relay behaviors and protocols have been developed and proven in the Mars program, and much of that technology can be inherited as reusable software. Arm-control algorithms from MER and MSL will be used.

Flight software also has a key role in system fault management. This mission concept includes a number of time-critical activities, including orbit insertions, critical maneuvers, and descent and landing, where the physics of motion through space constrains the time in which the activity must be completed without mission-limiting consequences. For this reason the FSW coordinates a system fault-management approach, consistent with current best practices, aimed at protecting essential resources, but trying to maintain scheduled operations using automatic fault responses such as resetting devices, switching to redundant devices, or selectively trimming subsets of planned activities.

The FSW is organized using the same layered architecture as the Carrier element, as shown in Figure D.2.4-5, and described in Section D.2.4.5.5. The Lander element software system includes modules within the instruments group for each of the science instruments, a distinct descent and landing module under the G&C package to provide coordinated closed-loop control of the descent and landing (including hazard avoidance) behavior, and another package to manage behaviors of the sample acquisition robot arm.

Science instrument software is developed by instrument providers using a spacecraft simulator (see Section D.2.7.1, Testbed Approach). All other software is developed in-house.

D.2.5.11 Europa Sampling System (ESS)

The Europa Lander requires a subsystem to acquire and transfer subsurface samples of the terrain for the science suite of instruments including the Mass Spectrometer, Raman Spectrometer, and the Microscopic Imager. The primary objective of the ESS is to acquire approximately one cubic centimeter of Euro-

pan subsurface material at two different depths into the near surface, where the influence and contamination of original materials from the Lander's hydrazine thrusters and from the natural incident radiation environment should be minimized.

The ESS concept is composed of two primary functional components. The first is the sampling device (SD), which interacts with Europa's surface, generating and extracting the desired "sample" from this native site. Second, the sampling device manipulator, which deploys the SD from its stowed position on the Lander, moves and orients the SD to the surface for sample acquisition; and then after sampling, returns the SD to the Lander instrument suite. Finally, in concert the SD and SD manipulator perform the last step of sample handling by depositing the acquired sample into each instrument's intended repository.

The ESS will deliver at least two samples to the instrument suite, approximately 1 cubic centimeter in volume, with the first sample acquired from a depth of 0.5 to 2 cm below the Europan surface, and the second sample acquired from a depth of between 5 and 10 centimeters below the surface. During each sampling operation, the temperature of the sample will be kept below a maximum bulk temperature of 150 K, which along with minimizing the time taken for sampling will allow a minimum of volatiles to escape from the sample prior to the science investigations. Since the surface topography of Europa is largely unknown, a challenging range of possible surface conditions is established. The final landed configuration of the vehicle from which the ESS must sample is defined as being a slope of between 0 degrees and a maximum of 25 degrees, and with the Lander on or in the vicinity of an obstacle, such as a boulder or a crater, of maximum height or depth of 1.5 meters. From previous NASA missions, the surface of Europa is known to be composed primarily of water ice, with inclusions or deposits of various hydrated salts, particu-

larly those of magnesium sulfate. The ESS must be able to successfully sample the material within its workspace with any mixture-ratio of those constituents. In addition, this surface material may be presented to the ESS as essentially bedrock, boulders, etc., down to the size of sand grains. The presumed range of strength of these near surface materials varies considerably from an Unconfined Compressive Strength (UCS) of 70 MPa (approximately that of concrete), down almost three orders of magnitude to 100 KPa. In addition, these near surface materials are believed to have porosities that can vary from a high of 40% down to 0%. Because of the astrobiological potential of the Europan environment, the engineering implementation of the system will require the capability of the ESS to meet stringent Planetary Protection specifications, necessitated by international treaty and most likely met through DHMR. And finally, because the environment of Europa is a very cold vacuum, with surface temperatures of approximately 100 K, radiation filled, and with low gravity (less than 14% of Earth's gravity); the ESS will be required to function in both this extremely alien environment, and in laboratory operation on Earth.

All of these requirements and constraints led to the architecture of the ESS composed of a rotary-percussive drill for the Sampling Device, and to a five-DOF robotic arm (RA) for the SD Manipulator. This combination of coring drill and autonomous manipulator results in no additional mechanization of the ESS to perform sample handling tasks. The rotary-percussive approach to a coring drill is chosen in order to facilitate the design intent of having a low-mass, low-force, low-power SD for the mission. A percussive coring drill intrinsically minimizes the "soil work" necessary to get the selected sample from the ground, because it minimizes the amount of collateral damage to the surrounding surface. In addition rotary-percussive drilling minimizes the abrasion or cutting of the terrain in

direct contact with the drill bit's kerf, thus reducing temperature rise, by instead utilizing the percussion aspect of the device to pulverize the ice, and the rotary action to essentially sweep away and expel the drill tailings. The coring drill will be implemented with the rotary mode and percussive modes separated in different mechanisms, which allows the percussive mode to be turned off if the surface contact is determined to be in very weak, soft, or friable material. The drill will be comprised of 3 motor-driven actuators; including the rotary DOF, the percussive DOF, and finally an inner bit extension and retraction linear actuator, which allows the SD to drill full-face until it gets to the intended depth, which once reached results in retraction of the inner bit, so that an annular or coring drill configuration is achieved. Once the full length core (~1 cm) is made, the same inner bit actuator, through hyper-extension causes the core to be snapped-off at the base material, and then retained in the coring bit for sample extraction. The mis-

sion life requirements even at the hardest end of the material strength spectrum (i.e., pure water ice at 100 K) is well understood therefore mission will fly with a single coring bit, and no bit replacement capability. Using design techniques from previous missions, the mechanisms and their actuators (e.g., lubricated motors, bearings, and gears) can be heated and kept above heritage levels of low AFTs (>218 K), while highly effective thermal isolation of the hardware of the coring bit itself will keep it well below the high Allowable Flight Temperature for the samples (<150 K) by thermal sinking to the environment. In Figure D.2.5-28 a series of pictures are shown which demonstrate the key functions of the drill bit.

The second major piece of the ESS architecture is the five-DOF robotic arm (RA), which is very similar in implementation to previous flight manipulators such as the MER Instrument Deployment Device (IDD) and the Phoe-
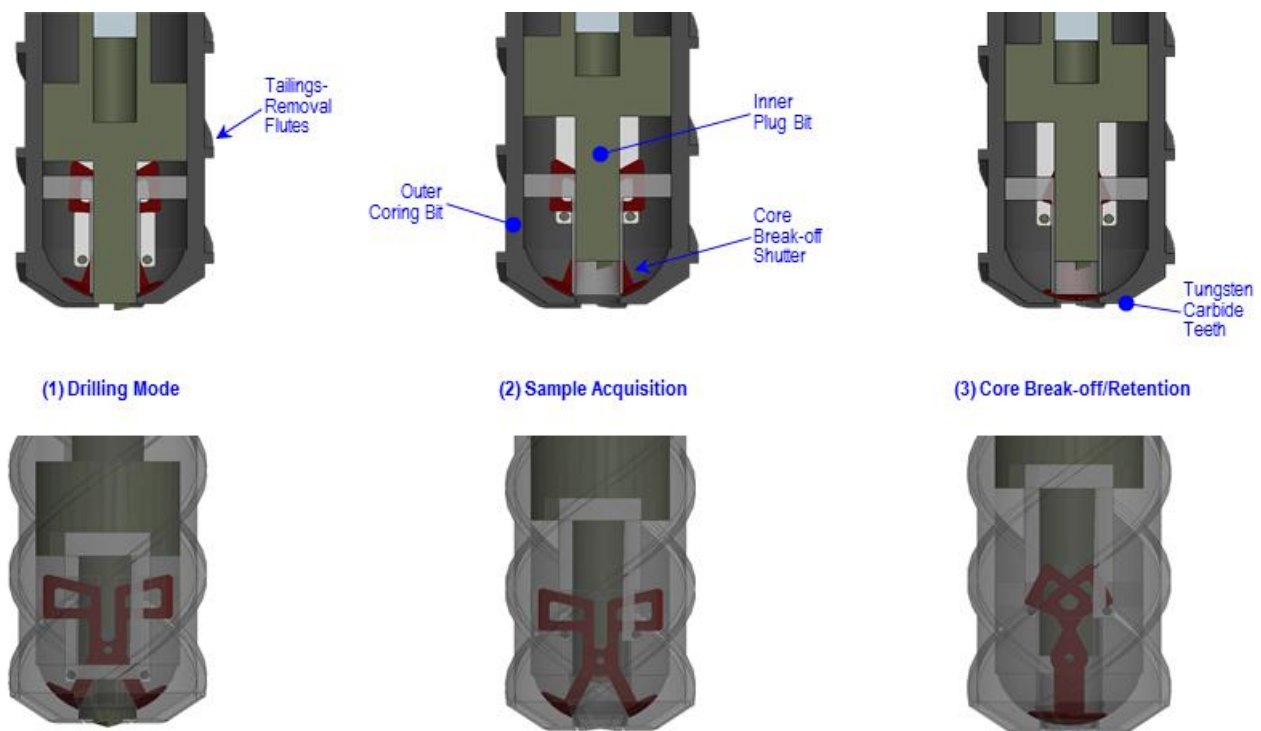

Figure D.2.5-28. The sampling system utilizes lessons learned from MER, Phoenix, and MSL. There are three steps in sample acquisition: (1) In drilling mode the outer coring bit rotates and is hammered to drill into the ice; (2) the inner plug bit allows a sample to enter while coring; (3) the core break-off shutter is activated to capture and retain the sample.

nix Robotic Arm. Specifically the envisioned design would essentially extend the total length of the MER IDD from its as-flown 0.75 meter length to an ESS required length of 2.0 meters. The larger length of the ESS RA is due to the need to extend the manipulator's workspace to include the terrain requirement of accessibility near 1.5 meter obstacles. The need for five DOF in the RA, which requires 5 separate motor-driven joints in the arm, is driven by the need for three DOF in translation in linear space, and two DOF in rotation for tip and tilt control of the SD to achieve alignment with the sampling site local surface normal. The increase in the ESS payload mass to 6 kg, from the MER IDD value of 2 kg, requires a substantial increase in actuator torque capacity which is reflected in the CBE mass. The addition of a force-torque sensor to the arm's end-effector or turret, allows the arm to be properly preloaded to the surface normal for drilling, and also to detect misalignment or side-loading of the drill bit during operations. The

mechanisms of the RA, and of the SD, are of extensive heritage in terms of materials and construction. Those mechanism components include brushless permanent magnet DC motors, planetary and harmonic gear drives, solenoid brakes, Hall-effect sensors, resolvers, PFPE lubricated bearings and gears, and finally Kapton-based flex print cabling. In Figure D.2.5-29 a view is shown of the deployed ESS with the SD in contact with the terrain.

The resulting ESS will have performance requirements that do not exceed the as-flown capabilities of the MER IDD including a positional repeatability of ±2 mm, a free space accuracy of ±5 mm, and a rotational or orientation accuracy of ±2 degrees. The RA capability for end-effector force application will be approximately 100 N, but the required minimum drill preload will be <40 N. The time required to take a full depth core will be <20 minutes. This design will result in a CBE mass of the robotic arm of 11.5 kg, and a CBE mass of the sampling device of 6 kg. The average power used by the robotic arm during placement is estimated to be <20 watts, with no power required for the arm to hold position with the power-off brakes employed. The average power of the drill is estimated to be <30 watts and the maximum data rate needed for subsystem telemetry will be <5 kbps.

As a new system, the Europa Lander ESS will require technology development, specifically with respect to the sampling device.
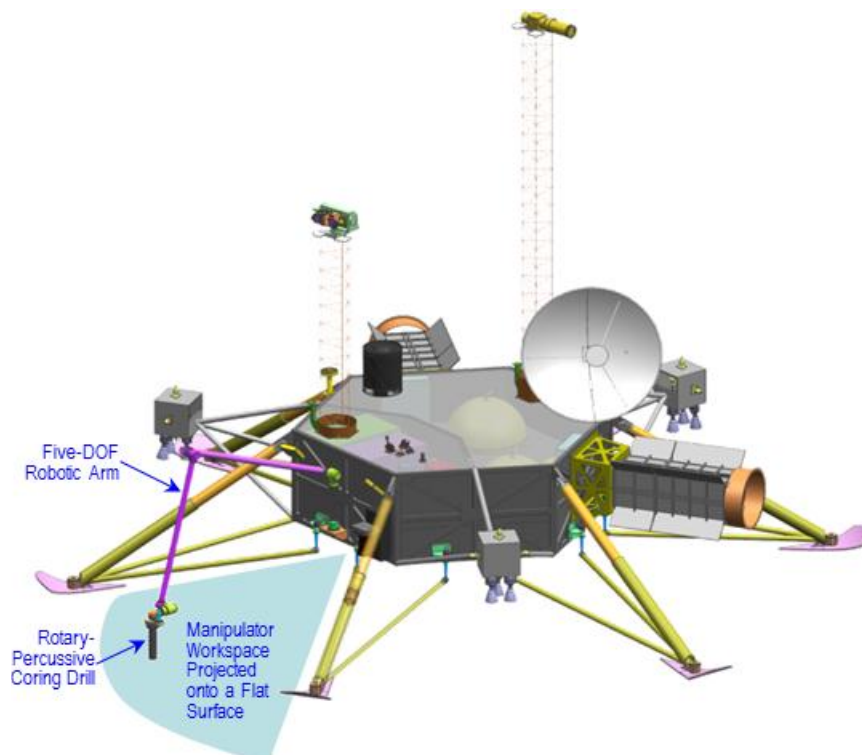

Figure D.2.5-29. The ESS is oversized so that we can support unknown surface conditions and meet the baseline science requirements for samples.

D.2.6   Technical Budgets

To minimize cost and schedule risk, the spacecraft has high levels of technical margin designed in.

Three primary technical margins are addressed here: mass, power/energy, and data balance. Other key technical margins are covered elsewhere in this report: Radiation tolerance margin is treated in Section D.2.9.1.The Europa Study Team's approach to technical resources is to model what we understand, then include conservative margin based on past experience to account for items not known well enough to model.

D.2.6.1   MEL and Mass Margins

The mass margin follows the definitions and conventions specified in the JPL DPs, Section 6.3.2 (JPL 2010a). The earliest milestone at which the DPs specify a mass margin, however, is the Project Mission System Review (PMSR), when 30% is required. In consideration of the fact that the Europa Lander Mission concept is in a much earlier phase, pre–Mission Concept Review (MCR), we have striven for a more conservative policy of 40% mass margin for this report. This policy is consistent with the expected evolution of JPL's institutional guidance. The mass margin is shown in three tables: Lander element (Table D.2.6-1), Carrier element (Table D.2.6-2), and integrated spacecraft (Table D.2.6-3).

Table D.2.6-1. Lander element has good mass margin.

Lander Mass Margin			
T. Bayer 25 Apr 2012	Deorbit, Descent, Landing		
Lander Model - Final Report Update	Mass, kg		
	CBE	Cont.*	MEV
Magnetometer	2	50%	3
Multi-Band Seismometer	6	50%	9
Mass Spectrometer	15	50%	22
Site Imaging System	3	50%	5
Raman Spectrometer	7	50%	10
Microscopic Imager	2	50%	3
Lander Payload	35	50%	52
Power	56	20%	68
C&DH	24	30%	31
Telecom	20	28%	26
Structures	191	34%	257
Thermal Control	35	30%	45
Propulsion	61	22%	74
GN&C	32	36%	43
Harness	39	50%	58
ASRG	66	30%	86
Lander	524	31%	689
Lander Total Dry	559	33%	741
DV Monopropellant	106	31%	139
TVC Monopropellant	5	25%	7
ACS Monopropellant	4	33%	5
Pressurant	5	25%	7
Residual and Holdup	2	31%	2
Lander Propellant	122	31%	159
Lander Total Wet	681	32%	900
SRM Casing and Inert	43	0%	43
Braking Stage Dry	43	0%	43
SRM Propellant	460	30%	600
Braking Stage Total Wet	503	28%	643
Lander System Total Stack	1183	30%	1543
Capability			1602
System Margins			
JPL DVVP (Capability - Max Prop - CBE Dry) / (Capability - Max Prop)			29%

For the purpose of calculating DP margin, the following definitions of "capability" are used:

1. "Capability" for the Lander is the maximum SRM propellant load for the STAR 30E plus the maximum dry mass this amount of propellant can push through the required deorbit and descent ΔV.

2. "Capability" for Carrier is #3 minus #1.

3. "Capability" for the integrated spacecraft at launch has the usual DP meaning: the maximum launchable wet mass on the chosen launch vehicle at the required C_3.

The dry mass CBE includes tanks sized to carry the maximum propellant load, radiation shielding, and the launch vehicle adapter (LVA). Each is discussed below.

D.2.6.1.1 Use of "Max Propellant"

The DPs explicitly require that the propellant load assumed for the margin calculation be that amount of propellant needed to provide the required ΔV for the maximum possible launch mass on that launch vehicle (LV) (JPL 2010a). In addition, the dry mass of the propellant tanks reflects tanks sized for this maximum propellant load. This approach gives an accurate reading of the overall dry mass margin, *assuming* that the flight system grows to the maximum launchable mass. Specifically for the three configurations of the Lander mission,

1. "Max Prop" for the Lander is the maximum SRM propellant load for the STAR 30E plus the liquid propellant fraction for the Lander after SRM sepa-

Table D.2.6-2. Carrier element has good mass margin.

Carrier Mass Margin			
T. Bayer 25 Apr 2012	Launch		
Carrier Model - Final Report Update	Mass, kg		
	CBE	Cont.*	MEV
Power	42	30%	54
C&DH	6	30%	8
Telecom	68	29%	87
Structures	270	30%	352
Thermal Control	29	30%	37
Propulsion	220	28%	280
GN&C	80	35%	107
Harness	70	50%	105
Radiation Monitor	8	30%	10
ASRGs (2)	66	30%	86
Carrier Total Dry	857	31%	1127
SRM Propellant	0	---	0
DV Bipropellant	2777	48%	4101
TVC Monopropellant	100	0%	100
ACS Monopropellant	40	0%	40
Pressurant	6	0%	6
Residual and Holdup	73	45%	106
Carrier Propellant	2995	45%	4352
Carrier Total Wet	3852	42%	5479
Capability			5503
System Margins			
JPL DVVP (Capability - Max Prop - CBE Dry) / (Capability - Max Prop)			28%

ration for the descent and landing trajectory.

2. "Max Prop" for the Carrier is the propellant fraction needed to impart the ΔV to the entire stack to get from LV separation down to the 5×200–km Lander release orbit.

3. "Max Prop" for the integrated spacecraft is the sum of #1 and #2 above.

The CBE propellant is computed using the CBE dry mass and CBE ΔV. The maximum expected value (MEV) propellant is computed using the MEV dry mass and the MEV ΔV.

Table D.2.6-3. Lander Mission (at launch) has good mass margin.

Lander Flight System Mass Margin			
T. Bayer 25 Apr 2012	**Launch**		
Lander Model - Final Report Update	**Flight System Mass, kg**		
Carrier Model - Final Report Update	**CBE**	**Cont.***	**MEV**
Lander Total Dry	559	33%	741
Lander Propellant	122	31%	159
Lander Total Wet	681	32%	900
Braking Stage Dry	43	0%	43
SRM Propellant	460	30%	600
Braking Stage Total Wet	503	28%	643
Lander System Total Stack	1183	30%	1543
Carrier Total Dry	857	31%	1127
Carrier Propellant	2995	45%	4352
Carrier System Total Wet	3852	42%	5479
Flight System Total Wet	5036	39%	7023
Capability (21-Nov-21 VEEGA)	Delta IV Heavy LVCap**		7105
System Margins			
JPL DVVP (Capability - Max Prop - CBE Dry) / (Capability - Max Prop)			28%

The max propellant is computed using the maximum possible dry mass and the CBE ΔV.

D.2.6.1.2   Radiation Shielding

The mass model tracks the amount of shielding necessary to protect each piece of sensitive electronics. This mass is accounted for at the appropriate level of assembly (card, box, or module), and shown as a payload and engineering total in each table.

D.2.6.1.3   Launch Vehicle Adapter

A standard Delta IV LVA is assumed. The mass shown in the Carrier and integrated spacecraft tables includes both the part that remains with the spacecraft and the part that remains with the upper stage but is considered by NASA Launch Services as "payload mass" for the purpose of LV performance. Spacecraft ΔV calculations carry only the part that remains with the spacecraft.

This margin calculation adds "growth contingency" mass to the CBE masses to arrive at an MEV mass and the propellant required for that mass, and then compares this value to the LV capability. For determination of contingency factors, the Europa Study Team has used the ANSI/AIAA Guide G-020-1992(American National Standards Institute 1992), applied at the component level. This document specifies the *minimum* contingency factor based on project phase and component sizing and maturity, and allows a higher factor where the project deems it appropriate. The guideline is consistent with traditional JPL practice, but provides a more rigorous grounding through its use of historical data.

A more detailed mass breakdown can be found in the Master Equipment List (MEL) Section D.4.3.

As can be seen in these three tables, the Europa Lander Mission has lower than the striven-for 40% mass margin. With further refinement of this concept it is expected that a mass margin of 35-40% could be achieved. These refinements will be studied in Phase A. There are multiple opportunities for reducing mass, with associated impacts in cost and risk, including:

- Spacecraft:
  - Composite overwrapped tanks (Carrier and Lander)
  - Composite structure (Carrier and Lander)
  - SSPA in lieu of TWTA (Carrier and Lander)
  - Refined shielding analysis (Carrier and Lander)
  - Bipropellant propulsion (Lander)
  - Digital Motor Control (Lander)
  - Avionics Integration (Lander)

- Mission design:
  - LV performance (estimated degradation)
  - Trajectory optimization
  - Lander campaign optimization

D.2.6.2   PEL and Power/Energy Margins

The Power Equipment List (PEL), captured in the system model, contains the CBE power needs for power loads in various modes with a contingency for maturity. The power modes are based on the mission scenarios described in Section D.2.3. Europa Lander Mission policy is to maintain 40% of the power source capability after a single ASRG failure as power margin on the load for all mission power modes. Each mission mode is assessed against the policy. The transient modes are assessed with the power margin on the load included and the JPL DPs DOD guidelines for actual battery capacity, assuming a single ASRG failure. A single mechanical failure can eliminate one of the two Stirling engines in the ASRG; this results in the power output being reduced by approximately 50%. Summary results of the mission mode power analysis are shown in Table D.2.6-4.

The PEL provides the CBE capabilities of the power source and its LEV for each mission mode. The power source estimate takes into account a degraded performance of the ASRG during launch due to the environmental conditions inside the shroud. The LEV of the ASRG assumes a failed Stirling converter after launch, effectively producing the power of 3.45 ASRGs. The PEL contains each load with a CBE, an estimated contingency based on maturity, and a maximum expected value (MEV). Each mode is identified in the PEL, along with a summation of all of the loads that are on in that mode. The mission mode total is compared to the power source capability for the same mission mode, with the power margin calculated per the JPL DPs approach of (Capability − CBE) / Capability (JPL 2010a). The transient modes are modeled to estimate the battery DOD with the actual battery capacity.

One mission mode that needs some investigation is the outer cruise safe mode, in which the power margin is slightly below the Europa Mission policy at 38%. This mode is steady-state and cannot rely on the battery. This mode will need further evaluation in Phase A to comply with the mission policy margin.

Table D.2.6-4. Carrier and Lander power analysis compares the power source capability to the estimated load for all phases of the mission. There are two mission modes that rely on the battery, and the DOD is displayed.

	Europa Lander Mission Power Analysis							
	ASRG Power, W		Flight System Power, W				Steady-State	Max Bat
Mission Phase	**Spec**	**LEV**	**CBE**	**Cont.**	**MEV**	**Margin, %**	**or Transient**	**DOD, %**
Launch	426	334	145	21%	175	57%	SS	
Inner Cruise	535	420	179	24%	223	57%	SS	
Inner Cruise (Safe)	535	420	247	23%	305	41%	SS	
Outer Cruise	514	403	234	24%	290	42%	SS	
Outer Cruise (Safe)	**514**	**403**	**251**	**23%**	**309**	**38%**	**SS**	
Orbit Insertion/TCM	505	396	434	24%	537	40%	Transient	17%
Europa—Communications	505	396	241	68%	405	40%	Transient	4%
Europa—No Communications	505	396	147	28%	188			
Carrier—Camera	252	229	181	28%	233	40%	Transient	75%
Carrier—Communications	252	229	189	28%	242			
Carrier—No Communications	252	229	95	21%	112			
Lander—Relay Baseline	252	166	See Charts					
Lander—DTE Baseline	252	166	See Charts					
Lander—DTE Floor	252	166	See Charts					

D.2.6.2.1   Transient Modes for Integrated Spacecraft and Carrier

The first integrated spacecraft transient mode is the obit insertion/TCM. Orbit insertion is not the defining mode for the either battery because of the combination of the integrated spacecraft power systems. The battery capacity is estimated to be 60 Ah with a 14-A discharge at 10°C at EOM. The load profile and battery DOD are shown in Figure D.2.6-1. The JPL DPs allow for a 70% DOD for events such as orbit insertion that are less than 100 cycles (JPL 2010a).

The next transient mode is for the integrated spacecraft in Europa orbit before Lander separation. In this scenario, the Carrier has 3.5 ASRGs (assuming one Stirling engine has failed) and is performing both Ka-band communication and reconnaissance imaging. The Telecom Subsystem is transmitting for half the orbit, and the camera is on continuously (see Figure D.2.6-2). The integrated spacecraft has only a 4% DOD during this event.

After landing, the Carrier element takes images of the landing site (one time only) and then enters relay mode with six UHF passes every 42 hours (every ½ Eurosol). In between UHF passes, the Carrier transmits for 45 minutes per orbit until the next UHF pass. The Carrier is assumed to have two ASRGs (assuming no Stirling engine failure). If a Stirling engine fails on one ASRG, then the Lander will rely on DTE communication. The initial camera mode requires some additional one-time energy storage of approximately 20 Ahr of primary battery. Once the Carrier is in relay mode, the maximum DOD is 10% with a 20-Ahr secondary battery (see Figure D.2.6-3).

Post-separation ASRG failure conditions will be studied in more detail in Phase A.
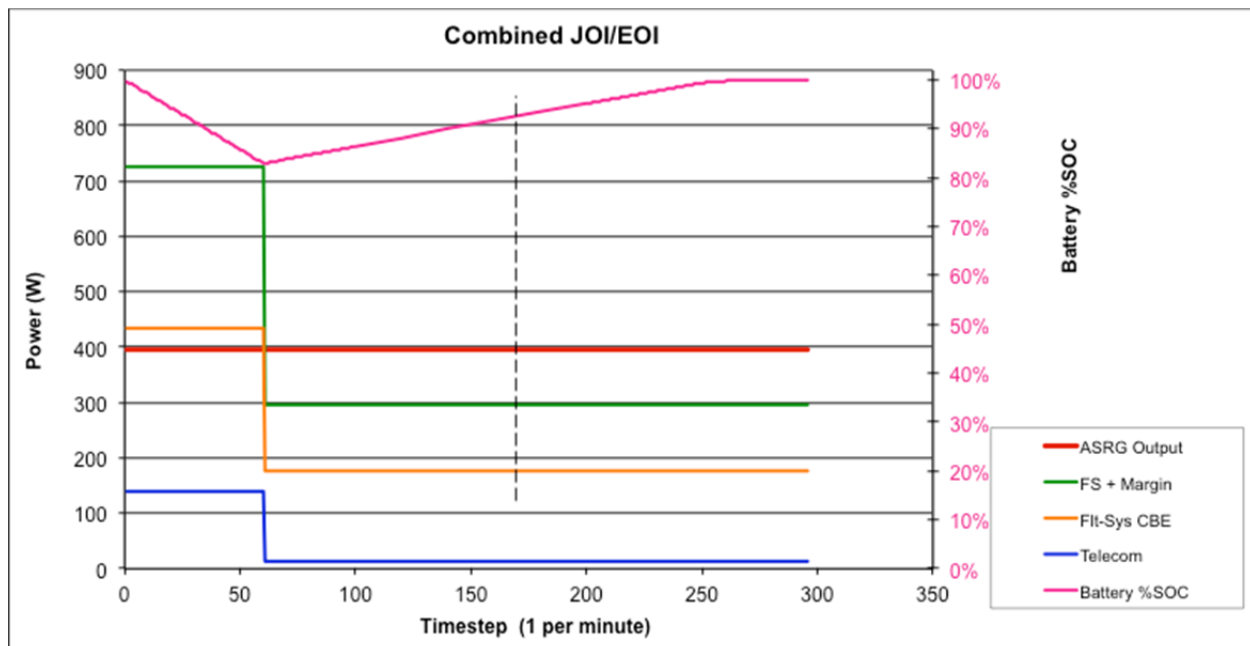

Figure D.2.6-1. JOI power analysis for the integrated spacecraft shows that a 1-hour discharge of the combined batteries achieve energy balance using the Europa Study policy of 40% margin on the load profile.
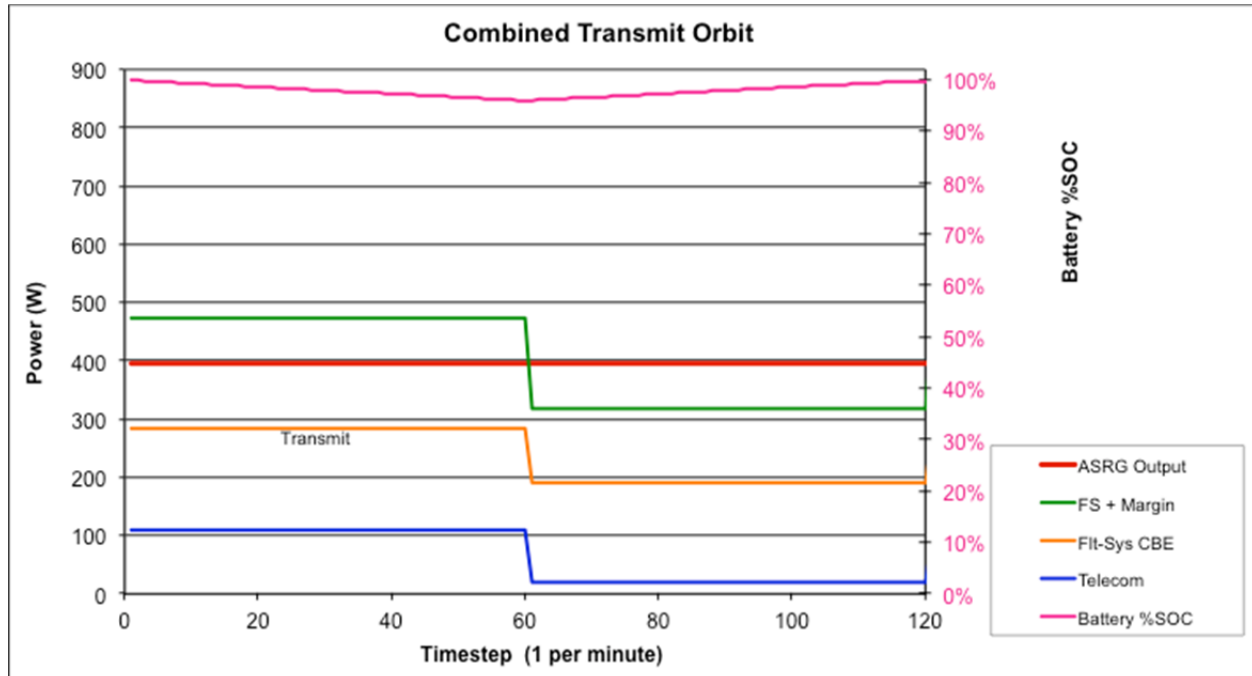
Figure D.2.6-2. Integrated spacecraft reconnaissance-mode power profile shows that the system achieves energy balance with Telecom transmitting for half of the orbit with a 4% DOD and the Reconnaissance Camera on.
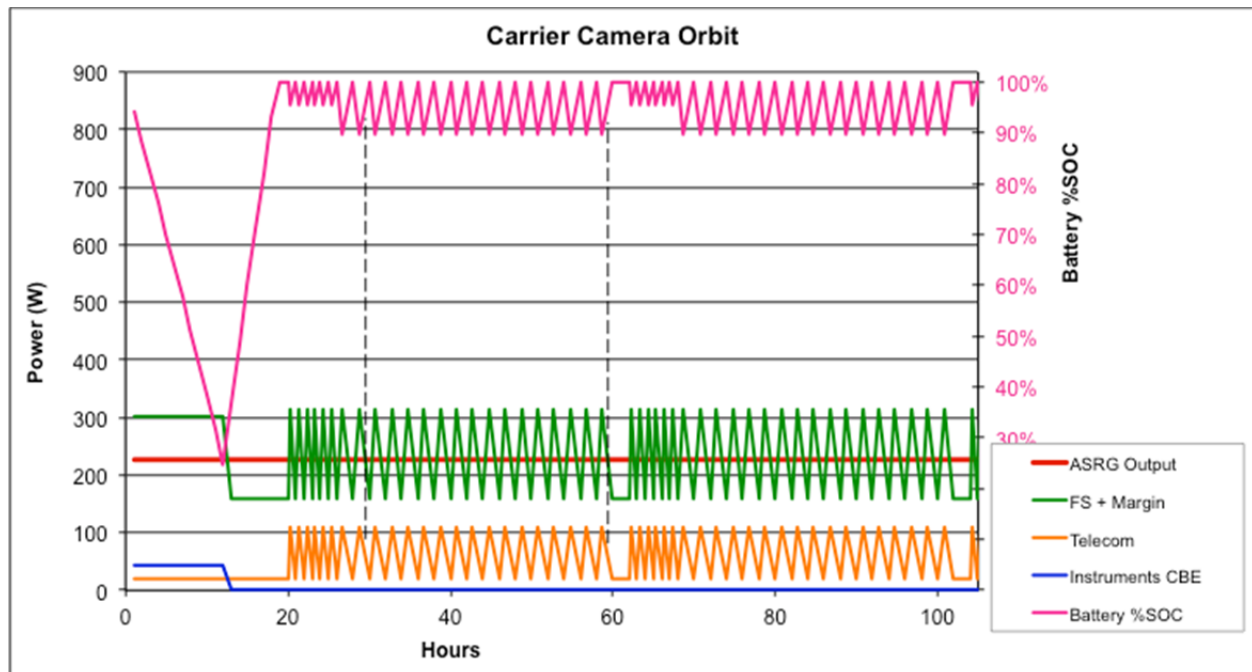

Figure D.2.6-3. Post-separation camera mode followed by relay mode requires an addition of 20 Ahr of primary battery to achieve energy balance for camera needs prior to relay mode. This is with two ASRGs and a 20-Ahr secondary battery.

D.2.6.2.2   Transient Modes for Lander

The Lander surface relay operation achieves energy balance with a failure in the ASRG. The initial 2-hour orbit after separation with the DDL defines the secondary battery size of 40 Ahr EOM. After the initial science in the first two Eurosols, the Power Subsystem runs power-positive (see Figure D.2.6-4).

If the Lander needs to operate in DTE X-band mode (assuming a dual failure in the Carrier), energy balance is achieved (Figure D.2.6-5).

The overall power budget is driven by the post-separation scenario for the both the Carrier and the Lander. Each Power Subsystem has the option of combining the secondary batteries with primary batteries to obtain an optimum solution for both mass and power margin. Further study in Phase A will refine the outer cruise safe-mode steady-state scenario and the post-separation Carrier transient scenario with 1.5 ASRG power source.

D.2.6.3   Data Balance

Mission data balance is driven primarily by two scenarios.

The first scenario describes the Lander science data return through the Carrier. The science objectives are described in Section D.2.1, and the corresponding relay operations strategy is described in Section D.2.5. The surface science mission phase is a driving case because of the time criticality to get the Lander science data back to Earth. Getting data back from the surface of Europa imposes many constraints, and the delivery process involves a multistep store-and-forward operation.

The second scenario is the prelanding site-certification phase. This phase also presents some data delivery driving requirements due to the need to collect a large volume of surface imaging data and deliver it to the ground quickly to support landing-site certification in the short time allocated in order to minimize the system radiation exposure prior to landing.

The site-certification phase (described in more
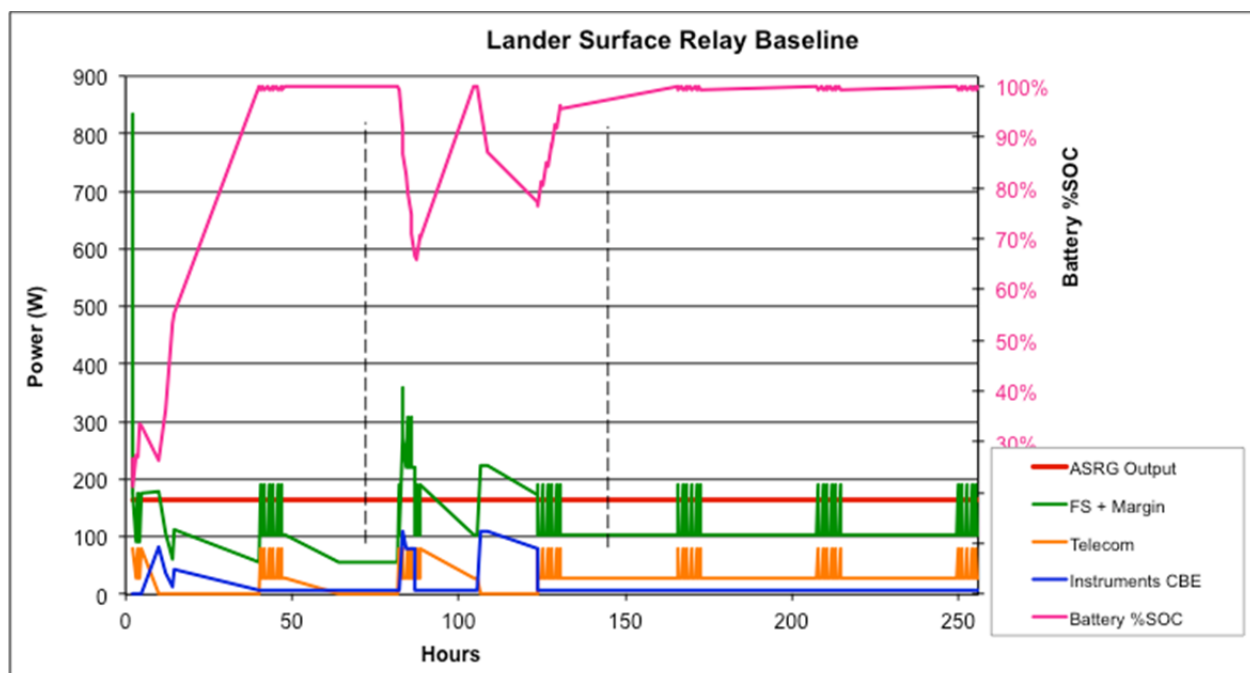

Figure D.2.6-4. Lander baseline science with relay; the battery sizing is driven by DDL and relies on a 40-Ahr EOM secondary battery. After science on the second Eurosol, the Power Subsystem is mostly power-positive with a 1% DOD.
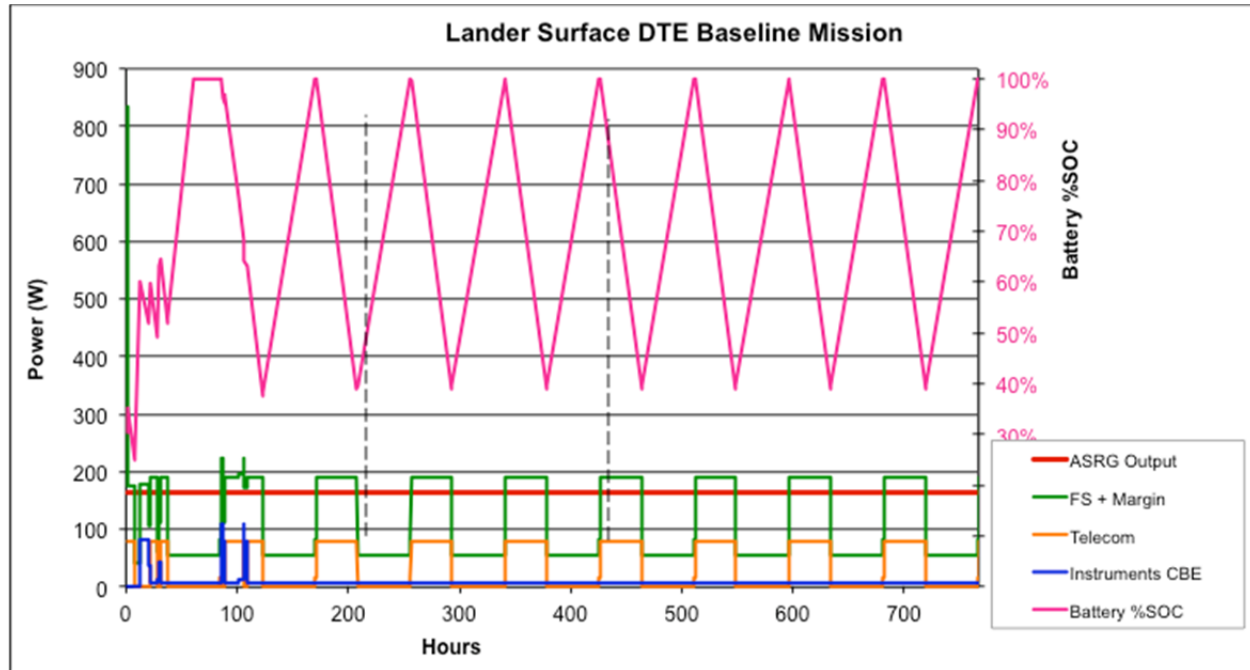
Figure D.2.6-5. Lander DTE baseline science data return is the defining scenario for the Lander power system with a 60% DOD for telecom transmit.

detail in Sections D.2.8.2.1 and D.2.8.2.3) begins immediately after EOI. The integrated spacecraft begins orbiting in a polar orbit that will take it over all four of the pretargeted science sites within the first half Eurosol (about 2 days). Within this period the Carrier will image all of the targeted landing sites using the RC (Section D.2.2.2), collecting a total of about 6.4 Gbit of imaging data.

The spacecraft will be operated in this phase using reaction wheels to provide precise camera and HGA pointing (additional power needed to do this is available from the Lander ASRGs in this phase). Using reaction wheels to point the HGA to Earth within 1 mrad enables the Ka-band telecom downlink to support a bit rate of 129 kbps through the 3-m HGA. At this rate it will take about 14 hours of downlink time to get all the imaging to the ground (about 3.5 hours, or about 3 orbits per site). Some of this data volume can be downlinked on orbits between imaging passes.

This capacity means that all of the site-certification data should be available on the ground within about 3 days of orbit insertion,

leaving the remainder of the 30-day site-certification period for analysis and planning, as well as imaging of other potential landing sites. Numerous retransmission opportunities exist on subsequent orbits because the spacecraft has no other objectives during the remainder of this phase.

For the surface science scenario the primary path to return science data is through the Carrier element acting as a store-and-forward relay. Relaying data to Earth through the Carrier element is the primary strategy during this phase, as described in Sections D.2.8.2.2 and D.2.8.2.3. The total amount of science data produced to meet the baseline requirements is about 4.6Gbit, mostly collected within the first two Eurosols after landing. The amount of data that can be relayed to the Carrier element using a conservative elevation angle visibility mask of 30° is about 3.7 Gbit per Eurosol, spread over 6 to 12 view periods per Eurosol. Note that if the Lander finds itself in a location with a clear view of the horizon data throughput could be more than double this amount. Over the 30-day surface mission

duration this results in a capacity to relay a minimum of 33.3 Gbit of data from the surface (86% margin over baseline requirement).

Data relayed to the Carrier element will be stored and queued for retransmission to Earth. Additional data will be produced on the Carrier as a result of its own operation and a science requirement to image the landing site post landing. This activity will add another 1.6 Gbit of data that the Carrier must return to Earth (for a total of about 6.6 Gbit). Due to power limitations the Carrier will typically operate the UHF relay link only during Lander over-flights, and operate the Ka-band downlink at other times when Earth is in view. The Ka-band downlink rate during this phase is 75 kbps using thrusters to maintain HGA pointing. Downlink durations are limited due to power constraints on the Carrier. The design concept has two ASRGs powering the space-craft after Lander separation. The total down-link capacity, based on data rate and usable downlink time, is about 83 Gbit (~92% margin over baseline requirement).

Two contingency cases are considered for the Lander relay scenario. First, if the Carrier loses half of one ASRG (one Stirling engine) the primary operational response will be to limit Ka-band downlink time available in each orbit (time was already restricted to 50% duty cycle due to occultations). In this case the total downlink capacity is reduced to about 6.8 Gbit (17% margin over requirement), which still meets the mission need.

In the second contingency case studied, if the Carrier element's relay capability fails entire-ly, the Lander retains the capability to transmit DTE using its own X-band transmitter and articulated HGA. Because of the lower power, smaller HGA, and less precise pointing, the Lander can achieve, this telecom system pro-duces a much weaker signal, and thus lower bandwidth link to Earth, than the Carrier ele-ment capability. This configuration requires 70-m-equivalent DSN tracking (four arrayed 34-m stations) to achieve a 9-kbps data rate,

and can be operated only when the landing site is within view of the Earth (view period calcu-lations assume the same 30° elevation mask as for relay communications). The total data delivery capacity of this system is about 7.8 Gbit over the 30-day surface mission. Because significantly more power must be dedicated to telecom in this contingency, science observations must be more carefully planned around downlink periods (science and telecom cannot operate concurrently). None-theless, this configuration provides about 41% margin over the baseline science requirement, and 83% margin over the floor science re-quirement of 1.3 Gbit.

Onboard data storage requirements for the two spacecraft elements is determined by the max-imum amount of data that can accumulate in onboard storage before it must be transmitted. On the Lander this maximum is driven by the desire to perform science observations soon after landing to mitigate fault risks associated with accumulated radiation dose over time. The largest volume of data is associated with the site imaging, about 3.5 Gbit. The actual data store is designed to provide significant margin over this quantity so that data can be redundantly stored in order to mitigate the risk of memory corruption. Figure D.2.6-6 shows a timeline for data accumulation on the Lander. Note that most of the science data is transmit-ted to the Carrier element within the first two Eurosols of landing. Additional data continues to flow from the MAG and seismometer ex-periments through the end of the mission.

The Carrier element storage is sized to ac-commodate the prelanding site-certification imaging data (about 6.4 Gbit). This quantity exceeds the quantity that will be returned from the surface. Another 1.6 Gbit of landing site imaging data are collected after landing when the Carrier is also relaying data from the Lander, but the data accumulated in this case never exceeds the amount collected during the earlier phase. Figure D.2.6-7 depicts a timeline of the data accumulation on the Carrier ele-
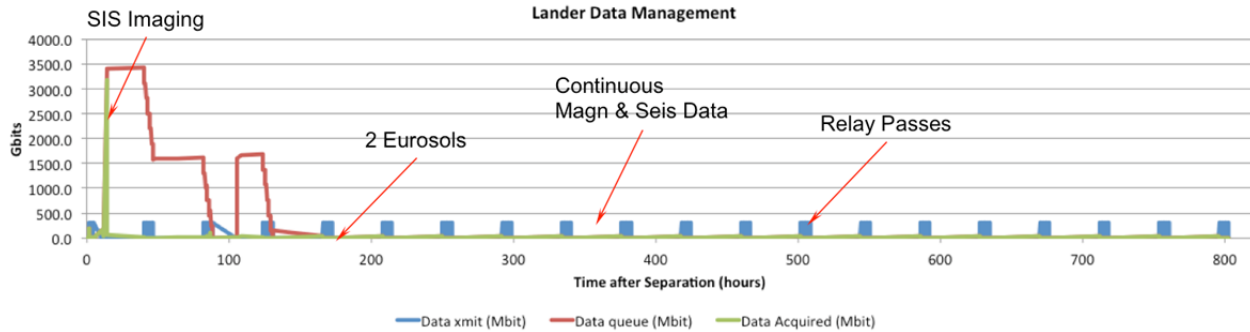
Figure D.2.6-6. All the baseline science data is downlinked after 2 Eurosols; this leaves an excellent margin of 7 Eurosols.

ment after landing. The scenario of a missed DSN pass (due to weather at the DSN) is not a driver for onboard Lander or Carrier data storage. A missed DSN pass is typically 8 hours. The Lander must store data between relay passes. The relay gaps are typically 42 hours. The Carrier must store Lander data taken at relay passes and then meter it out over the next few orbits; in the event of a missed DSN pass the Carrier data would still be downlinked prior to the next relay overflight.
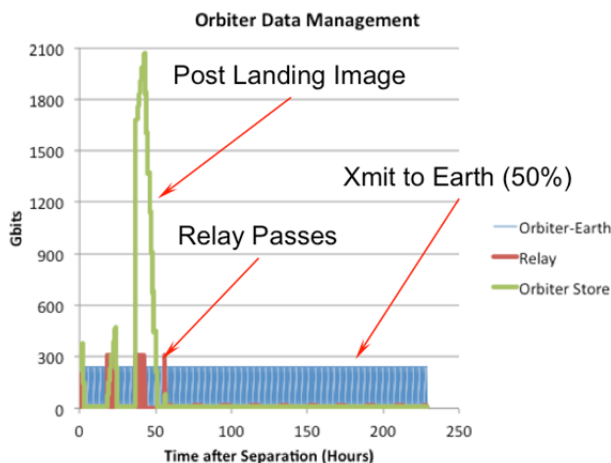

Figure D.2.6-7. The Carrier easily accommodates the Lander science relay needs even with a 50% duty cycle on the transmission back to Earth.

D.2.7　Development, Integration, and Test

Europa Lander Mission development, integration, and test leverages the module design of the Carrier and Lander to reduce project risks by simplifying interfaces, reducing schedule dependencies, and enabling a smooth funding profile.

For the Europa Lander Mission, the interfaces between the Lander element and the Carrier element are simple, permitting the Lander and the Carrier to be assembled and tested independently. The integration program for the spacecraft will use a developmental test model (DTM) Lander for the spacecraft test program during environmental test and verification, permitting the flight Lander to be delivered to the project at the launch site. This approach was done successfully for the Viking Project (1975) as well as the Cassini-Huygens Program (1997). Engineering Models of the requisite electronic components will be integrated during the System Integration and Test (SI&T) flow during both the Lander and the Carrier test programs to ensure functional compatibility as was done on the above-mentioned previous missions. Emulations of each element's electrical interfaces will be used to support element-level integration in each case.

The concept of operations for the development and test program is to have as much of the development performed at the module level as possible, permitting a high level of integration at the system level. The Carrier element is comprised of an Avionics Module and Propulsion Module. The Avionics Module is comprised of a radiation vault, that houses electronics equipment that requires radiation shielding, and the Upper Equipment Section (UES), which contains the attitude control sensors, actuators, and the RC. The Propulsion Module is comprised of propulsion hardware,

telecom antennas, ASRG, and LVA. The Avionics Module and Propulsion Module are built in parallel. The Carrier element will be subjected to thermal-vacuum tests, both stand-alone and with a DTM Lander element for thermal and launch environmental tests. The Lander element will be subjected to all landed environmental, functional, and deployment testing prior to being delivered for system integration at the launch site.

D.2.7.1   Testbed Approach

Consistent with current practice as demonstrated by MSL and SMAP, the Europa Lander Mission adopts a system integration approach supported by a set of software and hardware testbeds, enabling early and thorough integra-tion of key hardware and software interfaces prior to ATLO. This development and validation approach begins with scenario development during formulation and design and progresses incrementally to system validation using an ever-growing battery of regression tests that verify and validate system architecture as it is designed and developed. Figure D.2.7-1 depicts the proposed testbeds described in the following paragraphs.

Since science instruments are likely to be developed externally, instrument developers must be provided with a testbed environment that includes a spacecraft simulator (hardware and software for the Lander element) that simulates the power, data, and control inter-
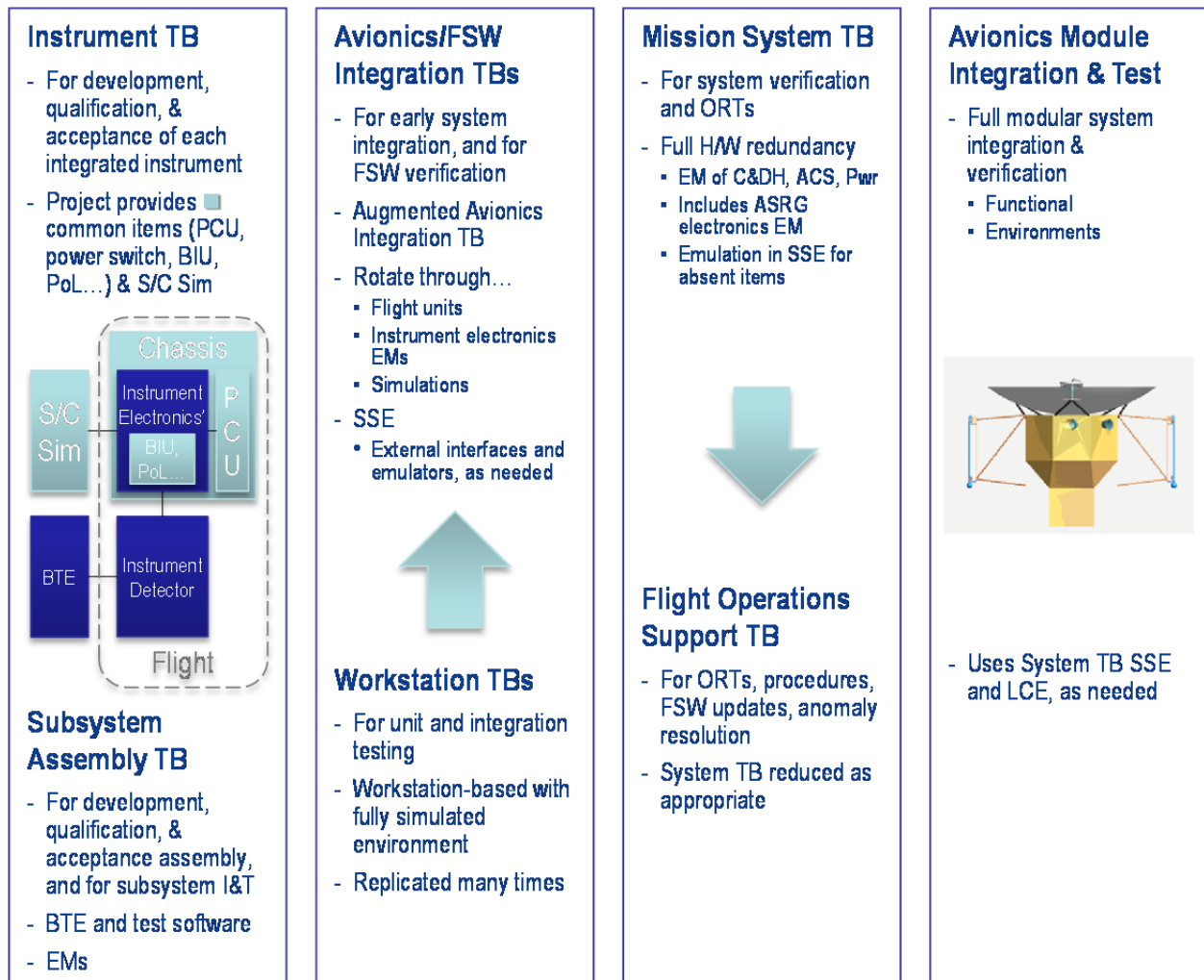

Figure D.2.7-1. System integration flow is designed to catch problems before the next level of integration.

faces with which the instrument must integrate. This ensures that all interface issues have been resolved prior to delivery, thereby helping to keep the ATLO work focused on system integration and on the concerns that can be verified only in an assembled system context. Similar subsystem assembly testbeds are provided for early integration testing of major subsystems (Telecom, Propulsion, Power, etc.).

This mission concept involves two distinct spacecraft system elements: a Lander element and a Carrier element, which must be developed, assembled, and tested separately up to the point of integration, and then finally tested as a single system. System testbeds must be able to support the separate parallel development of Carrier and Lander elements, validation of interfaces, and combined system functionality.

A high-fidelity model-based simulation capability (workstation test set [WSTS] on MSL and SMAP) is baselined for FSW development test and verification, fault-management development and test, attitude-control system-level verification and validation (V&V), and mission activity development and test. Several groups will exploit this capability, which can be replicated cheaply as often as necessary. The commonality of the flight computers and other avionics (storage, telecom, SpaceWire interfaces) between the two spacecraft elements enables the use of a common workstation-based development environment that can be configured in software to support either the Lander or Carrier system configuration (or both).

The software simulation of hardware must be of sufficient fidelity to allow seamless migration of FSW and test cases from simulation to hardware-in-the-loop testbeds. This capability is important and necessary because certain software services are needed to support the instrument testbeds and the testing and integration of devices. The first workstation-based spacecraft simulator version will be available

in time to support development of the first FSW release and will continue on with expanded capability to support testing of subsequent FSW builds. It is to be available on all software developers' and testers' workstations, and includes closed-loop spacecraft behaviors operating in nominal and off-nominal modes. These simulators are built to allow for interchangeability between software models and hardware engineering models (EMs) later in the "hardware-in-the-loop" testbeds in such a way that is transparent to the FSW, and test scripts, at least at the interface level. This enables use of the same test scripts whenever the testbed models are interchanged with EMs.

In addition to the simulation capability described above, the Europa Lander Mission has three system testbeds, each containing separate hardware for a Lander and a Carrier element. The first two are similarly configured with nonredundant avionics, and are depicted in Figure D.2.4-19 as the Avionics/FSW integration testbeds. These testbeds support, among other things, ground support equipment (GSE) hardware and software development and test, test scripts development and validation, and database maturation. First on line is the Real-Time Development Environment (RDE), which is dedicated to GSE hardware and software development and test. The next instances of this testbed, the Flight Software Testbeds (FSWTBs) become available later in the development process to allow V&V to proceed in parallel with FSW development. The Mission System Testbed (MSTB) is a dual-string high-fidelity testbed dedicated to system V&V, FSW fault tests, mission system tests, and ATLO support. Each of these three testbed sets has distinct hardware for a Lander and Carrier element that can be operated independently, or in a combined mode simulating the preseparation integrated spacecraft configuration.

These system testbeds include the C&DH, GN&C, Power, Telecom, and Harness subsystems, as well as Ground Data System (GDS)

hardware and software. The EM versions of all spacecraft engineering subsystems and instruments pass through the testbeds for integration and interface verification. No flight units are required to flow through the testbeds unless there are major modifications from the EM; however, the testbeds can support flight hardware integrations if needed. The V&V simulation environment can offload the hardware-in-the-loop testbeds and use the EM integration effort to help evaluate model fidelity. The simulation environment interfaces and procedures are compatible with those of the hardware testbeds. The testbeds are also used to train test analysts to support ATLO testing as well as to support ATLO procedure development and anomaly investigation. All FSW versions are verified on the testbeds prior to being loaded onto the spacecraft in ATLO or in operations. The spacecraft testbed transitions to operational use for this purpose after launch.

D.2.7.2 Assembly, Test, and Launch Operations (ATLO)—Carrier and Lander

Lander Element

The Lander element is developed separately and is delivered to the project at the launch site. The Lander element will be subjected the appropriate descent and landing functional and environmental tests, as well as the surface functional and environmental tests. The Carrier element is assembled and tested using the same methodology as described above but utilizing Lander engineering model (EM) hardware for functional/electrical test and Lander DTM hardware for the system environmental test program (including mass model for the deorbit Solid Rocket Motor (SRM). This approach was used on both the Viking-1975 and Cassini-Huygens (1997) test programs. A final verification of EMC will be performed at the launch site. Two phases of thermal-vacuum testing will be performed at JPL, for both the integrated configuration (Carrier and Lander) and the Carrier stand-alone configuration. All environmental testing of the Lander element is performed prior to delivery of the Lander to system integration and test. At the launch site, the DHMR operations will be performed on the Carrier element and the Lander element concurrently prior to fueling of each and integration of the deorbit SRM. The integration of the SRM will be performed with the SRM inverted.

Carrier Element

For the Carrier element, the ATLO phase begins with the delivery of the vault, UES, and Propulsion Module to ATLO. The vault and the UES (containing the RC, G&C sensors, and reaction wheels) will be integrated to each other using extender cables. Extender cables permit access to circuits for integration and troubleshooting as well as for connection of direct access equipment needed for closed-loop operation of the Attitude-Control Subsystem during mission scenario and comprehensive performance testing. During integration, interface signal characteristics will be measured and recorded for comparison with requirements.

Although thorough JPL-traditional electromagnetic compatibility (EMC)/ electromagnetic interference (EMI) systems engineering methods will be employed during development, the early integration of the Telecom Subsystem permits monitoring of spectral characteristics as other hardware is added to the system for detection and identification of any interfering spurious signals. A thorough telecom functional test is included in the flow to establish baseline performance while operating with the Propulsion Module.

The Propulsion Module is integrated next in the flow to demonstrate signal characteristics to propulsion valves and thrusters as well as an initial verification of proper phasing. The design of the extender cables and the layout of the modules in the test facility will minimize copper losses as appropriate. Phasing of propulsion components will be repeated after

spacecraft stacking to remove any influence of the extender cables.

We plan on having fully functional ASRGs that are electrically heated and can be used to verify end-to-end performance as well as verify integration procedures that will be used for the flight ASRG integration at KSC.

A Deep Space Network (DSN) compatibility test will be performed at this point with the DSN compatibility test trailer followed by an engineering baseline comprehensive performance test (CPT). This and other configuration-dependent baseline tests are performed throughout the ATLO program in order to detect performance changes resulting from either trending or environments.

A series of fault-management tests will be performed to establish correct operation of the fault-management system software in conjunction with the associated hardware detections and responses.

The first mission scenario test is the Launch Sequence Test executed both nominally as well as with selected fault and off-nominal conditions. Subsequently, a Trajectory Correction Maneuver Test (including orbit insertion) will be performed in both nominal and off-nominal conditions. Other capabilities of the spacecraft to support required operational modes, reconnaissance observations, and other noncritical mission scenarios will be incorporated in CPT(s) rather than specific scenario tests so that spacecraft capabilities, rather than point-design mission scenario verifications are established. Since all operations described above are first-time events, one month schedule margin is included at this point to ensure no delay to the environmental test program.

The environmental test program starts with the mating of the UES and the vault mechanically and electrically, to create the Avionics Module. Next the installation of the HGA to the PM occurs followed by the stacking of the Propulsion Module with the Avionics Module, the stacking of the spacecraft on the LVA, and

the installation of pyro devices needed for pyroshock testing. An abbreviated baseline CPT is performed as well as an RF radiation test using the flight antennas and a phasing test to demonstrate proper phasing without extender cables. This is the first time the Carrier element is in a flight-like electrical and mechanical configuration. A DTM of the Lander (which has thermal simulation) is installed.

Radiated emissions and radiated susceptibility tests are performed, as well as a self-compatibility test. Since very limited operation of the Lander element is planned during the cruise mission (preseparation), self-compatibility between the Carrier and the Lander can be simulated easily. EMC/EMI is followed by an alignment verification to establish pre-environmental alignment data. Thermal blankets and environmental test instrumentation are installed after the spacecraft is stacked on a noninterference basis.

The spacecraft is transported to the Environmental Test Lab (ETL), where acoustics tests and pyroshock tests are performed. The pyroshock test also verifies the launch vehicle separation mechanical interfaces.

The spacecraft is then moved to the 25-foot Space Simulator, where a baseline test is performed to verify configuration and performance prior to starting solar thermal-vacuum (STV) tests.

The STV test is primarily a verification of worst-case hot and cold performance as well as selected thermal balance conditions. Additional functional tests are performed during thermal transitions if they are not required for the worst-case thermal tests, which verify margins required by JPL DPs and FPPs.

After STV, the spacecraft is transported to the Spacecraft Assembly Facility (SAF), where post–environmental alignment verifications are performed followed by destacking to a system test configuration. A CPT is repeated for post–environmental performance verification. Launch sequence tests, Trajectory correc-

tion maneuver tests, countdown and scrub/recycle tests, and engineering and science performance tests are performed prior to shipment to KSC. Two months of schedule margin are included at this point to protect the ship date and KSC operations. Shipment to KSC is performed at the module level.

After arrival at the KSC Payload Hazardous Servicing Facility (PHSF), the spacecraft modules, interconnected with extender cables, undergo a system test configuration baseline CPT to establish the health of all spacecraft systems. The Lander element is included in this test. Spacecraft stacking is then performed, followed by a DSN compatibility test with MIL-71, alignment verification, and a phasing test using the launch version of flight software. A launch configuration baseline test is performed, followed by a launch sequence test from prelaunch through early cruise. Pyrotechnic devices (excluding spacecraft separation pyro) are installed. A dry-run installation of the flight ASRG(s) is performed as well. After the flight ASRG(s) are removed and secured, the spacecraft is transported to the KSC Operations and Checkout (O&C) facility for DHMR.

At the O&C the spacecraft is installed in the existing thermal chamber in the O&C high bay. Vacuum bakeout of the spacecraft is performed, followed by backfill to an appropriate convective atmospheric environment, either nitrogen or filtered air at the preference of the Planetary Protection Engineer. Spacecraft temperatures are elevated and verified, at which point the DHMR operation is conducted. Because of the uncertainty of the durations of each of these operations, five days of schedule margin are allocated at this point. The spacecraft is then transported back to the PHSF.

At the PHSF, a baseline test is performed to confirm the status of all spacecraft systems subsequent to DHMR. Final spacecraft close-outs and walk-down inspections are performed followed by fueling of the propulsion systems

for both the Lander and the Carrier. Three weeks of schedule margin are included at this point to protect the date of delivery to the launch vehicle for integrated operations.

At this point, the spacecraft is ready for integrated operations with the launch vehicle, including mating to the flight LVA and encapsulation with the fairing, transport to the launch pad, and ASRG installation for flight, countdown, and launch. Durations for integrated operations are, for reference, based on the actual Atlas V launch vehicle operations conducted for the MSL mission (we anticipate the Delta IV Heavy operations to be similar).

The ATLO flow described above has incorporate opportunities for parallel operations including the fact that the Lander and Carrier elements are assembled and tested in parallel. The flow described also includes the 20% schedule margin at JPL, and one day per week schedule margin at KSC, as required by the JPL DPs.

D.2.8   *Mission Operations*

The Europa Lander Mission would keep operations costs low by simplifying operations during cruise and focusing science operations on the surface element.

Europa and its vicinity present a challenging and hazardous environment for operating any science mission. Based on the cost-reduction mandate from the decadal survey for 2013–2022, and hand-in-hand with the design of the Europa Lander Mission and spacecraft, the operations strategies described herein have been developed principally to achieve the Europa science in Section D.1 at the lowest feasible cost. The central guiding theme of mission operations is to deliver the spacecraft to Europa safely, with a flight team fully capable of conducting science observations. No other activities are allowed to drive the design of the operations systems and concepts. All design decisions—be they for the spacecraft or operations—are studied, often with the applications of models and/or scenarios, to measure the cost,

performance, and risk across all phases of the project, including operations. The science is the driver of mission architecture. For the landed surface mission, operations consist of science observations that can be accomplished autonomously on the surface of Europa, and activities needed to return that data to Earth.

Operations development has drawn much wisdom from the many NASA-wide studies of Europa exploration from as early as 1997. In addition, two key studies in 2008 were conducted to capture relevant lessons learned from the past and present operations missions, incorporating members from JPL, APL, and NASA Ames. These studies focused in particular on flight and ground system capabilities needed to simplify science operations; early development of flight and ground concepts to ensure appropriate implementation; and postlaunch activities and development to ensure functional capabilities and simplified operations. All of the operations assessments, from the many studies and scenario work of highly experienced engineers, emphasize early consideration of operability issues in the system architecture and design. All system trades (spacecraft, operations, science, etc.) should be treated as mission trades to work toward the best cost/risk for the overall mission, rather than optimizing a single element and unknowingly adding significant cost/risk to another.

The data-relay operations leveraged in this concept derive from similar operations developed by the Mars Program. Both MER and MSL rely on data-relay capabilities provided by MRO and Odyssey spacecraft for most communication with the landers. This approach has proven to be very reliable and cost-effective, and it enables surface systems to deliver data to Earth at significantly lower energy cost. In the proposed Europa Lander Mission the coordination and planning of surface and relay operations would be greatly simplified by having both spacecraft operated by the same mission and project, as compared to MER where that project has to coordinate its relay operations

with other missions. Furthermore, the Carrier element in this concept would have no other purpose than to support surface science operations after landing, eliminating the need to coordinate with other objectives.

D.2.8.1 Interplanetary and Jupiter Cruise

After launch, mission focus will be on the checkout, characterization, and deployment of all flight systems. In the first few weeks, coverage will be continuous driven by real-time commanding for schedule flexibility based on the high uncertainties of early activities. Once postlaunch checkouts are complete, the mission will transition to sequence-based control.

Interplanetary cruise will be quiescent, save for elevated activity required for gravity assists and maneuvers. The spacecraft will be minimally operated, with basic telemetry expected only once per week; however, 24-hour coverage is expected around maneuvers, and daily to continuous tracking prior to gravity assists, particularly with those of Earth for planetary protection. In between gravity assists, the project will focus some of its efforts on development and improvement of operations processes and tools for Europa orbit and landing, as well as science team meetings to refine the Europa template of operations. After JOI, RC characterization and checkout will resume, and operations readiness tests and camera calibrations may be conducted at Jupiter system flybys prior to the EOI. All operations in this phase will be conducted via 34-m DSN stations.

D.2.8.2 Operations Concept

Operations at Europa consist of a two-phase approach, with both phases lasting approximately one month. The first month is dedicated to the landing site reconnaissance and certification and is performed by the Carrier. The second month (9 Eurosols) is dedicated to the landed operations, involving both the Carrier (for a data relay) and the Lander. Both the Carrier and the Lander operations are described in the following two subsections. The third subsection addresses the communi-

cations approach for the Carrier and Lander predescent, postdescent, and during the surface operations.

D.2.8.2.1   Operations Concept—Carrier

The Carrier element provides the ΔV needed to insert the vehicle into Europa orbit upon completion of the Jupiter cruise phase using its bi-propellant propulsion system (Section D.2.3). EOI occurs in three steps: first, capture into a 200 × 7000–km elliptical polar orbit with its node at ~10 a.m. local time; second, a plane change to shift the node to 7:30 a.m. local time; and third, circularization into a 200-km polar orbit.

The primary task for the Carrier immediately after EOI is to conduct reconnaissance of the set of pre-selected candidate landing sites to help ensure landing safety (Section D.2.4.1). Mission success requires that a landing site be identified that not only has high scientific interest but also for which we can ensure with high probability that it contain areas within it that are as large as our targeting error ellipse and in which sufficiently large and numerous

hazard-free areas are distributed that are within our descent targeting divert capability. Unfortunately, insufficient information currently exists to accomplish this objective, since the available data tell us nothing about what the surface of Europa looks like at spatial scales relevant to landing. The very best Galileo imaging data has a scale of only 6 m/pixel, and this imaging is limited to a single frame. Fifteen other frames with resolutions of about 10 m/pixel exist. But our Lander needs to identify and avoid hazards at a scale of 3 m across and 1.5 m high. Use of an onboard hazard detection and avoidance system to avoid hazards at this scale is planned, but with our current knowledge, we can't guarantee that any chosen site will, in fact, have any hazard-free areas within the landing error ellipse to which the system could be diverted. Figure D.2.8-1 illustrates the types of surface Europa might have everywhere in the worst case.

Therefore, additional site-certification data at the necessary spatial scale is needed prior to committing to releasing the Lander on its descent. The process of site certification in-
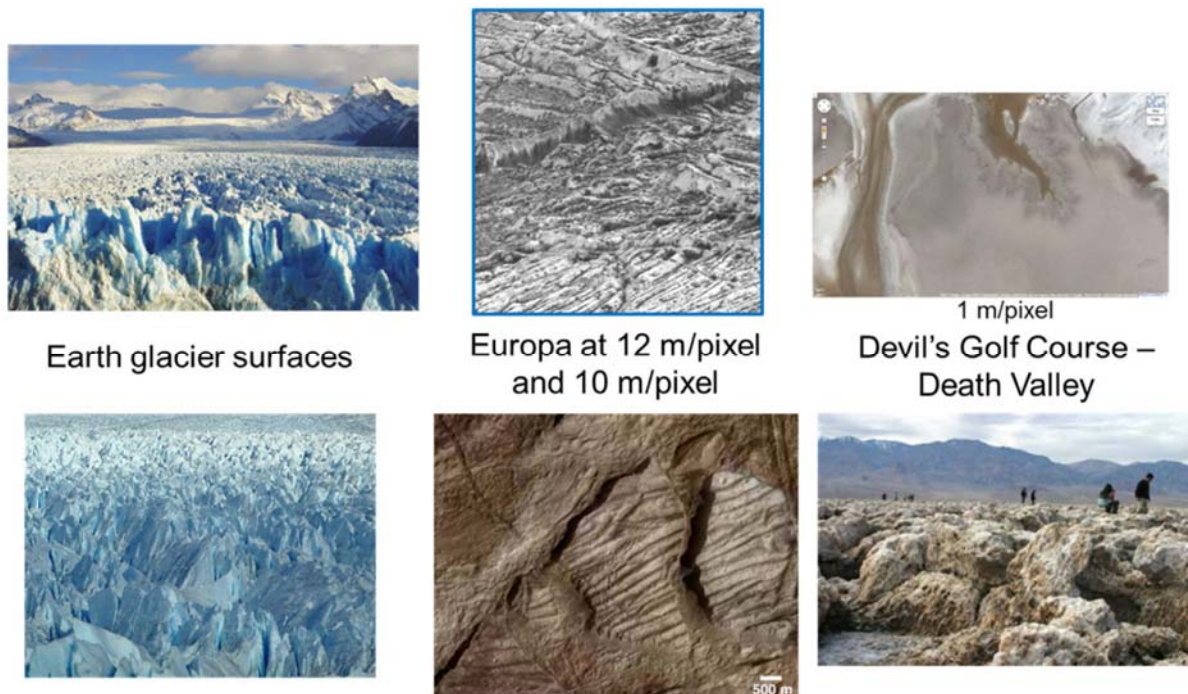

Figure D.2.8-1. Our current knowledge of Europa's surface cannot exclude the possibility of ubiquitous landing hazards such as these.

cludes ground activities as well as collection and return of suitable data from the Carrier element prior to landing. The process will begin even before launch with the selection of candidate landing sites of scientific interest, preferably in low-radiation zones on Europa's surface. In addition, measurable criteria will be established for defining a safe landing site. These criteria will be used to define the data products that need to be produced and the data processing system that will be needed to yield the necessary measurements. The criteria will not be flexible once they are adopted. During the cruise to Jupiter and the Jupiter orbital cruise periods, the data processing system will be thoroughly tested using Earth analog data and data from early flybys of Ganymede and Callisto. Operational readiness tests involving the ground data analysis personnel will be conducted to train the teams to accomplish the certification steps quickly and correctly. In addition, high-precision calibration of the RC, its alignment to the Carrier pointing coordinate system, and Carrier pointing knowledge and stability will be conducted.

For the current study, the SDT suggested four candidate landing sites outside of the trailing-side high radiation zone—Thera (45S,180W), Thrace (43S,175W), E17 (20S, 85W) and E25 (45N, 355W), as shown in Figure D.1.4-2.

Imaging of these sites needs to be acquired at a scale of 0.5 m/pixel or better to adequately characterize them at the scale relevant to landing safely. Figure D.2.8-2 shows a HiRISE image of Mars at a comparable spatial scale showing the Spirit rover vehicle and surrounding rough terrain. Slope and hazard quantification is best done with observations taken at low Sun elevation angles (between 10° and 30°) and at emission angles <30°. While stereo imaging may not be essential to the certification process, it is likely to provide significant additional confidence in the assessment of hazards.

The planned Carrier element capabilities are sufficient to support the landing-site certification activity envisioned (Section D.2.4.1). The telecom system data rate of 129 kbps will allow downlinking of 0.5-m/pixel imagery of a candidate site within a few hours (Section D.2.8.2.3). The Carrier mass margin is adequate to accommodate a RC of mass up to ~50 kg. The landing delivery error ellipse is 3 km cross-track by 6 km along-track prior to invoking any corrections based on surface remote-sensing during descent (Section D.2.3.4). Figure D.2.8-3 shows this error ellipse at the proper scale superimposed on two possible landing locations in the Thera region. The Lander system includes terrain-

Spirit rover

Figure D.2.8-2. This HiRISE image of Mars at 0.3 m/pixel illustrates the spatial resolution scale needed for Europa landing site certification.
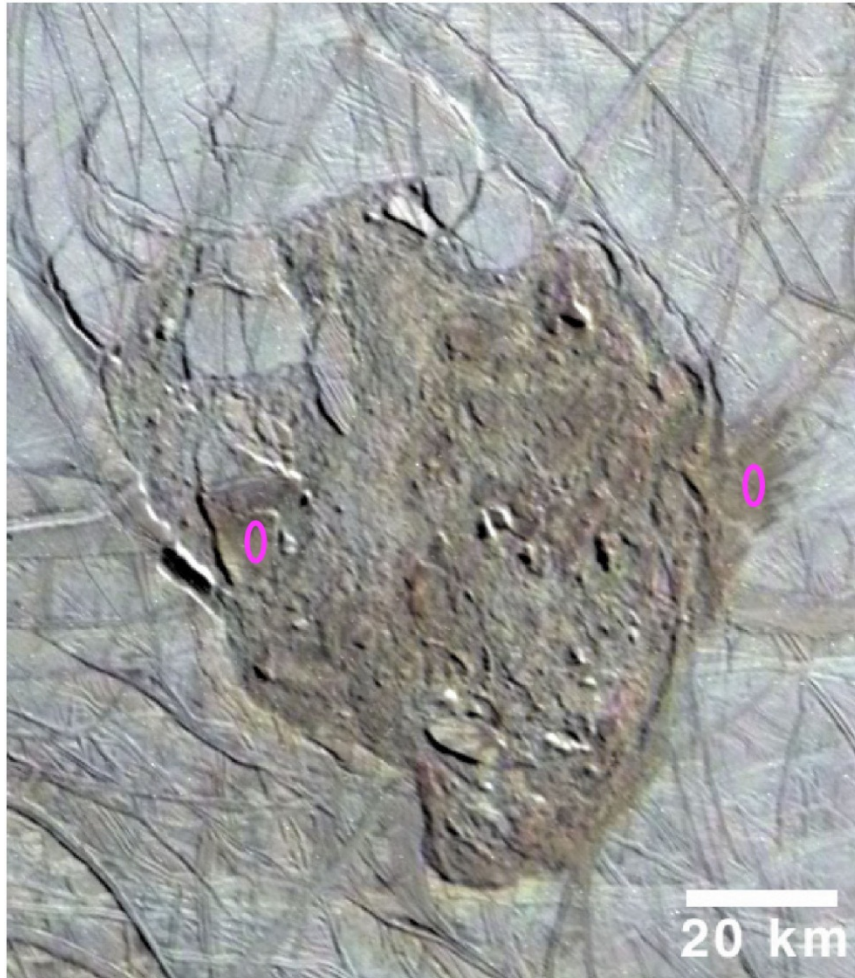
Figure D.2.8-3. Landing error ellipses positioned at two possible landing locations within the Thera area show that many scientifically acceptable placements are possible. This flexibility allows the site certification process to focus on safety for a quick decision.

relative navigation (TRN), which is used to redirect the Lander to its nominal target point during its descent. The TRN imaging will begin at an altitude of 4 km and will cover an area of 4 × 4 km, ample to recognize features around the landing site area to provide a navigational fix. The Lander element will be able to divert to a landing location up to 3 km from the location it is initially headed toward, sufficient to maneuver from the edge of the pre-deorbit error ellipse back to the center. A hazard detection and avoidance system will operate during the final descent. It will be able to detect hazards larger than 3 m wide and 1.5 m high and slopes in excess of 25°. It will

redirect the Lander up to 50 m laterally to the safest reachable 10 × 10–m landing zone.

Given these requirements and capabilities, the site-certification approach we have taken is to observe each site during the first Carrier overpass of its location after achieving the 200-km circular, 7:30 a.m.–node orbit. Imagery at 0.5 m/pixel is obtained using the RC described in Section D.2.2.2 over an area of 10 × 10 km centered on the nominal site location. This coverage is obtained in <10 seconds as each site is overflown. The 200-km altitude will permit viewing of any site at a side-looking emission angle of <30° from the Carrier on its closest overflight. For the ~2-hr orbital period of our 200-km circular orbit, successive ground tracks are displaced by ~230 km at the equator (~160 km at ±45° altitude). Therefore, a given site will be visible at low emission angles in daylight only once per Eurosol. The RC is designed to acquire coverage of the entire 10-km-wide swath in a single overflight to minimize the radiation dose accumulated while doing the reconnaissance by avoiding having to build up coverage over multiple Eurosols. The four sites will be imaged in sequence over the course of about one-half a Eurosol as Europa rotates beneath the inertially fixed orbit and each candidate site comes close to the Carrier ground track. Downlinking of the stored images (nominally compressed 3:1) occurs in the periods between image

acquisition. We <u>assume</u> that covering four sites with 10 × 10–km areas each will yield sufficiently high probability of finding a safe landing area in at least one location.

The site-certification process must be completed quickly to constrain the prelanding radiation dose. The required time for data acquisition, downlink, ground processing, analysis, and decisions is estimated to be 30 days. The timeline of activities for the four candidates sites initially specified is shown in Figure D.2.8-4. Data acquisition, downlink, and processing through the pipeline to produce products for analysis can be completed in about 3 days. Geologic mapping and hazard analysis of the four sites is competed by day 12. Automated hazard-detection software will be run, but time for validation of those results by human checking is allocated. Creation of the TRN maps from the site-certification imagery and corrections for existing cartographic errors goes on in parallel. Somewhat over two weeks is allocated for digestion and assessment of the results for these first four sites leading to a recommended landing site location for management approval. Landing can occur within 2 days after final site selection.

Although this is not shown in Figure D.2.8-4, there is no reason why continued reconnaissance imagery of both the first four sites and additional candidate sites could not be acquired on Eurosols subsequent to the first one after EOI. The Carrier has no other pressing

demands for use of its capabilities during this 30-day period. These data could include stereo imagery of previously observed sites or coverage of new candidate sites in other locations. These added data can be run through the processing pipeline and the automated hazard detection software and be waiting in the queue for further analysis as soon as one or more of the initial four sites is judged unacceptable. Or additional teams of analysts could be employed to study more than 4 sites in parallel. Stereo data can be run through a digital elevation map production system to provide supplemental data to the site-certification process.

The site-certification concept described above begins after EOI. An alternative approach that does site reconnaissance from a series of close flybys of Europa prior to EOI could be possible, but has not been studied in any detail. This alternative seems at first glance much more complicated since it would require numerous close approach daylight flyby points over a variety of specific site locations, preferably with low Sun-elevation angles. The sites would be spread over up to 180° of longitude on the leading side and over a range of latitudes. Off-nadir pointing would be needed to get coverage at the desired resolution. The higher ground speed (~4 km/s typically vs. 1.3 km/s in Europa orbit) makes image smear a concern. Stereo coverage becomes very difficult to obtain. However, if this alternative would prove feasible, it would allow substantially more time for data analysis and site
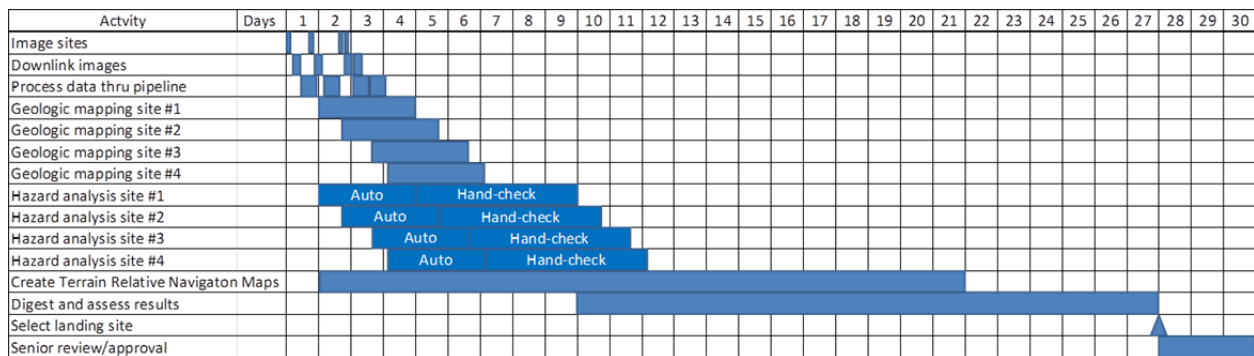

Figure D.2.8-4. The timeline for accomplishing site certification provides adequate time for data analysis and landing site specification.

selection prior to entering the high-radiation-dose-rate environment of Europa's orbit.

Upon completion of landing site selection, the Carrier will lower its orbital periapsis to 5 km and separate the Lander at the proper time and place (Section D.2.3). After successful landing, the Carrier will return to its 200-km circular orbit serving as a data relay between the Lander and Earth. The relay telecom concept is discussed in Section D.2.8.2.3.3. In addition, a post-landing image of the actual landing site location will be acquired by the RC and returned to Earth to provide accurate knowledge of the Lander location and context for interpretation of the surface science measurements. Due to the high power draw required to thermally stabilize the RC telescope, which precludes simultaneous telecom from the Carrier, acquisition of this image is scheduled to occur after all of the baseline Lander science data have been returned, i.e., two or more Eurosols after landing. The camera must be powered on in its standby mode for at least 12 hours prior to acquiring imagery to thermally stabilize the telescope at its nominal operating temperature.

D.2.8.2.2 *Operations Concept—Lander*

The operations for the Lander start with the DDL at the surface of Europa. The details on the landing sequence and navigation to the surface are described in Section D.2.3.4.

Once at the surface, the Lander will spend the rest of the mission lifetime acquiring the science data and transmitting it to the Carrier. The surface operations are divided into four main phases: Checkout and Commission Phase, Context Acquisition Phase, Sampling Phase, and Continuous Monitoring Phase. All of the phases are described below, with the times to perform the steps based on heritage estimates. The operations at the surface are a combination of ground-in-the-loop and automated sequences, with ample time periods for ground-in-the-loop allocated before all of the critical phases in the operations (e.g., sampling). The current concept described below is

success oriented with the main operations of sampling and imaging baselined to be accomplished in the first <u>two</u> Eurosols. If the science team needs additional time beyond the allocated ground-in-the loop times, or if there are problems with the Lander, the Context Acquisition and Sampling phases can be extended into seven additional Eurosols (or ~25 days), as long as the MAG and MBS are on, taking data. Moreover, because of the low radiation dose expected for the Lander and relatively long lifetimes and additional redundancy for all critical Lander components, the Lander should survive and operate longer than the Lander design lifetime of 9 Eurosols. The lifetime- limiting item is the Carrier since it is acquiring radiation damage at higher rates than the Lander, and, if it fails, it will prevent the Lander from downlinking data at higher telemetry rates. However, DTE communication for the Lander is still possible, and additional data can be downlinked using this mode, albeit at slower rates.

Checkout and Commission Phase

After the descent and landing sequence, which lasts less than 5 minutes, the Lander establishes a communications link with the Carrier and transmits the data from the descent. Based on the separation trajectory for the Carrier and Lander, the Carrier has three more passes over the landing site after touchdown, before ceasing communication with the Lander 40 hours later (see Figure D.2.8-5). 0.2 Gb of data acquired during the Lander descent can be transmitted to the Carrier element during these passes. Then the payload checkout and commission commences, including the SIS mast and MAG boom deployment. The one-time cover for the SIS would be opened as well. The payload checkout is expected to last ~6 hours, and at the end of that period the MAG and MBS are on, taking data for the rest of the landed operations. The aliveness of the ESS is checked out as well: The Lander unstows and actuates the arm, and possibly performs a blank measurement to make sure that
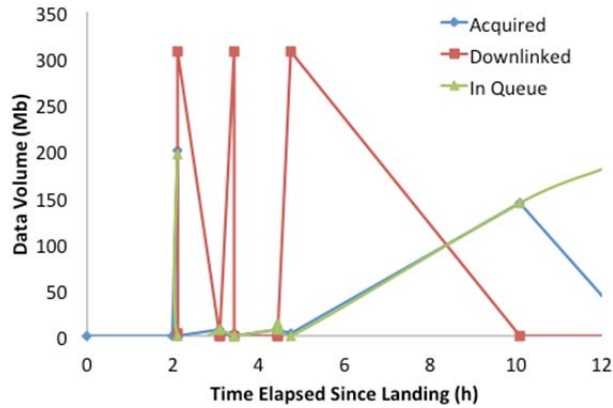
Figure D.2.8-5. Lander–Carrier relay telecom provides data return to inform the ground team before committing to the next phase of science activity.

the sample processing sequence operates as expected (~2 hours). The data from checkout is stored on the SSR for transmission during the next relay pass.

Context Acquisition Phase

At the beginning of the Context Acquisition Phase, the Carrier element is not within the view of the Lander. The SIS images the landing site with 10 a.m. lighting conditions and prepares for the first sample (~2.5 hr). These images are part of a stored sequence. Table D.2.8-5 shows the science data set that is acquired as part of this time period, including the priorities for data downlink and the image

Table D.2.8-5. Imaging data set expected to be acquired during the Context Acquisition Phase. Downlink priorities 1 through 4 are shown, as well as a compression factor for the images.

| Description	Priority	Comp	Data Volume (Gb)
foot pads	1	6	0.013
horizon	1	6	0.004
sun	1	6	0.002
near field regolith (adjacent regolith and portion of thruster pit) stereo (1 eye color)	1	3	0.034
site panorama, single eye, monochromatic	2	6	0.315
far field regolith (surface outside disrupted zone)	2	3	0.336
site panorama, color, single eye	3	3	1.887
stereo part of site panorama, other eye, no color	4	3	0.629
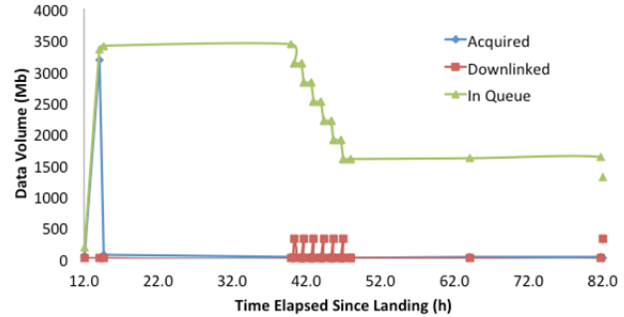
Figure D.2.8-6. Lander–Carrier relay telecom data return from the Context Acquisition Phase enables the decision to start the sampling activity.

compression. The worksite imager functions of the SIS in preparation for sampling supersede the fulfillment of geology science objectives. Also, for positioning of the ESS arm at the site of interest, stereo imaging is acquired. Priority-1 data is then transmitted during the first relay pass at ~39 hours since landing (see Figure D.2.8-6). The rest of the acquired data is then trickled out during the next 12 passes by the Carrier element. On the ground, as soon as the science team receives the priority-1 data, the "24-h " ground-in-the-loop mode commences for processing of the images and performing selection of the two sampling sites (see Figure D.2.8-6, 46 to 82 hours, providing additional margin). In the meantime, the MAG and MBS continue acquiring data and storing them on the SSR.

At the end of this phase, the science team has selected two sites to sample, and has produced and validated sequences on the ground to be uplinked to the Lander for the start of the Sampling Phase. The sequences for the first sampling site are then uplinked during the first relay pass at ~82 hours since landing (see Figure D.2.8-6).

Sampling Phase

At the start of the sampling phase, the Carrier is beginning a set of six overhead passes over a 12-hour time period. The data in queue from the Context Acquisition Phase are being transmitted to the Carrier; however, they are all lower priority than any sampling data

acquired during this phase. The Sampling phase begins with positioning of the arm with the rotary percussive drill onto the first sampling site selected by the science team. This operation is baselined at ~10 minutes based on MER estimates. The drill then penetrates into the surface and retrieves the sample from 0.5–2 cm below the surface (~10 minutes, based on MER estimates and also on the testing done by Honeybee Robotics for the rotary percussive drill for Mars Sample Return). The sample is then brought to the Lander, and is pushed out into an oven located on top of the Lander deck (~10 minutes based on MER estimate, with emphasis on minimizing that time). The sample is then analyzed in the following steps (for the total of ~2 hours of analysis):

1. The sample is placed in an oven with MS connected to it (see Figure D.2.8-7)
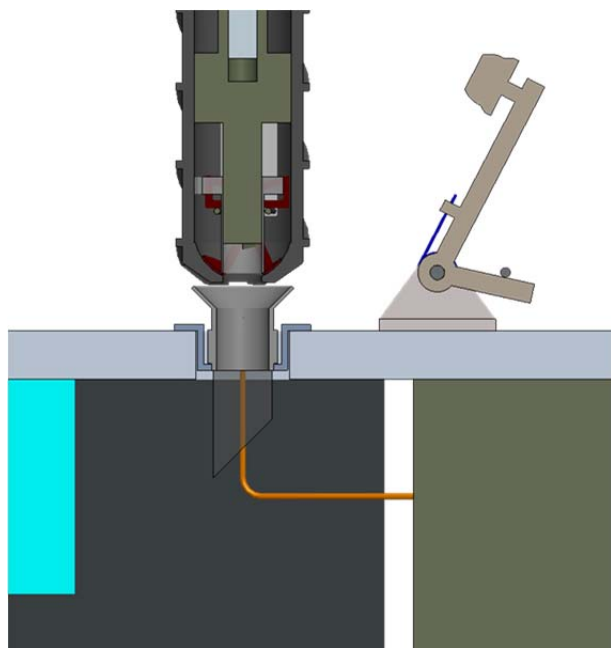2. The oven is sealed via pin-puller oper-

Figure D.2.8-7. A simple and reliable concept design for sample handoff is shown. The sample in the drill is shown positioned above the oven, with the oven door concept to the right. The oven has a window and a prism on the bottom to allow imaging by the MI and spectrum acquisition by RS. The capillary to transport evolved gas to MS and GC (orange) is shown as well.

ated door, and is kept at ambient vacuum
3. The sample is viewed by MI and Raman through a diamond window (~15 minutes)
4. The EGA/Pyrolysis/EI/MS and GC on sample is performed (~60 minutes)
   a. MS is run in headspace mode looking at natural volatile release as the temperature rises to steady state oven temperature (e.g., 200 K) for examination of low-temperature volatiles and the background (5 minutes)
   b. He regulation is started; oven manifold pressure and temperature of the valved hydrocarbon trap (HCT) are adjusted
   c. Pyrolysis ramp is started at the rate of ~40°C min^{-1} for EGA-EI-MS passing in order: light volatile release; water sublimation; organics via split pressure for balance between direct organic MS and HC trapping (for GCMS) in 100–400°C range; and inorganics up to 1100°C to capture all sulfates (total ramp time ~30 minutes); all lines are flushed, and MS is run in background mode
   d. HCT organics are released to GC injection and subsequent GCMS (20 minutes)

The collected data is then transmitted to the Carrier for as long as relays allow (82–88 hours, see Figure D.2.8-8). In the meantime, the Lander prepares for the second sample by imaging the disturbed location in addition to the second sampling site (~0.5 h). That data gets first priority and is transmitted to the ground in addition to the sampling data from the first site. The science team then uses another 16 hours to look at the data from the first site, and make a decision on whether to start sampling the picked out second site. The sequences are then uploaded to the Lander and
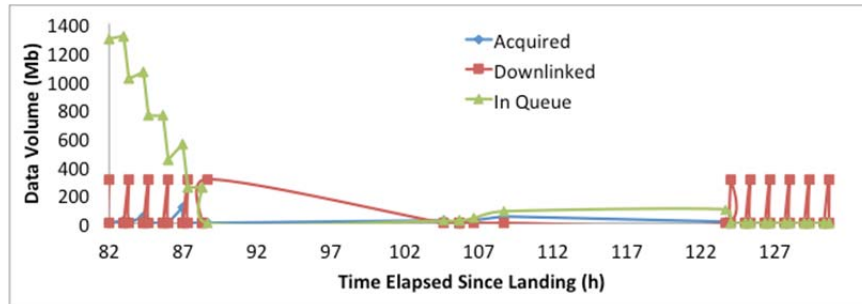
Figure D.2.8-8. Science data from sampling is downlinked by the end of the second Eurosol; this leaves 7 Eurosols of margin for extended science.

the sampling by drilling into 5–10 cm deep into the surface and analysis are repeated for the second site (see 105–107 hours, Figure D.2.8-8). At the end of the phase, the Carrier is overhead and data from the second sampling site is transmitted.

Continuous Monitoring Phase

During this phase, lasting from Eurosol 3 to Eurosol 9, the MBS and MAG are on and taking data continuously. The SIS will perform priority-5 imaging, acquiring ~0.05 Gb each Eurosol, with <2 relay passes required to transmit it. The priority-5 imaging data includes photometry in color taken with a single eye, and imaging selected locations, repeated at different times per day (nominally at four times per Eurosol). It also includes change-detection imaging of Europa's surface (mass wasting, front, sublimation) repeated two times per Eurosol. This data, together with the MBS and MAG data, is transmitted when the Carrier is overhead 12 times per Eurosol. Because of the low data volume acquired during this period, additional sample acquisition is possible.

D.2.8.2.3 Operations Concept—Telecom

Using the Carrier element to support delivery of science data from the Lander is a key feature of this mission concept. Communicating DTE from the surface is constrained by the mass, power, and complexity of having to point an HGA toward Earth, and by the amount of energy needed to transmit the data. System mass, and particularly the mass needed

to supply and store power, are particularly constrained in a Lander because of the system cost associated with delivering that mass to the surface safely. The rate at which data can be transmitted across a deep-space communications link is characterized by the power of the transmission, the sensitivity of the receiver, and the various gains and losses along the transmission path, particularly including the dissipation of radiated energy with distance. The fundamental insight of the relay concept is that it enables data to be delivered at high rates from the Lander to a nearby Carrier at very low energy cost to the Lander, thus reducing the need to provide and store that energy, and thus the Lander mass that must be delivered to the surface. This feature has a huge leverage in total system cost. The tradeoff requires that the Carrier carry the capability to support delivery of that data to Earth, but in this concept all of those capabilities were already needed to get the system to Europa and perform site certification, so the only direct cost is related to the need to continue to operate the Carrier for the 30-day surface mission.

Telecom hardware to support relay operations via UHF and the associated procedures and data management protocols have been developed by the Mars Program and successfully demonstrated by the MER and MSL rovers.

All communications modes in this concept were designed to work with 34-m DSN support with the exception of descent and landing tone reception and the contingency X-band Lander DTE downlink capability, both of which will require 70-m-equivalent DSN capability (achievable by arraying 34-m stations).

Preseparation Communications

From launch until the Lander separates from the Carrier element, the integrated spacecraft will primarily communicate with Earth via the telecom capabilities of the Carrier. LGAs are used to support X-band communications during early cruise, and tones during ME maneuvers including JOI and EOI. An MGA is used to support X-band communications during most of the rest of interplanetary cruise. During this phase the Lander and Carrier UHF capabilities can be tested to deliver Lander data through the UHF link even though the two are still attached.

The Carrier carries a 3-m HGA and 35-W Ka-band TWTA to support high downlink rates during the site-certification and science/relay phases. During the site selection phase when the two spacecraft remain joined and able to share power this system can employ the reaction wheels on the relay/Carrier element to enable precision pointing of the HGA to Earth, enabling a maximum data rate of about 129 kbps (the reaction wheels are primarily needed to support camera pointing during landing site imaging).

Descent and Landing

Once the spacecraft have separated the Lander will transmit tones DTE via X-band through LGAs, and engineering data to the Carrier via UHF. The intent of communicating in this phase is primarily diagnostic because the descent and landing behaviors must proceed autonomously from ground intervention. After separation the Carrier will remain in sight of the Lander during the brief DDL activity. All data collected during this phase will also be stored on the Lander for subsequent replay to the Carrier, if needed, on a subsequent relay pass.

Relay Communications Concept

Relay communications are primarily constrained by the geometry of the landing site and the relay orbit. A polar orbit allows the Carrier to overfly any potential landing site on the surface, but it minimizes the amount of time it will remain in sight of any particular landing sites other than the polar regions. The current concept retains a 200 × 200–km polar orbit to remain as flexible as possible to a landing site selection. The altitude is determined by a trade study that balanced achievable data throughput rates with ΔV and other costs. At much lower altitudes the instantaneous data rates can be higher but the view periods are so short and infrequent that they would become critical operations. In this arrangement the Carrier would pass within view of the Lander up to six times every half-Eurosol. That is, after the first set of passes Europa would rotate the landing site out from below the orbital path until they once again intersected nearly 180 degrees later on the dark side. The number and extent of view periods would be largely constrained by the Lander's view of the horizon, and the Carrier elevation above the horizon, since most passes will not pass directly overhead. Figure D.2.8-9 depicts what the duration of a set of view periods over one Eurosol achievable assuming a 30-degree elevation mask on visibility between the Lander and Carrier. Data balance is computed based on this conservative case. Power allocated to telecom sessions to support data relay is conservatively computed based on much longer view periods that would be possible if the horizon is unobstructed, in which case significantly more data could be delivered. Thus, data will be recorded on the Lander as science observations are performed, and then uplinked to the relay/Carrier element when it next passes overhead.

The UHF telecom capabilities include the ability to automatically adjust bit rates as a function of detected signal/noise ratio in real time, which enables the Lander and Carrier to coordinate with each other during each pass to maximize data throughput for the specific conditions they encounter.

Data delivered to the Carrier will be stored and forwarded to the ground using the Ka-band
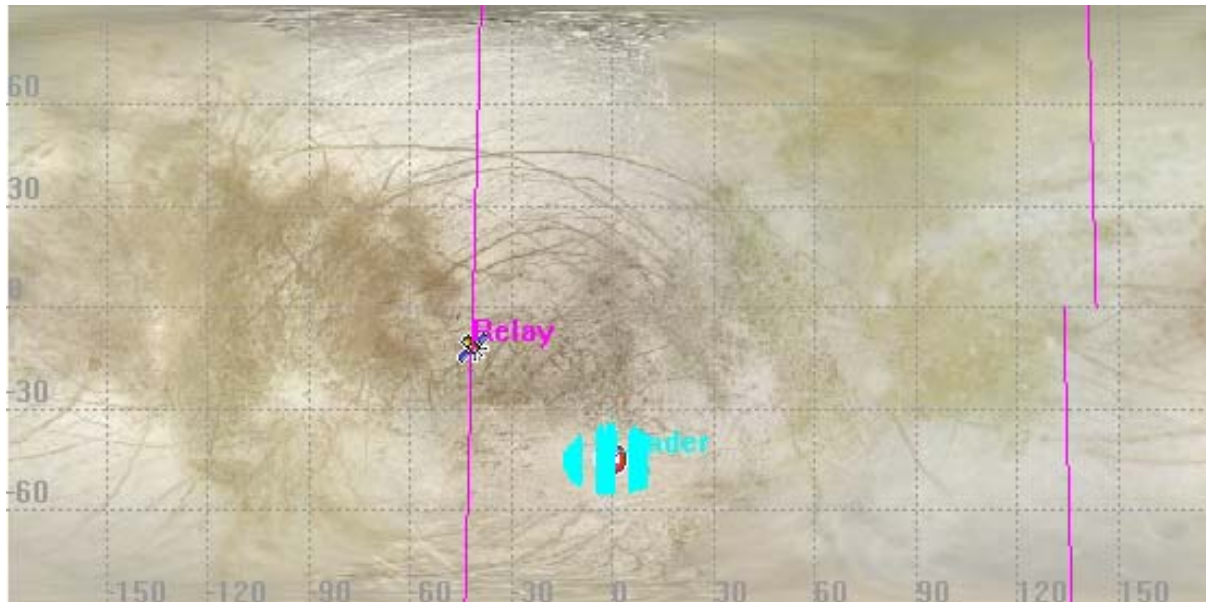
Figure D.2.8-9. The near-polar relay orbit enables a minimum of six consecutive contacts per half-Eurosol.

telecom capability and 3-m HGA on the Carrier element. Although the Carrier could support simultaneous communications with the Lander and Earth, this concept chooses to operate them sequentially in order to preserve power. Note that half of the overpasses will occur on the dark side of Europa when both spacecraft will be out of view of Earth, so simultaneous capability is moot there. During this phase the Carrier element is power-constrained and so uses thrusters rather than reaction wheels to maintain pointing. This limitation results in a lower maximum data rate through the Ka-band downlink system of about 75 kbps. This rate is much lower than the rates of up to 2 Mbps achievable across the UHF proximity link, but the time and energy available to transmit over this link is much less constrained.

Another benefit of the relay concept is the ability that it enables to precisely locate the Lander on the surface using radiometric ranging from orbit.

Lander Contingency DTE Communications

Because the Carrier will continue to be exposed to the highest-flux radiation in Europa orbit it presents a potential failure mode for the mission if it becomes unable to relay data from the Lander to the ground. For this reason the concept retains a DTE X-band telecom capability on the Lander as a contingency capability. In the event of a Carrier failure, data could be transmitted directly from the Lander at a maximum rate of about 9 kbps to a 70-m-equivalent DSN (four arrayed 34-m stations).

D.2.8.3 Development Supporting Europa Surface Operations

Each deep space flight project must address one key question concerning operations: how much of its flight capabilities must be developed and tested pre-launch. Many missions with short cruise periods develop the bulk of their flight and ground software, tools and processes pre-launch out of necessity, whereas some missions with longer cruise periods may leave science phase development largely untouched. These latter missions often suffer from "if we had only known" moments, where opportunities for more efficient operations concepts are lost because of the lack of operations scenario and modeling work done hand-in-hand with spacecraft and flight software development. Early consideration of operability issues in the system architecture and design is of great importance to the Europa Lander Mission.

Therefore, significant operations scenario development will occur during phases A–D. Science operations should be a strong element of the pre-launch flight systems engineering. Science operation scenarios need to be explored early and at a level of detail that permits flight system design choices to be better assessed. In particular, the uncertainty associated with the conditions that may be encountered on the surface will require a certain level of operational flexibility and autonomy of the landed system. Thus, the project will rely on a nominal operational plan to achieve baseline science goals that allows significant margins in time and other system resources to ensure that it can be completed. The project will develop the operations and ground system architecture, requirements, models and software to a level sufficient to support pre-launch development and flight system trade studies. The science planning tools should be developed such that they can be used to evaluate the ground and flight system requirements and capabilities. Based on these evaluations, refinements could be made in cruise and throughout the mission to the unified ground and flight system architecture and software requirements.

Modeling will be conducted to simulate representative key operations, primarily including surface and relay operations, and the ATLO phase will include the testing of at least one operational mode to be used during the Europa surface science phase. The product of these efforts should effect a net savings to the project over all life cycle phases, for the work will make possible more efficient operations and will uncover problems at a time when something can be done to mitigate them.

Furthermore, opportunities for process improvement will be built into the schedule after launch. A long cruise period has some challenges, among them skill retention and the dangers of obsolescence of ground systems. However, the varying level of intensity—lower between gravity assists, for example—also offers opportunities to improve processes,

software, IT infrastructure, operations concepts and the science template for Europa observations. The project aims to fill the "bathtubs" between major events in cruise with periods of further development. This approach dovetails a number of issues together well. First, it is impractical to staff the project up and down simply for major cruise events. Second, deferring some Europa operations development closer to the time of execution is a better design, taking advantage of available improvements in technology and work by a flight team more likely to be present during operations. Third, these periods of development and process improvement offer enticing opportunities to the flight team (in addition to spacecraft maintenance) to contribute the design of the operations system, and should improve skill and staff retention, in part so that their efforts can be seen to bear fruit in Jupiter orbit.

The gravity-assist flybys in the months before EOI also offer opportunities for operations readiness tests. Few, if any, surface behaviors can be executed prior to Lander separation, but some relay behaviors can be exercised to test both the flight and ground systems, and personnel readiness to begin science observations. These tests may also be perceived as a compromise to those members of the science team who may push for pre-Europa science. Some data would be collected during these tests that could prove scientifically valuable. However, no departure from the Europa template of activities will be tolerated, as that would allow non-Europa science to drive the design of the system. Furthermore, it is crucial that these in-flight exercises use the processes, procedures, software, and ground system capabilities in the same manner, to the extent possible, as will be used during Europa operations; otherwise the tests are less valid. Finally, there should be at least one ground software delivery, procedures update milestone, planned after these tests to take advantage of key lessons learned.

As far as staffing levels are concerned, after launch and initial checkouts, which should maintain approximately the phase C/D workforce level, cruise staffing will be relatively flat, with a moderate increase in development staff in the later portion of interplanetary cruise. As the navigation team must be fully capable for JOI, they would staff up to support Jupiter cruise levels at no later than JOI minus six months, along with any additional spacecraft system and subsystem support required to support navigation and maneuvering. The remainder of operations teams would staff up at some point post-JOI to test the final processes, science template, and software, with the first operations readiness tests for EOI and the start of science operations beginning about 12 months before EOI.

D.2.9   Systems Engineering

Systems engineering uses JPL's provided practices along with recent advancements in model-based engineering to design, develop, and integrate a complex Europa Lander Mission.

This section outlines the overall systems engineering approach and plan. The subsections that follow address three specific systems engineering challenges: radiation, planetary protection, and nuclear safety.

In general the Europa Lander Mission can be said to have the following technical and programmatic characteristics:

- Technical
  - Functioning in the presence of radiation flux, single-event effects (SEEs), damage to parts and materials
  - Satisfying planetary protection of the Europan ocean, as well as of Ganymede and Callisto, from delivered bioburden
  - Lifetime and reliability over a long mission
  - Maintaining conservative resource margins

- Integrating a complex suite of competitively selected science instruments from a diverse field of providers
- Integrating radioisotope power sources
- Thermal environments at Venus flyby vs. Jupiter
- Critical orbit insertion at Jupiter and Europa
- Identifying a scientifically yet safe location to land
- Dense science operations schedule at Europa after years of cruise
- Keeping a 10-year-plus "corporate memory" of the requirements, detailed design, and the rationales for design choices

- Programmatic
  - Succeeding in a cost- and cost-profile-constrained environment
  - Coordinating the efforts of a large, diverse engineering team
  - Integrating the project and design with competitively selected instruments
  - Multiinstitutional and potential multinational partnerships (JPL, APL, PIs)

- Overarching systems engineering objectives for formulation
  - By System Requirements Review (SRR), produce a Baseline System Specification (L1–L3 Baseline; L4 Preliminary; L5 Key and Driving), a committed systems engineering schedule and cost profile, and a committed mission architecture.
  - By Preliminary Design Review (PDR), produce a released set of procurement specifications, a fully-developed preliminary design, and a committed project schedule and cost.

Institutional project and line management is uniformly committed to making major strides in systems engineering, supporting and enforcing the following approach:

- Enforce rigorous engineering discipline. Expect engineering rationale to be documented as complete and logical chains of thought, and in appropriate tools
- Make use of emerging new systems engineering capabilities as appropriate, including system modeling language standards and tooling, model integration and exchange standards and tooling, and Web-based report generation.
- Starting from the beginning, build persistent and evolvable artifacts.
- Starting from the beginning, build a core team of systems engineers who can faithfully promulgate the architecture later as the project grows.
- Proactively align with forthcoming NPR 7120.5E (NASA 2012).
- Emphasize architecture and design space exploration through MCR. An architectural approach keeps the team properly focused on the "why," and design space exploration keeps us properly focused on the concept rather than a point design. In this endeavor, trusted models and analytical tools are essential investments.
- Make decisions by a process that is explicitly guided by Architecture, is timely and responsive, is transparent to all stakeholders, and includes balanced consideration of multiple experienced viewpoints.

The Europa Lander Mission is well positioned to move into pre-project formulation. The Europa Study Team has made key investments in infrastructure, engineering artifacts, and team-building, as described below:

- Infrastructure has been developed for the long term. Already set up and in

routine use are a collaborative Systems Modeling Language (SysML) environment (MagicDraw/Teamwork Server), a collaborative architecture development environment (Architecture Framework Tool), the project repository (DocuShare), and the project workflow management system (JIRA).
- Existing engineering and architectural artifacts provide a powerful head start. Key plans and processes are in place. Key parts of the architecture description are done. The system model is established.
- Our team processes and practices are mature and effective. Cost estimates, technical margin estimates, and configuration changes take a fraction of the usual time. Report autogeneration is already in routine use.

From this strong starting point, a plan that achieves robust maturity at SRR and PDR is constructed. The sketch of this plan, expressed as key artifacts per life-cycle phase through PDR, is shown in Tables D.2.9-1 through D.2.9-4. In these tables the changes from one table to the next are shown in blue font, and the parentheticals following the artifact names denote maturity levels:

- (A): Approach is defined, and possibly a sketch of the artifact.
- (K&D): Key and Driving cases are identified and covered.
- (P): Preliminary. A full version for review and discussion leading to a baseline version.
- (B): Baseline. The artifact is under configuration control.
- (U): Update.

After PDR, systems engineering focus changes from development to implementation: managing change control process, while maintaining architectural integrity; implementing the I&T and V&V programs; and preparing for flight operations.

Table D.2.9-1. Present maturity of systems engineering artifacts.

At Tech Review	Systems Engineering Plan: Key Artifacts per Life-Cycle Phase Artifact Type					
	Plan	**Scenario**	**Model**	**Analysis & Sim**	**Report**	**Spec**
Program (L1)						L1 Rqmts (K&D)
Project (L2)	Arch Dev Plan (P) SEMP (A) Model Mgt Plan (A)	Driving Mission (K&D)	Trajectory (P) Science Margin (A) Data Margin (P) FS Radiation (P)	ΔV/Prop (P) Science Margin (A) Data Margin (P) FS Radiation Life (P)	Concept Report (P) Msn Arch Descr (P) Ops Concept (A) Tech Assessment (A) Eng Dev Assess (A) Top Risks (A)	L2 Rqmts (A) Env Definition (A)
System (L3)		Flight Sys Ops (K&D)	FS Functional (P) FS Physical (P) FS Shielding (P) FS Power (P) FS Static Mech (P) FS Thermal (P) FS Telecom Link (P) FS Attitude Ctrl (P)	FS Mass Margin (P) FS Shield Mass (P) FS Pwr Margin (P) FS Mass Props (P) FS Therm Balance (P) FS Link Margin (P) FS Pntg Margin (P)		L3 Rqmts (A)
Subsystem (L4)			Power (K&D) Thermal (K&D) Propulsion (K&D) Telecom (K&D) Avionics (K&D) Structure (K&D)	Power Bus Sim (P) Therm Balance (P) JOI/EOI Perf (A) EIRP, G/T (P) C&DH Throughput (A) LV Static Envel (P)		
Component (L5)			Radiation Effects (P) DHMR Effects (P)	Component Life (P) Parts/Matl Issues (P)	Approved Parts (A) Approved Matls (A)	

SCOPE

Blue = Change (U) Update (B) Baseline (P) Preliminary (A) Approach (K&D) Key & Driving

Table D.2.9-2. Maturity of systems engineering artifacts at MCR. Acronyms will be defined in an appendix (Section B.4.2).]

At MCR	Systems Engineering Plan: Key Artifacts per Life-Cycle Phase — Artifact Type						
	Plan	Scenario	Model	Analysis & Sim	Report	Spec	
Program (L1)						L1 Rqmts (P)	
Project (L2)	Arch Dev Plan (B) SEMP (P) Model Mgt Plan (P) Integr Plan (A) V&V Plan (A)	Driving Mission (P)	Trajectory (B) Science Margin (B) Data Margin (B) FS Radiation (B)	ΔV/Prop (P) Science Margin (P) Data Margin (P) FS Radiation Life (P) Rqmt Traceability (P)	Concept Report (B) Msn Arch Descr (P) Ops Concept (P) Tech Assessment (P) Eng Dev Assess (P) Top Risks (P) Instrument AO PIP (B)	L2 Rqmts (P) Env Definition (P) External ICDs (K&D) Intersystem ICDs (K&D) S/C–P/L ICD (K&D)	Blue = Change (U) Update (B) Baseline (P) Preliminary (K&D) Key & Driving (A) Approach
System (L3)		Flight Sys Ops (P)	FS Functional (P) FS Physical (P) FS Shielding (P) FS Power (P) FS Static Mech (P) FS Thermal (P) FS Telecom Link (P) FS Attitude Ctrl (P) FS Behavior (P) FS Fault Contnmt (P)	FS Mass Margin (P) FS Shield Mass (P) FS Pwr Margin (P) FS Mass Props (P) FS Therm Balance (P) FS Link Margin (P) FS Pntg Margin (P)		L3 Rqmts (K&D) Intra-FS ICDs (K&D)	
Subsystem (L4)			Power (P) Thermal (P) Propulsion (P) Telecom (P) Avionics (P) Structure (P)	Power Bus Sim (P) Therm Balance (P) JOI/EOI Perf (P) EIRP, G/T (P) C&DH Throughput (P) LV Static Envel (P)			
Component (L5)			Radiation Effects (P) DHMR Effects (P)	Component Life (P) Parts/Matl Issues (P)	Approved Parts (P) Approved Matls (P)		

(Left side label: SCOPE)

Table D.2.9-3. Maturity of systems engineering artifacts at SRR.

At SRR	Systems Engineering Plan: Key Artifacts per Life-Cycle Phase Artifact Type						
	Plan	Scenario	Model	Analysis & Sim	Report	Spec	
Program (L1)						L1 Rqmts (B)	Blue = Change
Project (L2)	Arch Dev Plan (U) SEMP (B) Model Mgt Plan (B) Integr Plan (P) V&V Plan (P) S/W Mgt Plan (P)	Mission Plan (K&D)	Trajectory (U) Science Margin (U) Data Margin (U) FS Radiation (U)	ΔV/Prop (B) Science Margin (B) Data Margin (B) FS Radiation Life (B) Rqmt Traceability (B)	Concept Report (U) Msn Arch Descr (B) Ops Concept (B) Tech Assessment (B) Eng Dev Assess (B) Top Risks (B)	L2 Rqmts (B) Env Definition (B) External ICDs (B) Intersystem ICDs (P) S/C-P/L ICD (P)	(U) Update
System (L3)		Flight Sys Ops (B)	FS Functional (B) FS Physical (B) FS Shielding (B) FS Power (B) FS Static Mech (B) FS Thermal (B) FS Telecom Link (B) FS Attitude Ctrl (B) FS Behavior (B) FS Fault Contnmt (B)	FS Mass Margin (P) FS Shield Mass (P) FS Pwr Margin (P) FS Mass Props (P) FS Therm Balance (P) FS Link Margin (P) FS Pntg Margin (P) FS PRA (A) FS Func FMECA (A) FS TAYF Exceptions (A)	Ground Sys Arch (P) Payload Arch (P)	L3 Rqmts (B) Intra-FS ICDs (P) Procurement Specs (P)	(B) Baseline
Subsystem (L4)			Power (B) Thermal (B) Propulsion (B) Telecom (B) Avionics (B) Structures (B)	Power Bus Sim (P) Therm Balance (P) JOI/EOI Perf (P) EIRP, G/T (P) C&DH Throughput (P) LV Static Envel (P)		L4 Rqmts (P) Intrasubsystem ICDs (P)	(P) Preliminary
Component (L5)			Radiation Effects (B) DHMR Effects (B)	Component Life (P) Parts/Matl Issues (P)	Approved Parts (P) Approved Matls (P)		(K&D) Key & Driving

(Right margin label: SCOPE; legend column: Blue = Change, (U) Update, (B) Baseline, (P) Preliminary, (K&D) Key & Driving, (A) Approach)

Table D.2.9-4. Maturity of systems engineering artifacts at PDR.

At PDR	Systems Engineering Plan: Key Artifacts per Life-Cycle Phase Artifact Type						
	Plan	Scenario	Model	Analysis & Sim	Report	Spec	
Program (L1)						L1 Rqmts (B)	
Project (L2)	Arch Dev Plan (B) SEMP (U) Model Mgt Plan (U) Integr Plan (B) V&V Plan (B) S/W Mgt Plan (B)	Mission Plan (P)	Trajectory (U) Science Margin (U) Data Margin (U) FS Radiation (U)	ΔV/Prop (U) Science Margin (U) Data Margin (U) FS Radiation Life (U) Rqmt Traceability (U) Mission Fault Tree (P)	Concept Report (U) Msn Arch Descr (U) Ops Concept (U) Tech Assessment (U) Eng Dev Assess (U) Top Risks (U) Instrument AO PIP (B)	L2 Rqmts (B) Env Definition (B) External ICDs (B) Intersystem ICDs (B) S/C–P/L ICD (B)	
System (L3)		Flight Sys Ops (U)	FS Functional (B) FS Physical (B) FS Shielding (B) FS Power (B) FS Static Mech (B) FS Thermal (B) FS Telecom Link (B) FS Attitude Ctrl (B) FS Behavior (B) FS Fault Contnmt (B)	FS Mass Margin (B) FS Shield Mass (B) FS Pwr Margin (B) FS Mass Props (B) FS Therm Balance (B) FS Link Margin (B) FS Pntg Margin (B) FS PRA (P) FS Func FMECA (P) FS TAYF Exceptions (P)	Ground Sys Arch (B) Payload Arch (B)	L3 Rqmts (B) Intra-FS ICDs (B) Procurement Specs (B)	
Subsystem (L4)			Power (B) Thermal (B) Propulsion (B) Telecom (B) Avionics (B) Structures (B)	Power Bus Sim (B) Therm Balance (B) JOI/EOI Perf (B) EIRP, G/T (B) C&DH Throughput (B) LV Static Envel (B)	Subsys Des Desc (P) P/L Design Desc (P)	L4 Rqmts (B) Intrasubsystem ICDs (B)	
Component (L5)			Radiation Effects (B) DHMR Effects (B)	Component Life (B) Parts/Mat Issues (B)	Approved Parts (B) Approved Matls (B)	L5 Rqmts (P)	

SCOPE (left vertical label)

Right vertical labels: Blue = Change (U) Update (B) Baseline (P) Preliminary (K&D) Key & Driving (A) Approach

D.2.9.1   Radiation/Charging

The effects of radiation on the Carrier element and Lander would be mitigated by the efficient use of inherent shielding provided by the spacecraft itself and additional dedicated shield mass, combined with radiation-tolerant materials and electronics.

The Europa Lander Mission spacecraft is exposed to naturally occurring and self-generated radiation from launch to EOM. The self-generated radiation, composed of neutrons and gamma rays, is produced from the ASRGs. The naturally occurring radiation encountered during the cruise phase between launch and JOI consists of solar flare protons and background galactic cosmic ray heavy ions. Between JOI and EOI, the combined Carrier element and Lander is exposed to protons, electrons, and heavy ions trapped in the Jovian magnetosphere.

After EOI, the combined spacecraft and Lander will orbit Europa at an altitude of 200 kilometers, performing surface photo reconnaissance of potential landing sites for 30 days. During the orbital photo reconnaissance phase, the combined spacecraft will be exposed to protons, electrons, and heavy ions that are partially shielded by the effects of Europa within the Jovian magnetic field. At the end of the orbiting reconnaissance, the Carrier element and the Lander will separate, changing the configuration of the spacecraft shielding distribution for both elements and the radiation environment encountered by the Lander element.

After separation, the Carrier element will remain in Europa orbit for 32 days providing a telecommunications relay between the Lander and Earth. The external radiation environment will be the same as in the photo reconnaissance portion of the mission, but the internal environment will be more severe due to the removal of the shielding provided by the Lander. The Lander radiation environment for surface operations will be significantly lower due to the shielding effects of Europa.

The radiation encountered during the mission affects onboard electronics, nonmetallic materials, thermal control materials, and surface coatings by depositing energy through ionization, henceforth called total ionizing dose (TID), and causes noise in science instrument and star-tracker detectors due to the intense proton and electron flux encountered in the Jovian system. The expected accumulated TID from launch to EOM as a function of effective aluminum shielding thickness is shown in Table D.2.9-5 for the Carrier element and Table D.2.9-6 for the Lander. Peak unshielded electron and proton fluxes for the Carrier are shown in Table D.2.9-7. For the Lander surface operations the peak unshielded electron and proton fluxes are shown in Table D.2.9-8.

Table D.2.9-5. The Carrier electronics will be shielded to a TID of 50 krad, enabling the use of standard aerospace equipment. Expected Carrier element mission accumulated TID as a function of shield thickness.

Aluminum Thickness (mil)	Total Ionizing Dose (krad Si)				
	Cruise	Tour	Photo Recon	Telecom Relay	Total
100	5.1	125	359	383	872
200	2.9	52.0	157	168	380
400	1.8	20.2	57.8	61.7	142
600	1.5	12.1	30.5	32.5	76.6
800	1.3	9.0	19.3	20.6	50.2
1000	1.2	7.5	13.8	14.8	37.4
1200	1.2	6.8	10.8	11.6	30.3
1400	1.1	6.3	9.0	9.6	26.0
1600	1.1	6.0	7.8	8.4	23.3

Table D.2.9-6. The Lander electronics will be shielded so a TID of 50 krad, enabling the use of standard aerospace equipment. Expected Lander element mission accumulated TID as a function of shield thickness.

Aluminum Thickness (mil)	Total Ionizing Dose (krad Si)				
	Cruise	Tour	Photo Recon	Surface Ops	Total
100	5.1	125	359	33.0	522
200	2.9	52.0	157	22.5	235
400	1.8	20.2	57.8	21.5	101
600	1.5	12.1	30.5	21.0	65.1
800	1.3	9.0	19.3	20.6	50.2
1000	1.2	7.5	13.8	14.8	37.4
1200	1.2	6.8	10.8	11.6	30.3
1400	1.1	6.3	9.0	9.6	26.0
1600	1.1	6.0	7.8	8.4	23.3

Table D.2.9-7. The Carrier detectors are shielded so that exposure to this flux does not impact operations. Expected Carrier element mission peak unshielded electron and proton flux.

Particle Energy (MeV)	Flux (#>Energy cm^{-2} sec^{-1})	
	Electron	Proton
10	1.7 E6	1.7 E5
20	4.8 E5	3.6 E4
30	2.2 E5	9.1 E3
50	7.9 E4	8.6 E2
100	1.8 E4	1.5 E1

Table D.2.9-8. The Lander detectors are shielded so that exposure to this flux does not impact operations. Expected Lander surface operations peak unshielded electron and proton flux.

Particle Energy (MeV)	Flux (#>Energy cm^{-2} sec^{-1})	
	Electron	Proton
10	3.9 E5	8.5 E4
20	9.8 E4	1.8 E4
30	5.3 E4	4.6 E3
50	3.0 E4	4.3 E2
100	1.3 E4	7.5 E1

The selection of electronic parts with respect to their radiation tolerance and reliability in the Europa radiation environment will be achieved through a combination testing and analysis. The minimum acceptable TID hardness of electronic devices will be 100 kilorad. The minimum SEE hardness will be documented in a Parts Program Requirements (PPR) document. A combination of radiation testing (TID, DDD, and SEE) of electronic devices and buying vendor-guaranteed radiation-hardened parts that meet the minimum TID and SEE requirements will ensure that robust electronics will be used in spacecraft and instrument electronics. Radiation testing will be done at high-dose rates and at low-dose rate for electronic device types that are susceptible to enhanced low-dose-rate sensitivity (ELDRS) effects (primarily bipolar devices). Electronic part parameter degradation observed during radiation testing will be documented and used as input into the spacecraft and instrument electronics end of mission worst-case analysis (WCA). Electronic devices that do not meet the minimum TID and SEU hardness requirements will not be used within

the spacecraft electronics or instruments unless approved by a requirements waiver.

The selection guidelines of nonmetallic materials for radiation susceptibility and reliability has been documented by Willis (2011). Detailed evaluations will be performed for these materials after exposure to EOM radiation environment to ensure that end-of-life performance requirements are met. Radiation testing will be performed for materials that do not have available radiation data.

The Europa Lander Mission will develop an Approved Parts and Materials List (APML) to identify standard parts approved for flight equipment that are developed under the project's cognizance. The APML will be populated with EEE parts and materials, as well as many critical parts such as sensors, detectors, power converters, FPGAs, and nonvolatile memories. Each entry will be accompanied with a Worst-Case Datasheet (WCD) and application notes describing proper use of the part at selected radiation levels. Dissemination of this information early in the design process is critical to enable the spacecraft electronics and instrument providers to design adequately for the radiation environment.

Every approved part listed on the APML will meet the reliability, quality, and radiation requirements specified in the PPR. The APML will be updated as new radiation data becomes available. Parts not listed as approved on the APML are defined as nonstandard parts and will require a Nonstandard Parts Approval Request (NSPAR) for use on the Europa Lander Mission. All nonstandard parts will be reviewed, screened, and qualified to the requirements of PPR.

Every part on the APML will be approved by the Parts Control Board (PCB). The PCB recommends and approves parts for inclusion in the APML. Criteria will be based on absolute need, the number of subsystems requiring the part, qualification status, TID, SEE, and procurement specification review. Mission

designers should use standard parts to the maximum extent possible so that they can reduce the radiation testing and qualification expenditure to the minimum.

Radiation-induced effects on instrument detectors and other key instrument components ultimately impact the quality and quantity of the mission science return and the reliability of engineering sensor data critical to flight operations. High-energy particles found within the Europa environment will produce increased transient detector noise as well as long-term degradation of detector performance and even potential failure of the device. Transient radiation effects are produced when an ionizing particle traverses the active detector volume and creates charges that are clocked out during readout. Radiation-induced noise can potentially swamp the science signal, especially in the infrared wavebands, where low solar flux and low surface reflectivity result in a relative low signal. Both TID and DDD effects produce long-term permanent degradation in detector performance characteristics. This includes a decrease in the ability of the detector to generate signal charge or to transfer that charge from the photo active region to the readout circuitry; shifts in gate threshold voltages; increases in dark current and dark current non-uniformities, and the production of high-dark-current pixels (hot pixels or spikes). It is important to identify and understand both the transient and permanent performance degradation effects in order to plan early for appropriate hardware and operations risk mitigation to ensure mission success and high-quality science returns.

The JEO Detector Working Group (DWG) was formed in FY08 to evaluate the detector and laser components required by the planning payload and SRU. DWG participants included experienced instrument, detector, and radiation environment experts from APL and JPL. For each technology required for the payload, the DWG (i) reviewed the available radiation literature and test results, (ii) estimated the radiation environment incident on the component behind its shield, and (iii) assessed the total dose survivability (both TID and DDD) and radiation-induced transient noise effects during peak flux periods. The assessment included the following technologies: visible detectors, mid-infrared and thermal detectors, microchannel plates and photomultipliers, avalanche photodiodes, and laser-related components (pump diode laser, solid-state laser, fiber optics).

The DWG assessment, reported in Boldt et al. (2008), concluded that the radiation challenges facing the JEO notional payload (similar types to the Lander payload) and SRU detectors and laser components (Lidar HD on the Lander) are well understood. With the recommended shielding allocations, the total dose survivability of these components is not considered to be a significant risk. In many cases, the shielding allocation was driven by the need to reduce radiation-induced transient noise effects in order to meet science and engineering performance requirements. For these technologies—notably mid-infrared detectors, avalanche photodiode detectors, and visible detectors for star-tracking—the extensive shielding (up to 3-cm-thick Ta) for transient noise reduction effectively mitigates all concern over total dose degradation. For the remaining technologies, more modest shielding thicknesses (0.3–1.0 cm Ta, depending upon the specific technology) were judged to be sufficient to reduce the total dose exposure and transient noise impact to levels that could be further reduced with known mitigation techniques (detector design, detector operational parameters, algorithmic approaches and system-level mitigations). The DWG conclusions reached for the JEO are applicable for the science detectors and the SRU on board the Europa Lander Mission.

A rigorous "test-as-you-fly" policy with respect to detector radiation testing, including irradiation with flight-representative species and energies for TID, DDD, and transient

testing, will be adopted for the Europa Lander Mission.

The Jovian electron environment also causes dielectric materials and ungrounded metals to collect charge on the Carrier element and Lander external surfaces and within the spacecraft. This causes transient voltage and currents in the spacecraft when an electrostatic discharge (ESD) event occurs. Surface charging effects are mitigated by limiting the differential charging of external materials. This limitation is accomplished by using materials that have surface coatings and treatments that allow the accumulated charges to bleed to spacecraft ground. A significant number of such surface materials have been used extensively in severe charging environments for spacecraft with long lifetimes (typically geosynchronous communications spacecraft, but also Juno) and are usable for the Europa Lander Mission. These materials include

- Carbon-loaded Kapton thermal blankets
- Indium–tin-oxide-coated gold Kapton thermal blankets
- Germanium-coated, carbon-loaded Kapton thermal blankets
- Electrostatic-conductive white paint
- Electrostatic-conductive black paint
- Composite materials
- Metallic materials

When surface discharge does occur, the voltage and current transients are mitigated by shielding around harness lines and using interface electronic devices that can tolerate the energy from ESD-induced transients that couple into the harness center conductors.

Internal ESD is controlled by shielding to reduce the electron flux present at dielectric materials within the Carrier element and Lander (typically circuit boards) and by limiting the amount of ungrounded metal (ungrounded harness conductors, connector pins, device radiation shields, part packages). The shielding required to reduce the TID to ac-

ceptable levels for the Europa Lander Mission is more than sufficient to reduce the electron flux enough to preclude discharge events to circuit boards. Grounding of radiation shields, part packages, harness conductors, and connector pins through ESD bleed wires or conductive coatings limits the ungrounded metals to small areas that cannot store enough energy to cause discharges that can damage electronic devices.

The surface and internal charging methodology has been used extensively in a severe charging environment for spacecraft with long lifetimes and was used specifically on the Juno project.

The Carrier element and Lander's exposure to radiation is attenuated to acceptable levels by providing shielding between the external environment and the sensitive materials and electronic parts in the spacecraft. Most of the Carrier element avionics electronics are placed in a shielded vault. Carrier element sensor heads for the SRU and RC external to the vault have shielding to enable operation to the required levels. This shielding is tailored for their design and location on the spacecraft.

Efficient use of dedicated shield mass for the Carrier element is achieved through a nested shield design, shown in Figure D.2.9-1. Spacecraft structure, the placement of the Propulsion Subsystem hardware (fuel tanks, oxidizer tanks, helium pressurant tanks and propellant that remains in the tanks after JOI) and the Lander provide significant collateral shielding to the electronics packaged within the vault. The vault's wall thickness and material composition, 4.4-mm-thick aluminum, limit the Carrier element mission TID to 150 krad for the enclosed electronics. Localized shielding at the assembly level reduces the Carrier element mission TID from 150 krad to 50 krad at the device level for all electronics (inside or outside the vault).
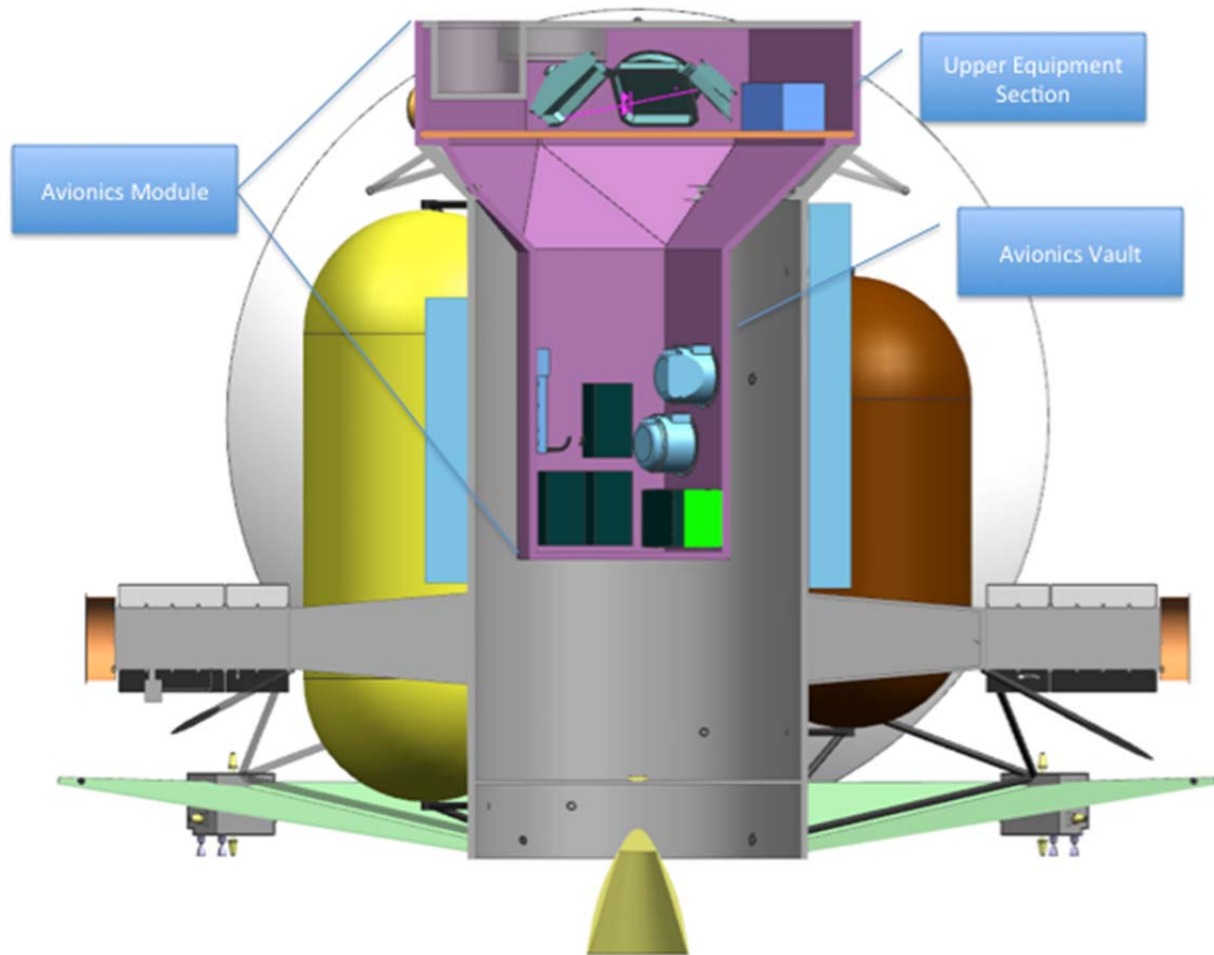
Figure D.2.9-1. Carrier element electronics are shielded by the spacecraft structure, propulsion tanks, and a dedicated vault. Note that the Lander structure above the Upper Equipment Section is not included in the figure.

Unlike the Carrier element, the Lander does not employ a vault to shield its electronics(see Figure D.2.9-2). The Lander avionics electronics and science instrument electronics are shielded from TID at the assembly level. Science instrument detector shielding to suppress radiation-induced background noise and permanent damage effects from the ASRGs is achieved through a combination of instrument-level shielding for detector support electronics and internal high-Z material shielding for the detector devices. The typical science detector is shielded by 1 cm aluminum, provided by the Lander structure and instrument housing and 1 cm tantalum shielding added around the detector device. The TID, DDD, and electron flux exiting the shield are shown in Table D.2.9-9.

Table D.2.9-9. Europa surface detector radiation environment within a 1-cm aluminum and 1-cm tungsten shield.

Europa Lander Detector Radiation Environment	
Total Ionizing Dose	6.2 krad Si; 8.0 krad InGaAs
Displacement Damage Dose	1.3E8 MeV/gram Si
Electron Flux inside Shield	7E3 electrons/(cm^2sec^1)

The dedicated shield mass for the Lander Mission is a total of 127 kg (TBR), as shown in Table D.2.9-10. The shield mass was calculated based on a detailed radiation transport analysis that takes into account the Carrier element and Lander configuration shown in Figures D.2.9-1 and D.2.9-2; material composition and thickness of the spacecraft structural
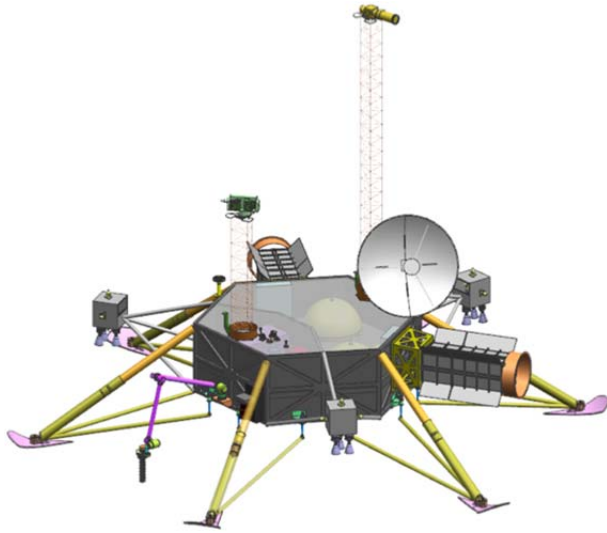
Figure D.2.9-2. Lander electronics and science instruments are shielded by the spacecraft structure with additional shielding added at the assembly level to limit exposure to 50 krad TID.

elements and propulsion tanks; and the locations of electronic units and science instruments. Analysts used the following process:

1. Generate Carrier and Lander configurations and locations from a CAD models. Three configurations were generated; an integrated Carrier element and Lander for analyses from launch to separation; a Carrier-element-alone configuration for the telecommunications relay phase; and a Lander-alone configuration for surface operations.

2. Explicitly calculate the shielding effectiveness of materials used in spacecraft structure, propulsion tanks, electronics unit chassis, dedicated vault, and added electronics assembly shielding based on material composition, density, and location using the NOVICE radiation transport code. For this analysis, the propulsion tanks are modeled as empty tanks.

3. To minimize the cost and risk of assuming electronic parts with higher radiation tolerance, assume all spacecraft electronics to use 100-krad-tolerant electronic parts.

4. Understand science instrument electronics colocated with detectors to have radiation tolerances that are instrument-specific (see Section D.2.2).

5. Through adjustments to assembly-level shielding mass, shield all spacecraft electronics assemblies to a TID of 50 krad or less at EOM (i.e., to account for environmental uncertainty, they are given an RDF greater than or equal to 2 at the end of the mission).

6. Shield science instrument electronics to have a minimum RDF of 2 for TID at the end of the mission.

7. To minimize cost, use aluminum shielding for all spacecraft electronics except science instrument and star-tracker detectors.

8. To minimize the radiation-induced noise at the detector location, shield science instrument and star-tracker detectors using high-atomic-number materials (such as tantalum) (see Section D.2.2).

9. At the individual assembly level, to allow the use of off-the-shelf electronics without modification, wrap shielding around each assembly rather than integrating it into the assembly chassis.

10. Model circuit boards within the electronic assemblies as unpopulated boards. (Modeling component layouts on boards will be performed as the project progresses into Phase B. Including component layout in the radiation transport model will further reduce TID at the device level.)

Significant opportunities to reduce the dedicated shield mass have been identified although they have been unexercised at this time. These opportunities include the following:

1. Change electronics unit placement within the vault to protect units with lower-TID-capable electronic parts (Carrier only).

2. Place electronics cards within units to provide the lowest local TID at the part level.
3. Use a more efficient shield material than aluminum.
4. Add rigor to the radiation transport model by including populated boards and individual device shielding.
5. Integrate the shielding into the electronics chassis.
6. Use multiple-material layered shielding.

The shield masses in Table D.2.9-10 have been incorporated into the spacecraft MEL.

Table D.2.9-10. Calculated shield masses (CBE values) to reduce the mission TID to 50 krad.

Item	Shield Mass (kg)
Carrier element	60.0
Lander element	47.3
Europa Lander Mission Total	127.3

D.2.9.2 Sample Contamination

The Lander mission success is based on the understanding of composition of Europa's surface and subsurface, which requires an ability to differentiate the native Europan composition from terrestrial contamination carried by the Lander. There are two main sources of contamination for the samples acquired by the ESS:

1. Hydrazine combustion byproducts mixing with the sampling site during landing
2. Spacecraft contamination in the sampling chain

In this section, both of these sources are addressed, along with the Lander approach for mitigating the resulting contamination.

D.2.9.2.1 *Hydrazine Contamination*

During the final approach to the landing site, the Lander will be firing its hydrazine mono-propellant thrusters toward the surface to ensure controlled descent and touchdown. Use of these thrusters will result in impingement of some of the exhaust products onto the Europan surface, creating cratering and contaminating the landing site. The un-decomposed hydrazine and potential impurities in the fuel will alter the composition of the landing site. Even if the fuel used in the thrusters is a high purity fuel (99% by weight), it still contains impurities such as water (<1%), ammonia (<0.3%), aniline (<0.003%) and trace organics (<0.005) (Plemmons et al. 2008). Furthermore, the thruster plumes are mainly composed of ammonia, water and molecular nitrogen, with some imidogen, amino radical, and oxygen present (Plemmons et al. 2008). All of these compounds will contaminate the surface and would be detected in the Lander sample by the MS and RS, since they would be present at high enough abundances and within the MS mass range and the RS spectral range. To combat detection of this contamination, the approach is to drill below the surface, and acquire multiple samples (one at 0.5–2 cm below the surface, and one at 5-10 cm below the surface). The samples at different depths enable the differentiation between the possible thruster-contamination and radiation-altered surface; pristine composition of the subsurface-based testing in Phases A and B can be used to demonstrate the extent of the hydrazine contamination below a test surface and whether it impacts the sample from 5–10 cm depth.

D.2.9.2.2 *Contamination in the Sampling Chain*

Critical to the mission success, the MS and the RS impose very stringent requirements on contamination of the pristine Europan sample by organics (<1 ppb), and inorganics (<1 ppm). Although many steps will be employed to minimize the contamination during spacecraft assembly, test, and launch activities, the spacecraft will inevitably bring some organic and inorganic contaminants to Europa. The plan is to leverage the lessons learned from Phoenix and MSL, and bring an organic-free blank that would sample any spacecraft contamination during the cruise, descent, and landing. Figure D.2.9-3 shows an example of such a blank used by the Phoenix mission as
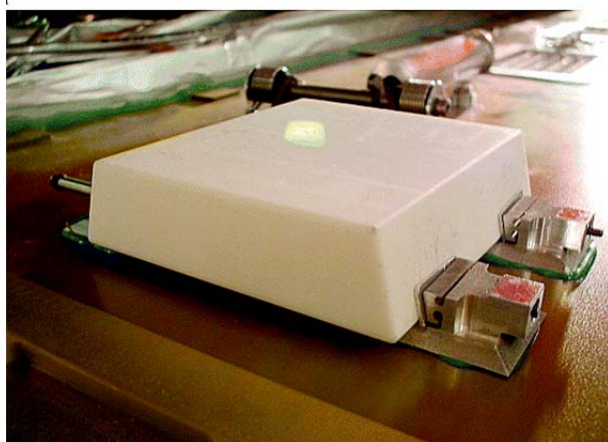
Figure D.2.9-3. Organics-free blank used for the Phoenix mission (Ming et al. 2008). A similar approach for calibrating out spacecraft contamination will be utilized for the Europa Lander Mission.

part of their sampling system and processing by the TEGA instrument (Ming et al. 2008). The exact composition of the blank would be defined in Phase A, however, there are a few requirements that the blank should meet. The ESS drill should be able to penetrate the blank and provide a 1-cm^3 sample to the MS oven within a 10-minute drilling time. The blank if uncontaminated should not release more than 1 ppb of organics (limit of detection for MS) during heating from ambient 150 to 1100 K. The blank lifetime will exceed the 8-year (cruise) and 9-Eurosol Lander lifetime. The ESS drill will acquire a sample from the blank, and deposit it into an extra oven carried by the MS for this purpose. The sample from the blank will then go through the same processing that is done for the Europan surface and subsurface samples: it will be imaged by the MI and analyzed by RS, before the EGA and pyrolysis for MS and GC. This process can be performed as part of the sampling system checkout, and it will not only test the sampling process at the surface of Europa, but also quantify the spacecraft contamination of the sampling system. Subsequently, the contamination can be calibrated out of the Europan surface sample spectra. Moreover, both MS and RS can also carry separate blanks for

their own processing to quantify the contamination within their instrument.

The two-pronged approach to mitigating the spacecraft contamination ensures that even if the Europan samples are not contamination free, the impact of the contamination on mission science will be quantified and minimized.

D.2.9.3   Planetary Protection

NASA Planetary Protection policy (NPR 8020.12C [NASA 2005]) specifies requirements for limiting forward contamination in accordance with Article IX of the 1967 Outer Space Treaty. Because Europa is a body of extreme interest to the astrobiological community as a possible location for the emergence of extra-terrestrial life, contamination of Europa with Earth derived biology must be carefully avoided.

The mission's plan for responding to planetary protection requirements is to perform DHMR on as much of the spacecraft as possible, as late in the integration flow as possible. DHMR involves raising the bulk temperature of the spacecraft above the survival threshold for microbes and their spores. For materials contamination reasons, this bake out is typically done in vacuum or inert gas (nitrogen). To the extent possible, all spacecraft components will be designed to accommodate late-integration DHMR without disassembly or recalibration. However, components or instrumentation unable to comply with DHMR requirements may be removed and cleaned through other means.

The extent to which DHMR and subsequent recontamination must reduce the spacecraft bioburden before liftoff is greatly influenced by the expected impact of postlaunch microbial reduction processes and contamination probabilities. These include

1. Probability of organism survival during interplanetary cruise
2. Probability of organism survival in the Jovian radiation environment
3. Probability of impacting Europa

4. Probability of organism survival on the surface of Europa before subsurface transfer

5. The duration required for transport to the Europan subsurface

6. Organism survival and proliferation after subsurface transfer

Each of these factors will be carefully examined to determine the ultimate allowable bioburden at launch and the required effectiveness of DHMR to maintain compliance with NASA regulation and international treaty.

D.2.9.4   Nuclear Safety

Missions to the outer solar system generally require the use of nuclear energy sources for electrical power and heating. The radioactive material used for this purpose is potentially hazardous to humans and the environment unless precautions are taken for its safe deployment. The following circumstances are of concern:

- Handling: People would be in the vicinity while nuclear sources (ASRGs or RHUs) are being constructed, transported, and installed on the spacecraft.
- Launch: In the event of a catastrophic LV failure, the spacecraft with its nuclear components would be potentially subject to explosion, fire, impact, or the heat and forces of immediate reentry.
- Injection: If injection into interplanetary flight is not achieved, the spacecraft may be left in an Earth orbit that could decay to reentry after some time, thus exposing nuclear components to reentry conditions.
- Earth Flyby: If unplanned trajectory errors cause the spacecraft to reenter Earth's atmosphere, nuclear components would be exposed to reentry conditions.

Safety from nuclear hazards in each of these circumstances is essential.

The National Environmental Policy Act of 1969 (NEPA) specifies measures intended to mitigate these concerns. Project compliance with NEPA is mandatory and is described in more detail below.

D.2.9.4.1   NEPA Compliance, Earth Flyby, Sufficiently High Orbit

Environmental review requirements are satisfied by the completion of a mission-specific Environmental Impact Statement (EIS) for the Europa Lander Mission. In accordance with the requirements of NPR 7120.5D and NPR 7120.5E and NPR 8580.1 (pending) (NASA 2007, 2012), the Record of Decision (ROD) for this EIS would be finalized prior to or concurrent with project PDR.

The Europa Lander Mission Launch Approval Engineering Plan (LAEP) would be completed no later than the Mission Definition Review (MDR). This plan describes the approach for satisfying NASA's NEPA requirements for the mission, and the approach for complying with the nuclear safety launch approval process described in Presidential Directive/National Security Council Memorandum #25 (PD/NSC-25) (1977) and satisfying the nuclear safety requirements of NPR 8715.3 (NASA 2010b). The LAEP provides a description of responsibilities, data sources, schedule, and an overall summary plan for preparing the following:

- A mission-specific environmental review document and supporting nuclear safety risk-assessment efforts
- LV and spacecraft/mission design data requirements to support nuclear risk assessment and safety analyses in compliance with the requirements of NPR 8715.3 (NASA 2010b) and the PD/NSC-25 nuclear safety launch approval process
- Support of launch site radiological contingency planning efforts
- Earth swing-by analysis

- Risk communication activities and products pertaining to the NEPA process, nuclear safety, and planetary protection aspects of the project.

It is anticipated that NASA HQ will initiate the Europa Lander Mission environmental review document development as soon as a clear definition of the baseline plan and option space has been formulated. The Department of Energy (DOE) provides a nuclear risk assessment to support the environmental review document, based upon a representative set of environments and accident scenarios compiled by the KSC Launch Services Program working with JPL. This deliverable might be modeled after the approach used for the MSL EIS.

DOE provides a Nuclear Safety Analysis Report (SAR) based upon NASA-provided mission-specific launch system and spacecraft data to support the PD/NSC-25 compliance effort. The SAR is delivered to an ad hoc Interagency Nuclear Safety Review Panel (INSRP) organized for the Europa Lander Mission. This INSRP reviews the SAR's methodology and conclusions and prepares a Safety Evaluation Report (SER). Both the SER and the SAR are then provided by NASA to the Environmental Protection Agency, Department of Defense, and DOE for agency review. Following agency review of the documents and resolution of any outstanding issues, NASA, as the sponsoring agency, would submit a request for launch approval to the Director of the Office of Science and Technology Policy (OSTP). The OSTP Director reviews the request for nuclear safety launch approval and can either approves the launch or defer the decision to the President.

As part of broader nuclear safety considerations, the Europa Lander Mission would adopt ATLO, spacecraft, trajectory (e.g., for sufficiently high orbit at launch, and for Earth flybys), and operations requirements that satisfy the nuclear safety requirements of NPR 8715.3 (NASA 2010b).

Development of coordinated launch site radiological contingency response plans for NASA launches is the responsibility of the launch site Radiation Protection Officer at KSC. Comprehensive radiological contingency response plans, compliant with the National Response Framework and appropriate annexes, is developed and put in place prior to launch as required by NPR 8715.2 and NPR 8715.3 (NASA 2009a, 2010b). The Europa Lander Mission supports the development of plans for on-orbit contingency actions to complement these ground-based response plans.

A project-specific Risk Communication Plan would be completed no later than the MDR. The Risk Communication Plan details the rationale, proactive strategy, process, and products of communicating risk-related aspects of the project, including nuclear safety and planetary protection. The communication strategy and process would comply with the approach and requirements outlined in the Office of Space Science Risk Communication Plan for Deep Space Missions (JPL D-16993, 1999).

D.3   Programmatics

D.3.1   Management Approach

The Europa Lander Mission concept employs JPL's integrated project controls to manage and control cost, schedule, and risk.

The management approach draws upon extensive experience from Galileo and Cassini. It follows NPR 7120.5E (NASA 2012) and incorporates NASA lessons learned. Recent JPL flight projects that have used this integrated project controls approach include Juno, GRAIL, MSL, and Phoenix.

The project approach includes a work breakdown structure (WBS), technical management processes conducted by veteran systems engineers, and integrated schedule/cost/risk planning and management. The project will take advantage of existing infrastructure for planning, acquisition, compliance with the National Environmental Policy Act (NEPA), compli-

ance with export control regulations (including International Traffic in Arms Regulations), independent technical authority (as called for in NPR 7120.5E), mission assurance, ISO 9001 compliance, and earned value management (EVM).

The Europa Lander Mission employs JPL's integrated project controls solutions to manage and control costs. Skilled business and project control professionals are deployed to projects, utilizing state of the art tools and executing processes that support the project cost, schedule, and risk management requirements. Key attributes of the project controls solution are as follows:

- The Business Manager, project focal point on all business management issues, and the project control staff lead project planners and managers in application of the most effective and efficient implementation of project control processes.
- Mature and successfully demonstrated cost and schedule tools are employed.
- Cost and schedule data are tied directly to work scope.
- "Early warning" metrics are provided monthly to key decision makers. Metrics include 1) cost and schedule variances based on the cost value of work performed and 2) critical-path and slack analysis derived from fully integrated end-to-end network schedules. Each end-item deliverable is scheduled with slack to a fixed receivable. Erosion of this slack value is tracked weekly and reported monthly.
- An integrated business management approach is applied to all system and instrument providers. This approach includes relative performance measurement data integrated into the total project database for a comprehensive understanding of project cost and schedule dynamics.

- Risk management processes are integrated with the liens management process for full knowledge of project reserve status. Early risk identification is maintained as a potential threat to project reserves. Reserve utilization decisions are made with the knowledge of risks and risk mitigation, project performance issues, and increases in scope.

Requirements for project controls evolve throughout the project life cycle. Pre–Phase A and Phase A will require less support than phases B, C, and D. During Phase B, the project controls capability is established at full strength to establish all the appropriate databases and gate products required for a successful Confirmation Review. During phases C and D, the project controls will be fully functioning with recurring performance measurement analysis and cost and schedule tracking reports. During phases E and F, the project controls function reduces to minimal levels.

D.3.2   Work Breakdown Structure (WBS)

The Europa Lander Mission work breakdown structure is designed to enable effective cost, schedule, and management integration.

The WBS is derived from JPL's Standard Flight Project WBS Version 5 and is fully compliant with NPR 7120.5E. This WBS is a product-oriented hierarchical division of the hardware, software, services, and data required to produce end products. It is structured according to modular design of the spacecraft, and reflects the way the work would be implemented, and the way in which project costs, schedule, technical and risk data are to be accumulated, summarized, and reported. The top-level WBS is shown Figures D.3.2-1 and D.3.2-2.
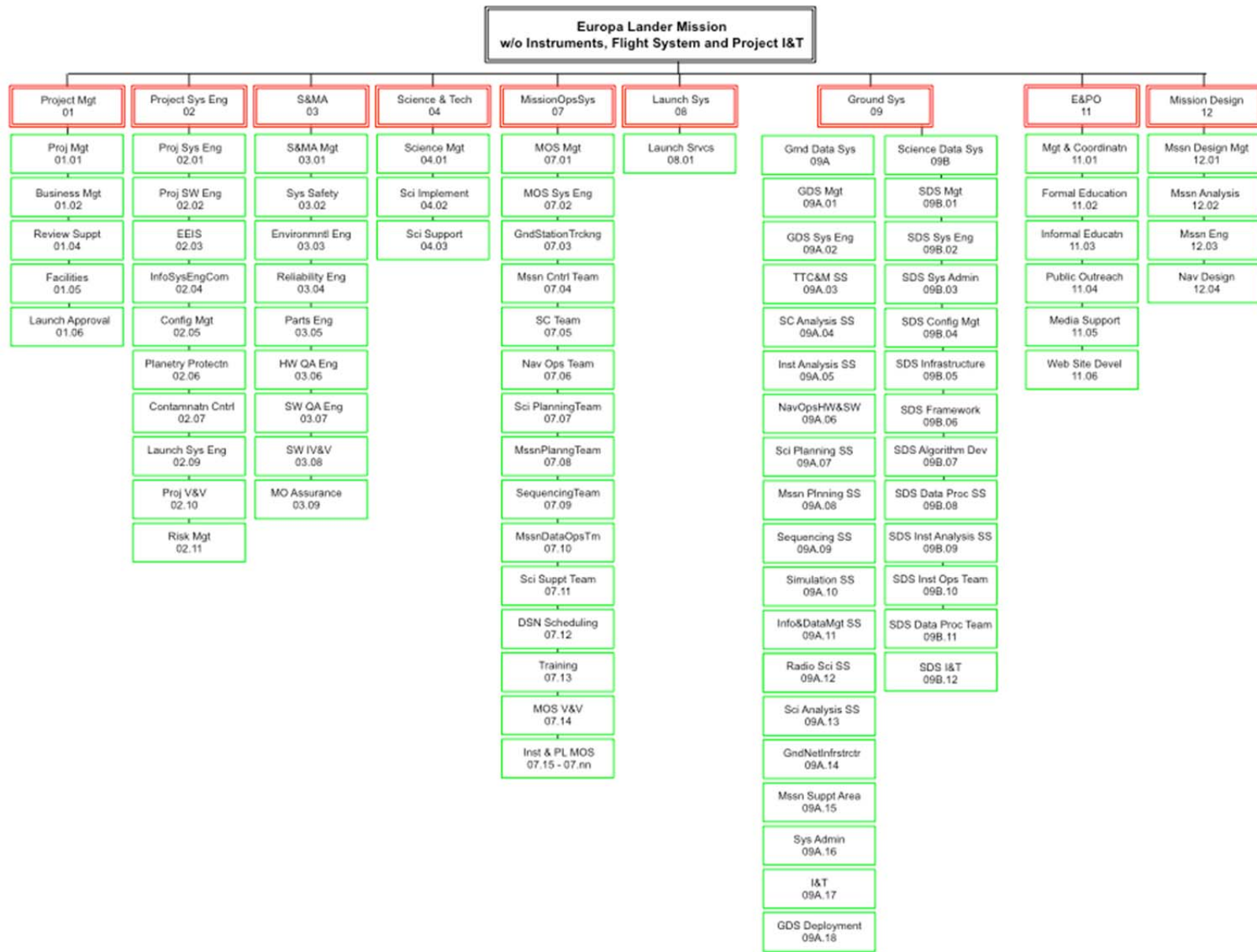
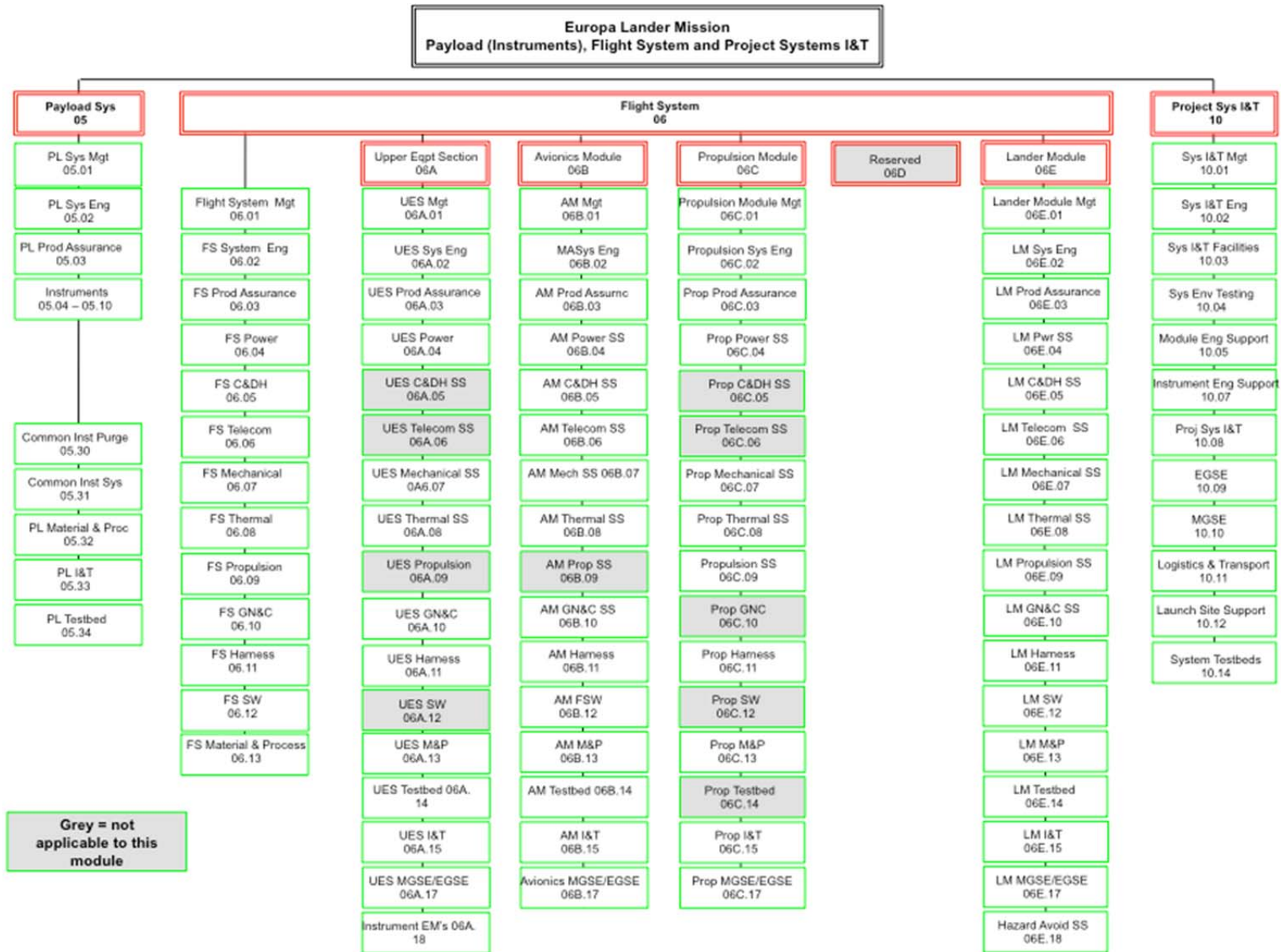**Figure D.3.2-1.** Lander Mission work breakdown structure (without 5, 6, and 10). [This is the 4/12/12 version.]

Figure D.3.2-2. Europa Lander Mission work breakdown structure: Payload, flight systems, I&T. This supports the modular design approach.

D.3.3   Schedule

The Europa Lander Mission schedule leverages the modular design to minimize dependencies; it also includes conservative schedule margin to mitigate risk.

A top-level schedule with implementation flow is shown in Figure D.3.3-1. The phase durations draw on experience from previous outer planets missions and are conservative. During Pre–Phase A, a bottom-up, WBS-based integrated schedule will be generated.

D.3.3.1   Pre–Phase A

Up to and including this report, many alternative concept studies have been conducted. Those studies form the basis of an assessment of alternatives that have resulted in the current mission concept and its readiness to complete Pre-Phase A. To complete Pre-Phase A, a pre-project team would be formed to refine the baseline mission concept and implementation plan in alignment with programmatic goals and objectives. This refinement, along with interactions with NASA and other potential stakeholders, would result in further definition of the mission concept and draft project-level requirements.

The Pre–Phase A activities include completion of NPR 7120.5D specified Pre-Phase A Gate Products, preparation of a Project Information Package (PIP) in support of NASA's development of an AO for instrument acquisition, and a Mission Concept Review leading to Key Decision Point (KDP) A. In addition to those activities required for transition to Phase A, the team will identify additional planning, advanced development and risk reduction tasks that, if funded, would provide a prudent and cost effective approach to early reduction of cost and schedule risk and which have the potential to reduce the estimated cost of Phase A. Primary activities would include reducing the radiation and planetary protection risks associated with instrument and spacecraft development.

There has been a great deal of work done on missions to Europa that this mission builds upon. The Prometheus/JIMO Program and the Jupiter Europa Orbiter provided comprehensive exploration of the mission option space and led to development of technologies for coping with the radiation environment. The immediate progenitors of this mission, which uses Venus and Earth gravity assist maneuvers and chemical propulsion, are the Europa Geophysical Explorer Concept Study in 2005, the Europa Explorer in 2006 and 2007 and the Jupiter Europa Orbiter in 2008. For this mission the ability to get the instruments selected and through design updates for radiation and planetary protection is the pacing item.

D.3.3.2   Phases A through F

The Phase A–F schedule reflects the total project scope of work as discrete and measurable tasks and milestones that are time phased through the use of task durations, interdependencies, and date constraints. To insure low risk, the schedule includes slack for all tasks.

The Project Manager will control the project schedule, with support from a Project Schedule Analyst. An Integrated Master Schedule will identify key milestones, major reviews, and receivables/deliverables (Rec/Dels). Schedule reserves for the November 2021 launch opportunity meet or exceed JPL DPs requirements (schedule reserves of 1 month per year for Phases A through D, with schedule reserves of 1 week per month for activities at the launch site). The project utilizes an integrated cost/schedule system in Phase B, in order to fully implement an EVM baseline in Phases C/D/E. Inputs will be supplied to NASA's CADRe support contractor for reporting at major reviews. Schedule and cost estimates at completion (EAC) will be prepared at regular intervals as part of the EVM process. Major project review milestones (not all shown) are consistent with NPR 7120.5E.
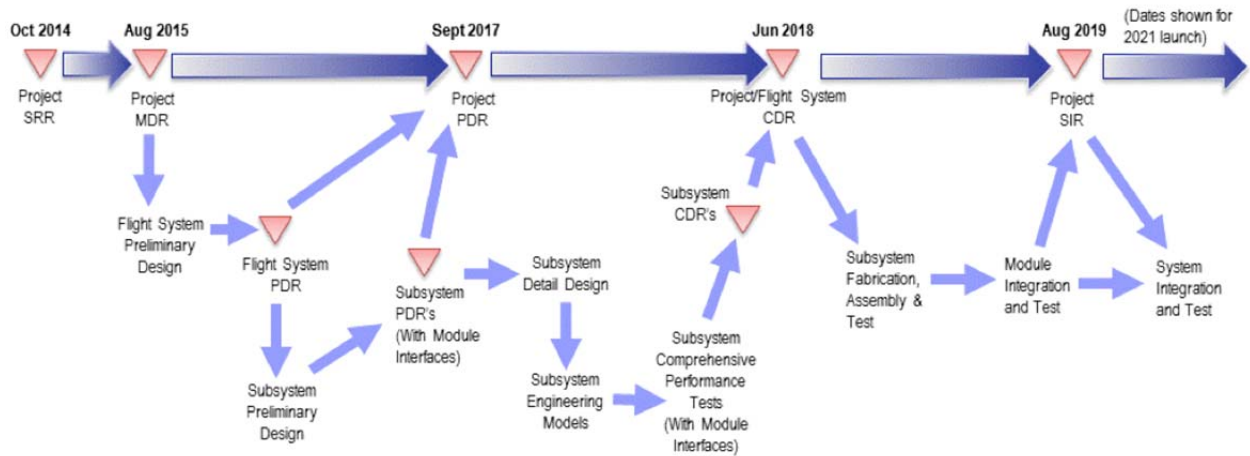
Figure D.3.3-1. Project implementation flow supports flow-down of requirements early.

D.3.3.3   Phases A–B

The length of Phases A and B (24 months for A, 26 months for B) is primarily driven by the schedule to select the instruments in response to the AO and advance the selected instruments to PDR level of maturity. In Phase A the primary tasks are completing the Gate Products required and facilitating the selection of the science instruments. The six-month period between instrument selection and the system requirements review/mission design review allows instrument designers to work directly with the project personnel on issues related to accommodation, requirements, radiation and planetary protection.

A milestone for a Planetary Protection decision has been inserted in Phase B. A basic approach to meeting the planetary protection requirements has been outlined and agreed to by the Planetary Protection Officer at NASA Headquarters. This milestone is anticipated to be a review of the more detailed implementation approach including any major outstanding issues related to mission design, spacecraft design or operations concepts. This review may ultimately be combined with the Project PDR if it is more effective to do so.

D.3.3.4   Phases C–D

The length of Phases C and D (27 months for C, 22 months for D) is primarily driven by the schedule to bring the spacecraft to launch readiness. Phase C is longer than typical due to the added time required to implement the radiation and planetary protection requirement mitigation aspects of the design. Phase D was developed using the Cassini model of ATLO and includes 1.5 months to perform the system-level DHMR.

A trailblazer activity is scheduled to occur at the launch facility in Phase D to ensure that the spacecraft design is compatible with the launch vehicle and facility limitations at the launch site for transporting and loading of the ASRGs. This activity starts at a very low level in Phase B and continues with increasing

activity until the approach to ASRG installation is validated in Phase D. In addition the trailblazer activity will dry run the system-level DHMR.

D.3.3.5   Phases E–F

Phase E (9.5 years) is driven by the interplanetary trajectory and science requirements at Europa. Phase F (6 months) is structured to carry out the EOM scenario and to complete data analysis and archiving.

D.3.4   Risk & Mitigation Plan

The Europa Lander Mission is unique and challenging; we understand the risks and have developed mitigation plans to address them.

The primary challenges of a mission to Europa's surface are Jupiter's radiation environment, planetary protection, high propulsive needs to get into Europa orbit, and the large distance from the Sun and Earth. Driving technical risks are

1   ASRG development
2   Radiation
3   Deorbit, decent, and landing (DDL)
4   Sample-handing system
5   Instrument development
6   Planetary protection
7   Internal charging

D.3.4.1   ASRG

NASA is developing the ASRG as the long-term solution for reducing the plutonium requirements for future planetary missions. Any problems with the development and validation of the ASRG could have a serious impact on the Europa Lander Mission, since it is baselining a radioisotope power system. ASRG development and qualification risks could have high consequences and are outside the control of the Europa project. The ASRGs are a new development and the likelihood of problems is not known; however, successful development of new radioisotope thermoelectric generators can be difficult. Risks to the mission associated with this development can be mitigated by achieving well-defined and

stable ASRG characteristics early in Phase A to allow the system designers to adequately incorporate it into the spacecraft system. If the characteristics are not known early in Phase A, late design changes and impacts on mass, power, cost, and schedule are likely. The Europa Study Team's close work with NASA to clearly delineate the mission requirements helps to mitigate ASRG risk. Mitigation of these risks also requires that the project work closely with the Program Executive at NASA Headquarters for the ASRG Development Program to ensure that the technology is flight-qualified no later than Phase B. A robust ground-test program is essential to mitigating the ASRG risks. The NASA ASRG development efforts are currently underway (see Section D.2.4.6).

D.3.4.2   Radiation

The radiation environment to which the Europa mission hardware will be exposed by EOM is significant. Radiation effects expected in the Europa mission are TID effects and SEE in electronic components, displacement damage (DD) effects in components and materials, and surface and internal charging. The primary risk considered here is the likelihood that component failure could have a serious impact on spacecraft functionality if the radiation problem is not addressed appropriately. Sensors for instruments used for pointing and navigation and in science instruments are particularly sensitive to radiation effects. Test techniques used to verify component suitability might over-predict component hardness due to inadequate accounting for radiation rate or source type effects that are negligible at lower doses. Also, unanticipated failure mechanisms might be present or might become important at high doses or at high DD levels that are not of concern for missions conducted at nominal total dose exposures. The measures taken here both reduce the likelihood and the consequences of such impacts, with designs for this radiation environment robust beyond the level normally accomplished for space flight design.

The Europa mission design uses an approach similar to that taken by Juno and utilizes a vault to shield the electronic components to a mission dose of 150 krad, thereby reducing the likelihood of radiation-related problems and parts availability. There has been significant effort exerted by experts to mitigate this risk over the past decade. In 2007, the Europa study team convened several review teams to assess the particular risks in each area. The results of that review were presented in Appendix C of the 2007 EE Study Report (Clark et al. 2007). As a result of those reviews, a Risk Mitigation Plan: Radiation and Planetary Protection [JPL D-47928] outlined in the Clark et al. 2007 report was further developed and executed to make strategic investments related to reducing the likelihood of component failure and degradation, and reducing the related radiation risk even further. Results of this work were reported in the 2008 JEO final report. An expanded systems engineering approach focuses on graceful degradation and will reduce the consequences of any component failures in electronic parts.

D.3.4.3   Deorbit, Decent, and Landing

Refer to Section D.2.8.2.1 for details on the DDL approach. If the coverage at the four sites does not yield a safe landing area, then other sites could be explored for potential landing. This data could be taken also during the first 30 days in orbit. A protracted site-certification process could impact the Lander lifetime on the surface, as radiation dose will accumulate over time.

If the Lander is deployed to a landing site that exceeds design specifications (maximum 47° effective landing surface angle) then the Lander may fail to execute science measurements or communicate results resulting in a failure to achieve mission objectives. A tiered risk-mitigation approach has been designed for the Lander. As discussed above, a predeployment of the Lander orbital reconnaissance at 50 cm/pixel will be performed and the project will execute a ground-site certification process

using the reconnaissance imagery. Then the Lander will be released and will perform a high precision deorbit maneuver, utilize a high altitude Terrain Relative Navigation (TRN) with 3-km divert capability (the reconnaissance imagery map is loaded in the TRN), followed by low altitude hazard avoidance with 50-m divert capability (using a LIDAR system), resulting in altimetry guided soft landing at 0.5 m/s. The pallet landing system has high stability along with crushable energy attenuation. Designing a landing system is challenging because little information exists about the surface on the scale of the Lander. The surface could range from hard crystalline surfaces to unconsolidated crunchy/fluffy surface layers atop hard surfaces. The implementation chosen for DDL attempts to overcome the Europa uncertainties with an extremely flexible and robust solution.

D.3.4.4   Sample Handling

The ESS (see Section D.2.5.11 for a description) is required to interact with the natural environment of Europa's surface, generating and extracting the "sample" from its native site using a rotary-percussive coring drill. It also includes mechanisms that deploy the sampling device from its stowed position on the Lander, move and orient the sampling device to the surface for sample acquisition; and after sampling, return the sampling device to the Lander instrument suite. Lastly, there is mechanization for the removal and transfer of the "sample" from the sampling device to the instrument suite. The sampling handing systems must be fully capable of working within the environmental specifications of the landed terrain; with obstacles up to 1.5 m in vertical dimension (concave or convex relative to a flat plane), on slopes up to 25° from horizontal, in the Jovian radiation environment, and in both Earth's and Europa's gravity fields. The sample handing system must be capable of sampling on terrain that has a compressive strength (UCS) ranging from 0.1–70 MPa,

porosity between 0 and 40%, and an ambient temperature range of 70–145 K.

The baseline plan is to use a rotary-percussive coring tool as the sampling device and a five-DOF robotic manipulator similar to the MER IDD, for sample device articulation and preloading, plus sample delivery. No technology development is required for the robotic manipulator; system-level and component-level technologies are all at TRL 7 to 9 due to development for previous flight projects. No technology development is required for the sample device mechanisms (brushless motor driven actuators similar to the robotic manipulator). Under the auspices of the Mars Program (JPL R&TD, NASA SBIRs, Mars Technology Program) low-force coring drills have been developed to function in soft and hard rock for sample acquisition, and that technology is currently within the range of TRL 4 to 5. Technology development is required for some sampling device components and system integration: inner and outer core bits, rotary and percussive performance, core break-off and retention, coring thermal characterization, and sample expulsion.

The sample handling system is critical to the success of the Lander Mission. If the Sample Handling System fails to provide a sample to the instrument suite, baseline science objectives will not be met. In order to mitigate this risk, items that require technology development will be funded early in the mission development to raise the TRL of the devices to TRL 7. Several full scale sample handling systems will be constructed during Phase B, environmentally tested, and tested extensively to verify operation over the range of conditions expected on the surface of Europa and with samples covering the range of expected surface properties. A second flight sample handling system will be built and used on the ground to validate the flight sequences just in advance of the sampling operations on Europa's surface.

D.3.4.5   Instrument Development

As is indicated by past experience, the instrument development and delivery will undoubtedly be on the critical path. The model planning payload selected for the Europa Lander study consists of a notional set of instruments including MS, MAG, MBS, SIS, RS, and MI. The RS is the least mature instrument in the payload suite and will require significant upfront time for development. The mass spectrometer could be constructed from elements of existing flight instrument, but will be a challenging development. The seismometer package is working in a frequency outside of current flight instruments, which will require some development. The rest of the payload are instruments based upon existing flight instruments.

An approved parts and materials list, including planetary protection and radiation characteristics, is planned in support of the instrument AO. In addition, design guidelines will be incorporated into the AO. This approach will allow maturation of the instrument concepts prior to final selection. The instruments in the planning payload are all based on mature technologies and if applied in a mission in the inner solar system would represent very low risk. For Europa, however, radiation can have a detrimental impact on instrument performance, although operation on the surface of Europa is in a more benign radiation environment. If these problems cannot be solved or, more importantly, if the solutions cannot be conveyed to instrument developers in a timely fashion, there is a risk that the science objectives of the mission will not be met. The project will assign instrument interface engineers to work with each instrument provider to ensure that the spacecraft accommodates the specific instrument needs. In addition, the instruments will be selected as early as possible in Phase A, and early funding will be made available to reduce development risks.

To reduce the likelihood that the instruments do not achieve their desired specifications or run into resource and schedule problems due to radiation issues, the typical interface engineering support will be augmented for each instrument with personnel experienced in the area of radiation design. Design guidelines will be generated for the instrument teams to describe radiation constraints and to provide recommendations for design issues and parts and material selection. Development of a knowledge base among potential instrument providers has already begun. Four instrument workshops were held to engage the instrument provider community in a dialogue on the Europa mission needs and potential driving requirements. Information regarding radiation and planetary protection requirements was disseminated. The Europa development schedule provides significant time and reserves for the instrument developer and the Project to work through and understand the actual design implications for radiation and planetary protection after selection. The project schedule allows ample time for the instruments to be developed and delivered to ATLO. In addition, the spacecraft module approach and a straightforward instrument interface allow instrument to be integrated last in the ATLO integration process.

D.3.4.6   Planetary Protection

The planetary protection requirements for a mission to Europa are significant and can be mission design, schedule, and cost driver. The mission will put a Lander on the Europan surface; therefore, the mission will be classified as Category III under current COSPAR and NASA policy (COSPAR 2002). To prevent Europa contamination, if prelaunch cleanliness levels prove difficult to meet, cost and schedule reserves might be required to address contamination problems late in the process. This risk is cross cutting and is mitigated by a review added in Phase B to confirm the approach and assess implementation. This risk is also mitigated by the previous Europa study activities. The approach to planetary protection compliance for the Europa mission concept, at

this time, is 1) prelaunch DHMR to control bioburden for those areas not affected by radiation in flight and 2) in-flight microbial reduction via radiation prior to EOI. The prelaunch microbial reduction method will be to perform full-system DHMR as one of the last steps in the ATLO process at KSC. A chamber has been identified at KSC that is capable of performing the system DHMR. A pathfinder activity is planned as a dress rehearsal to resolve any procedural challenges. The Europa Approved Parts and Materials List (APML) will evaluate the compliance of materials with the DHMR process. Hardware wherein there is conflict between radiation and DHMR compatibility for individual components might require that the instrument is actually "distributed"; that is, electronics and sensors physically separated on the spacecraft. If one sensor choice is much more robust than another in this context, the distribution solution might influence the choice of sensor technology for some instruments.

D.3.4.7 Internal Charging

The high levels of charged particles near Europa are a source of internal charging (see Section D.2.9.1) within spacecraft materials. The result of this charging is often an electrostatic discharge within the spacecraft that causes material damage and an electromagnetic pulse damaging to electronics. If not mitigated properly, discharges resulting from internal charging might result in mission degradation or failure. To mitigate this risk, proper choice of materials, the use of charge dissipating designs, and the robustness of electronic designs to internal discharge effects will greatly affect the frequency and consequence of internal discharges. Mitigations for this risk include the use of rigorous design guidelines for Electrostatic Discharge and grounding. For example, specifications on the maximum length of ungrounded wire length, specifications on the use of necessary bleed resistors and bleed-path analysis, and specifications regarding the restriction on the use of floating

(e.g., ungrounded) metal area. In addition, IC risk mitigation will include utilization of design experience from Galileo and Cassini, early testing of materials and processes to define acceptable use for a Europa mission, providing mission design guidelines in Pre–Phase A prior to release of the AO, and conducting design workshops to train designers on the environment and charging issues.

D.3.5 Cost

The Europa Lander Mission cost is estimated at $2.8B with a 70% confidence factor; this includes conservative margins of 40% on Phases A–D and 20% on Phases E–F.

D.3.5.1 Cost Summary

The Total Mission Cost for the Europa Lander Mission concept is estimated at $2.6B to $2.8B FY15, excluding the launch vehicle, which is costed separately. The mission baseline includes a Carrier element and a soft Lander carrying six instruments—Magnetometer (MAG), Multiband Seismometer Package (MBS), Mass Spectrometer (MS), Site Imaging System (SIS), Raman Spectrometer (RS), and Microscopic Imager (MI). The integrated spacecraft will spend 30 days in orbit performing reconnaissance imaging for potential landing sites, followed by science operations on the Europan surface. The Europa Lander Mission enables researchers to investigate Europa's potential habitability by sampling and analyzing surface materials *in situ*, and to advance Europa science through *in situ* geophysical and geological observations.

Table D.3.5-1 summarizes the Europa Lander Mission cost estimate at WBS level 2.

Table D.3.5-1. Europa Lander Mission cost summary by WBS (FY15$M).

WBS Element	PRICE-H	SEER
01 Project Management	79	74
02 Project System Engineering	70	65
03 Safety & Mission Assurance	76	71
04 Science	88	88
05 Payload System	97	97
06 Spacecraft System	894	792
ASRG	200	200

WBS Element	PRICE-H	SEER
Technology Development	195	195
07 Mission Operations System	237	237
08 Launch System	-	-
09 Ground Data System	55	55
10 Project System I&T	78	66
11 Education and Public Outreach	19	18
12 Mission Design	32	29
Subtotal (FY15$M)	**2,120**	**1,987**
Reserves	701	647
Total (FY15$M)	**2,821**	**2,634**

The Total Mission Cost is broken down into $2.3B to $2.4B FY15 for the Phase-A through -D development period and $0.4B for operations during Phases E and F. The Europa Lander Mission holds 37% in cost reserves, broken down into 40% for Phases A, B, C, and D, and 20% for Phases E and F.

The estimated cost is based on the implementation approach described in Section D.2, which includes the following key features in the baseline plan:

- Redundant flight system with selected cross-strapping
- Technology development of a precision landing system
- Experienced providers of key systems and subsystems

D.3.5.2   Cost Estimating Methodology

To estimate the cost for the Europa Lander Mission concept, JPL used its institutional cost estimation process applicable for the design maturity of a concept study in early formulation. This process focuses on using parametric cost models, analogies, and other nongrassroots estimating techniques, which provide the following advantages:

- Provide rapid turnaround of extensive trade studies
- Enable design-to-cost to narrow the trade space and define a baseline concept
- Establish reasonable upper and lower bounds around a point estimate

The cost estimation process begins once the technical design is closed, with the Europa

Study Team developing a Technical Data Package (TDP) that describes the science requirements, technical design, mission architecture, and project schedule. Next, all work is organized, defined, and estimated according to the NASA standard WBS. The Europa Study Team then tailors the WBS as needed for cost estimation and planning.

The institutional business organization uses the TDP and WBS to develop the cost estimate by applying estimating methods and techniques appropriate for each WBS element, based on the maturity of design and manufacturing requirements, availability of relevant historical information, and degree of similarity to prior missions. For the Europa Lander Mission, the tools and methods used include the following:

- Calibration of commercial, off-the-shelf (COTS) tools PRICE-H and SEER to Juno and Phoenix, the most relevant JPL planetary missions
- Use of the NASA Instrument Cost Model (NICM) for the notional payload, tailored for the Europa environment
- Use of the NASA Space Operations & Cost Model (SOCM) for Phases E and F
- Wrap factors based on analogous historical planetary missions for Project Management, Project Systems Engineering, Safety and Mission Assurance, and Mission Design

The Europa Study Team's estimate is a compilation of these multiple techniques. The Europa Study Team then vets the integrated cost rollup and detailed basis of estimate (BOE), and reviews the results for consistency and reasonableness with the mission design, WBS, and NASA requirements to ensure that technical and schedule characteristics are accurately captured and a consistent cost-risk posture is assumed.

To validate the resulting proposed cost, the Europa Study Team used Team X to cost independently the baseline concept with the JPL Institutional Cost Models (ICMs): 33 integrated, WBS Level-2 through -4 models built by JPL doing organizations to emulate their grassroots approach. The Europa Study Team also contracted with the Aerospace Corporation to perform an Independent Cost Estimate (ICE) and Cost and Technical Evaluation (CATE.) The Team X and Aerospace results are discussed in Section D.3.5.8.

The Europa Study Team then used an S-curve cost risk analysis to validate and bound the cost reserves. The reserves substantiation is discussed in Section D.3.5.9.

D.3.5.3   Basis of Estimate

The Europa Lander Mission cost estimate is based on the science and mission implementation approach described in Section D.2. In addition, the Master Equipment List (MEL) provided the key inputs for mass, quantities, and the quantification of electronics versus structures that are needed to run the parametric tools. The cost estimating methodologies and assumptions used to develop the Europa Lander Mission cost estimate are summarized in Table D.3.5-2.

D.3.5.4   Instrument Cost Estimates

The NICM system model with an augmentation to account for radiation and planetary protection was used to estimate instrument costs. Each notional instrument was characterized for performance establishing instrument type, aggregate power estimates, and subsystem-level mass. Table D.3.5-3 shows the input parameters used for each instrument for the NICM system model.

D.3.5.4.1   NICM Adjustments

NICM outputs at the 70th percentile were reported in FY15$. This reference cost estimate was then augmented for radiation and planetary protection. The NICM model does not have parameters or characteristics suffi-cient to model planetary protection requirements or radiation environments. A flat fee for planetary protection was added to each instrument, based on instrument complexity. An estimate for the number of electronic boards and detectors was made for each instrument, and an additional fee of $2M was assessed per detector for radiation redesign costs. The instrument radiation shielding masses were estimated separately in PRICE-H and SEER, and are included in WBS 06 spacecraft costs under Payload Radiation Shielding. Table D.3.5-4 summarizes the instrument cost-estimation process.

D.3.5.4.2   NICM Estimate

Table D.3.5-5 provides the final NICM system cost estimate, including all adjustments for radiation and planetary protection.

Table D.3.5-2. Cost estimation methodology.

WBS Element	Methodology
01 Project Management	Historical wrap factor based on analogous historical planetary missions. Estimate was augmented by $15M to account for Nuclear Launch Safety Approval (NLSA) and National Environmental Policy Act (NEPA) costs associated with usage of the advanced Stirling radioisotope generators (ASRGs).
02 Project Sys Engineering	Historical wrap factor based on analogous historical planetary missions.
03 Safety & Msn Assurance	Historical wrap factor based on analogous historical planetary missions.
04 Science	Expert-based estimate from the science team based on mission class, schedule, and the number and complexity of instruments. Cost estimate captures the level of effort for a Project Scientist, two Deputy Project Scientists, the Science Team, and participating scientists, with additional workforce requirements for Phases C and D, based on the size of the team, the number of meetings with the team, and the products required from this group. For Phases E and F, the cost estimate also assumes a science team for each instrument, with the estimated level of effort based on existing instrument teams supporting the current mission, and on the number of months in hibernation, cruise, and science operations.
05 Payload System	Historical wrap factor for Payload Management, Systems Engineering, and Product Assurance based on analogous historical planetary missions. Instrument costs developed using the NASA Instrument Cost Model (NICM), Version 5.0. The 70%-confidence-level estimate was selected as a conservative point estimate for each notional instrument. Instrument costs are then augmented for radiation shielding, detector radiation redesign, and planetary protection for any DHMR material properties issues. For payload radiation shielding, the cost was estimated separately using PRICE-H and SEER, and the cost is included under WBS 06 Spacecraft System. For planetary protection a flat fee was then added to each instrument based on instrument complexity. For radiation redesign, an additional fee of $2M was assessed per detector.
06 Spacecraft System	Historical wrap factor for Flight System Management, Systems Engineering, and Product Assurance based on analogous historical planetary missions. Combined wrap factor applied to spacecraft hardware and software for Carrier and Lander element Module Management, Systems Engineering, and Product Assurance. Carrier element hardware costs estimated using PRICE-H and SEER calibrated to Juno at the subsystem level. Reconnaissance imager estimate included under Carrier Guidance, Navigation, and Control (GN&C) Subsystem. Juno selected as an analogous mission for the calibration due to the operation of a comparable flight system in a comparable radiation environment. Lander element hardware costs estimated using PRICE-H and SEER calibrated to Phoenix at the subsystem level. Europa Sampling System (ESS) estimate included under Lander Mechanical Subsystem. Phoenix selected as an analogous mission for the calibration due to size, design complexity, required functionality, instrumentation, planetary protection requirements, and design lifetime. Software costs estimated using a wrap factor of 10% on the hardware cost. Additional $220M included for technology development of Raman Spectrometer, Multiband Seismometer Package, Precision Landing System, and ESS. ASRG cost provided by NASA Headquarters in the Europa Study Statement of Work, dated October 4, 2011 (NASA 2011). Estimate includes four ASRGs at $50M each (FY15$). Technology development for the ASRG is separately funded by NASA.
07 Mission Ops System	Team X estimate based on historical data for a Class A mission for Phases A–D; SOCM estimate for Phases E–F.
08 Launch System	Launch Vehicle costs, including nuclear processing costs, are not included and will be provided by NASA Headquarters as directed in the Europa Study Statement of Work (NASA 2011).
09 Ground Data System	Team X estimate based on historical data for a Class A mission for Phases A–D; SOCM estimate for Phases E–F.
10 Project Systems I&T	PRICE-H and SEER estimate calibrated to Juno and Phoenix.
11 Education & Public Outreach	1.0% wrap factor on the total mission cost excluding the launch system (WBS 08), ASRG, and DSN tracking costs. Based on the percentage prescribed in the recent AOs for Discovery 2010 and New Frontiers 2009 (NASA 2010, 2009).
12 Mission Design	Historical wrap factor based on analogous historical planetary missions.
Reserves	40% for Phases A–D and 20% for Phases E–F on the total mission cost excluding the launch system (WBS 08), ASRG, and DSN tracking costs.

Table D.3.5-3. NICM system model inputs for baseline.

Instrument Name	Magnetometer (MAG)	Multiband Seismometer Pkg (MBS)	Mass Spectrometer (MS)	Site Imaging System (SIS)	Raman Spectrometer (RS)	Microscopic Imager (MI)
Remote Sensing or In situ?	In situ	In situ	In situ	In situ	In situ	In situ
Remote Sensing Instrument Type	Fields	Passive Wave	Particles	Optical	Optical	Optical
Mission Destination	Planetary	Planetary	Planetary	Planetary	Planetary	Planetary
Total Mass (kg)	2.4	4.3	14.3	2	5.9	2.4
Max Power (W)	4	4.6	50	4	30	10
Number of Samples	N/A	N/A	4	N/A	4	4
Max Data Rate (kbps)	1.8	72	3.1	2,520	1.6	1,260
Number of Detectors	0	0	0	2	0	1

Table D.3.5-4. Instrument cost-estimation process.

Master Instrument Costing Matrix.	Instrument Cost (Excluding Radiation Shielding) (A)	Detector Radiation Design Costs (B)	Planetary Protection Fee (C)	TOTAL INSTRUMENT COST	Radiation Shielding Cost —Included in WBS 06
Instrument X	NICM 70th-percentile estimate	$2M per detector	Based on complexity	A+B+C	Estimated in PRICE-H/SEER

Table D.3.5-5. Instrument cost-estimation details (FY15$M).

Instrument	Acronym	NICM 70% Cost	Detector Radiation Design Costs	Planetary Protection Fee	TOTAL INSTRUMENT COST
Magnetometer	MAG	5.8	0.0	0.1	5.9
Multiband Seismometer Package	MBS	10.0	0.0	0.1	10.1
Mass Spectrometer	MS	28.2	0.0	0.3	28.5
Site Imaging System	SIS	6.5	4.0	0.3	10.8
Raman Spectrometer	RS	17.7	0.0	1.2	19.0
Microscopic Imager	MI	8.3	2.0	0.4	10.7
TOTAL (FY15$M)		76.5	6.0	2.4	84.9

D.3.5.5   Spacecraft Hardware Costs

The Europa Lander Mission spacecraft hardware costs were estimated using PRICE-H and SEER, calibrated to Juno for the Carrier element and Phoenix for the Lander element. The Carrier element is most closely analogous to the Juno spacecraft. Configuration, avionics subsystems, radiation environment, mission complexity, and design lifetime match closely to the corresponding aspects of the Juno mission.

The Lander element is most analogous to the Phoenix mission in terms of size, design complexity, required functionality, instrumenta-

tion, planetary protection requirements, and design lifetime. However, the Europa Lander is deployed to a vacuum environment and does not need the additional complexity associated with Martian atmospheric entry, parachute deployment, and landing uncertainty due to wind perturbations. In that regard, Phoenix should represent a conservative analogy with embedded cost for complexities entirely irrelevant to the Europa Lander.

D.3.5.5.1.1   PRICE-H and SEER Cost Estimates

The Spacecraft System costs generated from PRICE-H and SEER are shown in Ta-

ob **Table D.3.5-6.** PRICE-H and SEER cost estimates for the Europa Lander Mission.

Spacecraft System	PRICE-H (FY15$M)	SEER (FY15$M)
06A Carrier Element		
06A.04 Spacecraft Power SS	54	91
06A.05 Spacecraft C&DH SS	38	20
06A.06 Spacecraft Telecom SS	69	54
06A.07 Spacecraft Mechanical SS	33	22
06A.07a Spacecraft Radiation Shielding	9	6
06A.07b Payload Radiation Shielding	0	0
06A.08 Spacecraft Thermal SS	7	7
06A.09 Spacecraft Propulsion SS	64	47
06A.10 Spacecraft GN&C SS	85	68
06A.11 Spacecraft Harness SS	6	6
06A.12 Spacecraft Flight SW	36	32
06B Lander Element		
06B.04 Spacecraft Power SS	40	37
06B.05 Spacecraft C&DH SS	10	8
06B.06 Spacecraft Telecom SS	12	19
06B.07 Spacecraft Mechanical SS	95	91
06B.07a Spacecraft Radiation Shielding	6	4
06B.07b Payload Radiation Shielding	3	2
06B.08 Spacecraft Thermal SS	10	10
06B.09 Spacecraft Propulsion SS	33	28
06B.10 Spacecraft GN&C SS	35	20
06B.11 Spacecraft Harness SS	15	14
06B.12 Spacecraft Flight SW	26	23
06C RPS	**200**	**200**
10 I&T	**78**	**66**

ble D.3.5-6. The Spacecraft System comprises the Carrier element and the Lander element in WBS 06. The Payload Radiation Shielding is captured as part of the Lander System and the costs are bookkept under WBS 06B.07. The radioisotope power system (RPS) was estimated at a cost of $50M per ASRG unit as directed by NASA HQ, and included in WBS 06, separate from the Carrier element and Lander element costs. The I&T costs are kept in WBS 10. Spacecraft flight software was estimated as a 10% wrap factor based on hardware cost, which is a high-level rule of thumb derived from JPL's historical software cost data.

D.3.5.6 Technology Development

A single Lander mission to Europa, with no precursor, along with the science objectives set forth by the Europa Science Definition Team, requires some technology development costs to bring items employed in the mission to adequate maturity levels prior to PDR. These additional costs are listed in Table D.3.5-7.

Table D.3.5-7. Technology development costs for Europa Lander Mission.

Item	Description of Technology Development	Cost (FY15$M)
Raman Spectrometer	No Raman Spectrometer has been flown in space. Radiation testing campaign and technology development to meet radiation and planetary protection requirements of the Europa Lander Mission required.	50
Multiband Seismometer Package	MEMS seismometers have not been qualified or flown in a space environment. Technology development is required to adapt MBS to the Europa environment. Radiation testing campaign and technology development to meet radiation and planetary protection requirements of the Europa Lander Mission required.	20
Precision Landing System	Development of terrain-relative navigation/hazard avoidance system. Currently have over 10 years of development under Mars Program and Human Program, but will need additional development and tailoring to Europa radiation environment and planetary protection requirements.	100
Europa Sampling System	Leverage sampling technology from MER, Phoenix, and MSL. Technology development is required for some components of the sampling device for the anticipated Europa surface environment and surface properties. The sample device components requiring technology development include inner and outer core bits, rotary and percussive performance, core break-off and retention, coring thermal characterization, and sample expulsion.	25
TOTAL TECHNOLOGY DEVELOPMENT COSTS (FY15$M)		**195**

D.3.5.7 Phase E and F Cost Estimates

The NASA SOCM was used to estimate operations costs in Phases E and F. The Europa Study science team provided an expert-based estimate for WBS 04 (Science) based on schedule and the number and complexity of instruments. The Europa Lander Mission Phase E and F cost estimate is shown in Table D.3.5-8.

Table D.3.5-8. Phase E and F cost estimate for the Europa Lander Mission.

Phase E & F Costs by WBS	FY15$M
01 Project Management	13
02 Project Systems Engineering	13
03 Safety & Mission Assurance	13
04 Science	63
05 Payload	0
06 Spacecraft	0
07 Mission Operations	177
08 Launch System	0
09 Ground Data Systems	19
10 Project System Integration & Test	0
11 Education & Public Outreach	3
SUBTOTAL	**301**
DSN Tracking	18
20% Reserves (excluding DSN)	60
TOTAL	**380**

D.3.5.8 Estimate Reasonableness (Validation)

A JPL Team X cost session was used to assess the reasonableness of the parametrically derived PRICE-H and SEER-based Flight System (WBS 06) and Project Systems I&T (WBS 10) estimates and associated wraps. In addition, Aerospace Corporation independently ran an ICE and CATE. The results of the Team X cost session and Aerospace Corporation analysis are presented in Table D.3.5-9 along with the PRICE-H and SEER-based project estimates for comparison. The Aerospace CATE report is provided in Section D.4.4.

D.3.5.9 Cost-Risk Assessment and Reserve Strategy

The Europa Study Team conservatively applied project-level reserves of 40% for Phases A–D and 20% for Phases E and F on all elements except for Launch Services, ASRGs, and DSN tracking. These reserve levels are more conservative than the reserve guidelines set forward in JPL's FPPs (JPL 2010b).

The Europa Lander Mission cost-risk and -uncertainty assessment is a natural extension of the cost modeling discussed in Sections D.3.5.1–6, and is consistent with standard practice at NASA and JPL. This assessment considers the wide band of uncertainty that typically accompanies missions at early phases of development, as well as the technical risk and uncertainties of the Europa Lander Mission as understood at this time and as experienced on prior competed and directed missions (e.g., Juno, MRO, MSL).

The primary technique used for this assessment is an S-curve. This provides a statistically-based distribution of total project cost around the project's point estimate based on the cost models used in this analysis and the historical JPL data to which they are calibrated. Equivalently, this technique provides a probabilistic estimate of total project cost based on variability and uncertainties in the model-based estimates

An S-curve analysis was performed on the Europa Lander Mission cost estimate, and demonstrated a 70th-percentile cost estimate of $2.8B FY15 (Figure D.3.5-1). Comparing the Europa Study Team estimate (including cost reserves) to the S-curve indicates that the Europa Study Team estimate of $2.6B to $2.8B is at approximately the 70th percentile. Based on this analysis, the Europa Study Team reserves position of 37% overall (Phases A–F) is sufficient to meet the 70th percentile.

Table D.3.5-9. Comparison of Europa Study Team estimates with Team X and Aerospace Corporation estimates.

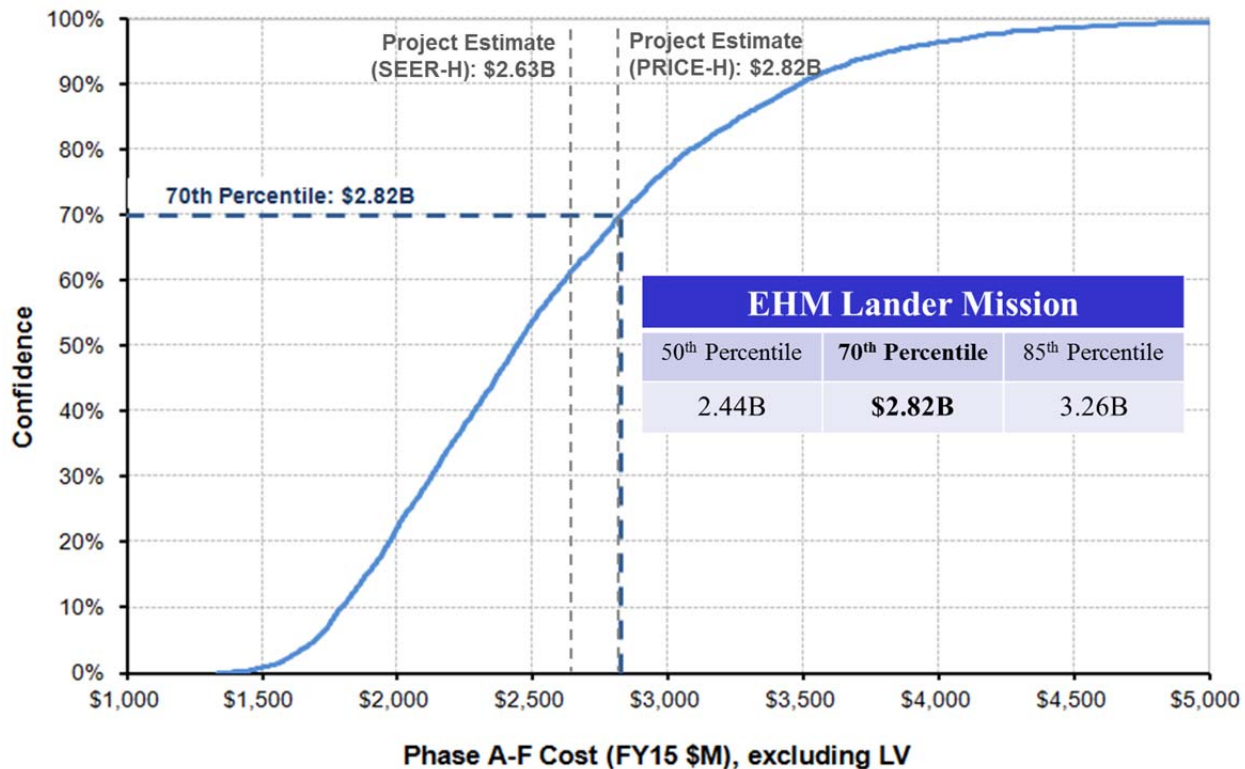| WBS Element	PRICE-H	SEER	Team X	Aerospace ICE	Aerospace CATE
Total (FY15$B)	2.8	2.6	2.1	2.8	3.0

Figure D.3.5-1. Europa Lander Mission cost estimate S-curve analysis.

D.4   Appendices

D.4.1   References

Acuña, M. H., Connerney, J. E. P., Ness, N. F., Lin, R. P., Mitchell, D., Carlson, C. W., McFadden, J., Anderson, K. A., Rème, H., Mazelle, C., Vignes, D., Wasilewsk, P., Cloutier, P. (1999). Global Distribution of Crustal Magnetization Discovered by the Mars Global Surveyor MAG/ER Experiment. Science 30, 790-793.

Agostinelli, S., et al., 2003. Geant4 Collaboration, Geant4-a simulation toolkit. Nucl. Instrum. Methods A 506, 250–303.

Alexander, C., Carlson, R., Consolmagno, G., Greeley, R., and Morrison, D. (2009), The exploration history of Europa. In *Europa* (R.T. Pappalardo, W.B. McKinnon, and K.K. Khurana, eds.), pp. 3–26. Univ. of Arizona Press, Tucson.

Alley, R.B., Blankenship, D.D., Bentley, C.R., Rooney, S.T., 1986. Deformation of till beneath Ice Stream B, West Antarctica, Nature 322, 57-59.

Allison, J., et al., 2006. Geant4 developments and applications. Nuclear Science, IEEE Transactions, 53, 270-278.

Alvarellos, J. K. Zahnle, A. Dobrovolskis, and P. Hamill, Transfer of mass from Io to Europa and beyond due to cometary impacts, Icarus 194, 636–646, 2008.

Anandakrishnan, S., Alley, R.B., 1997. Tidal forcing of basal seismicity of Ice Stream C, West Antarctica seen far inland. J. Geophys. Res. 102, 15183-15196.

Anderson, D.L., Miller, W.F., Latham, G.V., Nakamura, Y., Toksöz, M.N., Dainty, A.M., Duennebier, F.K., Lazarewicz, A.R., Kovach, R.L., Knight, T.C.D., 1977. Seismology on Mars. J. Geophys. Res. 82, 4524–4546, doi:10.1029/JS082i028p04524.

Bassis, J.N., Coleman, R., Fricker, H.A., Minster, J.B., 2005. Episodic propagation of a rift on the Amery Ice Shelf, East Antarctica, Geophys. Res. Lett. 32, L06502.

Bell, J.F. III, Squyres, S.W., Herkenhoff, K.E., Maki, J.N., Arneson, H.M., Brown, D., Collins, S.A., Dingizian, A., Elliot, S.T., Hagerott, E.C., Hayes, A.G., Johnson, M.J., Johnson, J.R., Joseph, J., Kinch, K., Lemmon, M.T., Morris, R.V., Scherr, L., Schwochert, M., Shepard, M.K, Smith, G.H., Sohl-Dickstein, J.N., Sullivan, R.J., Sullivan, W.T., Wadsworth, M., 2003. Mars Exploration Rover Athena Panoramic Camera (Pancam) investigation. JGR 108, E12, 8063.

Belton, M.J.S., Head, J.W. III, Ingersoll, A.P., Greeley, R., McEwen, A.S., Klaasen, K.P., Senske, D., Pappalardo, R., Collins, G., Vasavada, A.R., Sullivan, R., Simonelli, D., Geissler, P., Carr, M.H., Davies, M.E., Veverka, J., Gierasch, P.J., Banfield, D., Bell, M., Chapman, C.R., Anger, C., Greenberg, R., Neukum, G., Pilcher, C.B., Beebe, R.F., Burns, J.A., Fanale, F., Ip, W., Johnson, T.V., Morrison, D., Moore, J., Orton, G.S., Thomas, P., West, R.A., 1996. Galileo's first images of Jupiter and the Galilean Satellites. Science 274, 377–385

Bentley, C.R., 1964. The structure of Antarctica and its ice cover. In Odishaw, H., ed. Research in Geophysics. Vol. 2. *Solid Earth and Interface* Phenomena. Cambridge, Mass., Massachusetts Institute of Technology Press, 335-389.

Bierhaus, E.B., Zahnle, K., Chapman, C.R., 2009. Europa's crater distributions and surface ages. In: Pappalardo, R.T., McKinnon, W.B., Khurana, K.K. (Eds.), Europa, U. Arizona Press, Tucson, 161–180.

Bish, D.L., Blake, D., Sarrazin, P., Treiman, A., Hoehler, T., Hausrath, E., Midtkandal, I., Steele, A.,., Field XRD/XRF mineral analysis by the MSL Chemin instrument, Lunar and Planetary Science Conf. 37, Houston TX, Abstract #1163., 2007.

Blankenship, D.D., 1989. Seismological Investigations of a West Antarctic Ice Stream. PhD Thesis. The University of Wisconsin. Table 3.1.

Blankenship, D.D., Anandakrishnan, S., Kempf, J.L., Bentley, C.R., 1987. Microearthquakes under and alongside Ice Stream B, Antarctica, detected by a new passive seismic array. Annals Glac. 9, 30–34.

Blankenship, D.D., Bentley, C.R., Rooney, S.T., Alley, R.B., 1986. Seismic measurements reveal a saturated, porous layer beneath an active Antarctic ice stream. Nature 322, 54–57.

Boldt, J., et al., 2008. Assessment of radiation effects on detectors and key optical components. JPL D-48256.

Brajanovski, M., Müller, T.M., Gurevich, B., 2006. Characteristic frequencies of seismic attenuation due to wave-induced fluid flow in fractured porous media, Geophys. J. Int. 166, 574-578.

Brown, P., Hildebrand, A., Zolensky, M., Grady, M., Clayton, R., Mayeda, T., Tagliaferri, E., Spalding, R., MacRae, N., Hoffman, E., D. W. Mittlefehldt, J. F. Wacker, J. Bird, M. Campbell, R. Carpenter, H. Gingerich, M. Glatiotis, E. Greiner, M. Mazur, P. McCausland, H. Plotkin, and T. Mazur., 2000. The fall, recovery, orbit, and composition of the Tagish Lake meteorite: A new type of carbonaceous chondrite, Science 290, 320–325.

Brown, R. H., K. H. Baines, G. Bellucci, J. P. Bibring, B. J. Buratti, F. Capaccioni, P. Cerroni, R. N. Clark, A. Coradini, D. P. Cruikshank, P. Drossart, V. Formisano, R. Jaumann, Y. Langevin, D. L. Matson, T. B. Mccord, V. Mennella, E. Miller, R. M. Nelson, P. D. Nicholson, B. Sicardy, and C. Sotin, The Cassini Visual And Infrared Mapping Spectrometer (VIMS) investigation, Space Sci. Rev., 115, 111–168, 2004.

Brunetto, R., G. Baratta, M. Domingo, and G. Strazzulla. (2005), Reflectance and transmittance spectra (2.2–2.4 μm) of ion irradiated frozen methanol, *Icarus* 175, 226– 232.

Calvel, P., Catherine Barillot, Alain Porte, Gérard Auriel, Christian Chatry, Pierre-François Peyrard, Giovanni Santin, Robert Ecoffet, Thomas M. Jordan, 2008. Review of Deposited Dose Calculation Methods Using Ray Tracing Approximations, IEEE Transactions on Nuclear Science, 55, 3106–3113.

Cammarano, F., Lekic, V., Manga, M., Panning, M., Romanowicz, B., 2006. Long-period seismology on Europa: 1. Physically consistent interior models, J. Geophys. Res. 111, E12009.

Campagnola, S., Boutonnet, A., Schoenmaekers, J., Grebow, D.J., Petropoulos, A.E., Russell, R.P., 2012. Tisserand-leveraging transfers. AAS Paper No. 12-185, AIS/AIAA Spaceflight Mechanics Meeting, Charleston, SC January 29–February 2.

Carlson, R.W., 1999. A Tenuous carbon dioxide atmosphere on Jupiter's moon Callisto. Science 283, 820–821.

Carlson, R.W., 2001. Spatial distribution of carbon dioxide, hydrogen peroxide, and sulfuric acid on Europa. Bull. Amer. Astron. Soc. 33, 1125.

Carlson, R.W., Calvin, W.M., Dalton, J.B., Hansen, G.B., Hudson, R.L., Johnson, R.E., McCord, T.B., Moore, M.H., 2009. Europa's Surface Composition. In: Pappalardo, R.T., McKinnon, W.B., Khurana, K.K. (Eds.), Europa, U. Arizona Press, Tucson, 283–327.

Carlson, R.W., Anderson, M.S., Johnson, R.E., Smythe, W.D., Hendrix, A.R., Barth, C.A., Soderblom, L.A., Hansen, G.B., McCord, T.B., Dalton, J.B., Clark, R.N., Shirley, J.H., Ocampo, A.C., Matson, D.L., 1999a. Hydrogen peroxide on the surface of Europa. Science 283, 2062–2064.

Carlson, R.W., Johnson, R.E., Anderson, M.S., 1999b. Sulfuric acid on Europa and the radiolytic sulfur cycle. Science 286, 97–99.

Carlson, R.W., M. Anderson, R. Johnson, M. Schulman, and A. Yavrouian, 2002. Sulfuric acid production on Europa: The radiolysis of sulfur in water ice. Icarus 157, 456–463.

Carlson, R.W., ., M. Anderson, R. Mehlman, and R. Johnson., 2005. Distribution of hydrated sulfuric acid on Europa. Icarus 177, 461–471.

Carr, M.H., Belton, M.J.S., Chapman, C.R., Davies, M.E.., Geissler, R., Greenberg, R., McEwen, A.S., Tufts, B.R., Greeley, R., Sullivan, R., Head, J.W., Pappalardo, R.T., Klaasen, K.P., Johnson, T.V., Kaufman, J., Senske, D., Moore, J., Neukum, G., Schubert, G., Burns, J.A., Thomas, P., Veverka, J., 1998. Evidence for a subsurface ocean on Europa. Nature 391, 363–365.

Cassen, P., Reynolds, R.T., Peale, S.J., 1979. Is there liquid water on Europa? Geophys. Res. Lett. 6, 731–734.

Cassen, P.M., Peale, S.J., Reynolds, R.T., 1982. Structure and thermal evolution of the Galilean satellites., in D. Morrison (ed.), Satellites of Jupiter, University of Arizona Press, Tucson, pp. 93–128.

Chaban, G.M., Huo, W.M., Lee, T.J., 2002. Theoretical study of infrared and Raman spectra of hydrated magnesium sulfate salts. J. Chem. Phys. 117, 2532.

Chio, C.H., Sharma, S.K., Muenow, D.W., 2007. The hydrates and deuterates of ferrous sulfate ($FeSO_4$): A Raman spectroscopic study. J. Raman Spectrosc. 38, 87–99

Chyba, C. F., 2000. Energy for microbial life on Europa. Nature 403, 381–382.

Clark, B.E., Helfenstein, P., Veverka, J., Ockert-Bell, M., Sullivan, R.J., Geissler, P.E., Phillips, C.B., McEwen, A.S., Greeley, R., Neukum, G., Denk, T., Klaasen, K., 1998. Multispectral terrain analysis of Europa from Galileo images. Icarus 135, 95–106.

Clark, K., 2008. EJSM Europa Orbiter Mission Design and Architecture (presentation slides). Outer Planets Flagship Mission Instrument Workshop, June 3, 2008.

Clark, K., et al., 2007. Europa Explorer Mission Study: Final Report, JPL D-41283.

Clark, K., et al., 2008. Jupiter Europa Orbiter Mission Study 2008 Final Report, JPL D-48279.

Clark, K., et. al., 2009. Europa Jupiter System Mission Joint Summary Report, January 16, 2009.

Collins, G., Nimmo, F., 2009. Chaotic terrain on Europa. In: Pappalardo, R.T., McKinnon, W.B., Khurana, K.K. (Eds.), Europa, U. Arizona Press, Tucson, 259–282.

Collins, G.C., Head III, J.W., Pappalardo, R.T., Spaun, N.A., 2000. Evaluation of models for the formation of chaotic terrain on Europa. J. Geophys. Res. 105, 1709–1716.

Committee on the Limits of Organic Life in Planetary Systems, 2007. The Limits of Organic Life in Planetary Systems. Washington, D.C., National Academies Press, 116 pp.

Cooper, J.F., R.E. Johnson, B.H. Mauk, H.B. Garrett, N. Gehrels, (2001). Energetic ion and electron irradiation of the icy Galilean satellites, Icarus 149, pp. 133-159.

Coy, S. K. Killeen, J. Han, G. Eiceman, and I. Kanik, A microfluidics-hplc/differential mobility spectrometer macromolecular detection system for human and robotic missions, Lunar Planet. Sci. Conf.42, The Woodlands, Texas, Abstract # 1423.

Dalton, J. B. (2000), Constraints on the surface composition of Jupiter's moon Europa based on laboratory and spacecraft data, Ph.D. dissertation, University of Colorado, Boulder.

Dalton, J. B. (2007), Linear mixture modeling of Europa's non-ice material using cryogenic laboratory spectroscopy, Geophys. Res. Lett. 34, L21205.

Dalton, J. B., et al. (2005), Spectral comparison of heavily hydrated salts to disrupted terrains on Europa, Icarus 177, 472–490.

Delitsky, M. L. and A. L. Lane (1997), Chemical schemes for surface modification of icy satellites: A road map, J. Geophys. Res. 102, 16385–16390.

Delitsky, M. L., and A. L. Lane (1998), Ice chemistry on the Galilean Satellites, J. Geophys. Res. 103(E13):31,391–31,403.

Des Marais D.J., Nuth, J.A. 3rd, Allamandola L.J., Boss A.P., Farmer J.D., Hoehler T.M., Jakosky B.M., Meadows V.S., Pohorille A., Runnegar B., Spormann A.M. (2008). The NASA Astrobiology roadmap. Astrobiology 8, 715–730.

Doggett, T., Greeley, R., Figueredo, P., Tanaka, K., Weiser, S., 2009. Geologic stratigraphy and evolution of Europa's surface. In: Pappalardo, R.T., McKinnon, W.B., Khurana, K.K. (Eds.), Europa, U. Arizona Press, Tucson, 137–160.

Dyal, P., Parkin, C. W. and Sonett, C. P. (1970). Apollo 12 Magnetometer: Measurement of a steady magnetic field on the surface of the Moon. Science 21, 762-764.

Esposito, L., C. Barth, J. Colwell, G. Lawrence, W. McClintock, A. Stewart, H. Keller, A. Korth, H. Lauche, M. Festou, et al., The Cassini Ultraviolet Imaging Spectrograph Investigation, Space Sci. Rev. 115, 299–361, 2004.

Fagents, Sarah A. (2003) Considerations for effusive cryovolcanism on Europa: The post-Galileo perspective. J. Geophys. Res.108, 13-1.

Fagents, Sarah A.; Greeley, Ronald; Sullivan, Robert J.; Pappalardo, Robert T.; Prockter, Louise M.; The Galileo SSI Team, (2000). Cryomagmatic mechanisms for the formation of Rhadamanthys Linea, triple band margins, and other low-albedo features on Europa. Icarus, 144, 54-88.

Fall, A, Tattitch, B , Bodnar, RJ (2011). Combined microthermometric and Raman spectroscopic technique to determine the salinity of H_2O-CO_2-NaCl fluid inclusions based on clathrate melting. Geochem. Cosmochim. Acta 75, 951-964.

Figueredo, P.H., et al., 2002. Geology and origin of Europa's "Mitten" feature (Murias Chaos). J. Geophys. Res. 107, 5026.

Figueredo, P.H., Greely, R., 2004. Resurfacing history of Europa from pole-to-pole geological mapping. Icarus 167, 287–312.

Figueredo, P.H., Greeley, R., Neuer, S., Irwin, L., Schulze-Makuch, D., 2003. Locating potential biosignatures on Europa from surface geology observations. Astrobiology 3, 851–861.

Gaidos, E., and Nimmo, F. (2000). Tectonics and water on Europa. Nature 405, 637.

Geissler, P.E., Greenberg, R., Hoppa, G., Helfenstein, P., McEwen, A., Pappalardo, R., Tufts, R., Ockert-Bell, M., Sullivan, R., Greeley, R., Belton, M.J.S., Denk, T., Clark, B., Burns, J., Veverka, J., 1998a. Evidence for non-synchronous rotation of Europa. Nature 391, 368–370.

Geissler, P.E., Greenberg, R., Hoppa, G., McEwen, A., Tufts, R., Phillips, C., Clark, B., Ockert-Bell, M., Helfenstein, P., Burns, J., Veverka, J., Sullivan, R., Greeley, R., Pappalardo, R. T., Head, J. W., Belton, M. J. S., Denk, T., 1998b. Evolution of lineaments on Europa: Clues from Galileo multispectral imaging observations. Icarus 135, 107–126, doi: 10.1006/icar.1998.5980.

Glavin, D.P., et al., 2001. Detecting pyrolysis products from bacteria on Mars, Earth Planet. Sci. Lett. 185, 1–5.

Goesmann, F., Rosenbauer, H., Roll, R., Szopa, C., Raulin, F., Sternberg, R., Israel, G., Meierhenrich, U., Thiemann, W., Munoz-Caro, G., 2006. COSAC: The Cometary Sampling and Composition Experiment on Philae. Space Sci. Rev. 128, 257–280.

Grant, F.S., West, G.F., 1965. Interpretation theory in applied geophysics. New York: McGraw-Hill.

Grebow, D.J., Petropoulos, A.E., Finlayson, P.A., 2011. Multi-body capture to low-altitude circular orbits at Europa. AAS Paper No. 11-427, AAS/AIAA Astrodynamics Specialists Conference, Girdwood, Alaska, July 31–August 4.

Greeley, R., Collins, G.C., Spaun, N.A., Sullivan, R.J., Moore, J.M., Senske, D.A., Tufts, B.R., Johnson, T.V., Belton, M.J.S., Tanaka, K.L., 2000. Geologic mapping of Europa. J. Geophys. Res. 105, 22559–22578.

Greeley, R., Chyba, C.F., Head, J.W. III, McCord, T.B., McKinnon, W.B., Pappalardo, R.T., Figueredo, P., 2004. Geology of Europa. In: Bagenal, F., Dowling, T.E., McKinnon, W.B. (Eds.), Jupiter: The Planet, Satellites, and Magnetosphere, Cambridge U. Press, Cambridge, U.K., 329–362.

Greenberg, R.G., 2010. Transport rates of radiolytic substances into Europa's ocean: Implications for the potential origin and maintenance of life. Astrobiology 10, 275–283.

Greenberg, R., Hoppa, G.V., Tufts, B.R., Geissler, P., Riley, J., Kadel, S., 1999. Chaos on Europa. Icarus 141, 263–286.

Han, L., Showman, A.P., 2010. Coupled convection and tidal dissipation in Europa's ice shell. Icarus 207, 834–844.

Hand, K.P., Chyba, C.F., 2007. Empirical constraints on the salinity of the Europan ocean and implications for a thin ice shell. Icarus 189, 424–438.

Hand, K.P., Carlson, R.W., Chyba, C.F., 2007. Energy, chemical disequilibrium, and geological constraints on Europa. Astrobiology 7, 1–18.

Hand, K.P., Chyba, C.F., Priscu, J.C., Carlson, R.W., Nealson, K.H., 2009. Astrobiology and the potential for life on Europa. In: Pappalardo, R.T., McKinnon, W.B., Khurana, K.K. (Eds.), Europa, U. Arizona Press, Tucson, 589.

Hand, K.P., McKay, C.P., Pilcher, C., 2010. Spectroscopic and spectrometric differentiation between abiotic and biogenic material on icy worlds. Proc. IAU 6, 165–176.

Hansen, G., McCord, T.B., 2003. Amorphous and crystalline ice on the Galilean satellites: A balance between thermal and radiolytic processes. J. Geophys. Res. 109, doi: 10.1029/ 2003JE002149.

Head, J.W., Pappalardo, R.T., 1999. Brine mobilization during lithospheric heating on Europa: Implications for formation of chaos terrain, lenticula texture, and color variations. J. Geophys. Res., Planets 104, 27143–27155.

Head, J.W., Pappalardo, R.T., Sullivan, R., Galileo SSI Team, 1999. Europa: Morphological characteristics of ridges and triple bands from Galileo data (E4 and E6) and assessment of linear diapirism model, J. Geophys. Res. 24,223–24,236.

Hecht et al. (2009), Detection of perchlorate and the soluble chemistry of martian soil at the Phoenix Lander site, *Science* 325, 64–67.

Herkenhoff, K.E., Squyres, S.W., Bell, J.F. III, Maki, J.N., Arneson, H.M., Bertelsen, P., Brown, D.I., Collins, S.A., Dingizian, A., Elliott, S.T., Goetz, W., Hagerott, E.C., Hayes, A.G., Johnson, M.J., Kirk, R.L., McLennan, S., Morris, R.V., Scherr, L.M., Schwochert, M.A., Shiraishi, L.R., Smith, G.H., Soderblom, L.A., Sohl-Dickstein, J.N., Wadsworth, M.V., 2003. Athena Microscopic Imager investigation. J. Geophys. Res. 108, E12, 8065, doi: 10.1029/2003JE002076.

Hoehler, T. M., 2004. Biological energy requirements as quantitative boundary conditions for life in the subsurface. Geobiology 2, 205–215.

Hood, L.L., Coleman, P.J. Jr., Wilhelms, D.E., 1979. The Moon: Sources of the crustal magnetic anomalies. Science 204, 53–57.

Hood, L.L., Young, C.N., Richmond, N.C., Harrison, K.P., 2005. Modeling of major martian magnetic anomalies: Further evidence for polar reorientations during the Noachian. Icarus 177, 144–173.

Hoppa, G.V., Tufts, B.R., Greenberg, R., Geissler, P.E., 1999. Formation of cycloidal features on Europa. Science 285, 1899–1902.

Hudson, R.L., Moore, M.H., 1998. Infrared study of ion-irradiated water-ice mixtures with hydrocarbons relevant to comets. Icarus 136, 518–527.

Hurford, T.A., Sarid, A.R., Greenberg, R., Bills, B.G., 2009. The influence of obliquity on europan cycloid formation. Icarus 202, 197–215.

Iizuka, Y., et al. (2008). A relationship between ion balance and the chemical compounds of salt inclusions found in the Greenland Ice Core Project and Dome Fuji ice cores. J. Geophys. Res., 113, D07303, doi: 10.1029/2007JD009018

Ivanov, M. A., L.M. Prockter, B. Dalton (2011). Landforms of Europa and selection of landing sites, Advances in Space Research, 48, p. 661-677.

Jet Propulsion Laboratory, 2010a. Design, Verification/Validation and Ops Principles for Flight Systems (Design Principles), Rev. 4, JPL Rules! DocID 43913, September 20, 2010.

Jet Propulsion Laboratory, 2010b. Flight Project Practices, Rev. 8, JPL Rules! DocID 58032, October 6, 2010.

Johannesen, J., D'Amario, L., 1999. Europa orbit mission trajectory design. AAS Paper No. 99-360, AAS/AIAA Astrodynamics Specialists Conference, Girdwood, Alaska, August 15–19.

Johnson, M.R. and Smith, A.M., 1997. Seabed topography under the southern and western Ronne Ice Shelf, derived from seismic surveys, Antarctic Science 9, 201-208.

Johnson, R. E., R.W. Carlson, J.F. Cooper, C. Paranicas, M.H. Moore, M.C. Wong, (2004). Radiation effects on the surfaces of the Galilean satellites. In: Bagenal, F., Dowling, T.E., McKinnon, W.B. (Eds.), Jupiter: The Planet, Satellites, and Magnetosphere, Cambridge U. Press, Cambridge, U.K., 485–512.

Johnson, R.E. and T.I. Quickenden (1997), Photolysis and radiolysis of water ice on outer solar system bodies, J. Geophys. Res. 102, 10,985–10996.

Johnson, R.E., Burger, M.H., Cassidy, T.A., Leblanc, F., Marconi, M., Smyth, W.H., 2009. Composition and Detection of Europa's Sputter-induced Atmosphere. In: Pappalardo, R.T., McKinnon, W.B., Khurana, K.K. (Eds.), Europa, Univ. of Arizona Press, Tucson, pp. 507-527.

Kargel, J. S., et al. (2000), Europa's crust and ocean: Origin, composition, and prospects for life, Icarus 148, 226–265.

Kattenhorn, S.A., Hurford, T., 2009. Tectonics of Europa. In: Pappalardo, R.T., McKinnon, W.B., Khurana, K.K. (Eds.), Europa, U. Arizona Press, Tucson, 199–236.

Khurana, K.K., Dougherty, M.K., Russell, C.T., Leisner, J.S., 2007. Mass loading of Saturn's magnetosphere near Enceladus. J. Geophys. Res. 112, CiteID A08203.

Khurana, K.K., Kivelson, M.G., Stevenson, D.J., Schubert, G., Russell, C.T., Walker, R.J., Joy, S., Polanskey, C., 1998. Induced magnetic fields as evidence for subsurface oceans in Europa and Callisto. Nature 395, 777–780, doi: 10.1038/27394.

Kivelson, M.G., Khurana, K.K., Russell, C.T., Volwerk, M., Walker, R.J., Zimmer, C., 2000. Galileo magnetometer measurements: A stronger case for a subsurface ocean at Europa. Science 289, 1340.

Kivelson, M.G., Khurana, K.K., Stevenson, D.J., Bennett, L., Joy, S., Russell, C.T., Walker, R.J., Zimmer, C., Polanskey, C., 1999. Europa and Callisto: Induced or intrinsic fields in a periodically varying plasma environment. J. Geophys. Res. 104, 4609.

Klaasen, K., Clary, M., Janesick, J., 1984. Charge-coupled device television camera for NASA's Galileo mission to Jupiter. Optical Engineering 23, 334–342.

Klien, J.P., 1979. The Viking Mission and the search for life on Mars. Rev. Geophys. 17, 1655–1662.

Kohnen, H., 1974. Temperature dependence of seismic waves in ice. J. Glac. 67, 144-147.

Kovach, R.L., Chyba, C.F., 2001. Seismic detectability of a subsurface ocean on Europa. Icarus 150, 279–287.

Kwok, J. (Study lead) Jupiter System Observer Mission Study Final Report, JPL D-41284, November 1, 2007.

Lambrecht, A., Sandhäger, H., Vaughan, D.G., Mayer, C., 2007. New ice thickness maps of Filchner–Ronne Ice Shelf, Antarctica, with specific focus on grounding lines and marine ice. Antarctic Science 19, 521–532.

Lane, A.L., et al. (1981), Evidence for sulphur implantation in Europa's UV absorption band, Nature 292, 38–39.

Lock, R. EJSM Europa Orbiter Science Scenarios (presentation slides). Outer Planets Flagship Mission Instrument Workshop, June 3, 2008.

Lock, R. Concept of Operations (presentation slides), Jupiter Europa Orbiter Internal Mission Concept Review, June 7-9, 2010.

Lockheed Martin, 2011. ASRG User Interface Control Document. Lockheed Martin Contract No. DE-AC07-00SF22191, Specification #912IC002085, Rev. A, June 2011.

Lodders, K. and B. Fegley (1998), Presolar silicon carbide grains and their parent stars, Meteoritics Planet. Sci. 33, 871–880.

Loeffler, M., R. Hudson, M. Moore, and R. Carlson, Radiolysis of sulfuric acid, sulfuric acid monohydrate, and sulfuric acid tetrahydrate and its relevance to Europa, Icarus 25, 370–380, 2011.

Lorenz, R.D., 2011. Planetary seismology—Expectations for Lander and wind noise with application to Venus. Planet. Space Sci. 62, 86–96.

Lucchitta, B.K., Soderblom, L.A., 1982. The geology of Europa. In: Morrison, D. (Ed.), Satellites of Jupiter. The University of Arizona Press, Tucson, pp. 521–555.

Ludwinski, J. Galileo Mission Planning Office Closeout (Lessons Learned), JPL IOM 311.1/98/01, January 19, 1997.

Magnes, W., Oberst, M., Valacanoglou, A., Hauer, H., Hagen, C., Jerjej, I., Neubauer, H., Baumjohann, W., Pierce, D., Means, J., Falkner, P., 2008. Highly integrated front-end electronics for spaceborne fluxgate sensors. Meas. Sci. Technol. 19, 115801–115814.

Mahaffy, P. Exploration of the habitability of Mars: Development of analytical protocols for measurement of organic carbon on the 2009 Mars Science Laboratory. Space Sci. Rev. 135, 1-4, 2008.

Marion, G. M., C. H. Fritsen, H. Eicken, and M. C. Payne (2003), The search for life on Europa: Limiting environmental factors, potential habitats, and Earth analogies, Astrobiology 3, 785–812.

Marshall, S.T., Kattenhorn, S. A., (2005). A revised model for cycloid growth mechanics on Europa: Evidence from surface morphologies and geometries, Icarus 177, 341–366.

Mauk B. H., Williams D. J., McEntire R. W., Khurana K. K., and Roederer J. G. (1999). Storm-like dynamics of Jupiter's inner and middle magnetosphere. J. Geophys. Res. 104, 22759–22778.

McCarthy, C et al. (2007), Solidification and microstructures of binary ice-I/hydrate eutectic aggregates, Am. Mineralogist 92, 1550–1560.

McCollom T.M. and J.P. Ammend (2005), A thermodynamic assessment of energy requirements for biomass synthesis by chemolithoautotrophic microorganisms in oxic and anoxic environments, Geobiology 3, 135–144.

McCollom, T. M. (1999). Methanogenesis as a potential source of chemical energy for primary biomass production by autotrophic organisms in hydrothermal systems on Europa. J. Geophys. Res. 104, 30729–30742.

McCord, T.B., Carlson, R.W., Smythe, W.D., Hansen, G.B., Clark, R.N., Hibbitts, C.A., Fanale, F.P., Granahan, J.C., Segura, M., Matson, D.L., Johnson, T.V., Martin, P.D., 1997. Organics and other molecules in the surfaces of Callisto and Ganymede. Science 278, 271–275.

McCord, T.B., Hansen, G.B., Fanale, F.P., Carlson, R.W., Matson, D.L., Johnson, T.V., Smythe, W.D., Crowley, J.K., Martin, P.D., Ocampo, A., Hibbitts, C.A., Granahan, J.C., The NIMS Team, 1998a. Salts on Europa's surface detected by Galileo's Near Infrared Mapping Spectrometer. Science 280, 1242–1245.

McCord, T. B., Hansen, G.B., Clark, R.N., Martin, P.D., Hibbitts, C.A., Fanale, F.P., Granahan, J.C., Segura, M., Matson, D.L., Johnson, T.V., Carlson, R.W., Smythe, W.D., Danielson, G.E., The NIMS Team, 1998b. Non-water-ice constituents in the surface material of the icy Galilean satellites from the Galileo Near-Infrared Mapping Spectrometer investigation. J. Geophys. Res. 103, 8603–8626.

McCord, T.B., Matson, D.L., Johnson, T.V., Crowley, J.K., Fanale, F.P., Carlson, R.W., Smythe, W.D., Martin, P.D., Hibbitts, C.A., Granahan, J.C., Ocampo, A., 1999. Hydrated salt minerals on Europa's surface from the Galileo Near-Infrared Mapping Spectrometer (NIMS) investigation. J. Geophys. Res. 104, 11,827–11,851, doi: 10.1029/1999JE900005.

McCord, T.B., Hansen, G.B., Hibbitts, C.A., 2001a. Hydrated salt minerals on Ganymede's surface: Evidence of an ocean below, Science 292, 1523–1525.

McCord, T.B., Hansen, G.B., Hibbitts, C.A., 2001b. Thermal and radiation stability of the hydrated salt minerals epsomite, mirabilite, and natron under Europa environmental conditions. J. Geophys. Res. 106, 3311–3320.

McCord, T.B., Teeter, G., Wiley, W.R., Hansen, G.B., Sieger, M.T., Wiley, W.R., Orlando, T.M., 2002. Brines exposed to Europa surface conditions. J. Geophys. Res. 107, 5004–5009, doi: 10.1029/2000JE001453.

McCord, T., Hansen, G., Combe, J., Hayne, P. 2010. Hydrated minerals on Europa's surface: An improved look from the Galileo NIMS investigation. Icarus, 209, 639–650.

McEwen, A. S., Eliason, E.M., Bergstrom, J.W., Bridges, N.T., Hansen, C.J., Delamere, W.A., Grant, J.A., Gulick, V.C., Herkenhoff, K.E., Keszthelyi, L., Kirk, R.L., Mellon, M.T., Squyres, S.W., Thomas, N., Weitz, C.W., 2007. Mars Reconnaissance Orbiter's High Resolution Imaging Science Experiment (HiRISE), J. Geophys. Res. 112, E05S02, doi:10.1029/2005JE002605.

McKinnon, W. B. Convective instability in Europa's floating ice shell. Geophys. Res. Lett. 26, 951-954 (1999).

McKinnon, W. B., and M. E. Zolensky (2003), Sulfate content of Europa's ocean and shell: Evolutionary considerations and geological and astrobiological implications, Astrobiology 3, 879–897.

McMahon, K.L. and Lackie, M.A., 2006. Seismic reflection studies of the Amery Ice Shelf, East Antarctica: delineating meteoric and marine ice. Geophys. J. Int. 166, 757-766.

Mehta, M. et al. (2011), Explosive erosion during the Phoenix landing exposes subsurface water on Mars. Icarus 211, 172-194.

Mellon M. T., R. L Fergason, N. E. Putzig, The thermal inertia of the surface of Mars, in *The Martian Surface: Composition, Mineralogy, and Physical Properties*, J. F. Bell, ed., Cambridge U. Press, London, 399-427, 2008.

Merchant, B.J., 2009. MEMS applications in seismology. Seismic Instrumentation Technology Symposium, November.

Metzger, P.T, et al. (2011), Phenomenology of soil erosion due to rocket exhaust on the Moon and the Mauna Kea lunar test site, J. Geophys. Res. 116, E06005.

Mevel, L., and Mercier, E. Large-scale doming on Europa: A model of formation of Thera Macula. Planet. Space Sci. 55, 915-927 (2007).

Ming et al., Mars 2007 Phoenix Scout mission Organic Free Blank: Method to distinguish Mars organics from terrestrial organics, JGR, VOL. 113, E00A21, doi:10.1029/2007JE003061, 2008.

Mitri, G., Showman, A.P., 2008. A model for the temperature-dependence of tidal dissipation in convective plumes in icy satellites: Implications for Europa and Enceladus. Icarus 195, 758–764.

Miyamoto, H., Mitri, G., Showman, A.P., Dohmd, J. P. (2005) Putative ice flows on Europa: Geometric patterns and relation to topography collectively constrain material properties and effusion rates. Icarus 177 413–424.

Monnard, P.-A., Apel, C.L., Kanavarioti, A., and Deamer, D.W. (2002). Influence of ionic solutes on self-assembly and polymerization processes related to early forms of life: Implications for a prebiotic qaueous medium. Astrobiology 2, 213-219.

Moore, H.J., G.D. Clow, and R.E. Hutton (1982). A summary of Viking sample-trench analyses for angles of internal friction and cohesions. J. Geophys. Res. 87, 10,043–10,050.

Moore, J.M., E. Asphaug, R.J. Sullivan, J.E. Klemaszewski, K.C. Bender, R. Greeley, P.E. Geissler, A.S. McEwen, E.P. Turtle, C.B. Phillips, B.R. Tufts, J.W. Head III, R.T. Pappalardo, K.B. Jones, C.R. Chapman, M.J.S. Belton, R.L. Kirk, and D. Morrison (1998) Large impact features on Europa: Results from the Galileo nominal mission, Icarus 135, 127-145.

Moore, M. (1984), Studies of proton-irradiated SO_2 at low temperatures: Implications for Io, Icarus 59, 114–128.

Moore, M.H., Hudson, R.L., 2003. Infrared study of ion-irradiated N_2-dominated ices relevant to Triton and Pluto: Formation of HCN and HNC. Icarus 161, 486–500.

Moore, W.B. and Hussman, H. (2009). Thermal evolution of Europa's silicate interior. In: Pappalardo, R.T., McKinnon, W.B., Khurana, K.K. (Eds.), Europa, U. Arizona Press, Tucson, 369–380.

NASA, 2009. New Frontiers 2009 Announcement of Opportunity, NNH09ZDA007O, April 20, 2009.

NASA, 2010. Discovery 2010 Announcement of Opportunity, NNH10ZDA007O, June 7, 2010.

NASA 2011. Headquarters, October 4, 2011. Europa Study Statement of Work.

Navarro Gonzolez et al. (2011), Reanalysis of the Viking results suggests perchlorate and organics at midlatitudes on Mars, J. Geophys. Res. 116, E08011.

Nealson, K. (1997). The limits of life on Earth and searching for life on Mars. J. Geophys. Res. 102, 23675–23686.

Neave, K.G., Savage, J.C., 1970. Icequakes on the Athabasca Glacier, J. Geophys. Res. 75(8), 1351-1362.

Noll, K. S., H. A.Weaver, A. M. Gonnella (1995), The Albedo spectrum of Europa from 2200 to 3300, J. Geophys. Res. 100, 19,057–19,060.

O'Brien, D. P., Geissler, P., Greenberg, R. A melt through model for chaos formation on Europa. Icarus 156, 152-161 (2002).

O'Brien, H., Brown, P., Beek, T., Carr, C., Cupido, E., Oddy, T., 2007. A radiation tolerant digital fluxgate magnetometer. Meas. Sci. Technol.18, 3645–3650.

Ojakangas, G.W., Stevenson, D.J., 1989. Thermal state of an ice shell on Europa. Icarus 81, 220–241.

Orlando, T. M., et al. (2005), The chemical nature of Europa surface material and the relation to a sub-surface ocean, Icarus 177, 528–533.

Oudea, C., Poirot, P., Gaillard, R., Poivey, C., Marchand, L., 2009. Single event effects in MEMS accelerometers, IEEE Radiation Effects Data Workshop, 94–98,
doi: 10.1109/REDW.2009.5336309.

Paczkowski, B., et al., 2008. Outer Planets Flagship Mission Science Operations Concept Study Report, JPL D–46870. June 2008.

Panning, M., Lekic, V., Manga, M., Cammarano, F., Romanowicz, B., 2006. Long-period seismology on Europa: 2. Predicted seismic response. J. Geophys. Res. 111, E12008.

Pappalardo, R., Barr, A.C., 2004. The origin of domes on Europa: The role of thermally induced compositional diapirism. Geophys. Res. Lett. 31, L01701.

Pappalardo, R.T., Head, J.W., Greeley, R., Sullivan, R.J., Pilcher, C., Schubert, G., Moore, W.B., Carr, M.H., Moore, J.M., Belton, M.J.S., Goldsby, D.L., 1998. Geological evidence for solid state convection in Europa's ice shell. Nature 391, 365–368.

Pappalardo, R.T., Head, J.W., Greeley, R., Sullivan, R.J., Pilcher, C., et al., 1999. Does Europa have a subsurface ocean? Evaluation of the geological evidence. J. Geophys. Res. 104, 24,015–24,056.

Paranicas, C., Ratliff, J.M., Mauk, B.H., Cohen, C., Johnson, R.E., 2002. The ion environment of Europa and its role in surface energetics. Geophys. Res. Lett. 29, 2001GL014127.

Paranicas, C., Cooper, J.F., Garrett, H.B., Johnson, R.E., Sturner, S.J., 2009. Europa's radiation environment and its effects on the surface. In: Pappalardo, R.T., McKinnon, W.B., Khurana, K.K. (Eds.), Europa, U. Arizona Press, Tucson, 529–544.

Patterson, G.W., Paranicas, C., Prockter, L.M., 2012. Characterizing electron bombardment of Europa's surface by location and depth. Icarus, in press.

Pauer, F., Kipfstuhl, J., Kuhs, W.F., 1996. Raman spectroscopic study on the spatial distribution of nitrogen and oxygen in natural ice clathrates and their decomposition to air bubbles. Geophys. Res. Lett. 23, 177–180.

Pierazzo, E., Chyba, C., 2002. Cometary delivery of biogenic elements to Europa. Icarus 157, 120–127.

Pike W.T., Kumar S., 2007. Improved design of micromachined lateral suspensions using intermediate frames. J. Micromech. Microeng. 17, 1680–1694.

Pizzarello, S., Huang, Y., Becker, L., Poreda, R., Nieman, R., Cooper, G., Williams, M., 2001. The organic content of the Tagish Lake meteorite. Science 293, 2236–2239.

Plemmons, D.H., Mehta, M., Clark, B.C., Kounaves, S.P., Peach, L.L. Jr., Renno, N.O., Tamppari, L., Young, S.M.M., 2008. Effects of the Phoenix Lander descent thruster plume on the Martian surface. J. Geophys. Res. 113, E003059.

Prockter, L.M., Schenk, P., 2005. Origin and evolution of Castalia Macula, an anomalous young depression on Europa. Icarus 177, 305–326.

Prockter, L.M., Patterson, G.W., 2009. Morphology and evolution of Europa's ridges and bands. In: Pappalardo, R.T., McKinnon, W.B., Khurana, K.K. (Eds.), Europa, U. Arizona Press, Tucson, 237–258.

Prockter, L.M., Head, J.W. III, Pappalardo, R.T., Patel, J.G., Sullivan, R.J., Clifton, A.E., Giese, B., Wagner, R., Neukum, G., 2002. Morphology of europan bands at high resolution: A midocean ridge-type rift mechanism. J. Geophys. Res. 107, 10.1029/2000JE001458.

Rasmussen, R., 2009. System Architecture for JEO (presentation slides), EJSM Instrument Workshop, July 15–17.

Rathbun, J.A., Musser, G.S. Jr., Squyres, S.W., 1998. Ice diapirs on Europa: Implications for liquid water. Geophys. Res. Lett. 25, 4157–4160.

Rathbun, J.A., Rodriguez, N.J., Spencer, J.R., 2010. Galileo PPR observations of Europa: Hotspot detection limits and surface thermal properties. Icarus 210, 763–769.

Robin, G. de Q., 1958. Glaciology III. Seismic shooting and related investigations. *Norwegian-British-Swedish Antarctic Expedition, 1949-1952. Scientific Results V*. Norsk Polarinstitutt, Oslo, 134 pp.

Roethlisberger, H., 1972. Seismic Exploration in Cold Regions. Cold Regions Science and Engineering Monograph 11-A2a, Hanover, NH.

Rull, F., Maurice, S., Diaz, E., Tato, C., Pacros, A., the RLS Team, 2011. The Raman laser spectrometer on the Exo-Mars 2018 Rover Mission, 2400, 42nd Lunar and Planetary Science Conference.

Schenk, P. and Pappalardo, R.T. Topographic variations in chaos on Europa: Implications for diapiric formation. Geophys. Res. Lett. 31, L16703 (2004).

Schenk, P.M. and E.P. Turtle, 2009, Europa's Impact Craters: Probes of the Icy Shell. In: Pappalardo, R.T., McKinnon, W.B., Khurana, K.K. (Eds.), Europa, U. Arizona Press, Tucson, 259–282.

Schenk, P.M., 2009. Slope characteristics of Europa: Constraints for Landers and radar sounding. Geophys. Res. Lett. 36, L15204.

Schenk, P.M., Chapman, C.R., Zahnle, K., Moore, J.M., 2004. Ages and interiors: The cratering record of the Galilean satellites. In: Bagenal, F., Dowling, T.E., McKinnon, W.B. (Eds.), Jupiter: The Planet, Satellites, and Magnetosphere, Cambridge U. Press, Cambridge, U.K., 427–456.

Schmidt, B.E., Blankenship, D.D., Patterson, G.W., Schenk, P.M., 2011. Active formation of "chaos terrain" over shallow subsurface water on Europa. Nature 479, 502–505. doi: 10.1038/nature10608.

Shea, H., 2011. Effects of radiation on MEMS. Proc. SPIE, Vol. 7928.

Shirley, J.H., Dalton, J.B., Prockter, L.M., Kamp, L.W., 2010. Europa's ridged plains and smooth low albedo plains: Distinctive compositions and compositional gradients at the leading side-trailing side boundary. Icarus 210, 358–384.

Showman, A.P., Han, L., 2004. Numerical simulations of convection in Europa's ice shell: Implications for surface features. J. Geophys. Res. 109, E01010.

Showman, A.P., Han, L., 2005. Effects of plasticity on convection in an ice shell: Implications for Europa. Icarus 177, 425–437.

Siegel, B.Z., 1979. Life in the calcium chloride environment of Don Juan Pond, Antarctica. Nature 280, 828–829.

Smythe, W. D., et al. (1998), Galileo NIMS measurements of the absorption bands at 4.03 and 4.25 microns in distant observations of Europa. Bull. Am. Astron. Soc. 30, 1448.

Sotin, C., Head, J.W., Tobie, G. (2002) Tidal heating of upwelling thermal plumes and the origin of lenticulae and chaos melting. Geophys. Res. Lett. 29, 1233.

Spaun, N. A., J.W. Head, G.C. Collins, L.M. Prockter, and R.T. Pappalardo, Conamara Chaos region, Europa: Reconstruction of mobile polygonal ice blocks. Geophys. Res. Lett. 25, 4277–4280 (1998).

Spencer, J. R., L. K. Tamppari, T. Z. Martin, and L. D. Travis, Temperatures on Europa from Galileo Photopolarimeter-Radiometer: Nighttime thermal anomalies, *Science, 284*, 1514-1516, 1999.

Spencer, J. R., and W. M. Calvin (2002), Condensed O_2 on Europa and Callisto, Astron. J. 124, 3400–3403.

Spencer, J. Thermal segregation of water ice on the Galilean satellites, Icarus 69, 297–313, 1987.

Spengler, B. Microprobing and imaging MALDI for biomarker detection, in: Hillenkamp, F., Peter-Katalinic′, Jasna. (Eds.), *MALDI MS: A Practical Guide to Instrumentation, Methods and Applications*. Wiley-VCH, pp. 109–130, 2007.

Spitale, J.N. and Porco, C.C. Association of the jets of Enceladus with the warmest regions on its south-polar fractures. Nature 449, 695-697, 2009.

Spitzer, J., Poolman, B. The role of biomacromolecular crowding, ionic strength, and physicochemical gradients in the complexities of life's emergence. Microbiology and Molecular Biology Reviews, 73, 371–388, 2009.

Squyres, S.W., Reynolds, R.T., Cassen, P., Peale, S. J. Liquid water and active resurfacing on Europa. Nature 301, 225-226. (1983)

Strazzulla, G. et al. (2011), Cosmic ion bombardment of the icy moons of Jupiter, Nucl. Instrum. Meth. B 269, 842–851.

Sullivan, R., Greeley, R., Homan, K., Klemaszewski, J., Belton, M.J.S, Carr, M.H., Chapman, C.R., Tufts, R., Head, J.W. III, Pappalardo, R., Moore, J., Thomas, P., and the Galileo Imaging Team, 1998. Episodic plate separation and fracture infill on the surface of Europa. Nature 391, 371–373.

Thomas, N., Lüthia, B.S., Hviidb, S.F., Kellerb, H.U., Markiewiczb, W.J., Blümchenb, T., Basilevskyb, A.T., Smithc, P.H., Tannerc, R., Oquestc, C., Reynoldsc, R., Jossetd, J.-L., Beauvivred, S., Hofmanne, B., Rüfferf, P., Pillingerg, C.T., 2004. The microscope for Beagle 2. Planet. Space Sci. 52, 853–866.

Tobie, G., Choblet, G., Sotin, C., 2003. Tidally heated convection: Constraints on Europa's ice shell thickness. J. Geophys. Res. 108 (E11), 5124.

Tufts, B.R., Greenberg, R., Hoppa, G., Geissler, P., 2000. Lithospheric dilation on Europa. Icarus 146, 75–97.

Valavanoglou, A., Oberst, M., Magnes, W., Hauer, H., Neubauer, H., Baumjohann, W., Falkner, P., 2007. Magnetometer front-end ASIC (MFA). Geophys. Res. Abstracts 9, 06089.

Van den Broeke, M., Van de Berg, W. J., Van Meijgaard, E. (2008). Firn depth correction along the Antarctic grounding line. Antarctic Sci. 20, 513–517.

Vance, S. and Goodman. J., 2009. Oceanography of an ice-covered moon. In: Pappalardo, R.T., McKinnon, W.B., Khurana, K.K. (Eds.), Europa, U. Arizona Press, Tucson, 459–482.

Vance, S., J., Harnmeijer, J. Kimura, H. Hussmann, B. de Martin, and J. M. Brown, *2007*. Hydrothermal systems in small ocean *planets*. Astrobiology 7, 987-1005.

Volwerk M. et al. (2001), Wave activity in Europa's wake: Implications for ion pickup, J. Geophys. Res. 106, 26033–26048.

Wackett, L.P., Dodge, A.G., and Ellis, L.B.M. (2004). Microbial genomics and the periodic table. Appl. Environ. Microbio. 70, 647-655.

Wang, A., Haskin, L., Lane, A., Wdowiak, T., Squyres, S., Wilson, R., Hovland, L., Manatt, K., Raouf, N., Smith, C., 2003. Development of the Mars Microbeam Raman Spectrometer (MMRS), J. Geophys. Res. 108, E1, 5005, doi: 10.1029/2002JE001902.

Wang, A., L. A. Haskin, A. L. Lane, T. J. Wdowiak, S. W. Squyres, R. J. Wilson, L. E. Hovland, K. S. Manatt, N. Raouf, and C. D. Smith, Development of the Mars microbeam Raman spectrometer (MMRS), J. Geophys. Res., 108, 5005, 2003.

Weertman, J., 1974. Stability of the junction of an ice sheet and an ice shelf. J. Glac. 13, 3-11.

Willis, P.B., 2011. Materials Survivability and Selection for Nuclear Powered Missions. JPL D-34098.

Winberry, J.P., Anandakrishnan, S., Alley, R.B., 2009. Seismic observations of transient subglacial water-flow beneath MacAyeal Ice Stream, West Antarctica, Geophys. Res. Lett. 36, L11502.

Wuest, M., Managadze, G., Managadze, N., 2007. A combined Raman/laser ablation mass spectrometer instrument for exploration of small solar system objects, Adv. Space Res., 39, 477–39,481, 2007.

Zahnle, K., Dones, L., Levison, H.F., 1998. Cratering rates on the Galilean satellites. Icarus 136, 202–222.

Zahnle, K.J., Alvarellos, J.L., Dobrovolskis, A.R., Hamill, P., 2008. Secondary and sesquinary impact craters on Europa. Icarus 194, 660–674.

Zimmer, C., Khurana, K.K., Kivelson, M.G., 2000. Subsurface oceans on Europa and Callisto: Constraints from Galileo magnetometer observations. Icarus 147, 329, 2000.

Zolotov, M.Y., Shock, E.L., 2001. Composition and stability of salts on the surface of Europa and their oceanic origin. J. Geophys. Res. 106, 32815–32828.

Zolotov, M.Y. Shock, E.L., 2003. Energy for biologic sulfate reduction in a hydrothermally formed ocean on Europa. J. Geophys. Res. 108, 5022.

Zolotov, M.Y., Shock, E.L., 2004. A model for low-temperature biogeochemistry of sulfur, carbon, and iron on Europa. J. Geophys. Res. 109, E06003.

Zombeck, M.V, 1982. Handbook of Space Astronomy and Astrophysics. Cambridge U. Press, Cambridge, U.K.

D.4.2 Acronyms and Abbreviations

ΔV	delta velocity, delta-V
3D	three-dimensional
A	ampere
A	approach
A/D	analog to digital
ABSL	ABSL Power Solutions Ltd. used to be AEA Battery Systems, Ltd., where AEA stood for Atomic Energy Authority (a privatized branch of the U.K. AEA)
AC	alternating current
ACS	Attitude Control Subsystem
ACU	ASRG controller unit
ADC	analog-to-digital converter
AFT	allowable flight temperature
Ah	ampere-hour
AJ	anti-Jovian
AO	Announcement of Opportunity
APL	Applied Physics Laboratory
APML	Approved Parts and Materials List
APS	active pixel sensor
ASC	advanced Stirling converter
ASIC	application-specific integrated circuit
ASRG	Advanced Stirling Radioisotope Generator
ATK/PSI	
ATLO	assembly, test, and launch operations
B	baseline
BIU	bus interface unit
BOM	beginning of mission
BTE	bench-test equipment
C&DH	command and data handling/ Command and Data Handling Subsystem
C_3	injection energy per unit mass (V∞2), km^2/s^2
CAD	computer-aided design
CADRe	Cost Analysis Data Requirement
CATE	Cost and Technical Evaluation
CBE	current best estimate
CCD	charge-coupled device
CCSDS	Consultative Committee for Space Data Systems
CDR	Critical Design Review
CEM	channel electron multiplier
CFDP	CCSDS File Delivery Protocol
CG	center of gravity
CM	center of mass
CMMI	Capability Maturity Model Integration
CMOS	complementary metal-oxide semiconductor
COSPAR	Committee on Space Research
COT	crank over the top
CPT	comprehensive performance test
CRAM	chalcogenide random-access memory
CRISM	Compact Reconnaissance Imaging Spectrometer for Mars

CTS	coaxial transfer switch	EOI	Europa Orbit Insertion
CU	cleanup	EOM	end of mission
Da	dalton	ES	Europa Study
DBPM	digital baseband processing module	ESA	European Space Agency
		ESD	electrostatic discharge
DC	direct current	ESS	Europa Sampling System
DC/DC	direct current to direct current	ETL	Export Technical Liaison
DD	displacement damage	EVEE	Earth-Venus-Earth-Earth
DDD	displacement damage dose	FMECA	failure modes, effects, and criticality analysis
DDL	deorbit, descent, and landing		
DEM	digital elevation model	FOV	field of view
DHMR	dry-heat microbial reduction	FPGA	field-programmable gate array
DOD	depth of discharge		
DOE	Department of Energy	FPPs	Flight Project Practices
DOF	degree of freedom	FS	flight system
DPs	Design Principles	FSW	flight software
DSM	deep-space maneuver	FSWTB	flight software testbed
DSN	Deep Space Network	FWHM	full width at half maximum
DTM	developmental test model	G/T	gain to equivalent noise temperature
DWG	Detector Working Group		
EEE	electrical, electronic, and electromechanical	G-0	
		GC	gas chromatograph
EGA	Earth gravity assist	GDS	Ground Data System
EHS	electrical heater source	GHA	generator housing assembly
EIRP	effective isotropic radiated power	GM	product of gravitational constant and mass
EIS	Environmental Impact Statement	GN&C	guidance, navigation, and control
EJSM	Europa Jupiter System Mission	GPHS	General-Purpose Heat Source
		GRAIL	Gravity Recovery and Interior Laboratory
ELDRS	enhanced low-dose-rate sensitivity	GSE	ground-support equipment
EM	engineering model	H/W	hardware
EMI	electromagnetic interference		

HCIPE	High-Capability Instrument for Planetary Exploration	KBase	Knowledge Base
HCT	hydrocarbon trap	KSC	Kennedy Space Center
HEPA	high-efficiency particulate air	L1, L2	Level-1, Level-2, etc.
HGA	high-gain antenna	LAEP	Launch Approval Engineering Plan
HQ	NASA Headquarters	LAT	limited angle torque
HS	heat source	LCE	launch control equipment
HY	RF hybrid	LDEF	Long-Duration Exposure Facility
I&T	integration and test	LEV	lowest expected value
I/O	input/output	LGA	low-gain antenna
IC	internal charging	LORRI	Long-Range Reconnaissance Imager
ICD	Interface Control Document	LST	local solar time
ICE	Independent Cost Estimate	LVA	launch vehicle adapter
ICM	Institutional Cost Model	M3	Moon Mineralogy Mapper
ID	identification/identifier	MAG	Magnetometer
ID	inner diameter	MARCI	Mars Color Imager
IDD	Instrument Deployment Device	MARSIS	Mars Advanced Radar for Subsurface and Ionosphere Sounding
IFOV	instantaneous field of view	MBS	Multiband Seismometer Package
IMU	inertial measurement unit		
INMS	Ion and Neutral Mass Spectrometer	MCP	microchannel plate
IOM	interoffice memorandum	MCR	Mission Concept Review
IPR	Ice-Penetrating Radar	MDIS	Mercury Dual Imaging System
IR	infrared	MDR	Mission Definition Review
ITAR	International Traffic in Arms Regulations	MEL	Master Equipment List
I-V	current-voltage	MEMS	microelectromechanical system
JEO	Jupiter Europa Orbiter	MER	Mars Exploration Rover
JIRA	project workflow management system	MESSENGER	Mercury Surface, Space Environment, Geochemistry, and Ranging
JOI	Jupiter Orbit Insertion		
JPL	Jet Propulsion Laboratory		
K&D	key and driving		

MEV	maximum expected value		OPAG	Outer Planets Assessment Group
MFA	magnetometer front-end ASIC		ORT	operations readiness test
MGA	medium-gain antenna		OSTP	Office of Science and Technology Policy
MI	Microscopic Imager		OTS	off the shelf
MLI	multilayer insulation		P	preliminary
MMM	Moon Mineralogy Mapper		P/L	payload
MOLA	Mars Orbiter Laser Altimeter		P/N	part number
MPSS	multimission power switch slice		PBC	power bus controller
MRO	Mars Reconnaissance Orbiter		PCA	pressurant-control assembly
MS	Mass Spectrometer		PCB	Parts Control Board
MSL	Mars Science Laboratory		PCU	power converter unit
MSTB	Mission System Testbed		PDE	propulsion drive electronics (slice)
MTIB	minimum torque impulse bit		PDR	Preliminary Design Review
MVIC	Multispectral Visible Imaging Camera		PEL	Power Equipment List
NASA	National Aeronautics and Space Administration		PFC	pyro-firing card
			PHSF	Payload Hazardous Servicing Facility
NEPA	National Environmental Policy Act		PI	Principal Investigator
NICM	NASA Instrument Cost Model		PIA	propellant-isolation assembly
NIMS	Near-Infrared Mapping Spectrometer		PIP	Project Information Package
			PJR	perijove raise maneuver
NLS	NASA Launch Services		PMD	propellant-management device
NLSA	Nuclear Launch Safety Approval		PMSR	Project Mission System Review
NR	nonresonant, nonres		PoL	point of load
NSI	NASA Standard Initiator		PPR	Parts Program Requirements
NSPAR	Nonstandard Parts Approval Request		PRA	probablilistic risk assessment
			PRA	Project Resource Analyst
NTO	nitrogen tetroxide		PRICE-H	Parametric Review of Information for Costing and Evaluation—Hardware
O&C	operations and checkout			
OD	orbit determination			

PSA	Project Schedule Analyst		SDT	Science Definition Team
R&TD	research and technology development		SDU	shunt dissipater unit
			SEE	single-event effect
RAD750	radiation-hardened microprocessor		SEER	System Evaluation and Estimation of Resources
RAM	random-access memory		SEL	single-event latchup
RCS	Reaction-Control Subsystem		SEMP	Systems Engineering Management Plan
RDE	Real-Time Development Environment		SER	Safety Evaluation Report
RDF	radiation design factor		set point	
RF	radio frequency		SEU	single-event upset
RHU	radioisotope heater unit		SHARAD	Shallow Radar
RI	Rconnaissance Imager		SIS	Site Imaging System
R_J	Jovian radii		SMAP	Soil Moisture Active Passive
ROD	Record of Decision		SNR	signal-to-noise ratio
ROIC	readout integrated circuit		SOCM	Space Operations Cost Model
ROSINA	Rosetta Orbiter Spectrometer for Ion and Neutral Analysis		SQRT	mean radiation signal per pixel
RPS	radioisotope power system			
RS	Raman Spectrometer		SRAM	static random-access memory
RTG	radioisotope thermoelectric generator		SRR	System Requirements Review
RTOF	reflectron time-of-flight		SRU	stellar reference unit
RWA	reaction wheel assembly		SS	subsystem
S/N	signal-to-noise ratio		SSE	spacecraft support equipment
S/S	steady state		SSI	solid-state imager
SAF	Spacecraft Assembly Facility		SSPA	solid-state power amplifier
SAM	Sample Analysis at Mars		SSR	solid-state recorder
SAR	Safety Analysis Report		STV	solar thermal-vacuum
SBIR	Small Business Innovation Research (funding)		SWIRS	Shortwave Infrared Spectrometer
SD	sampling device		SysML	Systems Modeling Language
SDS	shunt driver slice		TAYF	test as you fly
SDST	small deep-space transponder			

TB	testbed
TCA	thruster cluster assembly
TCM	trajectory correction maneuver
TDP	Technical Data Package
TEGA	Thermal and Evolved Gas Analyzer
TI	Topographical Imager
TID	total ionizing dose
TOF	time of flight
TRL	technology readiness level
TVC	thrust vector control
TWTA	traveling-wave tube amplifier
U	update
UST	universal space transponder
V	volt, velocity, vector
V&V	verification and validation
VEE	Venus-Earth-Earth
VEEGA	Venus-Earth-Earth gravity assist
VIMS	Visual and Infrared Mapping Spectrometer
VRHU	variable radioisotope heating unit
W	watt
WBS	work breakdown structure
WCA	worst-case analysis
WCD	Worst-Case Datasheet
WDE	wheel drive electronics
WSTS	workstation testset
WTS	waveguide transfer switch

D.4.3   Master Equipment List

D.4.3.1   Carrier Spacecraft MEL

Master Equipment List (MEL) removed for compliance with export-control (ITAR) regulations. Available upon request.

D.4.3.2   Lander Spacecraft MEL

Master Equipment List (MEL) removed for compliance with export-control (ITAR) regulations. Available upon request.

D.4.4   Aerospace Independent Cost Estimate

AEROSPACE REPORT NO.
ATR-2012(5583)-6

Europa Habitability Mission: Lander Concept
CATE: Cost and Technical Evaluation

April 24, 2012

Randy Persinger[1], Robert Kellogg[2], Mark Barrera[3]
[1]Advanced Studies and Analysis Directorate, NASA Programs Division
[2]Space Architecture Department, Systems Engineering Division
[3]Vehicle Concepts Department, Systems Engineering Division

Prepared for:

Jet Propulsion Laboratory
4800 Oak Grove Drive
Pasadena, CA 91109

Contract No. 1393581

Authorized by: Civil and Commercial Operations

PUBLIC RELEASE IS AUTHORIZED.

.

AEROSPACE
Assuring Space Mission Success

Europa Habitability Mission: Lander Concept
CATE: Cost and Technical Evaluation

April 24, 2012

Randy Persinger[1], Robert Kellogg[2], Mark Barrera[3]
[1]Advanced Studies and Analysis Directorate, NASA Programs Division
[2]Space Architecture Department, Systems Engineering Division
[3]Vehicle Concepts Department, Systems Engineering Division

Prepared for:

Jet Propulsion Laboratory
4800 Oak Grove Drive
Pasadena, CA 91109

Contract No. 1393581

Authorized by: Civil and Commercial Operations

AEROSPACE REPORT NO.
ATR-2012(5583)-6

Europa Habitability Mission: Lander Concept
CATE: Cost and Technical Evaluation

April 24, 2012

Randy Persinger[1], Robert Kellogg[2], Mark Barrera[3]
[1]Advanced Studies and Analysis Directorate, NASA Programs Division
[2]Space Architecture Department, Systems Engineering Division
[3]Vehicle Concepts Department, Systems Engineering Division

Prepared for:

Jet Propulsion Laboratory
4800 Oak Grove Drive
Pasadena, CA 91109

Contract No. 1393581

Authorized by: Civil and Commercial Operations

PUBLIC RELEASE IS AUTHORIZED.

AEROSPACE
Assuring Space Mission Success

AEROSPACE REPORT NO.
ATR-2012(5583)-6

Europa Habitability Mission: Lander Concept
CATE: Cost and Technical Evaluation

Approved by:

Matthew J. Hart/Principal Director
Advanced Studies and Analysis Directorate
Ground Enterprise
NASA Programs Division
Civil and Commercial Operations

© The Aerospace Corporation, 2012.

ii

SL0082(1, 4320, 35, GN)

Acknowledgments

The following individuals are recognized for their contributions as authors, reviewers, and editors of the Cost and Technical Evaluation (CATE) for the Europa Habitability Mission: Lander concept.

David Bearden
Ray Nakagawa
Anh Tu
Mark Cowdin
Gary North

iii

iv

Contents

v

Figures

Tables

vi

1. Purpose

The Aerospace Corporation was tasked in November 2011 to participate as an independent party to review three separate, but related, Europa Habitability Mission (EHM) concepts under study by the Jet Propulsion Laboratory (JPL) to visit Europa in the continuing search for life in our solar system. The three concepts were being studied by JPL in the context of guidance provided by the National Research Council (NRC) Planetary Decadal Survey report released to the public in March 2011. In this report, a mission to the Jupiter/Europa system was rated very high with regard to science importance to the United States in the next decade. However, based on the expected high cost of the baseline reference mission evaluated by the NRC Planetary Decadal Steering Committee, the guidance was to descope the reference mission and significantly reduce mission cost while providing sufficient science investigation capability considered to be of paramount importance over the next decade. Aerospace, having participated as the NRC Cost and Technical Evaluation (CATE) contractor in the cost, technical, and schedule risk assessment of the planetary concepts evaluated by the Planetary Steering Committee was a logical choice to independently evaluate the three updated EHM concepts with the same CATE techniques, and processes. The three separate EHM mission concepts evaluated were: Orbiter, Flyby, and Lander. This report presents the cost, technical and schedule risk assessment for the **EHM Lander Mission** using the CATE process originally established by the NRC.

The key parameters of the EHM Lander Mission can be found in Figure 1.

Europa Lander and Carrier

Combined Carrier and Lander with Braking Stage

Lander Element

Carrier Element

Scientific Objectives:
- Explore Europa to investigate its habitability
- Key science themes cited:
  - *Composition*: Understand the habitability of Europa's ocean through composition and chemistry
  - *Geology*: Characterize a locality of high scientific interest to understand the formation and evolution of the surface at local scales
  - *Ocean & Ice Shell*: Characterize the local thickness, heterogeneity, and dynamics of any ice and water layers

Key Parameters:
- Model Payload (6 Lander instruments + 1 Carrier instrument)
  - *Composition: Mass Spectrometer, Raman Spectrometer*
  - *Composition & Geology: Site Imager, Microscopic Imager, Carrier Reconnaissance Imager*
  - *Ocean & Ice Shell: Magnetometer, Multi-band Seismometer Package*
- 2 Advanced Stirling Radioisotope Generators (ASRGs) on Lander + 2 ASRGs on Carrier
- Launch Mass: 6868 kg
- Launch Date: 2021 (on Delta IV Heavy)
- Orbit: 200 km Europa orbit Carrier + Europa landing
- Radiation Environment: 850 krad TID (100 mil Al Si) Carrier, 520 krad TID (100 mil Al Si) Lander
- Disposal Location: Europa

Key Challenges:
- Mass
  - *Insufficient launch margin for this phase of development*
- New Technology Development
  - *New science instrumentation*
  - *New spacecraft technologies*
- Radiation Environment
  - *Impact to external hardware and sensitive detectors*
- Planetary Protection
  - *Ability of hardware to withstand Dry Heat Microbial Reduction and/or sterilization*

Figure 1.   EHM Lander Mission Concept Overview

1

2

2. Executive Summary

The EHM Lander concept was found to have a Medium-High technical risk and will require several new developments for a landed mission to Europa. Mass margins for this concept are low on the Delta IV Heavy launch vehicle for this phase of development. Power margins are robust and the design incorporates modularity with well-defined interfaces. Multiple technology and engineering implementation developments are needed for this mission. Safe landing on the surface of Europa requires a new autonomous terrain relative navigation system. New instrumentation includes a Raman Spectrometer qualified for the Europa environment and a rotary percussive sample acquisition system for in situ sample collection. Concern does exist with the technology development of the radioisotope power source (ASRGs) currently under development by NASA. An additional concern is the selection of hardware that is tolerant to the dry heat microbial reduction process planned to ensure satisfaction of Planetary Protection requirements. The impact of radiation for this mission is also a concern, but has been mitigated by compartmentalization and modular design.

The CATE cost estimate for the EHM Lander concept is $3.0B in FY15 dollars excluding launch services. The EHM Lander CATE estimate, excluding launch services, is compared to the Project's cost estimate in Figure 2. Including a launch service cost of $543M, consistent with CATE estimates for the Planetary Decadal Survey Steering Committee, the CATE estimate including launch services is $3.6B. The cost estimate for four ASRGs is assumed to be $200M based on guidance provided by NASA. The cost risk associated with the ASRG technology development required for the EHM mission concepts has not been included in the CATE estimate.

The project schedule of 73 months is considered to be realistic, with the independent estimate being 71 months. The concept's use of modularity provides the opportunity to focus and minimize risk through parallel development paths.
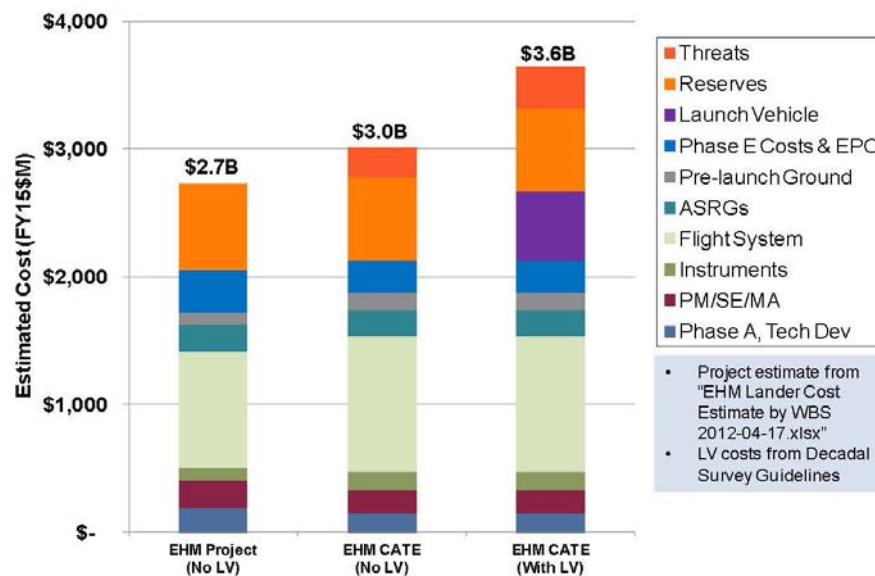
Figure 2.   Europa Lander Cost Estimates

3

4

3. CATE Background

The NRC Astro2010 Decadal Survey Steering Committee established the CATE process in June 2009. The CATE process was then used for three NRC Decadal Surveys: Astro2010, Planetary, and Heliophysics. Previous NRC Decadal Surveys had underestimated the costs associated with the recommended science priorities. The NRC and others recognized that mission costs were being underestimated, so the U.S. Congress mandated that an independent contractor be utilized to provide more realistic cost, technical and schedule risk assessment directly to the decadal steering committees for consideration and evaluation in executing their charter. Select portions of the Planetary Decadal report, *Vision and Voyages,* from Appendix C are provided below to summarize the CATE process. It is important to note that the CATE process is intended to inform future NASA Science Mission Directorate (SMD) budget decisions, not to decide if a specific concept meets a cost target or to decide if a specific mission concept should be selected for flight versus another mission. Because the CATE process is used for future budgetary decisions, it incorporates potential cost threats that may occur in the future based on concept maturity at the time of evaluation.

The CATE process focuses on cost and schedule risk assessment, but limited technical evaluation is also required to categorize concept maturity, technology development and the potential impact that insufficient margins and contingency (mass and power) may have on schedule or cost.

*__Vision and Voyages__, **Planetary Decadal Report, Appendix C:** The objective of the CATE process is to perform a cost and technical risk analysis for a set of concepts that may have a broad range of maturity, and to ensure that the analysis is consistent, fair, and informed by historical data. Typically, a concept evaluated using the CATE process is early in its life cycle and therefore likely to undergo significant subsequent design changes. Historically, such changes have resulted in cost growth. Therefore, a robust process is required that fairly treats a concept of low maturity relative to one that has undergone several iterations and review. CATEs take into account several components of risk assessment.*

The primary goal of the CATE cost appraisal is to provide independent estimates (in fiscal year [FY] 2015 dollars) that can be used to prioritize various concepts within the context of the expected NASA budgetary constraints for the coming decade. ... To be consistent for all concepts, the CATE cost process allows an increase in cost resulting from increased contingency mass and power, increased schedule, increased required launch vehicle capability, and other cost threats depending on the concept maturity and specific risk assessment of a particular concept. ... All cost appraisals for the CATE process are probabilistic in nature and are based on the NASA historical record and documented project life-cycle growth studies.

The evaluation of technical risk and maturity in the CATE process focuses on the identification of the technical risks most important to achieving the required mission performance and stated science objectives. The assessment is limited to top-level technical maturity and risk discussions. Deviations from the current state of the art as well as system complexity, operational complexity, and integration concerns associated with the use of heritage components are identified. Technical maturity and the need for specific technology development, including readiness levels of key technologies and hardware, are evaluated. ... The CATE technical evaluation is limited to high-level technical risks that potentially impact schedule and cost. The CATE process places no cost cap on mission concepts, and hence risk as a function of cost is not considered. Concept maturity and technical risk are evaluated in terms of the ability of a concept to meet performance goals within proposed launch dates with adequate mass, power, and performance margins.

To aid in the assessment of concept risk, independent schedule estimates are incorporated as part of the CATE cost estimate.

5

6

4.   Technical Evaluation

The EHM Lander technical risk rating is Medium-High. The mission will require multiple new technology and engineering implementation developments. Terrain relative navigation for landing hazard avoidance at Europa; Radioisotope, or ASRG, power source qualification; a Raman Spectrometer qualified for the Europa environment; a rotary percussive sample acquisition system; radiation mitigation for external hardware, bake stable treatment of detectors for planetary protection; qualification of the STAR 30BP solid rocket motor for long duration space exposure; and life qualification of the AMBR 890 N (HiPAT) engine will be some of the key challenges associated with this mission. Power margins and battery depth of discharge are adequate assuming two ASRGs on the Lander element and two ASRGs on the Carrier element. Mass margins are low for this phase of development with an average mass contingency of 30% for the bus and 50% for the instruments. The concept design is at risk of exceeding the capability of the Delta IV Heavy launch vehicle. A lack of existing high resolution imagery of the surface of Europa contributes to uncertainty in landing hazards, requiring a very robust landing system.

The top technical risks associated with the EHM Lander Mission are:

1.   Overall **System Mass** margin
2.   **Technology Development** impact on project schedule and cost
3.   Survival of flight system in **Radiation Environment**
4.   Development of hardware to withstand **Planetary Protection** methods

These top risks are discussed below. Figure 3 illustrates some key aspects of the EHM Lander concept.
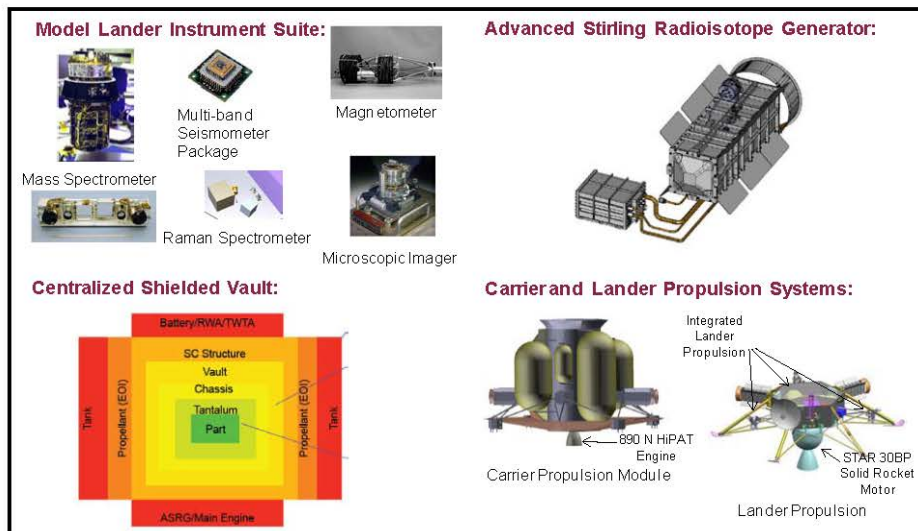
Figure 3.   EHM Lander Mission Concept Features

7

System Mass

The anticipated mass margins for the EHM Lander mission are low and system mass is at risk of exceeding the capacity of the Delta IV Heavy launch vehicle for the proposed mission design. As illustrated in Figure 4, the project estimate for launch mass is within 3% of the Delta IV Heavy capacity using an average of 30% mass growth on the spacecraft bus and 50% mass growth for the instruments. The CATE mass estimate assumes a higher average mass growth allowance of 50% for the spacecraft bus and 70% for the instruments, based on previous systems at a Pre-Phase A stage of design. Competitively chosen instruments may have higher mass or complexity than the model instruments for the EHM Lander concept and the spacecraft system is subject to additional modification at this stage of development. Anticipated risks include increased cost and schedule to maintain low mass and possible science instrument descopes to recover mass.
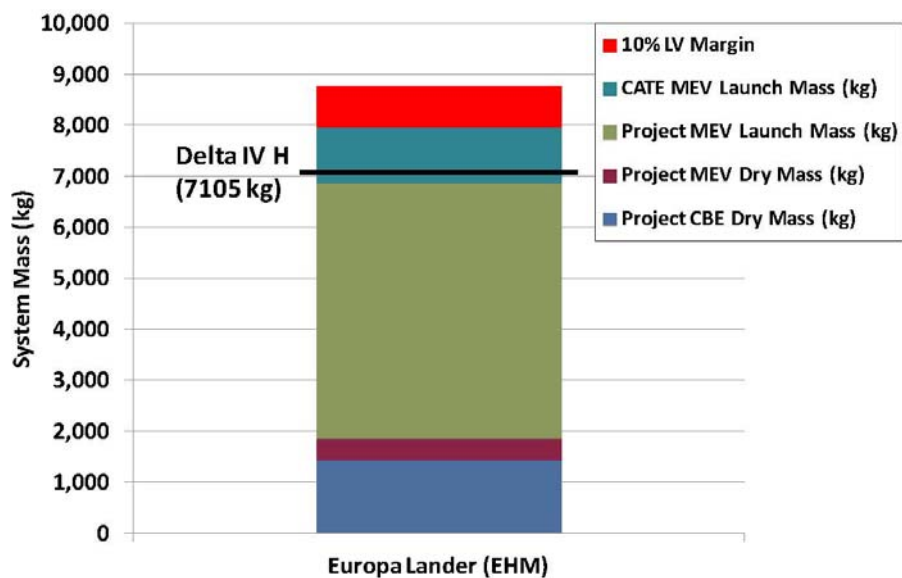
Figure 4.   EHM Lander Launch Mass Margin

Power margins during normal operations are acceptable assuming 2 ASRGs on the Carrier and 2 ASRGs on the Lander, as shown in Figures 5 and 6. There are small differences in the expected maximum battery depth of discharge due to differences in power growth allowances in CATE estimates versus project estimates; however, all estimated power margins are within acceptable limits. CATE estimates indicate battery depth-of-discharge is held to 27% or lower in the worst case for the combined Carrier/Lander stack at Jupiter orbit insertion, 8% for the Carrier communications relay phase, 72% on the Lander for the one time landing event, and 28% for Lander surface science.

Technology Development

Multiple new technology development items are proposed for the EHM Lander mission. The number and complexity of the proposed technology effort contributes to risk in the overall project schedule and cost. Technology development items for the EHM Lander mission include an autonomous terrain relative navigation system for landing hazard avoidance, development of the ASRG, a new Raman Spectrometer qualified for the Europa surface environment, a rotary-percussive coring tool for surface

8
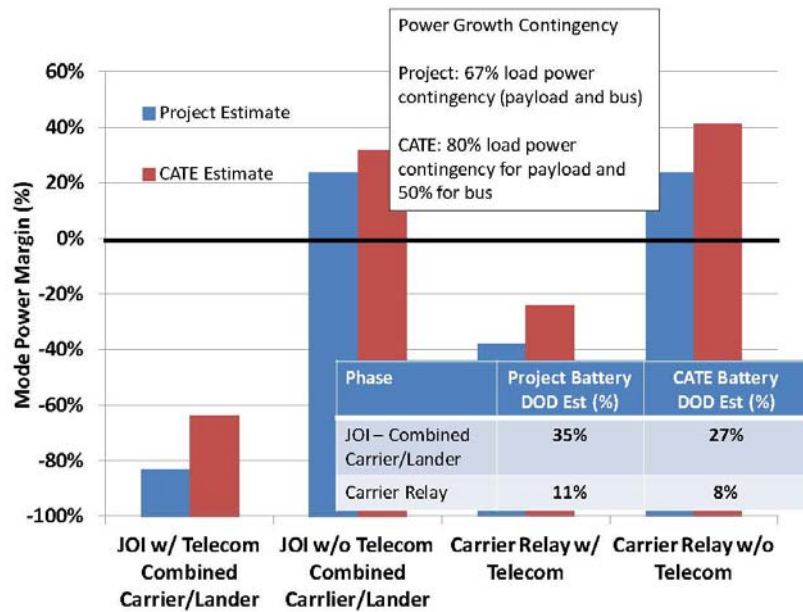
Figure 5.   EHM Carrier/Lander Power Margin
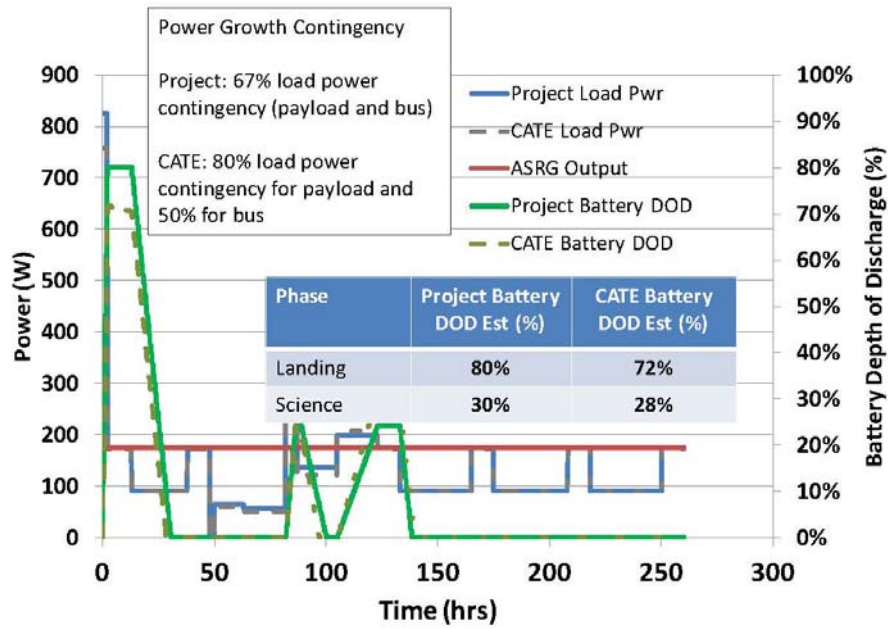
Figure 6.   EHM Lander Surface Power

9

sample acquisition, radiation-hardened detectors for the Europa mission environment, qualification of the STAR 30BP solid rocket motor for long-duration space exposure, and life qualification of the AMBR 890 N (HiPAT) engine. Terrain-relative navigation is currently estimated at TRL 4 based on work from the Autonomous Landing and Hazard Avoidance Technology (ALHAT) project toward development of instrumentation and software for lunar landing technology. A particular challenge for landing at Europa is the current level of uncertainty in the Europa surface characteristics. The Raman Spectrometer is currently estimated at TRL 4 based on laboratory demonstrations, and design effort is anticipated to adapt hardware for the Europa mission environment. Rotary-percussive sample acquisition is currently estimated at TRL 4 based on prototype development for future Mars missions and further design effort is anticipated to adapt this technology for the Europa surface properties. The ASRG is currently estimated at TRL 5 based on DoE engineering unit testing with further testing by NASA Glenn Research Center. Further life testing is anticipated as well as a modified housing design. An area of concern regarding the ASRGs is the impact of ASRG-induced jitter on mission imaging, such as the reconnaissance mapping prior to landing. Additional development of radiation-hardened detectors is anticipated to advance beyond TRL 5-6. The current level of maturity depends on the selected manufacturers and their proposed manufacturing techniques for hardening of CCD and CMOS type detectors. The AMBR engine is currently estimated at TRL 6, based on unit level environmental and performance testing, though additional performance and life testing is ongoing. The STAR 30BP rocket motor proposed for this mission is currently estimated at TRL 6-7 based on previous use in space missions with some possibility of modifications to perform as needed after a long storage period in space while in transit to Europa.

Radiation Environment

The radiation environment for the EHM lander mission contributes to uncertainty in mass, cost, and schedule. Hardware that is external to the radiation vault, particularly exposed sensor heads, will require qualification for the mission radiation environment. Delays in radiation qualification of sensor detectors or optics may adversely impact project cost and schedule. Hardware that is internal to the radiation vault may need to be assessed for compatibility (EMI and thermal) within the common enclosure. Additional systems engineering effort is anticipated for successful integration of electronics within the common radiation vault. The impact to the CATE cost estimate was considered by using the Juno mission as a cost analogy and adding a 5% multiplier to the bus and camera estimates for radiation issues.

Planetary Protection

The EHM Lander is intended for a Europa surface science mission and the Carrier is intended for disposal on the surface of Europa. As a result both the Lander and Carrier elements are subject to Planetary Protection Requirements. These requirements will place a stringent limit on spores on surfaces, in joints, and in the bulk of nonmetallic materials. Currently, the project plans to use dry heat microbial reduction to meet these requirements and possibly other means if necessary, such as H_2O_2 plasma sterilization. Hardware used on the EHM Lander and Carrier must be tolerant to the high heat (~110-125 C) microbial reduction process or other processes as needed. These requirements will constrain hardware selection and may result in adverse impacts to cost and schedule. In order to ensure satisfaction of Planetary Protection requirements, the project will need to implement a compliance effort throughout the system development. In order to account for instrument and bus planetary protection, a 5% multiplying factor was used in the cost estimate.

10

5.   Cost and Schedule Evaluation

Figure 7 illustrates the CATE cost estimating approach in the form of a flow diagram. The initial focus is to estimate, with multiple analogies and cost models, the concept hardware such as instruments and spacecraft bus. Following the estimation of other cost elements based on historical data, a probabilistic cost- risk analysis is employed to estimate appropriate cost reserves. To ensure consistency for all concepts, the cost estimates are updated with information from the technical team with regard to mass and power contingencies and potentially required additional launch vehicle capacity. Using independent schedule estimates, costs are adjusted using appropriate burn rates to properly reflect the impact of schedule delays or multiple work shifts to ensure meeting a launch date. Finally, the results are integrated, cross-checked with other independent cost and schedule estimating capabilities and verified for consistency.

Figure 7.   CATE Cost Estimating Process

Hardware Cost Estimates

The hardware cost elements estimated for the Europa Lander concept are the Carrier, the Lander, and the instruments. Multiple estimates are developed for each of these elements. Both parametric cost models and analogy-based estimates are used. Figure 8 illustrates the analogy-based estimating process, which uses a cost estimating relationship (CER) to adjust the actual costs of past missions. By using the actual costs of past missions, unique attributes of those missions or performing organizations, which are similar to the mission being estimated, can be captured. This can provide insight that is different from most parametric cost models, which are based more on an "industry average" approach.

Table 1 summarizes the cost estimate results for the Flight System. Comparisons between the project and CATE estimates are difficult at lower levels because of the differing breakouts of cost elements. At the total Flight System level, the agreement between the CATE estimate ($1,066M) and the project estimate ($915M) is reasonable.

11
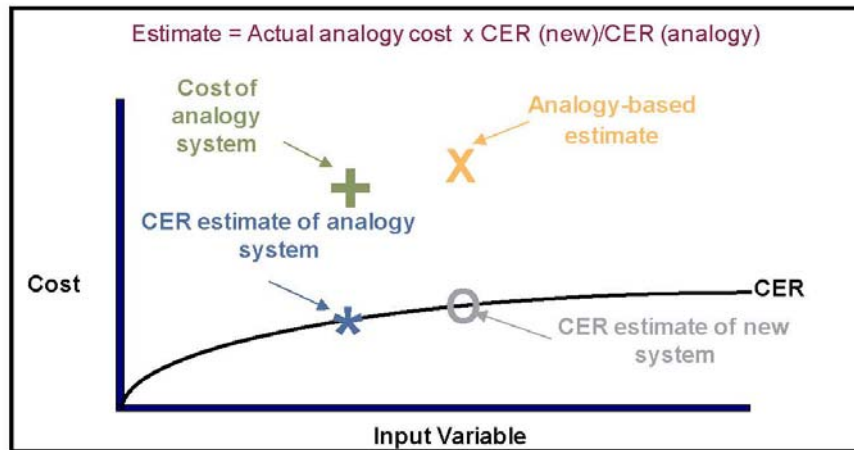
Figure 8.   Analogy-Based Estimating Process

Table 1.   Europa Lander Flight System Cost Estimates

WBS Element	Project Estimate		CATE Estimate		Basis of CATE Estimate
Flight System PM/SE	$	103			Included in Lander and Carrier estimates
Lander	$	309	$	354	NAFCOM11, PRICE, Phoenix, and MSL Descent Stage
Sample Acquisition System (SAS)			$	44	PRICE; MER, Phoenix, and MPL arms
TRNC			$	12	MICM, NICM, SOSCM, PRICE; MRO and MSL cameras
Flash Lidar (2 units)			$	47	MICM, NICM, MOLA, NLR, MLA
Carrier	$	428	$	454	NAFCOM11, PRICE, Juno, MRO
Radiation Monitoring System (on Carrier)			$	10	MICM, NICM, CRaTER, MARIE
Recon Imager			$	71	MICM, NICM, SOSCM, PRICE, HiRISE, LORRI, MOC
Braking Stage	$	3	$	3	Pass-through of Project Value
System I&T	$	72	$	72	Roll-up from lower level methods
Total	$	915	$	1,066	

For the Lander, a total of four estimates were developed using the NASA and Air Force Cost Model (NAFCOM), the PRICE-H cost model and analogy-based estimates using Phoenix and the MSL Descent Stage. The final CATE estimate is an average of these four estimates. The results of these estimates are depicted in Figure 9. The cost estimates shown include the Lander hardware, Project Management and Systems Engineering at the Lander and Flight System level, and Lander-level Integration and Test.

For the Carrier, a total of four estimates were developed using the NASA and Air Force Cost Model (NAFCOM), the PRICE-H cost model and analogy-based estimates using Juno and Mars Reconnaissance Orbiter (MRO). The final CATE estimate is an average of these four estimates. The results of these estimates are depicted in Figure 10. The cost estimates shown include the Carrier hardware, Project Management and Systems Engineering at the Carrier and Flight System level, as well as Carrier-level Integration and Test.

The Sample Acquisition System, the Flash Lidar, the TRNC, the Reconnaissance Imager, and the Radiation Monitoring System are estimated like instruments, and the results are included in the Flight System total. The cost estimates are based on either two or three parametric cost models and two to five analogy-based estimates. The parametric models used for the Lander instruments include the NASA Instrument Cost Model (NICM), The Multivariate Instrument Cost Model (MICM), and the Space-based Optical System Cost Model (SOSCM). Figures 11 to 15 show the results for each element.

12
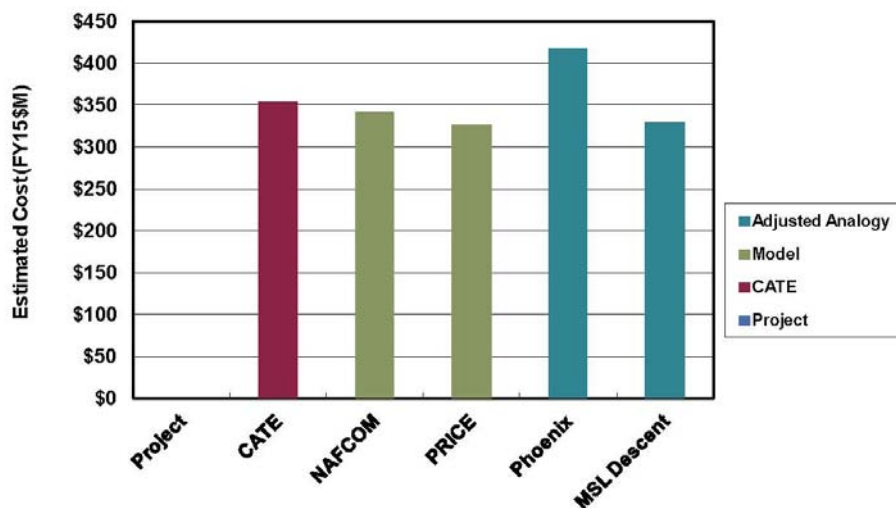
Figure 9.   Lander Cost Estimates
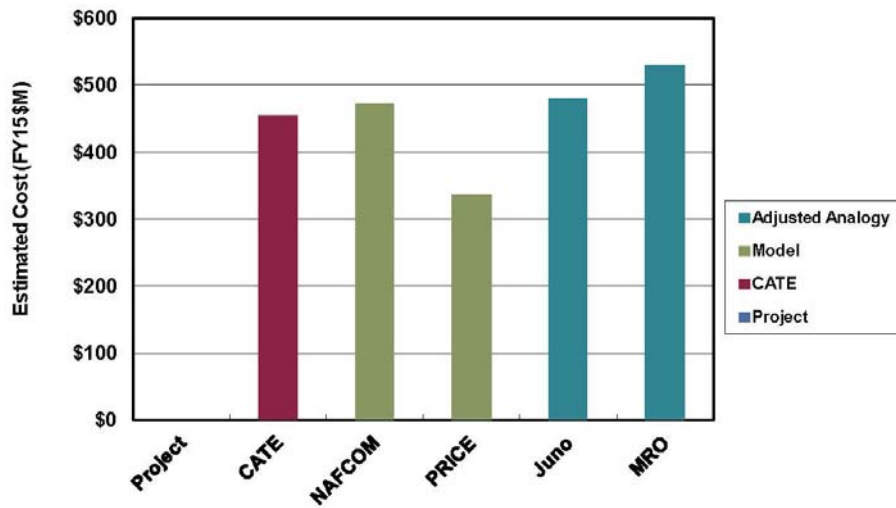
Figure 10.   Carrier Cost Estimates

13
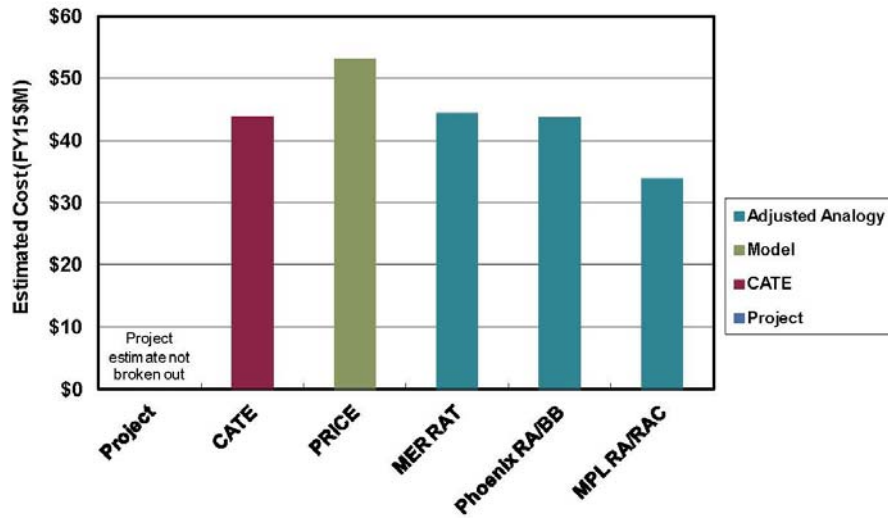
Figure 11. Sample Acquisition System Cost Estimates
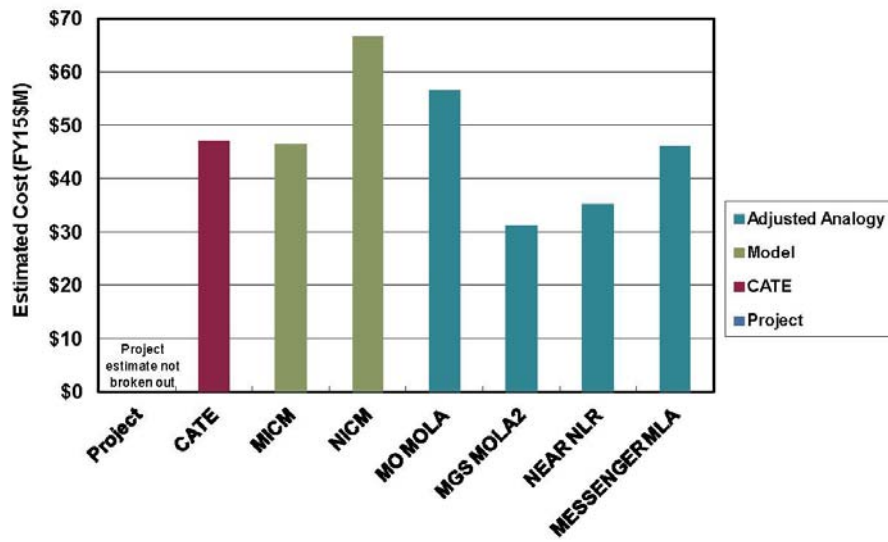

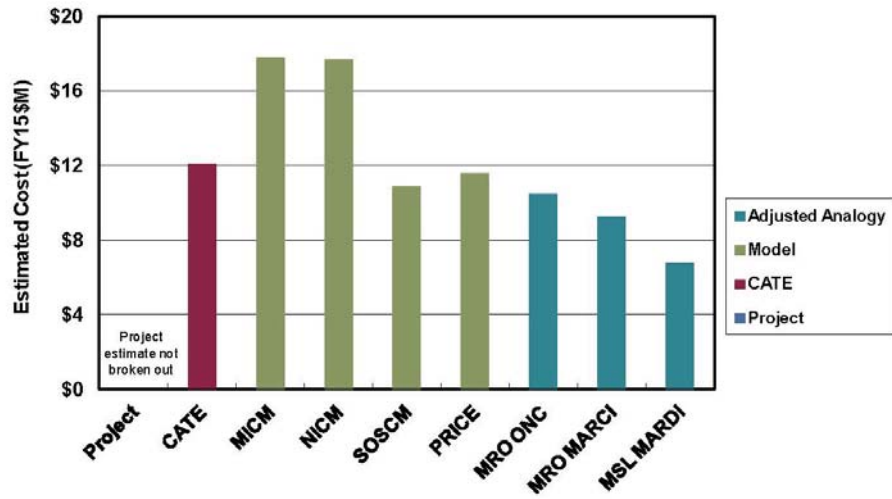Figure 12. Flash Lidar Cost Estimates
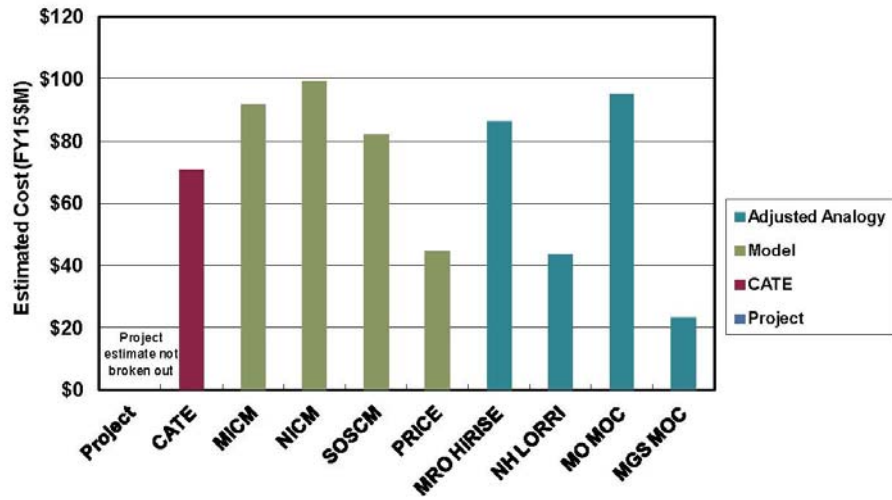
14

Figure 13. TRNC Cost Estimates

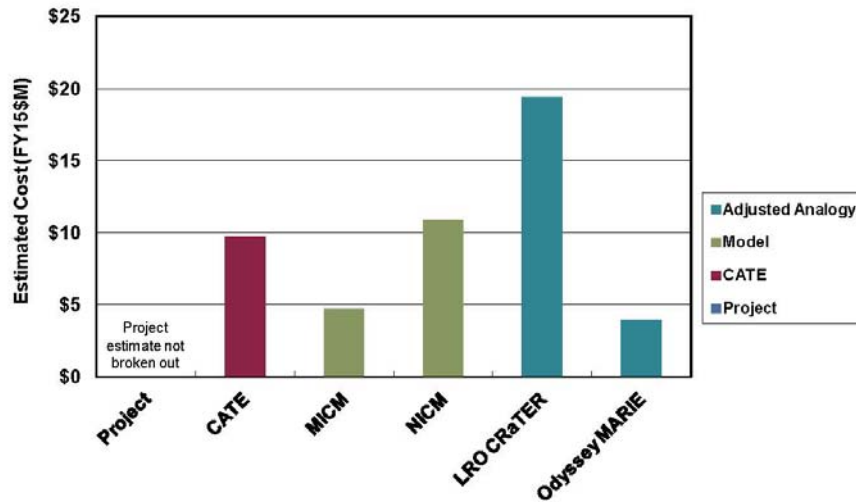Figure 14. Reconnaissance Image Cost Estimates

15

Figure 15. Radiation Monitoring System Cost Estimates

For the Lander science instruments, the cost estimates are based on either two or three parametric cost models and two to five analogy-based estimates. The parametric models used for the Lander instruments include the NASA Instrument Cost Model (NICM), The Multivariate Instrument Cost Model (MICM), and the Space-based Optical System Cost Model (SOSCM). In addition to the 6 Lander science instruments. The results for the instruments are depicted in Figures 16 to 21. In addition to the individual instrument estimates, the total payload estimate includes an estimate of the payload-level Project Management and Systems Engineering. For the total payload, the CATE estimate ($143M) is significantly higher than the project estimate ($97M), as shown in Figure 22. This difference is offset by the $70M project estimate for Technology Development of the Raman Spectrometer and Seismometer compared to the CATE estimate of $16M for these same elements.
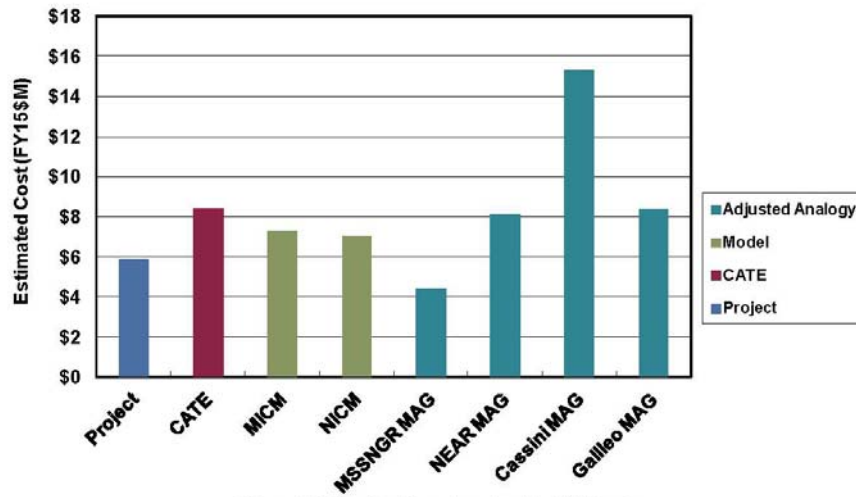
Figure 16. Lander Magnetometer Cost Estimates

16
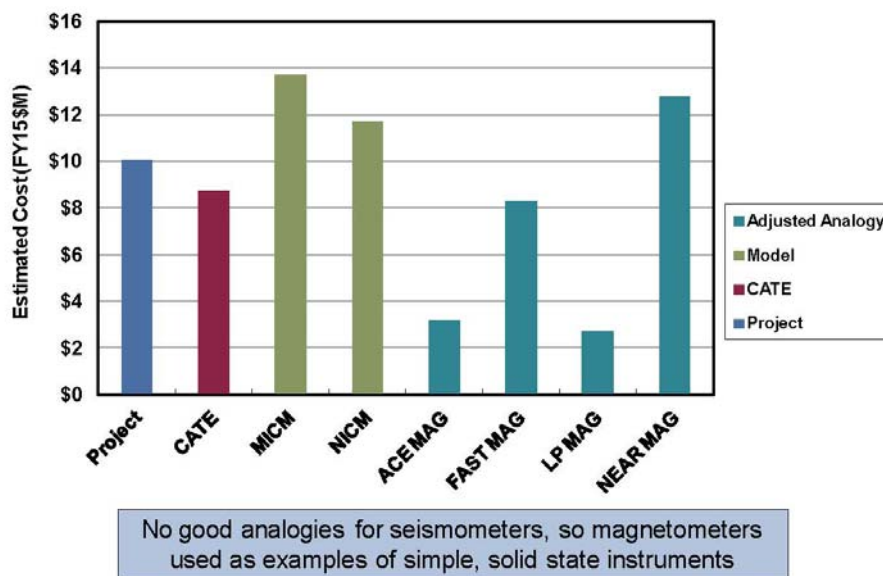
Figure 17. Lander Seismometer Cost Estimates
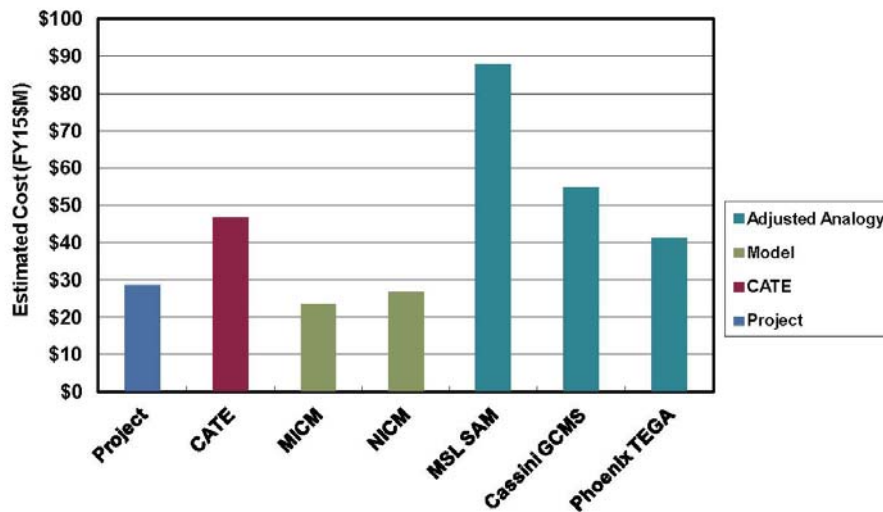
Figure 18. Lander Mass Spectrometer Cost Estimates

17
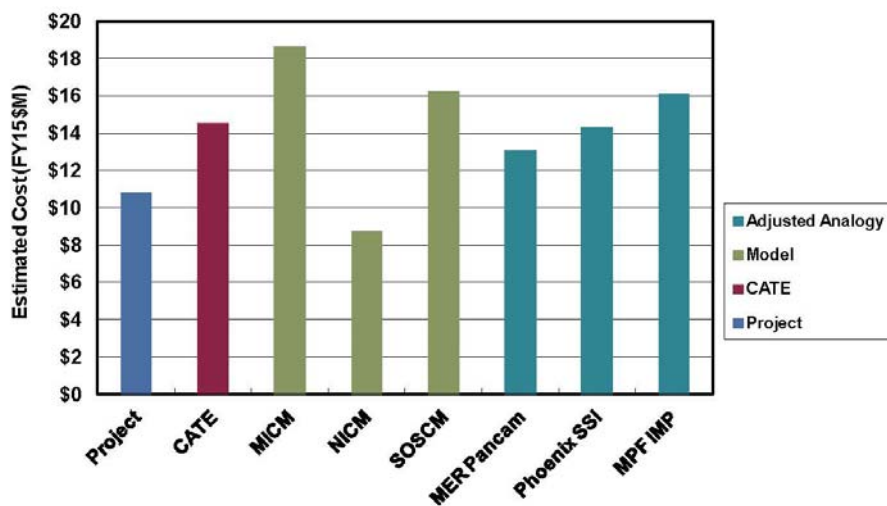
Figure 19. Lander Site Imaging System Cost Estimates
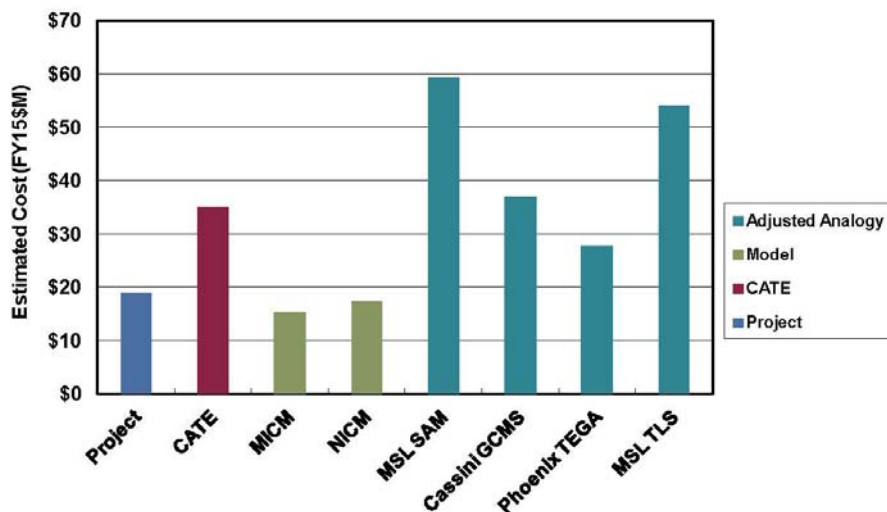
Figure 20. Lander Raman Spectrometer Cost Estimates
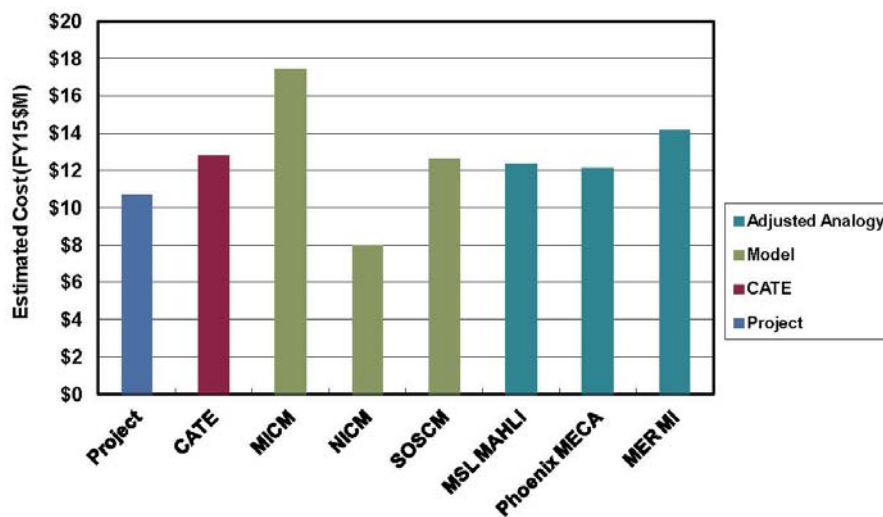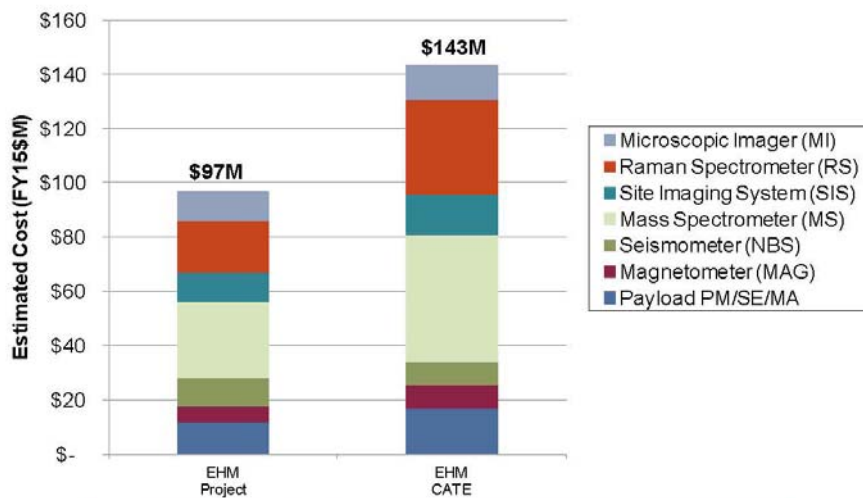
18

Figure 21. Lander Microscopic Imager Cost Estimates

Difference in Phase B-D instrument estimates is offset by significantly higher JPL technology development estimates

Figure 22. Total Payload Cost Comparison

19

Other Cost Elements

Other cost elements estimated for the EHM Lander concept include project-level Project Management, Systems Engineering, and Mission Assurance (PM/SE/MA), pre-launch Science and Ground System Development, Pre-Phase A/Phase A, Technology Development, Phase E, and Education and Public Outreach (EPO). Other cost elements included in the total cost estimate, but not independently estimated are the ASRGs, the braking stage, and launch vehicle.

PM/SE/MA was estimated as a single total using "wrap factors" based on similar historical projects. The historical missions used for the Lander PM/SE/MA estimate are Cassini, Juno, Mars Exploration Rover (MER), and MRO. The "wrap factors" are calculated as a percentage of hardware costs for the historical missions. These percentages are then applied to the estimated hardware cost of the Lander concept. Specifically, the average percentage wrap factor is applied to the total of the average estimate for each hardware element.

Pre-launch Science and Ground System Development estimate is similarly developed using wrap factors based on historical missions. The historical missions used are Cassini, Juno, MER, and MRO.

Pre-Phase A/Phase A costs are estimated using a rule of thumb of 1.5% of the Phase B-D development costs per year of Pre-Phase A/Phase A. For the EHM Lander concept, the total duration used was 40 months starting in June 2012 and ending in October 2015. This is actually earlier than the Phase A end date shown on the project schedule (Figure 23). However, significant activities are planned to start in October 2015. These activities have historically been a part of Phase B, so an adjusted Phase B start date is used for all schedule related analyses.
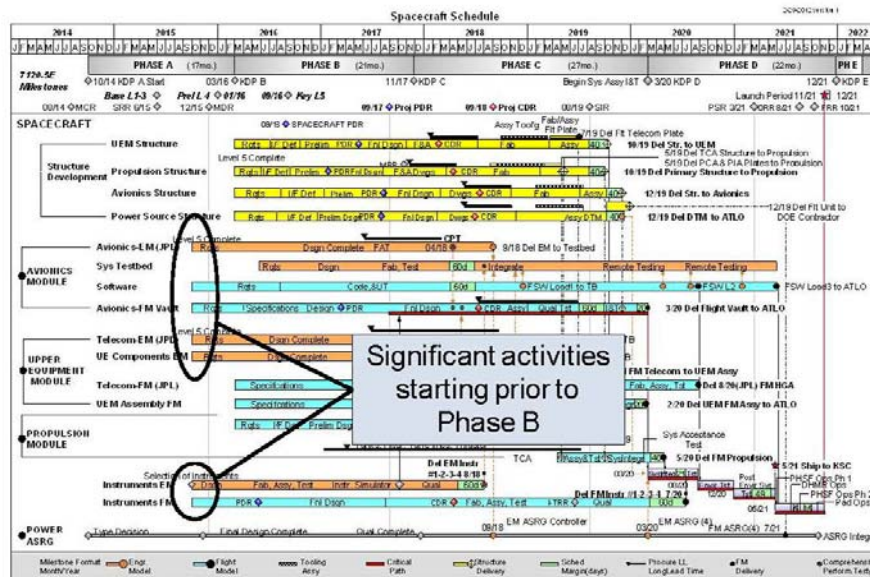

Figure 23. Europa Lander Planned Development Schedule

Technology Development costs were estimated using a table of percentage derived from past technology development efforts. The percentages are applied to the estimated cost of the item

20

requiring the Technology Development. For the EHM Lander, Technology Development was estimated for 4 items: the Raman Spectrometer, the Seismometer, the Precision Landing System, and the Sample Acquisition System.

Phase E costs were estimated using annual spend rates from similar historical projects. Because of the potentially different staffing required during cruise and encounter, these phases were estimated separately using historical rates appropriate for the respective phase. For the cruise phase, annual rates from MESSENGER, Juno, and New Horizons cruise phases were used. For the encounter phase, annual rates from MRO and the predicted annual rate from Juno encounter phases were used.

EPO costs were estimated as 1% of total project costs excluding launch vehicle.

For the ASRGs, the project estimate of $50M each, supplied by NASA HQ, was used in the CATE estimate and for the Braking Stage, the project estimate of $3.2M was used. For the Delta IV Heavy launch vehicle, a $543M estimate from the Planetary Decadal Survey was assumed for consistency.

Cost Reserves

Cost reserves are estimated using a process illustrated in Figure 24. For each Work Breakdown Structure (WBS) element, a triangular distribution of possible costs is developed. The cost values for the triangle are derived from the range of cost estimates as illustrated in the bus and instrument figures above. The lowest of the multiple estimates is used as the low value of the triangular distribution. The average of the multiple estimates is used as the mode or most-likely value of the triangular distribution. The high value of the triangular distribution starts with the highest of the multiple estimates but then adds an additional Design Maturity Factor (DMF). The DMF is a multiplier based on the maturity of the proposed design and the experience of the team. This factor helps ensure that the high value of the distribution truly represents a worst case.
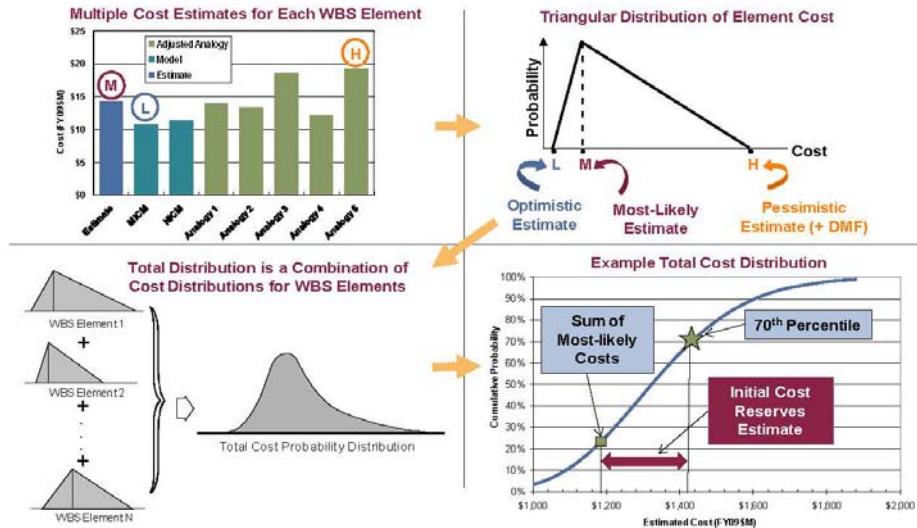

Figure 24. Cost Reserve Estimate Process Overview

21

Once the triangular distributions are developed for each WBS element, they are statistically combined to produce a total cost probability distribution. This distribution is typically plotted as a cumulative distribution which takes the familiar "S-curve" shape. The difference between the 70th percentile value from this curve and the sum of the most-likely estimates is the cost reserves estimate.

Mass and Power Contingency Threat

The mass and power contingency threat is a concept that was developed to support the CATE estimates, initially for the Astro2010 Decadal Survey, then later applied to the Planetary Science and Heliophysics Decadal Surveys. The motivation was to provide a methodology to account for the design evolution that has historically occurred from early conceptual design through development and launch. In order to assign a cost to these design changes, historical mass and power growth data was examined. This data showed values that were well above the typical guidelines of roughly 30% at Phase B start. Because data prior to Phase B start was sparse, the available data was extrapolated back to early conceptual phases.

Figure 25 shows an example of the data used for the mass and power contingency threats. This plot shows payload mass growth data for seven historical planetary missions. The red line is the average of this historical mission data. The black line is the CATE contingency that is used for the threat calculation.
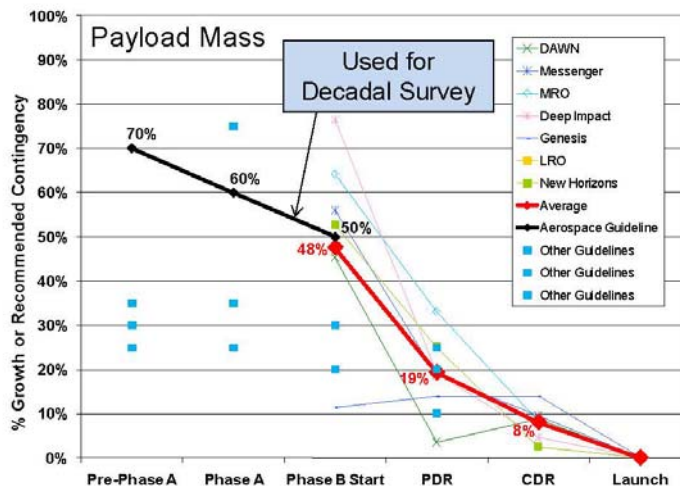

Figure 25. Contingency Values Used for Threat Estimates

To estimate the threat cost, the project-proposed mass and power contingencies (used in the hardware estimates described above) are replaced with the CATE contingencies. The estimates, including reserves, are then recalculated and the difference between this result and the result using project contingencies is recorded as the mass and power contingency threat.

For most projects, the CATE contingencies are well above the contingency values assumed in the proposed concept. The Europa Lander concept was no exception. The consequence of this is that the CATE estimate includes a significant mass and power contingency threat ($230M) as an estimate of the impact of potential future design changes. Table 2 is a summary of the mass properties used in the CATE assessment.

22

Table 2. Europa Leader Mass Properties

	Project CBE (kg)	Project Cont. (%)	Project MEV (kg)	CATE Cont. (%)	CATE MEV (kg)
EHM Lander System Total (Dry)	**1395.2**	**30%**	**1815.6**	**52%**	**2118.6**
Lander Payload Total	**44.2**	**46%**	**64.4**	**70%**	**75.2**
Magnetometer (MAG)	2.2	50%	3.3	70%	3.7
Narrow Band Seismometer (NBS)	5.8	50%	8.6	70%	9.8
Mass Spectrometer (MS)	14.8	50%	22.2	70%	25.2
Site Imaging System (SIS)	3.2	50%	4.8	70%	5.4
Raman Spectrometer (RS)	6.5	50%	9.8	70%	11.1
Microscopic Imager (MI)	2.3	50%	3.4	70%	3.8
Science Chassis	9.5	30%	12.4	70%	16.2
Lander Flight System Total	**514.1**	**30%**	**668.9**	**52%**	**779.5**
Mechanical + Shielding	181.9	33%	241.4	52%	276.7
Thermal	28.6	30%	37.0	50%	42.8
Propulsion	60.7	30%	78.7	50%	91.0
GN&C	31.8	36%	43.3	64%	52.1
C&DH	27.4	26%	34.6	50%	41.1
Telecom	23.0	32%	30.3	50%	34.4
Elect Power	94.9	24%	117.7	50%	142.4
ASRGs	66.0	30%	85.8	50%	99.0
Carrier Flight System Total	**836.9**	**29%**	**1082.3**	**51%**	**1264.0**
Mechanical + Shielding	266.2	30%	346.5	50%	399.3
Thermal	28.5	30%	37.1	50%	42.8
Propulsion	219.6	28%	280.1	50%	329.4
GN&C	72.8	35%	98.3	60%	116.1
C&DH	8.6	30%	11.2	50%	12.9
Telecom	55.5	22%	67.7	50%	83.3
Elect Power	111.8	30%	145.3	50%	167.6
ASRGs	66.0	30%	85.8	50%	99.0
Radiation Monitoring System	8.0	30%	10.4	70%	13.6

Schedule Threat

The base cost estimate described above uses the project-proposed development schedule. Historically, project schedule estimates have proven to be optimistic. As part of the CATE process, a probabilistic Independent Schedule Estimate (ISE) is developed. If the 70th percentile duration from the ISE is longer than project schedule, then a schedule threat is added.

Figure 26 illustrates the ISE process. The ISE is based on actual schedule durations from similar, historical missions. The duration of each schedule phase is treated as a triangular distribution, which can be statistically combined to yield a probability distribution of total project development time. The triangular distribution of durations for each phase is derived from the actual phase durations from the historical missions. The lowest duration is used as the low end of the triangular distribution, the average duration is used as the mode or most-likely value and the highest historical value is used as the high value of the triangular distribution.

Figure 27 compares the actual Phase B-D duration of the four analogous missions used in the ISE with the proposed Europa Lander Phase B-D duration. Figure 28 shows the results of the ISE as a cumulative probability distribution or s-curve. The 70th percentile ISE value is 71 months while the Europa Lander proposed value is 73 months (after adjusting the effective Phase B start date as described above). Figure 29 is a breakdown of the results by project phase. While the overall durations agree quite well, the 70th percentile historical duration for the start of spacecraft I&T to start of flight system I&T phase is significantly longer than the project value. Although this difference
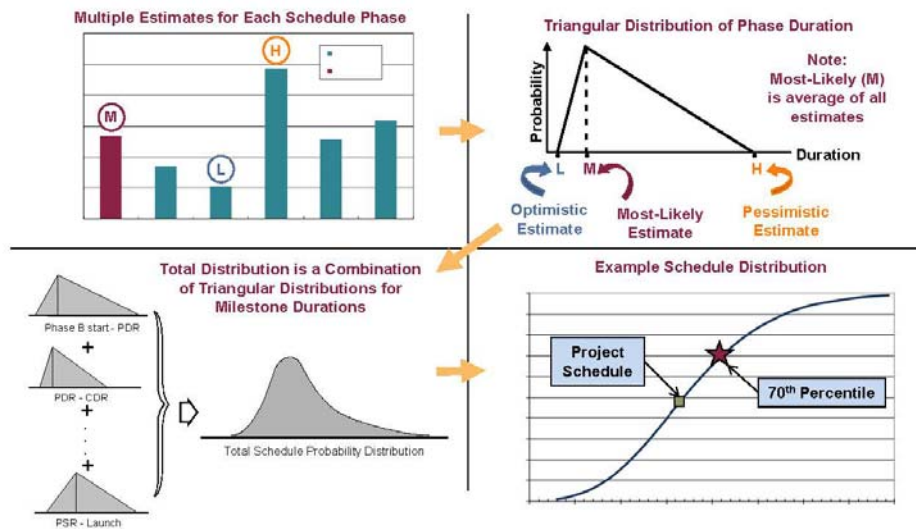
23

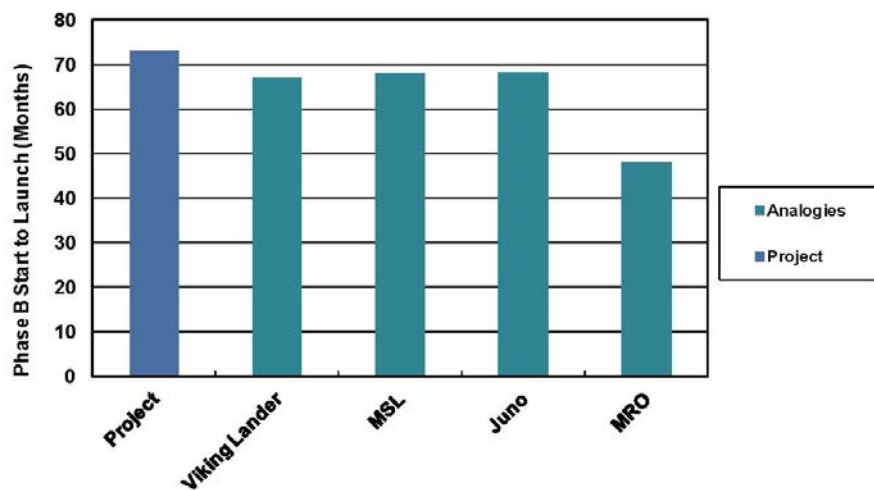Figure 26. Independent Schedule Estimate Process overview

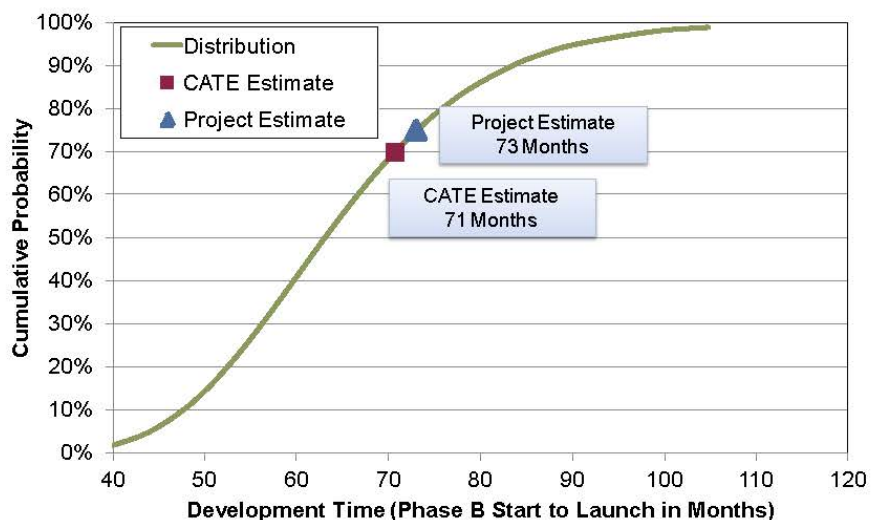Figure 27. Analogous Mission Development Time Comparison
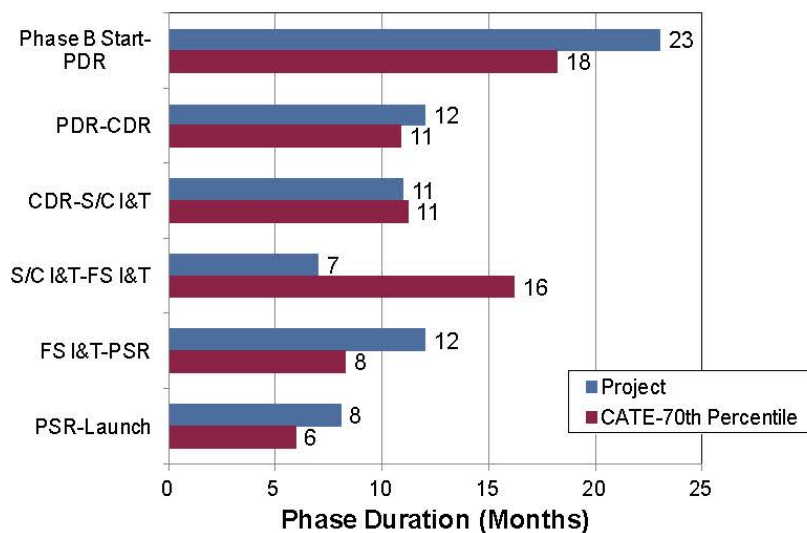
24

Figure 28. Europa Lander ISE S-Curve

Figure 29. Europa Lander Analogous Mission Phase Comparison

25

does not contribute to the CATE cost estimate, the plan for this phase should be examined to ensure its adequacy. Because the overall project schedule is longer than the ISE 70th percentile estimate, no schedule threat is added.

Results

Table 3 presents the final CATE cost results compared to the current Europa team cost estimate. The agreement between the two estimates is quite close in all WBS elements. Figure 30 and 31 present the same data in graphical form.

Table 3.   Europa Lander Cost Estimate Comparison (FY15$M)

| WBS Element	Project Estimate	CATE Estimate	Basis of CATE Estimate
Pre-Phase A, Phase A, Tech Dev	$ 195	$ 146	1.5% of Dev cost per year for 40 months + Tech Dev
Mission PM/SE/MA	$ 209	$ 184	Percentage of HW based on Cassini, Juno, MRO, MER + NEPA
Instruments	$ 97	$ 143	MICM, NICM, SOCM and analogies to planetary instruments
Flight System	$ 915	$ 1,066	NAFCOM11, PRICE and analogies to planetary systems
ASRGs	$ 200	$ 200	Project Value for 4 ASRGs
Pre-launch Ground and Science	$ 103	$ 138	Percentage of HW based on Cassini, Juno, MRO, MER
Phase E and EPO	$ 335	$ 250	Based on annual rates from MESSENGER, NH, Juno, MRO, MSL, and Phoenix
Total Reserves	$ 674	$ 647	70% from cost risk analysis
Mission Cost Before Threats	**$ 2,728**	**$ 2,774**	
Schedule Threats		$ -	Proposed schedule is adequate
Mass and Power Contingency Threats		$ 230	Aerospace contingency levels
LV Threats		$ 91	Based on a percentage of Delta IV H costs
Mission Cost With Threats	**$ 2,728**	**$ 3,095**	
Launch Vehicle/Services	$ 543	$ 543	Delta IV H cost from DS guidelines + nuclear processing
Total Mission Cost With Threats	**$ 3,271**	**$ 3,638**	
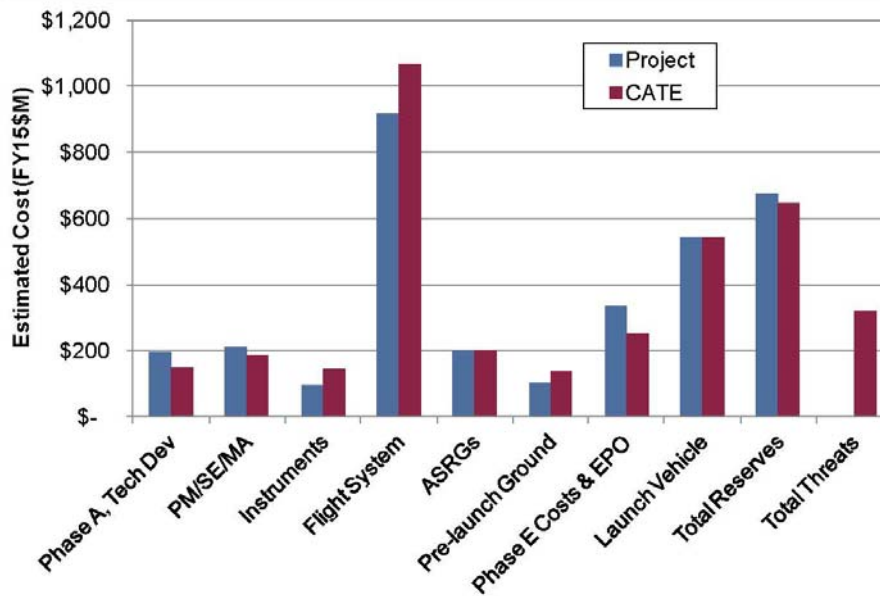
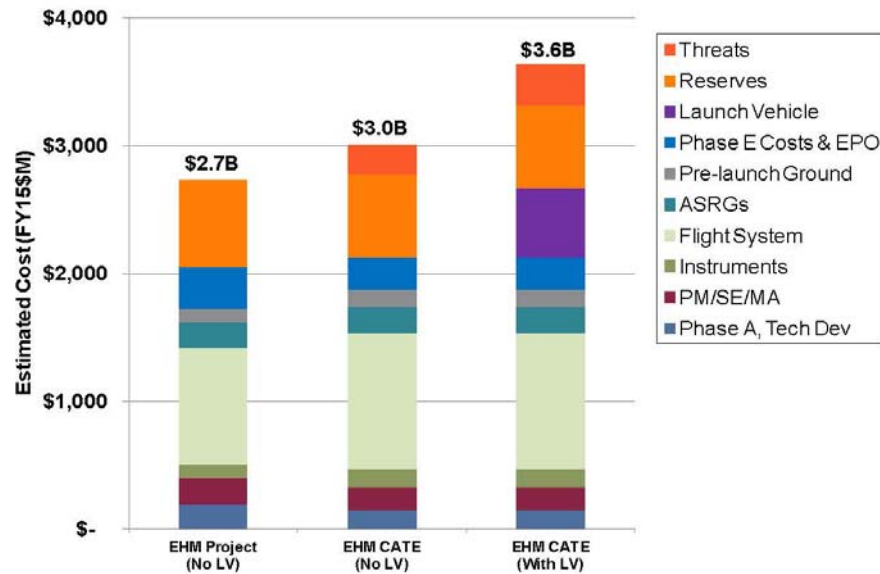Figure 30. Europa Lander Key Cost Element Comparison

26

Figure 31. Europa Lander Cost Estimates

Complexity-Based Risk Assessment (CoBRA)

As a cross-check of the CATE results, the Complexity-Based Risk Assessment (CoBRA) process was also applied to the Europa Lander concept. The CoBRA process uses technical and programmatic parameters from the conceptual design to calculate a complexity value for the design. This is done by ranking each of the individual parameters against a database of historical space missions. The calculated complexity values for the historical missions are plotted against development cost and schedule. The missions are classified as successful, partially successful, failed, or yet to be determined. A best fit line is drawn through the successful missions and the estimated cost and schedule of the Europa Lander concept can be compared to missions of similar complexity. Figures 32 and 33 show the CoBRA cost and schedule analysis results. Both the project and CATE cost estimates are slightly above the green trend line but in family with successful past missions of this complexity. Both the project and CATE schedule estimates are below the green trend line but above the blue trend line which is drawn through successful missions that had a planetary launch window constraint. Again, this result adds confidence that the Europa Lander schedule estimates are in family with comparable successful missions.
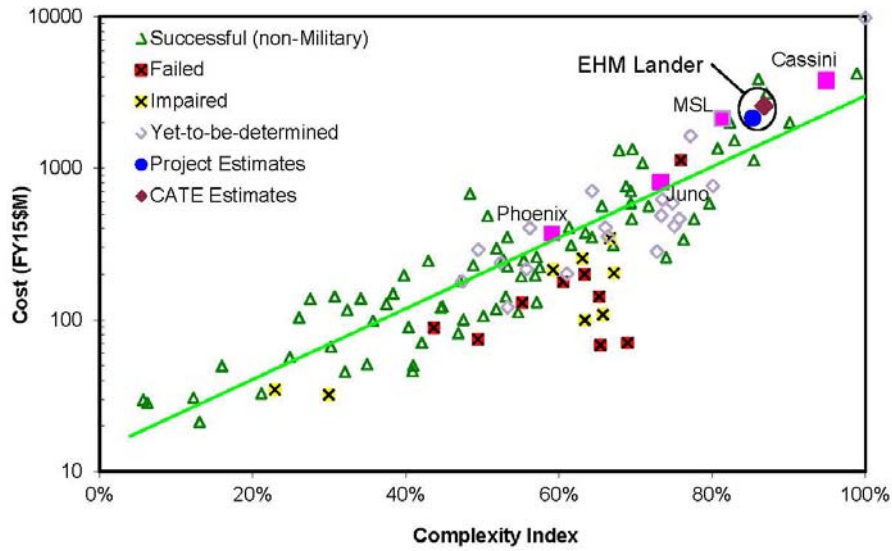
27

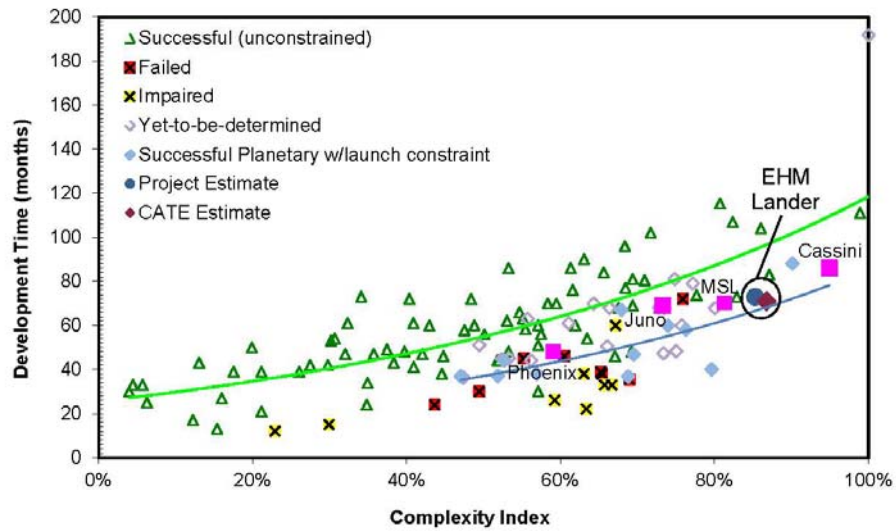Figure 32. Complexity-Base Risk Assessment Cost Analysis

Figure 33. Complexity-Based Risk Assessment Schedule Analysis

28

D.4.5   *Independent Technical Review Findings*

STANFORD
AERONAUTICS &
ASTRONAUTICS

DURAND BUILDING, 496 LOMITA MALL
STANFORD, CA 94305-4035
http://aa.stanford.edu
(650) 723-3317, fax: (650) 723-0279

Dr. Firouz Naderi   March 23, 2012
Solar System Exploration Directorate
JPL
Pasadena, CA

Dear Dr. Naderi

The recent Planetary Decadal Survey determined that the Europa Jupiter System Mission
(EJSM) would produce compelling science but was not affordable based on an
independent cost estimate of $4.8B provided to the National Research Council by The
Aerospace Corporation. The Decadal Survey recommended that the mission be descoped
to significantly reduce cost. In response, NASA created a Science Definition Team (SDT)
which recommended that EJSM be separated into two elements (Orbiter and Flyby) and
focused solely on Europa science. Subsequently, NASA augmented the SDT to allow for
the investigation of a soft lander mission concept. That latter option is the focus of this
letter report.

As requested by JPL and consistent with the direction from NASA HQs, a Review Board
was created to assess the viability of the three mission options to be provided to NASA
HQ. These options were to focus on Europa only and develop Orbiter, Flyby (multiple)
and Lander concepts, identifying the lowest achievable cost with a target value of ≈$1.5B
for each concept, not including launch vehicle. It was recognized by the Board that at a ≈
70% reduction in cost from the original EJSM concept any new mission design and
corresponding science content would be dramatically different and go far beyond the
usual meaning of a simple "descope".

In the charge to the Board, it was emphasized that the Board's responsibility was to
conduct an "existence proof" evaluation of a pre-pre Phase A concept. In addition, each
project was to be evaluated independently, not as one element of a program series.

The Board listed below was assembled and on March 15, convened at JPL to review the
Lander mission designs.

Scott Hubbard	Chair – NASA Ret.
Orlando Figeroa	NASA Ret.
Mark Saunders	NASA Ret.
Dave Nichols	JPL Div. 31
Jeff Srinivasan	JPL Div. 33
Barry Goldstein	JPL Div. 34
Cindy Kahn	JPL Div. 35

1

Leslie Tamppari	JPL Div. 32
Gentry Lee	JPL 4X Chief Engineer
Will Devereux	APL
Douglas Eng	APL

To assist the Board in assessing the concepts, members of the JPL staff provided presentations and responded to many questions. This entire effort was applauded by all of the members of the Board and contributed to a most successful meeting. In particular, many Board members specifically commented on the exceptional work that was conducted in a relatively short time to achieve a Lander concept that provided a scientific return and mission concept with detail equivalent to the Orbiter and Flyby studies.

The top level Europa Lander Review Board conclusions can be summarized in a few statements:

- If the scientific objectives could be met as outlined, the scientific return from an *in situ*, soft-landed instrument suite with coring and drilling capabilities would advance the knowledge of Europa habitability greatly.

- However, the Board was unanimous in concluding that the Lander concept does not satisfy the "existence proof" test as a project that could be conducted within the cost constraints provided and that would also have an acceptable risk posture.
    - Given the very limited information about the nature of the surface of Europa at a small (lander) scale, the scientific and engineering risk inherent in this mission is extremely high. To mitigate those risks, a series of technologies must be developed along with a site location process constrained by the radiation environment. The aggregate resulting cost for the mission estimated by JPL easily exceeds $2B without ELV and the JPL "S-curve" analysis at the 70% confidence level is $2.8B. The Aerospace Cost And Technical Evaluation (CATE) was not available at the time of the review but given the experience of the Decadal Survey, the CATE cost is likely to be higher.

- As a consequence of the finding above, the Board also unanimously recommended that rather than continuing Lander mission studies, a technology investment program be put into place whose goal would be to eventually retire the surface landing risks.
    - Several Board members commented that such a Lander mission would be better suited as a follow-on mission once the surface of Europa was far better characterized.

- As with the previous reviews, the Board identified two generic technical risks that impact all mission concepts:
    - The Advanced Sterling Radioisotope Generator (ASRG) poses a major risk to the project. The project is depending on the Phase 2 ASRG. *However, it appears certain that the ASRG product from Phase 1 will be unusable for a Europa mission.* The ability of the project to levy requirements (and therefore capability) in the first phase to bootstrap any future development

2

work is limited by the need of the ASRG program to meet its performance and delivery commitment to the NASA Discovery program. This exposes the Europa project to major technical, schedule and costs risk in acquiring ASRGs. We recommend that the ASRG plan be consistent with achieving TRL 6 as early in the phase B as possible, as opposed to waiting until PDR, as is normally expected.

o Detector Systems - Development and characterization of the detector systems, including front end and signal processing electronics, are a high-risk area for all of the mission concepts because of the extreme radiation environment requirement. It is recommended that a program be started early to verify the processes for their fabrication, integration, and end-to-end performance in representative environments, including repeatability of results. The viability and availability of detectors may require that their production and characterization be started early, possibly ahead of the AO. The design of the instruments may also be affected by what is learned about the detectors and their performance. An instrument accommodation assessment may be beneficial to the instrument-selecting officials for a more complete assessment of risk.

Programmatic and Management Approach
- Consistent with the above assessment, a Board consensus emerged that if any of the mission concepts move ahead, particular attention must be paid to the wording and schedule of an Announcement of Opportunity (AO) for the science investigations. An early AO release and selection will establish the PI-mission interface in critical areas such as total detector dose and enable the Europa mission system engineering team to do all the shielding and system integration trades as early in Formulation as possible. Such a process will allow the technology and engineering development needed to have a sound mission design by PDR and thus good cost and schedule estimates at both KDP B and KDP C (now a major emphasis of NASA's external stakeholders). This AO approach will greatly improve the probability mission success within cost constraints.

- Cost and Schedule – It was noted at the reviews for the orbiter and flyby that cost and schedule estimates had to be better integrated, and checked against representative past experiences. Time limitations did not allow for the review board to critically assess these areas to the same level of the technical aspects of the mission. However, the Project did exhibit an approach that appears to address the recommendation. We commend the Project for moving in the right direction.

- Margins – Some presenters made reference to the "AO Technique" to compare mass, and power margins. AO proposal concepts are (or supposed to be) submitted at a higher level of maturity than an early concept, and should not be used as a basis for comparison. Presenting such data invites inappropriate comparisons.

3

- Organization – The Project presented an organization structure that adds a much needed focus, emphasis, and visibility on cost planning and management. Such a structure is a particularly pressing issue for flagship missions, and these efforts are applauded. There was a perception, though, that the system engineering function was downplayed in the organization. The strength and expectations of system engineering needs to be stated and communicated clearly, as part of the Project' leadership team.

Detailed Considerations:
In the charter distributed to the Board prior to the review, we were asked to consider the following criteria:
- Ability of the mission to satisfy the Science Objectives
- Mission design approach
- Robustness of the mission and system architectures
- Robustness of mission and system margins; compliance with JPL design principles.
- Proposed scope, including available options, is consistent with funding target value to complete the mission
- Cost risk Project planning risks, including design, environment mitigation plans, integration and test plans, schedule and margins.

Within this overall review framework the following more specific comments were noted where at least two or more Board members addressed similar issues:

Advanced Technologies required to meet Science Objectives:
In addition to the landing site risk, this mission concept requires significant new technology and complex engineering developments that raise the overall technical and cost risk to undesirable levels. Listed below are comments on each of those areas:
- Optical terrain relative navigation (TRN) for space application is maturing; however significant technology work is still required to demonstrate this as part of a landing system.
- Flash-based LIDAR hazard avoidance technology is also maturing but has even more development required than TRN to be qualified for such a mission.
- The sampling drill needs to be qualified for the very challenging Europa environment
- The Raman spectrometer still requires significant technology work
- An integrated mass spectrometer, Raman spectrometer, and microscopic imager assembly for measuring the core sample is a very complex engineering development. There is currently no comparable instrument package that has been developed and flown.
- The seismometer assumed for this concept is very low technology readiness level.
- Planetary Protection would need to be considered much more carefully than was obvious from the charts.

Mission Design and Architecture
- At present there are only 15 Galileo images of Europa's surface at a resolution of 9-12 m/pixel and only 1 image at 6m/pixel. Because the existence of a 10-meter square area with mild slope and limited rock distribution (height, width, and concentration) is unknown, the mission would initially have to perform an orbital survey phase with

4

high-resolution (Mars Reconnaissance Orbiter "HiRise" scale) imagery. Given the intense radiation environment of Europa, the 30 days allocated to this survey prior landing presents an unacceptable mission risk that puts its feasibility into question. Such a survey would normally be allocated something more like 90 days. With data currently available, Europa appears to have very difficult landing terrain and it is conceivable that with the 30-day survey an acceptable landing site might not be found. The much lower risk approach would be to conduct a thorough orbital reconnaissance prior to a landed mission.
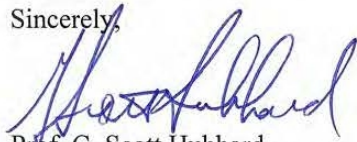
<u>Summary Comments</u>

Several Board members volunteered similar thoughts that address the method of assessing the three different concepts. To present the materials, the JPL Europa Team should develop a summary chart or charts that compare all of the mission concepts to the original JEO mission in the areas of overall science benefit, risk, and cost in a simple and understandable way to help make the recommendation clear to NASA decision makers.

One approach may be to devise figures of merit (FM) to compare the different mission (orbiter, flyby, lander) concepts. Such FMs might include.
- Degree to which the mission concept addresses the scientific goals/objectives defined by the NRC Decadal
- Degree to which the mission concept meets the schedule for earliest LRD ($\geq$70% confidence), commissioning, and completion of primary science campaign.
- Degree to which the mission concept meets the cost target including reserves at the 70% confidence level.
- Independent assessment of risks for environment in which the system is designed to operate

On behalf of the entire Board, I wish to express again our congratulations to the JPL team in the high quality of the studies. Please let us know if we may of any further assistance.

Sincerely,

Prof. G. Scott Hubbard
Chair, Europa Mission Review Board
Cc: Board members, Tom Gavin

5